THE JOURNAL OF PHYSICAL CHEMISTRY

Volume 73, Number 12 December 1969

Ionization and Dissociation of Pentafluorosulfur Chloride by Electron Impact . . . **P. Harland and J. C. J. Thynne** 4031

Charge Distribution in and Dipole Moments of Some Aliphatic Alcohols . . . **S. S. Krishnamurthy and S. Soundararajan** 4036

Vibrational Intensities. XX. Band Shapes of Some Fundamentals of Methyl Iodide-d_3 . . . **Tsunetake Fujiyama and Bryce Crawford, Jr.** 4040

Surface Orientation in Electrocapillarity. . . . . **A. Sanfeld, A. Steinchen, and R. Defay** 4047

Homogeneous Gas-Phase Thermolysis Kinetics. An Improved Flow Technique for Direct Study of Rate Processes in the Gas Phase . . . . **Harold Kwart, Stanley F. Sarner, and Jon H. Olson** 4056

Electron Attachment by Pyridine and the Diazines in γ Radiolysis. Experimental and Theoretical Consideration . . . **A. Grimison, G. A. Simpson, M. Trujillo Sánchez, and J. Jhaveri** 4064

Mean Activity Coefficient of Polyelectrolytes. XI. Activity Coefficients of Various Salts of Polyacrylic Acid and Carboxymethylcellulose . . . . **Kiyotsugu Asai, Katsuhiko Takaya, and Norio Ise** 4071

The Equation of State of Fluid Argon and Calculation of the Scaling Exponents . . . **Olav B. Verbeke, Vik Jansoone, Rik Gielen, and Jan De Boelpaep** 4076

Thermal Stabilities of Tungsten Oxyiodides . . . . **Suresh K. Gupta** 4086

Kinetics of the Addition of Ethyl, Isopropyl, *n*-Butyl, and Isopentyl Radicals to Ethylene . . . **K. W. Watkins and L. A. O'Deen** 4094

The Kinetics of Heterogeneous Catalytic Electrode Reactions. II. Charge-Transfer Kinetics . . . **J. D. E. McIntyre** 4102

On the Distinction between the Kinetics of Parallel and Hetereogenous Catalytic Electrode Reactions . . . **J. D. E. McIntyre** 4111

The Electrical Conductivities of Molten Bismuth Chloride, Bismuth Bromide, and Bismuth Iodide at High Pressure . . . . **A. J. Darnell, W. A. McCollum, and S. J. Yosim** 4116

Application of Density Matrix Methods to the Study of Spin Exchange. I. The Barrier to Internal Rotation in N-Acetylpyrrole . . . . **Kjell-Ivar Dahlqvist and Sture Forsén** 4124

The Interaction of the Ground and Excited States of Indole Derivatives with Electron Scavengers . . . **Robert F. Steiner and Edward P. Kirby** 4130

Proton Resonance in Alkali Nitrate Melts . . . . **Lieng Chen Siew and Benson R. Sundheim** 4135

Ion–Molecule Reactions in Propene . . . . **A. MacKenzie Peers** 4141

Nitrogen-14 Nuclear Magnetic Resonance Determination of the Quadrupole Coupling Constants of Methyl Isocyanide and Ethyl Isocyanide . . . . **William B. Moniz and C. F. Poranski, Jr.** 4145

Viscosity of a Vitreous Potassium Nitrate–Calcium Nitrate Mixture . . **R. Weiler, S. Blaser, and P. B. Macedo** 4147

The Oxidation of Bromide by Bromate in Fused Alkali Nitrates . . . . **James M. Schlegel** 4152

Kinetics and Mechanism for the Reaction between Alkyl Hydroperoxides and Tetranitromethane . . . **William F. Sager and John C. Hoffsommer** 4155

X-Ray Diffraction Studies of Mono- and Polynuclear Thorium(IV) Ions in Aqueous Perchlorate Solutions . . . **W. E. Bacon and Glenn H. Brown** 4163

Free Radical Formation in Hydrocarbon Crystals by γ Irradiation. Electron Spin Resonance Spectra of Some Alkyl Radicals . . . . **Tomas Gillbro, Per-Olof Kinell, and Anders Lund** 4167

Electron Spin Resonance Studies of Irradiated Heterogeneous Systems. V. Naphthalene, Anthracene, Phenanthrene, and Biphenyl Adsorbed on Porous Silica Gel . . . **Per-Olof Kinell, Anders Lund, and Akira Shimizu** 4175

Photochemistry of Complex Ions. VII. *trans*-4-Stilbenecarboxylatopentaamminecobalt(III) Ion . . . **Arthur W. Adamson, Arnd Vogler, and Ian Lantzke** 4183

Pulse-Radiolysis Studies of *p*-Hydroxyphenylpropionic Acid . . . . **J. Chrysochoos** 4188

Ionic Reactions in Gaseous Mixtures of Monosilane with Methane and Benzene . . **D. P. Beggs and F. W. Lampe** 4194

Solvent Exchange Rates of Solvent–Metal Complexes for Fe^{3+} in N,N-Dimethylformamide, Acetonitrile, and Ethanol and for Ni^{2+} in Ethanol by Proton Magnetic Resonance . . . . **F. W. Breivogel, Jr.** 4203

Pulse Radiolysis of Aliphatic Acids in Aqueous Solutions. I. Simple Monocarboxylic Acids . . . **P. Neta, M. Simic, and E. Hayon** 4207

Pulse Radiolysis of Aliphatic Acids in Aqueous Solutions. II. Hydroxy and Polycarboxylic Acids . . . **M. Simic, P. Neta, and E. Hayon** 4214

Absorption, Optical Rotatory Dispersion, and Circular Dichroism Studies of Some Sulfur-Containing Ribonucleosides . . . . . . **Kam-Khow Cheong, Yi-Chang Fu, Roland K. Robins, and Henry Eyring** 4219

Conformational Rigidity of the Amide Bond. A Variable-Temperature Nuclear Magnetic Resonance Study of the System Ag$^+$–N,N-Dimethylacetamide . . . . **P. A. Temussi, T. Tancredi, and F. Quadrifoglio** 4227

The Thermodynamic Properties of Carbon Tetrafluoride from 12°K to its Boiling Point. The Significance of the Parameter ν . . . . **John H. Smith and E. L. Pace** 4232

Micellar Effects on Acidity Functions . . . . **C. A. Bunton and L. Robinson** 4237

Spectroscopic Evidence for the Mixture Model in HOD Solutions . . . . **W. A. Senior and R. E. Verrall** 4242

Photochemistry of Complex Ions. VIII. Photoelectron Production . . . **W. L. Waltz and Arthur W. Adamson** 4250

Ultrasonic Investigation of the Conformal Changes of Bovine Serum Albumin in Aqueous Solution . . . **L. W. Kessler and F. Dunn** 4256

Enthalpy and Entropy of Sublimation of Tetraphenyltin and Hexaphenylditin. The Bond Dissociation Energy of Sn–C and Sn–Sn . . . . **D. Keiser and A. S. Kana'an** 4264

Adsorption on Hydroxylated Silica Surfaces . . . . **M. L. Hair and W. Hertl** 4269

Visible Circular Dichroism of Planar Nickel Ion Complexes of Peptides and Cysteine and Derivatives . . . **Joyce Wen Chang and R. Bruce Martin** 4277

The Effect of Charge Scavengers on Radiation-Induced Isomerization of Stilbene in Cyclohexane . . . . **Robert R. Hentz and H. P. Lehmann** 4283

Relative Cross Sections for the Quenching of Hg($^1P_1$) Atoms . . . **Albrecht Granzow, Morton Z. Hoffman, and Norman N. Lichtin** 4289

The Prediction of the Properties of Mixed Electrolytes from Measurements on Common Ion Mixtures . . . **P. J. Reilly and R. H. Wood** 4292

Heats of Mixing Aqueous Electrolytes. VIII. Prediction and Measurement of Charge-Asymmetric Mixtures of Three Salts . . . . **R. H. Wood, M. Ghamkhar, and J. D. Patton** 4298

Sublimation of Ammonium Perchlorate . . . . **Christiane Guirao and F. A. Williams** 4302

Extinction Coefficient of Azulene Anion Radical and the Yield of Scavengeable Electron in γ-Irradiated Organic Glass . . . . **Tadamasa Shida** 4311

Optical and Electron Spin Resonance Studies on Photolyzed and Radiolyzed Tetraphenylhydrazine and Related Compounds . . . . **Tadamasa Shida and Akira Kira** 4315

Excitation of Molecular Vibration on Collision. Oriented Nonlinear Encounters . . . . . . **Kyung Kyu Shin** 4321

Mass Spectrometric Determination of the Proton Affinities of Various Molecules . . . **Max A. Haney and J. L. Franklin** 4328

Singlet–Triplet Absorption Bands of Methyl-Substituted Ethylenes . . . **Michiya Itoh and Robert S. Mulliken** 4332

Heats of Dilution at 25° of Aqueous Solutions of the Bolaform Electrolyte $[Bu_3N{-}(CH_2)_8{-}NBu_3]X_2$ . . . **Siegfried Lindenbaum** 4334

Relationships between Arrhenius Activation Energies and Excitation Functions . . . . **Rodney L. LeRoy** 4338

Quantum Yield of Photonitrosation of Cyclohexane in Homogeneous System . . . **Hajime Miyama, Kuya Fukuzawa, Noriho Harumiya, Yoshikazu Ito, and Shigeru Wakamatsu** 4345

The Effects of a Homogeneous Chemical Reaction Preceding Electron Transfer on the Current–Time Curves and Current Integrals Obtained in Controlled-Potential Electrolysis . . . **Robert S. Rodgers and Louis Meites** 4348

Direct Determination of the Extinction Coefficients for Triplet ← Triplet Transitions in Naphthalene, Phenanthrene, and Triphenylene . . . . **Steven G. Hadley and Richard A. Keller** 4351

Direct Determination of the Singlet → Triplet Intersystem Crossing Quantum Yield in Naphthalene, Phenanthrene, and Triphenylene . . . . **Steven G. Hadley and Richard A. Keller** 4356

The Molecular *g* Values, Magnetic Susceptibility Anisotropies, and Molecular Quadrupole Moments in Propynal . . . **R. C. Benson, R. S. Scott, and W. H. Flygare** 4359

Electron Transfer from Dimeric Dianions of α-Methylstryene to Benz[*e*]pyrene . . . **H. Tokunaga, J. Jagur-Grodzinski, and M. Szwarc** 4364

The Study of the Thermal Decomposition of Methyl-Substituted Amine-Type Perchlorates
. . . **William A. Guillory and Morgan King** 4367

The Thermal Decomposition of Ammonium Chlorate . . . . **W. A. Guillory, M. King, and J. L. Mack** 4370

NOTES

Ion–Solvent Interactions. Conductance and Nuclear Magnetic Resonance Studies of Sodium Tetrabutylaluminate in the Presence of Benzene and Toluene . . . . **C. N. Hammonds, T. D. Westmoreland, and M. C. Day** 4374

Negative Ions Produced by Electron Capture in Phosphine . . . . **M. Halmann and I. Platzner** 4376

Competitive Reactions of Recoil Tritium Atoms with Methylsilanes and Alkanes
. . . **S. H. Daniel and Yi-Noo Tang** 4378

Photoconductivity of Electron Acceptors. II. 2,7-Dibromofluoren-$\Delta^{9\alpha}$-malononitrile . . . **Tapan K. Mukherjee** 4381

Potentiometric Titration of Stereoregular Poly(acrylic acids) . . . **Yoshikazu Kawaguchi and Mitsuru Nagasawa** 4382

Instability of Sorption Complexes in Synthetic Faujasites . . . . **Lothar Riekert** 4384

Analysis of Dielectric Measurements in the Presence of a Small Departure from Debye Behavior
. . . **Edward H. Grant** 4386

Line-Width Effects in the Electron Spin Resonance Spectrum of the 2,5-Dimethylhydroquinone Cation Radical
. . . **Paul D. Sullivan and James R. Bolton** 4387

Steric Effects in the Decomposition of Halogenated Nitrobenzene Anion Radicals
. . . **Wayne C. Danen, Terry T. Kensler, J. G. Lawless, M. F. Marcus, and M. D. Hawley** 4389

The Kinetics of the Hydrolysis of the Dichromate Ion. V. General Acid Catalysis
. . . **R. Baharad, Berta Perlmutter-Hayman, and Michael A. Wolff** 4391

Electron Impact Studies of Stannous Chloride and Stannic Chloride
. . . **A. S. Buchanan, D. J. Knowles, and D. L. Swingler** 4394

Deuterium Sulfide as an Electron Scavenger in the Radiolysis of Liquid Saturated Hydrocarbons
. . . **P. T. Holland and J. A. Stone** 4397

Field Independence of Photoinjection into Hydrocarbon Solution . . . . **A. Prock and M. Djibelian** 4398

Substituent Effects on the Nuclear Magnetic Resonance Spectra of Ethyl Acetates
. . . **Lana S. Rattet and J. H. Goldstein** 4400

Comparison of Methylene Radical Insertion Reactions with the Si–H Bonds of Methylsilane, Dimethylsilane, and Trimethylsilane . . . . **W. L. Hase, W. G. Brieland, and J. W. Simons** 4401

Further Consideration of the Moving Boundary Experiment for the Measurement of Transference Numbers
. . . **Richard J. Bearman and L. A. Woolf** 4403

Electron Paramagnetic Resonance of Nitrosodisulfonate Ion with Oxygen-17 and Sulfur-33 in Natural Abundance
. . . **J. B. Howell and Douglas C. McCain** 4405

Methyl Radical Reactions in Aqueous Solutions. I. Hydrogen Abstraction from Acetone
. . . **Issam A. I. Taha and Robert R. Kuntz** 4406

Solubility of Gases in Mixtures of Nonpolar Liquids . . . . **R. G. Linford and J. H. Hildebrand** 4410

The Limiting Behavior of the Integrand in the Robinson and Sinclair Equation . . . . **Chai-fu Pan** 4411

Identification of the Photochemically Active Species in Sulfur Dioxide Photolysis within the First Allowed Absorption Band . . . . . **Sachiko Okuda, T. Navaneeth Rao, David H. Slater, and Jack G. Calvert** 4412

Anion Exchange of Metal Complexes. XIX. Volumetric Studies of the Exchanger in Mixed Solvents
. . . **Y. Marcus, J. Naveh, and Mayo Nissim** 4415

Electronic Spin Resonance Study of Ultraviolet-Irradiated Di-*t*-butyl Peroxide in the Frozen State
. . . **P. Svejda and D. H. Volman** 4417

A Redetermination of the Thermoelectric Properties of the Bismuth–Bismuth Bromide System
. . . **Jordan D. Kellner, S. J. Yosim, and L. E. Topol** 4419

On the Surface Tension of Fused Salt Mixtures . . . . **George L. Gaines, Jr.** 4421

Concentration Dependence of Heats of Transfer between Heavy and Normal Water
. . . **Jerome Greyson and Harriet Snell** 4342

COMMUNICATIONS TO THE EDITOR

The Spectrophotometric Determination of Association Constants for $CuSO_4$ and $Cu(en)_2SO_3$ . . . **R. A. Matheson** 4425

On the Reliability of the Spectrophotometric Determination of Association Constants. The Case of $CuSO_4$ and $Cu(en)_2S_2O_3$ . . . . **Paul Hemmes and Sergio Petrucci** 4426

On the Determination of Average Pore Size of Membranes . . . . **N. Lakshminarayanaiah** 4428

The Chemistry of Nuclear Recoil Fluorine-18 Atoms. II. Energetic F-for-F and Ring-Attack Reactions in Perfluorocyclanes . . . . **Charles F. McKnight and John W. Root** 4430

Additions and Corrections 4433

Author Index to Volume 73, 1969 4435

Subject Index to Volume 73, 1969 4456

AUTHOR INDEX

Adamson, A. W., 4183, 4250
Asai, K., 4071

Bacon, W. E., 4163
Baharad, R., 4391
Bearman, R. J., 4403
Beggs, D. P., 4194
Benson, R. C., 4359
Blaser, S., 4147
Bolton, J. R., 4387
Breivogel, F. W., Jr., 4203
Brieland, W. G., 4401
Brown, G. H., 4163
Buchanan, A. S., 4394
Bunton, C. A., 4237

Calvert, J. G., 4412
Chang, J. W., 4277
Cheong, K.-K., 4219
Chrysochoos, J., 4188
Crawford, B., Jr., 4040

Dahlqvist, K.-I., 4124
Danen, W. C., 4389
Daniel, S. H., 4378
Darnell, A. J., 4116
Day, M. C., 4374
De Boelpaep, J., 4076
Defay, R., 4047
Djibelian, M., 4398
Dunn, F., 4256

Eyring, H., 4219

Flygare, W. H., 4359
Forsén, S., 4124
Franklin, J. L., 4328
Fu, Y.-C., 4219
Fujiyama, T., 4040
Fukuzawa, K., 4345

Gaines, G. L., Jr., 4421
Ghamkhar, M., 4298
Gielen, R., 4076
Gillbro, T., 4167
Goldstein, J. H., 4400
Grant, E. H., 4386
Granzow, A., 4289
Greyson, J., 4423
Grimison, A., 4064
Guillory, W. A., 4367, 4370
Guirao, C., 4302
Gupta, S. K., 4086

Hadley, S. G., 4351, 4356
Hair, M. L., 4269
Halmann, M., 4376
Hammonds, C. N., 4374
Haney, M. A., 4328
Harland, P., 4031
Harumiya, N., 4345
Hase, W. L., 4401
Hawley, M. D., 4389
Hayon, E., 4207, 4214
Hemmes, P., 4426
Hentz, R. R., 4283
Hertl, W., 4269
Hildebrand, J. H., 4410
Hoffman, M. Z., 4289
Hoffsommer, J. C., 4155
Holland, P. T., 4397
Howell, J. B., 4405

Ise, N., 4071
Ito, Y., 4345
Itoh, M., 4332

Jagur-Grodzinski, J., 4364
Jansoone, V., 4076
Jhaveri, J., 4064

Kana'an, A. S., 4264
Kawaguchi, Y., 4382
Keiser, D., 4264
Keller, R. A., 4351, 4356
Kellner, J. D., 4419
Kensler, T. T., 4389
Kessler, L. W., 4256
Kinell, P.-O., 4167, 4175
King, M., 4367, 4370
Kira, A., 4315
Kirby, E. P., 4130
Knowles, D. J., 4394
Krishnamurthy, S. S., 4036
Kuntz, R. R., 4406
Kwart, H., 4056

Lakshminarayanaiah, N., 4428
Lampe, F. W., 4194
Lantzke, I., 4183
Lawless, J. G., 4389
Lehmann, H. P., 4283
LeRoy, R. L., 4338
Lichtin, N. N., 4289
Lindenbaum, S., 4334
Linford, R. G., 4410
Lund, A., 4167, 4175

Macedo, P. B., 4147
Mack, J. L., 4370
Marcus, M. F., 4389
Marcus, Y., 4415
Martin, R. B., 4277
Matheson, R. A., 4425
McCain, D. C., 4405
McCollum, W. A., 4116
McIntyre, J. D. E., 4102, 4111
McKnight, C. F., 4430
Meites, L., 4348
Miyama, H., 4345
Moniz, W. B., 4145
Mukherjee, T. K., 4381
Mulliken, R. S., 4332

Nagasawa, M., 4382
Naveh, J., 4415
Neta, P., 4207, 4214
Nissim, M., 4415

O'Deen, L. A., 4094
Okuda, S., 4412
Olson, J. H., 4056

Pace, E. L., 4232
Pan, C., 4411
Patton, J. D., 4298
Peers, A. M., 4141
Perlmutter - Hayman, B., 4391
Petrucci, S., 4426
Platzner, I., 4376
Poranski, C. F., Jr., 4145
Prock, A., 4398

Quadrifoglio, F., 4227

Rao, T. N., 4412
Rattet, L. S., 4400
Reilly, P. J., 4292
Riekert, L., 4384
Robins, R. K., 4219
Robinson, L., 4237
Rodgers, R. S., 4348
Root, J. W., 4430

Sager, W. F., 4155
Sánchez, M. T., 4064
Sanfeld, A., 4047
Sarner, S. F., 4056
Schlegel, J. M., 4152
Scott, R. S., 4359
Senior, W. A., 4242
Shida, T., 4311, 4315
Shimizu, A., 4175
Shin, H. K., 4321
Siew, L. C., 4135
Simic, M., 4207, 4214
Simons, J. W., 4401
Simpson, G. A., 4064
Slater, D. H., 4412
Smith, J. H., 4232
Snell, H., 4423
Soundararajan, S., 4036
Steinchen, A., 4047
Steiner, R. F., 4130
Stone, J. A., 4397
Sullivan, P. D., 4387
Sundheim, B. R., 4135
Svejda, P., 4417
Swingler, D. L., 4394
Szwarc, M., 4364

Taha, I. A. I., 4406
Takaya, K., 4071
Tancredi, T., 4227
Tang, Y.-N., 4378
Temussi, P. A., 4227
Thynne, J. C. J., 4031
Tokunaga, H., 4364
Topol, L. E., 4419

Verbeke, O. B., 4076
Verrall, R. E., 4242
Vogler, A., 4183
Volman, D. H., 4417

Wakamatsu, S., 4345
Waltz, W. L., 4250
Watkins, K. W., 4094
Weiler, R., 4147
Westmoreland, T. D., 4374
Williams, F. A., 4302
Wolff, M. A., 4391
Wood, R. H., 4292, 4298
Woolf, L. A., 4403

Yosim, S. J., 4116, 4419

NOTICE TO AUTHORS

I. General Considerations

The Journal of Physical Chemistry is devoted to reporting both experimental and theoretical research dealing with fundamental aspects of physical chemistry. Space limitations necessitate giving preference to research articles dealing with previously unanswered basic questions in physical chemistry. Acceptable topics are those of general interest to physical chemists, especially work involving new concepts, techniques, and interpretations. Research that may lead to reexaminations of generally accepted views is, of course, welcome.

The Journal of Physical Chemistry publishes three types of manuscripts: *Articles, Notes,* and *Communications to the Editor.*

Authors reporting data should include, if possible, an interpretation of the data and its relevance to the theories of the properties of matter. However, the discussion should be concise and to the point and excessive speculation is to be discouraged. Papers reporting redeterminations of existing data will be acceptable only if there is reasonable justification for repetition: for example, if the more recent or more accurate data lead to new questions or to a reexamination of well known theories. Manuscripts that are essentially applications of chemical data or reviews of the literature are, in general, not suitable for publication in *The Journal of Physical Chemistry.* Detailed comparisons of methods of data analysis will be considered only if the paper also contains original data, or if such comparison leads to a genesis of new ideas.

Authors should include an introductory statement outlining the scientific rationale for the research. The statement should clearly specify the questions for which answers are sought and the connection of the present work with previous work in the field. All manuscripts are subject to critical review. It is to be understood that the final decision relating to a manuscript's suitability rests solely with the editorial staff.

Symposium papers are sometimes published as a group, but only after special arrangement with the editor.

Authors' attention is called to the "Handbook for Authors," available from the Special Issues Sales Department, American Chemical Society, 1155 Sixteenth St., N.W., Washington, D. C. 20036, in which pertinent material is to be found.

II. Types of Manuscripts

A. Articles should cover their subjects with thoroughness, clarity, and completeness. However, authors should also strive to make their *Articles* as concise as possible, avoiding unnecessary historical background. Abstracts to *Articles* should be brief—300 words is a maximum—and should serve to summarize the significant data and conclusions. The abstract should convey the essence of the *Article* to the reader.

B. Notes. Papers submitted in the category of *Notes* should report work that represents a complete and self-contained study of limited scope. *Notes* are a luxury in the present scientific literature; authors should not use a *Note* to report work that is part of a continuing study. *Notes* are not to be used for reporting preliminary results; reports of such work should be postponed until the work is completed or should be submitted as *Communications* if the results are of immediate or unusual interest to physical chemists. The same criteria of suitability for publication apply to *Notes* as to *Articles* (see General Considerations). The length of a *Note,* including tables, figures, and text, must not exceed 1.5 journal pages (1500 words or the equivalent). A *Note* should not be accompanied by an abstract.

C. Communications to the Editor are of two types, *Letters* and *Comments.* Both types are restricted to three-quarters of a page (750 words or the equivalent) including tables, figures, and text, and both types of *Communications* are subject to critical review, but special efforts will be made to expedite publication.

Letters should report preliminary results whose immediate availability to the scientific community is deemed important, and whose topic is timely enough to justify the double publication that usually results from the publication of a *Letter.*

Comments include significant remarks on the work of others. The editorial staff will generally permit the authors of the work being discussed to reply.

III. Introduction

All manuscripts submitted should contain brief introductory remarks describing the purpose of the work and giving sufficient background material to allow the reader to appreciate the state-of-knowledge at the time when the work was done. The introductory remarks in an *Article* should constitute the first section of the paper and should be labeled accordingly. In *Notes* and *Communications,* the introductory material should not be in such a separate section. To judge the appropriateness of the manuscript for *The Journal of Physical Chemistry,* the editorial staff will place considerable weight on the author's intentions as stated in the Introduction.

IV. Functions of Reviewers

The editorial staff requests the scientific advice of reviewers who are active in the area of research covered by the manuscript. The reviewers act only in an advisory capacity and the final decision concerning a manuscript is the responsibility of the editorial staff. The reviewers are asked to comment not only on the scientific content, but also on the manuscript's suitability for *The Journal of Physical Chemistry.* With respect to *Communications,* the reviewers are asked to comment specifically on the urgency of publication. All reviews are anonymous and the reviewing process is most effective if reviewers do not reveal their identities to the authors. An exception arises in connection with a manuscript submitted for publication in the form of a comment on the work of another author. Under such circumstances the first author will, in general, be allowed to review the communication and to write a rebuttal, if he so chooses. The rebuttal and the original communication may be published together in the same issue of the journal. Revised manuscripts are generally sent back to the original reviewers, who are asked to comment on the revisions. If only minor revisions are involved, the editorial staff examines the revised manuscript in light of the recommendations of the reviewers and without seeking further opinions. For the convenience of reviewers, authors are advised to indicate clearly, either in the manuscript or in a covering letter, the specific revisions that have been made.

V. Submission of Manuscripts

All manuscripts must be submitted at least in duplicate and preferably in triplicate to expedite handling. Manuscripts must be typewritten, double-spaced copy, on $8^1/_2 \times 11$ in. paper. Legal sized paper is not acceptable. Authors should be certain that copies of the manuscript are clearly reproduced and readable. **Authors submitting figures must include the original drawings or photographs thereof, plus two xerographic copies for review purposes. These reproductions of the figures should be on $8^1/_2 \times 11$ in. paper.** Graphs must be in black ink on white or blue paper. Lettering at the sides of graphs may be penciled in and will be typeset. Figures and tables should be held to a minimum consistent with adequate presentation of information. All original data which the author deems pertinent must be submitted along with the manuscript. For example, a paper reporting a crystal structure should include structure factor tables for use by the reviewers.

Footnotes and references to the literature should be numbered consecutively within the paper; the number should also be placed in parentheses in the left margin opposite the line in which the reference first appears. A complete list of references should appear at the end of the paper. Initials of the authors referred to in the citations should be included in the complete reference at the back of the paper. Nomenclature should conform to that used in *Chemical Abstracts* and mathematical characters should be underlined for italics, Greek letters should be annotated, and subscripts and superscripts clearly marked.

Papers should not depend for their usefulness on unpublished material, and excessive reference to material in press is discouraged. References not readily available (*e.g.*, private technical reports, preprints, or articles in press) that are necessary for a complete review of the paper must be included with the manuscript for use by the reviewers.

VI. Revised Manuscripts

A manuscript sent back to an author for revision should be returned to the editor within 6 months; otherwise it will be considered withdrawn and treated as a new manuscript when and if it is returned. Revised manuscripts returned to the editor must be submitted in duplicate and all changes should be made by typewriter. **Unless the changes are very minor, all pages affected by revision must be retyped.** If revisions are so extensive that a new typescript of the manuscript is necessary, it is requested that a copy of the original manuscript be submitted along with the revised one.

VII. Supplementary Material

By arrangement with the National Auxiliary Publications Service (NAPS) of the American Society for Information Science (ASIS), supplementary material, such as extensive tables, graphs, spectra, and calculations, can be distributed in the form of microfiche copies or photoprints readable without optical aids. This material should accompany the manuscript for review by the editors and reviewers. Upon acceptance, it will be sent by the editor to NAPS where it is assigned a document number. A deposit fee of $6.50 (for 60 manuscript pages or less) is required and should be included with the material sent to the editor. The check must be made payable to ASIS-NAPS. Further details may be obtained from NAPS c/o CCM Information Corp., 909 3rd Ave., New York, N. Y. 10022.

VIII. Proofs and Reprints

Galley proofs, original manuscript, cut copy, and reprint order form are sent by the printer directly to the author who submitted the manuscript. The attention of the authors is directed to the instructions which accompany the proof, especially the requirement that all corrections, revisions, and additions be entered on the proof and not on the manuscript. Proofs should be checked against the manuscript (in particular all tables, equations, and formulas, since this is not done by the editor) and returned as soon as possible. No paper is released for printing until the author's proof has been received. Alterations in an article after it has been set in type are made at the author's expense, and it is understood that by entering such alterations on proofs the author agrees to defray the cost thereof. The filled-out reprint form must be returned with the proof, and if a price quotation is required by the author's organization a request for it should accompany the proof. Since reprinting is generally done from the journal press forms, all orders must be filed before press time. None can be accepted later, unless a previous request has been made to hold the type. Reprint shipments are made a month or more after publication, and bills are issued by the printer subsequent to shipment. Neither the editors nor the Washington office keeps any supply of reprints. Therefore, only the authors can be expected to meet requests for single copies of papers.

A page charge is assessed to cover in part the cost of publication. Although payment is expected, it is not a condition for publication. Articles are accepted or rejected only on the basis of merit, and the editor's decision to publish the paper is made before the charge is assessed. The charge per journal page is $50.

THE JOURNAL OF
PHYSICAL CHEMISTRY

Registered in U. S. Patent Office © Copyright, 1969, by the American Chemical Society

VOLUME 73, NUMBER 12 DECEMBER 1969

Ionization and Dissociation of Pentafluorosulfur Chloride by Electron Impact

by P. Harland and J. C. J. Thynne

Chemistry Department, Edinburgh University, Edinburgh, Scotland *(Received July 31, 1969)*

Positive and negative ion formation as a result of the electron bombardment of pentafluorosulfur chloride has been studied. Various ionization processes have been suggested to account for the formation of the ions, and for several negative ions the dependence of their formation upon electron energy has been studied.

As part of a continuing study of positive and negative ion formation by molecules as a result of electron impact,[1,2] we have examined pentafluorosulfur chloride, SF_5Cl. This molecule is of particular interest from a negative ion standpoint since the closely related molecule sulfur hexafluoride readily forms the ion SF_6^- at low energies,[3,4] and it is of interest to observe if the SF_5Cl^- ion is formed similarly.

In electron impact studies, when the electron source is a heated filament, uncertainties arise in the evaluation of experimental ionization data because of the energy spread of the thermionically emitted electron beam; this is largely due to the ionization thresholds becoming smeared-out as a result of the high energy tail of the electron energy distribution. Analytical methods have been developed to reduce this problem for positive[5] and negative[2] ions, and we have applied this technique to the negative ions formed by SF_5Cl at low electron energies.

Experimental Section

The data were obtained using a Bendix time-of-flight mass spectrometer, Model 3015. The pressure in the ion source was usually maintained below 5×10^{-6} mm in order to reduce the possibility of ion formation due to ion–molecule reactions. The energy of the ionizing electrons was read on a Solatron digital voltmeter, Model LM 1619, and the spectra recorded on two 1-mV Kent potentiometric recorders.

In both the positive and negative ion studies, the electron current was maintained constant by automatic regulation over the whole energy range investigated. Ionization curves were usually measured three to five times, the appearance potentials for negative ions being reproducible to ±0.1 eV. The appearance potential of the O^- ion from SO_2 was used as the reference for energy scale calibration,[3] both the onset at 4.2 eV and the maximum of the resonance peak at 5.0 eV being taken as the calibration points.[6-8] For the positive ion studies argon was used to calibrate the energy scale, the method used for determining the appearance potentials being the semilogarithmic plot technique.

The electron energy distribution, which was required to be known for the deconvolution procedure,[2] was measured using the SF_6^- ion formed by sulfur hexafluoride.[3,4] It was found that performing 15 smoothing and 20 unfolding iterations on the basic experimental data enabled satisfactory evaluation of appearance po-

---

[1] K. A. G. MacNeil and J. C. J. Thynne, *Int. J. Mass Spec.*, **2**, 1 (1969).

[2] K. A. G. MacNeil and J. C. J. Thynne, *ibid.*, **2**, 35 (1969).

[3] W. M. Hickman and R. E. Fox, *J. Chem. Phys.*, **25**, 642 (1956).

[4] G. J. Schulz, *J. Appl. Phys.*, **31**, 1134 (1960).

[5] J. D. Morrison, *J. Chem. Phys.*, **39**, 200 (1963).

[6] K. Kraus, *Z. Naturforsch.*, **16a**, 1378 (1961).

[7] J. G. Dillard and J. L. Franklin, *J. Chem. Phys.*, **48**, 2349 (1968).

[8] F. H. Dorman, *ibid.*, **44**, 3856 (1966).

tentials, resonance peak maxima, and peak widths (at half-height) to be made.

Results and Discussion

(*1*) *Positive Ion Formation by Pentafluorosulfur Chloride.* In Table I we show the positive ion mass spectra for SF_5Cl and SF_6 measured at 70 eV. For both molecules, doubly charged fragments containing sulfur and fluorine are common, but it is noteworthy that for SF_5Cl few ions containing sulfur, fluorine, and chlorine are formed and these are generally of low abundance. A low intensity parent ion is formed in the case of SF_5Cl although the most probable ionization process involves the loss of a chlorine atom from the molecule. Positive ion appearance potential data for SF_6 have been reported by Dibeler and Mohler.[9] Results of mass spectra of SF_5Cl and SF_6 as shown in Table I.

Table I: Positive Ion Mass Spectrum of SF_5Cl and SF_6 for 70-V Electrons

	SF_5Cl		SF_6	
m/e	Ion	Rel. intensity	Ion	Rel. intensity
16	S^{2+}	0.14	S^{2+}	0.06
19	F^+	0.44	F^+	0.35
32	S^+	3.10	S^+	1.44
35	Cl^+	2.02		
	SF_2^{2+}	1.53	SF_2^{2+}	0.68
37	Cl^+	0.67		
44.5	SF_3^{2+}	0.04	SF_3^{2+}	0.01
51	SF^+	6.13	SF^+	4.65
54	SF_4^{2+}	0.44	SF_4^{2+}	0.39
63.5	SF_5^{2+}	<0.01		
67	SCl^+	1.57		
70	SF_2^+	6.77	SF_2^+	4.72
86	$SFCl^+$	0.63		
89	SF_3^+	36.8	SF_3^+	18.0
105	SF_2Cl^+	0.20		
108	SF_4^+	5.25	SF_4^+	3.17
124	SF_3Cl^+	<0.1		
127	SF_5^+	100	SF_5^+	100
143	SF_4Cl^+	11.0		
162	SF_5Cl^+	<0.1		

Energetics of Decomposition. For dissociation into atoms SF_6 and SF_6Cl require 20.3 and 18.9 eV, respectively.

$$SF_6 \longrightarrow S + 6F \qquad (1)$$

$$SF_5Cl \longrightarrow S + 5F + Cl \qquad (2)$$

If the S–F bonds have a constant bond energy, then $D(SF_5\text{–}F) - D(SF_6\text{–}Cl) = 1.4$ eV and, using the value of $\leqslant 3.4$ eV deduced for $D(SF_5\text{–}F)$ by Curran,[10] then $D(SF_5\text{–}Cl) \leqslant 2.0$ eV. This relatively low bond strength is compatible with the observation[11] that pentafluorosulfur chloride thermally decomposes at about 200°.

(*a*) *SF_5^+.* We have measured a value of 13.2 ± 0.2 eV for the appearance potential of the SF_5^+ ion.

$$SF_5Cl + e \longrightarrow SF_5^+ + Cl + 2e \qquad (3)$$

Dibeler and Mohler[9] have reported that, for SF_6, $A(SF_5^+) = 15.9 \pm 0.2$ eV. These results suggest that, neglecting possible excess energy contributions, $D(SF_5\text{–}F) - D(SF_5\text{–}Cl) = 2.5 \pm 0.4$ eV, a result which is in reasonable accord with the difference deduced above.

(*b*) *Cl^+.* Our data yield a value of 20.8 ± 0.3 eV for the appearance potential for the Cl^+ ion (Table II); possible ionization processes to explain the formation of the ion include

Table II: Appearance Potentials of Various Ions in the Mass Spectrum of SF_5Cl

m/e	Ion	A, eV
19	F^+	33.8 ± 0.3
32	S^+	33.2 ± 0.5
35	Cl^+	20.8 ± 0.3
127	SF_5^+	13.2 ± 0.2
143	SF_4Cl^+	15.9 ± 0.1

$$SF_5Cl + e \longrightarrow SF_5 + Cl^+ + 2e \qquad (4)$$

$$\longrightarrow SF_4 + F + Cl^+ + 2e \qquad (5)$$

$$\longrightarrow S + 5F + Cl^+ + 2e \qquad (6)$$

If $D(SF_5\text{–}Cl) \simeq 2.0$ eV, then the enthalpy requirements of reaction 4 are about 16.2 eV. Reactions 5 and 6 require minimum energies of 19.1 and 33.1 eV, respectively; it is therefore probable that reaction 5 is responsible for Cl^+ ion formation.

(*c*) *F^+.* An appearance potential of 33.8 ± 0.3 eV was obtained for this ion; in addition breaks in the F^- and Cl^- ionization efficiency curves were noted at 32.8 and 33.5 eV, respectively.

$$SF_5Cl + e \longrightarrow S + 4F + Cl + F^+ + 2e \qquad (7)$$

$$\longrightarrow S + 3F + Cl + F^+ + F^- + 2e \qquad (8)$$

$$\longrightarrow S + 4F + Cl^- + F^+ + 2e \qquad (9)$$

Reactions 7, 8, and 9 have minimum enthalpy requirements of 37.1, 33.7, and 33.5, respectively. Our data for $A(F^+)$, together with the observed breaks in the F^- and Cl^- curves, suggest that both reactions 8 and 9 are contributing to F^+ ion formation.

(*d*) *S^+.*

$$SF_5Cl + e \longrightarrow S^+ + 5F + Cl + 2e \qquad (10)$$

---

[9] V. H. Dibeler and F. L. Mohler, *J. Res. Nat. Bur. Stand.*, **40**, 25 (1948).

[10] R. K. Curran, *J. Chem. Phys.*, **34**, 1069 (1961).

[11] H. L. Roberts and N. H. Ray, *J. Chem. Soc.*, 665 (1960).

Table III: Appearance Potentials (A), Resonance Peak Maxima (M), and Half-Widths (PW) for Negative Ions Formed by SF_6[a]

Ion	A	M	PW	Process
SF_6^-	0	0.4 ± 0.1	0.6 ± 0.1	$SF_6 + e \rightarrow SF_6^-$
SF_5^-	0.1	0.5 ± 0.1	0.8 ± 0.1	$\rightarrow SF_5^- + F$
SF_4^-	5.0 ± 0.1	6.0 ± 0.1	1.7 ± 0.1	$\rightarrow SF_4^- + 2F$
F^-	4.3 ± 0.1	5.7 ± 0.1	1.4 ± 0.1	$\rightarrow SF_4 + F + F^-$
	7.8 ± 0.1	9.3 ± 0.1	~2	$\rightarrow SF_3 + 2F + F^-$
	10.5 ± 0.1	11.8 ± 0.1	1.6 ± 0.1	$\rightarrow SF_2 + 3F + F^-$

[a] All values in eV.

The enthalpy change for reaction 10 is 32.2 eV; this is in reasonable accord with the value of 33.2 ± 0.5 eV we have measured for the appearance potential of the S^+ ion. Any ion-pair process would have energy requirements at least 3.4 eV lower than this for (10) since it would involve F^- or Cl^- formation; we therefore attribute S^+ ion production to reaction 10.

(*e*) SF_4Cl^+.

$$SF_5Cl + e \longrightarrow SF_4Cl^+ + F + 2e \qquad (11)$$

$A(SF_4Cl^+) = 15.9 \pm 0.1$ eV; if we assume that $D(F\text{–}SF_4Cl)$ is the same as the S–F bond strength in SF_6, *i.e.*, ~3.4 eV, then a maximum value of 12.5 eV may be deduced for the ionization potential of SF_4Cl.

(*2*) *Negative Ion Formation.* (*a*) *O^- Ion Formation by Sulfur Dioxide.* The formation of negative ions by sulfur dioxide has been investigated by several workers, and the appearance potential of the O^- ion is sufficiently well established[6-8] at 4.2 eV to be used to calibrate the energy scale.

Our results for this ion are shown in Figure 1; the two resonance peaks observed have clear maxima but uncertain appearance potentials. Deconvolution of these data, using an electron energy distribution measured using SF_6^-/SF_6, give the results shown by the open circles. The threshold for the first peak is sharp and is separated from the peak maximum by 0.80 eV; this is in exact agreement with the difference obtained by Kraus[6] (using a retarding-potential-difference technique) and by Dillard and Franklin.[7]

The onset of the second resonance peak is not quite resolved; Kraus[6] also was unable to completely separate the two peaks. The onset of the first peak and the minimum between the resonance peaks are separated by 2.4 eV in both our work and that of Kraus.

(*b*) *Negative Ion Formation by Sulfur Hexafluoride.* The negative ions observed at 70 eV are F^-, S^-, F_2^-, SF^-, SF_2^-, SF_3^-, SF_4^-, SF_5^-, and SF_6^-, with F^- and SF_6^- being the most abundant. The formation of most of these ions is well known, in particular the SF_6^- ion which has been used to determine the electron energy distribution.[3,4] The data are presented in Table III.

(*i*) SF_5^-. The SF_5^- ion is formed abundantly, presumably by the dissociative capture reaction

$$SF_6 + e \longrightarrow SF_5^- + F$$

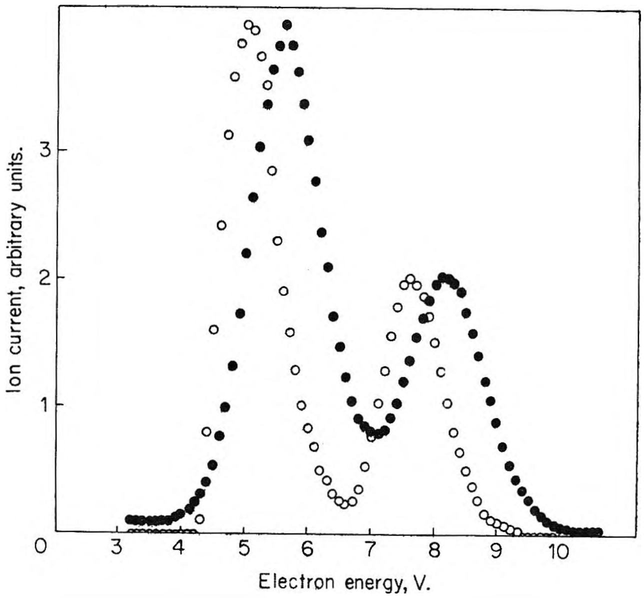

Figure 1. Ionization efficiency curve for O^- ion formation by sulfur dioxide. Full circles, original experimental results; open circles, deconvoluted results obtained using 15 smoothing and 20 unfolding iterations.

and we have measured an appearance potential of 0.1 eV for this ion, a result in good accord with those of other workers.[12,13]

(*ii*) SF_4^-.

$$SF_6 + e \longrightarrow SF_4^- + 2F \qquad (12)$$

Our experimental data indicate that $A(SF_4^-) = 5.0 \pm 0.1$ eV; if reaction 12 is responsible for ion formation, then a value of 1.7 eV may be estimated for the electron affinity of sulfur tetrafluoride, $E(SF_4)$.

(*iii*) F^-. Ion formation was observed initially at electron energies near to zero, indicating that $D(SF_5\text{–}F) \simeq E(F)$. Three other ionization processes were noted at 4.3, 7.8, and 10.5 eV, the process at 4.3 having considerably the largest cross section.

$$SF_6 + e \longrightarrow SF_4 + F + F^- \qquad (13)$$

$$\longrightarrow SF_3 + 2F + F^- \qquad (14)$$

$$\longrightarrow SF_2 + 3F + F^- \qquad (15)$$

---

(12) W. M. Hickman and D. Berg, *Advan. Mass Spectrometry*, 458 (1958).

(13) A. J. Ahearn and N. B. Hannay, *J. Chem. Phys.*, **21**, 19 (1953).

The minimum enthalpy requirements for reaction 13 are 3.3 eV, so we suggest that this reaction is responsible for the increase in ion current at 4.3 eV. Reactions 14 and 15 have higher energy requirements than 13 in both cases S–F bonds being broken which probably require ~3 eV. The energy difference observed between the ionization processes are 3.5 and 2.7 eV; this is close to the likely S–F bond energies and we tentatively suggest that reactions 14 and 15 also participate in ion formation.

(*c*) *Negative Ion Formation by SF_5Cl.* The negative ion mass spectra measured at (uncorrected) electron energies of 2 and 70 eV are shown in Table IV. F^- is the most abundant ion but, unlike SF_6, no parent negative ion is observed either at low electron energies (where it could be formed by primary electron capture) nor at higher energies where secondary electrons might be involved in the capture process. No ions which contain S, F, and Cl or S and Cl are formed. Some Cl^- and F^- ion formation occurs at ~0 eV as a consequence of thermal decomposition of the pentafluorosulfur chloride on the hot filament.

Table IV: Negative Ion Mass Spectrum of SF_5Cl at 2 and 70 eV

m/e	Ion	Rel. int. (2)	Rel. int. (70)
19	F^-	1000	1000
32	S^-	...	0.65
35	Cl^-	26.7	100
38	F_2^-	6.7	...
51	SF^-	2.2	8.0
54	FCl^-	2.2	2.0
70	SF_2^-	2.0	0.65
89	SF_3^-	2.2	16.2
108	SF_4^-	2.3	3.3
127	SF_5^-	20.0	24.1

(*i*) SF_5^-. This ion is observed at 0.2 ± 0.1 eV, the resonance peak attaining a maximum value a 0.7 eV. Ionization is attributed to the reaction

$$SF_5Cl + e \longrightarrow SF_5^- + Cl \qquad (16)$$

(*ii*) SF_4^-. Our appearance potential data for this ion are given in Table V.

$$SF_5Cl + e \longrightarrow SF_4^- + F + Cl \qquad (17)$$

If reaction 17 is responsible for ion formation, then we can estimate a value of 1.0 eV for $E(SF_4)$; this may be compared with the value of 1.7 eV deduced for $E(SF_4)$ in the experiments using SF_6.

(*iii*) SF_3^-. The dissociation energy into atoms of SF_4 is 14.0 eV; if we assume that the four S–F bonds have equal strengths, then $D(SF_3\text{–}F) \simeq 3.5$ eV and we may estimate that the heat of formation of SF_3, $\Delta H_f(SF_3) = -5.3$ eV.

$$SF_5Cl + e \longrightarrow SF_3^- + 2F + Cl \qquad (18)$$

$A(SF_3^-) = 7.9$ eV so that, from reaction 18, we may estimate the electron affinity of SF_3 to be 0.5 eV. The similarity of the appearance potentials of SF_3^- and FCl^- initially suggest the occurrence of the reaction

$$SF_5Cl + e \longrightarrow SF_3^- + F + FCl$$

but the energetic requirements for this reaction are such as to indicate $E(SF_3) < 0$, and so the reaction is neglected.

(*iv*) FCl^-. This ion must be formed either by an ion–molecule reaction involving F^- or Cl^-, *e.g.*

$$F^- + SF_5Cl \longrightarrow FCl^- + SF_5 \qquad (19)$$

or by rearrangement reactions such as

$$SF_5Cl + e \longrightarrow SF_4 + FCl^- \qquad (20)$$

$$\longrightarrow SF_3 + F + FCl^- \qquad (21)$$

$$\longrightarrow SF_2 + 2F + FCl^- \qquad (22)$$

A study of the pressure dependence of FCl^- ion formation at 7.6 eV showed it to be a primary ion, and we may therefore rule out secondary reactions such as (19).

Reactions 20 and 21 may also be neglected as sources of the FCl^- ion on energetic grounds. To estimate the energetics of (22) we require to know $\Delta H_f(SF_2)$. If we assume $D(SF_2\text{–}F) \simeq 3.3$ eV, then $\Delta H_f(SF_2) \simeq -2.8$ eV. Using this estimate we can calculate that $E(FCl) \simeq 1.5$ eV. We know of no value with which this may be compared but values of 2.8 and $\leqslant 1.7$ eV have been reported for $E(F_2)$[2] and $E(Cl_2)$,[14] respectively.

(*v*) Cl^-. Our data for this ion showed it to have an appearance potential at 4.0 eV, the broad resonance peak rising slowly with a much more intense resonance process having an appearance potential at 7.6 ± 0.2 eV, the peak maximum being attained at 9.1 eV. Some ion formation also occurred at electron energies ~0 eV, this may be due to thermal decomposition of SF_5Cl or to the occurrence of reaction 23 since $D(SF_5\text{–}Cl) < E(Cl)$.

$$SF_5Cl + e \longrightarrow SF_5 + Cl^- \qquad (23)$$

$$\longrightarrow SF_4 + F + Cl^- \qquad (24)$$

$$\longrightarrow SF_3 + 2F + Cl^- \qquad (25)$$

$$\longrightarrow SF_3 + F_2 + Cl^- \qquad (26)$$

$$\longrightarrow SF_2 + 3F + Cl^- \qquad (27)$$

The broad peak which has its onset at 4.0 eV may be attributable to reaction 26 for which the enthalpy requirements are ~3.2 eV. Reactions 25 and 27 would correspond to appearance potentials for Cl^- of 4.8 and 8.1 eV; we are therefore unable to identify the second

---

(14) N. S. Buchel'nikova, *Usp. Fiz. Nauk*, 65, 351 (1958).

Table V: Appearance Potentials (A), Resonance Peak Maxima (M) and Half-Widths (PW) for Negative Ions Formed by Pentafluorosulfur Chloride[a]

Ion	A	M	PW	Process
SF_5^-	0.2 ± 0.1	0.7 ± 0.1	0.8 ± 0.1	$SF_5Cl \rightarrow SF_5^- + Cl$
SF_4^-	4.1 ± 0.1	4.65 ± 0.1	1.0 ± 0.1	$\rightarrow SF_4^- + F + Cl$
SF_3^-	7.9 ± 0.2	8.9 ± 0.1	1.4 ± 0.2	$\rightarrow SF_3^- + 2F + Cl$
FCl^-	7.6 ± 0.1	9.1 ± 0.1	1.7 ± 0.1	$\rightarrow SF_2 + 2F + FCl^-$
Cl^-	4.0 ± 0.1	Uncertain	...	$\rightarrow SF_3 + F_2 + Cl^-$
	7.6 ± 0.2	9.1 ± 0.1	1.6 ± 0.1	$\rightarrow SF_2 + 3F + Cl^-$(?)
F^-	3.2 ± 0.1	5.1 ± 0.1	1.3 ± 0.1	$\rightarrow SF_3 + FCl + F^-$
	6.3 ± 0.2	6.5 ± 0.1	...	$\rightarrow SF_2 + F_2 + Cl + F^-$
	8.0 ± 0.1	9.4 ± 0.1	~1.5	$\rightarrow SF_2 + 2F + Cl + F^-$

[a] All values in eV.

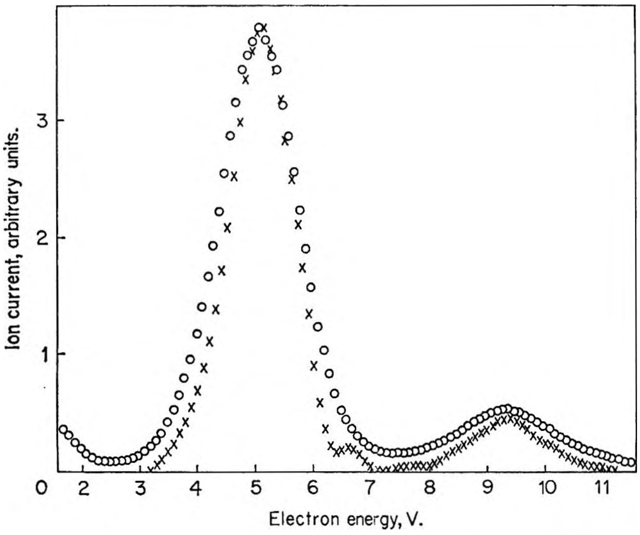

Figure 2. Ionization efficiency curve for F^- ion formation by SF_5Cl. Open circles, original experimental data; crosses, deconvoluted results.

ionization process more than tentatively and suggest that (27) is responsible.

(*vi*) F^-. A typical ionization efficiency curve for this ion before and after performing 15 smoothing and 20 unfolding iterations is shown in Figure 2. Ion formation of low intensity occurs at energies near to zero, presumably due to the reaction

$$SF_5Cl + e \longrightarrow SF_4 + Cl + F^-$$

A further dissociative capture process occurs at 3.3 eV, the resonance peak reaching a maximum value at 5.1 eV. A reaction of very low cross section, occurs at 6.3 eV and a further ionization process at 8.0 eV.

$$SF_5Cl + e \longrightarrow SF_3 + FCl + F^- \quad (28)$$

$$\longrightarrow SF_2 + F_2 + Cl + F^- \quad (29)$$

$$\longrightarrow SF_2 + 2F + Cl + F^- \quad (30)$$

Reaction 28 would require that $A(F^-) \simeq 2.4$ eV, in reasonable accord with the onset noted at 3.2 eV. Reactions 29 and 30 have minimum enthalpy requirements of 6.7 and 8.3 eV, respectively, which in view of the uncertainty associated with some of our thermochemical estimates, suggest that they may be assigned to the resonance processes occurring at 6.3 and 8.0 eV.

(*d*) *Thermochemical Data.* We have used the following values for heats of formation (at 298°K) in our calculations (in eV); SF_6, −12.7;[15] SF_5Cl, −10.9;[16] SF_4, −8.0;[16] FCl, −0.6;[17] Cl, 1.2;[17] S, 2.8;[17] F, 0.8.[17]

Acknowledgments. We thank the Science Research Council for a grant in aid of this work and Dr. H. L. Roberts of I. C. I. (Mond Division) for a gift of the pentafluorosulfur chloride.

---

(15) P. A. G. O'Hare, J. L. Settle, and W. N. Hubbard, *Trans. Faraday Soc.*, **62**, 558 (1966).

(16) National Bureau of Standards, Technical Note 270-3, Jan 1968.

(17) JANAF Thermochemical Tables, Dow Chemical Co., Midland, Mich., 1961.

Charge Distribution in and Dipole Moments of Some Aliphatic Alcohols

by S. S. Krishnamurthy and S. Soundararajan

Department of Inorganic and Physical Chemistry, Indian Institute of Science, Bangalore-12, India

(Received November 1, 1968)

Using the treatment of Smith, *et al.*,[1] charge distributions in several aliphatic alcohols and consequently their dipole moments have been evaluated. The dipole moments of trichloroethanol (2.04 D) and 1,3-dichloropropan-2-ol (2.11 D) have been measured in benzene solution at 35°. The results of evaluation and measurements are interpreted in terms of the occurrence of intramolecular interaction between the hydroxyl hydrogen and an acceptor atom X (halogen or oxygen) at the β-carbon atom.

Introduction

The study of conformational equilibria has attracted the attention of several workers in recent years.[2-8] Krueger and Mettee[2] have detected intramolecular hydrogen bonding in 2-cyano- and several nitroethanols while Urbanski[9,10] has thoroughly investigated the ability of nitro groups to act as proton acceptors. Baitinger, *et al.*,[7] have obtained unequivocal evidence for the formation of a six-membered intramolecular hydrogen bond in β-nitroalcohols and have refuted the earlier work of Ungnade, *et al.*,[11] which indicated the absence of any such intramolecular interaction. In their studies of conformational equilibria of 2-halo-,[3] 2,2-dihalo-, and 2,2,2-trihaloethanols[4] in dilute CCl_4 solutions, Krueger and Mettee have evaluated the thermodynamic parameters for the equilibria and have interpreted their results in terms of the stabilization of *gauche* structure by the formation of an X····H–O intramolecular hydrogen bond. More recently, Buckley, *et al.*,[12] have made an ir study of rotational isomerism in ethylene glycol and concluded that ethylene glycol exists wholly in the *gauche* form. The stability of this *gauche* form is caused by the presence of two adjacent O–H groups leading to two equivalent intramolecular H-bonded structures.

The present investigation attempts to analyze the available dipole moment data on aliphatic alcohols on the basis of the recently recognized notions of stabilization of intramolecularly H-bonded conformations in these systems. Since the inductive effects operating in the halo- and nitroethanols are considerable, we have calculated the theoretical moments of several aliphatic alcohols after allowing for induction by the method of Smith, *et al.*[1] Because of lack of data in the literature, we have determined the experimental moments of trichloroethanol and 1,3-dichloropropan-2-ol in benzene solution at 35°.

Experimental Section

Materials. Benzene was purified as described in the literature.[13] Trichloroethanol was donated by Cilag Chemie, Switzerland. 1,3-Dichloropropan-2-ol was distilled just prior to use, bp 169° (680 mm).

Apparatus and Methods of Measurement. One of our earlier publications[14] describes the equipment used for dielectric constant and density measurements and the method of computing the dipole moments from dielectric constant and density data. Table I summarizes the results of our measurements.

Results and Discussion

The parameters used for calculating the formal charge distribution by the Smith, *et al.*,[1] scheme are taken from the literature.[1,14,15] Table II shows the formal charge distributions in several aliphatic alcohols. The bond distances and the bond angles required for computing the dipole moments from charge distribution data are obtained from Sutton's "Tables of Interatomic Distances."[16] Table III gives the experimental dipole

---

(1) R. P. Smith, T. Ree, J. L. Magee, and H. Eyring, *J. Amer. Chem. Soc.*, **73**, 2263 (1951).

(2) R. J. Krueger and H. D. Mettee, *Can. J. Chem.*, **43**, 2888 (1965).

(3) P. J. Krueger and H. D. Mettee, *ibid.*, **42**, 326 (1964).

(4) P. J. Krueger and H. D. Mettee, *ibid.*, **42**, 340 (1964).

(5) P. J. Krueger and H. D. Mettee, *ibid.*, **42**, 347 (1964).

(6) P. J. Krueger and H. D. Mettee, *J. Mol. Spectrosc.*, **18**, 131 (1965).

(7) W. F. Baitinger, P. von R. Schleyer, T. S. S. R. Murthy, and L. Robinson, *Tetrahedron*, **20**, 1635 (1964).

(8) L. P. Kuhn and R. A. Wires, *J. Amer. Chem. Soc.*, **86**, 2161 (1964).

(9) T. Urbanski, *Tetrahedron*, **6**, 1 (1959).

(10) T. Urbanski in "Hydrogen Bonding," D. Hadzi, Ed., Pergamon Press, New York, N. Y., 1959, p 143.

(11) H. E. Ungnade and L. W. Kissinger, *Tetrahedron*, *Suppl.* **1**, **19**, 121 (1963).

(12) P. Buckley and P. A. Giguere, *Can. J. Chem.*, **45**, 397 (1967).

(13) A. Weissberger and E. Proskauer, "Organic Solvents," "Techniques of Organic Chemistry," Vol. VII, Interscience Publishers, New York, N. Y., 1955.

(14) S. S. Krishnamurthy and S. Soundararajan, *Tetrahedron*, **24**, 167 (1968).

(15) S. Soundararajan, *ibid.*, **19**, 2171 (1963).

Table I: Dielectric Constants and Density

Mole fraction $f_2 \times 10^4$	Dielectric constant, ϵ	Density, d
Trichloroethanol in benzene at 35 ± 0.02°[a]		
0.000	2.25320	0.86282
8.786	2.25672	0.86344
15.04	2.26155	0.86390
22.19	2.26522	0.86435
28.57	2.26798	0.86485
1,3-Dichlorohydrin in benzene at 35 ± 0.02°[b]		
0.000	2.25005	0.86284
9.620	2.25562	0.86332
20.08	2.26194	0.86376
29.06	2.26591	0.86425
34.80	2.27188	0.86471
49.83	2.27900	0.86531

[a] $\alpha_{\text{mean}} = 2.4093$, $\beta_{\text{mean}} = 0.8118$, $P_T^{\infty} = 110.9$ cc $MR_D = 27.2$ cc, $P_0 = 82.3$ cc, $\mu_D = 2.04$.

[b] $\alpha_{\text{mean}} = 2.6050$, $\beta_{\text{mean}} = 0.5761$, $P_T^{\infty} = 116.7$ cc, $MR_D = 27.1$ cc, $P_0 = 88.3$ cc, $\mu_D = 2.11$. (α and β are Hedestrand's constants, P_T^{∞} = total polarization, MR_D = molar refraction, P_0 = orientation polarization.)

moments and the moments calculated theoretically for various possible conformations of the aliphatic alcohols.

In simple unsubstituted alcohols, the observed moments agree well with the moments calculated assuming free rotation (Table III). This suggests that the barrier to free rotation in these molecules is low and that conformational heterogeneity is not significant as revealed by spectroscopic studies.[17]

In 2,2,2-trihaloethanols, only two extreme conformations arise[18]

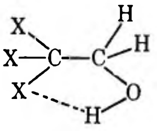

I (*cis*)

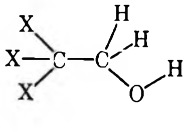

II (*trans*)

One can compute the equilibrium constant for isomerization *cis* ⇌ *trans* from a knowledge of the experimental and theoretical moments for the two conformers. For this computation we have used the equation[19]

$$\mu_{\text{mean}}^2 = (1 - x)\mu_{cis}^2 + x\mu_{trans}^2$$

where μ_{mean} is the "average" moment observed experimentally, μ_{cis} and μ_{trans} are the moments calculated theoretically for the *cis* and *trans* forms, respectively, and x is the mole fraction of the *trans* conformer. The equilibrium constants (K_x) for trichloroethanol and tribromoethanol at 35° turn out to be 0.606 and 0.474, respectively. The corresponding standard free energies of isomerization ($\Delta F = -RT \ln K_x$) are 307 and 458 cal/mol. The present results thus indicate that for trichloro- and tribromoethanols, the equilibrium lies to the left. This implies a stabilization of the *cis* structure (I) by intramolecular hydrogen bonding X···H–O. However, in tribromoethanol, the hydrogen-bonded form predominates to a greater extent than in trichloroethanol. From spectroscopic studies, Krueger and Mettee[4] have found that intramolecular hydrogen bonding in trihaloethanols increases in the order $F_3C < Cl_3C < Br_3C$, a trend which is the reverse of the normal accepted order of propensity of hydrogen bonding by halogens. These authors have listed a number of possible reasons for this unusual behavior.

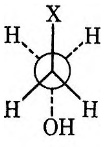

III

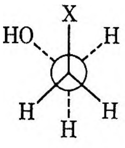

IV

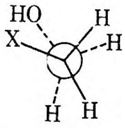

V

Spectroscopic studies have shown that 2-chloro- and 2-bromoethanols exist in *trans* and *gauche* forms in the gaseous state and in solution[3] (structures III and IV), the *cis* form (V) being ruled out.[20] Taking the azimuthal angle to be 64°,[21] we have calculated the moments for the *gauche* form (IV) of 2-chloroethanol both when the H of the O–H group points towards and away from chlorine. We obtain the values of 2.05 and 3.00, respectively. Similar calculation for 2-bromoethanol yields values of 2.04 and 2.93 D, respectively. The moments calculated for the *trans* conformations of 2-chloro- and 2-bromoethanols assuming free rotation of hydroxyl hydrogen, are 2.30 and 2.28 D, respectively. The experimental moments (1.96 for chloro- and 2.18 D for bromoethanol) can thus be reconciled with an equilibrium between the *trans* and *gauche* forms. Also the experimental value is much lower than the one calculated for the *gauche* form in which the hydroxyl hydrogen points away from halogen and, hence, rules out significant contributions from this structure. The spectroscopic results of Krueger, *et al.*,[3] which clearly indicate the presence of only one distinguishable *gauche* type conformer in 2-haloethanols with "bonded" OH, support our conclusion. In the *gauche* orientation the hydrogen bonds are strong enough to hold the H atom of the OH group in that position where it is nearest to the X atom.[22]

---

(16) L. E. Sutton, "Tables of Interatomic Distances and Configuration in Molecules and Ions," Special Publication No. 11, The Chemical Society, London, 1959.

(17) E. B. Wilson, *Advan. Chem. Phys.*, **2**, 367 (1959).

(18) The *cis* and *trans* refers to hydroxyl hydrogen being near or away from halogen.

(19) S. Mizushima, "Structure of Molecules and Internal Rotation," Academic Press, New York, N. Y., 1954, p 34.

(20) S. Mizushima, T. Shimanouchi, T. Miyazawa, K. Abe, and M. Yasumi, *J. Chem. Phys.*, **19**, 1477 (1951).

(21) P. Buckley, private communication.

(22) K. Kojima, T. Tokuhiro, Y. Takeoka, and E. Hirano, *Proc. Intern. Symp. Mol. Struct. Spectry. Tokyo*, **A222**, 1 (1964); *Chem. Abstr.*, **60**, 157146 (1964).

Table II: Formal Charge Distribution in Aliphatic Alcohols[a]

No.		$\epsilon_{C\alpha}$	$\epsilon_{C\beta}$	$\epsilon_{H\alpha}$	$\epsilon_{H\beta}$	ϵ_O	ϵ_X	$\epsilon_{H(alc)}$	$\epsilon_{C\gamma}$	H_γ
1	CH_3OH	0.368	...	0.0478	...	−2.230	...	1.720	...	...
2	CH_3CH_2OH	0.304	0.103	0.0395	0.0135	−2.245	...	1.718	...	...
3	$(CH_3)_2CHOH$	0.260	0.0886	0.0338	0.0115	−2.256	...	1.716	...	...
4	$(CH_3)_3COH$	0.227	0.0772	...	0.0100	−2.256	...	1.716	...	...
5	$ClCH_2CH_2OH$	0.489	0.685	0.0636	0.0891	−2.206	−1.004	1.724	...	...
6	Cl_2CHCH_2OH	0.608	1.045	0.0880	0.1361	−2.181	−0.748	1.728	...	...
7	Cl_3CCH_2OH	0.687	1.290	0.0894	...	−2.165	−0.574	1.731	...	...
8	$BrCH_2CH_2OH$	0.470	0.616	0.0611	0.0801	−2.211	−0.882	1.723	...	...
9	Br_2CHCH_2OH	0.561	0.897	0.0729	0.1171	−2.191	−0.628	1.727	...	...
10	Br_3CCH_2OH	0.617	1.074	0.0802	...	−2.180	−0.467	1.729	...	...
11	ICH_2CH_2OH	0.475	0.634	0.0618	0.0824	−2.209	−0.913	1.724	...	...
12	I_2CHCH_2OH	0.552	0.872	0.0718	0.1131	−2.192	−0.607	1.727	...	...
13	I_3CCH_2OH	0.595	1.006	0.0774	...	−2.184	−0.434	1.728	...	...
14	FCH_2CH_2OH	0.534	0.819	0.0695	0.1061	−2.197	−1.235	1.726	...	...
15	F_2CHCH_2OH	0.739	1.453	0.0961	0.1891	−2.154	−1.077	1.733	...	...
16	F_3CCH_2OH	0.922	2.019	0.120	...	−2.114	−0.935	1.740	...	...
17	$HOCH_2CH_2OH$	0.400	...	0.0520	...	−2.225	...	1.721	...	...
18	$H_2C{=}CHCH_2OH$	0.468	0.131	0.0608	0.0170	−2.505	...	1.674	0.0750	0.0097
19	$HC{\equiv}CCH_2OH$	0.298	0.0847	0.0387	...	−2.246	...	1.717	0.0606	0.0079
20	$CH_3OCH_2CH_2OH$[b]	0.450	0.555	0.0585	0.0721	−2.217	...	1.722	0.555	0.0721
21	$(NO_2)(CH_3)_2CCH_2OH$	0.614	1.063	0.0798	...	−2.179	−2.392	1.729	0.362	0.0471
22	$(ClCH_2)_2CHOH$	0.576	0.708	0.0749	0.0921	−2.187	−0.987	1.727	...	...

[a] ϵ denotes charge; carbon, hydrogen, etc., are designated α, β, γ with reference to the hydroxyl group. [b] $\epsilon_{O(OMe)} = -1.543$.

Table III: Calculated and Observed Electric Moments of Aliphatic Alcohols

Compound	μ_{exptl}	μ_{calcd}
CH_3OH	1.69	1.61
CH_3CH_2OH	1.67	1.80; 1.45; 1.64[a]
$(CH_3)_2CHOH$	1.68	1.79; 1.49; 1.65[a]
$(CH_3)_3COH$	1.69	1.65
$H_2C{=}CHCH_2OH$	1.63	1.95; 1.15; 1.60[a]
$HC{\equiv}CCH_2OH$	1.78	1.90; 1.38; 1.66[a]
$ClCH_2CH_2OH$	1.96	2.05; 2.30[b]
$BrCH_2CH_2OH$	2.18	2.04; 2.28[b]
Cl_3CCH_2OH	2.04[h]	0.40; 3.28[c]
Br_3CCH_2OH	1.73	0.34; 3.01[c]
F_3CCH_2OH	...	1.41; 1.81[c]
$(ClCH_2)_2CHOH$	2.11[h]	2.12[d]
$HOCH_2CH_2OH$	2.27	2.29; 1.30; 1.64; 1.10[e]
$CH_3OCH_2CH_2OH$	2.22	1.94; 2.86[f]
$(NO_2)(CH_3)_2CCH_2OH$	3.35	3.82, 5.38, 4.47, 4.30[g]

[a] The values are in the order for the skeletons

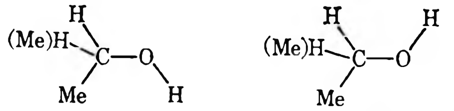

and for free rotation. [b] The values are, respectively, for structure IV with intramolecular H bond and III with free rotation of O-H. [c] The values are for structures I and II, respectively. [d] For structure VI. [e] The values are for structures VII, VIII, *gauche* form with the hydroxyl hydrogens *trans*, and *trans* form with the hydroxyl hydrogens *cis*. [f] For structures IX and X, respectively. [g] For structure XI; the other values in the row are for structures without an intramolecular bond, O-H···O_2N. [h] Present work; other values in the column are taken from literature [A. L. McClellan, "Tables of Electric Dipole Moments," Freeman, London, 1963]. The structures labeled I, II, etc., are shown in the text.

For 1,3-dichloropropan-2-ol, several structures are possible. The experimental value (2.11 D) is close to the one (2.12 D) calculated for the structure VI, with the two C-Cl bonds tilted 60° in the opposite sense from the H-C_α-C_β plane. Once again, this structure is stabilized by intramolecular hydrogen bonding O-H···Cl. Moreover, as the bulky chlorine atoms are away from each other, the steric repulsions are reduced to a minimum.

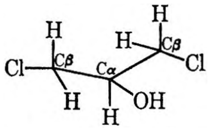

VI

For ethylene glycol, the dipole moment (2.29 D) calculated for the *gauche* form (azimuthal angle 64°) with the two O-H groups *cis-trans* to each other (conformation VIIa or b) agrees well with experimental value (2.27 D), thus corroborating the spectral data which reveal a rigid *gauche* conformation for this molecule.[12] The special stability of the *gauche* conformation arises out of the presence of the two equivalent structures VIIa and b. The earlier work Krueger, *et al.*,[6] have postulated two types of *gauche*

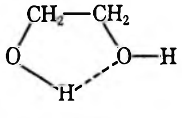

VIIa

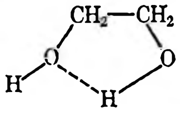

VIIb

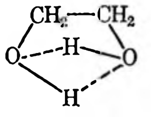

VIII

forms, VII and VIII for this molecule with the latter appreciably populated at low temperatures. Buckley, *et al.*,[12] have pointed out that the presence of species VIII with two intramolecular H bonds is unlikely in view of considerable strain in such a cyclic structure. The moment calculated for structure VIII turns out to be only 1.30 D different from the experimental value. Thus, the present results confirm the conclusions of Buckley, *et al.*,[12] that ethylene glycol exists wholly in the conformation VII.

For 2-methoxyethanol again, two conformations need be considered *gauche* and *trans* (IX and X).[8] In the *gauche* conformation (IX), the hydroxyl hydrogen will enter into hydrogen-bonding interaction with the methoxyl oxygen, while in the *trans* conformation (X), the O–H will be "free." The moment calculated for IX is 1.94 D when it is assumed that the H of the hydroxyl points towards methoxyl oxygen. The experimental value is 2.22 D, indicating that the predominant conformation is IX. The slightly higher experimental value can be explained on the basis of some slight contribution from the *trans* form (X) for which a moment of 2.86 D has been calculated. Spectroscopic studies[6,23] show that 2-methoxyethanol exists predominantly in the intramolecularly hydrogen-bonded *gauche* conformation, with the *trans* conformation slightly populated. The stability of the *gauche* form is not only due to attractive force of the hydrogen bond, but also due to the loss of repulsive interaction compared to the *trans* form.[8]

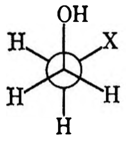

IXa

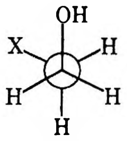

IXb

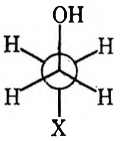

X

$X = -OCH_3$

The dipole moment (3.82 D) calculated for the intramolecularly hydrogen-bonded conformation of 2,2-dimethyl-2-nitroethanol (structure XI) is closer to the experimental value (3.35 D) than the moments calculated for the other conformations (Table III), indicating that for the nitroethanol, the preferred conformation is XI with a six-membered chelate ring resulting from intramolecular H bonding between hydroxyl proton and nitrooxygen. Spectroscopic studies by several authors, notably Baitinger, *et al.*,[7] and Urbanski,[9,10] confirm such an interaction.

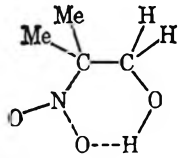

XI

The experimental moments of trifluoro-, dihalo-, and iodoalcohols are not available in the literature. However, for the sake of completeness, the charge distributions in these compounds have been evaluated, and the values are shown in Table II.

Acknowledgment. The authors thank Professor M. R. A. Rao for his keen interest and encouragement. S. S. K. thanks U. G. C. (India) for a fellowship.

---

[23] A. B. Foster, A. H. Haines, and M. Stacey, *Tetrahedron*, 16, 177 (1961).

Vibrational Intensities. XX.

Band Shapes of Some Fundamentals of Methyl Iodide-d_3

by Tsunetake Fujiyama and Bryce Crawford, Jr.

Molecular Spectroscopy Laboratory, Department of Chemistry, University of Minnesota, Minneapolis, Minnesota 55455

(Received November 18, 1968)

The refractive index, n, and extinction coefficient, k, have been measured by ATR techniques for the ν_3 and ν_6 bands of CD_3I, at 492 and 656 cm^{-1}, respectively. The band-shape and intensity data are examined both in comparison with simple "collision-damped" models, and through the correlation-function approach, comparison being made with the corresponding branch of CH_3I. The perpendicular band ν_6 of CH_3I shows noticeable effects of inertial rotation; the other three bands show little, if any, such effects. A rather full discussion is given of the reliability of correlation functions as calculated from spectroscopic data.

Introduction

One of the more challenging problems in vibration spectroscopy is the measurement of absolute intensities of absorption bands and the understanding of band shapes in liquids. We have found attenuated total reflection (ATR) spectroscopy advantageous since we can by this method measure the absolute intensity of bands in the condensed phase without introducing certain kinds of systematic error such as the base-line correction and the effects of refractive index.

The wing correction, however, is still a very important problem that remains to be solved; in this connection it would be valuable if we could establish some reasonable intensity distribution function as one which reproduces the shape of the absorption band. Recently, some authors have discussed absorption band shapes from the viewpoint of molecular motion in the liquid phase, and this seems to us a promising method of considering the problem quantitatively.

In the present report we extend to the ν_3 and ν_6 bands of heavy methyl iodide the recent similar study on normal methyl iodide.[1] Our main interest is to decide whether and under what circumstances it is reasonable to use the Lorentzian function as a fairly general experimental function of the band shape. We also seek to derive quantitative information about the molecular motion itself from the band shape.

Determination of Optical Constants

Experimental Conditions. The ATR spectrum of liquid methyl iodide-d_3 was observed, using the spectrometer constructed in this laboratory[2] for two fundamental bands, one the perpendicular e-type fundamental ν_6 at 656 cm^{-1}, and the other the a_1 parallel fundamental ν_3 at 492 cm^{-1}. These two bands were chosen because they are fairly well isolated from other bands and because the results obtained are directly comparable with the earlier results of methyl iodide.[1] The spectrometer was used at a resolution of 3–5 cm^{-1} at a temperature of about 27°.

The optical constants for these two bands were obtained from the ATR spectrum by a slightly improved version of the techniques previously described,[3] and the results obtained are given in Tables I and II. The reliability of the optical constants is checked using the Kramer–Kronig equation,[4] where $n(\nu')$ is the refractive

$$n(\nu') - n' = \frac{2}{\pi}\int_{\text{band}} \frac{k(\nu)\nu\cdot d\nu}{\nu^2 - \nu'^2} \qquad (1)$$

index at wave number ν' and n' is the contribution to the refractive index arising from transitions other than those under consideration here. The refractive indices calculated from the equation agree with the observed ones within the standard estimates of error, $\sigma(n)$, which are also given in Tables I and II.

Reduction to "True" Band Shape. In order to obtain parameters more amenable to theoretical interpretation, the effect of the dielectric field was eliminated by transforming the optical constant $\hat{n}$ into the local susceptibility

$$\hat{C} = C' + iC'' \qquad (2)$$

using the Lorentz–Lorenz field.[5] The imaginary part of the local susceptibility C'', after scaling, may be thought of as a "true" extinction coefficient, k_0,[6,7] where

$$k_0 = 2\pi\cdot C'' \qquad (3)$$

To demonstrate the effect of the dielectric field on the

---

(1) C. F. Favelukes, A. A. Clifford, and B. Crawford, Jr., *J. Phys. Chem.*, **72**, 962 (1968).

(2) A. C. Gilby, J. Burr, Jr., and B. Crawford, Jr., *ibid.*, **70**, 1520 (1966).

(3) A. C. Gilby, J. Burr, Jr., W. Krueger, and B. Crawford, Jr., *ibid.*, **70**, 1525 (1966).

(4) For instance, W. K. H. Panofsky and M. Phillips, "Classical Electricity and Magnetism," 2nd ed, Addison-Wesley, Reading, Mass., 1962.

(5) A. A. Clifford and B. Crawford, Jr., *J. Phys. Chem.*, **70**, 1536 (1966).

(6) N. G. Bakhshiev, O. P. Girin, and V. S. Libov, *Opt. Spectrosc.* (USSR) (English Transl.), **15**, 225, 336, 395 (1963); **16**, 549 (1964).

(7) W. C. Krueger, Ph.D. Thesis, University of Minnesota (1966).

Table I: Optical Constants for the 492-Cm^{-1} Band of Liquid Methyl Iodide-d_3

ν, cm^{-1}	k	$\sigma(k)$	n	$\sigma(n)$
521.1	0.0011	0.0003	1.5101	0.0014
519.9	0.0013	0.0003	1.5099	0.0014
518.9	0.0013	0.0003	1.5097	0.0014
518.0	0.0012	0.0003	1.5096	0.0014
517.1	0.0014	0.0003	1.5095	0.0014
516.2	0.0017	0.0003	1.5093	0.0013
514.9	0.0014	0.0003	1.5093	0.0014
514.0	0.0016	0.0003	1.5090	0.0013
513.1	0.0018	0.0003	1.5087	0.0013
511.9	0.0018	0.0003	1.5081	0.0013
511.1	0.0017	0.0003	1.5080	0.0013
509.9	0.0022	0.0003	1.5076	0.0013
509.0	0.0023	0.0003	1.5073	0.0013
508.1	0.0028	0.0003	1.5065	0.0014
507.0	0.0029	0.0004	1.5059	0.0014
506.1	0.0030	0.0004	1.5054	0.0015
505.0	0.0033	0.0004	1.5046	0.0016
504.1	0.0035	0.0004	1.5041	0.0016
503.0	0.0041	0.0004	1.5022	0.0019
501.9	0.0052	0.0004	1.4994	0.0021
501.0	0.0060	0.0005	1.4974	0.0022
499.9	0.0072	0.0005	1.4944	0.0023
499.1	0.0083	0.0005	1.4920	0.0023
498.0	0.0109	0.0006	1.4889	0.0023
497.0	0.0137	0.0007	1.4910	0.0025
495.9	0.0194	0.0009	1.4884	0.0027
495.1	0.0246	0.0011	1.4879	0.0029
494.0	0.0300	0.0013	1.4945	0.0030
493.5	0.0311	0.0014	1.4999	0.0031
493.0	0.0315	0.0015	1.5054	0.0031
491.9	0.0291	0.0016	1.5148	0.0031
490.9	0.0240	0.0015	1.5218	0.0030
490.1	0.0194	0.0015	1.5260	0.0029
489.1	0.0147	0.0014	1.5279	0.0029
488.1	0.0114	0.0012	1.5271	0.0027
487.1	0.0085	0.0011	1.5272	0.0026
486.1	0.0075	0.0008	1.5235	0.0024
485.1	0.0056	0.0008	1.5248	0.0024
484.1	0.0050	0.0007	1.5244	0.0024
482.9	0.0042	0.0005	1.5227	0.0023
482.1	0.0040	0.0005	1.5213	0.0022
480.9	0.0032	0.0004	1.5213	0.0022
479.9	0.0027	0.0004	1.5210	0.0022
479.0	0.0027	0.0004	1.5209	0.0022
478.0	0.0025	0.0004	1.5211	0.0022
477.1	0.0022	0.0003	1.5199	0.0022
475.9	0.0021	0.0003	1.5182	0.0021
475.0	0.0017	0.0003	1.5177	0.0021
474.1	0.0016	0.0003	1.5178	0.0021
472.0	0.0016	0.0003	1.5175	0.0021
472.0	0.0015	0.0003	1.5167	0.0020
471.1	0.0016	0.0003	1.5170	0.0021
470.0	0.0011	0.0003	1.5173	0.0021
469.1	0.0009	0.0003	1.5163	0.0020

Table II: Optical Constants for the 656-Cm^{-1} Band of Liquid Methyl Iodide-d_3

ν, cm^{-1}	k	$\sigma(k)$	n	$\sigma(n)$
740.5	0.0003	0.0002	1.5039	0.0022
734.8	0.0001	0.0002	1.5035	0.0022
730.2	0.0002	0.0002	1.5022	0.0021
724.7	0.0005	0.0003	1.5017	0.0021
720.3	0.0007	0.0003	1.5015	0.0021
715.1	0.0011	0.0003	1.5009	0.0021
710.0	0.0018	0.0003	1.5003	0.0021
705.1	0.0023	0.0004	1.5000	0.0021
700.2	0.0027	0.0004	1.4998	0.0021
694.7	0.0033	0.0004	1.4993	0.0021
690.1	0.0041	0.0005	1.4983	0.0022
684.8	0.0055	0.0006	1.4974	0.0023
680.4	0.0063	0.0006	1.4967	0.0023
678.2	0.0077	0.0008	1.4935	0.0028
676.0	0.0084	0.0008	1.4937	0.0028
673.9	0.0109	0.0007	1.4903	0.0026
671.8	0.0122	0.0007	1.4906	0.0027
669.7	0.0150	0.0008	1.4890	0.0028
668.4	0.0168	0.0009	1.4888	0.0029
666.3	0.0194	0.0010	1.4890	0.0031
664.3	0.0227	0.0011	1.4882	0.0031
662.3	0.0261	0.0013	1.4895	0.0034
660.3	0.0293	0.0015	1.4915	0.0036
658.3	0.0320	0.0017	1.4959	0.0038
656.4	0.0323	0.0018	1.5006	0.0040
653.8	0.0285	0.0017	1.5097	0.0041
651.9	0.0258	0.0016	1.5104	0.0040
650.0	0.0216	0.0015	1.5163	0.0042
648.1	0.0192	0.0013	1.5131	0.0039
645.7	0.0131	0.0009	1.5166	0.0027
643.9	0.0111	0.0009	1.5163	0.0026
642.0	0.0098	0.0009	1.5160	0.0025
639.7	0.0084	0.0009	1.5153	0.0025
637.9	0.0075	0.0009	1.5150	0.0024
636.1	0.0064	0.0008	1.5150	0.0024
634.4	0.0053	0.0008	1.5147	0.0024
632.1	0.0047	0.0008	1.5143	0.0023
629.8	0.0037	0.0008	1.5139	0.0023
624.8	0.0032	0.0008	1.5124	0.0022
620.1	0.0034	0.0005	1.5151	0.0024
615.2	0.0031	0.0004	1.5145	0.0023
609.9	0.0022	0.0004	1.5134	0.0023
604.8	0.0018	0.0003	1.5131	0.0023
600.2	0.0015	0.0003	1.5128	0.0017
595.3	0.0014	0.0003	1.5121	0.0017
590.1	0.0009	0.0003	1.5109	0.0017
585.0	0.0009	0.0003	1.5108	0.0017

optical constants, we show both k and k_0, the continuous line and the broken line, respectively, in Figures 1a and b. In general, the correction for dielectric effect causes not only a change in the magnitudes of k but also a shift of the absorption maximum and a change of band shape[7,8] although the effects are not so remarkable in the present case because of the weak bands and low polarity.

The integrated intensities of the two bands are summarized in Table III for both normal and heavy methyl iodide, Γ^k being obtained by the direct integration of the extinction coefficient, *i.e.*

$$\Gamma^k = (4\pi/c_m) \int k(\nu)\cdot d\nu \qquad (4)$$

---

(8) T. Fujiyama and B. Crawford, Jr., *J. Phys. Chem.*, **72**, 2174 (1968).

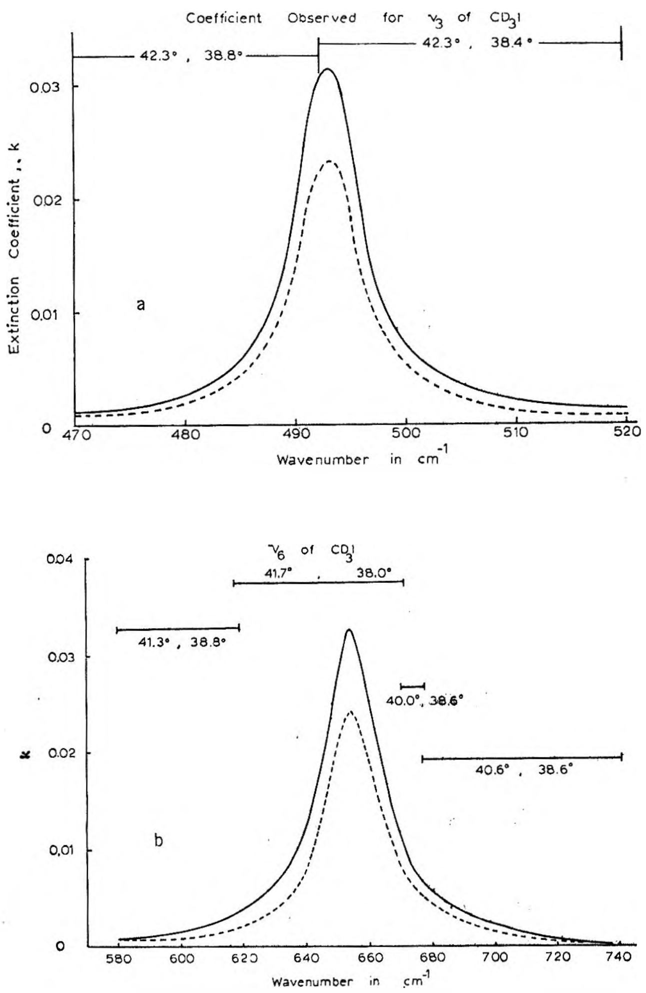

Figure 1. Extinction coefficients for liquid CD_3I. (a) Parallel band, ν_3, species a; (b) perpendicular band, ν_6, species e. Continuous lines, observed extinction coefficient, k; broken lines, corrected values, k_0.

where c_m is the molar concentration. Γ^{pw} is integrated intensity obtained from Γ^k by the Polo–Wilson method and $\Gamma^{c''}$ is the integrated intensity resulting from direct integration of the imaginary part of the local susceptibility.[8]

Comparison with Van Vleck and Weisskopf Theory and Spectral Parameters

The observed local susceptibility, $\hat{C}$, was compared with the collision theory of Van Vleck and Weisskopf.[6,9] The four parameters, namely, the damping constant γ, the resonant frequency ν_0, the strength factor S, and the contribution K to the local susceptibility from the outside of the band, were obtained by the least-squares method using the equation

$$\hat{C} = K + S\left[\frac{\nu_0 - i\gamma}{(\nu_0 - \nu) - i\gamma}\right] + \frac{\nu_0 + i\gamma}{(\nu_0 + \nu) + i\gamma} \qquad (5)$$

The calculated local susceptibilities are compared with the observed ones in Figures 2a and b, and they agree well within the experimental errors both for ν_3 and ν_6.

In Table III, the parameters obtained are given together with the earlier results for methyl iodide. The intensity values Γ^{vvw}, given by the relation

$$\Gamma^s = 8\pi^3\nu_0(M/d)S \qquad (6)$$

with M and d being molecular weight and density, respectively, are also included in the table.

We remind the reader that the imaginary part of eq 5 reduces to the well-known Lorentzian shape function

$$C'' = \text{constant}\cdot\frac{\gamma}{(\nu_0 - \nu)^2 + \gamma^2} \qquad (7)$$

if the ratio γ/ν_0 is small enough, and that γ is related to the half-band width $\Delta\nu_{1/2}$ by

$$\gamma = (1/2)\cdot\Delta\nu_{1/2} \qquad (8)$$

It will be noted in Table III that the half-band widths of the e-type bands are larger than those of the a-type bands and a remarkable decrease of half-band width is observed when passing from methyl iodide to methyl iodide-d_3 for both ν_3 and ν_6 fundamentals.

Table III: Spectral Parameters for ν_3 and ν_6 of Methyl Iodide and Methyl Iodide-d_3

CH_3I	
ν_3 (440–626 cm^{-1}, 290 points)	
ν_0: 521.64 cm^{-1}	Γ^k: 719.16 cm^2/mol
γ: 5.168 cm^{-1}	Γ^{pw}: 536.53
S: 0.608	$\Gamma^{c''}$: 537.27
K: 0.070	Γ^{vvw}: 489.87
ν_6 (750–1040 cm^{-1}; 249 poiints)	
ν_0: 884.16	Γ^k: 1969.65
γ: 15.975	Γ^{pw}: 1467.43
S: 1.016	$\Gamma^{c''}$: 1472.05
K: 0.070	Γ^{vvw}: 1388.50
CD_3I	
ν_3 (430–530 cm^{-1}; 243 points)	
ν_0: 492.61	Γ^k: 277.85
γ: 3.376	Γ^{pw}: 205.85
S: 0.281	$\Gamma^{c''}$: 206.43
K: 0.072	Γ^{vvw}: 213.65
ν_6 (535–760 cm^{-1}; 345 points)	
ν_0: 656.11	Γ^k: 805.0
γ: 11.179	Γ^{pw}: 598.9
S: 0.599	$\Gamma^{c''}$: 600.8
K: 0.071	Γ^{vvw}: 607.03

It is also worth noting here, for discussion later, that the band shape of ν_6 of methyl iodide is not well approximated by the Van Vleck–Weisskopf function, while ν_3 of methyl iodide is well fitted to the function.

Calculation of the Time-Correlation Function and the Estimation of Errors

Time-correlation functions are calculated as the

---

(9) J. H. Van Vleck and V. F. Weisskopf, *Rev. Mod. Phys.*, **17**, 227 (1945).

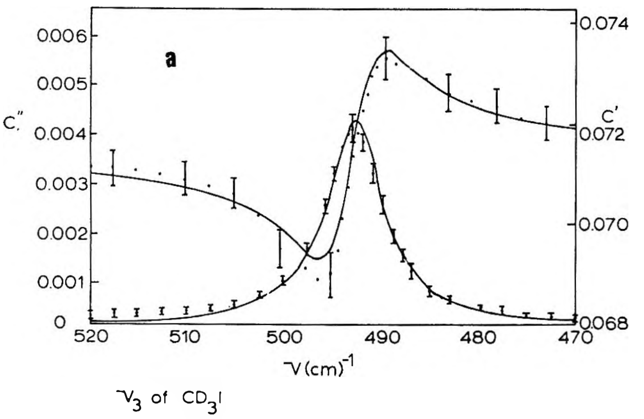

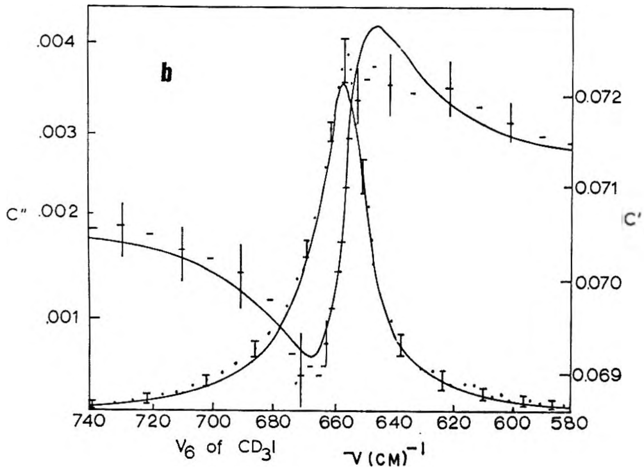

Figure 2. Comparison of local susceptibilities with VVW calculation. Solid lines, C' and C'' calcd; points, values from observation; vertical lines, standard errors, $\sigma(C')$ and $\sigma(C'')$. (a) parallel band, ν_3; (b) perpendicular band, ν_6.

Fourier integral of the spectral density distribution function[10]

$$\alpha(t) = \int_{\text{band}} \tilde{I}(\omega)\cdot\cos(\omega t)\cdot d\omega \qquad (9)$$

where $\tilde{I}(\omega)$ represents the normalized spectral density distribution function. We took the corrected C'' as the spectral density. In the actual numerical procedure we would use the summation

$$\alpha(t) = \sum_i \left[\frac{I(\omega_i)}{\sum_j I(\omega_j)\Delta\omega_j}\cos(\omega_i t)\right]\Delta\omega_i \qquad (10)$$

instead of eq 9. Several points regarding the reliability of time-correlation functions so calculated from infrared data seem worth discussion at this point.

Finite Resolution of Spectrometer. Let the resolution of the spectrometer be $\Delta\nu$; then one cannot obtain accurate information about phenomena which occur at times greater than $1/\Delta\nu$ along the time axis, from the Fourier analysis of the observed phenomena along the frequency axis. This uncertainty is *systematic* in type. Our spectrometer is used at a resolution of 3-5 cm^{-1} during the present experiment, and hence the limit of reliability of our results is confined to times less than 1-2 psec.

Numerical Procedure of Integration. This type of error is essentially systematic and sometimes leads to serious errors in the calculated absolute values because the integration is included in the denominator of eq 10. The magnitude of this error is easily estimated, and the effect is eliminated by choosing the proper numerical procedure and by taking enough data points. In this work about 300 points are used for each band. Thus the error is made negligibly small.

Truncation Effect. The calculated time-correlation functions are very sensitive to the actual extent of the region of integration which is indicated as *band* in eq 9. In the actual procedure, we are compelled to truncate the region of integration because of the overlap of bands or the increase of random errors in the wing parts. The effects are clarified by numerical study using the Lorentzian

$$f(\omega) = \frac{4}{\omega^2 + (11)^2} \qquad (11)$$

which closely represents the intensity distribution function of ν_6 of methyl iodide-d_3. In Figure 3, we show several calculated correlation functions, curves A, B, C, D, and E corresponding to the range of integration being truncated at one, two, three, four, and eight times the half-band width (22 cm^{-1}). The result of analytical integration (between $\pm\infty$) is indicated by F in Figure 3. It is seen that the truncation causes an oscillation effect in the calculated correlation function and the periodicity of the oscillation is roughly inversely proportional to the range of the integration. As the correlation function is normalized for unity at $t = 0$, the amplitude increases as t increases. In addition, the amplitude of oscillation with respect to the line F increases as the range of integration is decreased. These results lead to the conclusion that the region of integration should be more than eight or ten times the half-band width to have a reliable correlation function for the time less than ~2 psec.

Baseline Effect. The choice of baseline is also very critical. In order to investigate this effect, time-correlation functions were calculated by adding various constants to the function of eq 11. The effect of thus changing the baseline is demonstrated in Figure 4, where 1, 2, 3, and 4 correspond to the baselines being lowered 0, 0.0002, and 0.004 with respect to the original zero line, respectively; the region of integration is ten times the half-band width. We note that lowering the baseline 0.0002, which is about 0.5% of the maximum value of $f(\omega)$, causes a remarkable error in the time-correlation function. Let $f(\omega)$ be given by

---

[10] R. G. Gordon, *J. Chem. Phys.*, **43**, 1307 (1965).

$$f(\omega) = \frac{b}{\omega^2 + a^2} \tag{12}$$

Then the ratio of $f(\omega)$ to $f(0)$ is expressed by the equation

$$f(\omega)/f(0) = \frac{a^2}{\omega^2 + a^2} \tag{13}$$

If the region of integration is terminated at $\pm\omega_e$ corresponding to ten times the half-band width, $f(\omega_e)$ is about 1% of $f(0)$ and the errors expected for $f(\omega_e)$ should be less than $(^1/_2)f(\omega_e)$. Thus the effects of the truncation are safely eliminated when, and only when, the intensity distribution is measured over a frequency range at least ten times the half-band width and the intensity error of the wing parts is less than 50% of the absolute value of the wing intensity. It is difficult to satisfy this requirement for the usual infrared absorption bands and the common infrared absorption spectroscopy techniques.

As the actual band shape does not always follow a Lorentzian function, the situation may be more complicated and the necessary condition needed to be able to ignore safely the truncation effect may have to be made more severe. The region of integration we used for each band is given in Table III together with the number of data points included in the integration.

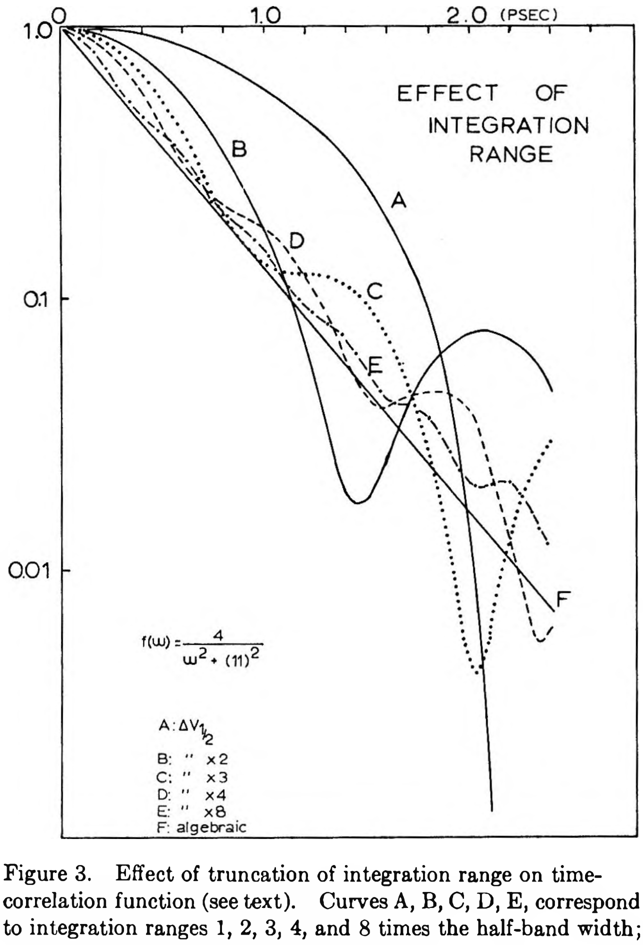

Figure 3. Effect of truncation of integration range on time-correlation function (see text). Curves A, B, C, D, E, correspond to integration ranges 1, 2, 3, 4, and 8 times the half-band width; F is the algebraic result with no truncation.

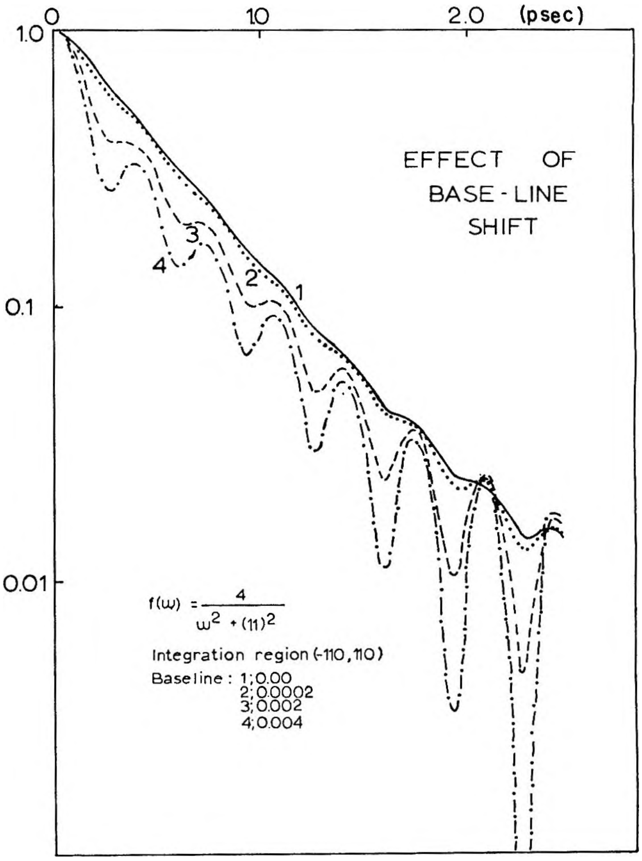

Figure 4. Effect of baseline shift on time-correlation function (see text). Curve 1 corresponds to the unshifted baseline; curves 2, 3, and 4 correspond to shifts of 0.0002, 0.003, and 0.004.

It must be emphasized here that the effect of truncation always occurs even in the region of short times but becomes worse as the time increases. These errors are systematic in type, and there is no way to eliminate them except to extend the observations of the wing intensity over a wider range of frequency with sufficiently high accuracy. Any mathematical techniques to eliminate the effect cause new systematic errors in the results.

Random Errors. We estimated the effects of experimental random errors on the calculated time-correlation functions by propagating the standard errors of the parameters of the VVW functions, eq 5, fitted to the observed intensity. These standard errors of the VVW parameters themselves are calculated in the least-squares procedure from the weight matrix determined by the $\sigma(n)$ and $\sigma(k)$ given in Tables I and II. The effect of the VVW-parameter errors on the time-correlation function can be seen by noting that the simplified eq 7 would correspond to the time-correlation function expressed

$$\alpha(t) = \exp(-\beta t) \tag{14}$$

If we express $\alpha(t)$ on the natural logarithmic scale, then

$$\ln\,[\alpha(t)] = -\beta t \qquad (15)$$

and the standard error for $\ln[\alpha(t)]$ is estimated as

$$\sigma[\ln\,(\alpha(t))] = \sigma(\alpha)\cdot t \qquad (16)$$

This estimate depends, of course, on the appropriateness of the VVW function to describe the data.

Results of Calculation. The calculated time-correlation functions are shown in Figure 5. The errors indicated by the vertical lines represent the contribution from the random errors only of the observed data, estimated as described above. We note that the systematic errors due to the truncation effect still remain clearly in all the results, and the systematic errors are at least comparable in magnitude with the random error.

Discussion of Results

General. Although the time-correlation functions obtained are not accurate enough to support detailed quantitative interpretation, some interesting information can be obtained.

The rotational motion of molecules having C_{3v} symmetry is characterized by two types of rotation; one about the symmetry axis which we take as the z axis and one about one of the perpendicular axes (x or y). The rotational time-correlation function obtained from the a_1-type band corresponds to the decay of polarization parallel to the z axis, this being the direction of the transition-moment vector of the vibration; thus, the two equivalent rotations about the x and y axes enter into the analysis of this time-correlation function. Similarly, the two different rotations about the z and x axes affect the time-correlation function for the e-type band. Before discussing the actual results, let us consider what we might expect in the way of differences between the time-correlation functions for methyl iodide and methyl iodide-d_3.

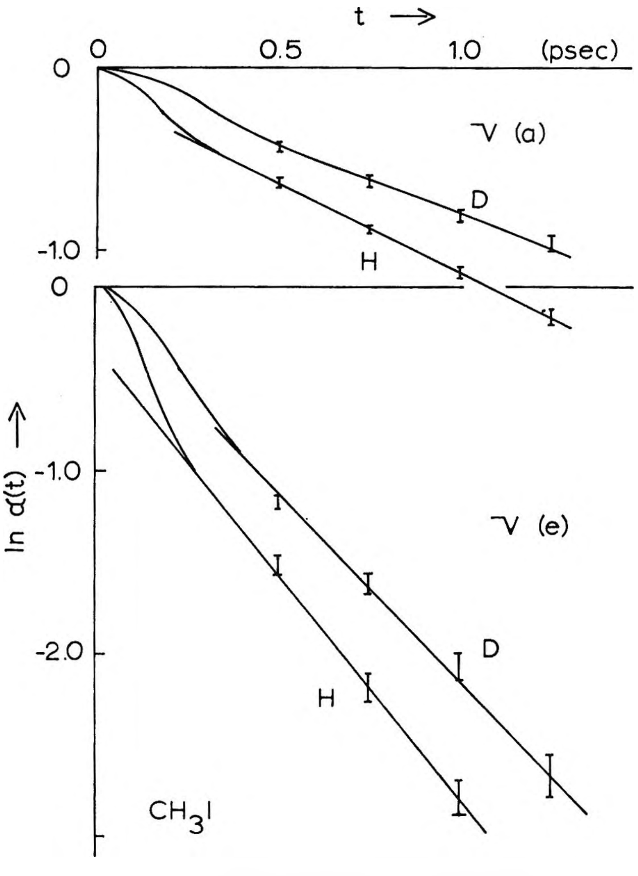

Figure 5. Time-correlation functions for the four bands studied. Vertical lines indicate estimates of random error effect as described in the text; D, curves for CD_3I bands; H, curves for CH_3I.

So far as the rotational motion is concerned, the chief differences between these two molecules are in the inertial rotational constants and in the position of the center of gravity along the z axis. The rotational constants reported for the gas phase are[11] $A_0 = 5.11_9$ and $B_0 = 0.250_2$ cm^{-1} for normal methyl iodide and $A_0 = 2.58_6$ and $B_0 = 0.201_4$ cm^{-1} for methyl iodide-d_3.

Following the recent theoretical treatments of the subject[10,12,13] we may distinguish two different limiting types of the decay process, one governed by a rotational diffusion and the other by inertial rotation. If the rotational motion of the molecules is essentially inertial and, hence, characterized by the rotational constants, then the behavior of the time-correlation function for an e-type band, involving both A_0 and B_0, should differ remarkably from methyl iodide to methyl iodide-d_3; that for an a-type band, involving only B_0, should be similar for both molecules. If, instead, the rotational motion is essentially a diffusion process, the time-correlation functions of a_1-type vibrations of the two molecules would be expected to differ, since the change of the center of gravity would cause a change in the drag force and therefore a change in the diffusion constants.

Time-Correlation Function. The time-correlation function should also reflect the nature of the decay process. A rotational diffusion mechanism should give an exponential decay, or logarithmic straight-line behavior for $\ln\,\alpha(t)$, as for any stochastic process.[14] If, on the other hand, most of the molecules are rotating fairly freely and the rotation is inertial, logarithmic time-correlation function $\ln\,\alpha(t)$ deviates from a straight line, especially at short times. In fact, as Figure 5 shows, all four rotational correlation functions observed in the present experiment behave exponentially at long times; moreover, the limiting long-time exponential curves can be extrapolated back close to unity at time $t = 0$, the deviation from unity being most marked in the case of the rotational correlation function for the e-type band of normal methyl iodide. These results imply that the molecular rotation of methyl iodide or methyl iodide-d_3

---

(11) E. W. Jones, R. J. L. Popplewell, and H. W. Thompson, *Proc. Roy. Soc.*, **A288**, 39, 50 (1965).

(12) H. Shimizu, *J. Chem. Phys.*, **43**, 2453 (1965).

(13) H. Shimizu, *Bull. Chem. Soc. Jap.*, **39**, 2385 (1966).

(14) "Investigations on the Theory of the Brownian Movement," R. Furth, Ed., Dover Publications, New York, N. Y., 1956.

ห้องสมุด กรมวิทยาศาสตร์

should be characterized essentially by a random reorientation process and the behavior of the rotational-correlation functions may be interpreted mainly by the diffusion equation.

Favro[15] reports a general theory of rotational diffusion for the case of a rotational-correlation function which is governed by the stochastic process. If we adapt his formula to the case of the symmetric-top molecule, we obtain for the a_1-type band shape

$$f(\omega) = \frac{1}{3\pi}\left[\frac{(A_z)^2(2D_x)}{\omega^2 + (2D_x)^2}\right] \tag{17}$$

and for the e-type

$$f(\omega) = \frac{1}{3\pi}\left[\frac{(A_x)^2(D_x + D_z)}{\omega^2 + (D_x + D_z)^2}\right] \tag{18}$$

where D_z and D_z are the rotational diffusion constants with respect to the parallel and perpendicular axes, respectively, while A_z and A_x represent the magnitude of the transition dipole moments along such axes. Thus the diffusion constants are related directly to the time derivative of the logarithmic correlation functions at long times. Since (17) and (18) are Lorentzian, we get

$$2D_z = \beta_z$$

and

$$D_x + D_z = \beta_x$$

that is

$$D_x = \beta_z/2$$

and

$$D_z = \beta_x - (\beta_z/2) \tag{19}$$

where β_z and β_x are the time derivatives of the logarithmic rotational correlation functions of a_1- and e-type bands, respectively.

In Table IV, the diffusion constants thus observed are given in units of psec^{-1}. The results show that the magnitude of the diffusion constants about the symmetry axes are four to five times larger than those about the perpendicular axes. The diffusion constants about symmetry axes have nearly the same values for methyl iodide and methyl iodide-d_3, while those about perpendicular axes differ considerably. The results seem reasonable in terms of the expectations discussed above.

Table IV: Diffusion Constants Obtained for Methyl Iodide and Methyl Iodide-d_3

	CH_3I	CD_3I
D_z	1.94	1.71
D_x	0.48	0.33

We now turn to the behavior of the time-correlation functions at short times. As the perpendicular rotational constants B_0 of the two molecules are nearly equal, the behavior of the two rotational correlation functions concerned with the a_1-type vibrations should be very similar if the rotation of these molecules is inertial. Actually, it is seen from Figure 5 that the two ν_3 functions are quite different even at very short times. The change of $\alpha(t)$ of methyl iodide-d_3 along the time axis is much slower than that of normal methyl iodide. From this we would conclude that the molecular rotations of these molecules in the liquid phase about their perpendicular axes must be strongly hindered, with the contribution of inertial rotation to the rotational-correlation function being very small.

The rotational-correlation functions for the e-type vibration at short times are more complicated, since both kinds of rotation, about parallel and perpendicular axes, contribute to them. From the present data we can draw no conclusion as to the contribution of inertial rotation to the short-time behavior of $\alpha(t)$. We can only conclude from the behavior of all four rotational correlation functions at short times, that the decay processes of methyl iodide and methyl iodide-d_3 cannot be completely explained by the stochastic process, noting, however, that deviation from the random reorientation picture is marked only for ν_6 of normal methyl iodide.

Band Shapes and Conclusion. As discussed above, the Van Vleck–Weisskopf theory and the diffusion theory lead essentially to the same band shape, the Lorentzian, although their theoretical approaches are quite different, and if the band shape is approximated well by the Lorentz function, the logarithmic time-correlation function obtained from it will be a straight line. The conclusion we reached from comparison of the observed band shapes with the Van Vleck–Weisskopf function is that the band shapes of ν_3 and ν_6 of methyl iodide and of ν_3 of methyl iodide-d_3 are approximated fairly well by a Lorentzian curve but not that of ν_6 of methyl iodide; this is consistent with our discussion of the time-correlation functions, which show predominantly the logarithmic straight-line behavior reflecting diffusional rotation, although inertial rotation, or free rotation, affects all the time-correlation functions a little in the short-time region and most noticeably that for ν_6 of CH_3I. We suspect we can reasonably assume, from these and earlier results, that the Lorentz function is rather generally applicable to liquids composed of typical organic molecules, when proper allowance is made for the dielectric effect by correction to the local susceptibility, C'' (or k_0). From the molecular viewpoint, the factor dominating the shape of the infrared absorption band should be the drag force which the molecule experiences during rotation diffusion in the liquid phase. The effect of inertial

---

(15) L. D. Favro, *Phys. Rev.*, **119**, 53 (1960).

rotation perturbs the band shape, especially the wing parts, as is seen for ν_6 of methyl iodide.

In concluding, we stress again that great care should be exercised in the calculation of time-correlation functions from observed band shapes, especially with regard to truncation effects. In order to obtain a reliable time-correlation function, the extension of accurate observations of the absorption coefficient to the wing region of the band is essential.

Acknowledgments. We are grateful to the National Science Foundation for financial support of this research through Grant GP-3411. We are also grateful to Dr. Roger Frech for general help and Mrs. Charlotte Smith for assistance with the calculations.

Surface Orientation in Electrocapillarity

by A. Sanfeld, A. Steinchen, and R. Defay

Free University of Brussels (Faculty of Applied Sciences), Brussels, Belgium *(Received February 7, 1969)*

In the multilayer thermodynamic framework, the authors show the influence of the dipole orientation in electrocapillary systems. In the case of a low rate of orientation in the surface layer, the electrocapillarity equation of Lipmann must be modified. The new terms allow an approach of the electrocapillary phenomena when the orientation is delayed.

Electrocapillary systems are usually treated as discontinuous media. In this approach, the system is divided into well-defined spatial regions. In each of these regions, electric and thermodynamic variables are continuous in space, but some of the intensive properties are discontinuous at the boundaries of the regions considered. This model has led to very good results in electrochemical kinetics, in colloid science, and in capillarity. It seems difficult, however, to describe quasi-microscopic discontinuous regions, as, for instance, interfacial layers with macroscopic variables. This difficulty disappears when the electrocapillary system is considered as a continuum, but the fundamental problem is then the mathematical formulation of the physical properties of this continuous system.

If the layer is many molecules thick, its composition may vary with position within the layer; these circumstances make it physically consistent to use the multilayer model developed by Defay and colleagues[1,2]—a model one could call intermediate between the continuous and discontinuous models.

The system is divided into uniform regions called phases. The nonuniform regions, such as the capillary layer, are subdivided into a number of laminae, each sufficiently thin to be considered homogeneous. Our purpose is to develop an electrocapillary theory based on the multilayer model with a view to deriving an explicit formulation of dipole orientation.[3] Some results have been partially published in a previous paper.[4] In fact, important properties of the interfacial layers find their origin in this molecular orientation (ref 5–7). Excluding all microscopic fluctuation effects, this work deals only with systems for which orientation equilibrium occurs after the establishment of the diffusion equilibrium.

All transport of matter from one region to another may be treated as a transfer of one or several components from one phase to another. The only entropy production sources are, on the one hand, the chemical reactions and the transport from one phase to another, and, on the other hand, the orientation of every component which occurs in the laminae. Thus, in addition to the classical electrochemical and transport affinities, we shall have orientation affinities. In Defay's work,[1,2] the orientation of the components is not treated as an independent variable. This means that the

---

(1) R. Defay, I. Prigogine, and A. Bellemans, "Surface Tension and Adsorption," D. H. Everett, trans., Longmans Green, New York, N. Y., 1966.

(2) R. Defay, *J. Chim. Phys.*, **46**, 375 (1949).

(3) I. Prigogine and P. Mazur, *Physica*, **17**, 661 (1951); S. Nakajima, *Proc. Int. Conf. Theoret. Phys., Kyoto, Tokyo*, Sept 1953.

(4) A. Sanfeld, *Koninkl. Vlaams, Acad. Wetenschap. Letter Schone Kunsten Belg. Colloq. Grenslaagverschijnselen Vloeistoffilmen, 1965* (1966); "Introduction to Thermodynamics of Charged and Polarized Layers," Monograph no. 10, "Statistical Physics," I. Prigogine, Ed., Wiley Interscience, Dec 1968.

(5) J. T. Davies and E. K. Rideal, "Interfacial Phenomena," Academic Press, New York, N. Y., 1961.

(6) J. Guastella, *J. Chim. Phys.*, **44**, 306 (1947); *Mem. Serv. Chim. Etat*, (1947); J. Michel, *ibid.*, **54**, 206 (1957).

(7) A. N. Frumkin, *ibid.*, **63**, 785 (1966); B. B. Damaskin, *Electrochim. Acta*, **9**, 231 (1964).

Table I

	$\langle \cos \beta_1 \rangle$	$\langle \cos \beta_2 \rangle$	$\langle \cos \beta_3 \rangle$	$\langle \cos^2 \beta_1 \rangle$	$\langle \cos^2 \beta_2 \rangle$	$\langle \cos^2 \beta_3 \rangle$
Vertical upward	1	0	0	1	0	0
Vertical downward	−1	0	0	1	0	0
Lying on random	0	0	0	0	$\neq 0$	0
Lying and mutually parallel	0	0 or $\neq 0$	0 or $\neq 0$	0	$\neq 0$ or 0	$\neq 0$ or 0
Nonoriented	0	0	0	$\neq 0$	$\neq 0$	$\neq 0$
One half vertical upward, the other vertical downward	0	0	0	1	0	0
Lying one half in one direction, the other half in the other direction	0	0	0	0	$\neq 0$	$\neq 0$

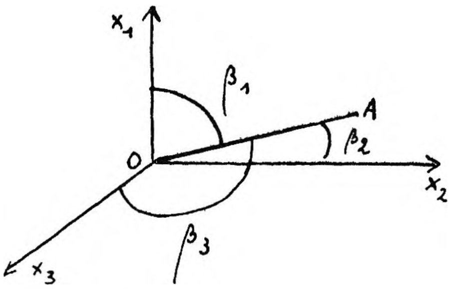

Figure 1. $\overline{\mathrm{OA}}$ is the unit vector on the axis of a dipole and β_i are the direction cosines of $\overline{\mathrm{OA}}$.

molecules, while moving from one phase to another, are always supposed to be in instantaneous orientation equilibrium with the dipole structure of the successive laminae. If, on the contrary, the orientation equilibrium is reached after the diffusion equilibrium, orientation variables independent of diffusion variables should clearly appear in the thermodynamic formalism. This will enable us to show how the Gibbs formula may easily be extended to these systems and, for illustrative purposes, we shall discuss a very simple example of surface orientation.

Orientation Variable

We consider an electrocapillary system composed of undeformable neutral polar and nonpolar molecules with charged molecules. We suppose that there are $1 \ldots \gamma \ldots c$ constituents in $1 \ldots \alpha$ phases. The orientations of the components in each phase are directly related to the chemical and electrical interactions.

Let $\overline{\mathrm{OA}}$ be a unit vector on the axes of a dipole (Figure 1)

$$\sum_{i=1}^{3} \cos^2 \beta_i = 1 \tag{1}$$

where the $\cos \beta_i$ are the direction cosines of $\overline{\mathrm{OA}}$.

We suppose that rotations of $\overline{\mathrm{OA}}$ around the coordinate axes are free. We shall introduce now the mean value of $\cos \beta$ defined by

$$\langle \cos \beta \rangle = \frac{\int \cos \beta f(\beta) \mathrm{d}\beta}{\int f(\beta) \mathrm{d}\beta} \tag{2}$$

where $f(\beta)$ is the distribution function on the angles and where the denominator is the normalization integral.

On the other hand, it is easy to see that the three mean cosines are insufficient to describe the orientation. If in addition we introduce the value of the mean-square direction cosine $\langle \cos^2 \beta_i \rangle$, we then obtain for different experimental situations the values listed in Table I. We conclude that the six mean values $\langle \cos \beta_i \rangle$ and $\langle \cos^2 \beta_i \rangle$ are at least necessary to describe all orientations.

Generally, the dipole length is not equal to unity, and thus we replace variables $\langle \cos \beta_i \rangle$ and $\langle \cos^2 \beta_i \rangle$ by the mean projection on x_i, $\langle m_{x_i\gamma}{}^{\alpha} \rangle$, and the mean-square projection on x_i, $\langle m_{x_i\gamma}{}^{\alpha 2} \rangle$ of the dipole moment, per mole of γ in the phase α.

The set of all mean variables and of all mean-square variables corresponding to all different values of $\alpha = 1,2 \ldots$ of $\gamma = 1,2, \ldots c$ and of $x_i = 1,2,3$ are respectively, represented by the abbreviated notations $\langle m_{x_i\gamma}{}^{\alpha} \rangle$ and $\langle m_{x_i\gamma}{}^{\alpha 2} \rangle$.

Remark. In fact, the distribution function of the orientation may not be described by only six projections $\langle m_{x_i} \rangle$ and $\langle m_{x_i}{}^2 \rangle$. We assume that the classical approximation of a Gaussian distribution is valid (the first projection gives the more probable value and the latter gives a way to calculate the dispersion around this value, *i.e.*, the fluctuation).

Thermodynamics of a Closed Electrocapillary System

We adopt the multilayer model in which each lamina within the surface layer is considered as a homogeneous phase of infinitesimal thickness. Let us consider now a system at uniform temperature and in mechanical equilibrium, unable to exchange molecules, ions, and electrons with the surrounding world. We include in the definition of the system all forms of electric energy including that of the field which the system creates around itself. The system is not subject to the influence of external charges since we include all relevant charges within the boundaries of the system. The system cannot, therefore, interact electrically with the surrounding world. In particular, for a system containing only one plane interface, the work done on the system by its surroundings is

$$\mathrm{d}W = -p_e\mathrm{d}V + \sigma\mathrm{d}\Omega \tag{3}$$

where p_e is the external (uniform) pressure acting on the system, $V = \sum_\alpha V^\alpha$ is the total volume, equal to the sum of the volumes of the individual phases, σ is the surface or interfacial tension, $\mathrm{d}\Omega$ is the increase of the area of surface Ω.

The equations, derived from the first and second principles of thermodynamics, have the form

$$\mathrm{d}\tilde{U} = \mathrm{d}Q - \sum_\alpha p_e\mathrm{d}V^\alpha + \sigma\mathrm{d}\Omega \tag{4}$$

and

$$\mathrm{d}\tilde{S} = \frac{\mathrm{d}Q}{T} + \frac{\mathrm{d}Q'}{T} = \mathrm{d}_e\tilde{S} + \mathrm{d}_i\tilde{S} \tag{5}$$

with $\mathrm{d}Q'/T = \mathrm{d}_i\tilde{S} \geqslant 0$.

The function $\tilde{S}$ is the total entropy including electrochemical effects and $\mathrm{d}Q' = T\mathrm{d}_i\tilde{S}$ the Clausius "uncompensated heat." Let us remember that if the orientation of the components is at each time in statistical equilibrium with the field (a reversible process), then $\tilde{S}$ may be replaced by S.[8] Because of the way in which the system has been defined (no thermal flux, no hydrodynamical motion), the only possible sources of entropy production are the chemical (including electrochemical) reactions, the diffusion of molecules or ions from one part of the system to another, and the orientation variations in each lamina within the surface layer.

The variations in orientation are due to the macroscopic electric field and to interactions between molecules or atoms belonging to the same lamina or to neighboring laminae.

We define now the degree of advancement introduced by de Donder[9] for all possible reactions (matter transport, *i.e.*, passage of one or more components from one phase to another, chemical and orientation reactions). We have

$$n_\gamma{}^\alpha - n_\gamma{}^{\alpha 0} = {}^{\alpha-1}\xi_\gamma{}^\alpha - {}^\alpha\xi_\gamma{}^{\alpha+1} + \sum_r \nu_{\gamma r}{}^\alpha \xi_r \tag{6}$$

$$\langle m_{x_i\gamma}{}^\alpha\rangle - \langle m_{x_i\gamma}{}^\alpha\rangle^0 = \xi_{x_i\gamma O}{}^\alpha \tag{7}$$

$$\langle m_{x_i\gamma}{}^{\alpha 2}\rangle - \langle m_{x_i\gamma}{}^{\alpha 2}\rangle^0 = \xi_{x_i\gamma Q}{}^\alpha \tag{8}$$

where ${}^{\alpha-1}\xi_\gamma{}^\alpha$ and ${}^\alpha\xi_\gamma{}^{\alpha+1}$ are, respectively, the degrees of advancement of the transport "reaction" of constituent γ from phase $\alpha - 1$ to phase α, and from α to $\alpha + 1$. Index r refers to the chemical reactions, superscript 0 to the time $t = 0$ (origin of ξ), subscripts O and Q refer, respectively, to $\langle m_{x_i\gamma}{}^\alpha\rangle$ and $\langle m_{x_i\gamma}{}^{\alpha 2}\rangle$, and $\nu_\gamma{}^\alpha$ is the stoichiometric coefficient of γ in α and in the chemical reaction. If the molecule orientation varies during the crossing from one lamina to another, then variables ${}^{\alpha-1}\xi_\gamma{}^\alpha$, $\xi_{x_i\gamma O}{}^\alpha$, and $\xi_{x_i\gamma Q}{}^\alpha$ vary together during the crossing.

Usually, in electrocapillary theory, orientation and diffusion are treated as independent variables, *i.e.*, the orientation and diffusion occur simultaneously.[2] We consider here the case of independent variables. Applying the de Donder and Prigogine method,[9] the entropy production $\mathrm{d}_i\tilde{S}$ can be written for all the possible reactions

$$T\mathrm{d}_i\tilde{S} = \sum_\rho \tilde{A}_\rho\mathrm{d}\xi_\rho + \sum_{x\gamma_i} \tilde{A}_{x_i\gamma O}{}^\alpha\mathrm{d}\xi_{x_i\gamma O}{}^\alpha + \sum_{x\gamma_i} \tilde{A}_{x_i\gamma Q}{}^\alpha\mathrm{d}\xi_{x_i\gamma Q}{}^\alpha \tag{9}$$

where the summation symbol $\sum_{x\gamma_i}$ represents the triple summation $\sum_\alpha\sum_\gamma\sum_{i=1}^3$. The coefficient $\tilde{A}_\rho$ is the electrochemical affinity[9] of the reaction ρ; subscript ρ, here, refers to all reactions except orientations (*i.e.*, passage and chemical reactions). The orientation affinities $\tilde{A}_{x_i\gamma O}{}^\alpha$ and $\tilde{A}_{x_i\gamma Q}{}^\alpha$ are related, respectively, to moments $\langle m_{x_i\gamma}{}^\alpha\rangle$ and $\langle m_{x_i\gamma}{}^{\alpha 2}\rangle$.

Combining (5), (9), and (4), we obtain

$$\mathrm{d}\tilde{F} = -\tilde{S}\mathrm{d}T - \sum_\alpha p_e\mathrm{d}V^\alpha + \sigma\mathrm{d}\Omega - \sum_\rho \tilde{A}_\rho\mathrm{d}\xi_\rho - \sum_{\alpha\gamma_i} \tilde{A}_{x_i\gamma O}{}^\alpha\,\mathrm{d}\xi_{x_i\gamma O}{}^\alpha - \sum_{\alpha\gamma_i} \tilde{A}_{x_i\gamma Q}{}^\alpha\,\mathrm{d}\xi_{x_i\gamma Q}{}^\alpha \tag{10}$$

where

$$\tilde{F} = \tilde{U} - T\tilde{S} \tag{11}$$

The free electrochemical energy becomes thus the function

$$\tilde{F} = \tilde{F}(T, V^\alpha, \Omega, \xi_\rho, \xi_{x_i\gamma O}{}^\alpha, \xi_{x_i\gamma Q}{}^\alpha) \tag{12}$$

where $\alpha = 1,2\ldots$; $\gamma = 1,2\ldots$ c, and $i = 1,2,3$.

The derivatives of $\tilde{F}$ with respect to one variable all others remaining constant, have for example the form

$$\frac{\partial\tilde{F}}{\partial T} = -\tilde{S}$$

$$\frac{\partial F}{\partial V^\alpha} = -p_e$$

$$\frac{\partial\tilde{F}}{\partial\Omega} = \sigma \tag{13}$$

$$\frac{\partial\tilde{F}}{\partial\xi_\rho} = -\tilde{A}_\rho \tag{14}$$

$$\frac{\partial\tilde{F}}{\partial\xi_{x_i\gamma O}{}^\alpha} = -\tilde{A}_{x_i\gamma O}{}^\alpha \tag{15}$$

$$\frac{\partial\tilde{F}}{\partial\xi_{x_i\gamma Q}{}^\alpha} = -\tilde{A}_{x_i\gamma Q}{}^\alpha \tag{16}$$

[8] A. Sanfeld and R. Defay, *Physica*, **30**, 2232 (1964).

[9] Th. de Donder, "L'affinité," P. Van Rysselberghe, Ed., Gauthier-Villars, Paris, 1936; I. Prigogine, "Introduction to Thermodynamics of Irreversible Processes," Charles C. Thomas, Springfield, Ill., 1955; R. de Groot, "Thermodynamics of Irreversible Processes," North-Holland, Amsterdam, 1951; P. Van Rysselberghe, "Thermodynamics of Irreversible Processes," Hermann, Paris, 1962.

This description implies the assumption that the relative disposition of the phases remains uchanged.

The relative position of the phases and the magnitude of the charges (ions and electrons) that they carry determine the electric field in the system. Therefore the energy of the system, including the energy of the electric field, will for a fixed arrangement of the phases be described by T, V^α, Ω, ξ_ρ, $\xi_{x_i\gamma O}{}^\alpha$, $\xi_{x_i\gamma Q}{}^\alpha$.

Extension to Open Systems

The previous discussion leads to the conclusion that $\tilde{F}$ is a function of the variables which determine the physico-chemical state of the phases, the mode of repartition of the components among the phases and their orientation within each phase

$$\tilde{F} = \tilde{F}(T,V^\alpha,\Omega,n_\gamma{}^\alpha,\langle m_{x_i\gamma}{}^\alpha\rangle,\langle m_{x_i\gamma}{}^{\alpha 2}\rangle) \qquad (17)$$

where the symbol $n_\gamma{}^\alpha$ represents $n_{1\cdots\alpha}^{1\cdots\alpha}$, the number of moles of each component in each phase of the system. The same will be true for an open system, provided that when a charged particle is removed from the system, it is taken to infinity so that the system is never subjected to a field of force. Similarly, when a charged particle is added to the system, it must be brought from infinity.

Let us remark now that the orientation variables are *intensive.* If the system is subjected to a transformation in which all $n_\gamma{}^\alpha$, $\langle m_{x_i\gamma}{}^\alpha\rangle$, and $\langle m_{x_i\gamma}{}^{\alpha 2}\rangle$ remain constant, the free energy will vary in exactly the same way as it would in a closed system where all ξ are constant. Equation 13 can thus be written

$$\sigma = \left(\frac{\partial \tilde{F}}{\partial \Omega}\right)_{T,V^\alpha,n_\gamma{}^\alpha,\langle m_{x_i\gamma}{}^\alpha\rangle,\langle m_{x_i\gamma}{}^{\alpha 2}\rangle} \qquad (18)$$

On the other hand, if the system is subjected to a transformation in which only $\langle m_{x_i\gamma}{}^\alpha\rangle$ vary, the free energy will vary in exactly the same way as it would in a closed system where all ξ are constant except $\xi_{x_i\gamma O}{}^\alpha$.

From (7) we obtain

$$\left(\frac{\partial \tilde{F}}{\partial\langle m_{x_i\gamma}{}^\alpha\rangle}\right)_{T,V^\alpha,\Omega,n_\gamma{}^\alpha,\langle m_{x_i\gamma}{}^{\alpha 2}\rangle} = \left(\frac{\partial \tilde{F}}{\partial \xi_{x_i\gamma O}{}^\alpha}\right)_{T,V^\alpha,\Omega,\xi_\rho,\xi_{x_i\gamma Q}{}^\alpha} = -\tilde{A}_{x\gamma O}{}^\alpha \qquad (19)$$

The same conclusion is valid for $\langle m_{x_i\gamma}{}^{\alpha 2}\rangle$, and from (8) we have

$$\left(\frac{\partial \tilde{F}}{\partial\langle m_{x_i\gamma}{}^{\alpha 2}\rangle}\right)_{T,V^\alpha,\Omega,n_\gamma{}^\alpha,\langle m_{x_i\gamma}{}^\alpha\rangle} = \left(\frac{\partial \tilde{F}}{\partial \xi_{x_i\gamma Q}{}^\alpha}\right)_{T,V^\alpha,\Omega,\xi_\rho,\xi_{x_i\gamma O}{}^\alpha} = -\tilde{A}_{x_i\gamma Q}{}^\alpha \qquad (20)$$

Furthermore, we define the quantity

$$\tilde{\mu}_\gamma{}^\alpha = \left(\frac{\partial \tilde{F}}{\partial n_\gamma{}^\alpha}\right)_{T,V^\alpha,\Omega,n_{\beta\neq\gamma}^{\delta\neq\alpha},\langle m_{x_i\gamma}{}^\alpha\rangle,\langle m_{x_i\gamma}{}^{\alpha 2}\rangle} \qquad (21)$$

as the electrochemical potential of component γ in the phase α for a state where the mean orientations have given values. When these mean orientations take their equilibrium values, the electrochemical potential reduces to the classical electrochemical potential.[4]

A derivative, in which only $n_\gamma{}^\alpha$ varies, means that component γ, added to phase α, takes in this phase the preexistent orientation. From (14) and (6), we have

$$\tilde{A}_\rho = -\sum_{\alpha\gamma}\frac{\partial\tilde{F}}{\partial n_\gamma{}^\alpha}\cdot\frac{\partial n_\gamma{}^\alpha}{\partial\xi_\rho} = -\sum_{\alpha\gamma}\nu_\gamma{}^\alpha\tilde{\mu}_\gamma{}^\alpha \qquad (22)$$

Equation 10 can thus be written

$$\mathrm{d}\tilde{F} = -\tilde{S}\mathrm{d}T - \sum_\alpha p_e\mathrm{d}V^\alpha + \sigma\mathrm{d}\Omega + \sum_{\alpha\gamma}\tilde{\mu}_\gamma{}^\alpha\mathrm{d}n_\gamma{}^\alpha - \sum_{\alpha\gamma i}\tilde{A}_{x_i\gamma O}{}^\alpha\mathrm{d}\langle m_{x_i\gamma O}{}^\alpha\rangle - \sum_{\alpha\gamma i}\tilde{A}_{x_i\gamma Q}{}^\alpha\mathrm{d}\langle m_{x_i\gamma Q}{}^{\alpha 2}\rangle \qquad (23)$$

For an electrochemical system to be in equilibrium, all electrochemical affinities, all phase-transfer affinities, and all orientation affinities, which can actually take place, must be zero

$$\tilde{A}_\rho = 0;\ \tilde{A}_{x_i\gamma O} = 0;\ \tilde{A}_{x_i\gamma O} = 0$$

Plane Interphase between Two Electrically Conducting Phases

Consider two phases I and II, each one becoming homogeneous at a sufficient distance from their interface (Figure 2).

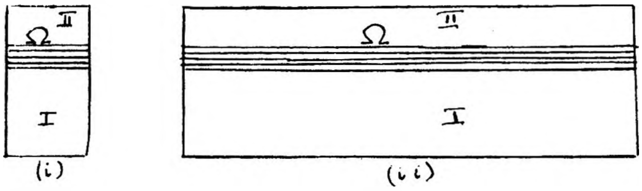

Figure 2. Two systems, on the same interface, of same height but of different interfacial areas *i* and *ii*.

If the phases are electrically conductive (ionic or electronic) and are at thermodynamical equilibrium, potentials φ^{I} and φ^{II} must be uniform in the homogeneous regions of these phases. If they were not, then charges would continue to move in the resultant field. In general, however, φ^{I} and $\varphi^{-\mathrm{I}}$ will not be equal.

The two homogeneous regions are separated by a heterogeneous region which constitutes the surface layer. We consider this layer as being made up of a number of laminae each of which can be treated as an infinitesimally thin homogeneous phase. The surface layer is in general a region in which there exists an intense electric field because in a very short distance (for example a few tenths of an angström in aqueous solutions) the value of φ changes form φ^{I} to φ^{II}. For a sufficiently large plane interface, the lines of force are normal to the surface. This is not strictly true at any instant on a molecular scale, but will be so on the average. Although the successive surface layers may have finite charges associated with them, from Gauss's theorem it is easy to see nevertheless that the interface is, as a whole, neutral.[1,2] This property is connected to the conductivity of the bulk of phases I and II (the field is zero in the bulk of these phases). If we cut out, on the same interface, two systems defined as in Figure 2, having the same height but different interfacial areas *i* and *ii;* and if area *ii* is *k* times area *i*, then the extensive variables values V^α, Ω and n_γ^α in system *ii* will be *k* times their values in system *i*.

The kinetic, structural, and chemical contributions to the free energies for the two systems will also be in the same ratio.

Furthermore, provided the dimensions of the surface are large compared with the thickness of the interfacial region, the electrostatic edge effects will be negligible.[1,2] Consequently, the electrostatic contributions from the surface will be proportional to the area.

In particular, we conclude that the function $\tilde{F}$ defined by eq 20 is a homogeneous function of the first degree in the variables V^α, Ω, n_γ^α and thus, from Euler's theorem and from eq 18 and 21

$$\tilde{F} = -\sum_\alpha p_e V^\alpha + \sigma\Omega + \sum_{\alpha\gamma} n_\gamma^\alpha \tilde{\mu}_\gamma^\alpha \tag{24}$$

where the electrochemical potentials $\tilde{\mu}_\gamma^\alpha$ depend on the orientations (see eq 21) and where the summation over α includes all bulk of both phases I and II, and all the surface layers.

By differentiating this expression and subtracting (23), we obtain

$$\mathrm{d}\sigma = -\frac{\tilde{S}\mathrm{d}T}{\Omega} + \frac{V\mathrm{d}p_e}{\Omega} - \sum_{\alpha\gamma} \frac{n_\gamma^\alpha}{\Omega}\mathrm{d}\tilde{\mu}_\gamma^\alpha - \frac{1}{\Omega}\sum_{\alpha\gamma i} \tilde{A}_{x_i\gamma O}{}^\alpha \mathrm{d}\langle m_{x_i\gamma}{}^\alpha\rangle - \frac{1}{\Omega}\sum_{\alpha\gamma i} \tilde{A}_{x_i\gamma Q}{}^\alpha \mathrm{d}\langle m_{x_i\gamma}{}^{\alpha 2}\rangle \tag{25}$$

The above proof does not assume the existence of equilibrium with respect to the distribution of components among the surface layers, but does assume mechanical and thermal equilibrium; p_e is the pressure applied externally and is equal to that in the bulk of the two homogeneous phases (*cf.* eq 4).

Equation 25 can thus be applied both to systems in equilibrium and to others, such as polarized electrodes, which are not in a true equilibrium state.

Partial Equilibrium in Systems Where Each Component May Be Present in All Surface Layers

In the case where orientation is much slower than diffusion, we can reach a partial equilibrium state and for each component γ,

$$\tilde{\mu}_\gamma^{\mathrm{I}} = \tilde{\mu}_\gamma^\alpha = \tilde{\mu}_\gamma^{\mathrm{II}} \tag{26}$$

although the orientation affinities are different from zero. The superscripts to $\tilde{\mu}_\gamma$, may then be dropped. Equation 25 reduces then to

$$\Omega\mathrm{d}\sigma = -\tilde{S}\mathrm{d}T + V\mathrm{d}p_e - \sum_\gamma n_\gamma \mathrm{d}\tilde{\mu}_\gamma - \sum_{\alpha\gamma i} \tilde{A}_{x_i\gamma O}{}^\alpha \mathrm{d}\langle m_{x_i\gamma}{}^\alpha\rangle - \sum_{\alpha\gamma i} \tilde{A}_{x_i\gamma Q}{}^\alpha \mathrm{d}\langle m_{x_i\gamma}{}^{\alpha 2}\rangle \tag{27}$$

where

$$\sum n_\gamma^\alpha = n_\gamma \tag{28}$$

This case better lends itself to the Gibbs treatment in which the interfacial layer is replaced by a geometrical division surface defining the volumes V' and V''.

In the bulk of phases I and II, each element of volume is neutral, without any electric field and in orientation equilibrium.

The potentials φ^{I} and φ^{II} must be uniform in the homogeneous regions of these phases and since the vector displacement obeys Poisson's electrostatic equation, the average net charge density must be zero in each element of volume in the homogeneous regions of phases I and II; hence

$$\sum_\gamma z_\gamma C_\gamma^{\mathrm{I}} = 0 \qquad \sum_\gamma z_\gamma C_\gamma^{\mathrm{II}} = 0 \tag{29}$$

and

$$\left.\begin{aligned} \sum_\gamma z_\gamma C_\gamma^{\mathrm{I}} F_a^{\mathrm{I}} \mathrm{d}\varphi &= 0 \\ \sum_\gamma z_\gamma C_\gamma^{\mathrm{II}} F_a \mathrm{d}\varphi &= 0 \end{aligned}\right\} \tag{30}$$

where z_γ is the elementary charge of the component γ and F_a the Faraday. We have thus the Gibbs–Duhem equation

$$\left.\begin{aligned} s_v^{\mathrm{I}}\mathrm{d}T - \mathrm{d}p_e + \sum C_\gamma^{\mathrm{I}}\mathrm{d}\tilde{\mu}_\gamma &= 0 \\ s_v^{\mathrm{II}}\mathrm{d}T - \mathrm{d}p_e + \sum C_\gamma^{\mathrm{II}}\mathrm{d}\tilde{\mu}_\gamma &= 0 \end{aligned}\right\} \tag{31}$$

These two equations are now added to (27), remembering that for the Gibbs model

$$n_\gamma = C'C_\gamma^{\mathrm{I}} + V''C_\gamma^{\mathrm{II}} + \Gamma_\gamma\Omega \tag{32}$$

$$\tilde{S} = V's_v^{\mathrm{I}} + C''s_v^{\mathrm{II}} + \Omega\hat{s}^a \tag{33}$$

while

$$V = V' + V'' \tag{34}$$

Dividing by Ω, we obtain

$$\mathrm{d}\sigma = -\tilde{s}^a\mathrm{d}T - \sum_\gamma \Gamma_\gamma \mathrm{d}\tilde{\mu}_\gamma - \frac{1}{\Omega}\sum_{\alpha\gamma i} \tilde{A}_{x_i\gamma O}{}^\alpha \mathrm{d}\langle m_{x_i\gamma}{}^\alpha\rangle - \frac{1}{\Omega}\sum_{\alpha\gamma i} \tilde{A}_{x_i\gamma Q}{}^\alpha \mathrm{d}\langle m_{x_i\gamma}{}^{\alpha 2}\rangle \tag{35}$$

This is an extension of the Gibbs equation to electrochemical systems where orientation reaches the equilibrium after a long time after the diffusion equilibrium.

At the true equilibrium (diffusion and orientation), $\tilde{A}_{x_i\gamma O}{}^{\alpha} = 0$ and $\tilde{A}_{x_i\gamma Q}{}^{\alpha} = 0$, and (35) reduces to the classical equation[1,2]

$$d\sigma = -\bar{s}^a dT - \sum_{\gamma} \Gamma_{\gamma} d\tilde{\mu}_{\gamma} \tag{36}$$

If the system is uncharged, the electrochemical functions ($\tilde{\mu}_{\gamma}$, $\tilde{A}_{x_i\gamma O}{}^{\alpha}$, $\tilde{A}_{x_i\gamma Q}{}^{\alpha}$) reduce to the corresponding chemical functions ($\bar{\mu}_{\gamma}$, $A_{x_i\gamma O}{}^{\alpha}$, $A_{x_i\gamma Q}{}^{\alpha}$) and, at uniform temperature, we have

$$d\sigma = -\sum_{\gamma} \Gamma_{\gamma} d\mu_{\gamma} - \frac{1}{\Omega} \sum_{\alpha\gamma i} \tilde{A}_{x_i\gamma O}{}^{\alpha} d\langle m_{x_i\gamma}{}^{\alpha}\rangle - \frac{1}{\Omega} \sum_{\alpha\gamma i} \tilde{A}_{x_i\gamma Q}{}^{\alpha} d\langle m_{x_i\gamma}{}^{\alpha 2}\rangle \tag{37}$$

Let us now suppose that we maintain a constant temperature, pressure, and composition of the bulk phase, *i.e.*, $d\tilde{\mu}_{\gamma} = 0$. The evolution of the surface from a state of partial equilibrium (*i.e.*, from a state where the orientation is not in equilibrium) would be given with the aid of (35)

$$d\sigma = -\frac{1}{\Omega} \sum_{\alpha\gamma i} \tilde{A}_{x_i\gamma O}{}^{\alpha} d\langle m_{x_i\gamma}{}^{\alpha}\rangle - \frac{1}{\Omega} \sum_{\alpha\gamma i} \tilde{A}_{x_i\gamma Q}{}^{\alpha} d\langle m_{x_i\gamma}{}^{\alpha 2}\rangle \tag{38}$$

This formula implies that each $\tilde{\mu}_{\gamma}$ is constant during the transformation, *i.e.*, that diffusion occurs quickly enough to ensure continually the equality (26), by balancing the influence of the change in orientation on the local $\tilde{\mu}_{\gamma}$.

For uncharged components, we obtain

$$d\sigma = -\frac{1}{\Omega} \sum_{\alpha\gamma i} \tilde{A}_{x_i\gamma O}{}^{\alpha} d\langle m_{x_i\gamma}{}^{\alpha}\rangle - \frac{1}{\Omega} \sum_{\alpha\gamma i} \tilde{A}_{x_i\gamma Q}{}^{\alpha} d\langle m_{x_i\gamma}{}^{\alpha 2}\rangle \tag{39}$$

Examples

We consider a system in a real equilibrium state. A short-impulse, transitory field is applied so as to avoid diffusion (in the bulk phase the temperature, the pressure, and the composition are constant and we suppose all the $\tilde{\mu}_{\gamma}$ uniform in the medium). Nevertheless, this field is able to turn over the molecules' orientation in certain laminae. When the field cancels out, the system returns to equilibrium in agreement with (38).

We could also consider the return to equilibrium after a perturbation due to friction or a motion laying down the molecules. This case may be related to the viscosity flow of monomolecular solutions.[10] The return to equilibrium follows eq 38 or 39.

On the other hand, Defay and Roba-Thilly,[11] Defay and Hommelen,[11] and Pétré and Debelle[12] show that the rate of adsorption of sebacic acid, azelaic acid, and diols at the air–aqueous solution interface is not only diffusion controlled. A barrier of potential energy between the substrate and the surface phase, related to the orientation of the adsorbed molecule, has to be taken into account in the evolution rate to the equilibrium state.

Now we suppose that only one component of the upper lamina orientates itself at the interface. Equation 38 may be then rewritten

$$d\sigma = -\left[\sum_{i} \tilde{A}_{x_iO}{}^{*} d\langle m_{x_i}\rangle + \sum_{i} \tilde{A}_{x_iQ}{}^{*} d\langle m_{x_i}{}^{2}\rangle\right] \tag{40}$$

where

$$\tilde{A}_{x_iO}{}^{*} = \frac{\tilde{A}_{x_iO}}{\Omega} \quad \text{and} \quad \tilde{A}_{x_iQ}{}^{*} = \frac{\tilde{A}_{x_iQ}}{\Omega}$$

Let us suppose that initially (out of equilibrium) one-half of the undeformable or rigid dipoles are directed vertically upwards and the other half vertically downwards, while at equilibrium all dipoles turn vertically downwards. If axis x_1 is perpendicular to the surface of the layer, the rigid moments $\langle m_{x_1}\rangle$ and $\langle m_{x_1}{}^2\rangle$ may be written as $m\langle\cos\beta_1\rangle$ and $m^2\langle\cos^2\beta_1\rangle$, where m is the arithmetic value of the dipole moment.

Furthermore, let us suppose that $\tilde{A}_Q$ varies only slowly with $\langle m\rangle$ in such a way that contribution of the second integral $\int_1^1 \tilde{A}_Q{}^{*} d\langle m^2\rangle$ can be neglected.

Integrating (40) from $\langle\cos\beta_1\rangle = 0$ to $\langle\cos\beta_1\rangle = -1$ and $\langle\cos^2\beta_1\rangle = 1$ to $\langle\cos^2\beta_1\rangle = 1$, one has then

$$\langle\tilde{A}_0{}^{*}\rangle = \frac{\Delta\sigma}{m} \tag{41}$$

where $\langle\tilde{A}_0{}^{*}\rangle$ is the mean value of the surface orientation affinity in the integration and $\Delta\sigma$ the variation of the surface or interfacial tension due to the change of orientation.

If by way of a perturbation, all the rigid dipoles are initially directed vertically upwards and if, while equilibrium takes place they turn downwards, then after integration eq 40 becomes

$$\langle\tilde{A}_0{}^{*}\rangle = \frac{\Delta\sigma}{2m} \tag{42}$$

A measure of the surface or interfacial tension for the two extreme positions of the orientation can give us a value of the mean affinity of orientation, as long as the dipoles are rigid and their moments are known.

Remark a. If we assume that only one of variables $\xi_{x_i\gamma}{}^{\alpha}$ varies, all others being kept constant in eq 10, and that moreover $\langle m_{x_1}\rangle$ varies from 0 to $-\langle m_{x_1}\rangle$ ($\langle\cos\beta\rangle$ varies from 0 to -1), there comes

---

[10] M. Joly, III Internationale Vortragstagung über grenzflächenaktive Stoffe, Mar 1966, Berlin.

[11] R. Defay and J. Roba-Thilly, *J. Colloid Sci., Suppl.*, 1, 48 (1954); R. Defay and J. R. Hommelen, *ibid.*, 13, 553 (1958); *ibid.*, 14, 401 (1959).

[12] G. Pétré and P. Debelle, Vth International Congress on Surface Activity, Barcelona, Sept 1968.

$$\Delta\tilde{F} = \int_0^{m_{x1}} \tilde{A}_{x10}\mathrm{d}\langle m_{x1}\rangle = \langle \tilde{A}_{x10}\rangle\langle m_{x1}\rangle = \Omega\langle \tilde{A}^*\rangle\langle m_{x1}\rangle \qquad (43)$$

Putting (43) in (41), we get

$$\langle \Delta\tilde{F}\rangle = \Omega\Delta\sigma \qquad (44)$$

Remark b. It is easy to compare now the mean affinity $\langle \tilde{A}_0^*\rangle/\Gamma$ with $RT/\langle m\rangle$, where Γ is the number of moles per cm². At 15°, $RT \simeq 2.3 \times 10^{10}$ erg/mol. Let us choose, for example, a binary liquid whose surface is covered by 10^{-10} mol/cm² (6×10^{-3} molecule/Å²) of the surfactants. We suppose now that if one-half of the surface molecules of the surfactant are turning, the experimental value of $\Delta\sigma$ is 5 dyn/cm. The variation of the mean affinity per mole being only due to the surfactant in the upper lamina (we exclude the orientation variation of the other component), it is easy to see, from eq 47 that $\langle \tilde{A}^*\rangle/\Gamma$ is of the order of magnitude of $2.2RT/\langle m\rangle$.

Ideal Polarized Electrode

For some metal solution interfaces, the surface can be regarded as consisting of two parts, only one of which is accessible to the constituents of the solution.

As an example, we consider mercury in contact with an aqueous solution (ideal polarized electrode). The thermodynamical properties of an ideal polarized electrode may be discussed conveniently by dividing the surface layer into two parts which we imagine to be separated by a surface impermeable to all components of the system as indicated below.[13] Here the plane B separates the surface layer of the mercury (AB) from the surface layer of the solution (BC). The fundamentally important feature of an ideal polarized electrode is that its potential drop $\varphi^{\mathrm{I}} - \varphi^{\mathrm{II}}$ can be notified without changing the concentration of the bulk of the phase.

We denote by h the components which can exist in mercury and in its surface layer (that is Hg, Hg$^+$, and e$^-$, together with any other metals dissolved in the mercury and their ions) and by l the components of the solution and its surface layer. The index θ is used to denote surface layers in the bulk mercury and its surface, while β denotes those associated with the solution of the bulk and surface. If there is a partial equilibrium between each phase bulk and the corresponding surface layer in such a way that:

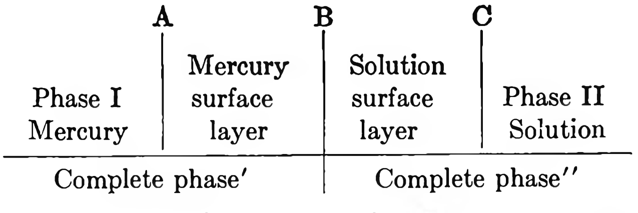

$$\tilde{\mu}_{\mathrm{h}}^{\theta} = \tilde{\mu}_{\mathrm{h}}^{\mathrm{I}}, \qquad \tilde{\mu}_{\mathrm{l}}^{\beta} = \tilde{\mu}_{\mathrm{l}}^{\mathrm{II}} \qquad (45)$$

and (25) may be written in the form

$$\begin{aligned}\mathrm{d}\sigma = &- \frac{\tilde{S}}{\Omega}\mathrm{d}T + \frac{V}{\Omega}\mathrm{d}p - \sum_{\theta\mathrm{h}} \frac{n_{\mathrm{h}}^{\theta}}{\Omega}\mathrm{d}\tilde{\mu}_{\mathrm{h}}^{\mathrm{I}} - \sum_{\beta\mathrm{l}} \frac{n_{\mathrm{l}}^{\beta}}{\Omega}\mathrm{d}\tilde{\mu}_{\mathrm{l}}^{\mathrm{II}} \\ &- \frac{1}{\Omega}\sum_{\theta\mathrm{h}_i} \tilde{A}_{x_i\mathrm{h}O}{}^{\theta}\mathrm{d}\langle m_{x_i\mathrm{h}}{}^{\theta}\rangle - \frac{1}{\Omega}\sum_{\beta\mathrm{l}_i} \tilde{A}_{x_i\mathrm{l}O}{}^{\beta}\mathrm{d}\langle m_{x_i\mathrm{l}}{}^{\beta}\rangle \\ &- \frac{1}{\Omega}\sum_{\theta\mathrm{h}_i} \tilde{A}_{x_i\mathrm{h}Q}{}^{\theta}\mathrm{d}\langle m_{x_i\mathrm{h}}{}^{\theta 2}\rangle - \frac{1}{\Omega}\sum_{\beta\mathrm{l}_i} \tilde{A}_{x_i\mathrm{l}Q}{}^{\beta}\mathrm{d}\langle m_{x_i\mathrm{l}}{}^{\beta 2}\rangle\end{aligned} \qquad (46)$$

We choose plane B as the Gibbs dividing surface, so that

$$\left.\begin{aligned}\Gamma_{\mathrm{h}} &= \frac{n_{\mathrm{h}}^{a}}{\Omega} = \frac{1}{\Omega}\left\{\sum_{\theta} n_{\mathrm{h}}^{\theta} - C_{\mathrm{h}}^{\mathrm{I}}V'\right\} \\ \Gamma_{\mathrm{l}} &= \frac{n_{\mathrm{l}}^{a}}{\Omega} = \frac{1}{\Omega}\left\{\sum_{\beta} n_{\mathrm{l}}^{\beta} - C_{\mathrm{l}}^{\mathrm{II}}V''\right\} \\ \bar{s}^{a} &= \frac{\tilde{S}^{a}}{\Omega} = \frac{1}{\Omega}\{\tilde{S} - s_v^{\mathrm{I}}V' - s_v^{\mathrm{II}}V''\}\end{aligned}\right\} \qquad (47)$$

where, as before, s_v^{I} and s_v^{II} refer to entropies per unit volume in the bulk of the phases and $\bar{s}^{a}$ is the surface entropy per unit area.

Applying the Gibbs–Duhem equation to the bulk phases which are neutral and are not subjected to an electric field, one has, combining (46), (47), and the expression of $\tilde{\mu}_{\gamma}$

$$\tilde{\mu}_{\gamma} = \mu_{\gamma} + z_{\gamma}F_a\varphi \qquad (48)$$

where φ is the Galvani potential

$$\begin{aligned}\mathrm{d}\sigma = &-\bar{s}^{a}\mathrm{d}T - \sum_{\mathrm{h}} \Gamma_{\mathrm{h}}\mathrm{d}\mu_{\mathrm{h}}^{\mathrm{I}} - \sum_{\mathrm{l}} \Gamma_{\mathrm{l}}\mathrm{dh}_{\mathrm{l}}^{\mathrm{II}} - \\ &q_M\mathrm{d}(\varphi^{\mathrm{I}} - \varphi^{\mathrm{II}}) - \frac{1}{\Omega}\sum_{\theta\mathrm{h}_i} \tilde{A}_{x_i\mathrm{h}O}{}^{\theta}\mathrm{d}\langle m_{x_i\mathrm{h}}{}^{\theta}\rangle - \\ &\frac{1}{\Omega}\sum_{\beta\mathrm{l}_i} \tilde{A}_{x_i\mathrm{l}O}{}^{\beta}\mathrm{d}\langle m_{x_i\mathrm{l}}{}^{\beta}\rangle - \frac{1}{\Omega}\sum_{\theta\mathrm{h}_i} \tilde{A}_{x_i\mathrm{h}Q}{}^{\theta}\mathrm{d}\langle m_{x_i\mathrm{h}}{}^{\theta 2}\rangle - \\ &\frac{1}{\Omega}\sum_{\beta\mathrm{l}_i} \tilde{A}_{x_i\mathrm{l}Q}{}^{\beta}\mathrm{d}\langle m_{x_i\mathrm{l}}{}^{\beta 2}\rangle\end{aligned} \qquad (49)$$

where q_M is the charge per unit surface area of the metal surface layer.

Because of the over-all neutrality of the system, q_M is equal but of opposite sign to the charge of the solution surface layer and is given by

$$q_M = \sum_{\mathrm{h}} \Gamma_{\mathrm{h}}z_{\mathrm{h}}F_a = -\sum_{\mathrm{l}} \Gamma_{\mathrm{l}}z_{\mathrm{l}}F_a \qquad (50)$$

At the real equilibrium, all the orientations affinities are zero and (49) reduces to the classical electrocapillary equation. Particularly, for equilibrium displacements keeping the temperature and the composition of the bulk phases constant, we find again the Lippmann equation

---

(13) D. C. Grahame, *Chem. Rev.*, **41**, 441 (1947); F. G. Koenig, *J. Phys. Chem.*, **38**, 339 (1934).

$$\mathrm{d}\sigma = -q_M\,\mathrm{d}(\varphi^{\mathrm{I}} - \varphi^{\mathrm{II}}) \qquad (51)$$

If, in the case of a partial equilibrium (45), without orientation equilibrium, $\varphi^{\mathrm{I}} - \varphi^{\mathrm{II}}$ can be varied without changing the temperature, the composition of bulk phases and the orientations in the layers (49) reduces also to Lippmann eq 51. Nevertheless, q_M has not necessarily the same value in both cases. If the composition of the bulk remains constant but not the orientation in the layers, then at constant temperature eq 49 reduces to

$$\mathrm{d}\sigma = -q_M\mathrm{d}(\varphi^{\mathrm{I}} - \varphi^{\mathrm{II}}) - \frac{1}{\Omega}\sum_{\theta\mathrm{h}i} \tilde{A}_{x_i\mathrm{h}O}{}^{\theta}\mathrm{d}\langle m_{x_i\mathrm{h}}{}^{\theta}\rangle - \frac{1}{\Omega}\sum_{\beta\mathrm{l}i} \tilde{A}_{x_i\mathrm{l}O}{}^{\beta}\mathrm{d}\langle m_{x_i\mathrm{l}}{}^{\beta}\rangle - \frac{1}{\Omega}\sum_{\theta\mathrm{h}i} \tilde{A}_{x_i\mathrm{h}Q}{}^{\theta}\mathrm{d}\langle m_{x_i\mathrm{h}}{}^{\theta 2}\rangle - \frac{1}{\Omega}\sum_{\beta\mathrm{l}i} \tilde{A}_{x_i\mathrm{l}Q}{}^{\beta}\mathrm{d}\langle m_{x_i\mathrm{l}}{}^{\beta 2}\rangle \qquad (52)$$

Let us suppose now that only the orientation affinity $\tilde{A}_{x\mathrm{l}O}{}^{\beta}$ of one constituent 1 in one interfacial lamina layer β is different from zero. We denote this affinity by symbol A_0 and the mean dipole moment by $\langle m\rangle$. From (52), we get

$$\mathrm{d}\sigma = -q_M\mathrm{d}(\varphi^{\mathrm{I}} - \varphi^{\mathrm{II}}) - \tilde{A}_0{}^*\mathrm{d}\langle m\rangle \qquad (53)$$

In the neighborhood of orientation equilibrium, let us adopt the classical hypothesis that the orientation affinity is proportional to the orientation rate. Equation 53 now reads

$$\frac{\mathrm{d}\sigma}{\mathrm{d}t} = -q_M\frac{\mathrm{d}}{\mathrm{d}t}(\varphi^{\mathrm{I}} - \varphi^{\mathrm{II}}) - R_0\left(\frac{\mathrm{d}\langle m\rangle}{\mathrm{d}t}\right)^2 \qquad (54)$$

where R_0 is the "resistance" coefficient. Experimentally, it is possible to keep constant in time an arbitrary value of the imposed tension $(\varphi^{\mathrm{I}} - \varphi^{\mathrm{II}})$. If the orientation is slow, we could watch the time evolution of σ towards its value in the orientation equilibrium state.

The evolution in time of function $\sqrt{R_0}\mathrm{d}\langle m\rangle/\mathrm{d}t$ being thus known the variation with time of the orientation rate $v_0 = \mathrm{d}\langle m\rangle/\mathrm{d}t$ is indicated.

Integral $\int\sqrt{R_0}(\mathrm{d}\langle m\rangle/\mathrm{d}t)\mathrm{d}t$ is thus computable between two limits, and we could, for instance, plot function $\langle\sqrt{R_0}\rangle(\langle \mathrm{m}\rangle_{\mathrm{eq}} - \langle m\rangle_{t_0})$ for each value of the imposed tension $(\varphi^{\mathrm{I}} - \varphi^{\mathrm{II}})$ [$\langle m\rangle_{\mathrm{eq}}$ is the value of the moment at orientation equilibrium,[14-17] $\langle m\rangle_{t_0}$ its value at the initial time].

However, such a conclusion is only possible when the orientation rate is much slower than the transfer rates, in such a way that after an evolution due to the diffusion and to the transfer, the system reaches a state of partial equilibrium which is then controlled by the orientation rate. The question now is what is the meaning of a single orientation affinity?

In a state of three-dimensional space, we consider a random orientation; the related variables of a single component in the considered laminae have then the following values (taking the z axis perpendicular to the surface and $|m| = 1$)

$$\langle m_x\rangle = 0,\ \langle m_y\rangle = 0,\ \langle m_z\rangle = 0,\ \langle m_x{}^2\rangle = a_m,\ \langle m_y{}^2\rangle = a_m,\ \langle m_z{}^2\rangle = a_m \qquad (55)$$

where a_m is a positive mean value lying between 0 and 1.

When all the molecules will have orientated perpendicularly to the surface in the direction $(-z)$, we will have

$$\langle m_x\rangle = 0,\ \langle m_y\rangle = 0,\ \langle m_z\rangle = -1,\ \langle m_x{}^2\rangle = 0,\ \langle m_y{}^2\rangle = 0,\ \langle m_z{}^2\rangle = 1 \qquad (56)$$

Variables $\langle m_x\rangle$ and $\langle m_y\rangle$ have remained equal to zero, but the four others have changed.

Rigorously, in (53) terms related to the evolution of the three mean quadratic moments should have been added.

As these mean quadratic moments are invariable under a complete rotation of 180° of all the molecules it is expected that, in this case, they will not play an important role in an evolution towards a determined direction and so we can neglect them in (53).

However, these mean quadratic moments may not be neglected in other phenomena as when a chain molecule, having two identical chemical ends, has a tendency to lie flat on the surface. One then goes from a three-dimensional disorder to a two-dimensional one which state is characterized by

$$\langle m_x\rangle = 0,\ \langle m_y\rangle = 0,\ \langle m_z\rangle = 0,\ \langle m_x{}^2\rangle = a_m{}',\ \langle m_y{}^2\rangle = a_m{}',\ \langle m_z{}^2\rangle = 0 \qquad (57)$$

By comparing (55) and (57), one sees that this phenomenon depends essentially on the evolution of $\langle m^2{}_z\rangle$. Here the $\tilde{A}_{x_iO}$ affinities can be neglected. The approximation thus depends on the special studied cases.

Electrocapillary Maximums in the Case of Partial Equilibrium[18]

Let us now consider the case of slow orientation and keeping the approximation leading to (53).

By following the evolution from partial equilibrium to complete equilibrium, keeping the temperature and the compositions of the bulk phase constant, it could be possible, for each constant value of $\varphi^{\mathrm{I}} - \varphi^{\mathrm{II}}$, to build the curve $\sigma(t)$ where t represents the age of the surface. By taking all the σ values corresponding to a same t

---

(14) C. J. F. Böttcher, "Theory of Electric Polarization," Elsevier, Amsterdam, 1952.

(15) J. Barriol, "Les Moments Dipolaires," Gauthier-Villars, Paris, 1957.

(16) H. Fröhlich, "Theory of Dielectrics," Clarendon Press, Oxford, 1959.

(17) M. Mandel, *Bull. Soc. Chim. Fr.*, **7**, 1018 (1955).

(18) A. Sanfeld, A. Steinchen, and R. Defay, Vth International Congress on Surface Activity, Barcelona, Sept 1968.

value, one can build a $\sigma(\varphi^{\mathrm{I}} - \varphi^{\mathrm{II}})$ curve at constant t. It will be *the electrocapillary curve of a given age surface.* The last of these curves, *i.e.*, corresponding to $t = \infty$ *is the equilibrium electrocapillary curve.*

It is probable that, at least for states neighboring complete equilibrium, the curves correspond to a given age, will also have an electrocapillary maximum of the same age.

In order to analyze these curves, one could suppose as a first approximation that the surfaces having the same age have the same orientation. The curves of a given age will then be curves at constant $\langle m\rangle$ and following (53), their slope

$$\frac{\mathrm{d}\sigma}{\mathrm{d}(\varphi^{\mathrm{I}} - \varphi^{\mathrm{II}})} = -q_M \tag{58}$$

will give the charge per unit area of the metal surface layer at the considered time. By studying all these curves, one could then study the evolution of the charge *vs.* time.

If the surfaces of same age are in the same orientation state, the charge will be zero at each electrocapillary maximum.

One could then also compare the points of zero charge corresponding to the maximum of the various curves. On a line joining the maximum, one will have

$$\mathrm{d}\sigma_{\max} = \left(\frac{\partial\sigma}{\partial\langle m\rangle}\right)_{\varphi^{\mathrm{I}}-\varphi^{\mathrm{II}}} \mathrm{d}\langle m\rangle + \frac{\partial\sigma}{\partial(\varphi^{\mathrm{I}} - \varphi^{\mathrm{II}})_{\langle m\rangle}} \frac{\mathrm{d}(\varphi^{\mathrm{I}} - \varphi^{\mathrm{II}})}{d\langle m\rangle} \mathrm{d}\langle m\rangle \tag{59}$$

where the second term is zero. Thus, at each point of this extreme curve

$$\frac{\mathrm{d}\sigma_{\max}}{\mathrm{d}\langle m\rangle} = \left(\frac{\partial\sigma}{\partial\langle m\rangle}\right)_{\varphi^{\mathrm{I}}-\varphi^{\mathrm{II}}} = -\tilde{A}_0^* \tag{60}$$

Remarks

(*a*). Following the classical hypothesis, $\mathrm{d}\langle m\rangle/\mathrm{d}t$ is proportional to the orientation affinity $\tilde{A}_0^*$; eq 53 may be rewritten

$$\frac{\mathrm{d}\sigma}{\mathrm{d}t} = -q_M \frac{\mathrm{d}(\varphi^{\mathrm{I}} - \varphi^{\mathrm{II}})}{\mathrm{d}t} - \tilde{L}_0\tilde{A}_0^{*2} \tag{61}$$

where L_0 is the "straight" phenomenological coefficient. The knowledge of the instantaneous values of $\varphi^{\mathrm{I}} - \varphi^{\mathrm{II}}$ permits us to calculate the time variation of the orientation affinity. Equation 60 also becomes

$$\frac{\mathrm{d}\sigma_{\max}}{\mathrm{d}\langle m\rangle} = \left(\frac{\partial\sigma}{\partial\langle m\rangle}\right)_{\varphi^{\mathrm{I}}-\varphi^{\mathrm{II}}} = -R_0v_0 \tag{62}$$

(*b*). If there is a coupling between the various orientations, one should introduce interference coefficients.

(*c*). A more careful analysis of the influence of orientation on the electrochemical potential would perhaps separate the terms related to pure orientation and to pure diffusion. The orientation in an external field could then be studied with the aid of the relaxation polarization effect.[19]

(*d*). From the experimental point of view, the influence of orientation in the mercury electrode process has been developed by Volke[20] and by Smolders.[21]

Acknowledgment. The work was performed under the auspices of the Fonds de La Recherche Fondamentale Collective.

(19) S. R. de Groot and P. Mazur, "Non-equilibrium Thermodynamics," North-Holland, Amsterdam, 1962, p 349.

(20) J. Volke, *Chem. Listy*, 62, 497 (1968).

(21) C. A. Smolders, Thesis, Utrecht, 1961, pp 41–45.

Homogeneous Gas-Phase Thermolysis Kinetics. An Improved Flow Technique for Direct Study of Rate Processes in the Gas Phase

by Harold Kwart, Stanley F. Sarner, and Jon H. Olson

Departments of Chemistry and Chemical Engineering, University of Delaware, Newark, Delaware 19711

(Received February 13, 1969)

The operational parameters of an improved flow method for direct determination of the kinetics of gas-phase thermolysis reactions have been evaluated. A scheme has been devised for rapidly estimating the rates of first-order decompositions in a single series of simple measurements at an established reactor temperature. The activation parameters for decomposition of ethyl acetate and dicyclopentadiene have been determined in this fashion and compared with the corresponding values reported by earlier authors applying a variety of kinetic techniques. The use of a gold-surfaced reactor and a highly diluted reaction medium has simplified (or eliminated) the problem of residual wall reaction.

Introduction

The application of flow methods to the study of the kinetics of homogeneous gas-phase reactions is highly advantageous since a time-invariant concentration gradient is generated.[1-4]

The reactor described herein is a flow reactor in which many difficulties present in other designs have been eliminated. On entering the system the reactant is immediately diluted with a large volume of helium, thus precluding intermolecular reactions, simplifying the analysis to considerations of unimolecular mechanisms, and rendering the effects of volume changes during reaction (due to changes in the number of moles) negligible. The design results in laminar flow with a low degree of axial diffusion in the reactor, thereby simplifying the kinetics to the case of the static reactor model under normal operating conditions.

The reactor system is equipped with a preliminary gas chromatograph, so that samples may be purified and directly transferred to the reactor, and a second gas chromatograph providing for automatic analysis of the reaction products. The helium flows in the three sections of the system (GC1, reactor, and GC2) are separate, allowing each gas chromatograph to be operated under optimum conditions for analysis while providing for maximum variability of reactor residence time.

The elements of the design of this reactor system and its application to kinetic measurements are discussed below. Data obtained for the thermolysis of ethyl acetate and dicyclopentadiene are also presented and compared to those in the literature obtained by other methods.

Apparatus and Operation

The reactor system is similar to the model described by Levy.[5] The basic block diagram is shown in Figure 1, and the flow diagram of the reactor module is shown in Figure 2. In a typical experiment a sample is injected into GC1 and a normal chromatogram is obtained using a nondestructive thermal conductivity detector. The 4-port 2-position selector valve (A) in the position shown simply vents the output of GC1. Upon rotation of this valve 90° clockwise, the sample plus helium from GC1 is directed into the reactor module. The valve is then returned to its original position, and the regulated helium flow of the reactor module assumes control of the sample. Alternatively, a sample can be directly injected into a port in line with the reactor helium flow, and this will be directed into the reactor without rotating the valve. The sample is moved through the delay coil (D) into port 1 of the 4-port 2-position bypass valve (B), out of port 2 into the reactor coil, and then back through the bypass valve (ports 4 and 3) to the indicator thermal conductivity cell. If the bypass valve is rotated 90°, the reactor coil is bypassed for system checking or calibration of GC2. From the indicator cell, the sample is directed into port 4 of the transfer valve (C), out of port 5, and through the transfer coil (E) back through ports 2 and 3 of the transfer valve to the other side of the indicating cell, and then vented. This latter path through the indicating cell can be eliminated if desired since the path volume after the first indication is known and the transfer time can be determined from the volume flow rate. With two indications, the determination of the time at which the

---

(1) W. D. Walters in "Technique of Organic Chemistry," Vol. 8, Interscience Publishers, New York, N. Y., 1953, p 231.

(2) A. Maccoll in "Technique of Organic Chemistry," Vol. 8, Interscience Publishers, New York, N. Y., 1953, p 427.

(3) H. B. Young and L. P. Hammet, *J. Amer. Chem. Soc.*, **72**, 280 (1950); J. Suldick and L. P. Hammet, *ibid.*, **72**, 283 (1950); L. B. Rand and L. P. Hammet, *ibid.*, **72**, 287 (1950).

(4) J. DeGraaf and H. Kwart, *J. Phys. Chem.*, **67**, 1458 (1963); J. DeGraaf, Thesis, Leiden, Netherlands, 1961.

(5) E. J. Levy and D. G. Paul, *J. Gas Chromatogr.*, **5**, 136 (1967).

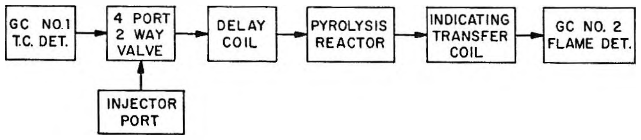

Figure 1.

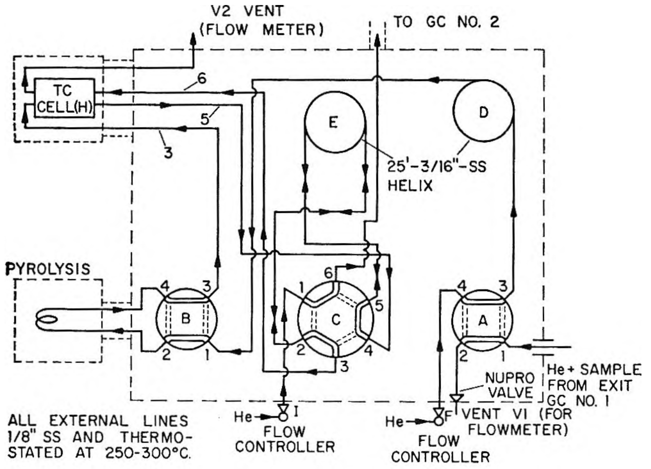

ALL EXTERNAL LINES 1/8" SS AND THERMOSTATED AT 250-300°C.

Figure 2.

sample (now reacted) is in the center of the transfer coil is simplified as shown in Figure 3.

For succeeding runs under the same conditions, the same procedure is followed until the predetermined time (from Figure 3) at which the reaction products are in the center of the transfer coil. At this time, the transfer valve (C) is rotated 60° so that the GC2 helium flow back flushes the sample in the transfer coil into GC2 for analysis. At the same time, the reactor flow is directed to the indicating cell, and the lack of any further display (Figure 3b) shows that no portion of the sample has failed to be transmitted to the GC2.

The operation of chromatographs GC1 and GC2 is no different than normal, except that the output from port 6 of the transfer valve is fitted to the injection port of GC2 for automatic transfer rather than requiring sample collection and subsequent injection. The inclusion of the transfer coil and valve allows each of the three flows in the system (GC1, reactor, and GC2) to be entirely independent, so that each chromatographic flow can be optimized for the required separations and so that the reactor flow can be varied to obtain a variety of reaction conditions. In one of the systems used in this investigation, GC1 is a programmed temperature gas chromatograph (Hewlett-Packard Model 700 series with Model 240 temperature programmer), equipped with a nondestructive dual thermal conductivity detector, and GC2 is a programmed temperature gas chromatograph (Hewlett-Packard Model 5750) with a dual flame ionization detector for increased sensitivity. In two other systems, no GC1 is employed, and GC2 uses a thermal conductivity detector.

The reactors consist of gold coils helically wound on stainless steel cores 1.75 in. in diameter and extending past the ends of the helices so that all gradients are beyond the reactor coils. In two systems, the coils have inside diameters of 0.0937 in. and lengths of 36 and 32.5 in., resulting in volumes of 4.07 and 3.67 ml, respectively. The third reactor coil in use has a 0.221 in. i.d. and is 33.25 in. long, giving a volume of 20.90 ml. They are heated by means of cartridge heaters and regulated by temperature controllers (Hewlett-Packward Model 220 or equivalent) and can accurately maintain desired reaction temperatures up to 675°.

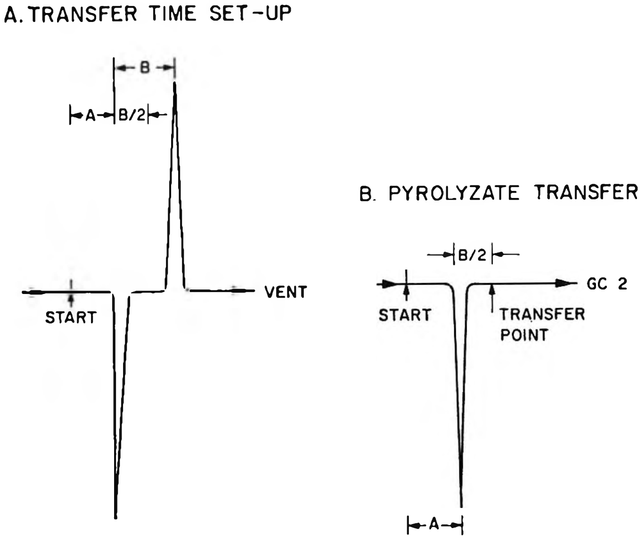

Figure 3.

The delay and transfer coils are $^3/_{16}$-in. o.d. stainless steel, with the latter being 25 ft in length; all internal connecting lines are 0.125-in. i.d. stainless steel tubing; the valves have glass-filled Teflon seats; the external connections and the reactor module are thermostated at a suitable temperature between the condensation and reaction temperatures. The delay coil must be sufficiently long to contain a complete peak so that the selector valve (A) may be turned to allow control of the flow by the reactor flow prior to entry to the reactor.

A modification has been made in one of the systems presently in use to split the reactor flow after the first indication to direct half the flow through another valve for a detailed thermal conductivity detected analysis on a second column in addition to the main analysis on GC2. This section provides added information on smaller molecules such as CH_4, CO, CO_2, H_2O, NH_3, HCl, HBr, C_2H_4, C_2H_6, and C_3H_6, for which results under CG2 conditions optimized for larger molecule analyses may not be definitive. This reaction was not required in this work except to determine that no "small molecule" other than C_2H_4 was present and will not be described here.

Recently, Levy and Paul[5] described a model of this reactor system from which the present equipment is an outgrowth. Their results, in experiments using the reactor in free-radical pyrolytic cracking of hydrocarbons and long-chain molecules with functional group terminations, showed that the thermolytic dissociation patterns were independent of sample size, reproducible under standardized conditions, correlatable with the molecular structure of the reactant, and agreed with the results predicted by the modified Rice free-radical mechanism theory.[6] Thus, it was anticipated that this experimental approach would be applicable to homogeneous gas-phase kinetic reactions.

Data Acquisition

Basically, only three parameters are required to characterize the reaction kinetics, *i.e.*, the contact time, the reaction temperature, and the extent of reaction. The first is easily obtained from the known reactor volume and the volume flow rate. This latter is measured under ambient conditions using a soap film meter and vents provided in the apparatus for such measurement. The reactor temperature is measured *via* a chromel–alumel thermocouple and a potentiometer. These are combined to give the residence time as

$$\tau = \frac{V}{F} \cdot \frac{T_m}{T_r} \cdot \frac{P_r}{P_m} \tag{1}$$

where V is the reactor volume, F is the volume flow rate measured by the soap film meter, T is temperature, P is pressure, and the subscripts m and r refer to the soap film meter and reactor measurements, respectively. For this work, the ratio P_r/P_m was taken as unity, since both the reactor and the soap film meter were at ambient pressure.

The extent of the reaction is determined either by an internal standard technique or by reference to the total integral. In the first case, accurate mixtures of the reactant and an unreactive standard are made and diluted with an unreactive solvent until the chromatographic response to variation in concentration ratios of reactant to standard is linear over the desired range. Comparison of the reactant to standard ratio between bypass and thermolysis conditions on the same sample then gives the ratio of reactant concentrations before and after thermolysis under the experimental conditions. In the second method, where pure substrate only is transferred from GCl, the total product integral can be taken equal to the unreacted substrate, and the same ratio can be determined.

Analysis of the operating conditions of the reactors as given below has established that the systems are essentially static reactors. Thus, at any temperature, the specific reaction rate constant, k, is given by

$$k = \frac{-\ln (C/C_0)}{\tau} \tag{2}$$

where C_0 and C are the initial and final substrate concentrations, respectively, and τ is the residence time. It should be noted that C/C_0 will be determined chromatographically and is subject to errors of the order of 3%. Inspection of the relationship of C/C_0 *vs.* $-\ln (C/C_0)$ will show that at small values of C/C_0 the determination of the rate constant is subject to the largest errors from this source. Similarly, since the Arrhenius relationship will ultimately be used, and $\ln k$ involved, inspection of the relationship of C/C_0 *vs.* $\ln(-\ln(C/C_0))$ will show that errors in $\ln k$ become largest at both small and large values of C/C_0. Thus, it is recommended that for accurate determinations, C/C_0 should preferably be near 0.5, and within limits of 0.2 to 0.8. This can readily be accomplished by means of the variable reaction conditions: the flow rate of carrier gas and the choice of thermolysis temperature.

Reactor Model

The performance of the flow tube thermolysis apparatus has been carefully established to ensure that data are given correct interpretation. It will be shown that the reactor behaves very nearly as an ideal static reactor. This extremely simple result is developed from the axial dispersion model of mixing for a tubular reactor operated at the conditions of these experiments.

The flow in the reactor is clearly laminar, for the maximum Reynolds number is 3.2. From the Graetz[7] solution for heat transfer from the wall to the flowing fluid, the cold gas entering the reactor attains (within 0.1°) the wall temperature in less than 1 cm. In addition, the parabolic velocity profile also is achieved in less than 0.1 cm of tube length. The pressure drop across the reactor is so small that the flow is incompressible. Thus the flow in the reactor is fully developed laminar (parabolic velocity profile), isothermal, and incompressible.

Taylor[8] developed the axial dispersion model for laminar flow in long tubes. In this model the fluid is considered to flow as a piston in a cylinder. Radial diffusion interacts with the parabolic velocity profile to provide an axial diffusive flux relative to the assumed piston flow. Strictly, the model only applies to systems which satisfy the inequality

$$(N_{Re}/N_{Sc}) < 30(l/d) \tag{3}$$

where N_{Re} is the Reynolds number, N_{Sc} is the Schmidt number (kinematic viscosity divided by diffusivity), d is the inside tube diameter, and l is the reactor length. This inequality is most certainly valid after 1-cm length in these experiments. In addition, Farrell and Leonard[9] developed an analysis for mixing in the entrance region of pipe in laminar flow; it was shown that the mixing is greater in the entrance region than in the zone for which the Taylor model applies. Thus the use of the Taylor model for mixing in the reactor appears to be well justified but slightly conservative.

---

[6] F. O. Rice, "Free Radicals" (Collected Papers), The Catholic University Press, Washington, D. C., 1958.

[7] H. Grober, S. Erk, and U. Grigull, "Fundamentals of Heat Transfer," McGraw-Hill Book Co., Inc., New York, N. Y., 1961.

[8] G. I. Taylor, *Proc. Roy. Soc.*, **A219**, 186 (1953); **A225**, 473 (1954).

[9] M. J. Farrell and E. F. Leonard, *A.I.Ch.E. J.*, **9**, 160 (1962).

The thermolysis reaction is kinetically first order and thus the reactor performance is uniquely specified by the residence time distribution. In dimensionless form the component material balance for the reactor is written as

$$P\frac{\partial^2 C}{\partial Z^2} - \frac{\partial C}{\partial Z} - \frac{\partial C}{\partial T} - KC = 0 \qquad (4)$$

where

$P = \frac{D_{ax}}{vl}$, the axial dispersion parameter
$K = \frac{k}{v}$, the kinetic reaction parameter
$Z = z/l$, dimensionless length
$T = tv/l$, dimensionless time
$C = C/C_{ref}$, dimensionless concentration

Thus the performance of the reactor is described by two parameters: K, the reaction rate parameter which is the object of this study, and P, the axial dispersion parameter which is estimated from the Taylor model.

The boundary conditions for eq 4 have been discussed extensively,[10] and for this study are chosen as

$$F(t) = C - P\frac{\partial C}{\partial Z} \text{ at } Z = 0 \qquad (5)$$

and

$$\frac{\partial C}{\partial Z} = 0 \text{ at } Z = 1 \qquad (6)$$

The initial condition for an empty reactor is $C(Z,0) = 0$. Equation 5 is written in terms of an arbitrary forcing function, $F(t)$. Physically $F(t)$ is the pulse of reactant in carrier gas which is injected into the reactor. The solution to eq 4 is obtained by Laplace transformation with respect to T and solution of the ordinary differential equation subject to the boundary conditions, eq 5 and 6. Denoting transform variables by overbars, the result is

$$\bar{C}(Z) = \bar{F}\left\{\frac{r_1 e^{r_1 + r_2 Z} - r_2 e^{r_2 + r_1 Z}}{(r_1 e^{r_1} - r_2 e^{r_2}) - P r_1 r_2 (e^{r_1} - e^{r_2})}\right\} \qquad (7)$$

where

$$r_1 = \frac{1 + \sqrt{1 + 4P(s + K)}}{2P}$$

$$r_2 = \frac{1 - \sqrt{1 + 4P(s + K)}}{2P}$$

and s = Laplace transform variable. The term in brackets is the transfer function for the reactor. A simple way of relating this transfer function to the measured parameters of the experiment is through moment analysis. The measured values are the area of the chromatographic peak for reactant prior to entering the reactor and the area of this peak after passing through the reactor. These areas are equivalent to the zeroth moments of $\bar{F}$ and $\bar{C}$. The zeroth moments are found directly by taking the limit as s approaches zero. Denoting the moments as M_0^C, etc., the general equation is

$$M_0^C = M_0^F M_0^T \qquad (8)$$

Thus M_0^T, the zeroth moment of the reactor transfer function, is the fraction of the reactant remaining. In terms of the parameters of the problem

$$M_0^T = e^{-K}\left(\frac{Re^{A+K}}{(A + K)\sinh R + R\cosh R}\right) \qquad (9)$$

where $A = (2P)^{-1}$ and $R = \sqrt{1 + 4PK}/2P$. The e^{-K} term of eq 9 is the performance of an ideal static reactor, and the term in parentheses is a correction factor for axial dispersion. Three limiting values of M_0^T are found easily and are listed as

ideal static reactor: $M_0^T = e^{-K}$ as $P \rightarrow 0$

ideal stirred tank reactor: $M_0^T = \frac{1}{1 + K}$ as $P \rightarrow \infty$

zero reaction rate: $M_0^T = 1$ for $K = 0$ and any P

The zero reaction rate limit is a statement of conservation of mass.

When the axial dispersion parameter P is small the correction term in eq 9 can be expanded to yield

$$\frac{Re^{A+K}}{(A + K)\sinh R + R\cosh R} \approx \left(1 + K^2P + \left(\frac{K^2}{2} - 2\right)K^2P^2 \ldots\right) \qquad (10)$$

The terms in eq 10 will converge rapidly where P is less than 0.01 for the values of K used in this experimental work. The analysis which follows demonstrates that the correction to the static model is small enough to be ignored.

The apparent rate constant for a static reactor is defined as

$$\begin{aligned} K_{app} &= -\ln M_0^T \\ &= K - \ln\left(1 + K^2P + \left(\frac{K^2}{2} - 2\right)K^2P^2 \ldots\right) \\ &= K - K^2P + 2K^2P^2 \ldots \qquad (11) \end{aligned}$$

Equation 11 is a quadratic expression for the true K in terms of the apparent K. Upon expanding the final form of eq 11 one finds

---

[10] F. J. Wehner and R. H. Wilhelm, *Chem. Eng. Sci.*, 6, 89 (1956); 8, 309 (1958).

Table I: Mixing Correction Factors

T, °K	M_0^T	K_{app}	Inverse Peclét no., D/vd	$P \times 10^3$	Correction factor	K_{true}
793	0.706	0.348	0.089	1.11	1.000387	0.348
793	0.661	0.414	0.114	1.15	1.000477	0.414
823	0.665	0.405	0.030	0.68	1.000275	0.405
823	0.483	0.727	0.058	0.82	1.000597	0.727
844	0.455	0.787	0.031	0.69	1.000543	0.787
866	0.242	1.419	0.031	0.69	1.000979	1.420
872	0.363	1.013	0.016	0.62	1.000629	1.014
883	0.263	1.336	0.016	0.62	1.000829	1.337
893	0.206	1.578	0.016	0.62	1.000979	1.579

Table II: Gas-Phase Thermolysis Kinetics of Ethyl Acetate

Temp, °C	$10^3/T$, °K	Flow rate,[a] ml/min	Residence time, sec	C/C_0	k, sec^{-1}	ln k
472.0	1.342	9.56	10.22	0.711	0.033	−3.40
				0.704	0.034	−3.37
		7.35	13.29	0.661	0.031	−3.47
498.6	1.296	28.20	3.34	0.674	0.118	−2.14
				0.660	0.124	−2.09
				0.666	0.122	−2.11
		14.58	6.47	0.485	0.112	−2.19
				0.483	0.113	−2.18
				0.482	0.113	−2.18
517.5	1.265	28.04	3.28	0.446	0.246	−1.40
				0.448	0.245	−1.41
				0.450	0.243	−1.41
				0.467	0.232	−1.46
				0.465	0.233	−1.46
537.1	1.234	28.20	3.19	0.237	0.452	−0.79
				0.248	0.438	−0.83
				0.242	0.446	−0.81
				0.241	0.447	−0.81
543.0	1.225	55.07	1.62	0.356	0.638	−0.45
				0.370	0.614	−0.49
				0.363	0.626	−0.47
552.4	1.211	55.07	1.60	0.259	0.844	−0.17
				0.266	0.828	−0.19
				0.264	0.832	−0.18
561.3	1.198	55.07	1.58	0.210	0.985	−0.015
				0.196	1.029	−0.029
				0.213	0.977	−0.023

[a] Flow rate corrected for measurement at 25.0°.

$$K = K_{app}(1 + K_{app}P(1 - 2P)\ldots) \qquad (12)$$

The application of eq 12 for data reduction requires estimates of the axial dispersion parameter. Taylor[8] developed a theoretical model for the effective diffusivity which was carefully tested in the experimental work of Bournia, Coull, and Houghton.[11] Figure 4 shows these results combined with additional experimentation. There is a shallow minimum in the group, Pl/d, for inverse Peclét numbers (D_m/vd) in the range 0.01 to 0.1. There is no current theoretical model for this curve although the asymptotes have proper values. This empirical correlation was used to estimate P.

Table I lists the data used in the examination. The correction factor is the term $1 + K_{app}P(1 - 2P)$, the ratio by which the apparent rate constants must be multiplied to obtain the true value. The correction factor ordinarily is unity within experimental error limits. Thus, the thermolysis reactor effectively is a static reactor with a reaction time equal to the pulse residence time, and the dimensionless rate parameter, K, is found from the simple static reactor model as

$$K = k\tau = -\ln (C/C_0) \qquad (13)$$

---

[11] A. Bournia, J. Coull, and G. Houghton, *Proc. Roy. Soc.*, **A261**, 227 (1961).

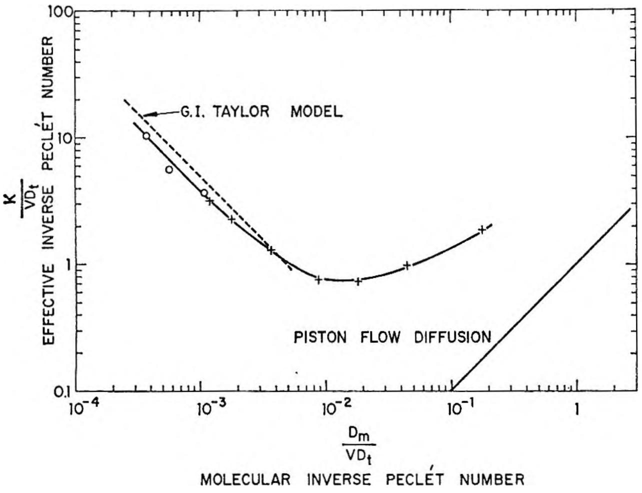

Figure 4.

Thermolysis of Ethyl Acetate as a Test Case

The thermolysis of ethyl acetate was chosen as a test reaction due to its simplicity and the abundance of kinetic data available in the literature for comparison.[4,12–17] The mechanism has been established as a *cis* elimination (Figure 5) proceeding through a six-membered ring cyclic transition state to the acid and olefin. Thus, the only species present should be ethyl acetate, acetic acid, and ethylene, in addition to any standards and/or solvents used. Examination of both flame ionization detector traces and the "small molecule" thermal conductivity chromatograms proved this to be the case.

Data were obtained for a range of temperatures from 472 to 561° and at flow rates of about 7–55 ml/min. The results (Table II) were fitted by regression analysis to the basic Arrhenius equation with the results

$$k = 1.87 \times 10^{12} e^{-46,700/RT}\ \mathrm{sec}^{-1}$$

$$E = 46.7 \pm 0.7\ \mathrm{kcal/mol}$$

$$\ln A = 28.26 \pm 0.46\ \mathrm{sec}^{-1}$$

$$\log A = 12.27 \pm 0.20\ \mathrm{sec}^{-1}$$

$$\Delta S^{\ddagger} = -6.3 \pm 1.0\ \mathrm{eu}$$

As can be seen from Table III and Figure 6, this result is in excellent agreement with previous values and lies about midway in the range of values previously obtained.

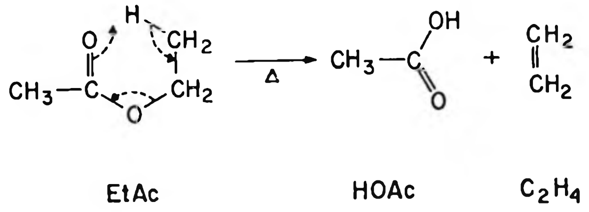

Figure 5.

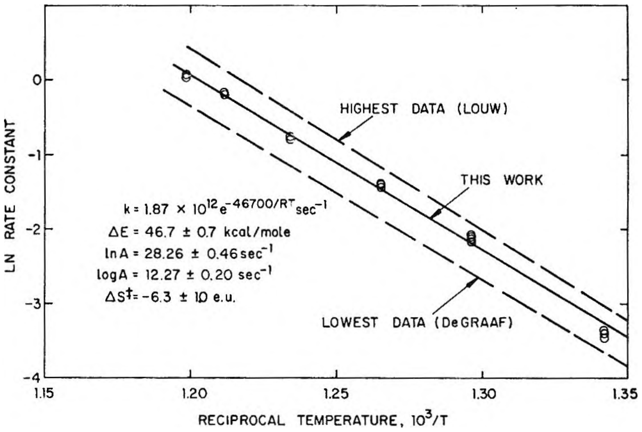

Figure 6.

Table III: Comparison of Ethyl Acetate Thermolysis Data

Temp range, °C	Arrhenius parameters: log A, sec^{-1}	Arrhenius parameters: ΔE, kcal/mol	Reference
386–487	12.84	48.3	17
500–603	12.59	48.0	13
514–610	12.49	47.7	14
433–461	12.47	47.7	16
437–465	12.38	47.4	16
472–561	12.27	46.7	This work
452–537	12.10	46.5	12
434–531	11.97	46.3	4

Thermolysis of *endo*-Dicyclopentadiene as a Test Case

The thermolysis of *endo*-dicyclopentadiene is another excellent test case since reliable data exist in the literature,[18,19] and since the reaction is also a simple one involving only the fission of dicyclopentadiene into two cyclopentadiene molecules. Since the presence of highly acidic products was not desired in one of the systems, this reaction was chosen as an additional test case and as a check on the comparability of data obtained from different reactors. In the two smallest reactors (4.07 and 3.67 cm^3) data were obtained over the temperature ranges of 244–282 and 240–280°, while in the largest reactor the range of 200–250° was investigated (see Tables IV–VI).

Since each set of data was taken over a comparatively

---

(12) J. C. Scheer, E. C. Kocyman, and F. L. J. Sixma, *Rec. Trav. Chim.*, **82** (11), 1123 (1963); J. C. Scheer, Thesis, Amsterdam, Netherlands, 1961.

(13) A. T. Blades and P. W. Gilderson, *Can. J. Chem.*, **38**, 1407 (1960).

(14) A. T. Blades, *ibid.*, **32**, 366 (1954).

(15) C. H. DePuy and R. W. King, *Chem. Rev.*, **60**, 431 (1960).

(16) C. A. Cramers, Thesis, Eindhoven, Netherlands, 1967; C. A. Cramers and A. I. M. Keulemans, *J. Gas Chromatogr.*, **5**, 58 (1967).

(17) R. Louw, Thesis, Leiden, Netherlands, 1964.

(18) J. B. Harkness, G. B. Kistiakowsky, and W. H. Mears, *J. Chem. Phys.*, **5**, 682 (1937).

(19) W. C. Herndon, C. R. Grayson, and J. M. Manion, *J. Org. Chem.*, **32**, 526 (1967).

Table IV: Gas-Phase Thermolysis Kinetics of Dicyclopentadiene (4.07-cm^3 Reactor)

Temp, °C	$10^3/T$, °K	Flow rate, ml/min	Residence time, sec	C/C_0	k, sec^{-1}	ln k
244.0	1.934	8.803^a	16.25	0.481	0.045	−3.10
244.0				0.497	0.043	−3.15
251.1	1.908	25.81^b	5.35	0.703	0.066	−2.72
251.2	1.907			0.679	0.072	−2.63
259.6	1.877	22.76^a	6.10	0.457	0.128	−2.05
259.7				0.452	0.130	−2.04
270.2	1.840	25.81^b	5.16	0.281	0.246	−1.40
270.4				0.286	0.243	−1.42
276.5	1.819	40.17^b	3.28	0.281	0.387	−0.95
				0.263	0.408	−0.90
		53.26^b	2.47	0.375	0.397	−0.92
				0.364	0.408	−0.90
				0.373	0.399	−0.92
280.5	1.806	57.01^a	2.34	0.245	0.600	−0.51
280.8	1.805			0.227	0.633	−0.46
281.6	1.803	40.17^b	3.25	0.183	0.523	−0.65
281.8	1.802			0.179	0.530	−0.63

[a] Flow rate corrected for measurement at 30.0°. [b] Flow rate corrected for measurement at 23.5°.

Table V: Gas-Phase Thermolysis Kinetics of Dicyclopentadiene (3.67-cm^3 Reactor)

Temp, °C	$10^3/T$, °K	Flow rate, ml/min	Residence time, sec	C/C_0	k, sec^{-1}	ln k
240	1.949	10	12.80	0.739	0.024	−3.74
				0.737	0.024	−3.74
250	1.911	10	12.56	0.534	0.050	−3.00
				0.527	0.051	−2.98
		20	6.28	0.691	0.059	−2.83
				0.709	0.055	−2.90
260	1.876	10	12.32	0.338	0.088	−2.43
				0.330	0.090	−2.41
		20	6.16	0.545	0.099	−2.32
				0.537	0.101	−2.29
		40	3.08	0.746	0.095	−2.35
				0.747	0.095	−2.35
270	1.841	20	6.05	0.348	0.175	−1.74
				0.345	0.176	−1.74
		40	3.02	0.575	0.183	−1.70
				0.569	0.186	−1.68
280	1.808	10	11.88	0.033	0.287	−1.25
				0.032	0.289	−1.24
		20	5.94	0.179	0.290	−1.24
				0.159	0.310	−1.17
		40	2.97	0.376	0.330	−1.11

short temperature interval, it was deemed preferable to compare the data directly with those from the literature, rather than to compare activation energies and preexponentials from each set. The data of Harkness, Kistiakowsky, and Mears,[18] and of Herndon, Grayson, and Manion[19] are shown in Figure 7 along with the data obtained in this work. The former report

$$k = 1.0 \times 10^{13}e^{-33{,}700/RT}\ \mathrm{sec}^{-1}$$

but linear regression techniques applied to their data (omitting their three lowest temperature points as they did) result in

$$k = 1.56 \times 10^{13}e^{-34{,}600/RT}\ \mathrm{sec}^{-1}$$

Herndon, Grayson, and Manion[19] report

$$k = 10^{13}e^{-34{,}000/RT}\ \mathrm{sec}^{-1}$$

in agreement with values obtained by linear regression, and the data obtained in this work are within experimental error of these values.

The entire set of available data from both the literature[18,19] and this work (Tables IV–VI) over the entire range of temperatures from 152 to 282° was used in linear regression techniques to derive the relationship

Table VI: Gas-Phase Thermolysis Kinetics of Dicyclopentadiene (20.90-cm³ Reactor)

Temp, °C	$10^3/T$, °K	Flow rate, ml/min	Residence time, sec	C/C_0	$k \times 10^2$, sec⁻¹	ln k
200	2.113	40	19.76	0.967	0.170	−6.38
		40		0.967	0.171	−6.37
		30	26.34	0.958	0.165	−6.41
		30		0.956	0.172	−6.37
		20	39.51	0.935	0.171	−6.37
		20		0.935	0.170	−6.38
210	2.070	40	19.35	0.915	0.461	−5.38
		40		0.915	0.461	−5.38
		30	25.80	0.890	0.451	−5.40
		30		0.890	0.451	−5.40
		20	38.69	0.842	0.445	−5.41
		20		0.843	0.441	−5.42
220	2.028	40	18.95	0.838	0.936	−4.67
		40		0.837	0.939	−4.67
		30	25.27	0.787	0.949	−4.66
		30		0.789	0.936	−4.67
		20	37.91	0.706	0.919	−4.69
		20		0.703	0.928	−4.68
230	1.987	30	24.77	0.629	1.87	−3.98
		30		0.633	1.84	−3.99
		20		0.521	1.75	−4.04
240	1.949	20	36.43	0.261	3.69	−3.30
250	1.911	20	35.74	0.0825	6.98	−2.66

$$k = 1.48 \times 10^{13} e^{-34{,}400/RT}\ \text{sec}^{-1}$$

$$\Delta E = 34.4 \pm 0.3\ \text{kcal/mol}$$

$$\ln A = 30.32 \pm 0.26\ \text{sec}^{-1}$$

$$\log A = 13.17 \pm 0.11\ \text{sec}^{-1}$$

$$\Delta S^{\ddagger} = -1.3 \pm 0.8\ \text{eu}$$

correlation coefficient = 0.998

Of related interest are the data of Herndon, Grayson, and Manion[19] for thermolysis of the *exo* isomer of dicyclopentadiene to the same product, for which they report

$$k = 5.25 \times 10^{13} e^{-38{,}600/RT}\ \text{sec}^{-1}$$

and the work of Khambata and Wasserman,[20] who report for thermolysis of pure liquid dicyclopentadiene

$$k = 4 \times 10^{13} e^{-35{,}300/RT}\ \text{sec}^{-1}$$

and for thermolysis of liquid dicyclopentadiene in paraffin solution

$$k = 10^{13} e^{-34{,}200/RT}\ \text{sec}^{-1}$$

Conclusions

We have tentatively deduced that wall catalysis of ester decomposition, which was noted as a problem in the measurements conducted in glass apparatus,[4,12,13] has been effectively eliminated in our system. It would appear that a combination of the use of a gold-surfaced reactor and a highly diluted reaction medium has substantially reduced if not completely eliminated all residues of a "wall reaction." It is well known that gold affords a "neutral" wall. On the other hand, the wall of a hot glass vessel is regarded as decidedly alkaline or acid depending on the presence of adventitious impurities. A catalytic effect was particularly difficult to eliminate in glass apparatus designs previously used,[4,12,13] because the substrate under study had to be volatilized by dropping onto a very high temperature glass surface and the resulting vapors had to be transported *in toto* through the thermolyzing area and thence to the analyzer.[4,12] No allowance could be made for

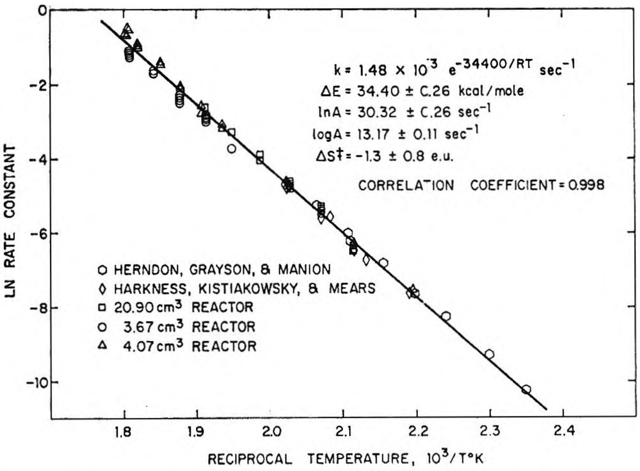

Figure 7.

---

(20) B. S. Khambata and A. Wasserman, *J. Chem. Soc.*, 375 (1939).

the amount of catalyzed decomposition prevalent with very high boiling substrates which were only sluggishly volatilized in the glass evaporator.

We conclude that in our apparatus not only does the surface of the thermolytic reactor possess a minimal catalytic influence, but the design has avoided all possibility of passing any (already) thermolyzed material into the reactor. The upstream GCl can be used to effectively separate all the peaks emerging from the evaporator section and pass into the reactor section only the substrate peak selected for thermolysis, along with inert reference-standard materials. The additional advantages of purification of the reactant subsequent to its volatilization and thermolysis in a vessel characterized by very minimal wall effects are clearly inherent in the design elements of our system. Moreover, the presence of the reactor bypass flow valve ensures that no prior thermolysis has taken place by allowing check runs through the entire system, eliminating only the reactor. These runs, furthermore, are used as the standards against which the thermolytic reactions are compared. The great simplicity of determining reaction rates under well-specified reaction conditions also recommends application of this rapid method of studying thermolytic reactions in the gas phase. Further studies applying this system and method of operation to a wide variety of reactions are presently in progress in these laboratories.

Acknowledgment. We are greatly obliged for very helpful, critical discussions and many useful suggestions contributed by Dr. Eugene Levy during the preparation of this article.

Electron Attachment by Pyridine and the Diazines in γ Radiolysis. Experimental and Theoretical Consideration[1a]

by A. Grimison, G. A. Simpson, M. Trujillo Sánchez, and J. Jhaveri

Puerto Rico Nuclear Center[1b] *and Departments of Chemistry and Physics, University of Puerto Rico, San Juan, Puerto Rico 00935*
(Received February 14, 1969)

Absorption spectra characterizing the radical anions of pyridine, pyrimidine, pyrazine, and pyridazine have been produced by γ radiolysis of the parent compounds in a 2-methyltetrahydrofuran matrix at 77°K. These spectra are in good agreement with those obtained by chemical reduction or electrolysis, but some additional transitions at longer wavelengths have been observed. Pariser–Parr–Pople calculations of the theoretical doublet–doublet transitions of the radical anions yield good correlations with the experimental transitions. The best correlation is obtained by not including configuration interaction, at least for a very limited number of configurations.

Our primary interest is in the production and characterization of ionic intermediates formed by the γ radiolysis of heterocyclic molecules. This identification can provide important information on the effects of radiation on biological systems. The technique being used is that of isolation in a solid matrix at liquid nitrogen temperature.[2] From the chemical viewpoint, perhaps the most intriguing aspect of such work is the extreme simplicity of the final processes forming these intermediates. Thus the work of Hamill and coworkers[3] has indicated how radical anions can be formed by attachment of low-energy electrons to solute molecules. Radical cations can apparently be produced by a simple positive charge exchange between the matrix and the solute molecule.[4,5] In a previous publication,[5] we have described one radiolytic technique suitable for the production and stabilization of radical cations. By this means, absorption maxima measured at 77°K were assigned to the radical cations of pyridine, pyrrole, and thiophene.[5] In general, the production of radical-anion intermediates is experimentally much less difficult. Thus Hush and Hopton have reported the absorption spectra of the radical anions of pyridine, pyrazine, pyrimidine, and

---

[1] (a) Presented in part at the Second Interamerican Radiochemistry Conference, Mexico City, Mexico, Apr 1968. (b) Puerto Rico Nuclear Center is operated by the University of Puerto Rico for the U. S. Atomic Energy Commission under Contract AT(40-1)-1833.

[2] A. M. Bass and H. P. Broida, "Formation and Trapping of Free Radicals," Academic Press, Inc., New York, N. Y., 1960.

[3] M. R. Ronayne, J. P. Guarino, and W. H. Hamill, *J. Amer. Chem. Soc.*, **84**, 4230 (1962).

[4] T. Shida and W. H. Hamill, *J. Chem. Phys.*, **44**, 2369 (1966).

[5] A. Grimison and G. A. Simpson, *J. Phys. Chem.*, **72**, 1776 (1968).

pyridazine, produced by reduction with sodium metal in tetrahydrofuran at room temperature.[6] Kimmel and Strauss[7] reported the optical spectra of the same radical anions, produced by electrolysis in liquid ammonia solutions. The observation of a λ_{max} at 330 nm from alkali metal solutions in anhydrous pyridine at room temperature is in good agreement with the earlier reports for the pyridine anion.[8] The present paper describes the effects of γ irradiation on the optical spectra of pyridine and the diazines in methyltetrahydrofuran (MTHF) glasses at 77°K. The major process observed under these conditions is shown to be the attachment of an electron to the neutral azine molecule to form the radical anion. The experimentally observed optical transitions from the different experimental techniques are shown to be in excellent accord. Finally, the semiempirical theoretical excitation energies for the radical anions, calculated by us, by Hush and Hopton,[6] and by Kimmel and Strauss,[7] are compared with the experimental values.

Experimental Techniques

Pyridine, Eastman Spectrograde, was distilled from barium oxide before use in absorption spectra determination.

Pyrazine, pyridazine, and pyrimidine were best commercial grade and were used without further purification. MTHF was purified by passage over alumina and stored under vacuum in a storage vessel containing Na–K alloy.

Solutions of required concentrations were prepared from the purified MTHF on the vacuum line by standard techniques.

γ Irradiations were performed in the PRNC 2700-Ci ^{60}Co source, using the Fricke technique for dosimetry.

Absorption spectra were obtained with the apparatus and techniques described previously.[5] Optical bleaching was effected with a 250-W quartz–iodine lamp and appropriate transmission filters.

Theoretical Calculations

Theoretical excitation energies and oscillator strengths corresponding to doublet–doublet electronic transitions in the azine anions have been carried out using the semiempirical Pariser–Parr–Pople (PPP) self-consistent field technique.[9] Recent nonempirical calculations on the excited states of the ethylene molecule[10] including σ–π interaction have given a sorely needed justification for the reduction of the π-electron integrals in the PPP method below the theoretical values. This can be considered as taking account of the effect of screening of the π-electron repulsions by the σ-electron distribution. In heterocyclic molecules, there is no reason to expect the similarity between radical-anion and radical-cation spectra suggested for the alternate hydrocarbon systems.[11] In particular, in calculating the electronic properties of the azine radical cations, some thought must be given to whether the missing electron has been removed from a lone-pair orbital or from a π orbital. However, for the radical anions, the additional electron enters a π-antibonding orbital, so that the use of a π-electron calculation in predicting electronic excitations is justified.

Input wave functions for the PPP calculation were obtained from Hückel calculations on the appropriate neutral heterocyclic molecule, using conventional parameter values. As a variant on this approach in some preliminary calculations, wave functions from a 10-iteration ω-technique calculation[12] on the actual radical anions were used as input to the PPP program. However, the comparative "weakness" of the ω technique in making electron density corrections to the Coulomb integrals was immediately apparent. Thus, after one iteration of the PPP calculation, identical results were obtained from Hückel and ω-input wave functions.

The parameter values which were used in the PPP calculations are listed in Table I. A limited configuration interaction (CI) was also carried out among the ground state and five excited doublet states. The diagonal and off-diagonal CI matrix elements were obtained from formulas derived using the Longuet-Higgins and Pople approximation.[11] In view of the heavy parametrization of the Pariser–Parr method and the relatively limited configuration interaction,[13] it can be expected that CI actually causes a slight deterioration of the agreement between theory and experiment.

Results and Discussion

Pyridine. The spectrum shown in Figure 1 illustrates the absorption bands produced on radiolysis of MTHF solutions of pyridine. The 1200-nm band corresponds to the position of the trapped electron band in pure MTHF. The band at 340 nm is characteristic of pyridine in MTHF. Liberation of electrons by photolysis into the trapped electron band is expected to increase authentic radical-anion absorption bands, as the liberated electrons are captured by unreacted neutral solute molecules.[3] Bleaching the trapped electron band in irradiated pyridine–MTHF solutions causes an increase in the band near 340 nm, as shown in Figure 1. Addition of 2 × 10^{-2} *M* trifluoroethanol, an electron

---

(6) (a) J. W. Dood, F. J. Hopton, and W. S. Hush, *Proc. Chem. Soc.*, 61 (1962); (b) F. J. Hopton, Ph.D. Thesis University of Bristol, England, 1962.

(7) P. I. Kimmel and H. L. Strauss, Abstracts, 155th National Meeting of the American Chemical Society, San Francisco, Calif., Mar 1968, p S-151, and private communication from H. L. Strauss.

(8) C. D. Schmulbach, C. C. Hinckley, and D. Wasmund, *J. Amer. Chem. Soc.*, **90**, 6600 (1968).

(9) R. G. Parr, "The Quantum Theory of Molecular Electronic Structure," W. Benjamin, New York, N. Y., 1963.

(10) T. H. Dunning and V. McKoy, *J. Chem Phys.*, **47**, 1733 (1967).

(11) H. C. Longuet-Higgins and J. A. Pople, *Proc. Phys. Soc.*, **A68**, 591 (1955).

(12) A. Streitweiser, Jr., "Molecular Orbital Theory for Organic Chemists," John Wiley & Sons, Inc., New York, N. Y., 1961, p 115.

(13) N. L. Allinger and T. W. Stuart, *J. Chem. Phys.*, **47**, 4611 (1967).

Table I: Parameter Values in Pariser–Parr–Pople Calculations

Molecule	Coulomb and resonance integrals, eV	Repulsion integrals, eV
Pyridine, pyridine radical anion	$H_{NN} = -45.865$ $H_{22}, H_{66} = -42.535$ $H_{33}, H_{55} = -42.374$ $H_{44} = -42.343$ $H_{CN} = -2.62$ $H_{CC} = -2.29$	(NN/NN) = 12.340 (CC/CC) = 11.130 (11/22), (11/66) = 7.770 (11/33), (11/55) = 5.608 (11/44) = 4.989 (22/33), (33/44), (44/55), (55/66) = 7.549 (22/44), (22/66), (33/55), (44/66) = 5.548 (22/55), (33/66) = 4.960
Pyrazine, pyrazine radical anion	$H_{NN} = -51.502$ $H_{22}, H_{33}, H_{55}, H_{66} = -42.706$ $H_{CN} = -2.62$ $H_{CC} = -2.29$	(NN/NN) = 12.340 (CC/CC) = 11.130 (11/22), (11/66), (33/44), (44/55) = 7.776 (11/33), (11/55), (22/44), (44/66) = 5.615 (11/44) = 10.600 (22/33), (55/66) = 7.565 (22/55), (33/66) = 5.030 (22/66), (33/55) = 5.56
Pyrimidine, pyrimidine radical anion	$H_{NN} = -50.736$ $H_{22} = -42.862$ $H_{44}, H_{66} = -42.610$ $H_{55} = -42.550$ $H_{CN} = -2.62$ $H_{CC} = -2.29$	(NN/NN) = 12.340 (CC/CC) = 11.130 (11/22), (11/66), (22/33), (33/44), = 7.776 (11/33) = 10.460 (11/44), (33/66) = 4.989 (11/55), (33/55) = 5.615 (22/44), (22/66), (44/66) = 5.560 (22/55) = 5.030 (44/55), (55/66) = 7.565
Pyridazine, pyridazine radical anion	$H_{NN} = -48.755$ $H_{33}, H_{66} = -42.595$ $H_{44}, H_{55} = -42.403$ $H_{NN} = -2.25$ $H_{CN} = -2.62$ $H_{CC} = -2.29$	(NN/NN) = 12.340 (CC/CC) = 11.130 (11/22) = 10.660 (11/33), (11/55), (22/44), (22/66) = 5.608 (11/44), (22/55) = 4.989 (11/66), (22/33), = 7.770 (33/44), (44/55), (55/66) = 7.549 (33/55), (44/66) = 5.548 (33/66) = 4.960

scavenger, to the pyridine–MTHF solution prior to irradiation results in the nonappearance of the 340-nm band. Figure 2 shows the dependence of the absorption at 340 and at 1200 nm on the initial pyridine concentration. The net absorption at 1200 nm falls off very sharply with increasing pyridine concentration and reaches a limiting but nonzero value. The concentration at which the one-half limiting yield occurs is approximately 7.0×10^{-3} *M*. This indicates that the efficiency of pyridine in competing for electrons against solvent traps is fairly high. Simultaneously, the 340-nm absorption increases and, within the precision of the data, reaches a limiting value at the same pyridine concentration. By equating the concentrations of the species responsible for the changes in absorption seen in Figure 2, neglecting the contribution of MTHF intermediates to the absorption at 340 nm, and using the value of the extinction coefficient reported by Dainton and Salmon[14] for the trapped electron in MTHF, a value of the extinction coefficient of the species absorbing at 340 nm is obtained which is some 15% higher than that reported by Hopton[6b] for the pyridine anion.

At concentrations greater than 4×10^{-2} *M*, a component of the absorption can also be observed with a max-

---

[14] F. S. Dainton and G. A. Salmon, *Proc. Roy Soc.*, **A285**, 319 (1965).

Table II: Transition Energies (eV) for the Pyridine Anion

Experimental values			Calculated values			
Ref 6b	Ref 7	This work	Ref 6b	Ref 7	This work	
					Without CI	With CI
		~1			0.26 (0.000)	0.27
		2.5	2.66 (0.067)		2.25 (0.231)	1.88
3.7 (0.078)[a]	3.46 (0.071)	3.65		3.07 (0.07)	4.29 (0.195)	4.15
					4.65 (0.200)	4.67
	4.75 (0.25)		5.05 (0.007)			
					5.40 (0.173)	5.83
5.08 (0.120)			5.23 (0.830)	5.26 (0.007)		

[a] Oscillator strength values in parentheses.

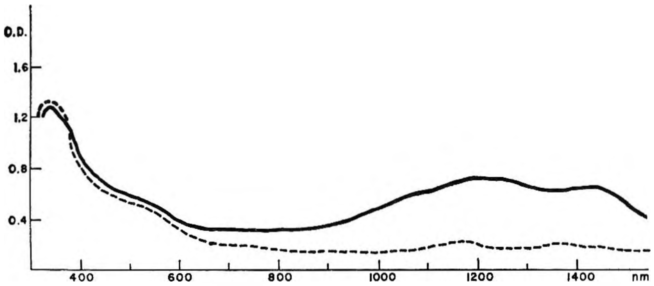

Figure 1. Absorption spectrum of an irradiated solution of pyridine, 2.4×10^{-2} *M*, in MTHF: —, after dose of 1.7×10^{22} eV/l.; -----, after 5-min bleach, λ ≥650 nm (Corning No. CS 2-64 filter).

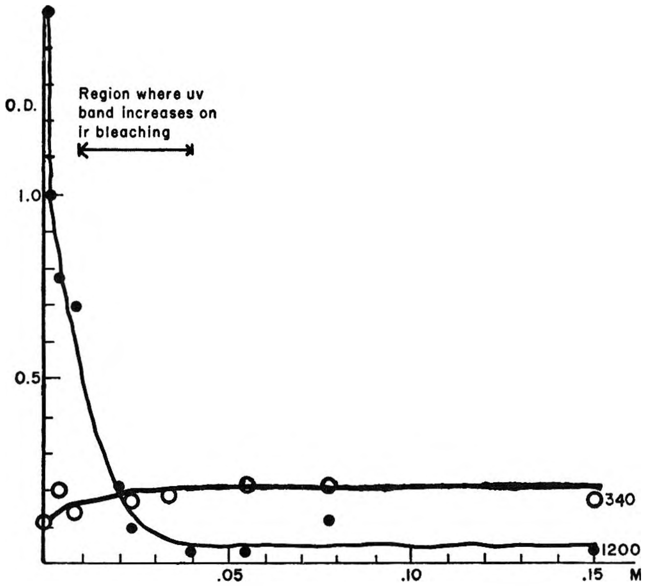

Figure 2. Concentration dependence of absorption bands produced on radiolysis of pyridine in MTHF, dose = 2.0×10^{21} eV/l.: ○, optical density at 340 nm; ●, optical density at 1200 nm.

imum at 500 nm. Only in the concentration region 8×10^{-3} to 4.0×10^{-2} *M* does bleaching the trapped electron band result in an increase of the 340-nm band.

The fact that the 340-nm band can be increased on bleaching the trapped electron band and is decreased on addition of an electron scavenger demonstrates the presence of an anionic intermediate of pyridine. This absorption is assigned to the pyridine radical anion, formed by the attachment of an electron to pyridine in competition with matrix trapping of the electron in MTHF. However, the fact that an increase in the 340-nm absorption following trapped electron bleaching does not occur at high pyridine concentrations requires some discussion. One explanation is to assume a weak optical transition of the pyridine anion at wavelengths greater than 1000 nm, which can give rise to a photoejection process. Thus, the bleaching process at pyridine concentrations greater than 4×10^{-2} *M* would cause two competing processes: capture of electrons released from matrix traps and photoejection from pyridine anions. Where there is a low trapped electron yield, the photoejection process dominates the capture of trapped electrons released by photostimulation, and a decrease in the 340-nm absorption results. Supporting evidence for the existence of a long wavelength transition of the pyridine anion may be taken from the appearance of the limiting concentration yields of the trapped electron band in Figure 2. The nonzero value of the absorption suggests that the extinction coefficient of the pyridine anion at 1200 nm may be as high as 20% of the value at 340 nm.

Table II gives a summary of the transitions attributed to the pyridine radical anion in this work, and the experimental assignments of Hush and Hopton[6] and Kimmel and Strauss.[7] The agreement on the position of the near-uv band is excellent, considering the very different experimental techniques. Thus Hush and Hopton's (HH) results refer to solution in tetrahydrofuran at room temperature, and Kimmel and Strauss (KS) results to spectra obtained in liquid ammonia solutions. These other workers observe additional shorter wavelength transitions which cannot be verified under our experimental conditions. The theoretically predicted doublet–doublet transitions of the pyridine radical anion calculated with and without configuration interaction are collected on the right of Table II. Our results without configuration interaction give high os-

Table III: Transition Energies (eV) for the Pyrazine Anion

Experimental values			Calculated values			
Ref 6b	Ref 7	This work	Ref 6b	Ref 7	This work	
					Without Cl	With Cl
					0.49 (0.000)	0.49
		2.45	2.90 (0.066)		2.28 (0.188)	2.11
3.4 (0.078)[a]	3.58 (0.091)	3.65		3.15 (0.053)		
					4.70 (0.253)	4.21
			5.16 (0.215)			6.03
4.98 (0.215)	5.21 (0.25)			5.22 (0.113)	5.54 (0.238)	6.24

[a] Oscillator strength values in parentheses.

Table IV: Transition Energies (eV) for the Pyrimidine Anion

Experimental values			Calculated values			
Ref 6b	Ref 7	This work	Ref 6b	Ref 7	This work	
					Without Cl	With Cl
					0.29 (0.003)	0.24
		3.1	2.86 (0.081)		2.53 (0.193)	2.36
3.75 (0.077)[a]	3.72 (0.065)	3.9		3.01 (0.169)	4.04 (0.216)	4.07
4.97 (1.94)	5.11 (0.25)		5.09 (0.10)	5.36 (0.15)	4.73 (0.181)	4.37
			5.47 (0.060)		4.94 (0.169)	5.81

[a] Oscillator strength values in parentheses.

Table V: Transition Energies (eV) for the Pyridazine Anion

Experimental values			Calculated values			
Ref 6b	Ref 7	This work	Ref 6b	Ref 7	This work	
					Without Cl	With Cl
		1.45			0.27 (0.000)	0.3
		2–3	2.73 (0.051)		2.13 (0.168)	1.79
3.52 (0.052)[a]	3.64 (0.065)	3.5		3.20 (0.132)	4.54 (0.185)	4.21
			4.59 (0.030)		4.93 (0.235)	5.46
5.13 (0.182)			5.24 (0.062)	5.63 (0.125)	5.27 (0.210)	5.60

[a] Oscillator strength values in parentheses.

cillator strengths as expected and are in reasonable accord with the experimental results. The calculations with configuration interaction shown here and in Tables III–V are generally in no better, and for a few levels are in worse, agreement with the experimental results than the calculations without configuration interaction. Thus, the entire discussion will be restricted to a comparison with the calculation without configuration interaction.

The band at 3.65 eV is calculated at 4.29, whereas KS results give 3.07 eV and HH have no corresponding band. The band observed by HH at 5.08 eV and by KS at 4.75 eV is calculated by HH at 5.23 eV (allowed band), by KS at 5.26 eV, and by us at 5.40 eV. The suspected band at 2.5 eV (500 nm) corresponds to a predicted pyridine anion absorption at 2.66 (HH) or at 2.25 eV (this work). Finally, our calculations alone suggest a forbidden long wavelength transition. By using the extinction coefficient of HH[6] for the 3.65-eV band, we estimate a G value of 3.0 for the production of pyridine anion at high pyridine concentration. The difference between this value and the value reported by Ronayne, Guarino, and Hamill[3] for the yield of trapped electrons in MTHF is ascribed to error in the value of the extinction coefficient of the pyridine anion at 77°K.

Pyrazine. Figure 3 shows the absorption spectrum at 77°K after γ radiolysis of pyrazine in a MTHF glass and the result of bleaching the trapped electron band. An absorption maximum is produced near 345 nm, and in a suitable concentration region an increase in this absorption is produced by bleaching the trapped electron band.

A rigorous concentration dependence study of these bands is complicated by the occurrence of an apparent shift in the position of the short wavelength band, but it can be reported that the concentration of pyrazine reduces the trapped electron band by half is $7 \pm 2 \times 10^{-3}$ M. Specifically, a λ_{max} of 320 nm is found at a

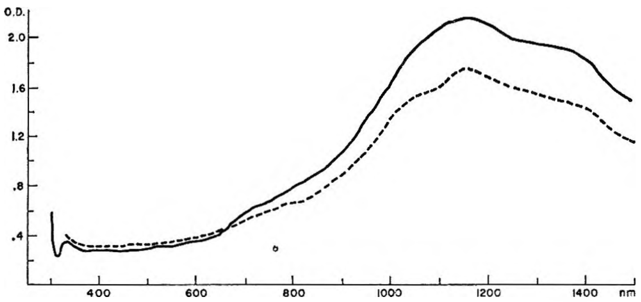

Figure 3. Absorption spectrum of irradiated solutions of pyrazine, 1.0×10^{-2} M in MTHF: —, after dose of 7.4×10^{21} eV/l.; ----, after 15-min bleach, $\lambda \geq 1000$ nm (Schott RG-1000 filter).

concentration of 1×10^{-4} M, which increases monotonically with concentration to a λ_{max} of 345 nm at a concentration of 3×10^{-2} M. We attribute this effect to an artifact of the technique of determining spectra. Difference spectra are obtained in the usual manner by subtracting the initial glass spectrum from that after irradiation, and the absorption after irradiation at every wavelength is greater than the initial spectrum. Nevertheless, the technique is unreliable if the parent heterocyclic concentration is decreased appreciably during radiolysis. Pyrazine has been found to have a λ_{max} at 315 nm in MTHF at room temperature in comparison with the value of 328 nm (ϵ 7.5×10^2 M^{-1} cm^{-1})[6b] in cyclohexane. The marked blue shift characterizes the n–π^* nature of the transition.[15] The pyrazine anion has been found to have λ_{max} at 365 nm (ϵ 3.0×10^3 M^{-1} cm^{-1}) in tetrahydrofuran at room temperature.[6b] Thus, depletion of pyrazine at low initial concentrations can cause a shift in the apparent position of the nearby absorption of the pyrazine intermediate. This was demonstrated further by repeated irradiation of the same solution to successively higher doses. On obtaining difference spectra in the usual manner, a shift in the λ_{max} to shorter wavelengths with increasing dose was observed. The position of the near-uv band of the radiation-induced intermediate of pyrazine is thus assigned to be equal to or greater than that observed at the highest concentration studied. As a result of the above observations, an absorption maximum at 345 nm is assigned to an anionic intermediate of pyrazine. This is believed to be the pyrazine radical anion, formed by electron attachment to pyrazine. The general features of the concentration dependence of the spectra show qualitative similarities to that observed for pyridine. At high concentration ($>10^{-2}$ M) a maximum is resolved at 500 nm. Also at these concentrations the 340-nm band decreases on bleaching the trapped electron band. This suggests the existence of an unobserved long wavelength transition of the pyrazine anion.

Table III compares the above assignment for the pyrazine radical anion with the results of HH[6] and KS.[7] Again there is substantial accord among the three groups of investigators for the near-uv band, remembering that our experimental value represents an upper limit to the transition energy. Again the theoretical excitation energies provide a reasonable account of the observed transitions. All three calculations give excellent accord with the high-energy transition near 5 eV. For the band near 3.5 eV, KS (3.15) are in good agreement, whereas our value of 4.70 eV is very high, and that of HH is very low (2.90 eV). This latter value may be related to the suggested 2.45-eV (500 nm) band, for which we calculate 2.28 eV. A forbidden long wavelength transition is predicted near 0.5 eV, which is suggested by our bleaching experiments. By using the extinction coefficient of HH for the near-uv band, we estimate a G value of 1.7 for the production of the pyrazine anion at the highest concentration of pyrazine reported here.

Pyrimidine. Figure 4 illustrates the absorption bands produced by radiolysis of pyrimidine in MTHF at 77°K and the result of bleaching the trapped electron band. An absorption maximum is produced near 320 nm, which is increased by bleaching the trapped electron band for a suitable initial pyrimidine concentration. As for pyrazine, a shift was observed in the position of the λ_{max} with increasing initial pyrimidine concentration at constant dose. This effect is again attributed to depletion of the underlying neutral pyrimidine absorption. The band is assigned a λ_{max} of 320 nm in MTHF at 77°K. For concentrations above 2×10^{-2} M, a further absorption band can be resolved near 400 nm. The concentration of pyrimidine which reduces the trapped electron absorption by half is $5 \pm 3 \times 10^{-3}$ M.

Table IV compares our results for the pyrimidine radical anion with those of HH[6] and KS.[7] Again our experimental transition energy for the near-uv band is very slightly higher than the values of these other workers, for the reason explained earlier. Our theoretical calculation gives a predicted band at 4.04 eV, in

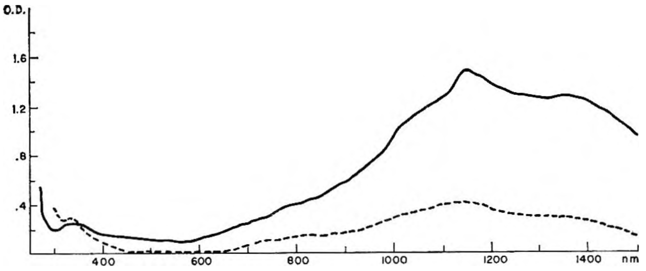

Figure 4. Absorption spectra of an irradiated solution of pyrimidine, 5.2×10^{-3} M in MTHF: —, after dose of 4.0×10^{21} eV/l.; ----, after 2-min bleach, $\lambda > 1000$ nm (Schott RG-1000 filter).

---

(15) M. Kasha, "A Symposium of Light and Life," Johns Hopkins University Press, Baltimore, Md., 1961, p 31.

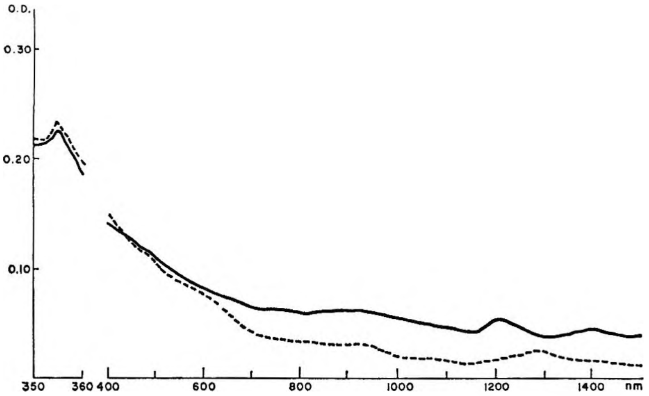

Figure 5. Absorption spectrum of an irradiated solution of pyridazine, 0.15 M in MTHF: —, after dose of 1.3 × 10^{22} eV/l.; -----, after 3-min unfiltered exposure to quartz–iodine lamp.

better accord with the experimental value of 3.8 eV than the result of HH (2.86 eV) or of KS (3.01 eV). For the band near 5 eV, the values of HH (5.09 or 5.47 eV), those of KS (5.36 eV), and our value, 4.73 or 4.94 eV, are all in reasonable accord with experiment. In addition, the existence of a transition near 3 eV (400 nm) reported by us is supported by calculated transitions at 2.86 (HH), 3.01 (KS, but may refer to the 3.8-eV band), and at 2.53 eV (this work). A virtually forbidden long wavelength transition is again predicted. Using the extinction coefficient of HH for the near-uv band, we estimate a G value for the production of the pyrimidine anion of 2.1 at the highest pyrimidine concentration reported here.

Pyridazine. Figure 5 shows the absorption bands produced by radiolysis of pyridazine in MTHF at 77°K and the results of bleaching the trapped electron band. An absorption band is produced with $\lambda_{\max}$ at 354 nm, whose intensity is increased on bleaching the trapped electron band. The absorption maximum at 354 nm is therefore assigned to the pyridazine radical anion. Figure 5 also shows other overlapping absorption bands at 900 nm and between 400 and 700 nm.

The data in Table V indicate the excellent agreement for the near-uv band of the pyridazine radical anion among the different groups. Our theoretical excitation energy value of 4.54 eV does not correspond very well with the experimental value of 3.5–3.6 eV. The value of KS (3.20 eV) is satisfactory, but HH have no closely corresponding band. The band found by HH at 5.13 eV is satisfactorily accounted for in all three calculations. In addition, the possible existence of bands at 2–3 (400–700 nm) and at 1.45 eV is partly supported by a calculated band at 2.73 (HH) and at 2.13 eV (this work). Using the extinction coefficient of HH for the near-uv band, we estimate a G value of 0.8 for the production of the pyridazine radical anion shown in Figure 5.

Conclusion

The results of these investigations, taken jointly with the measurement of "authentic" radical anion spectra by two other groups of workers, demonstrate the formation of the azine radical anions in γ radiolysis at 77°K. The high yields of these anions, produced in competition with trapped electrons, and the results of the bleaching experiment indicate their production *via* simple electron attachment.

$$\text{azine} + e^- \rightarrow (\text{azine})^-$$

The efficiency for electron capture by the azines is similar to that of the aromatics.[3]

The experimental absorption spectra of the four azine radical anions are, therefore, fairly well established. The reasonable accord between the experimental transitions and the theoretical transitions, in the π-electron approximation, confirms that the additional electron enters a π^*-antibonding level. In the present calculations, no direct account was taken of the σ reorganization expected as a result of this additional electron. We feel that specific inclusion of this effect would provide a more adequate account of the electronic structure of the radical anions, and we are currently investigating this possibility.

Acknowledgments. This work was supported by a research grant from the Division of Biology and Medicine of the U. S. Atomic Energy Commission. We wish to acknowledge the kindness of Professor Hush and Professor Strauss in communicating unpublished results and to thank Professor Hamill for helpful discussions.

Mean Activity Coefficient of Polyelectrolytes. XI. Activity Coefficients of Various Salts of Polyacrylic Acid and Carboxymethylcellulose[1]

by Kiyotsugu Asai, Katsuhiko Takaya, and Norio Ise

Department of Polymer Chemistry, Kyoto University, Kyoto, Japan *(Received February 19, 1969)*

The osmotic and (mean) activity coefficients of propionates, polyacrylates (PAA), and carboxymethylcellulose (CMC) salts of various gegenions in aqueous media have been determined at 25° by means of the isopiestic vapor pressure measurement. As had been found in previous works, a marked specificity of gegenions was noted. For propionates, the osmotic and activity coefficients decreased in the order $N(n\text{-}C_4H_9)_4 > N(CH_3)_4 > K > Na > Li$. For polyacrylates at high degrees of neutralization, the order was $N(n\text{-}C_4H_9)_4 > N(n\text{-}C_3H_7)_4 > N(C_2H_5)_4 > N(CH_3)_4 > Li > K > Na$. In the case of a CMC sample of a higher degree of substitution ($DS = 0.95$) the order was $N(n\text{-}C_4H_9)_4 > N(CH_3)_4 > Na$. Lowering of the DS value changed the order. At $DS = 0.78$, $NR_4(R = \text{alkyl}) \approx K > Na > Li$ and at $DS = 0.68$ $N(CH_3)_4 > Na > N(n\text{-}C_4H_9)_4$. The order $Na > N(n\text{-}C_4H_9)_4$ was also found for polyacrylates at a degree of neutralization of 0.2. These results could be accounted for in terms of the structural influence of ions on water by taking into consideration balancing of two "counteracting" effects of hydrophobic and ionic groups. The electrostrictional structure formation effect, which was predominant at a highly charged state, could be screened off by the cage-like structure formation of hydrophobic parts at low degrees of neutralization or substitution. Comparison of the PAA and CMC ions suggested that the former is more hydrophobic than the latter.

Introduction

In previous papers from this laboratory,[2] the mean activity coefficients of a variety of synthetic polyelectrolytes having various gegenions have been measured. The results have shown that the mean activity coefficients are largely influenced not only by the character of macroions but also by that of gegenions; the specificity of macroions and gegenions was successfully, though qualitatively, accounted for in terms of the structural influence of ions on water. Furthermore, it was concluded that the solvent–solute interaction is more important than the gegenion association, though the reverse was often believed to be true. While we intend to extend the measurements to biologically important polyelectrolytes, we want to report here the mean activity coefficient data of various salts of polyacrylic acid (PAA) and carboxymethylcellulose (CMC). No other types of salts than the sodium salt of PAA[3,4] have been measured previously. The salts of CMC were thought interesting because the CMC molecule contains a number of polar groups and is believed to be comparatively stiff.

Experimental Section

The NaPAA was a gift from the Toa Gosei Chemicals Co., Nagoya. Its weight-average degree of polymerization was 640. The NaCMC was kindly furnished from the Daiichi Kogyo. The degree of polymerization was estimated by the supplier to be about 400. The NaPAA and NaCMC solutions were purified by passing through cation- and anion-exchange resins. Propionic acid was twice distilled at reduced pressure in a nitrogen atmosphere (42 mm, 65.1°). The polyacid solution thus obtained was neutralized with the aid of conductometric titration with an aqueous solution of reagent grade LiOH, NaOH, KOH, $(CH_3)_4NOH$, $(C_2H_5)_4NOH$, $(n\text{-}C_3H_7)_4NOH$, or $(n\text{-}C_4H_9)_4NOH$. The polymer concentration was determined by the titration data.

The isopiestic measurements were carried out at 25 ± 0.005° by using an apparatus and experimental procedures described previously.[5]

Results and Discussion

The measured concentrations of the solutions of PAA salts and potassium chloride (reference electrolyte) in isopiestic equilibria are listed in Table I. The corresponding data for propionates and CMC salts are given in Tables II and III, respectively.

The practical osmotic coefficient of the electrolyte was calculated by the condition of equal solvent vapor pressure, as previously described.[4] The osmotic coefficients of potassium chloride solutions were taken from the literature.[6] The osmotic coefficients of pro-

---

(1) Presented at the 21st Annual Meeting of the Chemical Society of Japan, Tokyo, Japan, April 1968, and at the 17th Annual Meeting of the Society of High Polymers, Japan, May 1968.

(2) (a) N. Ise and T. Okubo, *J. Phys. Chem.*, **71**, 1886 (1967); (b) N. Ise and T. Okubo, *ibid.*, **72**, 1361 (1968); (c) N. Ise and K. Asai, *ibid.*, **72**, 1366 (1968); (d) N. Ise and T. Okubo, *ibid.*, **72**, 1370 (1968).

(3) N. Ise and T. Okubo, *ibid.*, **69**, 4102 (1965).

(4) N. Ise and T. Okubo, *ibid.*, **71**, 1287 (1967).

(5) T. Okubo, N. Ise, and F. Matsui, *J. Amer. Chem. Soc.*, **89**, 3697 (1967).

(6) R. A. Robinson and R. H. Stokes, "Electrolyte Solutions," Butterworth and Co., Ltd., London, 1959, pp 476, 481.

Table I: Concentrations of Isopiestic Solutions of Potassium Chloride and Polyacrylates at 25°[a]

1. PAA Salts at a Degree of Neutralization = 1

m_{KCl}	Li	K	$N(CH_3)_4$	$N(C_2H_5)_4$	$N(n\text{-}C_3H_7)_4$	$N(n\text{-}C_4H_9)_4$
0.0962	0.504	0.550	0.352	0.326	0.300	0.266
0.123	0.667	0.731	0.448	0.408	0.375	0.325
0.151	0.809	0.872	0.542	0.491	0.450	0.392
0.164	0.869	0.933	0.669	0.612	0.554	0.496
0.200	1.03	1.10	0.754	0.685	0.623	0.562
0.241	1.18	1.26	0.945	0.858	0.773	0.707
0.332	1.56	1.65	1.23	1.11	0.986	0.922

2. NaPAA and $N(n\text{-}C_4H_9)_4PAA$ at Degrees of Neutralization of 0.2, 0.4, 0.6, and 0.8

	NaPAA				$N(n\text{-}C_4H_9)_4PAA$			
m_{KCl}	0.2	0.4	0.6	0.8	0.2	0.4	0.6	0.8
0.105	0.248	0.320	0.430	0.523		0.267		
0.139	0.331	0.414	0.550	0.668	0.377	0.338	0.356	0.377
0.216	0.503	0.606	0.792	0.969	0.626	0.471	0.481	0.503
0.268	0.628	0.733	0.958	1.17	0.825	0.560	0.560	0.578
0.342	0.819	0.923	1.19	1.43	1.11	0.683	0.660	0.671
0.428	1.03	1.13	1.45	1.73	1.46	0.828	0.778	0.779
0.475	1.14	1.23	1.55	1.84	1.62	0.891	0.824	0.821
0.543	1.31	1.42	1.73	2.03	1.86	0.995	0.901	0.892
0.695	1.63	1.72	2.10	2.41		1.24	1.07	1.05
0.851	1.95	2.07	2.46	2.76		1.47	1.23	1.17
1.36	2.75	2.93	3.40	3.64			1.72	1.56
1.53	3.00	3.19	3.69	3.87			1.92	1.71
2.01	3.62	3.86	4.36	4.47				

[a] m_{KCl} is in molality; polymer concentration is in equiv/1000 g of water.

Table II: Concentrations of Isopiestic Solutions of Potassium Chloride and Propionates at 25°

m_{KCl}	Na	Li	K	$N(CH_3)_4$	$N(n\text{-}C_4H_9)_4$
0.144	0.143	0.145	0.142	0.131	0.128
0.188	0.185	0.187	0.185	0.169	0.165
0.420	0.386	0.405	0.381	0.364	0.347
0.880	0.800	0.836	0.777	0.729	0.660

pionates (ϕ) are given in Figure 1, together with the ϕ values of the sodium salt reported previously (given by the filled circles).[7] The osmotic coefficients of polyacrylates (ϕ_z)[8] are given in Figure 2. The ϕ_z values for NaPAA were obtained from the results previously published by using the observed value of the polymer charge fraction.[4] Figure 3 gives the ϕ_z as a function of polyelectrolyte concentrations for salts of CMC of a degree of substitution (*DS*) of 0.95 (carboxymethyl groups per glucose unit). From Figures 1, 2, and 3, it is seen that alkali metal salts of electrolytes have lower osmotic coefficient values than tetraalkylammonium salts. For CMC salts having lower *DS* values, however, the situation is different; as shown in Figure 4, at *DS* = 0.78, the ϕ values of the tetraalkylammonium salts fell on a curve and were as large as those of KCMC. It is seen from Figure 5 that at *DS* = 0.68 $N(n\text{-}C_4H_9)_4$CMC showed smaller ϕ_z values than $N(CH_3)_4$CMC, whereas the reverse was the case in Figures 1, 2, and 3. Figure 6 gives the ϕ_z values of sodium salts of the poly-

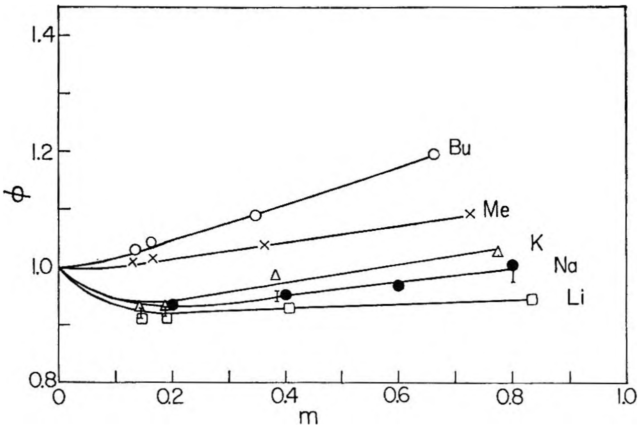

Figure 1. Osmotic coefficients of aqueous solutions of $N(n\text{-}C_4H_9)_4$-, $N(CH_3)_4$-, K-, Na-, and Li propionates (25°). ●: data for the sodium salt taken from the work cited in ref 6.

---

(7) Taken from ref 6, p 484, Appendix 8.10.

(8) The ϕ_z values were calculated on the assumption that the electrolyte is fully dissociated. For polyelectrolytes, it is possible to define another osmotic coefficient on the basis of the number of free gegenions, which has been denoted by ϕ without suffix in a series of our work. We note that it is not necessary to distinguish between ϕ and ϕ_z for simple electrolytes, since the so-called gegenion association does not so markedly occur for this kind of electrolytes as for polyelectrolytes. We further note that the mean activity coefficient γ^* to be discussed in the present paper corresponds to ϕ_z by the fundamental thermodynamic relation, but not to ϕ.

Table III: Concentrations of the Isopiestic Solutions of Potassium Chloride and Salts of Carboxymethylcelluloses at 25°[a]

1. CMC (*DS* = 0.78)

m_{KCl}	Na	K	Li
0.143	0.333	0.239	0.391
0.176	0.456	0.329	0.493
0.219	0.598	0.425	0.636
0.305	0.741	0.524	0.783
0.424	0.964	0.676	1.03
0.623	1.38	0.924	1.47
0.956	1.99	1.30	2.15

2. CMC (*DS* = 0.78)

m_{KCl}	$N(CH_3)_4$	$N(C_2H_5)_4$
0.155	0.260	0.276
0.195	0.328	0.345
0.255	0.400	0.419
0.336	0.535	0.553
0.459	0.740	0.762
0.665	0.964	0.997

3. CMC (*DS* = 0.95 and 0.68)

	DS = 0.95			*DS* = 0.68		
m_{KCl}	Na	$N(CH_3)_4$	$N(n\text{-}C_4H_9)_4$	Na	$N(CH_3)_4$	$N(n\text{-}C_4H_9)_4$
0.108	0.364	0.271	0.243	0.258	0.228	0.293
0.128	0.430	0.325	0.288	0.308	0.268	0.340
0.209	0.637	0.472	0.406	0.477	0.386	0.479
0.244	0.749	0.546	0.466	0.566	0.446	0.550
0.268	0.840	0.616	0.520			0.621
0.338	1.01	0.722	0.601	0.767	0.581	0.716
0.427	1.24	0.855	0.703	0.927	0.689	0.854
0.493	1.43	0.987	0.794	1.07	0.747	0.979
0.672	1.80	1.21	0.972	1.35	0.914	1.21

[a] m_{KCl} is in molality; CMC concentration is in equiv/1000 g of water.

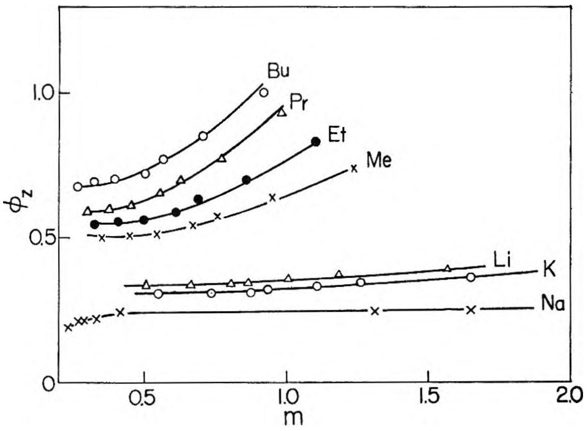

Figure 2. Osmotic coefficients of aqueous solutions of $N(n\text{-}C_4H_9)_4$-, $N(n\text{-}C_3H_7)_4$-, $N(C_2H_5)_4$-, $N(CH_3)_4$-, Li-, K-, and Na polyacrylates (25°).

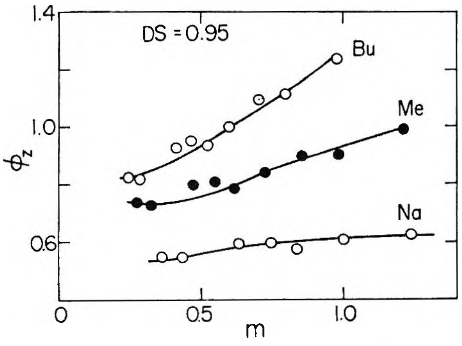

Figure 3. Osmotic coefficients of aqueous solutions of $N(n\text{-}C_4H_5)_4$-, $N(CH_3)_4$-, and NaCMC at a degree of substitution of 0.95 (25°).

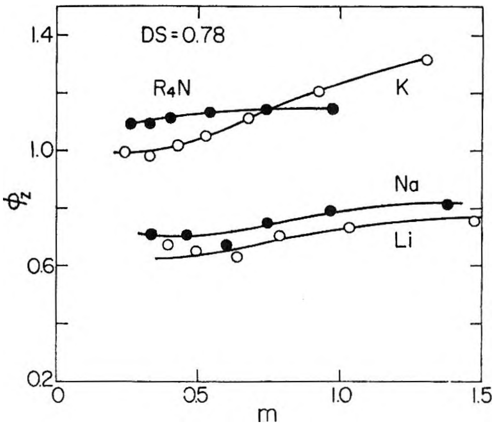

Figure 4. Osmotic coefficients of aqueous solutions of $N(n\text{-}C_4H_9)_4$-, $N(CH_3)_4$-, K-, Na-, and LiCMC at a degree of substitution of 0.78 (25°).

acrylic acid at degrees of neutralization of 0.2, 0.4, 0.6, and 1.0 and of carboxymethylcellulose samples at approximate degrees of substitution of 0.7, 0.8, and 1.0. For both PAA and CMC, the ϕ_z becomes larger as the charge density on the polymer chain decreases.

The mean activity coefficient was calculated using the Gibbs–Duhem relation, as reported previously.[4] The assumptions involved in the calculation of the coefficient of the polyelectrolytes were, again, that (1) the cube-root rule holds down to infinite dilution and (2) the polyelectrolytes have the same activity coefficient at infinite dilution (γ_0^*), irrespective of the gegenion, the degree of substitution, or the degree of neutraliza-

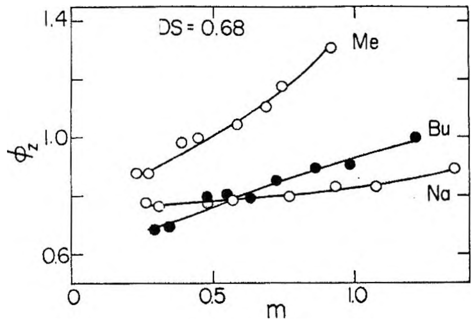

Figure 5. Osmotic coefficients of aqueous solutions of $N(CH_3)_4$-, $N(n\text{-}C_4H_9)_4$-, and NaCMC at a degree of substitution of 0.68 (25°).

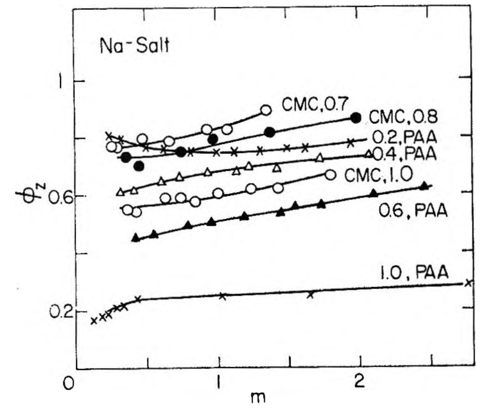

Figure 6. Osmotic coefficients of sodium salts of carboxymethylcellulose and polyacrylic acid at various degrees of neutralization and of substitution (25°). CMC, 0.7, 0.8, and 1.0 denote the samples at degrees of substitution of 0.68, 0.78, and 0.95, respectively. 0.2, 0.4, 0.6, and 1.0 PAA denote the degrees of neutralization of 0.2, 0.4, 0.6, and 1.0, respectively.

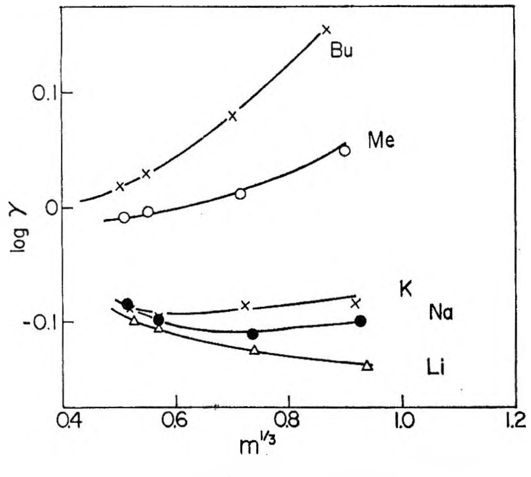

Figure 7. The cube-root plot of the activity coefficients of propionates (25°).

tion. Obviously the second assumption is questionable and will be considered in the latter part of this paper.

Figure 7 gives the activity coefficients of propionates as a function of the cube root of electrolyte concentration. It is seen that the cube-root rule is not valid in the concentration range studied.[9] Furthermore, the activity coefficient decreased in the order

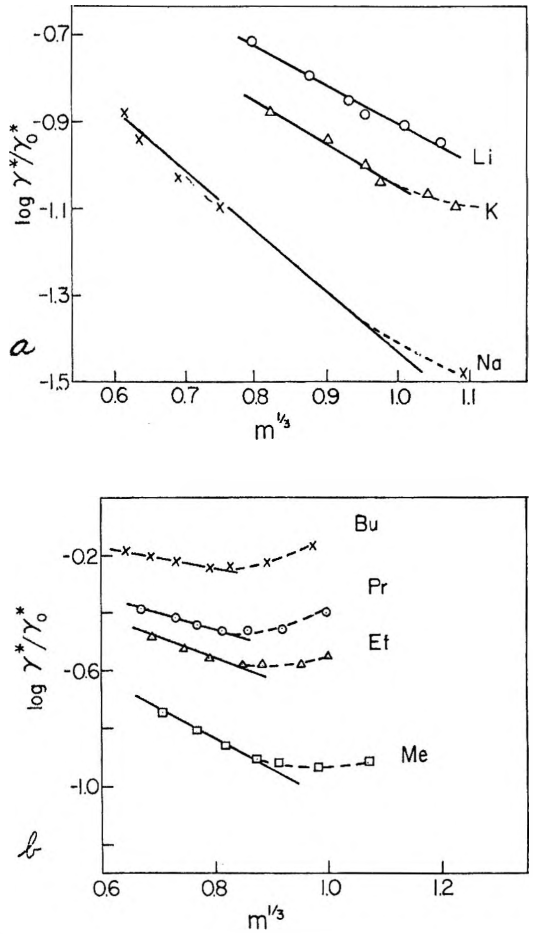

Figure 8. The cube-root plot of the activity coefficients of polyacrylates at a degree of neutralization of 1.0 (25°).

$$K \approx Na > Li \tag{A}$$

and

$$N(n\text{-}C_4H_9)_4 > N(CH_3)_4 \tag{B}$$

The order (A) is the same as found for acetates,[10] and is the reverse of that observed for polyvinyl sulfates, polystyrenesulfonates, polyethylenesulfonates, and polyphosphates.[2] The order (B) was also found for all these polyelectrolytes examined so far[2] and for tetraalkylammonium halides in a dilute region.[11] Figures 8a and 8b give the mean activity coefficients of alkali metal salts and tetraalkylammonium salts of the polyacrylic acid, respectively. The cube-root rule is seen to hold at low concentrations. The upper bound of the range of fit of the rule is about 1 equiv/1000 g of water for the inorganic salts and about 0.5 equiv/1000 g of water for the organic salts. The slopes are −0.82, −1.00, −1.30, −0.40, −0.60, −0.80, and −0.95 for Li-, K-, Na-, $N(n\text{-}C_4H_9)_4$-, $N(n\text{-}C_3H_7)_4$-, $N(C_2H_5)_4$-, and $N(CH_3)_4$-PAA, respectively. The activity coefficients of polyacrylates decreased in the order

---

[9] For earlier references on the cube-root rule of the activity coefficient of electrolytes and for the related problem, see H. S. Frank and P. T. Thompson, "The Structure of Electrolytic Solutions," W. J. Hamer, Ed., John Wiley and Sons, Inc., New York, N. Y., 1959, Chapter 8.

[10] Reference 7, pp 492, 494.

[11] (a) S. Lindenbaum and G. E. Boyd, *J. Phys. Chem.*, 68, 911 (1964); (b) W. Y. Wen, S. Saito, and C. M. Lee, *ibid.*, 70, 1244 (1966).

$$\mathrm{Li} > \mathrm{K} > \mathrm{Na} \qquad \text{(C)}$$

and

$$N(n\text{-}C_4H_9)_4 > N(n\text{-}C_3H_7)_4 > N(C_2H_5)_4 > N(CH_3)_4 \qquad \text{(D)}$$

While the order (D) was already found for polyelectrolytes studied so far,[2] for tetraalkylammonium halides[11] and for the propionates, the order (C) is new in two respects: it differs from the order (A) found for propionates or acetates, and also from the order Li > Na > K observed for polyelectrolytes studied in this laboratory.[2] According to the existing theories of structural influences of ions on water,[11b,12-14] the structural salting-out and salting-in effects result in the high-lying and low-lying activity coefficient concentration curves, respectively. The observed order for propionates (K > Na > Li) indicates that the propionate ion is a structure-former in the same sense as for Li^+ ion. As was earlier suggested by Gurney,[15] the acetate ion is a structure-former. Therefore, the propionate ion would be structure-forming also, though probably even less so than the acetate ion because of the presence of an ethyl group which is a structure former of a mode incompatible with the carboxylate group.[16] The order (C) for the polyacrylates (Li > K > Na) suggests that the polyacrylate ion is a weaker structure former than the propionate ion. This would be understood as follows. The $-CH_2-\underset{|}{CH}$ groups present in the polymer chain could show a stronger cage-like structure-forming tendency than the CH_3-CH_2 groups in the corresponding monomer unit, *i.e.*, the propionate ion. In other words, we can expect a cooperative influence by the repeating units in the polymer chain on the water structure. As a consequence, the electrostrictional influence of the carboxylate group would be weakened more strongly for the polyacrylates than for the propionates. Thus, the order (C) differs from the order (A). As for the orders (B) and (D), which agree to each other, it is useful to point out that the organic ions are strong cage-like structure formers. The incompatibleness of the modes of the water structure around the organic ions and the propionate or polyacrylate ions gave rise to the observed order.

The foregoing discussion was clearly based on two "counteracting" structural influences on water structure, namely the cage-like structure formation by the hydrophobic part (methyl and ethyl groups for acetates and propionates) and the electrostrictional structure formation by the ionic part (carboxylate ion for acetates and propionates). The relative magnitudes of these two effects determine the position of the activity (or osmotic) coefficient–concentration curves.[17] Thus, the CMC salts of *DS* = 0.95 (Figure 3) showed in the order

$$N(n\text{-}C_4H_9)_4 > N(CH_3)_4 > \mathrm{Na} \qquad \text{(E)}$$

which agrees with the finding for the polyacrylates. When the charge density (or the degree of substitution) is lowered, the contribution of the electrostrictional factor becomes smaller and the hydrophobic influence becomes more important. In other words, the structure-forming character of the CMC ions becomes closer to that of the organic gegenions with decreasing *DS*. Therefore $N(n\text{-}C_4H_9)_4$–CMC at *DS* = 0.68 has smaller osmotic coefficients than $N(CH_3)_4$–CMC, as shown in Figure 5

$$N(CH_3)_4 > \mathrm{Na} \approx N(n\text{-}C_4H_9)_4 \qquad \text{(F)}$$

The CMC salts at *DS* = 0.78 represent an intermediate feature, as seen from Figure 4. At this degree of substitution, the osmotic coefficients of the tetraalkylammonium salts fell on the same curve; no observable difference was observed between $N(n\text{-}C_4H_9)_4$ and $N(CH_3)_4$ salts.

It would be interesting to examine the order of the

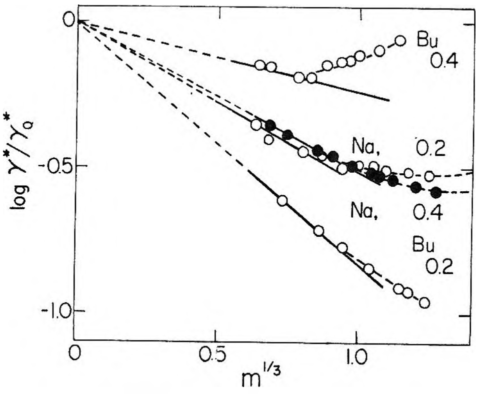

Figure 9. The cube-root plot of the activity coefficients of $N(n\text{-}C_4H_9)_4$- and Na polyacrylate at degrees of neutralization of 0.4 and 0.2.

---

(12) H. S. Frank and W.-Y. Wen, *Discussions Faraday Soc.*, **24**, 133 (1957).

(13) H. S. Frank, *J. Phys. Chem.*, **67**, 1554 (1963).

(14) H. S. Frank, *Z. Phys. Chem.* (Leipzig), **228**, 364 (1965).

(15) R. W. Gurney, "Ionic Processes in Solution," McGraw-Hill Book Co., Inc., New York, N. Y., 1953, Chapter 16.

(16) The reasoning that the structure-forming tendency of the propionate ion is weaker than that of the acetate ion is substantiated by the fact that sodium propionate has larger activity coefficients than sodium acetate. See ref 6, p 484, Appendix 8.10.

(17) The structural influences can be discussed in terms of the osmotic coefficient, instead of the activity coefficient. When comparison of various polyelectrolytes is sought, the use of the osmotic coefficient is convenient because the activity coefficient at infinite dilution varies from sample to sample. The activity coefficients of CMC samples are not given in the present paper, because the isopiestic data were not reliable enough at higher dilutions to allow the cube-root extrapolation.

activity coefficients of PAA salts at lower degrees of neutralization. Figure 9 shows that at a degree of neutralization = 0.4 we have the order

$$N(n\text{-}C_4H_9) > Na \qquad (G)$$

which is the same as found at a degree of neutralization = 1 (see Figures 8a and 8b). However, when we go down to 0.2, we have

$$Na > N(n\text{-}C_4H_9) \qquad (H)$$

In words, the inversion of the order of the activity (or osmotic) coefficients can occur not only for CMC salts but also for PAA salts. This fact strongly supports the validity of the above-mentioned explanation in terms of the shift of balance between the structural influences of ionic and hydrophobic groups with varying charge density.

Finally, we compare the ϕ_z values of the PAA and CMC. As was mentioned before, the linear charge density of a CMC having a $DS = 1.0$ is about the same as that of a PAA of a degree of neutralization of 0.3. Figure 6 shows that the ϕ_z of this PAA sample is larger than that of the corresponding CMC salt. This result indicates that the PAA anions are more hydrophobic than the CMC anions. This is consistent with the information derived from the solubility measurements of naphthalene and biphenyl in solutions of water-soluble polymers.[18]

Acknowledgments. The sodium polyacrylate and sodium salts of carboxymethylcellulose were gifts of the Toa Gosei Chemicals Co., Nagoya, and the Daiichi Kogyo Seiyaku Co., Kyoto, respectively.

(18) T. Okubo and N. Ise, *J. Phys. Chem.*, **73**, 1488 (1969).

The Equation of State of Fluid Argon and Calculation of the Scaling Exponents

by Olav B. Verbeke,

Institute for Molecular Physics, University of Maryland, College Park, Maryland

Vik Jansoone, Rik Gielen, and Jan De Boelpaep

Fysisch Instituut, Universiteit van Leuven, Leuven, Belgium *(Received February 19, 1969)*

Experimental $P-V-T$ data of fluid argon are presented. Most of the data cover the volume range from 28 to 132 cm^3 in the range from 90 to 200°K and below 150 atm. Special attention is paid to the critical region. One isochore, however, is measured up to 2000 atm and in the high-density range. In the high-density range with molar volumes below 38 cm^3 a Tait-like equation of state is fitted to the data. In the range from 40 to 132 cm^3/mol, a new type of equation of state is proposed which fits the data through the critical point. It is shown that the latter equation is compatible with the power laws, and the exponents are derived. From these equations different thermodynamic properties are calculated.

Apparatus and Method

The apparatus used for this experiment is a modification of the equipment used with liquid hydrogen by Van Itterbeek, *et al.*[1] (See Figure 1.) The 99.996% purity gas is liquefied in a formerly evacuated high-pressure volume HP in a cryostat K. By means of thermal compression the experimental volume VM is filled through K1 to the desired pressure while K2 is closed. This pressure can be 2000 atm in one stroke, under the condition that VM has already been filled with liquid up to 150 atm at the desired final temperature. Care must be taken in order to avoid the melting curve and blocking of the capillary tubing CT. While pressurizing at pressures in excess of 200 atm, care must be taken of the differential gauge DM since the pressure difference across the membrane may not exceed 200 atm. Subsequently, valve K1 will be closed and by changing the temperature in cryostat K and measuring pressure and temperature, pseudo-isochores can be determined.

The quantity of gas can be determined by subsequent expansion of the fluid at room temperature and at 1 atm in the so-called expansion volumes VE1 and VE2 while measuring temperature of thermostat T and of the pressure by means of the oil-differential gauge D and the mercury gauge M.

Temperature measurement in the experimental

---

[1] A. Van Itterbeek, O. Verbeke, F. Theeuwes, and V. Jansoone, *Physica*, **32**, 1591 (1966).

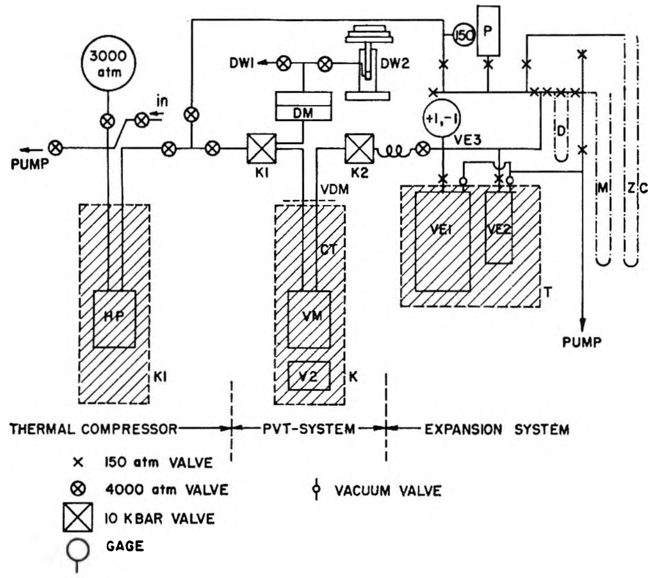

Figure 1. Schematic drawing of the apparatus.

volume VM is carried out by means of a Tinsley thermometer calibrated at N.P.L. (England). Absolute accuracy of the temperature determination is about 0.003°K but reproducibility of the readings is 0.001°K. The temperature regulating system and the cryostat have been described by Verbeke, *et al.*[2] The differential gauge has been described by Van Itterbeek, *et al.*,[3] but has been modified since then in order to allow overpressurization of the membrane by about 200 atm without shifts of its zero position of more than 0.02 atm. The modified differential gauge is shown in Figure 2. Since the determination of the change in equilibrium position is carried out in a capacitive way, on the oil-side it was necessary to account for the change in dielectricity constant by means of an external variable condensor. Zero calibration as a function of pressure is carried out before and after each run by means of a mercury gauge at about 3 atm. Zero shifts of more than 0.010 atm have never been detected.

Pressure is measured by means of two pressure balances, one in the 300-atm range (Barnett Co., England and one in the 3000-atm range (Hart, The Netherlands). We estimate the final reproducibility and the accuracy of the pressure readings to be better than 0.01 atm in the 150-atm range. At the higher pressures the reproducibility and accuracy are much dependent on the differential gauge and no clear relation between reproducibility and pressure can be given, but we expect the error in pressure to be no more than 0.3 atm at 2000 atm.

Corrections

Special attention is paid to corrections on the readings due to expansion of the volume VM, the fluid contained in the capillary tubing CT and in the differential gauge and connections at room temperature, VDM, and the hydrostatic pressure head in capillary tube CT.

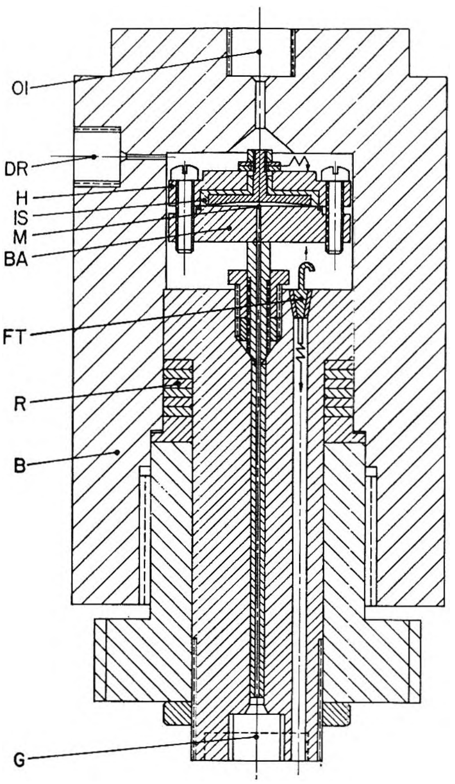

Figure 2. The differential gauge.

From the readings of temperature on the platinum thermometer, pressure from the pressure balances, and the expanded quantity of fluid mass, the temperature and pressure in VM and the molar volume are computed. In the program, pressure and temperature dependence of VM, a subroutine for an approximate equation of state of argon, the thermal conductivity integrals for the material of the capillary tube (AIS1 316) and all dimensions necessary to calculate P, the pressure in VM, and V, the molar volume at pressure P and temperature T, were included. The different values of the volumes and their pressure and temperature dependence are listed in Table I. The correction for the gas in DM and leads at room temperature was much more important than the correction for the fluid in the capillary tube. Maximum values for the gas correction, the fluid correction, and the hydrostatic head are given in Table II.

Extension of Earlier Measurements on the Vapor Pressure Curve. Values of the vapor pressure curve additional to those determined in a former publication by Van Itterbeek, *et al.*,[4] were determined. These values

---

(2) O. Verbeke, A. Van Itterbeek, P. Dirven, and J. De Boelpaep, Supplement an Bulletin de l'Institut international du Froid, Commission 1, Boulder, Colo., 1966.

(3) A. Van Itterbeek, F. Theeuwes, O. Verbeke, and K. Staes, *Cryogenics*, **6**, 85 (1965).

(4) A. Van Itterbeek, J. De Boelpaep, O. Verbeke, F. Theeuwes, and K. Staes, *Physica*, **30**, 2119 (1964).

Table I: Dimensions and Temperature and Pressure Dependence of the Volumes of the Apparatus

Symbo	Explanation	Value (cm^3 or cm)[a]
VM	Experimental volume for the 150-atm range	$0.57424 \times 10^2 + 0.74213 \times 10^{-5}T^2 + 0.2925 \times 10^{-3}P + 0.1052 \times 10^{-6}PT$
	Experimental volume for the 3000-atm range	$0.16847 \times 10^2 + 0.180 \times 10^{-5}T^2 + 0.254 \times 10^{-4}P + 0.108 \times 10^{-7}PT$
VE1	First expansion volume	0.10200×10^6
VE2	Second expansion volume	0.19923×10^4
VE3	Volume of valves and leads to the expansion volume	0.22×10^2
CT	Volume of the capillary tube	0.4002×10^{-1}
CTL	Length of the capillary tube	0.96×10^2
VDM	Dead volume of DM, valves and capillary tubing at room temperature	0.958

[a] P is in kg cm^{-2}; T is in °K.

Table II: Maximum Value for Different Corrections in the 150-Atm Range and Corresponding Pressure and Temperature of VM

Correction	Max value	T, °K	P, atm
Gas	0.2437	. . .	153
Fluid	0.305×10^{-1} g	91.999	152.6
Hydrostatic pressure head	0.810×10^{-1} atm	91.999	152.6

Table III: Vapor Pressure Curve near the Critical Point

T, °K	P, atm
149.780	46.335
150.773	48.166
150.653	47.936
150.499	47.644
149.227	45.360
149.911	46.577
149.434	45.715
150.206	47.108
150.639	47.912

Table IV: Density of Argon on the Vapor Tension Curve (Graphical Determination of Intersection Point of Isochores and Vapor Pressure Curve)

T, °K	ρ, mol/cm^3	T, °K	ρ, mol/cm^3
87.02	0.035031	148.80	0.018635
91.02	0.034431	149.21	0.018150
96.55	0.033541	149.57	0.017668
102.06	0.032613	149.85	0.017220
107.30	0.031682	150.08	0.016779
112.37	0.030705	150.31	0.016260
116.90	0.029800	150.40 ± 0.03	0.015773
121.30	0.028868	150.50 ± 0.03	0.015307
125.41	0.027928	150.55 ± 0.04	0.014841
129.58	0.026943	150.66 ± 0.07	0.014324
133.50	0.025797	150.65 ± 0.07	0.012459
136.97	0.024718		
140.00	0.023596		
142.81	0.022498		
145.13	0.021349		
147.12	0.020114		

are listed in Table III. The molar volume along the vapor pressure curve is shown in Table IV. They are determined by graphical determination of the intersection points of the isochores with the vapor pressure curve. Near the critical point, a special graph was used in which $P_{\text{exp}} - P_0(T)$ was drawn as a function of temperature. $P_0(T)$ is a straight line which was estimated to be very near the tangential to the vapor tension curve in the critical point.

$$P_0(T) = -241.0918 + 1.918465T \qquad (1)$$

The actual graph itself is shown in Figure 3.

PVT Data on Argon. The distribution of the experimental points in a P–T diagram is shown in Figure 4. About 100 of these points cluster together in the neighborhood of the critical point and are shown in Figure 3. The experimental data are tabulated in Table V. The determination of each point took about 1.5 hr owing to the time needed to reach equilibrium.

To illustrate the curvatures in the isochores, basic to the behavior of C_v, their deviation curves from the tangentials to the isochores at the vapor pressure are given in Figure 5.

Analysis of the Data in the High-Density Range. Thermodynamic quantities can be obtained from an

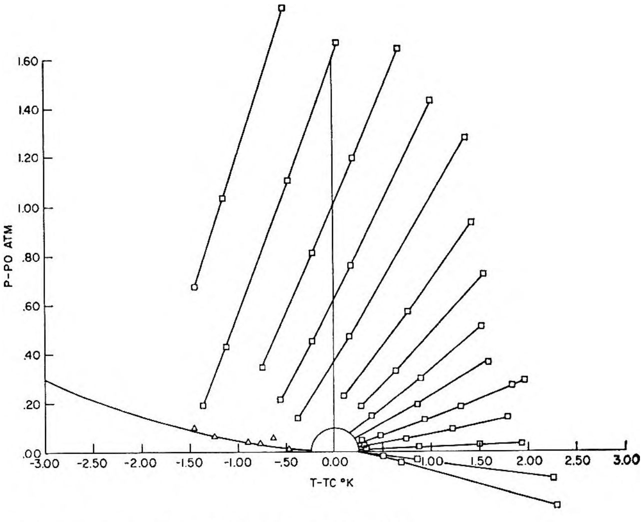

Figure 3. $P - P_0$ as a function of $T - T_c$.

Table V: Experimental Data for Argon

T, °K	P, atm	V, cm³/mol	T, °K	P, atm	V, cm³/mol	T, °K	P, atm	V, cm³/mol	T, °K	P, atm	V, cm³/mol
174.356	92.935	75.8877	112.580	10.270	32.5709	153.805	76.141	46.9300	152.095	51.579	61.4349
163.469	72.201	75.7514	114.823	36.660	32.6017	158.653	97.486	46.9816	150.774	48.394	61.4216
147.349	42.233	75.5576[a]	116.244	53.276	32.6201	162.243	113.375	47.0197	151.439	49.985	61.4280
137.778	28.414	75.4643[a]	118.551	80.059	32.6498	168.849	142.612	47.0908	151.309	49.509	63.3175
140.436	31.845	75.4884[a]	121.107	109.387	32.6819	169.008	125.725	49.9462	150.950	48.681	63.3140
143.863	36.706	75.5209[a]	123.386	135.344	32.7102	147.684	43.882	49.7221	152.224	51.607	63.3271
150.047	46.857	75.5879[a]	124.533	148.264	32.7245	150.758	55.296	49.7529	152.196	51.336	65.2527
157.467	60.890	75.6783	124.504	147.929	32.7242	155.494	73.273	49.8024	150.689	48.046	65.2372
168.730	82.182	75.8170	124.519	91.360	33.6532	161.002	94.537	49.8608	151.061	48.848	65.2409
182.843	109.011	75.9945	117.945	21.309	33.5701	165.275	111.143	49.9061	151.565	49.940	65.2459
202.291	145.687	76.2479	117.168	12.981	33.5595	173.558	143.483	49.9959	151.536	49.787	67.2906
202.367	134.707	83.2102	119.704	40.203	33.5929	173.871	128.565	53.4645	150.703	48.059	67.2821
195.315	123.040	83.1142	121.489	59.277	33.6155	150.076	48.788	53.2116	150.763	48.182	67.2827
186.648	108.635	82.9965	123.049	75.857	33.6351	154.536	63.247	53.2587	152.263	51.322	67.2985
179.351	96.472	82.8995	126.620	113.348	33.6789	159.513	79.816	53.3101	152.511	51.703	69.7251
170.640	81.846	82.7835	128.643	134.384	33.7034	165.040	98.485	53.3693	151.975	50.611	69.7190
161.702	66.788	82.6688	129.983	148.223	33.7196	170.481	116.993	53.4277	151.150	48.940	69.7101
158.168	60.802	82.6198	129.892	96.168	34.7473	178.431	144.116	53.5153	150.839	48.312	69.7068
151.882	50.093	82.5365	123.099	30.563	34.6643	177.849	128.360	57.4577	150.773	48.166	69.7061[a]
151.990	49.977	90.9884	121.621	16.095	34.6451	151.819	51.935	57.1754	150.653	47.936	69.7049[a]
157.587	58.460	91.0676	124.963	48.741	34.6875	156.995	66.650	57.2315	150.499	47.644	69.7033[a]
164.529	68.769	91.1664	126.722	65.756	34.7098	162.504	82.765	57.2893	149.227	45.360	69.6911[a]
172.505	80.483	91.2773	128.161	79.575	34.7264	167.020	96.101	57.3384	149.911	46.577	69.6976[a]
180.477	92.048	91.3895	131.347	110.069	34.7646	171.766	110.209	57.3902	149.434	45.715	69.6930[a]
190.274	106.242	91.5290	132.991	125.661	34.7841	183.821	145.910	57.5253	150.206	47.108	69.7004[a]
192.436	100.887	102.2495	134.406	139.111	34.8008	183.701	132.720	62.2147	150.752	48.133	69.7059
186.127	93.039	102.1508	134.181	93.283	35.9112	152.289	51.964	61.8627	150.802	48.232	69.7064
173.510	77.257	101.9575	125.464	16.508	35.8061	156.616	62.658	61.9107	150.839	48.305	69.7068
162.058	62.679	101.7868	126.255	23.554	35.8162	161.578	75.256	61.9640	150.951	48.539	69.7080
156.313	55.233	101.6956	128.053	39.473	35.8382	169.331	95.245	62.0509	151.603	49.850	69.7148
156.503	53.745	114.6036	130.484	60.875	35.8676	177.964	117.644	62.1486	152.640	51.958	69.7265
159.970	57.632	114.6617	132.775	80.988	35.8947	189.667	148.093	62.2841	152.467	51.488	72.0128
166.605	64.974	114.7795	132.851	81.703	35.8956	189.133	130.511	69.6859	151.893	50.357	72.0061
176.190	75.340	114.9315	134.955	100.274	35.9207	153.191	53.134	69.2587	151.415	49.421	72.0008
186.193	85.994	115.0980	137.276	120.228	35.9474	160.266	68.119	69.3419	150.992	48.594	71.9962
196.343	96.694	115.2707	140.290	146.195	35.9829	168.676	86.221	69.4394	150.639	47.912	71.9924[a]
197.184	87.832	132.7366	140.324	104.438	37.3190	175.145	100.229	69.5171	150.711	48.051	71.9932
180.617	73.273	132.4271	131.433	34.339	37.2161	181.439	113.897	69.5925	150.742	48.109	71.9935
166.339	60.389	132.1633	130.090	23.676	37.1999	195.971	145.208	69.7718	150.973	48.554	71.9960
153.993	48.925	131.9349	132.835	45.427	37.2327	194.477	118.829	85.3870	150.830	48.281	71.9944
91.172	133.423	28.2625	135.405	65.760	37.2633	177.810	92.186	85.1594	150.998	48.592	74.4225
91.337	136.068	28.2646	137.759	84.307	37.2897	185.254	104.125	85.2601	150.929	48.459	74.4217
91.999	147.793	28.2742	141.045	110.089	37.3273	94.205	127.379	28.6542	150.823	48.248	74.4205
91.121	3.033	29.0449	143.244	127.243	37.3523	87.077	2.089	28.5471	150.825	48.256	74.4205
92.066	19.051	29.0607	145.591	145.479	37.3795	88.032	18.862	28.5632	150.750	48.125	74.4197
93.813	48.441	29.0868	145.714	109.464	38.9025	88.701	31.012	28.5738	150.807	48.224	74.4203
95.551	77.484	29.1120	133.973	26.747	38.7694	89.209	40.044	28.5814	150.774	48.174	74.4200
96.662	95.012	29.1271	135.815	39.774	38.7905	89.714	49.033	28.5891	150.795	38.202	74.4202
96.770	97.679	29.1294	137.948	54.777	38.8149	89.200	40.075	28.5814	150.789	48.202	74.4202
98.194	120.763	29.1492	140.704	74.178	38.8462	89.192	39.993	28.5814	151.523	49.576	74.4283
99.595	143.531	29.1689	143.384	93.076	38.8764	89.280	38.840	28.5805	152.177	50.827	74.4360
96.787	6.271	29.8180	148.380	127.980	38.9321	89.996	54.107	28.5933	152.608	51.641	74.4411
97.173	12.309	29.8243	150.400	142.044	38.9548	87.134	3.047	28.5482	151.547	49.635	74.4286
98.388	31.340	29.8427	150.217	110.490	40.6020	88.219	22.366	28.5664	151.557	49.600	77.3740
99.439	47.441	29.8577	139.774	44.946	40.4871	91.074	73.220	28.6093	151.167	48.885	77.3695
99.453	47.585	29.8578	136.952	27.398	40.4553[a]	92.791	103.323	28.6344	150.849	48.299	77.3657
99.455	47.590	29.8578	137.252	29.164	40.4585	93.656	118.384	28.6467	150.712	48.053	77.3642
100.833	68.735	29.8773	142.012	59.006	40.5116	94.796	137.733	28.6627	150.810	48.227	77.3653
102.262	90.485	29.8970	145.193	78.978	40.5468	150.797	50.824	53.6173	150.840	48.290	77.3657
103.290	105.822	29.9109	148.269	98.284	40.5808	150.760	50.680	53.6169	150.907	48.408	77.3664
103.316	106.383	29.9114	153.574	131.481	40.6388	149.529	46.869	53.6051	152.181	50.759	77.3817
104.886	129.768	29.9325	156.456	149.354	40.6690	150.158	48.825	53.6110	152.927	52.096	77.3908
106.116	148.035	29.9492	156.733	123.768	42.5606	149.228	45.934	53.6022	152.960	52.029	80.1533
106.196	62.227	30.7241	140.892	35.595	42.3891	150.725	49.750	55.0444	151.360	49.205	80.1332
102.215	6.055	30.6672	143.330	49.040	42.4153	149.307	45.600	55.0309	150.807	48.219	80.1265
102.810	14.645	30.6766	145.867	63.153	42.4436	149.554	46.304	55.0332	150.796	48.193	80.1264
104.150	33.552	30.6959	148.918	80.130	42.4760	150.206	48.202	55.0394	150.715	48.049	80.1254
107.454	79.892	30.7410	153.392	105.126	42.5244	151.350	51.595	55.0507	150.929	48.433	80.1280
108.274	91.115	30.7519	159.928	141.548	42.5953	151.362	51.644	55.0508	150.844	48.275	80.1269
109.178	103.452	30.7637	159.782	119.128	44.6289	151.355	50.901	56.5503	150.803	48.221	80.1265
110.847	126.207	30.7856	143.605	39.082	44.4561	149.925	46.913	56.5365	150.811	48.226	80.1266
112.462	148.239	30.8069	145.728	49.445	44.4786	150.874	49.546	56.5455	150.816	48.244	80.1267
112.443	147.941	30.8066	149.195	66.494	44.5167	150.457	48.380	56.5415	150.862	48.315	80.1272
112.381	70.803	31.6340	153.257	86.613	44.5589	150.449	48.005	58.0027	151.724	49.848	80.1376
107.438	7.193	31.5662	157.486	107.663	44.6042	149.780	46.335	57.9966[a]	124.85	1415.8	26.803[b]
108.078	15.504	31.5758	163.541	137.983	44.6694	150.116	47.143	57.9996	139.28	1701.0	26.868[b]
110.209	43.130	31.6054	165.893	149.498	44.6940	150.850	49.066	58.0066	153.67	1972.2	26.928[b]
115.248	107.044	31.6712	165.968	129.889	47.0595	151.691	51.320	58.0150	162.69	2135.7	26.964[b]
122.604	126.574	32.7007	145.678	40.963	46.8448	150.835	48.753	59.5272	172.01	2298.6	26.997[b]
113.730	23.741	32.5870	149.355	56.746	46.8830	150.297	47.408	59.5221	130.52	1528.5	26.832[b]
						152.039	51.814	59.5393			

[a] These data are on the vapor pressure curve. [b] Partial high-pressure data.

Table VI: Constants, Root-Mean-Square Error, and Maximal Error for Eq 3 (Argon)

Constant	Value	Errors
V_1	29.500	$\sqrt{\frac{\Sigma\Delta V_i^2}{N}} = 0.029$
P_{00}	$-0.16687370E + 04$	
P_{01}	$0.17741882E + 02$	
A_0	$-0.18415472E + 01$	
A_1	$-0.14207086E - 02$	
A_2	$-0.32813317E - 03$	$\lvert\Delta V_{max}\rvert = 0.0923$ cm^3/mol
B_0	$0.11975025E + 04$	at $P = 113.375$ atm
B_1	$-0.12803259E + 02$	and $T = 162.243$ °K
B_2	$0.30093923E - 01$	

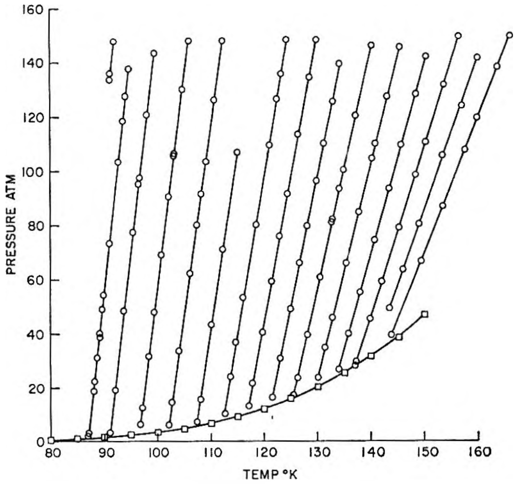

Figure 4. Distribution of the points of region A in the P–T diagram.

Table VII: Constants A_{ij}, Root-Mean-Square Error, and Maximal Error for Eq 2 (Argon), $n = 4$ ($T_0 = 90$°K)[a]

i/j	0	1	2	3	4
0	$-0.75900238E - 02$	$0.71584393E - 03$	$-0.75196106E - 05$	$0.20306236E - 07$	$-0.65710489E - 10$
1	$-0.12717845E - 01$	$0.16048266E - 04$	$0.55845763E - 06$	$0.34423535E - 08$	$-0.39070570E - 10$
2	$0.15295170E - 02$	$-0.10201680E - 05$	$-0.29457961E - 06$	$0.27616452E - 08$	$-0.66056574E - 11$
3	$-0.65689337E - 04$	$0.55700661E - 06$	$0.63552902E - 08$	$-0.99358067E - 10$	$0.30689139E - 12$
4	$0.86843559E - 06$	$-0.13887073E - 07$	$0.34276596E - 10$	$0.53428864E - 12$	$-0.24061742E - 14$

[a] Errors: $\Sigma(\Delta V_i^2)/N = 0.0078$ cm^3/mol; $\lvert\Delta V_{max}\rvert = 0.023$ cm^3/mol at $P = 66.494$ atm, $T = 149.195$°K.

equation of state either by interpolation methods (graphical or mathematical) or from an analytical expression fitted to the data. The latter approach is followed in this publication. For the high-density range, limited to the isochores shown in Figure 4, an analytical expression described by Verbeke, *et al.*,[5] was used in order to determine different derivatives and the thermodynamic quantities

$$V = V_1 + (A_0 + A_1T + A_2T^2) \times \log\frac{B_{00} + B_{11}T + B_{22}T^2 + P}{B_{00} + B_{11}T + B_{22}T^2 + P_{00} + P_{01}T} + \sum_{=0}^{n}\ \sum_{i=0}^{n} A_{ij}(T - T_0)\,P_j \quad (2)$$

The constants, the root-mean-square error, and the maximal error for the first part of eq 2

$$V = V_1 + (A_0 + A_1T + A_2T^2) \times \log\frac{B_{00} + B_{11}T + B_{22}T^2 + P}{B_{00} + B_{11}T + B_{22}T^2 + P_{00} + P_{01}T} \quad (3)$$

are given in Table VI.

The constants A_{ij} in the case where $n = 4$ and the corresponding errors are tabulated in Table VII and for the case where $n = 5$ in Table VIII.

Analysis of the Data in the Critical Region. Since $\delta V/\delta P_T{}'$, as calculated from eq 3, is infinite in all the points in the P–T diagram corresponding to

$$P = -(B_{00} + B_{11}T + B_{22}T^2)$$

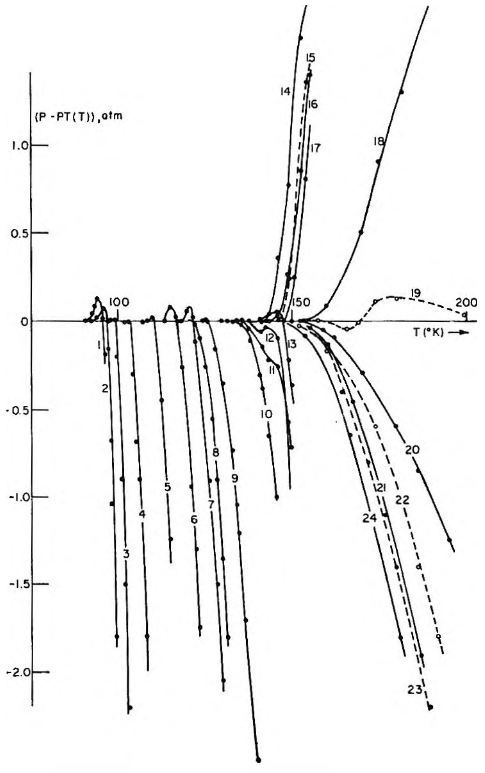

Figure 5. Deviated pressure curves of isochores from the tangentials to the isochores at the vapor pressures.

---

(5) O. Verbeke, A. Van Itterbeek, V. Jansoone, F. Theeuwes, and J. De Boelpaep, Communications of the "Kon VI. Academie voor Wetenschappen" 28, 2 (1966).

Table VIII: Constants A_{ij}, Root-Mean-Square Error, and Maximal Error for Eq 2 (Argon), $n = 5$ ($T = 90$°K)[a]

i/j	0	1	2	3	4	5
0	$0.26873287E - 03$	$0.21366147E - 02$	$-0.11776210E - 03$	$0.24884925E - 05$	$-0.20481240E - 07$	$0.56155933E - 10$
1	$-0.11270204E - 01$	$-0.22261861E - 04$	$0.13674242E - 04$	$-0.46191754E - 06$	$0.46019095E - 08$	$-0.14084985E - 10$
2	$0.59032223E - 03$	$-0.11115187E - 04$	$0.65690172E - 07$	$0.18410739E - 07$	$-0.25540331E - 09$	$0.88886116E - 12$
3	$0.26064731E - 04$	$-0.48390853E - 07$	$-0.32864666E - 07$	$-0.11876686E - 11$	$0.45132522E - 11$	$-0.20808169E - 13$
4	$-0.21419079E - 05$	$0.41665353E - 07$	$0.52575284E - 09$	$-0.71732554E - 11$	$-0.84347443E - 14$	$0.16726970E - 15$
5	$0.31823553E - 07$	$-0.85634203E - 09$	$0.29778178E - 11$	$0.35600057E - 13$	$-0.13325317E - 15$	$-0.30525966E - 18$

[a] Errors: $\Sigma(\Delta V_i^2)/N = 0.0062$ cm^3/mol, $\Delta V_{max} = 0.0159$ cm^3/mol at $P = 149.195$ atm and $T = 66.494$ °K.

a more suitable PVT relation is needed in that region.

Recently, much work has been carried out on critical phenomena.[6-10] One of the important results is the fact that one should be able to describe the deviations of different quantities from their value at the critical point or the quantities themselves by simple laws involving only two constants of the forms

$$|A_i| \text{ or } |A_i - A_{ic}| = C_i|T - T_c|^{\pm\epsilon_i}$$

or

$$|A_i| \text{ or } |A_i' - A_{ic}'| = C_i'|\rho - \rho_c|^{\pm\epsilon_i'}$$

The laws which represent a similar behavior are often referred to as power laws and people are inclined to believe that the exponents ϵ_i should be identical for the corresponding quantities of critical phenomena as different as for instance superfluidity, ferromagnetism, binary mixtures and, in this case, the vapor–liquid transition.

Important in connection to our data are, for instance, the temperature dependence of $|\rho_s - \rho_m|$, the difference of the saturated density and the mean value of the coexisting densities of liquid and gas; K_{TS}, the isothermal compressibility along the vapor pressure curve; K_{TC}, the isothermal compressibility along the critical isochore, $\delta^2P_s/\partial T^2{}_s$, the second derivative of the vapor pressure with respect to temperature; C_{VC}, the specific heat along the critical isochore, and C_{VS}, the specific heat along the vapor pressure curve in the single phases.

Also important is the pressure dependence of $|\rho - \rho_c|$, the difference of the density and the critical density along the critical isotherm.

The exponents corresponding to these quantities and their estimated magnitude are given in Table IX.[8]

In this way, limiting ourselves to the critical region, we tried to develop an equation with the following features: 1, small number of constants; 2, covering the obvious features of the isochoric behavior near the critical point as visible on Figures 3 and 5; 3, implicating what could be called the scaling laws and the nonanalytic behavior near the critical point; and 4, presenting no contradiction when extrapolating the equations so that further extensions are possible. The equation presented here has the form

$$P = P_S(T_S(\rho)) + B(\rho)(T - T_S(\rho)) + A\rho \frac{\rho - \rho_t}{|\rho - \rho_t|} |\rho - \rho_t|^{\lambda}\{[T + T_C - 2T_s(\rho)]^{1+\mu} - [T_c - T_s(\rho)]^{1+\mu}\} \quad (4)$$

---

(6) H. W. Habgood and W. G. Schneider, *Can. J. Chem.*, **32,** 98 (1954).

(7) E. F. Carome, C. B. Cybowski, J. F. Havlice, and P. A. Swyk, *Physica*, **38,** 307 (1968).

(8) P. Heller, *Progr. Phys.*, **30,** 731 (1967).

(9) R. B. Griffiths, *Phys. Rev. Letters*, **14,** 623 (1965).

(10) M. Vincentini-Missoni, J. M. H. Levelt-Sengers, M. S. Green, *ibid.*, **22,** 389 (1969).

Table IX: Exponents for the Power Laws as Given by the Literature

Quantity A_i or A_i'	Notation for exponent	Sign of exponent	Estimated value	Last known value (Wilcox)
General form: $\lvert A_i\rvert \propto \lvert T - T_C\rvert^{\pm\epsilon_i}$				
$\rho_S - \rho_m$	β	+	0.33–0.36	0.343 ± 0.003
K_{TS}	γ'	−	$\geqslant 1.2$	
K_{TC}	γ	−	>1.1	1.29 ± 0.07
$\left[\dfrac{d^2P_S}{dT_S^2}\right]$	α^*	−	$\geqslant 0$	
C_{VS}	α	−	$0 \leqslant \alpha \leqslant \cdot 2$	0.04 ± 0.04
C_{VC}	α'	−	$\geqslant 0$ (log)	
General form $\lvert A_i'\rvert \propto \lvert\rho - \rho_c\rvert^{\pm\epsilon_i'}$				
$P - P_C$	δ	+	$3.5 \longleftrightarrow 5$	4.76

where P is the pressure in atmospheres, T is the temperature in °K, ρ is the density in mol/cm^3, P_s is the vapor pressure, $T_s(\rho)$ is the intersection temperature of an isochore of density ρ with the vapor pressure curve, ρ_c is the critical density, and $\rho_m(T_s)$ is the mean of the saturated densities of the gas and the liquid at temperature T_s. The relationships $T_s(\rho)$, $\rho_m(T_s)$, $P_s(T_s)$, and $B(\rho)$ have to be defined and are given by

$$T_s = T_c - [C|\rho - \rho_m|]^{1/\beta} \tag{5}$$

where T_c is the critical temperature

$$P_s = P_{s0} + P_{s1}T_s + (T_c - T_s)^{\omega}P_{s2} \tag{6}$$

with $\omega = \beta\lambda + 1 + \mu$.

$$\rho_m = \rho_c - (T_s - T_c)\rho_{m1} = \rho_c + [C|\rho - \rho_m|]^{1/\beta}\rho_{m1} \tag{7}$$

$$B = B_0 + B_1(\rho - \rho_m)|\rho - \rho_m|^{\kappa} + B_2(\rho - \rho_m)^3 + B_3(\rho - \rho_m)^4 + B_4(\rho - \rho_m)^5 \tag{8}$$

with $\kappa = \lambda - 1 + \mu/\beta$ and

$$\rho_t = \rho_m + \rho_{t0}|T - T_s|^{\beta} \tag{9}$$

Since power law behavior is required from the equation, B_0 must be equal to P_{s1}

Equation 4 as described here is consistent with all scaling laws and will consequently be used for the analysis of data near the critical point and for the determination of the critical exponents. This version will be called eq 4, version 1.

In a wider range $B(\rho)$ and $\rho_t(T,\rho)$ as given by eq 8 and 9 are not very suitable, especially not the term with $|\rho - \rho_m|^{\kappa}$. Equations 8 and 9 are then replaced by

$$B = B_0 + B_1(\rho - \rho_m) + B_2(\rho - \rho_m)^2 + B_3(\rho - \rho_m)^3 + B_4(\rho - \rho_m)^4 \tag{8'}$$

and

$$\rho_t = \rho_m - \rho_{t1}(T - T_s)^2 + \rho_{t2}(T - T_s)^3 \tag{9'}$$

This version of eq 4 will be called eq 4, version 2. A schematic survey of the equation is given by Table X.

In fact, eq 4 yields P as a function of the two independent variables ρ and T. It consists of three parts. The first part gives the vapor pressure corresponding to the density ρ; the second part gives the bulk of the slope of the isochore of density ρ times $T - T_s$; the last part gives the curvature of the isochores and part of their slope near the vapor pressure curve. Equation 7 is not solvable for ρ_m and iterations have to be used in order to determine ρ_m. This iteration can be carried out by replacing ρ_m, in the right side of the equation, by using ρ_c as a first approximation.

Equation 8 is a very crude expression which possibly can be modified and even simplified in order to meet more strict requirements (as for instance experiments with lower experimental errors or expansion of the range of the experiments).

Application of the Equation on Argon. The constants of the two versions for eq 4, 5, 6, and 8 are given in Table XI together with the root-mean-square error and the maximum error. Version 2 applies to the whole range B (Figure 6) and version 1 applies to 100 data points in the immediate vicinity of the critical point (Figure 3).

Application of the Equation to the Data of Habgood and Schneider.[6] These authors claim an accuracy of 0.002°K on the temperature and 0.002 atm on the pressure. They have measured isotherms (86 data points) and isochores (196 data points). The isochoric data were used to approximate the constants of eq 4, version 1, and the results, with inclusion of the errors, are given in Table XII. The error is remarkably low.

When applying the resulting equation on the isotherms of the same author, slightly higher errors are obtained ($\Sigma(\Delta P_i)^2/N = 0.0043$ atm and $|\Delta P|_{\max} = 0.011$ atm at $T = 289.735$°K and $P = 57.713$ atm). This in-

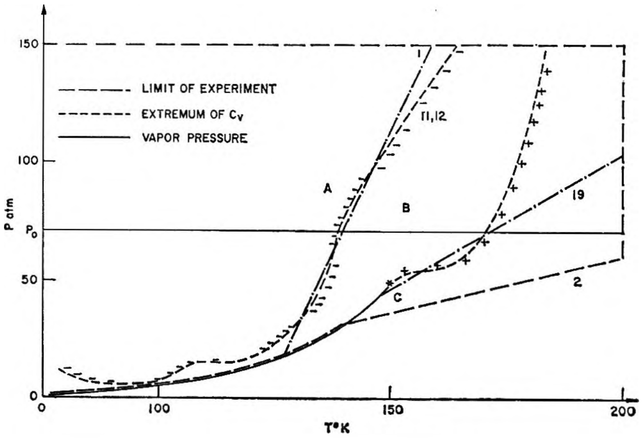

Figure 6. Division of the P–T diagram for the application of eq 2 (A) and 4 (B). Behavior of C_v (+ for maximum, − for minimum).

Table X: Equation of State Near the Critical Point[a]

$P_S(T_S)$

$$P_S = P_{S0} + P_{S1}\underline{T_S} + (T_O - \underline{T_S})^{\omega}P_{S2} \text{ with } \omega = \beta\lambda + 1 + \mu \qquad \underline{T_S} = T_C - [C|\rho - \rho_m|]^{1/\beta}$$

$+ B(\rho)(T - T_S)$

$$B = B_0 + B_1(\rho - \rho_m)|\rho - \rho_m|^{\kappa} + B_2(\rho - \underline{\rho_m})^3 + B_3(\rho - \rho_m)^4 \qquad \underline{\rho_m} = \rho_C + [C|\rho - \rho_m|]^{1/\beta}\rho_{m1}$$

$$+B_4(\rho - \rho_m)^5 \text{ (version 1)}$$

$$\text{with } \kappa = \lambda - 1 + \frac{\mu}{\beta} \qquad P_{S1} = B_0$$

or

$$B = B_0 + B_1(\rho - \rho_m) + B_2(\rho - \rho_m)^3 + B_3(\rho - \rho_m)^2 + B_4(\rho - \rho_m)^4$$

version 2)

$$+ A\rho\frac{\rho - \rho_t}{|\rho - \rho_t|}|\rho - \rho_t|^{\lambda} \times \qquad \rho_t = \rho_m + \rho_{t0}(T - T_S)^{\beta} - \rho_{t1}(T - T_S)^2 + \rho_{t2}(T - T_S)^3$$

$$\{[T + T_C - 2T_S]^{1+\mu} - [T_C - T_S]^{1+\mu}\} \qquad \text{With} \begin{cases} \rho_{t1} = \rho_{t2} = 0 \\ \text{(version 1)} \\ \rho_{t0} = 0 \text{ (version 2)} \end{cases}$$

||

P

Extrinsic constants	Number of constants
P_{S0}, P_{S2} for vapor pressure curve	2
C, β, ρ_{m1} for density on vapor pressure curve	3
ρ_C, T_C critical parameters	2
Intrinsic constants	
B_0, B_1, B_2, B_3, B_4	5
ρ_{t1}, ρ_{t2} or ρ_{t0}	1 or 2
A, λ, μ	3

[a] Note: β, λ, μ, will be used for the determination of the exponents of the scaling equation.

Table XI: Constants of the Two Versions of Eq 4 (Argon)

Constant	Version 1 100 data points	Version 2 165 data points	Errors
P_{S0}	$-0.23190965E + 03$	$-0.23988877E + 03$	Version 1:
			$\sqrt{\frac{\Sigma(\Delta P_i^2)}{N}} = 0.0058$ atm
P_{S2}	$-0.29339334E + 00$	$-0.19322434E - 01$	
C	$0.28278334E + 03$	$0.26695619E + 03$	$\lvert\Delta P_{max}\rvert = 0.017$ atm
β	$0.24185447E + 00$	$0.41048025E + 00$	
ρ_{m1}	$0.23233912E - 03$	$-0.10775245E - 04$	at $\rho = 0.01863$ mol/cm^3
ρ_C	$0.12742505E - 01$	$0.13289408E - 01$	and $T = 150.760$°K
T_C	$0.15062575E + 03$	$0.15100651E + 03$	
B_0	$0.18575542E + 01$	$0.19104314E + 01$	Version 2:
B_1	$0.20942681E + 06$	$0.10810675E + 03$	
			$\sqrt{\frac{\Sigma(\Delta P_i^2)}{N}} = 0.062$ atm
B_2	$-0.38247378E + 08$	$0.42450496E + 05$	
B_3	$0.88916376E + 10$	$0.41158392E + 06$	$\lvert\Delta P_{max}\rvert = 0.284$ atm
B_4	$-0.85042335E + 12$	$0.17671372E + 08$	
ρ_{t1}	0	$0.14729426E - 06$	at $\rho = 0.01738$ mol/cm^3
ρ_{t2}	0	$0.14937277E - 08$	
ρ_{t0}	$0.34451075E - 03$	0	$T = 183.821$ °K
A	$0.12314683E + 05$	$0.46190615E + 04$	
λ	$0.10737425E + 01$	$0.10331957E + 01$	$P = 145.910$ atm
μ	$0.28088459E + 00$	$0.17745256E + 00$	

Table XII: Constants of Version 1 of Eq 4 on the Isochores (All Data Points) of Xenon of Habgood and Schneider[8]

Constant		Constant		Errors
P_{s0}	$-0.28421922E + 03$	B_1	$0.19992770E + 04$	$\sqrt{\frac{\Sigma(\Delta P_i^2)}{N}} = 0.0024$ atm
P_{s2}	$0.46886764E - 01$	B_2	$0.64366998E + 06$	
		B_3	$0.66489489E + 09$	$\lvert\Delta P_{max}\rvert = 0.008$ atm
C	$0.49896403E + 03$	B_4	$0.56842250E + 11$	at $\rho = 0.00658$ mol/cm^3
β	$0.38017756E + 00$	ρ_ω	$-0.11855380E - 03$	and $T = 289.14$°K
ρ_{m1}	$0.61400000E - 04$	A	$0.51892559E + 04$	
ρ_C	$0.85338014E - 02$	λ	$0.91702329E + 00$	
T_C	$0.28976934E + 03$	μ	$0.27636974E + 00$	
B_0	$0.11798741E + 01$			

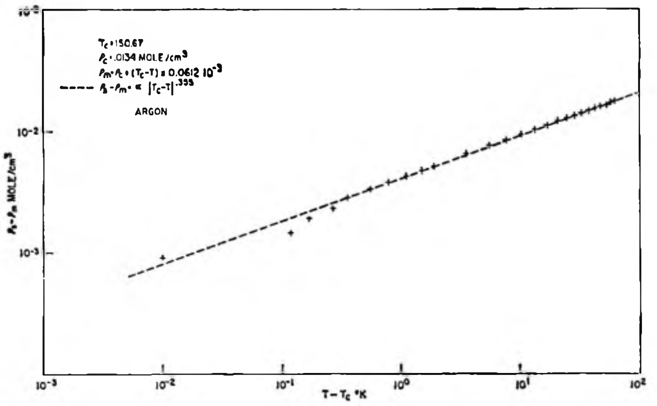

Figure 7. $\rho - \rho_m$ as a function of $T - T_0$ along the vapor pressure curve.

dicates a possible minor shift between the isotherms and the isochores.

Exponents of the Scaling Laws as Determined from the Equation. The exponents for the temperature dependence of

$$|\rho_s - \rho_m| \text{ and } \left(\frac{d^2P}{dT^2}\right)S$$

can be determined directly from eq 4 and 5, and 6 as being β and $2 - \omega$, respectively. The behavior for $\rho_s - \rho_m$ is shown in Figure 7. Expressions for the temperature dependence of C_{VS}, C_{VC}, K_{TS}, and K_{TC} can be derived from eq 4. It is clear, however, that some of these expressions do not give pure scaling laws since more than one term is involved; in the immediate neighborhood of the critical point these expressions simplify to the most important term.

$$K_{TC} \propto \left(\frac{\delta P}{\delta \rho}\right)_T^{-1} \propto |T - T_C|^{-\gamma};\ \gamma = \beta(\lambda - 1) + 1 + \mu$$

$$K_{TS} \propto |T - T_C|^{-\gamma};\ \gamma = \beta(\lambda - 1) + 1 + \mu$$

$$C_{VS} \propto |T - T_C|^{-\alpha};\ \alpha = -\left(\lambda + \frac{\mu - 1}{\beta} + 1\right)\beta$$

$$C_{VC} \propto |T - T_C|^{-\alpha};\ \alpha = -\left(\lambda + \frac{\mu - 1}{\beta} + 1\right)\beta$$

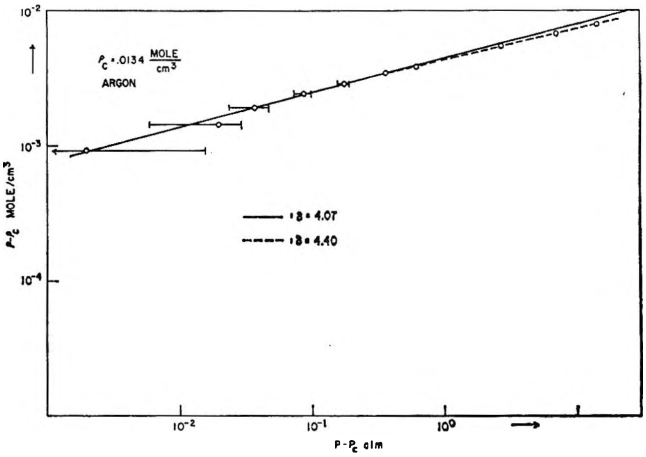

Figure 8. $\rho - \rho_0$ as a function of $P - P_0$ for points along the critical isotherm.

The pressure dependence of $\rho - \rho_c$ at the critical temperature (see Figure 8) is given by

$$p - p_0 \propto |\rho - \rho_0|^\delta;\ \delta = \lambda + \frac{1 + \mu}{\beta}$$

The specific heat at the critical temperature can also be calculated from eq 4. The calculation yields

$$C_{VTC} \propto |\rho - \rho_0|^\tau\ \ \tau = \left(\lambda + \frac{\mu - 1}{\beta} + 1\right)$$

(the specific heat along the critical isotherm) and

$$C_{VS} \propto C_{VC} \propto |T - T_c|^{-\alpha};\ \alpha = -\beta\left(\lambda + \frac{\mu - 1}{\beta} + 1\right)$$

A summary of all these results is given in Table XIII; also included in Table XIII is an internal check on the exponents of the scaling equation.

Conclusion

We can stress that the primary goals of the equation are obtained at least in version 1 of eq 4. This was only possible if certain requirements are fulfilled which can be summarized as follows. (1) The slope of the vapor pressure curve and the slope of the critical isochore near the

Table XIII: Comparison of Values of Exponents to Results of a Preliminary Calculation

				Result of Calculation		
			Relation imposed	Argon		Xenon
Notation	Sign	Value	by equation	Version 1	Version 2	ref 6
β	+	0.33–0.36	β	0.242	0.410	0.3802
γ'	−	$\geqslant 1.2$	$\beta(\lambda - 1) + 1 + \mu$	1.298	1.191	1.244
γ	−	$\geqslant 1.1$ (1.29)	$\beta(\lambda - 1) + 1 + \mu$	1.298	1.191	1.244
α^*	−	$\geqslant 0$	$-(\beta\lambda - 1 + \mu)$	0.46	0.399	0.375
α	−	$0 \leqslant \alpha \leqslant \cdot 2$	$-\left(\lambda + \frac{\mu - 1}{\beta} + 1\right)\beta$	0.242	−0.011	−0.005
α'	−	$\geqslant 0$	$-\left(\lambda + \frac{\mu - 1}{\beta} + 1\right)\beta$	0.242	−0.011	−0.005
δ	+	3.5–5(4.76)	$\lambda + \frac{1 + \mu}{\beta}$	6.30	3.904	4.274

Check on thermodynamic equalities

1. $\underline{\beta(\delta + 1)} = \beta\left(\lambda + \frac{1 + \mu}{\beta} + 1\right) = \beta\lambda + 1 + \mu + \beta = 2 - \alpha.$
2. $\underline{\gamma + 2\beta} = \beta\lambda - \beta + 1 + \mu + 2\beta = \beta\lambda + 1 + \mu + \beta = 2 - \alpha$

critical point must be identical ($P_{S1} = B_0$). (2) The line of maxima of C_v is not coinciding with the critical isochore ($\rho_t \neq \rho_c$). (3) $(\partial B/\partial \rho)_{\rho=\rho_c}$ and $(\partial^2 B/\partial \rho_t)_{\rho=\rho_c}$ are zero.

The results for the exponents in the case of argon may look poor especially when we compare β as determined from the densities on the vapor pressure curve (0.355) to the value obtained from the equation, version 1 (0.250). The reason for this is that for argon only the high-density side of the critical point has been investigated. By doing so, too much freedom is left for the constants describing the vapor pressure curve.

For version 2, the result is better (0.400) because here some data points at lower density have also been introduced in the calculations.

At this point, a few final remarks must be made. It turns out that λ is never much different from 1.0 (1.07 or 1.03 for argon and 0.92 for xenon); when λ is different from 1.0 some discontinuity is introduced for $(\partial P/\partial \rho)_T$ at the critical isochore. This must be avoided and, consequently, λ should be put equal to 1.0 in future calculations.

α^* obeys the relation: $\alpha^* = \alpha' + \beta$; this refers to the weak inequality, $\alpha^* < \alpha' + \beta$, put forward by Griffiths.[9] Independent tests have shown that, near T_c, α^* should become equal to α', and, consequently, rather obey the inequality, than obey the above equality. This point has recently been clarified theoretically by Vincentini-Missoni, *et al.*[10]

Acknowledgments. We wish to express our thanks to the Computer Science Center of the University of Maryland which granted us the use of the IBM 7094 Computer. We also thank the Computer Center of the University of Leuven, where the initial calculations (region A) were carried out (IBM 360). We are also indebted to ARPA for partial financing of the project. Dr. J. M. H. Sengers-Levelt pointed out several errors in the preprint for which we want to express our thanks.

Thermal Stabilities of Tungsten Oxyiodides

by Suresh K. Gupta

Lamp Research Laboratory, General Electric Co., Cleveland, Ohio 44112 *(Received February 24, 1969)*

A mass spectrometric and Knudsen effusion investigation of the W–O–I system at high temperatures has been conducted. Vaporization of solid WO_2I_2 has been observed to involve its partial dissociation to molecular iodine. Iodine pressures over solid WO_2I_2 in a Knudsen cell exhibit strong effusion orifice dependence. The enthalpy of WO_2I_2 vaporization = 45.2 ± 1.0 kcal/mol at 298°K has been derived. A decomposition reaction assumed as $WO_2I_2(s) = WO_2I(s) + {}^1/_2I_2(g)$ has given -136 ± 5 kcal/mol as $\Delta H_f°$ of solid WO_2I at 550°K. WOI_3 has been observed as a minor gaseous species over solid WO_2I_2 in an effusion cell. From our extensive study of the WO_2–I_2 reaction, -102.8 ± 2.0 kcal/mol and 90.1 ± 2.0 eu have been evaluated as $\Delta H_f°$ and $S°$, respectively, of $WO_2I_2(g)$ at 298°K.

Introduction

Thermodynamic studies of tungsten halogen chemistry are considered vital in view of the growing technological importance of tungsten as an important refractory metal. Such data are of significant theoretical value because of known similarities in the chemical behavior of group VIa elements of the periodic table.

Among oxyhalides, WOX_4 and WO_2X_2 have been established as the prominent tungsten(VI) compounds.[1] Lower oxidation state oxyhalides, WOX_3 and WOX_2, have also been reported.[1] However, most of these investigations have been restricted to fluorides, chlorides, and bromides. Recently, WO_2I_2 has been reported as a stable tungsten oxyiodide.[2,3] The present investigation has been prompted with a view to establish the existence of tungsten oxyiodides and to obtain their thermochemical stabilities using mass spectrometric and Knudsen effusion techniques.

During the course of the present work, a series of three papers on the W–O–I system have been published.[4–6] Comparisons of the results have been made wherever appropriate.

Experimental Section

A. Vapor Pressure Determination. An Ainsworth automatic recording semimicrobalance Model AU-2 with a sensitivity of 0.02 mg was used in Knudsen effusion vapor pressure work. The apparatus included a specially designed 2 in. i.d. and 14 in. long resistance furnace. A 7 in. long copper liner in the middle of the furnace provided a 3 in. long central constant-temperature zone. Voltage regulation with a Sola transformer and minimization of air convections through the furnace provided temperature stabilities of about 1°. A pressure of less than 10^{-5} Torr was maintained during the course of a run.

The effusion cell was supported on a molybdenum pan rest suspended by a 0.015-in. diameter molybdenum wire. Temperature of the cell was continuously measured on a dual pen strip-chart recorder using a calibrated Pt—Pt-Rh thermocouple. The thermocouple bead was positioned as near as possible without contact to the cell. In separate experiments, the reliability of this technique was verified by comparing temperatures from the thermocouple in contact with the cell and the one positioned near it.

In a typical experiment, the sample was outgassed at an average temperature of the entire range of investigation. Both the weight of the cell and the temperature were continuously monitored. A few initial measurements were always discarded to eliminate outgassing contributions to the weight loss and only data corresponding to constant temperature periods were used. The vapor pressure of zinc was measured to establish the reliability of the experimental setup. Graphite effusion ovens with screw-type covers containing 0.025- and 0.070-in. orifices were employed after outgassing at 1100°K under vacuum ($\sim 10^{-5}$ Torr). Zinc shot of 99.999% purity[7] were used in these measurements in the temperature range 530–630°K. Diameter and length of orifices were obtained through their highly magnified photographs in a horizontal plane and at 45° inclination. Orifice areas were corrected for expansion due to heating in the evaluation of vapor pressures using the Knudsen effusion equation[8]

$$\text{rate of effusion } \frac{\mathrm{d}m}{\mathrm{d}t} = \alpha W a P_e \times \sqrt{\frac{M}{2\pi RT}}$$

where M, P_e, and α are the molecular weight, equilibrium pressure, and condensation coefficient, respec-

---

(1) J. E. Ferguson in "Halogen Chemistry," Vol. III, V. Gutman, Ed., Academic Press, New York, N. Y., 1967, p 227.

(2) J. Tillack, P. Eckerlin, and J. H. Dettingmeijer, *Angew. Chem.*, **78**, 451 (1966).

(3) B. McCarroll, *J. Chem. Phys.*, **47**, 5077 (1967).

(4) J. H. Dettingmeijer and B. Meinders, *Z. Anorg. Allg. Chem.*, **357**, 1 (1968).

(5) J. Tillack, *ibid.*, **357**, 11 (1968).

(6) H. Schäfer, D. Geigling, and K. Rinke, *ibid.*, **357**, 25 (1968).

(7) Supplied by Alfa Inorganics, Inc., Beverly, Mass.

(8) M. Knudsen, *Ann. Phys.*, **29**, 179 (1909).

tively, of the vapor molecule at T°K; a is the effusion area; and W is the Clausing correction factor[9] for an orifice of finite length. Zinc has been known to sublime predominantly as monatomic vapor with condensation coefficient about unity.[10,11] The present vapor pressures were about 10% higher than the reported values. Least-squares treatment of the data gave for the enthalpy of sublimation of zinc at 298°K a second-law value of 32.0 ± 1.0 kcal/mol as compared to the published quantity of 31.2 kcal/mol.[11] The agreement is satisfactory and well within experimental uncertainty.

Tungsten oxydiodide, WO_2I_2, was prepared from tungsten, tungsten trioxide, and iodine by the method described by Tillack, *et al.*[2] High-purity tungsten powder was supplied by General Electric Co. and the reagent grade iodine by Fisher Scientific Co. Tungsten trioxide was obtained by additional dehydration of Fisher technical anhydrous tungstic acid at 800° in a platinum crucible. Chemical analysis of tungsten and X-ray emission spectral determination of W:I molar ratio were performed with alkaline WO_2I_2 solution. The W:O:I ratio obtained was 1:2.04:1.96 as compared to the theoretical value of 1:2:2. WO_2I_2 was always stored under vacuum and handled carefully as it is susceptible to slow attack by moisture.

The vapor pressure data on WO_2I_2(s) were obtained employing Hastelloy C effusion cells with 0.024-, 0.010-, and 0.003-in. orifices, subsequently referred to as cells 1, 2, and 3, respectively. Hastelloy C was found fairly inert to chemical attack by WO_2I_2 or I_2, and only cell 3 tarnished slightly at the highest temperatures.

B. Mass Spectrometric Technique. A 12-in., 90° single-focusing mass spectrometer built by Nuclide Corporation was employed in the present investigation. The instrument is equipped with a high-temperature assembly which includes a Knudsen effusion oven heated by radiation from two individually controlled circular tungsten ribbon filaments. Temperatures greater than 1000°K were attained by electron bombardment heating and tantalum radiation shields helped maintain constant temperatures. Two Pt—Pt-Rh thermocouples spot-welded at the top and bottom of the oven continuously monitored its temperature on a Moseley variable range strip-chart recorder.

Gaseous species entering the ion source are ionized by electron bombardment, and positive ions are withdrawn perpendicular to both the electron and molecular beams. The repeller was held at the potential of the ion box, while the electron trap was biased 75 V positive. The ion accelerating potential usually employed was 3 kV. A 16-stage Cu–Be electron multiplier, vibrating-reed electrometer, and strip-chart recorder formed the ion-detection system. Ion currents could also be measured on a retractable Faraday cup to evaluate ion multiplier efficiencies.

A movable shutter, located between the ion source of the mass spectrometer and effusion oven, was used to distinguish molecules generating out of the crucible and the surroundings. The original shutter system on the instrument consisted of a movable plate with 0.100-in. hole covered by a collimating "hat" (0.18 in. i.d. and 0.38 in. long) with a 0.040-in. exit orifice. Shutter profile of $WO_2I_2^+$ and I_2^+ with this arrangment exhibited two uneven maxima around the center. Replacement of the "hat" with either a knife-edged 0.040-in. orifice or a 0.050 × 0.100-in. rectangular slit eliminated the anomalous shutter effect, which is believed to arise from the condensation behavior of I_2 and WO_2I_2 vapors on the shutter surfaces. The condensation coefficient of a diatomic or complex molecule, in general considerably less than unity, strongly depends on the nature of the molecule, the substrate, the temperature, etc.[12] Silver and gold vapors, which are known to have a condensation coefficient near unity, do not exhibit an anomalous shutter effect.[13] Thus, the condensation coefficients of I_2 and WO_2I_2 vapors on stainless steel surfaces, under the present experimental conditions, may be considerably less than unity.

In the investigation of the WO_2(s)–I_2(g) reaction, the shutter plate with a 0.040-in. orifice was used. A somewhat different type of shutter effect was observed during these experiments, but it was restricted primarily to I_2^+ ion currents. The position of the shutter profile "maximum" on I_2^+ remained unchanged with an increase in the temperature of the cell from 25° to 800°, and broad peaks developed on either side of the "maximum." A positive temperature and time dependence was exhibited by these auxiliary peaks whose rate of decay on stopping the iodine supply was found considerably slower than that for the "maximum." At temperatures above 500° and pressures used in Knudsen cells, molecular iodine would dissociate appreciably. Hence, it is believed that these auxiliary shutter peaks of I_2^+ mostly arise from iodine atoms desorbing as molecular iodine from surfaces near the shutter and radiation shields. In the measurement of shuttered I_2^+ ion currents, this effect was taken into consideration.

An external gas inlet was provided to the crucible to study solid–gas reactions. A 0.125-in. o.d. Monel or molybdenum tubing connected the crucible to a 0.25-in. o.d. Monel inlet tubing welded to a greaseless all-Monel Nupro controlling valve outside the Knudsen cell housing. Pyrex gas containers were coupled to the valve using Teflon gasketed stainless steel flanges and Pyrex to stainless steel graded seals.

---

(9) P. Clausing, *Ann. Phys.*, **12**, 961 (1932).

(10) K. H. Mann and A. W. Tickner, *J. Phys. Chem.*, **64**, 251 (1960).

(11) R. Hultgreen, R. L. Orr, P. D. Anderson, and K. K. Kelley, "Selected Values of Thermodynamic Properties of Metals and Alloys," John Wiley & Sons, Inc., New York, N. Y., 1963.

(12) F. M. DeVienne in "The Solid–Gas Interface," Vol. II, E. A. Flood, Ed., Marcel Dekker, Inc., New York, N. Y., 1967, p 815.

(13) A. Kant, private communication.

Table I: Ion Intensities and Appearance Potentials of Observed Ions in Vaporization of WO_2I_2(s)

Ion	Relative intensity[a]	Appearance potential, eV		Molecular precursor
		Present work	Lit.	
$WO_2I_2^+$	100	10.4 ± 0.4	13.4[c]	WO_2I_2
WOI_2^+	5			WO_2I_2
WI_2^+	1.5			WO_2I_2
WO_2I^+	35	12.5 ± 0.5	14.4[c]	WO_2I_2
WOI^+	12			WO_2I_2
WI^+	5			WO_2I_2
WO_2^+	10			WO_2I_2
WO^+	12			WO_2I_2
W^+	8			WO_2I_2
I_2^+	b	1st: 9.4 ± 0.5 2nd: 15.0 ± 0.8	9.5,[c] 9.35[d]	WO_2I_2,I_2
I^+	b	1st: 9.1 ± 0.5 2nd: 12.0 ± 0.5	10.5,[c] 8.68[d] 12.0[d]	WO_2I_2,I_2
WOI_3^+	0.5			WOI_3

[a] Ionizing electron energy = 50 V; temperature of the cell, 300°. Data reported in ref 6 are in agreement with these values. [b] Relative ion currents of I_2^+ and I^+ were cell temperature and orifice dependent. [c] Reference 6. [d] Reference 19.

Molybdenum, tungsten, and Hastelloy C effusion ovens were used in the WO_2I_2 evaporation investigations. The reactions of solid WO_2 with gaseous iodine were studied in a tungsten crucible with an external gas inlet connection. A tungsten cup inside the crucible contained solid WO_2. Hydrogen reduction of WO_3(s) at 1000° produced WO_2 which was further verified by an X-ray diffraction pattern.[14] Iodine was purified and dried by sublimation over dehydrated magnesium perchlorate.

Results and Discussion

A. Gaseous Molecular Species over Solid WO_2I_2. The ionic species observed in the mass spectra of vapors from solid WO_2I_2 are listed in Table I. The identity of ions was established by mass counting and tungsten isotopic abundance analysis. Relative intensities of observed ions are in fair agreement with those recently reported by Schäfer, *et al.*,[6] who used an open crucible and did not detect WOI_3^+. The mass spectra are also quite similar to those reported in the vaporization studies of solid WO_2Cl_2 and WO_2Br_2,[15] except for the presence of WOI_3 and the absence of dimeric species in WO_2I_2 vapors. Relative ion currents for I_2^+ and I^+ are not given in the table since these were found to be cell orifice and temperature dependent. Within the limited temperature range, 450–620°K, the $WOI_3^+/WO_2I_2^+$ ratio exhibited only a slight positive temperature dependence. Pressure ratio $P_{WOI_3}/P_{WO_2I_2}$ in the cell was estimated about 2×10^{-3} at 575°K. Other ions relative to $WO_2I_2^+$, within the experimental error, were found to be temperature independent. The existence of molecular and atomic iodine was investigated using their temperature dependence and appearance potential data.

The appearance potentials (A.P.) listed in Table I were evaluated using the vanishing current method with argon or krypton as a calibrating medium.[16] The assigned uncertainties are well above their experimental reproducibilities. Obviously, there are differences in our A.P.'s and Schäfer's published values.[6] Their use of linear extrapolation technique may account for part of the discrepancy, but large differences in A.P.'s for $WO_2I_2^+$ and for WO_2I^+ cannot be explained. The two A.P.(I_2^+) values at 9.4 and 15.0 eV correspond to the ionization of I_2(g) in the WO_2I_2 vapors and the fragmentation of WO_2I_2, respectively. The difference of 5.6 eV in these values compares well with the dissociation energy $D(WO_2\text{–}I_2)$ of 6.0 eV computed from the present thermodynamic data.[17] Thresholds for ion pair formation of I^+ from I_2 have been reported at 8.85 and 8.68 eV in photoionization[18] and electron impact work,[19] respectively. Our value of 9.1 eV for the first A.P. (I^+) suggests ion pair formation from I_2, while the second A.P. observed at 12.0 eV apparently is the onset of dissociative ionization of I_2. A.P. for I_2^+ and I^+ on electron impact of I_2 were also measured during the present work using mercury for voltage calibration. Comparison with the published data in Table II indicate that our results for I^+ are slightly higher. In view of rather low ionization cross section for ion pair process, the discrepancy is well within the experimental errors encountered in electron impact work. The mass spectrum of I_2 gave an I_2^+/I^+ ratio

---

(14) J. A. M. van Liempt, *Z. Anorg. Allg. Chem.*, **126**, 183 (1923).

(15) C. G. Barraclough and J. Stals, *Aust. J. Chem.*, **19**, 741 (1966).

(16) J. W. Warren and C. A. McDowell, *Discussions Faraday Soc.*, **10**, 53 (1951).

(17) Dissociation energy (WO_2–I_2) in WO_2I_2 can be estimated from the enthalpy of reaction $WO_2I_2(g) = WO_2(s) + I_2(g)$ and heat of vaporization of WO_2(s) from Janaf tables, ref 26.

(18) J. D. Morrison, H. Hurzeler, and M. G. Inghram, *J. Chem. Phys.*, **33**, 821 (1960).

(19) D. C. Frost and C. A. McDowell, *Can. J. Chem.*, **38**, 407 (1960).

Table II: Electron Impact Data on Gaseous Iodine

	Relative intensity[a]		Appearance potential, eV			
Ion	Present work	Lit.[b]		Present work	Lit.	
I_2^+	100	50		9.3 ± 0.3	9.3,[c]	9.35[d]
I^+	10	100	1st:	9.1 ± 0.5	8.85,[c]	8.68[d]
			2nd:	12.2 ± 0.5		12.02[d]

[a] Ionizing electron energy = 50 V. [b] Reference 20. [c] Reference 18. [d] Reference 19.

much higher than that reported elsewhere.[20] Low values of I_2^+/I^+ would result unless the I^+ contribution from the background HI and iodine dissociation at the hot filament are duly substracted. With iodine effusing out of the cell, the shutter was used to obtain I^+ ion current only from the ionization of I_2. The ionization efficiency curve for I^+ from the WO_2I_2 vapors compared well with that obtained from gaseous I_2, but it failed to reveal any distinct step at 10.4 eV corresponding to the ionization potential of atomic iodine. At the cell temperatures below 500°K employed in the appearance potential measurements, the expected dissociation (about 8%) of the molecular iodine would easily elude detection. The presence of such minor quantities of atomic iodine in the WO_2I_2 vapors could not be ascertained from the temperature dependence data due to inevitable fragmentation contribution to I^+ ion currents from molecular iodine. Fragmentation contribution to I^+ from WO_2I_2 is expected to begin at electron energies greater than 14.1 eV, as the calculated dissociation energy $D(WO_2I-I)$ is 3.7 eV.

Table III: Variation of $P_{I_2}/P_{WO_2I_2}$ with Temperature and Effusion Orifice

Cell no.	Cell material	Orifice diameter, in.	Temp range °K	Obsd $P_{I_2}/P_{WO_2I_2}$ range
4	Molybdenum	0.040	460–520	3–1.5
5	Tungsten	0.027	490–540	4–1.7
2	Hastelloy C	0.010	520–580	25–15
3	Hastelloy C	0.003	520–630	60–17

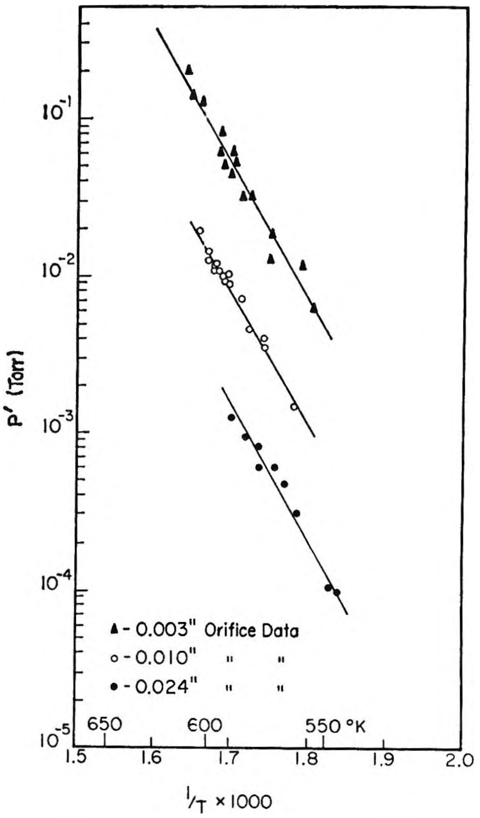

Figure 1. Apparent vapor pressure data on solid WO_2I_2.

B. Vaporization of Solid WO_2I_2. It is apparent from section A that WO_2I_2 and I_2 are the major species while WOI_3 and I are the minor vapor species over solid WO_2I_2. The WO_2I_2 decomposition to I_2, besides being temperature variant, was observed to exhibit a strong inverse dependence on the effusion orifice area. The results are summarized in Table III. Ion intensities were used to obtain I_2 and WO_2I_2 pressure ratios using the relation

$$\frac{P_{WO_2I_2}}{P_{I_2}} = \frac{I_{WO_2I_2^+}}{I_{I_2^+}} \frac{\sigma_{I_2}}{\sigma_{WO_2I_2}} \frac{S_{I_2^+}}{S_{WO_2I_2^+}}$$

where I_{x^+} is the total ion current of species x at partial pressure, P_x, in effusion cell at T°K; σ_x is its ionization cross section; and S_{x^+} is its multiplier detection efficiency. Ion currents for I_2^+ and $WO_2I_2^+$, measured at electron energies 2.6 ± 0.3 eV above their ionization thresholds, were taken as their total ion currents because the observed fragmentation contributions were only about 1%. Contributions to I_2^+ from electron impact of WO_2I_2 molecules should be negligible at these electron energies, since the dissociation energy $D(WO_2-I_2)$ is estimated about 6.0 eV.[17] Electron multiplier efficiencies measured for I_2^+ and $WO_2I_2^+$ ions, surprisingly, were found to be identical within experimental error. The ionization cross section ratio was estimated by the additivity rule[21] using recently published atomic ionization cross sections.[22] In view of the known deviations of the additivity rule[23] to obtain molecular ionization cross section and experimental errors, these derived pressure ratios are estimated to be accurate within a factor of 2.

Knudsen effusion weight loss measurements on vaporization of solid WO_2I_2 were treated assuming $M = 470$ (molecular weight of WO_2I_2) in the Knudsen effusion

(20) Compilation of Mass Spectral Data, American Petroleum Institute Project 44, Washington, D. C.

(21) J. W. Otvos and D. P. Stevenson, *J. Amer. Chem. Soc.*, **78**, 546 (1956).

(22) J. B. Mann, *J. Chem. Phys.*, **46**, 1646 (1967).

(23) R. F. Pottie, *ibid.*, **44**, 916 (1966).

equation. Apparent pressures, P', thus obtained and plotted in Figure 1, clearly show their strong effusion orifice dependence. However, the mass spectrometrically obtained $P_{I_2}/P_{WO_2I_2}$ in Table III suggest that only I_2 pressures may show significant orifice dependence. The presence of minor quantities of atomic iodine in the cell would result from the I_2 dissociation, which is expected to be less than 0.5% in cell 3, about 1% in cell 2, and a maximum of 5% in cells 1, 4, and 5. Using the following modified version of the effusion equation

$$P' = P_{WO_2I_2}\left(1 + \frac{P_{I_2}}{P_{WO_2I_2}}\sqrt{\frac{M_{I_2}}{M_{WO_2I_2}}}\right)$$

WO_2I_2 partial pressures were evaluated to investigate their orifice dependence. The effect of the minor presence of gaseous WOI_3 and atomic iodine on these calculations is expected to be negligible. $P_{WO_2I_2}$ was calculated as 2.1×10^{-7} atm at 560°K by combining the observed pressure ratio, $P_{I_2}/P_{WO_2I_2}$ (Table III), with P' values obtained from the 0.024-in. diameter orifice cell. Assuming invariance of $P_{WO_2I_2}$ with effusion orifice, pressure ratios from P' data were calculated as 11 and 84 for cells with 0.010 and 0.003-in. diameter orifices, respectively. Comparison with the observed ratios (Table III) suggest nonexistence of any appreciable orifice size dependence of $P_{WO_2I_2}$. Rather unusual variations were observed in the $P_{I_2}/P_{WO_2I_2}$ values from one set of measurements to another in any particular series of experimental runs even after appropriate conditioning of the sample. These variations are well above the range of instrumental reproducibility. Tillack's effusion data also show a similar phenomenon; for example, the pressure ratio changed from about 1 to 3 at 597°K as the measurement with the same sample was repeated at a later time.[5] Our pressure ratios failed to reveal any specific trend with time and thus the formation of solid solutions is discounted. An intermediate condensed phase produced from the dissociation of solid WO_2I_2 has been reported by Schäfer, *et al.*,[6] as WO_2I, which undergoes further decomposition to the stabler phase of WO_2(s). It is believed that these condensed phases do not attain equilibrium with one another at the experimental temperatures due to kinetic factors and could give rise to the observed variations in the $P_{I_2}/P_{WO_2I_2}$ values. An identical situation in a different system has recently been reported.[24]

In view of the observed variations in the $P_{I_2}/P_{WO_2I_2}$ ratios, only a few $P_{WO_2I_2}$ were calculated from P' data obtained with the effusion cell having a 0.024-in. orifice. These derived WO_2I_2 pressures were found a factor of about 25 smaller than those reported by Tillack.[5] Discrepancies of somewhat lesser order have sometimes been reported in Knudsen effusion data obtained in different laboratories. At present, it is not possible to offer a reasonable explanation for the discrepancy.

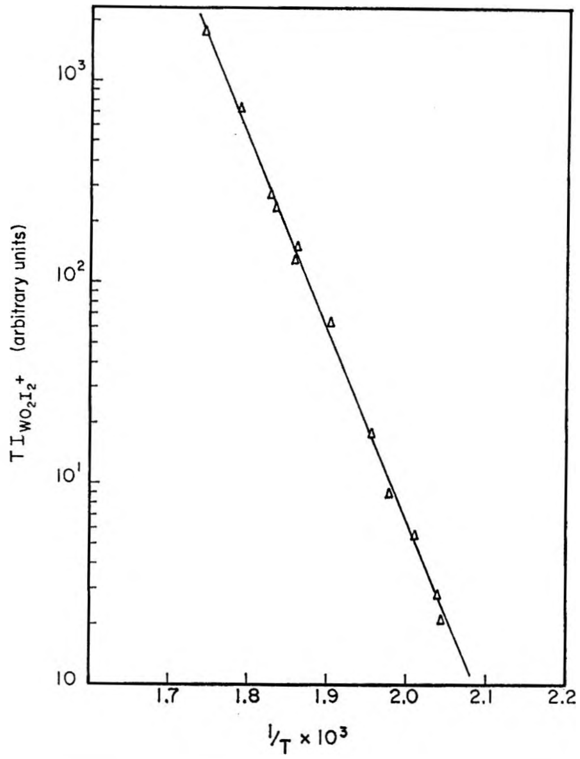

Figure 2. Mass spectrometric determination of the enthalpy of sublimation of solid WO_2I_2.

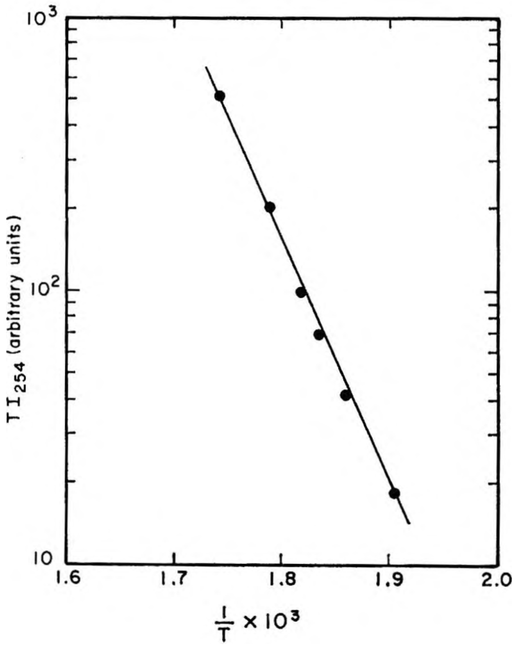

Figure 3. Mass spectrometric determination of the heat of WO_2I_2(s) decomposition.

The presence of WOI_3 in the vapor phase over solid WO_2I_2 is significant since no such species have been

---

(24) E. D. Cater, E. G. Rauh, and R. J. Thorn, *J. Chem. Phys.*, **49**, 5244 (1968).

detected in the WO_2Cl_2 and WO_2Br_2 studies,[15] although the solid $WOCl_3$ and $WOBr_3$ have been synthesized by other methods.[25] In the mass spectrometric study, the ion current ratio $WOI_3^+/WO_2I_2^+$ has been observed to increase from 2.4×10^{-3} to 1.1×10^{-2} as the temperature is raised from 500 to 630°K. Thus, large quantities of gaseous WOI_3 are possible at high WO_2I_2 pressures and elevated temperatures. The formation of WOI_3 from WO_2I_2 may involve reaction with iodine and evolution of oxygen.

C. Thermodynamics of the Evaporation Reactions of $WO_2I_2(s)$. Besides the sublimation reaction

$$WO_2I_2(s) = WO_2I_2(g) \qquad (1)$$

the following possible decomposition reactions are considered

$$2WO_2I_2(s) = 2WO_2I(s) + I_2(g) \qquad (2a)$$

$$WO_2I_2(s) = WO_2(s) + I_2(g) \qquad (2b)$$

The heat of sublimation, $\Delta H_1°$, was obtained mass spectrometically by a second-law procedure. Since $P \propto TI$, log $TI_{WO_2I_2}{}^+$ *vs.* $1/T$ were plotted to evaluate $\Delta H_1°$. A typical set of data is shown in Figure 2. Table IV lists $\Delta H_1°$ values obtained by least-squares evaluation of three independent sets of data, which provided a mean value of 43.7 ± 0.7 kcal/mol at 510°K. From WO_2Cl_2 data,[26] $\Delta C_p°$ for reaction 1 was estimated as 7 cal/mol deg, and $\Delta H_1° = 45.2 \pm 1.0$ kcal/mol at 298°K was obtained. The agreement between this and Tillack's result of 43.2 ± 1.2 kcal/mol[5] is satisfactory in view of the different experimental techniques employed.

Table IV: Enthalpy of Vaporization of $WO_2I_2(s)$

Knudsen cell	Temp range, °K	$\Delta H_{vap}°$ kcal/mol[a]
4	455–510	43.0 ± 0.5
5	490–550	44.4 ± 0.7
5	490–570	43.7 ± 0.2

[a] Mean $\Delta H_{vap}° = 43.7 \pm 0.7$ kcal mol at 510°K.

As was noted earlier, the extent of dissociation of WO_2I_2 to I_2 exhibited strong cell orifice dependence. Decomposition processes of this nature have been known to show such behavior.[27,28] In these cases the condensation coefficient, α, of the gas on solid phase has been found to be considerably smaller than unity. For molecular iodine, the condensation coefficient on solid WO_2I_2 is estimated about 10^{-6}. This suggests that iodine pressures may not be equilibrium pressures, a conclusion also reached by Tillack.[5] However, with an effective orifice to sample surface ratio of $\sim 10^{-5}$ (cell 3), the degree of unsaturation may be assumed to be small and independent of the temperature in a narrow range. Table III shows that in this cell, iodine comprises 95 to 97% of the total pressure. A second-law plot of P', on least-squares evaluation, gave $\Delta H_2° = 40 \pm 3$ kcal/mol, which should correspond to the enthalpy change of the decomposition reaction 2 at mean $T = 580$°K. In the mass spectrometric study, log $TI_{I_2}{}^+$ *vs.* $1/T$ (see Figure 3) was plotted to derive $\Delta H_2°$. Two independent sets of data gave a mean value of 39.8 ± 1.0 kcal/mol for $\Delta H_2°$ at 530°K. Agreement between the mass spectrometric and effusion data values is fairly good.

Existence of WO_2I as a solid phase between WO_2I_2 and WO_2 has been established by synthesis and analysis.[5,6] In the present mass spectrometric work, WO_2I as a gaseous molecular species was not detected even up to a cell temperature 720°K. X-Ray diffraction powder patterns of WO_2I_2 sample heated in a Knudsen cell up to various temperatures were obtained to identify the solid phase. However, the existence of WO_2I as a solid phase could not be ascertained on the basis of X-ray powder patterns for WO_2I reported by Tillack.[5] Good X-ray patterns were difficult to obtain with samples that had been heated long in Knudsen cells. The only additional lines observed were due to the WO_2 phase. One WO_2I_2 sample heated up to 410° in the Knudsen cell gave a predominantly WO_2 pattern, while another sample heated up to 310° gave W:I as 1:1.1 on chemical analysis and the X-ray diffraction pattern failed to show lines due to WO_2I or WO_2. Since tungsten oxydihalides have been postulated to be polymeric in solid phase,[15,29] thermal decomposition of WO_2I_2 with evolution of iodine may be a process involving a number of steps. This is typical of a number of decomposition or vaporization reactions where condensation coefficients of the gaseous species are considerably less than unity.[30] If WO_2I produced in a Knudsen cell is a polymeric amorphous solid phase, it may elude detection by X-ray diffraction techniques. It may be pointed out that Schäfer, *et al.*,[6] conducted experiments up to 6 days in order to obtain a crystalline variety of WO_2I.

It is believed that solid WO_2I, initially produced from WO_2I_2 decomposition, later dissociates to $WO_2(s)$ above 620°K. Therefore $\Delta H_2° = 40 \pm 3$ kcal/mol, obtained in the effusion study, was taken as the enthalpy for reaction 2a. Combining $\Delta H_2°$ with the present thermochemical data for $WO_2I_2(s)$ and available

---

(25) G. W. A. Fowles and J. L. Frost, *Chem. Commun.*, 252 (1966).

(26) "Janaf Thermochemical Tables," Dow Chemical Co., Midland, Mich, 1967.

(27) D. L. Hildenbrand and W. F. Hall, *J. Phys. Chem.*, **67**, 888 (1963).

(28) G. A. Somorjai in "Condensation and Evaporation of Solids," E. Rutner, P. Goldfinger, and J. P. Hirth, Ed., Gordon and Beach, New York, N. Y., 1964, p 417.

(29) D. M. Adams and R. G. Churchill, *J. Chem. Soc. A*, 2310 (1968).

(30) D. W. Jepsen and G. A. Somorjai, *J. Chem. Phys.*, **39**, 1665 (1963).

Table V: Thermochemical Calculations for the Reaction: $WO_2(s) + I_2(g) = WO_2I_2(g)$

Series	T, °K	I_{254},[a] (12.0 eV)	I_{470},[a] (13.0 eV)	K_3	$\Delta G_3°$, kcal/mol	$\Delta H_3°$ (298°K),[b] kcal/mol
I	783	78.0×10^4	240	59.2×10^{-5}	11.6	22.9
	819	72.0×10^4	450	12.0×10^{-4}	11.0	22.8
	867	42.0×10^4	630	28.9×10^{-4}	10.0	22.5
	889	19.5×10^4	330	32.5×10^{-4}	10.1	22.9
	918	9.6×10^4	205	41.1×10^{-4}	10.0	23.2
	921	11.4×10^4	270	45.6×10^{-4}	9.9	23.0
II	717	17.3×10^4	12.3	13.7×10^{-5}	12.7	23.1
	750	58.0×10^4	81.0	26.9×10^{-5}	12.3	23.1
	757	141.0×10^4	260	35.5×10^{-5}	12.0	22.9
	785	19.8×10^4	60.0	58.3×10^{-5}	11.6	23.0
	839	87.0×10^3	70.0	15.5×10^{-4}	10.8	22.9
	861	34.5×10^4	330	18.4×10^{-4}	10.8	23.1
	912	32.0×10^3	75.0	45.1×10^{-4}	9.8	22.8
	927	33.5×10^3	105	61.2×10^{-4}	9.4	22.6
III	806	58.0×10^4	210	69.6×10^{-5}	11.6	23.3
	826	33.0×10^4	235	13.7×10^{-4}	10.8	22.7
	844	4.0×10^4	42.0	20.2×10^{-4}	10.4	22.6
	942	11.4×10^4	435	73.4×10^{-4}	9.2	22.7
IV	921	15.9×10^4	390	47.2×10^{-4}	9.8	23.0
	927	48.0×10^3	160	64.1×10^{-4}	9.3	22.6

[a] m/e = 254 and 470 correspond to I_2^+ and the predominant $WO_2I_2^+$ ion peaks, respectively. [b] Mean $\Delta H_3° = 22.9 \pm 0.5$ kcal/mol at 298°K.

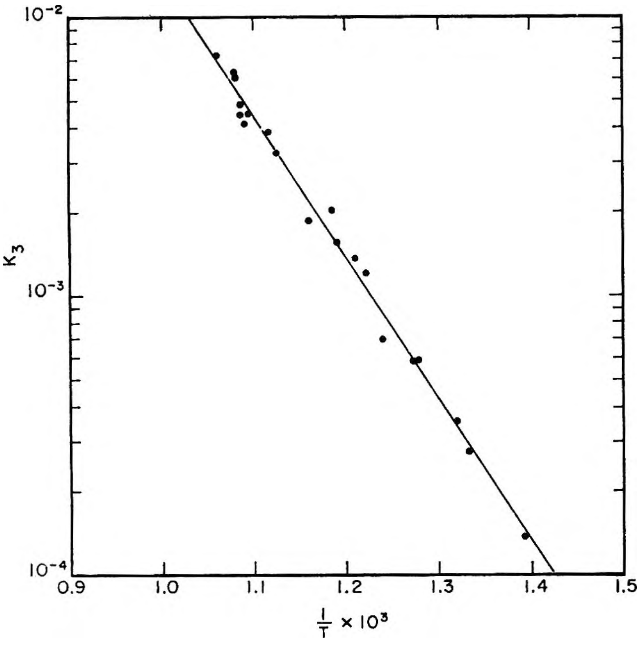

Figure 4. Equilibrium constant data for the reaction $WO_2(s) + I_2(g) = WO_2I_2(g)$ studied in the mass spectrometer.

data for I_2,[26] $\Delta H_f°(WO_2I(s)) = -136 \pm 5$ kcal/mol at 550°K was derived. This is larger than Schäfer's approximate value of −147 kcal/mol, which changes to −143 kcal/mol if our $\Delta H_{vap}°(WO_2I_2)$ is used.[6] In view of the assumptions involved, the discrepancy is not great. $\Delta H_2°$ could also be interpreted as the activation energy for reaction 2b, which would have an estimated enthalpy of only 21 kcal/mol.[26]

D. $WO_2(s) + I_2(g)$ Reaction. In the mass spectrometric investigation of the WO_2–I_2 reaction in a tungsten effusion cell, WO_2I_2 was identified as the only product. At cell temperatures above 700°K, dissociation of molecular iodine into atoms was observed as expected since the effusion cell pressures are kept below 1 Torr. It was not possible to study the reaction at temperatures above 950°K because the iodine dissociation became appreciable, resulting in lower WO_2I_2

$$WO_2(s) + I_2(g) = WO_2I_2(g) \qquad (3)$$

pressures. Equilibrium constants for the reaction may be written as

$$K_3 = \frac{P_{WO_2I_2}}{P_{I_2}}$$

Ion current data were used to evaluate the equilibrium constants. The procedure for converting ion current data to pressure ratios has been outlined in section B. Equilibrium constants, thus derived, are estimated to have an absolute uncertainty of a factor of 2. These data, along with thermochemical calculations, are presented in Table V and illustrated in Figure 4 as a second-law plot. Least-squares evaluation of the data gave

$$\log K_3 = -\frac{5045 \pm 123}{T} + 3.197 \pm 0.15$$

which provided the following second-law quantities: $\Delta H_3° = 23.1 \pm 0.6$ kcal/mol and $\Delta S_3° = 14.6 \pm 0.7$ eu at mean T = 830°K.

Third-law analysis of the equilibrium data was also performed using the relation

$$\Delta H_3°(298°\text{K}) = \Delta G_3° - T\Delta\left(\frac{G°_T - H°_{298}}{T}\right)_3$$

where $\Delta G_3°$ is the observed free energy change and $\Delta(G°_T - H°_{298}/T)_3$ is the change in free energy functions for reaction 3.

Molecular parameters and fundamental vibrational frequencies were estimated for the WO_2I_2 molecule in order to compute its free-energy functions, $S°$, and $C_p°$. The structure of WO_2I_2 molecule has not been examined, but infrared and Raman spectra of solid WO_2Cl_2 and molybdenum oxydihalides have been reported.[15,29] Recent attempts to obtain infrared spectra of gaseous WO_2I_2 have failed due to its poor thermal stability.[31] Molecular structure was assumed as distorted tetrahedral similar to that of MoO_2Cl_2. Isostructural molecules, *e.g.*, CrO_2Cl_2, SO_2Cl_2, and the corresponding fluorides, have been studied in great detail.[32] Using these data the following vibrational frequencies for WO_2I_2 molecule were estimated: $\nu_1 = 770$, $\nu_2 = 210$, $\nu_3 = 340$, $\nu_4 = 70$, $\nu_5 = 140$, $\nu_6 = 800$, $\nu_7 = 200$, $\nu_8 = 230$, and $\nu_9 = 250$ cm^{-1}. The estimated WO_2I_2 molecular parameters obtained from the WO_2Cl_2 values[26] are: bond distance W–I = 2.54 Å and W–O = 1.81 Å; bond angle I–W–I = 113°, O–W–O = 109.47°, and O–W–I = 90°. Thermodynamic functions, computed from these estimates, are presented in Table VI. Free-energy functions of $WO_2I_2(g)$ were combined with available functions[26] for $WO_2(s)$ and $I_2(g)$ to produce $\Delta H_3°(298°\text{K}) = 22.9 \pm 0.5$ kcal/mol. The second-law enthalpy, derived using the $C_p°$ data, was 23.6 ± 0.6 kcal/mol at 298°K. In view of uncertainties in measured equilibrium constants and other possible sources of errors, we assign an absolute uncertainty of ±2.0 kcal/mol to these derived enthalpies. Second- and third-law $\Delta H_3°$ values agree well within the experimental error indicating that the computed thermodynamic functions for $WO_2I_2(g)$, based on estimated parameters, are not appreciably in error.

Table VI: Thermodynamic Functions for Gaseous WO_2I_2

$T°$, K	$C_p°$, cal/mol deg	$-(G°_T - H°_{298})/T$, cal/mol deg	$S°$, eu
298	22.00	89.09	89.09
400	23.29	89.97	95.76
500	24.05	91.67	101.05
600	24.53	93.61	105.48
700	24.84	95.59	109.28
800	25.06	97.51	112.62
900	25.21	99.36	115.58
1000	25.32	101.11	118.24

Dettingmeijer and Meinders,[4] in a recent transpiration study of reaction 3, have reported a second-law evaluated $\Delta H_3° = 23.9$ kcal/mol at 298°K, which is modified to 23.3 kcal/mol with use of the present $C_p°$ for WO_2I_2. As can be seen, agreement between the two investigations is very good. From these $\Delta H_3° = 23.2 \pm 2.0$ kcal/mol at 298°K is taken as the "best" value, which is combined with $\Delta H_f°(298°\text{K})$ for $WO_2(s)$ and $I_2(g)$, −140.94 and 14.92 kcal/mol, respectively,[26] to give $\Delta H_f°(WO_2I_2(g)) = -102.8 \pm 2.0$ kcal/mol at 298°K. Our value is much larger than −108.7 ± 2.2 kcal/mol reported by Tillack from a calorimetric determination of heat of solution of $WO_2I_2(s)$.[5] However, using the present $\Delta H_{vap}°(WO_2I_2)$ of 45.2 kcal/mol, his value is changed to −106.7 ± 2.2 kcal/mol. Our thermochemical data give $\Delta H_f°(WO_2I_2(s)) = -148.0 \pm 2.0$ kcal/mol at 298°K as compared to the reported value of −151.9 ± 1.0 kcal/mol.[5] Tillack has pointed out that absolute uncertainties in these derived quantities are much greater than the assigned values due to lack of well-defined available thermochemical data on $Na_2WO_4(s)$ and H_2WO_4.[5] In view of this the discrepancy is within the experimental errors.

Entropy change for reaction 3, $\Delta S_3° = 14.6$ eu at mean $T = 830°$K, has been obtained in the present work. This quantity is changed to 15.7 ± 2.0 eu at 298°K with the use of calculated thermodynamic functions for $WO_2I_2(g)$ and available data[26] for $WO_2(s)$ and $I_2(g)$. The assigned uncertainty of ±2.0 eu is estimated to include experimental and other possible sources of errors. Dettingmeijer and Meinders have reported their second-law $\Delta S_3° = 18.1 \pm 1.4$ eu at 298°K,[4] which is reduced to 17.2 eu on the basis of present WO_2I_2 thermodynamic functions. Although this value is slightly higher than the present one, the discrepancy is well within the experimental errors. Since agreement between the enthalpy values obtained in the two studies is quite good, it is likely that the discrepancy in $\Delta S_3°$ may be real. A comparison of the data shows that their equilibrium constants are about a factor of 2 higher than the present values. Thus, their $\Delta S_3°$ would be expected to be higher by $R \ln 2$, *i.e.*, 1.4 eu, while the observed discrepancy is 1.5 eu. It is believed that WOI_3 quantities in their experiment would not be negligible since they have used fairly high iodine pressures, although it is doubtful if a factor of 2 difference in the equilibrium constants can be accounted for by such considerations alone.

The present $\Delta S_3°$ is combined with entropies[26] of $WO_2(s)$ and $I_2(g)$ to give $S°(WO_2I_2(g)) = 90.1 \pm 2.0$ eu at 298°K, as compared to the computed value of 89.1 eu. Agreement between these is quite good. Tillack has obtained 93.6 ± 4 eu for $S°$ of $WO_2I_2(g)$ at 298°K from a second-law evaluation of WO_2I_2 vapor pressure data and an estimation of solid WO_2I_2 entropy.[5] Dis-

---

(31) B. G. Ward and F. E. Stafford, *Inorg. Chem.*, **7**, 2569 (1968).

(32) (a) H. Stammereich, K. Kawai, and Y. Tavares, *Spectrochim. Acta* **9**, 438 (1959); (b) F. A. Miller, G. L. Carlson, and W. B. White, *ibid.*, **9**, 709 (1959).

crepancy between the two values, although within experimental errors, could partly arise from an error in the estimated entropy of solid WO_2I_2.

Acknowledgment. Helpful discussions with Drs. E. G. Zubler and L. V. McCarty are gratefully acknowledged.

Kinetics of the Addition of Ethyl, Isopropyl, *n*-Butyl, and Isopentyl Radicals to Ethylene[1]

by K. W. Watkins and L. A. O'Deen

Department of Chemistry, Colorado State University, Fort Collins, Colorado 80521 *(Received March 7, 1969)*

Kinetic parameters for the addition of ethyl, isopropyl, *n*-butyl, and isopentyl radicals to ethylene have been determined. Azoethane and azoisopropane were irradiated in the presence of ethylene in the temperature range 68–140°. Products were identified and measured quantitatively by a detailed gas chromatographic analysis. The products were interpreted as arising from the addition of ethyl and isopropyl radicals to ethylene. Products resulting from the addition to ethylene of the *n*-butyl and isopentyl radicals produced in these systems were also identified. The rate constants found here are compared with previous results. An activated complex is proposed which fits the observed *A* factors for the addition of ethyl radical to ethylene and its reverse reaction, the decomposition of *n*-butyl radical. Published rate parameters for the decomposition of *n*-butyl radical are combined with the present results to estimate thermodynamic properties for the *n*-butyl radical: $\Delta H_f^\circ \cong 16.8$ kcal/mol; $S^\circ \cong 79.1$ eu (standard state, 1 atm); $D(n\text{-}C_4H_9\text{–}H) \cong 99.1$ kcal/mol.

Introduction

There have been few detailed kinetic studies of the addition of alkyl radicals to unsaturated hydrocarbons. Most of the work reported before 1961 has been reviewed.[2] The addition of ethyl radicals to ethylene was studied by Lampe and Field,[3] who used azoethane photolysis as a source of ethyl radicals, and by Kerr and Trotman-Dickenson,[4] who used the photolysis of propionaldehyde as a source of ethyl radicals. Lampe and Field found an activation energy for addition of 5.5 kcal/mol, while the latter workers reported the activation energy to be 8.6 kcal/mol. The addition of isopropyl and *n*-butyl radicals to ethylene has been studied only once previously.[5,6] The photolysis of isobutyraldehyde and valeraldehyde was used as the source of isopropyl and *n*-butyl radicals, respectively. More recently, Endrenyi and LeRoy[7] have reported a study of the addition of methyl and *n*-propyl radicals to ethylene. They used the photolysis of acetone as the methyl radical source. Isopentyl radical reactions have not been studied previously.

In the present work, the rate constants for addition of ethyl, isopropyl, *n*-butyl, and isopentyl (3-methyl-1-butyl) radicals to ethylene have been determined. Photolysis of azoethane and azoisopropane was used as the source of ethyl and isopropyl radicals, respectively. The experimental method required that the radicals produced by addition (the *n*-butyl and isopentyl radicals) be accounted for quantitatively. By using gas chromatography we have made an essentially complete product analysis. Azoalkanes were chosen instead of ketones and aldehydes because, in the temperature range studied, ketones on photolysis yield some acyl radicals as well as alkyl radicals. Aldehydes upon photolysis yield alkyl and formyl radicals. The formyl radicals can decompose to hydrogen atoms and carbon monoxide. The only radicals produced by photolysis of azoalkanes are alkyl radicals. Also, the radicals formed by photolysis of azoalkanes with 3660-Å light appear to behave as thermalized radicals.[8] Since alkyl radicals and nitrogen are the only primary products resulting from the photolysis of azoalkanes,

---

(1) Presented at the 1968 Midwest Regional Meeting of the American Chemical Society, Manhattan, Kansas, Paper 508.

(2) J. A. Kerr and A. F. Trotman-Dickenson, *Progr. Reaction Kinetics*, **1**, 107 (1961).

(3) F. W. Lampe and F. H. Field, *Can. J. Chem.*, **37**, 995 (1959).

(4) J. A. Kerr and A. F. Trotman-Dickenson, *J. Chem. Soc.*, 1609 (1960).

(5) J. A. Kerr and A. F. Trotman-Dickenson, *Trans. Faraday Soc.*, **55**, 921 (1959).

(6) J. A. Kerr and A. F. Trotman-Dickenson, *J. Chem. Soc.*, 1602 (1960).

(7) L. Endrenyi and D. J. LeRoy, *J. Phys. Chem.*, **71**, 1334 (1967).

(8) J. E. Calvert and J. N. Pitts, Jr., "Photochemistry," John Wiley and Sons, Inc., New York, N. Y., 1966, p 462.

Table I: Experimental Results, Ethyl–Ethylene System[a,b]

No.	*T*, °K	*t*, sec	(Azoethane)$_0$	$(C_2H_4)_0$	1-C_4H_8	*n*-C_6H_{14}	*n*-C_4H_{10}	C_6H_{12}	3-MH[c]	*n*-C_8H_{18}[d]
1	348.2	240	0.53	2.28	0.991	17.5	272	0.06	0.27	0.65
2	350.2	240	0.403	3.75	1.13	20.6	149	0.195	0.61	1.4
3	369.0	240	0.508	2.06	...	27.3	218	0.03	0.79	1.0
4	372.2	240	0.486	2.14	1.35	29.3	215	0.59	0.90	0.98
5	386.5	240	0.525	2.18	2.45	42.1	201	0.58	2.2	2.0
6	395.7	240	0.384	2.08	2.22	38.6	143	0.80	4.0	2.3
7	397.2	240	0.569	1.93	2.65	47.9	218	1.08	3.8	2.3
8	352.2	240	0.490	2.00	1.25	18.0	254	0.180	0.29	0.52
9	354.4	480	0.323	1.88	0.755	13.1	144	0.045	0.31	0.44
10	354.7	240	0.406	1.92	1.08	18.4	265	0.104	0.43	0.70
11	354.7	480	0.422	1.77	0.835	15.1	229	0.11	0.22	0.36
12	358.0	480	0.430	1.59	0.811	12.9	204	0.046	0.17	0.22
13	383.2	240	0.408	2.04	2.43	35.6	206	0.36	2.11	2.16
14	385.7	260	0.473	2.04	2.79	43.5	243	0.33	2.73	2.70
15	387.7	240	0.448	1.81	3.55	32.9	169	0.66	2.34	2.12
16	396	240	0.376	2.04	2.52	44.2	189	0.84	3.94	3.33
17	396.7	240	0.376	2.03	2.43	40.3	154	0.88	3.75	3.12
18	399.7	480	0.454	1.84	2.21	36.3	166	0.70	3.24	2.40
19	404.7	240	0.489	1.63	2.53	45.0	196	0.75	3.82	3.06
20[e]	385	240	0.0446	0.193	0.060	1.09	18.9	0.008	0.042	0.020

[a] Reagent concentrations are expressed in moles cm^{-3} × 10^6. [b] Products are expressed in terms of their rates of formation in moles cm^{-3} sec^{-1} × 10^{12}. [c] 3-MH = 3-methylheptane. [d] For runs numbered 1–7 the relative amounts of 3-MH and *n*-C_8H_{18} are only an estimate because these products were not completely resolved using the 3-ft silica gel column. The total of 3-MH + *n*-C_8H_{18} however is accurate. [e] 114-cm^3 reactor.

the interpretation of the product analysis from radical addition reactions is usually without complication.

There are very few thermochemical data on free radicals. Most values for enthalpies of formation are deduced from kinetic measurements, whereas entropies are calculated from statistical thermodynamics. By combining the present results for rate parameters for addition of ethyl radical to ethylene with published data for the decomposition of *n*-butyl radical, we have estimated several thermodynamic quantities for the *n*-butyl radical.

Besides the study of addition reactions, the systems reported here provide new data for some of the reactions of long-chain (C_4 and higher) alkyl radicals. The addition of an alkyl radical to ethylene produces a new radical which has two more carbon atoms than the original alkyl radical. Long-chain radicals are difficult to produce cleanly due to the lack of a suitable precursor. Very little work on alkyl radicals C_5 and longer has been reported. The problem of suitable alkyl radical sources has been reviewed by Kerr and Trotman-Dickenson.[2] Our results indicate that reactions of long-chain alkyl radicals can be studied in detail. The cross disproportionation-to-combination rate constant ratios of ethyl–*n*-butyl and isopropyl–isopentyl radicals are reported. Also, the rate constants for addition of *n*-butyl and isopentyl radicals to ethylene were determined, and in a separate publication we have reported rate parameters for the isomerization of *n*-hexyl radicals.[9] The *n*-hexyl radicals were produced by the addition of *n*-butyl to ethylene.

Experimental Section

Azoethane and azoisopropane were prepared by the method of Leitch,[10] and stored in the vapor phase in blackened 500-cc flasks. Ethylene was Phillips research grade. All gas handling was performed with a conventional vacuum system. Azoalkane and ethylene were measured separately for each run. Azoalkane at a concentration of about 0.5 × 10^{-6} mol cm^{-3} was irradiated in the presence of about 2 × 10^{-6} mol cm^{-3} of ethylene. The exact concentrations used appear in Table I. Unfiltered light from a Hanovia 550-W high-pressure mercury arc lamp was used for the irradiation. The reaction vessel was a 10.0-cm^3 Pyrex cylinder. In several runs a 114-cm^3 reactor was used. The amount of azoalkane consumed was usually between 15 and 25%, and the ethylene consumed was always less than 0.5% of the initial ethylene. Since azoalkanes have an absorption maximum at about 3600 Å, the use of Pyrex reactors does not result in the important radiation being cut out by the reactor walls.

After an irradiation time of either 4 or 8 min, the entire reactant–product mixture was analyzed by gas chromatography, using a 3-ft silica gel column and a flame ionization detector. A 6-ft silica gel column was used for runs numbered 8–20. Temperature programming from room temperature to about 160° was required. Reaction products were identified from elution temperatures of known standards on the silica gel column. Many of the products were also identified by their retention time on other columns (Apiezon L, diisodecylphthalate, and dimethylsulfolane). The azoalkane was retained by the silica gel column and seemed to decompose on standing. Before a series of analyses, the column was conditioned at 200°. This procedure eliminated all bogus peaks. Quantitative determinations were based on calibrations of peak areas using measured amounts of C_2, C_4, and C_6 hydrocarbon standards. The use of hydrocarbon standards containing varying numbers of carbon atoms showed that the response (peak area) per mole of hydrocarbon was directly proportional to the number of carbon atoms per molecule.

---

[9] K. W. Watkins and L. A. Ostreko, *J. Phys. Chem.*, **73**, 2080 (1969).

[10] R. Renaud and L. C. Leitch, *Can. J. Chem.*, **32**, 545 (1954).

Results and Rate Constant Calculations

Kinetics of the Ethyl–Ethylene System. The products listed in Table I can be explained by the following reaction scheme.

$$C_2H_5N_2C_2H_5 + h\nu \longrightarrow 2C_2H_5 + N_2 \qquad (1)$$

$$C_2H_5 + C_2H_4 \longrightarrow n\text{-}C_4H_9 \qquad (2)$$

$$2C_2H_5 \longrightarrow n\text{-}C_4H_{10} \qquad (3)$$

$$2C_2H_5 \longrightarrow C_2H_4 + C_2H_6 \qquad (4)$$

$$n\text{-}C_4H_9 + C_2H_5 \longrightarrow n\text{-}C_6H_{14} \qquad (5)$$

$$n\text{-}C_4H_9 + C_2H_5 \longrightarrow 1\text{-}C_4H_8 + C_2H_6 \qquad (6)$$

$$n\text{-}C_4H_9 + C_2H_5 \longrightarrow n\text{-}C_4H_{10} + C_2H_4 \qquad (7)$$

$$n\text{-}C_4H_9 + C_2H_4 \longrightarrow n\text{-}C_6H_{13} \qquad (8)$$

$$2n\text{-}C_4H_9 \longrightarrow n\text{-}C_8H_{18} \qquad (9)$$

$$2n\text{-}C_4H_9 \longrightarrow 1\text{-}C_4H_8 + C_4H_{10} \qquad (9a)$$

$$n\text{-}C_6H_{13} + C_2H_5 \longrightarrow n\text{-}C_8H_{18} \qquad (10)$$

$$n\text{-}C_6H_{13} + C_2H_5 \longrightarrow 1\text{-}C_6H_{12} + C_2H_6 \qquad (11)$$

$$n\text{-}C_6H_{13} + C_2H_5 \longrightarrow n\text{-}C_6H_{14} + C_2H_4 \qquad (12)$$

The reactions of ethyl radicals with azoethane (abstraction and addition) have not been included because the products from these reactions which are mostly ethane and tetraethylhydrazine should not affect the interpretation of the results.

The rate constant ratio k_6/k_5 was measured from the ratio $R(1\text{-}C_4H_8)/R(n\text{-}C_6H_{14})$, where R refers to the rate of formation of the product in mol cm^{-3} sec^{-1}. The average of 20 runs gave $k_6/k_5 = 0.060 \pm 0.006$ independent of temperature in the range 70–140°. This is about the value expected considering that k_6/k_5 should be one-half of the disproportionation to combination ratio for n-alkyl radicals, which is about 0.12–0.15.

The relative contributions to $R(C_4H_{10})$ by reactions 3 and 7 could not be directly measured. However, on the basis of the number of hydrogen atoms available for disproportionation, k_7/k_5 should be 0.090. Thus the contribution to $R(C_4H_{10})$ by R_7 is only 1% at 70° and less than 2% at 140°; therefore, the contribution to $R(C_4H_{10})$ by reaction 7 was neglected. We assumed $R(C_4H_{10}) = k_3\,(C_2H_5)^2$ for all calculations.

The Reaction $C_2H_5 + C_2H_4 \rightarrow n\text{-}C_4H_9$. From the reaction scheme $R(n\text{-butyl}) = k_2[C_2H_5][C_2H_4]$. The ethyl radical concentration was obtained from $[C_2H_5] = R^{1/2}(C_4H_{10})/k_3^{1/2}$; therefore

$$\frac{k_2}{k_3^{1/2}} = \frac{R(n\text{-butyl})}{R^{1/2}(n\text{-}C_4H_{10})[C_2H_4]} \qquad \text{(i)}$$

$R(n\text{-butyl})$ is equal to $R(n\text{-butyl products})$. From the reaction scheme

$$R(n\text{-butyl products}) = R_5 + R_6 + R_7 + 2R_9 + R(n\text{-hexyl})$$

Since $R_5 + R_6 + R_7 = (k_5 + k_6 + k_7)\ [n\text{-}C_4H_9][C_2H_5]$, dividing by $R_5 = k_5[n\text{-}C_4H_9][C_2H_5]$ we obtain

$$\frac{R_5 + R_6 + R_7}{R_5} = \frac{(k_5 + k_6 + k_7)}{k_5}$$

or

$$R_5 + R_6 + R_7 = \frac{k_5 + k_6 + k_7}{k_5} R(n\text{-}C_6H_{14})$$

where $R_5 = R(n\text{-}C_6H_{14})$. Using the rate constant ratios discussed above, $(k_5 + k_6 + k_7)/k_5 = 1.15$. The calculation of $R(n\text{-hexyl})$ is explained in the next section. The quantity R_9 is simply the octane produced in reaction 9. The octane produced in reaction 9 was found from the equation

$$R_9 = k_9[n\text{-}C_4H_9]^2$$

which can be shown[9] to be

$$R_9 = \frac{k_3 k_9}{k_5^2}\,\frac{R^2(n\text{-}C_6H_{14})}{R(C_4H_{10})}$$

According to simple collision theory, the ratio k_3k_9/k_5^2 is equal to $^1/_4$ for reactions with no activation energy. Most of the available data are in agreement with this prediction.[2] Therefore

$$R(n\text{-butyl}) = 1.15R(\text{hexane}) + R(n\text{-hexyl}) + 2R_9 \qquad \text{(ii)}$$

In the calculation of $k_2/k_3^{1/2}$ initial ethylene concentrations were used because at most only about 8×10^{-8} mol of ethylene was consumed in a run. This corresponds to about 0.5% of the initial ethylene.

A plot of log $k_2/k_3^{1/2}$ *vs.* $1/T$ is shown in Figure 1. The activation energy E_2 was calculated from the slope which is equal to $-(E_2 - {}^1/_2\ E_3)/2.3R$. E_3 was assumed to be zero. The preexponential factor A_2 was calculated from the intercept which is equal to log

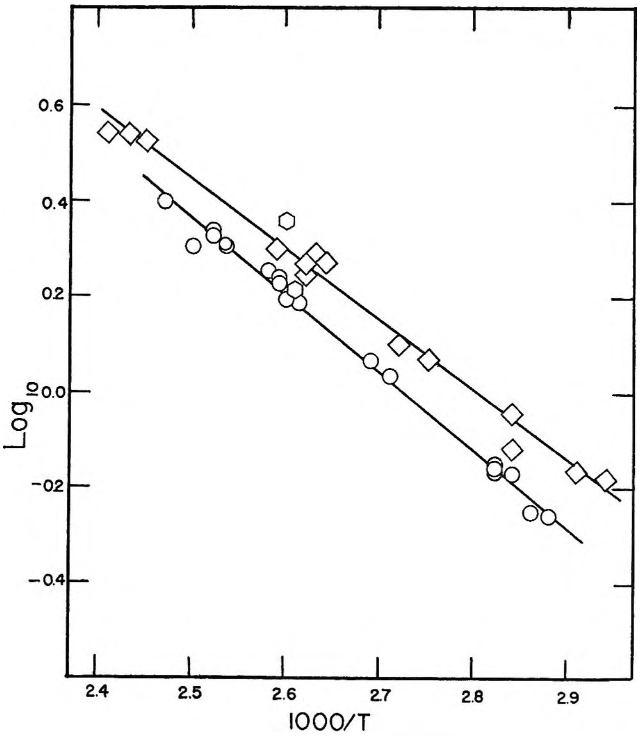

Figure 1. Addition of ethyl, ○, and isopropyl, ◇, to ethylene. Arrhenius plots for $k_2/k_3^{1/2}$ and $k_{18}/k_{19}^{1/2}$; ⌀, 114-cm^3 reactor.

$(A_2/A_3^{1/2})$. A_3 was reported[11] to be 2.2×10^{13} mol^{-1} cm^3 sec^{-1}. A least-squares calculation was used to determine the rate constant. The value found was log $k_2 = 11.17 - (7560/2.3RT)$.

As a test of the mechanism, one reaction was carried out in a 114-cm^3 reactor. The increase in reactor size has the effect of changing the concentration of ethylene and the rates of formation of products in mol cm^{-3} sec^{-1}, but $k_2/k_3^{1/2}$ should remain constant. The rate constant ratio $k_2/k_3^{1/2}$ was not affected by the reactor size. The point from this run is shown in Figure 1.

The Reaction n-C_4H_9 + C_2H_4 → n-C_6H_{13}. As either the temperature or ethylene concentration was increased, the products from the addition of n-butyl to ethylene (reaction 8) increased relative to ethyl-n-butyl cross disproportionation and combination. Hexene and some of the n-octane were assumed to result from n-hexyl radical reactions with ethyl radicals (reactions 10, 11, 12). The detection of a product with the same retention time as the hydrocarbon 3-methylheptane was taken as evidence that some n-hexyl radicals isomerized to *sec*-hexyl.

$$n\text{-}C_6H_{13} \longrightarrow sec\text{-}C_6H_{13} \qquad (13)$$

sec-Hexyl radicals react predominantly with ethyl radicals by reactions 14, 15, and 16.

$$sec\text{-}C_6H_{13} + C_2H_5 \longrightarrow C_8H_{18}(\text{3-methylheptane}) \qquad (14)$$

$$sec\text{-}C_6H_{13} + C_2H_5 \longrightarrow \text{1- \& 2-}C_6H_{12} + C_2H_6 \qquad (15)$$

$$sec\text{-}C_6H_{13} + C_2H_5 \longrightarrow n\text{-}C_6H_{14} + C_2H_4 \qquad (16)$$

The products 1- and 2-hexene, formed in reactions 10 and 14, could not be resolved from each other on the silica gel column. Therefore, their total amount is reported in Table I. The rate constant for the unimolecular isomerization k_{13} is reported elsewhere.[9]

The quantity R(n-hexyl) was set equal to

$$R(n\text{-hexyl}) = R_{10} + R_{12} - R_{16} + R(\text{3-methylheptane}) + R(\text{hexene}) \qquad \text{(iii)}$$

The n-hexane produced in reactions 12 and 16 could not be distinguished from the n-hexane produced in reaction 5. Therefore, the hexane produced in reactions 12 and 16 was estimated by assuming the disproportionation-to-combination rate constant ratios k_{12}/k_{10} and k_{16}/k_{14} were 0.10 and 0.15 respectively.[12] Thus

$$R(n\text{-hexyl}) = 1.10R_{10} + 1.15R(\text{3-methylheptane}) + R(\text{1- \& 2-hexene}) \qquad \text{(iv)}$$

The ratio R(n-hexyl)/R(n-hexane) was used to calculate the activation energy for addition of n-butyl to ethylene

$$\frac{R(n\text{-hexyl})}{R(n\text{-hexane})} = \frac{k_8[C_4H_9][C_2H_4]}{k_5[C_4H_9][C_2H_5]}$$

After setting $[C_2H_5] = R^{1/2}(C_4H_{10})/k_3^{1/2}$ and substituting, the expression becomes

$$\frac{k_8k_3^{1/2}}{k_5} = \frac{R^{1/2}(C_4H_{10})R(n\text{-hexyl})}{[C_2H_4]_0R(\text{hexane})} \qquad \text{(v)}$$

A plot of log $(k_8k_3^{1/2}/k_5)$ *vs.* $1/T$ is shown in Figure 2. The slope is equal to $-(E_8 + {}^1/_2\,E_3 - E_5)/2.3R$ and the intercept is log $(A_8A_3^{1/2}/A_5)$. The activation energy E_8 was calculated by assuming that the activation energies E_3 and E_5 for the radical combination reactions were essentially zero. To calculate the preexponential factor A_8, it was necessary to assume that $A_5 = A_3 = 2.2 \times 10^{13}$ mol^{-1} cm^3 sec^{-1} since the preexponential factor A_5 has not been reported in the literature. The rate constant determined from a least-squares calculation was log $k_8 = 10.34 - (6700/2.3RT)$.

Kinetics of the Isopropyl-Ethylene System. The products listed in Table II can be explained by reactions 17-27.

$$C_3H_7N_2C_3H_7 + h\nu \longrightarrow 2i\text{-}C_3H_7 + N_2 \qquad (17)$$

$$i\text{-}C_3H_7 + C_2H_4 \longrightarrow i\text{-}C_5H_{11}(\text{isopentyl}) \qquad (18)$$

$$2i\text{-}C_3H_7 \longrightarrow C_6H_{14}(\text{2,3-dimethylbutane}) \qquad (19)$$

$$2i\text{-}C_3H_7 \longrightarrow C_3H_6 + C_3H_8 \qquad (20)$$

$$i\text{-}C_5H_{11} + i\text{-}C_3H_7 \longrightarrow C_8H_{18}(\text{2,5-dimethylhexane}) \qquad (21)$$

---

[11] A. Shepp, *J. Chem. Phys.*, 24, 939 (1956). A_3 was assumed to be given by the rate constant for the recombination of methyl radicals.

[12] k_{12}/k_{10} should be very similar to k_7/k_5, therefore $k_{12}/k_{10} \simeq 0.10$. k_{16}/k_{14} was estimated in ref 9 to be ~0.15.

$$i\text{-}C_5H_{11} + i\text{-}C_3H_7 \longrightarrow CH_{10}(\text{3-methyl-1-butene}) + C_3H_8 \quad (22)$$

$$i\text{-}C_5H_{11} + i\text{-}C_3H_7 \longrightarrow i\text{-}C_5H_{12} + C_3H_6 \quad (23)$$

$$i\text{-}C_5H_{11} + C_2H_4 \longrightarrow C_7H_{15}(\text{isoheptyl}) \quad (24)$$

$$i\text{-}C_7H_{15} + i\text{-}C_3H_7 \longrightarrow C_{10}H_{22}(\text{2,7-dimethyloctane}) \quad (25)$$

$$i\text{-}C_7H_{15} + i\text{-}C_3H_7 \longrightarrow C_7H_{14}(\text{5-methyl-1-hexene}) + C_3H_8 \quad (26)$$

$$i\text{-}C_7H_{15} + i\text{-}C_3H_7 \longrightarrow i\text{-}C_7H_{16}(\text{2-methylhexane}) + C_3H_6 \quad (27)$$

The products 3-methyl-1-butene, isopentane, and 2,5-dimethylhexane were assumed to be produced by reactions 21–23. These are the cross disproportionation and combination of isopropyl and isopentyl radicals. The ratios k_{23}/k_{21} and k_{22}/k_{21} were obtained from the expressions

$$\frac{k_{23}}{k_{21}} = \frac{R(\text{isopentane})}{R(\text{2,5-dimethylhexane})}$$

$$\frac{k_{22}}{k_{21}} = \frac{R(\text{3-methyl-1-butene})}{R(\text{2,5-dimethylhexane})}$$

The results give $k_{23}/k_{21} = 0.24 \pm 0.01$ and $k_{22}/k_{21} = 0.082 \pm 0.005$. The ratio k_{22}/k_{21} is constant over the entire temperature range studied, 70–140°. k_{23}/k_{21} was constant below 112°, but increased slightly at 135°. The increase was probably due to hydrogen atom abstraction from azoisopropane or ethylene by isopentyl.

The Reaction $i\text{-}C_3H_7 + C_2H_4 \rightarrow i\text{-}C_5H_{11}$. The rate of formation of isopentyl radicals is given by $R(\text{isopentyl}) = k_{18}[C_3H_7][C_2H_4]$. The isopropyl radical concentration was obtained from $[C_3H_7] = R^{1/2}(\text{2,3-dimethylbutane})/k_{19}^{1/2}$; therefore

$$\frac{k_{18}}{k_{19}^{1/2}} = \frac{R(\text{isopentyl})}{R^{1/2}(\text{2,3-dimethylbutane})[C_2H_4]_0} \quad \text{(vi)}$$

R(isopentyl) is given by R(isopentyl products), where R(isopentyl products) = R(2,5-dimethylhexane) + R(3-methyl-1-butene) + R(isopentane) + R(isoheptyl). Defining $R_{22} = R$(3-methyl-1-butene), $R_{23} = R$(isopentane) and $R_{21} = R$(2,5-dimethylhexane), then $R_{21} + R_{22} + R_{23} = (k_{21} + k_{22} + k_{23})\,[C_5H_{11}][C_3H_7]$, and $R_{21} + R_{22} + R_{23} = (k_{21} + k_{22} + k_{23})/k_{21} \times R$(2,5-dimethylhexane). Using the rate constant ratios given in the previous section $(k_{21} + k_{22} + k_{23})/k_{21} = 1.32$.

Similarly, R(isoheptyl) = R(2,7-dimethyloctane) + R(5-methyl-1-hexene) + R(2-methylhexane), and

$$R_{25} + R_{26} + R_{27} = \frac{k_{25} + k_{26} + k_{27}}{k_{27}} R(\text{2-methylhexane})$$

The ratio of rate constants $(k_{25} + k_{26} + k_{27})/k_{27}$ could not be determined experimentally because an analysis of the probable products 5-methyl-1-hexene and 2,7-dimethyloctane was not obtained. 5-Methyl-1-hexene was not observed because its retention time was the same as 2,5-dimethylhexane which was present in a much greater amount. No standard of 2,7-dimethyloctane was available to identify the peak due to that product. The product 2-methylhexane was observed and its rate of formation was used as the basis of the calculation. Because of the similarity of the radicals involved, it was assumed that $k_{27}/k_{25} = k_{23}/k_{21} = 0.24$ and $k_{27}/k_{26} = k_{23}/k_{22} = 3.0$. Thus $(k_{25} + k_{26} + k_{27})/k_{27} = 5.6$. Finally, we have

$$\frac{k_{18}}{k_{19}^{1/2}} = \frac{1.32R(\text{2,5-dimethylhexane}) + 5.6R(\text{2-methylhexane})}{R^{1/2}(\text{2,3-dimethylbutane})[C_2H_4]_0} \quad \text{(vii)}$$

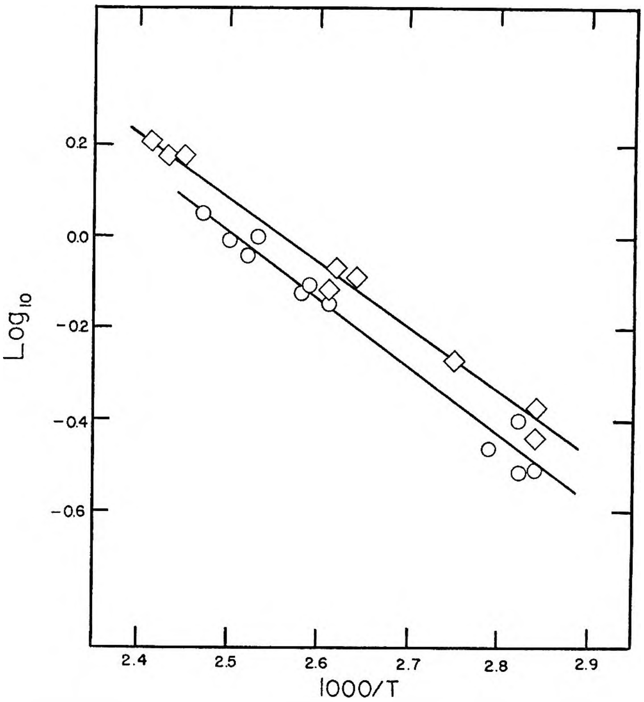

Figure 2. Addition of n-butyl, ○, and isopentyl, ◇, to ethylene. Arrhenius plots for $k_8k_3^{1/2}/k_5$ and $k_{24}k_{19}^{1/2}/k_{21}$.

In the calculations, initial ethylene concentrations were used. At most, about 8×10^{-8} mol of ethylene was consumed in a run, which corresponds to about 0.4% of the initial ethylene. As in the ethyl–ethylene system, the mechanism was tested by using a different size reactor in order to alter the concentrations of reactants. In this case the substitution of a 114-cm³ reactor for the 10-cm³ reactor did not affect $k_{18}/k_{19}^{1/2}$.

The slope of a plot of log $k_{18}/k_{19}^{1/2}$ *vs.* $1/T$ (Figure 1) leads to a value for the activation energy difference, $E_{18} - {}^1/_2E_{19}$, of 6.93 kcal/mol. Since E_{19} has previously been shown to be essentially zero,[13] $E_{18} = 6.93$ kcal/

---

(13) E. L. Metcalfe and A. F. Trotman-Dickenson, *J. Chem. Soc.*, 4620 (1962).

Table II: Experimental Results, Isopropyl–Ethylene System[a,b]

No.	T, °K	t, sec	[Azoisopropane]$_0$	$[C_2H_4]_0$	i-C_5H_{12}[c]	MIB	2,5-DMH	2,3-DMB	2-MH
25	340.2	240.0	0.38	2.24	2.63	0.83	11.3	109	0.08
26	343.7	240.0	0.41	2.21	2.49	0.83	11.6	109	...
27	352.2	240.0	0.36	1.88	2.20	0.71	9.66	62.9	0.18
28	352.7	240.0	0.40	3.83	3.83	1.3	14.3	53.4	0.50
29	363.4	240.0	0.42	2.20	3.9	1.3	17.5	94.6	0.39
30	367.7	240.0	0.39	2.36	5.12	1.8	20.6	98.8	...
31	379.7	240.0	0.37	3.18	8.3	2.9	35.0	84.1	1.8
32	380	240.0	0.41	0.587	2.3	0.75	9.33	126	...
33	381.7	240.0	0.37	2.08	5.8	2.5	24.7	89.6	0.83
34	382.	240.0	0.38	1.04	3.91	1.3	14.6	119	...
35	384.7	240.0	0.37	2.16	6.7	3.0	28.4	95.0	0.92
36	408.2	240.0	0.42	2.02	10.5	3.1	34.7	70.0	2.2
37	411.2	240.0	0.38	1.95	12.3	3.2	40.3	90.0	2.2
38	413.8	240.0	0.40	1.95	11.3	...	35.8	75.5	2.3
39[d]	384	240.0	0.028	0.166	0.19	0.073	0.868	8.50	0.008

[a] Reagent concentrations are expressed in mol $cm^{-3} \times 10^6$. [b] Products are expressed in terms of their rates of formation in mol $cm^{-3} sec^{-1} \times 10^{12}$. [c] 3-MIB = 3-methyl-1-butene; 2, 5-DMH = 2,5-dimethylhexane; 2,3-DMB = 2,3-dimethylbutane; 2-MH = 2-methylhexane. [d] 114-cm^3 reactor.

mol. The intercept is equal to log $A_{18}/A_{19}^{1/2}$. Figure 1 gives log $A_{18}/A_{19}^{1/2} = 4.32$. Using $A_{19} = 10^{13.8}$ $mol^{-1}\ cm^3\ sec^{-1}$, $A_{18} = 10^{11.22}\ mol^{-1}\ cm^{-3}\ sec^{-1}$. The rate constant found was log $k_{18} = 11.22 - (6930/2.3 \cdot RT)$.

The Reaction i-C_5H_{11} + C_2H_4 → i-C_7H_{15}. As either the temperature or C_2H_4 concentration was increased, the product from the addition of isopentyl to ethylene (2-methylhexane) increased relative to isopentyl–isopropyl cross disproportionation and combination. The ratio R(2-methylhexyl)/R(2,5-dimethylhexane) was used in the calculation of the activation energy for the addition of isopentyl to ethylene.

$$\frac{R(\text{2-methylhexyl})}{R(\text{2,5-dimethylhexane})} = \frac{k_{24}[C_5H_{11}][C_2H_4]}{k_{21}[C_5H_{11}][C_3H_7]}$$

Using the steady-state concentration of isoheptyl and the relationship $[C_3H_7] = R^{1/2}(\text{2,3-dimethylbutane})/k_{19}^{1/2}$, we obtain the expression

$$\frac{k_{24}k_{19}^{1/2}}{k_{21}} = \left[\frac{k_{25} + k_{26} + k_{27}}{k_{27}}\right]\frac{R^{1/2}(\text{2,3-DMB})R(\text{2-MH})}{[C_2H_4]_0R(\text{2,5-DMH})} \tag{viii}$$

Figure 2 is a plot of log $(k_{24}k_{19}^{1/2}/k_{21})$ *vs.* $1/T$. The slope should equal $-(E_{24} + {}^{1}/{}_{2}E_{19} - E_{21})/2.3R$ and the intercept will equal log $(A_{24}A_{19}^{1/2}/A_{21})$. A least-squares treatment gave $(E_{24} + {}^{1}/{}_{2}E_{19} - E_{21}) = 6.43$ kcal/mol. On the assumption that E_{19} and E_{21} are essentially zero, $E_{24} = 6.43$ kcal/mol. Log $(A_{24}A_{19}^{1/2}/A_{21})$ was found to be 3.59. A_{21} has never been measured, and so it was assumed that $A_{21} = A_{19} = 6.3 \times 10^{13}\ mol^{-1}\ cm^3\ sec^{-1}$; thus, $A_{24} = 10^{10.5}\ mol^{-1}\ cm^3\ sec^{-1}$. The rate constant is log $k_{24} = 10.5 - (6430/2.3RT)$.

Table III lists all the calculated relative rate constants for the four addition reactions, and the corresponding Arrhenius parameters.

Table III: Relative Rate Constants and Corresponding Arrhenius Parameters

T, °K	$k_2/k_3^{1/2}$[a]	$k_8k_3^{1/2}/k_5$[b]	T, °K	$k_{18}/k_{19}^{1/2}$	$k_{24}k_{19}^{1/2}/k_{21}$
348.2	0.563		340.2	0.671	...
350.2	0.570		343.7	0.698	...
352.2	0.681	0.32	352.2	0.780	0.37
354.0	0.707	0.31	352.7	0.918	0.43
354.7	0.720	...	363.4	1.18	0.54
354.7	0.687	0.41	367.7	1.28	...
358.0	0.690	0.35			
369	0.1.10		379.7	1.91	0.82
372.2	1.18		380	1.96	...
383.2	1.57	0.71	381.7	1.80	0.86
385	1.70	...	382	1.88	
385.7	1.77	0.78	384	2.35	...
386.5	1.73		384.7	2.05	0.78
387.7	1.83	0.74	408.2	3.55	1.48
395.7	2.10		411.2	3.71	1.49
396	2.14	0.95	413.8	3.77	1.61
396.7	2.17	0.88			
397.2	2.24				
399.7	2.06	0.97			
404.7	2.58	1.09			
Log A[c] =	4.50	3.67		4.32	3.59
E[d] =	7.56	6.70		6.92	6.43

[a] In ($cm^3\ mol^{-1}\ sec^{-1}$). [b] Runs numbered 1–7 are not included. [c] $A = A_2/A_3^{1/2}$, etc. [d] In kcal/mol.

Discussion

Alkyl Radical Addition to Ethylene. Measurements of the rate parameters for the addition of ethyl radicals to ethylene have been made in several previous studies. Those results, together with results for the addition of several other alkyl radicals to ethylene, and the present results are summarized in Table IV. The rate parameters found in this work for the addition of ethyl radicals to ethylene differ from those found by previous workers. The activation energy reported here is 2 kcal/mol higher than that of both Pinder and LeRoy,[14] and Lampe and Field,[3] but is 1 kcal/mol lower than the value reported by Kerr and Trotman-Dickenson.[4] Kerr and Trotman-Dickenson[2] have suggested that their value "may not be very accurate because of the difficulty of disentangling the *n*-butane" produced by two different reactions in their system. *n*-Butane was produced by the combination of ethyl radicals and by the abstraction of a hydrogen atom from propionaldehyde by *n*-butyl radicals that result from the addition of ethyl radicals to ethylene. The activation energy of 8.6 kcal/mol and preexponential factor of 12.1 mol^{-1} cm^3 sec^{-1} seem high when compared with the rate parameters for other alkyl radical additions reactions.

Table IV: Kinetic Parameters for Addition Reactions of Alkyl Radicals to Ethylene

Radical	Temp range, °C	Log *A*	*E*	Ref
Ethyl	75–132	11.17	7.56	This work
	100–200	12.1	8.6	4
	58–123	10.0	5.5	14
	125–175	10.3	5.5	3
Isopropyl	67–140	11.22	6.93	This work
	90–180	11.4	6.9	5
n-Butyl	79–132	10.34	6.7	This work
	84–171	11.1	7.3	6
Isopentyl	67–140	10.49	6.4	This work
Methyl	130–230	11.10	6.84	7
n-Propyl	105–200	10.9	6.5	18
	130–230	10.4	5.1	7

The activation energy and preexponential factor found by Lampe and Field are probably low, because they did not account for essentially all of the *n*-butyl radicals. They used ratios of azoethane to ethylene in the range of 1.6 to 8.0. With this excess of azoethane over ethylene, a considerable fraction of the butyl radicals probably added to azoethane, rather than adding to ethylene or combining with ethyl radicals. Radicals that add to azoethane most likely end up as part of a tetraalkylhydrazine molecule. Addition of *n*-butyl radicals to azoethane should compete with addition to ethylene since the activation energies for the addition of methyl radicals to azomethane and ethyl radicals to azoethane have been reported to be 6.3 and 6.0 kcal/mol, respectively.[15,16] In our experiments, the ratio of azoethane to ethylene was between 0.1 and 0.2; therefore, *n*-butyl radicals either combined with ethyl or *n*-butyl radicals or added predominantly to ethylene rather than to azoethane.[17]

The addition of *n*-butyl radicals to ethylene has been reported previously by Kerr and Trotman-Dickenson, who used the photolysis of valeraldehyde over the temperature range 85–170° as the source of *n*-butyl radicals.[6] Their results appear in Table IV. The rate parameters reported here are probably lower limits of the actual values because as the temperature increases between 70 and 140° the fraction of *n*-hexyl radicals (~10%) that adds to ethylene increases. The hexyl radicals that add to ethylene eventually produce *n*-decane. Since we could not analyze for *n*-decane, all of the *n*-hexyl radicals were not accounted for, and so *R*(*n*-hexyl products) is slightly low.

This failure to account for subsequent addition reactions is also a possible explanation of the "low" values of 5.1 kcal/mol for the activation energy for addition of *n*-propyl radicals to ethylene reported by Endrenyi and LeRoy,[7] since some of the resulting *n*-pentyl radicals would add to ethylene and eventually give rise to *n*-octane. They did not report *n*-octane in their analysis; thus the *n*-pentyl radicals that added to ethylene were not taken into account. Kerr and Trotman-Dickenson[18] found $E = 6.5$ kcal/mole for the addition of *n*-propyl radical to ethylene.

The only previously published study of the addition of isopropyl radicals to ethylene was that of Kerr and Trotman-Dickenson,[4] who used the photolysis of isobutyraldehyde as the source of isopropyl radicals. Their results appear in Table IV. The results are based on the assumption of $A_{19} = 10^{14}$ mol^{-1} cm^3 sec^{-1} and $E_{19} = 0$. In later experimental work[13] they found $A_{19} = 10^{13.8}$ and $E_{19} = 0$. Their value of $k_{18}/k_{19}^{1/2}$ was also obtained from expression vi; however, in their system the products resulting from isopentyl radicals were isopentane by hydrogen atom abstraction from isobutyraldehyde, and isoheptane resulting from *n*-heptyl radicals formed by the addition of isopentyl radicals to ethylene.

The addition of isopentyl radicals to ethylene has not been studied previously. Our values of A_{24} and E_{24} are probably slightly low due to the fact that not all isoheptyl radicals react with isopropyl radicals. About 10% add to ethylene. Because we did not analyze for C_{12} hydrocarbons, we could not account for those isoheptyl radicals which added to ethylene to form isononyl radicals.

From the values in Table IV it appears that the ac-

---

(14) J. A. Pinder and D. J. LeRoy, *Can. J. Chem.*, **35**, 588 (1957).

(15) M. H. Jones and E. W. R. Steacie, *J. Chem. Phys.*, 21, 1018 (1953).

(16) H. Cerfontain and K. O. Kutschke, *Can. J. Chem.*, **36**, 344 (1958).

(17) Assuming addition of *n*-butyl to azoethane has the same rate constant as addition to ethylene, then by our product analysis which does not detect alkyl hydrazines we have accounted for ~98% of the *n*-butyl radicals.

(18) J. A. Kerr and A. F. Trotman-Dickenson, *Trans. Faraday Soc.*, **55**, 572 (1959).

tivation energy for addition of alkyl radicals to ethylene is independent (within 1 kcal/mol) of the alkyl radical. Most of the activation energies are between 6.8 and 7.6 kcal/mol. The preexponential factors are also very similar. Most of the values are between 7×10^{10} and 2×10^{11} mol^{-1} cm^3 sec^{-1}.

Cross Disproportionation and Combination of Isopropyl and Isopentyl Radicals. The ratio of rate constants k_{23}/k_{22} compares the rate of transfer of a hydrogen atom from isopropyl to isopentyl radical, to the rate of transfer of a hydrogen atom from isopentyl to isopropyl radical in a disproportionation reaction. The ratio $k_{23}/k_{22} = 2.96 \pm 0.02$ is in close agreement with the ratio of hydrogen atoms available for disproportionation which is 3.0. Isopropyl can transfer one of six hydrogen atoms to isopentyl, and isopentyl can transfer one of two hydrogen atoms to isopropyl. The observation that k_{23}/k_{22} is essentially equal to the ratio of available hydrogen atoms compares with previous data for the cross disproportionation-to-combination ratios for ethyl and isopropyl radicals.[2,19]

$$C_2H_5 + i\text{-}C_3H_7 \longrightarrow i\text{-}C_5H_{12} \qquad (28)$$

$$\longrightarrow C_2H_4 + C_3H_8 \qquad (29)$$

$$\longrightarrow C_2H_6 + C_3H_6 \qquad (30)$$

k_{29}/k_{28} was reported to be 0.19 while $k_{30}/k_{28} = 0.43$. Thus, $k_{30}/k_{29} = 2.3$. The ratio of available hydrogen atoms is 2.0. Additional data will be required to show whether or not the relative rates of the cross disproportionation reaction for alkyl radicals can be predicted from the number of available hydrogen atoms in each radical.

Thermochemistry. Thermochemical quantities are directly related to the Arrhenius parameters for the forward and reverse reaction rates. The unimolecular decomposition of n-butyl radical to ethylene and ethyl radical has been studied by Morganroth and Calvert.[20]

$$n\text{-}C_4H_9 \longrightarrow C_2H_5 + C_2H_4 \qquad (-2)$$

They found $k_{-2} = 3.73 \times 10^{13} \exp(-28.7/RT)$ sec^{-1}.

Using the value of k_2 reported here and the result for k_{-2}, the enthalpy change of reaction 2 should be $\Delta H_2 = E_2 - E_{-2} - RT = -21.7$ kcal/mol; reasonable thermal data give $\Delta H_2° = -22.8$ kcal/mol at 25°.

The relation between A factors for the forward and reverse reactions and the overall entropy change for the reaction

$$\Delta S_2° = R \ln \left(\frac{A_2}{A_{-2}}\right)$$

was used to calculate $\Delta S_2°$. It was found to be -24.7 eu for a standard state of 1 mol/l. Using the equation $\Delta S°$ (1 atm) $= \Delta S°$ (1 mol/l.) $+ \Delta nR + \Delta nR \ln (0.082\, T)$ from Benson,[21] $\Delta S_2°$ was calculated to be -33.1 eu for a standard state of 1 atm. This result is in agreement with the estimate of $\Delta S_2° = -34.7$ eu calculated from reasonable thermal data.[8] The above equation has not always been expressed correctly, and this has led to confusion among literature values.

The data for $S°(n\text{-}C_4H_9)$ and $S°(C_2H_5)$ are estimates and are probably in error by ±1 eu.[8,21] A different calculation of $\Delta S_2°$ is suggested. Since $\Delta S_2° = S°(n\text{-}C_4H_9) - S°(C_2H_5) - S°(C_2H_4)$ it should be more accurate to estimate the difference $S°(n\text{-}C_4H_9) - S° \cdot (C_2H_5)$ rather than to estimate each absolutely. Let $S°(n\text{-}C_4H_9) - S°(C_2H_5) = S°(n\text{-}C_4H_{10}) - S°(C_2H_6) = 74.12 - 54.85 = 19.27$ eu. With $S°(C_2H_4) = 52.45$ eu, $\Delta S_2° = -33.18$ eu in excellent agreement with the $\Delta S°$ from kinetics. Using $\Delta S_2° = -33.1$ eu and $S°(C_2H_5) = 59.8$ eu,[21] we calculate $S°(n\text{-}C_4H_9) = 79.1$ eu.

In the case of $\Delta H_2°$, we can also estimate the difference $\Delta H_f°(n\text{-}C_4H_9) - \Delta H_f°(C_2H_5)$ from $\Delta H_f°(n\text{-}C_4H_{10}) - \Delta H_f°(C_2H_6) = -9.91$ kcal/mol. This leads to $\Delta H_2° = -22.4$ kcal/mol compared to -21.7 kcal/mol from kinetics. Using $\Delta H_2° = -21.7$ kcal/mol and $\Delta H_f°(C_2H_5) = 26.0$ we estimate $\Delta H_f°(n\text{-}C_4H_9) = 16.8$ kcal/mol. A previous estimate was 15.9 kcal/mol.[8] These data can be used with $\Delta H_f°(n\text{-}C_4H_{10})$ and $\Delta H_f°(H)$ to estimate the bond dissociation energy of the primary C–H bond in $n\text{-}C_4H_{10}$ to be about 99.1 kcal/mol.

The Activated Complex. According to the principle of microscopic reversibility the activated complex should be the same for forward and reverse elementary processes. The agreement of thermochemical quantities calculated above is consistent with this conclusion. We have also assigned frequencies for an activated com-

Table V: Frequency Assignments[a] (cm^{-1}) and the Entropy of Activation

Mode	n-Butyl	Complex	$\Delta S_1^{\ddagger}$
CH_2 rock	721	515	0.35
	721	515	0.35
C–C–C bending	431	306	0.53
	271	192	0.62
Torsion CH_3CH_2–	225	225	...
–$CH_2CH_2\cdot$	102	197	−1.27
–CH_2CH_2–	102	51	1.36
C–C stretch, reaction coord	1000	...	−0.09
–CH_2–$CH_2\cdot$	850	1300	−0.15
		$\Delta S^{\ddagger}$ =	1.70

[a] Only molecule frequencies which change in the complex are given.

---

(19) P. J. Bobby and J. P. Robb, *Proc Roy. Soc.*, **A249**, 5 (1959).

(20) W. E. Morganroth and J. G. Calvert, *J. Amer. Chem. Soc.*, **88**, 5387 (1966).

(21) S. W. Benson, "Thermochemical Kinetics," John Wiley & Sons, Inc., New York, N. Y., 1968, p 9.

(22) S. Glasstone, K. J. Laidler, and H. Eyring, "The Theory of Rate Processes," McGraw-Hill Book Co., Inc., New York, N. Y., 1941.

(23) J. H. Schachtschneider and R. G. Snyder, *Spectrochem. Acta*, **19**, 117 (1963).

plex for reaction 2, and used activated complex theory[22] to calculate the A factors for the forward (2) and reverse (-2) reactions for comparison with experiment. n-Butane was used as a model for n-butyl radical.[23]

In the activated complex the four bending and rocking frequencies were lowered to $^1/_{1.4}$ of their value in butane. This is the effect of lowering the force constants for these vibrations by a factor of 2. Two of the three torsions were adjusted. The torsion about the partial double bond was increased by 1.4 of the difference between its frequency in n-butane (102 cm^{-1}) and its frequency about a double bond (578 cm^{-1}). The torsion about the partial single bond was lowered by $^1/_2$. The frequencies and entropy of activation are shown in Table V.

This simplified description of frequency changes can nevertheless provide realistic calculated values of the A factors. The calculated value $\Delta S^{\ddagger} = 1.70$ eu leads to an A factor for reaction -2 of $10^{13.60}$ sec^{-1} at 298°K, in good agreement with the experimental value $10^{13.57}$ sec^{-1}. Using $\Delta S_2° = -33.2$ eu, this leads to an A factor for the association reaction 2 of about $10^{11.17}$ cc mol^{-1} sec^{-1}, which is fortuitously exactly equal to the experimental value.

Acknowledgments. The authors gratefully acknowledge the financial support of the Faculty Improvement Committee of Colorado State University, and the Research Corporation, Burlingame, California. We thank Mr. D. R. Lawson, who prepared the azoisopropane.

The Kinetics of Heterogeneous Catalytic Electrode Reactions.

II. Charge-Transfer Kinetics

by J. D. E. McIntyre

Bell Telephone Laboratories, Incorporated, Murray Hill, New Jersey *(Received March 20, 1969)*

The kinetic behavior of an electrochemical reaction coupled with a heterogeneous chemical regenerative reaction is analyzed. The steady-state current–voltage curve for this electrode process contains a catalytic current component over the complete potential range in which reduction of the electroactive species occurs. Methods of determining the kinetic parameters of the charge-transfer reaction, *per se*, are presented with particular reference to use of the rotating disk electrode. This analysis provides a basis for the elucidation of the kinetics and mechanism of an oxygen electrode reaction where hydrogen peroxide is formed as an intermediate reduction product which undergoes a surface-catalyzed decomposition.

The kinetic behavior of an electrochemical reaction which is coupled with a surface-catalyzed chemical regenerative reaction was analyzed in a preceding communication[1] with particular reference to the kinetics of the regenerative process. The course of this heterogeneous catalytic electrode reaction (HCER) can be represented schematically as

$$\mathrm{O} + ne \underset{k_{-1}}{\overset{k_1}{\rightleftharpoons}} \mathrm{R} \qquad \text{(Ia)}$$

$$p\mathrm{R} \xrightarrow{k_h} \mathrm{O} + q\mathrm{S} \qquad \text{(Ib)}$$

On defining the regeneration rate fraction[2] to represent that fraction of the electrolysis product, R, consumed in the regenerative cycle after each successive occurrence of the electrolysis reaction, it was shown that the over-all electrode process can be represented in the simple form

$$\theta = \frac{pk_h[C_R(0,t)]^p}{J_R(0,t) + pk_h[C_R(0,t)]^p} = \frac{pk_h[C_R(0,t)]^p}{i/nF} \qquad (1)$$

$$\mathrm{O} + \left(\frac{p}{p-\theta}\right) ne \longrightarrow (1-\theta)\left(\frac{p}{p-\theta}\right)\mathrm{R} + \left(\frac{\theta}{p-\theta}\right) q\mathrm{S} \qquad \text{(II)}$$

The equivalent number of Faradays of charge, n^*, required to reduce each mole of O supplied to the electrode by either mass transport or regeneration is thus given by eq 2.

---

[1] J. D. E. McIntyre, *J. Phys. Chem.*, 71, 1196 (1967).

[2] The symbols and sign conventions used in reaction scheme I and eq 1 are defined in ref 1.

$$n^* = \left(\frac{p}{p - \theta}\right) n \qquad (2)$$

The parameter n^* is mass transport dependent.

The kinetics of the HCER differ significantly from those of a catalytic electrode process in which regeneration occurs *via* a *homogeneous* chemical reaction within the diffusion layer at the electrode surface, owing to the different forms of the equations of continuity.[1] The kinetic behavior of the HCER is exemplified by the electrochemical reduction of oxygen on solid electrode surfaces which catalyze decomposition of the intermediate electrolysis product, hydrogen peroxide (*cf.* references cited in ref 1).

A complete description of the reaction mechanism and electrocatalytic properties of the electrode substrate material for such a process requires a knowledge of the kinetic parameters characteristic of the charge-transfer reaction Ia as well as those for the surface-catalyzed chemical regenerative reaction Ib. In the simple model considered here, the heterogeneous rate constant of the regenerative reaction is assumed to be potential independent.[3] The current–voltage (i–E) curve for this electrode process thus contains a catalytic current component over the complete potential range in which reduction of O occurs. To obtain kinetic parameters characteristic of the electrochemical reaction Ia, *per se*, the rate of regeneration of O *via* reaction Ib must be taken into account.

In the present communication, we extend the previous kinetic analysis for the limiting-current region[1] to the region of mixed chemical kinetic, mass transport, and potential control and examine the form of the steady-state i–E curves for various types of regenerative reactions. Methods for determing the characteristic kinetic parameters of the electrolysis reaction are presented with particular reference to use of the rotating disk electrode (RDE). The case of consecutive electrochemical reactions coupled with a surface-catalyzed regenerative process is considered as well. Finally, the kinetic behavior of the HCER is contrasted with that of the case in which O is reduced in mutally independent parallel reactions.

Theory

For a flux of O, $J_O(0,t)$, at the electrode surface, the cathodic current density for reaction scheme II is

$$i = -nF\left(\frac{p}{p - \theta}\right) J_O(0,t) = -n^*FJ_O(0,t) \qquad (3)$$

Since

$$\lim_{k_h \to 0} \theta = 0 \qquad (4a)$$

and

$$\lim_{k_h \to \infty} \theta = 1 \qquad (4b)$$

it is evident that

$$1 \leq \frac{n^*}{n} \leq \frac{p}{p - 1} \qquad (5)$$

The steady-state flux of O at an RDE, assuming a *uniform* current density over the entire disk surface, is[4–7]

$$J_O(0) = -\frac{i}{n^*F} = -L_O\omega^{1/2}[C_O^\circ - C_O(0)] \qquad (6)$$

where L_i, the Levich constant, is given by[8]

$$L_i = \frac{0.62048D_i^{2/3}\nu^{-1/6}}{1 + 0.2980(D_i/\nu)^{1/3} + 0.14514(D_i/\nu)^{2/3}} \qquad (i = \text{O,R},\ldots) \qquad (7)$$

Although the chemical rate constant, k_h, is assumed here to be independent of potential, it will become evident in the following that θ and n^* can be functions of potential. We therefore denote n^*_{lc} as the value of n^* in the limiting current region where θ and n^* are potential invariant. The limiting current density (lcd) of the HCER is

$$i_{lc} = n_{lc}^*FL_O\omega^{1/2}C_O^\circ \qquad (8)$$

Hence, from eq 6 and 8, the steady-state surface concentration of O is

$$C_O(0) = \frac{1}{L_O\omega^{1/2}F}\left(\frac{i_{lc}}{n_{lc}^*} - \frac{i}{n^*}\right) = \frac{1}{L_O\omega^{1/2}F}\left(\frac{i_d}{n} - \frac{i}{n^*}\right) \qquad (9)$$

where i_d is the normal diffusion-limited current density when $k_h = 0$.

From eq 3 and the general boundary conditions

$$\frac{i}{nF} = -J_O(0,t) + k_h[C_R(0,t)]^p = J_R(0,t) + pk_h(C_R(0,t)]^p \qquad (10)$$

we obtain a general relation for the surface concentration of R. If the bulk solution concentration of R is zero, then

$$C_R(0) = \frac{i}{nFL_R\omega^{1/2}}\left[\frac{pn}{n^*} - (p - 1)\right] \qquad (11)$$

When the electrode is polarized in the cathodic direction, $C_O(0)$ decreases while $C_R(0)$ increases. On rewriting eq 1 as

---

[3] Potential-dependent adsorption of the reaction constituents can be taken into account if the forms of the appropriate adsorption isotherms are known.

[4] V. G. Levich, "Physicochemical Hydrodynamics," Prentice-Hall Inc., Englewood Cliffs, N. J., 1962.

[5] Owing to the complexity of the current-voltage relations for this type of electrode process, the effects of a nonuniform current distribution (*cf.* ref 6 and 7) are not considered here.

[6] J. Newman, *J. Electrochem. Soc.*, **113**, 501 (1966); **115**, 1235 (1966); **114**, 239 (1967).

[7] W. J. Albery and J. Ulstrup, *Electrochim. Acta*, **13**, 281 (1968).

[8] J. Newman, *J. Phys. Chem.*, **70**, 1327 (1966).

$$\theta = \frac{1}{1 + \{L_R\omega^{1/2}/pk_h[C_R(0)]^{p-1}\}} \qquad (1a)$$

it is evident that when $p = 1$, θ and n^* are independent of $C_R(0)$. For this case, $n^* = n^*_{lc}$ over the complete potential range of interest and the ratio n^*/n at a given rotational speed is equal to the ratio i_{lc}/i_d.

When $p > 1$, however, θ and n^* are functions of potential in the region of mixed mass transport, chemical kinetic, and potential control. In this region, n^* varies continuously with potential, increasing monotonically from the value n at the foot of the current wave to the value n^*_{lc} at the lcd plateau, while the catalytic component of the current density increases from zero to its maximum value ($i_{lc} - i_d$).

For an irreversible charge-transfer reaction

$$\frac{i}{nF} = k_1C_O(0) = k_1{}^\circ \exp\left(-\frac{2.3}{b_c}E\right)C_O(0) \qquad (12)$$

where the symbols $k_1{}^\circ$, b_c, E, and F have their usual significance. General analytic expressions for the surface concentrations of O and R can be obtained, for the case of the RDE, by solution of eq 6, 10, and 12. We find

$$C_O(0) = \frac{C_C{}^\circ + (k_h/L_O\omega^{1/2})[C_R(0)]^p}{1 + (k_1/L_O\omega^{1/2})} \qquad (13)$$

For the case $p = 1$

$$C_R(0) = \frac{(k_1 + L_O\omega^{1/2} - 1)C_O{}^\circ}{\left[k_h + L_R\omega^{1/2} + \dfrac{k_h/L_O\omega^{1/2}}{1 + (k_1/L_O\omega^{1/2})}\right]} \qquad (14)$$

When $p = 2$

$$C_R(0) = \frac{-b + (b^2 - 4ac)^{1/2}}{2a} \qquad (15)$$

where

$$a = k_h[2 + (k_1/L_O\omega^{1/2})] \qquad (15a)$$

$$b = L_R\omega^{1/2}[1 + (k_1/L_O\omega^{1/2})] \qquad (15b)$$

$$c = -k_1C_O{}^\circ \qquad (15c)$$

From eq 5 and 9 it is apparent that at potentials in the rising part of the current wave, the primary effect of the regenerative process is to enhance $C_O(0)$ and, hence, the current, in comparison with the normal case ($k_h = 0$). The forms of the relations involving n^* are particularly useful for conceptual purposes. For generation of steady-state i–E curves with a computer, eq 13, 14, and 15 are employed.

From eq 8, 9, and 12, the ratio of the current density for the catalytic case to that for the normal case, at a fixed potential, is

$$\frac{i}{i_n} = \frac{1 + (k_1/L_O\omega^{1/2})}{1 + (n/n^*)(k_1/L_O\omega^{1/2})} \qquad (16)$$

It is apparent from eq 16 that the ratio i/i_n is only equal to the ratio n^*/n in the lcd region, where $k_1/L_O\omega^{1/2} \gg 1$.

I. Steady-State Current–Voltage Curves. The formal standard electrochemical rate constant, k_s, of the electrolysis reaction Ia is defined as

$$k_s = k_1{}^\circ \exp\left(-\frac{2.3}{b_c}E_c{}^\circ\right) = k_{-1}{}^\circ\left(\frac{2.3}{b_a}E_c{}^\circ\right) \qquad (17)$$

where $E_c{}^\circ$ is the formal standard potential. For an irreversible electrode reaction, the current density is

$$i = nFk_s \exp[-2.3(E - E_c{}^\circ)/b_c]C_O(0) \qquad (18)$$

From eq 9 and 18 we obtain two equivalent forms of the steady-state i–E curve for an irreversible HCER at an RDE

$$E = E_c{}^\circ + b_c \log\left(\frac{k_s}{L_O\omega^{1/2}}\right) + b_c \log\left(\frac{i_{lc}/n^*_{lc}}{i/n} - \frac{n}{n^*}\right) \qquad (19a)$$

$$E = E_c{}^\circ + b_c \log\left(\frac{k_s}{L_O\omega^{1/2}}\right) + b_c \log\left(\frac{i_d}{i} - \frac{n}{n^*}\right) \qquad (19b)$$

These relations may be compared to that for the normal case ($k_h = 0$)

$$E = E_c{}^\circ + b_c \log\left(\frac{k_s}{L_O\omega^{1/2}}\right) + b_c \log\left(\frac{i_d}{i} - 1\right) \qquad (20)$$

a. First-Order Catalytic Reaction. When $p = 1$, $n^* = n^*_{lc}$ for all E and eq 19 can be written as

$$E = E_c{}^\circ + b_c \log\left(\frac{k_s}{L_O\omega^{1/2}}\right) - b_c \log\left(\frac{n^*_{lc}}{n}\right) + b_c \log\left(\frac{i_{lc}}{i} - 1\right) \qquad (21)$$

For this case, a plot of log ($i_{lc}/i - 1$) *vs.* E is linear and has a slope equal to the reciprocal of the Tafel parameter, b_c. The half-wave potential, $E_{1/2}$, where $i = i_{lc}/2$, is given by

$$E^{1/2} = E_c{}^\circ + b_c \log\left(\frac{k_s}{L_O\omega^{1/2}}\right) - b_c \log\left(\frac{n^*_{lc}}{n}\right) \qquad (22)$$

Since $n^*_{lc} > n$, the effect of the coupled catalytic reaction is to shift $E_{1/2}$ cathodically from its normal value when $k_h = 0$. This shift reflects the extension of the range of potential control by the action of the chemical regenerative process.

b. Higher-Order Catalytic Reactions. When $p > 1$, n^* is a complicated function of both potential and mass transport rate for intermediate values of ω and cannot be simply evaluated from the steady-state current–voltage curves. The effects of the variation of n^* with potential can be revealed by recasting eq 19 in the form

$$E = E_c{}^\circ + b_c \log\left(\frac{k_s}{L_O\omega^{1/2}}\right) + b_c \log\left(\frac{i_{lc}}{i} - 1\right) - b_c \log\left[\frac{(i_{lc}/i) - 1}{(i_d/i) - (n/n^*)}\right] \qquad (23)$$

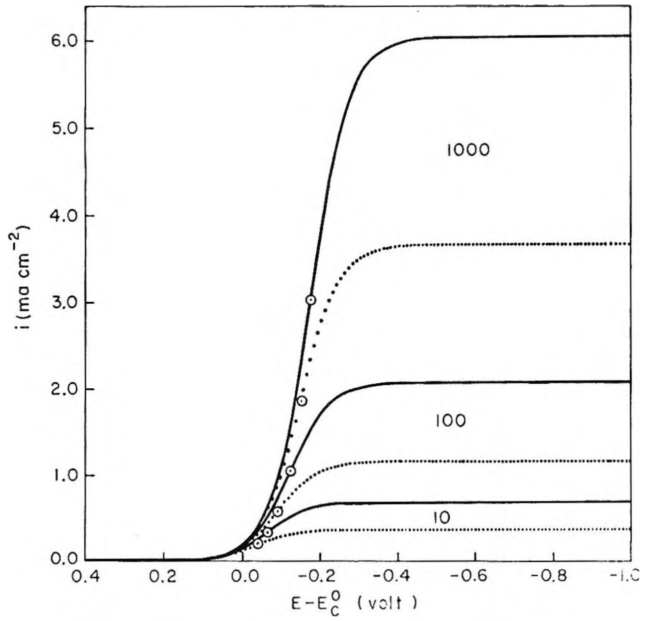

Figure 1. Steady-state current-voltage curves for heterogeneous catalytic ($p = 2$, $k_h = 10^4$ cm^4 mol^{-1} sec^{-1}) and normal ($k_h = 0$) electrode reactions on an RDE for the disk angular velocities $\omega = 10$, 100, and 1000 radians sec^{-1}: ——, HCER; ·······, normal case; ⊙, half-wave potentials.

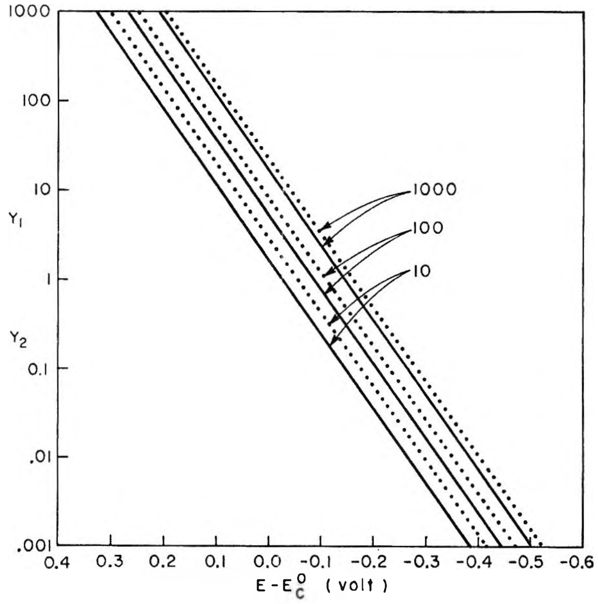

Figure 2. Exact and approximate plots for determination of the Tafel parameter, b_c, of an HCER with $p = 2$, $k_h = 10^4$ cm^4 mol^{-1} sec^{-1}, and $\omega = 10$, 100, and 1000 radians sec^{-1}: ——, exact: $Y_1 = i_d/i - n/n^*$; ·······, approximate: $Y_2 = i_{lc}/i - 1$.

The last term on the right side varies only slightly with potential in the range of interest, since the shape of the i–E curve for the HCER closely resembles that for the normal case ($k_h = 0$). To a good approximation, a plot of log $(i_{lc}/i - 1)$ *vs.* E simply represents a lateral displacement (to more negative potentials) of a graph of log $[(ni_{lc}/n^*_{lc}i) - (n/n^*)]$ *vs.* E, coupled with a slight decrease in slope (*ca.* 2%). The Tafel parameter b_c can thus be determined with reasonable accuracy from the reciprocal slope of a plot of log $(i_{lc}/i - 1)$ *vs.* E. An alternative method of determining b_c is discussed in a following section.

Figure 1 illustrates[9] the form of the steady-state i–E curves at disk angular velocities of 10, 100, and 1000 radians sec^{-1} for the case $p = 2$ and the parametric values: $n = 2$, $D_O = D_R = 10^{-5}$ cm^2 sec^{-1}, $\nu = 10^{-2}$ cm^2 sec^{-1}, $C_O{}^\circ = 10^{-6}$ mol cm^{-3}, $k_s = 10^{-3}$ cm sec^{-1}, $\alpha = 0.5$, $b_c = 0.118315$ V, and $T = 25.0°$. The dotted curves indicate the normal form when $k_h = 0$; the solid curves represent the behavior of a catalytic electrode reaction with $k_h = 10^4$ cm^4 mol^{-1} sec^{-1}. Half-wave potentials are indicated by open circles. The extension of the range of potential control and the enhancement of the current due to increasing mass transport rate and the action of the catalytic reaction are apparent. As the electrode is polarized cathodically, the i–E curve for the HCER appears to grow out of the curve for the normal case, reflecting the increase in n^* with increasing $C_R(0)$. The catalytic component of the current density attains its maximum value at the *l*cd plateau. From Figure 1 it is apparent that the relative enhancement of the current is greater at low rotational speeds, in accord with the variation of θ and $n_{lc}{}^*$ with ω. The kinetic behavior of this lcd region has already been discussed in detail (*cf.* ref 1).

In Figure 2, graphs of $Y_1 = (i_d/i - n/n^*)$ and $Y_2 = (i_{lc}/i - 1)$ are plotted on a logarithmic scale as functions of $E - E_c{}^\circ$ for the HCER discussed above. From this figure, it is apparent that "approximate" plots of log Y_2 *vs.* E (dotted lines), which can readily be constructed from experimental data, are very nearly linear and almost parallel to the theoretical "exact" plots of log Y_1 *vs.* E (solid lines). It should be noted that the exact plots are independent of k_h and $C_O{}^\circ$ (*cf.* eq 19).

II. Evaluation of Kinetic Parameters. The method of evaluating the heterogeneous rate constant, k_h, of the chemical regenerative reaction was discussed in a preceding communication.[1] To determine kinetic parameters characteristic of the charge-transfer reaction Ia, *per se*, the effects of electrode polarization due to the rate of mass transfer and depolarization due to the regenerative reaction must be taken into account. The steady-state RDE method is particularly well suited to this application. By measuring the current density as a function of rotational speed at a series of potentials in the rising part of the steady-state i–E curve and extrapolating the results to infinite rotational speed, the effects of mass transfer and chemical kinetic control on the rate of the electrolysis reaction can be completely removed. The definition of n^* in eq 2 enables a kinetic treatment to be developed which is similar to those em-

---

(9) All illustrations in this article were automatically generated with a General Electric 645 computer.

ployed for RDE studies of other less-complicated types of electrode processes.[10-13]

For an irreversible discharge reaction, we obtain, from eq 9 and 12, the relation

$$\frac{1}{i} = \frac{1}{nFk_1C_O^\circ} + \frac{1}{n^*FL_OC_O^\circ}\left(\frac{1}{\omega^{1/2}}\right) \qquad (24)$$

At constant electrode potential, k_1 is fixed and eq 24 represents a curve with a local slope of $1/n^*FL_OC_O^\circ$ and intercept, on the $1/\omega^{1/2} = 0$ axis, of

$$\frac{1}{i_\infty} = \frac{1}{nFk_1C_O^\circ} \qquad (25)$$

which corresponds to an infinite mass-transfer rate constant. Since

$$\lim_{\omega \to 0} \theta = 1 \qquad (26a)$$

$$\lim_{\omega \to 0} \theta = 0 \qquad (26b)$$

and

$$n^* = \left(\frac{p}{p - \theta}\right) n$$

it is evident for the case $p = 2$, the slope of the curve doubles between the limits $\omega = 0$ and $\omega = \infty$. The limiting slope for *all* p at the $1/\omega^{1/2} = 0$ axis is $1/nFL_OC_O^0$.

The value of the intercept, $1/i_\infty$, is completely independent of parameters pertaining to mass transport and the kinetics of the regenerative process; the variation of i_∞ with E is solely due to charge-transfer polarization. From eq 17 and 25

$$i_\infty = nFk_sC_O^\circ \exp[-2.3(E - E_c^\circ)/b_c] \qquad (27)$$

Hence

$$\log i_\infty = \log nFk_sC_O^\circ - (E - E_c^\circ)/b_c \qquad (28)$$

A plot of log i_∞ *vs.* E is analogous to a conventional Tafel plot and has a slope equal to the reciprocal of the Tafel parameter, b_c. By extrapolating this plot to the standard potential, E_c°, the value of the standard electrochemical rate constant, k_s, of reaction Ia can be determined. The standard exchange current density is defined by

$$i_s^\circ = nFk_s \qquad (29)$$

The apparent exchange current density under the actual experimental conditions is defined by

$$i^\circ = nFk_s \exp[-2.3(E_r - E_c^\circ)/b_c]C_O^\circ \qquad (30)$$

and can be evaluated by extrapolation of the plot of log i_∞ *vs.* E to the hypothetical reversible potential, E_r.[14]

Figure 3 illustrates the form of the $1/i$ *vs.* $1/\omega^{1/2}$ plots for an HCER with $p = 2$ and $k_h = 10^4$ cm^4 mol^{-1} sec^{-1}. The dotted lines indicate the kinetic behavior for the normal case ($k_h = 0$); the solid curves refer to the catalytic reaction. It is important to note the changes in curvature which occur as the electrode is polarized more cathodically. For potentials near the foot of the current wave (upper curves) the curvature in the plot of $1/i$ is gradual as the $1/\omega_{1/2} = 0$ axis is approached. At more negative potentials (lower curves), the curvature becomes increasingly sharper. In the limit, the solid curves become tangential to the dotted lines since $\theta \rightarrow 0$ as $\omega \rightarrow \infty$. To avoid serious errors in the extrapolation of experimental plots, it is necessary to obtain data at high disk rotational speeds (10,000 rpm or greater). Incorrect extrapolation will yield Tafel slopes, b_c, which are too high and standard rate constants, k_s, which are too low.

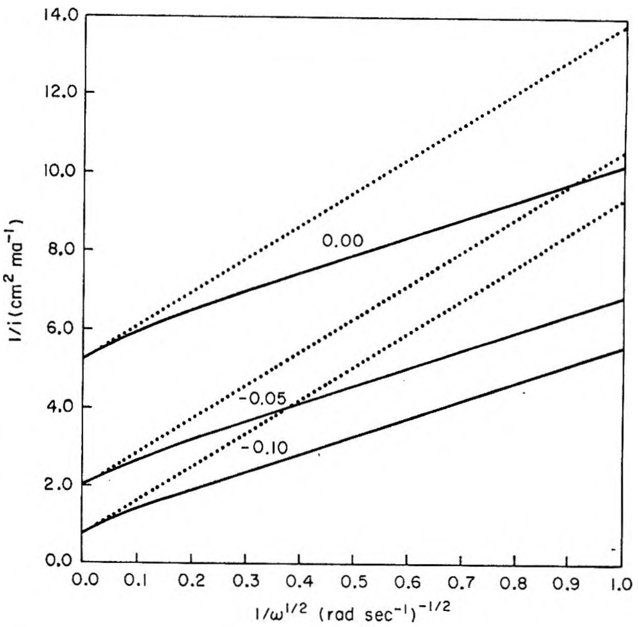

Figure 3. Variation of $1/i$ with $1/\omega^{1/2}$ for an HCER ($p = 2$, $k_h = 10^4$ cm^4 mol^{-1} sec^{-1}) and a normal electrode reaction at the potentials, $E - E_c^\circ$ (volts), indicated: ——, HCER; ·····, normal case.

III. Consecutive Electrochemical Reactions. The kinetic behavior of two consecutive electrochemical reactions which are coupled with a heterogeneous chemical regenerative reaction is now considered. The reaction scheme is

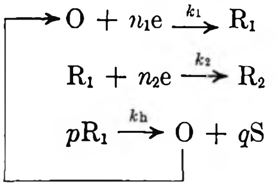

$$O + n_1e \xrightarrow{k_1} R_1 \qquad (IIIa)$$

$$R_1 + n_2e \xrightarrow{k_2} R_2 \qquad (IIIb)$$

$$pR_1 \xrightarrow{k_h} O + qS \qquad (IIIc)$$

---

(10) A. N. Frumkin and G. Tedoradse, *Z. Elektrochem.*, **62**, 251 (1958).

(11) D. Jahn and W. Vielstich, *J. Electrochem. Soc.*, **109**, 849 (1962).

(12) Z. Galus and R. N. Adams, *J. Phys. Chem.*, **67**, 866 (1963).

(13) A. C. Riddiford, "Advances in Electrochemistry and Electrochemical Engineering," Vol. 4, P. Delahay, Ed., Interscience Publishers, New York, N. Y., 1966, p 96.

(14) In experimental studies of the HCER, it is usually expedient to make $C_R^\circ = 0$ to avoid a continuous decomposition of R *via* reaction Ib. The hypothetical values of E_r and i° correspond to the case $C_R^\circ = C_O^\circ$.

All reactions are assumed to be irreversible. The components of the total current density which correspond to the rates of the individual charge-transfer steps IIIa and IIIb are denoted by i_1 and i_2.

The flux boundary condition for reaction III is

$$J_O(0) + J_{R_1}(0) + J_{R_2}(0) + (p - 1)k_h[C_{R_1}(0)]^p = 0 \quad (31)$$

and the regeneration rate fraction now becomes

$$\theta = \frac{pk_h[C_{R_1}(0)]^p}{J_{R_1}(0) + J_{R_2}(0) + pk_h[C_{R_1}(0)]^p} \quad (32a)$$

i.e.

$$\theta = \frac{pk_h[C_{R_1}(0)]^p}{i_1/n_1F} \quad (32b)$$

It follows that

$$\frac{i_1}{n_1F} = -\left(\frac{p}{p - \theta}\right)J_O(0) \quad (33)$$

We define, as before, the quantity n^*_1 to represent the number of Faradays of charge which are required to reduce (*via* steps IIIa and IIIc) each mole of O supplied to the electrode surface by either mass transport or regeneration. Thus

$$n_1^* = \left(\frac{p}{p - \theta}\right)n_1 \quad (34)$$

On denoting i_{lc_1} as the lcd for reaction IIIa and $n^*_{lc_1}$ as the corresponding value of n^*_1, the surface concentration of O is given by

$$C_O(0) = \frac{1}{L_O\omega^{1/2}F}\left(\frac{i_{lc_1}}{n^*_{lc_1}} - \frac{i_1}{n^*_1}\right) \quad (35a)$$

i.e.

$$C_O(0) = \frac{1}{L_O\omega^{1/2}F}\left(\frac{i_{d1}}{n_1} - \frac{i_1}{n^*_1}\right) \quad (35b)$$

where i_{d1} is the normal diffusion-limited current density of reaction IIIa when $k_h = 0$. When the bulk solution concentration of R_1 is zero, the surface concentration of R_1 is

$$C_{R_1}(0) = \frac{1}{L_{R_1}\omega^{1/2}F}\left\{\left[p\left(\frac{n_1}{n^*_1}\right) - (p - 1)\right]\frac{i_1}{n_1} - \frac{i_2}{n_2}\right\} \quad (36)$$

General analytic expressions for the surface concentration of O and R_1 can be obtained by a procedure similar to that used for reaction I, for generating steady-state *i–E* curves with a computer.

The total current density of reaction III is

$$i = i_1 + i_2 \quad (37)$$

The steady-state *i–E* curve for reaction III at an RDE is then given by

$$i = \frac{n_1k_{s1}}{L_O\omega^{1/2}}\exp\left[-\frac{2.3}{b_{c_1}}(E - E_{c1}°)\right]\left(\frac{i_{lc_1}}{n^*_{lc_1}} - \frac{i_1}{n^*_1}\right) + \frac{n_2k_{s2}}{L_{R_1}\omega^{1/2}}\exp\left[-\frac{2.3}{b_{c2}}(E - E_{c2}°)\right]\left\{\left[\frac{pn_1}{n^*_1} - (p - 1)\right]\frac{i_1}{n_1} - \frac{i_2}{n_2}\right\} \quad (38)$$

where k_{s1}, k_{s2}, $E_{c1}°$, and $E_{c2}°$ are the formal standard rate constants and potentials of reactions IIIa and IIIb, and b_{c1} and b_{c2} are the corresponding cathodic Tafel slopes.

When the values of k_1, k_2, and k_h are such that the steady-state *i–E* curve exhibits two well-defined limiting current regions, the kinetic parameters for the successive steps can be found. For potentials more positive than the limiting current region of the first wave, i_2 is negligibly small and the second term on the right side of eq 36 can be neglected. The method of determining the kinetic parameters for the first step is then identical with that discussed previously for reaction I.

For potentials in the second wave, the variation of i_2 with potential is given by

$$i_2 = \frac{n_2k_{s2}}{L_{R_1}\omega^{1/2}}\exp\left[-\frac{2.3}{b_{c2}}(E - E_{c2}°)\right]\left\{\left[\frac{pn_1}{n^*_1} - (p - 1)\right]\frac{i_1}{n_1} - \frac{i_2}{n_2}\right\} \quad (39)$$

When $p = 2$

$$E = E_{c2}° + b_{c2}\log\left(\frac{k_{s2}}{L_{R_1}\omega^{1/2}}\right) + b_{c2}\log\left[\frac{n_2}{n_1}\left(\frac{2n_1}{n^*_1} - 1\right)\frac{i_1}{i_2} - 1\right] \quad (40)$$

Figure 4 illustrates the form of the steady-state *i–E* curves for consecutive electrochemical reactions at disk rotational speeds of 10, 100, and 1000 radians sec^{-1}, with $n_1 = n_2 = 2$, $k_{s2} = 10^{-3}$ cm sec^{-1}, $k_{s2} = 10^{-20}$ cm sec^{-1}, $b_{c1} = b_{c2} = 0.118315$ V, and $E_{c1}° - E_{c2}° = 1.0$ V.[15] Other parameters have the same values as for Figure 1. The solid curves represent the kinetic behavior of an HCER with $p = 2$ and $k_h = 10^4$ cm^4 mol^{-1} sec^{-1}; the dotted lines illustrate the normal behavior when $k_h = 0$. Dashed curves show the variation of the component, i_1, with potential.

Two well-defined current waves are evident in Figure 4. The kinetic behavior of the first wave is identical with that discussed for reaction I. At the foot of the second wave, $i_1 = i_{lc_1}$ and $n^*_1 = n^*_{lc_1}$. At more negative potentials, however, $C_{R_1}(0)$ falls due to the increased rate of consumption of R_1 *via* step IIIb. As a

---

(15) Note particularly in this example that $E_{c2}°$ is more positive than $E_{c1}°$, as is the case for the reactions

$$O_2 + 2H^+ + 2e \rightleftarrows H_2O_2 \quad E° = 0.713 \text{ V}$$

$$H_2O_2 + 2H^+ + 2e \rightleftarrows 2H_2O \quad E° = 1.77 \text{ V}$$

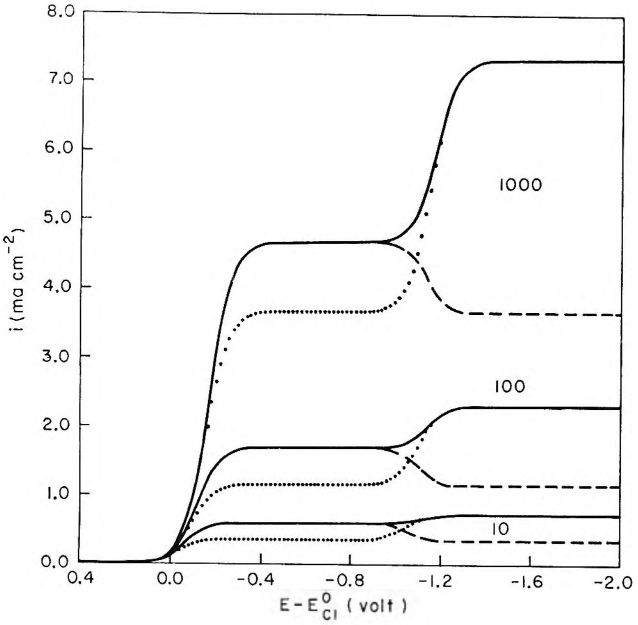

Figure 4. Steady-state current-voltage curves for consecutive electrochemical reactions coupled with a heterogeneous chemical regenerative reaction (p = 2, k_h = 10^4 cm^4 mol^{-1} sec^{-1}) on an RDE for ω = 10, 100, and 1000 radians sec^{-1}: HCER: ----, i_1; ——, $i = i_1 + i_2$; normal case (k_h = 0): ······, i.

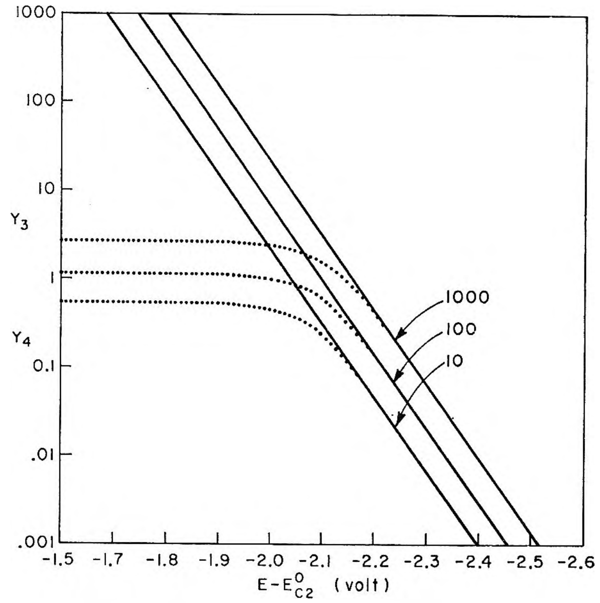

Figure 5. Exact and approximate plots for determination of the Tafel parameter, b_{c2}, of the second electrochemical reaction of an HCER with p = 2, k_h = 10^4 cm^4 mol^{-1} sec^{-1}: ——, exact: $Y_3 = \{(n_2i_1/n_1i_2)[pn_1/n_1{}^* - (p - 1)] - 1\}$; ·······, approximate: $Y_4 = [(i_{d2} - i_{d1})/(i - i_{d1}) - 1]$.

result, the rate of regeneration of O by the catalytic reaction IIIc decreases. As the potential is scanned cathodically through the second wave, i_1 and $n^*{}_1$ recede from their maximum values of i_{lc_1} and $n^*{}_{lc_1}$ in the lcd region of the first wave until finally, in the lcd region of the second wave, they become equal to i_{d1} and n_1 as $C_{R_1}(0)$ becomes zero.

In the second wave, the potential span of the rising section is shortened owing to the enhancement of the limiting current of the first wave by the regenerative reaction IIIc. The exaltation of the total current by the catalytic reaction persists well into the second wave, until the electrode potential becomes sufficiently negative that the rate of consumption of R_1 by the charge-transfer reaction IIIb greatly exceeds that due to reaction IIIc. Finally, the second wave coalesces again with that for the normal case as the current density approaches its limiting value, i_{d2}. For the catalytic electrode reaction, the height of the limiting current plateau of the first wave varies relative to that of the second, according to the variation of θ and $n^*{}_{lc1}$ with the angular velocity of the disk. The value of the lcd of the second wave, i_{d2}, is independent of the kinetics of the catalytic reaction and thus affords a convenient reference level for determining i_{d1} and the magnitude of the catalytic component of the current density in the lcd region of the first wave. From the latter value, the heterogeneous chemical rate constant, k_h, of the regenerative reaction can be evaluated.[1]

The Tafel parameter, b_{c2}, of reaction IIIb can be determined, in principle, from the reciprocal slope of a graph of log $\{(n_2i_1/n_1i_2)\ [(pn_1/n^*{}_1) - (p - 1)] - 1\}$ *vs.* E for potentials in the rising part of the second wave (*cf.* eq 39). In this region, to a good approximation (*cf.* eq 16)[16]

$$\frac{i_1}{n^*{}_1} = \frac{i_{lc_1}}{n^*{}_{lc_1}} = \frac{i_{d1}}{n_1} \tag{41}$$

The quantity, $n^*{}_1$, and the individual current density components, i_1 and i_2, cannot be directly determined from the experimental i–E curves, however, owing to the recession of i_1 from its maximum value (*cf.* Figure 4). In the second wave, therefore, $n^*{}_1 \neq n^*{}_{lc_1}$, $i_1 \neq i_{lc_1}$, and $i_2 \neq (i - i_{lc_1})$.

From eq 39 and 41, we obtain for the case p = 2

$$E = E_{c2}{}^\circ + b_{c2} \log\left(\frac{k_{s2}}{L_{R_1}\omega^{1/2}}\right) + b_{c2} \log\left[\frac{(i_{d2} - i_{d1})(2 - n^*{}_1/n_1)}{i_2} - 1\right] \tag{42}$$

Near the limiting current of the second wave, $n^*{}_1 \rightarrow n_1$ and $i_2 \rightarrow (i - i_{d1})$. Thus an "approximate" plot of log $[(i_{d2} - i_{d1})/(i - i_{d1}) - 1]$ *vs.* E has a slope which approaches $1/b_{c2}$ at potentials in this region and can be used for the analysis of experimental data. Figure 5 illustrates the form of the exact (eq 42) and approximate plots for the HCER whose steady-state i–E curves are illustrated in Figure 4. At potentials near the foot of the wave, $i \approx i_{lc_1}$, and the approximate plots

---

[16] Equation 41 is only valid for potentials equal to or more negative than those in the lcd region of the first wave, *i.e.*, where $k_1/L_O\omega^{1/2} \gg 1$.

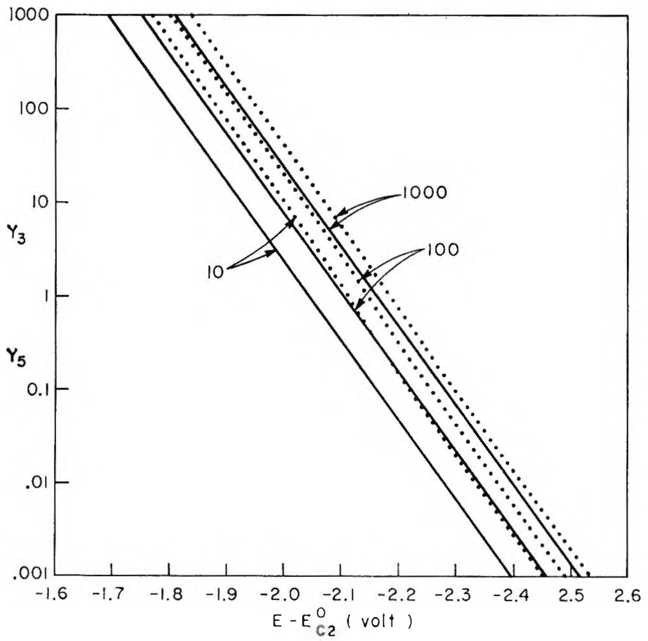

Figure 6. Exact and approximate plots for determination of b_{c2}: ——, exact: $Y_3 = \{(n_2 i_1/n_1 i_2)[pn_1/n_1 - (p - 1)] - 1\}$; ·······, approximate: $Y_5 = [(2 - n_{1c1}^*/n_1)(i_{d2} - i_{d1})/(i - i_{1c1}) - 1]$.

(dotted curves) have an almost constant value. At more negative potentials, they merge with the exact plots (solid lines). It is evident that the approximation becomes increasingly better as the rotational speed is increased and the effects of the regenerative reaction, IIIc, are minimized. In Figure 6, the dotted curves represent "approximate" plots of log $[(2 - n^*_{1c_1}/n_1)(i_{d2} - i_{d1})/(i - i_{1c_1}) - 1]$ *vs.* E Comparison with the exact plots (solid lines) indicates that the dotted curves are shifted to more negative potentials, as was the case in Figure 1. The slopes of the approximate plots, however, provide a very good estimate of the value of $1/b_{c_2}$, at potentials near the foot of the wave. Even at potentials near the lcd region, the approximation remains surprisingly good, in spite of the recession of i_1, owing to a cancellation of errors in the ratio $(2 - n^*_{1c_1})/(i - i_{1c_1})$.

The standard rate constant, k_{s2}, and exchange-current density, i_s°, of reaction IIIb can be evaluated by a method similar to that described for the first wave. From eq 39 and 41, we have for the case $p = 2$

$$\frac{1}{i_2} = \frac{1}{(2 - n^*_1/n_1)n_2Fk_2(L_O/L_{R_1})C_O^\circ} + \frac{1}{(2 - n^*_1/n_1)n_2FL_OC_O^\circ}\left(\frac{1}{\omega^{1/2}}\right) \tag{43}$$

Since $n^*_1 \rightarrow n_1$ as $\omega \rightarrow \infty$, the reciprocal of the intercept of the curve represented by eq 43 on the $1/\omega^{1/2} = 0$ axis for the HCER (solid curves) and those for the normal case (dotted lines) for three potentials in the rising part of the second wave. The solid curves lie above the corresponding dotted lines, since i_2 for the catalytic electrode process is less than that for the normal case, in contrast to the behavior of i_1 in the first wave (*cf.* Figure 3). The separation of curve and line decreases as the electrode potential is made more negative, reflecting the decrease of θ and n^*_1 with increasing $C_{R_1}(0)$. It should be noted that at constant potential both

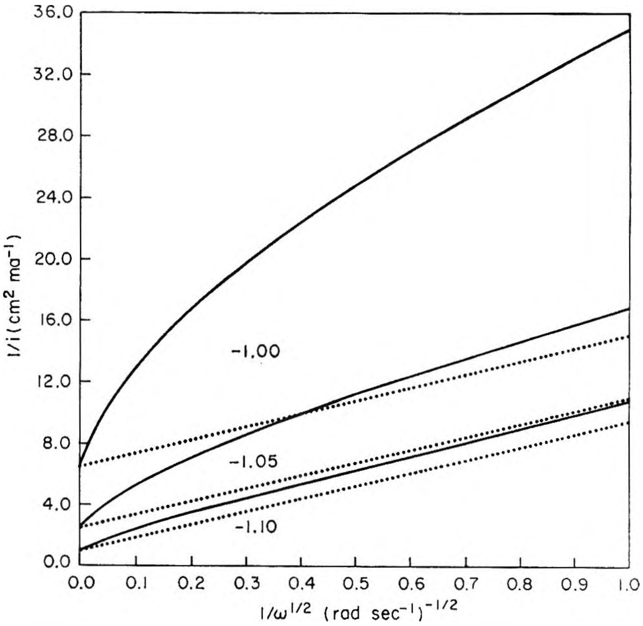

Figure 7. Variation of $1/i$ with $1/\omega^{1/2}$ for the second waves of an HCER ($p = 2$, $k_h = 10^4$ cm^4 mol^{-1} sec^{-1}) and normal consecutive electrochemical reactions at the potentials, $E - E_{c2}^\circ$ (volts), indicated: ——, HCER; ·······, normal.

$$\lim_{\omega \to 0} (2 - n^*_1/n_1) = 1 \tag{44a}$$

and

$$\lim_{\omega \to 0} (2 - n^*_1/n_1) = 1 \tag{44b}$$

The latter result arises since for fixed potentials in the second wave, n^*_1 passes through a maximum as ω is increased from 0 to ∞. This variation in n^*_1 is made more evident by observing how a constant-potential line cuts through the second waves of the steady-state i–E curves in Figure 4. At low rotational speeds the intersection occurs near the lcd plateau, where $n^*_1 \rightarrow n_1$ since $C_{R_1}(0) \rightarrow 0$. At high rotational speeds the line crosses the i–E curve near the foot of the second wave, where $n^*_1 \rightarrow n^*_{1c_1}$. It will be recalled that as $\omega \rightarrow \infty$, $n^*_{1c_1} \rightarrow n_1$.

The dotted lines in Figure 7 represent approximate experimental plots of $1/(i - i_{1c_1})$ *vs.* $1/\omega^{1/2}$. These plots have the same intercepts on the $1/\omega^{1/2} = 0$ axis as the exact plots and enable values of $i_{2\infty}$ to be determined as a function of potential.

Discussion

The preceding kinetic analysis is particularly relevant to studies of the kinetics and mechanism of oxygen reduction on solid electrodes which act as catalysts for the heterogeneous chemical decomposition of the intermediate electrolysis product, hydrogen peroxide. Determination of all the kinetic parameters pertinent to this complex electrode process is essential for a detailed understanding of how the mechanism is affected by the pH of the electrolyte and the electrocatalytic properties of the electrode substrate material. Steady-state forced-flow techniques such as the RDE method are particularly useful since they often permit kinetic parameters to be determined in a potential region where the electrode is not covered (or is only partially covered) by a surface oxide film.

It is important to distinguish between the kinetic behavior of the HCER discussed here and that of an electrode process in which O is reduced to the final product S and the intermediate R_1 by simple *parallel* reactions which are *not* coupled through an intermediate. The latter case has recently been analyzed by Damjanovic, Genshaw, and Bockris[17] for studies of the kinetics of oxygen electrode reactions using an RDE with a concentric ring electrode.[18-20] The ratio of the rates of consumption of O *via* the two parallel paths is denoted by x. For simple parallel reactions, the value of x is dependent on potential but not on mass transport rate. For the HCER, however, the quantity, x, is dependent on potential, mass transport rate, and chemical kinetics. The analysis of the form of the diagnostic plots of $I_{\text{disk}}/I_{\text{ring}}$ *vs.* $\omega^{-1/2}$ for the HCER is considerably more complex than that for the simple parallel reactions although the plots for these two types of mechanism have several features in common. The distinction between the kinetics of heterogeneous catalytic and parallel electrode reactions is discussed in detail elsewhere.[21]

A close similarity also exists between the kinetic behavior of an HCER and that of an ECE mechanism

$$\begin{tikzcd}
O \arrow[r, "n_1e"] & R_1 \arrow[r, "n_2e"] \arrow[d, "k_d"] & R_2 \\
& X \arrow[r, "n_3e"] & S
\end{tikzcd}$$

in which the rate of reduction of the intermediate, R_1, to S is controlled by a heterogeneous *chemical* decomposition step. Methods of distinguishing between these two reaction types will be presented in a forthcoming communication.

Acknowledgment. It is a pleasure to acknowledge helpful discussions with Dr. P. C. Milner and assistance in computer programming by W. F. Peck, Jr.

(17) A. Damjanovic, M. A. Genshaw, and J. O'M. Bockris, *J. Chem. Phys.*, **45**, 4057 (1966).

(18) A. Damjanovic, M. A. Genshaw, and J. O'M. Bockris, *J. Phys. Chem.*, **70**, 3761 (1966); **71**, 3722 (1967).

(19) A. Damjanovic, M. A. Genshaw, and J. O'M. Bockris, *J. Electrochem. Soc.*, **114**, 466, 1107 (1967).

(20) M. A. Genshaw, A. Damjanovic, and J. O'M. Bockris, *J. Electroanal. Chem.*, **15**, 163, 173 (1967).

(21) J. D. E. McIntyre, *J. Phys. Chem.*, **73**, 4111 (1969).

On the Distinction between the Kinetics of Parallel and Heterogeneous Catalytic Electrode Reactions

by J. D. E. McIntyre

Bell Telephone Laboratories, Incorporated, Murray Hill, New Jersey *(Received March 20, 1969)*

The kinetic behavior of a heterogeneous catalytic electrode reaction can be described in terms of a "pseudo-parallel" reaction scheme which is analogous in form to that for simple parallel reactions. Such kinetic schemes are currently employed in studies of the complex mechanism of the oxygen electrode reaction. Criteria are developed for distinguishing between these two types of reaction mechanism with particular reference to use of a rotating ring-disk electrode system.

In a recent communication,[1] Damjanovic, Genshaw, and Bockris have discussed the use of the rotating disk electrode (RDE) with a concentric ring electrode for distinguishing between intermediates and products evolved in parallel electrochemical reactions. It is the purpose of this article to show that the diagnostic plots for a heterogeneous catalytic electrode reaction (HCER) have features in common with those for simple parallel reactions and to provide criteria for establishing the actual reaction mechanism.

Theory

I. Parallel Electrochemical Reactions. An electrode process consisting of parallel electrochemical reactions which yield the same final product can be represented schematically as[2-4]

$$\mathrm{O} + n_1\mathrm{e} \xrightarrow{k_1} \mathrm{R} \tag{Ia}$$

$$\mathrm{R} + n_2\mathrm{e} \xrightarrow{k_2} \mathrm{S} \tag{Ib}$$

$$\mathrm{O} + n_3\mathrm{e} \xrightarrow{k_3} \mathrm{S} \tag{Ic}$$

where k_1, k_2, k_3, and n_1, n_2, n_3 represent the formal heterogeneous electrochemical rate constants and the number of electrons transferred in the individual steps, respectively. The partial current densities corresponding to the rates of these steps on the disk electrode will be denoted as i_1, i_2, and i_3 and are assumed to be *uniform* over the entire disk surface (*cf.* ref 3). Cathodic currents and fluxes directed away from the electrode surface ($x = 0$) are taken as positive.

The ring-electrode current corresponds to the diffusion-limited rate of reoxidation to O of that fraction of the intermediate species, R, which escapes from the disk and is transported to the ring by convective diffusion. The collection efficiency, N, of the ring electrode is a function of the geometry of the ring and disk but is independent of the angular velocity of the assembly.[5-8] A general relation for the ratio of the disk current to the ring current for reaction I is obtained as follows.

Since the flux of R (moles per square centimeter per second) at the disk surface is

$$J_{\mathrm{R}}(0) = \frac{i_1}{n_1F} - \frac{i_2}{n_2F} \tag{1}$$

the *absolute* value of the ring current is given by

$$I_{\mathrm{r}} = n_1FNAJ_{\mathrm{R}}(0) \tag{2}$$

where F is the Faraday constant and A is the geometric surface area of the disk. Hence

$$I_{\mathrm{r}} = N[I_1 - (n_1/n_2)I_2] \tag{3}$$

where I_1 and I_2 are the partial disk currents corresponding to reaction steps Ia and b. The total disk current is

$$I_{\mathrm{d}} = I_1 + I_2 + I_3 \tag{4}$$

From eq 3 and 4

$$I_{\mathrm{d}} = [1 + (n_2/n_1)]I_1 - (n_2/n_1)(I_{\mathrm{r}}/N) + I_3 \tag{5}$$

We now define the quantity, x, to represent the ratio of the rates of consumption of O *via* reactions Ia and c

$$x = \frac{n_1I_3}{n_3I_1} \tag{6}$$

---

(1) A. Damjanovic, M. A. Genshaw, and J. O'M. Bockris, *J. Chem. Phys.*, **45**, 4057 (1966).

(2) For consistency with previous treatments[3,4] of the kinetics of the HCER, it has been necessary to alter the numbering of the steps in the reaction scheme used by Damjanovic, *et al.*[1] The parameters n_3 and k_3 in their communication are identical with n_2 and k_2 in reaction scheme I above.

(3) J. D. E. McIntyre, *J. Phys. Chem.*, **71**, 1196 (1967).

(4) J. D. E. McIntyre, *ibid.*, **73**, 4102 (1969).

(5) Yu. B. Ivanov and V. G. Levich, *Dokl. Akad. Nauk SSSR*, 126, 1029 (1959).

(6) V. G. Levich, "Physicochemical Hydrodynamics," Prentice-Hall, Inc., Englewood Cliffs, N. J., 1962, p 329.

(7) A. C. Riddiford, "Advances in Electrochemistry and Electrochemical Engineering," Vol. 4, P. Delahay, Ed., Interscience Publishers, New York, N. Y., 1966, p 108.

(8) W. J. Albery and S. Bruckenstein, *Trans. Faraday Soc.*, **62**, 120 (1966).

From eq 5 and 6

$$I_1 = \frac{I_d + (n_2/n_1)(I_r/N)}{(n_3/n_1)x + (n_2/n_1) + 1} \qquad (7)$$

The steady-state flux of a species i at an RDE is

$$J_i(0) = L_i\omega^{1/2}[C_i(0) - C_i^0] \qquad (8)$$

where $C_i(0)$ and $C_i°$ are the surface and bulk solution concentrations of this species. The Levich constant, L_i, is given by[9,10]

$$L_i = \frac{0.62048 D_i^{2/3}\nu^{-1/6}}{1 + 0.2980(D_i/\nu)^{1/3} + 0.14514(D_i/\nu)^{2/3}} \qquad (i = \mathrm{O, R}, \ldots) \qquad (9)$$

where D_i is the diffusion coefficient of species i in the supporting electrolyte with kinematic viscosity, ν. The product, $L_i\omega^{1/2}$, is equal to the ratio of D_i to the diffusion-boundary layer thickness, δ_i.

The partial current density, i_2, is given by

$$i_2 = n_2Fk_2C_R(0) \qquad (10)$$

With $C_R° = 0$, we have from eq 1, 2, 8, and 10

$$I_1 = [1 + (k_2/L_R\omega^{1/2})](I_r/N) \qquad (11)$$

Hence from eq 7 and 11, the ratio of the disk current to the ring current is

$$\frac{I_d}{I_r} = \frac{1}{N}\left[\left(\frac{n_3}{n_1}\right)x + 1\right] + \frac{1}{N}\left[\left(\frac{n_3}{n_1}\right)x + \frac{n_2}{n_1} + 1\right]\left(\frac{k_2}{L_R\omega^{1/2}}\right) \qquad (12)$$

Equation 12 is a more general form of the diagnostic relation originally derived by Damjanovic, Genshaw, and Bockris.[1] These authors have analyzed reaction scheme I and deduced the form of plots of I_d/I_r *vs.* $\omega^{1/2}$ for several possible combinations of the rate constants k_1, k_2, and k_3. For this scheme, the rates of the parallel electrochemical reactions are coupled through the variation of $C_O(0)$, which is a function of both potential and mass transport rate. However, the quantity, x, which expresses their relative velocity, is independent of mass transport; x is potential dependent, if the Tafel parameters, b_{c1} and b_{c3}, of reaction steps Ia and c are different. This analysis has been employed[11-13] to provide diagnostic criteria for the elucidation of the mechanism of the electrochemical reduction of oxygen on noble metal electrodes and to establish the role of the intermediate electrolysis product, hydrogen peroxide. To determine the actual mechanism for this complex electrode process, it is particularly important to distinguish between the results of the diagnostic analysis for parallel electrochemical reactions[1] and those for a heterogeneous catalytic electrode reaction.

II. Heterogeneous Catalytic Electrode Reactions. The HCER is represented schematically as

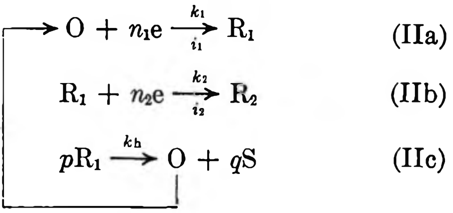

$$\mathrm{O} + n_1\mathrm{e} \underset{i_1}{\xrightarrow{k_1}} \mathrm{R_1} \qquad (\mathrm{IIa})$$

$$\mathrm{R_1} + n_2\mathrm{e} \underset{i_2}{\xrightarrow{k_2}} \mathrm{R_2} \qquad (\mathrm{IIb})$$

$$p\mathrm{R_1} \xrightarrow{k_h} \mathrm{O} + q\mathrm{S} \qquad (\mathrm{IIc})$$

Reaction IIc represents a surface-catalyzed *chemical* regenerative reaction of order p (with respect to R_1) and with a heterogeneous chemical rate constant, k_h, which is independent of potential. The kinetic behavior of the HCER has been analyzed in detail in recent communications.[3,4] It is particularly relevant to studies of the kinetics and mechanism of oxygen reduction on solid metal electrodes which act as catalysts for the heterogeneous chemical decomposition of hydrogen peroxide (*cf.* references cited in ref 3 and 4). On defining the steady-state regeneration rate fraction of reaction II as

$$\theta = \frac{pk_h[C_{R_1}(0)]^p}{J_{R_1}(0) + J_{R_2}(0) + pk_h[C_{R_1}(0)]^p} = \frac{pk_h[C_{R_1}(0)]^p}{i_1/n_1F} \qquad (13)$$

it was shown[4] that reactions IIa and c can be combined as

$$\mathrm{O} + n_1^*\mathrm{e} \rightarrow (1 - \theta)\left(\frac{p}{p - \theta}\right)\mathrm{R_1} + \left(\frac{\theta}{p - \theta}\right)q\mathrm{S} \qquad (\mathrm{III})$$

where n_1^*, the equivalent number of Faradays of charge required to reduce each mole of O supplied to the electrode by either mass transport or regeneration, is given by

$$n_1^* = \left(\frac{p}{p - \theta}\right)n_1 \qquad (14)$$

On rearranging, reaction III can be resolved into two "pseudo-parallel" reactions corresponding to the limiting cases obtained when $k_h = 0, \theta = 0$, and $k_h = \infty$, $\theta = 1$, respectively. The kinetic behavior of the HCER can then be expressed in terms of a "parallel" reaction scheme which is equivalent in over-all stoichiometry and kinetics to reaction II but which is identical in form with the simple parallel reaction scheme I[14]

$$\mathrm{O} + n_1\mathrm{e} \rightarrow \mathrm{R_1} \qquad (\mathrm{IVa})$$

---

[9] Reference 6, p 69.

[10] J. Newman, *J. Phys. Chem.*, **70**, 1327 (1966).

[11] A. Damjanovic, M. A. Genshaw, and J. O'M. Bockris, *ibid.*, **70**, 3761 (1966); *ibid.*, **71**, 3722 (1967).

[12] A. Damjanovic, M. A. Genshaw, and J. O'M. Bockris, *J. Electrochem. Soc.*, **114**, 466, 1107 (1967).

[13] M. A. Genhsaw, A. Damjanovic, and J. O'M. Bockris, *J. Electroanal. Chem.*, **15**, 163, 173 (1967).

[14] The species R_2 and S may be chemically identical. Here they are denoted as separate entities for mathematical convenience.

$$\mathrm{R_1} + n_2\mathrm{e} \rightarrow \mathrm{R_2} \qquad \text{(IVb)}$$

$$\mathrm{O} + \left(\frac{p}{p-1}\right)n_1\mathrm{e} \rightarrow \left(\frac{q}{p-1}\right)\mathrm{S} \qquad \text{(IVc)}$$

It must be emphasized that the ratio of the velocities of reactions IVa and c is not simply dependent on the potential, as is the case for reactions Ia and c, but rather is a complex function of potential, mass transport rate, and chemical kinetics.

The rates of consumption of O *via* the two parallel paths are equal to the velocities of the reactions IVa and c. Now

$$v_{\mathrm{IVa}} = J_{\mathrm{R_1}}(0) + J_{\mathrm{R_2}}(0) \qquad (15)$$

and

$$v_{\mathrm{IVc}} = \left(\frac{p-1}{q}\right)J_{\mathrm{S}}(0) \qquad (16)$$

The quantity, x, for the HCER is therefore given by

$$x = \frac{v_{\mathrm{IVc}}}{v_{\mathrm{IVa}}} \qquad (17)$$

Now for reaction II

$$J_{\mathrm{S}}(0) = qk_{\mathrm{h}}[C_{\mathrm{R_1}}(0)]^p \qquad (18)$$

Hence from eq 16 and 18

$$v_{\mathrm{IVc}} = (p-1)k_{\mathrm{h}}[C_{\mathrm{R_1}}(0)]^p \qquad (19)$$

For the HCER, the surface concentration of O is[4]

$$C_{\mathrm{O}}(0) = \frac{C_{\mathrm{O}}^{\circ} + (1/L_{\mathrm{O}}\omega^{1/2})k_{\mathrm{h}}[C_{\mathrm{R_1}}(0)]^p}{1 + k_1/L_{\mathrm{O}}\omega^{1/2}} \qquad (20)$$

The normal component of i_1 (the value of i_1 when $k_{\mathrm{h}} = 0$) is

$$i_{n1} = \frac{n_1Fk_1C_{\mathrm{O}}^{\circ}}{1 + k_1/L_{\mathrm{O}}\omega^{1/2}} \qquad (21)$$

When $k_{\mathrm{h}} > 0$, we define

$$i_{\mathrm{cat}} = i_1 - i_{n1} \qquad (22)$$

From eq 20, 21, and 22

$$\frac{i_{\mathrm{cat}}}{n_1F} = \left(\frac{k_1/L_{\mathrm{O}}\omega^{1/2}}{1 + k_1/L_{\mathrm{O}}\omega^{1/2}}\right)k_{\mathrm{h}}[C_{\mathrm{R_1}}(0)]^p \qquad (23)$$

Therefore

$$v_{\mathrm{IVc}} = (p-1)\left(\frac{1 + k_1/L_{\mathrm{O}}\omega^{1/2}}{k_1/L_{\mathrm{O}}\omega^{1/2}}\right)\left(\frac{i_{\mathrm{cat}}}{n_1F}\right) \qquad (24)$$

The current density, i_1, is

$$i_1 = n_1Fv_{\mathrm{IVa}} + [p/(p-1)]n_1Fv_{\mathrm{IVc}} \qquad (25)$$

From eq 22 and 24

$$v_{\mathrm{IVa}} = \frac{i_{n1}}{n_1F} - \left[\frac{p}{k_1/L_{\mathrm{O}}\omega^{1/2}} + (p-1)\right]\frac{i_{\mathrm{cat}}}{n_1F} \qquad (26)$$

The total rate of consumption of O is thus

$$v_{\mathrm{IVa}} + v_{\mathrm{IVc}} = \frac{i_{n1}}{n_1F} - \left(\frac{1}{k_1/L_{\mathrm{O}}\omega^{1/2}}\right)\frac{i_{\mathrm{cat}}}{n_1F} \qquad (27)$$

Examination of eq 24 and 26 reveals that the rates of consumption of O *via* the equivalent parallel reactions IVa and c are *not* simply equal to i_{n1}/n_1F and $[(p-1)/p]i_{\mathrm{cat}}/n_1F$, respectively. When $k_{\mathrm{h}} > 0$, the rate of reaction IVa and the absolute flux of O to the surface are *less* than their normal value, i_{n1}/n_1F. The total current density is *greater* than normal, however, since more charge is consumed in reducing O by reaction IVc than by reaction IVa.

To find the quantity, x, it is most convenient to express $C_{\mathrm{O}}(0)$ as[4]

$$C_{\mathrm{O}}(0) = \frac{C_{\mathrm{O}}^{\circ}}{1 + (n_1/n_1^*)k_1/L_{\mathrm{O}}\omega^{1/2}} \qquad (28)$$

It follows that

$$\frac{i_{\mathrm{cat}}}{n_1F} = \left(\frac{k_1/L_{\mathrm{O}}\omega^{1/2}}{1 + k_1/L_{\mathrm{O}}\omega^{1/2}}\right)\left[\frac{1 - n_1/n_1^*}{1 + (n_1/n_1^*)k_1/L_{\mathrm{O}}\omega^{1/2}}\right]k_1C_{\mathrm{O}}^{\circ} \qquad (29)$$

$$v_{\mathrm{IVa}} = \left[\frac{1 - p(1 - n_1/n_1^*)}{1 + (n_1/n_1^*)k_1/L_{\mathrm{O}}\omega^{1/2}}\right]k_1C_{\mathrm{O}}^{\circ} \qquad (30)$$

$$v_{\mathrm{IVc}} = \left[\frac{(p-1)(1 - n_1/n_1^*)}{1 + (n_1/n_1^*)k_1/L_{\mathrm{O}}\omega^{1/2}}\right]k_1C_{\mathrm{O}}^{\circ} \qquad (31)$$

From eq 17, the ratio of the rates of consumption of O is then given by the simple relation

$$x = \frac{(p-1)(1 - n_1/n_1^*)}{1 - p(1 - n_1/n_1^*)} \qquad (32)$$

Since the equivalent parallel reaction scheme IV for the HCER is of the same form as that for the "simple parallel" reactions I, the form of plots of $I_{\mathrm{d}}/I_{\mathrm{r}}$ *vs.* $\omega^{-1/2}$ for the HCER can be determined from the diagnostic expression, eq 12 and the value of x given by eq 32.

Figure 1 illustrates[15] the form of the steady-state current–voltage (i–E) curve of the HCER depicted in reaction scheme II for the case $p = 2$, disk angular velocities of 10, 200, and 1000 radians sec^{-1} and the parametric values: $n_1 = n_2 = 2$, $k_{\mathrm{s1}} = 10^{-3}$ cm sec^{-1}, $k_{\mathrm{s2}} = 10^{-20}$ cm sec^{-1}, $b_{\mathrm{c1}} = b_{\mathrm{c2}} = 0.118315$ V, $E_{\mathrm{c1}}^{\circ} - E_{\mathrm{c2}}^{\circ} = -1.0$ V, $p = 2$, $k_{\mathrm{h}} = 10^4$ cm^4 mol^{-1} sec^{-1}, $C_{\mathrm{O}}^{\circ} = 10^{-6}$ mol cm^{-3}, $D_{\mathrm{O}} = D_{\mathrm{R1}} = D_{\mathrm{R2}} = 10^{-5}$ cm^2 sec^{-1}, $\nu = 10^{-2}$ cm^2 sec^{-1}, and $N = 0.4$, where k_{s1}, k_{s2} and E_{c1}°, E_{c2}° are the formal standard rate constants and potentials of reactions IIa and IIb, respectively. The solid curves represent the behavior of the HCER with $k_{\mathrm{h}} = 10^4$ cm^4 mol^{-1} sec^{-1}, the dashed curves show the current corresponding to the sum of the reaction velocities, v_{IVa} and v_{IVb}, while the dotted curves illustrate the

---

[15] All illustrations were generated automatically with a General Electric 645 computer.

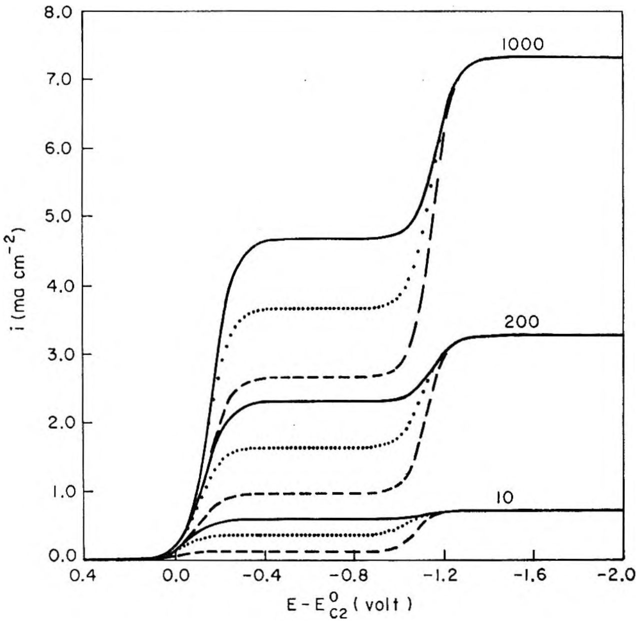

Figure 1. Steady-state current–voltage curves for heterogeneous catalytic ($p = 2$, $k_h = 10^4$ cm^4 mol^{-1} sec^{-1}) and normal ($k_h = 0$) electrode reactions on an RDE for disk angular velocities ω = 10, 200, and 1000 radians sec^{-1}: HCER: ——, i; ––––, $n_1Fv_{IVa} + n_2Fv_{IVb}$; normal: ......, i.

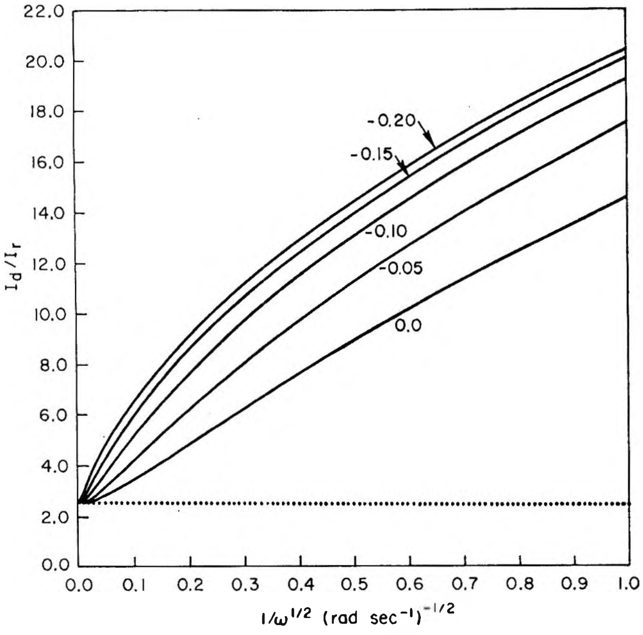

Figure 2. Variation of I_d/I_r with $\omega^{-1/2}$ for an HCER ($p = 2$, $k_h = 10^4$ cm^4 mol^{-1} sec^{-1}) and a normal electrode reaction at potentials, $E - E_{c1}°$ (volts) in the first current wave: ——, HCER; ......, normal case.

normal form when $k_h = 0$. The values of the rate constants are such that the i–E curves exhibit two well-defined limiting current regions. The detailed characteristics of the curves have been discussed previously.[4]

In Figure 2, the ratio I_d/I_r is plotted as a function of $\omega^{-1/2}$ for a series of potentials on the rising section of the first current wave of Figure 1. The solid curves correspond to the HCER, the single dotted line to the normal case. In this potential region, $k_2 \approx 0$, and since there is no catalytic current for the normal case, $x = 0$ as well. The normal ratio I_d/I_r is independent of both potential and mass transport and has a constant value equal to $1/N$. The variation of I_d/I_r for the HCER is revealed

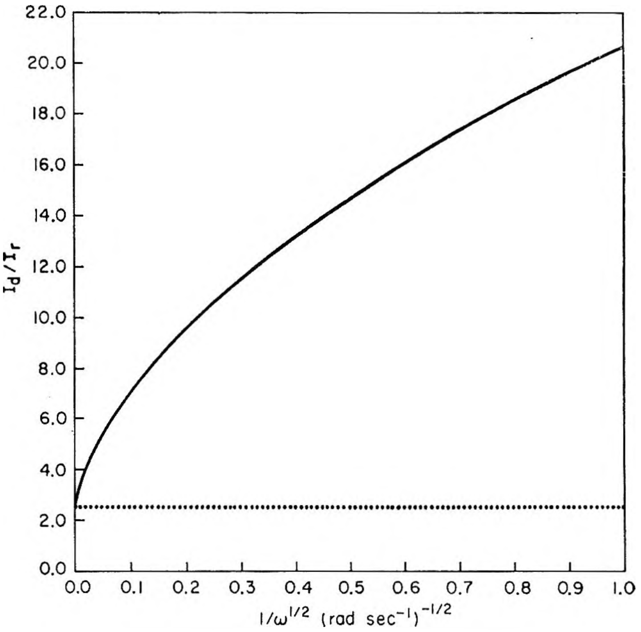

Figure 3. Variation of I_d/I_r with $\omega^{-1/2}$ for an HCER ($p = 2$, $k_h = 10^4$ cm^4 mol^{-1} sec^{-1}) and a normal electrode reaction at potentials in the lcd region of the first wave: ——, HCER; ......, normal case.

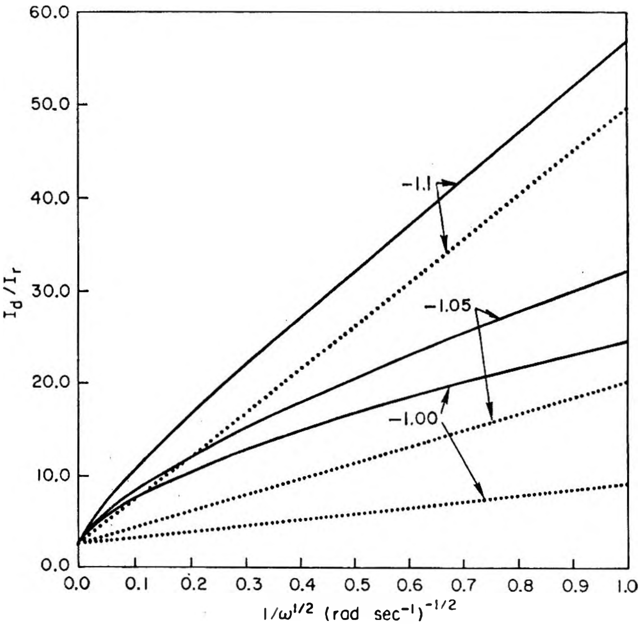

Figure 4. Variation of I_d/I_r with $\omega^{-1/2}$ for an HCER ($p = 2$, $k_h = 10^4$ cm^4 mol^{-1} sec^{-1}) and a normal electrode reaction at potentials, $E - E_{c2}°$ (volts), in the second current wave: ——, HCER; ......, normal case.

by examination of eq 12 and 32. As the disk potential is scanned cathodically through the first wave with ω held constant, the value of n_1^* increases monotonically from n_1, at the foot of the wave, to its maximum value $n_{1\text{cl}}^*$ at the limiting current density (lcd) plateau. Simultaneously I_d/I_r increases from the value $1/N$, when $x = 0$, to the value $(1/N)$ $[1/(2 - n_{1\text{cl}}^*/n_1)]$. A constant potential plot of I_d/I_r *vs.* $\omega^{-1/2}$ has an intercept equal to $1/N$ on the $\omega^{-1/2} = 0$ axis since $n_1^* \rightarrow n_1$ and $x \rightarrow 0$ as $\omega \rightarrow \infty$. As $\omega \rightarrow 0$, $\theta \rightarrow 1$, and $J_{\text{R}_1}(0) \rightarrow 0$; hence, $I_r \rightarrow 0$ and $I_d/I_r \rightarrow \infty$.

In the lcd region where x is independent of potential, the constant potential curves coalesce to form a single curve with $I_d/I_r = (1/N)$ $[1/(2 - n_{1\text{cl}}^*/n_1)]$. Figure 3 shows the variation of I_d/I_r with disk angular velocity in this region.

Finally, Figure 4 illustrates the form of plots of I_d/I_r *vs.* $\omega^{-1/2}$ for potentials in the rising part of the second current wave. In this region, $k_2 > 0$ and R_1 is partially consumed by the consecutive electrochemical reaction IIb. The slopes of the plots for both the normal and catalytic electrode reactions increase as the potential is made more negative. At fixed potential, the ratio I_d/I_r is greater for the HCER since R_1 is consumed by both the electrochemical reduction process IIb and the chemical regenerative reaction IIc. The curvature of the solid plots for the HCER reflects the variation in n_1^* with ω. For potentials near the lcd region of the second wave, $n_1^* \rightarrow n_1$ and $x \rightarrow 0$; the solid curves for the HCER tend to merge with the dotted lines for the normal case. In the lcd region, R_1 is totally consumed on the disk and $I_r = 0$.

Discussion

Although the rate constant, k_h, of the reaction IIc, by which S is formed is independent of potential, the rate of consumption of R_1 by this reaction varies with potential in the rising sections of *both* the first and second current waves since the surface concentration, $C_{\text{R}_1}(0)$, is potential dependent. As a result, the plots of I_d/I_r *vs.* $\omega^{-1/2}$ for the HCER exhibit features characteristic of several of the "diagnostic" forms deduced[1] for the simple parallel reaction scheme (*cf.* Figure 1, ref 1).

For the rising section of the first wave of the HCER, $x > 0$ but $k_2 = 0$. In the medium-to-high rotational speed range ($\omega^{-1/2} \approx 0.03$–$0.2$ sec$^{-1/2}$), the constant potential curves for the HCER closely resemble the family of lines for reaction I with $k_2 > 0$ and $x = 0$. At low rotational speeds, the plots for the HCER are similar to those for reaction I when $k_1 > 0$, $k_2 > 0$, $k_3 > 0$, and $x > 0$. In the limit at very high rotational speeds, the HCER plots become tangential to the line, $I_d/I_r = 1/N$, corresponding to the behavior of reaction I when $k_1 > 0$, $k_2 = k_3 = 0$, and $x = 0$.

For the rising section of the second current wave of the HCER, $k_1 > 0$, $k_2 > 0$, and $x > 0$. At low rotational speeds, the constant potential plots of I_d/I_r *vs.* $\omega^{-1/2}$ for the HCER resemble those for reaction I when $k_1 > 0$, $k_2 > 0$, $k_3 > 0$, and $x > 0$; the latter have intercepts greater than $1/N$ on the $\omega^{-1/2} = 0$ axis. At high rotational speeds, $x \rightarrow 0$ as $\omega \rightarrow \infty$; the constant-potential plots for the HCER then resemble those for reaction I when $k_1 > 0$, $k_2 > 0$, $k_3 = 0$, and $x = 0$.

In the restricted range of rotational speeds commonly employed in kinetic studies with the ring–disk electrode system, the plots of I_d/I_r *vs.* $\omega^{-1/2}$ for an HCER bear a close resemblance to those for simple parallel electrochemical reactions. To gain a detailed understanding of the actual reaction mechanism and the catalytic role of the electrode substrate, it is essential to distinguish between these two kinetic schemes. The characteristic curvature of HCER plots can only be revealed properly by obtaining data over a wide range of disk angular velocities, sufficient to alter the diffusion layer thickness, δ_{O}, and the value of the ratio, $k_h/L_{\text{O}}\omega^{1/2}$, by at least a factor of 10. A rotational speed range of 100–10,000 rpm or more is required. HCER plots exhibit the greatest curvature for potentials in the lcd region of the first wave. A simpler procedure, which does not require the use of a ring–disk assembly, is to examine the form of the Levich plots of $i_{1\text{cl}}$ *vs.* $\omega^{1/2}$ for curvature and/or nonzero intercepts on the $\omega^{1/2} = 0$ axis (*cf.* ref 3).

A comparison of the kinetics of the HCER and those of an ECE mechanism with a rate-controlling chemical step which is noncatalytic will be presented in a separate article. Application of these kinetic analyses to the interpretation of the kinetics and mechanism of the oxygen electrode reaction will be discussed in forthcoming communications.

The Electrical Conductivities of Molten Bismuth Chloride, Bismuth Bromide, and Bismuth Iodide at High Pressure[1]

by **A. J. Darnell, W. A. McCollum, and S. J. Yosim**

Atomics International Division, North American Rockwell Corporation, Canoga Park, California 91304

(Received March 27, 1969)

The electrical conductivities of molten $BiCl_3$, $BiBr_3$, and BiI_3 were measured at temperatures up to 886° at a pressure of 5.4 kbars. At this elevated pressure the specific conductivity (κ) varies exponentially with $1/T$, *i.e.*, $\kappa \propto e^{-E_\kappa/RT}$. This is in contrast to the behavior of these molten salts at low pressures ($P < 0.1$ kbar) where Grantham and Yosim (1963) found a maximum in κ *vs.* T curves. The isothermal electrical conductivity of molten $BiCl_3$, $BiBr_3$, and BiI_3 was examined at pressures from 3 to 14 kbars. At temperatures above the temperature of maximum conductivity at ordinary pressures, κ increases with increasing pressure. It is concluded that pressure inhibits the association of these salts at high temperature. This effect is predominant over the decreased conductivity expected from the lower ionic mobility in liquids at these elevated pressures.

Introduction

Negative temperature coefficients of specific electrical conductivity have been reported for the bismuth salts $BiCl_3$[2a,b], $BiBr_3$[2a], and BiI_3.[2a] Negative coefficients have also been found in molten HgI_2,[3] $InCl_3$[4] and $InBr_3$.[4] This behavior of these salts has been considered anomalous, but other work by Grantham and Yosim[5] has shown that many molten salts which show conventional positive temperature coefficients near the melting point, exhibit negative temperature coefficients if their conductivities are measured over a wide enough temperature range. Since in the conductivity measurements of Grantham and Yosim[2a,b,5] the samples expanded while they were heated, a simultaneous variation of temperature and volume took place. These authors point out that this negative temperature coefficient probably arises due to increased covalency or ionic association of the molten salt as a result of the increased volume rather than just increased temperature. The reduction in the number of ionic carriers offsets the increase in ionic mobility with increased temperature to give a negative temperature coefficient of conductivity at high temperatures.[5]

Measurement of the electrical conductivity at constant volume over a wide range of temperatures, particularly at temperatures where the molten salts exhibit a negative temperature coefficient of conductivity, would be useful towards a better understanding of ionic transport in these bismuth halides. If Grantham's and Yosim's explanation of the conductivity maximum were correct, one would not expect maxima when these salts are heated at constant volume.

Estimates from thermal expansion of the liquid at pressures near atmospheric[6-8] and the compressibility of the solid[9] indicate that pressures up to 25 kbars would be required to maintain constant volume of the liquid as the temperature is raised to as much as 300° above the melting point. Neither the experimental apparatus nor the *PVT* data are currently available with which to carry out constant volume conductivity measurements on these salts over such a pressure and temperature interval. We have, however, made the following measurements in order to better understand the conduction process in these molten salts. Electrical conductivities were determined as a function of temperature at a constant but relatively high pressure of 5.4 kbars. Thus, if there is an increase in specific volume of the salt as a result of ionic association,[10,11] then such extreme pressures would be expected to decrease this association[12] and thus displace or eliminate the negative temperature coefficient of electrical conductivity which has been observed in these salts at relatively low pressures.[1,2] In addition the effect of pressure on the isothermal electrical conductivity of these molten salts was examined. Temperatures above the temperature of maximum conductance exhibited by the salts at pressures near the salts' own vapor pressures were selected for these isothermal studies. The molten salts examined in this study were subjected to a pressure variation of approximately 10 kbars. This pressure variation should, by comparison with the compression of the solid salts,[9] be sufficiently large to change the specific volume of the molten salts from 5 to 15%. Such a volume change would in all likelihood affect the conduction by an amount great enough to be detected by our high-pressure experimental technique.

---

[1] This work was supported by the Research Division of the U. S. Atomic Energy Commission and was presented in part at the Pacific Conference on Chemistry and Spectroscopy, Third Western Regional Meeting of the American Chemical Society, Anaheim, Calif., Nov. 1, 1967.

[2] (a) L. F. Grantham and S. J. Yosim, *J. Phys. Chem.*, **67**, 2506 (1963); (b) L. F. Grantham and S. J. Yosim, *ibid.*, **72**, 762 (1968).

[3] I. K. Delimarskii and B. F. Markov, "Electrochemistry of Fused Salts," Sigma Press, Washington, D. C., 1961, pp 12, 15.

[4] W. Klemm, *Z. Anorg. Chem.*, **152**, 252 (1926).

[5] L. F. Grantham and S. J. Yosim, *J. Chem. Phys.*, **45**, 1192 (1966).

[6] J. W. Johnson and D. Cubicciotti, *J. Phys. Chem.*, **68**, 2235 (1964).

[7] J. W. Johnson, D. Cubicciotti, and W. J. Silva, *ibid.*, **69**, 1989 (1965).

[8] F. J. Keneshea, Jr., and D. Cubicciotti, *ibid.*, **63**, 1472 (1959).

[9] A. J. Darnell and B. B. Owens, Abstracts, 150th National Meeting of the American Chemical Society, Atlantic City, N. J., Sept 1965, p 51V.

[10] W. Fischer, K. Heinzinger, W. Herzog, and A. Klemm, *Z. Naturforsch.*, **17a**, 799 (1962).

[11] H. A. Levy and M. D. Danford in "Molten Salt Chemistry," M. Blander, Ed., Interscience Publishers, Inc., New York, N. Y., 1964, pp 109–125.

[12] S. D. Hamann, "Physico-Chemical Effects of Pressure," Butterworth and Co., Ltd., London, 1957, pp 141–144.

The bismuth trihalides were selected for these high-pressure, high-temperature conductivity studies because (a) of their unusual conduction properties at low pressures,[2a,b] (b) their relatively low melting temperatures probably offer less experimental containment problems than would salts with higher melting points, and (c) resistance ratio measurements upon molten BiI_3 indicated that the temperature coefficient is normal or positive at elevated pressures.[13] The pressure-temperature dependence of the melting point and, thus, the extent of the liquid range is known.[13]

Experimental Section

A. Materials. Reagent grade salts were purified by multiple distillation and sublimation under vacuum and under a partial pressure of oxygen. These purified salts were loaded into the conductivity cells in an argon atmosphere. This procedure introduces ~0.02 wt% argon into the high pressure conductivity cell from argon gas present in the void space (20 to 30% of the cell volume) between the solid salt particles in the cell. This entrapped argon probably dissolves in the salt when it is melted in the high pressure cell. The dissolution of 0.3 atm of Ar is not expected to change the specific conductance of these molten salts to a measurable extent. This is by analogy with the relatively small effect which dissolved Ar has on the specific conductance of molten $NaNO_3$ as found by Copeland and Zybko.[14]

B. Apparatus and Procedure. The electrical conductivity studies on the bismuth trihalides at elevated pressures and temperatures were carried out in a piston–cylinder high pressure chamber similar to the apparatus of Coes,[15] Hall,[16] and Kennedy, *et al.*[17] A conductivity cell (shown schematically in Figure 1) made of fused quartz or of boron nitride with either tungsten, platinum or graphite electrodes was designed to fit within a graphite sleeve furnace, all contained within the high pressure chamber. A metallic-sheathed, MgO-insulated thermocouple junction is located within a well in the upper electrode. This junction is at most 0.5 mm from the molten salt–electrode interface. The conductance cell is approximately 1 mm in diameter and from 7 to 10 mm long. This cell is positioned in the central, most isothermal portion of a graphite sleeve furnace. This furnace is approximately four times the length of the conductivity cell. The method used for determining the pressure and temperature within the high pressure chamber has been described previously.[13]

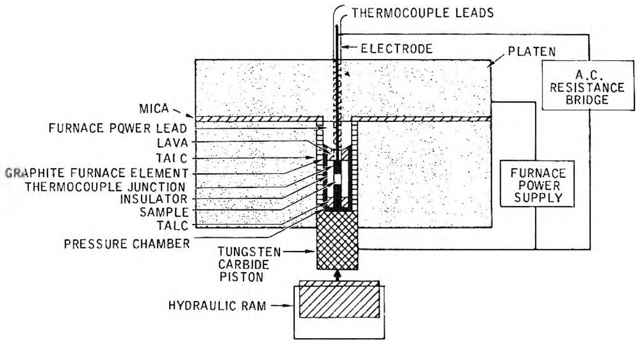

Figure 1. Schematic drawing of high-pressure, high-temperature conductivity cell.

Electrical conductivity measurements were made with a General Radio Type 1650-A impedance bridge. To check the accuracy of the conductivity bridge under conditions similar to the fused salt impedance measurements, calibrated resistors were substituted for the cell within the pressure chamber at ambient pressure. Thus, all the circuit components external to the cell were equivalent. Lead resistance corrections were also made in these calibration tests. These substituted resistors ranged from 10 ohms to 10^4 ohms, which is greater than the range of resistances encountered in the fused salt measurements (~30–300 ohms). Within these limits, the resistance measured by the impedance bridge agreed to ±2% of the value of the calibrated resistors.

The conductivity data reported for the salts $BiCl_3$, $BiBr_3$, and BiI_3 were measured at a frequency of 1000 Hz. However, the effect of frequency on the conductivity of molten BiI_3 was measured at a pressure of 5.4 kbars at a temperature of 580° in a quartz cell employing graphite electrodes. These conductivity measurements upon molten BiI_3 were made over the frequency range 500–10,000 Hz with a General Radio Type 1311-A audio oscillator and a Type 1232-A tuned amplifier and null detector in conjunction with the Model 1650-A impedance bridge. The conductivity of molten BiI_3 at infinite frequency (from an extrapolation of the linear relationship found between κ *vs.* frequency$^{-1/2}$) differed by less than 2% from the conductivity measured at 1000 Hz. No correction was made for this relatively small frequency dependence of κ.

---

[13] A. J. Darnell and W. A. McCollum, *J. Phys. Chem.*, **72**, 1327 (1968).

[14] J. L. Copeland and W. C. Zybko, *ibid.*, **70**, 181 (1966).

[15] L. Coes, *J. Amer. Ceram. Soc.*, **38**, 298 (1955).

[16] H. T. Hall, *Rev. Sci. Instrum.*, **29**, 267 (1958).

[17] G. C. Kennedy and P. N. LaMori in "Progress in Very High Pressure Research," F. P. Bundy, W. R. Hibbard, and H. M. Strong, Ed., John Wiley and Sons, Inc., New York, N. Y., 1961, p 30.

Tests made with boron nitride and quartz blanks showed that the conductivity contribution from the shunt path of the high pressure conductivity cell and its input leads was no greater than 1.5% of the conductance of the molten salt at all temperatures and pressures considered in these measurements. This shunt resistance does, however, become significant at higher temperatures than employed here, *i.e.*, 1000°. Brown and Porter[18] have found that fused fluorides penetrate boron nitride at elevated temperature (*i.e.*, 1000°). Visual inspection and X-ray photography of cross sections of our boron nitride cells indicated no detectable penetration of the boron nitride by the fused bismuth trihalides occurred during a run. Furthermore, results with boron nitride and with quartz cells were essentially the same which also suggests that salt penetration did not take place in the BN cells. Irreversible changes in cell resistance were observed in other runs to higher temperatures (*i.e.*, 1000–1100°) than considered here. It is not known, however, whether this irreversible resistance change was due to salt decomposition or to salt–electrode and/or salt–cell interaction.

The two-probe rather than the usual four-probe method was used in these conductivity measurements. Lead resistance corrections for this two-probe method were obtained from *in situ* measurements with tungsten and nickel blanks substituted in place of the salt sample. Data for these lead resistance corrections as a function of temperature applicable at a pressure of 5.4 kbars are given in Figure 2. This correction consists primarily of the resistance of the leads into the high pressure chamber. These leads, of necessity, must be of relatively small diameter. This lead resistance at 25° is 1.8 ohms. From Figure 2 it is seen that the total resistance from the *in situ* test at high pressure with the tungsten or nickel blank is 2.2 ohms. The difference, 0.4 ohms, is attributed to the two electrode–Ni or electrode–W contact resistances. Electrode–fused salt contact resistances of approximately this same value were found by Grantham[19] for identical size tungsten electrodes in contact with molten $BiCl_3$ and $BiBr_3$ at near atmospheric pressure. Grantham[19] found that temperature has little, if any, effect on this contact resistance. We have assumed that this tungsten–fused salt contact resistance remains small (*i.e.*, 0–0.2 ohm) at the elevated pressures considered here. Graphite electrodes were also used with the salts $BiCl_3$ and BiI_3. Here, the same contact resistance correction as was used for tungsten electrodes was employed. The lowest resistance encountered in these fused salt cells is ~30 ohms. An uncertainty of 0.4 ohm arising from uncertainty of two of the electrode–fused salt contact resistances would therefore amount to an uncertainty of ~1% in the resistance of the fused salt cell. However, further measurements would be required in order to establish the effect of pressure on these electrode–fused salt contact resistances.

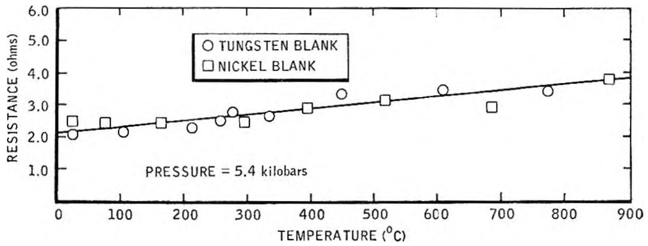

Figure 2. Lead and contact resistance of tungsten and nickel blanks as a function of temperature.

The cell constant of the high-pressure conductivity cell was determined from its dimensions taken from X-ray profiles after its removal from the high-pressure chamber. Two longitudinal profiles, displaced by 90°, were used to determine the diameter and length of the cell. As a further check, the cell volume was also calculated from the weight of the salt and its density at 25°. The cell volume determined by this procedure and from the dimensions of the cell agreed to within ±5%. The effects which compression (from 1 bar to 5.4 kbars) and thermal expansion (from 25° to the melting point) have upon the cell constant are not known for lack of high-pressure, high-temperature *PVT* data for these salts. These two effects however, compensate for each other to some extent. This cell constant for the solid salt was used to calculate the cell constant of the molten salt at its melting point by assuming the cell dimensions increase proportionally in all directions by an amount determined by the volume of fusion of the salt.[13] Furthermore, the cell constant calculated for the liquid salt at its melting point is used for the entire temperature interval. In the kind of experimental arrangement shown in Figure 1, the amount of salt between the electrodes remains constant both with a variation in pressure and with temperature. It is expected, however, that the conductivity cell dimensions change with a change in temperature and with pressure. If both the diameter and length of the cylindrical conductivity cell change dimensions proportional to the volume change of the molten salt (from thermal expansion and/or compression), then the fractional change in cell constant is approximately equal to the cube root of the fractional volume change due to the change in temperature or pressure. No high-pressure expansivity data are available from which to make these cell constant adjustments. The near atmospheric thermal expansion data of these molten salts[6–8] should, however, give an esti-

---

(18) E. A. Brown and B. Porter, Bureau of Mines Report R. I. 6500, U. S. Department of the Interior, Washington, D. C., 1963.

(19) L. F. Grantham, private communication.

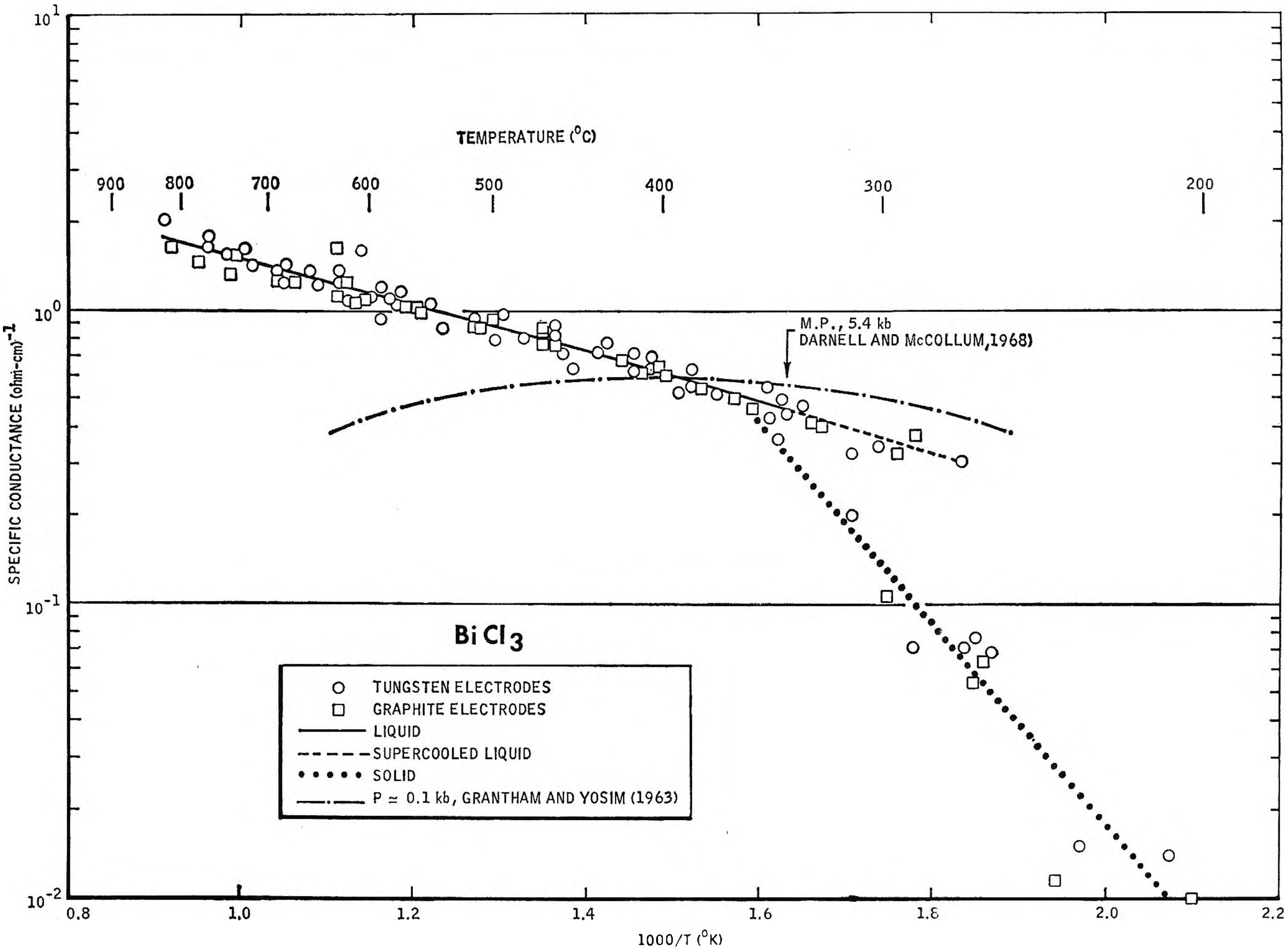

Figure 3. Log κ (ohm-cm)$^{-1}$ *vs.* $1/T$ (°K) for $BiCl_3$.

mate for the change in cell constant with temperature. For $BiCl_3$ this correction would decrease the specific conductance at most by 15% at 800° since the expansivity at a pressure of 5.4 kbars would be expected to be less than the expansivity at atmospheric pressure. The specific conductivities were calculated using the cell constant obtained for the liquid salt at its melting point.

It is realized this procedure yields cell constants for the liquid salt which are only approximate and that consideration of only the resistance ratios of the salts are necessary for the interpretation of the results given below. However, since the cell conductance is directly proportional to the cell constant, determination of the cell constant gives some measure of the agreement between the isobaric specific conductivities measured on different samples, and on the agreement in the conductivity data between the isobaric and isothermal tests. More significantly, however, specific conductivities give a means of comparison with the conductivity data of Grantham and Yosim[2a] at pressures near atmospheric.

Results

The isobaric specific electrical conductivities of $BiCl_3$, $BiBr_3$, and BiI_3 at a pressure of 5.4 kbars are shown in Figures 3–5. The isothermal specific conductivities of these salts at pressures from 3 kbars up to pressures as high as 14 kbars in the case of $BiBr_3$ are shown in Figure 6. The specific electrical conductivity data of Grantham and Yosim,[1,2] taken at a pressure equal to or somewhat greater than the salts' own vapor pressures (*i.e.*, $P < 0.1$ kbar) are shown for comparison with the isobaric and isothermal data in Figures 3–6.

$BiCl_3$. The specific conductance data for $BiCl_3$ were obtained through use of quartz cells with either tungsten electrodes or graphite electrodes and with a boron nitride cell with tungsten electrodes. The specific conductance obtained with tungsten electrodes is ~10% higher than with the use of graphite electrodes. However, this difference may be due to the uncertainty which arises in the measurement of the cell constant for the two samples. In both cases, conductivity measurements were made from room temperature to 700–800°, then back to room temperature. There appears to be

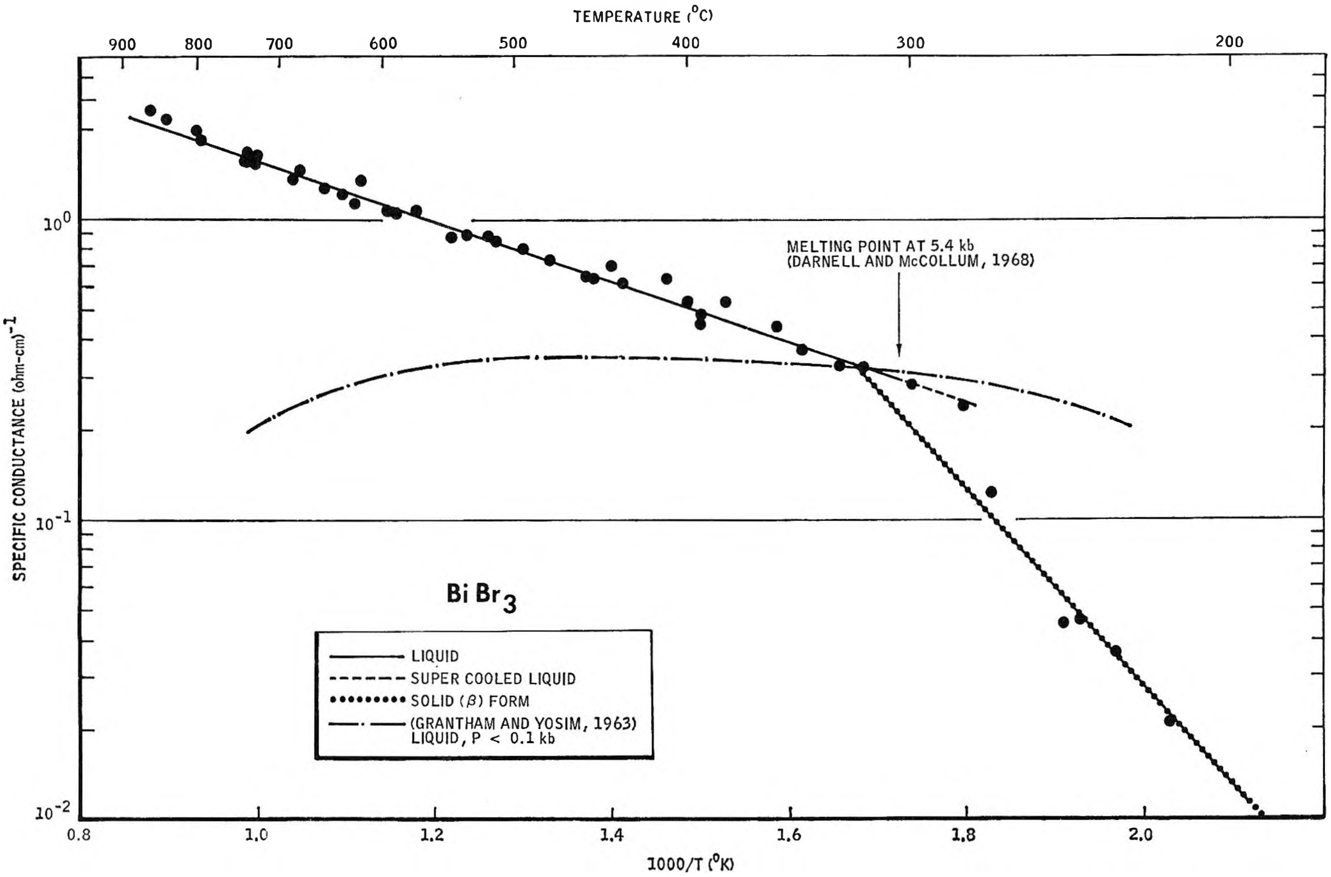

Figure 4. Log $\varkappa$ (ohm-cm)$^{-1}$ *vs.* $1/T$ (°K) for $BiBr_3$.

no detectable difference in the specific conductance obtained from these consecutive runs. This suggests that neither corrosion nor irreversible deformation occurs in these cells in a given run.

The data for the logarithm of the specific conductance *vs.* $1/T$ (°K) for both liquid and solid $BiCl_3$, are shown in Figure 3. The intersection of these log $\varkappa$ *vs.* $1/T$ curves for the solid and the liquid is at 368°. The melting point obtained by differential thermal analysis is 336° at this pressure.[13] The conductivity ratio for the liquid and solid phases at 336° is 1.5. Conductivity measurements for the liquid phase are shown in Figure 3 at temperatures as much as 70° below the melting temperature at this pressure. These measurements for the liquid phase below 336° were obtained on cooling only and are therefore attributed to supercooling of liquid $BiCl_3$. Mayer, *et al.*,[20] also experienced rather severe supercooling with this salt in their cryoscopic experiments.

The contrast in the behavior of the specific conductance of molten $BiCl_3$ at a pressure of 5.4 kbars (from measurements in this work) and at a pressure of $\sim$0.1 kbar[2a,b] is illustrated in Figure 3. As can be seen from Figure 3, the temperature dependence of the isobaric specific conductance of liquid $BiCl_3$ can, to a first approximation, be represented by the Arrhenius equation

$$\varkappa = A \exp(-E_\varkappa/RT) \qquad (1)$$

The values for the constant A and for the activation energy $E_\varkappa$ were determined empirically by method of least squares from the log $\varkappa$ *vs.* $1/T$ data for the liquid and solid phases. In this case, the conductivity data obtained from use of tungsten and graphite electrodes were given equal weight. Values obtained for A and

Table I: Constants in the Arrhenius Equation, $\varkappa$ (ohm-cm)$^{-1}$ $= Ae^{-E_\varkappa/RT}$, for the Salts $BiCl_3$, $BiBr_3$, and BiI_3 at a Pressure of 5.4 kbars

Salt	A, (ohm-cm)$^{-1}$	$E_\varkappa$, kcal/mol	T, °C
$BiCl_3$,			
solid	6.67×10^4	15.0 ± 2.2	212–336
liquid	9.51	3.68 ± 0.09	273–830[a]
$BiBr_3$,			
β form	9.97×10^4	15.1 ± 1.5	206–315
liquid	16.2	4.62 ± 0.08	282–864[a]
BiI_3,			
β form	6.85×10^{10}	42.5 ± 4.3	468–502
liquid	...	11	502–886

[a] Includes supercooled liquid.

---

[20] S. W. Mayer, S. J. Yosim, and L. E. Topol, *J. Phys. Chem.*, **64**, 238 (1960).

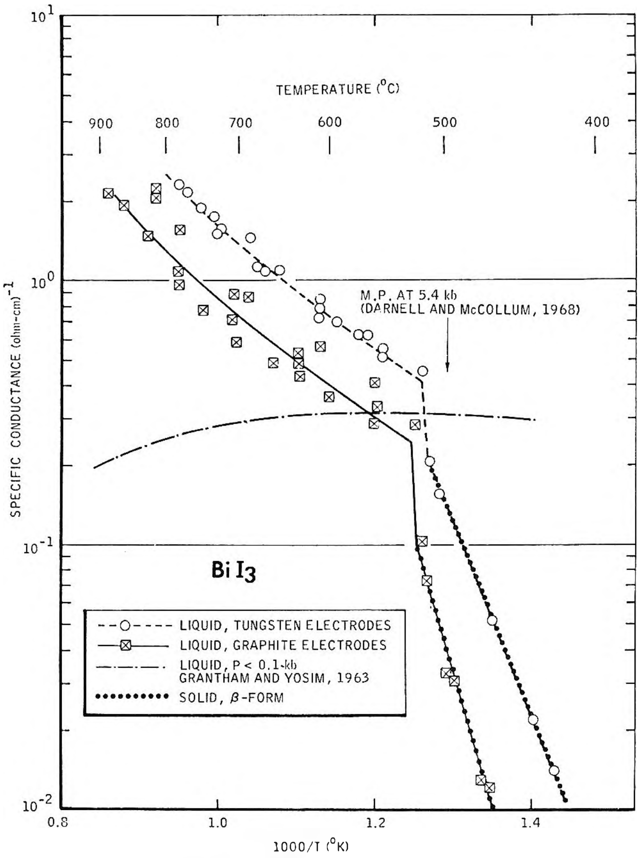

Figure 5. Log $\varkappa$ (ohm-cm)$^{-1}$ *vs.* $1/T$ (°K) for BiI_3.

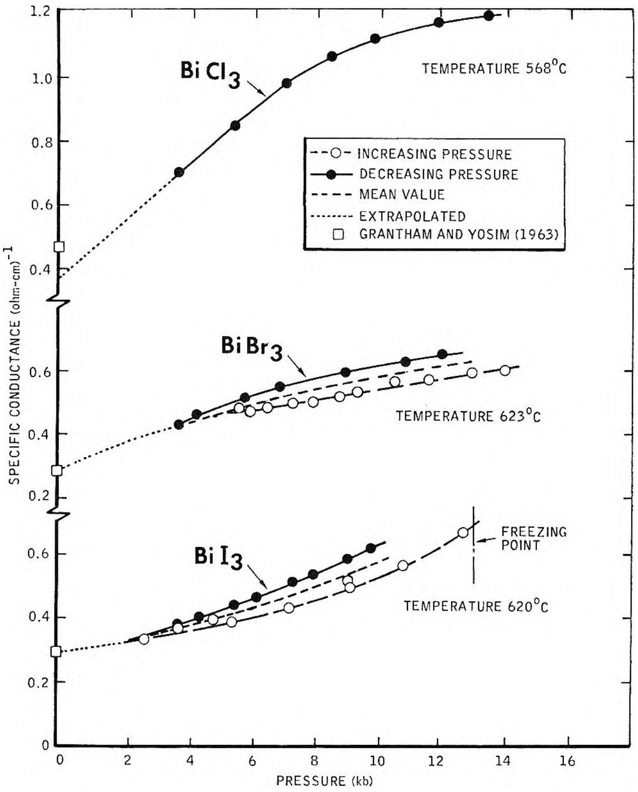

Figure 6. Isothermal specific conductance ($\varkappa$) of liquid $BiCl_3$, $BiBr_3$, and BiI_3 as a function of pressure.

$E_\varkappa$ are shown in Table I. The activation energies for solid and liquid $BiCl_3$ are 15.0 ± 2.2 and 3.68 ± 0.09 kcal/mol respectively.

Isothermal conductivity measurements at 568° were made on liquid $BiCl_3$ at pressures from 13.5 to 4 kbars. These conductivity data are shown in Figure 6. The specific conductance at 568° is 0.83 (ohm-cm)$^{-1}$ at a pressure of 5.4 kbars. This specific conductance is lower than was obtained from the isobaric experiment at this same pressure and temperature, [1.04 (ohm-cm)$^{-1}$]. These isothermal specific conductance data taken at a temperature of 568° were extrapolated to $P = 0$ in order to make a comparison with the specific conductance at low pressure.[1,2] The extrapolated value of $\varkappa$ at $P = 0$ is 0.38 (ohm-cm)$^{-1}$; the measured value[2a,b] at this temperature and pressure is 0.50 (ohm-cm)$^{-1}$.

$BiBr_3$. The specific conductance of $BiBr_3$ was measured at a pressure of 5.4 kbars using a boron nitride cell with tungsten electrodes. The isobaric (5.4 kbars) specific conductance data for $BiBr_3$ are shown in Figure 4. The low pressure conductivity data of Grantham *et al.*,[2a] are shown for comparison. Log $\varkappa$ *vs.* $1/T$ for liquid $BiBr_3$ is linear at a pressure of 5.4 kbars. These log $\varkappa$ *vs.* $1/T$ data for the liquid and β-$BiBr_3$ phases were each treated by method of least squares in order to evaluate the constants A and $E_\varkappa$ in eq 1. The activation energies for β-$BiBr_3$ and liquid $BiBr_3$ are 15.1 ± 1.5 and 4.62 ± 0.08 kcal/mol, respectively (Table I). The curves for the solid and liquid intersect at 322°. The melting point obtained at this pressure from differential thermal analysis is 315°.[13] The conductivity ratio of the liquid and solid at 315° is 1.33. Data for supercooled liquid $BiBr_3$ are also shown in Figure 4, but the extent of supercooling is not as great as was found in $BiCl_3$.

Isothermal conductivity measurements were made on $BiBr_3$ over the pressure interval 3.6–14 kbars at a temperature of 623°. These data are shown in Figure 6. In the case of $BiCl_3$ described above, conductivity measurements were made only on the decompression step. However, it was found that if the pressurization cycle was first carried out on the solid salt it could then be carried out on the molten salt. This preliminary pressurization upon the solid salt probably results in a better seal between the electrode and the boron nitride container. As can be seen in Figure 6, hysteresis was observed in the conductivities taken on the compression and decompression cycles. This hysteresis is due to a difference between the actual and indicated pressures on both the compression and decompression procedures. A similar hysteresis effect is also observed in volume *vs.* pressure curves taken with this same type of piston-cylinder apparatus.[13,17] An averaged $\varkappa$ *vs.* P curve has been drawn from the separate $\varkappa$ *vs.* P curves from the compression and decompression cycles. The specific conductance from the isobaric (5.4 kbars) measurement was 1.20 (ohm-cm)$^{-1}$. The mean value for the specific conductance at a pressure of 5.4 kbars from this isothermal experiment at 623° is considerably lower, being only 0.50 (ohm-cm)$^{-1}$. Extrapolation of this curve for the mean value of the isothermal conductivity to $P = 0$ gives $\kappa = 0.30$ (ohm-cm)$^{-1}$. Grantham and Yosim[2a] give 0.28 (ohm-cm)$^{-1}$ for the specific conductance of $BiBr_3$ at this temperature and pressure.

BiI_3. The specific conductance of BiI_3 was measured at a pressure of 5.4 kbars using quartz cells with either tungsten or graphite electrodes or with a boron nitride cell with tungsten electrodes. The specific conductance found with use of tungsten electrodes is almost twice the value obtained with the use of graphite electrodes (Figure 5). This difference in specific conductance of BiI_3 from the use of tungsten and of graphite electrodes is much greater than was found in the case of $BiCl_3$. This difference in κ may be due to a reaction between the salt and one of the types of electrodes. On the other hand, it could be due to an initial impurity in one of the samples; probably the one which has the higher conductivity. The temperature coefficient of κ for the liquid phase is, however, approximately the same in both cases. When graphite electrodes were used, the specific conductance from the isobaric experiments agreed with the specific conductance from the isothermal experiments [*i.e.*, at 620° and 5.4 kbars the specific conductance from the isobaric and isothermal experiments are 0.45 and 0.41 (ohm-cm)$^{-1}$, respectively]. Both sets of data are shown in Figure 5; however, only the data from the cell with graphite electrodes were used to obtain the activation energy E_κ reported in Table I. The log κ *vs.* $1/T$ curves for molten $BiCl_3$ and $BiBr_3$ were approximately linear at a pressure of 5.4 kbars. This curve for liquid BiI_3 on the other hand shows a curvature with a steeper slope (and thus higher E_κ) at higher temperatures. Since E_κ changes with temperature, its value was determined from the slope of log κ *vs.* $1/T$ at the median temperature (690°) of the measurements on the liquid. E_κ for the liquid phase is 11 kcal/mol. From a least-squares treatment the activation energy E_κ for the β phase at a pressure of 5.4 kbars is 42.5 ± 4.3 kcal/mol.

BiI_3 has a larger discontinuity in its log κ *vs.* $1/T$ curve at its melting point than does $BiCl_3$ and $BiBr_3$. The ratio of conductivities for the liquid and solid phases is $\sim$3.0. This larger discontinuity in the log κ *vs.* $1/T$ curves and the pressure gradient normally found along the axis of the high pressure conductivity cell[21] probably accounts for the difference in the melting point indicated by these conductivity measurements and the differential thermal analysis results.[13] Little, if any, supercooling occurs in BiI_3 since the conductivity *vs.* temperature data upon melting and freezing are very nearly identical.[13] This was not the case in $BiCl_3$ and $BiBr_3$ where supercooling is extensive.

Isothermal conductivity measurements were made at 620° over the pressure interval 2.5 to 12.6 kbars (Figure 6). These conductivity measurements on liquid BiI_3 were limited to pressures below 13 kbars since BiI_3 solidifies at this pressure at 620°.[13] As with $BiBr_3$ discussed above, hysteresis was also experienced in the κ *vs.* P curves (taken from the compression and decompression cycles). An average κ *vs.* P curve was constructed from these separate κ *vs.* P curves. Extrapolation of this averaged curve to $P = 0$ yields a specific conductance [0.30 (ohm-cm)$^{-1}$] which is in good agreement with κ measured at low pressures [0.30 (ohm-cm)$^{-1}$].[2a]

Discussion

The molten salts $BiCl_3$, $BiBr_3$, and BiI_3 show an exponential increase in specific conductance with decreasing $1/T$ at a pressure of 5.4 kbars. This "normal" or positive temperature coefficient of conductivity at this elevated pressure is in contrast to the behavior of the conductivity as a function of temperature at pressures approximately equal to the salts, own vapor pressures[2a,b] *i.e.*, $P < 0.1$ kbar. At such relatively low pressures, the specific conductivity of these salts was found to exhibit a maximum at a temperature $\sim$150° above the melting point.[2a,b] A maximum in the electrical conductivity *vs.* temperature of the liquid phase has also been found for several other salts.[3-5] Usually an increase in temperature increases the ionic conductivity of a molten salt. This increased conductivity is attributed to an increase in fluidity and thus an increase in the mobility of the ions with increased temperature. Grantham and Yosim[5] suggest that the negative temperature coefficient which they find at extremely high temperatures in several of the salts examined is due to increased covalency or more probably ionic association at high temperature. There are several indications that this increase in covalency results in a decrease in density of the molten salt.[10,11] If the specific volume of the liquid salt increases at high temperatures due to increased ionic association, for example, by a process such as

$$xM^+ + yA^- \rightleftharpoons M_xA_y \tag{2}$$

because the molar volume of the associated species is greater than the sum of the molar volumes of the ions from which it is formed, *i.e.*,

$$V_{M_xA_y} > xV_{M^+} + yV_{A^-}, \tag{3}$$

then application of an external pressure should, from the principle of Le Chatelier, suppress the association reaction 2.[12] In the absence of other factors, iso-

---

(21) M. Tamayama and H. Eyring, *Rev. Sci. Instrum.*, 38, 1009 (1967).

thermal compression would then be expected to increase the specific conductance of partially associated salts due to an increased ionic dissociation. On the other hand, in salts which are highly ionized at ordinary pressures, isothermal compression would not be expected to increase the number of ionic species. High pressure would, however, be expected to increase the viscosity[22] and thus to decrease the mobility of the ions.

Both the dissociation effect and the increased viscosity effect appear to be demonstrated in the bismuth trihalides when the high pressure, isobaric, specific conductance data obtained in this work are compared with the low pressure specific conductance data of Grantham and Yosim.[2a,b] To illustrate, in Figures 3–5 the log $\varkappa$ *vs.* $1/T$ curves for $P = 5.4$ kbars and $P \leq 0.1$ kbar intersect at temperatures T_i of 390, 322, and 560° for $BiCl_3$, $BiBr_3$, and BiI_3 respectively. Thus at temperature T_i, the specific conductivity of the liquid salt is the same at these two pressures, *i.e.*, $\varkappa_{P=5.4\ \mathrm{kbars}} = \varkappa_{P \leq 0.1\ \mathrm{kbar}}$. At temperatures below T_i, the specific conductance $\varkappa$ at $P = 5.4$ kbars is less than $\varkappa$ at $P \leq 0.1$ kbar; here the effect of pressure is to decrease the specific conductance of the molten salt, at least up to a pressure of 5.4 kbars. This decrease in $\varkappa$ is probably due to an increase in viscosity and thus a decrease in mobility of the ions. At temperatures greater than T_i pressure would still be expected to raise the viscosity and therefore lower the conductivity. However, from Figures 3–5 it can be seen that $\varkappa_{P=5.4\ \mathrm{kbars}} > \varkappa_{P \leq 0.1\ \mathrm{kbar}}$ when $T > T_i$. Thus the effect which pressure has upon dissociation is in all likelihood the predominant factor at temperatures greater than T_i. The ratio (α), $\varkappa_{P=5.4\ \mathrm{kbars}}/\varkappa_{P \leq 0.1\ \mathrm{kbar}}$ becomes larger at higher temperatures. This is probably due to a greater degree of ionic association at the lower pressure.

In Table II the conductivity ratio at $P = 5.4$ and $P \leq 0.1$ kbar is compared at (a) the normal melting point,[23] (b) at the temperature of maximum conductance when the salt is under its own vapor pressure,[2a,b] and (c) at the critical temperature of the salt. In the last case, conductivity data at $P \leq 0.1$ kbar are available only for $BiCl_3$.[2b] The effect of pressure on the conductivity at the critical temperature is large; for $BiCl_3$, $\alpha = 480$.

The isothermal conductivity experiments were, for all the salts considered here, carried out at temperatures greater than T_i. As a further check, it would be useful to examine the pressure dependence of the specific conductance $(\partial\varkappa/\partial P)_T$ of the liquid phase at temperatures below T_i. These measurements were not carried out since the apparatus used here is not suitable for the rather limited and low pressure range required at these low temperatures.

The effect of pressure on $(\partial\varkappa/\partial P)_{T=568°}$ for $BiCl_3$ decreases with increasing pressure and is approaching zero at $P = 13.5$ kbars. This result could be due to almost complete dissociation of $BiCl_3$ at this high pressure. However, it is possible that the viscosity effect may become predominant at these high pressures. If this were the case, then a maximum in the $\varkappa$ *vs.* P curve might be expected at still higher pressures ($BiCl_3$ solidifies at 24 kbars at this temperature). In the case of $BiBr_3$, the coefficient $(\partial\varkappa/\partial P)_{T=623°}$ is diminishing but still greater than zero at the highest pressure attained (14 kbar). Bismuth tribromide solidifies at a pressure of 29 kbar at this temperature. The pressure coefficient $(\partial\varkappa/\partial P)_{T=620°}$ for BiI_3, on the other hand, increases with increasing pressure. Thus both coefficients $(\partial\varkappa/\partial P)_{T=620°}$ and $(\partial\varkappa/\partial T)_{P=5.4\ \mathrm{kbars}}$ for BiI_3, unlike those for $BiBr_3$ and $BiCl_3$, increase with increasing pressure and temperature.

The difference in behavior of the specific conductance of molten BiI_3 from $BiBr_3$ and $BiCl_3$ at high pressure may be due to the effect of pressure on the stability of these molten salts. For example, there is an increase in volume in the formation of BiI_3 (l) from its elements at $P = 1$ atm, *i.e.*, $V_{BiI_3(l)}$ at its melting point is 127 cm³/mol;[8] $V_{Bi(l)} + 3/2V_{I_2(l)}$ is only 111 cm³/mol. Thus liquid BiI_3 should become less stable with respect to its elements with an increase in pressure. The molar vol-

Table II: The Specific Conductance Ratio [$\alpha \equiv \varkappa_{P=5.4\ \mathrm{kbars}}/\varkappa_{P=0.1\ \mathrm{kbar}}$] for Molten $BiCl_3$, $BiBr_3$, and BiI_3 at Several Temperatures[a]

Salt	α at the normal melting point (hypothetical)[b] t, °C	α	α at temp of max. conductance when $P \simeq 0.1$ kb t, °C	α	α at T_{critical} t, °C	α
$BiCl_3$	232	0.75	425	1.15	905	480
$BiBr_3$	218	0.96	425	1.69		...
BiI_3	408	0.36	525	0.81		...

[a] Data for specific conductance at $P = 0.1$ kbar from Grantham and Yosim.(2a,b) [b] Conductivity curve for liquid phase at pressure of 5.4 kbars was extrapolated to a temperature corresponding to the melting point at atmospheric pressure.

Table III: Arrhenius Activation Energy for Conduction in Liquid $BiCl_3$, $BiBr_3$, and BiI_3 at 5.4 kbars and at Pressure Equal to or Less than 0.1 kbar

Salt	$E_\varkappa$ at $P = 5.4$ kbars, kcal/mol	$E_\varkappa$[a] at $P \leq 0.1$ kbar, kcal/mol
$BiCl_3$	3.68	3.6
$BiBr_3$	4.62	4.2
BiI_3	11	3

[a] Calculated from data in ref 1. $E_\varkappa$ at $P \leq 0.1$ determined from the slope of log $\varkappa$ *vs.* $1/T$ at temperatures immediately above the melting point.

---

(22) Reference 12, p 81.

(23) For purposes of comparison, the log $\varkappa$ *vs.* $1/T$ curve for the liquid at a pressure of 5.4 kbars has been extrapolated to the temperature of the normal or atmospheric melting point.

umes of $BiBr_3$ (l)[7] and $BiCl_3$ (l)[6] are, significantly smaller than the sum of the molar volumes of their respective elements from which they are formed. On this basis, BiI_3 (l) would show a tendency to disproportionate at high pressures whereas $BiBr_3$(l) and $BiCl_3$(l) become more stable. This difference in stability with pressure could account for the difference in behavior of the log $\varkappa$ vs $1/T$ and $\varkappa$ vs. P curves of BiI_3 from those of $BiBr_3$. and $BiCl_3$.

The activation energies ($E_\varkappa$) for $BiCl_3$, $BiBr_3$, and BiI_3 at $P \leq 0.1$ kbar were estimated from the slope of the log $\varkappa$ vs. $1/T$ curves for these salts from data given by Grantham and Yosim[2a] at temperatures immediately above the melting point. These estimated values of $E_\varkappa$ at $P \leq 0.1$ kbar are compared with $E_\varkappa$ at $P = 5.4$ kbars in Table III. The activation energies at these two pressures are essentially identical in the cases of $BiCl_3$ and $BiBr_3$; for BiI_3, $E_\varkappa$ at 5.4 kbars is almost four times its value at $P = 0$. This difference in $E_\varkappa$ between bismuth triiodide and the tribromide and trichloride may be due to a greater effect of pressure upon ionic association in the case of BiI_3.

Application of Density Matrix Methods to the Study of Spin Exchange. I. The Barrier to Internal Rotation in N-Acetylpyrrole

by Kjell-Ivar Dahlqvist and Sture Forsén

Division of Physical Chemistry, The Lund Institute of Technology, Chemical Center, Lund 7, Sweden

(Received April 1, 1969)

The density matrix theory of the effects of rate processes on complex nmr spectra, developed by Kaplan, has been applied to a study of the barrier to internal rotation in N-acetylpyrrole. Theoretical spectra of the four-spin system of the ring protons give excellent fits to the experimental lineshapes in the temperature region -65 to $+30°$. The activation parameters for the rotation of the acetyl group were found to be $E_a = 12.6 \pm 0.5$ kcal/mol, $\Delta H^{\ddagger} = 12.0 \pm 0.5$ kcal/mol, $\Delta F_{298°K}^{\ddagger} = 12.1 \pm 0.2$ kcal/mol and $\Delta S^{\ddagger} = -0.6 \pm 2.3$ eu. The Arrhenius activation energy, E_a, is about 7 kcal/mol lower than that for N,N-dimethylacetamide, which indicates that the lone-pair electrons on the nitrogen atom in N-acetylpyrrole are to a large extent localized in the pyrrole ring.

Introduction

Comparatively high values for the barrier to internal rotation about formal single bonds have been observed in a number of molecules. Examples of bonds and compounds in which this effect is manifest are the $\geqslant$C–N$<$ bond in amides[1-3] thioamides[4] and vinylogous amides[5,6] the $=$N–N$<$ bond in nitroso amines[7,8], the $\geqslant$C–C$\leqslant$ bond in aromatic aldehydes,[9] and the $=$N–C$\leqslant$ bond in aromatic or conjugated nitroso compounds.[10] In all of these compounds, the main contributor to the barrier is assumed to be conjugative interaction between π electrons on both sides of the single bond that exhibits restricted rotation.

The rotational barrier about the $>$N–C$\leqslant$ bond in amides ((I), X = 0) is among those most extensively investigated, mainly by nmr spectroscopy.

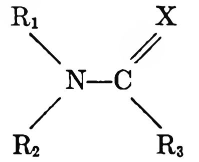

I

In compounds of this type, high barriers have been found when R_1, R_2, and R_3 are small alkyl groups which do not prevent the molecule from being essentially planar in the ground state. Increased bulkiness of the substituents is found to lower the barrier, presumably due primarily to steric crowding in the ground state.

A systematic study of the influence of R_3 on restricted rotation in thioamides ((I), X = S) was carried out by Sandström.[4] Electron donating +M substituents such as CH_3S– and CH_3O– were found to de-

---

[1] H. S. Gutowsky and C. H. Holm, *J. Chem. Phys.*, **25**, 228 (1956).

[2] A. Allerhand and H. S. Gutowsky, *ibid.*, **41**, 2125 (1964).

[3] M. T. Rogers and J. C. Woodbrey, *J. Phys. Chem.*, **66**, 540 (1962).

[4] J. Sandström, *ibid.*, **71**, 2318 (1967).

[5] H. E. A. Kramer and R. Gompper, *Z. Phys. Chem.*, (Frankfort am Main), **43**, 292 (1964).

[6] H. E. A. Kramer and R. Gompper, *ibid.*, **43**, 349 (1964).

[7] C. E. Looney, W. D. Philips, and R. Reilly, *J. Amer. Chem. Soc.*, **79**, 6136 (1957).

[8] D. J. Blears, *J. Chem. Soc.*, 1964, 6256.

[9] F. A. L. Anet and M. Ahmad, *J. Amer. Chem. Soc.*, **86**, 119 (1964).

[10] D. D. MacNicole, R. Wallace, and J. C. D. Brand, *Trans. Faraday Soc.*, **61**, 1 (1965).

crease the barrier, and electron attracting −M substituents such as –C≡N and COOEt were found to increase the barrier. Hückel-type MO calculations indicate that the more strongly the substituent R$_3$ interacts with the thiocarbonyl group, the lower is the barrier to rotation about the >N–C⩽ bond. An interesting observation has been made by Anet and coworkers,[11,12] who have shown the ring protons in N-acetylaziridine (II) to give only one sharp nmr signal at temperatures down to −150°. The barrier in the C–N bond in (II)

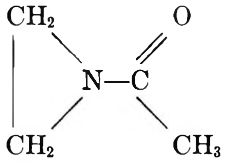
II

can be estimated to be lower than that in an ordinary N,N-dialkylsubstituted analogue by at least 10 kcal/mol, which indicates that the "lone pair" electrons on the nitrogen atom in (II) are predominantly localized in the three-membered ring.

If the nitrogen atom in an amide also forms part of an aromatic system, a low barrier in the >N–C⩽ bond may be expected. In order to test the validity of this idea, we have evaluated the activation parameters for rotation of the acetyl group in N-acetylpyrrole (III).

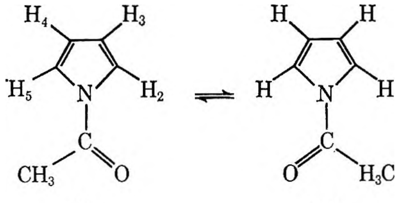
IIIa IIIb

The evaluation of rate parameters from pmr spectra of N,N-dialkylamides can in most cases be made using the adiabatic Gutowsky–McConnell approach.[13,14] In order to determine accurately the interconversion rate in N-acetylpyrrole (III) from the four-spin nmr spectrum of the ring protons, it is however, necessary to apply the density matrix theory developed by Kaplan.[15,16] The applicability of this theory to intramolecular exchange in a four-spin system has recently been demonstrated.[17]

Experimental Section

N-Acetylpyrrole was prepared according to Dennstedt[18] and purified by distillation, bp 181–182°. The deuterated methylene chloride (CD$_2$Cl$_2$) used as solvent was of commercial quality (Merck Sharpe & Dohme of Canada, Ltd.) and used without further purification. A 10% solution of N-acetylpyrrole in CD$_2$Cl$_2$ containing 1% tetramethylsilane (TMS) was used in the present investigation. The sample tubes used were standard 5 mm pyrex nmr tubes, and the sample was degassed and sealed before use.

The sample temperatures were obtained from the temperature-dependent shift difference between the signals from the hydroxyl and methylene protons in a 50% solution of ethylene glycol in acidified CD$_3$OD. This solution was placed in a sealed capillary which in turn was fixed in the center of the sample tube by means of two teflon plugs. The temperature-dependent shift between the OH and the methylene signals in the solution was separately calibrated against a copper–constantan thermocouple according to a procedure described elsewhere.[19] The temperatures obtained in this way are estimated to be accurate to ±0.5°. The nmr spectra were recorded between −60 to +30° using a Varian A 60 nmr spectrometer equipped with a variable temperature probe and a V 4343 variable temperature controller. The resolution of the spectrometer was maintained approximately constant by adjusting the homogeneity so as to always obtain the same half width (*ca.* 0.35 Hz) in the triplet from the traces of CDHCl$_2$ in the CD$_2$Cl$_2$ solvent. Shifts were measured by means of the ordinary side-band technique using a Hewlett-Packard Model 202 C Audio Oscillator and a Hewlett-Packard Model 5512 Electronic Counter.

The Nmr Spectra of N-Acetylpyrrole

The ring protons of N-acetylpyrrole give rise to an ABXY spectrum at −70° and an AA′XX′ spectrum at +50°. These spectra were analyzed using the LAOCOON II computer program developed by Castellano and Bothner-By.[20] The ABXY spectrum at −70° consists of two "quartets" in the region 420 Hz to 450 Hz (from TMS) and a "triplet" at 378 Hz. The two "quartets" in the low temperature spectrum are due to H-2 and H-5 in conformer IIIa. The assignment of H-2 and H-5 is dependent on the model for the diamagnetic anisotropy effects of carbonyl groups. We have tentatively assigned the low field "quartet" (at 446.3 Hz) to H-2 and the high field "quartet" (at 427.5 Hz) to H-5. The signals from H-3 and H-4 are found as a triplet centered at 377.8 Hz (from TMS). The chemical shift between H-3 and H-4 obtained from the iterative computer analyses is only

---

(11) F. A. L. Anet and J. M. Osyany, *J. Amer. Chem. Soc.*, **89**, 352 (1967).

(12) F. A. L. Anet, R. D. Trepka, and D. J. Cram, *ibid.*, **89**, 357 (1967).

(13) H. S. Gutowsky, D. McCall, and C. P. Slichter, *J. Chem. Phys.*, **21**, 279 (1953).

(14) H. M. McConnell, *ibid.*, **28**, 430 (1958).

(15) J. Kaplan, *ibid.*, **28**, 278 (1958).

(16) J. Kaplan, *ibid.*, **29**, 462 (1958).

(17) K-I. Dahlqvist and S. Forsén *J. Magnetic Resonance*, in press.

(18) C. Dennstedt, *Ber.*, **16**, 2353 (1883).

(19) T. Drakenberg, K-I. Dahlqvist, and S. Forsén, *Acta Chem. Scand.*, in press.

(20) S. Castellano and A. A. Bothner-By, *J. Chem. Phys.*, **41**, 3863 (1964).

$\simeq$0.8 Hz, which makes it difficult to obtain any assignment of the relative shifts for these protons. At 30° the two "quartets" from H-5 and H-2 have coalesced into a "triplet" which forms the AA′ part of the AA′XX′ spectrum. The methyl protons of the acetyl group give at room temperature a singlet at 150.6 Hz (from TMS). The parameters for the ring protons obtained from the computer analyses are given in Table I.

Table I: Chemical Shifts from TMS at 60 MHz and Spin Coupling Constants for the Ring Protons in N-Acetylpyrrole

Temp −70°		Temp 50°		
Proton	Shift, Hz	Proton	Shift, Hz	Spin coupling constants, Hz
H-2	446.3	H-2	435.9	$J_{23} = 3.00$
H-3 or H-4	378.2	H-3	375.6	$J_{24} = 1.42$
H-4 or H-3	377.4	H-4	375.6	$J_{25} = 2.06$
H-5	427.5	H-5	435.9	$J_{34} = 3.00$
				$J_{35} = 1.47$
				$J_{45} = 3.15$

Evaluation of the Interconversion Rate

The interconversion rate between (IIIa) and (IIIb) has been evaluated from the nmr spectrum of the ring protons. This spectrum is converted from an ABXY-type spectrum on slow rotation of the acetyl group into an AA′XX′-type spectrum on fast rotation. Intramolecular exchange in a spin system can according to Kaplan[15,16] be represented by an exchange operator R

$$\psi \longrightarrow R\psi \qquad (1)$$

Here ψ and $R\psi$ are the wave functions for the spin system before and after the exchange.

The density matrix before and after exchange may similarly be represented by

$$\rho = R\rho R \qquad (2)$$

The time dependence of the density matrix in the absence of exchange is given by

$$\frac{d\rho}{dt} = \frac{i}{\hbar}[\rho,H] \qquad (3)$$

where the brackets on the right hand side denote the commutator of the density matrix and the Hamiltonian of the spin system. According to Kaplan the exchange may be accounted for, by adding a "damping term" $(R\rho R - \rho)/\tau$ (where τ is the mean lifetime of the nuclei in each site) to eq 3

$$\frac{d\rho}{dt} = \frac{R\rho R - \rho}{\tau} + \frac{i}{\hbar}[\rho,H] \qquad (4)$$

The relaxation processes are accounted for by adding a term $1/T_2$ (where T_2 is the spin-spin relaxation time) to eq 4. The time dependence of the density matrix element for the transition between the states k and l may now be written using the notation of Johnson[21]

$$\begin{aligned}\frac{d\rho_{kl}}{dt} = \Big(\sum_{n,m} R_{kn}\rho_{nm}R_{ml} - \rho_{kl}\Big)\Big/\tau - \frac{\rho_{kl}}{T_2} - \\ i\rho_{kl}\Big[\sum_i(\omega_i - \omega)[(I_z{}^i)_{kk} - (I_z{}^i)_{ll}] + \\ \sum_{i<j} J_{ij}[(I_z{}^iI_z{}^j)_{kk} - (I_z{}^iI_z{}^j)_{ll}]\Big] + \\ + \frac{i}{2}\sum_{i<j} J_{ij}[\rho,I_+{}^iI_-{}^j + I_+{}^jI_-{}^i]_{kl} + \\ i\omega_r(\rho_{kk} - \rho_{ll})\sum_i(I_x{}^i)_{kl} \qquad (5)\end{aligned}$$

When the spectrum is recorded using a weak radiofrequency field, only transitions between those states for which $\Delta M = +1$ need be considered. Under "slow passage" conditions we may put $d\rho/dt = 0$ and eq 5 then leads to 56 linear equations in the present four-spin case. However, the corresponding 56 × 56 coefficient matrix decomposes into diagonal blocks, two of dimension 24 × 24 and two of dimension 4 × 4, and these must be inverted for every point in the spectrum. This may be done by means of a digital computer.

The absorption intensity of the nmr-spectrum $I(\omega)$, is given by the expectation value of I_y in the rotating frame[21]

$$I(\omega) = \langle I_y \rangle = k\mathrm{Im}\ \mathrm{Tr}(\rho\Sigma I_+{}^j) \qquad (6)$$

where k is a proportionality factor, Tr denotes the trace, Im stands for the imaginary part and $I_+{}^j$ is the raising operator $(I_x + iI_y)$ for nucleus j. Since eq 6 contains the trace of $(\rho\Sigma I_+{}^j)$, $I(\omega)$ will be independent of the representation used for the basis functions in eq 1–6. For convenience we have chosen simple product functions for this representation.

A computer program named DENSMAT has been developed[22] by means of which eq 5 and 6 may be solved numerically for up to four-spin systems. For a given set of τ, T_2, chemical shifts, and spin coupling constants, theoretical spectra were calculated using a CDC 3600 computer and plotted on Calcomp plotter Type 565. The rate of rotation for the acetyl group at each temperature was determined by visual fitting of theoretical spectra to experimental ones. A single point in the theoretical spectrum required about 1.7 sec computation time on a CDC 3600 computer. In general a complete spectrum of the AB part was made up of about 700 points and the XY part of about 200 points, thus demanding *ca* 20 min and 6 min of computation time respectively. In all approximately 150 spectra, some of which however, were cal-

---

(21) C. S. Johnson, Jr., "Advances in Magnetic Resonance," Vol. 1, Academic Press, New York, N. Y., 1965, p 33.

(22) K-I. Dahlqvist, S. Forsén, and T. Alm, *Acta Chem. Scand.*, in press.

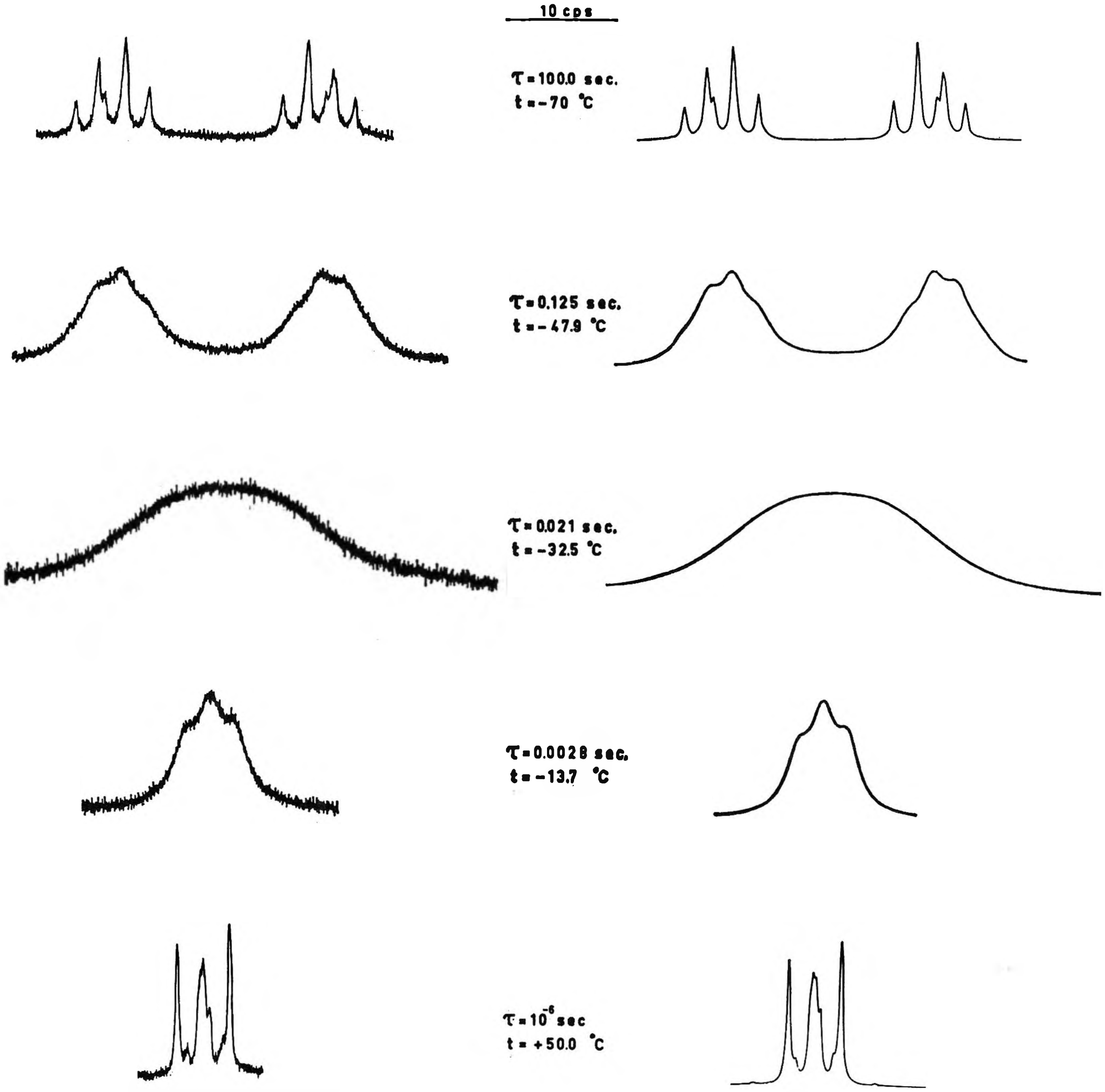

Figure 1. Examples of experimental and theoretical spectra of H-2 and H-5 protons in N-acetylpyrrole.

culated over a small region of the spectrum with less than 700 points, were calculated during the present investigation, and the total computation time for the whole investigation was about 25 to 30 hr.

The transverse relaxation time, T_2, was obtained by visual fitting of theoretical curves to the experimental ones obtained at the slow and fast exchange limits where the value of the exchange rate no longer affects the line width. The theoretical spectra at these limits were calculated with the computer program DENSMAT with input parameters obtained in the following way. The chemical shifts and spin-spin coupling constants were obtained by the LAOCOON II analyses, and τ values appropriate for each limit were chosen. The theoretically reproduced line widths are found to depend mainly on T_2. (See spectra at −70 and +50° in Figure 1.) Since both the high- and low-temperature spectra could be well reproduced with the same set of T_2 (0.65 sec) and spin-spin coupling constants (see Table I), these parameters were used for calculation of theoretical spectra at all intermediate temperatures.

The shift difference, $\Delta\nu_{AB-XY} = (\nu_A + \nu_B)/2 - (\nu_X + \nu_Y)/2$, between the AB part and the XY part of the spectrum showed a small temperature dependence and was 1.2 Hz larger at +50° than at −70°. As calculated spectra with $\Delta\nu_{AB-XY} \pm 2$ Hz showed no detectable difference in the exchange broadened region the low temperature value of $\Delta\nu_{AB-XY}$ was used for all temperatures.

The XY part of the N-acetylpyrrole spectrum could

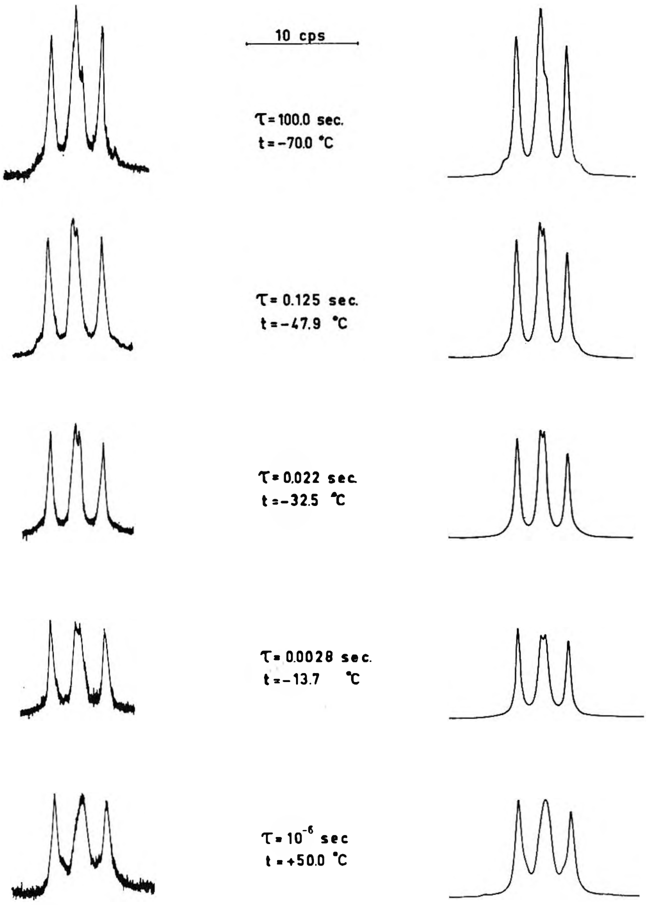

Figure 2. Examples of experimental and theoretical spectra of the H-3 and H-4 protons in N-acetylpyrrole

at all temperatures be well reproduced using the same value of $\delta\nu_{XY}$ (0.8 Hz). A variation in $\delta\nu_{XY}$ of the order of ±0.2 Hz had no detectable effect on the lineshape of either the XY part or the AB part of the spectrum, and the value 0.8 Hz was used for $\delta\nu_{XY}$ throughout the investigation.

The τ value at each temperature was evaluated only from the AB part of the spectrum since the lineshape of the XY part was very insensitive to variations in τ due to the small value of $\delta\nu_{XY}$. In the temperature region below the coalescence temperature both τ and $\delta\nu_{AB}$ could be determined independently by curve fitting. Above this temperature the spectrum contains too little information to permit the simultaneous evaluation of $\delta\nu_{AB}$ and τ.

The $\delta\nu_{AB}$ values obtained by direct curve fitting are most accurate at the slow exchange limit where the spectrum contains fine structure. The accuracy in the determination of $\delta\nu_{AB}$ decreases gradually as the exchange broadening increases and the fine structure disappears. At −70°, $\delta\nu_{AB}$ could thus be determined within about ±0.1 Hz, at −47.9° within about ±0.2 Hz and at the coalescence temperature within about ±0.3–0.4 Hz, (*cf.* Figure 1.) Within these error limits no significant temperature dependence in $\delta\nu_{AB}$ was found, and a mean value of the shifts determined at temperatures below the coalescence point were used for the calculation of spectra at higher temperatures.

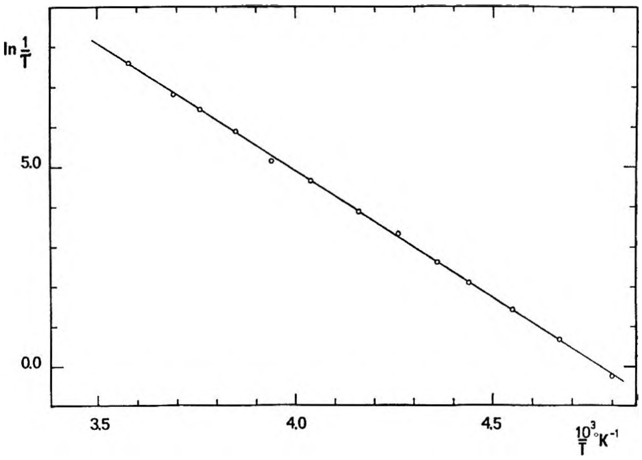

Figure 3. Arrhenius plot of the kinetic data obtained from the lineshape of the H-2 and H-5 protons in N-acetylpyrrole.

The evaluation of τ is, on the other hand, most accurate at the coalescence point, but the precision decreases with decreasing exchange broadening both toward the slow and fast exchange limits. The relative error in τ at the coalescence point was about ±1–2% and the Arrhenius plot close to the slow and fast exchange limits was terminated when the relative errors amounted to about ±4–5%.

Results and Discussion

The ring proton spectrum of N-acetylpyrrole is not a pure ABXY spectrum since N-acetylpyrrole contains seven protons and one nitrogen, and is therefore actually the ABXY part of an eight-spin system. However, the spectrum of the ring protons could be well reproduced at the slow and fast exchange limits by neglecting the spin–spin interactions with the acetyl protons and the nitrogen. Furthermore the absorption lines in the limiting spectra were relatively sharp ($\delta\nu_{1/2} \simeq$ 0.5 Hz). It therefore appears that no additional errors should result from a phenomenological treatment of all these couplings as contributing only to the apparent T_2 values.

A comparison between experimental and calculated spectra for N-acetylpyrrole (Figures 1 and 2) shows the same excellent agreement for all exchange rates determined between the slow and fast exchange limits.

The τ-values obtained by visual fitting of theoretical spectra to experimental ones are plotted as $\ln(1/\tau)$ *vs.* $1/T$ in Figure 3. The activation parameters for the $>$N–C$\lessdot$ rotation in N-acetylpyrrole calculated from the theory of absolute reaction rates are given in Table II. The errors in these activation parameters were calculated assuming only random errors and are probably too low. An investigation of the sources of

Table II: Activation Parameters for the Internal Rotation of the N-Acetyl Group in N-Acetylpyrrole[a]

Compound	T, °K	E_a, kcal/mol	$\Delta H^\ddagger$, kcal/mol	$\Delta F_{298°K}{}^\ddagger$, kcal/mol	$\Delta S^\ddagger$, eu	Ref
(III)	298.2	12.55 ± 0.09	11.96 ± 0.09	12.14 ± 0.10	−0.6 ± 0.6	present investigation
N,N-Dimethylacetamide	298.2	19.0 ± 0.4	18.3 ± 0.4	18.0 ± 0.2	0.9 ± 1.3	22

[a] The errors given for these parameters have been calculated assuming only random errors. More realistic errors are E_a and $\Delta H^\ddagger$, ± 05 kcal/mol; $\Delta F^\ddagger$, ± 0.2 kcal/mol; $\Delta S^\ddagger$, ± 2.3 eu (*cf.* text). For comparison, corresponding values for the internal rotation of the N–$(CH_3)_2$ group in N-dimethylacetamide are also given in the table.

error in the evaluation of the $\geqslant$C–N< barrier in N,N-dimethyltrichloroacetamide[19] shows that more realistic values for the errors in E_a and in $\Delta H^\ddagger$ are ±0.5 kcal/mol, in $\Delta F^\ddagger$ ±0.2 kcal/mol, and ±2.3 eu in $\Delta S^\ddagger$.

A comparison of the activation parameters for the restricted >N–C$\leqslant$ rotation in N-acetylpyrrole and N-dimethylacetamide (IV) (see Table II) shows that E_a, $\Delta H^\ddagger$, and $\Delta F^\ddagger$ are about 7 kcal/mol lower in (III) than in (IV). As the steric interactions between the acetyl group and the rest of the molecule should be quite similar in both of these molecules, and since the interaction between the lone pair on the nitrogen and the carbonyl group is believed to give the main contribution to the restricted >N–C$\leqslant$ rotation in amides, we may conclude that the lone pair on the nitrogen in (III) is to a great extent localized in the pyrrole ring.

The entropy of activation for the >N–C$\leqslant$ rotation in compound (III) was found to be zero within the experimental errors. Careful measurements of the barrier to internal rotation in (IV) and other simple alkylsubstituted amides[23] have also yielded activation entropies close to zero.

Acknowledgments. The authors wish to thank Dr. E. Forslind for his kind interest in this work. Thanks are also due to Dr. R. E. Carter for helpful linguistic criticism and to Dr. R. A. Hoffman for valuable discussions and criticism. The cost of the nmr spectrometer was defrayed by a grant from the Knut and Alice Wallenberg Foundation.

(23) T. Drakenberg, K-I. Dahlqvist, and S. Forsén, *Acta Chem. Scand.*, in press.

The Interaction of the Ground and Excited States of Indole Derivatives with Electron Scavengers[1]

by Robert F. Steiner and Edward P. Kirby

Laboratory of Physical Biochemistry, Naval Medical Research Institute, National Naval Medical Center, Bethesda, Maryland 20014 *(Received April 1, 1969)*

The quantum yields and fluorescent lifetimes of a series of indole derivatives are reduced in the presence of a wide range of substances which are efficient scavengers of hydrated electrons. Deactivation of the excited state of the indole ring, which is solvated in polar or polarizable solvents, requires a direct collisional interaction with the scavenger. One possible mechanism for quenching is by abstraction of an electron from the excited indole by the scavenger although other mechanisms cannot be excluded. At higher concentrations of added quencher, ground state complexes of the scavenger with the indole may be formed in some cases.

Introduction

In earlier investigations by this and other laboratories, the fluorescence properties of many indole derivatives have been found to be dependent upon the nature of the chemical modification, as well as upon the temperature and solvent composition.[2a-6] Under a particular set of conditions, the quantum yield and excited lifetime of fluorescence depend upon the competition between the emission of fluorescent radiation and any radiationless processes which deactivate the excited state. The possible factors which can contribute to radiationless deactivation include intramolecular quenching by a group in chemical attachment to the indole, intermolecular quenching by an external molecule or ion, electron ejection to the solvent,[7] "tunneling" from the excited to the ground state, and intersystem crossing to the triplet state.

If all of the processes which deactivate the excited singlet are first order with respect to the excited state

$$Q = \text{quantum yield} = k_f/(k_f + \Sigma k_i) \tag{1}$$

where k_f and the set of k_i are the rate constants for emission of fluorescence and for the various radiationless deactivation processes, respectively. The fluorescence lifetime, τ, is given by

$$\tau = 1/(k_f + \Sigma k_i) \tag{2}$$

or

$$Q/\tau = k_f \tag{3}$$

For a series of tryptophan derivatives formed by substitution on the α-amino or α-carboxyl group, the approximate constancy of Q/τ[2a] and of the spectral distribution of fluorescence[2b] indicate that the basic characteristics of the indole excited state are not greatly changed by substitution of the non-indole portion and that the variation in fluorescence parameters arises primarily from the nonradiative processes.

The present paper is concerned with the intermolecular quenching of indole derivatives and with the bearing which this might have upon the intramolecular and other nonradiative quenching processes which terminate the excited state. We have been particularly interested in the possibility of quenching by electron transfer.

The latter interest has led us to examine the effects upon the fluorescence of indole derivatives of a series of compounds known to be active electron scavengers.[7,8] The rates of combination with free solvated electrons, usually produced by pulse radiolysis of water, have been determined for over 300 substances of very diverse chemical nature and provide an index of their relative efficiency in electron capture.[8] In brief, all the electron scavengers examined have been found to be quenchers of fluorescence and quenching by these agents generally occurs primarily by interaction with the excited state.

Experimental Section

Methods. Measurements of relative fluorescence intensity and of the spectral distribution of fluorescence were made with an Aminco-Bowman spectrofluorometer, equipped with a spectral compensator to correct for the wavelength dependence of the instrument sensitivity. Energy-corrected spectra were obtained.[2a] If no change in the shape or wavelength position of the emission band occurred, the effects of additives upon the fluorescence intensity were assessed by measurements at the wavelength of maximum emission. The intensity for each level of additive was compared with that of a control solution containing no additive but otherwise identical. All experiments were run at room temperature. A correction was applied for any attenuation by absorption of the incident or emitted beam, as described elsewhere.[9] If the correction for attenuation was large (>20%), the extent of quenching was also measured for excitation at longer wavelengths.

---

[1] From Bureau of Medicine and Surgery, Navy Department, Research task MR005.06-0005. The opinions in this paper are those of the authors and do not necessarily reflect the views of the Navy Department or the naval service at large.

[2] (a) I. Weinryb and R. F. Steiner, *Biochemistry*, **7**, 2488 (1968); (b) R. W. Cowgill, *Arch. Biochem. Biophys.*, **100**, 36 (1963).

[3] R. W. Cowgill, *Biochim. Biophys. Acta*, **75**, 272 (1963).

[4] R. W. Cowgill, *ibid.*, **133**, 6 (1967).

[5] M. S. Walker, T. W. Bednar, and R. Lumry, *J. Chem. Phys.*, **47**, 1020 (1967).

[6] J. A. Gally and G. M. Edelman, *Biochim. Biophys. Acta*, **60**, 499 (1962).

[7] L. I. Grossweiner and H. I. Joschek, Advances in Chemistry Series No. 50, American Chemical Society, Washington, D. C., 1965, p 279.

[8] M. Anbar, Advances in Chemistry Series No. 50, American Chemical Society, Washington, D. C., 1965, p 55.

Measurements of absorbance at a single wavelength were normally made with a Gilford 2000 spectrophotometer. Difference spectra were measured with the Cary 14 spectrophotometer, using a set of fused tandem quartz cells.

Excited lifetimes were determined using the TRW system (TRW Instruments, El Segundo, Calif).[2a,10]

Materials. Purified preparations of tryptophan (Trp), indole, acetyl tryptophan (AcTrp), acetyl tryptophan amide (AcTrp NH_2), and tryptophan ethyl ester (TrpEt) were purchased from Sigma and from Cyclo. No differences in properties were observed between preparations from the two sources.

All other preparations were reagent grade. Glass redistilled water was used for the preparation of all aqueous solutions. Solvents were Matheson Coleman and Bell "Spectroquality" reagents.

Results

Table I summarizes the effects upon the fluorescence of acetyl tryptophan of the electron scavengers examined. All of the more than two dozen molecules and ions with electron-capturing ability which were tested were found to show significant quenching activity, although their efficiencies varied widely. Table I includes the corresponding values of the rate constants for electron capture.[8]

Table I: Quenching of Acetyltryptophan in Water

Reagent	Molarity for 50% quenching[a]	τ/τ_0 for 50% quenching[b]	$k_e{}^c \times 10^{-10}$	Ref
H^+	0.02		2.3	8
D^+	0.02			
Cu^{2+}	0.026		3	8
Na fumarate	0.028		0.8	13
Acrylamide	0.035	0.49	2	13
NO_3^-	0.038	0.46	3	8
IO_3^-	0.06		0.8	8
Acetone	0.07		0.6	13
Pb^{2+}	0.08		4	8
Cysteamine	0.09		2	8
Histidine	0.09	0.52	0.7	15
Chloroform	0.10		2	13
Thiourea	0.10		0.3	8
Cysteine	0.17	0.46	0.9	15
Cd^{2+}	0.37		1	8
Proline	0.41		0.002	15
Mn^{2+}	0.52		0.008	8
Glycylglycine	0.58		0.025	18
Arginine	0.67		0.015	15
Glycine	1.1		0.0008	15
$H_2PO_4^-$	1.2		0.15	8
Lysine	1.3	0.48	0.002	15
Alanine	2		0.005	15
β-Alanine	2.2		0.0004	15

[a] The solvent is 0.1 *M* KCl, 0.01 *M* KOAc, pH 5.0, except in the cases of Cu^{2+} and Mn^{2+}, for which the pH is 4.50, and that of Pb^{2+}, for which the solvent is 0.01 *M* KOAc, pH 4.50. For Cu^{2+}, H^+, D^+, and Pb^{2+}, acetyl tryptophan amide replaced acetyl tryptophan. $\lambda_{ex} = 295$ mμ; $\lambda_f = 350$ mμ. [b] The ratio of the excited lifetime at 50% quenching to the value in the absence of quencher. [c] The second-order rate constant for electron capture.

Quenching by Cations. Hydrogen and deuterium ions quench the fluorescence of acetyl tryptophan amide to an equivalent degree below pH 2 (Table I). Since this derivative contains no site which ionizes in the pH range 0–12, the observed quenching cannot be due to protonation of the ground state and must reflect an interaction of hydrogen or deuterium ion with the excited state of indole.[11,12] It is pertinent that $H_3{}^+O$ is a very efficient electron scavenger.[8]

The metallic cations Cu,$^{2+}$ Pb,$^{2+}$ Cd,$^{2+}$ and Mn^{2+} are effective electron scavengers and efficient quenchers of the fluorescence of tryptophan derivatives (Table I). In contrast, Na^+, K^+, Mg,$^{2+}$ $NH_4{}^+$, and Ba^{2+} (supplied as the chlorides) are inactive both as electron scavengers (8) and as quenchers at concentrations up to 1 *M*.

Quenching by Anions. The anions NO_3^-, IO_3^-, and fumarate are highly efficient as both electron scavengers[8] and quenchers, while $H_2PO_4^-$ (but not $HPO_4{}^{2-}$) is moderately active in both respects (Table I). The following anions, which are unreactive with solvated electrons[8,13] exhibited no quenching activity when supplied as the sodium or potassium salt: CNS^-, CH_3COO^-, $HCOO^-$, $SO_4{}^{2-}$, and citrate. (Acetate and formate were tested at pH 7.0, where the unionized species are absent.

The second-order rate constant for the quenching of acetyl tryptophan by NO_3^- (as computed from eq 4 below) was 5.2×10^9, which approaches that predicted for a diffusion-controlled reaction (6.5×10^9) of an ion of this size. As shown in Table I, the excited lifetime

---

(9) R. F. Steiner, J. Roth, and J. Robbins, *J. Biol. Chem.*, **241**, 560 (1966).

(10) R. F. Chen, G. G. Vurek, and N. Alexander, *Science*, **156**, 949 (1967).

(11) A. White, *Biochem. J.*, 71, 217 (1959).

(12) G. Weber, in "Light and Life," W. McElroy and G. Glass, Ed., Johns Hopkins Press, Baltimore, Md., 1961.

(13) E. J. Hart, J. K. Thomas, and S. Gordon, *Radiat. Res. Suppl.*, **4**, 74 (1964).

is reduced to approximately the same extent as the fluorescence intensity for 50% quenching. Since interaction of NO_3^- with the ground state to form a nonfluorescent complex would not alter the lifetime, this implies that NO_3^- interacts directly with the excited state. This model was confirmed by the failure of any significant difference spectrum to appear for mixtures of acetyl tryptophan (4×10^{-4} M) with 0.1 M $NaNO_3$.

Quenching by Sulfur-Containing Compounds. The sulfur-containing molecules carbon disulfide, thiourea, cysteine, and cysteamine combine with electrons at rates which approach those predicted for diffusion-controlled processes.[7,8,13] All four are also very efficient quenchers of the fluorescence of acetyl tryptophan (Table I).

The reduction of fluorescence intensity by cysteine is accompanied by an equivalent fall in excited lifetime (Table I), suggesting that the quenching process involves primarily an interaction of cysteine with the excited state. However a barely perceptible difference spectrum was developed for a mixture of 4×10^{-4} M acetyl tryptophan and 0.5 M cysteine, with a small positive peak at 292 mμ, whose magnitude was about 1% of the total absorbance at 280 mμ. This raises the possibility of some minor degree of interaction of cysteine with the ground state of indole.

The quenching by cysteine of four tryptophan derivatives was analyzed according to the Stern–Volmer equation[14]

$$\frac{I_0}{I} = 1 + K_{SV}[B] = 1 + k_2\tau[B] \qquad (4)$$

where I_0 and I are the intensities of fluorescence in the absence and presence of quencher, respectively; K_{SV} is a constant given by the slope of the line; k_2 is the second order rate constant for deactivation of the excited state; τ is the excited lifetime in the absence of quencher; and $[B]$ is the concentration of quencher.

The variation of I_0/I with cysteine concentration was linear for all four derivatives, with slopes decreasing in the order AcTrp > Trp, $AcTrpNH_2$ > Trp > TrpEt (Table II), which is that expected from the respective values of τ (1). However the values of k_2, as computed from eq 4 were of a similar order of magnitude for all derivatives (Table II).

Table II: Rate Constants for Quenching of Tryptophan Derivatives by Cysteine

Compound	K_{SV}	$k_2 \times 10^{-9}$
Trp	3.2	1.1
AcTrp	5.6	1.1
$AcTrpNH_2$	2.9	0.75
TrpEt	0.26	0.52

The solvent is 0.1 M KCl 0.01 M KOAc, pH 5.0. The values of k_2 are computed from eq 4. Estimated accuracy of k_2 is ±20%.

Quenching by Histidine. Histidine, cysteine, and cystine are the only amino acids whose rate constants for electron capture approach collisional values.[8,15] Shinitzky and coworkers have already reported the quenching of indole derivatives by imidazole-containing compounds, which they attributed to the formation of a nonfluorescent charge transfer complex by the ground state.[16]

Histidine was likewise found in this study to be an efficient quencher of the fluorescence of acetyl tryptophan (Figure 1 and Table I). However the parallel fall of excited lifetime with fluorescence intensity (Figure 1) indicates that deactivation of the excited state by interaction with histidine is a major factor in the quenching. The association constant for ground state complex formation by indole and histidine (~2) or by tryptophan and histidine (1.7) is too low to account for all of the quenching,[16,17] predicting that only 13–15% of the acetyl tryptophan is complexed at the histidine level sufficient for 50% quenching.

The pH profile of the quenching of acetyl tryptophan amide by histidine (Figure 1) parallels those for electron capture (Figure 2 of ref 15) and for the ionization of imidazole (pK 6), suggesting that it is the protonated imidazole ring which is effective in both electron capture and in quenching.

Quenching by Other Amino Acids and Peptides. None of the remaining amino acids approach cysteine, cystine, or histidine in either electron capture efficiency or quenching effectiveness (Table I). Arginine is much more effective in both respects than glycine, alanine, lysine, or β-alanine (Table I). However, proline, whose rate constant for electron capture is the same as that of lysine, is significantly more efficient as a quencher. This may be a consequence of ground state complex formation between proline and tryptophan derivatives.[17]

Mixtures of acetyl tryptophan with proline, lysine, and arginine all gave small but significant difference spectra, which were qualitatively similar. Arginine gave the largest absorbance change, the magnitude of the small positive peak developed at 293 mμ being about 2% of the total absorbance at 280 mμ (Figure 2). Thus ground state complexing may make a finite contribution to the quenching by all three compounds.

Formation of a peptide bond by glycine promotes both electron capture[18] and fluorescence quenching (Table I). $(Gly)_2$ is more effective than glycine.

---

[14] O. Stern and M. Volmer, *Phys. Z.*, **20**, 183 (1919).

[15] R. Braams, *Radiat. Res.*, **27**, 319 (1966).

[16] M. Shinitzky, E. Katchalski, V. Grisano, and N. Sharon, *Arch. Biochem. Biophys.*, **116**, 332 (1966).

[17] S. C. K. Su and J. A. Shafer, *J. Amer. Chem. Soc.*, **90**, 3861 (1968).

[18] R. Braams, *Radiat. Res.*, **31**, 8 (1967).

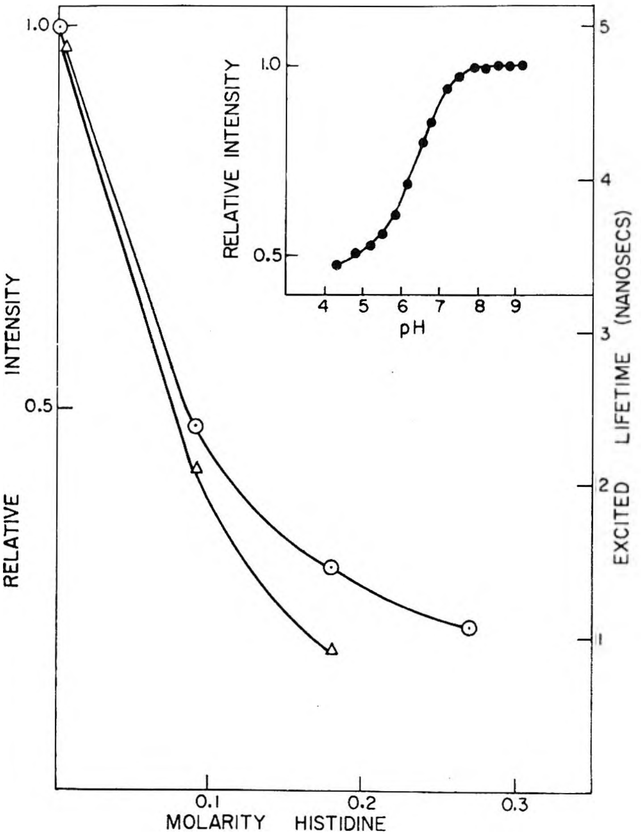

Figure 1. Variation of relative fluorescence intensity (⊙) and of fluorescence lifetime (△) for acetyl tryptophan (0.01 mg/ml) as a function of histidine concentration in 0.1 M KCl, 0.01 M KOAc, pH 5.0. (1) Inset. pH variation of relative fluorescence intensity for acetyl tryptophan amide (0.009 mg/ml) in the presence of 0.19 M histidine in 0.1 M KCl.

Quenching by Uncharged Aliphatic Compounds. The chlorinated hydrocarbon chloroform, which combines with free electrons at a diffusion-controlled rate,[8] is also an efficient quencher of the fluorescence of tryptophan derivatives in water (Table I). The parallel decrease of fluorescence intensity and excited lifetime and the absence of any detectable difference spectrum (for 4×10^{-4} M acetyl tryptophan plus 0.05 M chloroform) suggest that extensive ground state complexing is absent and that quenching occurs predominantly by interaction with the excited state. Similar statements can be made with respect to quenching by acrylamide (Table I), whose efficiency in electron capture has been attributed to its conjugation.[8] Acetone is likewise effective both as an electron scavenger and as a quencher (Table I).

The following compounds, which are inactive in electron capture, did not quench tryptophan derivatives at concentrations up to 1 M: sucrose, ethanol, ethylene glycol, and urea.

Solvent Effects on Quenching of Indole Fluorescence. The quenching of indole and its derivatives by electron scavengers is not confined to aqueous solutions. The fluorescence of indole in dioxane is quenched by low levels of carbon disulfide, chloroform, carbon tetrachloride, and acetone (Table III), all of which react with solvated electrons in water at collisional or near-collisional rates.[8] Acetic acid quenches at a somewhat reduced efficiency (Table III).

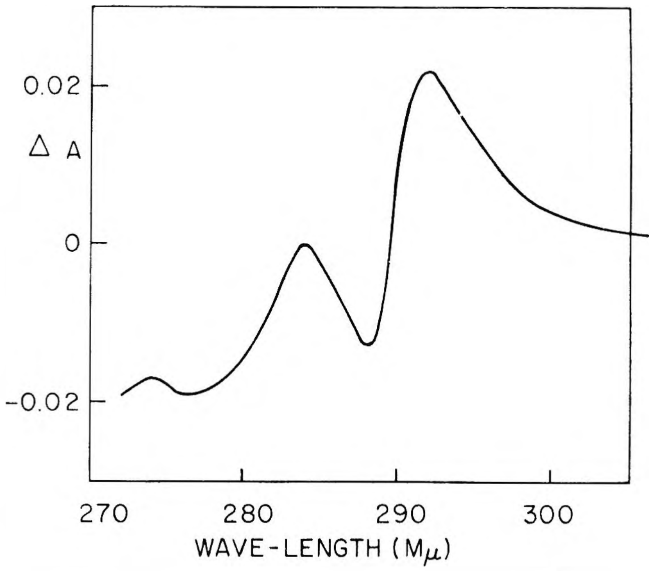

Figure 2. Difference spectrum developed by 3×10^{-4} M acetyl tryptophan plus 0.3 M arginine in 0.1 M KCl, 0.01 M KOAc, pH 5.0, with respect to the unmixed components.

Table III: Quenching of Indole in Dioxane

Reagent	Molarity for 50% quenching	$k_e{}^a$ 10^{-10}
Acetone	0.004	0.6
Carbon tetrachloride	0.005	2
Carbon disulfide	0.02	2
Chloroform	0.04	2
Acetic acid	0.08	0.02

[a] Data of Hart, Thomas, and Gordon (1964).

Table IV compares the rate constants for quenching of indole by chloroform in a series of non-aqueous solvents, as computed from the Stern–Volmer equation using the limiting slopes at low chloroform concentrations.[14] A significant degree of upward curvature was observed for chloroform concentrations above 0.1 M. The rate constant in methanol was an order of magnitude larger than in propylene glycol, which has a similar dielectric constant, presumably as a consequence of the 60-fold higher viscosity of the latter solvent. The rate constant was highest in the nonpolar solvent cyclohexane, which is the only solvent of this series in which "exciplex" formation cannot occur.[5]

Discussion

It is clear from the preceding results that the group of molecules and ions which have been found by pulse radiolysis studies to be efficient electron scavengers are also effective quenchers of the fluorescence of indole derivatives. All of the more than twenty members of this class which were studied were found to quench to some degree. (R. Lumry (private communication) has found that the scavenger N_2O at a concentration of $\sim$0.008 M does not quench indole fluorescence.)

In all the cases which were examined, the parallel decrease of the excited lifetime and the quantum yield suggests that radiationless deactivation of the excited state is a dominant mechanism. However, several of the amino acids, including arginine, histidine, proline, and cysteine, appear to form complexes to some extent with the ground state of tryptophan in water. This may also make a contribution to the observed intermolecular quenching by these molecules.

It should be stressed that a particular molecule may quench by more than one mechanism; that its quenching efficiency may be influenced by several other factors (such as the nature of the substitution on the indole derivative, the size and charge density of the quencher, steric factors, etc.), and that quenching and solvated electron capture are different processes. Hence it is not to be expected that the quenching efficiencies should vary monotonically with the rate constants for electron capture. If the data of Table I are displayed graphically in a log–log plot, the computed correlation coefficient between the rate constants for electron capture and the molarities for 50 per cent quenching is 0.82 ± 0.05.

It is not unreasonable to suggest that the quenching of the fluorescence of indole derivatives by this series of compounds may result, at least in part, from electron transfer from the excited state of indole to the acceptor molecule or ion. The evidence for an electron transfer mechanism for quenching is indirect and inferential, and cannot be regarded as conclusive. It may, however, serve as a convenient working hypothesis, pending more definitive information.

It would be premature to attempt to elaborate the electron transfer hypothesis in any detail. Quenching might occur by (1) transfer of an electron by collisional contact of the quencher with an excited indole, (2) preliminary ejection of an electron from an excited indole to vicinal solvent molecules, combination with a scavenger being competitive with respect to recapture by the indole or escape into the free, solvated state, or (3) the formation of a transient complex of the charge-transfer type between excited indole and the quencher. (For case (3) the electron would not necessarily be retained by the quencher upon dissociation of the complex.)

The exact nature of the most probable donor in any electron transfer process is uncertain. In a nonpolar solvent the donor would presumably be the excited indole ring itself, but in polar solvents a more specific transient complex is formed with the solvent of the "exciplex" type postulated by Walker, Bednar, and Lumry.[5,19]

There are several instances where a molecule which acts as an intermolecular quencher of indole derivatives is also known to suppress fluorescence when in chemical combination. Cowgill has reported that a series of tryptophan derivatives containing a sulfhydryl or disulfide group in proximity to the indole are all characterized by very low quantum yields of fluorescence.[20] Similarly, Shinitzky and Goldman have found that a series of derivatives of the dipeptide HisTrp have low quantum yields ($\sim$0.02–0.03) when the imidazole group of histidine is protonated.[21] The pH profile of quenching parallels the titration of histidine closely. Of the amino acids examined in the present study, only cysteine and histidine were highly effective as intermolecular quenchers. (Cystine could not be examined because of its low solubility). It is of interest that the only amino acids which combine with electrons with very high efficiency ($k_e > 10^9$) are cysteine, cystine, and histidine.[15] In these cases, there is a strong possibility that the inter- and intramolecular quenching processes occur by similar mechanisms, which may include electron transfer as a factor. It is worthy of mention in this connection that Dose has reported that ultraviolet irradiation of mixed solutions of tryptophan and cystine results in photodecomposition of tryptophan, accompanied by a reduction of cystine.[22]

Table IV: Solvent Effects on Quenching of Indole Fluorescence by Chloroform

Solvent	τ (nsec)	K_{SV}	$k_2 \times 10^{-9}$ for $CHCl_3$
Water	4.1	23.2	5.7
Methanol	3.5	32.3	9.2
Propylene glycol	4.4	3.9	0.9
Ethanol	3.8	29.8	7.8
Isopropyl alcohol	4.0	26.1	6.5
n-Butyl alcohol	3.7	23.5	6.4
Dioxane	4.5	35.0	7.8
Cyclohexane	5.1	65.5	12.8

The estimated accuracy of τ is ±0.3 nsec. K_{SV} was determined from Stern–Volmer plots as the slope of the line at concentrations of $CHCl_3$ less than 0.1 M. The estimated acuracy of k_2 is ±20%.

The quenching of indole derivatives by hydrogen ions deserves special comment. A combination with indole in the ground state can here be ruled out for the

---

[19] M. S. Walker, T. W. Bednar, and R. Lumry, *J. Chem. Phys.*, **45** 3455 (1966).

[20] R. W. Cowgill, *Biochim. Biophys. Acta*, **140**, 37 (1967).

[21] M. Shinitzky and R. Goldman, *European J. Biochem.*, **3**, 139 (1967).

[22] D. Dose, *Photochem. Photobiol.*, **7**, 671 (1968).

range of hydrogen ion concentrations in which quenching occurs (pH 1–3). Two alternative mechanisms may be proposed. (a). Quenching might occur by attachment of a proton to the excited indole ring. This mechanism may suffer somewhat in plausibility from the failure of the existing molecular orbital calculations[23] to indicate an obvious locus of excess negative charge on the excited indole ring. (b). In view of the high electron-capturing efficiency of hydrogen ion (8) it may be that the proton acts by abstracting an electron from the excited indole ring, thereby deactivating it. It has also been suggested that hydrogen ions may be the effective quenching agent for several tryptophan derivatives which contain a potential proton donor group.[2a,11,12]

The question may also be raised as to whether the reduced quantum yield of zwitterionic tryptophan (indole-3-alanine) in water, as compared with indole,[4] is related to the general intermolecular quenching caused by amino acids, including glycine and alanine, and whether the mechanism involves electron transfer, either directly to the protonated amino group or to the hydrogen ion donated by this group. The two mechanisms are not, of course, mutually exclusive. The parallel increase of inter- and intramolecular quenching and of electron capture efficiency upon peptide bond formation is also suggestive.

Acknowledgment. The authors wish to acknowledge the able technical assistance of Mr. Theodore Lutins and Mr. Richard Kolinski. This work was partially supported by ONR Grant No. NR108-815.

---

[23] P.-S. Song and W. E. Kurtin, *Photochem. Photobiol.*, **9**, 175 (1969)

Proton Resonance in Alkali Nitrate Melts[1]

by Lieng Chen Siew and Benson R. Sundheim

Department of Chemistry, New York University, New York, New York 10003

(Received April 3, 1969)

The viscosity, density, electrical conductivity, chemical shift, and proton relaxation times were determined for solutions of HNO_3 in the $LiNO_3$–KNO_3–$NaNO_3$ eutectic. Over the temperature range 140 to 220°, pronounced changes in many of these properties were noted at a composition near mole fraction of HNO_3 equal to one-third. The data are interpreted as showing the presence of a more-than-two coordinated proton in this region and of the hydrogen dinitrate ion in dilute solutions.

Introduction

Nuclear magnetic resonance measurements have been widely used in the study of chemical systems. Under favorable circumstances it is possible to obtain information about the nature of bonding, the identity and concentration of the various species in the system and of the lifetime of some of these species. Very little application of this technique has been made to the study of fused salt systems. Hafner and Nachtrieb[2] first investigated the chemical shifts in fused thallium salts as a function of temperature and anions. There have also been rather extensive studies made on the structure of mineral acids, sulfuric,[3,4a] nitric,[4b] and perchloric.[4b] Here the various ways in which the proton can be bound were studied by coupling with other physical measurements such as infrared spectroscopy and electrical conductivity.

In connection with the studies of the structure of liquid nitric acid near room temperature, Happe and Whittaker[5] examined the proton resonance spectrum of nitric acid and of solutions of potassium nitrate in nitric acid. A systematic chemical shift dependent on concentration was observed and it was suggested that this is associated with a systematic change in structure.

Studies on fused alkali nitrates have established that the cations are octahedrally surrounded by six oxygen atoms in a fairly regular pseudo-lattice.[6] By comparison with the behavior of other molten salt systems, it seems not unlikely that nitric acid when dissolved in

---

[1] Extracted in part from a dissertation by L. C. Siew submitted to the Graduate School of Arts and Science, New York University, in partial fulfillment of the requirements for the degree of Doctor of Philosophy, Feb 1969.

[2] S. Hafner and N. H. Nachtrieb, *J. Chem. Phys.*, **40**, 2891 (1964).

[3] H. S. Gutowsky and A. Saika, *ibid.*, **21**, 1688 (1953).

[4] (a) G. C. Hood and C. A. Reilly, *ibid.*, **27**, 1126 (1957); (b) G. C. Hood, O. Redlich, and C. A. Reilly, *ibid.*, **22**, 2067 (1954).

[5] J. A. Happe and A. G. Whittaker, *ibid.*, **30**, 417 (1959).

[6] (a) D. Gruen, P. Graf, S. Fried, and R. L. McBeth, *Pure Appl. Chem.*, **6**, 23 (1963); (b) K. E. Johnson and T. S. Piper, *Discussions Faraday Soc.*, **32**, 32 (1961).

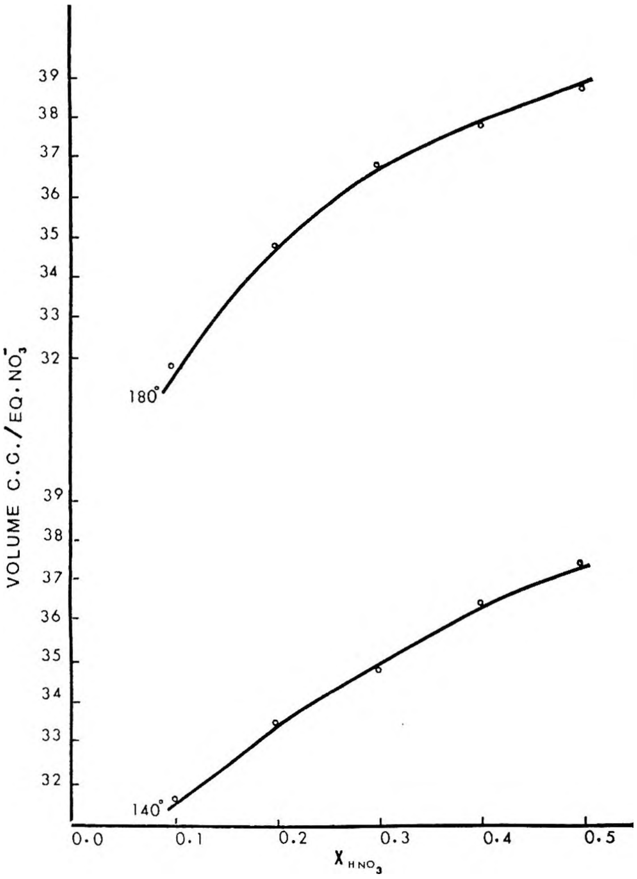

Figure 1. Volume/equiv of NO_3 of solutions of HNO_3 in $LiNO_3$–KNO_3–$NaNO_3$ as a function of X_{HNO_3}.

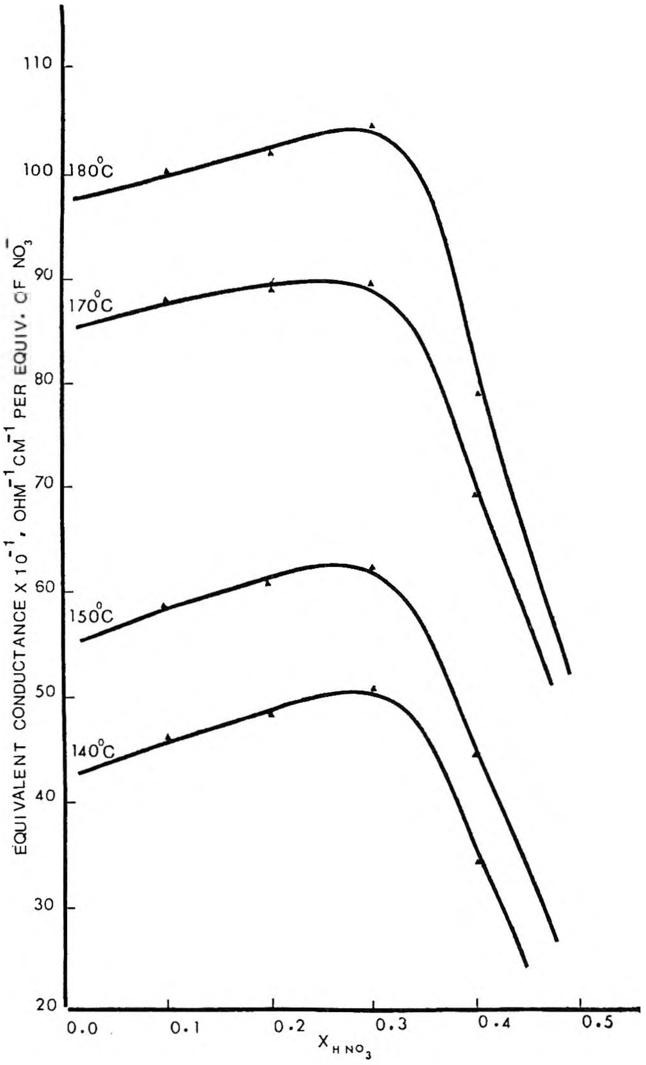

Figure 2. Equivalent conductance of solutions of HNO_3 in $LiNO_3$–KNO_3–$NaNO_3$ as a function of X_{HNO_3}.

small amounts of molten alkali nitrates would lead to a proton solvated in some fashion within the octahedral cavity. The proton might be specifically associated with one, two or perhaps an entire set of oxygen atoms.

The work reported here consists of an investigation of nuclear magnetic resonance spectra, nuclear magnetic resonance relaxation times, densities, viscosities and electrical conductivities of solutions of nitric acid in molten $LiNO_3$–KNO_3–$NaNO_3$ eutectic over the composition range from 10 mol % HNO_3 to 50 mol % and the temperature range from 140 to 220° (below 10 mol % no nmr signals could be reliably measured and above 50 mol % the vapor pressure becomes excessive).

Experimental Procedures

In order to extend the liquid range as far down in temperature as possible, all of the experiments reported herein were performed with the ternary eutectic of $NaNO_3$–KNO_3–$LiNO_3$ (20.7:53.5:14.5) to which anhydrous HNO_3 was added. The compositions are reported in terms of X, the mole fraction of HNO_3, taken as one component, the eutectic mixture being thought of as the other component. Measurements were made of the density, the electrical conductance, the viscosity and the infrared spectra by conventional means. The results are given in Figures 1–3. The proton magnetic resonance was determined on a Varian Model A-60 using a conventional high temperature cavity. Tetramethylsilane was used to calibrate the instrument at room temperature. At higher temperatures ethylene glycol was used as a standard for temperature measurements within the cavity.[7] The chemical shifts reported were corrected for the bulk magnetic susceptibility.

Approximate values of the spin–lattice relaxation time T_1 were obtained by direct method.[8] The absorbing system was first saturated by increasing the amplitude H_1 of the radiofrequency field. When H_1 was abruptly reduced to a nonsaturating value, the approximately exponential recovery of the magnetic resonance signal was followed and its half-life taken as T_1. Values of T_2 were obtained from measurements of the half-width of the (Lorentzian) line. In all cases,

---

(7) Varian Associates, Instrument Division, Technical Information Publication No. 87-100-120, Palo Alto, Calif.

(8) A. L. Van Geet and D. N. Hume, *Anal. Chem.*, 37, 983 (1965).

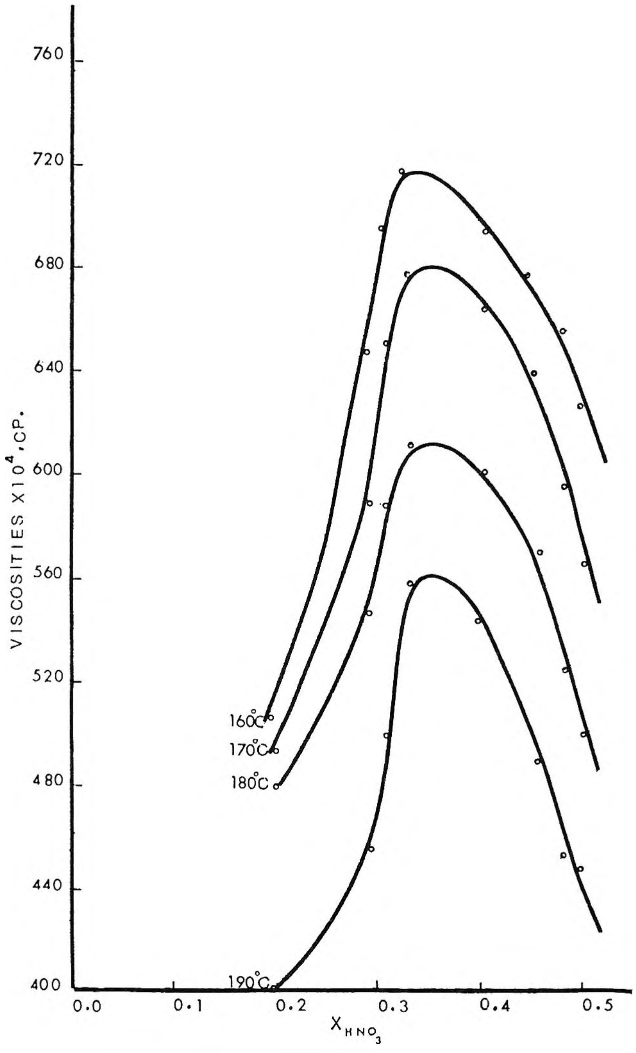

Figure 3. Viscosity of solutions of HNO_3 in $LiNO_3$-KNO_3-$NaNO_3$ as a function of X_{HNO_3}.

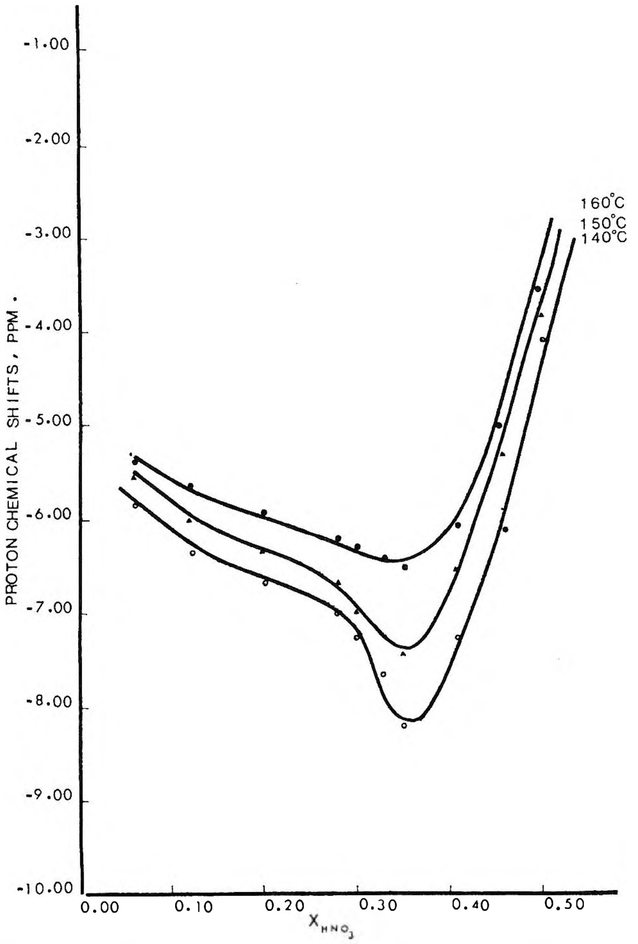

Figure 4. Chemical shift (τ scale, corrected) of the proton in solutions of HNO_3 in $LiNO_3$-KNO_3-$NaNO_3$ as a function of X_{HNO_3}.

only a single resonance line was observed. The results of the measurements of the chemical shift (τ scale) and relaxation times are given in Figure 4–6.

The salts were analytical reagents which had been carefully dried. The HNO_3 was freshly vacuum distilled for each experiment. By adding up to 1% H_2O it was shown that small traces of water produced no visible effect. Further details of these and other experiments may be found in the dissertation.

Discussion

Examination of the main experimental results shows that most of the properties undergo substantial changes in the region $X = 0.3$–0.4. (In addition, some further changes occur in the temperature range 155–165°.) In particular, the viscosity varies dramatically with composition and temperature, passing through a sharp maximum between $X = 0.3$ and 0.35. Experience with the viscosities of alkali halides and alkali nitrate melts[9] has generally shown that the viscosity follows a more or less linear course with mole fraction, the deviations from linearity being of the order of 10%. Here the viscosity approximately doubles over a short composition range and then returns nearly to its previous value. It appears that an important change in the structure of the liquid takes place in this region. There is a distinct deviation of the molal volume from linearity in this region, although the accuracy of the density data does not warrant numerical calculation of the partial molal volumes. Any proposed structure also must take into account the somewhat increased ionic mobilities indicated by the maximum in the electrical equivalent conductivity which is reached at a slightly lower value of X. The large increase in viscosity presumably signals the formation of more extended aggregates such as would be formed if the proton served as a bridge between nitrate groups; that is, if hydrogen bonds are formed between oxygen atoms on adjacent anions, the viscosity would be expected to rise because of the increase in average ionic size. As the concentration of nitric acid rises, the possibility of a still more extended network must be entertained. In

---

(9) J. P. Frame, E. Rhodes, and A. R. Ubbelohde, *Trans. Faraday Soc.*, 55, 2039 (1959).

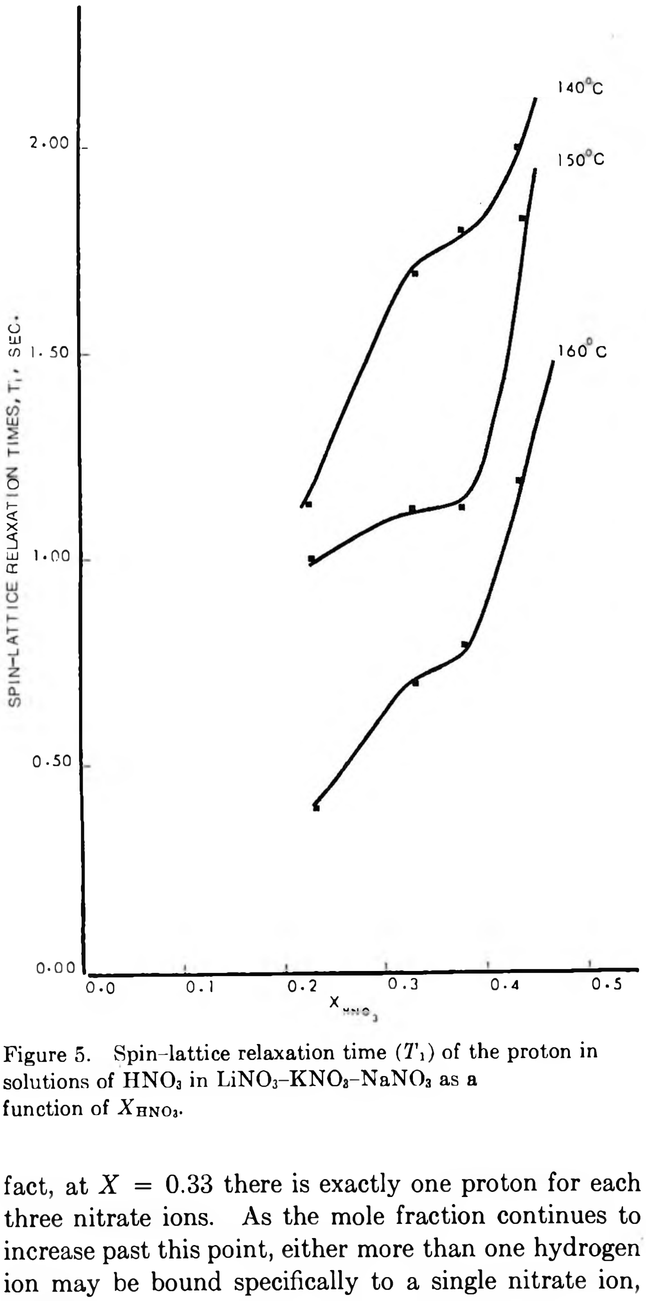

Figure 5. Spin-lattice relaxation time (T_1) of the proton in solutions of HNO_3 in $LiNO_3$-KNO_3-$NaNO_3$ as a function of X_{HNO_3}.

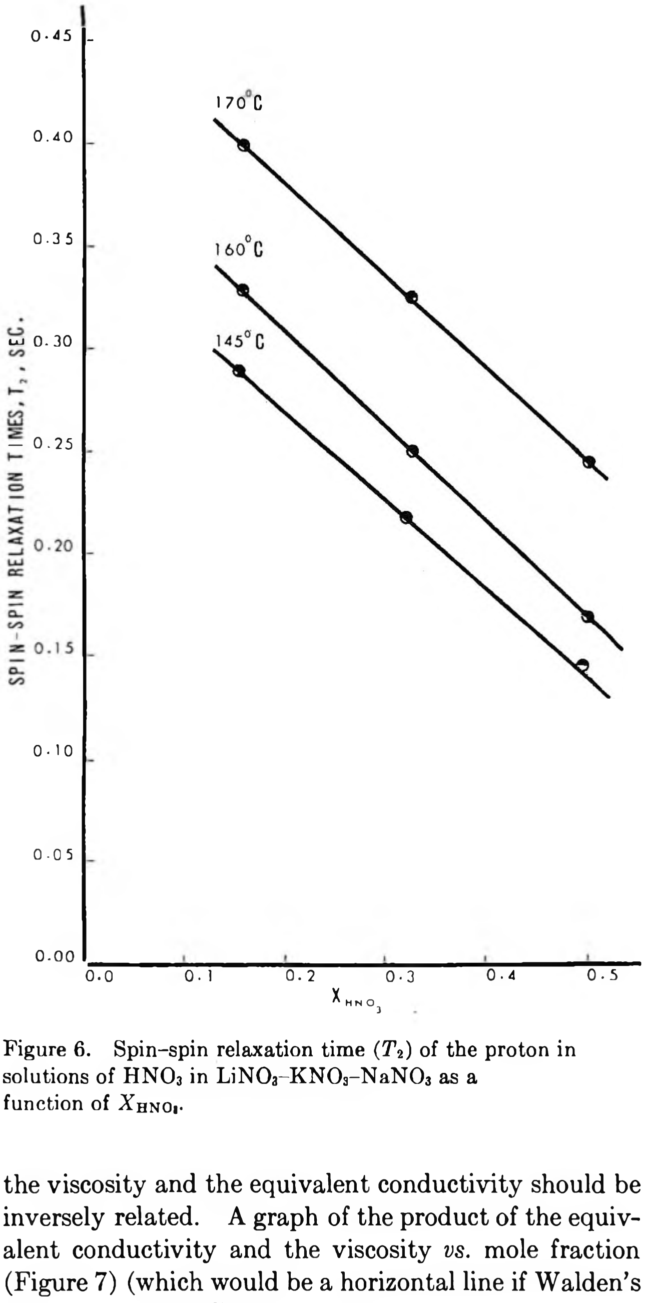

Figure 6. Spin-spin relaxation time (T_2) of the proton in solutions of HNO_3 in $LiNO_3$-KNO_3-$NaNO_3$ as a function of X_{HNO_3}.

fact, at $X = 0.33$ there is exactly one proton for each three nitrate ions. As the mole fraction continues to increase past this point, either more than one hydrogen ion may be bound specifically to a single nitrate ion, breaking up the network, or else multiple bridging may take place so that a single nitrate ion forms several hydrogen bonds simultaneously. The fall-off in the viscosity shows that multiple bridging does not occur, but rather that the structure becomes relatively less extended.

The mobility of an ionic species can be viewed as the reciprocal of the frictional retarding force it experiences when moving through the liquid. In dilute solutions it is fruitful to measure the frictional forces in terms of the bulk viscosity (and ionic radii). This view leads to Walden's rule which predicts that the product of the equivalent conductance of an ion and the viscosity will be a constant (which is proportional to the reciprocal of the ionic radius). Passing over the further complications related to transference numbers, etc., we are still led in the present case to the expectation that the viscosity and the equivalent conductivity should be inversely related. A graph of the product of the equivalent conductivity and the viscosity *vs.* mole fraction (Figure 7) (which would be a horizontal line if Walden's rule were followed) reveals a striking absence of correlation.

Since the variation in electrical conductivity with composition is not explicable in terms of the changing viscosity, it must be due to changes in the structure of the liquid, to changes in the size of the conducting species, to changes in the mode of conduction, or to some combination of these.

The maximum in the equivalent conductivity–viscosity product near the critical composition indicates that the extended structure postulated above offers an unusually high mobility for the hydrogen ions. There immediately springs to mind the possibility that bridge structures involving protons may facilitate a cooperative transfer of protons in the spirit of the well-known Grotthus model used to explain the high mobility of hydrogen ions in solvents like water. This situation is not

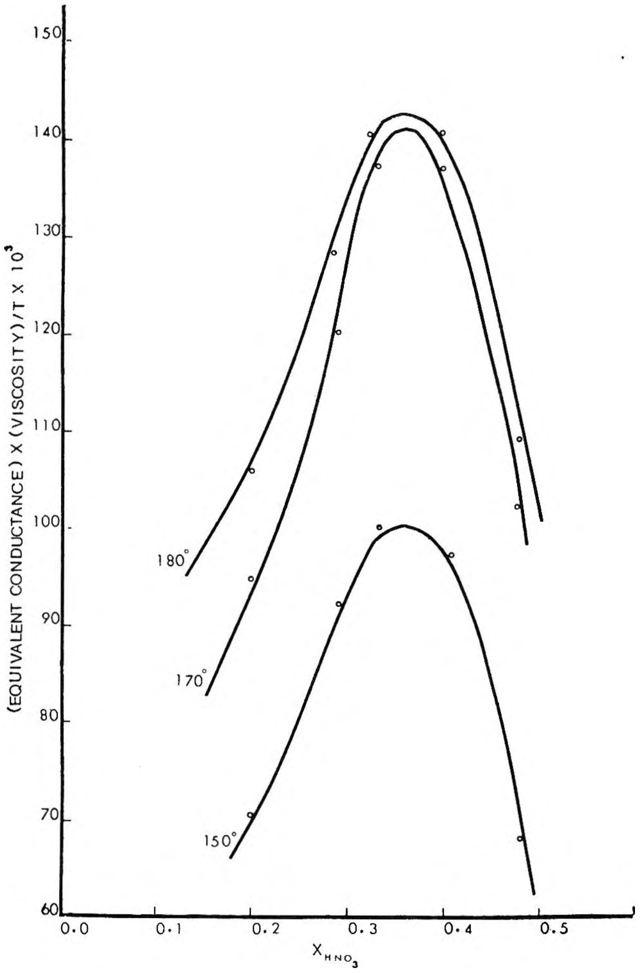

Figure 7. "Walden product" for solutions of HNO_3 in $LiNO_3$-KNO_3-$NaNO_3$ as a function of X_{HNO_3}.

strictly analogous, but one can readily imagine a number of ways in which the protons can be passed along, *e.g.*, by a concerted rotation of the nitrate ions or by transfer of the bridge to another adjacent pair.

The spin resonance results confirm this general picture. The system is presumably at all times in a state of rapid exchange since only one proton resonance line is ever observed. The sharp minimum in the chemical shift indicates the occurrence of a highly deshielded proton just at the concentration where the viscosity peaks sharply. If, in fact, more than one species is present at this composition, the deshielding is even greater. The value observed at the minimum is approximately 13.2 ppm less than liquid H_2O at 0° and 6 ppm less than liquid HNO_3 at 25°; therefore, it must represent a quite unusual degree of deshielding.

The fact that the equivalent electrical conductivity near $X = 0$ rises sharply with increasing X means the proton in this region is involved in an ionic structure. (Conductivity in the high X region, where the principal species is HNO_3, falls off to much lower values.) The chemical shift extrapolated to $X = 0$ is -5.0 (τ scale) and is more or less independent of temperature, whereas the chemical shift seen for high values of X at high temperatures (present work) extrapolates to values near $+2$ (τ scale). (At 27° the corresponding solution has a shift of -2.5) The decrease in the negative shift at higher temperatures presumably reflects a decrease in hydrogen bonding associated with increasing rotation in the liquid.

Thus it appears that the proton in these solutions occurs in (at least) three different states characterized, respectively, by chemical shifts of about -8.5, -5.0 and $+2.0$. The highest algebraic value clearly belongs to the undissociated nitric acid molecule. Nmr studies in the high X, low temperature region,[5] ir measurements on the pure acid and the very low equivalent conductivity support this conclusion. We are then left with the problem of identifying the species associated with the two most negative τ values.

A series of solid compounds with the general formula *trans* $(MA_4X_2{}^+NO_3{}^-)\cdot HNO_3$, where M = Co or Rh, A = pyridyl or bipyridyl, and X = Cl or Br, have been described[10] as containing the hydrogen dinitrate ion (O_2N-O-H-O-NO_2). Furthermore, one member of this series has been subjected to an X-ray analysis[11] and the presence of the hydrogen dinitrate ion confirmed directly. The X-ray and infrared data are taken to indicate that the hydrogen ion is in a "pseudo-tetrahedral environment." Compounds of the type $(R_4M^+NO_3{}^-)\cdot HNO_3$, where R = phenyl, benzyl or methyl, and M = P or As, have been assumed to contain a symmetrical hydrogen dinitrate ion.[12] This study also reports nmr spectra on tetraphenylarsonium hydrogen dinitrate dissolved in CH_3CN and in CH_3NO_2. The acidic proton displays a chemical shift varying between -6.6 and -7.05 (τ scale). An X-ray analysis of the same compound[13] shows that there are "short" hydrogen bonds. X-ray analysis[14] of crystals of $NH_4NO_3\cdot 2HNO_3$ reveals a dihydrogen trinitrate ion. The bond lengths and bond angles are similar to those later found in the hydrogen dinitrate ion.[13]

Therefore, we conclude that a "short bond" hydrogen dinitrate ion is a plausible species to postulate in the fused salt system. The most negative chemical shift (-7.05) reported in the solids described above falls midway between the two ranges of values found in the fused salt system (-8.5 and -5.0). Direct comparison is not easy in view of the differences in solvent and temperature and partly because it is not clear whether the reported values include diamagnetic corrections. However, it is reasonable to assume that the molten salt system will be, on the average, less accurately maintained in a given structure so that we tend to feel that the −7.05 value found for the hydrogen dinitrate should be thought of as corresponding to the −5.0 for the molten salt system. (We must note, however, that the nmr studies on the tetraphenylarsonium salt are done on a solution and the X-ray studies on a crystal so that the structures may be slightly different.) The substantial deshielding of the proton is then taken to result from its bridging between two oxygen atoms on adjacent nitrate ions.

---

[10] R. D. Gillard and R. Ugo, *J. Chem. Soc.* (*A*), 549 (1966).

[11] G. C. Dobinson, R. Mason, and D. R. Russell, *Chem. Commun.*, 62 (1967).

[12] B. D. Faithful, R. D. Gillard, D. G. Tuck, and R. Ugo, *J. Chem. Soc.* (*A*), 1185 (1966).

[13] B. D. Faithful and J. C. Wallwork, *Chem. Commun.*, 1211 (1967).

[14] J. R. C. Duke and F. J. Llewellyn, *Acta Cryst.*, **3**, 305 (1950).

We turn now to the third species whose τ value is approximately 3.5 ppm more negative than the one just attributed to the hydrogen dinitrate ion. This species becomes prominent at nearly the same composition as the maximum in the viscosity and a rapid change in the electrical conductivity. The simultaneous requirements for a more extended structure and a more negative chemical shift cannot be met by extending linear polymers of HNO_3 through the liquid, since it is reasonable to expect that a proton on a nitrate which is simultaneously bonded to two protons will not be less shielded than one which is bound to a nitrate which is not bound to another proton. Thus the dihydrogen trinitrate ion is not expected to lead to further deshielding of the proton.

In order to account for the large downfield shift, it seems necessary to postulate that the proton comes under the influence of a third center in addition to two nitrate groups. We imagine this third center to be either another nitrate group or, alternatively, one of the alkali metal ions. It is possible to rule out the cations by consideration of the spin–lattice relaxation times. Since the cationic mixture contains a substantial fraction of ions with nuclear spins (Li^7, Na^{23}), it would be expected that the close association of the cation with the proton would introduce dipole–dipole coupling as an important mode of relaxation. In the region where the greatest downfield shift occurs the spin–lattice relaxation time shows no sudden change.

The fact that the spin–lattice relaxation times, T_1, and the spin–spin relaxation times, T_2, differ from each other probably reflects a proton exchange phenomenon. The quantity $1/T^* = 1/T_2 - 1/T_1$ is shown in Figure 8. It appears that $1/T^*$, which represents the contribution to relaxation from the exchange process, is near zero for low values of X and rises more or less linearly with X. It does not in fact show any unusual changes in the vicinity of the maximum in the viscosity. If the exchange process in question is simply the dipolar interaction of protons with each other, then the dependence upon X is readily understood. The lack of dependence on viscosity may simply indicate that the diffusion coefficient of the hydrogen ions does not decrease when the viscosity increases.

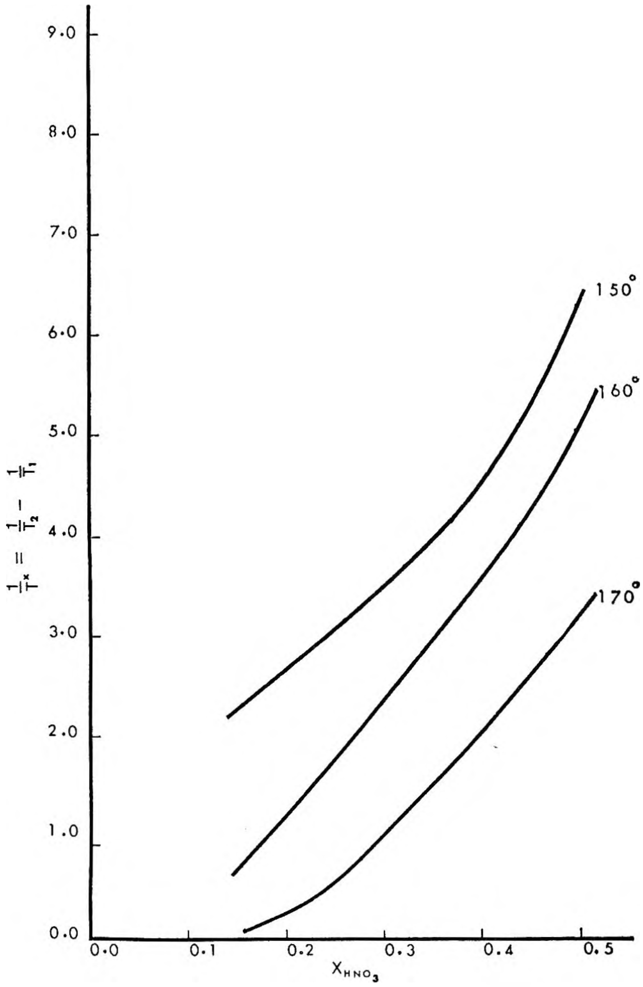

Figure 8. $1/T^*$ for the the proton in solutions of HNO_3 in $LiNO_3$–KNO_3–$NaNO_3$.

Since the behavior of the relaxation times seems to rule out alkali-metal ions as the postulated third center, we conclude that in the region near $X = 0.33$ the proton comes under the influence of three or more oxygen atoms simultaneously. Further support for this view is afforded by the fact that the maximum downfield shift is found in just the composition region where there are three nitrate groups to each proton. Some indication of the possible occurrence of such a more-than-two coordinated structure is found in the X-ray studies of nitrate salts of large cations. A "pseudo-tetrahedral" structure is postulated in one set of compounds.[11] The configuration found in another set[13] is readily converted to a more-or-less tetrahedral one if the nitrate ions are permitted to rotate more freely in the liquid than in the solid state.

There are two general kinds of arrangements to be considered. In one, three or more nitrate groups are involved. In the other, two oxygen atoms from one nitrate ion share the proton with one or more oyxgen atoms on another nitrate ion. In both cases, there are more than two oxygen atoms coordinating with the proton and producing an unusual degree of deshielding.

If the assignments to the −5.0 and −8.5 chemical shifts had been reversed, it would then have been necessary to find a species more shielded than the hydrogen dinitrate ion with a high electrical conductivity and low viscosity. Although the assignments chosen here are necessarily quite tentative, it seems to be reasonable and self-consistent to identify the species in dilute solution as hydrogen dinitrate, as undissociated nitric acid in concentrated solution, and as a structure with a more-than-two coordinated proton near $X = 0.33$.

Finally, we may note the analogy between these solutions and those of metals in liquid ammonia, allowing for the charge reversal, *i.e.*, the nitrate ion is equivalent to the ammonia molecule and the proton to the electron. Given the mass difference, it is not likely that a proton can be "smeared out" as is the electron. Perhaps the proton is primarily coordinated to some pair of oxygen atoms at any given time and experiences secondary effects from the others. Nevertheless, the analogy is striking and may be used to rationalize the experimental results reported here. Further experiments to try to confirm the structure postulated here are being planned.

Acknowledgment. It is a pleasure to acknowledge assistance to this work from the Office of Naval Research, Contract Nonr 285-37.

Ion-Molecule Reactions in Propene

by A. MacKenzie Peers

Laboratoire Curie, Institut de Physique Nucléaire, Paris 5, France *(Received April 4, 1969)*

Recent studies of ion-molecule reactions in propene, using tandem and single-stage mass spectrometers, are compared and some additional information is obtained from the combined results. Ion-molecule complex structure, charge transfer, and the measurement of disappearance cross sections are discussed.

A recent study by Abramson and Futrell[1] of ionic reactions in propene, using single-stage and tandem mass spectrometers, provides some interesting comparisons with published[2] and unpublished results from this laboratory. In addition, the tandem results may be combined with those from our single-stage instrument to provide some additional information.

In general, the tandem measurements do not upset the parent ion assignments which we had made,[2] but they do bring to light a number of reactions which could not be detected with the more simple instrument. (Some of these reactions, incidentally, were predicted on the basis of analogy with observed processes.[2]) In particular, the absence of $C_6H_7^+$ from the reaction products of $C_3H_5^+$ supports our preference for the alternative precursor, $C_3H_4^+$. The formation of $C_6H_7^+$ from $C_3H_5^+$ had been proposed by Harrison[3] and Fuchs[4] and, more recently, by Aquilanti, *et al.*[5] It might be mentioned here that the conclusions of Aquilanti[5] regarding the reactions of $C_3H_4^+$ and $C_2H_3^+$ are in striking disagreement with those of other workers.[1-3]

Both laboratories have proposed structures for the intermediate ion-molecule complex, $C_6H_{12}^+$. From the isotopic composition of $C_6H_9^+$ (X = H or D) formed by reaction of $C_3H_6^+$ with C_3D_6, Abramson and Futrell[1] suggested that the complex has the structure

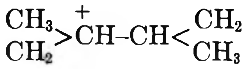

$$\begin{matrix}CH_3\\CH_2\end{matrix}\!>\overset{+}{C}H\text{-}CH<\begin{matrix}CH_2\\CH_3\end{matrix}$$

I

but later[6] concluded in favor of a linear hexene ion form on the basis of the similarity of the fragmentation pattern of 3-hexene to the distribution of reaction products of the $C_3H_6^+ + C_3H_6$ reaction. We have also concluded[2] in favor of a linear arrangement, specifically

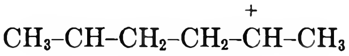

$$CH_3\text{-}CH\text{-}CH_2\text{-}CH_2\text{-}\overset{+}{C}H\text{-}CH_3$$

II

but on rather different grounds. Briefly, the reasons were as follows: (i) whatever structure is taken for the complex, one may assume that fragmentation products which involve only the breaking of a C-C

---

(1) F. P. Abramson and J. H. Futrell, *J. Phys. Chem.*, **73**, 1994 (1968).

(2) A. M. Peers and P. Vigny, *J. Chim. Phys.*, **65**, 805 (1968).

(3) A. G. Harrison, *Can. J. Chem.*, **41**, 236 (1963).

(4) R. Fuchs, *Z. Naturforsch.*, **A16**, 1026 (1961).

(5) V. Aquilanti, A. Galli, A. Giardini-Guidoni, and G. G. Volpi, *Trans. Faraday Soc.*, **64**, 124 (1968).

(6) F. P. Abramson and J. H. Futrell, *J. Phys. Chem.*, **72**, 1826 (1968).

bond are more probable than those requiring a preliminary net transfer of hydrogen to one side or the other of the C–C bond to be broken (net transfer must not be confused with exchange, which may or may not be rapid compared to bond rupture); (ii) we have shown experimentally[2] for six primary ions, $C_3H_n^+$ (n = 1–6), that the most probable reaction is addition of CH_2 to the ion. In view of (i), (ii) is most easily understood if the ion adds to the terminal carbon of the molecule as in structure II. The above reasons also lead us to prefer (II) to the structure $CH_3{-}CH_2{-}\dot{C}H{-}\overset{+}{C}H{-}CH_2{-}CH_3$ proposed by Abramson and Futrell.[6]

With regard to the observation of "stable" complexes in propene, we have reported[2] $C_6H_{11}^+$ and $C_6H_{12}^+$, whereas Abramson and Futrell remark that only $C_3H_7^+$ gave stable intermediates with the olefin systems investigated. This would appear to be a question of sensitivity, not a fundamental disagreement. Table III of Abramson and Futrell shows, incidentally, that the complexes $C_6H_9^+$ from $C_3H_3^+ + C_3H_6$ and $C_5D_4H_6^+$ from $C_3H_6^+ + C_2D_4$ were also observed, although this would appear to be in contradiction with the text.

Recent modifications to the ion source of our single-stage spectrometer now permit the measurement of absolute cross sections for the formation and disappearance of ions. The field in the ion chamber is presumably known and nearly constant, the ion path length is 4.7 mm, a McLeod gauge is directly connected to the ion chamber, and strong differential pumping is employed. Table I compares some formation cross sections recently obtained with relative cross sections measured by Abramson and Futrell with the tandem instrument.[1] The average ion kinetic energy in our work (exit energy = 0.88 eV) was fairly close to that employed with the tandem machine (0.3 eV) and the agreement is excellent. The sum of 100 Å² is fortuitous. As shown by our earlier results[2] and by the tandem measurements of Abramson and Futrell,[1] the product ions in Table I account for at least 99% of the reactive collisions of $C_3H_6^+$. The only processes of appreciable importance missing from Table I are thus charge transfer and simple scattering of the incident $C_3H_6^+$. The cross sections for these two processes, however, can be estimated by combining our results with the tandem measurements for $C_3H_6^+$ and the target gas C_3D_6. These measurements showed[1] that charge transfer plus the formation of $C_3H_7^+$ accounts for 50% of all the processes involving $C_3H_6^+$, excluding simple scattering. Since $\sigma^f(C_3H_7^+)$ = 26 Å² (Table I), a simple calculation gives a cross section for charge transfer of 48 Å². With this result and the help of two simple assumptions, we are now in the rare situation where a low-energy ion–molecule collision cross section may be estimated from a complete sum of the cross sections of the outgoing channels. The first assumption is that charge transfer cannot take place when the centers of mass of ion and molecule are further apart than the radius of the circular orbit[7] for the charge-induced dipole interaction. (Charge transfer is thus obliged to compete with the processes requiring intimate collision.) The second assumption is that, in the symmetric resonant case, charge transfer occurs with a probability of one-half at each nonreactive collision.[8a,9] Thus the collision cross section is found to be 100 + 48 + 48 = 196 Å². This value, however, is so much greater than the theoretical result (125 Å²), based on the charge-induced dipole interaction, that it would seem that at least one of the two assumptions is mistaken. If the collision cross section is, in fact, less than 196 Å², we may estimate the distance, d (between centers of mass), for which electron transfer must be possible. For this purpose, we assume[8a,b] that the probability of charge transfer over a distance, x, is given by a step function such that the probability is one-half for all $x < d$, except when a reactive collision intervenes, and zero for all $x > d$. In terms of the impact parameter, b, we thus have $\pi b^2 = 100 + 2(48) = 196$ Å². For this value of b, the system cannot overcome the rotational barrier and the particles will separate after reaching a distance of closest approach, which is also the maximum distance d, over which charge transfer occurs. For the charge-induced dipole potential and a noncollision trajectory, the distance of closest approach is related to the impact parameter by $\pi b^2 = \pi d^2(1 + e^2\alpha/2d^4E)$, where e is the charge of the electron, α is the polarizability of the molecule, and E is the initial barycentric kinetic energy.[10] With $\pi b^2 = 196$ Å² and an average laboratory energy of (0.88/4) eV, the above equation gives d = 7.45 Å for the $C_3H_6^+/C_3H_6$ system. Subtracting the "hard-sphere" collision diameter for propene (4.68 Å), obtained from viscosity data with the help of the

Table I

Reaction	Abramsom and Futrell (%)	This work $10^{16}\,\sigma^f$ (cm^2)
$C_3H_6^+ + C_3H_6 \rightarrow C_3H_7^+$	27	26
$\rightarrow C_4H_7^+$	18	19
$\rightarrow C_4H_8^+$	34	33
$\rightarrow C_6H_9^+$	21	22
Total	100%	100 Å²

---

[7] G. Gioumousis and D. P. Stevenson, *J. Chem. Phys.*, 29, 294 (1958).

[8a] D. Rapp and W. E. Francis, *ibid.*, 37, 2631 (1962); (b) F. A. Wolf and B. R. Turner, *ibid.*, 48, 4226 (1968).

[9] This second assumption has recently received some experimental support from ion cyclotron resonance measurements by Bowers, *et al.* [M. T. Bowers, D. D. Elleman, and J. L. Beauchamp, *J. Phys. Chem.*, 72, 3599 (1968)]. *I.e.*, taking the probability of charge exchange to be one-half, these authors find that the collision rate for $C_2H_4^+$ in C_2D_4 is independent of ion kinetic energy, in agreement with the prediction of the charge-induced dipole model.[7] The prediction may not be entirely reliable, however, since the ion kinetic energies involved would appear to exceed those for which the model is applicable.[10]

[10] A. M. Peers, *Int. J. Mass Spectrom. Ion Phys.* (in press).

Lennard-Jones 6–12 potential,[11] the foregoing distance corresponds to an ion–molecule separation of ~2.8 Å for the electron jump. Since the step function is a fairly crude simplification and the Lennard-Jones diameter is probably too large when one of the molecules is ionized, 2.8 Å may be taken to be a lower limit. We attach a certain credence to these estimates, since our present ion source gives disappearance cross sections for $CH_4^+ + CH_4$ which are in very good agreement with the accepted rate constant, confirmed by many workers.[12–15] Although the importance of charge transfer has been demonstrated[1] in the case of $C_3H_6^+$, disappearance cross sections larger than the presumed collision cross section may not always be associated with resonant charge transfer. As possible examples, we have included in Table II the disappearance cross sections of C^+, C_2^+, C_2H^+, C_3^+, and C_3H^+, all of which exceed the theoretical collision cross sections by amounts greater than the expected experimental error. From the ionization potentials of the radicals,[16] charge transfer with C_3H_6 can be expected to be exothermic for all of these ions. Of course, it may be supposed that accidental resonance is readily achieved for polyatomic systems,[9] but it should be borne in mind that known, thermal energy, exothermic, fast charge transfer cross sections would appear to be often as large as but seldom, if ever, greater than the charge-induced dipole collision cross sections.[17] This would suggest that a strongly coupled intermediate complex is usually necessary for asymmetric charge transfer, or that the maximum separation at which electron tunneling can occur is, fortuitously, nearly always sufficiently small compared with the collision cross sections at these low relative velocities. In Table II, the only ion for which the experimental recombination energy[18] shows accidental resonance to be likely is $C_2H_4^+$ and it can be seen that very good agreement with the collision cross section is obtained. Abramson and Futrell, on the other hand, show that charge transfer accounts for about 95% of the disappearance of $C_2H_4^+$ in butene,[1] but the disappearance cross section, according to their measurements, appears to exceed the collision cross section by a factor of 3. More work in this area would seem to be required.

Table II

		$10^{16}\ \sigma^d$ (cm²), (exit energy = 0.88 eV)		
Ion	*m/e*	Abramson and Futrell[a]	This work	Theor. collision cross section[b]
C^+	12	. . .	139	101
C_2^+	24	. . .	154	111
C_2H^+	25	. . .	139	112
$C_2H_2^+$	26	. . .	113	113
$C_2H_3^+$	27	90	84	114
$C_2H_4^+$	28	. . .	114	115
C_3^+	36	. . .	180	121
C_3H^+	37	. . .	153	122
$C_3H_2^+$	38	. . .	133	122
$C_3H_3^+$	39	. . .	29(?)	123
$C_3H_4^+$	40	>280	105	124
$C_3H_5^+$	41	47	53	124
$C_3H_6^+$	42	56(?), 102[c]	97	125

[a] Corrected from an ion exit energy of 3.1 eV. [b] Charge-induced dipole collision cross section.[7] [c] See text.

Although single-stage, "high-pressure" instruments were used in both studies,[1,2] comparison of the disappearance cross sections is not straightforward, since the ion exit energies were not the same (0.88 and 3.1 eV). For Table II, however, we make the usual assumption that the cross sections vary inversely with the square root of the ion kinetic energy[7] (although this is only approximately so for many organic systems[19]) and the results of Abramson and Futrell are given for an exit energy of 0.88 eV. The agreement is quite good for $C_2H_3^+$ and $C_3H_5^+$, but very bad for $C_3H_4^+$. Our own figures agree quite well with earlier measurements made with a different ion source[20] and do not exceed the charge-induced dipole collision cross section calculated for these experimental conditions. As mentioned above, Abramson and Futrell do suggest that disappearance cross sections larger than collision cross sections may be accounted for by charge transfer (as we have also supposed elsewhere[20] for $C_4H_2^+$), but this does not take care of the large discrepancy between the two measurements for $C_3H_5^+$. With regard to $C_3H_6^+$, the disagreement is within the range of uncertainty of the kinetic energy correction,[19] but the disappearance cross section of Abramson and Futrell would appear to be unreliable, since the data of Figure 2 in ref 1 do not fall too well on a straight line. In these circumstances, one may estimate the disappearance cross section of $C_3H_6^+(42^+)$ from the formation cross section of a secondary ion whose contribution to the disappear-

---

(11) R. C. Reid and T. K. Sherwood, "The Properties of Gases and Liquids," McGraw-Hill Book Co., Inc., New York, N. Y., 1966, Appendix G.

(12) V. L. Talroze and E. L. Frankevich, *Zh. Fiz. Khim.*, **34**, 2709 (1960).

(13) C. W. Hand and H. von Weyssenhoff, *Can. J. Chem.*, **42**, 195 (1964).

(14) K. Birkinshaw, A. J. Masson, D. Hyatt, L. Matus, I. Opauszky, and M. Henchman, *Advan. Mass Spectrom.*, **4**, 379 (1968).

(15) S. K. Gupta, E. G. Jones, A. G. Harrison, and J. J. Myher, *Can. J. Chem.*, **45**, 3107 (1968).

(16) V. I. Vedeneyev, L. V. Gurvich, V. N. Kondrat'yev, V. A. Medvedev, and Ye. L. Frankevich, 'Bond Energies, Ionization Potentials and Electron Affinities," Edward Arnold, London, 1966.

(17) E. E. Ferguson, *Advan. Electron. and Electron Phys.*, **24**, 1 (1968).

(18) E. Lindholm, Advances in Chemistry Series, No. 58, American Chemical Society, Washington, D. C., 1966, p 1.

(19) J. H. Futrell and F. P. Abramson, Advances in Chemistry Series, No. 58, American Chemical Society, Washington, D. C., 1966, p 107.

(20) A. MacKenzie Peers and P. Vigny, *Int. J. Radiat. Phys. Chem.*, **1**, 99 (1969).

ance cross section is known. For $C_4H_8^+(56^+)$, the limiting slope of $I(56^+)/I(42^+)$, using the data of Figure 1 in ref 1, gives a formation cross section of 18.5 A^2 for 56^+. Since the tandem measurements[1] have shown $C_4H_8^+$ to account for 34% of the disappearance of $C_3H_6^+$, one obtains for the latter 18.5/0.34 = 54.5 Å^2. The inverse square root correction for kinetic energy then gives 102 Å^2, in good agreement with our own result. It should be noted that our measurements were carried out at much lower pressures (0.1 to 10 μ) than those of Abramson and Futrell and that changes of slope of the semilog plots of ionic intensity *vs.* pressure were not observed. Abramson and Futrell have found, however (ref 1, Figure 3), that the curves for $C_3H_5^+$ and $C_3H_6^+$ exhibit changes of slope when the intensities have fallen to about 20% of their initial values. It is common practice in high-pressure mass spectrometry to calculate disappearance cross sections from the slope of the linear segment at the lower pressures, but such a procedure is not always justified. Only cross sections obtained from data showing a single slope over a very large drop in ionic intensity can be taken as certain, unless the reason for the change of slope is known and an appropriate correction applied when necessary. For example, when the intensity is given by the sum of two exponentially decreasing terms, the larger of the two exponential coefficients cannot be obtained from the slope at lower pressures without correction for the effect of the more slowly varying term. The two terms may evidently represent two distinct species with the same mass/charge ratio (*e.g.*, structural isomers) but may also represent a special case of the ionic intensity being partly of secondary origin. When part of the intensity of P_1^+ is due to the reaction $P_2^+ + M \rightarrow P_1^+ + F$, we may write[20]

$$I_1 = I_1^0 \exp-(\sigma_1^dNx) + \frac{I_2^0\sigma_2^1}{\sigma_1^d - \sigma_2^d}[\exp-(\sigma_2^dNx) - \exp-(\sigma_1^dNx)]$$

where I_n^0 is the rate of formation of P_n^+ at $x = 0$, σ_n^d is the disappearance cross section of P_n^+, N is the gas concentration, x is the length of the ion trajectory in the source, and σ_2^1 is the cross section of the reaction written above. The foregoing expression may be rearranged to

$$I_1 = (I_1^0 - I_2^0\sigma_2^1/\Delta)\exp-(\sigma_1^dNx) + (I_2^0\sigma_2^1/\Delta)\exp-(\sigma_2^dNx)$$

where $\Delta = \sigma_1^d - \sigma_2^d$. When Δ is positive and $I_1^\circ > I_2^0\sigma_2^1/\Delta$, the rearranged equation shows that a semilog plot will have two linear sections, the slope at higher pressures being proportional to σ_2^d. In the case of $C_3H_5^+$ in particular, the tandem measurements[1] have shown it to be produced in part by the reaction of $C_3H_3^+$ with C_3H_6. Assuming, therefore, that the second slope for $C_3H_5^+$ (ref 1, Figure 3) is equal to $-\sigma_{39}^dx$, one obtains $\sigma_{39}^d \simeq 14$ Å^2. When corrected to an exit energy of 0.88 eV, this gives 27 Å^2, in agreement with our result (Table II). The disappearance cross section of $C_3H_5^+$, on the other hand, according to this interpretation, can be obtained by extrapolating the second linear section to zero pressure and subtracting the extrapolated curve from the total intensity. The slope of the curve thus obtained from the data of Abramson and Futrell gives about 79 Å^2 for σ_{41}^d, which is not an unreasonable value.[20] Unfortunately, the results of Abramson and Futrell also suggest (Figure 1) that σ_{39}^d is approximately zero in the pressure range where the second linear segment for $C_3H_5^+$ is observed. In addition, our own low-pressure value of σ_{39}^d is rather uncertain, since it may be necessary (as the preceding remark indicates) to correct the observed intensity by subtracting a fixed current, due to the presence of a stable form of $C_3H_3^+$.[20] Until the reasons for the changes of slope can be ascertained, the cross sections for 39^+, 41^+, and 42^+ must be considered to be doubtful, although we are inclined to accept our result for σ_{42}^d, since it agrees with the sum of the formation cross sections in Table I.

Nitrogen-14 Nuclear Magnetic Resonance Determination of the Quadrupole Coupling Constants of Methyl Isocyanide and Ethyl Isocyanide

by **William B. Moniz and C. F. Poranski, Jr.**

Naval Research Laboratory, Washington, D. C. 20390 *(Received April 7, 1969)*

Nitrogen-14 nmr line width data for liquid MeNC and EtNC are indicative of nitrogen quadrupole coupling constants of 0.27 and 0.30 MHz, respectively. The substantial difference from the previously reported microwave value of 0.483 MHz for MeNC in the gas phase is considered to be real and to reflect alterations in electron distribution associated with the condensed phase.

The quadrupole coupling constant of methyl isocyanide is elusive. The upper limits of 1[1] and 0.5 MHz[2] were lowered to 0.3 MHz by the work of Loewenstein and Margalit.[3] Subsequently, Kemp, Pochan, and Flygare[4] reported a value of 0.483 ± 0.017 MHz. Loewenstein and Margalit based their calculation on the N^{14} nmr line width in liquid CH_3NC, while Kemp, Pochan, and Flygare observed microwave high-resolution nuclear quadrupole rotational transitions in the vapor state.

While a change in quadrupole coupling constant may well be expected in going from the vapor phase to the condensed phase, a decrease of 40% is unusual. Moreover, the issue is clouded somewhat by the agreement found between the microwave-determined coupling constant of Kemp, Pochan, and Flygare and the approximate coupling constant estimated by Gore and Gutowsky[5] from the liquid phase N^{14} T_1 data.

In the present study, we report N^{14} nmr line width studies for liquid MeNC and EtNC which are in support of coupling constants smaller than 0.5 MHz, and for MeNC, smaller than the 0.3 MHz upper limit of Loewenstein and Margalit.

Experimental Section

Samples. Ethyl isocyanide was prepared by the method of Jackson and McKusick.[6] The cut distilling at 77–78° (uncor) (lit. bp 79°) was used.

Two methyl isocyanide samples were employed for the nmr studies, one kindly supplied by Dr. L. Paolillo, the other prepared by a modification of the Jackson and McKusick[6] method in which four times the theoretical amount of MeI was added, with refluxing for 48 hr. Both samples were *ca.* 90% pure, MeCN and MeI being the major contaminants. The MeNC sample employed for viscosity measurements, prepared according to the procedure of Schuster, Scott, and Casanova,[7] was determined by nmr measurements to be *ca.* 98% pure.

Nmr Spectra. Initially, N^{14} spectra were obtained in the HR mode on a Varian HA-100 spectrometer operating at 7.22 MHz. Under these conditions, reproducible half-height line widths of 0.4 Hz were observed for MeNC. Subsequently, frequency sweep field-lock spectra were obtained with the isocyanide in the annulus of a spinning 5-mm o.d. Wilmad cell containing a concentric fixed capillary of tetranitromethane from which the locking signal was derived. Because the required offset frequencies exceeded the capabilities of the manual oscillator in the HA-100, a Hewlett-Packard 204B audio oscillator was substituted. The minimum reproducible half-height line width observed in the HA field-lock mode was 0.26 Hz; it is not known whether this value was limited by relaxation or by the field inhomogeneity.

Viscosity Measurements. The viscosity of MeNC was measured at 25° using a Cannon-Manning semimicroviscometer. The low viscosity of MeNC, 0.27 cP, resulted in a relatively short efflux time. However, comparison with a liquid of similar viscosity (acetone) showed the kinetic energy correction term to be negligible.

Results and Discussion

With knowledge of T_1, the spin-lattice relaxation time, and τ_q, the correlation time for quadrupolar relaxation, it is possible to directly extract the value of

---

(1) H. Ring, H. Edwards, M. Kessler, and W. Gordy, *Phys. Rev.*, **72**, 1262 (1947).

(2) M. Kessler, H. Ring, R. Trambarulo, and W. Gordy, *ibid.*, **79**, 54 (1950).

(3) A. Loewenstein and Y. Margalit, *J. Phys. Chem.*, **69**, 4152 (1965).

(4) M. K. Kemp, J. M. Pochan, and W. H. Flygare, *ibid.*, **71**, 765 (1967).

(5) E. Gore and H. S. Gutowsky, reported in ref 4.

(6) H. L. Jackson and B. C. McKusick, *Org. Syn.*, **35**, 62 (1955).

(7) R. E. Schuster, J. E. Scott, and J. Casanova, Jr., *ibid.*, **46**, 75 (1966).

the quadrupole coupling constant, e^2qQ/h, according to the expression[8]

$$1/T_1 = {}^3/_8(e^2qQ/\hbar)^2\tau_q \qquad (1)$$

An observed line width is a measure of T_2^*, the apparent spin–spin relaxation time. Contributions from inhomogeneity broadening lead to the inequality $T_2^* \leq T_2$. But inasmuch as $T_2 \leq T_1$ ($T_2 = T_1$ in the motional narrowing region), the substitution of T_2^* for T_1 in eq 1 can only result in an underestimate of T_1, and therefore, in an overestimate of e^2qQ/h.

Loewenstein and Margalit[3] and Gore and Gutowsky[4,5] made the reasonable assumption that the τ_q for MeNC is about the same as that for MeCN. Thus, knowing e^2qQ/h for acetonitrile, which is well established, and the N^{14} line width[3] or T_1[5] for acetonitrile, a value of τ_q was found using eq 1. This τ_q was then employed with the corresponding N^{14} data for MeNC to yield values for its quadrupole coupling constant.[9] As noted earlier, Loewenstein and Margalit obtained $e^2qQ/h < 0.3$ MHz, while the N^{14} T_1 data of Gore and Gutowsky[5] yielded $e^2qQ/h = 0.5$ MHz. It should be emphasized that there can be no question about the validity of the gas phase microwave value of 0.483 ± 0.017 MHz[4] inasmuch as no assumptions are involved in its determination.

The figure shows representative field-lock N^{14} spectra of neat samples of MeNC and EtNC. Resolution is sufficient to partially resolve the overlapping lines due to spin coupling to nitrogen of the CH_3– and –CH_2– protons in EtNC. Table I contains the parameters determined from numerous such spectra. Assuming a Lorentzian line shape,[10] the line width data of Table I were converted into T_2^* values of 1.2 sec for MeNC and 1.0 sec for EtNC.

Table I: N^{14} Nmr Parameters of MeNC and EtNC at 24° in the Neat Liquids

Compound	Line width at half-height, Hz[a]	Chemical shift, ppm[b]
MeNC	0.26 ± 0.02[c]	219.6 ± 0.1[c]
EtNC	0.31 ± 0.03	205.1 ± 0.1

[a] Based on 40 line width measurements for MeNC and 37 for EtNC. [b] Upfield from externally referenced nitromethane. [c] Standard deviation of the mean.

For comparative purposes we have calculated the e^2qQ/h of all three nmr studies using a common basis. Improvement can be made in the assumption that τ_q for MeNC is the same as that for MeCN by employing the Debye–BPP relationship[11] for rotational correlation time $\tau_c = 4\pi\eta a^3/3kT$. With knowledge of the viscosity, η, and the molecular radius, a (estimated from the molar volume), it was calculated that $(\tau_c)_{MeNC}/(\tau_c)_{MeCN} = 0.79$. In addition, the quadrupole coupling constant of acetonitrile in the solid phase (3.74 MHz)[12] was used rather than the gas phase value (4.21 MHz).[4] This is based on the observation that, in general, the N^{14} coupling constant of the solid is 10–15% less than that of the gas.[8] Presumably, the solid phase intermolecular interactions more closely resemble those of the liquid. The calculated values of e^2qQ/h are listed in Table II.

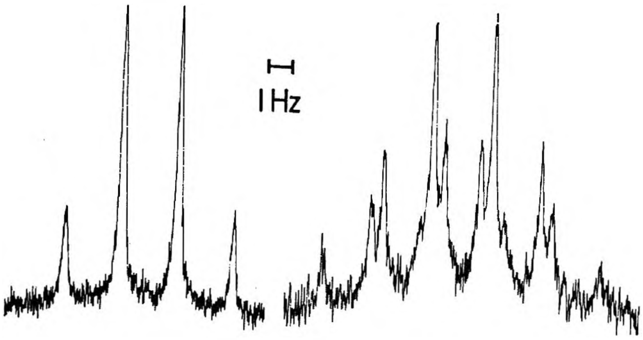

Figure 1. 7.22-MHz field-lock N^{14} nmr spectra of MeNC (left) and EtNC (right).

Table II: Relaxation Times and Quadrupole Coupling Constants in Liquid MeNC and EtNC

Compound	T_1, sec	T_2^*, sec	$e^2/qQ/h$, MHz[a]	Reference
MeNC	...	0.64	0.34	3
MeNC	0.35	...	0.46	4
MeNC	...	1.2	0.27	This study
EtNC	...	1.0	0.30	This study

[a] Calculated from eq 1 assuming $(T_1)_{MeCN} = 5$ msec, $(e^2qQ/h)_{MeCN} = 3.74$ MHz, and $(\tau_q)_{RNC} = 0.79(\tau_q)_{MeCN}$.

The difference between the quadrupole coupling constant calculated from T_1 data[5] and that calculated from our T_2^* data is well beyond the expected limits of error. Furthermore, by a method which does not involve correlation times or relaxation data, Yannoni[13] has determined a quadrupole coupling constant of 0.277

---

(8) W. B. Moniz and H. S. Gutowsky, *J. Chem. Phys.*, **38**, 1155 (1963).

(9) The alternative possibility is that the quadrupole coupling constant of MeNC in the gas and liquid phases is approximately the same and that the τ_q of MeNC is about one-third that of MeCN. As shown below, however, the Debye–BPP correlation times for MeNC and MeCN differ only by about 20%. While it is well known that the Debye-BPP relationship overestimates rotational correlation times by a factor of from five to ten, it seems improbable that the factors which apply to MeCN and MeNC would differ significantly in view of the similar size and shape of the two molecules.

(10) E. R. Andrew, "Nuclear Magnetic Resonance," Cambridge University Press, London, 1955, p 105.

(11) N. Bloembergen, E. M. Purcell, and R. V. Pound, *Phys. Rev.* **73**, 679 (1948).

(12) P. A. Casabella and P. J. Bray, *J. Chem. Phys.*, **29**, 1105 (1958).

(13) C. S. Yannoni, private communication.

MHz for MeNC aligned in the nematic phase. Inasmuch as the independent T_2^* measurements of Loewenstein and Margalit[3] also support our results, a remeasurement of the N^{14} T_1 of MeNC is desirable.[14] We conclude, therefore, that there is a real difference between the e^2qQ/h of MeNC in the gas phase (0.483 ± 0.017 MHz)[4] and that in the liquid phase (0.27 MHz).

In the case of EtNC, an upper limit to e^2qQ/h of 0.5 MHz has been determined from the gas phase microwave spectrum.[15] It would be premature to conclude that the liquid phase value of 0.30 MHz is significantly smaller than the gas phase value until higher resolution microwave data can be obtained.

As noted above, e^2qQ/h for nitrogen compounds generally is 10–15% less in the solid than in the gas. In the compounds in which this decrease is observed, the nitrogen atom has been subject to large electric field gradients, resulting in quadrupole coupling constants of the order of 4 MHz. It is entirely possible that the effect is not a relative one, but an absolute one. That is, e^2qQ/h may be reduced in magnitude by about 0.4–0.6 MHz in going from the gas phase to the condensed phase. In any case, the observed difference in the values of e^2qQ/h for MeNC in the liquid and gas phases may reflect alterations in the field gradient caused by interactions with neighboring molecules.

The dipole moment (μ) of MeCN in the gas phase (3.92 D)[16] is substantially larger than that of the liquid in benzene solution (3.47 D).[17] The observed decrease in the μ of MeCN in going from the gas to the condensed phase parallels the decrease in e^2qQ/h in going from the gas to the solid. It appears that a change in μ of comparable magnitude occurs in the case of MeNC. MeNC in the gas phase has a μ of 3.83 D.[16] While the μ of MeNC in the condensed phase has not been reported, that of EtNC in benzene is 3.47 D.[18] Thus, it seems reasonable that the change in electron distribution associated with the alteration of μ would be reflected in different nitrogen quadrupole coupling constants for gaseous and liquid MeNC. The lack of an observable N^{14} nmr resonance in solid MeNC[3] suggests that further changes in electron distribution occur upon solidification.

---

(14) H. S. Gutowsky, private communication.

(15) R. J. Anderson and W. D. Gwinn, *J. Chem. Phys.*, **49**, 3988 (1968).

(16) S. N. Ghosh, R. Trambarulo, and W. Gordy, *ibid.*, **21**, 308 (1953).

(17) J. W. Smith and L. B. Witten, *Trans. Faraday Soc.*, **47**, 1304 (1951).

(18) R. G. A. New and L. E. Sutton, *J. Chem. Soc.*, 1415 (1932).

Viscosity of a Vitreous Potassium Nitrate–Calcium Nitrate Mixture

by R. Weiler, S. Blaser, and P. B. Macedo

Vitreous State Laboratories, Catholic University of America, Washington, D. C. *(Received April 14, 1969)*

Viscosity measurements were made between 10^{-1} and 10^8 P over the temperature range from 79 to 200° in 60% KNO_3–40% $Ca(NO_3)_2$ (mole per cent). The data departed from the Fulcher equation as one lowered the temperature below 120°. The departure was similar to that observed in B_2O_3 and *n*-propyl alcohol, indicating that the viscosity tended to a low-temperature Arrhenius region. The existence of such an Arrhenius region in so many different types of liquids shows a major deficiency in the existing viscosity theories.

Introduction

Many of the viscosity equations can be approximated by the Fulcher[1] equation

$$\ln \eta = A + B/(T - T_0) \qquad (1)$$

in which η is the viscosity and A, B, and T are material constants. This expression predicts the temperature dependence of any structural relaxation time, be it involved in shear, volume, dielectric, or conductivity processes. Thus the original equation now has a much more general application in determining the structural kinetics of liquids.

Of the many viscosity models which predict this relationship there are three most prominent ones which will be reviewed here. Cohen and Turnbull[2] assumed that the limiting mechanism for an irreversible diffusional motion was the ability that the "lattice cell" would expand to permit molecules to "jump" over each other.

---

(1) G. S. Fulcher, *J. Amer. Ceram. Soc.*, **8**, 339 (1925).

(2) M. H. Cohen and D. Turnbull, *J. Chem. Phys.*, **31**, 1164 (1959).

They calculated the distribution of excess or free volume by maximizing the entropy of mixing. By a further assumption that there was a minimum volume below which no motion could occur, they calculated the temperature dependence of the viscosity (or any other structural relaxation time) to be

$$\ln \eta = A + B'/(V - V_0) \simeq A + B/(T - T_0) \quad (2)$$

where V is the actual volume and V_0 is the close-packed volume. The approximation used here is that the expansion coefficient, α, is temperature independent ($B = B'/\alpha$).

A second approach is due to Adam and Gibbs.[3] They proposed that in order to have viscous flow, a flow unit had to overcome a potential barrier. In addition, depending upon the configurational entropy, more than one flow unit might have to perform the "jump" at a time. This led to an equation of the form

$$\ln \eta = A + B''/[T(S - S_0)] \quad (3)$$

in which $(S - S_0)$ is the configurational entropy, S_c. This equation is equivalent to the Fulcher equation if one assumes that

$$S_c \simeq \Delta c_p(T - T_0)/T \quad (4)$$

where Δc_p is the relaxational part of the specific heat and $B = B''/\Delta c_p$. When Gibbs[4] proposed the approximation in equation (4), he implicitly expected a second order transition at T_0, and an infinite relaxation time at $T = T_0$ was identified with the presence of this second order transition.[5]

A third approach grew from the hybrid concept of Macedo and Litovitz.[6] There it was proposed that the "jump" probability was the product of the probability of obtaining sufficient energy to break the bonds and the probability of having the appropriate structural configuration which permitted such rearrangements. The ability to obtain such a structural rearrangement could be quantitatively expressed in terms of the excess entropy or free volume, giving an equation of the form

$$\ln \eta = A + H/RT + V/(V - V_0) \quad (5)$$

Angell[5] had also considered the relative roles of structural configuration and bond energy in terms of the Adam–Gibbs equation. He associated the parameter B'' (of eq 3) to relative bond strength and $(T - T_0)$ with the excess entropy.

The conclusion of all these approaches can best be seen from the shape of the curve on an Arrhenius plot ($\log \eta$ *vs.* $1/T$). It is expected that at equivalent viscosities, the weaker the intermolecular bonding, the higher will be the curvature. Also, as the temperature is made to approach the vicinity of T_g (*i.e.*, $(T - T_0)$ gets smaller), the curvature increases. This latter feature had not been observed in B_2O_3, where a second Arrhenius region was found at low temperatures, but since KNO_3–$Ca(NO_3)_2$ mixture has minimum bonding, it is expected to follow the Fulcher equation. In fact, Angell[7] has reported that the electrical conductivity of this mixture does follow the Fulcher equation over a limited temperature range. We therefore propose to test the validity of the Fulcher equation for this mixture over nine decades of viscosity.

Experimental Method

(*1*) *Sample Preparation.* The composition of the sample was 60% KNO_3 and 40% $Ca(NO_3)_2$ (mole per cent) and was prepared by a method similar to that of Ubbelohde.[8] The $Ca(NO_3)_2$ (certified reagent grade) was dried a minimum of 12 hr at approximately 230° before being placed in weighing bottles. The bottles were replaced in the oven for 2–4 hr to drive out the moisture contaminated during filling, then cooled in a desiccator under vacuum. The salt was weighed and the amount of KNO_3 necessary for the given composition was calculated. The KNO_3 (primary standard) was dried for 3–5 hr at 130° and cooled in a desiccator, under vacuum, before weighing. The sample was prepared by melting the KNO_3 over a flame and allowing the $Ca(NO_3)_2$ to dissolve the KNO_3 melt.

(*2*) *Measurements.* Viscosity of the sample was measured over the temperature range 79–200°. A Pyrex test tube holding the sample was placed in a bath, consisting of a glass dewar fitted with an electric stirrer and filled with glycerol. The temperature of the bath was controlled by a Fisher proportional temperature control unit, with an accuracy of ±0.01° and reproducibility of ±0.02°. Temperature measurements were done by a mercury thermometer, to the nearest tenth of a degree.

Three methods were used to measure the viscosity over various ranges. The Cannon–Fenske (capillary) method produced data, reproducible to within 1%, for viscosities up to about 750 P. The small volume of sample used, as well as the short duration of a complete run, eliminated most of the problem of crystallization.

A Brookfield rotating cylinder viscometer was used to measure higher viscosities. The outer cylinder remained stationary in the temperature bath while the inner cylinder was rotated at a known angular velocity. The general equation of motion for the viscometer is

$$I\frac{d^2\theta}{dt^2} + \eta K_1\frac{d\theta}{dt} + K_2\theta = 0 \quad (6)$$

where I is the moment of inertia of the inner cylinder,

---

[3] G. Adam and J. H. Gibbs, *J. Chem. Phys.*, **43**, 139 (1965).

[4] J. H. Gibbs, "Modern Aspects of the Vitreous State," Butterworth and Co., Ltd., London, 1960, Chapter 7.

[5] C. A. Angell, *J. Amer. Ceram. Soc.*, **51**, 117 (1968); C. A. Angell, *ibid.*, **51**, 125 (1968).

[6] P. B. Macedo and T. A. Litovitz, *J. Chem. Phys.*, **42**, 245 (1965).

[7] C. A. Angell, *J. Phys. Chem.*, **65**, 1917 (1964).

[8] E. Rhodes, W. E. Smith, and A. R. Ubbelohde, *Proc. Roy. Soc.*, **A285**, 263 (1965).

θ is its angular displacement, η is the dynamic viscosity, and K_1 and K_2 are constants of the apparatus. The first term represents the resistance to acceleration which is negligible, the system being overdamped. The second term is the viscous drag, and the third term represents as elastic torque produced by the angular displacement of the suspension.

For viscosities up to 7 × 10^4 P the Brookfield was used in the conventional rotation mode. The spindle was rotated at a constant angular velocity so that it experienced a torque (proportional to the angular displacement) which was produced by the viscous drag of the sample. The equation of motion of this mode reduced to

$$\eta = C_1\theta/\left(\frac{d\theta}{dt}\right) \tag{7}$$

where $C_1 = K_2/K_1$ and was obtained in units of P-rev/min per scale division by calibrating the viscometer. $d\theta/dt$ was obtained from the rpm rotation of a synchronous motor, with an error of 0.1% or less.

The range of the Brookfield was extended by using the decay mode. In this method the spindle was displaced and allowed to return to its equilibrium position by the torque of the suspension system. The equation of motion for this mode is

$$\eta K_1 \frac{d\theta}{dt} + K_2\theta = 0 \tag{8}$$

or

$$\eta = C_2(t_2 - t_1)/\ln(\theta_1/\theta_2) \tag{9}$$

where $C_2 = K_2/K_1$ with a conversion to units of P rev/sec per radian. It was necessary to extrapolate the scale to read 575 divisions per 360° in order to obtain the proper conversion factor for θ. This constant was calculated by direct calibration with a standard oil. For this mode $(t_2 - t_1)/\ln(\theta_1/\theta_2)$ was calculated by finding the slope of a plot of the logarithm of the displacement *vs.* time (Figure 1). The slope could be calculated to within 1% uncertainty. Agreement between measurements of η made at the same temperature by the two modes was within 0.8%. Using a spindle with a diameter of 0.118 cm, the range of the viscometer was extended to approximately 10^8 P.

Crystallization was a major problem with the Brookfield viscometer. The large volumes of sample needed and the presence of the rotating spindle tended to speed up the crystallization process so that it was generally impossible to leave the sample in the apparatus overnight. This problem particularly increased for temperatures around and above 100°.

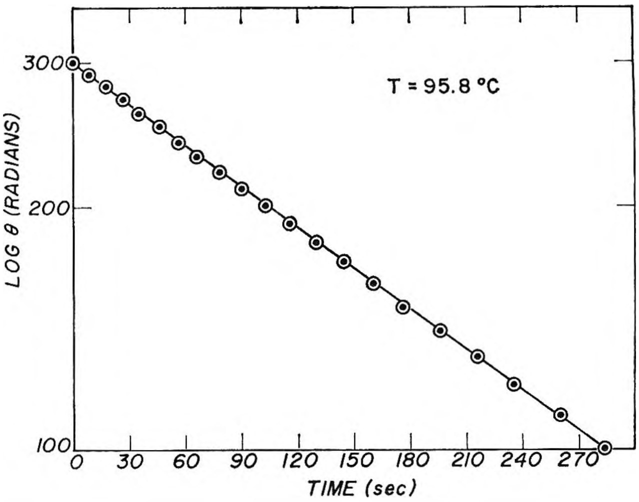

Figure 1. Logarithm of the angular displacement of the spindle of the Brookfield viscometer (used in the decay mode) as a function of time.

Table I: Viscosity Data as a Function of Temperature

T, °K	Log η P	T, °K	Log η P
Cannon–Fenske		Rotation method	
473.4	−0.240	384.8	3.199
466.1	−0.129	383.0	3.350
459.7	−0.022	380.0	3.662
454.0	−0.094	377.3	3.981
449.0	0.193	374.6	4.309
441.6	0.351	372.4	4.599
435.3	0.513	371.0	4.763
430.7	0.642		
425.4	0.814		
		Decay method	
419.8	1.039	369.0	5.085
414.8	1.226	366.8	5.377
413.0	1.309	364.6	5.748
411.1	1.552	362.5	6.115
406.9	1.610	361.2	6.378
404.0	1.792	360.0	6.634
400.5	1.976	359.0	6.781
399.2	2.046	357.6	7.029
397.8	2.140	356.7	7.202
397.6	2.154	355.9	7.371
395.2	2.346	354.1	7.826
392.9	2.468	354.8	7.608
390.6	2.636	352.5	8.134
387.8	2.868		

Results

The measured values and methods of measurement are given in Table I. These results represent several melts but since sample reproducibility was within the accuracy of the viscometer, sample identification was dropped.

The results from the Cannon–Fenske method give viscosity in Stokes which was converted to poises by multiplying each value of η by the density of the sample at that temperature. The densities, D, were calculated from the graph of Dietzel[9] using the equation

$$D = 2.2344 - 0.79364 \times 10^{-3}T \tag{10}$$

in which T is the temperature in degrees Centigrade.

---

[9] A. Dietzel and H. J. Poegel, Proceedings of the Third International Glass Congress, Venice, 1963, p 319.

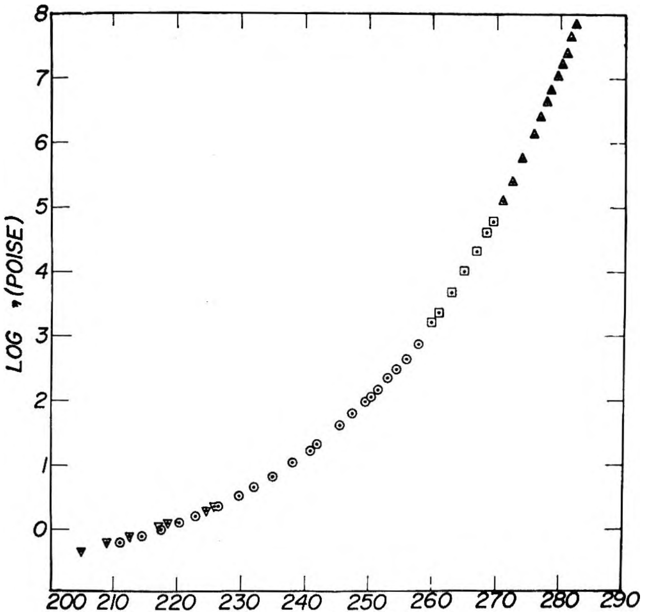

Figure 2. Arrhenius plot of the temperature dependence of viscosity: ▽, Ubbelohde's data; ⊙, Cannon-Fenske viscometer; ⊡, Brookfield (rotation mode); ⟁, Brookfield (decay mode).

In Figure 2, the logarithm of the viscosity is plotted *vs.* $1/T$. The values obtained by the Cannon-Fenske method are in fair agreement with Ubbelohde's[8] data, the latter plotted as inverted triangles in Figure 2. Unfortunately, ref 8 does not include any "raw" data. It seems that the worst deviations between their curve and the presently reported values are about 10%. The results from the Brookfield viscometer, operated in both modes, join smoothly with each other as well as with the low viscosity values obtained from the Cannon-Fenske viscometer.

In order to fit the Fulcher equation to the data by a least-squares fit method, eq 1 has to be linearized[10] to the form

$$\log \eta = A + \frac{1}{T}(B - AT_0) + \frac{T_0}{T}\log \eta \qquad (11)$$

Obtaining an initial set of values A', B', T_0' for the adjustable coefficients in eq 11, an improved set A, B, and T_0 can be calculated by a simple iterative procedure. Differentiating eq 11 and rearranging terms, one has

$$\Delta \log \eta = \Delta A + \Delta B/(T - T_0) + \Delta T_0 B/(T - T_0)^2 \qquad (12)$$

Performing successive least-squares fits on eq 12 to obtain a best set of values for ΔA, ΔB, and ΔT_0, one finally has

$$A = A' + \Delta A \quad B = B' + \Delta B \quad T_0 = T_0' + \Delta T_0$$

The standard deviations of A, B, and T_0 are those of ΔA, ΔB, and ΔT_0, respectively. If the initial values of the coefficients A', B', and T'_0 are taken from a least-squares fit to eq 11, then the second set of coefficients ΔA, ΔB, and ΔT_0 in eq 12 are comparable to their standard deviations and only a few further iterations are necessary.

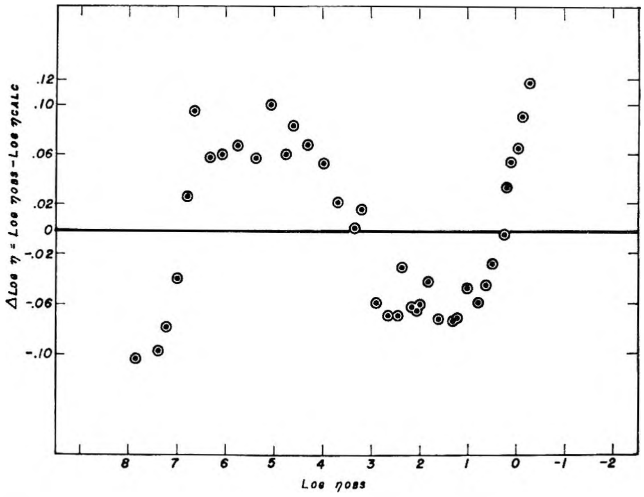

Figure 3. Deviation of the viscosity data from the Fulcher equation.

If the viscosity data are limited to the same temperature range as that of Angell's conductivity measurements (*i.e.*, roughly up to 76° above T_0), it follows the Fulcher equation to within the experimental standard deviation. The best fit is obtained with the following values of the unknown parameters; $A = -2.234 \pm 0.062$, $B = 635 \pm 11°\mathrm{K}^{-1}$, $T_0 = 334.8 \pm 1.8°\mathrm{K}$, where ± denotes the standard deviation in each case, and the overall standard deviation of the data is 0.5%. In fact, the conductivity as well as the viscosity data can be fitted to the same T_0 indicating that both transport processes display the same curvature in an Arrhenius plot (Figure 2). Thus taking $T_0 = 324.4°\mathrm{K}$ from ref 7, the limited viscosity data can be fitted to the Fulcher equation with $A = -2.602 \pm 0.024$ and $B = 798 \pm 5°\mathrm{K}^{-1}$. However, this shows that the value of the constant B from viscosity measurements is 1.30 ± 0.02 times larger than the value of B obtained from Angell's conductivity data, which was processed in the same manner. This ratio is somewhat larger than that obtained by Ubbelohde, who found it to be 1.20 at higher temperatures, and over a much smaller range of viscosity and conductivity.

If instead of stopping at 76° above T_0, we use all our data (which extends up to 35° above T_0), the Fulcher equation overestimates the data by a factor of 500. The data over the entire temperature range can be fitted to the Fulcher equation using the described least-squares technique, where now $A = -3.245 \pm 0.088$, $B = 1066 \pm 11°\mathrm{K}^{-1}$, and $T_0 = 312.6 \pm 0.9°\mathrm{K}$.

---

[10] P. B. Macedo, Mechanical and Thermal Properties of Ceramics: Proceedings of a Symposium, (U. S. Department of Commerce, National Bureau of Standards Special Publication 303, 1969) p 169.

The new fit requires the lowering of T_0 by 22° and an increase of 68% in B. Even so, this new fit has the characteristic "S" shape[11] (Figure 3) indicating that the discrepancy between the data and the Fulcher equation is well outside the experimental uncertainty.

Conclusion

The failure of the Fulcher equation to fit the data as one approaches the glass transition has many implications. First, the relaxation time will not extrapolate to infinity at a finite T_0. This raises the question as to whether or not a second order transition exists below T_g, as has been proposed by several authors.[3,5,6,11] The low-temperature Arrhenius behavior seems to be a general liquid feature, since it has been observed in molten oxides (B_2O_3) and organic liquids such as *n*-propyl alcohol[12] as well.

Secondly, Macedo and Napolitano[11] showed that in B_2O_3 (a melt with strong covalent bonds) the kinematics of viscous flow was controlled by the activation energy, rather than the structural effects. This also seems to be the case in the KNO_3–$Ca(NO_3)_2$ melts, a rather unexpected conclusion.[5,6,13]

Thirdly, even though the Fulcher equation fails markedly to fit the data near the glass transition, it still represents a good fit to the high-temperature data. Even more significantly, Angell[14] has shown that the parameters A and B are concentration independent in this system and T_0 varies linearly with concentration. Thus the Fulcher equation may have a deeper physical significance, beyond that of a purely empirical expression. However, the significances proposed so far[2,3,5,6] are inconsistent with the data.

Acknowledgment. This work was sponsored by Air Force Office of Scientific Research—Grant No. AFOSR-68-1376.

---

(11) P. B. Macedo and A. Napolitano, *J. Chem. Phys.*, **49**, 1887 (1968).

(12) A. C. Ling and J. E. Willard, *J. Phys. Chem.*, **72**, 1918 (1968).

(13) C. A. Angell, L. J. Pollard, and W. Strauss, *J. Chem. Phys.*, **50**, 2694 (1969).

(14) C. A. Angell, *ibid.*, **46**, 4673 (1967).

The Oxidation of Bromide by Bromate in Fused Alkali Nitrates

by James M. Schlegel

Rutgers, The State University, Newark College of Arts and Sciences, Newark, New Jersey

(Received April 16, 1969)

The oxidation of bromide by bromate in a dichromate solution of fused alkali nitrates can be expressed by the over-all reaction

$$Cr_2O_7^{2-} + BrO_3^- + Br^- = 2CrO_4^{2-} + Br_2 + O_2 \tag{1}$$

when the concentrations of BrO_3^-, Br^-, and CrO_4^{2-} are in excess compared to $Cr_2O_7^{2-}$. However, if the chromate concentration is kept at a minimum the over-all stoichiometry of this reaction approaches

$$3CrO_7^{2-} + BrO_3^- + 5Br^- = 6CrO_4^{2-} + 3Br_2 \tag{2}$$

This reaction was studied quantitatively under conditions which favored reaction 1, and it was found to follow a rate law which is first order in bromate and second order in bromide. The mechanism proposed for this reaction is

$$CrO_7^{2-} + BrO_3^- \overset{k_1}{\rightleftharpoons} BrO_2^+ + 2CrO_4^{2-} \quad \text{(rapid equilibrium)}$$

$$BrO_2^+ + 2Br^- \overset{k_2}{\rightleftharpoons} BrO_2^- + Br_2 \quad \text{(rapid equilibrium)}$$

$$BrO_2^- \xrightarrow{k} Br^- + O_2 \quad \text{(slow step)}$$

Introduction

The oxidation of bromide by bromate in aqueous solution is first order in bromate, second order in hydrogen ion, and either first order or second order in bromide. Edwards[1] suggests that the "super acid" ion $H_2BrO_3^+$ or the anhydrous acceptor form BrO_2^+ is formed by the reaction of bromate with protons. The postulated intermediate is Br_2O_2, formed either by displacement of a water molecule from $H_2BrO_3^+$ by Br^- or by a collision between BrO_2^+ and Br^-. If this intermediate decomposes unimolecularly after its formation, the reaction is first order in Br^-. However, if this intermediate collides with a Br^- to form products, the reaction is second order in bromide. Both of these mechanisms have been postulated.[2,3]

Protons are not available in fused salt media. However, the anhydrous acceptor form, BrO_2^+, is formed directly in fused nitrates through an equilibrium between dichromate and bromate[4]

$$Cr_2O_7^{2-} + BrO_3^- \rightleftharpoons BrO_2^+ + 2CrO_4^{2-} \tag{3}$$

Reactions 1 and 2 closely parallel the bromate–bromide reaction in aqueous solution except $Cr_2O_7^{2-}$ is the oxide ion acceptor rather than H^+. Our studies show that the rate law for reaction 1 is similar to a rate law which has been postulated in aqueous solution; however, reaction 2 best represents the stoichiometry for this reaction in aqueous solution. A possible explanation for this behavior will be presented later.

Experimental Section

Materials and Apparatus. ACS reagent grade chemicals were used. They were dried and stored in a desiccator until needed. All reactions were carried out in a thick-walled Pyrex tube equipped with gas inlet and outlet tubes affixed into the ground joint stopper of the tube. The solvent for each run was a 50-g eutectic mixture of KNO_3–$NaNO_3$. A large volume of identical composition was employed as a source of constant temperature. Gaseous products of the reaction were pased through "sulfite scrubber." The scrubbers were wide-mouthed erlenmeyer flasks fitted with rubber corks bored to receive a test tube containing glass beads with an exit hole at the bottom. Seven of these scrubbers were employed each with its own three-way stopcock and detachable ball and socket joint arm. This arrangement allowed removal of the flasks for titration while the reaction was still in progress. Prior to each run the scrubbers were charged with sulfite solution prepared by passing SO_2 through water.

Procedure. The limiting reactant, dichromate, was added to a KNO_3–$NaNO_3$ eutectic melt containing relatively high concentrations of Br^-, BrO_3^-, and CrO_4^{2-} compared to the concentrations of $Cr_2O_7^{2-}$. One mole of Br_2 was recovered for every mole of dichromate consumed in the reaction. Therefore, the rate of the reaction was studied by following the appearance of Br_2 with time. The evolved Br_2 was swept out of the reaction vessel with N_2 at a constant rate and allowed to pass

---

(1) J. O. Edwards, *Chem. Rev.*, **50**, 455 (1952).

(2) R. H. Clark, *J. Phys. Chem.*, **10**, 679 (1906); **11**, 353 (1907).

(3) A. Skrabal and S. R. Schreiner, *Monatsh.*, **36**, 213 (1934).

(4) F. R. Duke and J. M. Schlegel, *J. Phys. Chem.*, **67**, 3487 (1963).

through sulfite scrubbers in order to reduce the Br_2 to Br^-. The Br^- in solution was then titrated against a standard silver nitrate solution using eosin as an indicator. From this information the disappearance of total acid, $T_A = Cr_2O_7^{2-} + BrO_2^+ + BrO_2^-$, may be calculated. The rate of the reaction was found to depend on the flow rate of the purge gas, N_2. Therefore, the flow rate of nitrogen was varied from 0.20 to 0.70 l./min. At flow rates above 0.70 l./min, the scrubbers do not efficiently reduce Br_2 to Br^- and, in most cases, the rate of the reaction proceeds too fast to follow experimentally. An analysis of the melt was carried out by first dissolving the melt in water and precipitating the chromate formed as $BaCrO_4$. This precipitate was dried and weighed to constant weight. The melt was then analyzed for Br^- using silver nitrate and eosin indicator. The remaining bromate was determined iodimetrically.

Results and Discussion

Preliminary studies were made to allow the selection of proper temperature and concentration ranges for convenient study. The experimental data gave a first-order plot in the disappearance of total acid. The addition of chromate retarded the rate which indicated that a reversible reaction is involved. Varying the bromide concentration and plotting the logarithm of the rate constant obtained at fixed concentrations of BrO_3^- and CrO_4^{2} *vs.* the logarithm of the bromide concentration gave an order of two in bromide over a wide range of flow rates (Figure 1). This result is surprising in view of the results obtained by Duke and Lawrence for a similar reaction.[5] They report a first-order dependence in Br^- when studying the oxidation of Br^- by NO_3^- in a dichromate solution of fused nitrates.

We observed that the rate of reaction increased if the flow rate of the purge gas, N_2, was increased. Rate studies were made to distinguish between two possible explanations for this flow rate dependence; namely, (1) the rate is determined by the rate of diffusion of Br_2 to the surface of the melt, or (2) the rate is determined by solubility of Br_2 in the melt. If explanation 1 applies, then the rate would be independent of the reactant concentrations and would increase to a maximum value as the flow rate is increased. We found that the rate of the reaction increased without limit as the flow rate was increased. Also, the same dependence of the rate of the reaction on the Br^- and CrO_4^{2-} concentration was found at flow rates varying from 0.20 to 0.70 l./min. In view of these observations, we proposed that an equilibrium exists between bromine in the melt and the reactants and that the rate of the reaction is determined by the solubility of the bromine in the melt. If one assumes that the solubility of bromine in the melt is proportional to the partial pressure of the bromine above the melt and that the partial pressure of the bromine is inversely proportional to the flow rate of the purge gas, then one can relate the concentration of bromine in the melt to the flow rate of the purge gas $[Br_2] = C/\text{flow rate}$. A plot of $1/k'$ *vs.* the reciprocal of the flow rate of N_2 yields straight lines all having approximately the same ordinate intercept.

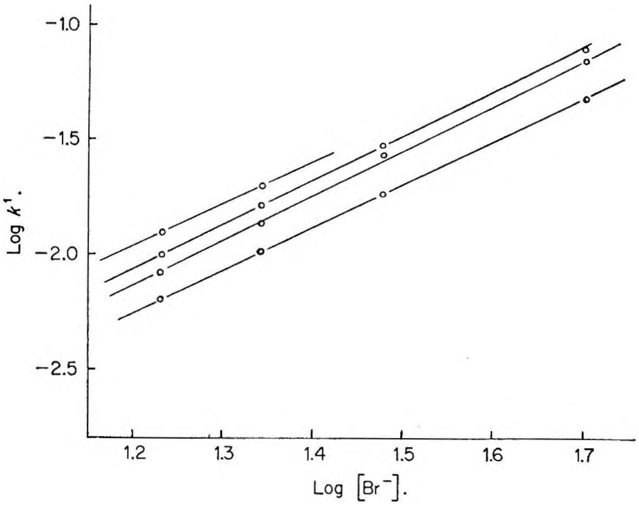

Figure 1. Plot of log k' *vs.* log $[Br^-]$. The flow rates of the carrier gas are 0.20, 0.29, 0.38, and 0.55 l./min.

A mechanism for this reaction can be written as

$$Cr_2O_7^{2-} + BrO_3^- \overset{K_1}{\rightleftharpoons} BrO_2^+ + 2CrO_4^{2-}$$

$$BrO_2^+ + 2Br^- \overset{K_2}{\rightleftharpoons} BrO_2^- + Br_2$$

$$BrO_2^- \xrightarrow{k} Br^- + O_2$$

where

$$K_1 = \frac{[BrO_2^+][CrO_4^{2-}]^2}{[Cr_2O_7^{2-}][BrO_3^-]}$$

and

$$K_2 = \frac{[BrO_2^-][Br_2]}{[BrO_2^+][Br^-]^2}$$

The rate is

$$-\frac{dT_A}{dT} = k[BrO_2^-]$$

where

$$T_A = Cr_2O_7^{2-} + BrO_2^+ + BrO_2^-$$

Substituting $[Cr_2O_7^{2-}] = T_A - [BrO_2^+] - [BrO_2^-]$ into the first equilibrium expression

$$K_1[BrO_3^-]T_A = [BrO_2^+][CrO_4^{2-}]^2 + K_1[BrO_3^-][BrO_2^+] + K_1[BrO_3^-][BrO_2^-]$$

and eliminating $[BrO_2^+]$ between this expression and the second equilibrium expression, one obtains

---

[5] F. R. Duke and W. Lawrence, *J. Amer. Chem. Soc.*, **83**, 1269 (1961).

$$[BrO_2^-] = \frac{K_1K_2[BrO_3^-][Br^-]^2}{K_1[BrO_3^-][Br_2] + [CrO_4^{2-}]^2[Br_2] + K_1K_2[BrO_3^-][Br^{-2}]}T_A$$

The rate law now becomes

$$-\frac{dT_A}{dT} = \frac{kK_1K_2[BrO_3^-][Br^-]^2}{K_1[BrO_3^-][Br_2] + [CrO_4^{2-}]^2[Br_2] + K_1K_2[BrO_3^-][Br^-]^2}T_A = k'T_A$$

Incorporating the relationship between the flow rate of purge gas and the concentration of bromine in the melt into the above equation, one obtains

$$1/k' = 1/k + C/F\frac{1}{kK_2[Br^-]^2} + \frac{[CrO_4^{2-}]^2}{kK_1K_2[BrO_3^-][Br^-]^2}$$

F is the flow rate and C is the proportionality constant between the flow rate and the concentration of bromine in the melt. The above equation is consistent with the experimental data (Figure 2). Most of the points in Figure 2 represent an average of at least two runs. The average deviation of all duplicate runs did not exceed 5%.

The rate constant can be obtained directly from Figure 1 and its value is 0.25 min^{-1} at 260°. To obtain the other constants, the slopes in Figure 1 were plotted against $[CrO_4^{2-}]^2$ (Figure 3). The slope of each line is equal to $C/kK_1K_2[BrO_3^-]$ and the intercept is C/kK_2. Dividing the intercept by the slope yields K_1 $[BrO_3^-]$. The concentration of bromate is 0.20 m and therefore K_1 equals 5.5×10^{-3}. Only the ratio C/K_2 can be obtained from the data; this ratio is equal to 0.12.

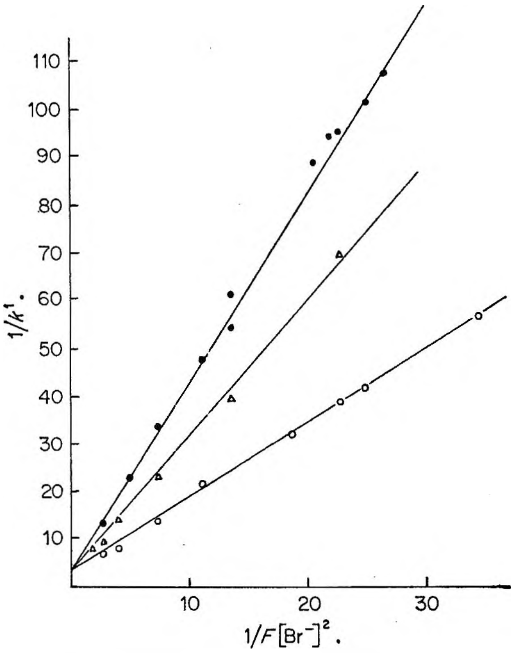

Figure 2. Plot of $1/k'$ *vs.* $1/F[Br^-]^2$ at various chromate concentrations: ○, 0.05 *m;* △, 0.070 *m;* ●, 0.092 *m.*

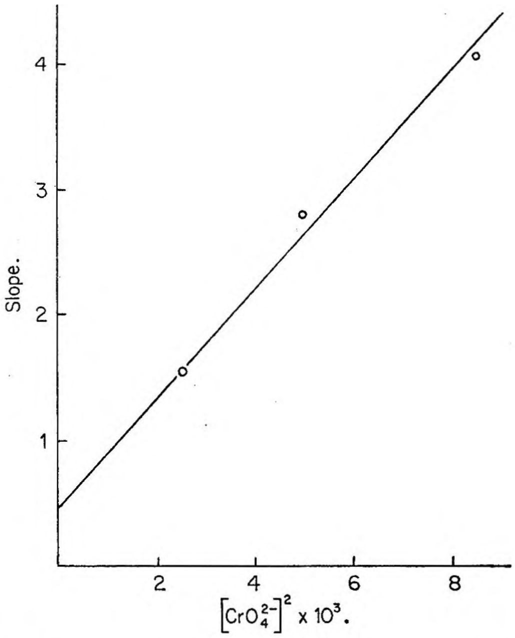

Figure 3. Plot of the slopes of the lines in Figure 2 *vs.* $[CrO_4^{2-}]^2$.

Although most of the data were obtained at 260°, this reaction was also studied at 250 and 276°, and an activation energy of 19.8 kcal/mol was obtained. This relatively high value indicates that this reaction is not controlled by the diffusion of bromine to the surface of the melt.

The stoichiometry of the reaction was determined by analyzing all the reactants and products during the course of the run. The oxygen was measured monometrically, and, under the conditions that this study was made, the ratio of Br_2 to O_2 was always one. However, if the initial chromate concentration was decreased to a value below 0.20 m, this ratio increased. As the initial chromatecon centration was successively decreased below 0.20 m, the ratio increased approaching a limit such that 3 mol of bromine and very little oxygen were liberated for every mole of bromate consumed. Analysis of the melt indicates that the stoichiometry of this reaction is best described by eq 2 when the concentration of chromate is kept at a minimum and bromine is not swept out of the melt. We suspect that under these conditions, bromite is kept in the melt for a sufficient length of time to react with dichromate, thereby producing more bromine and less oxygen. We are presently studying this aspect of the reaction.

Kinetics and Mechanism for the Reaction between Alkyl Hydroperoxides and Tetranitromethane[1]

by William F. Sager[2] and John C. Hoffsommer

U. S. Naval Ordnance Laboratory, White Oak, Silver Spring, Maryland 20910 *(Received April 18, 1969)*

The kinetics and activation parameters for the reaction between ROOH (where R = hydrogen, ethyl, isopropyl, cumene, and *t*-butyl) and tetranitromethane (TNM) in water in the pH range, 5.8–8.0, at 12.50, 25.14, and 37.10° have been investigated. Product analysis shows that ROOH reacts with TNM

$$C(NO_2)_4 + ROO^- + H_2O \longrightarrow C(NO_2)_3^- + NO_2^- + H^+ + ROH + O_2$$

Rates of reaction were followed spectrophotometrically from the trinitromethide, NF, concentration with time. Good second-order rate constants, k_2, were obtained from the expression

$$-d(TNM)/dt = +d(NF)/dt = k_1(TNM) = k_2(ROO^-)(TNM) = k_2K_a(ROOH)(TNM)(H^+)^{-1},$$

where k_1 is the pseudo-first-order rate constant with excess hydroperoxide, and K_a is the hydroperoxide acid dissociation constant. ROO^- reacted with TNM 10^3 to 10^4 times faster than OH^-, and, in general, the rates were found to follow the Brönsted free energy relationship with pK_a. Labeling experiments with $H_2{}^{18}O$ indicate that nucleophilic attack by ROO^- on TNM occurs at oxygen of the NO_2 group rather than at carbon or nitrogen.

Introduction

Tetranitromethane (TNM) has been used primarily as a color complexation reagent for the detection of carbon–carbon unsaturation in a wide variety of organic compounds.[3] In addition, TNM is known to react with hydrogen peroxide and potassium hydroxide in aqueous solution to produce nitroform.[4] Since unsaturated organic compounds often contain varying amounts of alkyl hydroperoxides, we thought it worthwhile to investigate the possibility of a hydroperoxide—TNM interaction. Reaction between TNM and the alkyl hydroperoxides would be theoretically interesting from a mechanistic standpoint, since reaction sites at carbon, nitrogen, as well as oxygen are all available for attack in TNM. We now wish to report our findings concerning the reaction between alkyl hydroperoxides and TNM.

Experimental Section and Results

Hydroperoxides. Ninety per cent *t*-butyl hydroperoxide in aqueous solution was obtained commercially (Lucidol Division of Wallace and Tierman, Inc., Buffalo, N. Y.) and was purified by distillation under reduced pressures.

Ethyl hydroperoxide was prepared in 37% yield from ethyl sulfate and aqueous potassium hydroperoxide based on methods of Baeyer and Villiger,[5] and Rieche and Hitz.[6] The hydroperoxide was obtained as a 53% aqueous solution by weight after distillation at reduced pressures.

Isopropyl hydroperoxide was prepared in 40% yield from diisopropyl sulfate[7] and aqueous potassium hydroperoxide based on the methods of Medvedev and Alexejewa.[8] The hydroperoxide was obtained as an 8% aqueous solution after distillation at reduced pressures.

Cumene hydroperoxide was obtained commercially from the Hercules Powder Co., Wilmington, Del., and found to contain 73% active oxygen by iodometric analysis. The pure hydroperoxide was obtained by fractional distillation and a middle fraction boiling at 65° (0.18 mm) was collected.[9]

Dilute aqueous hydrogen peroxide solutions were prepared from both commercially available 30% (Baker Analyzed Reagent) and 90% (Becco Chemical Division, Buffalo, N. Y.) aqueous hydrogen peroxide.

---

[1] Work taken in part from the Ph.D. dissertation of J. C. H., George Washington University, Washington, D. C., 1964.

[2] Department of Chemistry, University of Illinois at Chicago.

[3] A. Werner, *Ber.*, **42**, 4324 (1909); I. Ostromisslensky, *ibid.*, **43**, 197 (1910); E. M. Harper and A. K. MacBeth, *J. Chem. Soc.*, **107**, 1824 (1915); D. Ll. Hammick and R. P. Young, *ibid.*, **149**, 1463 (1936); E. Heilbronner, *Helv. Chem. Acta*, 1121 (1953); K. Miescher, *ibid.*, **29**, 743 (1946); L. F. Fieser and M. Fieser, "Reagents for Organic Synthesis," John Wiley & Sons, Inc., New York, N. Y., 1967, pp 1147–48.

[4] Method of K. Schimmelschmidt, reported by K. Klager and M. B. Frankel, Aerojet Report No. 494, Aerojet Engineering Corporation, Azusa, California, p 3 (1951). See also J. W. Copenhaver and M. H. Bigelow, "Acetylene and Carbon Monoxide Chemistry," Reinhold Publishing Corp., New York, N. Y., 1949, p 24.

[5] A. Baeyer and V. Villiger, *Ber.*, **34**, 738 (1901).

[6] A. Rieche and R. Hitz, *ibid.*, **62**, 2469 (1929).

[7] W. R. Ormandy and E. C. Craven, *J. Soc. Chem. Ind.*, **49**, 363T (1930).

[8] S. Medvedev and E. N. Alexejewa, *Ber.*, **65**, 132 (1932).

[9] D. Barnard and K. R. Hargrave, *Anal. Chim. Acta.*, **15**, 476 (1951).

Table I: Experimental pK_a Values for Ethyl Hydroperoxide in Water at 25.14°

			Buffered pH[b]					
			11.09		11.56		11.78	
Wavelength, mμ	ϵ_{HA}[a]	ϵ_A	ϵ	pK_a	ϵ	pK_a	ϵ	pK_a
260	8.74	98.5	40.7	11.35	62.7	11.36	73.8	11.36
265	6.75	78.2	31.3	11.34	48.3	11.37	57.4	11.32
270	5.18	60.8	23.9	11.34	37.2	11.38	44.2	11.32
275	3.94	47.1	18.6	11.33	28.5	11.37	34.2	11.31
280	3.02	36.1	14.1	11.34	21.9	11.36	26.2	11.31
				11.34		11.37		11.33

Combined av 11.35 ± 0.02

[a] ϵ_{HA}, ϵ_A, and ϵ are extinction coefficients for the undissociated, completely dissociated, and buffered ethyl hydroperoxide. [b] Phosphate buffers, ionic strength = 0.100.

Tetranitromethane. Tetranitromethane (TNM) was prepared in these laboratories by nitration of acetic anhydride, and purified by distillation at reduced pressures. The freezing point of the TNM used was 14.1°. Dilute aqueous solutions of TNM were analyzed quantitatively according to the method of Glover and Landsman[10] which is based on the quantitative reaction between TNM and hydrazine to produce nitroform (λ_{max}, 350 mμ; ϵ, 14,418).

Hydroperoxide Analysis. Dilute aqueous stock solutions, 0.03 to 0.05 M in hydroperoxide, were analyzed iodometrically immediately before use. Solutions of hydrogen peroxide were analyzed according to the procedure of Kolthoff and Sandell,[11] while the alkyl hydroperoxide solutions were determined in hot isopropyl alcohol solutions containing glacial acetic acid and potassium iodide.[12]

Dissociation Constants. Dissociation constants of the alkyl hydroperoxides in water were measured by a modification of the general procedure of Everett and Minkoff.[13] Extinction coefficients of the dissociated, ϵ_A, and undissociated hydroperoxides, ϵ_{HA}, were determined between 260 and 310 mμ in matched 5-cm quartz cells which were thermostated to within ±0.05° in the cell compartment of a Beckman, Model DU, spectrophotometer. Extinction coefficients, ϵ, of the hydroperoxides in phosphate buffers in the pH range, 10.9 to 12.10, for which the pH was known as a function of temperature[14] were measured at the same temperature and wavelengths as ϵ_A and ϵ_{HA}. The ionic strength of each buffered solution was maintained at 0.100 by the amount of buffer added, and the pK_a was calculated from the equation, $pK_a = pH + \log(\epsilon_A - \epsilon)/(\epsilon - \epsilon_{HA})$. Buffered solutions were checked with a Beckman, model G, pH meter. For each buffered hydroperoxide at a specific temperature and pH, the pK_a values obtained at 4 or 5 different wavelengths were found to be essentially constant and agreed reasonably well with pK_a values obtained in the buffer range, pH 10.9 to 12.0, at the same temperature. Alkyl peroxyanion extinction coefficients, ϵ_A, were obtained by measuring the optical densities of 2 to 5 M aqueous sodium hydroxide solutions which were 2 to 3 × 10^{-3} M in hydroperoxide. The data for ethyl hydroperoxide are illustrative of the general method employed for the determination of pK_a values for all the hydroperoxides studied and are shown in Table I.

Although aqueous solutions of the alkyl hydroperoxides were found to be stable in the pH range 10 to 12, and at temperatures, 12.5 to 37.1°, solutions of hydrogen peroxide were rapidly decomposed under these conditions.[15] Therefore, a modification of the procedure used for the alkyl hydroperoxides was used to obtain the pK_a's of hydrogen peroxide. Optical density measurements of aqueous phosphate-buffered solutions of hydrogen peroxide in the pH range 11 to 12 were made at 270 mμ as a function of time. Extrapolated values of log optical density, at time, t = 0, were taken as log ϵ, at the specific buffered pH and temperature, and used to obtain the pK_a from the buffer equation, as described. Plots of log optical density *vs.* time were found to be linear to about 10 minutes depending on the pH. The pK_a values and calculated thermodynamic parameters for all the hydroperoxides are shown in Table II.

Kinetics. Aliquots of aqueous stock hydroperoxide solutions together with sufficient phosphate buffer to make the ionic strength of the finally diluted solution equal to 0.1 were thermostated in 100 ml volumetric flasks at least 0.5 hr prior to each kinetic run. At the same time, separate aqueous solutions of 2.0 to 5.0 ×

---

(10) D. J. Glover and S. G. Landsman, *Anal. Chem.*, **36**, 1690 (1964).

(11) I. M. Kolthoff and E. B. Sandell, "Textbook of Quantitative Inorganic Analysis," The Macmillan Co., New York, N. Y., 1948, p 630.

(12) V. R. Kokatnur and M. Jelling, *J. Amer. Chem. Soc.*, **63**, 1432 (1941).

(13) A. J. Everett and G. J. Minkoff, *Trans. Faraday Soc.*, **49**, 410 (1953).

(14) H. T. S. Britton, "Hydrogen Ions," Vol. I, D. Van Nostrand Co., Inc., New York, N. Y., 1956, p 359.

(15) F. R. Duke and T. W. Haas, *J. Phys. Chem.*, **65**, 304 (1961).

Table II: Thermodynamic Parameters for the Dissociation of Alkyl Hydroperoxides in Water

R–OOH	T, °C ± 0.05	pK_a, ± 0.02[a]	ΔH, kcal/mol	ΔS, cal/deg
t-Butyl–	12.50	12.74	6.4 ± 0.02	−36 ± 1
	25.14	12.54		
	37.10	12.35		
H–	12.50	11.85	8.9 ± 0.3	−23 ± 1
	25.14	11.54		
	37.10	11.31		
Isopropyl–	12.50	12.07	7.5 ± 1.8	−28 ± 6
	25.14	11.74		
	37.10	11.61		
Cumene–	12.50	12.60	8.8 ± 0.3	−27 ± 1
	25.14	12.33		
	37.10	12.07		
Ethyl–	12.50	11.56	5.0 ± 1.0	−35 ± 3
	25.14	11.35		
	37.10	11.25		

[a] Ionic strength = 0.100.

Table III: Observed First-Order Rate Constants, k_1, for the Rate of Disappearance of TNM with Excess Ethyl Hydroperoxide in Aqueous Solution[a]

%Completion	t, min[b]	OD$_t$[c]	$k_1 \times 10^{-3}$, sec^{-1} [d]
2.6	1.49	0.015	0.243
	4.11	0.034	0.234
15.9	11.45	0.089	0.243
	14.27	0.106	0.239
	21.19	0.150	0.242
	28.23	0.187	0.239
42.8	39.05	0.239	0.237
	69.25	0.351	0.237
	81.57	0.384	0.237
71.4	87.60	0.399	0.237
	104.86	0.431	0.234
	125.47	0.462	0.232
85.5	137.54	0.478	0.234
	147.86	0.489	0.234
	182.35	0.519	0.240
94.6	207.24	0.529	0.234
100	overnight, ∞	0.559	. . .
		Av	0.237 ± 0.003

[a] TNM, 3.86×10^{-5} M; ethyl hydroperoxide, 2.43×10^{-2} M; pH, 7.00; 25.14°C. [b] Obtained with an automatic timer, Precision Scientific Co., Chicago, Ill. [c] Optical density of nitroform anion, $C(NO_2)_3^-$, at 350 mμ. [d] $k_1 = 1/t \ln (OD_\infty)/(OD_\infty - OD_t)$.

10^{-3} M TNM were similarly thermostated. Sufficient distilled water was added to the volumetric flasks containing the buffered hydroperoxides so that on addition of the TNM aliquot, the total volume of solution would be exactly 100 ml.[16] The contents of the flask were thoroughly mixed, poured into dry 1-cm quartz optical cells, stoppered, and immediately placed into the cell compartment of the spectrophotometer. The compartment was specially designed so that the optical cells could be immersed in circulating distilled water maintained at the desired temperature by means of an external constant temperature bath. A calibrated and certified National Bureau of Standards thermometer which could be read to within ±0.02°C was fitted tightly into the cell compartment. Temperatures during the kinetic runs were controlled to within ±0.05°C. Reference cells contained the same amount of buffer and hydroperoxide as the kinetic run. Cell blanks were negligible.

TNM was found to react quantitatively[17] with excess hydroperoxide in buffered aqueous solutions in the pH range 5.8 to 8.0 to produce yellow solutions containing trinitromethide (nitroform) and nitrite ions. From a large scale reaction between TNM and t-butyl hydroperoxide, oxygen gas and t-butyl alcohol were isolated (later section). And, although the isolation of these products was not quantitative, these products indicate the following general reaction

$$C(NO_2)_4 + ROO^- + H_2O \longrightarrow C(NO_2)_3^- + NO_2^- + H^+ + ROH + O_2 \quad (1)$$

whereas the rate of reaction between TNM and hydrazine was found to be practically instantaneous, the rate between TNM and excess hydroperoxide was found to be much slower and could be measured as a function of nitroform concentration with time from its molar absorption at 350 mμ. Under pseudo-first-order conditions with excess hydroperoxide, the rates of disappearance of TNM were found to obey first-order kinetics in the buffered pH range 5.8 to 8.0. The first-order rate constants, k_1, obtained for the rate of disappearance of TNM for the reaction between 3.86×10^{-5} M TNM and 2.43×10^{-2} M ethyl hydroperoxide in water at pH 7.00 and 25.14° were typical and are shown in Table III.

The rate of disappearance of TNM, $-d(TNM)/dt$, was followed from the observed rate of nitroform ion formation, $+d(NF)/dt$. Concentrations of TNM at any time were known from $(OD_\infty - OD_t)/\epsilon_{NF}$, where OD_∞ and OD_t were the optical density values after at least 10 half-lives and at time, t, respectively, and ϵ_{NF}, the extinction coefficient of nitroform anion in water. At a constant pH, the first-order rate constants, k_1, varied with initial hydroperoxide concentration and indicated first order dependency with respect to hydroperoxide, Table IV. In addition, the observed first-order rate constants, k_1, were found to vary with the pH of the buffered solution. These results indicated that

---

(16) Care must be exercised in working with aqueous solutions of TNM, since even at room temperatures, TNM is quite volatile and easily lost.

(17) Nitroform produced agreed within 1% to the nitroform obtained by the hydrazine method for the quantitative determination of TNM.[10]

Table IV: Order with Respect to Hydroperoxide for Reaction with TNM

R–OOH × 10^{-3} *M*	TNM × 10^{-5} *M*	pH	k_1, sec^{-1}	Order[a]
H–				
9.64	3.06	7.2	0.482	
18.6	4.42	7.2	0.904	1.00
21.6	3.95	7.2	1.12	
Ethyl–				
25.5	2.18	7.4	0.625	0.96
12.1	4.47	7.4	0.307	
t-Butyl–				
10.8	4.58	7.8	0.137	1.02
15.7	4.07	7.8	0.202	

[a] Value of x from, $(k_{1-1})/(k_{1-2}) = (\mathrm{ROOH_1/ROOH_2})^x$, where k_{1-1} and k_{1-2} are first-order rate constants for the respective hydroperoxide concentrations, $ROOH_1$ and $ROOH_2$.

the alkyl peroxyanion, ROO^- was the reactive nucleophile in attack on TNM.

Second-order rate constants, k_2, for the rate of disappearance of TNM, $-\mathrm{d(TNM)}/\mathrm{d}t = k_2(\mathrm{ROO^-})(\mathrm{TNM})$, were calculated from the derived expression, $k_2 = k_1(\mathrm{H^+})/K_a(\mathrm{ROOH})$, in terms of k_1, the observed first-order rate constant, and K_a, the acid dissociation constant of the alkyl hydroperoxide determined at the same ionic strength and temperature. Observed k_1 and calculated k_2 rate constants for the reaction between hydrogen peroxide and TNM in water at 25.14°C as a function of pH and concentration are shown in Table V. Rate data and thermodynamic activation parameters for the reactions between five hydroperoxides and TNM in water are shown in Table VI. Each second-order rate constant, k_2, is the average of at least three kinetic runs in at least two different buffered solutions in the pH range, 5.8 to 8.0.

Table V: First- and Second-Order Rate Constants, k_1 and k_2 for the Reaction Between TNM and Excess Hydrogen Peroxide in Water at 25.14°

TNM × 10^{-5} *M*[a]	H_2O_2 × 10^{-2} *M*	pH	$k_1 \times 10^{-3}$[c]	$k_2 \times 10^{3}$[d]
3.38	0.482	7.40	0.403	1.16
3.95	2.16	7.20	1.12	1.13
4.42	1.86	7.20	9.904	1.06
4.29	1.86	7.20	0.904	1.06
2.18	1.86	7.20	0.938	1.10
3.06	0.964	7.20	0.482	1.10
4.25	3.09	7.00	0.850	0.960
4.15	0.964	7.00	0.273	1.16
4.08	0.482	7.00	0.146	1.06
4.09	4.66	5.86	0.123	1.26
			Av	1.10 ± 0.05

[a] Concentration of TNM determined after at least ten half-lives from nitroform ion concentration. [b] Phosphate buffers, total ionic strength = 0.100. [c] In sec^{-1}. [d] In l. mol^{-1} sec^{-1}.

Product Analysis. Solutions were analyzed for nitrite ion by the method of Snell and Snell.[18] Under acidic conditions the nitrite ion was converted to nitrous acid. The nitrous acid produced was used to form the diazotization product of sulfanilic acid which was then coupled with 1-aminonaphthalene. Nitrite ion concentration was determined spectrophotometrically by measuring the absorption of the purple coupled product at 520 mμ and comparing to a standard curve. Beer's law was found to hold in the range of nitrite ion concentration, 1.0 to 6.0 × 10^{-6} *M*.

It was essential that all peroxides be destroyed prior to the nitrite analysis to prevent oxidation of nitrite ion to nitrate under the acidic conditions of the determination. Hydrogen peroxide and *t*-butyl hydroperoxide were completely decomposed in aqueous solutions after adjusting the pH of the solution between 11 and 12 with dilute aqueous sodium hydroxide and warming on the steam bath for 20 min. Ethyl, isopropyl, and cumene hydroperoxides were only partially decomposed under these conditions and, consequently, the nitrite analyses were somewhat low. For example, $(\mathrm{NO_2^-})/(\mathrm{C(NO_2)_3^-}$ ratios obtained from the kinetic runs for hydrogen peroxide and *t*-butyl hydroperoxide were found to be 1.00 and 0.96, respectively, while ratios of 0.81, 0.48, and 0.24 were found for the kinetic runs with ethyl, isopropyl and cumene hydroperoxides. However, similar ratios were obtained on analyses of synthetic solutions containing equal concentrations of NO_2^- and $C(NO_2)_3^-$ ions together with each of these hydroperoxides separately, and indicate that the ratio, $(\mathrm{NO_2^-})/(\mathrm{C(NO_2)_3^-}$ was close to unity in each kinetic run.

The pseudo-first-order rate constant, k_1, for the formation of NO_2^- ion from the reaction between 5.02 × 10^{-5} *M* TNM and 4.20 × 10^{-3} *M* H_2O_2 at pH 7.40 was found to be 0.28 × 10^{-3} sec^{-1}. This result paralleled the value obtained for the pseudo-first-order rate constant, k_1 (0.25 × 10^{-3} sec^{-1}), for the formation of nitroform ion for this run. Nitrite analyses were determined on aliquot samples taken from the reaction solution at various time intervals. Prior to the analyses, unreacted TNM was extracted with chloroform, and unreacted hydrogen peroxide was destroyed by adjusting the pH to 11.6 and heating on the steam bath for 20 min.

Oxygen gas and *t*-butyl alcohol were isolated and identified from a large scale reaction at room temperature between TNM and *t*-butyl hydroperoxide, buffered at pH, 11.56. The oxygen gas was collected and measured by displacement of water and identified by gas chromatography. Tertiary butyl alcohol was isolated by distillation, followed by extraction of the aqueous dis-

---

(18) F. D. Snell and C. T. Snell, "Colorimetric Methods of Analysis," Vol. 2, 3rd ed, D. C. Van Nostrand Co., Inc., New York, N. Y., 1949, pp 802–804.

Table VI: Second-Order Rate Constants and Activation Parameters for Reaction between Alkyl Hydroperoxides and TNM in Water

R-OOH	T, °C	$k_2 \times 10^3$ [a]	$\Delta F^{\ddagger}$ [b]	$\Delta H^{\ddagger}$ [c]	$\Delta S^{\ddagger}$ [d]
t-Butyl-	12.50	0.623 ± 0.02	12.9 ± 0.3	17.7 ± 0.2	15.1 ± 0.5
	25.14	2.25 ± 0.07			
	37.10	7.66 ± 0.02			
H-	12.50	0.530 ± 0.02	13.3 ± 0.3	12.6 ± 0.2	−2.8 ± 0.8
	25.14	1.10 ± 0.05			
	37.10	3.23 ± 0.02			
Isopropyl-	12.50	0.249 ± 0.003	13.5 ± 0.4	16.9 ± 0.2	10.4 ± 0.5
	25.14	0.811 ± 0.04			
	37.10	2.72 ± 0.05			
Cumene-	12.50	0.139 ± 0.006	13.9 ± 0.2	16.1 ± 0.2	6.5 ± 1.0
	25.14	0.435 ± 0.007			
	37.10	1.36 ± 0.010			
Ethyl-	12.50	0.0673 ± 0.001	14.3 ± 0.2	18.8 ± 0.2	16.5 ± 0.9
	25.14	0.217 ± 0.007			
	37.10	1.04 ± 0.03			

[a] l. mol^{-1} sec^{-1}. [b] kcal mol^{-1}. [c] kcal mol^{-1}. [d] cal deg^{-1}. Errors in footnotes c and d were estimated by the method of E. L. Purlee, R. W. Taft, and C. A. De Fazio, *J. Amer. Chem. Soc.*, **77,** 837 (1955). See also L. L. Schaleger and F. A. Long, in "Advances in Physical Organic Chemistry," Vol. I, V. Gold, Ed., Academic Press, New York, N. Y., 1963, pp 7–9.

Table VII: Large Scale Reaction between t-Butyl Hydroperoxide and TNM in Water

Reaction mixture, mol[a]			Reaction products, mol			
TNM	$(CH_3)_3COOH$	pH[b]	$C(NO_2)_3^-$	NO_2^-	O_2	$(CH_3)_3COH$[c]
0.128	0.198	11.56	0.101	0.0873	0.097	0.034

[a] Reaction mixture was heterogeneous. [b] Buffer, 0.60 mol of potassium dihydrogen phosphate and 0.90 mol of sodium hydroxide in 500 ml of water. [c] Isolated yield. No other organic fragment other than t-butyl alcohol was found.

tillate with ether and drying over anhydrous magnesium sulfate. The pure alcohol was obtained by fractional distillation and had an identical boiling point and infrared spectrum with authentic t-butyl alcohol. Nitrite ion concentration was determined on an aliquot sample as previously described. The results of a large scale reaction between t-butyl hydroperoxide and TNM are shown, Table VII.

^{18}O *Labeling Experiments.* Since TNM possesses three possible sites for nucleophilic attack by the hydroperanion nucleophile, we considered it worthwhile to investigate the labeled products resulting from the reaction between t-butyl hydroperoxide and TNM under basic conditions in $H_2{}^{18}O$. After optimizing conditions in ordinary unlabeled $H_2{}^{16}O$, the following experiments were carried out. A total of 4.12×10^{-2} mol of t-butyl hydroperoxide (5.3 g of 70% hydroperoxide in ordinary water) was dissolved at 20° in a solution containing 8.33×10^{-1} mol Volk, 5.09 excess atom % "normalized," $H_2{}^{18}O$, 6.44×10^{-1} mol of ordinary water and 0.100 mol (4.05 g 97.7%, reagent grade) of sodium hydroxide.[19] To this stirred solution was added in one portion, 9.19×10^{-3} mol (1.80 g) of TNM. The mixture was stirred vigorously for 0.5 hr until the gas evolution (oxygen) stopped and a portion collected. Tertiary butyl alcohol was obtained by distillation from the reaction mixture and purified as previously described. The results of the ^{18}O mass spectral analyses[20] are shown (where the numbers indicate % ^{18}O excess)

Reaction mixture

$$\underset{0}{(CH_3)_3COO^-} + \underset{0}{C(NO_2)_4} + \underset{2.69}{H_2{}^{18}O} \longrightarrow$$

Products

$$C(NO_2)_3^- + \underset{0.003}{O_2} + NO_2^- + \underset{0.024}{(CH_3)_3COH} + H^+ \qquad (2)$$

Obviously, the ^{18}O labeling in the O_2 and t-butyl alcohol

---

(19) The $H_2{}^{18}O$ was analyzed by conversion to $C_2H_5{}^{18}OH$ by the basic hydrolysis of ethyl sulfate (M. Anbar, I. Dostrovsky, D. Samuel, and A. D. Yoffe, *J. Chem. Soc.*, 3609 (1954)). Mass spectral analyses of the $C_2H_5{}^{18}OH$ were kindly performed by F. E. Saalfeld of the Naval Research Laboratory, Washington, D. C. Result is average of ten determinations.

(20) Mass analyses were performed by A. S. Ostashever, Analytical Corporation, New York, N. Y.

products was practically insignificant. We then decided to look for ^{18}O labeling in the nitrite ion by the method of Anbar and Taube[21] according to eq 3, by mass spectral analysis of N_2O. Also, Anbar and Taube found no exchange between NO_2^- and $H_2{}^{18}O$ in the buffer pH range, 2.5 to 3.5

$$HN^{18}O_2 + HN_3 \xrightarrow{\text{pH } 2.5-3.5} N_2{}^{18}O + N_2 + H_2{}^{18}O \qquad (3)$$

A total of 3.0×10^{-3} mol of TNM was allowed to react with 1.40×10^{-2} mol of *t*-butyl hydroperoxide in 0.277 mol of 5.09 excess atom % $H_2{}^{18}O$, 0.232 mol of ordinary distilled water and 3.70×10^{-2} mol of sodium hydroxide. After completion of the O_2 gas evolution, one-third of the resulting mixture was buffered[22] between pH 2.5–3.5 with 9.8×10^{-3} mol of potassium acid phthalate, and 1.4×10^{-2} mol of HCl in 0.85 mol of ordinary water. To this stirred solution was added 1.54×10^{-3} mol of sodium azide in one portion, whereupon a rapid evolution of gas (N_2O) ensued. Mass spectral analyses[23] showed the N_2O to possess 1.34 atom % excess ^{18}O. The ^{18}O labeling in the original $HN^{18}O_2$ would, therefore, be expected to be 2.68 atom % excess ^{18}O since the $HN^{18}O_2$ is converted to both $N_2{}^{18}O$ and $H_2{}^{18}O$ (eq 3). The results for the TNM–*t*-butyl hydroperoxide reaction are summarized (where the numbers indicate % ^{18}O excess)

Reaction mixture

$$\underset{0}{(CH_3)_3COO^-} + \underset{0}{C(NO_2)_4} + \underset{2.59}{H_2{}^{18}O} \longrightarrow$$

Products

$$C(NO_2)_3^- + \underset{2.68}{N^{18}O_2^-} + O_2 + (CH_3)_3COH + H^+ \qquad (4)$$

Also, had exchange between HNO_2 and $H_2{}^{18}O$ taken place inadvertently before or during the reaction with hydrazoic acid, the ^{18}O labeling in N_2O would be expected to be at most, 0.16% excess ^{18}O. Synthetic mixtures of *t*-butyl hydroperoxide, sodium hydroxide, nitroform, and *t*-butyl alcohol in water were found not to interfere with the conversion of nitrous acid to N_2O with hydrazoic acid.

Discussion

TNM reacts quantitatively with excess hydroperoxide to form trinitromethide and nitrite ions, with the liberation of O_2 gas and formation of the corresponding alcohol (eq 1). The rate of disappearance of TNM obeys second-order kinetics overall, first order in TNM and alkyl peroxyanion, (Tables III and IV) according to $-d(\text{TNM})/dt = k_2(\text{TNM})(\text{ROO}^-)$. Evidence for ROO^- attack on TNM as the rate determining step is demonstrated by the pH dependancy on the first-order rate constant, (Table V). Logarithms of the second-order rates, log k_2, follow the Brönsted free energy relationship with pK_a, in general (Figure 1) and also indicate attack on TNM by ROO^-. Although the fit of the data to a straight line is somewhat imprecise, this is not entirely unexpected since the R group of ROO^- is quite close to the reactive center of the peroxyanion oxygen, and since there is considerable variation in the entropies of activation (Table VI). In this plot, hydrogen peroxide has been statistically corrected for its two hydrogens by dividing the second-order rate constant by two.

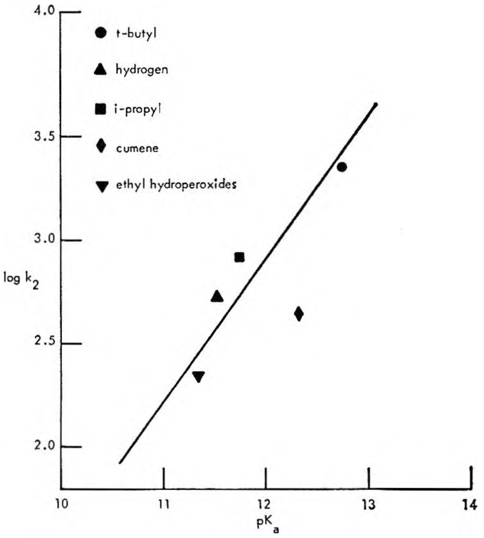

Figure 1. Brönsted relationship for the reaction of several hydroperoxides and TNM.

The kinetics, however, do not distinguish the point of nucleophilic attack by the peroxyanion, ROO^-, which in TNM may occur at any one or combination of three different atoms, namely, carbon, nitrogen, or oxygen to form I, II, or III

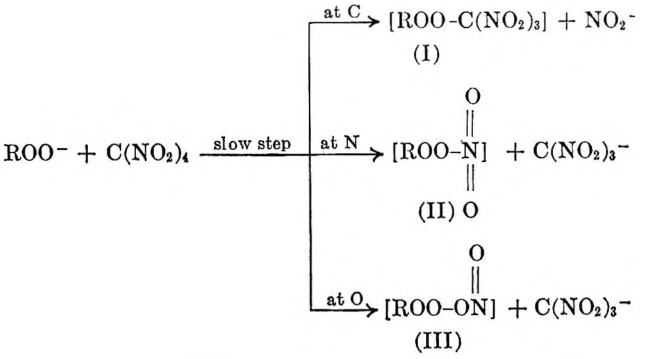

$$ROO^- + C(NO_2)_4 \xrightarrow{\text{slow step}} \begin{cases} \xrightarrow{\text{at C}} \underset{(I)}{[ROO\text{-}C(NO_2)_3]} + NO_2^- \\ \xrightarrow{\text{at N}} \underset{(II)}{[ROO\text{-}\overset{\overset{O}{\|}}{\underset{\underset{O}{\|}}{N}}]} + C(NO_2)_3^- \\ \xrightarrow{\text{at O}} \underset{(III)}{[ROO\text{-}O\overset{\overset{O}{\|}}{N}]} + C(NO_2)_3^- \end{cases}$$

Subsequent rapid decomposition of the intermediates I, II, or III by H_2O or OH^- could yield the other products

---

[21] M. Anbar and H. Taube, *J. Amer. Chem. Soc.*, **76**, 6243 (1954).

[22] The pH of the buffered solution was checked before and after the run with a Beckman, Model G, pH meter.

[23] Mass analyses by F. E. Saalfeld, Naval Research Laboratory, Wash., D. C. Atom $\%^{18}O = (I_{46}/I_{44})/(I_{46}/I_{44} + I_{44}/I_{44}) \times 100$, where I_i = ion current observed for $m/e = i$. Results are average of ten determinations.

Table VIII: Relative Rates and Activation Parameters for Nucleophilic Attack by OOH^- and OH^- on TNM and Benzonitrile

Substrate	Nucleophile	$k_2 \times 10^{-1}$ [a]	$k_2(OOH^-)/k_2(OH^-)$	$\Delta H^{\ddagger}$ [a]	$\Delta S^{\ddagger}$ [a]
TNM[b]	OH^- [c]	3.51	3,130	16.7 ± 0.3	−4.5 ± 1.0
	OOH^-	11,000		12.6 ± 0.2	−2.8 ± 0.8
Benzonitrile[d]	OH^-	0.00112	65,000	20.5 ± 0.7	−13.0 ± 2.0
	OOH^-	73		22.0 ± 1.0	+5.0 ± 4.0

[a] k_2, l.-mol^{-1} sec^{-1}; $\Delta H^{\ddagger}$, kcal mol^{-1}; $\Delta S^{\ddagger}$, cal deg^{-1}. [b] Solvent, water at 25.14°. [c] Results of D. J. Glover, this laboratory. A detailed report of the kinetics of the OH^-–TNM reaction is in preparation. [d] Solvent, 50% acetone: water, by volume, at 50°. Data of K. B. Wiberg, *J. Amer. Chem. Soc.*, **77**, 2519 (1955).

$$\text{I, II, or III} \xrightarrow{H_2O,\ OH^-} O_2 + HNO_2 \text{ or } HC(NO_2)_3 + ROH$$

Attack of TNM by the nucleophile, OH^- has been postulated to take place at either carbon or nitrogen depending on the hydroxide ion concentration.[24] In strong base, nucleophilic attack by OH^- on nitrogen was suggested to account for the formation of 1 mol each of nitrate and trinitromethide ions, while in dilute base, OH^- attack on carbon was rationalized to account for the formation of 4 mol of nitrite and 1 mol of carbonate ions. The details of the catalytic reaction of nitrite ion with TNM and the kinetic investigation of the hydroxide–TNM reaction will be reported separately by D. J. Glover.[25]

Since *t*-butyl hydroperoxyanion reacts with TNM in basic $H_2{}^{18}O$ to produce almost complete ^{18}O labeling in the nitrite ion to the exclusion of ^{18}O labeling in the *t*-butyl alcohol and O_2 gas, eq 2 and 4, initial nucleophilic attack by the *t*-butyl peroxyanion on the oxygen atom of TNM seems most plausible followed by a subsequent rapid attack by $^{18}OH^-$ on the nitrogen of intermediate, III, to produce the products as indicated

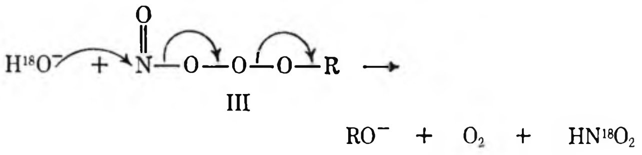

$$H^{18}O^- + N(=O)\text{–O–O–O–R} \longrightarrow RO^- + O_2 + HN^{18}O_2$$

Rationales involving nucleophilic attack by $H_2{}^{18}O$ or $^{18}OH^-$ on various sites of intermediates I or II produce either $R^{18}OH$ or $^{18}O_2$ and labeled or unlabeled nitrate ion and are at variance with experimental evidence.

Alternatively, perhaps the most attractive mechanism involves attack by ROO^- on the oxygen of the nitro group in TNM in a slow equilibrium step

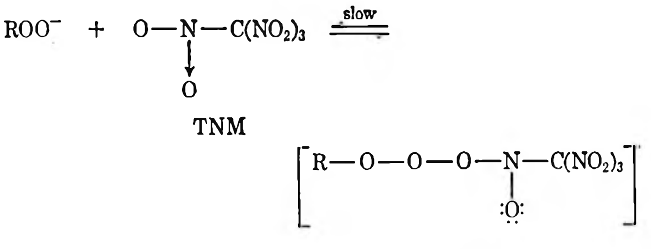

$$ROO^- + O\text{–}N(\rightarrow O)\text{–}C(NO_2)_3 \underset{}{\overset{slow}{\rightleftharpoons}} \left[R\text{–O–O–O–}N(\text{–}\ddot{O}\text{:})\text{–}C(NO_2)_3\right]^-$$

(IV)

A rapid, concerted decomposition of intermediate IV would then form O_2 gas and trinitromethide ion, $C(NO_2)_3{}^-$, as the driving force of the reaction

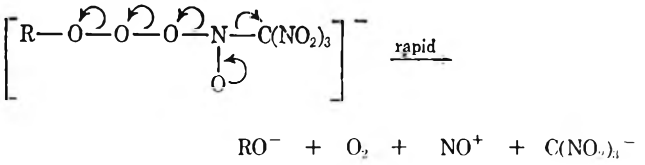

$$[R\text{–O–O–O–N(O)–C}(NO_2)_3]^- \xrightarrow{rapid} RO^- + O_2 + NO^+ + C(NO_2)_3{}^-$$

NO^+ then rapidly reacts with $^{18}OH^-$ to form exclusive labeling in the nitrite, as observed

$$NO^+ + {}^{18}OH^- \xrightarrow{rapid} HN^{18}O_2$$

Besides the convincing $H_2{}^{18}O$ experiments for peroxyanion attack on oxygen, some justification for considering that OOH^- and OH^- ions attack TNM at different sites is derived from a comparison of the activation parameters involving the substrates TNM and benzonitrile, Table VIII. Whereas the rates for nucleophilic attack by OOH^- on both TNM and benzonitrile are greater by a factor of 3 to 65 × 10^3 than rates for OH^- attack,[26] the activation energy for the OOH^-–TNM reaction is about 4 kcal mol^{-1} less than that for the OH^-–TNM reaction. On the other hand, the activation energies for both OOH^- and OH^- reacting with benzonitrile are about the same where attack occurs at carbon. The more positive entropies of activation for nucleophilic attack by OOH^- relative to OH^- has been rationalized[27] as a solvation effect, whereby OOH^- is less solvated than OH^-, thus requiring less reorientation of solvent molecules around OOH^- in the transition state.

With the exception of the hydroperoxyanion, all the alkyl peroxyanions possess positive entropies and have greater activation energies than the hydroperoxyanion in reaction with TNM, Table IX. $\Delta H^{\ddagger}$ is found to vary fairly linearly with $\Delta S^{\ddagger}$, with a slope of 330°K,

---

(24) E. Schmidt, *Ber.*, **52B**, 400 (1919).

(25) D. J. Glover, *J. Phys. Chem.*, **72**, 1402 (1968).

(26) Attributable to the so called "alpha effect;" J. O. Edwards and R. G. Pearson, *J. Amer. Chem. Soc.*, **84**, 16 (1962); T. C. Bruice, A. Donzel, R. W. Huffman, and A. R. Butler, *ibid.*, **89**, 2106 (1967); M. J. Gregory and T. C. Bruice, *ibid.*, **89**, 4400 (1967).

(27) C. A. Bunton in "Peroxide Reaction Mechanisms," J. O. Edwards, Ed., Interscience Publishers, Inc., New York, N. Y., 1962, p 25.

Table IX: Relative Activation Parameters for the Reaction of Alkyl Peroxy Anions with TNM in Water

R-OO⁻	$\Delta\Delta H^{\ddagger}$, kcal mol⁻¹	$\Delta\Delta S^{\ddagger}$, cal deg⁻¹
H–	0	0
$C_6H_5C(CH_3)_2$–	3.5	9.3
i-C_3H_7–	4.3	13.2
t-C_4H_9–	5.1	17.9
C_2H_5–	6.2	19.3

as the isokinetic temperature[28] for the reaction, and implies a single mechanism for peroxyanion attack on TNM.

Although one can readily rationalize on steric grounds the greater activation energies of the alkyl peroxyanions, as a class, relative to the hydroperoxyanion in reaction with TNM, it is somewhat more difficult to explain the ordering among the alkyl peroxyanions themselves. For instance, cumene hydroperoxyanion is the most sterically crowded of the alkyl peroxyanions, and yet has the lowest activation energy for attack on TNM, while just the converse is true for the ethyl peroxyanion. A rationale for these observations is offered in terms of a proposed "activated complex" resulting from nucleophilic peroxyanion oxygen attack on the oxygen of TNM

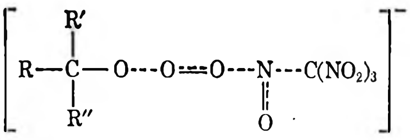

$$\left[\begin{array}{ccccc} & R' & & & \\ & | & & & \\ R- & C & -O\cdots O{=}O\cdots & N & \cdots C(NO_2)_3 \\ & | & & \| & \\ & R'' & & O & \end{array}\right]^-$$

Activated complex

The rather diffuse negative charge distribution in the proposed activated transition state relative to the more oriented and concentrated charge of the peroxyanion in the ground state would account, in part, for the positive entropies observed. Maximum p electron orbital overlap of the peroxyanion oxygen with the nitro oxygen orbital is required in forming the incipient O–O bond at the expense of weakening the old N–C and O–O peroxide bonds. The driving force of the reaction could now arise by the formation of $C(NO_2)_3^-$ ion and O_2 gas, and subsequent reaction of NO^+ with $^{18}OH^-$ as previously outlined.

Examination of molecular models for each of the peroxyanions indicate that the C–C and C–O bond rotations, C–R (R′, R″) and (R)(R′)(R″)–C–O are free and ordinarily do not interfere with the peroxyanion oxygen except in those cases where the R groups are quite bulky as in cumene peroxyanion. Here, rotations about the C–C bonds and especially the C–O bond are somewhat restricted in the ground state and, therefore, less energy and hence, lower $\Delta H^{\ddagger}$ would be required to "freeze out" the proper orientation for maximum oxygen p orbital electron overlap. Conversely, more energy, and greater $\Delta H^{\ddagger}$ would be required for the less sterically crowded ethyl peroxyanion where C–C and C–O bond rotations in the ground state are essentially free. Similar arguments have been offered to explain the $\Delta H^{\ddagger}$ and $\Delta S^{\ddagger}$ values obtained for the decompositions of a series of t-butyl peresters.[29]

Although all the peroxyanions would be expected to be solvated by water, the alkyl peroxyanions, ROO^-, most likely would be solvated about the same extent, but somewhat less than the hydroperoxyanion, HOO^-, where hydrogen bonding to itself as well as to water is possible.

---

[28] J. E. Leffler, *J. Org. Chem.*, **20**, 1202 (1955).

[29] J. E. Leffler and E. Grunwald, "Rates and Equilibria of Organic Reactions," John Wiley & Sons, Inc., New York, N. Y., 1963, pp 358 See also P. D. Bartlett and R. R. Hiatt, *J. Amer. Chem. Soc.*, **80**, 1398 (1958).

X-Ray Diffraction Studies of Mono- and Polynuclear Thorium(IV) Ions in Aqueous Perchlorate Solutions

by **W. E. Bacon and Glenn H. Brown**

Department of Chemistry, Kent State University, Kent, Ohio 44240 *(Received April 21, 1969)*

X-ray diffraction study of aqueous solutions of thorium(IV) oxyperchlorate has established the presence of polynuclear species containing clusters of four thorium atoms. The thorium–thorium distance is 4.00 Å. Thorium(IV) perchlorate in acid media is found to contain mononuclear species. The thorium(IV) has a coordination number of 11 in both thorium(IV) oxyperchlorate and thorium(IV) perchlorate solutions.

Introduction

Solutions of many salts of the actinide elements in water lead to the formation of polynuclear or mononuclear ions.[1] Hydrolysis of these solutions often lead to polynuclear complexes[2-4] containing two or more metal cations linked by hydroxo bridges

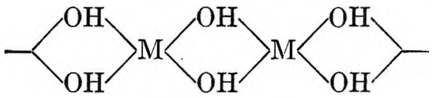

The X-ray crystal structures of the acid-hydrolysis products of thorium(IV) and uranium(IV) salts show the presence of infinite chains of zig-zag rows of the actinide ions situated on alternate sides of a double row of hydroxide ions.[3,4] Similar chains are reported from the crystal structure determination of $Th(OH)_2(NO_3)_2xH_2O$ by Johansson.[5]

Dinuclear species were recently shown to form in aqueous solutions of basic thorium nitrate.[5] In light of the interesting papers which we have cited, it seemed of interest to investigate the structure of concentrated aqueous solutions of thorium(IV) perchlorate and thorium(IV) oxyperchlorate. The radial distribution method was used to interpret the data obtained from the scattering of X-rays by the respective solutions as a function of the scattering angle (2θ).

Experimental Procedures

Method of Handling Data. The radial distribution method[6] of analysis of the X-ray diffraction data as applied to polyatomic liquids was used throughout this investigation. Radial distribution functions were calculated using the Waser and Schomaker[7] modification functions.

Materials. The samples of thorium(IV) perchlorate were prepared by heating Baker and Adamson reagent grade thorium(IV) nitrate tetrahydrate with an excess of 70% perchloric acid employing the method of Kolthoff and Ikeda.[8] The solution process was continued at 100–125° until the solid residue contained the theoretical amount of thorium for thorium(IV) perchlorate. The thorium content was established by titration with EDTA.[9] Solutions of thorium(IV) perchlorate were prepared by weight in a drybox; a dry atmosphere was necessary because of the hydroscopic nature of the perchlorate. The acidity of the solution was determined by titration with standard sodium hydroxide. The compositions of solutions used in this study are recorded in Table I.

Thorium(IV) oxyperchlorate was prepared by the method of Murthy and Patel;[10] thorium(IV) perchlorate hydrate was heated at 275–285° until the thorium content matched the theoretical amount of thorium in thorium(IV) oxyperchlorate.

Apparatus. All X-ray diffraction data were collected using a Picker X-ray Instrument Model No. 6238E equipped with a θ–θ diffractometer. The diffractometer had the Bragg–Brentano parafocusing arrangement. Molybdenum radiation at 36 kV, 20 mA was monochromated by use of a matched filter system of zirconium metal and yttrium foil and a pulse-height analyzer. The time-count-diffraction angle data were recorded from a digital printout for step-scan increments of $^4/_{15}$°, up to 28°, 1° increments from 28 to 40°, and 2° increments from 40 to 110° of the scattering angle, 2θ. Scatter and divergence slits of 0.1, 0.4, and 1° were used with these step-scan increments, respectively. Scaling factors to convert all measured data to the same slit opening were obtained from measurements in overlapping regions.

---

(1) J. J. Katz and G. T. Seaborg, "The Chemistry of the Actinide Elements," John Wiley & Sons, Inc., New York, N. Y., 1957, p 52.

(2) G. Lundgren and L. G. Sillen, *Ark. Kemi*, **1**, 277 (1949).

(3) G. Lundgren, *ibid.*, **2**, 535 (1950).

(4) G. Lundgren, *ibid.*, **4**, 421 (1952).

(5) G. Johansson, *Svensk Kem. Tidskr.*, **78**, 9 (1966).

(6) R. F. Kruh, *Chem. Rev.*, **62**, 319 (1962).

(7) J. Waser and V. Schomaker, *Rev. Mod. Phys.*, **25**, 671 (1953).

(8) I. M. Kolthoff and S. Ikeda, *J. Phys. Chem.*, **65**, 1020 (1961).

(9) H. A. Flaschka, "EDTA Titrations, An Introduction to Theory and Practice," Pergamon, New York, N. Y., 1959, p 81.

(10) P. R. Murthy and C. C. Patel, *Indian J. Chem.*, **3**, 134 (1955).

Table I: Composition of Solutions

No.	Compound	d_4^{20}	Atom ratio per thorium Th	 Cl	 O	 H
1	$ThO(ClO_4)_2$	2.5016	1.00	2.04	19.50	21.11
2	$ThO(ClO_4)_2$	2.5812	1.00	2.05	17.50	16.70
3	$ThO(ClO_4)_2$	2.7017[a]	1.00	2.13	17.33	15.77
4	$Th(ClO_4)_4$	2.3288[b]	1.00	5.17	25.80	11.30
5	$Th(ClO_4)_4$	2.3558[a]	1.00	4.75	22.30	7.68

[a] Crystals precipitated after standing 1 week. [b] Solvent is 1.0 *M* perchloric acid.

The cell holder was machined from Plexiglas and the X-radiation was scattered from the free surface of the stationary sample contained in a tray. The tray was enclosed in a Plexiglas cover with walls about 2 mils thick. The enclosure preserved the composition of the solutions.

Procedure. All diffraction data were recorded as the time necessary for a fixed number of counts (100,000) for each scattering angle measured. The initial step in treatment of the data is the conversion of the time-count record of X-ray intensities to a common basis, counts per second. The averaging of these intensity data for replicate samples included six or seven samples at a given concentration. These data were then corrected for absorption,[11] instrument background count, and polarization. Diffraction by the Plexiglas cover could be ignored since both the incident and measured beams were always perpendicular to the section of the cover which they intersected. The coherent scattering factors for thorium and chlorine were corrected for dispersion.[12] The incoherent scattering factors for thorium were calculated by the method of Bewelogua.[13] The measured intensities after correction were normalized to the theoretical intensities calculated for a stoichiometric unit of solution containing one thorium atom. The corrected experimental intensity data were normalized using the methods of Krogh-Moe[14] and Norman.[15]

The normalized experimental intensity has units of electron volts based on the theoretical independent atomic scattering, $\Sigma_i f_i^2(s)$, from a stoichiometric unit of solution containing one thorium atom. The summation is over the atoms contained in this unit. A reduced intensity function based upon this unit was obtained from

$$si(s) = s[I(s) - \Sigma f_i^2(s)]M(s) \qquad (1)$$

Here $I(s)$ represents the observed scattering after correction and the quantity in the brackets represents the interatomic part of the scattered intensity in electron volts. $M(s)$, a modification function, is included to sharpen the distribution function obtained by Fourier inversion.[7] This function has the effect of removing some of the breadth arising from the characteristic electron distribution of the atoms. The modification function used in this work is

$$M(s) = [f_{Th}^{(0)}/f_{Th}(s)]^2 \exp(-bs)^2 \qquad (2)$$

where f_{Th} is the form factor for thorium and $f_{Th}^{(0)}$ is its value at $s = 0$. Here s, Å^{-1} is defined as $4\pi \sin \theta/\lambda$ and the scattering angle is 2θ. The exponential assures convergence of the Fourier integral over the accessible range of s,Å^{-1}. The particular modification function used in this study was of a form similar to the one employed by Levy, Danford, and Agron.[16]

The radial distribution function expressed in units of electrons squared per ångstrom was calculated from the following equation

$$D(r) = 4\pi r^2 \rho_0 + 2r/\pi \int_0^{s_{max}} si(s) \sin srds \qquad (3)$$

where ρ_0 is the average scattering density of the solution in units of electrons squared per unit volume, and s_{max} is the upper limit of integration. $D(r)$ represents a superposition of modified pair distribution functions for the various kinds of atom pairs. The modification of a given pair distribution function ρ is expressed by Waser and Schomaker[7]

$$D_{ij}(r) = 4\pi r \int_{-\infty}^{+\infty} \mu \rho_{ij}(\mu) T_{ij}(\mu - r) d\mu \qquad (4)$$

with

$$T_{ij}(r) = \frac{1}{\pi} \int_0^{s_{max}} f_i f_j M(s) \cos(sr) ds \qquad (5)$$

and f_i and f_j being the form factors for atoms of kind i and j. The function $T_{ij}(r)$ is the so-called shape function.[7]

Results

Aqueous Solution of Thorium(IV) Oxyperchlorate. The measured intensity curve after correction for instrument background noise, polarization, and Compton scattering is shown in Figure 1, for a 3.95 *M* solution of thorium(IV) oxyperchlorate plotted as a function of

---

(11) M. E. Milberg, *J. Appl. Phys.*, **29**, 64 (1958).

(12) C. H. Dauben and D. H. Templeton, *Acta Crystallogr.*, **8**, 841 (1955).

(13) L. Bewelogua, *Phys. Z.*, **32**, 740 (1931).

(14) J. Krogh-Moe, *Acta. Crystallogr.*, **9**, 951 (1956).

(15) N. Norman, *ibid.*, **10**, 370 (1957).

(16) H. A. Levy, M. D. Danford, and P. A. Agron, *J. Chem. Phys.*, **31**, 1458 (1959).

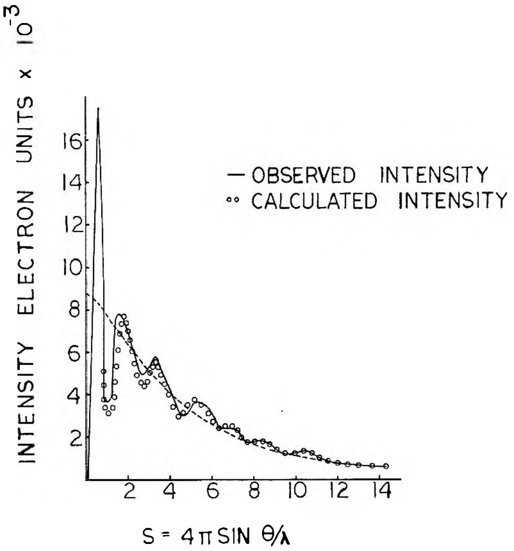

Figure 1. Observed and calculated intensity curves for a solution of $ThO(ClO_4)_2$. The circles represent the calculated intensities for $Th_4(OH)_6^{10+}$. The dotted line is independent atomic scattering.

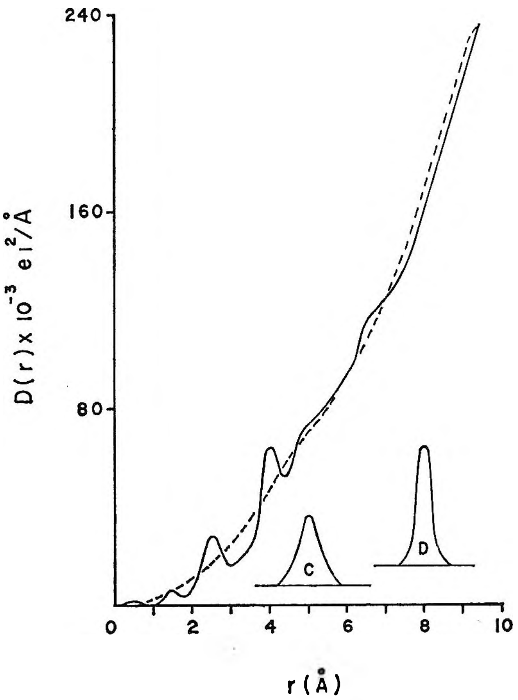

Figure 2. X-Ray radial distribution function for a solution of $ThO(ClO_4)_2$.

s,$Å^{-1}$. The dotted line indicates the theoretical independent atomic scattering calculated for a unit of solution containing one thorium atom. The radial distribution curve calculated from eq 3 is shown in Figure 2. The three maxima occur at distances of 1.50, 2.50, and 4.00 Å. The radial distance of 1.50 Å represents the bond distance of Cl–O in the perchlorate ion. This distance is reported as 1.49 Å in ammonium perchlorate[17] and 1.47 Å in potassium perchlorate.[18] The peak at the radial distance of 2.50 Å is equivalent to the Th–O bond distance reported for basic thorium sulfate[3] and chromate.[4] This distance is slightly shorter than the 2.6 Å for the Th–O interaction in thorium oxide–thorium nitrate solutions reported by Johansson.[19]

In addition to the Th–O interactions within the area beneath the 2.50 Å peak the O–O interactions from the perchlorate ion,[20] reported at 2.40 Å, and from water[16] at 2.70 Å are included. The contribution of these interactions to the area can be calculated from eq 5, and the stoichiometry of the solution, Table I, No. 1, considering the tetrahedral structures of the perchlorate ion and the water molecule. Curve C, Figure 2, represents the total contribution of the O–O interactions from the perchlorate ion, the water molecule and eleven Th–O interactions per Th atom. This indicates a coordination number of eleven for thorium similar to thorium(IV) nitrate pentahydrate[21] and the basic thorium(IV) nitrate.[19]

The peak in the radial curve at 4.00 Å is attributed to Th–Th interactions. This bond distance is very nearly the same as that found in crystals of basic thorium salts in which two thorium atoms are bonded by a double hydroxo bridge.[3,4,19] The radial distribution curves for basic thorium(IV) nitrate in solution also show a sharp peak at 4.00 Å assigned to Th–Th interactions.[19] Curve D of Figure 2 shows the peak shape and size, computed from eq 5, to be expected from three Th–Th interactions at a single sharp separation. Comparison with the radial distribution curve shows that the thorium atoms in the solution complex must be arranged at a specific distance and the number of Th neighbors at 4.00 Å is 3. The geometric figure which can describe three first neighbor Th–Th interactions per Th at equal distance is a tetrahedron with each corner occupied by a Th atom. The Th atoms are linked together by hydroxo bridges. A model assumed for $Th_4(OH)_6^{10+}$ may be constructed by joining each thorium atom with an OH group along the edge of the tetrahedral arrangement with the Th–O distance of 2.50 Å and Th–Th distance of 4.00 Å.

Theoretical Intensity Function. In an effort to check the proposed model further, a detailed analysis was undertaken to calculate the theoretical intensity curve of the model for comparison with the experimental curve. Theoretical intensity curves for the arrangement corresponding to the intramolecular part of the intensity were calculated from the equation

$$I(s) - \sum_i f_i^2 = \sum_i \sum_{\substack{j \\ i \neq j}} f_i f_j \exp(-b_{ij}s^2) \frac{\sin sr_{ij}}{sr_{ij}} \qquad (6)$$

---

(17) C. Gattfried and C. Schusterius, *Z. Kristallogr.*, **84**, 65 (1932).

(18) N. V. Mami, *Proc. Indian Acad. Sci.*, **46A**, 143 (1957).

(19) G. Johansson, *Acta Chem. Scand.*, **22**, 399 (1968).

(20) F. S. Lee and G. B. Carpenter, *J. Phys. Chem.*, **63**, 279 (1959).

(21) T. Ueki, A. Zalkin, and D. H. Templeton, *Acta Crystallogr.*, **20**, 836 (1966).

where r_{ij} is the distance separating atoms i and j of the model, and b_{ij}, the temperature factor coefficient, is one-half the mean square variation in r_{ij}. Interatomic distances shown in Table II, were calculated from the coordinates of the atoms. The intensities calculated from the model were then normalized to the experimental intensities, *i.e.*, to a stoichiometric unit of solution containing one thorium atom. The comparison of the calculated and the experimental intensities is shown in Figure 1. The calculated and experimental curves show good agreement at high values of s. At smaller values, the curves deviate because the contribution from intermolecular interactions are omitted from the model.[16]

Table II: Distance and Number of Interactions for the Model of $Th_4(OH)_6^{10+}$

d, Å		N
	Th–O	
2.50		12
4.58		12
	Th–Th	
4.00		6
	O–O	
3.49		9
4.49		3
5.28		3

The tetrahedral model may arise by a combination of two dinuclear complexes similar to those found by Johansson in basic thorium(IV) nitrate solutions;[19] however, this point awaits evidence. Although the Th–Th distance of 4.00 Å is close to that found in the cubic ThO_2 structure, 3.96 Å, it does not appear related to this structure in which the Th atoms have a face-centered arrangement.

The linear complexes such as are found in the basic thorium salts,[3,4] *i.e.*, $Th(OH)_2SO_4$ and $Th(OH)_2CrO_4 \cdot H_2O$, are not evident in the thorium(IV) oxyperchlorate solution. The size of the 4.00-Å peak and the absence of a second distance at 6.00 Å indicate that linear complexes do not form.

Thorium(IV) Perchlorate in Perchloric Acid Solution. A 2.79 M solution (Table I, No. 4) was investigated by the same procedure used for thorium(IV) oxyperchlorate. The purpose of the study is to determine if polynuclear species are present.

The radial distribution curve calculated from eq 3 is shown in Figure 3. The two maxima, one at 1.50 Å and the other at 2.50 Å, correspond to the Cl–O and the Th–O interactions, respectively. The latter peak corresponds to the average Th–O distance reported in the X-ray crystal structure data of thorium(IV) nitrate pentahydrate as Th–O (nitrate) distance of 2.57 Å and Th–O (water) distance of 2.46 Å.[21] The absence of a peak at 4.00 Å indicates the thorium species is mononuclear. In addition to the Th–O interactions at 2.50 Å, the O–O interactions from the perchlorate ion and the solvent are also included. Thus, to calculate the coordination number of the thorium atom, it is necessary to subtract the area due to the O–O interactions as was done for the thorium(IV) oxyperchlorate solutions. The area due to the O–O interactions was calculated with eq 5, considering the tetrahedral structures of the perchlorate ion and water along with the stoichiometry of the solution from Table I. The difference between this area and the area beneath the 2.50-Å peak is equivalent to 11 Th–O interactions. The total area calculated from eq 5, for the O–O interactions and 11 Th–O interactions is shown as the insert curve in Figure 3.

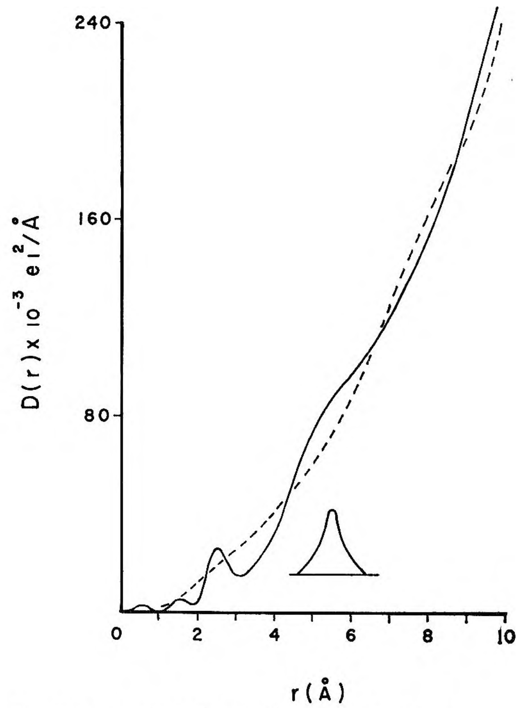

Figure 3. X-Ray radial distribution function for a solution of $Th(ClO_4)_4$.

Two studies which support the conclusion of the mononuclear species are by Hentz and Johnson[22] and by Larsen and Brown.[23] From ultracentrifugation studies of thorium(IV) perchlorate in perchlorate media, Hentz and Johnson support the presence of the mononuclear thorium(IV) species.[22] The investigation of thorium(IV) nitrate in acidic media using X-ray techniques showed only mononuclear thorium(IV) species.[23]

Acknowledgments. The authors wish to thank Dr. Richard J. De Sando, Monsanto Research Corp., Miamisburg, Ohio, and Dr. L. W. Gulrich, E. I. du Pont de Nemours Co., Wilmington, Del., for their helpful discussions and interest in this work.

---

(22) F. C. Hentz, Jr., and J. S. Johnson, *Inorg. Chem.*, **9**, 1337 (1966).

(23) R. D. Larsen and G. H. Brown, *J. Phys. Chem.*, **68**, 3060 (1964).

Free Radical Formation in Hydrocarbon Crystals by γ Irradiation.

Electron Spin Resonance Spectra of Some Alkyl Radicals

by **Thomas Gillbro,**

Section for Nuclear Chemistry, AB Atomenergi, Studsvik, Nyköping, Sweden

Per-Olof Kinell, and Anders Lund

The Swedish Research Council's Laboratory, Studsvik, Nyköping, Sweden *(Received April 22, 1969)*

Single crystals and polycrystalline samples of the *n*-alkanes, pentane, hexane, heptane, nonane, decane, and undecane, were prepared by a freezing technique. The crystals were irradiated at 77°K with ^{60}Co γ rays to a dose of 3 Mrads. Electron spin resonance in the X band and Q band demonstrated that $CH_3-CH-CH_2-R$ is the predominant radical species in all hydrocarbons except for undecane. The measured coupling constants found are the isotropic $a_1 = 25 \pm 1$ G (quartet), $a_2 = 33 \pm 1$ G (triplet), and the orientation dependent doublet splitting $a_3 = 12.5 - 33$ G. A complexity in the central region of the spectrum from undecane is thought to indicate the presence of additional alkyl radicals. Cleavage of the carbon chain is improbable. An irreversible decrease in line width with temperature has been explained in terms of a disappearance of the dipolar interaction between radicals some 30 Å apart. In single crystals indications of radical pair formation have been found.

Introduction

Radicals formed by the action of ionizing radiation in various hydrocarbons in the pure state have been extensively studied both from the point of view of their paramagnetic behavior[1-6] and with respect to their role in forming final radiolysis products.[7] An increased knowledge has been obtained regarding the formation of ionic and excited states in hydrocarbons and their decay and fragmentation pattern.[8-10] Some studies have also been made on saturated hydrocarbons adsorbed on solid inorganic supports.[11,12]

Esr spectra obtained after irradiation of polycrystalline samples often exhibit broad overlapping lines.[1-3,6] This makes it rather difficult and in many cases almost impossible to assign the lines correctly. In the liquid state, the anisotropies of the g and the hyperfine coupling tensors are averaged out and well-resolved lines may accordingly be observed. Thus Fessenden and Schuler[4,5] have unambiguously identified a series of radicals formed from hydrocarbons in the liquid state. In the single crystal state the radicals are located at specific sites in the unit cell and are related by the symmetry of the lattice. The esr spectrum will then be rather simple, but it will change with the orientation of the crystal axes with respect to the magnetic field direction. By rotating the crystal it is possible to determine the elements of the g and the hyperfine coupling tensors.

The present study is concerned with radical formation in some solid alkanes. It was initiated in connection with an investigation of the radiolysis of hexane in the adsorbed state.[11,12] Because of the broadness of the esr lines in this case, no final assignments of the spectra could be made. The only species identified was an ethyl radical which appeared at intermediate coverages.[12] It seems likely that the mobility of molecules in the adsorbed state can differ from that in the pure liquid and pure solid states.[13,14] A knowledge of the radical structure in solid hydrocarbons was therefore judged to be a valuable complement to the knowledge obtained from the liquid state[4,5] in making assignments of the spectra from the adsorbed hydrocarbons. In the present study, single crystals of alkanes were prepared. Irradiation gave rise to spectra with resolutions which permitted unambiguous assignments. Spectra from polycrystalline samples, however, could not easily be analyzed.

The action of ionizing radiation produces a heterogeneous distribution of regions (spurs, blobs, short

---

(1) B. Smaller and M. S. Matheson, *J. Chem. Phys.*, **28**, 1169 (1958).

(2) A. V. Topchiev, "Radiolysis of Hydrocarbons," Elsevier, Amsterdam, 1964.

(3) P. B. Ayscough, A. P. McCann, C. Thomson, and D. C. Walker, *Trans. Faraday Soc.*, **57**, 1487 (1961).

(4) R. W. Fessenden and R. H. Schuler, *ibid.*, **33**, 935 (1960).

(5) R. W. Fessenden and R. H. Schuler, *ibid.*, **39**, 2147 (1963).

(6) F. Thyrion, J.-P. Dodelet, C. Fauquenoit, and P. Claes, *ibid.*, **65**, 227 (1968).

(7) T. Gäumann and J. Hoigné, Ed., "Aspects of Hydrocarbon Radiolysis," Academic Press, London, 1968.

(8) R. E. Rebbert and P. Ausloos, *J. Chem. Phys.*, **46**, 4333 (1967).

(9) P. Ausloos and S. G. Lias, *Ber. Bunsenges. Phys. Chem.*, **72**, 187 (1968).

(10) P. Ausloos and S. G. Lias, *Radiat. Res. Rev.*, **1**, 75 (1968).

(11) P.-O. Kinell and G. Adolfsson, unpublished results.

(12) P.-O. Kinell, A. Lund, and T. Vänngård, *Acta. Chem. Scand.*, **19**, 2113 (1965).

(13) D. E. Woesner, *J. Phys. Chem.*, **70**, 1217 (1966).

(14) H. Winkler and H. Pfeifer, paper presented at XVth Colloque A.M.P.E.R.E., Grenoble, 1968.

tracks) containing primary species.[15] Initially, the species are in fairly close proximity to each other but with time they experience radial diffusion. In a solid the diffusion process is rather slow. The high local concentration of radicals formed by fragmentation of the primary species is therefore likely to be maintained for a considerable period of time if the temperature is kept suitably low. Thus it has been observed[16] that radicals can occur in pairs separated by a distance of 5–10 Å. Differences in the mechanism of pair formation may occur, depending upon the nature of the molecules and their arrangement in the crystal structure. The elucidation of their formation may, however, yield a contribution to the understanding of the structure of the primary regions. In the present study, radical pairs have been observed in single crystals of some of the *n*-alkanes. This observation has also been made in single crystal studies of certain vinyl compounds.[17] Dipolar interaction between radicals situated 15–30 Å apart can lead to line broadening in the esr spectra; such radicals will diffuse away from each other upon annealing and from the thermally irreversible decrease in line width, the original mean distance between them can be estimated. Evidence for such effects was obtained in the present study.

Experimental Section

The following normal hydrocarbons were used: pentane, hexane, heptane, nonane, decane, and undecane. Pentane and heptane of *pro analysi* and *purissimum* grade (minimum 99 mol% pure) were obtained from AB Kebo, Stockholm. The hexane was taken from a 99.96 mol% pure fraction (Phillips Petroleum Co.). Nonane, decane, and undecane with purities of 99.68, 99.34, and 99.33 mol%, respectively, were supplied by Fluka AG.

The hydrocarbons were transferred to Suprasil quartz tubes with an outer diameter of 4 mm. The samples were degassed and sealed under vacuum. For single crystal preparation the bottom of the tubes extended to form a thin capillary tube. The sample was lowered with a speed of 1.5–4 mm/hr into a cooling bath maintained 5–20° below the melting point of the hydrocarbon. In this way, it was possible to obtain a transparent solid. The sample was then slowly cooled to 77°K. During this operation the solid became opaque, suggestive of intracrystalline fracture. Crystals of hexane, nonane, decane, and undecane were prepared. Polycrystalline samples were obtained from the degassed hydrocarbons by rapid freezing to 77°K.

Samples were irradiated at 77°K with ^{60}Co γ rays to a dose of normally 3 Mrads at a dose rate of 180 krads/hr. In a special study of line broadening effects in decane, a range up to 15 Mrads was covered. The spectra were recorded at 77°K with a Varian V-4502-11 X-band spectrometer. The magnetic sweep was calibrated using the known splittings in the $NO(SO_3)_2^{2-}$ radical. The crystalline samples could be rotated around the tube axis, perpendicularly to the magnetic field direction. Selected samples thus mounted exhibited well-resolved spectra with anisotropic lines, showing that the radicals were trapped in an ordered environment. Some of the samples were warmed by a nitrogen stream passed through a double-walled quartz tube placed in the cavity, until the signal strength began to decay rapidly. This occurred 1–5° below the melting points of the hydrocarbons. The samples were then cooled to 77°K and the esr spectra were recorded again. The spectra of some polycrystalline samples were recorded at Q band with a Varian V-4503 spectrometer.

Crystal Structure

The crystal structures of the lower hydrocarbons have been determined by Norman and Mathisen.[18] Hexane, octane, and decane form triclinic crystals with one molecule in the unit cell. The space group is P$\bar{1}$ for hexane and octane and probably also for decane. The carbon chain is planar and the molecules contain a center of symmetry. Of the odd-numbered alkanes, heptane and nonane form triclinic crystals with two molecules in the unit cell; they probably belong to the space group P$\bar{1}$. Undecane crystallizes with orthorhombic symmetry, the unit cell containing four molecules. The carbon chains extend along the *c* axis. Pentane also crystallizes in the orthorhombic system, space group Pbcn, with four molecules in the unit cell. The carbon chains are not parallel to the c axis or to each other.

Results

Single Crystal Spectra. Hexane. Two of the first derivative spectra recorded at 77°K from a hexane single crystal are shown in Figure 1. The separation between the outermost lines is at a maximum in Figure 1a. The *g* factor has the value of about 2.0020 in this and in the other hydrocarbons investigated. The *g*-tensor anisotropy is negligible at the X band. The stick plot shown is a reconstruction with couplings a_1 = 25.9 G (quartet), a_2 = 33.6 G (triplet), and a_3 = 33.2 G (doublet). Binominal intensities of the lines were assumed. Using these coupling constants, the spectrum in Figure 1a′ was simulated on a computer.

The spectrum represented in Figure 1b was recorded with the sample rotated about the vertical axis through an angle of 90° from the first orientation. In this case a minimum in the overall spectral width was observed.

A stick plot analysis shows that the spectrum can be accounted for by the following coupling constants; a_1 =

---

[15] A. Mozumder and J. L. Magee, *Radiat. Res.*, **28**, 203 (1966).

[16] Y. Kurita, *J. Chem. Phys.*, **41**, 3926 (1964).

[17] T. Gillbro, P.-O. Kinell, and A. Lund, to be published.

[18] (a) N. Norman and H. Mathisen, *Acta Chem. Scand.*, **15**, 1747-1755 (1961); (b) *ibid.*, **18**, 353 (1964); (c) Central Institute for Industrial Research, Final Technical Report. Publication No. 334, Blindern, Oslo, 1961.

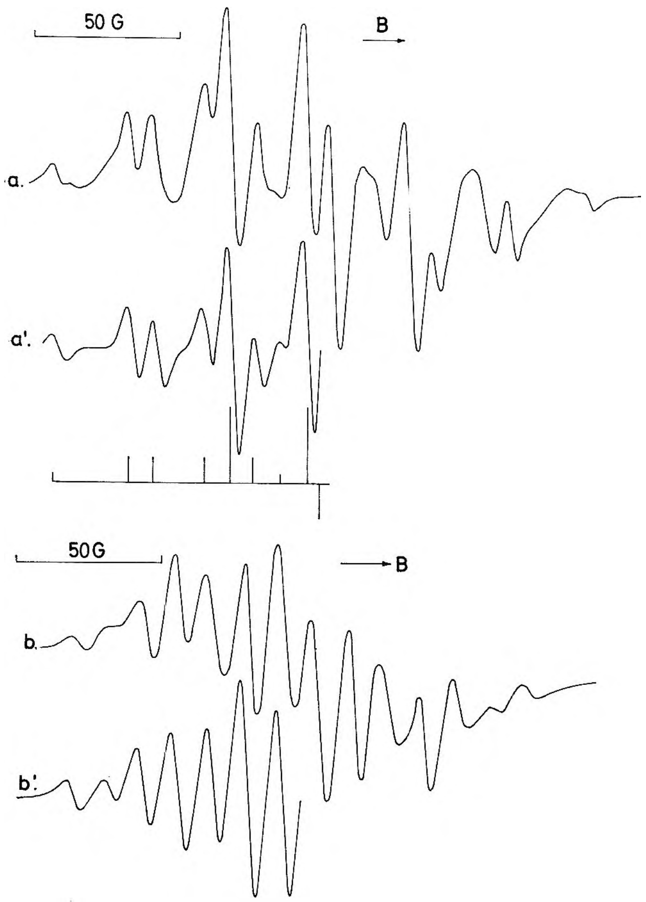

Figure 1. Esr spectra at 77°K from γ-irradiated *n*-hexane single crystals rotated at different angles around a vertical axis (a) with the field direction corresponding to maximum overall separation $\theta' = 0°$, (*b*) $\theta' = 90°$. a' and b' are calculated line shapes for the 2-hexyl radical with a line width ΔH_{pp} measured between the maximum and the minimum of the derivative line: (a') $a_1 = 25.9$ G (quartet), $a_2 = 33.6$ G (triplet), $a_3 = 33.2$ G (doublet), $\Delta H_{pp} = 5$ G (Gaussian shape); (b') $a_1 = 23.8$ G, $a_2 = 34.3$ G, $a_3 = 12.5$ G, $\Delta H_{pp} = 5.5$ G (Lorentzian shape).

23.8 G (quartet), $a_2 = 34.3$ G (triplet), and $a_3 = 12.5$ G (doublet). Good agreement is obtained in a line shape simulation with these parameters, Figure 1b'.

With the sample rotated through intermediate angles about the vertical axis, spectra were less well resolved. This made it difficult to measure the angular variation of the coupling constants. The reason for the large line width, $\Delta H_{pp} = 7$ G, may be a slight change in the orientation of the crystal parts obtained when the original crystal cracks during the cooling before irradiation. Clearly the maximum broadening by a mosaic structure will occur when the splitting varies most rapidly with the orientation.

Attempts to prepare crystals with a different orientation in the ampoule were unsuccessful. In all cases, the same angular variation was observed, indicating a preferential growth along the same crystal direction in the sample tube.

Nonane. The spectra from irradiated nonane are less completely resolved than those from hexane, as is illustrated in Figure 2, which shows the line shape at an orientation corresponding to maximum separation. Splitting constants used are of the same magnitude as those for the spectrum from hexane at maximum total width, *i.e.* $a_1 = 25.5$ G, $a_2 = a_3 = 33.5$ G, and are in reasonable agreement with the experimental spectrum, as is illustrated by the stickplot diagram. At other orientations the resolution is poor, which indicates the presence of several species with overlapping spectra.

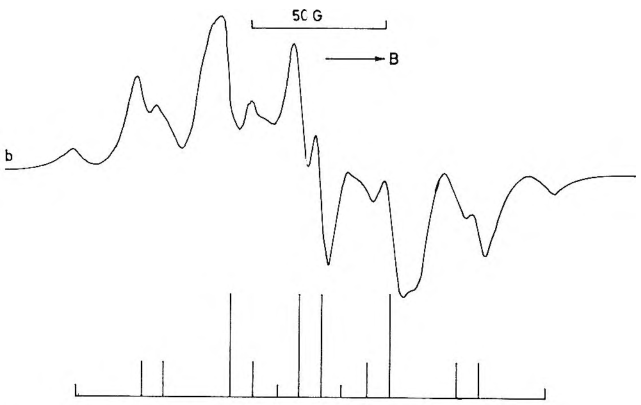

Figure 2. Esr spectrum from single crystal nonane, conditions as described in Figure 1, $\theta' = 0°$.

Decane. The spectrum from irradiated crystals of decane recorded at 77°K with the maximum separation between the outermost lines is shown in Figure 3a. This line shape is clearly very similar to that observed for hexane, Figure 1a, and the parameters $a_1 = 25.6$ G (quartet), $a_2 = 33.3$ G (triplet), and $a_3 = 33.3$ G (doublet) fit the experimental spectrum quite well as is shown by Figure 3a'. A sextet structure with $a_2 = 33.3$ G (quintet) and $a_3 = 33.3$ G (doublet) as in Figure 3a' seems to make a rather small contribution. The spectrum in Figure 3b is obtained when the doublet splitting, $a_3 = 13.2$ G, is at a minimum while $a_1 = 23.7$ G and $a_2 = 34.2$ G.

A better resolution was obtained after warming the sample to a temperature a few degrees below the melting point. The intensity of the absorption diminishes and the intensity is only 0.01 of the original in the spectrum shown in Figure 4, recorded at 77°K. The spectra which exhibited the maximum and minimum splitting when the sample was rotated about the vertical axis are shown in Figure 4a and b, respectively. For the simulated spectrum in Figure 4a' the values are $a_1 = 25.6$ G, $a_2 = 33.3$ G, and $a_3 = 33.3$ G, while in Figure 4b' the values are $a_1 = 23.7$ G, $a_2 = 34.2$ G, and $a_3 = 13.2$ G. As in the case of hexane, a_1 and a_2 are approximately constant, while the doublet splitting value varies with the angle θ as shown in Figure 5.

Undecane. In the direction which exhibits maximum total separation, Figure 6, the spectrum from undecane, has the same overall width and the corresponding main lines on the wings as the spectrum from decane, Figure

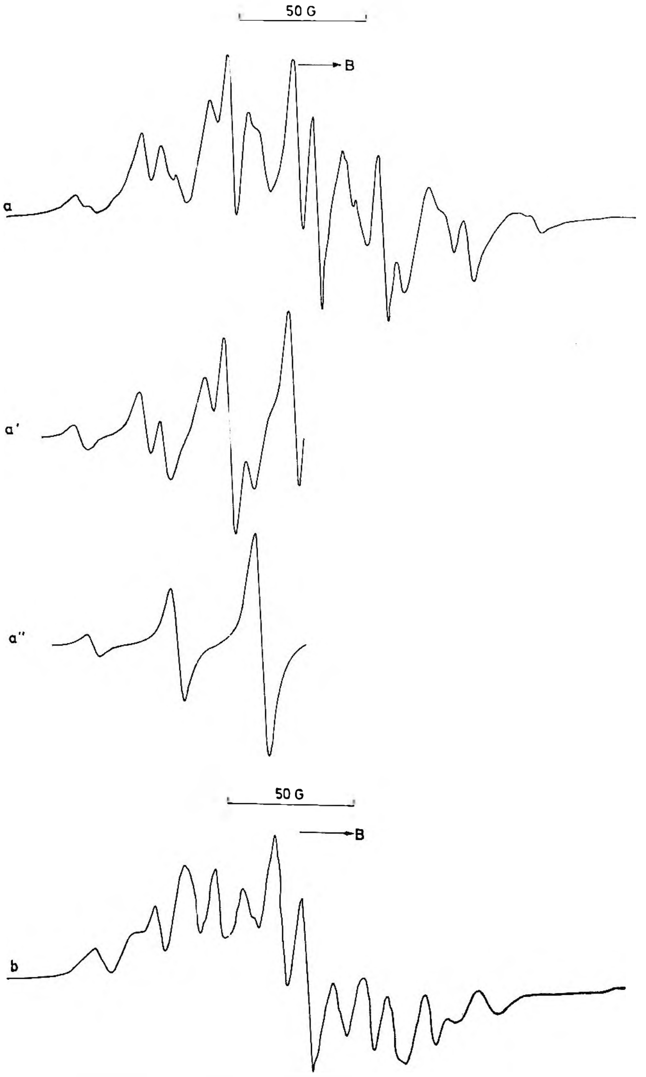

Figure 3. Esr spectrum from single crystal decane, conditions as described in Figure 1, (a) $\theta' = 0°$, (b) $\theta' = 90°$, (a') calculated spectrum with $a_1 = 25.6$ G, $a_2 = 33.3$ G, $a_3 = 33.3$ G, $\Delta H_{pp} = 4.9$ G (Lorentzian shape), (a'') calculated spectrum with $a_2 = 33.3$ G (triplet), $a_3 = 33.3$ G (doublet), $\Delta H_{pp} = 4.9$ G (Lorentzian shape).

4a, but in the central region the components differ considerably. At other orientations, the resolution is so poor that as yet no analysis has been possible.

Spectra from Polycrystalline Samples. The appearance of the spectra at 77°K changes gradually through the series from pentane to undecane, as is illustrated in Figure 7 for the C_5, C_{10}, and C_{11} hydrocarbons. When the samples were annealed as described in the experimental section, irreversible changes in the line shapes occurred, the effect being most pronounced in undecane, Figure 7c. After annealing, the spectra were quite similar to each other. In the case of pentane and hexane, neither the number of components nor their relative intensities exhibit noticeable change. There, is, however, an appreciable improvement in the resolution, which could be studied in some detail in the spectrum from powdered hexane. Figure 8a and b

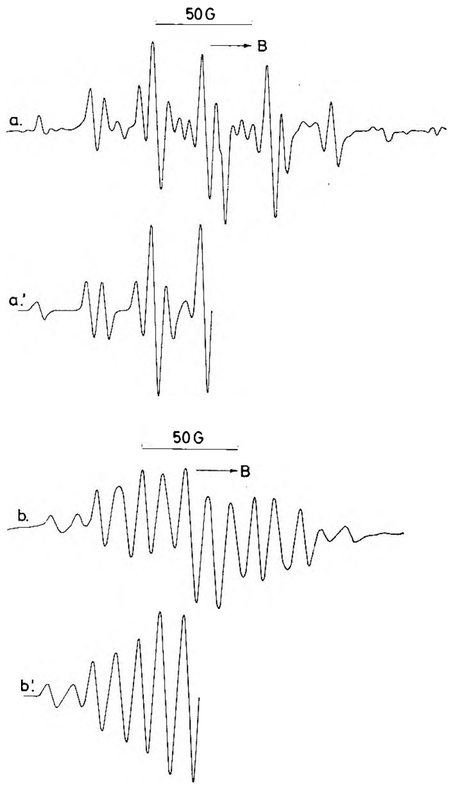

Figure 4. Esr spectrum from the same sample used in Figure 3 at 77°K after annealing, (*a*) $\theta' = 0°$, (b) $\theta' = 90°$, calculated spectra (a') $a_1 = 25.6$ G, $a_2 = 33.3$ G, $a_3 = 33.3$ G, $\Delta H_{pp} = 3.8$ G (Gaussian shape), (b') $a_1 = 23.7$ G, $a_2 = 34.2$ G, $a_3 = 13.2$ G, $\Delta H_{pp} = 4.7$ G (Gaussian shape).

shows the X- and Q-band spectra from an annealed sample recorded at 77 and 90°K, respectively. The line shape at Q band has a pronounced asymmetry. The profiles of the outermost lines, magnified in the recorded spectra, are also different at the two wavelengths.

Line Shape Simulation. An analysis was attempted on the line profiles obtained from the powder spectra of thermally annealed hexane, Figure 8. The outermost lines were expected to resemble those of a CH fragment contained in a rigid matrix. Line shapes for this fragment were synthesized using the computer program prepared by Lefebvre and Maruani.[19] Typical values of the proton coupling tensor were used,[19-21] and the influence of the direct field on the nucleus[19] was included. It proved difficult to reproduce the experimental shape, particularly at the Q band. In this case the *g*-tensor anisotropy must also be included. The degree of resolution, which approximately corresponds to a single crystal line width of 3.5 G, is insufficient to allow an experimental determination of the tensor

---

(19) R. Lefebvre and Y. Maruani, *J. Chem. Phys.*, **42**, 1480 (1965).

(20) H. Fischer, "Magnetic Properties of Free Radicals, Landolt–Bornstein. Numerical Data and Functional Relationships in Science and Technology," New Series, Group 2, Vol. 1. Springer-Verlag, Berlin, 1965.

(21) J. R. Morton, *Chem. Rev.*, **64**, 453 (1964).

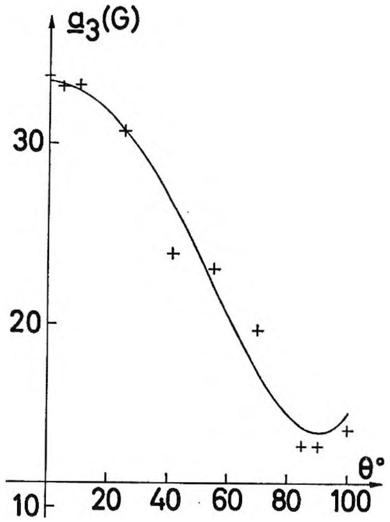

Figure 5. Angular dependence of a_3 from the sample used in Figure 4 with the crystal rotated at different angles θ relative to the vertical axis. The solid line represents a least-square fit of the experimental points to the relation $a_3^2 = \alpha + \beta \cos 2\theta + \gamma \sin 2\theta$.

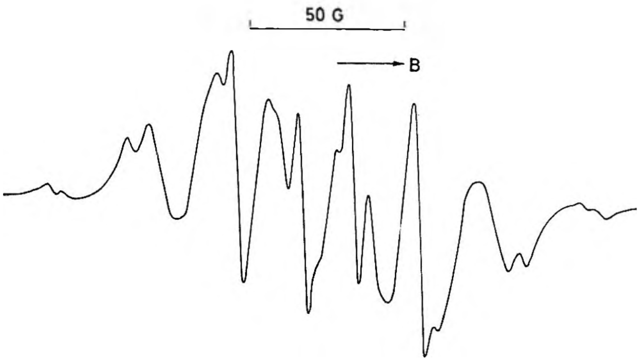

Figure 6. Esr spectrum from single crystal undecane, conditions as described in Figure 1, $\theta' = 0°$.

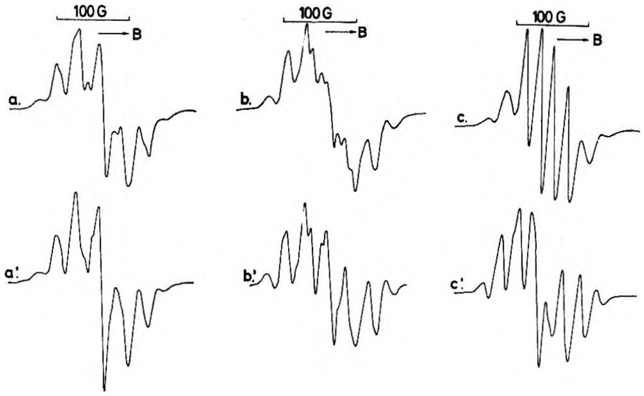

Figure 7. Spectra from polycrystalline samples of (a) pentane, (b) decane, and (c) undecane, irradiated and recorded at 77°K; (a')-(c') represent spectra of the same samples at 77°K after annealing at temperatures just below the melting points so that the integrated absorption intensity decreased.

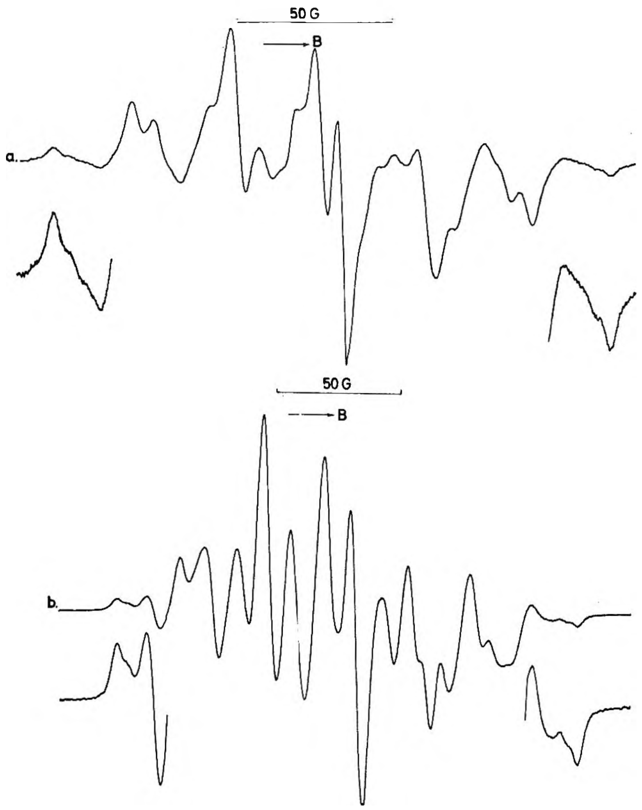

Figure 8. Spectra from an annealed polycrystalline sample of hexane recorded at (a) X-band and 77°K, (b) Q-band and 90°K.

components. Before annealing, the line width is about 5 G and the analysis becomes even more difficult. In order to obtain accurate measures of the hyperfine interaction and g tensors, a complete study based on a single crystal rotation about three axes seems to be necessary.

Discussion

Structure of the Radicals. The analysis of the single crystal spectra of hexane and decane gives evidence for a radical species with two approximately isotropic couplings $a_1 = 25 \pm 1$ G (quartet) and $a_2 = 33 \pm 1$ G (triplet). In addition, there exists an orientation-dependent doublet splitting which ranges between 33 and 12.5 G. These parameters are strong evidence for the occurrence of a radical of the type

$$CH_3\text{-}\dot{C}H\text{-}CH_2\text{-}R \qquad (I)$$

which may form by hydrogen abstraction at carbon atom 2. The magnitude and the equivalence of the methyl proton couplings suggest that this group rotates freely about the C(1)-C(2) bond.[5,21] Free rotation of end methyl groups has also been inferred from an nmr investigation of pentane and hexane in the solid state,[22] although it has not been supported by diffraction data.[18] The presence of a rotation also accords with observations made on the radical $CH_3\text{-}\dot{C}(COOH)_2$ in methyl-

---

(22) F. A. Rushworth, *Proc. Roy. Soc.*, **A222**, 526 (1954).

malonic acid single crystals,[23] where the rotation occurs even at 4°K.

The extent of methylene proton splittings may be estimated from the relationship[24]

$$a_\beta = B + A \cos^2 \theta$$

where θ is the angle between the perpendicular to the radical plane and the projection of the C(β)–H bond on a plane orthogonal to the C(α)–C(β) bond. Following the suggestion by Fessenden and Schuler,[5] A is made $= 2a_1 = 50$ G and B is neglected so that $\theta = 32.°$ This indicates that the hydrogen atoms are symmetrically disposed with respect to the radical plane. This configuration is to be expected if the atoms retain the positions featured in the juvenile crystal. Here the carbon chain is planar and the methylene hydrogen atoms are most probably symmetrically oriented with respect to this plane. Alkyl radicals in alkylhalide matrices seem to have a conformation which gives different coupling constants for the methylene protons.[25,26] It has been suggested that this applies also to the radicals trapped in *n*-hexadecene-1 and *n*-hexadecane.[3] In polyethylene, both symmetric and unsymmetric steric configuration at the C(β) atoms have been proposed.[27]

Pentane yields a powder spectrum which is essentially identical with that from hexane, Figures 7a and 8a, and radicals of type I are accordingly likely to predominate in this hydrocarbon also.

The complexity of the central regions of the powder spectra increases with increasing length of the carbon chain and this indicates that in the C_7–C_{11} alkanes, contributions are made by types of radicals other than the 2-alkyl radical, Figure 7b, c. The nature of these radicals could not be determined since neither the powder nor the single crystal spectra were sufficiently well resolved. Radicals of type II may give a spectrum

$$R\text{-}CH_2\text{-}\dot{C}H\text{-}CH_2\text{-}R' \qquad \text{(II)}$$

similar to that computed in Figure 3a″ where the four methylene protons and the α-proton are all equivalent. Clearly the II radicals may contribute to some extent, but the I radicals still make the predominant contribution to the absorptions. This does not apply to undecane, Figures 6 and 7c, where the central regions of the single-crystal and powder spectra differ in the number of components, line separation, and line width from those of pentane and hexane. Unfortunately, the single crystal spectra are poorly resolved and no assignments could be made. Radicals of type II were detected in the esr spectra of liquid *n*-alkanes[5] and they are possibly formed in the solid state as well. The line separation of 20 G, however, is not in accordance with the observed splitting of 30 G in, for instance, irradiated polyethylene.[28] The nature of the radicals can only be clarified by the study of well-resolved, single-crystal spectra. Attempts to prepare high-quality crystals of alkanes will therefore be continued.

Influence of Crystal Structure. The single crystal spectra are resolved to various degrees in the different hydrocarbons. When chemically equivalent radicals are formed, each with a different orientation in the crystal, site splittings or at least line broadenings can occur. In the triclinic hexane crystal the molecules have a common orientation. Furthermore, a radical centered on atom C_i is magnetically equivalent to that centered on atom C_{6-i} since they are symmetry related by the center of inversion and the esr spectrum does not depend on the polarity of the magnetic field. The same reasoning applies to decane. In this case, however, similar although not identical radicals are possible, as, for instance, those of type II. Three radicals of this type, not necessarily oriented in the same way, could be formed in decane crystals. In the odd-numbered alkane chains, there is no center of symmetry and therefore chemically equivalent radicals can differ in orientation, thus yielding different spectra. No additional complications are expected for nonane with its triclinic structure. In pentane and undecane with four molecules in the orthorhombic unit cell, overlapping can occur.

The conformation and the structure of the radicals which are formed may be affected by the freezing procedure if different polymorphic modifications of the crystals are possible. The simultaneous presence of different modifications would influence the resolution of the spectra. This could be of importance in compounds which feature phase transitions at temperatures above 77°K. Since no differences were observed between the *n*-alkane samples treated in various ways before irradiation,[6] such an effect is improbable in the present instance.

Irreversible Effects. Several types of radicals are clearly present in the C_7–C_{11} alkanes, as evidenced by the irreversible changes which occur in the central regions of the powder spectra on annealing (Figures 7b and c). The remaining radicals seem to be of type I, since all the spectra became closely similar to those obtained from pentane and hexane. The decay of other types of radicals, however, cannot explain the improved resolution obtained in hexane. (Figures 2 and 3 in ref 12 and Figure 8b.) Here, it is seen that the number of components and their relative intensities do

---

(23) C. Heller, *J. Chem. Phys.*, **36**, 175 (1962).

(24) C. Heller and H. M. McConnell, *ibid.*, **32**, 1535 (1960).

(25) P. B. Ayscough and C. Thomson, *Trans. Faraday Soc.*, **58**, 1477 (1962).

(26) J. E. Bennett and A. Thomas, *Proc. Roy. Soc.*, *A*280, 123 (1964).

(27) S. Nara, S. Shimada, H. Kashiwabara, and J. Somha, *Rept. Progress Polymer Phys. Japan*, **10**, 483 (1967).

(28) E. J. Lawton, J. S. Balwit, and R. S. Powell, *J. Chem. Phys.*, **33**, 395 (1960).

not change, which indicates that the type of radical remains the same.

Another possibility is that at 77°K radicals are formed which differ somewhat in their conformation.[3,27] In polyethylene, these were thought to be trapped in regions with various degrees of crystallinity.[27] Annealing would then favor the decay of the less stable species or a reorientation to a more stable conformation, giving rise to a change in the line shape.

Line broadening can be due to imperfect single crystals and to a spread in the orientation of the fragments formed when crystals fracture on cooling to 77°K. The decrease in line width is of the same magnitude in both single-crystal and powder spectra. It is therefore highly improbable that any change in orientation of crystallites and crystal fragments with temperature would influence the line width to any appreciable extent.

Radicals formed in close proximity to each other can exhibit a dipolar interaction. This would be the case, for instance, along the tracks of electrons released by the Compton scattering of the ionizing radiation. Line broadening would, therefore, arise due to this effect. Upon annealing the diffusion rate would increase and radicals trapped in positions close to each other could either recombine or diffuse away. In both cases, the line width would decrease irreversibly with temperature. Quantitatively, the degree of interaction can be estimated by its contribution to the second moment of the spectral lines.[29-31]

If one assumes that the different contributions to the line width add quadratically,[32] the broadening ΔH_s due to the dipolar interaction may be estimated from $\Delta H_s = \{(\Delta H_b)^2 - (\Delta H_a)^2\}^{1/2}$. ΔH_b and ΔH_a are the widths between maximum and minimum slopes before and after annealing, respectively. For decane ΔH_b is found to increase linearly with the dose to 15 Mrads. The concentration N of radicals within a track is estimated from the expression[29-31]

$$\Delta H_s = 8.1 \times 10^{-20} N$$

The formula applies to the case when the magnetic centers are equivalent and have a random angular distribution. Using $\Delta H_b = 4.9$ G and $\Delta H_a = 3.8$ G as obtained from the single-crystal spectra of decane, $N = (3.8 \pm 1.2) \times 10^{19}$ radicals/cm³. The error comes mostly from the uncertainty of ΔH_b. An exact fit of the experimental spectra was not possible using either a Gaussian (Figure 1a) or a Lorentzian (Figure 3a) shape. The obtained figure agrees well with the local concentration in clusters of radicals trapped in H_2O_2–H_2O glasses,[30] $N = (2.9 \pm 1.2) \times 10^{19}$ radicals/cm³. Other models give numerical values of the same magnitude. Also, the mean separation of 30 Å is in reasonable agreement with the estimated density of ionized or excited species formed in the spur[15] created by an electron with an energy of about 100 eV. The G value for radical formation and the total radiation dose gives an average separation between the radicals of 50 Å. This corresponds to a dipolar contribution to the width $\Delta H_s = 0.65$ G which would broaden the line with a negligible amount. This model, however, does not take into account the heterogeneous nature of the primary events.

Radicals may also be trapped in pairs in an ordered way, permitting satellite peaks to be resolved.[16] The distance between two radicals is then about 5–10 Å and exchange interaction will be possible. In such cases, theory predicts hyperfine splittings which are equal to one-half of those for the isolated radicals. In the single-crystal hydrocarbons investigated, evidence has been found for such a pair-wise trapping of radicals. This problem is under further investigation.

Free Radical Formation. There is at present strong evidence for the idea that the fragmentation of hydrocarbons occurs from ionized and superexcited states.[9,10] Furthermore, in view of the increased excitation energy, fragmentation of C–H and C–C bonds is more probable than molecular processes. Quenching of ionic states occurs more frequently at increased pressure, but a higher molecular weight makes this process more difficult.

The formation of free radicals in liquid hydrocarbons has been studied in some detail using either scavenger techniques or the analysis of final products.[2,7] It is generally concluded from these studies that the formation of normal and secondary parent radicals, *i.e.*, cleavage of C–H bonds, is three to five times more frequent than fragmentation of the carbon chain. Furthermore, secondary radicals are more easily formed than normal radicals. There is a tendency for the yield of parent radicals to increase with the molecular weight. The types of secondary radical that can be formed have been studied for *n*-hexane and *n*-hexane-d_{14}.[7,33] The following G values have been obtained: C(1)–H, 0.09; C(2)–H, 0.21; and C(3)–H, 0.18. Almost the same values are obtained for the deuterated hexane. Moreover, the temperature influence is rather small. The yields for carbon chain cleavage are C(3)–C(4), 0.08, C(2)–C(3), 0.08, and C(1)–C(2), 0.01; all of these values are rather low. From esr studies of liquid hydrocarbons simultaneously with irradiation[5] the conclusion has been reached that carbon chain cleavage is of some importance only in branched molecules.

---

(29) C. Kittel and E. Abrahams, *Phys. Rev.*, **90**, 238 (1953).

(30) (a) R. C. Smith and S. J. Wyard, *Nature* **191**, 897 (1961); (b) S. J. Wyard *Proc. Phys. Soc.*, **86**, 587 (1965).

(31) A. I. Mikhailov and Ya. S. Lebedev, *High Energy Chem.*, **1**, 347 (1967).

(32) D. G. Hughes and D. K. C. MacDonald, *Proc. Phys. Soc.*, **78**, 75 (1961).

(33) T. Gäumann and B. Reipso, "Radiation Chemistry 2," Advances in Chemistry Series, No. 82, American Chemical Society, Washington, D. C., 1968, p 441.

There are almost no experimental data for hydrocarbon fragmentation in the solid state. Cleavage of C–C bonds occurs with low efficiency,[2] which may be attributed to a cage effect since the fragments have limited possibilities for diffusing away from each other. In long-chain hydrocarbons, it has been observed that the retractive force within the fragments may draw the chains apart and in this way stabilize radical pairs.[34] The results obtained in the present study demonstrate that in solid hexane the C(2)–H bonds are most easily ruptured by irradiation. This applies also to the other hydrocarbons in the series pentane to decane, but not to undecane, where other radicals may also be formed. In liquid hexane, an inductive effect of the methyl group on the C(2)–H bond has been proposed to explain the different yields for C–H bond cleavage.[7] The present results make it likely that this inductive effect will be more pronounced in the solid state.

Decay of Free Radicals. As yet no quantitative study has been made of the decay of the various free radicals which were observed. However, in the case of undecane, a change in the spectrum with temperature, Figure 7c, indicates the presence of at least two types of radical designated R_1 and R_2. A decay mechanism which yields the products R_1R_1, R_2R_2, and R_1R_2 with equal rate constants[2] gives $R_1(t)/R_2(t) = R_1(0)/R_2(0)$ and hence no change ought to occur in the esr spectrum. It is evident that either the assumption of equal rate constants is not justified or the decay scheme is incomplete. An isomerization reaction, $R_1 \rightarrow R_2$, might possibly occur, where R_2 in the present case is of the type I while the nature of R_1 is at present unknown. Evidence for similar reactions has been found in irradiated alkylhalides,[25,26] where a transformation from normal to secondary alkyls occurs at 77°K. A complete kinetic analysis would contribute to the clarification of the decay mechanism.

Conclusions

The present investigation shows that single crystals of several straight-chain alkanes can be prepared at low temperature. Some fracture of the crystals seems inevitable on lowering the temperature to 77°K. Esr spectra from irradiated crystals of hexane, nonane, and decane and from powder samples of pentane and heptane reveal the preponderant formation of I radicals. In undecane, other secondary alkyl radicals may also be formed. An irreversible decrease in line width with temperature has been explained in terms of a disappearance of dipolar interaction between radicals which are about 30 Å apart. In single crystals, indications have been found of radical pair formation.

Acknowledgment. The authors thank Mr. O. Edlund, Mr. G. Börjesson, and Mr. L. Björn for valuable help in the experimental work and Mrs. I. Edvardsson for her expert handling of the manuscript. Financial support has been obtained from the Swedish Atomic Research Council.

---

(34) M. Iwasaki and T. J. Ichikawa, *J. Chem. Phys.*, **46**, 2851 (1967)

Electron Spin Resonance Studies of Irradiated Heterogeneous Systems. V. Naphthalene, Anthracene, Phenanthrene, and Biphenyl Adsorbed on Porous Silica Gel[1]

by Per-Olof Kinell, Anders Lund, and Akira Shimizu

The Swedish Research Council's Laboratory, Studsvik, Nyköping 1, Sweden *(Received April 22, 1969)*

Naphthalene, anthracene, phenanthrene, and biphenyl adsorbed on silica gel have been irradiated with ^{60}Co γ rays at a dose rate of 200 krads/hr to a total dose of 3 Mrads. The amount of adsorbed material was 0.1–1%. Aromatic cations were detected by their esr spectra at 77–300°K. The singly charged naphthalene dimer and biphenyl monomer were unambiguously identified. The coupling constants of the naphthalene cation are similar to the solution values. The splittings of the biphenyl cation are a_{para} = 6.6 G, a_{ortho} = 2.8 G. Neutral radicals formed seem to react at higher temperatures to yield secondary radicals which are persistent above room temperature.

Introduction

In two previous papers,[2a,b] the electron spin resonance spectra of the singly charged monomeric and dimeric cation radicals have been observed at 77°K in a γ irradiated benzene–silica gel system. In this case, irradiation of the system is necessary for the formation of the radicals, while on other adsorbents[3–5] the ions are formed by direct interaction with the solid. Thus esr spectra of anthracene and perylene cations adsorbed on the surface of silica–alumina were observed by Rooney and Pink,[3] who failed, however, to observe cations in the lower homologs of aromatics such as benzene and naphthalene. Muha[4] made a detailed study of the same system. Turkevich, *et al.*,[5] investigated the formation of the cation radical of triphenyl amine on the surface of synthetic zeolites. This indicates that the mechanism of cation formation may be different on the surface of the silica gel from that on silica–alumina or zeolite. Wong and Willard[6] have interpreted esr and optical spectra from naphthalene and biphenyl on silica gel as due to anion radicals.

One of the aims of the present study was to evolve a more systematic approach to the formation mechanism of ion radicals, by investigating several aromatic hydrocarbons with different ring structures. Furthermore, the previous work[2a,b] showed that cyclohexadienyl radicals are formed probably by hydrogen addition to the benzene nucleus. Hence, it was also of interest to study the correlation between the formation of such radicals and the free valence in different positions on aromatic rings. In this investigation the following compounds were used: naphthalene, anthracene, phenanthrene, and biphenyl.

In the previous study,[2b] the change of spectra with increasing temperature suggested that an addition of cyclohexadienyl to benzene molecules yielded a growing-chain type of radical. In order to examine the general applicability of this behavior the investigation was carried further with other aromatic hydrocarbons.

Experimental Section

The aromatic compounds used in the experiments were commercially obtained. Naphthalene, anthracene, phenanthrene, and biphenyl of *purum* grade (AB Kebo) were recrystallized twice from methanol. The silica gel was of chromatographic grade, 100–200 mesh (AB Kebo). The BET surface area was 667 m^2/g.

A detailed description of the experimental technique is given in a previous paper.[2b] After drying the silica gel in a quartz tube of 4 mm diameter at 500° for 18 hr under vacuum, the aromatic compound was added and absorbed on the silica gel by sublimation in vacuum. Anthracene and phenanthrene were added to the dried silica gel in the presence of air and the sample was again evacuated; in this case, the addition by sublimation was difficult. The amount of aromatic material added to the silica gel was about 1 wt% unless otherwise stated. At least two samples with the same hy-

---

(1) The previous papers in this series are I: P.-O. Kinell, A. Lund, and T. Vänngård, *Acta Chem. Scand.* **19,** 2113 (1965); II: O. Edlund, P.-O. Kinell, A. Lund, and A. Shimizu, *J. Chem. Phys.*, **46,** 3679 (1967); III: O. Edlund, P.-O. Kinell, A. Lund, and A. Shimizu, *Polymer Lett* **6,** 133 (1968); IV: O. Edlund, A. Lund, P.-O. Kinell, and A. Shimizu, Advances in Chemistry Series, No. 82, American Chemical Society, Washington, D. C., 1968, p 311.

(2) (a) O. Edlund, P.-O. Kinell, A. Lund, and A. Shimizu, *J. Chem. Phys.*, **46,** 3678 (1967). (b) O. Edlund, P.-O. Kinell, A. Lund, and A. Shimizu, Advances in Chemistry Series, No. 82, American Chemical Society, Washington, D. C., 1968, p 311.

(3) J. J. Rooney and R. C. Pink, *Trans. Faraday Soc.*, **58,** 1632 (1962).

(4) G. M. Muha, *J. Phys. Chem.*, **71,** 633 (1967).

(5) D. N. Stamires and J. Turkevich, *J. Amer. Chem. Soc.*, **86,** 749 (1964).

(6) P. K. Wong and J. E. Willard, *J. Phys. Chem.*, **72,** 2623 (1968).

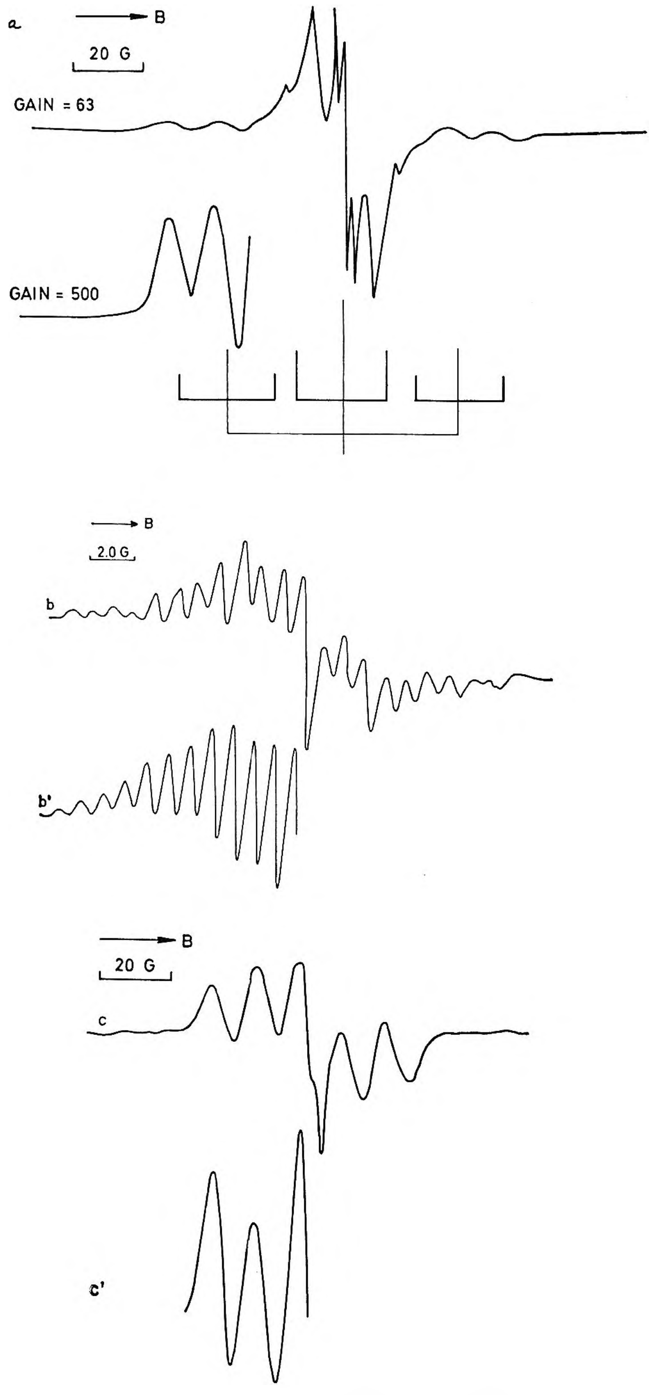

Figure 1. a, Esr spectrum of naphthalene adsorbed on silica gel and γ irradiated to 3.4 Mrads at 77°K; b, the central part of the spectrum at 251°K; b′, computed spectrum with $a_1 = 2.77$ G (8 protons) $a_2 = 0.96$ G (8 protons), line width $\Delta H_{pp} = 0.85$ G (Gaussian shape); c, the remaining spectrum at 295°K, c′, calculated powder line shape. The components of the coupling tensors for the assumed structure (II) are $A_H = (-5.8, -18.9, -11.7)$ G for the *ortho* and *para* hydrogens. The intermediate principal value is along the axis common to the tensors. The other axes are rotated through 120° relative to each other. A direct field of 5.04 G at the protons was used and the single crystal line width $\Delta H_{pp} = 6$ G.

drocarbon content were prepared to ensure reproducibility.

Irradiation with ^{60}Co γ rays at a dose rate of 200 krads/hr was carried out at 77°K. The dose was 3.4 Mrads. The esr spectra were measured with a Varian X-band spectrometer, V-4502-11, using 100-kHz field modulation, ordinarily within 2 hr after the irradiation was stopped. The esr signal from the Suprasil sample tube at $g = 2.0010$, $\Delta H_{pp} = 3$ G, was too weak to contribute significantly to the spectra recorded at 77°K following the irradiation. Generally this absorption had disappeared after warming the samples to room temperature; it might interfere somewhat in the low-intensity spectrum of naphthalene recorded at 251°K.

Results

Naphthalene. The esr first derivative spectrum of the irradiated naphthalene–silica gel system at 77°K is shown in Figure 1a. It contains two components, one observed in the central part with 40 G span and another with weaker and broader lines on the wings. The spectrum is similar to that observed by Hughes, *et al.*,[7] in the X-ray irradiated naphthalene–boric acid glass system. The two weak lines on the wings have a splitting of 13 ± 1 G. A third line is indicated as a shoulder on the central absorption. The line positions are in agreement with the outer triplets from the cyclohexadienyl type of radical, R in scheme I, observed by Koski, *et al.*[8] The stick plot shown in Figure 1a has the coupling constants 32.5 G for the methylene protons in the 1 position and 13 G for the ring protons in the 2 and 4 positions, which are similar to those observed in an alcoholic matrix.[8] These coupling constants are in good agreement with those calculated (Table II) by the molecular orbital method of McLachlan (*cf.* also ref 8). Similar calculations indicate that the isomeric radical formed by hydrogen attachment at carbon atom 2 does not contribute to the spectrum. For this structure, a much larger splitting than that observed is predicted for the methylene protons.

The assignment of the central absorption at 77°K is not entirely obvious. Similar signals in the central part of the spectra have also been observed for the other aromatics, as will be mentioned later. At 77°K the absorption due to silica gel defects is weak by comparison with that from the radicals. Measurements at higher temperatures give a better resolution. The spectrum measured at 251°K is shown in Figure 1b. At this temperature, the weak triplets on both wings due to $C_{10}H_9$ have decayed. The spectrum is somewhat asymmetric and lines which are symmetrically displaced from the center are better resolved on the low field side. The asymmetric central line in Figure 1b is partly due to the silica gel signal superimposed on the naphthalene signal. At these temperatures the intensity of the silica gel absorption is comparable with that of naphthalene, due to a difference in decay rates. In accordance with the finding from the benzene–silica gel system, it is reasonable to attribute the absorption to ionized naphthalene. However, a calculated spectrum for the monomeric cation[9] does not fit the experimental spectrum. On the other hand, a computed spectrum for the cation dimer shown in Figure 1b′ with a_1 = 2.77 G (8 protons) and a_2 = 0.96 G (8 protons) is in good agreement with the experimental spectrum. These values compare favorably with those found for the cation dimer of naphthalene formed by the oxidation of naphthalene by $SbCl_5$[9] $a_1 = 2.77$ G, $a_2 = 1.03$ G. Furthermore, the measured value of $g = 2.0020$ does not differ significantly from the value in the liquid state, $g = 2.0023$. A sample with naphthalene concentration of 0.1% also gave a dimer cation spectrum. The color of the sample was slightly purple after the irradiation at 77°K, but disappeared at around 250°K where the cation absorption decays.

---

[7] F. Hughes, R. D. Kirk, and F. W. Patten, *J. Chem. Phys.*, **40**, 872 (1964).

[8] J. A. Leone and W. K. Koski, *J. Amer. Chem. Soc.*, **88**, 656 (1966).

At 295°K the naphthalene cation has almost completely decayed revealing a five-component spectrum with approximately equal spacings, Figure 1c. The outer four lines could be saturated more easily than the central line by increasing the microwave power. On allowing the sample to warm up to 370°K the outer four lines began to decay and only the central absorption due to defects in the silica gel remained. In the systems biphenyl–silica gel (see below) and *n*-hexane–silica gel[10] it was observed that the only remaining silica gel defect gives a narrow line at $g = 2.0008$. In Figure 1c the central component is broader and also asymmetrical, showing that there must be an additional line. The five-line spectrum can be reasonably explained as being due to a radical in the hydrocarbon phase. From the line shape it is difficult to establish its structure. However, there are only a few radicals which are likely to be formed during radiolysis or after subsequent radical reactions. One of these is the naphthyl radical. In this case, the α and β isomers are possible products. The spectrum of α-naphthyl has been briefly reported;[11] it consists of two lines separated by 17 G. The assignment is supported by spin density calculations.[11] However, experimental values for the coupling constants of the related phenyl radical depend on the composition of the matrix in which the radicals are prepared,[12–14] and the calculations are also contradictory.[15] An attempt was therefore made to prepare α-naphthyl by photolysis and radiolysis of α-iodonaphthalene and α-bromonaphthalene, resulting in an unresolved asymmetric single-line spectrum. The same spectrum was obtained by photolysis of material in the absorbed state. These findings indicate that the five-line spectrum is not due to naphthyl radicals. In the system benzene–silica gel[2b] no evidence for the analogous phenyl radical was found. It has been suggested that a propagating radical occurs in this system. It seems very likely that in this case also the spectrum is caused by a propagating type of radical formed according to the scheme

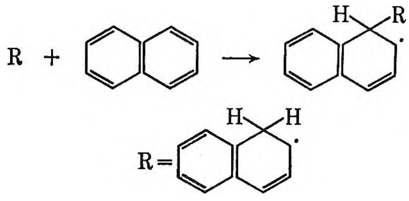

(1)

The couplings to the ring protons 2 and 4 of the radical (I) are probably anisotropic. Characteristic coupling tensors for CH fragments are known.[16] These typical values should be reduced proportionally to correspond to an isotropic splitting of 12 G for both protons. Using the computer program prepared by Lefebvre and Maruani,[16] a theoretical line shape has been calculated with the inclusion of an additional isotropic splitting of 23 G. The simulated curve in Figure 1c predicts relative line intensities deviating from the 1:2:2:2:1 ratio expected from a stick plot diagram. In particular the center line is narrower. In view of the roughness of the estimate of the coupling tensors, the agreement with observation is quite satisfactory, encouraging belief in the assignment.

Biphenyl. The spectrum at 77°K obtained from an irradiated sample of biphenyl–silica gel is shown in Figure 2a. The green color of the sample suggests the presence of ionic species. The central part of the spectrum seems to be composed of an odd number of lines, Figure 2b, as was the one observed by Hughes, *et al.*,[7] in the X-ray irradiated system of biphenyl–boric glass at 77°K. The average separation between the lines is 3.5 G. Although the hyperfine splitting constants of the biphenyl cation have not been reported previously, those of the biphenyl anion are $a_2 = 2.66$ G and $a_4 = 5.31$ G, and very small for *meta* protons.[17] Approximate estimates of the coupling constants for the biphenyl cation can be obtained from the values for the anion and McConnell's relationship between coupling constants and spin density $a = Q\rho$. According to

---

(9) I. C. Lewis and L. S. Singer, *J. Chem. Phys.*, **43**, 2712 (1965).

(10) P.-O. Kinell, A. Lund, and T. Vänngård, *Acta Chem. Scand.*, **19**, 2113 (1965).

(11) R. W. Lloyd, F. Magnotta, and D. E. Wood, *J. Amer. Chem. Soc.*, **90**, 7942 (1968).

(12) V. A. Tolkachev, I. I. Chkheidze, and N. Ya. Buben, *Zh. Strukt. Khim.*, **3**, 709 (1962).

(13) (a) S. Ohnishi, T. Tanei, and I. Nitta, *J. Chem. Phys.*, **37**, 2402 (1962); (b) T. Tanei, *Bull. Chem. Soc. Jap.*, **40**, 2456 (1967); (c) T. Tanei, *ibid.*, **41**, 833 (1968).

(14) J. E. Bennett, B. Mile, and A. Thomas, *Proc. Roy. Soc.*, **A293**, 246 (1966).

(15) (a) K. Morokuma, S. Ohnishi, T. Masuda, and K. Fukui, *Bull. Chem. Soc. Jap.*, **36**, 1228 (1963); (b) W. T. Dixon, *Mol. Phys.*, **9**, 201 (1965); (c) N. M. Atherton and A. Hincliffe, *Mol. Phys.*, **12**, 349 (1967).

(16) R. Lefebvre and J. Maruani, *J. Chem. Phys.*, **42**, 1480 (1965).

(17) H. Fischer, "Magnetische Eigenschaften freie Radikale," Landolt-Börnstein Gruppe II, Band 1, Springer-Verlag, 1965.

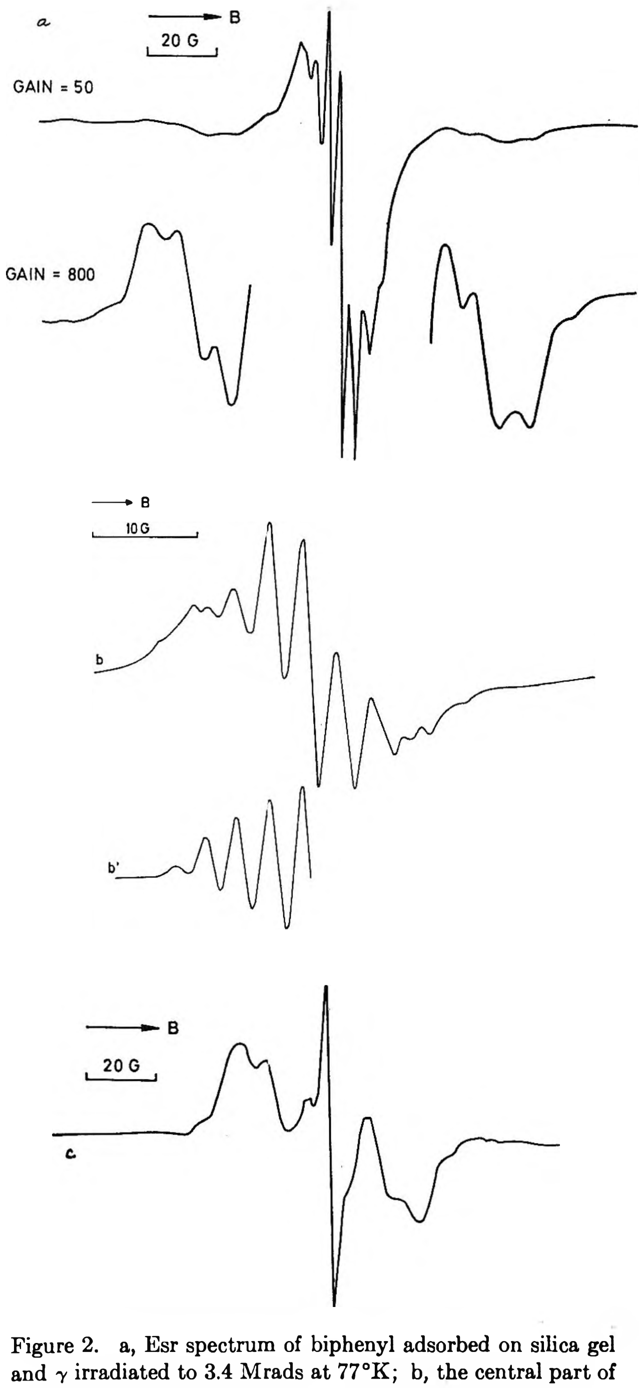

Figure 2. a, Esr spectrum of biphenyl adsorbed on silica gel and γ irradiated to 3.4 Mrads at 77°K; b, the central part of the spectrum at 77°K; b', computed spectrum with $a_1 = 6.6$ G (2 protons) $a_2 = 2.8$ G (4 protons) line width $\Delta H_{pp} = 2.0$ G (Gaussian shape); c, the remaining spectrum after heating the sample to 237°K.

Lewis and Singer,[9] the best value for Q, using Hückel spin densities is $Q^+ = 35.7$ G for the aromatic cations and $Q^- = 28.6$ G for the anions. In the Hückel approximation the densities in the positive and the negative ion are equal, yielding $a^+ = 1.25\ a^-$. Alternatively, the spin density can be computed from the Colpa–Bolton relationship $a^{\pm} = -(Q \cdot \rho \pm \mathrm{K} \cdot \rho^2)$ using the parameters[9] $Q = 32.2$ G, $K = 16$ G. From the experimental splitting a^- of the negative ion a theoretical estimate of a^+ is obtained. Table I gives the coupling constants of some aromatic ions together with the calculated values of a^+. The splittings predicted for the positive ions from the Colpa–Bolton relationship are correct to about 5%, indicating that for biphenyl $a_4^+ = 6.5 \pm 0.3$ G. The coupling constants in the adsorbed state $a_4 = (6.6 \pm 0.2)$ G, $a_2 = (2.8 \pm 0.2)$ G were estimated by fitting a computed line shape to the five lines of Figure 2b which are clearly resolved. The value $a_4 = 5.31$ G for the negative ion is too small to fit the experimental spectrum. It seems unlikely that the difference is caused by matrix effects. For instance, the influence of the solvent on the coupling constants[9,17] of ionic species is of the order 1–2% and likewise the splittings in the adsorbed state are close to those in the solution.[4] The absorption is, therefore, most probably caused by biphenyl cations. This conclusion does not conform with the findings of Wong and Willard,[6] who interpreted the couplings constants found, $a_2 = 2.86$ G and $a_4 = 5.72$ G, as evidence for the existence of anion radicals. These authors also present evidence from optical spectra. In view of results obtained by Hamill and coworkers[18] on biphenyl in 3-methylpentane glass and in polycrystalline carbon tetrachloride, the spectra could, however, as well be interpreted as due to cation radicals.

Table I: Experimental and Calculated Hyperfine Splittings for Some Aromatic Ions

Compound	a_H^-, G	a_H^+, G	$a_H^{+\,a} = 1.25a^-$, G	$a_H^{+\,a}$(C–B), G
Perylene	3.49	4.05	4.35	3.80
Anthracene	5.34	6.53	6.67	6.38
Naphthacene	4.23	5.06	5.27	4.85
Pyrene	4.75	5.38	5.94	5.56
Benzene	3.75	4.44	4.70	4.23
Biphenyl	5.46	6.6 ± .2	6.80	6.46

[a] $a_H^+ = 1.25\ a^-$ is obtained from McConnell's relation while a_H^+ (C–B) is computed by the Colpa–Bolton relation. In those ions where several groups of protons interact only the largest couplings are considered.

Apart from the central lines due to the cation, weak absorptions on the wings are observed at 77°K as shown in Figure 2a. The line shape resembles a partly resolved triplet with binomial intensities, as far as can be judged from compiled spectra.[19] The triplet splitting is about 9 G. The separation between the two absorptions on the wings is 80 G. This spectrum may be due to a cyclohexadienyl type of radical, *i.e.*, phenyl-

---

[18] T. Shida and W. G. Hamill, *J. Chem. Phys.*, **44**, 2375 (1966); J. B. Gallivan and W. H. Hamill, *ibid.*, **44**, 2378 (1966).

[19] Ya. S. Lebedev and V. V. Voevodskij, "Atlas spektrov elektronnogo paramagnitnogo rezonansa, Academy of science USSR, Moscow, 1962.

Table II: Free Valence Index F of Aromatic Compounds, Computed Spin Densities, ρ_i, and Coupling Constants a_i in Free Radicals of Cyclohexadienyl Type

			Spin density[a] and line separation, G					
			Location of CH_2 group					
Compound	Position	Free value index	ρ_i	a_i	ρ_i	a_i	ρ_i	a_i
			1		2			
Naphthalene	1	0.452			0.542	14.6		
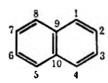	2	0.404	0.416	11.3				
	3		−0.108	2.9	0.138	3.7		
	4		0.394	10.6	−0.048	1.3		
	5		0.100	2.7	−0.048	1.3		
	6		−0.034	0.9	0.124	3.4		
	7		0.095	2.6	−0.049	1.3		
	8		−0.034	0.9	0.135	3.6		
	H_2		0.134	33.8	0.174	44.0		
			1		2		9	
Anthracene	1	0.459			0.554	15.0	−0.039	1.1
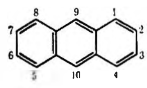	2	0.408	0.413	11.2			0.116	2.9
	3		−0.106	2.9	0.067	1.8	−0.039	1.1
	4		0.390	10.5	−0.023	0.6	0.122	3.3
	5		0.045	1.2	−0.027	0.7	0.122	3.3
	6		−0.018	0.5	0.055	1.5	−0.039	1.1
	7		0.041	1.1	−0.026	0.7	0.116	2.9
	8		−0.020	0.5	0.062	1.7	−0.039	1.1
	9	0.520	−0.031	0.8	−0.242	6.5		
	10		0.175	4.7	−0.042	1.1	0.478	12.9
	H_2		0.109	27.5	0.144	36.2	0.070	17.6
Phenanthrene	1	0.450						
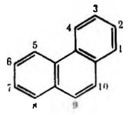	2	0.403						
	3	0.408						
	4	0.441						
	9	0.452						
Biphenyl			2		3		4	
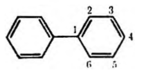	1							
	2	0.436			0.363	9.8	−0.087	2.5
	3	0.395	0.312	8.4			0.306	8.3
	4	0.412	−0.087	2.4	0.355	9.6		
	5		0.290	7.8	−0.104	2.8	0.306	8.3
	6		−0.087	2.4	0.336	9.1	−0.087	2.5
	H_2		0.173	43.5	0.200	50.4	0.175	44.1

[a] The spin density on the methylene protons ρ_{H_2} is equally distributed on both atoms and is therefore divided by 2 before being converted to a splitting constant.

cyclohexadienyl, similar to the cases of benzene[2b] and of naphthalene, as mentioned above. The central component of the spectrum could very well be masked by the cation absorption. In order to explain the triplet structure on the wings, spin density calculations were performed by applying the method of McLachlan.[20] According to these, the methylene group is in the 2 or 4 position (Table II), but a distinction between these two possibilities could not be made due to the bad resolution of the spectrum. Details of the calculations are given below.

Upon heating the sample to 273°K, the absorptions due to the cations and the phenylcyclohexadienyl decayed, and the spectrum shown in Figure 2c was obtained. This persisted up to 340°K. The central narrow line is caused by a defect in the silica gel, also observed in the irradiated n-hexane–silica gel system.[10] The lines on the wings are most probably due to radicals in the hydrocarbon phase. There is no indication of a central component of this spectrum which accordingly consists of a main doublet, separation 29 G, with some additional structure. There are two reasons for believing that the spectrum is due to a propagating type of radical obtained by the addition of phenylcyclohexadienyl to biphenyl. First, evidence for an analogous radical has been found in the cases of benzene[2b] and naphthalene under similar conditions. Secondly, the formation of quaterphenyl has been reported in the radiolysis study of biphenyl by Sweeney, *et al.*[21]

---

(20) A. D. McLachlan, *Mol. Phys.*, **3**, 233 (1959).

(21) M. A. Sweeney, K. L. Hall, and R. O. Bolt, *J. Phys. Chem.*, **21**, 1564 (1967).

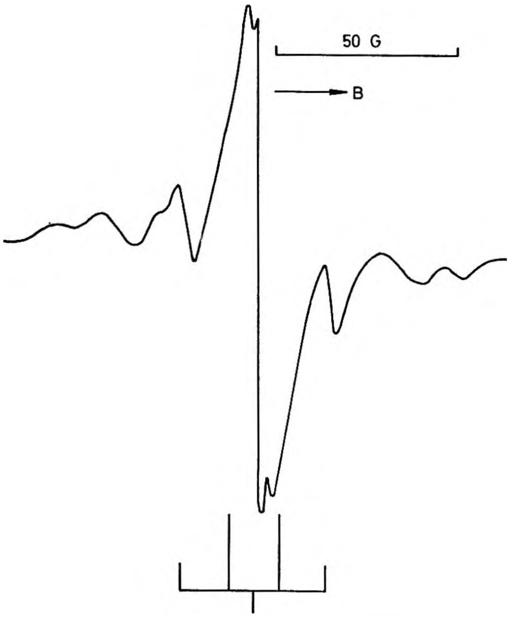

Figure 3. Esr spectrum of anthracene adsorbed on silica gel and γ irradiated to 3.4 Mrads at 77°K. The coupling constants in the stick plot are those given[21] for the radical derived from anthracene by hydrogen addition to the 9 position. The spectrum of phenanthrene is very similar.

Anthracene and Phenanthrene. Anthracene and phenanthrene were studied under the same conditions as above. The central parts of the spectra contain several lines at 77°K which attain a better resolution at higher temperatures. These absorptions may be due to the cations of the aromatics, as in the case of naphthalene and biphenyl. In these instances, however, poor resolution of the spectra prevents a detailed analysis.

In addition to the central part, several weaker lines were observed at 77°K for these aromatics (Figure 3) similar to those of naphthalene and biphenyl. These might be the outer components of cyclohexadienyl types of radical.

It does not seem possible to assign the observed spectra to a single radical. Thus, with the methylene group at carbon atom 9 of anthracene, a spectrum with the coupling constants $a_{H_2} = a_{10} = 14.8$ G is reported[22] while the observed total span is considerably larger. The other two isomers (methylene group in position 1 or 2) would yield spectra with a larger overall width, Table II, and it seems reasonable that they are also present. A similar conclusion holds for phenanthrene.

The absorptions observed at 77°K decayed almost completely at 260°K and a weak five-line spectrum remained. The spectral lines were broad and difficult to assign. However, the conditions are similar to those under which a propagating radical of naphthalene was observed and it seems likely that the spectra are due to analogous types of radical.

Molecular Orbital Calculations. Estimates of spin densities were obtained using the theory of McLachlan.[20] With this method, the predicted magnitudes of the methylene proton splittings are correct to within 10%.[8,23] The Hückel parameters are[23] $\alpha_C(H_2) = -0.1\,\beta$, $\alpha_{H_2} = -0.5\,\beta$, $\beta_{C-H_2} = 2.5\,\beta$ for the hyperconjugation model of the CH_2 group, and the value of $\lambda = 1.0$ was used. The spin densities were converted to coupling constants using McConnell's relationship $a = Q\rho$ with $|Q| = 27$ G for the ring protons and $|Q| = 505$ G for the methylene protons. The possibility of assigning the spectra with the aid of the computed couplings has been discussed above. There is apparently no significant difference between the total π electron energy of the different isomeric radicals; accordingly no special structure is favored on energetic grounds.

Discussion

Spectra of Ionized Molecules. The central absorptions, mainly due to the cationic species, are not well resolved at 77°K but the resolution becomes better at temperatures around 223–273°K. This is partly due to the decay of superimposed signals of the less stable cyclohexadienyl types of radical. Motional averaging of the anisotropic hyperfine coupling and the g tensor should also be more efficient at higher temperatures. Muha[4] has found that a modulation of these quantities gives a reasonable explanation for the variation in line widths observed for adsorbed cation radicals. A related explanation was offered in ref 1 supported by nmr measurements on similar systems[24] where it was suggested that adsorbed benzene ions rotate around the sixfold axis.

Other possible line broadening mechanisms include interactions with counterions.[4] In the present systems, it is possible that the electrons liberated during the ionization of the adsorbed hydrocarbons become trapped in the silica gel. If the ionized molecule and the trapped electron are close to each other, dipolar splittings may occur similar to those observed in radical pairs.[25] No $\Delta M_S = 2$ transitions of the triplet state were observed in the benzene–silica gel system. A smaller spin–spin interaction broadens the hyperfine lines. When the sample is heated, some recombination between electrons and ions, essentially those trapped close to each other, may accompany diffusion. The lines should accordingly become narrower after annealing. In the present systems other irreversible changes also occur, namely dimeric ion formation. However, the line width of the central component in the benzene–silica gel system remained unchanged at 0.4 G after

---

(22) L. A. Harrah and R. C. Hughes, *Mol. Cryst.*, **5**, 141 (1968).

(23) R. J. Cook, J. R. Rowlands, and D. H. Whiffen, Proceedings of the Sixth International Symposium on Free Radicals, Paper S, Cambridge, 1963.

(24) (a) D. E. Woesner, *J. Phys. Chem.*, **70**, 1217 (1966). (b) H. Winkler and H. Pfeifer, Paper presented at XV Colloque A.M.P.E.R.E., Grenoble (1968).

(25) (a) Y. Kurita, *J. Chem. Soc. Jap., Pure Chem. Sect.*, **85**, 833 (1964); (b) *J. Chem. Phys.*, **42**, 3926 (1964).

annealing. This indicates that dipolar broadening is unimportant.

It has been suggested that charge transfer complexes are formed when molecules are adsorbed on synthetic zeolites.[5] The electrons are thought to be trapped at electron acceptor sites on the solid catalyst. Exchange interactions between the electron site and the aromatic ion may lead to line broadening. Shifts in the g factors are expected[26] in charge-transfer complexes with strong exchange interaction. No such shifts could be detected within the limits of experimental accuracy. This indicates that the interaction, if any, is weak. Weak couplings are difficult to differentiate from the effects arising from an anisotropic g tensor and hyperfine couplings at the resolution obtainable in the spectra. Detailed line shape analysis of the better resolved spectra such as that of the positive benzene ion may help to elucidate these problems.

The observed splittings agree reasonably well with those measured for the positive ions in the solution. For the biphenyl cation the splittings agree well with those predicted theoretically.[9] Thus, no major redistribution of spin density takes place under the influence of the adsorbent. This is in accordance with previous observation.[4]

The positive ions show a tendency to form dimers, especially at increased temperature. A simple HMO treatment[27] shows that the singly charged dimer has a somewhat lower energy than the separated monomer ion and neutral molecule. Thus, the reaction seems to be favored on energetic grounds.

Previous studies of the oxidation of molecules on solid catalysts[3,5,28–30] have suggested that this process occurs at certain acidic or electron acceptor sites. Barter, *et al.*,[29] have reported that the acidity of silica gel is increased under the influence of ionizing irradiation. It was not apparent from the present experiments whether or not the silica gel is acidic, but naphthalene adsorbed on a preirradiated silica gel at 250°K did not show any esr absorption. No detectable amount of aromatic radical ions was found in the pure hydrocarbons irradiated at 77°K. This indicates that γ-ray irradiation of the composite system is a prerequisite for the formation of ionic species. Tanei[13c] recently observed benzene ions following uv illumination of benzene in the adsorbed state. The existence of acidic sites capable of oxidizing hydrocarbon is unlikely in this case, and the silica gel presumably acts merely as a stabilizing agent for the ions. The ionization potentials are probably lower in the adsorbed state, and the molecules may thus be more easily ionized. The silica gel plays the role of a trap for the ejected electrons, possibly at certain acceptor sites as suggested in ref 5 and also behaves as a stabilizing agent for the cations created on the surface.

No paramagnetic absorption due to radiolytically released electrons was detected in the benzene–silica gel system, even when the sample was kept in the dark and the spectrum was recorded at low microwave power to avoid bleaching and saturation. This could mean that its spectrum is too broad to detect.

Energy transfer may take place in addition to direct ionization. The yields were not measured in the present investigation, but the absorptions due to cations were strong. It is probable that the phenomenon occurs here as well as in the systems[2,10] previously studied.

Neutral Radicals. In all the compounds studied here, the cyclohexadienyl type of radical is observed. These radicals exhibit triplet splittings due to the methylene protons; the assignment is made possible by the observation of the outer two components of the spectrum. In the present studies, no direct evidence regarding the mechanism of their formation was obtained. If the central absorption is interpreted as being caused by anions, a reaction between these and protons from acidic sites of the gel may yield the observed neutral radicals. (We are indebted to the referee for this suggestion.) This would corroborate the acidic nature of irradiated silica gel.[29] There is no indication of any reaction after the irradiation was stopped; the central part of the biphenyl spectrum recorded 2 hr after the end of the irradiation was identical with regard to both intensity and shape to that obtained 6 days later. Therefore, if the cyclohexadienyl type of radical is formed by this mechanism, it seems that the reaction occurs at such early stage that it is not detectable with the present technique.

As previously reported,[31,32] hydrogen atoms are released from surface hydroxyl groups of the silica gel when irradiated with γ rays. These hydrogen atoms may react with adsorbed hydrocarbon molecules like ethylene.[31] Strelko and Suprunenko[32] observed the formation of C_6H_6D from irradiated benzene and deuterated silica gel. Further they interpreted the presence of $\equiv$Si—O· radicals as originating from the scission of the O–D bond of surface hydroxyl groups. Deuterium atoms would then be released which could react with the adsorbed hydrocarbon.

It seems reasonable that a similar reaction may account for the formation of the cyclohexadienyl types of radical in the present case. To elucidate this problem further, an investigation of effects arizing from differences in gel structure is presently attempted.

---

(26) M. Kinoshita, *Bull. Chem. Soc. Jap.*, **36**, 307 (1963).

(27) P.-O. Kinell and A. Lund, to be published.

(28) H. W. Kohn, *J. Phys. Chem.*, **66**, 1185 (1962).

(29) C. Barter and C. D. Wagner, *ibid.*, **68**, 2381 (1964).

(30) H. Arai, Y. Saito, and Y. Yoneda, *Bull. Chem. Soc. Jap.*, **40**, 318 (1967).

(31a) V. B. Kazanskii, G. B. Pariiskii, and V.V. Voevodskii, *Kinet. Katal.*, **1**, 539 (1960); (b) V. B. Kazanskii and G. B. Pariiskii, Proceedings of Sixth International Symposium on Free Radicals, Paper P, Cambridge, 1963.

(32) V. V. Strelko and K. A. Suprunenko, *Khim. Vys. Energ.* **2**, 258 (1968).

The hydrogen atoms are expected to add to the aromatic rings at carbon atoms with large free valence index.[33] In anthracene and phenanthrene several carbon atoms have a large free valence (see Table II) and addition probably occurs at several positions, as may be the case in biphenyl. In naphthalene and styrene (unpublished results) the addition takes place at the most reactive atom.

Free Radical Reactions. Evidence presented in this communication and in the previous paper[2b] suggests that a propagating type of radical, illustrated by (I) is produced at increased temperatures. This hypothesis is strongly supported by the radiolysis study of biphenyl,[21] in which the main final products were quaterphenyl and hydrogenated quaterphenyl. These are obtained by disproportionation of radicals formed when the biphenyl radical adds to biphenyl, in the same manner as is suggested here for the phenylcyclohexadienyl radical.

The splittings assigned to *ortho* and *para* protons are similar to those in the cyclohexadienyl radical, indicating that the distribution of spin density is not greatly changed. The coupling constant of the β proton, however, is smaller than that of the cyclohexadienyl type of radical. The β proton in 1-hydroxycyclohexadienyl[17] also shows a weaker interaction, namely 36 G compared to 48 G for C_6H_7. This indicates that the splitting depends markedly on the substituent at the β carbon. Molecular orbital theory predicts the correct magnitude of the methylene proton coupling in cyclohexadienyl. Detailed valence bond calculations[34] show that these splittings depend critically on the assumed geometry. A bulky substituent like $C_{10}H_8$ in (I) certainly affects the steric arrangement; furthermore, the calculations do not account for its effect on the spin density at the β proton. In view of these facts, it is not surprising that the splitting in (I) deviates from that of $C_{10}H_9$. No attempt to establish the radical geometry was made. For such an estimate, it is highly desirable to use data from a single crystal.

Conclusions

The observation of electron spin resonance spectra from irradiated systems of aromatic hydrocarbons–silica gel makes it possible to detect and identify reactive paramagnetic species such as radical cations, which become stabilized on the gel surface. The resolution is better than in the homogeneous phase, which makes it possible to identify the radical structure. Neutral radicals react further with other molecules at increased temperatures, yielding propagating types of radical; this gives evidence for the mechanism suggested by other authors for the formation of final dimeric products.

Acknowledgments. We are indebted to Mr. O. Edlund for valuable help in the experimental work and to Mrs. I. Edvardsson for typing the manuscript. Financial support has been obtained from the Swedish Atomic Research Council and the Swedish Technical Research Council.

---

(33) R. Daudel, R. Lefebvre, and C. Moser, "Quantum Chemistry," Interscience, 1959, p 242.

(34) K. Morokuma and K. Fukui, *Bull. Chem. Soc. Jap.*, **36**, 534 (1963).

Photochemistry of Complex Ions. VII.

trans-4-Stilbenecarboxylatopentaamminecobalt(III) Ion

by Arthur W. Adamson, Arnd Vogler, and Ian Lantzke[1]

Department of Chemistry, University of Southern California, Los Angeles, California 90007

(Received April 28, 1969)

The aqueous ion $Co(NH_3)_5(TSC)^{2+}$, where TSC denotes *trans*-4-stilbenecarboxylate, appears in most respects to be a normal member of the carboxylatopentaamminecobalt(III) family. The second ligand field band is masked, however, by a strong absorption at 320 mμ, essentially identical with that for the free TSC molecule. The first singlet–singlet transition of the TSC moiety thus appears to function as an isolated chromophoric group of the complex. Irradiation of the 320-mμ band of the free TSC ligand leads to *trans* to *cis* isomerization; however, irradiation of this same band in the complex produces cobalt(II) in a quantum yield of 0.16 and both some free (unisomerized) and some oxidized TSC ligand. Other members of the carboxylatopentaamminecobalt(III) series are nearly inert to this wavelength of irradiation. Free TSC^- ion shows a peak fluorescent emission at 400 mμ, which is partially quenched in the presence of $Co(NH_3)_5(H_2O)^{3+}$ and essentially completely so when the ligand is coordinated. It is concluded that an intramolecular excitation energy transfer occurs, probably to produce a charge transfer triplet excited state of the complex, which then undergoes redox decomposition. The suggested process is one of intersystem crossing from the first singlet excited state of the TSC ligand.

Introduction

The present investigation was undertaken to determine whether an intramolecular transfer of excitation energy leading to photolysis could be observed for a Werner-type complex ion. Certain cobalt(III) and other chelates have been reported to quench organic triplet excited states,[2-4] but the effect could be attributed to a catalysis of the radiationless return of the donor to the ground state. Excitation energy transfer clearly occurs, however, in the case of certain rare earth chelates, for which irradiation of ligand localized absorption bands lead to emission characteristic of the rare earth ion.[5] Similar evidence has been reported for solid $[Cr(urea)_6][Cr(CN)_6]$; in this case low-temperature irradiation of a cation absorption band led to emission characteristic of the anion.[6] Finally, in low-temperature but not rigid media, organic donors were found to sensitize the characteristic phosphorescent emission of $Cr(NCS)_6^{3-}$.[7]

The above are all spectroscopic situations; we were interested in whether excitation energy transfer could lead to chemical reaction. This was partly to establish the occurrence of such a process and partly as a potentially valuable approach to the study of excited state photochemistry of coordination compounds. At the time this work was initiated, it was felt that a search for intramolecular excitation energy transfer would be more likely to be successful than one for intermolecular transfer. Recently, however, sensitized photoredox decompositions of cobalt(III) ammines have been found to be facile.[8]

The complex selected for study was *trans*-4-stilbene carboxylatopentaamminecobalt(III), to be referred to as species I.

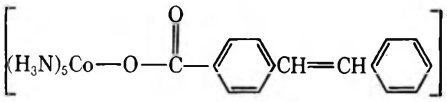

(I)

Although not a known compound, the preparation of I was not anticipated to be difficult, and the choice offered several advantages. The photochemistry of stilbene and of many of its derivatives had been studied extensively (see references 9 and 10); excitation in the region of the first singlet–singlet absorption band leads to isomerization *via* intersystem crossing to the first triplet excited state. Likewise, both the photochemistry and the thermal reaction chemistry of aqueous cobalt(III) ammine complexes of the type $Co(NH_3)_5X^{2+}$ were well known (see ref 11 and 12). The first two ligand field bands of such complexes correspond to the

---

(1) The University, Newcastle upon Tyne, England.

(2) G. S. Hammond and R. P. Foss, *J. Phys. Chem.*, **68**, 3739 (1964).

(3) L. Lindquist, *Acta Chem. Scand.*, **20**, 2067 (1966).

(4) A. J. Fry, R. S. H. Liu, and G. S. Hammond, *J. Amer. Chem. Soc.*, **88**, 4781 (1966).

(5) G. A. Crosby, R. E. Whan, and R. M. Alire, *J. Chem. Phys.*, **34**, 743 (1961).

(6) H. Gausmann and H. L. Schläfer, *ibid.*, **48**, 4056 (1968).

(7) D. J. Binet, E. L. Goldberg, and L. S. Forster, *J. Phys. Chem.*, **72**, 3017 (1968).

(8) A. Vogler and A. W. Adamson, *J. Amer. Chem. Soc.*, **90**, 5943 (1968).

(9) J. G. Calvert and J. N. Pitts, Jr., "Photochemistry," John Wiley and Sons, Inc., New York, N. Y., 1966.

(10) G. S. Hammond, J. Saltiel, A. A. Lamola, N. J. Turro, J. S. Bradshaw, D. O. Cowan, R. C. Counsell, V. Vogt, and C. Dalton, *J. Amer. Chem. Soc.*, **86**, 3197 (1964).

(11) F. Basolo and R. G. Pearson, "Mechanisms of Inorganic Reactions," 2nd ed, John Wiley and Sons, Inc., New York, N. Y., 1967.

(12) A. W. Adamson, W. L. Waltz, E. Zinato, D. W. Watts, P. D. Fleischauer, and R. D. Lindholm, *Chem. Rev.*, **68**, 541 (1968).

transitions ${}^1A_{1g} \rightarrow {}^1T_{1g}$ and ${}^1A_{1g} \rightarrow {}^1T_{2g}$ in O_h symmetry, and will be called here the L_1 and L_2 bands, respectively. If X is not an easily oxidizable ligand, *i.e.*, if the energy is large for the reaction

$$X^- = X + e^- \tag{1}$$

then the L_1 and L_2 bands are of normal intensity for d–d transitions (extinction coefficients of about 70 M^{-1} cm^{-1} at the band maxima), and the complexes are only slightly photosensitive in this wavelength region. Thus for X = Cl or SO_4, photolysis quantum yields are around 10^{-3} in the 370-mμ and longer wavelength region.[13] The same is true for $Co(NH_3)_6{}^{3+}$[8,13] and $Co(NH_3)_5(H_2O)^{3+}$,[8] and would be expected to be true if X were a carboxylato ligand, X = RCOO. Thus it was anticipated that irradiation of I could be made in the visible and near-ultraviolet without there being any appreciable complication due to direct photolysis of the complex.

The general expectation was that either irradiation of the L_1 band of complex I might lead to *trans* to *cis* isomerization of the stilbene moiety, or that irradiation of the singlet–singlet band of the ligand might result in either aquation or in redox decomposition of the complex. It will be seen that the latter process occurs, but apparently not the former.

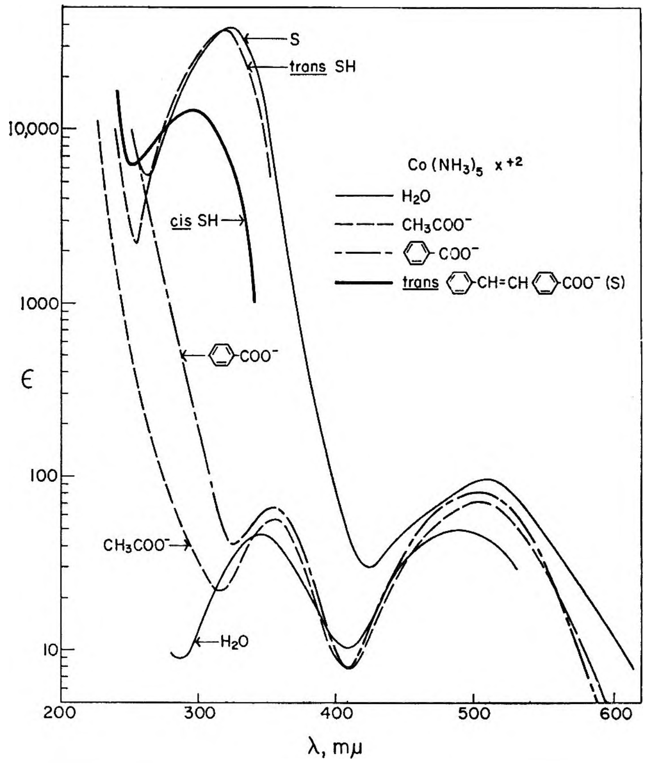

Figure 1. Absorption spectra for aqueous complexes of the type $Co(NH_3)_5X^{2+}$ (after A. W. Adamson, *Coordin. Chem. Rev.*, **3**, 169 (1968)).

Experimental Section

Preparations. The sodium salt of *trans*-4-stilbenecarboxylate, NaTSC, was prepared from α-bromo-*p*-toluic acid by a literature procedure,[14] the latter similarly having been prepared from *p*-toluic acid.[15] The corresponding acid, HTSC, was also obtained; its melting point was 239–246°, compared to the reported value of 247–249°.[16] While the HTSC was evidently not entirely pure, the pmr spectrum was closely similar to that for *trans* stilbene itself,[17] and no resonances attributable to the *cis* isomer were observed. The visible and ultraviolet spectrum of the HTSC agreed within experimental error with the published one.[16]

The perchlorate salt of I, $[Co(NH_3)_5(TSC)](ClO_4)_2$, was prepared as follows. Equimolar amounts of $[Co(NH_3)_5(H_2O)](ClO_4)_3$ and NaTSC were dissolved in a minimum volume of dimethylacetamide and the mixture was heated on a water bath at 80° for 3 hr. The reaction mixture was shaken periodically; light was excluded. The crude product was obtained by pouring the reaction mixture into three to four volumes of dilute perchloric acid and then filtering off the precipitated complex. The product was recrystallized from hot (90°) water, using added sodium perchlorate to reduce the solubility. The solution was then filtered, the precipitate washed twice with cold water, once with a small volume of ethanol, and several times with ether; it was then vacuum dried over magnesium perchlorate (in the dark). The whole recrystallization procedure was repeated to remove traces of uncomplexed HTSC. *Anal.* Calcd for $[Co(NH_3)_5(O_2C_{15}H_{11})](ClO_4)_2$: C, 31.5; H, 5.1; N, 12.3. Found: C, 31.8; H, 4.6; N, 12.4. The absorption spectrum of the aqueous solution of I is included in Figure 1.

The *cis* isomer of 4-stilbenecarboxylic acid, HCSC, was prepared by irradiating a dioxane solution of HTSC for several hours with a mercury arc lamp. The product was isolated by the procedure of ref 16.

Benzoatopentaamminecobalt(III) perchlorate was prepared by the method of Gould and Taube,[18] and recrystallized twice from water. *Anal.* Calcd for $[Co(NH_3)_5(O_2C{-}C_6H_5)](ClO_4)_2 \cdot 2H_2O$: C, 16.80; H, 4.80; N, 14.00; Co, 11.80. Found: C, 17.06 H, 4.77; N, 13.86; Co, 12.10. A sample of pure acetatopentaamminecobalt(III) perchlorate was kindly supplied by Dr. M. Barret. The spectra of these last two complexes are included in Figure 1.

General Procedures. The light source was a water-cooled General Electric A-H6 mercury arc, mounted

---

(13) A. W. Adamson, *Discussions Faraday Soc.*, **29**, 163 (1960).

(14) D. H. Wadsworth, O. E. Schupp, E. J. Sens, and J. A. Ford, Jr., *J. Org. Chem.*, **30**, 680 (1965).

(15) W. Davies and W. H. Perkins, *J. Chem. Soc.*, 2202 (1922).

(16) G. Berti and F. Bottari, *Gazz. Chim. Ital.*, **89**., 2371 (1959).

(17) "Catalogue of NMR Spectra," Varian Associates, Palo Alto, Calif., spectra no. 305 and 306.

(18) E. S. Gould and H. Taube, *J. Amer. Chem. Soc.*, **86**, 1318 (1964).

on an optical bench, with collimating lenses, etc., as previously described.[19] A UG11 Schott glass filter was used for the irradiations of the stilbene absorption band; this filter transmitted light between 250 and 385 mμ, but since Pyrex optics were used, the net wavelength spread of the light reaching the solution was limited to the range 340 to 385 mμ. Two Corning glass filters, CS-370 and CS-496, were used in combination for irradiation of the L_1 bands of the complexes; this combination transmitted light between 500 and 600 mμ.

The photolyses were carried out in a 10-cm cylindrical spectrophotometer cell, using solutions of such known concentration (around 0.001 M) as to have complete absorption of the incident light. To avoid pH increases during photolyses, which might lead to base catalyzed hydrolysis of the complexes, the solutions were also 0.01 M in perchloric acid. In addition, the photolyses were limited to about 10% reaction, to avoid undue inner filter effects and, in the case of solutions of I, to minimize loss of light from scattering by the insoluble HTSC produced. Incident light intensity was determined by Reineckate actinometry.[20]

Emission spectra were measured by means of an American Instrument Company spectrofluorometer, and the visible and ultraviolet absorption spectra by means of a Cary Model 14 spectrophotometer or a Beckman Model DU instrument. Proton resonance spectra were obtained with a Varian A60 instrument.

Analytical Procedures. Carbon, hydrogen, and nitrogen analyses were made commercially by standard microanalytical procedures (Elek Microanalytical Laboratories, Torrance, Calif.).

The photolyzed solutions were analyzed for the various possible products as follows. Cobalt(II) was determined by dilution of an aliquot of the solution into acetone containing ammonium thiocyanate, and the optical density due to $Co(NCS)_4^{2-}$ measured at 625 mμ.[21] Free HTSC released during the photolyses was present as a suspension since the acid is quite insoluble in acidified water. It was extracted with ether, the ether solution evaporated, and the residue triturated with 2 M sodium hydroxide and the mixture filtered. The remaining precipitate consisted of NaTSC, which is insoluble under these conditions. The solid was converted to HTSC by the addition of dilute aqueous hydrochloric acid and dissolved in ethanol; its identity was confirmed by its absorption spectrum, and the amount present by the absorbance at 319 mμ.[16]

The filtrate from the above separation contained any NaCSC present, as established by tests with a sample of known material. Where such product was present, it was then precipitated as the acid, filtered off, dissolved in ethanol, and determined spectrophotometrically.

A further possible product was $Co(NH_3)_5(H_2O)^{3+}$. The photolyzed solution was passed through a Dowex 50 ion-exchange column, and any cobaltous ion and aquopentaammine complex present was then eluted with 10% aqueous hydrochloric acid. The aquo complex was then determined from the visible and ultraviolet absorption spectrum of the effluent solution.

Results

The principal results are summarized in Table I. Both the acetato- and the benzoatopentaammine complexes showed the expected low sensitivity to light in the region of either the L_1 or the L_2 absorption bands. A small yield of the aquation product, $Co(NH_3)_5(H_2O)^{3+}$, appeared to be present, but insufficient for an accurate determination. An upper limit to the amount could be set, however, which was adequate for the purposes of this investigation.

Table I: Photolysis of Certain Carboxylatopentaamminecobalt(III) Complexes (25°, 0.01 M Aqueous Perchloric Acid)

	Quantum yields[a]	
Complex	340–385 mμ	500–600 mμ
$Co(NH_3)_5(acetate)^{2+}$	$\phi_R < 7 \times 10^{-4}$	$\phi_R < 1 \times 10^{-4}$ $\phi_A < 0.01$
$Co(NH_3)_5(benzoate)^{2+}$	$\phi_R < 3 \times 10^{-3}$ $\phi_A < 0.01$	$\phi_A < 0.01$
$Co(NH_3)_5(TSC)^{2+}$	$\phi_R = 0.16$ $\phi_L = 0.090$ $\phi_A < 0.04$ *b*	$\phi_R < 1 \times 10^{-4}$ $\phi_A < 0.05$

[a] ϕ_R, ϕ_A, and ϕ_L denote the quantum yields for Co(II), aquopentaamminecobalt(III), and free TSC ligand, respectively. [b] The quantum yield for isomerization of the released TSC was less than 1×10^{-3}, and less than 5×10^{-4} for that which remained coordinated.

By contrast, complex I was quite light sensitive in the region 340 mμ to 385 mμ. The principal reaction was one of redox decomposition to give cobalt(II); the actual oxidation products were not determined, but the TSC ligand was affected in part since the yield of free HTSC was only about half of that of cobalt(II). Again, it was established that only a small proportion of the photolysis led to formation of $Co(NH_3)_5(H_2O)^{3+}$ and also therefore that this reaction mode was not responsible for any important fraction of the free HTSC found. Ammonia analyses were not accurate enough to determine whether some $Co(NH_3)_4(H_2O)(TSC)^{2+}$ might have been formed, analogous to the reported behavior of $Co(NH_3)_5Cl^{2+}$ [22] and $Co(NH_3)_5$-

---

(19) E. Zinato, R. Lindholm, and A. W. Adamson, *J. Amer. Chem. Soc.*, **91**, 1076 (1969).

(20) E. Wegner and A. W. Adamson, *ibid.*, **88**, 394 (1966).

(21) R. E. Kitson, *Anal. Chem.*, **22**, 664 (1959).

(22) L. Moggi, N. Sabbatini, and V. Balzani, *Gazz. Chim. Ital.*, **97**, 980 (1967).

N_3^{2+}[23] (in these last two cases, however, 254 mμ radiation was used, so that a charge-transfer band was irradiated).

It was established that no isomerization of the TSC occurred. The free TSC ligand contained no appreciable amount of *cis* form. The second possibility, namely that ligand isomerization occurred but with the TSC remaining coordinated, was ruled out by photolyzing a solution of I to complete decomposition. Again, no *cis* ligand was found (the free HTSC produced in the irradiation remained suspended as insoluble material, and hence was not subject to any appreciable photoisomerization itself).

As indicated in Table I, complex I was virtually insensitive to light around 500 mμ in wavelength, as was the acetatopentaammine species. Finally, it should be mentioned that the dark thermal aquation of the various complexes was small enough that no correction for this was needed. Also, in the case of I, deaeration of the solution did not affect the photochemical behavior.

The results of the emission studies, using 330 mμ stimulating light, are shown in Figure 2. The free ligand, as NaTSC, showed the expected fluorescent emission centered at 400 mμ, characteristic of the first excited singlet state.[24] No phosphorescent emission was observed, nor expected, in terms of the behavior of stilbenes generally in room temperature solution.[25]

As shown in the figure, quite appreciable quenching of the fluorescence occurred in the presence of added $Co(NH_3)_5(H_2O)^{3+}$, and emission was essentially absent in the case of compound I. The small residual emission shown in Figure 2 for this last case is almost certainly due to the presence of some free TSC produced by photodecomposition. The results are for a 50% water–ethanol mixture as solvent; this medium was chosen as one in which all of the species had a reasonable solubility and yet would still be largely aqueous.

Discussion

The immediate conclusion from the above results seems to be that intramolecular energy transfer occurs with I, to provide an example of an internally sensitized photolysis of a coordination compound. The basis for this conclusion follows.

The fact that the absorption band of I at 320 mμ is essentially unaltered from that for free HTSC indicates that the singlet–singlet transition has remained largely and perhaps entirely isolated in the ligand moiety. Alternatively, it does not seem tenable to view the 320-mμ band in I as a charge-transfer band of the type found in acidopentaammine complexes (CTTM), not only for the above reason, but also because the other carboxylatopentaammines show a normal intensity L_2 absorption in that wavelength region. It could be argued that the extended π system of the TSC ligand might shift the first CTTM band of I to the 370-mμ region, and it is true that some bathochromic shift appears to occur in the case of the benzoatepentaammine complex, relative to the acetatopentaammine one. However, the virtually intact minimum in the absorption spectrum of I at about 250 mμ should not then be present. From a comparison of the minima for I and for free TSC, a maximum of a few per cent contribution from a hidden CTTM band might be present, or not enough for absorption by such a hidden band to account for the observed quantum yield of 0.16.

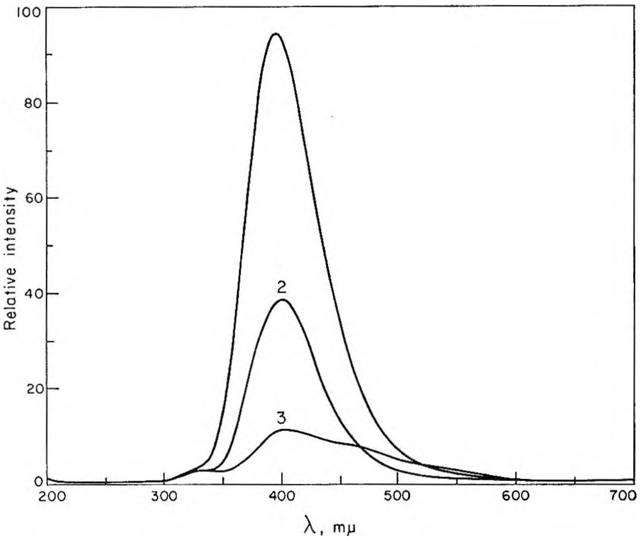

Figure 2. Emission from *trans*-4-stilbenecarboxylate ion (330 mμ exciting radiation; 50% ethanol–water solution): 1, 0.001 *M* NaTSC; 2, 0.001 *M* NaTSC + 0.005 *M* $Co(NH_3)_5(H_2O)^{3+}$; 3, 0.001 *M* complex I.

As confirmation that the carboxyl group as a ligand does not introduce appreciable CTTM character to the L_2 band, the acetato- and benzoatopentaammine complexes show about the same low photosensitivity in the 340 to 385-mμ region as do the hexaammine and aquopentaammine species.

It seems clear, then, that the redox photolysis that occurs with I should not be ascribed to any disposition toward such reaction of the excited state first reached by absorption in 320-mμ band. As further discussed below, the fact that the observed reaction is one of redox decomposition strongly suggests that the excited state of the coordinated cobalt system which is populated by energy transfer is one having CTTM character.

To elaborate on the above conclusion, the partial quenching of the fluorescent emission from TSC by $Co(NH_3)_5(H_2O)^{3+}$ and the essentially complete quenching when TSC is coordinated in I probably represent analogous processes. In the first case, the quenching is accompanied by redox decomposition of the aquopentaammine complex,[8] and in the second, by the redox decomposition of I. Both effects could be supposed to be due to a catalyzed deactivation of the singlet excited state of the TSC group, but then the associated photolysis would have to be attributed to a hot ground state reaction of the complex. Were this the case, aquation would be the expected reaction as this is an easier thermal process than is redox decomposition. As with acidopentaammines of cobalt(III) generally, the carboxylatopentaammines show a slow thermal aquation of the acido group, but no detectable redox decomposition.

---

[23] J. F. Endicott and M. Z. Hoffman, *J. Amer. Chem. Soc.*, **90**, 4740 (1968).

[24] H. Dyck and D. S. McClure, *J. Chem. Phys.*, **36**, 2326 (1962).

[25] D. Schulte-Frohlinde, H. Blume, and H. Güsten, *J. Phys. Chem.*, **66**, 2486 (1962).

It seems necessary, then, to ascribe the quenching to an excitation energy transfer rather than to deactivation catalysis. A second supposition would be that the produced excited state was a cobalt(III) ligand field state, *i.e.*, one derived from the $^1T_{1g}$ or $^1T_{2g}$ states of O_h symmetry. This supposition can also be ruled out on the grounds that the observed photochemistry is inappropriate to it. Thus direct population of such excited states by absorption in the region of the L_1 or L_2 bands of the acetato- and benzoatopentaammine complexes, and of the L_1 band of complex (I) leads only to very low quantum yield processes, probably mainly aquation in nature. Such population by energy transfer should do likewise, contrary to the high photoredox yield found for I.

It thus seems necessary to conclude not only that excitation energy transfer has occurred, but also that produced state is a CTTM state of the cobalt(III)–ligand system. The spectroscopically observed first CTTM band for the carboxylatopentaammine complexes lies around 200 mμ, however, and it does not seem possible to populate this state through the singlet excited state of the TSC group, on energy grounds. As previously noted,[8] though, there must exist a set of triplet CTTM excited states of cobalt(III) complexes which are nonspectroscopic (*i.e.*, are not seen in absorption spectroscopy), but which might be reached by intersystem crossing processes. It appears to us that in the present system as well as in those involving intermolecular sensitization, it is a low-lying, nonspectroscopic triplet CTTM state which is responsible for the observed photoredox reaction.

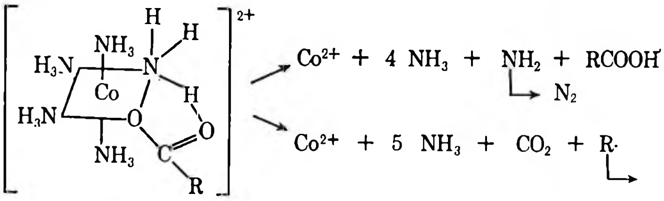

$$\mathrm{Co^{2+} + 4\ NH_3 + \underset{\hookrightarrow N_2}{NH_2} + RCOOH} \qquad (2)$$

$$\mathrm{Co^{2+} + 5\ NH_3 + CO_2 + R\cdot} \qquad (3)$$

A remaining question is whether the above state is produced directly from the TSC singlet excited state or whether the latter first converts to a TSC triplet state which then undergoes the excitation energy transfer. The second alternative was considered to be the more likely in the case of the biacetyl sensitized decomposition of $Co(NH_3)_6^{3+}$,[8] since in the presence of this complex, the biacetyl phosphorescence was quenched, but not the fluorescence. In the case of TSC, however, fluorescence quenching is observed, which indicates that the singlet excited state has been intercepted.

A further point is that in the ordinary photochemistry of the stilbenes, the observed *trans* to *cis* photoisomerization is considered to occur *via* the triplet excited state (see ref 9 and 10), produced from the singlet excited state by intersystem crossing. In our system we observe no isomerization either of the TSC which remains coordinated or of that which is released, which suggests that the triplet excited state of TSC was not populated. We therefore conclude that most probably the triplet CTTM state of the complex is formed from the singlet excited state of the TSC ligand by an intramolecular crossing process. The spin conservation rule is not of ubiquitous importance; it is violated, for example, in singlet to triplet intersystem crossing processes.

A remaining speculation concerns the *chemical* mechanism of the redox decomposition of I. It follows from the quantum yield results that production of cobalt(II) leads to free TSC ligand only about 55% of the time. The implication is that 55% of the primary acts lead to oxidation either of ammonia or of solvent, and 45%, to oxidation of the TSC. As illustrated by the mechanistic scheme below, the primary process might be reaction 2 part of the time. This is apparently what occurs in the 254-mμ photolysis of $Co(NH_3)_5(H_2O)^{3+}$, for which the final products are cobalt(II) and nitrogen.[26] Hydrogen bonding between the carboxyl oxygen and an adjacent ammonia group is likely, and a reaction of type 2 might be assisted by a hydrogen atom transfer to the TSC ligand. Reaction 3 shows possible products if the acido group is oxidized directly. The ultimate fate of possible fragments such as R· was not sought for in the present investigation.

Acknowledgment. These investigations were supported in part by Contract No. DA-31-124-ARO-D-343 between the University of Southern California and the U. S. Army Research Office (Durham).

---

[26] J. F. Endicott and M. Z. Hoffman, *J. Amer. Chem. Soc.*, **87**, 3348 (1965).

Pulse-Radiolysis Studies of *p*-Hydroxyphenylpropionic Acid[1]

by J. Chrysochoos

Department of Chemistry, The University of Toledo, Toledo, Ohio 43606 *(Received April 28, 1969)*

The pulse radiolysis technique has been used to investigate the initial radiolysis products of aqueous *p*-hydroxyphenylpropionic acid (S). The transient absorption spectra show that OH and H adducts are formed initially in acidic and near-neutral solutions while in alkaline solutions both addition products and phenoxyl radicals are formed simultaneously. The decay of the addition products in acidic and near-neutral solutions is accompanied by a parallel formation of phenoxyl radicals by a process obeying first-order kinetics with $k = (2.7 \pm 0.3) \times 10^3$ sec^{-1}. Both the OH and H adducts have overlapping intense uv absorptions. Their molar extinction coefficients at 320 and 330 mμ are 5.0×10^3, 3.5×10^3 and 3.4×10^3, 4.1×10^3 M^{-1} cm^{-1}, respectively. The reaction rate constants of H atoms with *p*-hydoxyphenylpropionic acid is $(1.5 \pm 0.3) \times 10^9$ M^{-1} sec^{-1}. Evidence was obtained for reactions of O_2 with the phenoxyl type radicals in alkaline solutions of *p*-hydroxyphenylpropionic acid and L(−)-tyrosine, and with the OH adduct of DL-phenylalanine.

Introduction

A variety of pulse-radiolysis studies have been made on the reactivity of aromatic compounds with the initial water radiolysis products. Addition of OH radicals and H atoms to the benzene ring lead to cyclohexadienyl-type radicals which have similar intense uv absorption bands.[2-6] Addition of OH radicals to aromatic rings carrying hydroxyl groups is particularly interesting because of the possibility of elimination of water from the OH adduct to form phenoxyl-type radicals.[7] Such a reaction was not observed in the pulse radiolysis of L(−)-tyrosine in either acidic or basic solutions.[8] However, some evidence for water elimination was obtained in near-neutral solutions of L(−)-tyrosine.[8]

The purpose of this investigation is to obtain additional information on the water elimination reaction in *p*-hydroxyphenylpropionic acid, to study the reactions of this molecule with H atoms, and to determine the molar extinction coefficients of the OH and H adducts.

Experimental Procedure

The irradiation source was a linear accelerator providing 1-μsec pulses of 30-MeV electrons at a dose of 1560 rads/pulse as determined with the modified Fricke dosimeter.[9] The samples were contained in a 5 cm long cylindrical fused silica cell which could be evacuated to 2×10^{-6} Torr. The transient spectra were taken by monitoring the transmission changes using an Osram XBO-450 xenon arc and a Hilger E498 spectrograph with the E720 photoelectric scanning unit. Details of the electronic and optical arrangements are given elsewhere.[10,11] Transient changes were monitored to a Tektronix 535 oscilloscope using three time scales, namely 10, 50, and 200 μsec/cm. In this way, the buildup and decay at various wavelengths were readily studied.

Triply distilled water was used. The other chemicals were of reagent grade and they were used without further purification. To study reactions with O_2, air-saturated solutions were used, containing 2.5×10^{-4} M O_2 at 20°.

Results

Transient Spectra. The transient absorption spectra obtained under various experimental conditions in the pulse radiolysis of *p*-hydroxyphenylpropionic acid are given in Figures 1A and 1B. In almost neutral deaerated solutions (pH 6.0) a broad absorption band was observed 5 μsec after the pulse with an absorption maximum below 320 mμ and a broad shoulder at about 345 mμ (Figure 1A-a). Similar results were observed at pH 4.3 with a possible absorption maximum located at about 300 mμ (Figure 1B-a). However, absorption spectra measured 45 μsec after the pulse show a slight decrease in the intensity of the broad band and the appearance of another weak band with a possible peak maximum at about 415 mμ (Figure 1A-b). This observation was verified in all cases in which the pH was below 7. On the other hand, transient absorption spectra taken 5 μsec after the pulse in alkaline solution (pH 11.4) show intense and broad bands at both 415 mμ and below 360 mμ (Figure 1A-c). In the presence

---

[1] The experimental work was carried out at the Department of Radiation Therapy, Michael Reese Hospital and Medical Center, Chicago, Ill.

[2] (a) L. M. Dorfman, I. A. Taub, and R. E. Bühler, *J. Chem. Phys.*, **36**, 3051 (1962); (b) D. F. Sangster, *J. Phys. Chem.*, **70**, 1712 (1966).

[3] R. Wander, P. Neta, and L. M. Dorfman, *ibid.*, **72**, 2946 (1968).

[4] M. C. Sauer, Jr., and B. Ward, *ibid.*, **71**, 3971 (1967).

[5] K. D. Asmus, B. Cercek, M. Ebert, A. Henglein, and A. Wigger, *Trans. Faraday Soc.*, **63**, 2435 (1967).

[6] P. Neta and L. M. Dorfman, *J. Phys. Chem.*, **73**, 413 (1969).

[7] E. J. Land and M. Ebert, *Trans. Faraday Soc.*, **63**, 1181 (1967).

[8] J. Chrysochoos, *Radiat. Res.*, **33**, 465 (1968).

[9] L. M. Dorfman and M. S. Matheson, *Progr. Reaction Kinetics*, **3**, 237 (1965).

[10] J. Chrysochoos, *Chim. Chronica*, **31A**, 94 (1966).

[11] J. Chrysochoos, J. Ovadia, and L. I. Grossweiner, *J. Phys. Chem.*, **71**, 1629 (1967).

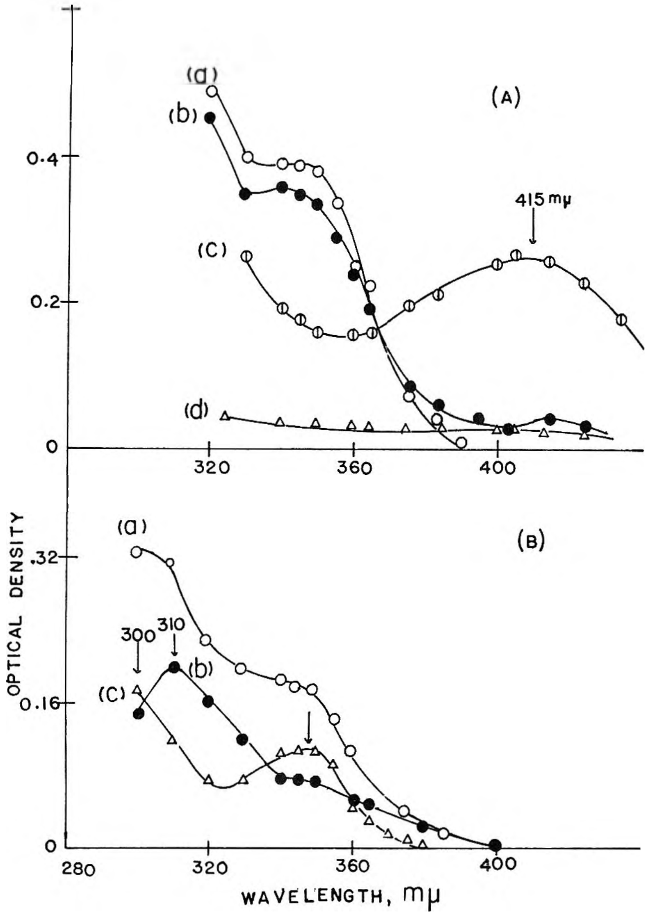

Figure 1. Transient spectra from the pulse radiolysis of p-hydroxyphenylpropionic acid. (A) 5.0 mM deaerated p-hydroxyphenylpropionic acid buffered with OHNa, optical length 10.4 cm: ○, 5 μsec after the pulse; ●, 45 μsec after the pulse (both at pH 6.0); ◐, 5 μsec after the pulse; (pH 11.4); △, 5 μsec after the pulse; pH 11.4, 0.1 M $HCOO^-$. (B) 0.1 mM p-hydroxyphenylpropionic acid buffered with OHNa; pH 4.3, optical length 10.4 cm: ○, 5 μsec after the pulse, deaerated; ●, 5 μsec after the pulse; 0.25 mM O_2 (OH adduct); △, difference of curves (a) and (b) (H adduct).

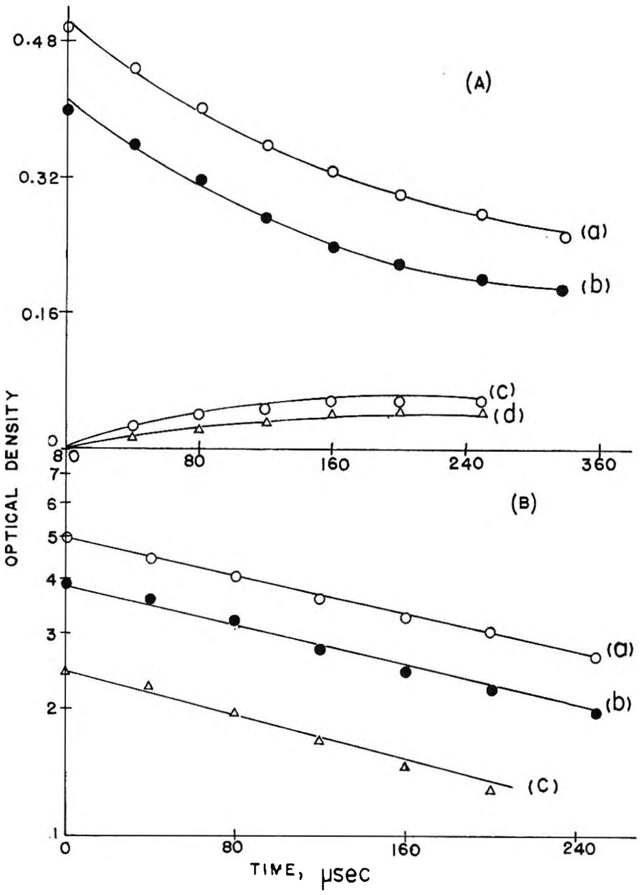

Figure 2. Variation of transient optical densities with time. 5.0 mM p-hydroxyphenylpropionic acid, pH 6.0, optical length 10.4 cm. (A) Decay of the addition products at 320 mμ (a) and 340 mμ (b) and formation of the phenoxyl radicals at 415 mμ (c) and 405 mμ (d). (B) First-order plot of the decay of the addition product at 320 (a), 340 (b), and 360 mμ (c).

of 0.1 M formate, the absorption bands were almost completely quenched (Figure 1A-d) in either acidic or basic solutions. Therefore, the transient species formed are attributed to the reactions of OH radicals and H atoms with the substrate. The absorption band below 360 mμ is attributed to OH and H adducts, while the band at 415 mμ is attributed to a phenoxyl-type radical. The latter was not observed in the pulse radiolysis of DL-phenylalanine,[8] a molecule which does not have a hydroxyl group in the aromatic ring.

The transient spectra obtained in aerated solutions at pH 4.3 (0.25 mM O_2) are attributed to the OH adducts (Figure 1B-b) since under these conditions about 98% of the H atoms are scavenged by O_2 (see text). The reaction of e_{aq}^- with the substrate is very slow[8] ($k \leq (0.9 \pm 0.2) \times 10^7\ M^{-1}\ \text{sec}^{-1}$) and therefore, the conversion of e_{aq}^- to H atoms in deaerated solutions at pH 4.3 is complete ($t_{1/2}(e_{aq}^-) \simeq 2$ μsec). In aerated solutions e_{aq}^- are partly converted to H atoms and partly scavenged by $O_2(t_{1/2}(e_{aq}^-) \simeq 1$ μsec and $t_{1/2}$(H) $\simeq 2$ μsec). The difference between spectra a and b in Figure 1B represents the absorption spectrum of the H adducts (Figure 1B-c) with two peak maxima, one at almost 350 mμ and another one below 300 mμ.

The decay of the OH adducts and the simultaneous buildup of the phenoxyl radicals at pH 6 during the early stages are depicted in Figure 2A. In the later stages, both the decay at 320–360 mμ and buildup at 400–425 mμ become more complex due to the slower formation of the H adduct ($t_{1/2}(e_{aq}^-) \simeq 50$ μsec) and the decay of the phenoxyl radicals. However, during the first 200 μsec the OH adducts decay by a first-order process, studied at 320, 340, and 360 mμ, with rate constants 2.6×10^3, 2.6×10^3, and 2.8×10^3 sec^{-1}, respectively (Figure 2B). Since the phenoxyl radicals are produced *via* the OH adducts, a plot of log ($D_\infty - D_t$), *vs.* t, where D_∞ is the maximum optical density due to phenoxyl radicals, should yield rate constants similar to those mentioned above. However, the behavior of the phenoxyl is more complex due to its own decay, and D_∞ cannot be determined with accuracy.

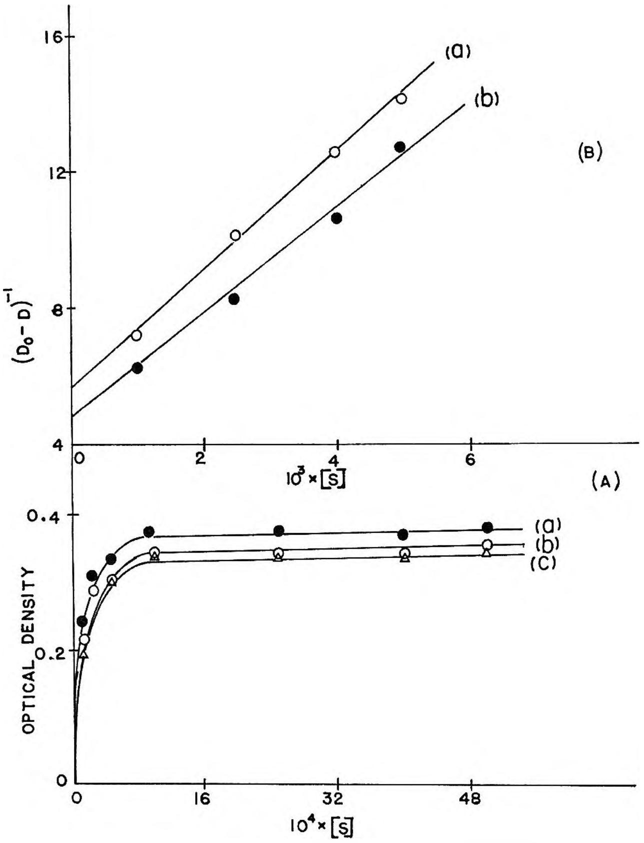

Figure 3. (A) Dependence of the transient optical density upon the initial concentration of the substrate at 320 (a), 330 (b), and 340 mμ (c). Deaerated solutions, pH 2.0–2.3, 20 μsec after the pulse, L = 10.4 cm. (B) Dependence of $\{D_0 - D\}^{-1}$ on the initial concentration of the substrate at 320 (a) and 330 mμ (b); 0.25 mM O_2, pH 2.0–2.3, 20 μsec after the pulse, L = 10.4 cm.

Reactions with H Atoms. The transient absorptions at 320, 330, and 340 mμ in deaerated solutions and at pH 2.0–2.3 (OH and H adducts) increase with increasing concentration of the substrate and at concentrations larger than 1 mM, they attain constant values (Figure 3A). These spectra, taken 20 μsec after the pulse, indicate that 1 mM substrate completely scavenges all the OH radicals and the H atoms produced during the electron pulse. If D_0 represents the maximum optical density at a wavelength λ, we will have

$$D_0 = (D_0)_{\mathrm{SOH\cdot}} + (D_0)_{\mathrm{SH\cdot}} = [\mathrm{OH}]_0 L\epsilon_{\mathrm{SOH\cdot}} + [\mathrm{H}]_0 L\epsilon_{\mathrm{SH\cdot}} \qquad (\mathrm{I})$$

where $[OH]_0$ and $[H]_0$ represent the total amount of OH radicals and H atoms formed during the pulse, L is the optical path and $\epsilon_{SOH\cdot}$ and $\epsilon_{SH\cdot}$ represent the molar extinction coefficients of the OH and H adducts, respectively, at the given wavelength. The values of $[OH]_0$ and $[H]_0$ are calculated from the dose and are based on the G values of OH, H, and e_{aq}^-, namely[9] $G_{OH} = 2.6$; $G_H + G_{e_{aq}^-} = 3.2$. Under these conditions we obtain $[OH]_0 = 4.3\ \mu M$ and $[H]_0 = 5.2\ \mu M$.

In the presence of O_2 there will be a competition for H atoms between the substrate, S, and O_2

$$\mathrm{S + H \longrightarrow SH\cdot} \qquad (1)$$

$$\mathrm{O_2 + H \longrightarrow HO_2} \qquad (2)$$

$$\mathrm{S + OH \longrightarrow SOH\cdot} \qquad (3)$$

If the concentration of the substrate is high enough to completely scavenge OH radicals (*i.e.*, larger than 1 mM) the optical density at any wavelength will given by

$$D = (D_0)_{\mathrm{SOH\cdot}} + (D)_{\mathrm{SH\cdot}} = (D_0)_{\mathrm{SOH\cdot}} + [\mathrm{H}]_0 L\epsilon_{\mathrm{SH\cdot}}[k_1[\mathrm{S}]/(k_1[\mathrm{S}] + k_2[\mathrm{O_2}])]$$

Therefore

$$D = (D_0)_{\mathrm{SOH\cdot}} + (D_0)_{\mathrm{SH\cdot}} - [\mathrm{H_0}]L\epsilon_{\mathrm{SH\cdot}}[k_2[\mathrm{O_2}]/(k_1[\mathrm{S}] + k_2[\mathrm{O}]_2)] \qquad (\mathrm{II})$$

Combining (I) and (II) we obtain

$$(D_0 - D)^{-1} = [[\mathrm{H}]_0 L\epsilon_{\mathrm{SH\cdot}}]^{-1} + [[\mathrm{H}]_0 L\epsilon_{\mathrm{SH\cdot}}]^{-1}(k_1/k_2[\mathrm{O_2}])[\mathrm{S}] \qquad (\mathrm{III})$$

By plotting $(D_0 - D)^{-1}$ *vs.* [S] we can determine the values of both k_1 and $\epsilon_{SH\cdot}$. The results of the competition are plotted according to eq III in Figure 3B at 320 and 330 mμ leading to the values

$$k_1 = (1.50 \pm 0.3) \times 10^9\ M^{-1}\ \mathrm{sec}^{-1} \text{ based on } k_2 = 1.9 \times 10^{10}\ M^{-1}\ \mathrm{sec}^{-1}$$

$$(\epsilon_{\mathrm{SH\cdot}})^{320} = 3.4 \times 10^3\ M^{-1}\ \mathrm{cm}^{-1} \text{ and } (\epsilon_{\mathrm{SH\cdot}})^{330} = 4.1 \times 10^3\ M^{-1}\ \mathrm{cm}^{-1}$$

Introducing the values of $\epsilon_{SH\cdot}$ into eq I we obtain

$$(\epsilon_{\mathrm{SOH\cdot}})^{320} = 5.0 \times 10^3\ M^{-1}\ \mathrm{cm}^{-1} \text{ and } (\epsilon_{\mathrm{SOH\cdot}})^{330} = 3.5 \times 10^3\ M^{-1}\ \mathrm{cm}^{-1}$$

Reactions with O_2. The presence of O_2 in the pulse radiolysis of *p*-hydroxyphenylpropionic acid not only suppresses the formation of the H adducts due to the scavenging of H atoms and e_{aq}^- but also alters the rate of formation and decay of the transient species formed. The decay of the phenoxyl radical is much faster in air-saturated than in deaerated solutions at pH 11.4. This fast decay is accompanied by an almost parallel buildup of a transient absorption at 300–340 mμ which is completed at about 400 μsec. The initial formation of both the phenoxyl and the cyclohexadienyl radicals, due to the reactions of the initial radiolysis products of water, is completed within 20 μsec. The slow buildup of the transient absorption at 300–340 mμ is given in terms of $D_t - D_{20}$, where D_t is the absorption at time t at any wavelength λ and D_{20} is the initial absorption at 20 μsec (*i.e.*, OH and partly H adducts). The presence of formate ion does not alter this behavior but only reduces the maximum absorptions at 20 μsec of both the phenoxyl and the OH adducts. Figure 4A depicts both the fast decay of the phenoxyl in the absence (d) and presence of formate

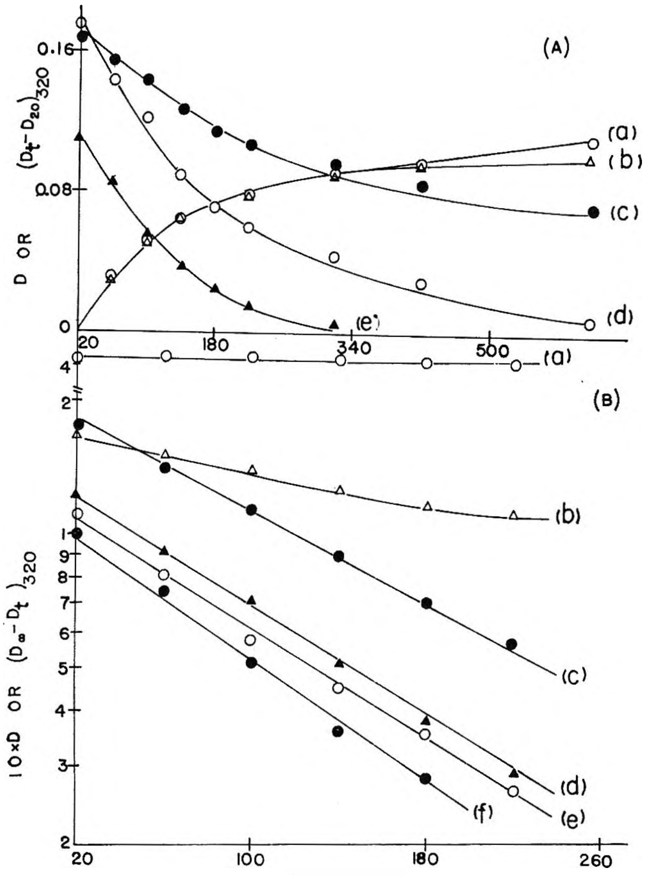

Figure 4. (A) Variation of transient optical densities with time: 0.2 m*M* *p*-hydroxyphenylpropionic acid, 0.25 m*M* O_2, pH 10.6, $L = 10.4$ cm. Slow buildup of the optical density at 320 mμ, given in terms of $(D_t - D_{20})_{320}$ in the absence of formate ion (a) and in the presence of 0.2 m*M* formate ion (b); decay of the phenoxy radical in the absence of formate at 405 mμ (d), and in the presence of 0.2 m*M* formate ion at 400 mμ (e); (c) decay of the phenoxyl at 405 mμ in the pulse radiolysis of 0.1 m*M* deaerated substrate at pH 10.6. (B) First-order kinetics for the decay of the phenoxyl and the appearance of the transient absorption at 320 mμ; 0.2 m*M* substrate, 0.25 m*M* O_2, pH 10.6, $L = 10.4$ cm. Decay of the phenoxyl at 405 mμ in the absence of formate (c) and at 400 mμ in the presence of 0.2 m*M* formate ion (d); appearance of the transient absorption at 320 mμ in terms of $(D_\infty - D_t)_{320}$ in the absence of formate (e) and in the presence of 0.2 m*M* formate ion (f); decay of the phenoxyl at 405 mμ in 0.1 m*M* deaerated substrate at pH 10.6 (b); decay of the addition product at 320 mμ in 5 m*M* deaerated substrate at pH 11.4 (a).

ion (b) whereas curves (a) and (b) represent the corresponding behavior of $D_t - D_{20}$ with time at 320 mμ. Curve (c) shows the decay of the phenoxyl in deaerated solutions. Both the decay of the phenoxyl and the slow buildup at 320 mμ obey first-order kinetics (Figure 4B). The latter is given in terms of $D_\infty - D_t$, where D_∞ represents the maximum optical density attained at 320 mμ. The decay of the cyclohexadienyl radicals at 320 mμ in deaerated solutions is very slow (Figure 4B-a) and therefore it does not interfere with the slow buildup at this wavelength. The half-times measured at 405 and 320 mμ in air-saturated solutions are 120 and 110 μsec, respectively, while the half-times at 400 and 320 mμ in air-saturated solutions containing 0.2 m*M* formate ion have the values of 105 and 100 μsec, respectively (Figure 4B-c-f). Curve b shows the decay of the phenoxyl radicals in deaerated solutions.

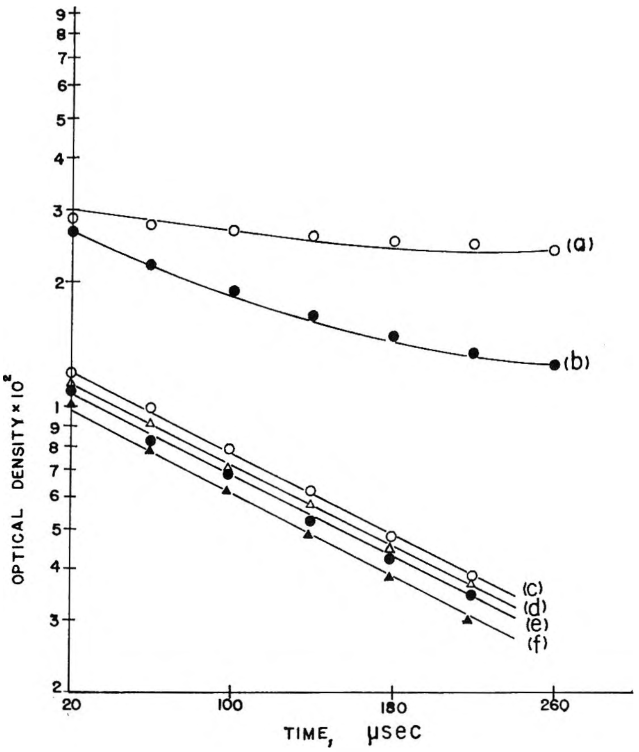

Figure 5. First-order kinetics for the decay of the phenoxyl and the appearance of the absorption at 320 mμ given in terms of $(D_\infty - D_t)_{320}$, curves c to f, in the pulse radiolysis of 0.2 m*M* aqueous L(−)-tyrosine; 0.25 m*M* O_2, pH 10.6, $L = 10.4$ cm; (c) 415 mμ in the absence of formate ion; (d) 320 mμ in the presence of 0.2 m*M* formate ion; (e) 320 mμ in the absence of formate ion; (f) 415 mμ in the presence of 0.2 m*M* formate ion; curves (a) and (b) depict the decay of the addition products and phenoxyl radical in deaerated solutions plotted as simple, first-order processes at 330 and 415 mμ, 5.0 m*M* L(−)-tyrosine, pH 10.0; $L = 10.4$ cm.

Similar results were observed with L(−)-tyrosine at pH 10.6 (Figure 5). However, the decay of the cyclohexadienyl radicals in DL-phenylalanine is faster in the presence of O_2. Since the latter amino acid does not have a hydroxyl group (no phenoxyl radical formed), the slow buildup at 300–340 mμ observed in both *p*-hydroxyphenylpropionic acid and L(−)-tyrosine is attributed to the reactions of O_2 with the phenoxyl radicals

$$\text{phenoxyl} + O_2 \longrightarrow \text{oxidation product} + O_2^- \quad (4)$$

The rate constants for (4) are determined from the decay of the phenoxyl radicals (Figure 4B). The values of (2.6 ± 0.4) × 10^7 and (2.4 ± 0.4) × 10^7 M^{-1} sec^{-1} are obtained for *p*-hydroxyphenylpropionic acid and L(−)-tyrosine, respectively.

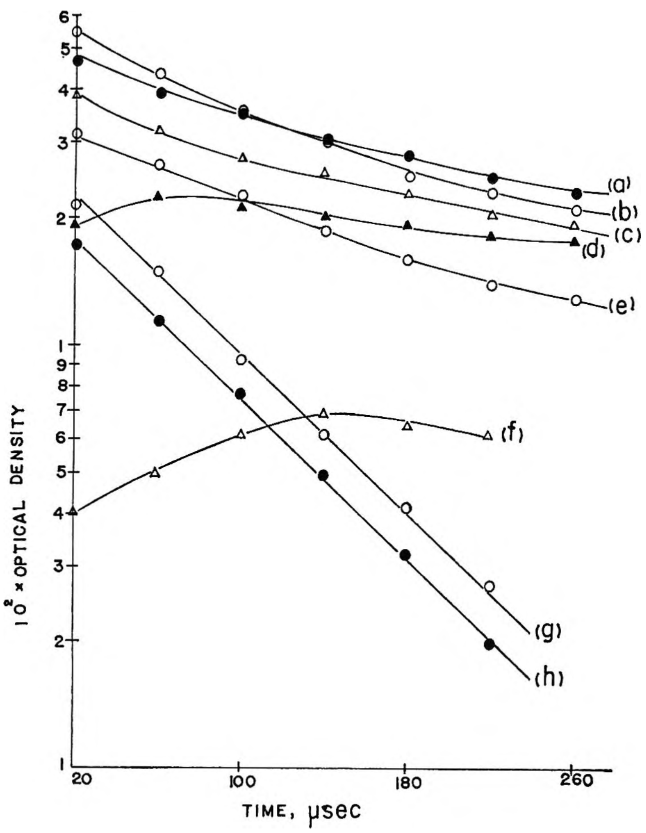

Figure 6. Kinetics of the decay of various transient species in the pulse radiolysis of DL-phenylalanine; 5 mM substrate, L = 10.4 cm. (a) 320 mμ, pH 10.0, deaerated solution; (b) 320 mμ, pH 2.0, deaerated solution; (c) 300 mμ, pH 10.0, deaerated solution (e) 300 mμ, pH 2.0, deaerated solution; (d) 300 mμ, pH 10.0, 0.25 mM O_2; (f) 300 mμ, pH 2.0, 0.25 mM O_2; (g) 320 mμ, pH 2.0, 0.25 mM O_2; (h) 320 mμ, pH 10.0, 0.25 mM O_2.

Possible reactions of O_2 with the OH adducts in p-hydroxyphenylpropionic acid and L(−)-tyrosine cannot be studied in these systems, because if such reactions do occur, they will be masked by reaction 4. However, evidence for such reactions was obtained in the case of DL-phenylalanine in which case reaction 4 does not participate. The decay of the cyclohexadienyl radicals at 320 mμ in aerated solutions of DL-phenylalanine (pH 2.0 and 10.0) is faster than in deaerated solutions and it obeys first-order kinetics (Figure 6). The first-order decay at 320 mμ is accompanied by a parallel increase in the optical density at 300 mμ. In deaerated solutions, the decay at 320 mμ is slower than in aerated solution and it does not obey first-order kinetics. The fast decay at 320 mμ in the presence of O_2 is attributed to the reaction

$$\text{cyclohexadienyl radical} + O_2 \longrightarrow \text{hydroperoxy radical} \quad (5)$$

with a rate constant $k_5 = 4.6 \times 10^7\ M^{-1}\ \text{sec}^{-1}$. The increase in optical absorption at 300 mμ is attributed to the hydroperoxy radical. Since the latter might also absorb to some extent at 320 mμ, the value of k_5 is taken as a lower limit; $k_5 \geq 4.6 \times 10^7\ M^{-1}\ \text{sec}^{-1}$.

Discussion. The transient spectra indicate that in acidic and near-neutral solutions, OH and H addition to the benzene ring leading to cyclohexadienyl radicals are the predominant processes between the substrate and the initial radiolysis products of water. The cyclohexadienyl radicals are transformed, at least during the early stages, to phenoxyl-type radicals by elimination of water.

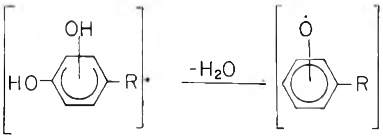

(6)

The value of k_6, $(2.7 \pm 0.3) \times 10^3\ \text{sec}^{-1}$, is comparable to the corresponding values of 5.8×10^3 and $4.7 \times 10^3\ \text{sec}^{-1}$ measured from the decay of the OH adduct of phenol at 330 mμ at pH 6.3 and 7.15 (buffered), respectively.[7]

In alkaline solution, in which the hydroxyl group is ionized, OH radicals both add to the benzene ring and react with the OH group simultaneously.

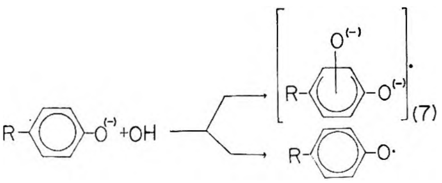

The decay of the phenoxyl radical produced in (7) is very fast while the decay of the OH adducts is extremely slow. It is not clear whether the phenoxyl radicals produced in (6) are exactly identical with those produced in (7) because elimination of water can remove either hydroxyl group from the cyclohexadienyl radicals (reaction 6).

The reactivity of H atoms toward p-hydroxyphenylpropionic acid, *i.e.*, $(1.5 \pm 0.3) \times 10^9\ M^{-1}\ \text{sec}^{-1}$, is a little lower than the reactivity of the OH radicals under similar conditions, *i.e.*, $(3.7 \pm 0.6) \times 10^9\ M^{-1}\ \text{sec}^{-1}$,[8] and it is comparable to the reactivity of H atoms toward phenylacetic acid and p-OH-C_6H_4COOH, namely 1.01×10^9 and $1.45 \times 10^9\ M^{-1}\ \text{sec}^{-1}$, respectively.[6]

The OH and H adducts not only have overlapping uv absorptions but they also have comparable molar extinction coefficients. The corresponding values at 320 and 330 mμ, namely $(\epsilon_{\text{SOH}\cdot})^{320} = 5.0 \times 10^3$, $(\epsilon_{\text{SOH}\cdot})^{330} = 3.5 \times 10^3$, $(\epsilon_{\text{SH}\cdot})^{320} = 3.4 \times 10^3$, and $(\epsilon_{\text{SH}\cdot})^{330} = 4.1 \times 10^3\ M^{-1}\ \text{cm}^{-1}$ compare well with the molar extinction coefficients of OH and H adducts of phenol measured at 330 mμ,[7] namely 4.4×10^3 and $3.8 \times 10^3\ M^{-1}\ \text{cm}^{-1}$. Molar extinction coefficients cannot be determined in alkaline solutions since both the phenoxyl and cyclohexadienyl radicals are formed

Table I: Summary of Rate Constants[a]

Substrate	H + substrate, M^{-1} sec^{-1}	Water elimination from OH adducts, sec^{-1}	Phenoxyl + O_2, M^{-1} sec^{-1}	OH adducts + O_2, M^{-1} sec^{-1}	Ref
p-Hydroxyphenylpropionic acid	$1.5 \pm 0.3 \times 10^9$ (2.0–2.3)	$2.7 \pm 0.3 \times 10^3$ (6)	$2.6 \pm 0.4 \times 10^7$ (11.4)		This work
L-(—)-Tyrosine			$2.4 \pm 0.4 \times 10^7$ (10.6)		This work
DL-Phenylalanine				$\geq 4.6 \times 10^7$	This work
Phenol		5.8×10^3; 4.7×10^3 (6.3) (7.15)			7
p-Hydroxyphenylacetic acid	1.45×10^9				6
Benzene				$5.0 \pm 0.6 \times 10^8$	2a

[a] Figures in parentheses indicates pH.

simultaneously. The aforementioned molar extinction coefficients in acidic and near-neutral solutions do not refer to a single species since more than one cyclohexadienyl radical can be formed. These values should be taken as average molar extinction coefficients

$$\bar{\epsilon} = \sum_i c_i \epsilon_i / \sum_i c_i \qquad \text{(IV)}$$

where ϵ_i represents the actual molar extinction coefficient of the species, i, at λ, and c_i the corresponding concentration.

The reactivity of O_2 with the cyclohexadienyl radicals in DL-phenylalanine, *i.e.*, $k_5 \geq 4.6 \times 10^7\ M^{-1}$ sec^{-1} is lower than the corresponding value determined in benzene, namely $(5.0 \pm 0.6) \times 10^8\ M^{-1}$ sec^{-1}. The peroxy radical formed was not studied but it is assumed to be responsible for the absorption buildup observed at about 300 mμ.

A summary of the rate constants determined in this work and relevant values from the literature is given in Table I.

Ionic Reactions in Gaseous Mixtures of Monosilane with Methane and Benzene[1]

by D. P. Beggs[2] and F. W. Lampe

Department of Chemistry, The Pennsylvania State University, University Park, Pennsylvania 16802

(Received May 1, 1969)

In ionized mixtures of methane and monosilane, the only major ions that are observed to undergo collision reactions with the opposite molecule are CH_3^+, CH_4^+, SiH_2^+, and SiH_3^+. Both CH_4^+ reacting with SiH_4 and SiH_2^+ reacting with CH_4 form $SiCH_2^+$, $SiCH_3^+$, and $SiCH_5^+$; in addition CH_4^+ forms $SiCH_4^+$ on collision with SiH_4 but this product was not detected in collisions of SiH_2^+ with CH_4. CH_3^+ reacts on collision with SiH_4 to give $SiCH_2^+$, $SiCH_3^+$, and $SiCH_4^+$, but not $SiCH_5^+$. The product(s) of SiH_3^+ reactions with CH_4 could not be ascertained, but are energetically limited to $SiCH_3^+$ and $SiCH_5^+$. The reactions of CH_4^+ with SiH_4 are by far the fastest and include, in addition to those mentioned, a collision-stabilized SiH_5^+ product ion. In ionized mixtures of benzene and monosilane, the only major ion undergoing such cross-reactions is $C_6H_6^+$ that is excited to at least 2.3 eV above the ground state. The reaction products are $SiC_6H_5^+$, $SiC_6H_6^+$, $SiC_6H_7^+$, $SiC_6H_8^+$, and $SiC_6H_9^+$. Rate constants are given for the various reactions.

Introduction

As a part of our program concerned with the radiation chemistry of silane systems, we have previously studied the ion-molecule reactions occurring in pure monosilane,[3] in monosilane-acetylene mixtures,[4a] in monosilane-ethylene mixtures,[4b] and, in addition, have reported the formation of SiH_5^+ in monosilane-methane mixtures.[4c] In this paper we report further details of the monosilane-methane system and, in addition, we report our results on ionic reactions in monosilane-benzene mixtures.

A number of studies of the ionic reactions in gaseous methane[5-24] and gaseous benzene[25-31] have been reported in the literature and there seems to be general agreement as to the identification of the bimolecular reactions and the specific reaction rates occurring in these one-component systems. This investigation is concerned with the identification of the "cross-reactions" (reactions between ions of one compound with molecules of the other) in monosilane-methane and monosilane-benzene mixtures and measurement of their specific reaction rates.

Experimental Section

The studies involving the effects of variation in the ion-source pressure and in reaction time available to thermal energy ions were conducted in a somewhat modified Bendix Model 14-101 time-of-flight mass spectrometer. Ionization efficiency curves and appearance potentials were obtained from studies utilizing a Nuclide 12-90-G magnetic sector mass spectrometer.

The basic design and modifications of the time-of-flight mass spectrometer have been described previously.[32-34] The ion-source pressures were read directly from a McLeod gauge which had been calibrated by measurement of the extent of formation of CD_5^+ in CD_4 which occurs *via* an ion-molecule reaction of a known rate constant.[35] It was found (in the pressure range of 1–50 μ) that the McLeod gauge readings were higher than the actual ion source pressures by a factor of 5.0 ± 0.9. A few measurements of total ionization produced in argon by 75-eV electrons yielded a factor of 6 ± 1 which agrees, within the combined precisions, with the calibration by the ion–molecule reaction rate. From all combined effects, we estimate the maximum uncertainty in ion-source pressure to be ±20%.

---

[1] AEC Document No. NYO-3570-11.

[2] Based in part on a thesis by D. P. Beggs submitted to The Pennsylvania State University in partial fulfillment of the requirements for the Ph.D. degree.

[3] G. G. Hess and F. W. Lampe, *J. Chem. Phys.*, **44**, 2257 (1966).

[4] (a) D. P. Beggs and F. W. Lampe, *J. Phys. Chem.*, **73**, 3307 (1969); (b) D. P. Beggs and F. W. Lampe, *ibid.*, **73**, 3315 (1969); (c) D. P. Beggs and F. W. Lampe, *J. Chem. Phys.*, **49**, 4230 (1968).

[5] V. L. Tal'roze and A. K. Lyubimova, *Dokl. Akad. Nauk SSSR*, **86**, 909 (1952).

[6] D. P. Stevenson and D. O. Schissler, *J. Chem. Phys.*, **24**, 926 (1956).

[7] F. H. Field, J. L. Franklin, and F. W. Lampe, *J. Amer. Chem. Soc.*, **79**, 2419 (1957).

[8] F. W. Lampe and F. H. Field, *ibid.*, **79**, 4244 (1957).

[9] G. G. Meisels, W. H. Hamill, and R. R. Williams, *J. Phys. Chem.*, **61**, 1456 (1957).

[10] C. D. Wagner, P. A. Wadsworth, and D. P. Stevenson, *J. Chem. Phys.*, **28**, 517 (1958).

[11] V. L. Tal'roze and E. L. Frankevich, *Zh. Fiz. Khim.*, **34**, 2709 (1960).

[12] R. Fuchs, *Z. Naturforsch.*, **16a**, 1026 (1961).

[13] S. Wexler and N. Jesse, *J. Amer. Chem. Soc.*, **84**, 3425 (1962).

[14] A. Henglein and G. A. Muccini, *Z. Naturforsch.*, **18a**, 753 (1963).

[15] F. H. Field, J. L. Franklin, and M. S. B. Munson, *J. Amer. Chem. Soc.*, **85**, 3575 (1963).

[16] G. A. Derwish, A. Galli, A. Giardini-Guidoni, and G. G. Volpi, *J. Chem. Phys.*, **40**, 5 (1964).

[17] C. W. Hand and H. von Weyessenhoff, *Can. J. Chem.*, **42**, 195 (1964).

[18] M. S. B. Munson and F. H. Field, *J. Amer. Chem. Soc.*, **87**, 4242 (1965).

[19] T. W. Shannon, F. Meyer, and A. G. Harrison, *Can. J. Chem.*, **43**, 159 (1965).

[20] K. R. Ryan and J. H. Futrell, *J. Chem. Phys.*, **42**, 824 (1965).

[21] H. von Koch, *Arkiv Fysik*, **28**, 529 (1965).

[22] F. H. Field and M. S. B. Munson, *J. Amer. Chem. Soc.*, **87**, 3289, (1965).

A variable time-delay circuit, described earlier,[34,36] was employed which permitted variation of the time between the end of the electron pulse and the onset of the ion draw-out pulse. During this delay time the entire reaction chamber is field-free, so that reactions occurring during this time interval do so under purely thermal conditions. The temperature of the source was 70°.

The electron beam was pulsed at 10 kilocycles for all the experiments reported, using a pulse width of 0.25 μsec and an ion draw-out pulse width of 3.9 μsec. The 250-V ion draw-out pulse was applied after a delay of 0–1 μsec from the electron-beam cutoff. The maximum delay time used was less, by a factor of at least 5, than the average primary-ion transit time to a wall of the ion source.

At the longer delay times, there is a diminution in all ion currents due to thermal drift of the ions out of the collectable region of the ionization chamber; this ion-current decrease is mass dependent and a correction is necessary. Correction factors for this effect were determined by observing the ion-current time-delay dependence of *m/e* 84, 58, 40, 28, and 20 from krypton, acetone, argon, nitrogen, and neon, respectively. The corrections were applied as described previously.[34] In all pressure and time-delay dependence studies, the energy of the electron beam was 100 eV and no collimating magnetic field was used on the ion source. We found that the various ion-drift losses with delay time could be reproduced and understood theoretically only when the ion source was free from the effects of such a collimating magnetic field.

The retarding potential difference technique (RPD)[37] was adopted for appearance potential and ionization efficiency curve measurement on the Nuclide instrument. A basic description of this instrument, its modifications, and the technique was reported earlier.[4a] It was found that a retarding potential difference, ΔE_P, of 0.2 eV gave the best results when observing ionization efficiency curves of secondary ions.

A correction must be made for the naturally occurring isotopes of silicon (^{28}Si, 92.2%; ^{29}Si, 4.7%; ^{30}Si, 3.1%) and carbon (^{12}C, 98.9%; ^{13}C, 1.1%). In the benzene–silane mixtures cross-reaction products are found at *m/e* 105, 106, 107, 108, and 109. The corrections are based on the observation that since there are no ions at *m/e* 103 or 104, the ion fraction at *m/e* 105 must be made up of $^{28}Si^{12}C_6H_5^+$. Then *m/e* 106 must be made up of $^{29}Si^{12}C_6H_5^+$, $^{28}Si^{13}C^{12}C_5H_5^+$, and $^{28}Si^{12}C_6H_6^+$. After determining the amount of $^{29}Si^{12}C_6H_5^+$ and $^{28}Si^{13}C^{12}C_5H_5^+$ from the isotopic abundances, the amount of $^{28}Si^{12}C_6H_6^+$ is easily calculated. The intensity of $^{28}Si^{12}C_6H_7^+$ is then easily obtained by correcting the intensity of *m/e* 107 for contributions from $^{30}Si^{12}C_6H_5^+$, $^{29}Si^{12}C_6H_6^+$, and $^{28}Si^{13}C^{12}C_5H_6^+$; the intensities of $^{28}Si^{12}C_6H_8^+$ and $^{28}Si^{12}C_6H_9^+$ are obtained by applying analogous corrections to *m/e* 108 and 109.

The methane (Research Grade, 99.54% pure) was purchased from the Phillips Petroleum Company and the benzene (Baker Analyzed, 99.9% pure) from the J. T. Baker Chemical Co. The silane was obtained from Air Products, Inc., while the dimethyl mercury was supplied by the Eastman Organic Chemicals Co. Methane-d_4 (minimum isotopic purity of 99%) was acquired from Stohler Isotope Chemicals, Ltd., while the silane-d_4 was prepared by the action of $LiAlD_4$ on $SiCl_4$ that had been purchased from the Peninsular Chemical Co. All gases were fractionated on the vacuum line and checked mass spectrometrically for satisfactory purity before use.

Methane–Silane System

A. Reaction Identification. 1. Bimolecular Reactions. A typical mass spectrum of the silane–methane system is shown in Table I while most of the major ions of interest are shown in an ion fraction *vs.* pressure plot in Figure 1. The data shown in Table I and Figure 1 are not corrected for the various isotopic contributions, since the purpose of these data is simply to establish the products of cross reactions and the primary ions that are reacting; it is sufficiently accurate for this purpose to assume that each ion is composed only of ^{28}Si and ^{12}C. In the determination of the rate constants isotopic corrections were, of course, made. Examination of this plot shows that CH_3^+, CH_4^+, and SiH_2^+ are re-

---

(23) F. P. Abramson and J. H. Futrell, *J. Chem. Phys.*, **45**, 1925 (1966).

(24) I. Szabo, *Arkiv Fysik*, **35**, 339 (1967).

(25) A. Henglein, *Z. Naturforsch*, **17a**, 44 (1962).

(26) F. H. Field, P. Hamlet, and W. F. Libby, *J. Amer. Chem. Soc.*, **89**, 6035 (1967).

(27) R. Barker, *Chem. Ind.* (London), 233 (1960).

(28) L. J. Bone and J. H. Futrell, *J. Chem. Phys.*, **47**, 4366 (1967).

(29) S. Wexler and R. P. Clow, *J. Amer. Chem. Soc.*, **90**, 3940 (1968).

(30) A. Giardini-Guidoni and F. Zocchi, *Trans. Faraday Soc.*, **64**, 2342 (1968).

(31) C. Lifshitz and B. G. Reuben, *J. Chem. Phys.*, **50**, 951 (1969).

(32) W. C. Wiley and I. H. McLaren, *Rev. Sci. Instrum.*, **26**, 1150 (1955).

(33) G. B. Kistiakowsky and P. H. Kydd, *J. Amer. Chem. Soc.*, **79**, 4825 (1957).

(34) P. M. Becker and F. W. Lampe, *J. Chem. Phys.*, **42**, 3857 (1965).

(35) V. L. Tal'roze and E. L. Frankevich, *Zh. Fiz. Khim.*, **34**, 2709 (1960).

(36) C. W. Hand and H. von Weyssenhoff, *Can. J. Chem.*, **42**, 195 (1964).

(37) R. E. Fox, W. M. Hickam, D. J. Grove, and T. Kueldans, *Rev. Sci. Instrum.*, **26**, 1101 (1955).

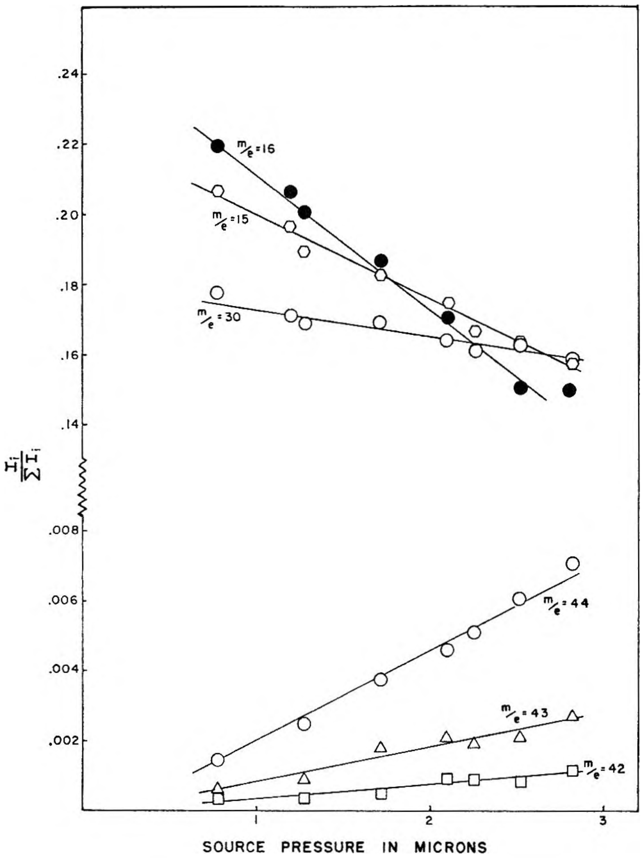

Figure 1. Dependence of ion fraction on source pressure in monosilane–methane mixtures. $[CH_4]/[SiH_4] = 1.5$.

Table I: Spectrum of SiH_4–CH_4 Mixture[a]

m/e	$I_i/\Sigma I_i$	Ion
13	0.019	CH^+
14	0.057	CH_2^+
15	0.173	CH_3^+
16	0.177	CH_4^+
17	0.040	CH_5^+
28	0.087	Si^+, $C_2H_4^+$
29	0.100	SiH^+, $C_2H_5^+$
30	0.147	SiH_2^+
31	0.149	SiH_3^+
32	0.024	Isotope, SiH_4^+
33	0.011	Isotope, SiH_5^+
42	0.00106	$SiCH_2^+$
43	0.00252	$SiCH_3^+$
44	0.00656	$SiCH_4^+$
45	0.00282	$SiCH_5^+$

[a] 1.0 μsec delay time, 2.8×10^{-3} Torr, $CH_4/SiH_4 = 1.5$.

actants in this system. The products of bimolecular cross-reactions appear at m/e 42, 43, 44, and 45. Secondary ions were also observed at m/e 41 and 46; however, their very small intensity deemed them as insignificant in comparison with the aforementioned products. SiH_3^+ is also observed as a product, but this has been observed and reported earlier in the pure silane system.[4a] There is no indication that SiH_3^+ is being formed by any process other than the homo-reaction[3]

$$SiH_2^+ + SiH_4 \longrightarrow SiH_3^+ + SiH_3 \qquad (1)$$

It has been found that SiH_3^+ also reacts to a small extent in methane–silane mixtures. Numerous homoreactions in methane were also observed, but since there was every indication that the products of these reactions (m/e 17, 26, 27, 28, and 29) were unique to these homoreactions, they were not studied further. Data such as shown in Figure 1 indicate that Si^+ and SiH^+ are neither products nor reactants in the system.

As an aid in the elucidation of the secondary cross reactions, we have compared the appearance potentials of the products with the appearance potentials of the possible reactants. The primary ion which has an appearance potential closest to that of the product ion is taken to be the reactant ion provided the reaction is energetically feasible. If more than one primary ion is responsible for production of a product ion, a change in the slope of the ionization efficiency curve often denotes the onset of a reaction involving a different reactant ion.

The ionization efficiency curves of the bimolecular

Table II

Typical Secondary Spectra of Pure Silane[1]

m/e	Relative intensity	Ion identity
57	11	Si_2H^+
58	60	$Si_2H_2^+$
59	41	$Si_2H_3^+$
60	100	$Si_2H_4^+$
61	18	$Si_2H_5^+$
62	8	Isotope

Typical Secondary Spectra of Pure Methane[7]

m/e	Relative intensity	Ion identity
17	100	CH_5^+
26	1.5	$C_2H_2^+$
27	9.4	$C_2H_3^+$
28	9.2	$C_2H_4^+$
29	55.6	$C_2H_5^+$
30	1.7	$C_2H_6^+$

Typical Secondary Spectra of Pure Benzene[31]

m/e	Relative intensity	Ion identity
103	6.8	$C_8H_7^+$
115	34	$C_9H_7^+$
127	47	$C_{10}H_7^+$
128	100	$C_{10}H_8^+$
129	33	$C_{10}H_9^+$
139	5.5	$C_{11}H_7^+$
152	11	$C_{12}H_8^+$
153	42	$C_{12}H_9^+$
154	31	$C_{12}H_{10}^+$
155	91	$C_{12}H_{11}^+$

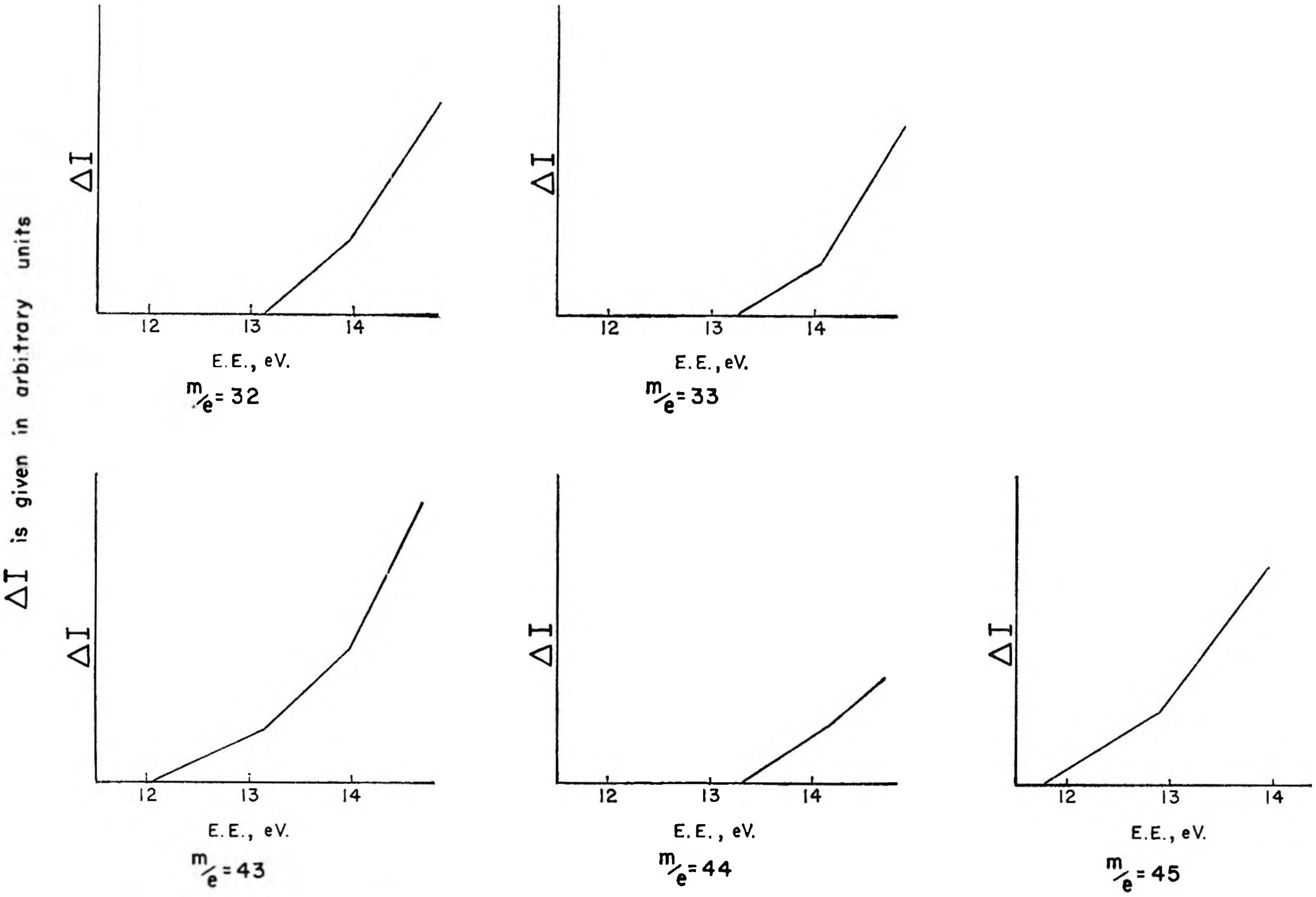

Figure 2. Ionization efficiency curves of various product ions in methane–monosilane mixtures. (Individual points do not appear since the curves are traced directly from the continuous RPD curves drawn by the X-Y recorder.)[37] Threshold potentials reproducible to ±0.2 eV.

product ions are shown in Figure 2. By comparing the onset and "breaks" of these curves with the known appearance potentials of the primary reactants (SiH_2^+, 11.9 eV; CH_4^+, 13.1 eV; CH_3^+, 14.3 eV)[38,39] the precursors may be identified. For example, the ionization-efficiency curve of m/e 43 shows an onset of 12.0 eV indicating SiH_2^+ as a precursor, a break at 13.2 eV indicating CH_4^+ as a precursor, and another break at 14.1 eV suggesting CH_3^+ also as a precursor. As will be discussed later, experiments with $(CH_3)_2Hg$ mixtures strengthen our conclusion that CH_3^+ is also a precursor. The low intensity of m/e 42 prohibited the collection of reliable enough ionization efficiency data near onset; however, kinetic data discussed later indicate that all three reactants are precursors. Similar appearance potential and kinetic considerations were used to establish the precursors to m/e 43, 44, and 45. The bimolecular cross-reactions established are summarized below.

$$\mathrm{SiH_2^+ + CH_4} \longrightarrow \left\{ \begin{array}{ll} \longrightarrow \mathrm{SiCH_2^+ + 2H_2} & (2) \\ \longrightarrow \mathrm{SiCH_3^+ + H_2 + H} & (3) \\ \longrightarrow \mathrm{SiCH_5^+ + H} & (4) \end{array} \right.$$

$$\mathrm{CH_3^+ + SiH_4} \longrightarrow \left\{ \begin{array}{ll} \longrightarrow \mathrm{SiCH_2^+ + 2H_2 + H} & (5) \\ \longrightarrow \mathrm{SiCH_3^+ + 2H_2} & (6) \\ \longrightarrow \mathrm{SiCH_4^+ + H_2 + H} & (7) \end{array} \right.$$

$$\mathrm{CH_4^+ + SiH_4} \longrightarrow \left\{ \begin{array}{ll} \longrightarrow \mathrm{SiCH_2^+ + 3H_2} & (8) \\ \longrightarrow \mathrm{SiCH_3^+ + 2H_2 + H} & (9) \\ \longrightarrow \mathrm{SiCH_4^+ + 2H_2} & (10) \\ \longrightarrow \mathrm{SiCH_5^+ + H_2 + H} & (11) \end{array} \right.$$

The notations used here for the secondaries are for convenience only; they should not be taken as denoting an established structure of the ion. Typical secondary spectra of pure compounds appear in Table II.

2. SiH_5^+ Formation. We have reported previously[4] that SiH_5^+ is formed in CH_4–SiH_4 mixtures by the reaction

$$\mathrm{CH_4^+ + SiH_4 + M \longrightarrow SiH_5^+ + CH_3 + M} \qquad (12)$$

---

[38] W. C. Steele, L. D. Nichols, and F. G. A. Stone, *J. Amer. Chem. Soc.*, **84**, 4441 (1962).

[39] F. H. Field and J. L. Franklin, "Electronic Impact Phenomena," Academic Press, Inc., New York, N. Y., 1957.

where M may be either CH_4 or SiH_4. Additional appearance potential studies using the RPD technique have confirmed the conclusion[4c] that CH_4^+ is the ionic precursor to SiH_5^+ (Figure 2). While the appearance potential of *m/e* 32 in the high-pressure CH_4–SiH_4 mixtures (Figure 2) suggests that SiH_4^+ is formed in a third body stabilized charge-transfer reaction from CH_4^+, we have been unable to confirm this in pressure variation studies.

B. Kinetics. As was shown earlier,[4a] the rate of change of a reactant ion may be written

$$X_{\mathrm{R}} = X_{\mathrm{R}}^0\, e^{-\frac{(k_c\Gamma + k_h)[M]t}{1+\Gamma}} \approx X_{\mathrm{R}}^0\left[1 - \frac{(k_c\Gamma + k_h)[M]t}{1+\Gamma}\right] \quad (13)$$

where X_{R} = ion fraction of reactant ion at time *t*, X_{R}^0 = initial ion fraction of reactant ion, k_h = sum of homo-reaction rate constants of reactant ion, k_c = sum of cross-reaction rate constants of reactant ion, $[M]$ = concentration of molecules of all kinds, and t = reaction time. Further

$$\Gamma = \gamma' = \frac{[CH_4]}{[SiH_4]}$$

if the reactant ion is SiH_2^+ and

$$\Gamma = \gamma = \frac{[SiH_4]}{[CH_4]}$$

if the reactant ion is CH_3^+ or CH_4^+. Similarly, the time and pressure dependencies of the intensity of a product ion at the pressures used in this work were shown to be approximated[4a] by

$$X_p \approx \frac{X_{\mathrm{R}}^0 k_p[M]t}{1+\Gamma} \quad (14)$$

where X_p = ion fraction of the secondary ion and k_p = specific reaction rate for formation of the secondary ion. From (14) it can be seen that the quantity $(k_pt)_{\mathrm{total}}$ is obtained from the slope of a plot of $I_i/\sum_i I_i$ *vs.* total pressure of $[M]$ (Figure 1). As was discussed in an earlier paper,[3] a plot of $(k_pt)_{\mathrm{total}}$ *vs.* delay time should produce a straight line whose slope is $(k_p^{\mathrm{th}})_{\mathrm{total}}$, the thermal rate constant. Such a plot is shown in Figure 3.

The total ion fraction of any bimolecular product ion is the sum of the contributions from each different cross reaction, *viz.*

$$(X_p)_{\mathrm{total}} = (X_p)_{\mathrm{RiH_2^+}}^{\mathrm{CH_4}} + (X_p)_{\mathrm{CH_4^+}}^{\mathrm{SiH_4}} + (X_p)_{\mathrm{CH_3^+}}^{\mathrm{SiH_4}} \quad (15)$$

where one or more of these contributions may be zero. Combining (14) and (15) and applying to *m/e* 43, as an example, we have

$$\frac{(X_p)_{\mathrm{total}}}{[M]t} = \frac{k_3X_{\mathrm{SiH_2^+}}^0}{1+\gamma} + \frac{k_9X_{\mathrm{CH_4^+}}^0}{1+\gamma'} + \frac{k_6X_{\mathrm{CH_3^+}}^0}{1+\gamma'} \quad (16)$$

Using different mixture ratios, k_3 may be calculated; however, only the sum of k_9 and k_6 can be determined, since the ratio $X_{\mathrm{CH_4^+}}^0/X_{\mathrm{CH_3^+}}^0$ does not change with a variation in $[CH_4]/[SiH_4]$. The ratio-plot method[40,41] was not successful in this case, since $X_{\mathrm{CH_4^+}}^0/X_{\mathrm{CH_3^+}}^0$ is not sufficiently dependent on electron energy at energies high enough to give sufficient intensity. The rate constants of the reactions of methyl ions with silane were, therefore, determined independently by studying the ion–molecule reactions in a 1:1 mixture of dimethyl mercury and silane. In this mixture the secondary ions at *m/e* 42–45 should be due only to reactions of CH_3^+ with SiH_4 and the rate constants calculated for this mixture, according to eq 14, are shown in Table III along with those of SiH_2^+ and CH_4^+ ions. No secondary product was found at *m/e* 45 in the mixture of dimethyl mercury and silane, indicating that CH_3^+ is not involved in the formation of $SiCH_5^+$. Knowledge of the rate constants of CH_3^+ allows us to calculate the rate constants for reactions 8–11. For example, in eq 16 k_6 is known from the dimethyl mercury–silane study, k_3 may be calculated from different reactant-ratio experiments, and all other values except k_9 are known for a given reactant ratio, $[CH_4]/(SiH_4]$. The rate constants of all the reactions in the methane–silane

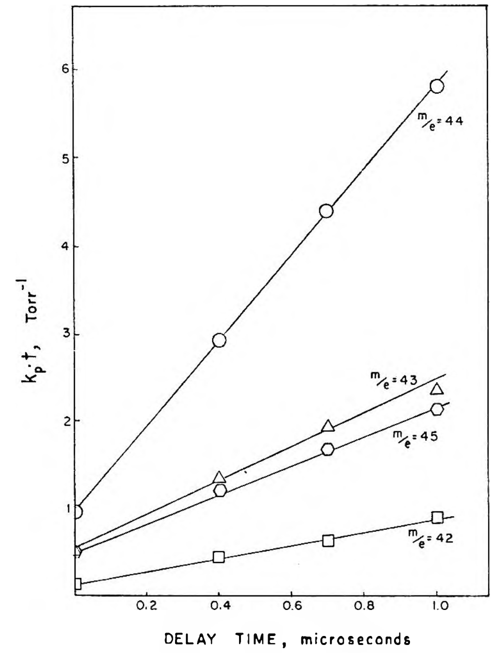

Figure 3. Effect of delay time on $(kt)_{\mathrm{total}}$ for product ions in monosilane mixtures.

---

(40) D. Hutchison, A. Kupperman, and L. Pobo, paper presented at A.S.J.M. Committee E-14 Meeting, Chicago, Ill., June 1961.

(41) A. G. Harrison and J. M. S. Tait, *Can. J. Chem.*, **40**, 1986 (1962).

Table III: Specific Reaction Rates of Cross Reactions in Methane–Silane Mixtures

Reaction	No.	$k \times 10^{10}$, cm³/mol·sec
$SiH_2^+ + CH_4 \rightarrow SiCH_2^+ + 2H_2$	(2)	0.11
$\rightarrow SiCH_3^+ + H_2 + H$	(3)	0.04
$\rightarrow SiCH_5^+ + H$	(4)	0.18
$CH_3^+ + SiH_4 \rightarrow SiCH_2^+ + 2H_2 + H$	(5)	0.65[a]
$\rightarrow SiCH_3^+ + 2H_2$	(6)	0.12[a]
$\rightarrow SiCH_4^+ + H_2 + H$	(7)	1.40[a]
$CH_4^+ + SiH_4 \rightarrow SiCH_2^+ + 3H_2$	(8)	0.54
$\rightarrow SiCH_3^+ + 2H_2 + H$	(9)	2.86
$\rightarrow SiCH_4^+ + 2H_2$	(10)	7.47
$\rightarrow SiCH_5^+ + H_2 + H$	(11)	2.20
		$k \times 10^{26}$, (cm³/mol)²/sec
$CH_4^+ + SiH_4 + M \rightarrow SiH_5^+ + CH_3 + M$	(12)	2.0

[a] Determined from $(CH_3)_2Hg$–SiH_4 mixture.

system are shown in Table III. Analogous to eq 14, the ion fraction for the tertiary reaction 12 in a 1:1 mixture of CH_4–SiH_4 may be written

$$X_p = \frac{(X_{CH_4^+}{}^0)k_{12}[M]^2t}{1+\gamma} \qquad (17)$$

and the rate constant determined in a manner similar to what has been described. The rate constant obtained for the SiH_5^+ formation is also given in Table III.

C. Discussion. Perhaps the most interesting cross reaction in this system is the proton transfer between CH_4^+ and SiH_4 to form SiH_5^+ as shown by (12). Reaction 18, *viz.*

$$CH_4^+ + CH_4 \longrightarrow CH_5^+ + CH_3 \qquad (18)$$

has been studied extensively[5–24] and has been shown to be definitely second order. The absence of SiH_5^+ as a secondary ion in ionized SiH_4[1,42 43] may be attributed to the virtual absence of SiH_4^+ as a primary ion in the mass spectrum of SiH_4. A simple comparison of the thermochemistry of ionic reactions in the methane and methane–silane mixtures suffices to explain the termolecular nature of (12). Since the reaction

$$CH_4^+ + CH_4 \longrightarrow CH_3^+ + H_2 + CH_3 \qquad (18a)$$

is endothermic by 28 kcal,[39] and since decomposition of CH_5^+ to $CH_3^+ + H_2$ is its lowest-energy decomposition, the CH_5^+ formed in (18) cannot decompose unimolecularly in any energetically feasible reaction. However, the reaction

$$CH_4^+ + SiH_4 \longrightarrow SiH_3^+ + H_2 + CH_3 \qquad (12a)$$

is *exothermic* by 18 kcal,[38,39] so that decomposition of an intermediate SiH_5^+ is energetically feasible unless a third body stabilizes it before decomposition. It has generally been assumed that the very observation of an ion–molecule reaction at ion-source pressures of the order of 10^{-2} Torr means that the reaction is exothermic or thermoneutral.[39,44,45] Applying such a consideration to (12) leads us to the conclusion that the proton affinity of SiH_4 is at least 4.9 eV.

In order to investigate the degree of randomization of hydrogen atoms that occurs in the intermediate complexes whose decomposition paths lead to the observed bimolecular product ions, 1:1 mixtures of SiD_4–CH_4 and SiH_4–CD_4 have been studied. A comparison of the experimentally observed distributions with those calculated using the rate constants of Table III and the simple assumption that the complex break-up is statistical, are shown in Table IV. Neither the SiD_4–CH_4 nor the SiH_4–CD_4 results agree with the calculated distributions, indicating that, for one reaction, at least mixing of hydrogen atoms is not extensive. In view of the relative magnitudes of the rate constants in Table III, the reactions of CH_4^+ or CD_4^+ will dominate the observed distribution and so we may conclude that in reactions of CH_4^+ with SiH_4, the hydrogen atoms are not equivalent. It is to be noted that there is a trend in the observed and calculated distributions. In the SiD_4–CH_4 mixture, the experimental results indicate a greater tendency toward loss of D rather than an H in comparison with the calculated distribution. Likewise, the loss of H over D atoms is favored in the CD_4–SiH_4 mixture; this suggests that Si–H bonds are weaker than C–H bonds and is in accord with the findings of Steele, *et al.*,[39] who have reported the H_3Si–H bond dissociation energy to be 94 kcal/mol, as compared with the generally accepted value of 102 kcal/mol for the H_3C–H bond energy.

Table IV: Hydrogen–Deuterium Distribution in Product Ions of SiD_4–CH_4 and SiH_4–CD_4 Mixtures

	CH_4–SiD_4		CD_4–SiH_4	
m/e	Calcd	Obsd	Calcd	Obsd
42	0.016	0.049	0.021	0.04
43	0.062	0.070	0.062	0.04
44	0.108	0.240	0.107	0.11
45	0.204	0.435	0.224	0.11
46	0.323	0.073	0.320	0.14
47	0.209	0.116	0.181	0.25
48	0.068	0.014	0.072	0.22
49	0.010	0.003	0.013	0.09

---

(42) D. P. Stevenson, private communication, 1962.

(43) F. H. Field and M. J. Henchman, private communication, 1967.

(44) F. W. Lampe and F. H. Field, *Tetrahedron*, **7**, 189 (1959).

(45) V. L. Tal'roze and E. L. Frankevich, *Dokl. Akad. Nauk SSSR*, **111**, 376 (1956).

H_2^- transfer reactions to form SiH_2^+ have been observed in previous studies of C_2H_2–SiH_4[4a] and C_2H_4–SiH_4[4b] mixtures, but a similar reaction was not observed in this system. Although CH^+ and CH_2^+ are energetically suitable reactants for such a reaction, their relatively small intensity limits the possibility of observing such a reaction.

As was mentioned earlier, SiH_3^+ is a product of reaction (1) but also reacts to a small extent with methane. Observation of SiH_3^- as a reactant has not been made in pure monosilane[3] or other hydrocarbon–silane mixtures.[4a,b] We were unable to determine the product(s) of this reaction because of its small extent but energetic considerations limit the choice of observed products to $SiCH_5^+$ and $SiCH_3^+$ only. Upper limits to the standard heats of formation of the product ions may be calculated following the assumption that the reactions must be exothermic or thermoneutral to be observed. Such limits are presented in a later section.

It is of interest to point out that various analogs to the observed cross-reactions (in which Si is replaced by C) in this investigation have been observed in studies of ion–molecule reactions in pure methane. Rudolph and Melton[46] observed production of acetylene by the reaction of CH_4^+ (definitely) or CH_3^+ (probably) with methane. Abramson and Futrell[23] report CH_4^+ as a precursor to $C_2H_4^+$ and $C_2H_5^+$; these same authors[23] and Fuchs[12] report $C_2H_3^+$ to be a product of CH_3^+ and methane. Field, Franklin, and Munson[15] and Wexler and Jesse[13] have observed the reaction of CH_3^+ with methane to produce $C_2H_4^+$. Wexler and Jesse[13] and Field, Franklin, and Munson[15] have reported CH_4^+ as a precursor to $C_2H_6^+$; the analogous product in our system, $SiCH_6^+$, was observed but at only a very small intensity.

It is perhaps of even more interest to note that one of the major ion–molecule reactions in pure methane,[5–24] namely

$$CH_3^+ + CH_4 \longrightarrow C_2H_5^+ + H_2 \qquad (19)$$

has no cross-reaction analog that is a major reaction, since CH_3^+ does not react with SiH_4 to yield $SiCH_5^+$. It is possible, as mentioned previously, that the reaction

$$SiH_3^+ + CH_4 \longrightarrow SiCH_5^+ + H_2 \qquad (20)$$

occurs to a small extent.

Silane–Benzene System

A. Reaction Identification. Secondary products in silane–benzene mixtures were found at *m/e* 43, 54–60, 79, 89, 91, 105–109, 115, and 127–129.

Kinetic analysis of various different mixture ratios as well as comparison with studies in pure benzene[25–31] and silane[3] sufficed to determine that only those ions at *m/e* 43, 54–57, and 105–109 were products of cross reactions. Of these, the intensities of the ions at *m/e* 43 and 54–57 were very small and are accounted for by the ion–molecule reactions of $C_2H_2^+$ with SiH_4 previously reported in ethylene–silane[4b] and acetylene–silane[4a] mixtures; the ionic precursor to these reactions, namely $C_2H_2^+$, is present in the benzene spectrum in small abundance and because of the resulting low intensities of these product ions they were not studied in detail. The remaining secondary ions (*m/e* 105–109) were attributed to cross-reactions unique to benzene–silane mixtures. Some of these ions are shown in a plot of ion fraction *vs.* source pressure in Figure 4. The possibility of a cross reaction to produce $C_6H_7^+$ was noted, since a small peak at *m/e* 80 ($C_6H_6D^+$) was observed in the SiD_4–C_6H_6 mixture. However, the low intensity of this ion points to a very slow reaction that was not studied kinetically.

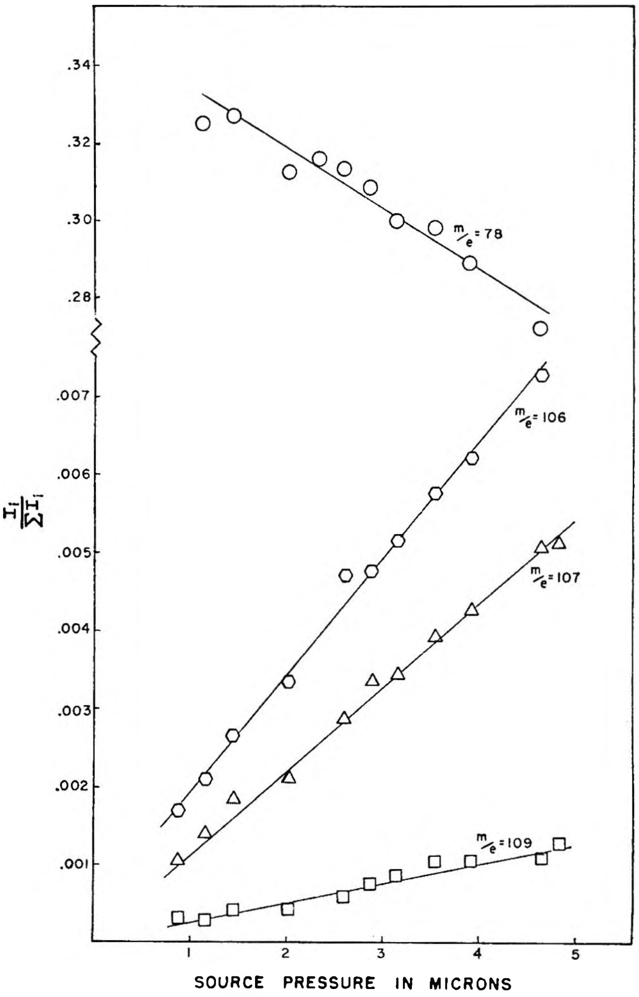

Figure 4. Dependence of ion fraction on source pressure in monosilane–benzene mixtures. $[C_6H_6]/[SiH_4] = 1.0$.

Several primary ions were observed to decrease with an increase in pressure and/or delay time indicating they were reactants; the largest change was noted in the benzene parent ion which is in contrast to pure benzene in which $C_6H_6^+$ is only a very minor reactant.

---

[46] P. S. Rudolph and C. E. Melton, *J. Phys. Chem.*, 71, 4572 (1967).

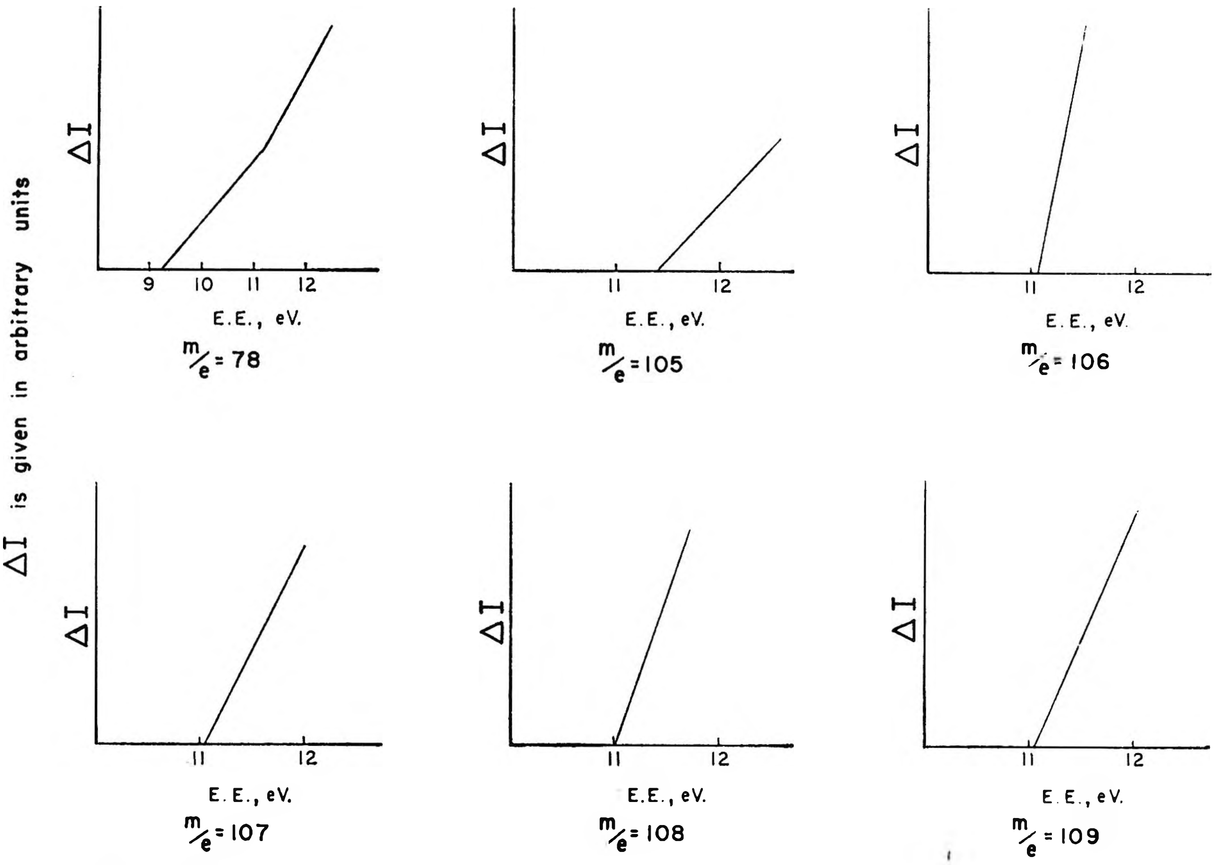

Figure 5. Ionization efficiency curves of various ions in monosilane–benzene mixtures. (Individual points do not appear since the curves are traced directly from the continuous RPD curves drawn by the X-Y recorder.)[37] Threshold potentials reproducible to ±0.2 eV.

Appearance potential measurements from ionization efficiency curves (Figure 5) of the secondary cross-products indicate that they all are formed by the same ionic precursor whose appearance potential is 11.1 ± 0.2 eV. Since the lowest appearance potential of any fragment ion in benzene is 14.1 eV,[31] we must conclude, in accord with the results of pressure variation studies, that the ionic reactant in the cross-reactions with SiH_4 is $C_6H_6^+$. Yet the first ionization potential of benzene is known to be 9.25 eV,[39] so the reactant $C_6H_6^+$ must be in an excited state. In accord with our finding that the appearance potentials of the product ions of $C_6H_6^+$ reactions with SiH_4 are 11.1 ± 0.2 eV, we find a break in the ionization efficiency curve of m/e 78 ($C_6H_6^+$) at 11.2 ± 0.2 suggesting the onset of an excited state of $C_6H_6^+$. Although the energies fall just outside our error estimates, we believe that this is probably the same excited state of $C_6H_6^+$ that has been reported by Fox and Hickam (11.5 eV);[47] El-Sayed, Kasha, and Tanaka (11.5 eV);[48] Dibeler and Reese (11.49 eV);[49] Brehm (11.4 eV);[50] Dewar and Worley (11.5 eV);[51] and Jonsson and Lindholm (11.4 eV).[52] This onset energy has been attributed[48,49] to ionization of an electron from an $(a_{2u})\pi$ molecular orbital of benzene. However, more recently Jonsson and Lindholm[52] have proposed that an onset energy of 11.4 eV corresponds to removal of an electron from a $(3e_{2g})$ t molecular orbital. Since the ground state of $C_6H_6^+$ has an onset of 9.25 eV and the only other state lying close to our appearance potentials of the secondary ions has an onset of 12.1 eV, our assignment is the most reasonable possible.

Thus the secondary cross-reactions observed in the benzene–silane system are

$$(C_6H_6^+)^* + SiH_4 \left| \begin{array}{ll} \rightarrow SiC_6H_5^+ + 2H_2 + H & (21) \\ \rightarrow SiC_6H_6^+ + 2H_2 & (22) \\ \rightarrow SiC_6H_7^+ + H_2 + H & (23) \\ \rightarrow SiC_6H_8^+ + H_2 & (24) \\ \rightarrow SiC_6H_9^+ + H & (25) \end{array} \right.$$

Again, the notations here for the secondaries are for convenience only and should not be construed as indicating structure.

B. Kinetics. We have already discussed in the sec-

---

(47) R. E. Fox and W. M. Hickam, *J. Chem. Phys.*, **22**, 2059 (1954).

(48) M. A. El-Sayed, M. Kasha, and V. Tanaka, *ibid.*, **34**, 334 (1961).

(49) V. H. Dibeler and R. M. Reese, *J. Res. Natl. Bur. Stand.*, **68a**, 409 (1964).

(50) B. Brehm, *Z. Naturforsch.*, **21a**, 196 (1966).

(51) M. J. S. Dewar and S. D. Worley, *J. Chem. Phys.*, **50**, 654 (1969).

(52) B. Jonsson and E. Lindholm, *Arkiv Fysik*, **39**, 65 (1969).

tion on methane–silane mixtures the kinetic equations pertinent to determination of the specific reaction rates from the pressure and delay-time data, and with modification these apply to the benzene–silane mixtures. Thus we may use (13) and (14) to represent the ion fractions of $C_6H_6^+$ and of a product ion, respectively. However, it must be borne in mind that the measured ion fraction, $X_{C_6H_6^+}$, refers to all ions of m/e 78 and from the appearance potentials of the product ions we know that only $C_6H_6^+$ excited to at least 2.3 eV will undergo reaction with SiH_4. Hence rate constants determined from the observed $X_{C_6H_6^+}$ (in the manner described for the methane–silane case) will be lower limits to the true rate constants since a portion of the $C_6H_6^+$ ions will not contain sufficient energy. Such limits are shown in Table V.

Table V: Specific Reaction Rates of Cross Reactions in Benzene–Silane Mixtures

Reaction		No.	$k \times 10^{10}$, cm³/mol·sec Lower limit	Estimated value
$(C_6H_6^+)^* + SiH_4$	$\rightarrow SiC_6H_5^+ + 2H_2 + H$	(21)	0.19	0.26
	$\rightarrow SiC_6H_6^+ + 2H_2$	(22)	2.52	3.44
	$\rightarrow SiC_6H_7^+ + H_2 + H$	(23)	1.77	2.42
	$\rightarrow SiC_6H_8^+ + H_2$	(24)	0.083	0.11
	$\rightarrow SiC_6H_9^+ + H$	(25)	0.31	0.42

Fox and Hickam[47] have studied the electron-impact ionization efficiency curve of $C_6H_6^+$ from onset to 18 eV and have reported four direct ionization processes in this range. Our kinetic experiments were performed at 100 eV electron energy. If we assume (1) that the relative probabilities of forming $C_6H_6^+$ in the various states is proportional to the slopes of the ionization efficiency curves, (2) that these relative probabilities are the same at 100 eV as at onset, and (3) that all states with onset energies above 11.5 eV react in the same way with SiH_4 regardless of the form of the excitation (electronic or vibrational) at the time of collision of $C_6H_6^+$ with SiH_4, we estimate the rate constants to be higher by a factor of $\sim^4/_3$ than the lower limits. These estimated values are given also in Table V but they are quite uncertain.

Table VI: Hydrogen–Deuterium Distribution in Product Ions of a 1:1 SiD_4–C_6H_6 Mixture

m/e	Ions	Relative intensity Obsd	Calcd
105	$SiC_6H_5^+$	0.025	0.001
106	$SiC_6H_6^+$, $SiC_6H_4D^+$	0.163	0.012
107	$SiC_6H_3D_2^+$, $SiC_6H_5D^+$	0.164	0.077
108	$SiC_6H_4D_2^+$, $SiC_6H_6D^+$	0.321	0.241
109	$SiC_6H_3D_3^+$, $SiC_6H_5D_2^+$	0.203	0.306
110	$SiC_6H_4D_3^+$, $SiC_6H_6D_2^+$	0.028	0.220
111	$SiC_6H_5D_3^+$	0.008	0.071
112	$SiC_6H_4D_4^+$, $SiC_6H_6D_3^+$	0.085	0.032
113	$SiC_6H_5D_4^+$	0.003	0.038

C. Discussion. In order to examine the possibility of randomization of hydrogen atoms in the intermediate complex which leads to the observed products, we have measured the distribution of secondary ions in a 1:1 mixture of SiD_4–C_6H_6. Table VI shows a comparison of the experimentally observed distribution with that calculated, using the rate constants of Table V and the simple assumption that the complex break-up is statistical. It is at once apparent that the calculated and experimental distributions are widely divergent. In view of the observations of Rylander, *et al.*,[53] and Theard and Hamill,[54] who found, respectively, that the tropylium ion, $C_7H_7^+$, was formed by electron impact on toluene and by the reaction of methyl ion with benzene, one might expect a similar incorporation of the silicon atom into the aromatic ring. In the case of the tropylium ion,[53,54] all the carbon atoms become equivalent and likewise all the hydrogen atoms. However, in our study it is quite apparent that the hydrogens attached to the benzene ring are not equivalent to those attached to silicon in the intermediate complex; this is consistent with the reported difficulties of preparing aromatic silicon compounds.[55] Actually, what is ob-

Table VII:[a] Upper Limits of the Heat of Formation for Observed Secondary Ions

A. Methane–Silane Mixtures

m/e	Secondary ion	$\Delta H_f <$
33	SiH_5^+	258
42	$SiCH_2^+$	217
43	$SiCH_3^+$	212
44	$SiCH_4^+$	217
45	$SiCH_5^+$	212

B. Benzene–Silane Mixtures

m/e	Secondary ion	$\Delta H_f <$
105	$SiC_6H_5^+$	206
106	$SiC_6H_6^+$	258
107	$SiC_6H_7^+$	206
108	$SiC_6H_8^+$	258
109	$SiC_6H_9^+$	206

[a] The heats of formation of the reactants and neutral products used to calculate these limits were obtained from Steele, *et al.*,[38] Rossini, *et al.*,[56] Field and Franklin,[39] and Gunn and Green.[57]

---

(53) P. N. Rylander, S. Meyerson, and H. M. Grubb, *J. Amer. Chem. Soc.*, **79**, 842 (1957).

(54) L. P. Theard and W. H. Hamill, *ibid.*, **84**, 1134 (1962).

(55) R. A. Benkeser and G. M. Stanton, *ibid.*, **85**, 834 (1963).

served is an overwhelming tendency for D loss rather than H loss in this SiD_4–C_6H_6 mixture. This suggests that the Si remains as a side group to the ring and that the preferential D loss is a result of the Si–D bonds being weaker in general than the C–H bonds in the ring.

The observation of $C_6H_6D^+$ in mixtures of C_6H_6–SiD_4 indicates that either $C_6H_6^+$ abstracts a hydrogen atom from SiH_4 or that ions from silane (SiH_3^+, SiH_2^+) transfer a proton to benzene. The intensity of this product ion is too small to determine unambiguously its precursor. If the reaction is that of hydrogen atom abstraction from silane by $C_6H_6^+$ ion, then energetic considerations make it clear that the $C_6H_6^+$ ions must have at least 1.9-eV excitation energy. The present state of the thermochemistry of monosilane, particularly with regard to the dissociation energies $D(H_2Si–H)$ and $D(HSi–H)$, is sufficiently well established to rule out protonation of benzene by SiH_3^+ and SiH_2^+.

Employing again the assumption that the ion–molecule reactions observed are exothermic or thermoneutral,[39,44,45] upper limits for the heats of formation of the observed product ions may be established. These are tabulated in Table VII.[56,57]

Acknowledgment. This work was supported by Contract No. AT (30-1)-3570 with the United States Atomic Energy Commission. We also wish to thank the National Science Foundation for providing funds to assist in the original purchase of the mass spectrometers.

---

(56) F. D. Rossini, *et al.*, "Selected Values of Chemical Thermodynamic Properties," National Bureau of Standards Circular 500, U. S. Government Printing Office, Washington, D. C., 1952.

(57) S. R. Gunn and L. G. Green, *J. Phys. Chem.*, **65**, 779 (1961).

Solvent Exchange Rates of Solvent–Metal Complexes for Fe^{3+} in N,N-Dimethylformamide, Acetonitrile, and Ethanol and for Ni^{2+} in Ethanol by Proton Magnetic Resonance

by F. W. Breivogel, Jr.

Department of Chemistry, Clippinger Laboratories, Ohio University, Athens, Ohio 45701 *(Received May 1, 1969)*

The transverse relaxation rates have been measured for the solvent protons in ethanol solutions of Fe^{3+} and Ni^{2+}, and N,N-dimethylformamide and acetonitrile solutions of Fe^{3+} by high-resolution nmr techniques. From the temperature dependence of the relaxation rates the rates and activation parameters have been determined for the exchange of solvent molecules between the first coordination sphere of the metal ion and the bulk solvent. The present results, together with previous work, show that for water, dimethyl sulfoxide, N,N-dimethylformamide, and acetonitrile solutions of Fe^{3+} the solvent exchange rates are all about 0.006 times the corresponding rate in Ni^{2+} solutions, while in methanol and ethanol solutions of Fe^{3+} the solvent exchange rates are twice as fast as in the corresponding Ni^{2+} solutions. This is attributed to steric effects.

I. Introduction

The rate of exchange of solvent molecules between the first coordination sphere of transition metal ions and the bulk solvent has been studied extensively by nmr line-broadening techniques.[1] The solvents which have been most widely studied are water,[2,3] methanol,[4-6] and N,N-dimethylformamide (DMF).[7-9] For the divalent ions which have been studied the *relative* exchange rates are about the same in all three solvents. However, the relative exchange rate for Fe^{3+} in methanol[6] is three orders of magnitude greater than in water[10] or dimethyl sulfoxide (DMSO)[11,12] when compared to the divalent ions.

---

(1) For a recent review, see T. R. Stengle and C. H. Langford, *Coordin. Chem. Rev.*, **2**, 349 (1967).

(2) T. J. Swift and R. E. Connick, *J. Chem. Phys.*, **37**, 307 (1962); **41**, 2553 (1964).

(3) R. E. Connick and D. N. Fiat, *ibid.*, **44**, 4103 (1966).

(4) Z. Luz and S. Meiboom, *ibid.*, **40**, 1058, 1066, 2686 (1964).

(5) H. Levanon and Z. Luz, *ibid.*, **49**, 2031 (1968).

(6) F. W. Breivogel, Jr., *ibid.*, **51**, 445 (1969).

(7) J. S. Babiec, C. H. Langford, and T. R. Stengle, *Inorg. Chem.*, **5**, 1362 (1966).

In a continuation of this investigation the exchange rates have been measured for Fe^{3+} in DMF and ethanol and an upper limit placed on the exchange rate in acetonitrile (AN). Since no other exchange rates have been reported in ethanol, the exchange rate has also been measured for Ni^{2+} in ethanol for comparison.

II. Experimental Section

Absolute ethanol was dried over Drierite and 50 ml of it was heated with iodine and magnesium until the iodine disappeared. An additional liter of ethanol was added, and the solution was distilled. Some of the ethanol was acidified by bubbling dry HCl gas through it. DMF was dried by distilling over BaO under reduced pressure. The AN was spectrograde and used without further purification.

Solutions were prepared by dissolving anhydrous metal chlorides in the solvent together with an amount of anhydrous silver perchlorate sufficient to precipitate all of the chloride ion. The preparation and transfer of solutions were carried out in a dry nitrogen atmosphere. The anhydrous salts were obtained commercially and dried over P_2O_5 under reduced pressure at 110° for 24 hr.[13] For each system studied at least three independently prepared solutions of different concentrations were employed. The range of concentrations employed for each system studied was P_M = 0.012–0.039 for Fe^{3+} in AN, P_M = 0.0018–0.019 for Fe^{3+} in DMF, P_M = 0.0019–0.0076 for Fe^{3+} in ethanol, and P_M = 0.018–0.040 for Ni^{2+} in ethanol, where P_M is the mole fraction of solvent molecules coordinated to the metal ion. A coordination number of 6 was assumed in all cases.

Nmr spectra of solvent protons were obtained on a Varian A-60 spectrometer equipped with a V-6040 variable temperature controller. The temperature was determined by measuring the peak separation in ethylene glycol or methanol. Chemical shift measurements were made using tetramethylsilane as an internal standard.

No separate peaks were observed belonging to solvent molecules coordinated to the metal ions. The observed lines corresponded either to free solvent molecules or to an average of free and bound solvent molecules, depending on the exchange rate. In most cases the line widths ranged between 10 and 60 Hz. The transverse relaxation rates T_2^{-1} were calculated from the nmr spectra using the equation

$$T_2^{-1} = \pi\delta\nu \qquad (1)$$

which applies for a Lorentzian line shape where $\delta\nu$ is the full line width in Hz at half-maximum. The contribution, T_{2P}^{-1}, to the line width due to the presence of paramagnetic ions is obtained by taking the difference between T_2^{-1} and T_{2a}^{-1}, the line width in the absence of paramagnetic ions.

III. Results

Transverse relaxation rates were measured for the CH_3 protons of AN, the formyl proton of DMF, and the CH_2 protons of ethanol in Fe^{3+} solutions and for the OH and CH_2 protons in ethanol solutions of Ni^{2+}. The results are shown in Figures 1–4 where logarithmic plots of $T_{2P}^{-1}P_M^{-1}$ *vs.* T^{-1} are given.

Spin–spin splittings in ethanol complicated the analysis of the data in that solvent. For both the Ni^{2+} and Fe^{3+} solutions it was necessary to use different values of T_{2a}^{-1} for different metal ion concentrations to obtain consistent values of T_{2P}^{-1}. The value of T_{2a}^{-1} used decreased as the metal ion concentration was increased. This can be attributed to a partial spin decoupling due to the presence of the paramagnetic ion.[14]

For each of the solutions studied $T_{2P}^{-1}P_M^{-1}$ increases as the temperature decreases in the low-temperature region. This is a region of very slow exchange, and the dominant relaxation mechanism is interaction between the metal ion and the solvent molecules in the second coordination shell. For Fe^{3+} in AN this appears to be the dominant relaxation mechanism throughout the entire liquid temperature range. In Figure 1 the slope in the high- and low-temperature regions is quite different. The straight lines represent the limiting high- and low-temperature slopes. It appears in Figure 1 that the slope undergoes a discontinuous change, but the fact that the points lie almost on the two straight lines is undoubtedly coincidental. The apparent activation energy is −1.4 kcal/mol at low temperatures and −3.2 kcal/mol at higher temperatures. At high temperatures diffusion controls the correlation time, while at low temperatures the electronic relaxation controls the correlation time. Electronic relaxation typically has an activation energy of about 1 kcal/mol, while diffusion has an activation energy of 3–5 kcal/mol.[4] For Fe^{3+} in DMF and ethanol the observed activation energies are −3.5 and −4.8 kcal/mol, respectively, corresponding to diffusion.

At higher temperatures $T_{2P}^{-1}P_M^{-1}$ increases as the temperature increases for the solutions of Fe^{3+} in

---

(8) N. A. Matwiyoff, *Inorg. Chem.*, **5**, 788 (1966).

(9) J. S. Babiec, Ph.D. Thesis, University of Massachusetts, Amherst, Mass., July 1966.

(10) M. R. Judkins, Ph.D. Thesis, University of California, Berkeley, Calif., May 1967. (Available as Lawrence Radiation Laboratory Report UCRL-17561).

(11) C. H. Langford and F. M. Chung, *J. Amer. Chem. Soc.*, **90**, 4485 (1968).

(12) S. Thomas and W. L. Reynolds, *J. Chem. Phys.*, **46**, 4164 (1967).

(13) In the work reported in ref 6 in methanol solutions the salts were not dried before preparing the solutions. This work has since been repeated after drying the salts as described above. The results for the divalent ions were not affected, but for Fe^{3+} in methanol the results were changed somewhat. The new results are $k_1 = 2.4 \times 10^3$ sec^{-1} at 25°, $\Delta H^{\ddagger}$ = 10.7 kcal/mol, and $\Delta S^{\ddagger}$ = −7 eu.

(14) L. S. Frankel, *J. Chem. Phys.*, **50**, 943 (1969).

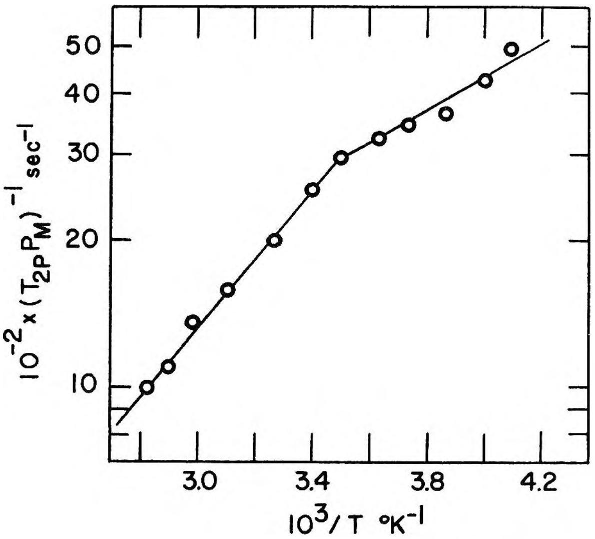

Figure 1. Temperature dependence of $T_{2P}^{-1}P_M^{-1}$ for the protons in acetonitrile solutions of Fe^{3+}.

DMF and ethanol and Ni^{2+} in ethanol. This is a region where chemical exchange is appreciable, and there is an incomplete averaging of the nmr spectra of the free and bound solvent. Under these conditions the relaxation rate is given by[2]

$$T_{2P}^{-1} = P_M\tau^{-1} \qquad (2)$$

where τ is the mean lifetime of a solvent molecule in the first coordination sphere of the metal ion. The variation of τ with temperature is given by

$$\tau^{-1} = k_1 = (kT/h)\exp(\Delta S^{\ddagger}/R - \Delta H^{\ddagger}/RT) \qquad (3)$$

where $\Delta S^{\ddagger}$ and $\Delta H^{\ddagger}$ are the entropy and enthalpy of activation, respectively, for the first-order exchange reaction.

Using these equations the activation parameters and the value of k_1 at 25° were calculated from Figures 2 to 4 in the region where there is a large negative slope after correcting for the outer coordination effects. The results are given in Table I.

Table I: Rate Constants and Activation Parameters for the Exchange of Solvent Molecules between the First Coordination Sphere of the Metal Ion and the Bulk Solvent

Metal ion	Solvent	k_1, sec^{-1} (at 25°)	$\Delta H^{\ddagger}$, kcal/mol	$\Delta S^{\ddagger}$, eu
Fe^{3+}	Ethanol	2.0×10^4	6.2 ± 1.5	-18 ± 5
Fe^{3+}	DMF	33	12.5 ± 1.5	-10 ± 5
Fe^{3+}	AN	<40		
Ni^{2+}	Ethanol	1.1×10^4	10.8 ± 1.5	-4 ± 5

For Ni^{2+} in ethanol the solution was not acidified. The OH and CH_2 data gave the same exchange rate within experimental error; the OH results are given in Table I since they are more accurate. In addition to the relaxation mechanisms mentioned above a different mechanism is apparent in the Ni^{2+} solutions where at high temperatures $T_{2P}^{-1}P_M^{-1}$ decreases as the temperature increases. In this region relaxation is dominated by the change in precessional frequency of the solvent protons during the exchange process. In theory the exchange rate could also be calculated from the relaxation rate in this region. Unfortunately, the data in this region cannot be represented by one of the limiting equations derived in ref 2. This is indicated since the straight line through the points at the left side of Figure 4 intersects the other straight line only slightly above the experimental points. If both straight lines accurately represented one of the limiting equations, the intersection should occur a factor of 2 greater than the experimental points. The complete equation derived in ref 2 cannot be employed since all of the parameters are not known.

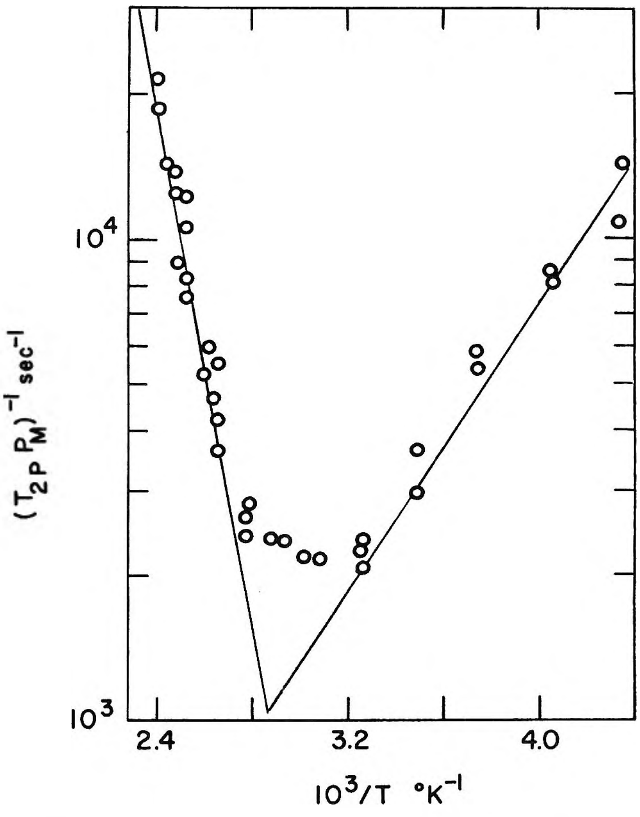

Figure 2. Temperature dependence of $T_{2P}^{-1}P_M^{-1}$ for the formyl proton in N,N-dimethylformamide solutions of Fe^{3+}.

Chemical shift measurements were made on ethanol solutions of Ni^{2+} in the high-temperature region where exchange is rapid. At 78° the chemical shifts divided by P_M are 2000 Hz for the OH proton, 1150 Hz for the CH_2 protons, and 550 Hz for the CH_3 protons.

For Fe^{3+} in ethanol it was anticipated that the OH proton would exchange more rapidly than the ethanol molecule itself, so only the CH_2 protons were studied. (This was the case in methanol solutions of Fe^{3+}.) The solutions were 0.02 *m* in acid to re-

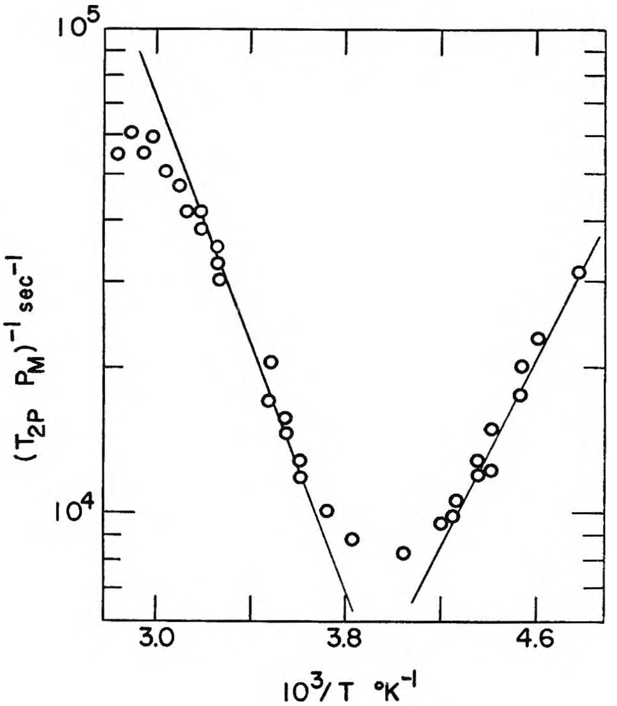

Figure 3. Temperature dependence of $T_{2P}^{-1}P_M^{-1}$ for the CH_2 protons in ethanol solutions of Fe^{3+}.

press acid dissociation of the complex. In previous studies of methanol solutions of Fe^{3+} measurements were carried out over a wide range of acid concentrations, and the exchange rates were found to be independent of the acid concentration.[6] Therefore, in the present work only a single low acid concentration was used.

For Fe^{2+} in AN only an upper limit to the exchange rate could be determined. No deviation from a straight line is observed in the high-temperature region (see Figure 1). At 78°, $T_{2P}^{-1}P_M^{-1} = 1 \times 10^3$ sec^{-1}, and we estimate that $k_1 \leq 300$ sec^{-1}. Assuming an activation energy of 8 kcal/mol, we calculate that at 25°, $k_1 < 40$ sec^{-1}.

IV. Discussion

With the results obtained in the present work exchange rates have been measured for Fe^{3+} complexes in six solvents. These results are summarized in Table II and are compared with the corresponding Ni^{2+} exchange rates. As mentioned above, relative exchange rates for the divalent ions are about the same for all the solvents studied. Comparison is made with Ni^{2+} since it has been more widely studied than any other divalent ion.

Table II shows that except for methanol and ethanol the relative exchange rates for Fe^{3+} are quite constant when compared to the corresponding Ni^{2+} exchange rates. For methanol and ethanol the relative exchange rates for Fe^{3+} are between two and three orders of magnitude greater than for the other solvents.

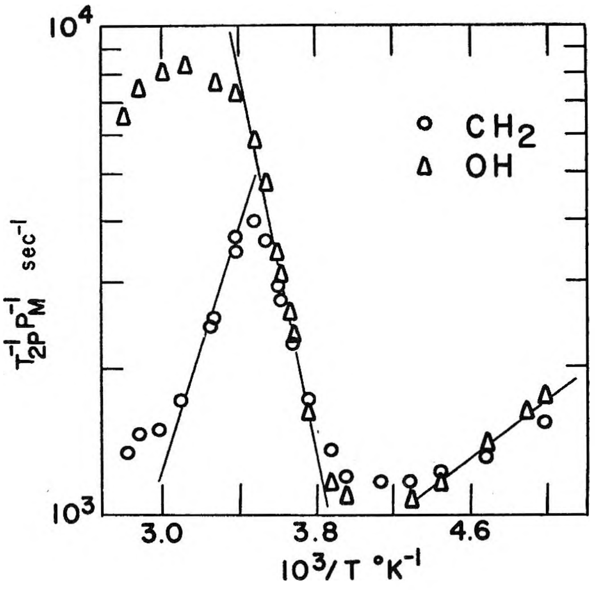

Figure 4. Temperature dependence of $T_{2P}^{-1}P_M^{-1}$ for the OH and CH_2 protons in ethanol solutions of Ni^{2+}.

Table II: Comparison of Rate Constants for Solvent Exchange at 25° for Fe^{3+} and Ni^{2+}

Solvent	$k_{Ni^{2+}}$, sec^{-1} (at 25°)	$k_{Fe^{3+}}$, sec^{-1} (at 25°)	$k_{Fe^{3+}}/k_{Ni^{2+}}$
H_2O	2.7×10^4 [a]	1.5×10^2 [b]	0.0055
DMSO	7.5×10^3 [c]	50[d]	0.0067
DMF	7.7×10^3 [e]	33	0.0043
	3.8×10^3 [f]		0.0087
AN	3.9×10^3 [g]	<40	<0.01
Methanol	1.0×10^3 [h]	2.4×10^3 [i]	2.4
Ethanol	1.1×10^4	2.0×10^4	1.8

[a] See ref 2. [b] See ref 10. [c] See ref 12. [d] See ref 11. [e] See ref 7. [f] See ref 8. [g] N. A. Matwiyoff and S. V. Hooker, *Inorg. Chem.*, **6**, 1127 (1967). [h] See ref 4. [i] See ref 13.

We attribute this to steric crowding around the small Fe^{3+} ion. For DMF, AN, and DMSO the atom through which the solvent coordinates to the metal ion is bonded to only one atom in the solvent molecule, while in methanol and ethanol the oxygen atom is bonded to two atoms in the solvent. Steric effects can be invoked to explain the decreasing tendency of Cr^{3+} to bind methanol and ethanol as more methanol and ethanol molecules are bound[15,16] and to account for the fact that methanol does not compete for coordination positions in $Cr(H_2O)_6^{3+}$ nearly as well as does DMSO.[17] It has been shown in a number

---

(15) J. C. Jayne and E. L. King, *J. Amer. Chem. Soc.*, **86**, 3989 (1964).

(16) D. W. Kemp and E. L. King, *ibid.*, **89**, 3433 (1967).

(17) K. R. Ashley, R. E. Hamm, and R. H. Magnuson, *Inorg. Chem.*, **6**, 413 (1967).

(18) C. H. Langford and T. R. Stengle, *Ann. Rev. Phys. Chem.*, **19**, 193 (1968).

of studies that the introduction of bulky organic groups around the metal ion will frequently increase the rate of substitution reactions.[18]

Acknowledgment. This work was supported, in part, by a grant from the Ohio University Research Committee.

Pulse Radiolysis of Aliphatic Acids in Aqueous Solutions. I.

Simple Monocarboxylic Acids

by P. Neta,[1] M. Simic,[1] and E. Hayon

Pioneering Research Laboratory, U. S. Army Natick Laboratories, Natick, Massachusetts 01760

(Received May 1, 1969)

Transient optical absorption spectra due to carboxyalkyl radicals have been observed on pulse radiolysis of aqueous solutions of some aliphatic acids (formic, acetic, propionic, *n*- and isobutyric, and trimethyl acetic acids). These radicals were produced as a result of dehydrogenation by H atoms and OH radicals at the α and/or β positions. The assignment of these radicals was supported by the results obtained from the reaction of e_{aq}^- with the corresponding monochloroaliphatic acids when dechlorination takes place. The α-carboxyalkyl radicals (C_2–C_4) studied have absorption maxima in the region 290–350 nm, while the β radicals (C_3–C_5) have maxima below 250 nm. The observed change with pH in the transient absorption spectra of these radicals was attributed to the dissociation of the carboxyl group. The p*K* values of these radicals were determined spectrophotometrically and were found to correspond in most cases to the p*K* values of the parent aliphatic acids. The extinction coefficients and decay rates were also found to be dependent upon pH. The reactivity of $\dot{C}H_2OH$, $CH_3\dot{C}HOH$, $\cdot CH_2C(CH_3)_2OH$, $\cdot CH_2COO^-$, and $\cdot CO_2^-$ radicals with $\cdot CO_2^-$ and $\cdot CH_2COO^-$ was investigated.

Introduction

The radiation chemistry of a number of simple aliphatic carboxylic acids in aqueous solution has been examined and many of the products formed have been determined (for general review, see Allen[2]). These products resulted from the reactions of the acids with the reactive species formed in the radiolysis of water.

$$H_2O \rightsquigarrow e_{aq}^-, OH, H, H_2, H_2O_2$$

The main radiolytic products from formic acid were H_2, CO_2 and/or oxalic acid depending on the pH of the solution. The main products from acetic acid were hydrogen and succinic acid. Carbon dioxide, methane and biacetyl were also found, the yields of which become significant only at high concentrations ($\geqslant 1$ *M*). The yields of H_2 and CO_2 from the radiolysis of higher acids were also studied.[3]

From the product analysis it was concluded that the main reactions taking place in these systems are hydrogen abstraction by OH radicals and H atoms

$$R_2CHCOOH + OH \longrightarrow R_2\dot{C}COOH + H_2O \quad (1)$$

$$R_2CHCOOH + H \longrightarrow R_2\dot{C}COOH + H_2 \quad (2)$$

At higher concentrations (>0.1 *M*) these acids were suggested[4] to react with hydrated electrons to produce carbonyl compounds and CO.

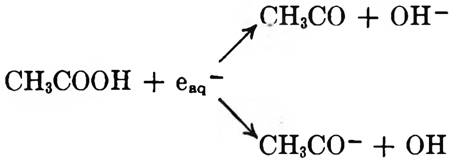

$$CH_3COOH + e_{aq}^- \longrightarrow CH_3CO + OH^- \quad (3a)$$

$$CH_3COOH + e_{aq}^- \longrightarrow CH_3CO^- + OH \quad (3b)$$

A transient absorption spectrum assigned to CO_2^- has been obtained on pulse radiolysis of formic acid solutions,[5] but none of the higher aliphatic acids has been investigated. This paper presents a pulse-radiolysis study of aqueous solutions of formic, acetic, propionic, *n*- and isobutyric, and trimethylacetic acids. The observed transients were produced mainly by reaction with OH radicals and H atoms. The e_{aq}^- was converted to OH radicals or H atoms by reaction with N_2O or H_3O^+.

---

(1) National Academy of Sciences National Research Council Research Associate at Natick.

(2) A. O. Allen, "The Radiation Chemistry of Water and Aqueous Solutions," D. Van Nostrand, Company, Inc., Princeton, N. J., 1961.

(3) H. Fricke, E. J. Hart, and H. P. Smith, *J. Chem. Phys.*, 6, 229 (1938).

(4) E. Hayon and J. Weiss, *J. Chem. Soc.*, 5091 (1960).

(5) J. P. Keene, Y. Raef, and A. J. Swallow, in "Pulse Radiolysis," M. Ebert, J. P. Keene, A. J. Swallow, and J. H. Baxendale, Ed., Academic Press, New York, N. Y., 1965, p 99.

Experimental Section

This work was carried out using a Febetron 705 pulsed radiation source, and the experimental conditions have been described[6] in detail. Briefly, this source produces an electron beam of 2.3 MeV energy and single pulses of ~30 nsec duration. The monitoring light source was an Osram XBO 450W xenon lamp, and the light output from the lamp was increased by a factor of 25–30 times by increasing the current to the lamp with pulses of ~1.2 msec duration. Two high-intensity Bausch and Lomb monochromators were used in series to reduce scattered light.

Solutions were prepared using water purified by triple distillation, radiolysis, and photolysis. Analytical reagent grade and spectrograde chemicals were employed as supplied by Baker and Adamson, Mallinckrodt, and Eastman. Solutions were buffered using perchloric acid, potassium hydroxide, sodium tetraborate (1–5 mM) and potassium phosphate (1–5 mM). Carbon dioxide was supplied by Matheson and was further purified on a vacuum line. Dosimetry was carried out[6] using a 0.1 M KCNS solution and the $(CNS)_2^-$ radical formed was observed at 500 nm using $\epsilon_{500} = 7600$ M^{-1} cm^{-1}. Doses of 8–36 krad/pulse were used and were derived on the basis of $g(e_{aq}^-) = g(OH) = 2.8$. Due to the high dose per pulse, the choice of solute concentration was made on the basis of known radical–radical and radical–solute rate constants[7] at the various pH values studied. This was also checked by varying the concentration of the acids. Full scavenging of the radicals was also ensured in the determination of the OD *vs.* pH curves.

Results and Discussion

Pulse radiolysis of aqueous solutions of aliphatic acids was carried out in N_2O–saturated (1 atm) solutions to convert practically all (~98%) the e_{aq}^- into OH radicals

$$e_{aq}^- + N_2O \longrightarrow N_2 + OH^- + OH \qquad (4)$$

Solutions at lower pH were studied under conditions such that all the e_{aq}^- would react with H_3O^+ to form hydrogen atoms

$$e_{aq}^- + H_3O^+ \longrightarrow H_2O + H \qquad (5)$$

Both H atoms and OH radicals are considered to dehydrogenate carboxylic acids and their ions in a similar way, reactions 1 and 2. Since the reactivity of carboxylic acids with H atoms is relatively low, high concentrations (up to 1 M) of these acids were used to assure full scavenging of both hydrogen atoms and hydroxyl radicals.

The nature of the transient species produced in the pulse radiolysis of these monocarboxylic acids was established in a number of cases by irradiating the corresponding α- or β-chloroaliphatic acids. These are known[8] to react with e_{aq}^- to form halogen ions

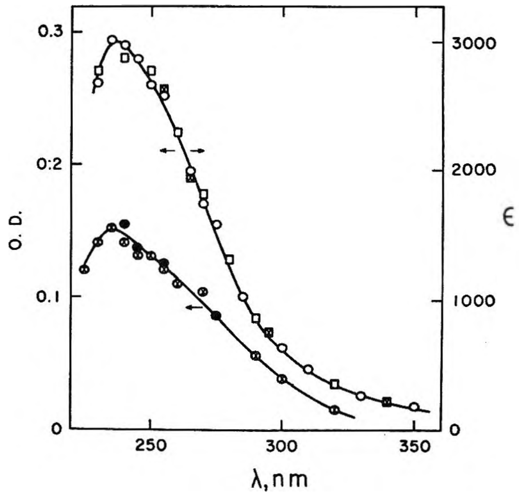

Figure 1. Absorption spectrum of CO_2^- in irradiated aqueous solutions (8 krads/pulse). ϵ is given in M^{-1} cm^{-1} units. □, 0.03 M HCOONa, N_2O (1 atm), pH 9; ⊠, 0.03 M HCOONa, N_2O (1 atm), pH 13; ○, 0.03 M HCOONa, CO_2 (1 atm), pH 3.1; ⊗, 0.1 M EtOH, CO_2 (1 atm), pH 5; ●, 0.2 M MeOH, CO_2 (1 atm), pH 5.

$$R_2CClCOOH + e_{aq}^- \longrightarrow R_2\dot{C}COOH + Cl^- \qquad (6a)$$

$$R_2CClCH_2COOH + e_{aq}^- \longrightarrow R_2\dot{C}CH_2COOH + Cl^- \qquad (6b)$$

To eliminate the reaction of OH radicals with the chloroaliphatic acids, *t*-butanol was used to scavenge the OH radicals. Tertiary butanol was chosen for this purpose since it was shown[6] to form a transient with low absorption above 250 nm and a spectrum independent of pH. In all the cases presented in this paper, the absorption due to the *t*-butanol radical was subtracted from the total absorption of the transient species observed. Furthermore, the $\cdot CH_2C(CH_3)_2OH$ radical was found to be unreactive with the chloroaliphatic acids. This was shown by irradiating solutions of *t*-BuOH + N_2O + $ClCH_2COO^-$ or $CH_3CHClCOO^-$ under conditions such that $RCHClCOO^-$ would not react with either e_{aq}^- or OH. Only $\cdot CH_2C(CH_3)_2OH$ radicals were observed with no absorption in the region where the α-carboxyalkyl radicals absorb.

Transient absorption spectra of aliphatic acid radicals, with the exception of $\cdot CO_2^-$, are in acidic solutions invariably different from those in alkaline solution. By following the change in absorption of the transient

---

[6] M. Simic, P. Neta, and E. Hayon, *J. Phys. Chem.*, 73, 3794, 1969.

[7] M. Anbar and P. Neta, *Int. J. Appl. Radiat. Isotopes*, 18, 493 (1967).

[8] E. Hayon and J. Weiss, *Proc. 2nd Intern. Conf. Peaseful Uses At. Energy, Geneva*, 39, 80 (1958); E. Hayon and A. O. Allen, *J. Phys. Chem.*, 65, 2181 (1961).

Table I: Absorption Maxima, Extinction Coefficients, Decay Rate Constants, and Dissociation Constants for the Carboxyalkyl Radicals Produced in Pulse Radiolysis of Aqueous Solutions of Some Aliphatic Acids

Acid	pH	λ_{max}, nm	ϵ, M^{-1} cm^{-1}[a]	$2k$, M^{-1} sec^{-1}[a]	Radical	pK_a of radical[b]	pK_a of acid
Formic	3.1	235	3000	1.5×10^9	[c]	[c]	3.77
	9	235	3000	1.5×10^9	CO_2^-		
	13			1.7×10^9	CO_2^-		
Acetic	3	320	650	1.8×10^9	$\dot{C}H_2COOH$	4.5	4.76
	10	350	800	1.0×10^9	$\dot{C}H_2COO^-$		
Propionic	3	300	700	2.2×10^9	$CH_3\dot{C}HCOOH$	4.9	4.88
	10, 13.5	335	950	1.2×10^9	$CH_3\dot{C}HCOO^-$		
n-Butyric	3	~280	....	$\sim 10^9$	$CH_3CH_2\dot{C}HCOOH$	4.8	4.82
	9	335	900	$\sim 10^9$	$CH_3CH_2\dot{C}HCOO^-$		
Isobutyric	3	~295	....	$\sim 10^9$	$(CH_3)_2\dot{C}COOH$	5.8	4.85
	9	325	....	$\sim 10^9$	$(CH_3)_2\dot{C}COO^-$		
Trimethylacetic	3	<240	....	1.3×10^9	$\dot{C}H_2C(CH_3)_2COOH$	4.8	5.02
	9	240	1800	9.3×10^8	$\dot{C}H_2C(CH_3)_2COO^-$		

[a] Deviation ±15%. In all cases the rate constants were derived near the maximum. [b] Deviation ±0.2. [c] See Discussion.

with pH at a suitable wavelength, the corresponding pK values of the radicals were derived.

Formic Acid. Identical absorption spectra and decay rates were obtained on pulse radiolysis of solutions containing $HCO_2^- + N_2O$ or $HCO_2^- + CO_2$ in the pH range 3–13 (Figure 1 and Table I). This demonstrates the equivalence of the carboxyl radical formed by either

$$HCO_2^- + OH \longrightarrow \cdot CO_2^- + H_2O \qquad (7)$$

or

$$CO_2 + e_{aq}^- \longrightarrow \cdot CO_2^- \qquad (8)$$

Our results at $\lambda > 260$ nm are in agreement with the results of Keene, *et al.*[5] However, we find the absorption maximum at 235 instead of 250 nm, with $\epsilon_{235} = 3000\ M^{-1}\ cm^{-1}$. This difference is probably due to the relatively high correction factor for scattered light used in the earlier experiments.[5]

The equivalence of the products from reactions 7 and 8 could also be demonstrated in γ-irradiated aqueous solutions of 0.5 M $HCO_2Na + N_2O$ and 0.5 M HCO_2Na + 0.5 M $NaHCO_3$ ($HCO_3^- \rightleftarrows CO_2 + OH^-$) at pH values between 6 and 9. The yield of oxalic acid, produced by dimerization of $\cdot CO_2^-$, was determined by precipitation as calcium oxalate. Identical yields were found[9] in both systems, with G(oxalic) = 3.4 and 3.2 ± 0.2, respectively.

Aqueous solutions of MeOH + CO_2 and EtOH + CO_2 were also irradiated (Figure 1). After correcting for the absorption due to the alcohol transient, which originates from the reaction of OH radicals with the alcohol, the spectrum was found to be identical with that in formic acid solutions, supporting further the above view. The transient absorption in the alcohol + CO_2 solutions was about one-half that in $HCO_2^- + N_2O$ solutions, in agreement with the relative yields of e_{aq}^- and $e_{aq}^- + OH + H$.

In acid solution (pH <3) the carboxyl radical is believed to disproportionate,[3] giving CO_2. At pH >3 a decrease of the CO_2 yield[3] and an increase in the oxalic acid yield[9] was observed, suggesting preferential dimerization of the radicals. Since no changes in the absorption spectra and decay rates of the carboxyl radical were observed down to pH 3 (this work) and pH 2.4,[5] it is possible that $\cdot CO_2H$ and $\cdot CO_2^-$ have identical spectra and decay rates. The pK value for the dissociation of this radical might also be below 2.4, and an explanation for the change in the nature of the products produced would have to be found.

A transient absorption down to 260 nm, similar to that of $\cdot CO_2^-$, was observed on pulse radiolysis of aqueous solution of oxalate ions saturated with N_2O at pH 9. Complete scavenging could not be achieved due to the low reactivity of OH radicals with oxalate ions. This spectrum could be assigned either to $\cdot CO_2$–CO_2^- or to $\cdot CO_2^-$. However, using the extinction coefficient of $\cdot CO_2^-$, the decay rate of the oxalate transient was found to be identical with that of $\cdot CO_2^-$.

Acetic Acid. The transient absorption spectrum produced on pulse radiolysis of aqueous solutions of acetate ions saturated with N_2O showed a broad absorption band with a maximum at 350 nm (Figure 2). This transient species is considered to be due to the $\cdot CH_2COO^-$ radical, and support for this assignment was obtained from the pulse radiolysis of chloroacetate ions. The spectra obtained from solutions of $CH_3COO^- + ClCH_2COO^-$ and of *t*-BuOH + $ClCH_2COO^-$ were identical with those obtained from $CH_3COO^- + N_2O$ solution. The absorption in the *t*-BuOH + $ClCH_2COO^-$ system was about one-half that in the other two systems, in accord with the relative radical yields.

On pulse radiolysis of acetic acid or chloroacetic acid

[9] M. Simic and G. Scholes, unpublished results.

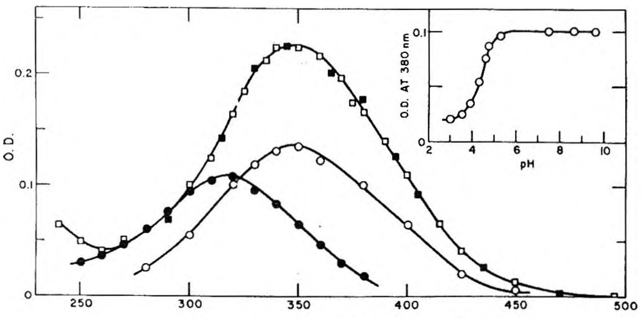

Figure 2. Absorption spectra and OD *vs.* pH curve of $\cdot CH_2COOH$ and $\cdot CH_2COO^-$ radicals in irradiated aqueous solutions (30 krads/pulse). □, 1 *M* CH_3COONa, N_2O (1 atm), pH 9; ■, 1 *M* CH_3COONa, 0.02 *M* $ClCH_2COONa$, pH 9; O, 0.1 *M* $ClCH_2COONa$, 1 *M* *t*-BuOH, pH 9; ●, 0.1 *M* $ClCH_2COOH$, 1 *M* *t*-BuOH, pH 3; *p*H curve: 0.1 *M* $ClCH_2COOH$, 1 *M* *t*-BuOH.

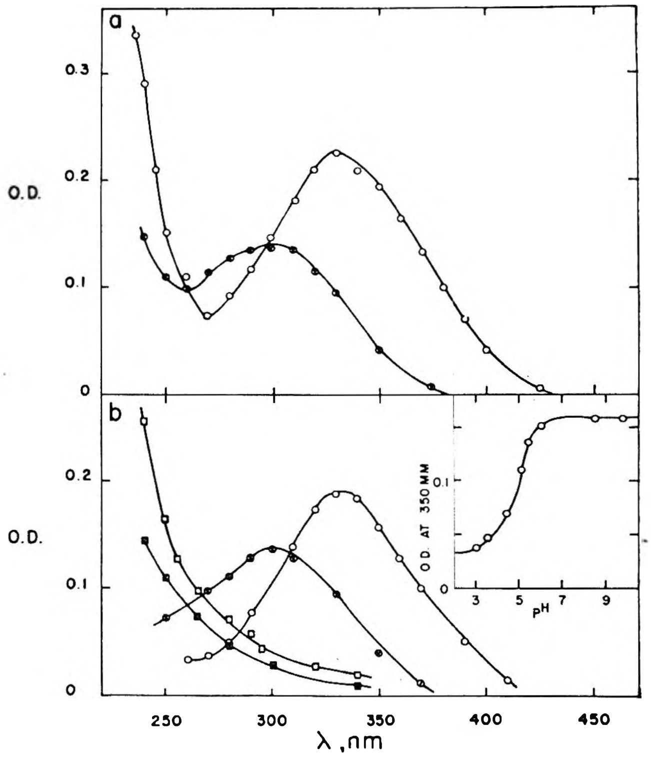

Figure 3. Absorption spectra and OD *vs.* pH curve of transients produced on pulse radiolysis of aqueous solutions of propionic and chloropropionic acids (36 krads/pulse). a. O, 0.25 *M* CH_3CH_2COONa, N_2O (1 atm), pH 9 and pH 13.5; ⊗, 0.5 *M* CH_3CH_2COOH, N_2O (1 atm), pH 3 and pH 1. b. O, 0.05 *M* $CH_3CHClCOONa$, 1 *M* *t*-BuOH, pH 9; ⊗, 0.05 *M* $CH_3CHClCOONa$, 1 *M* *t*-BuOH, pH 3.1; □, 0.1 *M* $ClCH_2CH_2COONa$, 1 *M* *t*-BuOH, pH 9; ⊠, 0.1 *M* $ClCH_2CH_2COOH$, 1 *M* *t*-BuOH, pH 4; pH curve: 0.05 *M* $CH_3CHClCOONa$, 1 *M* *t*-BuOH.

solutions at pH 3, the peak of the transient absorption is shifted to 320 nm, and the extinction coefficient is found to be about 20% lower than that at pH 9 (Figure 2). This absorption is assigned to the $\cdot CH_2COOH$ radical, since its formation was found to be dependent on the dissociation of the acid (see below).

It is evident from these results that the site of reaction of the OH radical with the dissociated or undissociated acid is primarily at the C–H bond (under the experimental conditions used). An attack on the carboxyl group, if taking place, has only a minor contribution. This is in agreement with previously reached conclusions from product analysis,[2] kinetic measurements,[10] and esr studies.[11,12]

The p*K* value of the $\cdot CH_2COOH$ radical has been derived by monitoring the transient absorption at 380 nm in irradiated solutions of *t*-BuOH + $ClCH_2COOH$ (inset in Figure 2). It was found to be p*K* = 4.5, in agreement with the p*K* value for acetic acid itself (Table I).

The second-order decay rate constants of the acetic acid transients were determined in N_2O-saturated solutions at pH 3 and pH 10. The rate was found to be about twice faster for the undissociated radical compared to the dissociated one (Table I), in general agreement with the relative rates of reaction of neutral and singly charged species.

Propionic Acid. The transient absorption spectrum obtained on irradiation of aqueous solutions of propionate ions in the presence of N_2O (1 atm) at pH 10–13 had a broad maximum at 330 nm and a second absorption with a peak below 230 nm (Figure 3). To demonstrate that the composite structure of this spectrum arises from two species, possibly the α- and β-carboxyalkyl radicals, these radicals were produced independently from the pulse radiolysis of the α- and β-chloropropionic acids. On irradiation at pH 9, the α radical formed shows a broad peak at 330 nm, whereas the β radical has a maximum below 240 nm (Figure 3). The peak of the β radical could not be observed due to high absorption of β chloropropionate ions below 240 nm. By comparing the absorption obtained in irradiated solution of $CH_3CH_2COO^-$ + N_2O with those of the α and β radicals produced from chloropropionic acids (Figure 3) it can be estimated that the extent of hydrogen abstraction by OH radicals at the α position is about 55%, in fair agreement with a previous estimate.[10]

In acid solutions of propionic and α- and β-chloropropionic acids, the absorption spectra are shifted toward lower wavelengths (Figure 3). The maximum of the α radical was shifted to 300 nm and its extinction coefficient is reduced by ~25%. These changes are attributed to the formation of the undissociated radicals $CH_3\dot{C}HCOOH$ and $\cdot CH_2CH_2COOH$. Comparing the spectrum obtained from CH_3CH_2COOH + N_2O with

---

(10) M. Anbar D. Meyerstein, and P. Neta, *J. Chem. Soc., B*, 742 (1966).

(11) W. T. Dixon, R. O. C. Norman, and A. L. Buley, *J. Chem. Soc.*, 701 (1964).

(12) H. Taniguchi, K. Fukui, S. Ohnishi, H. Hatano, H. Hasegawa, and T. Maryuaura, *J. Phys. Chem.*, 72, 1926 (1968).

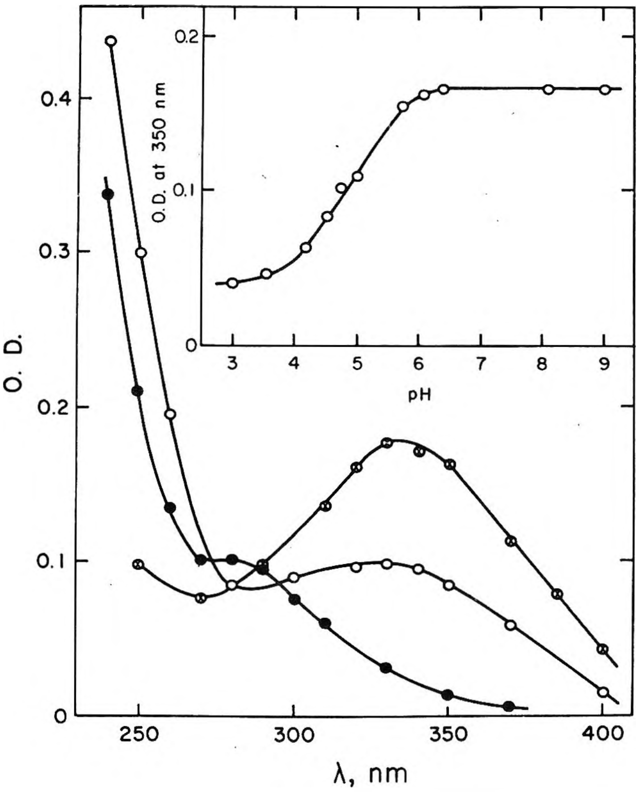

Figure 4. Absorption spectra and OD *vs.* pH curve of transients produced on pulse radiolysis of aqueous solutions of *n*-butyric and α-chloro-*n*-butyric acids (36 krads/pulse). ○, 0.1 *M* $CH_3CH_2CH_2COONa$, N_2O (1 atm), pH 9; ●, 0.1 *M* $CH_3CH_2CH_2COOH$, N_2O (1 atm), pH 3.15; ⊗, 0.05 *M* $CH_3CH_2CHClCOONa$, 1 *M* *t*-BuOH, pH 9.

those from $CH_2CHClCOOH$ + *t*-BuOH and $ClCH_2CH_2COOH$ + *t*-BuOH it is found that H abstraction from propionic acid takes place ~35% at the α position. This result is in agreement with that obtained in esr study[12] at pH 2. The different reactivity of the α C–H bonds in CH_3CH_2COOH and $CH_3CH_2COO^-$ toward OH radicals is probably due to a difference in the extent of the inductive effect of the –COOH and $-COO^-$ groups.

The p*K* of the $CH_3\dot{C}HCOOH$ radical was determined at 350 nm in irradiated solutions of α chloropropionic acid + *t*-BuOH, and was found to be 4.9, identical with the p*K* of propionic acid itself (Table I).

The second-order decay rate constants of the α and β radicals were measured in solutions of $CH_3CH_2COO^-$ + N_2O, where they are both formed in approximately the same yield. Following the decay in the 330- and the 250-nm region it was found that both radicals decay at the same rate. Otherwise, the α and β radicals could be formed independently from the chloropropionic acids in the presence of *t*-BuOH. The effect of the *t*-BuOH radicals on the decay of the acid radicals was found to be small for acetic acid (see below) and is probably even smaller for propionic acid. Indeed, the decay rates of both the α and the β radicals mixed with *t*-BuOH radicals were found to be very close to the rate found in solution of propionate + N_2O. In all cases a value of $(1.2 \pm 0.4) \times 10^9$ M^{-1} sec^{-1} was obtained for the dissociated radicals. The decay rate for the undissociated radicals was higher $\sim 2.2 \times 10^9$ M^{-1} sec^{-1} (Table I).

n-Butyric Acid. The transient absorption spectra from irradiated solutions of *n*-butyric acid and α-chloro-*n*-butyric acid are presented in Figure 4. A broad absorption with λ_{max} ~335 nm was observed in solution of *t*-BuOH + $CH_3CH_2CHClCOO^-$ at pH 9, and was assigned to the α radical, $CH_3CH_2\dot{C}HCOO^-$. In solutions of $CH_3CH_2CH_2COO^-$ + N_2O at the same pH a peak at 335 nm was also observed, in addition to a strong absorption below 280 nm. Attempts were made to unambiguously identify this increasing absorption below 280 nm as an absorption due to the β and γ radicals. However, exact measurements of these spectra were not possible due to impurities present in the commercially available β- and γ-chlorobutyric acids, which could not be eliminated. The main impurity seemed to be crotonic acid and when aqueous solutions of crotonic acid were irradiated a very strong absorption with λ_{max} 275 nm and ϵ ~10,000 M^{-1} cm^{-1} was obtained. This absorption was also found in the impure β-chlorobutyric acid. Nevertheless, it was possible to conclude that both the β and γ radicals exhibit strong absorption below 270 nm with $\lambda_{max} <$ 250 nm.

A comparison of the transient absorption obtained in irradiated solutions of *n*-butyrate + N_2O and α-chloro-*n*-butyrate + *t*-butanol (Figure 4) shows that the reaction of OH radicals with *n*-butyrate results in 25% hydrogen abstraction in the α position. This is in good agreement with a previous estimate (30%).[10] As it was found for propionic acid, the fraction of attack on the α position appears to be smaller for the undissociated acid. A value of 12% was suggested from the esr experiments at pH 2.[12]

The p*K* of the $CH_3CH_2\dot{C}HCOOH$ radical was monitored at 350 nm in irradiated solutions of *n*-butyric acid + N_2O (Figure 4) and found to be 4.8, identical with that of *n*-butyric acid itself.

The rate constants for the α radical interaction were derived from the decay of the transient absorption in solutions of *n*-butyric acid + N_2O at pH 3 and pH 9 and are of the order of $\sim 10^9$ M^{-1} sec^{-1}.

Isobutyric Acid. The results from irradiated solutions of isobutyric acid + N_2O (Figure 5) are similar to those of *n*-butyric acid. The peak at 325 nm was assigned to the α radical and the increase in absorption below 280 nm to the β radical. The α- and β-chloro derivatives were not available for confirmation of these assignments. In acid solution a shift of the spectrum was observed for both the α and β radicals. The p*K* of the α radical was derived by monitoring the transient at 335 nm, and a value of 5.8 was obtained, which is higher than p*K* = 4.85 for the acid itself.

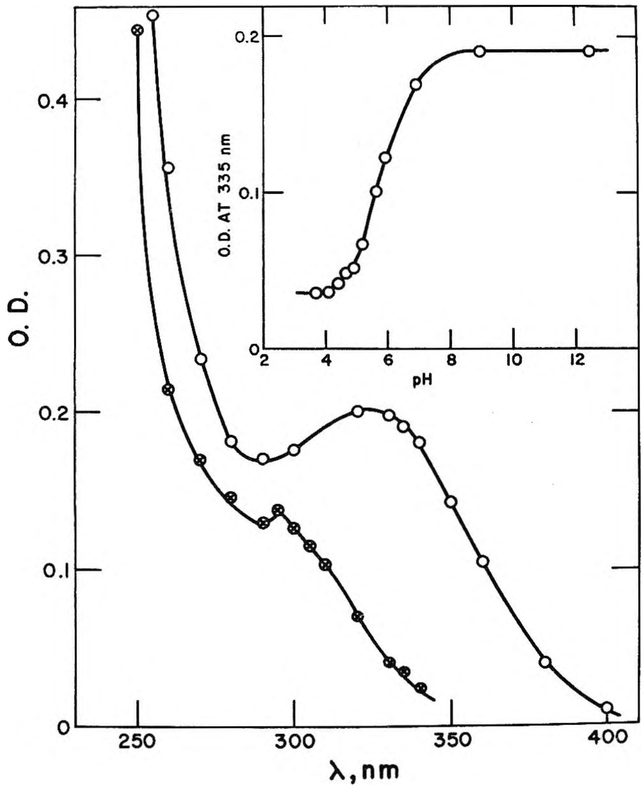

Figure 5. Absorption spectra and OD *vs.* pH curve of transients produced on pulse radiolysis of aqueous solutions of isobutyric acid (36 krads/pulse); 0.1 M $(CH_3)_2CHCOOH$, N_2O (1 atm); ○, pH 9; ⊗, pH 3.

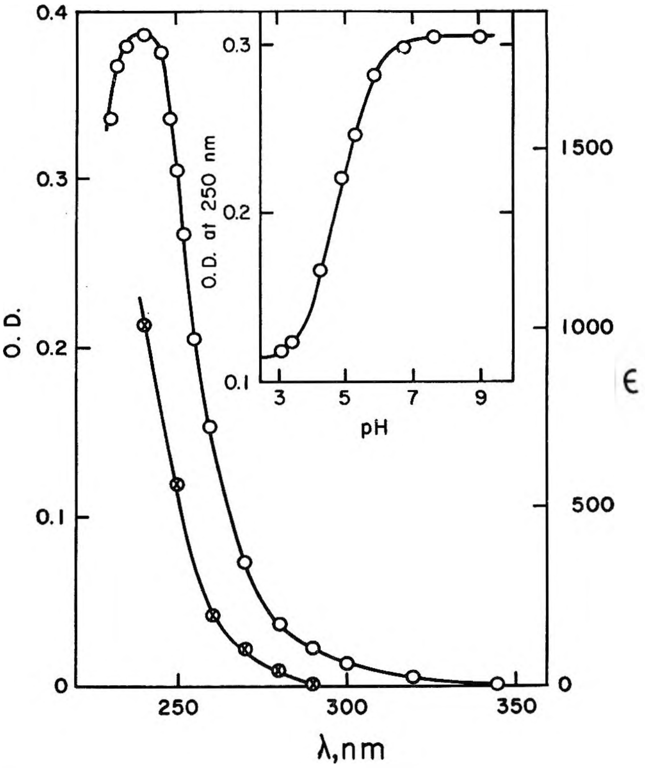

Figure 6. Absorption spectra and OD *vs.* pH curve of the transient produced on pulse radiolysis of aqueous solutions of trimethylacetic acid (19 krads/pulse); ϵ is given in M^{-1} cm^{-1} units; 0.2 M $(CH_3)_3CCOOH$, N_2O (1 atm) at pH 9, ○; pH 3.1, ⊗.

The decay rate constant was estimated to be about 10^9 M^{-1} sec^{-1}. This could not be calculated accurately because both α and β radicals are formed from isobutyric acid in appreciable amounts.[12] These radicals could not be formed separately from the chloro derivatives, and therefore only an approximate value for the extinction coefficient could be derived.

Trimethylacetic Acid. This acid has no α C–H bonds and a reaction with OH radicals is expected therefore to lead to the exclusive formation of a β radical. The transient absorption spectra obtained in the presence of N_2O are shown in Figure 6. No absorption was found in the 300–400-nm region. At pH 9 a maximum at 240 nm was obtained and is suggested to be due to the $\cdot CH_2C(CH_3)_2COO^-$ radical. In acid solutions at pH 3.1 the absorption maximum appears to be shifted toward lower wavelengths. The peak in acid solution could not be observed due to the increase in absorption of the acid at lower wavelengths. However, the pK of the radical could be derived at 250 nm (Figure 6) and was found to be 4.8, compared to 5.0 for the acid itself. The second-order decay rate constants at the dissociated and undissociated radicals are 9.3×10^8 and 1.3×10^9 M^{-1} sec^{-1}, respectively.

Reactivity of $\cdot CO_2^-$ *and* $\cdot CH_2COO^-$ *Radicals.* Reaction rates of $\cdot CO_2^-$ and $\cdot CH_2COO^-$ with each other and with various alcohol radicals have been followed. The $\cdot CO_2^-$ radical was produced either by reaction 7 or 8 at pH 5, and the initial decay was followed at 255 nm where the absorption of the other radicals[6] present contribute less than 15%. The $\cdot CH_2COO^-$ radical was produced by the reaction of chloroacetate with e_{aq}^- at pH 9, and the decay was followed at 350 nm where the contribution of other radicals was negligible. The alcohol radicals were formed by the reaction of OH with alcohols. Decay rates were estimated under initial conditions (first half-life), where the concentration of the two radicals was approximately the same, and represent a composite value of $k(R_1 + R_2)$ and $k(R_1 + R_1)$. In all cases, the decay rates of $\cdot CO_2^-$ and $\cdot CH_2COO^-$ radicals were found to be higher in the presence of an alcohol radical ($\cdot CH_2OH$, $CH_3\dot{C}HOH$, and $\cdot CH_2C(CH_3)_2OH$) by a factor of 3–5, indicating a substantial interaction between these radicals. The reactivity of $\cdot CH_2^-$ and $\cdot CH_2COO^-$ radicals was found to be the lowest with the t-BuOH radicals.

Although very little is known about the kinetics of interaction of two different radicals in pulse radiolysis, the existence of such reactions has been deduced from product analysis in radiation chemistry. In γ radiolysis of aqueous solutions of alcohols in the presence of CO_2, formation of various α-hydroxycarboxylic acids was reported.[13-15] For instance, glycolic acid with $G = 2.2$ was formed in CO_2-saturated solutions of methanol,[14,15] by the reaction of $\cdot CH_2OH$ with $\cdot CO_2^-$. Lactic acid was similarly formed from $CH_3\dot{C}HOH$, and malonic acid from $\cdot CH_2COO^-$.[13]

Our results show that the carboxylation reaction, that is combination of CO_2^- with organic radicals, is not sufficiently fast with some radicals to prevent partial recombination of like radicals. However, in some cases, substantial yields can be expected. It can also be seen that the $\cdot CH_2COO^-$ radical reacts with different alcohol radicals, and β-hydroxycarboxylic acids are expected to be formed.

Conclusions

The absorption spectra of the α- and β-carboxyalkyl radicals have been found to be easily distinguishable. The dissociated α radicals $R_2\dot{C}COO^-$ have absorption maxima in the region 325–350 nm, relatively independent of the number of carbon atoms in the alkyl group, with extinction coefficients of ~800–950 M^{-1} cm^{-1}. The undissociated radicals $R_2\dot{C}COOH$ show similar absorption spectra with maxima shifted toward lower wavelengths by about 30 nm and extinction coefficients 20–30% lower.

The β-carboxyalkyl radicals have absorption maxima $\leq$240 nm with extinction coefficients considerably higher than those of the α radicals. The spectra of the undissociated form are in all cases shifted toward lower wavelengths. It appears that γ radicals absorb in the same region.

In contrast to the carboxyalkyl radicals, $\cdot CO_2^-$ shows an absorption maximum at 235 nm with high extinction coefficient, 3000 M^{-1} cm^{-1}, independent of pH between pH 3 and 13.

The second-order decay rate constants for the carboxyalkyl radicals are of the order of 10^9 M^{-1} sec^{-1}. In all cases the dissociated form reacts about twice slower, in general agreement with the predicted rates for reactions of singly charged and neutral species according to Debye's equation. These changes in the rate constants are significantly greater than the changes which could result from variations in the ionic strength of the solutions. It appears that both α and β radicals decay at the same rate.

The pK values for the dissociation of the carboxyalkyl radicals (both α and β) were found to be identical with those of the parent acids, except that for the carboxyl radical $\cdot CO_2^-$ which remains unknown, and the isobutyric acid radical which appears to be higher. This increase could be explained as due to the hyperconjugation of the unpaired electron with the CH_3 groups, which would induce a partial negative charge on the α carbon atom. This is supported by the coupling constants of this unpaired electron as measured in esr studies.[11,12]

The attack of OH radicals on aliphatic carboxylic acids is directed primarily to the C–H bonds at different positions, the distribution being dependent on the relative reactivities. The fraction of the α radicals produced was found to be considerably lower for the undissociated acids. This is probably due to the difference in the inductive effect of $-COOH$ and $-COO^-$ groups on the α position and the electrophilic nature of the OH radical.

Acknowledgment. Partial financial support received from the U. S. Army Research Office, Durham, is gratefully acknowledged.

[13] G. Scholes, M. Simic, and J. J. Weiss, *Nature*, **188**, 1019 (1960).

[14] A. Appleby, J. Holian, G. Scholes, M. Simic, and J. J. Weiss, Proceedings of the 2nd International Congress of Radiation Research, (1962).

[15] F. Gütlbauer and N. Getoff, *Int. J. Appl. Radiat. Isotopes*, **16**, 673 (1965).

Pulse Radiolysis of Aliphatic Acids in Aqueous Solutions.

II. Hydroxy and Polycarboxylic Acids

by M. Simic, P. Neta, and E. Hayon

Pioneering Research Laboratory, U. S. Army Natick Laboratories, Natick, Massachusetts 01760

(Received May 1, 1969)

Pulse radiolysis of aqueous solutions of aliphatic hydroxycarboxylic acids (glycolic, lactic, tartaric, and citric) leads to the formation of hydroxycarboxyalkyl radicals. Similarly, polycarboxyalkyl radicals are formed from polycarboxylic acids (malonic, succinic, and tricarballylic). These radicals are formed as a result of hydrogen abstraction by OH radicals and H atoms and have characteristic transient absorption spectra dependent on pH. This dependence is attributed to the sequential dissociation of the carboxyl and α-hydroxyl groups. The pK values for the carboxyl group in the hydroxycarboxyalkyl radicals are higher than those of the parent acids and are close to the pK values of the nonsubstituted acids and their radicals, inferring a diminution of the inductive effect of the OH group on the radical. The pK values for the dissociation of the OH group in an α position to the unpaired electron in hydroxycarboxyalkyl radicals are lower than those of the corresponding α-hydroxyalkyl radicals. The second-order decay rates of the various carboxyalkyl radicals were found to be strongly dependent on the number of charges on the radicals.

Introduction

The radiation chemistry of hydroxy- and polycarboxylic acids in aqueous solutions has not been studied in detail. The main radiolytic products in aqueous solutions of glycolic acid were hydrogen[1] ($G = 4.2$) and tartaric acid[2] ($G = 2.1$). The products from lactic acid were not fully investigated; the only ones reported were hydrogen and pyruvic acid[3] ($G = 0.5$). Beside hydrogen, a small amount of CO_2 was reported for γ-irradiated solutions of glycolic, tartaric, malonic, and succinic acids,[4] with $G(CO_2)$ increasing substantially only at high concentrations of these acids.

On the basis of these investigations it was proposed that these acids, similar to the monocarboxylic acids, react with OH radicals and H atoms by a hydrogen abstraction mechanism

$$\mathrm{RCH(OH)COOH + OH \longrightarrow R\dot{C}(OH)COOH + H_2O} \quad (1)$$

$$\mathrm{RCH(OH)COOH + H \longrightarrow R\dot{C}(OH)COOH + H_2} \quad (2)$$

The organic radicals formed then dimerize and/or disproportionate, leading to the observed products. The mechanism for the formation of CO_2 was explained partly by the attack of the OH radicals on the carboxyl groups and partly by direct action of radiation on the solute molecules at the higher concentrations.

The absorption spectra and dissociation constants of various hydroxyalkyl and monocarboxyalkyl radicals produced on pulse radiolysis of aqueous solutions of alcohols[5,6] and monocarboxylic acids[7] have recently been investigated. It was of interest, therefore, to study the absorption spectra and, in particular, the sequential proton dissociation of radicals that combine those features. The radicals produced on pulse radiolysis of aqueous solutions of hydroxycarboxylic acids and also radicals having more than one carboxyl group, produced on pulse radiolysis of polycarboxylic acid solutions, were investigated.

Experimental Section

This work was done using the Febetron 705 pulsed radiation source. All the pertinent information on the experimental conditions and setup has been previously described.[6,7]

Results and Discussion

The pulse radiolysis of aqueous solutions of some hydroxy and polycarboxylic acids was studied under conditions such that only H atoms and OH radicals were reacting with these acids. The e_{aq}^- formed in the radiolysis of water was converted ($\geqslant 98\%$) into H atoms by reaction with H_3O^+ at pH <3, or into OH radicals by reaction with N_2O (1 atm) at pH >3. The concentration of the acids used in this work was sufficiently high to ensure complete scavenging of OH radicals and H atoms.

---

(1) E. Hayon and J. Weiss, *J. Chem. Soc.*, 5091 (1960).

(2) P. M. Grant and R. B. Ward, *ibid.*, 2654, 2659 (1959).

(3) G. R. A. Johnson, G. Scholes, and J. Weiss, *ibid.*, 3091 (1953).

(4) H. Fricke, E. J. Hart, and H. P. Smith, *J. Chem. Phys.*, **6**, 229 (1938).

(5) K. D. Asmus, A. Henglein, A. Wigger, and G. Beck, *Ber. Bunsenges. Phys. Chem.*, **70**, 756 (1966); J. Lilie, G. Beck, and A. Henglein, *ibid.*, **72**, 529 (1968).

(6) M. Simic, P. Neta, and E. Hayon, *J. Phys. Chem.*, **73**, 3794 (1969).

(7) P. Neta, M. Simic, and E. Hayon, *ibid.*, **73**, 4207 (1969).

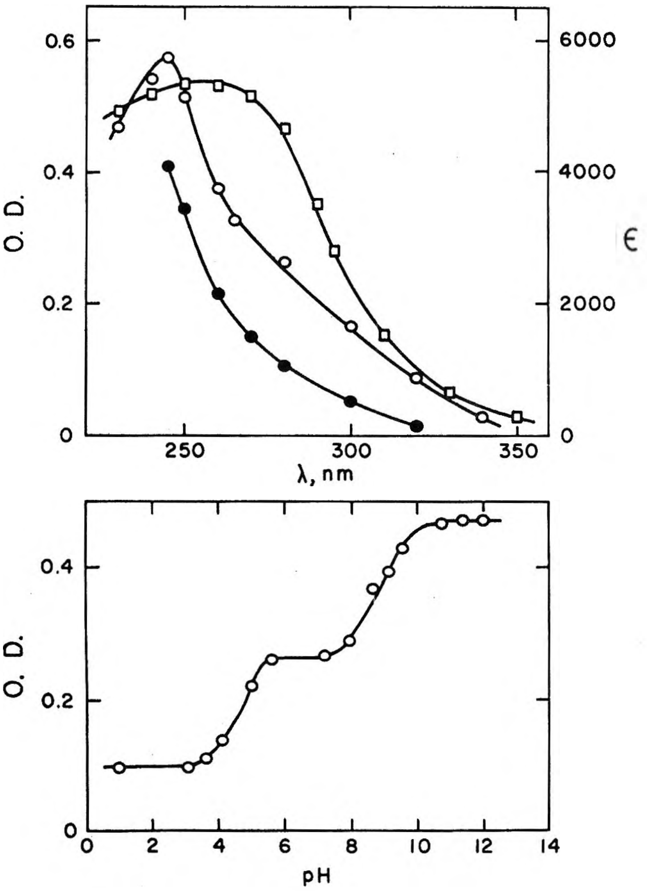

Figure 1. Absorption spectra and OD *vs.* pH curve of transients produced on pulse radiolysis of glycolic acid in aqueous solutions. 8 krads/pulse; ε is given in M^{-1} cm^{-1} units: ●, 0.5 *M* glycolic acid, pH 1; ○, 0.05 *M* glycolate, N_2O (1 atm), pH 7.2; □, 0.05 *M* glycolate, N_2O (1 atm), pH 12.

Hydroxycarboxylic Acids

Glycolic Acid. Three characteristic absorption spectra were observed on pulse radiolysis of aqueous solutions of glycolic acid at different pH values (Figure 1). At pH 7.2, the transient species has a maximum at 245 nm, and at pH 12.0 the peak is shifted to λ_{max} ~255 nm. At pH 1, the absorption maximum could not be established, $\lambda_{max} \leqslant 245$ nm, due to considerable absorption by glycolic acid. The concentration of the acid at pH 1 was sufficiently high to scavenge >90% of the H atoms. On the basis of the results obtained on pulse radiolysis of monocarboxylic acids[7] and of alcohols[6] and in the esr studies,[8] this spectrum has been assigned to the carboxyhydroxymethyl radical $\mathrm{HO\dot{C}HCOOH}$. By increasing the pH of the solution, dissociation of the carboxyl group takes place and at pH 7.2 the spectrum is due entirely to the $\mathrm{HO\dot{C}HCOO^-}$ radical. The p*K* of the dissociation of this group was determined by monitoring the absorption of the transient at 280 nm (Figure 1) and found to be 4.6. This is considerably higher than the p*K* = 3.83 of glycolic acid.

The $\mathrm{HO\dot{C}HCOO^-}$ radical beside being an α-carboxy radical has the unpaired electron in the α position to the OH group. Therefore the p*K* for the dissociation of this hydroxyl group in the radical $\mathrm{HO\dot{C}HCOO^-}$ is expected to be lower than the p*K* of that group in glycolic acid itself, as was found for a number of alcohols.[5,6] The p*K* of the $\mathrm{\dot{C}H_2OH}$ radical is 10.7[5] and the presence of a carboxyl group attached to this α radical would be expected to lower the p*K* of the dissociation of the OH group. Indeed, a p*K* = 8.8 has been found for the dissociation of the hydroxyl group of the glycolate radical (see Figure 1). At pH 12 the spectrum observed is due to the $\mathrm{^-O\dot{C}HCOO^-}$ radical.

The decay rates of the transients at pH 1, 7.2, and 12 (Table I) are also in agreement with the expected relative rates for neutral, mono- and dinegatively charged radicals. The spectra of the dissociated radicals are shifted toward the visible region. The extinction coefficients of the three radicals (ε ~6000 M^{-1} cm^{-1}) are considerably higher than those observed for both α-hydroxyalkyl radicals[6] (ε <2000 M^{-1} cm^{-1}) and α-carboxyalkyl radicals[7] (ε <1000 M^{-1} cm^{-1}).

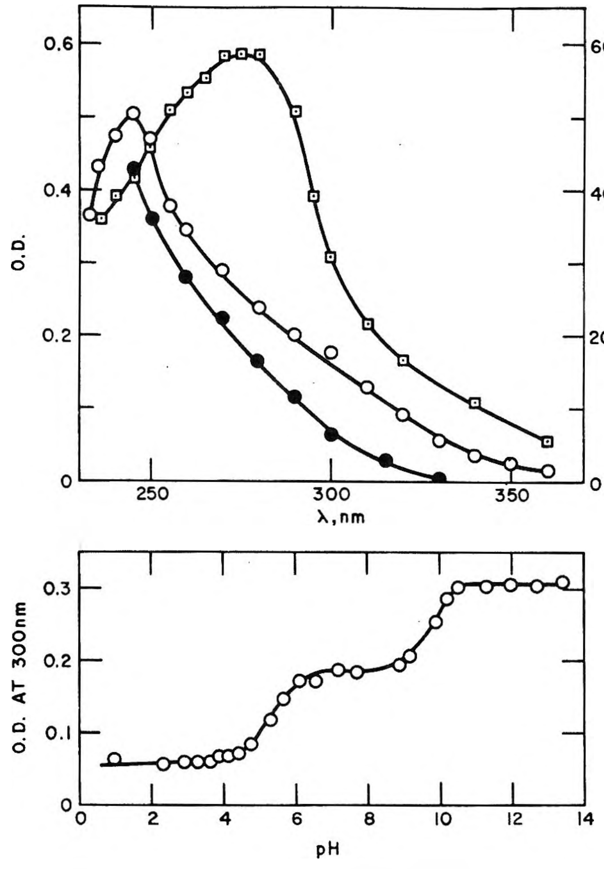

Figure 2. Absorption spectra and OD *vs.* pH curves of transients produced on pulse radiolysis of lactic acid in aqueous solutions. 8 krads/pulse; ε is given in M^{-1} cm^{-1} units: ●, 0.5 *M* lactic acid, pH 1; ○, 0.2 *M* lactate, N_2O (1 atm), pH 8.9; □, 0.1 *M* lactate, N_2O (1 atm), pH 12.

---

(8) W. T. Dixon, R. O. C. Norman, and A. L. Buley, *J. Chem. Soc.*, 3625 (1964).

Table I: Absorption Maxima, Extinction Coefficients, Decay Rate Constants, and Dissociation Constants of the Radical Produced on Pulse Radiolysis of Aqueous Solutions of some Polyfunctional Acids

Acid	pH	λ_{max}, nm	ϵ_1, M^{-1} cm$^{-1\,a}$	$2k$, M^{-1} sec$^{-1\,a}$	Radical	pK_a of radical^b	pK_a of acid
Glycolic	1	<245	...	1.1×10^9	$HO\dot{C}HCOOH$		3.83
					⇅		
	7.2	245	5700	8.5×10^8	$HO\dot{C}HCOO^-$	4.6	
					⇅		
	12	255	5400	1.5×10^7	$^-O\dot{C}HCOO^-$	8.8	
Lactic	1	<245	...	6.4×10^8	$HO\dot{C}(CH_3)COOH$		3.87
					⇅	5.3	
	8.9	245	5100	1.6×10^8	$HO\dot{C}(CH_3)COO^-$		
					⇅	9.8	
	12	275	5800	6.8×10^6	$^-O\dot{C}(CH_3)COO^-$		
Tartaric	1.3	<245	...	1.5×10^8	$HOOCCH(OH)\dot{C}(OH)COOH$		3.0; 4.3
					⇅	4.5	
	9.4	248	6500	5.8×10^6	$^-OOCCH(OH)\dot{C}(OH)COO^-$		
					⇅	12.4	
	13.2	255	9000	2.3×10^5	$^-OOCCH(OH)\dot{C}(O^-)COO$		
Citric	1	...	...	4.7×10^8	$\dot{C}HCOO^-$ | $HOCCOO^-$ | CH_2COO^-	...	3.1; 4.8; 6.4
	7.4	...	...	3.5×10^6			
	13.0	...	...	3.6×10^6			
Malonic	1	340	~400	$\sim 1 \times 10^9$	$HOOC\dot{C}HCOOH$		2.86
	4	340	400	5.5×10^8	⇅	5.7	5.70
	11	340	1000	5.7×10^7	$^-OOC\dot{C}HCOO^-$		
Succinic	11	...	...	8.5×10^7	$^-OOCCH_2\dot{C}HCOO^-$	...	4.2, 5.6
Tricarballylic	11	...	...	$\sim 6 \times 10^5$		...	

^{a} Deviation ±15%. In all cases the rate constants were derived near the maximum. ^{b} Deviation ±0.2

Lactic Acid. Dehydrogenation of lactic acid by H atoms and OH radicals is expected to take place predominantly at the α position to give a methyl-substituted glycolic acid radical. In fact, the transient absorption spectra obtained at pH 1.0, 8.9, and 12.0 (Figure 2) closely resemble those obtained on pulse radiolysis of glycolic acid. In acid solutions, the maximum is <245 nm, and is shifted to 245 nm and 275 nm at pH 8.9 and 12.0, respectively.

The dissociation constant of the $CH_3\dot{C}(OH)COOH$ radical to $CH_3\dot{C}(OH)COO^-$ has a pK = 5.3, which is higher than the pK = 3.87 of lactic acid; *i.e.*, the α radical is a weaker acid than the parent acid. The pK of the hydroxyl group of the radical $CH_3\dot{C}(OH)COO^-$, pK = 9.8, is lower than the pK of the corresponding alcohol radical $CH_3\dot{C}HOH$ (pK = 11.6). With both the $HO\dot{C}HCOO^-$ and $CH_3\dot{C}(OH)COO^-$ radicals, the pK of the hydroxyl group is about two units lower than the pK of the corresponding alcohol radicals.

The extinction coefficients and decay rates of the three different radicals produced (Table I) show general resemblance to those of the glycolic acid radicals.

Tartaric Acid. The two C–H bonds of tartaric acid are both in the α and β position to the hydroxyl and the carboxyl groups. Dehydrogenation at these positions by an OH radical is expected to take place on the basis of the high reactivities of these bonds. There is, however, only one radical produced due to the symmetry of the molecule. The general features of the transients produced on pulse radiolysis of tartaric acid in aqueous solutions (Figure 3 and Table I) are similar to those already described for glycolic and lactic acid radicals. The radical formed from tartaric acid has two carboxyl and two hydroxyl groups associated with the unpaired electron on the carbon atom. The decay rate of this polyfunctional radical ($2k$ = 1.5×10^8 M^{-1} sec^{-1}) is somewhat lower than those for other neutral radicals and could be due to as teric effect or to a resonance stabilization of the radical by the functional groups.

Both carboxyl groups of the radical are expected to dissociate, but due to the closeness of the pK values for the acid itself (pK_1 = 3.0, pK_2 = 4.3), the pK values of the radical were expected to be close also. The optical density method is not sufficiently sensitive for evaluation of close overlapping pK values. The derived overall pK value of 4.5 could perhaps be split into two values about 4 and 5 (Figure 3).

The change of the absorption spectrum above pH 9 is attributed to the dissociation of the hydroxyl group attached to the carbon atom carrying the unpaired electron, *i.e.*

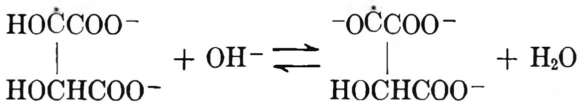

$$\begin{matrix} HO\dot{C}COO^- \\ | \\ HOCHCOO^- \end{matrix} + OH^- \rightleftharpoons \begin{matrix} ^-O\dot{C}COO^- \\ | \\ HOCHCOO^- \end{matrix} + H_2O$$

with $pK_a = 12.4$.

The 20-fold decrease of the decay rate constant of the dissociated radical at pH 13.2, compared to that at pH 9.4, is in agreement with the increased negative charge on the radical. The hydroxyl group at the β-position to the unpaired electron is not expected to dissociate in the same pH region,[6] but closer to the pK value of the OH group in tartaric acid itself (probably above 14).

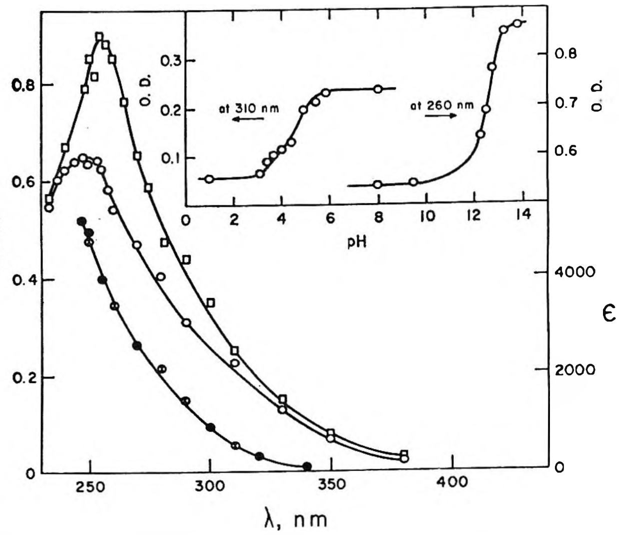

Figure 3. Absorption spectra and OD *vs.* pH curves of transients produced on pulse radiolysis of tartaric acid in aqueous solutions. 8 krads/pulse; 0.2 M tartaric acid, ϵ is given in M^{-1} cm^{-1} units: ●, pH 1; ⊗, pH 3, N_2O (1 atm); ○, pH 9.4, N_2O (1 atm); □, pH 13.2, N_2O (1 atm).

Citric Acid. The attack of the OH radical on citric acid is expected to take place at the CH_2 group, thus forming a single radical. This radical combines features of α-, β-, and γ-carboxyalkyl radicals, and indeed the spectrum (Figure 4) resembles that of the tricarballylic acid transient. This radical is at the same time a β-hydroxy radical and the main contribution of this hydroxyl group to the absorption spectrum of the transient is expected to be below 250 nm.[6]

At pH 1, the spectrum of the transient was very similar to that at pH 7.4, but due to incomplete scavenging of the H atoms even in 1 M solutions, no quantitative results could be obtained. Nevertheless, it appears that a shift of the spectrum (about 30 nm) toward lower wavelengths is observed in the 350–450-nm region. An attempt to obtain the pK values for the carboxyl groups of the citric acid radical was not made due to the closeness of the pK values of the acid.

The spectrum at pH >7.4, where all the carboxyl groups of the acid are already dissociated, can be assigned to the $^-OOCCH_2C(OH)(COO^-)\dot{C}HCOO^-$ radical. The hydroxyl group of this radical, being in a β position to the unpaired electron, is not expected[6] to dissociate much below the pK value of the same group in citric acid itself. No change in spectrum and decay rate (Table I) was observed up to pH 13.

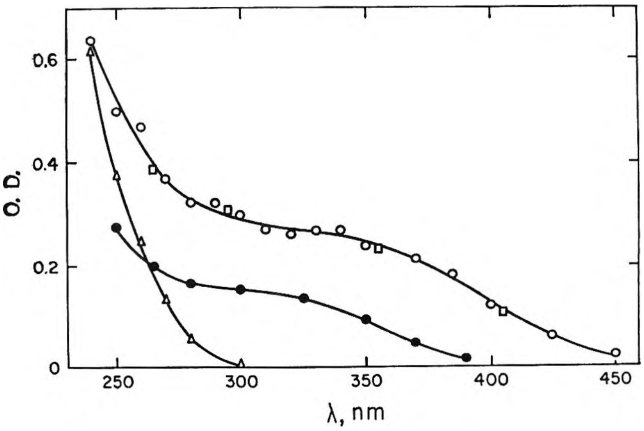

Figure 4. Absorption spectra of transients produced on pulse radiolysis of citric acid in aqueous solutions. 19 krads/pulse, 0.2 M citric acid, N_2O (1 atm): ○, pH 7.4, initial; △, pH 7.4, after 0.1 sec; □, pH 13, initial; ●, pH 1, partial scavenging at 1 M citric acid.

In addition to the relatively fast-decaying transient, a species with a slow first-order decay ($k = 3.8 \times 10^{-1}$ sec^{-1}) absorbing below 300 nm was observed at pH 7.4. The OD of this transient was measured at 0.1 sec after the electron pulse (Figure 4). The nature of this species is not known at present.

Polycarboxylic Acids

Malonic Acid. A broad transient spectrum with λ_{max} 340 nm was observed in alkaline solutions (Figure 5). No shift of the peak takes place in acid solutions although the absorption is decreased considerably. Only one pK = 5.7, attributed to the dissociation of carboxyl groups of the $\cdot CH(COOH)_2$ transient, was derived. This value is identical with the second pK of malonic acid. It is possible that the inductive effect of the COOH group is greatly reduced by the odd electron, resulting in much closer, or even identical, pK values for the two COOH groups of the radical. The transient absorption in alkaline solutions could have been due to the formation of $\cdot CH_2COO^-$ radicals, as suggested from esr study. However, the derived decay rate constant is considerably lower than that of the acetate radical or that expected for a singly charged radical. This transient absorption is therefore assigned to the $\cdot CH(COO^-)_2$ radical. Another transient was observed below 280 nm with a first-order decay in acid solutions. Due to considerable technical difficulties in that region, a complete study could not be made.

Succinic and Tricarballylic Acids. Only the fully dissociated transients have been investigated. A broad absorption in the region 260–400 nm was observed for both the succinic and tricarballylic acid transients (Figure 6). These spectra are considerably different

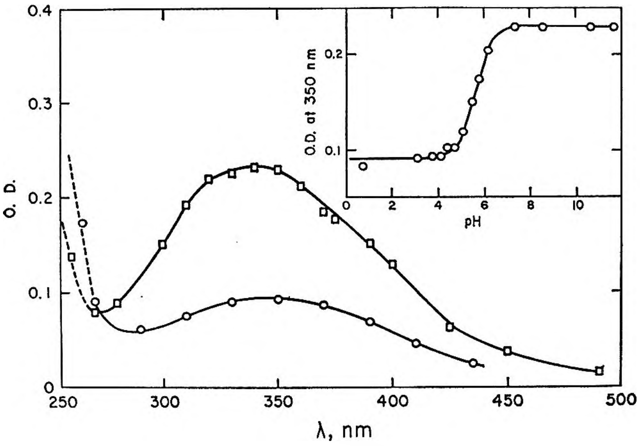

Figure 5. Absorption spectra and OD *vs.* pH curve of transients produced on pulse radiolysis of malonic acid in aqueous solutions. 19 krads/pulse, 0.2 *M* malonic acid, N_2O (1 atm): ○, pH 4; □, pH 11.

from the spectra of α-carboxyalky radicals.[7] Hydrogen abstraction from succinic acid gives rise to a single radical $\cdot CH(COO^-)CH_2COO^-$. As an α-carboxyalkyl radical, it is expected to absorb in the 330-350-nm region.[7] However, this radical is also a β-carboxyalkyl radical, and these latter radicals are expected to have an absorption below 280 nm. The effect of both of these contributions is expected to result in a composite absorption spectrum. Similarly, the tricarballylic acid radicals $\cdot CH(COO^-)CH(COO^-)CH_2COO^-$ and $CH_2(COO^-)\dot{C}(COO^-)CH_2COO^-$ are at the same time α-, β-, and γ- or α- and β-carboxyalkyl radicals, respectively.

The second-order decay rate constant of the succinate radical is close to that of the malonate radical (Table I) in accord with their similar structures and the same number of negative charges. On the other hand, the radicals produced in alkaline solutions of tricarballylic acid have three negatively charged groups and a lifetime two orders of magnitude longer, in general accord with the Debye relationship for the reaction rates of charged species.

The extinction coefficients of the succinic and tricarballylic radicals at 350 nm are 700 and 740, and at 270 nm are 1000 and 1800 M^{-1} cm^{-1}, respectively.

Conclusions

The α-carboxy-α-hydroxyalkyl radicals have characteristic absorption spectra with λ_{max} at about 250 nm and with high extinction coefficients. These absorption maxima lie between those of the α-hydroxy ($\leqslant$230 nm)[6] and the α-carboxyalkyl radicals (320-350 nm).[7] The extinction coefficients are about 5000-9000 M^{-1} cm^{-1}, considerably higher than those of either the alcohol (<2000 M^{-1} cm^{-1})[6] or the acid (<1000 M^{-1} cm^{-1})[7] radicals.

The absorption spectra of the polycarboxyalkyl radicals have features of the monocarboxyalkyl radicals. The malonic acid radical is an α,α-dicarboxyalkyl radical with an absorption spectrum similar to that of α-carboxyalkyl radicals. The carboxyl groups of polycarboxyalkyl radicals can also be in β and/or γ positions. The absorption spectra of these radicals have been found to combine the features of each functional group; *e.g.*, the spectrum of the succinic acid transient is a combination of those of α- and β-carboxyalkyl radicals. The transients of tricarballylic and citric acids combine features of α-, β-, and γ-carboxyalkyl radicals. The OH group in the β position to the unpaired electron of citric acid radical does not appear to have an effect on the absorption spectrum of the radical.

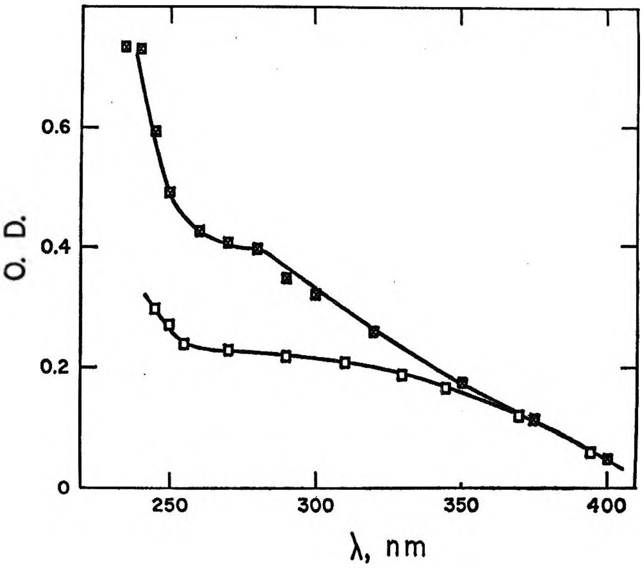

Figure 6. Absorption spectra of transients produced on pulse radiolysis of succinic and tricarballylic acids in aqueous solutions. 19 krads/pulse, 0.2 *M* acid, N_2O (1 atm), pH 11: □, succinic; ⊠, tricarballylic.

Due to the closeness of the p*K* values of the polycarboxylic acids, the corresponding p*K* values for the radicals could not be resolved. The p*K* values for the α-carboxy-α-hydroxyalkyl radicals appear to be higher than those of the parent acids. This is probably due to the delocalization of the unpaired electron by the OH group at the α position. The presence of such OH groups has been shown[8] to affect significantly the magnitude of the coupling of the unpaired electron with C_2 protons and has been attributed to a hyperconjugation mechanism. In other words, in α-hydroxy-α-carboxyalkyl radicals the inductive effect of the OH group on the dissociation of the COOH group is smaller than that in the parent acids. A similar effect could take place in α,α-dicarboxyalkyl radicals.

The p*K* values for the dissociation of the OH group of the α-hydroxycarboxyalkyl radicals are expected to be much lower than those of the parent molecules, as has been the case for simple alcohol radicals.[6] The p*K* of ROH is considerably lowered by the presence of an unpaired electron and also by the presence of electron-withdrawing substituents[6] (such as –COOH). Indeed, the pK values for the dissociation of the hydroxyl group in glycolic and lactic acid radicals are 8.8 and 9.8, respectively. The pK of β-hydroxyl group (in the citric acid radical) is not affected by the unpaired electron, as expected.[6]

The dissociation of both the COOH and the OH groups results in a shift of the transient spectrum toward higher wavelengths.

The decay rate constants of the uncharged polyfunctional radicals are of the order of $10^9\ M^{-1}\ \text{sec}^{-1}$, similar to the hydroxyalkyl and carboxyalkyl radicals. Some large radicals were found to have slower decays, *e.g.*, the tartaric acid radical. This could be due either to a steric effect, where the site of the unpaired electron is screened by various functional groups, or to resonance stabilization of the radical by those functional groups. Dissociation of the radicals has a large effect on the decay rates, and the triply charged species decay at rates lower than $10^6\ M^{-1}\ \text{sec}^{-1}$.

Absorption, Optical Rotatory Dispersion, and Circular Dichroism Studies on Some Sulfur-Containing Ribonucleosides

by Kam-Khow Cheong, Yi-Chang Fu, Roland K. Robins, and Henry Eyring

Department of Chemistry, University of Utah, Salt Lake City, Utah 84112 *(Received May 2, 1969)*

The uv absorption, and in some cases, the optical rotatory dispersion and circular dichroism data of some sulfur-containing nucleosides are reported. Both the pH effect and the correlation of spectral data with the non-sulfur containing nucleosides show that the intense absorption bands in the 300 to 350 mμ region are due to the $\pi \rightarrow \pi^*$ intramolecular charge-transfer transition by moving the charge from the sulfur-containing substituents to the purine ring.

Introduction

Sulfur-containing nucleic acid bases and nucleosides are of considerable importance. For example, 6-mercaptopurine[1] had been demonstrated to have an inhibitory effect on the growth of experimental tumors and human neoplasia and has been used as an antileukemia agent. 6-Mercaptopurine ribonucleoside is inhibitory at a lower dosage[2] than 6-mercaptopurine in adenocacinoma 755. In addition, 9-alkyl-2-amino-6-purinethiols,[3] 6-alkylthio-2-aminopurines,[4] and the corresponding purine 9-ribosides[5] have been reported to have antitumor activities. Recently, some sulfur-containing bases and their derivatives[6] have been found to occur in nature. The presence of sulfur adds to the biological interest of these molecules. A large number of closely related nucleosides have been synthesized but very little study of their electronic structure is reported. The present paper provides useful information for future work on the structures of related compounds.

The absorption spectra of purine and pyrimidine bases, as well as some substituted purines, show three or four bands between 180 and 300 mμ.[7] These bands have been related in the various bases and are presumably $\pi \rightarrow \pi^*$ transitions. Because of the high intensity of these bands, one cannot rule out the possibility that low intensity transitions, such as n $\rightarrow \pi^*$, are also present. With the aid of circular dichroism spectra,[8-12] the absorption curve of uridine was also

---

(1) "6-Mercaptopurine," *Ann. N. Y. Acad. Sci.*, **60**, 183 (1954).

(2) H. E. Skipper, J. A. Montgomery, J. R. Thomson, and F. M. Schabel, Jr., *Cancer Research*, **19**, 425 (1959).

(3) C. W. Noell and R. K. Robins, *J. Med. Pharm. Chem.*, **5**, 558 (1962).

(4) G. D. Daves, Jr., C. W. Noell, R. K. Robins, H. C. Koppel, and A. G. Beaman, *J. Amer. Chem. Soc.*, **82**, 2633 (1960).

(5) C. W. Noell and R. K. Robins, *J. Med. Pharm. Chem.*, **5**, 1074 (1962).

(6) (a) J. A. Carbon, L. Hung, and D. S. Jones, *Proc. Natl. Acad. Sci., U. S.*, **53**, 979 (1965); (b) M. N. Lipsett, *J. Biol. Chem.*, **240**, 3975 (1965); (c) L. Baczynskyj, K. Biemann, and R. H. Hall, *Science*, **159**, 1481 (1968).

(7) L. B. Clark and I. Tinoco, Jr., *J. Amer. Chem. Soc.*, **87**, 11 (1965).

(8) D. W. Miles, R. K. Robins, and H. Eyring, *Proc. Natl. Acad. Sci., U. S.*, **57**, 1138 (1967).

(9) D. W. Miles, R. K. Robins, and H. Eyring, *J. Phys. Chem.*, **71**, 3931 (1967).

(10) D. W. Miles, S. J. Hahn, R. K. Robins, M. J. Robins, and H. Eyring, *ibid.*, **72**, 1483 (1968).

(11) D. W. Miles, M. J. Robins, R. K. Robins, M. W. Winkley, and H. Eyring, *J. Amer. Chem. Soc.*, **91**, 824 (1969).

resolved into four bands. Clark and Tinoco[7] correlated the electronic transition of all bases in the near ultraviolet region to the B_{2u}, and B_{1u}, and the E_{1u} transitions of benzene.[7] There is also observed in pyridine-N-oxide[13-20] and some N-heteroaromatic compounds[21,22] with an electron donating substituent an absorption in the region of 300 mμ. This is thought to be due to a $\pi \rightarrow \pi^*$ transition having the character of an intramolecular charge transfer from the substituent to the ring.

In the present paper, the uv absorption, optical rotary dispersion (ORD), and circular dichroism (CD) properties of some sulfur-containing nucleosides are examined. The bands which mainly involve local excitation in the ring are correlated to the benzene transitions and will be labeled simply B_{2u}, B_{1u}, and E_{1u}[7] respectively. The longest wave absorption band between 300 and 350 mμ is considered a $\pi \rightarrow \pi^*$ intramolecular charge-transfer transition.

Experimental Section

All compounds under investigation were prepared and purified in the laboratory of Professor Roland K. Robins, or were donated or commercial samples of high purity. Details of the preparation and characterization of these compounds are given elsewhere.[23] Spectrophotometric grade solvents were used.

The absorption curves were determined with the Cary 14 recording spectrophotometer. The optical rotary dispersion data were measured with the automatic recording Cary Model 60 spectropolarimeter. The circular dichroism measurements were performed with the Cary Model 6001 circular dichroism accessory for the Cary 60 recording spectropolarimeter. A Beckman Model 96 Zeromatic pH meter was used for pH measurements.

The ORD data are expressed in terms of molecular rotation, (M), and the CD data in terms of molecular ellipticity, (θ). Usually ORD and CD studies of purine and pyrimidine nucleosides are discouraging because the corresponding chromophoric systems have a comparatively unfavorable anisotropy factor. Within the optical transition band, the signal-to-noise ratios are customarily smaller than those in the off-transitional region. The ORD and CD curves reported in the present paper are reproducible and within the 15% accuracy range. Another difficulty of these studies is that some of the compounds have very small solubilities in water. The concentrations of the solutions were usually 10^{-4} to 10^{-5} *M* so that further dilution did not alter the shape of the curves. Solutions were allowed to stand for at least 2 hr before performing the measurements to ensure the attainment of equilibrium conditions. The ultraviolet absorption spectra are presented in terms of the molar extinction coefficient. All data were recorded at room temperature. The results and configurations are shown in Figures 1–11.

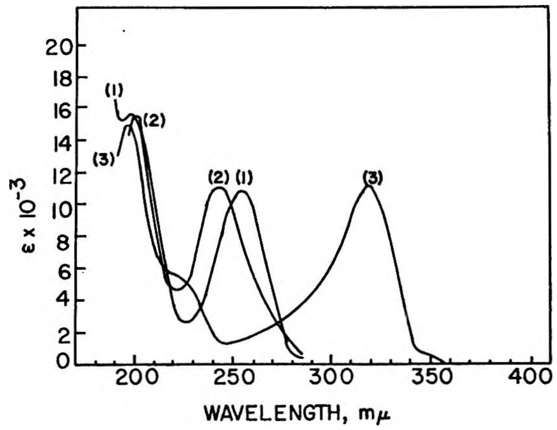

Figure 1. The absorption spectra of 6-amino-9-β-D-ribofuranosylpurine, (1); 9-β-D-ribofuranosylpurin-6-one, (2); and 9-β-D-ribofuranosylpyrine-6-thione, (3) measured at pH 7.

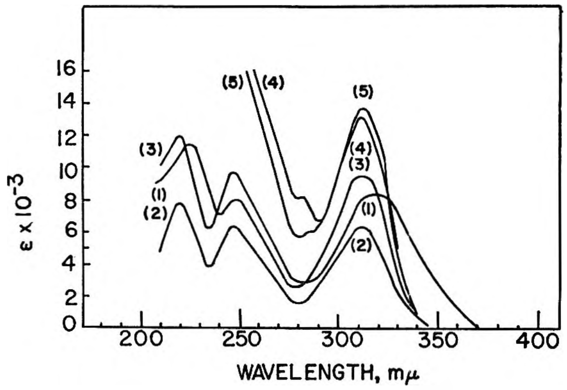

Figure 2. The absorption spectra of 2-amino-6-isobutylthio-9-β-D-ribofuranosylpurine measured at pH 2, (1); pH 7, (2); pH 11, (3); methanol, (4); and 1:1 *n*-butane:cyclohexane solution, (5).

Results and Discussion

The absorption spectra of 6-amino-9-β-D-ribofuranosylpurine (adenosine, (I), 9-β-D-ribofuranosylpurin-6-one, (inosine, II), and9-β- D-ribofuranosyl-purin-6-

(12) D. W. Miles, M. J. Robins, R. K. Robins, and H. Eyring, *Proc. Natl. Acad. Sci., U. S.*, **62**, 22 (1969).

(13) T. Kubota, *J. Chem. Soc. Jap.*, **79**, 930 (1958); **80**, 578 (1959).

(14) T. Kubota, *Bull. Chem. Soc. Jap.*, **35**, 946 (1962).

(15) M. Ito and N. Hata, *ibid.*, **28**, 260 (1955).

(16) M. Ito and W. Mizushima, *J. Chem. Phys.*, **24**, 495 (1956).

(17) J. Sidman, *Chem. Rev.*, **58**, 689 (1958).

(18) J. N. Murrell, "Theory of the Electronic Spectra of Organic Molecules," Methuen and Co., London, Ltd., 1963, p 188.

(19) H. H. Jaffe and M. Orchin, "Theory and Applications of Ultraviolet Spectroscopy," John Wiley & Sons, Inc., New York, N. Y., 1962.

(20) E. M. Evleth, *Theoret. Chim. Acta*, **11**, 145 (1968).

(21) S. F. Mason, *J. Chem. Soc.*, 219 (1960).

(22) M. Godfrey and J. N. Murrell, *Proc. Roy. Soc.*, **A278**, 57 (1964).

(23) (a) J. J. Fox, D. V. Praag, I. Wempen, I. L. Doerr, L. Cheong, J. E. Knoll, M. L. Eidinoff, A. Bendich, and G. B. Brown, *J. Amer. Chem. Soc.*, **81**, 178 (1959); (b) J. J. Fox, I. Wempen, A. Hampton, and I. L. Doerr, *ibid.*, **80**, 1669 (1958); (c) R. E. Holmes and R. K. Robins, *ibid.*, **86**, 1242 (1964); (d) T. A. Khwaja and R. K. Robins, *ibid.*, **88**, 3640 (1966).

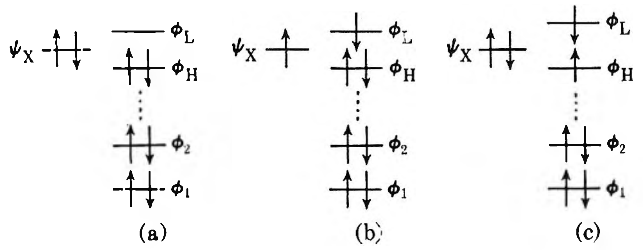

Figure 3. The electronic configurations of the substituted purine nucleosides or pyrimidines: (a) ground configuration; (b) charge-transfer configuration; (c) locally-excited configuration.

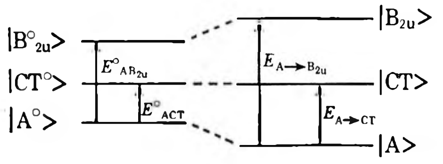

Figure 4. The energy level diagrams.

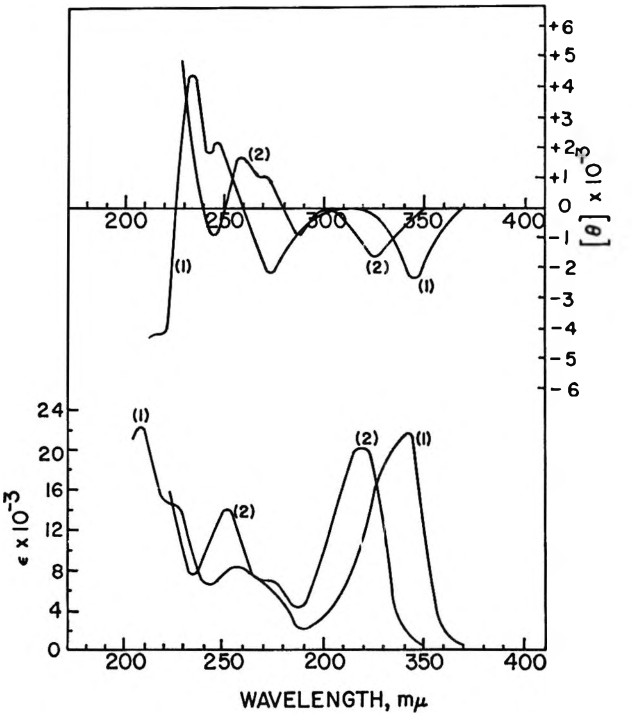

Figure 5. The circular dichroism and absorption spectra of 2-amino-9-β-D-ribofuranosylpurin-6-thione at pH 7, (1) and pH 11, (2).

thione (III) are shown in Figure 1. The broad composite long wavelength bands of I and II appearing around 240–260 mμ have been resolved by both the study of the circular dichroism spectrum[8–12] and the theoretical molecular orbital calculation[24–26] and have been designated as B_{1u} for the shorter wavelength and the B_{2u} for the longer wave length transition bands, respectively. While for compound III, in addition to two weak bands localized around 240–270 mμ, there is a high intensity transition appearing at the markedly longer wavelength of 315 mμ (ϵ 24 × 10^3). In the region 240–270 mμ, the absorption band of 6-sulfur-containing purines is intensified by introducing a substituent at position 2 or 8. This band is split into two (Figures 5, 9), with a weak intensity at the longer wavelength (155–275 mμ) and a moderately strong absorption at the shorter wavelength (245–255 mμ, ϵ 6–10 × 10^3). These two bands are analogous to the B_{2u} and B_{1u} absorption bands of I and II.

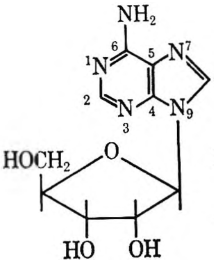

I

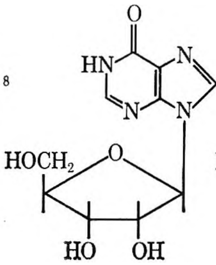

II

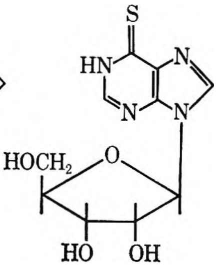

III

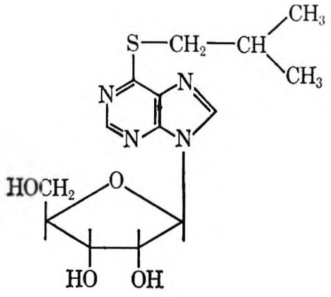

IV

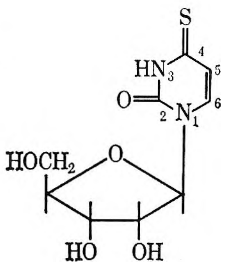

V

With the aid of the circular dichroism spectrum,[8] the absorption curve of uridine was resolved into four bands that can also be related to the B_{2u}, B_{1u}, and E_{1u} transitions of the benzene chromophore. Their maxima are at 267, 240, 210, and 190 mμ, respectively. In 4-thiouridine (V), analogous absorption bands are observed (Figure 6). Their corresponding locations are at 270, 234, 209, and 195 mμ (Table I). In addition, two more cotton effects located at 338 and 291 mμ are observed. The absorption curve shows a high intensity maximum at 332 mμ (ϵ_{max} 22 × 10^3).

It has been observed that for purine nucleosides, the B_{2u} band is seen to have an increasing blue shift as we proceed up along the series of substituents (–H, –Cl, $-NH_2$, $-OCH_3$) at the 6-position[7–10] (Table II). The ionization potentials of these substituents decrease along the series. A similar tendency is also observed for the 2-aminopurine series. With an increase in the perturbing power at the 6-position for the sequence –H, $-NH_2$ and =O (Table II)[7,23b] the B_{2u} band of 2-amino-9-β-D-ribofuranosylpurine, centered at 304 mμ, is blue

---

(24) J. W. Kwiatkowski, *J. Mol. Phys.*, **12**, 197 (1967).

(25) M. Tanaka and S. Nagakura, *Theoret. Chim. Acta*, **6**, 320 (1966).

(26) H. Berthord, C. Giessrer-Prettre, and A. Pullman, *ibid.*, **5**, 53 (1966).

Table I: Circular Dichroism and Absorption Spectral Data and Assignment of Bands

			λ, mμ				
Compound	Solvent	Spectra	CT	B_{2u}	B_{1u}	E_{1u}	Other
Uridine[a]	pH 7	UV		260 (10)[b]		204 (10)	
		CD		267 (+14)[c]	240 (−7)	210 (−8), 190 (+13)	
Cytidine[a]	pH 7	UV		268		200 (24),	235
		CD		271 (+16)		218 (−16)	
	pH 1	UV		280		215 (10)	
		CD		280 (+15)		217 (−14)	
4-Thiouridine	pH 7	UV	332 (22)		247 (5)	200 (15)	
		CD	338 (+1.8)	270 (+3)	234 (−7)	209 (−7.5), 195 (+10.4)	291 (−1.60)
	pH 11	UV	317 (22)				
		CD	316 (+7)	278 (+5.5)	239 (−3.5)		

[a] See reference 8. [b] The value given in parentheses for ε must be multiplied by 10^3 in order to get molar extinction coefficients. [c] The values given in parentheses for θ must be multiplied by 10^3 in order to get molar ellipticities.

Table II: Spectroscopic Data and Assignment of Bands

		λ, mμ (ε)[a]			
Compound	Solvent	CT	B_{2u}	B_{1u}	E_{1u}
2-Amino-9-β-D-ribofuranosylpurine[b]	pH 7		304 (6.9)	243 (6.2)	
2,6-Diaminopurine[c]	pH 6		280	242	215, 202
9-Ethylguanine[c]	pH 6.6		275 (9.6)	252 (13.6)	205 (s20), 188 (26)
2-Amino-6-isobutylthio-9-β-D-ribofuranosylpurine	pH 7	312 (6.2)	262 (s)	247 (6.2)	220 (7.8)
6-Thioguanosine[b]	pH 7.53	340 (21)	270 (7.5)	253 (9.0)	224 (14.3), 208
6-Thioguanine[b]	pH 9.6	340 (19.5)	268 (6.8)	242 (8.4)	
6-Thioxanthosine[d]	pH 7	342 (24)	269 (5.5)	255 (8.0)	222 (15), 201 (17.5)
Purine[c]	TMP		265 (6.9)	240 (3.0)	200 (18.1), 188 (21.1)
6-Aminopurine[c]	TMP		260 (12.6)		208 (18.7), 185 (15.8)
6-Chloropurine[c]	TMP		265 (8.2)	245 (s3.9)	205 (19), 193 (24.2)
6-Methoxypurine[c]	TMP		251 (7.3)		200 (16.7), 190 (18)
6-Mercaptopurine[d]	pH 9.5	312 (18.0)	250 (3.2)	230	

[a] The values given for ε must be multiplied by 10^3 in order to get molar extinction coefficients. [b] See ref 23(b). [c] See ref 7. [d] R. K. Robins, *et al.*, unpublished data.

shifted to 275 mμ for 9-ethylguanine. The ionization potentials of $HSCH_2CH(CH_3)_2$ and H_2S are smaller than those of H_2, NH_3, $HOCH_3$, and H_2O. All of these provide strong evidence for assigning the B_{2u} and B_{1u} bands to the 245–275 mμ region with their composite absorption bands for both the 6-sulfur-containing ribonucleosides and 4-thiouridine.

Further, there is a shoulder appearing around 320–330 mμ accompanying the strong band for the 6-sulfur-containing purine nucleoside (Figures 2, 9). Figure 9 shows that even in either the basic (pH 11) or the acidic solutions (pH 2), this shoulder does not disappear nor does it have an isobestic point. These facts rule out the possibility that the shoulder originates from either the absorption due to the anion or due to the cation form which exist in equilibrium with the neutral form in basic or acidic solutions,[23b] respectively. The only possible assignment for this shoulder is the n → π* transition which may arise from the excitation of the nonbonding electrons in a ketone, a mercaptan,[19] a thione, or the pyridine-type nitrogen. X-ray crystallographic examination of the guanine cation[27,28] indicates that the proton location is probably at N_7. This suggestion has further been proved by proton magnetic resonance studies.[29] If 6-mercapto-9-β-D-ribofuranosylpurin-2-one also have the same basic center at N_7, then, upon protonation, the transition arising from this pyridine-type nitrogen should be shifted to the blue side and the intensity of this band should be decreased and disappear.[17,30] But Figure 9 shows no such effect. In addition, Figure 2 indicates that in the nonpolar solvent, 2-amino-6-*S*-butylthio-9-β-D- ribofuranosylpurine was a shoulder around 320 mμ which is seen to be shifted by increasing the polarity of the solvent.[30] All of these

(27) W. Cochran, *Acta Cryst.*, **4**, 81 (1951).

(28) J. M. Broomhead, *ibid.*, 1, 324 (1948); **4**, 92 (1951).

(29) C. D. Jardetzky and O. Jardetzky, *J. Amer. Chem. Soc.*, **82**, 222 (1960).

(30) H. McConnell, *J. Chem. Phys.*, **20**, 700 (1952).

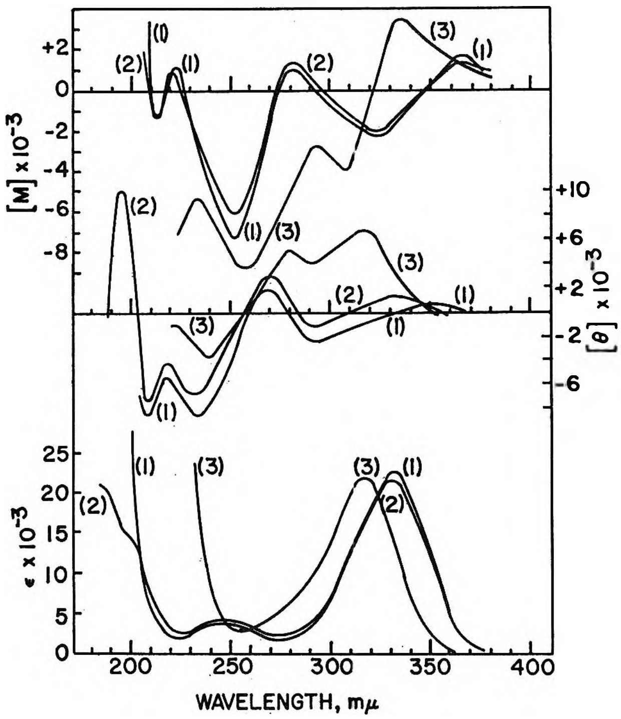

Figure 6. The optical rotatory dispersion, circular dichroism and absorption spectra of 4-thiouridine measured at pH 2, (1); pH 7, (2); and pH 11, (3).

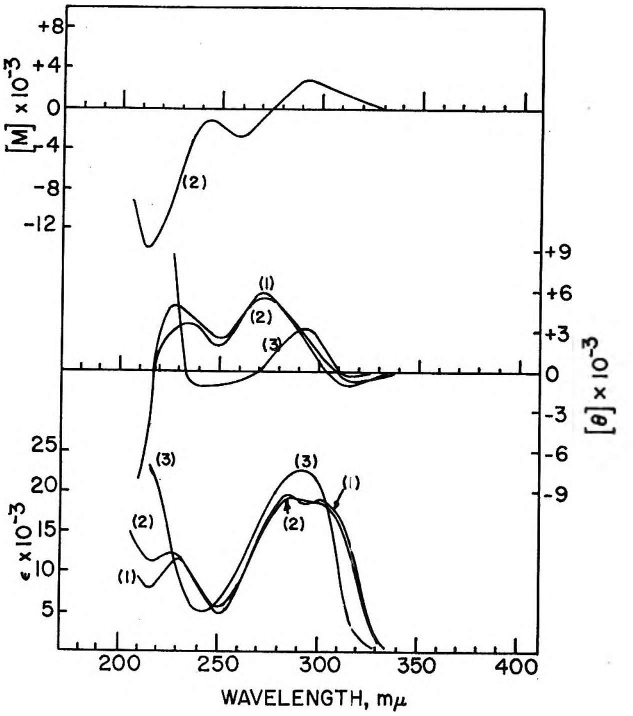

Figure 7. The optical rotatory dispersion, circular dichroism, and absorption spectra of 8-thioguanosine measured at pH 2, (1); pH 7, (2); and pH 11, (3).

findings indicate that the n → π* transition band for the 320–330 mμ shoulder comes from the excitation of a nonbonding electron on the sulfur atom to the extended π molecular orbital.

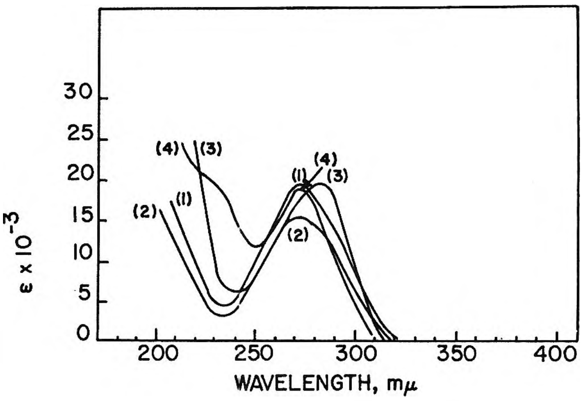

Figure 8. The absorption spectra of 8-methylthioguanosine measured at pH 2, (1); pH 7, (2); pH 11, (3); and methanol, (4) solutions.

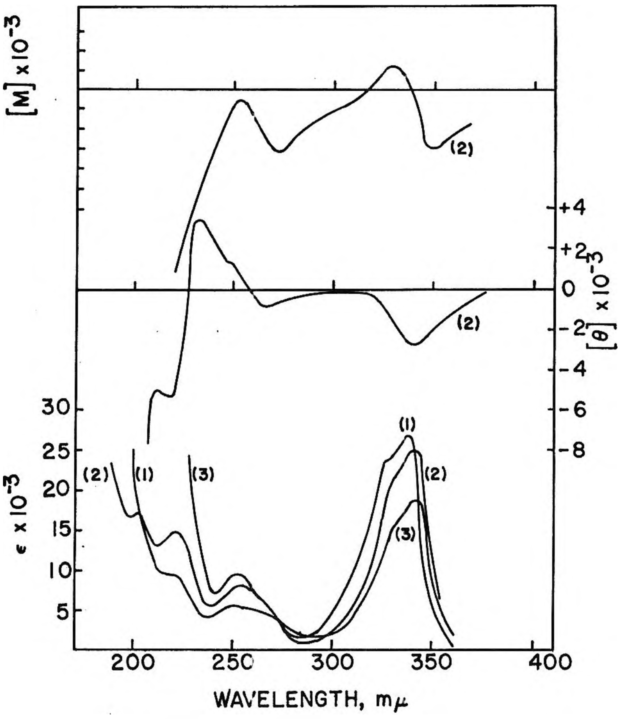

Figure 9. The optical rotatory dispersion, circular dichroism and absorption spectra of 6-thioxanthosine measured at pH 2, (1); pH 7, (2); and pH 11, (3).

As mentioned before, 4-thiouridine and all the 6-sulfur-containing purine nucleosides show an intense absorption band around 310–340 mμ. This extraordinary characteristically strong transition band is neither clearly visible nor existent in the nonsulfur-containing purine nucleosides. The origin of this band is worth discussing.

The intramolecular charge transfer band has been discussed both theoretically and experimentally.[31-33] A

---

(31) S. Nakakura, *J. Mol. Phys.*, **3**, 105 (1960).

(32) H. C. Longuet-Higgins and J. N. Murrell, *Proc. Phys. Soc.*, **A68**, 601 (1955).

(33) J. A. Shellman and E. B. Nielsen, *J. Phys. Chem.*, **71**, 3914 (1967).

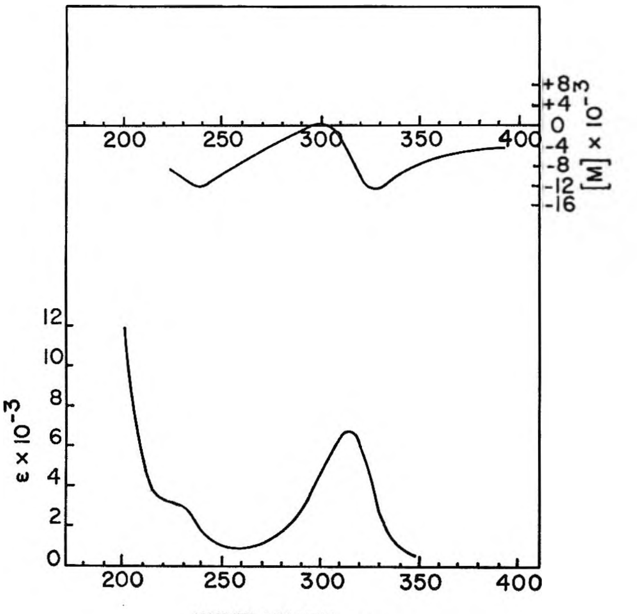

Figure 10. The optical rotatory dispersion and absorption spectra of 1-methyl-9-β-D-ribofuranosylpurine-6-thione measured at 1:1 aqueous methanol solution.

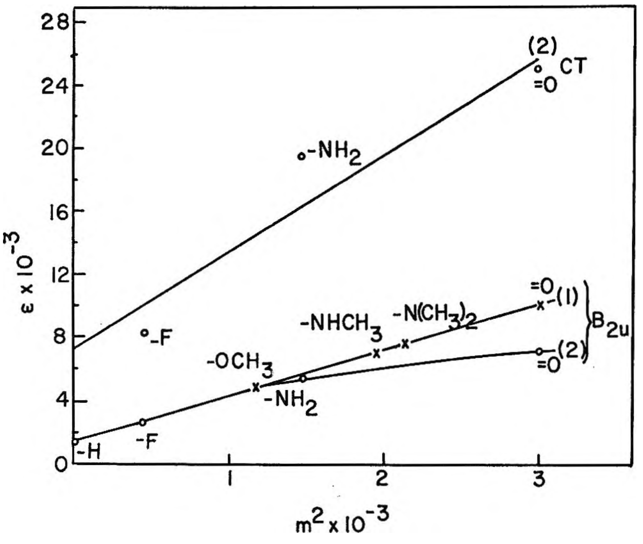

Figure 11. The observed extinction coefficient, ϵ_{max}, of B_{2u} and intramolecular charge transfer bands, plotted against the square of the spectroscopic moment, m^2, of the substituents, ×, at C_6 for the two series; (1) 2-X-9-β-D-ribofuranosylpurine-6-one (X = $-OCH_3$, $-NHCH_3$, $-N(CH_3)_2$, = O), (2) 2-X-9-β-D-ribofuranosylpurine-6-thione. (X = -F, $-NH_2$, =O).

substituent which has a small ionization potential will be expected to exert a strong mesomeric effect. In addition, a new intramolecular charge transfer band may also appear in the spectrum.[18,34] If the ionization potential of the substituent is large, then, in general, there will be only a weak mesomeric effect. In analogy to charge transfer, S. F. Mason proposed a benzyl anion model.[21] In this model, the lone-pair electrons of the amino, hydroxy, or mercapto group, delocalized over the pyrimidine nucleus in the ground state, are excited by the absorption of light to an unoccupied π-orbital.

It is not reasonable to assign the tremendously intense absorption band of 6-sulfur-containing purine ribonucleoside and 4-thiouridine at 310–340 mμ to the n → π* transition.[20] Probably it is chiefly due to the movement of charge upon excitation from the sulfur to the purine or the pyrimidine bases.[35] We propose calling this intramolecular charge transfer.

Let us think of the molecule as consisting of two parts, the substituent, X and the remaining purine ribonucleoside or pyrimidine part, P. X is an electron-donor group consisting of a lone pair of electrons in the atomic orbital, ψ_X, perpendicular to the purine or the pyrimidine ring. If X is a thione group, the electron available for the charge transfer is in the π orbital localized in the bond between X and P. We take account of the π electrons only. ϕ_i denotes the ith molecular orbital of P. ϕ_H is the highest occupied and ϕ_L is the lowest vacant π orbital of P. We can construct the electronic configuration by taking an antisymmetrized product of occupied orbitals. The ground configuration can be represented by a Slater determinant[34]

$$|A^0\rangle = (n!)^{-1/2}|\psi_X\bar{\psi}_X\phi_1\bar{\phi}_1\cdots\phi_H\bar{\phi}_H| \quad (1)$$

The representation of the singlet charge-transfer configuration is

$$|CT^0\rangle = (2!n!)^{-1/2}[|\psi_X\phi_1\bar{\phi}_1\cdots\phi_H\bar{\phi}_H\bar{\phi}_L| + |\bar{\phi}_X\phi_1\bar{\phi}_1\cdots\phi_H\bar{\phi}_H\phi_L|] \quad (2)$$

while

$$|B_{2u}{}^0\rangle = (2!n!)^{-1/2}[|\psi_X\bar{\psi}_X\phi_1\bar{\phi}_1\cdots\phi_H\bar{\phi}_L| + |\psi_X\bar{\psi}_X\phi_1\bar{\phi}_1\cdots\bar{\phi}_H\phi_L|] \quad (3)$$

corresponds to the first singlet locally-excited configuration, where n is the total number of π electrons in the molecule. All of these configurations[31] for the substituted purine ribonucleoside or pyrimidines are shown in Figure 3.

Neglecting the substitution of the sugar at the N_9 position, the electronic configuration $|A^0\rangle$, $|CT^0\rangle$ and $|B_{2u}{}^0\rangle$ are of A′ symmetry with respect to the plane of the purine or pyrimidine rings. After the interaction between the electron donor and electron acceptor groups, all the configurations will be mixed together.[36]

$$|A\rangle = |A^0\rangle + \sum_i{}'\alpha_{A^0 i}|i^0\rangle \quad (4)$$

$$|CT\rangle = |CT^0\rangle + \sum_i{}'\alpha_{CT^0 i}|i^0\rangle \quad (5)$$

---

(34) J. N. Murrell, *Proc. Phys. Soc.* **A68**, 969 (1955).

(35) (a) H. P. Koch, *J. Chem. Soc.*, 401 (1949); (b) G. B. Elion, W. H. Lange, and G. H. Hitchings, *J. Amer. Chem. Soc.*, **78**, 2858 (1956).

(36) H. Eyring, J. Walter, and G. E. Kimball, "Quantum Chemistry," John Wiley & Sons, Inc., New York, N. Y., 1944.

$$|B_{2u}\rangle = |B_{2u}{}^0\rangle + \sum_i{}' \alpha_{B^0_{2u}i} |i^0\rangle \qquad (6)$$

where $|A\rangle$, being the ground state function, has mixed in the charge transfer configuration as well as some other configurations and is stabilized with a decrease in energy, while the energy of the $|B_{2u}\rangle$ state will be expected to be increased by mixing in the charge transfer configuration. The relative energy levels of these states are shown in Figure 4.

Setting the energy of $|A^0\rangle$ equal to zero, the energy for exciting the ground state to the charge-transfer state will be[36]

$$E_{A \rightarrow CT} = E_{CT} - E_A = E^0_{CT} + (H^{(1)}_{CTCT} - H^{(1)}_{AA}) \qquad (7)$$

Where $H^{(1)}$ is the perturbation potential and E^0_{CT} is the energy of the charge transfer configuration and can be expressed as[34]

$$E^0_{CT} = I - A - \int \frac{\psi_X{}^2(1)\psi_L{}^2(2)}{r_{12}} d\tau_1 d\tau_2 \qquad (8)$$

I is the ionization potential of the substituent, and A is the electron affinity of the purine or the pyrimidine bases.

For most of the 6-substituted purine-ribonucleosides (*i.e.*, X = H, OH, Cl, NH_2, =O) the charge transfer absorptions bands are not observed. This may be due to the small value of the transition moment, or the merging of charge-transfer bands with the other strong transition bands, or their appearance in the far uv region. On the other hand, all the 6-sulfur-containing purine ribonucleosides show this strong charge transfer absorption at the long wave length (310–340 mμ), because the ionization potential of the electron in a sulfur containing group is small. From eq 7 and 8, it can be seen that the charge transfer band will be shifted to the red relative to the analogous but unobserved CT bands in compounds where X is not sulfur, and is, thus, separated from the other absorption bands. The intensity of the absorption may be due to the mixing of the sulfur's vacant 3d atomic orbital into its 3p orbital.[37] However, the charge transfer involves a significant charge displacement and this is probably sufficient to explain the observed intensity.

It has been pointed out previously, that by increasing the perturbing power with a substituent at C_6 on the purine base, instead of the red shift, the B_{2u} band is shifted to the blue. This may be explained as mixing in the charge transfer configuration in the ground state.

Additional evidence supporting the strong charge transfer absorption assignment at the long wave length for the 6-sulfur-containing purine nucleoside is provided by a study of the pH effect.

Figure 5 shows both the CD and uv spectra of 6-thioguanosine. In the basic solution (pH 11), the proton at N_1 is abstracted[38]

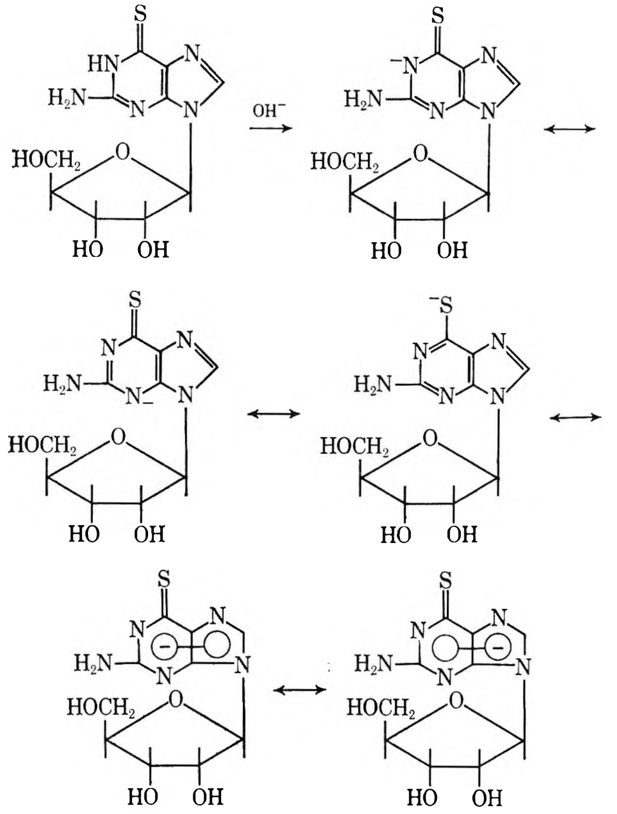

The delocalization of the extra electron around the purine ring will decrease the electron affinity and thus will shift the charge transfer absorption band to the shorter wavelength. While the ground state is less stabilized than the excited state by increasing the energy of the charge transfer configuration, the B_{2u} absorption band will have a bathochromic shift.

In the basic solution, the λ_{max} (312 mμ) of the charge transfer band of 2-amino-6-*sec*-butylthio-9-β-D-ribofuranosylpurine does not change, while in the acidic solution, this band is shifted to the longer wave length. The following equilibrium could occur.[39]

The protonation on the purine ring increases its electron affinity and thus causes the bathochromic shift of the charge-transfer band (320 mμ). For certain cases, steric effects have been adjudged[19] important but that does not explain the differences in intensities observed in Figure 2. Comparing the sulfur compounds in Table I, we can see a sharp decrease in intensity from $\epsilon \sim 2.0 \times 10^3$ of 6-thio to ϵ 9×10^3 of 6-isobutylthio. The steric effect probably disturbs somehow the $3p_z$ atomic orbital of sulfur thus becoming the most important cause of the decrease in intensity.

The absorption spectra, optical rotatory dispersion and the circular dichroism curves of compound 4-thio-

---

[37] (a) H. H. Jaffe, *J. Chem. Educ.*, **33**, 25 (1956); (b) H. C. Longuet-Higgins, *Trans. Faraday Soc.*, **45**, 173 (1949); (c) W. C. Price and A. D. Walsh, *Proc. Roy. Soc.*, **A179**, 201 (1941).

[38] B. Pullman and A. Pullman, "Quantum Biochemistry," Interscience, New York, N. Y., 1963.

[39] H. Morita and S. Nagakura, *Theoret. Chim. Acta*, **11**, 279, 1968.

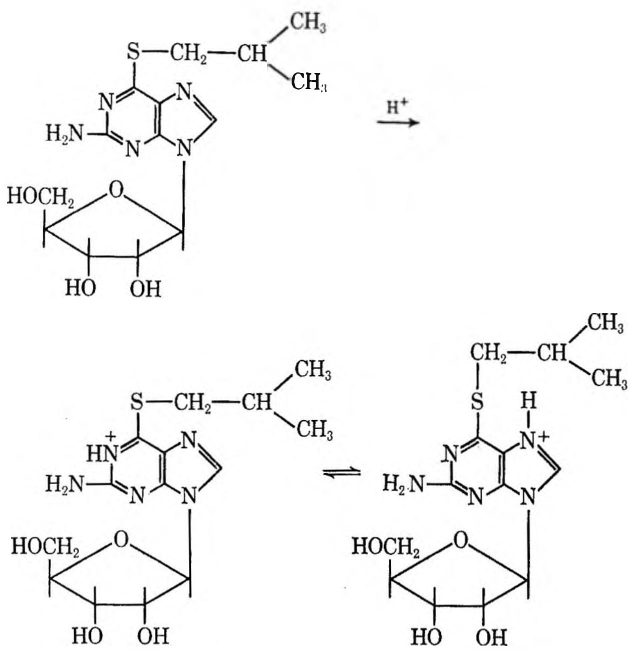

uridine are shown in Figure 6. The cotton effect appearing at 332, 291, 270, and 233 mμ are believed to correspond to the charge transfer, n → π*, B_{2u}, and B_{1u} transitions respectively. In basic solution, the existence of the following equilibria delocalizes the electron in the pyrimidine nucleus. Thus the blue shift of the charge transfer band (315 mμ) and the red shift of the B_{2u} band (279 mμ) occur as is to be expected.

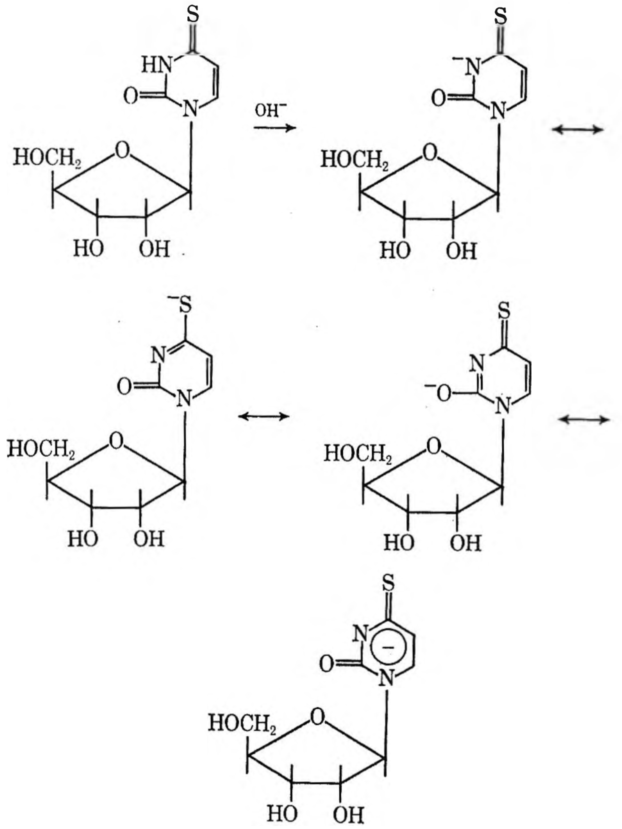

It has been proved that hypoxanthine is essentially in the lactam form.[38,39] In principle, two tautomers could exist in 6-thioinosine (III). The absorption spectrum of 6-thioinosine appears at 314 mμ and 230 mμ respectively, while the corresponding bands of 1-methyl-6-thioinosine (VI) appear at 315 mμ and 228 mμ. The analogies in the uv spectra suggest that in aqueous solution and at room temperature, 6-thioinosine is predominately in the 6-thione form.[40,41]

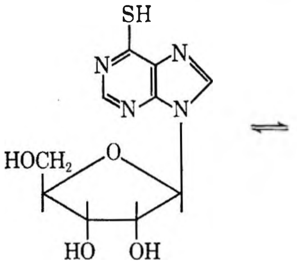

(III) Thiol

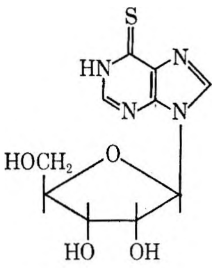

Thione

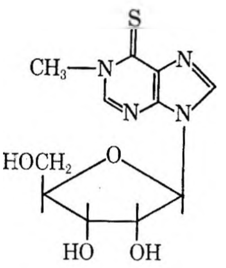

(IV)

The intensity changes and the polarization directions of the B_{2u} benzene bands on substitution has been given by Sklar,[42] Forster,[43] and Platt.[44] The induced intensity in the transition will be proportional to the square of the vector sum of the individual spectroscopic moments of the various substituents. The polarization direction also can be determined by the vector sum of the individual spectroscopic moments. On the other hand, from molecular orbital consideration, Song[45] has calculated the polarization directions of various transition of the purine and some of its derivatives. For purine and 6-purinone the B_{2u} band is polarized approximately along the line parallel to the N_1 to N_9 axis. If we also assume the same polarization direction of the B_{2u} bands for both 6-purinone and 6-purinethione ribonucleosides the absorption intensity of this transition will be proportional to the square of the vector sum of the spectroscopic moment, $\vec{m}$, of the substituent at the position 2 and the original resultant spectroscopic moment $\vec{M}$.

---

[40] R. A. Morton and A. L. Stubbs, *J. Chem. Soc.*, 1321 (1939).

[41] J. W. Ledbetter, Jr., *J. Phys. Chem.*, **72**, 4111 (1968).

[42] A. L. Sklar, *J. Chem. Phys.*, **10**, 135 (1942); *Rev. Modern Phys.*, **14**, 232 (1942).

[43] Th. Forster, *Z. Naturforsch.*, **2a**, 149 (1947).

[44] J. R. Platt, *J. Chem. Phys.*, **17**, 484 (1949); *J. Chem. Phys.*, **19**, 263 (1951).

[45] P. S. Song, *Intern. J. Quantum Chem.*, **II**, 281 (1968).

$$I = k(\vec{m} + \vec{M})^2 + I_0$$
$$= km^2\left(1 + 2\left(\frac{M}{m}\right)\cos\theta + \left(\frac{M}{m}\right)^2\right) + I_0 \qquad (9)$$

I is the absorption intensity of the substituted compound; θ is the angle between $\vec{m}$ and $\vec{M}$. For the case when $|\vec{m}| > |\vec{M}|$, I is proportional to m^2. Figure 2 shows a straight line for the two series of both 6-one and 6-thione purine ribonucleosides. The same plot is shown for the charge transfer band of purine-6-thione ribonucleoside derivatives. The intensity of the charge transfer band is seen to be more sensitive toward the substituents. The spectroscopic moment of the substituents are obtained from Petruska for benzene,[46] while that of ketone ($m = 51$) is taken by fitting it to the experimental intensity data.

Acknowledgments. The authors are grateful to Dr. Dennis J. Caldwell, Dr. Morris J. Robins and Professor Pete D. Gardner for helpful discussions. This investigation has been supported by the National Institutes of Health Grant GM 12862-02; National Science Foundation Grant GP 6496; Army Ordinance Contract DA-31-124-G618; and the National Cancer Institute of the National Institutes of Health, CA-08109-04, U. S. Public Health Service.

---

(46) J. Petruska, *J. Chem. Phys.*, **34**, 1120 (1961).

Conformational Rigidity of the Amide Bond. A Variable-Temperature Nuclear Magnetic Resonance Study of the System Ag^+–N,N-Dimethylacetamide

by P. A. Temussi, T. Tancredi, and F. Quadrifoglio

Istituto Chimico dell'Università di Napoli, Naples, Italy *(Received May 6, 1969)*

Nmr variable-temperature studies of the internal rotation of N,N-dimethylacetamide-d_3 in water and of its complex with $AgNO_3$ in water by high resolution nmr spectroscopy gave, respectively, the activation parameters $E_a = 21.0$ kcal/mol, $\log A = 13.6$, $\Delta G^{\ddagger} = 19.3$ kcal/mol, and $E_a = 19.0$ kcal/mol, $\log A = 13.9$, $\Delta G^{\ddagger} = 17.9$ kcal/mol. These results are discussed in terms of different possible structures of the complex. The data for dimethylacetamide in water are also discussed with respect to recent literature data for organic media.

Introduction

Complexes formed by simple amides and inorganic cations have been studied by means of various physicochemical techniques.[1-6] Many of these studies have been undertaken with the aim of understanding the influence of salts on conformational transitions of polyaminoacids. A direct interaction of lithium salts with the polymer amide groups has been invoked, for instance, to explain the helix–coil transition of poly-L-alanine and poly-L-methionine induced by various lithium salts.[7] Although considerable evidence has been collected pointing to complexation of cations at the oxygen of amides in the solid state,[1,5] it can not be excluded that complexes with cations linked to nitrogen may be of some importance in solution, at least as transition states. Complexation at the nitrogen can greatly influence the rigidity of the amide N–C bond, reducing the barrier to rotation. As reported previously,[8] there are indications that at least small amounts of a complex of Ag^+ linked to the nitrogen of N,N-dimethylacetamide (DMA) actually exist in aqueous solutions of the system $AgNO_3$–DMA.

Here we report a complete line shape analysis of the nmr spectra (at various temperatures) of the system $AgNO_3$–DMA in aqueous solution which gives the activation parameters connected with rotation around the N–C bond of the amide. For sake of comparison, the isomerization of pure DMA in water has been also studied.

---

(1) W. E. Bull, S. K. Madan, and J. E. Willis, *Inorg. Chem.*, **2**, 303 (1963).

(2) A. Fratiello and D. P. Miller, *Mol. Phys.*, **11**, 37 (1966).

(3) A. Fratiello, D. P. Miller, and R. Schuster, *ibid.*, **12**, 111 (1967).

(4) J. Bello and H. R. Bello, *Nature*, **190**, 440 (1961).

(5) J. Bello and H. R. Bello, *ibid.*, **194**, 681 (1962).

(6) P. D. Crispin and R. L. Werner, *Aust. J. Chem.*, **20**, 2589 (1967).

(7) J. S. Franzen, C. Bobik, and J. B. Harry, *Biopolymers*, **4**, 637 (1966).

(8) P. A. Temussi and F. Quadrifoglio, *Chem. Commun.*, 844 (1968).

Experimental Section

Materials. $AgNO_3$ (reagent grade) was purchased from C. Erba and used without further purification. DMA was purchased from C. Erba and distilled under N_2 before use. $(CH_3)_2N(C{=}O)CD_3$ (DMA-d_3) was prepared by reacting acetyl chloride-d_3 and dimethylamine.[9] The obtained DMA-d_3 was purified by filtration through a basic alumina column. The solutions of the system $AgNO_3$–DMA–D_2O were 4.36 *M* in $AgNO_3$ and 1.07 *M* in DMA. The solutions of the system $AgNO_3$–DMA-d_3–D_2O were 4.36 *M* in $AgNO_3$ and 1.04 *M* in DMA-d_3. The solutions of the system DMA-d_3–D_2O were 1.04 *M* in DMA-d_3. D_2O was employed instead of H_2O only to avoid strong side bands of the solvent.

Apparatus and Procedures. The high-resolution nmr spectra were recorded on a Varian A-60-A spectrometer equipped with a V-6040 variable-temperature accessory. Temperatures were determined using methanol and ethylene glycol samples. Temperature readings were taken before and after each run. The samples were allowed at least 10 min to attain thermal equilibrium before spectra were recorded.

Nmr Results

As mentioned above, evidence has been given[8] of the existence of an Ag^+–DMA complex both in a solution of DMA itself and in aqueous solution. The spectral changes observed at probe temperature[8] (*ca.* 40°) are consistent with the presence of varying amounts (for increasing Ag^+ concentrations) of two types of DMA molecules, bulk and complexed, in rapid equilibrium, characterized by different N–CH_3 doublet separations. The variable temperature study reported in the present paper has been restricted to aqueous solutions with a ratio of Ag^+ to DMA concentrations equal to *ca.* 4.1.

The N–CH_3 resonance is temperature dependent and can be used to extract exchange rates at different temperatures. It has been amply demonstrated[9,10] that the only method capable of furnishing reliable exchange rates from steady-state, high-resolution nmr spectra is the one based on complete line-shape analysis of the spectra. In the case of DMA, a calculation of the N–CH_3 resonance without any simplifying approximation amounts to the treatment of an eight-site problem, that is if one wants to take explicitly into account the coupling between the C–CH_3 and each of the N–CH_3 groups. Such a calculation, although not difficult to program on a digital computer, is certainly rather time consuming. This is why all couplings have generally been neglected in calculating the exchange rates of most amides. However, as shown by a recent paper,[11] the influence on the activation parameters of altogether neglecting these couplings can be quite large. In a preliminary study we have tried to take into account the effect of couplings with the C–CH_3 group of DMA in an empirical way, by assuming fictitious $T_2°$ values for the two N–CH_3 lines. For each calculation, the line width in absence of exchange ($1/T_2°$) was first taken equal to the apparent line width of the envelope of the quartet at the lowest studied temperature (*i.e.*, ignoring that this line width depends mostly on the coupling constant $J_{\mathrm{N-CH_3,C-CH_3}}$) and it was subsequently allowed to vary by small amounts in order to optimize the fit between calculated and experimental resonance lines. The spectra were calculated by using the GMS formulation,[12] with individual relaxation times for each of the two resonances of the N–CH_3 groups. Comparison with digitized experimental spectra was performed with the aid of an IBM 1620 computer, as described in previous papers.[13,14]

The calculated exchange rates are reported in Table I, along with the corresponding $\Delta G^{\ddagger}$'s calculated by means of the Eyring formulation. The $\Delta G^{\ddagger}$'s calculated from points of the straight line determined by least-squares treatment of the Arrhenius equation (Figure 1) are also given for comparison. A 10% confidence limit was taken for the exchange rates on the basis of previous experience.[14] An accuracy of ±2°K was assumed for all temperatures. All the activation parameters derivable from the Arrhenius plot are reported in Table II. The unusually high value of $\Delta S^{\ddagger}$, if real, would point to a mechanism of isomerization qualitatively different from that of the pure amide either in organic solutions[9] or in aqueous solution (*vide*

Table I: Temperature Dependence of the Isomerization Rate of Ag^+–DMA[a]

T, °K	*K*, sec^{-1}	$\Delta G^{\ddagger}_{\mathrm{sl}}$, kcal/mol	$\Delta G^{\ddagger}_{\mathrm{exptl}}$, kcal/mol
310	1.0	18.2 ± 0.5	18.2 ± 0.5
315	1.8	18.1 ± 0.5	18.1 ± 0.5
326	6.0	17.9 ± 0.5	17.9 ± 0.5
333	17.0	17.8 ± 0.5	17.7 ± 0.5
338	18.0	17.7 ± 0.5	17.9 ± 0.5
349	80.0	17.4 ± 0.6	17.5 ± 0.6
371	1000.0	17.0 ± 0.6	16.8 ± 0.6
383	2000.0	16.7 ± 0.6	16.8 ± 0.6

[a] Data include corresponding free energies of activation determined by complete line-shape analysis. $\Delta G^{\ddagger}_{\mathrm{sl}}$'s are calculated from points of the Arrhenius straight line; $\Delta G^{\ddagger}_{\mathrm{exptl}}$ values are calculated from experimental rates at the same temperature.

---

[9] R. C. Neuman, Jr., and V. Jonas, *J. Amer. Chem. Soc.*, **90**, 1970 (1968).

[10] A. Allerhand, H. S. Gutowsky, J. Jonas, and R. A. Meinzer, *J. Amer. Chem. Soc.*, **88**, 3185 (1966).

[11] A. Pines and M. Rabinovitz, *Tetrahedron Letters*, 3529 (1968).

[12] G. S. Johnson, Jr., in "Advances in Magnetic Resonance," J. S. Waugh, Ed., Academic Press, New York, N. Y., 1965, pp 33–101.

[13] J. Jonas, A. Allerhand, and H. S. Gutowsky, *J. Chem. Phys.*, **42**, 3396 (1965).

[14] P. A. Temussi and T. Tancredi, *J. Phys. Chem.*, **72**, 3581 (1968).

Table II: Activation Parameters[a]

T_c, °K	A, sec^{-1}	E_a, kcal/mol	$\Delta H^{\ddagger}$, kcal/mol	$\Delta G^{\ddagger}$, kcal/mol	$\Delta S^{\ddagger}$, eu
338	5×10^{17}	25.2 ± 0.5	24.6 ± 0.5	17.7 ± 0.5	+20.4

[a] Determined from the temperature dependence of isomerization rate of Ag^+–DMA.

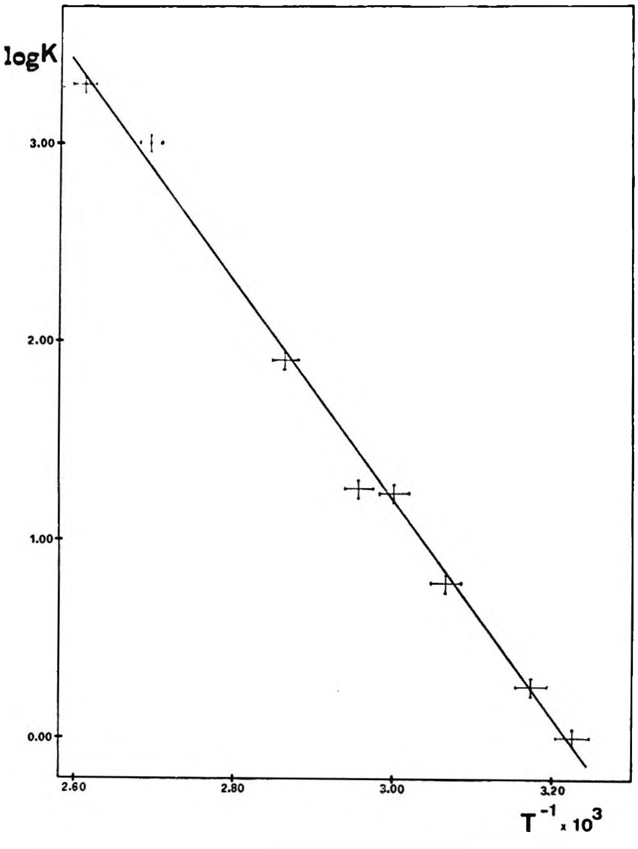

Figure 1. An Arrhenius plot of the isomerization rate of Ag^+–DMA as obtained from an nmr complete line-shape analysis.

infra). The documented[15] influence of incorrect $T_2°$ values on the activation parameters led us to suspect the $\Delta S^{\ddagger}$ value rather to be an artifact, due to the empirical way of accounting for long range couplings. This was actually shown to be the case by the study of the system $AgNO_3$–$(CH_3)_2N(C{=}O)CD_3$ in which the influence of long range couplings is almost negligible. In Figure 2 and Figure 3, the spectra of DMA, DMA-d_3, Ag^+–DMA and Ag^+DMA-d_3 are shown for comparison. The exchange rates for the system Ag^+DMA-d_3 are reported in Table III; the Arrhenius plot and the activation parameters are reported respectively in Figure 4 and Table IV. Since no detailed variable temperature nmr study of DMA itself in aqueous solution existed in the literature, the system DMA-d_3 in water was also studied in order to be able to judge the relative influence of Ag^+ on the rigidity of the N–C bond.

The relevant data of the chemical exchange study of DMA-d_3 are reported in Tables III and IV and in Figure 4. It must be noted that the somewhat high values of the standard errors in all activation parameters reported in this paper are attributable to the limited number of experimental points. Nevertheless, the uncertainties in the quoted parameters are not so high as to prevent a useful comparison between DMA and the complex Ag^+–DMA.

Table III: Temperature Dependence of the Isomerization Rate of Ag^+–DMA-d_3 and of DMA-d_3[a]

T, °K	K, sec^{-1}	$\Delta G^{\ddagger}_{sl}$, kcal/mol	$\Delta G^{\ddagger}_{exptl}$, kcal/mol
		Ag^+–DMA-d_3	
323	5.0	17.9 ± 0.7	17.9 ± 0.7
328	8.0	17.9 ± 0.7	17.9 ± 0.7
331	10.0	17.9 ± 0.7	17.9 ± 0.7
337	18.0	17.9 ± 0.7	17.9 ± 0.7
343	29.0	17.9 ± 0.7	17.9 ± 0.7
349	45.0	17.9 ± 0.8	17.9 ± 0.8
354	70.0	17.9 ± 0.8	17.8 ± 0.8
360	100.0	17.8 ± 0.8	17.9 ± 0.8
366	170.0	17.8 ± 0.8	17.8 ± 0.8
		DMA-d_3	
345	4.0	19.4 ± 0.9	19.3 ± 0.9
350	6.0	19.3 ± 0.9	19.4 ± 0.9
355	9.0	19.3 ± 0.9	19.4 ± 0.9
361	14.0	19.3 ± 0.9	19.4 ± 0.9
362	18.0	19.3 ± 0.9	19.2 ± 0.9
366	23.0	19.3 ± 0.9	19.3 ± 0.9
372	30.3	19.3 ± 1.0	19.4 ± 1.0
378	54.5	19.3 ± 1.0	19.3 ± 1.0
382	85.0	19.3 ± 1.0	19.2 ± 1.0
383	78.0	19.3 ± 1.0	19.3 ± 1.0

[a] Includes corresponding free energies of activation, determined by complete line-shape analysis. $\Delta G^{\ddagger}_{sl}$'s are calculated from points of the Arrhenius straight line; $\Delta G^{\ddagger}_{exptl}$'s are calculated from experimental rates at the same temperature.

Discussion

DMA-d_3. Before comparing the data of the pure amide and those of the complex, a few words of comment on the parameters of DMA-d_3 are in order. The electronic structure of the amide bond is generally described[16] as a resonance hybrid between the following structures

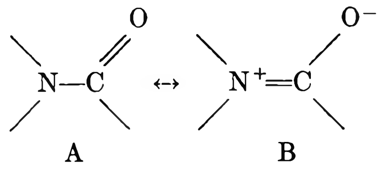

Table IV: Activation Parameters[a]

System	T_c, °K	A, sec^{-1}	E_a, kcal/mol	$\Delta H^{\ddagger}$, kcal/mol	$\Delta G^{\ddagger}$, kcal/mol	$\Delta S^{\ddagger}$, eu
Ag^+–DMA-d_3	337	4×10^{13}	19.0 ± 0.7	18.4 ± 0.7	17.9 ± 0.7	±1.4
DMA-d_3	366	8×10^{13}	21.0 ± 0.9	20.3 ± 0.9	19.3 ± 0.9	±2.7

[a] Data determined from the temperature dependence of isomerization rate of Ag^+–DMA-d_3 and of DMA-d_3.

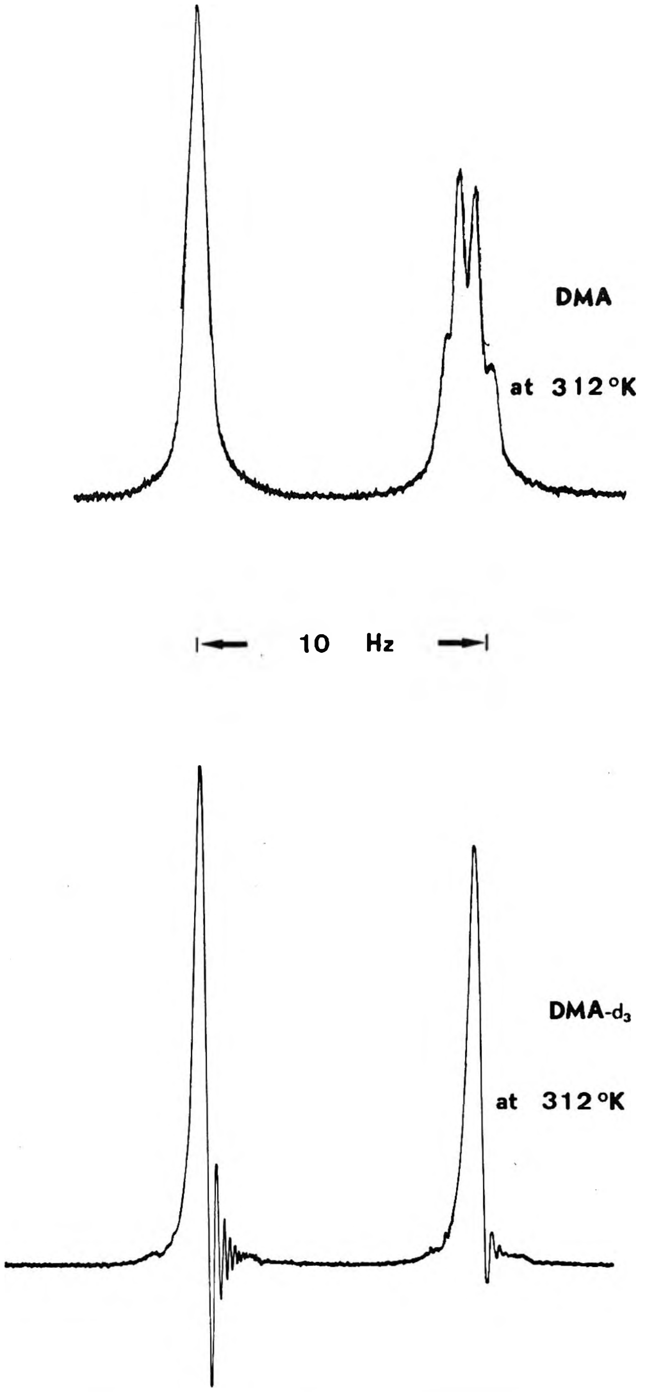

Figure 2. The experimentally observed N–CH_3 resonance signals for solutions of DMA and of DMA-d_3 in D_2O.

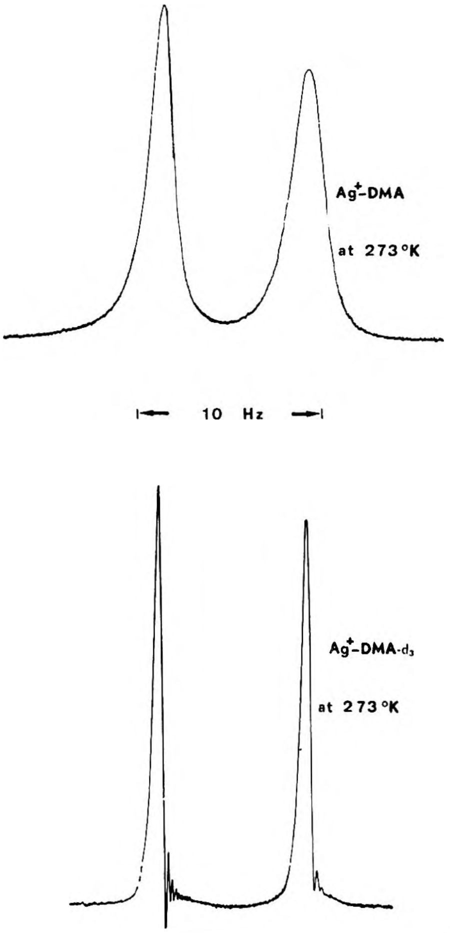

Figure 3. The experimentally observed N–CH_3 resonance signals for solutions of Ag^+–DMA and of Ag^+–DMA-d_3 in D_2O.

In other words a partial delocalization of the C=O double bond on the N–C bond is assumed to be the main cause of the rigidity of the amide bond. The relative importance of B should increase when the amide is dissolved in highly polar liquids. The nmr spectral changes in going from organic to aqueous solutions of amides (compare, for instance, Figure 2 of this paper and Figure 1 of ref 9) are accordingly interpreted as an indication of a pronounced increase of the polar character of the amide bond in water. An enhanced conformational rigidity has been generally associated to this increase in polarization. A comparison (Table V) of the activation parameters of DMA-d_3 in water with those of neat DMA-d_3 and in dimethyl sulfoxide

---

(15) Z. M. Holubec and J. Jonas, *J. Amer. Chem. Soc.*, **90**, 5986 (1968).

(16) L. Pauling, "The Nature of the Chemical Bond," Cornell University Press, Ithaca, N. Y., 1960.

Table V: Comparison of Activation Parameters of Various Solutions of DMA-d_3

Solvent	A, sec^{-1}	E_a, kcal/mol	$\Delta H^\ddagger$, kcal/mol	$\Delta G^\ddagger$, kcal/mol	$\Delta S^\ddagger$, eu	Ref
DMA-d_3	6×10^{13}	19.6	19.0	18.2	+2.7	9
DMSO-d_6	2×10^{14}	20.6	20.0	18.6	+4.7	9
D_2O	8×10^{13}	21.0	20.3	19.3	+2.7	This work

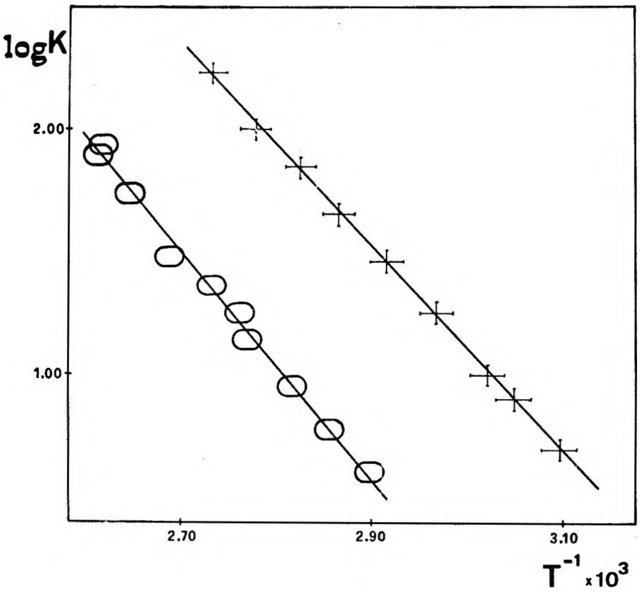

Figure 4. Arrhenius plots of the isomerization rate of Ag$^+$-DMA-d_3 and of DMA-d_3 as obtained from an nmr complete line-shape analysis: +, Ag$^+$-DMA-d_3; ○, DMA-d_3.

(DMSO) shows that the increase of rigidity of the amide bond is not very high.

By this we do not imply that DMA is not more polarized in water than in DMSO or in DMA itself. The increase in the long range coupling constants between each of the N-CH$_3$ groups and the C-CH$_3$ group clearly speaks in favor of an increased double bond character of the N-C bond. It should be concluded that the increase in double bond character is not paralleled by a large increase in the energy difference between the ground state form (the resonance hybrid) and the transition form (very likely structure A). A similar behavior has been recently observed[14] also in methyl nitrite whose activation barrier seems to be almost insensitive to the value of dielectric constant of the medium.

Ag$^+$-DMA-d_3. All relevant activation parameters of the amide are lowered[17] by the presence of silver ions, as shown in Table IV. The differences between corresponding activation parameters, being almost comparable with the errors, can not be discussed in any quantitative fashion. However they certainly indicate a reduced rigidity of the amide bond which can eventually be interpreted in terms of different possible complexes. Infrared evidence[1] points to complexation of the cation at the oxygen for many complexes of DMA (including that formed by Ag$^+$) in the solid state. A complex of formula

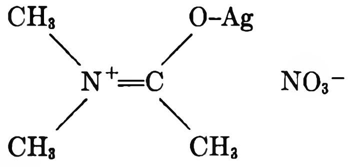

I

does not account for the lowering of the barrier. Only complexation of the nitrogen[18] or binding of the anion[18]

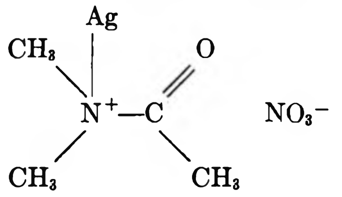

II

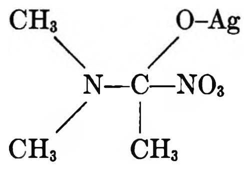

III

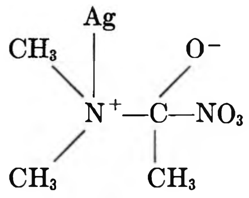

IV

can account for the observed lowering of E_a, $\Delta H^\ddagger$ and $\Delta G^\ddagger$. It has been shown[8] that by increasing the ratio Ag$^+$/DMA, the separation of the N-CH$_3$ doublet is reduced but the chemical exchange rate remains essentially unaltered. That is, increased amounts of Ag$^+$-DMA at 40° do not alter appreciably the rigidity of the amide bond. On the other hand, the temperature dependence of the spectra is greatly affected by relatively small amounts of Ag$^+$. Such a behavior can be interpreted, in our opinion, by means of mechanism similar to that suggested by Berger, *et al.*,[19] to explain the hydrogen catalyzed lowering of the barrier of DMA. The most important equilibrium in solution should be

---

[17] The lowering of $\Delta G^\ddagger$ is not so marked as reported in ref 8. The discrepancy is due to the fact that in the quoted paper the $\Delta G^\ddagger$'s had only been estimated on the basis of coalescence temperatures. This once again emphasizes the need of using complete line-shape analysis in extracting exchange rates from steady-state, high-resolution nmr spectra.

[18] See W. E. Stewart, Ph.D. Thesis, Florida State University, 1966.

[19] A. Berger, A. Loewenstein, and S. Meiboom, *J. Amer. Chem. Soc.*, 81, 62 (1959).

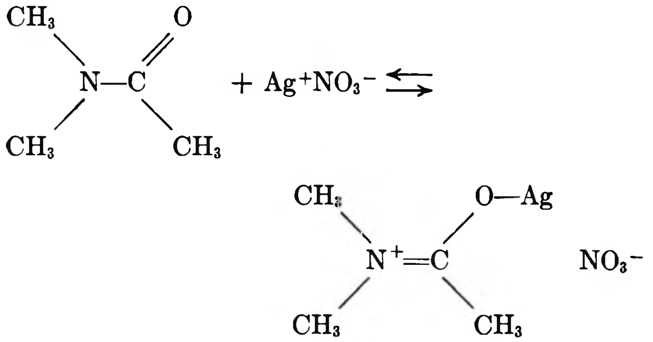

Only small amounts of either II, III, or IV are present at any temperature but can act as transition forms in the isomerization

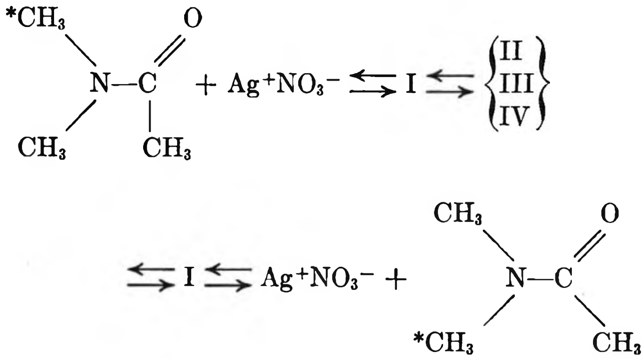

Acknowledgment. It is a pleasure to acknowledge the skillful help of Mrs. A. Hermann.

The Thermodynamic Properties of Carbon Tetrafluoride from 12°K to Its Boiling Point. The Significance of the Parameter ν

by John H. Smith[1] and E. L. Pace

Department of Chemistry, Case Western Reserve University, Cleveland, Ohio *(Received May 7, 1969)*

Low-temperature heat capacity data for carbon tetrafluoride of 99.985 mol % purity in the temperature range from 12 to 145.12°K are presented. Values were also derived experimentally for the entropies and temperatures of the solid transition, fusion, and vaporization (1 atm) as follows: $\Delta S_{tr} = 5.387$ cal/(mol °K), $T_{tr} = 76.23$°K; $\Delta S_f = 1.901$ cal/(mol °K), $T_f = 89.56$°K; $\Delta S_v = 19.457$ cal/(mol °K), $T_v = 145.12$°K. The calorimetric entropy for carbon tetrafluoride is found to be 54.04 ± 0.13 cal/(mol °K), a value in excellent agreement with the statistical value of 54.037 cal/(mol °K). The results are discussed in terms of the theory of Pople and Karasz. The parameter ν is calculated for carbon tetrafluoride and used to account for the temperatures, entropies, and volume increments for the fusion and transition anomalies.

Introduction

Carbon tetrafluoride in the solid form is commonly classified[2] as a plastic crystal which undergoes an orientationally disordering transition below the melting point due to a globular or spherically symmetric shape of its molecular envelope.

Previous low-temperature heat capacity data are given by Eucken, *et al.*,[3] and Kostryukov, *et al.*[4] In the former work an entropy discrepancy of 0.38 cal/(mol °K) between the calorimetric and spectroscopic entropy is in evidence at 298°K. This discrepancy is caused to a large extent by use of an incorrect value of the moment of inertia of the molecule. The latter work presents heat capacity data from 12°K to the melting point and offers no comparison between the statistical and calorimetric entropy involved. The purity of the samples used was in one case not stated and in the other slightly over 99%. Therefore, the present investigation was undertaken in part to obtain reasonably definitive thermodynamic data on this classic compound.

A possible interpretation of the transition and fusion anomalies in carbon tetrafluoride is offered by a theory due to Pople and Karasz[5] as an extension of the original works of Lennard-Jones and Devonshire.[6,7] This

---

(1) Department of Chemistry, Butler University, Indianapolis, Ind.

(2) J. Timmermans, *J. Phys. Chem. Solids*, **18**, 1 (1961).

(3) A. Eucken and E. Schroeder, *Z. Phys. Chem.*, **B41**, 307 (1938).

(4) U. N. Kostryukov, O. P. Samorukov, and P. G. Strelkov, *Zh. Fiz. Khim.*, **32**, 1354 (1958).

(5) (a) J. A. Pople and F. E. Karasz, *J. Phys. Chem. Solids*, **18**, 28 (1961); (b) *ibid.*, **20**, 294 (1961).

(6) J. E. Lennard-Jones and A. F. Devonshire, *Proc. Roy. Soc.*, **A169**, 317 (1939).

(7) J. E. Lennard-Jones and A. F. Devonshire, *ibid.*, **A170**, 464 (1939).

theory predicts both the appearance of a first-order transition in the solid-state heat capacity on the loss of orientational order and, at higher temperatures, a fusion anomaly, which marks the loss of positional order in the crystal lattice. The parameter ν, which gives the relative tendency for this loss of orientational and positional order, may be calculated from the potential barriers hindering the respective disordering processes.

Experimental Section

The Sample. The sample of carbon tetrafluoride, purchased from E. I. DuPont de Nemours Co., contained approximately 2% of nitrogen impurity and required purification by low-temperature distillation. A Podbielniak Series 8700 distillation apparatus was used for this operation and the resultant purity was determined by gas chromatographic analysis[8] utilizing a Burrel Kromo-Tog Model KD gas chromatograph. The impurity as determined in this manner was approximately 0.03 mol %. A calorimetric triple-point study was then carried out on the sample, the results of which are given in Table I.

Table I: Triple-Point Equilibrium Temperatures *vs.* Reciprocal of Fraction Melted, r

Temp, °K	$1/r$
88.866	11.21
89.499	4.94
89.521	2.78
89.531	1.93
89.538	1.40
89.548	1.05
89.56[a]	1.00

[a] Extrapolated.

The liquid-soluble, solid-insoluble impurity was estimated to be 0.015 mol % and the triple-point temperature was 89.56°K. This may be compared with previous values of 88.44°K[4] and 89.47°K.[3]

Procedure. A quantity of 1.0092 mol of purified CF_4 was condensed into the previously described adiabatic calorimeter[9] and thermal measurements were taken in the usual manner[10-12] from 12.88°K to the normal boiling point of 145.12°K. The saturated molar heat capacity is presented in Table II at the experimental temperatures and in Table III at rounded temperatures. Saturation corrections were determined for these data by utilizing the density relationship

$$d = 2.39 - 0.00538T \text{ g/cc} \qquad (1)$$

obtained from various literature values[13-16] and the vapor pressure relationship

$$\ln P(\text{mm}) = 28.519868 - \frac{1752.3637}{T} - 1.9705635 \ln T \qquad (2)$$

obtained experimentally in a manner previously described.[10,11] The values of the vapor pressure calculated with this equation are presented in Table IV for comparison with the values obtained experimentally at various temperatures.

Table II: Experimental Values of the Saturated Molar Heat Capacity of Carbon Tetrafluoride

Series	Temp, °K	C_s, cal/(mol °K)	Series	Temp, °K	C_s, cal/ (mol °K)
H II	12.88	1.951	N II	74.77	23.75
H I	14.62	2.694		Transition	
H II	15.07	2.867	N IV	79.96	15.93
H I	17.04	3.703	N III	81.33	16.08
H II	17.43	3.860	N IV	81.41	16.07
H II	19.79	4.820	N III	82.42	16.10
H I	20.27	4.999	N IV	83.93	16.26
H II	22.31	5.760	N III	85.09	16.26
H I	23.11	6.035	N IV	87.32	16.35
H II	25.75	6.919		Fusion	
H I	26.24	7.078	L II	91.99	18.61
H I	29.98	8.147	L I	94.44	18.66
H II	30.05	8.149	L II	96.26	18.52
H I	33.99	9.176	L I	97.29	18.52
H II	34.64	9.244	L II	100.88	18.46
H I	38.22	9.980	L I	102.00	18.46
H II	39.27	10.17	L II	104.92	18.49
H I	42.81	10.81	L I	107.11	18.43
H II	43.97	11.00	L II	109.53	18.43
H II	48.22	11.73	L I	112.30	18.42
H II	52.10	12.35	L II	114.39	18.42
N I	53.19	12.37	L I	117.41	18.44
N II	55.09	12.81	L II	119.47	18.48
H II	55.89	12.97	L I	122.44	18.50
N II	56.79	13.12	L II	124.63	18.55
N I	60.56	13.90	L I	127.41	18.58
N II	61.80	14.10	L II	129.71	18.62
N I	65.03	15.12	L I	132.44	18.69
N II	66.58	15.46	L II	134.86	18.75
N I	69.34	16.44	L I	137.55	18.79
N II	71.09	17.26	L II	139.94	18.93
N I	73.22	18.78			

A solid-solid orientationally disordering transition of the carbon tetrafluoride was encountered over the temperature range of 45 to 76.23°K and the enthalpy change for this transformation determined by incremental and continuous heating periods. The experimental enthalpy values and the fraction of carbon tetra-

---

(8) R. H. Campbell and B. J. Gudzinowicz, *Anal. Chem.*, **33**, 842 (1961).

(9) E. L. Pace, L. Pierce, and K. S. Dennis, *Rev. Sci. Instrum.*, **26**, 20 (1955).

(10) L. Pierce and E. L. Pace, *J. Chem. Phys.*, **22**, 1271 (1954).

(11) E. L. Pace and R. V. Petrella, *ibid.*, **36**, 2991 (1962).

(12) E. L. Pace and B. F. Turnbull, *ibid.*, **43**, 1953 (1965).

(13) O. Ruff, *Z. Anorg. Allg. Chem.*, **210**, 173 (1933).

(14) W. Klemm and P. Henkel, *ibid.*, **207**, 73 (1932).

(15) O. Ruff, *ibid.*, **201**, 255 (1931).

(16) Bulletin X-19 (1961) Freon Products Division, E. I. DuPont de Nemours, Inc., Wilmington, Del.

Table III: Smoothed Saturated Molar Heat Capacity of Carbon Tetrafluoride at Rounded Temperatures

Temp, °K	C_s, cal/(mol °K)
13	2.003
15	2.845
17	3.683
20	4.899
25	6.677
30	8.137
35	9.327
40	10.31
45	11.17 (11.15)[a]
50	12.02 (11.87)[a]
55	12.79 (12.51)[a]
60	13.74 (13.11)[a]
65	14.92 (13.66)[a]
70	16.73 (14.19)[a]
75	28.00 (14.69)[a]
Transition	
80	15.92
83	16.21
86	16.32
88	16.41
Fusion	
91	18.63
95	18.55
100	18.42
105	18.45
110	18.44
115	18.45
120	18.49
125	18.57
130	18.67
135	18.80
140	18.96
145	19.14

[a] Pretransition extrapolated heat capacity.

Table IV: Vapor Pressure of Carbon Tetrafluoride (Pressures in mm)

Temp, °K	P_{obsd}	P_{calcd}[a]	$P_{calcd} - P_{obsd}$
115.225	52.34	52.34	0.0
118.327	74.86	74.00	−0.86
121.928	107.62	108.03	0.41
125.012	146.27	146.60	0.33
128.347	200.27	200.35	0.08
131.685	269.11	269.23	0.12
135.245	362.73	362.59	−0.14
138.781	479.21	479.40	0.19
142.113	615.86	615.12	−0.74
143.215	665.81	666.13	0.32
145.714	793.97	794.12	0.15

[a] Calculated by eq 2.

Table V: Various Heats of Transition of Carbon Tetrafluoride

Determination	Enthalpy of solid transition cal/mol	(T_1, T_2), °K	Lattice enthalpy, cal/1.00915 mol	Pretransition enthalpy, cal/1.00915 mol
1	408.69[a]	(64.338, 82.691)	414.97	7.47
2	407.57[a]	(60.404, 77.768)	371.02	4.03
3	408.75[b]	(52.111, 78.304)	533.96	.76
4	408.93[b]	(58.223, 80.015)	467.00	2.74
Av	408.5			
T_{tr}	87.23°K			

	Enthalpy of fusion, cal/mol	(T_1,T_2), °K	Lattice enthalpy, cal/1.00915 mol
1	170.61	(83.926, 96.588)	345.18
2	169.45	(79.171, 90.715)	296.28
3	170.62	(79.364, 92.464)	340.47
Av	170.2		
T_f	89.56°K		

	Enthalpy of vaporization, cal/mol	Temp of vaporization, °K
1	2822.7	145.039
2	2824.0	145.615
3	2825.1	145.346
4	2822.7	145.840
Av	2823.6	
T_v	145.12°K(1 atm)	

[a] Continuous heating. [b] Incremental heating.

Table VI: Equilibrium Temperatures of the Transition of 1.0092 Mol of Carbon Tetrafluoride

Temp, °K	% transformed
61.80	1.69
66.58	3.51
71.09	6.76
74.77	13.36
76.22	35.67
76.23	62.52
76.23	80.40
76.27	100.00

fluoride transformed as a function of temperature are given in Tables V and VI, respectively. The average molar heat of transition was 408.5 cal/mol with a mean absolute deviation of 0.5 cal/mol. The pretransition enthalpy was encountered prior to the particular determination and is added to the experimental enthalpy value.

The heat of fusion of carbon tetrafluoride was determined from three separate measurements, the results of which are given in Table V. The average molar heat of fusion was 170.2 cal/mol at the triple point of 98.56°K with a mean absolute deviation of 0.5 cal/mol.

Heat of vaporization measurements on the carbon tetrafluoride are reported in Table V. The average of four determinations yields a value of 2823.6 cal/mol for the heat of vaporization of carbon tetrafluoride, corrected to the normal boiling point of 145.12°K by the Kirchoff relation.[10]

All of the preceding data have been recorded on the basis of a molecular weight of 88.0048 g/mol of carbon tetrafluoride, 1 cal equal to 4.1840 absolute J, and 0°C defined as 273.15°K.

Entropy

Residual or zero-point entropy is of course not expected for the carbon tetrafluoride molecule and complete correspondence between the calorimetric and spectroscopic entropy at the normal boiling point verifies the reliability of the data obtained.

A summary of the calorimetric entropy contributions is given in Table VII. The entropy increment for the transition ΔS_{tr} is assumed to arise from two separate portions of the transition heat-capacity curve, the nonisothermal adiabatic section from 45 to 76.23°K and the remainder, which is considered an isothermal process, occurring at 76.23°K. The expression for the entropy of transition is therefore

Table VII: Calorimetric Entropy of Carbon Tetrafluoride

	Entropy, cal/(mol °K)
0–13°K Debye extrapolation (θ_D = 102.31, 7°F)	0.715 ± 0.05
13–76.23°K, graphical	14.840 ± 0.07
76.23°K, transition	5.39 ± 0.02
76.23–89.56°K, graphical	2.587 ± 0.09
89.56°K, fusion	1.901 ± 0.013
89.56–145.12°K, graphical	8.975 ± 0.02
145.12°K, vaporization	19.457 ± 0.017
145.12°K, gas imperfection correction	0.175 ± 0.02
Total entropy	54.04 ± 0.13

$$\Delta S_{\text{tr}} = \int_{45}^{74} \frac{\Delta C_s}{T}\,\mathrm{d}T + \frac{\Delta H_{\text{tr}} - \int_{45}^{74} \Delta C_s\,\mathrm{d}T}{T_{\text{tr}}} \qquad (3)$$

where ΔC_s is the difference between the experimental and extrapolated molar heat capacities, ΔH_{tr} is 408.48 cal/(mol °K), and T_{tr} is 76.23°K as previously noted. The extrapolated heat capacities were determined by second differences and are given in Table III. The gas imperfection correction was estimated by assuming adherence to a Berthelot equation of state using critical constant values of 227.7°K and 36.96 atm for T_c and P_c, respectively.[16]

The statistical entropy of carbon tetrafluoride at the normal boiling point and 1 atm pressure is calculated as the sum of the translational, rotational, and vibrational entropy contributions given, respectively, as[17]

$$S_t = 6.8634 \log M + 11.4390 \log T - 2.3141 \qquad (4)$$

$$S_r = 6.8634 \log T + 2.2878 \log (I_A I_B I_C \times 10^{117}) - 4.5756 \log \sigma - 0.0330 \qquad (5)$$

$$S_v = R \sum_i \left[\frac{x_i}{e^{x_i} - 1} - \ln (1 - e^{x_i})\right] \qquad (6)$$

In these relationships, M is the molecular weight of the molecule, 88.0048; T is the normal boiling point, 145.12°K; $I_A I_B I_C$ is the product of the three principal moments of inertia,[18] 3.24×10^{-114} g^3 cm^6; σ is the symmetry number of the molecule, 12; x_i are the $i = 9$ values of $1.4387\ \omega_i/T$, where the quantities ω_i are the normal vibration frequencies of the carbon tetrafluoride molecule.[19] The sum of the entropy contributions was thus computed by use of these formulas to be 54.037 cal/(mol °K) and the comparison with the calorimetric entropy of 54.04 cal/(mol °K) gives the expected confirmation of the Third Law.

Discussion

Carbon tetrafluoride is seen to undergo an orientationally disordering transition at 76.23°K and a positionally disordering fusion at 89.56°K. The behavior of such physically crystalline materials is predicted by the theory of Pople and Karasz[5] for all compounds which have a value of the parameter ν less than 0.325. This parameter indicates the relative tendency of a molecule in the solid lattice to undergo a disordering process by either of two methods: (1) a reorientation from an α_1 to an α_2 orientation, or (2) a translation from an ordered set of α lattice sites to a set of β lattice sites which interstitially interpenetrate the α set. A tendency to undergo the first type of disordering process over the second gives rise to the plastically crystalline phase in which molecular libration occurs prior to the fusion. The carbon tetrafluoride molecule may therefore be thought of as residing in two potential wells having corresponding potential barriers hindering, respectively, the molecule's libration on its lattice site and its translation to an interstitial site. The ratio of these two potential barriers may be calculated as the parameter ν and permits the calculation of the thermodynamic properties for carbon tetrafluoride.

In a previous work,[20] the barrier hindering molecular libration of the carbon tetrafluoride molecule in the solid state was estimated by assuming a hindered rotor model and a frequency of oscillation described by an Einstein function. The two sets of alternating maxima and minima given by the assumed potential function

---

(17) D. D. Wagman, J. E. Kilpatrick, W. J. Taylor, K. S. Pitzer, and F. D. Rossini, *J. Res. Nat. Bur. Stand.*, **34**, 143 (1945).

(18) E. Gelles and K. S. Pitzer, *J. Amer. Chem. Soc.*, **75**, 5259 (1953).

(19) P. W. Schatz and D. F. Hornig, *J. Chem. Phys.*, **21**, 1516 (1953).

(20) J. Smith and E. L. Pace, *J. Phys. Chem.*, in press.

$$U = \frac{1}{2} U_0 (1 - \cos n\theta) \quad (7)$$

can be identified with the two orientations α_1 and α_2. The depth of the potential well U_0 therefore represents the potential energy required for such a reorientation process and appears as the numerator of the parameter ν. The barrier height, U_0 = 5420 cal/mol, was calculated for the lowest temperatures and applies only for the intermolecular separation prevalent at T approaches 0°K; *i.e.*, it is not a function of the lattice volume.

The denominator of the parameter ν, the barrier restricting molecular translation, is defined[5a] by the quantity ZW, where Z is the number of β sites immediately surrounding any α site and W is the interaction energy experienced by two molecules on neighboring α and β sites. An approximate value of W can be determined from a knowledge of the interaction potential between two carbon tetrafluoride molecules. The most precise intermolecular potential expression for globular molecules is given in terms of the spherical shell model.[21,22] However, a Lennard-Jones 6–12 interaction potential was considered adequate for the molecular interaction for two reasons. First, it has been found[21] that a Lennard-Jones potential can be adjusted to the spherical shell potential simply by adjusting its minimum parameters of potential and intermolecular distance ϕ_0 and r_0. Second, the 6–12 potential gives an excellent fit to the second virial coefficient data over a large temperature range.[23] Assuming such a potential, therefore, the parameter ϕ_0 may be calculated from the expression[7]

$$\phi_0 = \frac{\theta_D^2 k^2 4\pi^2 r_0^2 M}{483.7h^2} \quad (8)$$

The quantity θ_D, the Debye θ of translational motion, was calculated[20] as 79.6°K and r_0, the intermolecular distance of minimum potential energy, as 5.28 Å.[23] The quantity M is the molecular weight of carbon tetrafluoride, 88.00 g/mol, and k and h are, respectively, the Boltzmann and Planck constants. The further approximation is now made[6]

$$W \cong 2\phi_0 \quad (9)$$

which gives the value of W when complete positional disorder has set in, and assumes a change of crystal structure from an ordered face-centered lattice to a disordered cubic one. The denominator for the parameter ν (using a value of Z = 6 for a face-centered lattice) is thus calculated to be 16,000 cal/mol. The consequent value of ν = 0.34 results from the ratio of these orientational and positional barriers.

The correspondence with the predictions of the Pople–Karasz theory[5b] is quite good. The theory predicts the simultaneous loss of orientational and positional order at a value of ν = 0.325. Using, therefore, the value of ν calculated above, the theoretical value of the ratio of the transition temperature to the melting temperature is approximately 1.0, and it compares favorably to the experimental value of 0.86. Thus carbon tetrafluoride is seen to possess characteristics which are partially nonplastically crystalline in nature, *i.e.*, a tendency to lose both positional and orientational order at the same temperature of 76.23°K, the temperature of transition. The Pople–Karasz theory predicts further that the isothermal entropy increment of fusion passes from a value of 2.5 cal/mol when ν is slightly less than 0.325 to over 5.0 cal/mol for ν values greater than 0.325. The experimental entropies of 1.9 and 5.1 cal/mol for the melting and solid transition are consistent with the interpretation that orientational and some positional order are simultaneously lost in the transition. This conclusion, that the transition process has taken on to some degree the characteristics of a melting process in destroying not only orientational but also positional order, is supported by nmr measurements in which a sudden narrowing of the line at a temperature of 76°K indicates that migration as well as rotation of the molecules is occurring in the transition.[24]

The change in volume for the fusion of carbon tetrafluoride is also lower than one would expect for the loss of all lattice positional order at 89.56°K. A value of $\Delta V/V^*$ = 0.022 where ΔV is the volume change and V^* is the volume of the solid before fusion, is calculated from the density of the liquid, 1.92 g/cc (eq 3) and the solid,[13] 1.96 g/cc. The expected value of $\Delta V/V^*$ = 0.090 (using ν = 0.325) is thus diminished by the loss of positional order occurring at the transition point. The transition value however, calculated as $\Delta V/V^*$ = 0.053 from literature values,[25] is enhanced, indicating again the predominant role of the solid–solid transition in the loss of both positional and orientational order in solid carbon tetrafluoride.

Acknowledgments. Acknowledgment is made to the donors of the Petroleum Research Fund, administered by The American Chemical Society, for support of this work with Grant No. 1976-A5. The authors are also indebted to Dr. B. Jepson, who assisted in taking the data.

---

(21) R. Balescu, *Physica*, **22**, 224 (1956).

(22) A. DeRocco and W. Hoover, *J. Chem. Phys.*, **36**, 916 (1962).

(23) K. MacCormack and W. Schneider, *ibid.*. **19**, 849 (1951).

(24) J. G. Aston, Q. R. Stottlemeyer, and G. R. Murray, *J. Amer. Chem. Soc.*, **82**, 1281 (1960).

(25) J. W. Stewart and R. I. LaRock, *J. Chem. Phys.*, **28**, 425 (1958).

Micellar Effects on Acidity Functions[1]

by C. A. Bunton and L. Robinson

Department of Chemistry, University of California at Santa Barbara, Santa Barbara, California 93106

(Received May 9, 1969)

An anionic detergent, sodium lauryl sulfate (NaLS), increases $-H_R$, based on the ionization of tri-*p*-anisylmethanol, by up to 2.5 units, and $-H_0'$, based on the protonation of *p*-nitroaniline or 1-amino-4-nitronaphthalene, by up to 1.0 unit. Salts decrease the micellar effect on these acidity functions in the sequence: no salt > LiCl ≈ NaBr ≈ NaCl ≫ $(CH_3)_4NCl$. Added cetyltrimethylammonium bromide (CTABr) decreases both $-H_R$ and $-H_0'$, with 10^{-3} *M* CTABr decreasing $-H_R$ by 1.4 units and 10^{-2} *M* CTABr decreasing $-H_0'$ by 0.3 unit in 0.1 *M* HCl. These results show that anionic micelles stabilize and cationic micelles destabilize a triaryl cation much more than an ammonium ion.

Introduction

Long chain molecules or ions can aggregate in water to form micelles in which the polar or ionic end is exposed to the solvent. Ionic micelles are typically surrounded by a sheath of counterions, and therefore the ability of a micelle to incorporate organic substrate and to attract or repel ionic reagents at its surface changes the probability of many ion–molecule reactions.[2-7]

The acidity at the surface of an ionic micelle should be different from that in the bulk of the solution, and it has been shown that the ionization of indicators is different in the micellar and aqueous phases,[8] and the apparent pK_a of a Schiff's base is larger in an anionic and smaller in a cationic micelle than in water, based on the measured pH in the aqueous solution.[3] However, micellar effects upon the ionization of an indicator should depend not only upon the acidity, as measured by hydrogen ion activity or pH, but also upon the activity coefficients of the indicator and its conjugate acid or base in the micellar as compared with the aqueous phase (*cf.* ref 9). We can test this possibility by examining the protonation of two different bases, *e.g.*, a primary amine and a tertiary alcohol, which have been used to establish the H_0' and the H_R scales.[10-12]

H_0'

$$\mathrm{ArNH_2 + H^+ \rightleftharpoons Ar\overset{+}{N}H_3}$$

$$H_0' = \mathrm{p}K_a - \log(C_{\mathrm{BH^+}}/C_{\mathrm{B}}) = -\log(a_{\mathrm{H^+}}f_{\mathrm{B}}/f_{\mathrm{BH^+}})$$

$$(\mathrm{B} = \mathrm{ArNH_2})$$

H_R

$$\mathrm{Ar_3COH + H^+ \rightleftharpoons Ar_3\overset{+}{C} + H_2O}$$

$$H_R = \mathrm{p}K_{\mathrm{ROH}} - \log(C_{\mathrm{R^+}}/C_{\mathrm{ROH}}) = \frac{\log a_{\mathrm{H^+}}f_{\mathrm{ROH}}}{a_{\mathrm{H_2O}}f_{\mathrm{R^+}}}$$

$$(\mathrm{ROH} = \mathrm{Ar_3COH})$$

For a given solution the hydrogen ion activity will depend upon the presence of micelles, but not upon the indicator provided that it is in very low concentration, and therefore by using different indicator systems we can find the extent to which interactions between the micelles and indicator bases and conjugate acids are important. We used tri-*p*-anisylmethanol as the H_R indicator, and *p*-nitroaniline and 1-amino-4-nitronaphthalene as Hammett indicators. The naphthylamine has not been used as a Hammett indicator before, but we used it in this work so that we could observe any effect of a bulky organic residue in the base.

Our interest in this problem was stimulated by the fact that the relation between the various acidity scales depends on the strong acid, for example the difference between the H_R and H_0' scales is greater for perchloric than sulfuric or hydrochloric acid.[12] These differences have been shown to arise from the ability of a low charge density monoanion, such as perchlorate, to stabilize a carbonium relative to an anilinium ion, whereas a high charge density monoanion, such as chloride, does not have this ability.[13] It therefore seemed probable that ionic micelles should have differential effects upon the equilibria between indicators and conjugate acids of different chemical structure. It is also

---

(1) Support of this work by the National Science Foundation is gratefully acknowledged.

(2) E. F. Duynstee and E. Grunwald, *J. Amer. Chem. Soc.*, **81**, 4540, 4542 (1959).

(3) M. T. A. Behme and E. H. Cordes, *ibid.*, **87**, 260 (1965); M. T. A. Behme, J. G. Fullington, R. Noel, and E. H. Cordes, *ibid.*, **87**, 266 (1965).

(4) F. M. Menger and C. E. Portnoy, *ibid.*, **89**, 4698 (1967).

(5) L. R. Romsted and E. H. Cordes, *ibid.*, **90**, 4404 (1968).

(6) C. A. Bunton, E. J. Fendler, L. Sepulveda, and K-U. Yang, *ibid.*, **90**, 5512 (1968).

(7) C. A. Bunton and L. Robinson, *ibid.*, **90**, 5972 (1968).

(8) P. Mukerjee and K. Banerjee, *J. Phys. Chem.*, **68**, 3567 (1964).

(9) C. A. Bunton, L. Robinson, and L. Sepulveda, *J. Amer. Chem. Soc.*, **91**, 4813 (1969).

(10) M. A. Paul and F. A. Long, *Chem. Rev.*, **57**, 1 (1957).

(11) N. C. Deno, J. J. Jaruszelski, and A. Schreisheim, *J. Amer. Chem. Soc.*, **77**, 3044 (1955).

(12) E. M. Arnett and G. W. Mach, *ibid.*, **88**, 1177 (1966).

(13) C. A. Bunton, J. H. Crabtree, and L. Robinson, *ibid*, **90**, 1258 (1968).

possible that ionic micelles, like simple electrolytes, could affect the rates of A1 and A2 reactions differently,[13] but this aspect of the problem could not be studied until the indicator equilibria were understood.

Experimental Section

Materials. The preparation and purification of most of the indicators and the detergents has been described.[6,13] 1-Amino-4-nitronaphthalene had mp 191° (ref 14, 191°), after recrystallization from aqueous ethanol.

Measurement of Indicator Ratios. The indicator ratios, $I = C_B/C_{BH^+}$ or C_{ROH}/C_{R^+} were measured spectrophotometrically,[10-12] using a Gilford spectrophotometer as already described.[13] The wavelengths were approximately 3800 Å for *p*-nitroaniline, 4420 Å for 1-amino-4-nitronaphthalene and 4820 Å for tri-*p*-anisylmethanol. For each measurement, a range of wavelengths was used to allow for spectral shifts caused by the detergent. For each acid concentration, the absorbances at λ_{max} were measured for the acid–detergent mixture and for the detergent alone; the differences between these values were taken as the absorbance of the colored species. The indicator concentrations were: *p*-nitroaniline, 3×10^{-5} *M;* 1-amino-4-nitronaphthalene, 2.5×10^{-5} *M;* tri-*p*-anisylmethanol, 3×10^{-6} *M*.

One serious problem in these measurements is that it is virtually impossible to follow a greater than tenfold change in the value of *I*.[10] This problem is not particularly serious for the measurements of H_0' using the nitroamines because the detergents do not have very large effects upon the protonation of the indicators. However, the detergent effects upon the ionization of trianisylmethanol are so large that with 0.1–0.15 *M* acid, relatively low concentrations of NaLS are sufficient to lead to essentially complete ionization of the alcohol, and therefore we could not measure the maximum increase in $-H_R$ which could be brought about by the detergent. In order to avoid this problem, we studied the effect of NaLS upon $-H_R$ in both 0.01 and 0.1 *M* HCl, although in the absence of detergent, the value of *I* is inconveniently high in 0.01 *M* HCl. However, the experimental value of *I* for tri-*p*-anisylmethanol in 0.01 *M* HCl is almost exactly 10 times that in 0.1 *M* HCl.

With trianisylmethanol in 0.1 *M* HCl the ionization is almost completely suppressed by 10^{-3} *M* CTABr, and useful determinations of I could not be made at higher detergent concentrations.

So far as we know the pK_a value of 1-amino-4-nitronaphthalene has not been determined. We measured it spectrophotometrically[10] using 0.1–1.2 *M* HCl. A plot of $\log(C_{HB^+}/C_B \cdot C_{H^+})$ against C_{HCl} was linear and exactly parallel to the corresponding plot for *p*-nitroaniline[10] and extrapolated to pK_a = 0.36, as compared with 0.98–1.00 for *p*-nitroaniline.[10] This difference in basicity is understandable in terms of the electronic effects of a phenyl as compared with a naphthyl group.

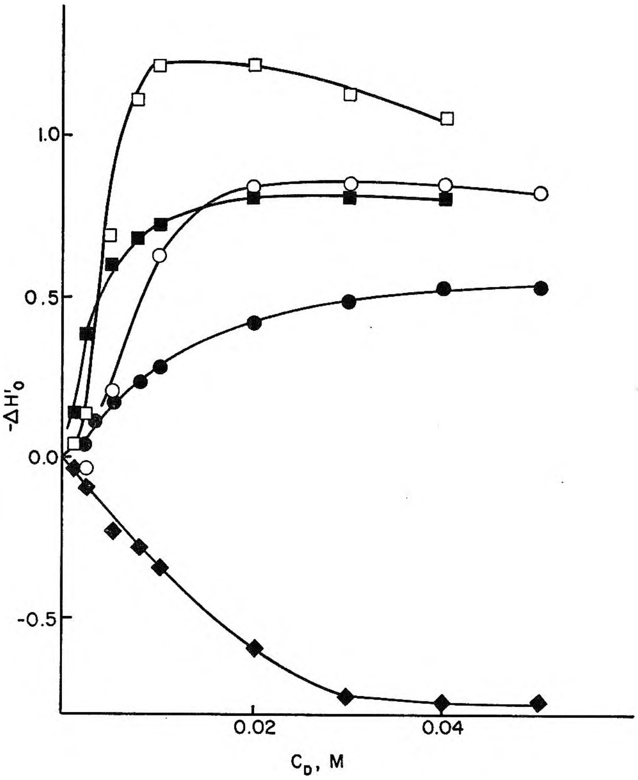

Figure 1. Variation of H_0' with detergent at 25°. Solid points 0.1 *M* HCl; open points 0.01 *M* HCl: ◆, CTABr with *p*-nitroaniline; ●, ○, NaLS with *p*-nitroaniline; ■, □, NaLS with 1-amino-4-nitronaphthalene.

Solubility Measurements. The solubilities of the indicator bases in aqueous detergents were measured by saturating the detergent solutions with the indicators by leaving the solutions for several days at 25.0° with occasional shaking.[7] The solutions were then filtered. For the experiments with the nitroamines, portions of the solution were diluted with water to bring the detergent concentrations below the cmc (critical micelle concentration), and the nitroamines were determined spectrophotometrically.

For tri-*p*-anisylmethanol the solutions were diluted with aqueous acid, sufficient to ionize the alcohol completely. Sulfuric acid was used with CTABr and perchloric with NaLS. Control tests were carried out to make sure that Beer's law was obeyed in these detergent solutions.

Results

The values of log *I* and $\Delta H_0'$ are given for *p*-nitroaniline and 1-amino-4-nitronaphthalene in 0.01 and 0.1 *M* HCl in Table I and Figure 1. The values of log *I* are given to show the range of indicator ratios used in the work. The values of $-\Delta H_0'$ increase to a plateau

---

(14) C. C. Price and S-T. Voong, "Organic Syntheses," Coll. Vol. III, John Wiley & Sons, Inc., New York, N.Y., 1955, p 664.

Table I: Effect of NaLS upon $H_0'^a$

Acid 10^3C_D, M	0.01 M HCl Log I^b	$-\Delta H_0'^b$	Log I^c	$-\Delta H_0'^c$	0.10 M HCl Log I^b	$-\Delta H_0'^b$	Log I^c	$-\Delta H_0'^c$
0.00	0.97		1.62^d		−0.03		0.62	
1.00			1.58	0.04	−0.03	0.00	0.62	0.00
1.50					−0.04	0.02	0.48	0.14
2.00					−0.07	0.04		
2.50	1.02	−0.05	1.50	0.12			0.24	0.38
3.00					−0.14	0.11		
5.00	0.78	0.19	0.94	0.68	−0.20	0.17	0.03	0.59
7.50			0.52	1.10	−0.26	0.23	−0.06	0.68
10.0	0.35	0.62	0.41	1.21	−0.31	0.28	−0.10	0.72
20.0	0.14	0.83	0.41	1.21	−0.45	0.42	−0.18	0.80
30.0	0.12	0.85	0.49	1.13	−0.51	0.48	−0.18	0.80
40.0	0.13	0.84	0.57	1.05	−0.56	0.53	−0.18	0.80
50.0	0.16	0.81			−0.55	0.52		

[a] In aqueous acid at 25.0°. [b] p-Nitroaniline. [c] 1-Amino-4-nitronaphthalene. [d] Calculated value.

Table II: Effect of NaLS upon H_R^a

Acid 10^3C_D, M	0.01 M HCl Log I	$-\Delta H_R$	0.1 M HCl Log I	$-\Delta H_R$	0.15 M HClO$_4$ Log I	ΔH_R
0.00	1.27		0.25		−0.17	
0.10			0.44	−0.19	−0.17	0.00
0.25			0.47	−0.22		
0.30					−0.23	0.06
0.50			0.19	0.06	−0.34	0.17
0.70					−0.64	0.47
0.75			−0.10	0.35		
1.00	1.25	0.02	−0.67	0.92	−1.32	1.15
2.00	0.78	0.49				
3.00	0.61	0.66				
4.50	−0.43	1.70				
5.00	−1.09	2.36				
6.00	−1.29	2.56				
7.50	−1.23	2.50				
9.00	−1.34	2.61				

[a] In aqueous acid at 25.0°.

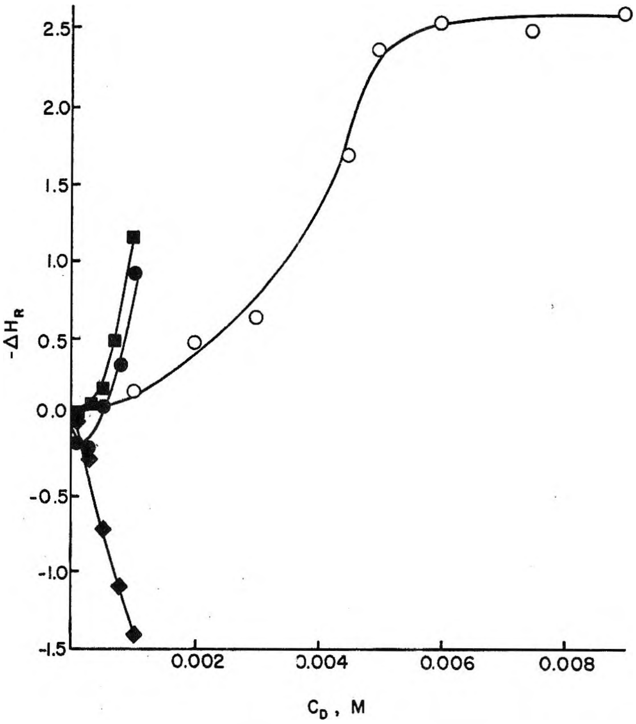

Figure 2. Variation of H_R with detergent at 25° using tri-p-anisylmethanol: ◆, CTABr in 0.1 M HCl; ■, NaLS in 0.15 M HClO$_4$; ●, NaLS in 0.1 M HCl; ○, NaLS in 0.01 M HCl.

and in some cases give a slight maximum. Relatively high concentrations of detergent could be used with these indicators, so that the indicator concentrations were always less than those of the detergents, and the detergent concentrations were generally considerably greater than the cmc. For NaLS the cmc = 4×10^{-3} M in water,[15] and 2.5×10^{-3} M in 0.05 M NaOH,[7] and the cmc should be considerably lower in 0.1 M than in 0.01 M acid because an increase in ionic strength decreases the cmc of an ionic detergent by stabilizing the ionic micelle.[16] The results given in Table II and Figure 2 show that in 0.1 M HCl and 0.15 M HClO$_4$ $-H_R$ is increased sharply by relatively low concentrations of NaLS, but with 0.01 M HCl where the cmc is higher than in 0.1 M HCl the values of $-\Delta H_R$ do not increase sharply until the detergent concentration becomes close to the cmc. However, the acidities increase at detergent concentrations below the cmc, possibly submicellar aggregates can stabilize the organic cations, just as they can be catalytically effective in reactions.[5,6,7,17] In addition organic solutes can pro-

---

(15) M. L. Corrin and W. D. Harkins, *J. Amer. Chem. Soc.*, **69**, 679 (1947).

(16) P. H. Elworthy, A. T. Florence, and C. B. Macfarlane, "Solubilization by Surface-Active Agents," Chapman and Hall, London, 1968, Chapter I.

(17) T. C. Bruice, J. Katzhendler, and L. R. Fedor, *J. Amer. Chem. Soc.*, **90**, 1333 (1968).

mote micellization.[18] One unexpected observation was that with 0.1 M HCl NaLS in low concentration at first decreases $-\Delta H_R$. We do not understand this anomaly, but effects on the cmc of the detergent may be important. In all the systems which we have examined the plateau values of $-\Delta H_0'$ or $-\Delta H_R$ are greater for 0.01 than for 0.1 M HCl, simply because when there are sufficient protons in the solution to occupy the Stern layer of the detergent, additional protons have very little effect, and the increase in ionic strength should increase the aggregation number of the micelle and therefore decrease the concentration of micelles for a given detergent concentration.

Both $-H'_0$ and $-H_R$ are decreased by the cationic detergent CTABr (Table III and Figures 1 and 2). The cmc for this detergent is 7.8×10^{-4} M in water and 3.2×10^{-4} M in 0.05 M NaOH.[7] The effects of added salts are shown in Table IV.

Table III: Effect of CTABr and H_0' and H_R[a]

10^3C_D, M	Log I[b]	$\Delta H_0'$[b]	Log I[c]	ΔH_R
0.00	−0.03		0.25	
0.10			0.28	0.03
0.25			0.47	0.22
0.50	0.01	0.04	0.97	0.72
0.75			1.35	1.10
1.00	0.01	0.04	1.66	1.41
2.50	0.06	0.09		
5.00	0.20	0.23		
7.50	0.25	0.28		
10.0	0.31	0.34		
20.0	0.56	0.59		
30.0	0.72	0.75		
40.0	0.75	0.78		
50.0	0.74	0.77		

[a] In 0.10 M HCl at 25.0°. [b] For p-nitroaniline. [c] For trianisylmethanol.

Table IV: Effect of Salts upon $\Delta H_0'$ and ΔH_R[a]

	Indicator			
	p-nitroaniline[b]		tri-p-anisylmethanol[c]	
Salt	Log I	$-\Delta H_0'$	Log I	$-\Delta H_R$
	0.12	0.85	−1.29	2.56
LiCl	0.21	0.76	−0.87	2.14
NaCl	0.23	0.74	−0.76	2.03
$(CH_3)_4NCl$	0.40	0.57	0.16	1.11
NaBr	0.21	0.76	−0.80	2.07

[a] With 0.03 M salt in 0.01 M HCl and NaLS at 25.0°. [b] 0.03 M NaLS. [c] 0.006 M NaLS.

Solubilities. The detergents solubilize both the nitromines and tri-p-anisylmethanol (Figure 3), but the effect is much greater with the tertiary alcohol, probably because of its higher molecular weight. In addition, the solubility of the alcohol in water will be decreased by steric hindrance to hydration of the hydroxyl group by the aryl groups, whereas there should be little steric hindrance to hydration of the amino group. In other systems we have used solubility measurements to determine the equilibrium constant for partitioning of the solute between the aqueous and micellar phases.[7] The treatment requires the assumption that the solute does not change the nature of the micelle significantly, and this assumption may not be valid for tri-p-anisylmethanol because the overall concentration of alcohol in 5×10^{-2} M NaLS is 6×10^{-4} M, and in 5×10^{-2} M CTABr it is 9×10^{-4} M, and we cannot assume that the solute will not affect the properties of the micelle.

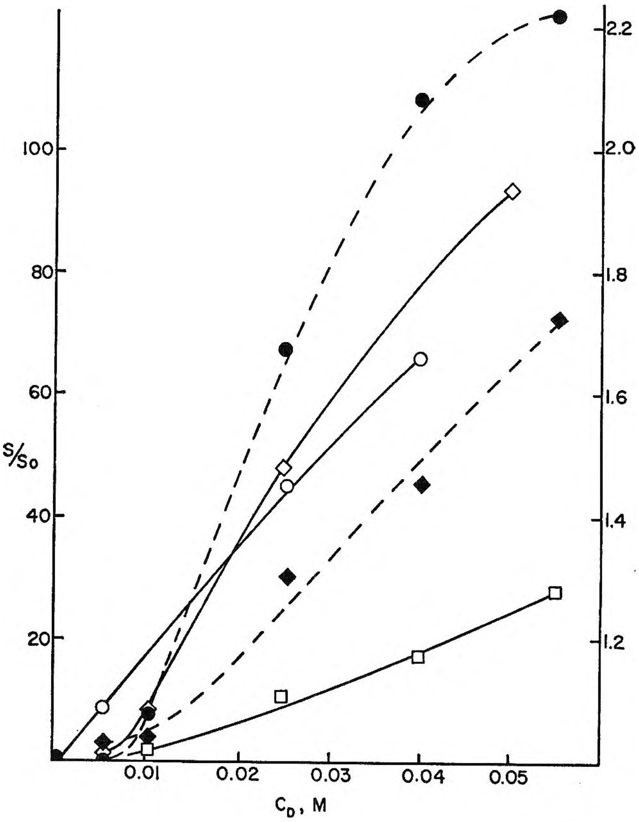

Figure 3. Solubilities of the indicators in detergent solutions at 25°. Left hand scale is for tri-p-anisylmethanol and 1-amino-4-nitronaphthalene; right hand scale is for p-nitroaniline: □, 1-amino-4-nitronaphthalene in NaLS; ○, tri-p-anisylmethanol in CTABr, and ◇ in NaLS; ●, p-nitroaniline in CTABr, and ◆ in NaLS.

Discussion

Relation between Acidity and Detergent Concentration. At a given acid concentration, the values of $-H_0'$ and $-H_R$ reach plateaus with increasing detergent concentrations, and these limiting values should be reached when the base and its conjugate acid are wholly in the micellar phase.[2-7] At lower concentrations of deter-

---

[18] P. Mukerjee and K. J. Mysels, *J. Amer. Chem. Soc.*, **77**, 2937 (1955).

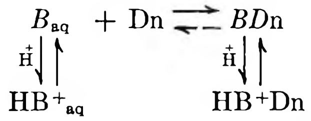

$$\begin{tikzcd}B_{aq} + \mathrm{Dn} \arrow[r, shift left] \arrow[d, shift right, "\overset{+}{\mathrm{H}}"'] & B\mathrm{Dn} \arrow[l, shift left] \arrow[d, shift right, "\overset{+}{\mathrm{H}}"'] \\ \mathrm{HB}^{+}_{aq} \arrow[u, shift right] & \mathrm{HB}^{+}\mathrm{Dn} \arrow[u, shift right]\end{tikzcd}$$

(Dn = micellized detergent)

gent, the values of $-H_0'$ and $-H_R$ will depend in part upon the solubilities of the bases and conjugate acids in the aqueous and micellar phases, and on the way in which the micelles affect the properties of water and hence, the equilibria in the aqueous phase, and the relations between $-H_0'$ and $-H_R$ and detergent concentrations will be very complicated. For these reasons it is the values of $-H_0'$ and $-H_R$ in the plateau region which are most informative.

We could not use one concentration of acid for all our experiments, but NaLS increases $-H_R$ much more than $-H_0'$ in the plateau region (Figures 1 and 2). The difference must depend upon the relative stabilities of the bases and their conjugate acids in the micellar phase, and it is probable that the triarylmethyl cation gains more stability in the micellar phase than does the anilinium ion. An ammonium ion gains much of its stability in water by hydrogen bonding, which would be lost, at least in part, if the positive charge were to be close to the surface of the anionic micelle. On the other hand, the large carbonium ion, in which the charge is delocalized over aryl groups, should not have a large solvation energy, and should gain considerable stability by incorporation into the micelle.[19] Anionic micellar effects upon H_0' and H_R are therefore similar to, but much larger than, the effects of a large, low charge density anion, such as perchlorate, which increases $-H_R$ much more than $-H_0$.[13] This similarity does not necessarily mean that there is direct association between carbonium and perchlorate ions in water, but in a 1 M lithium or sodium perchlorate solution, a large amount of water will be closely bound to the inorganic cation, and average interionic distances will be relatively small, even for free ions,[21] and the perchlorate and carbonium ions will be surrounded by loosely held layers of water which will be released if the ions come close enough. The free energy gained by the increasing entropy of the water, plus the electrostatic interaction of the ions, could offset the loss of hydration energy of the ions or ionic micelles. (This association is therefore analogous to hydrophobic bonding between nonpolar solutes.)[22]

The increase of $-H_0'$ (1.05 as compared with 0.85 for 0.01 M HCl) in NaLS is only slightly greater when 1-amino-4-nitronaphthalene rather than p-nitroaniline is used as the indicator, showing that the size of the organic residue is not particularly important; in agreement with our assumption that we are seeing a difference between the two indicator systems which depends on the difference between a carbonium and an anilinium ion.

The decrease of acidity brought about by the cationic detergent, CTABr, is easily understood, because incorporation of the base into the micellar phase will protect it from protonation and the ammonium or carbonium ions will be less stable in the micellar as compared with the aqueous phase.[2-7]

Our experiments show that we cannot use indicator measurements to determine micellar effects upon the "inherent" acidity or basicity of the medium *i.e.*, the ability of the medium to donate or accept hydrogen ions, because, as in any system, the measured effect depends not only upon the hydrogen ion activity, but upon the indicator base and its conjugate acid. We cannot estimate how much of the micellar effects upon H_0' and H_R are due to changes in hydrogen ion activity and how much to changes in the activity coefficient ratio of the base and its conjugate acid, but the large differences between $-\Delta H_0'$ and $-\Delta H_R$ show that this second effect must at least be large for the alcohol and its carbonium ion.

One problem in evaluating the effects is that $-H_R$ includes the water activity, but all the evidence suggests that the solutes will be in the water rich outer layer of the micelle,[23] so that the bulk water activity should not be an important factor (*cf.* ref 12).

Salt Effects. Counterions inhibit catalysis by ionic micelles,[5-7,9,24] and their efficiency increases with decreasing charge density of the ion. The same pattern is exhibited in the present systems (Table IV), for example tetramethyl-ammonium suppresses the acidity much more than does lithium, (based on either H_0' or H_R values in the plateau region) and in both cases it is the bulky low charge-density ions which are the most effective, because they interact most strongly with the micelle and prevent it interacting with the reactive ions. The effect on H_R is much greater than on H_0'.

A small contributory factor could be that it is the small ions which increase acidity most in aqueous acids,[10,13,25] in part by decreasing water activity and salting out the indicator base. However the effect of 0.03 M salt upon acidity is very small and should be negligible as compared with that caused by the micelle–salt interaction.

---

[19] The importance of hydrogen bonding in determining the differences between the various acidity scales has been noted by many workers.[12,20]

[20] R. W. Taft, *J. Amer. Chem. Soc.*, **82**, 2965 (1960).

[21] E. M. Kosower, "An Introduction to Physical Organic Chemistry," John Wiley & Sons, New York, N. Y., 1968, p 345.

[22] G. Nemethy and H. A. Scheraga, *J. Phys. Chem.*, **66**, 1173 (1962).

[23] J. C. Eriksson and G. Gilberg, *Acta Chem. Scand.*, **20**, 2019 (1966); *cf.*, M. Muller and R. H. Birkhahn, *J. Phys. Chem.*, **71**, 957 (1967).

[24] C. A. Bunton and L. Robinson, *J. Org. Chem.*, **34**, 773, 780 (1969).

[25] C. Perrin, *J. Amer. Chem. Soc.*, **86**, 256 (1964); B. J. Huckings and M. D. Johnson, *J. Chem. Soc.*, 5371 (1964).

Spectroscopic Evidence for the Mixture Model in HOD Solutions

by W. A. Senior[1a] and R. E. Verrall[1b]

Mellon Institute, Pittsburgh, Pennsylvania *(Received May 9, 1969)*

The significance of isosbestic points in spectral studies is established and the results of this investigation applied to the ir spectrum of HOD in solution over the temperature range 25–90°. The results suggest the existence of an equilibrium between two states of the OD group ("bonded" and "nonbonded") and a van't Hoff ΔH value of 2.3 ± 0.4 kcal/mol corresponding to the bond breaking process is derived.

Introduction

The idea that liquid water may be a mixture of at least two species of water molecules was apparently first put forward by Rowlands and elaborated by Roentgen in 1892.[2] Since that time, a great deal of effort has gone into calculating theoretically the thermodynamic properties of liquid water using a variety of mixture models.[3-8]

At the same time a number of authors have adhered to an essentially "uniformist" average model.[9,10] No clear-cut decision between the two paths has been possible because of the lack of direct evidence to indicate the simultaneous presence of more than one type of water molecule in liquid water.[11]

In general, the mixture models postulate an equilibrium between two or more types of water molecules roughly corresponding to a transition from a nonhydrogen-bonded species to a hydrogen-bonded type such as might be found in an ice structure. In model terms, this is usually visualized as corresponding to the formation of a "cluster"[6] with a limited lifetime probably between 10^{-11} and 10^{-7} sec.

If these lifetimes are essentially correct (and it is difficult to visualize a molecular rearrangement process taking place in much less than 10^{-11} sec), then spectroscopic studies at frequencies in excess of $\simeq 10^{12}$ cps should show the presence of more than one component in the system. The evidence at present available is extensive but not conclusive. The work of Luck[12] in the near ir shows that the temperature behavior of the spectra is consistent with the idea of a mixture of components in equilibrium but the complexities of assignment in the overtone region leave room for doubt. Similarly, the Raman and ir studies of the fundamental region of liquid water also depend on a particular band assignment.

The one region which appears to be accepted by most spectroscopists to be relatively free of doubt in assignment is the OD stretching vibration of the HOD molecule in solution in H_2O. With the proper concentration conditions, this band offers the best opportunities for deciding between continuum and mixture models. Although at first sight the appearance of a single band seems to support the continuum model[11,13] we believe this to be a hasty conclusion for two reasons. Firstly, the Raman results on the same system show very definite evidence of at least two components[14] and secondly the ir band exhibits an isosbestic point when several curves, obtained at different temperatures, are superimposed. This isosbestic behavior is most generally found in two component systems although, as we shall show, it may occur in other systems.

In an attempt to clarify the appearance of the OD band contour and its temperature behavior, we shall first investigate the general significance of isosbestic points and later look in detail at the ir band contour of HOD at 2500 cm^{-1}.

A. Isosbestic Points

The occurrence of a point on the absorption spectrum of a two component system (in which the two components are in chemical equilibrium) which is invariant with respect to the relative concentration of the two components was apparently first noted in 1924 by Thiel[15] who called this point the "isosbestic point"

---

[1] (a) On leave of absence from Unilever Research Laboratory, Port Sunlight, Cheshire, England. (b) University of Saskatchewan, Saskatoon, Saskatchewan, Canada.

[2] H. S. Frank, First International Symposium on Water Desalination, Washington, D. C., 1965.

[3] (a) G. Nemethy and H. A. Scheraga, *J. Chem. Phys.*, **36**, 3382 (1962); (b) H. S. Frank, *Fed. Proc.*, **24**, No. 2, Part III, Supp. 15, 1 (1965).

[4] R. P. Marchi and H. Eyring, *J. Phys. Chem.*, **68**, 221 (1964).

[5] V. Vand and W. A. Senior, *J. Chem. Phys.*, **43**, 1869, 1873, 1878 (1965).

[6] H. S. Frank and W. Y. Wen, *Discussions Faraday Soc.*, **24**, 133 (1957).

[7] C. M. Davis and T. A. Litovitz, *J. Chem. Phys.*, **42**, 2563 (1965).

[8] M. D. Danford and H. A. Levy, *J. Amer. Chem. Soc.*, **84**, 3965 (1962).

[9] J. Lennard-Jones and J. A. Pople, *Proc. Roy. Soc.*, **A205**, 155 (1951).

[10] J. A. Pople, *Proc. Roy. Soc.*, **A205**, 163 (1951).

[11] T. T. Wall and D. F. Hornig, *J. Chem. Phys.*, **43**, 2079 (1965).

[12] W. A. P. Luck, *Ber. Bunsenges Phys. Chem.*, **67**, 186 (1963).

[13] M. Falk and T. A. Ford, *Can. J. Chem.*, **44**, 1699 (1966); **46**, 3579 (1968).

[14] G. E. Walrafen, *J. Chem. Phys.*, **48**, 244 (1968).

[15] A. Thiel, *Fortschr. Chem. Phys. Phys. Chem.*, **18**, 38 (1924).

(the point of same extinction). Since that time, such a point has been found in many studies on equilibrium systems, notably those involving the spectra of indicators in systems of variable pH.[15,16] More recently, apparent isosbestic points have been found in the spectra of water and aqueous solutions[12,17,18] as the temperature is varied.

Although some of the conditions necessary for isosbestic points to occur have been established[19] only a limited range of conditions has been covered. We believe our investigations to be of a more general nature although by no means completely comprehensive.

We shall show that in general an isosbestic point may occur in a system of any number of components but that the chance of it occurring in a system of other than two components is remote.

For a system which obeys Beer's law, the total optical density $y(\nu)$ at any frequency ν in the absorption spectrum of a system of n components can be written

$$y(\nu) = \sum_{i=1}^{n} g_i(\nu)\cdot x_i \tag{1}$$

where x_i = mole fraction of the ith component and the $g_i(\nu)$ is the optical density of the ith component at frequency ν.

If the n components are involved in an equilibrium with one another, then their concentrations must obey the conservative condition

$$\sum_{i=1}^{n} x_i = 1 \tag{2}$$

Combining equations 1 and 2 we obtain

$$y(\nu) = g_1(\nu) + \sum_{i=2}^{n} x_i\{g_i(\nu) - g_1(\nu)\} \tag{3}$$

In general, to observe an isosbestic point we require that for at least one particular frequency ν_c, the optical density of the system be independent of some external variable t (t may be temperature, pressure, pH, etc.) *i.e.*, we require

$$\left[\frac{dy}{dt}\right]_{\nu=\nu_c} = 0$$

from which it follows quite generally that

$$\frac{dg_1(\nu)}{dt} + \sum_{i=2}^{n}\{g_i(\nu) - g_1(\nu)\}\frac{dx_i}{dt} + \sum_{i=2}^{n} x_i\left\{\frac{dg_i(\nu)}{dt} - \frac{dg_1(\nu)}{dt}\right\} = 0 \tag{4}$$

for at least one frequency $\nu = \nu_c$.

Equation 4 is the general equation governing isosbestic behavior in systems of any complexity. We shall, however, be concerned with only certain special cases governed by (4).

I. One-Component Systems. In these cases, eq 4 reduces to

$$\frac{dg_1(\nu)}{dt} = 0 \text{ or } g_1(\nu) = \text{constant}$$

for at least one frequency $\nu = \nu_c$. For a Gaussian band this requires

$$\epsilon_t \exp -\left\{\frac{\nu_c - \nu_t}{\Delta\nu_t}\right\}^2 = \alpha = \text{constant} \tag{5}$$

which may be satisfied if ϵ_t, ν_t, and $\Delta\nu_t$ are all constant or if they vary in the manner prescribed by (5). Such behavior is difficult to achieve. Equation 5 is the least restrictive one to allow an isosbestic point and more usually it is probably necessary to impose the additional condition that the integrated area remains constant (*i.e.*, constant oscillator strength) which requires

$$\epsilon_t\Delta\nu_t = \gamma = \text{constant} \tag{6}$$

Combining (5) and (6), the more restrictive condition is found to be

$$\nu_c - \nu_t = \pm\Delta\nu_t\{\ln\gamma - \ln(\alpha\Delta\nu_t)\}^{1/2} \tag{7}$$

which is probably somewhat more difficult to satisfy than (5). We conclude, therefore, that although an isosbestic point is possible in a pure material, it is extremely unlikely. More probably a pseudo-isosbestic region will be found and this region will grow larger as the range of variable t is extended.

II. Two-Component Systems. For a two-component system we must return to the general isosbestic eq 4. Although there are a number of ways in which (4) may be satisfied, only one of these is of real importance. This is the case when $dg_i(\nu)/dt = 0$, *i.e.*, the intrinsic band shapes of each component are independent of t. Because, in general, we know that the equilibrium constant will depend on t, it follows that $dx_i/dt \neq 0$ and therefore to satisfy (4) we must have $g_1(\nu_c) = g_2(\nu_c)$ which for Gaussian bands requires

$$\epsilon_1 \exp -\left\{\frac{\nu_c - \nu_1}{\Delta\nu_1}\right\}^2 = \epsilon_2 \exp -\left\{\frac{\nu_c - \nu_2}{\Delta\nu_2}\right\}^2 \tag{8}$$

and thus the frequencies ν_c of the isosbestic points are the solutions of

$$\nu_c^2\left\{\frac{1}{\Delta\nu_2^2} - \frac{1}{\Delta\nu_1^2}\right\} - 2\nu_c\left\{\frac{\nu_2}{\Delta\nu_2^2} - \frac{\nu_1}{\Delta\nu_1^2}\right\} + \left\{\frac{\nu_2^2}{\Delta\nu_2^2} - \frac{\nu_1^2}{\Delta\nu_1^2} - \ln\left[\frac{\epsilon_2}{\epsilon_1}\right]\right\} = 0 \tag{9}$$

Although eq 9 can be solved for ν_c, the isosbestic frequency, the form of the solutions does not easily indicate what happens when the band parameters are altered. A more convenient method is to inspect the

---

(16) R. P. Bauman, "Absorption Spectroscopy," John Wiley and Sons, Inc., New York, N. Y., 1962, p 419 ff.

17) K. A. Hartman, Jr., *J. Phys. Chem.*, **70**, 270 (1966).

(18) J. D. Worley and I. M. Klotz, *J. Chem. Phys.*, **45**, 2869 (1966).

(19) J. Brynestad and G. P. Smith, *J. Phys. Chem.*, **72**, 296 (1968).

part, Q, of the solution which occurs under the square root sign and see when this leads to real and imaginary solutions. This quantity Q is simply

$$Q = (\nu_2 - \nu_1)^2 + (\Delta\nu_1^2 - \Delta\nu_2^2) \ln (\epsilon_2/\epsilon_1) \quad (10)$$

the solutions proper being of the form

$$\nu_c = a \pm bQ^{1/2} \quad (11)$$

where a and b are constants determined by the band parameters. A number of different cases must now be considered.

(*i*) *Two Bands of Identical Shape*

$$\epsilon_1 = \epsilon_2;\ \Delta\nu_1 = \Delta\nu_2$$

$\therefore \ln\{\epsilon_2/\epsilon_1\} = 0$ and Q is a perfect square and it can be shown that there is only one isosbestic point which lies midway between the two bands.

(*ii*) *Two Bands of the Same Extinction Coefficient*

$$\epsilon_1 = \epsilon_2;\ \Delta\nu_1 \neq \Delta\nu_2$$

Again, $\ln\{\epsilon_2/\epsilon_1\} = 0$ and Q is a perfect square, but since $\Delta\nu_1 \neq \Delta\nu_2$ there are now always two isosbestic points if $\nu_1 \neq \nu_2$, although in practice for bands of not too different shape, $\Delta\nu_1 \simeq \Delta\nu_2$ and one isosbestic is well away from the main band area and in a region of very low absorption. If $\nu_1 = \nu_2$ only one isosbestic occurs and this at the frequency of maximum absorption, *i.e.*, $\nu_c = \nu_1 = \nu_2$.

(*iii*) *Bands of Equal Width*

$$\Delta\nu_1 = \Delta\nu_2;\ \epsilon_1 \neq \epsilon_2$$

Again, Q is a perfect square and it is easily shown that in this case there is only one isosbestic point which may lie between or outside the two maxima, depending on the relative intensity of the two bands.

(*iv*) *Bands of Equal Area* (*e.g.*, constant oscillator strength)

$$\epsilon_1\Delta\nu_1 = \epsilon_2\Delta\nu_2$$

Equation 10 can now be rewritten as

$$Q = (\nu_2 - \nu_1)^2 + (\Delta\nu_1^2 - \Delta\nu_2^2) \ln(\Delta\nu_1/\Delta\nu_2) \quad (12)$$

If $\Delta\nu_1 \neq \Delta\nu_2$, the second term in (12) is always >0 and hence Q is always >0 and there are two isosbestic points for all values of $(\nu_2 - \nu_1)^2$. As $\nu_1 \rightarrow \nu_2$ they become more symmetrically placed on each side of the band maximum.

(*v*) *One Strong Sharp Band and One Weak Broad Band*

$$\Delta\nu_1 < \Delta\nu_2 \text{ and } \epsilon_1 > \epsilon_2 \text{ or } \Delta\nu_1 > \Delta\nu_2 \text{ and } \epsilon_1 < \epsilon_2$$

The second term in (10) is always >0 and thus Q is always >0. Thus there are always two isosbestic points. Again, as $\nu_1 \rightarrow \nu_2$ they become more symmetrically placed around the band maximum.

(*vi*) *One Weak Sharp Band and One Strong Broad Band*

$$\Delta\nu_1 < \Delta\nu_2 \text{ and } \epsilon_1 < \epsilon_2 \text{ or } \Delta\nu_1 > \Delta\nu_2 \text{ and } \epsilon_1 > \epsilon_2$$

The first term in (10) is always >0 and the second term is always <0. Thus Q may be >0, = 0 or <0 depending on the relative magnitudes of these two terms. If Q is >0 two isosbestics occur exactly similar in form to cases (iv) and (v). If $Q = 0$ only one isosbestic occurs very similar to case (iii). If $Q < 0$ no isosbestics occur. This happens when

$$(\nu_2 - \nu_1)^2 < (\Delta\nu_2^2 - \Delta\nu_1^2) \ln (\epsilon_2/\epsilon_1) \quad (13)$$

As a simple example consider the case $\epsilon_2 = e\epsilon_1$ $\ln \epsilon_2/\epsilon_1 = 1$ and if $(\nu_2 - \nu_1)^2 < (\Delta\nu_2^2 - \Delta\nu_1^2)$ there will be no isosbestic point. For two typical bands one might have $\Delta\nu_2 = 100$ cm^{-1} and $\Delta\nu_1 = 50$ cm^{-1} so that if the band centers are separated by $<\simeq 85$ cm^{-1} no isosbestic point will occur. This situation is shown schematically in Figure 1 where a typical set of curves for various t values is presented. Note that both bands obey Beer's Law exactly and yet no isosbestic occurs. Spectra closely resembling this type have been observed by both Luck[12] and Klotz and Worley[18] in their studies on water. In itself, of course, this is not evidence of an equilibrium between distinct species.

III. Multicomponent Systems. Where multiple components are involved in equilibria with one another, the general situation is extremely complex. In general, one must take into account such factors as the stoichiometry of the reaction, changes in molar volume, the number of independent equilibrium constants which exist and the presence of inert solvents. However, for reactions of the type A $\leftrightarrows$ B $\leftrightarrows$ C $\leftrightarrows$ D ······ in which there are n components and $(n - 1)$ equilibrium constants, the general condition necessary for isosbestic behavior when the band parameters are independent of t is

$$g_i(\nu_c) = \text{constant } i = 1, 2, \cdots n \quad (14)$$

i.e., there must be at least one frequency at which all components have the same optical density. This

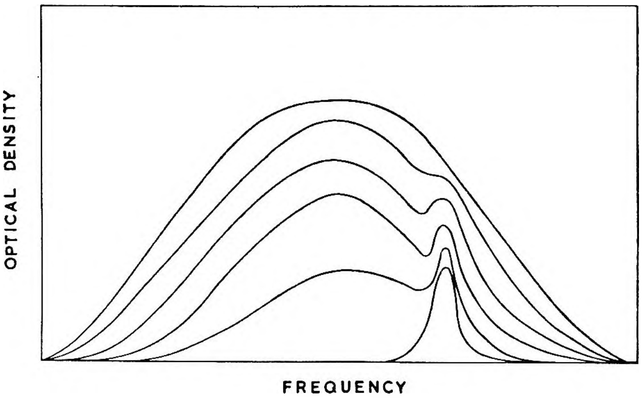

Figure 1. Nonoccurrence of an isosbestic point in a two-component equilibrium system. Both components obey Beer's law.

means that the band profiles of all components present must intersect in one unique point and this condition is almost impossible to satisfy even for only three component systems. Systems of this type containing more than three components must be completely unable to meet this condition.

Another type of multicomponent system which is of interest is of the form $A + B + C \cdots \rightleftarrows D + E + F \cdots\cdots$. This type of system can exhibit isosbestic points under special conditions, *e.g.*, since there is only one equilibrium constant and if only one component on each side of the equilibrium is absorbing, an isosbestic may exist—mathematically it behaves as a two component system. This type of equilibrium can also be varied by addition of one or more of the component materials. In this instance, the law of mass action plays a part and introduces certain special relationships between the amounts of the various components. If, at the same time, other special relations are observed, *e.g.*, keeping the total number of moles of material constant, isosbestic points can be made to occur.[20]

If, however, the equilibrium is not constrained by very special conditions and is varied only by altering the equilibrium constant (or constants), *i.e.*, by varying P and T then isosbestic points will only occur if relations of the form (14) hold between the band profiles.

In multicomponent systems, one might observe a pseudoisosbestic region if the equilibrium conditions are altered only by a small amount. However, the extent of this region would increase as the range of variation of the equilibrium conditions was widened.

If the band parameters vary as the equilibrium conditions are altered, perfect isosbestic behavior would only be observed if very stringent requirements were obeyed. In general, it appears that a dependence of this type would again lead to the existence of an isosbestic region, if the band parameters varied only slightly.

IV. Significance of Isosbestic Points. In sections I–III of this paper we have examined some of the most relevant conditions under which isosbestic points might occur. Somewhat surprisingly it is possible, although rather improbable, to observe isosbestic behavior in a system containing only one pure component so long as the band shape is reasonably sensitive to the external variable t. In a two component system, a genuine isosbestic is probable only if the band shapes and positions are very insensitive to t and the equilibrium constant is dependent on t. In addition, in two component systems one should point out that it is entirely possible that no isosbestic will occur even though the equilibrium is rigidly obeyed and even though both components have absorption bands which obey Beer's Law. In systems of high complexity (three or more components) it seems extremely unlikely that an isosbestic point would be found, except in rather special circumstances.

Bearing in mind the foregoing, it seems reasonably safe to state the case as follows. The existence of an isosbestic point implies the presence of either a one or two component system. If, in addition, it can be established that the observed band is composed of two subbands then the existence of the isosbestic point is virtual proof of a two component equilibrium system.

On the other hand, the absence of an isosbestic point has little or no significance in any type of system.

One should point out that we have been concerned only with theoretical conditions necessary for isosbestic points to occur. In many practical cases, a genuine isosbestic point may be present theoretically but may not be observable if, for instance, it occurs in a region of very low absorption. Again, in real situations, any isosbestic is almost certain to occur as a pseudo-isosbestic region rather than a mathematically precise point. In these circumstances, it is essential to use a wide enough range of conditions to establish that the isosbestic region has a limited area. Our investigations lead us to believe that if the area of the isosbestic region is greater than 1% of the total band area, it would be dangerous to conclude that any equilibrium exists without other information to support the conclusion.

B. Infrared Investigations of the O–D Stretching Vibration in H_2O–D_2O Solutions

Having established the significance of isosbestic points in spectroscopic investigations, we are now in a position to examine in detail the experimental results we have obtained on the O–D stretching vibration of the HOD molecule in solution over a range of temperature.

I. Experimental Section

The spectrometer used was a Beckman IR-9 which was continually purged with dry nitrogen to minimize any spurious absorptions due to water vapor and CO_2. The spectra were recorded with the instrument operating in the double beam mode using a pen response time of 0.1 sec at a scanning speed of 60 cm^{-1}/min. Samples were prepared in RIIC cells (Model No. FH01) fitted with LiF windows and used with an electrically heated thermostat jacket supplied by RIIC. Cell temperatures were recorded continuously and were kept constant to ±1° over the 10-min period of each run. Spectra were recorded on both the heating and cooling cycles to establish that no loss of sample occurred at the elevated temperatures.

The concentration and cell thickness conditions are, we believe, very important. The band to be observed has its maximum absorption at ~2500 cm^{-1} and because of the excess water (H_2O) in the system, there are additional bands about 2150 (fairly weak) and at 3420 cm^{-1} (very intense). The result is that if a very low D_2O concentration is used with a compensating path

---

(20) C. F. Timberlake and P. Bridle, *Spectrochim. Acta*, **23A**, 313 (1967).

length to make the band observable, there is a very large curved background which must be taken into account. The desired spectrum is then the small difference between two very large signals and correction procedures are extremely difficult. At the other end of the scale, *i.e.*, a high D_2O concentration, the solution contains a considerable number of D_2O molecules and these absorb radiation at exactly the same frequency as the HOD molecules.

In the concentration range 5–10 mol % D_2O in H_2O the contribution from any remaining D_2O molecules can be kept below 2% of the observed band and, at the same time, the background correction can be held to less than 5% of the total band. By comparison with a spectrum for pure H_2O obtained under the same conditions it was established that the background in this region is almost exactly a straight line and the correction used was of this type. Under these conditions a cell thickness in the range 1–2μ is necessary and this is not too difficult to achieve.[21] We have therefore worked in this concentration and cell thickness range.

At the D_2O concentrations used, the presence of HOD–HOD pairs is substantial. There are, however, a number of reasons why we believe this type of coupling to have no influence on our results. Firstly, Raman results obtained on similar systems by Bernstein[22] and Walrafen[23] indicate that the asymmetry is independent of the isotope concentration within the range 1–10 mol %. Secondly, the observed splitting of ± 25 cm^{-1} found by Haas and Hornig[24] in ice and attributed by them to this coupling effect is likely to be a maximum value as the coupling effects are almost certain to be strongest in the solid state. Our observed frequency difference between the two components is 125 cm^{-1} and it is very unlikely, therefore, that this splitting can be accounted for in terms of HOD–HOD coupling. Finally, the work of Schultz and Hornig[25] on ionic solutions indicates that whereas the O–H vibrations of water are sensitive to anions, they are very insensitive to cations, suggesting that the O atom of the molecule has a very considerable screening effect. Therefore, it seems rather unlikely that the central molecule can distinguish whether its nearest neighbors possess H or D atoms except perhaps in the solid state where the intermolecular coupling will be strongest. We therefore believe our results to be characteristic of the uncoupled OD group.

II. Experimental Results

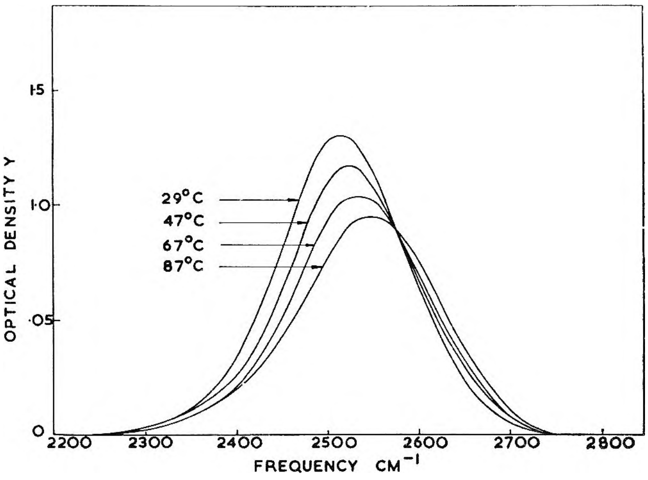

Figure 2. Plot of optical density *vs.* frequency for the ir absorption of HOD at ~2500 cm^{-1} for various temperatures. The presence of an isosbestic point at ~2575 cm^{-1} is clearly shown.

Figure 2 shows the experimental results obtained in the temperature range 29–87°. Taken individually, the curves show little or no sign of any asymmetry which might indicate the presence of more than one component. The remarkable feature of the set, of course, is the almost mathematically precise isosbestic point which occurs, and in view of our preceding analysis we must take further steps to decide whether or not our system contains more than one component. The frequency of the isosbestic point is 2575 cm^{-1} which coincides almost exactly with that found by Walrafen[14] in his Raman studies on the same band. In the Raman effect also, there seems to be no doubt of the existence of at least two components as the results show a fairly obvious shoulder, ~2650 cm^{-1}, in addition to the main maximum at ~2525 cm^{-1}. Hartman's[17] results on the OH band of HOD in D_2O also exhibit an isosbestic point.

In order to try and establish the structure of the ir band we have used a numerical differentiation technique. The observed curves were carefully measured over the frequency range 2200–2800 cm^{-1} at 10 cm^{-1} intervals. Successive differences are then taken between adjacent points and the modulus of the difference is plotted *vs.* the mean frequency of the interval. In this way, numerical differentiation of the observed curves is carried out which has the advantage that no assumption about band shape need be made.

Because the differential of a curve is much more sensitive to noise fluctuations on the data than the curve itself, we have found it advantageous to smooth our raw data before carrying out the numerical differentiation. This is done in the following way. Starting from point 1, a parabola is fitted through the first N points (where N determines the degree of smoothing required and, in our case, was 6) using a standard least squares method. The resulting equation is used to calculate the Y value at point 1 and this value replaces the original value. The process is then

---

(21) W. K. Thompson, *Trans. Faraday Soc.*, **61**, 2635 (1965).

(22) W. F. Murphy, W. Holzer, and H. J. Bernstein, *Raman Newsletter*, No. 1, 10 (1968).

(23) G. E. Walrafen, *J. Chem. Phys.*, **50**, 560 (1969).

(24) C. Haas and D. F. Hornig, *ibid.*, **32**, 1763 (1960).

(25) J. W. Schultz and D. F. Hornig, *J. Phys. Chem.*, **65**, 2131 (1961).

repeated starting from point 2, etc. Using the corrected points, the first derivative is then obtained as outlined above.

We have tested these procedures by truncating a 5-figure error table at the third decimal place. This procedure gives rise to random errors ~0.2% on the standard error curve (at half-height) which, in turn, gives rise to ~5–10% errors in the first derivative obtained by our method. When the initial data is smoothed as above and then differentiated, the resultant error in the differential is ~0.5%. A judicious choice of the measuring interval and the N value (number of smoothing points) is necessary to obtain best results. This is easily done after one or two trials.

Using the above procedure we have obtained the first differentials ($|\Delta Y|$) for the set of curves in Figure 2 and these results are shown in Figure 3. On the low frequency side of the minimum, all the curves behave as one would expect from the differential of a single component band. However, on the high frequency side of the minimum there is a distinct inflection at ~2690 cm^{-1} which occurs at all temperatures and which becomes more pronounced as the temperature is raised. The position of this inflection is consistent with the presence of a second component in the original band at about 2650 cm^{-1}. This agrees very well with the observed band at 2650 cm^{-1} in the Raman effect.

We conclude, therefore, that the -OD ir band of HOD liquid contains at least two components with positions 2525 and 2650 cm^{-1}. This is, then, in complete agreement with the observed Raman results. The positions of these bands are also consistent with the idea of two states of the OD group, *i.e.*, a hydrogen-bonded OD group having a vibrational frequency ~2525 cm^{-1} and a non-hydrogen-bonded OD group with a frequency ~2650 cm^{-1}. The behavior of the two bands as the temperature is varied is also quite consistent with this assignment. Further analysis indicates that the peak positions and half band width of both components are practically independent of temperature. Again, Walrafen's Raman results[14] show exactly similar behavior.

Of further interest is the experimental result obtained by Kecki *et al.*,[26] in a systematic infrared study of the effect of electrolytes on the OD and OH stretching band intensity in HDO–H$_2$O and HDO–D$_2$O solutions. In the case of NaClO$_4$, the OD stretching band of HDO is split into two components having frequencies of 2530 cm^{-1} and 2640 cm^{-1}. The position of the high frequency component is invariant to perchlorate concentration but its intensity increases at the expense of the low frequency component as the perchlorate concentration is increased. These frequencies agree rather well with those obtained in this paper on the salt free HDO–H$_2$O solutions. Perchlorate anion was the only anion in the above study[26] which exhibited this effect on the OD stretching band.

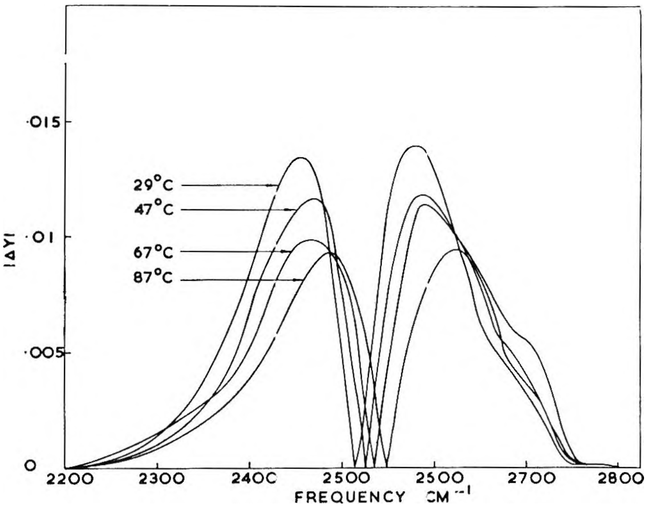

Figure 3. Moduli of the first differentials of the ir spectra of HOD (Figure 2) as obtained by the numerical differentiation and smoothing technique outlined in the text. The asymmetry at ~2690 cm^{-1} is clearly shown.

On balance, one might speculate that the effect of the perchlorate anion consists mainly in breaking the "normal" hydrogen bonds and therefore increases the concentration of nonhydrogen-bonded OD component at the expense of the bonded component. It appears that the unique behavior of perchlorate anion in aqueous solution, compared to other anions of similar size, may be related to its tetrahedral symmetry. The results of this work and ref 26 appear to support the concept of a mixture model for liquid water much better than they do that of the continuum model.

It is interesting to note that the peak position of the high frequency component (~2650 cm^{-1}) is well below the Q-branch O–D absorption of HOD vapor at 2720 cm^{-1}. This finding further substantiates the results of Franck and Roth[27] on the O–D absorption of HOD under supercritical conditions. If a $\nu_{\max}$ *vs.* T curve of their results for $\rho = 1.0$ g/cm^3 is extrapolated to higher temperatures it approaches an asymptotic value well below 2700 cm^{-1}, indeed at about 2650 cm^{-1}.

The implication is that nonhydrogen-bonded molecules in the liquid (or dense fluid) state are in no way comparable to free water molecules in the vapor phase.

One other feature of the experimental results is worthy of comment—the broadness of the observed ir and Raman bands. It is certain that this broadness arises from geometrical factors, *i.e.*, at a certain instant in time if one could examine the detailed structure of the liquid it would be found that in the "bonded" material hydrogen bonds of a wide range of lengths existed. This suggestion is supported by the width of

---

(26) Z. Kecki, P. Dryjanski, and E. Kozlowska, *Roczniki Chem.*, **42**, 1749 (1968).

(27) E. U. Franck and K. Roth, *Discussions Faraday Soc.*, **43**, 108 (1967).

the peaks found in the X-ray radial distribution function for water, (*e.g.*, the peak at ~2.90 Å has a width at half-height of ~0.5 Å[28] and by the fact that the radial distribution function can be derived from the Raman spectra.[11] Vand and Senior's[5] assumption of broadened energy bands is exactly equivalent to the above suggestion.

In view of our conclusions in section A.IV therefore, it seems fairly certain that an equilibrium between two states of the OD group does exist, particularly since the Raman evidence entirely supports this proposition.

III. Thermodynamic Quantities

Assuming the conclusions of section B.II to be correct, our next step is to try and determine the enthalpy change involved between the two states. Normally this is done by decomposing the total band into its two components at a series of temperatures and assuming the band areas (or peak heights) of each component to be proportional to the number of molecules in each state.

A simple plot of log A_1/A_2 *vs.* $1/T$ then gives the van't Hoff ΔH for the process from its slope. The main difficulty with this procedure is the band resolution step. This is usually accomplished by more or less refined techniques of curve fitting multiple Gaussian or Lorentzian bands to the observed band profile. At best, this means an arbitrary choice of band shape and, at worst, one has no guarantee that the final solution is unique. It seems likely that this technique is satisfactory if the bands do not overlap too strongly (*i.e.*, in the Raman case where two peaks can be distinguished) but there must be serious doubts about it in the type of situation we have in the ir spectrum. However, we have used the above method using both Gaussians and Lorentzians to derive a van't Hoff ΔH value of 4.5 ± 0.8 kcal/mol for the process OD(H-bonded) → OD-(non-H-bonded).

We have, however, found an alternative method of extracting this information which needs no assumptions about the band shapes. The only requirement is that we must be able to find a frequency range in the observed band at which one component has little or no absorption compared to the other. Consider the system A $\leftrightarrows$ B where the mole fraction concentrations of A and B are X_A and X_B respectively. The optical density at the same frequency at which the absorption of say B is zero is then purely determined by X_A and the absorption coefficient of A, G_A, giving

$$Y = G_A X_A \tag{15}$$

Defining the equilibrium constant for the reaction as

$$K = X_B/X_A = (1 - X_A)/X_A = C \exp - \Delta H/RT \tag{16}$$

or

$$\ln\{(1 - X_A)/X_A\} = \ln C - \Delta H/RT \tag{17}$$

Now

$$\ln[(1 - X)/X] = \ln[X(1 - X)/X^2] = \ln[X(1 - X)] - \ln X^2$$

or

$$\ln[(1 - X)/X] = \ln X(1 - X) - 2\ln X \tag{18}$$

Combining (18) and (17) we obtain

$$\ln X_A = \ln[X_A(1 - X_A)]^{1/2} - \ln C^{1/2} + \Delta H/2RT \tag{19}$$

or *via* (15)

$$\ln Y = \ln[X_A(1 - X_A)]^{1/2} + \ln[G_A/C^{1/2}] + \Delta H/2RT \tag{20}$$

The function $\ln[X_A(1 - X_A)]^{1/2}$ is a very slowly varying function of X_A and for values of X_A in the range 0.3–0.7 is constant to within ±5%. For X_A in the range 0.2–0.8 it is constant to within ±12.5%. Therefore for values of X_A in the range 0.3–0.7 a plot of $\ln Y$ *vs.* $1/T$ will be a straight line with a slope $\Delta H/2R$. If the X_A values lie far outside the above range then the plot will be a curve not a straight line.

Similarly, if a wavelength has been chosen such that condition (15) is not obeyed, this is also obvious from the graphical presentation, a peculiar S-shaped type of curve being obtained. In practice, therefore, the ln Y *vs.* $1/T$ graphs are plotted for a number of wavelengths covering the range of absorption of the band and a set of

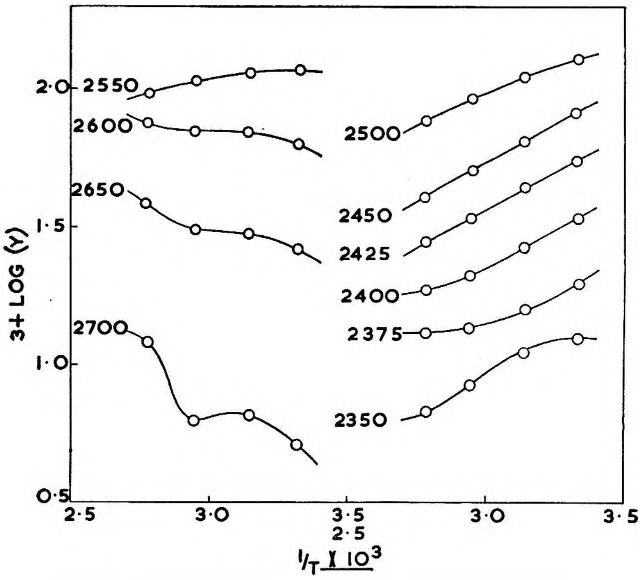

Figure 4. Plot of log (optical density) *vs.* $1/T$ at various frequencies across the HOD absorption band ~2500 cm⁻¹. The numbers at the left of each curve give the frequency at which the measurements were made.

---

[28] J. Morgan and B. E. Warren, *J. Chem. Phys.*, **6**, 666 (1938).

two or three lines are found in the regions where eq 15 is obeyed and where $\ln [X_A(1 - X_A)]^{1/2}$ is constant. A set of such curves obtained from our data is shown in Figure 4. Note that the set of lines lie in the region ~2425 cm^{-1} where indeed we would expect to find eq 15 best satisfied. The very low curvature also indicates that the condition $\ln [X_A(1 - X_A)]^{1/2}$ is constant is well satisfied.

The deviations from linearity at higher frequencies are due to the presence of the 2650 cm^{-1} component and those at ~2350 cm^{-1} and below are almost certainly caused by the presence of small amounts of CO_2 gas in the instrument. CO_2 gas has a strong absorption at 2350 cm^{-1} which is very difficult to eliminate even in double beam instruments.

The van't Hoff ΔH value obtained using this alternative method is 2.3 ± 0.4 kcal/mol and is the van't Hoff heat associated with the disruption of the $O-D\cdots O$ unit. This value of 2.3 kcal/mol is to be compared with the value of 2.5 kcal/mol obtained by Walrafen[14] in his Raman studies of the same process, as well as with the value of 2.4 kcal/mol obtained by Worley and Klotz[18] from near infrared studies of HDO in D_2O.

Using this method one cannot obtain the actual concentrations of the two components unless some assumption is made about the relative extinction coefficients of the species. However, the high degree of linearity of the $\ln Y$ *vs.* $1/T$ plots in the region where (15) holds indicates that the concentration ratios are probably about 2:1 or 1:1 with the bonded state being the most abundant.

The apparent discrepancy between the numerical values of the van't Hoff ΔH obtained in this work by two different methods requires further comment. It must be pointed out that, because of differences in the mode of presentation, the comparable results from the two methods of analysis are 2.25 and 2.3 kcal/mol; *i.e.*, there is close agreement between them. However, for reasons mentioned previously in this section, we feel the second method offers a more objective analysis of the data.

One other point concerning the variation of the van't Hoff heat values obtained from spectral studies is worthy of mention. This argument is not presented to account for any difference in the ΔH values of the present work but, rather as a possible reason for the general inconsistency among results to date. It has been shown[29] that, for cooperative hydrogen bonding phenomena in helix-coil transitions of some synthetic polypeptides, the transition involving hydrogen bonding can take place over a narrow or wide range of temperature depending on the degree of difficulty in starting an ordered region. An "equilibrium constant" constructed in the ordinary way would therefore show a temperature dependence which would vary depending upon the degree of cooperativeness of the process of hydrogen bond formation. Frank[30] has suggested that an analogous situation might arise in the 3-dimensional case of the equilibrium between bonded and unbonded species in liquid water, giving rise to different van't Hoff ΔH values from studies of different properties. The important implication is that the van't Hoff heat for hydrogen bond formation may be different from the calorimetric value, and that the latter might well be considerably smaller in absolute value than has sometimes been imagined.[31]

C. General Conclusions

In conclusion, it appears to us that the weight of spectroscopic evidence supports the idea of a two state model for the OD group of the HOD molecule in solution in H_2O. It follows that at least two states of the H_2O molecule must be present in liquid water. The detailed geometrical structures involved remain to be resolved in the future.

Acknowledgments. Both of us are deeply indebted to Professor H. S. Frank for his most helpful encouragement, advice, and friendly criticism during the course of this work. We wish to thank Dr. G. E. Walrafen for providing us with details of his work prior to publication. R. E. V. acknowledges the award of a N.A.T.O. Fellowship from the National Research Council of Canada and W. A. S. is grateful for financial support from the Office of Saline Water, Department of Interior, under Contract 14-01-001-403, which sponsored this work.

---

[29] B. H. Zimm and J. K. Bragg, *J. Chem. Phys.*, **31**, 526 (1959).

[30] H. S. Frank, private communication.

[31] Nemethy and Scheraga (ref 3a) have given an illuminating discussion of why this might be expected to be true.

Photochemistry of Complex Ions. VIII. Photoelectron Production

by W. L. Waltz and Arthur W. Adamson

Department of Chemistry, University of Southern California, Los Angeles, California 90007 *(Received May 9, 1969)*

An investigation of the photolytic production of hydrated electrons from aqueous solutions containing transition metal cyanide complexes and also $IrCl_6^{3-}$ is reported. A transient identified as due to e_{aq}^- has been observed in flash photolysis experiments with aqueous $Fe(CN)_6^{4-}$, $Mo(CN)_8^{4-}$, $W(CN)_8^{4-}$, and $Ru(CN)_6^{4-}$. In addition, steady illumination experiments have been made using N_2O as electron scavenger, to obtain the quantum yields ϕ_{N_2} $(=\phi_{e_{aq}^-})$ for the above complexes and for $IrCl_6^{3-}$. Values ranging from 0.031 to 0.66 are reported, using 254-mμ radiation. In the case of $Mo(CN)_8^{4-}$, ϕ_{N_2} drops to essentially zero with irradiation at greater than 300 mμ. The results are interpreted as confirming previously suggested criteria for systems likely to show photoelectron production. The qualitative product analyses suggest, however, that in addition to the oxidized complex of the same stoichiometry as the starting material, there may also in some cases be produced a partly aquated species in the same or next higher oxidation state as that of the starting material.

Introduction

An interesting and fairly recent observation has been that irradiation of aqueous solutions containing simple anions can lead to the eventual formation of hydrated electrons (see for example ref 1–4). The same type of process has been proposed to occur with $Fe^{2+}(aq)$ in acidic media.[5] The present investigation was stimulated by the additional finding that the same process occurred with $Fe(CN)_6^{4-}$ (ref 3–7) presumably according to eq 1. An immediate question was whether

$$Fe(CN_6)^{4-} \xrightarrow{h\nu} Fe(CN)_6^{3-} + e_{aq}^- \quad (1)$$

ferrocyanide ion was unique among complex ions in showing this phenomenon, and further, whether the process is associated with irradiation of a particular type of absorption band and whether reaction 1 indeed represents the typical primary process.

For the case of $Fe(CN)_6^{4-}$, for which photoaquation is also known to occur (see ref 8), it now seems established that photoaquation and photoelectron production do proceed from different excited states. In particular, irradiation in the region of the d–d absorption bands leads primarily to aquation while irradiation in the region of the first charge transfer (CT) bands leads to reaction 1.

A preliminary answer to the general question was given by a communication from this laboratory[9] which reported photoelectron production to occur with ultraviolet irradiation of aqueous $Mo(CN)_8^{4-}$ and $W(CN)_8^{4-}$. The present paper completes the presentation of these results and adds $Ru(CN)_6^{4-}$ and $IrCl_6^{3-}$ to the group of photoelectron producing complex ions. We have also addressed ourselves to the more difficult secondary questions raised above.

Experimental Section

Materials. The compounds $K_3[IrCl_6]\cdot 3H_2O$ and $K_4[Ru(CN)_6]\cdot 3H_2O$ were obtained commercially (Alfa Inorganic, Inc.) and used as pure substances. Reagent grade (Baker and Adamson) $K_4[Fe(CN)_6]\cdot 3H_2O$ was recrystallized before use. The complex $K_4[Mo(CN)_8]\cdot 2H_2O$ was prepared according to Furman and Miller;[10] $K_4[W(CN)_8]\cdot 2H_2O$, further recrystallized before use, was kindly supplied by Professor C. S. Garner; their purity was determined by redox titration with Ce(IV) solution, using ferron indicator: *Anal.* Calcd for $K_4[Mo(CN)8]\cdot 2H_2O$: Mo, 19.32. Found: 19.5. Calcd for $K_4[W(CN)_8]\cdot 2H_2O$: W, 31.47. Found: 31.8. The visible and ultraviolet spectra of the octacyano complexes agreed well with those previously reported.[11]

The water purification has been described elsewhere.[9] As a double guard against the presence of oxidizable material in the case of the scavenger experiments with N_2O (aside from those with $Fe(CN)_6^{4-}$), potassium persulfate was added to the water before the final distillation. The N_2O was obtained from J. T. Baker Chemical Co. and was purified immediately before its use by means of trap-to-trap distillation.

---

(1) J. R. Huber and E. Hayon, *J. Phys. Chem.*, **72**, 3820 (1968).

(2) J. Jortner, M. Ottolenghi, and G. Stein, *ibid.*, **68**, 247 (1964).

(3) M. S. Matheson, W. A. Mulac, and J. Rabini, *ibid.*, **67**, 2613 (1963).

(4) (a) J. J. Weiss, "The Chemistry of Ionization and Excitation," G. R. A. Johnson and G. Scholes, Ed., Taylor and Francis Publishers, London, 1957, p 17; (b) R. Devonshire and J. J. Weiss, *J. Phys. Chem.*, **72**, 3815 (1968).

(5) P. D. Airey and F. S. Dainton, *Proc. Roy. Soc.*, **A291**, 340, 478 (1966).

(6) S. Ohno, *Bull. Chem. Soc. Jap.*, **40**, 1770, 1776, 1779 (1967).

(7) (a) G. Stein, "Solvated Electron," Advances in Chemistry Series, No. 50, American Chemical Society, Washington, D. C., 1965, p 250; (b) M. Shirom and G. Stein, *Nature*, **204**, 778 (1964).

(8) A. W. Adamson, W. L. Waltz, E. Zinato, D. W. Watts, P. D. Fleischauer, and R. D. Lindholm, *Chem. Rev.*, **68**, 541 (1968).

(9) W. L. Waltz, A. W. Adamson, and P. D. Fleischauer, *J. Amer. Chem. Soc.*, **89**, 3923 (1967).

(10) N. H. Furman and C. O. Miller, "Inorganic Synthesis," Vol. 3, L. F. Audrieth, Ed., McGraw-Hill Book Co., Inc., New York, N. Y., 1950, p 160.

(11) J. R. Perumareddi, A. D. Liehr, and A. W. Adamson, *J. Amer. Chem. Soc.*, **85**, 249 (1963).

Apparatus. The flash photolysis equipment, *ca.* 600 J per flash, is described in detail elsewhere.[9,12] The quartz photolysis cell (1.5 × 15 cm) was mounted between the two flash tubes; transients were observed by following the decay of the absorption of a monitoring light beam which was directed longitudinally through the cell, using a photomultiplier–oscilloscope detector. The monitoring light was restricted to 675 mμ (*ca.* 20 mμ half-width) by means of interference and glass blocking filters (Bausch and Lomb, 680-mμ interference filter and Corning glass filter, CS 2-59).

The 254-mμ photolyses under steady illumination conditions were made with the use of a low pressure mercury lamp (Pen-ray Model 11SC-1, 0.75 watt; Ultra-Violet Products, Inc.), and those at wavelengths greater than 300 mμ, by means of a water cooled high pressure mercury are (General Electric AH-6). Ferrioxalate actinometry was used (see ref 8).

Procedures. Three types of experiments were performed: flash photolyses, to look for e_{aq}^- transients; steady illumination photolyses, with added N_2O scavenger, to obtain quantum yields for e_{aq}^- production; and photolyses to study the nature of the products. In each case the basic glassware consisted of an irradiation vessel or cell and an attached degassing bulb. The entire unit could be attached to a vacuum line, and the concentrations of dissolved oxygen and carbon dioxide in the solutions were reduced to a tolerable level with respect to their electron scavenging by at least three freeze–pumping–thaw cycles before the solutions were delivered into the irradiation cell. In the case of the flash photolyses and many of the other experiments, the unit employed could be cleaned by thorough washing, followed by baking at 500°. Where the irradiation cell also served as a spectrophotometer cell, heat treatment was not possible, and the unit was cleaned by soaking it in hot dilute nitric acid, followed by repeated rinsings (at least ten times) with purified water.

In the case of the N_2O scavenging experiments, a rectangular quartz cell (about 6 × 8 cm in cross section and 1.6 cm deep) was used. The photolysis lamp was placed next to and parallel with the large face of the cell, and the two were mounted together in a water bath held at 25.1 ± 0.2°; stirring was by means of a magnetic bar, teflon coated, for the experiments with $Fe(CN)_6^{4-}$ but then replaced by a glass encased one.

Where a quantitative measurement of nitrogen production was to be made, partially deaerated water was equilibrated with the same pressure of N_2O as was to be used for the final solution; this served as a means of ensuring complete removal of dissolved nitrogen, which tends to be displaced by N_2O.[13] After the degassing of the solution by freeze-thaw cycles, the desired amount of N_2O was dissolved in the solution by establishing the appropriate N_2O pressure (with correction for the partial pressure of water). The solubility was taken to be 3.12×10^{-5} *M*/Torr at 25°.[14]

The collection of nitrogen gas produced during photolysis was by means of an automatic Sprengel pump of the type described by Bartocha, Graham, and Stone.[15] After concentration, the amount of collected gas was measured by means of a gas buret, and the purity of the gas confirmed by mass spectrometric analysis.

Results

Flash Photolysis Experiments. The occurrence of the hydrated electron on flashing deaerated solutions of $Fe(CN)_6^{4-}$, $Mo(CN)_8^{4-}$, and $W(CN)_8^{4-}$ at 1-2 × 10^{-4} *M* has been reported in a previous communication.[9] Under similar conditions, the flash photolysis of a deaerated solution of $Ru(CN)_6^{4-}$ (2 × 10^{-4} *M*) gives rise to a transient signal at 675 mμ of about the same duration and intensity as for ferrocyanide. This similarity and the greatly diminished signal on aeration of the previously deaerated solution indicate the presence of e_{aq}^-.

Using a Pyrex sleeve on the irradiation cell to cut off light below about 300 mμ, no transient could be observed on flashing $Ru(CN)_6^{4-}$. This result, which is also found for the other cyano complexes,[9] suggests that the production of e_{aq}^- is associated with the CT type bands.

In the case of $Mo(CN)_8^{4-}$, the concentration dependence of the intensity and duration of the transient was reported, suggesting this complex also acts as a scavenger for e_{aq}^-.[9] A calculation from the above effect gives a scavenging rate constant of about 5 × 10^8 M^{-1} sec^{-1}. This is now to be compared with the directly measured value, using pulse radiolysis, of 4.0 ± 0.8 × 10^8 M^{-1} sec^{-1} (and 2.0 ± 0.4 × 10^8 M^{-1} sec^{-1} for $W(CN)_8^{4-}$).[16]

Photoelectron Yields from N_2O Scavenging. Because of the difficulty in obtaining a quantitative measure of e_{aq}^- production from the flash experiments, the method of N_2O scavenging was used. The reaction, given by eq 2, has a rate constant of 8.67 × 10^9 M^{-1} sec^{-1} at 25°[17]—large enough that competition from other scavengers should not be important. The nitrogen yields should thus correspond to those for e_{aq}^-.

$$H_2O + N_2O + e_{aq}^- \longrightarrow N_2 + OH + OH^- \quad (2)$$

---

(12) P. D. Fleischauer, Ph.D. Dissertation, University of Southern California, 1968.

(13) D. A. Head and D. C. Walker, *Can. J. Chem.*, **45**, 2051 (1967).

(14) W. S. Watt, Ph.D. Dissertation, University of Leeds, 1962; see F. S. Dainton and S. R. Logan, *Proc. Roy. Soc.*, **A287**, 281 (1965).

(15) B. Bartocha, W. A. G. Graham, and F. G. A. Stone, *J. Inorg. Nucl. Chem.*, **6**, 119 (1958).

(16) Data kindly obtained by Dr. D. Meyerstein, Argonne National Laboratory.

(17) S. Gordon, E. J. Hart, M. S. Matheson, J. Rabani, and J. K. Thomas, *Discussions Faraday Soc.*, **36**, 193 (1963).

Table I: Photoelectron Production from N_2O Scavenging

Complex (Absorption max or shoulder mμ/ extinction coefficient)	k_e,[a] M^{-1} sec^{-1}	Concentrations		% photolysis[b]	Wavelength of irrad. mμ	ϕ_{N_2}	ϵ^0v[c]
		Complex $M \times 10^{-3}$	N_2O $M \times 10^{-2}$				
$Fe(CN)_6^{4-}$ (422/4.73; 322.5/302.0; 270 sh/$\sim 10^3$; 218/24,200; 200/23,700)[d]	$<10_5$[e]	1.5	2.2	12	254	0.66 0.46[f]	−0.356[g]
$Ru(CN)_6^{4-}$ (323/—; 206/9,550; 192/—)[d]	$<10^7$[h]	3.0	2.2	3	254	0.36	−0.86[i]
$Mo(CN)_8^{4-}$ (510 sh/2.7; 431 sh/69; 367.6/170; 308.2 sh/262; 267.4 sh/1350; 240.0/15,540)[j]	4.0×10^8[k]	1.5	2.2	11	254	0.28	−0.726[g]
		1.5	1.6	10	254	0.26	
		1.0	2.2	100	>300	<0.01	
$W(CN)_8^{4-}$ (625.0 sh/1.9; 502.4 sh/4.8; 434.8/-111.0; 370.3/251.0; 303.1 sh/520; 273.7 sh/3000; 249.0/25,060)[j]	2.0×10^8[k]	0.75	2.2	19	254	0.34	−0.457[l]
$IrCl_6^{3-}$ (400 sh/480; $\sim$365/6820; 206/28,000)[m]	9.4×10^9[n]	1.0	2.2	6	254	0.031	−1.02[o]

[a] Rate constants for reaction with e_{aq}^-. [b] Per cent photolysis calculated from the nitrogen yield on the basis that hydroxyl radical oxidized a second molecule of complex. [c] Standard half-cell potential for oxidation. [d] Taken in part from J. J. Alexander and H. B. Gray, *Coord. Chem. Rev.*, **2,** 29 (1967). [e] M. Anbar, *Chem. Commun.*, 416 (1966). [f] A minimum value as small misalignment of the lamp and reaction cell was noticed after the experiment. [g] I. M. Kolthoff and W. J. Tomsicek, *J. Phys. Chem.*, **39,** 945 (1935); *ibid.*, **40,** 247 (1936). [h] M. Anbar, E. M. Fielden, and E. J. Hart, unpublished results cited in M. Anbar and P. Neta, *J. Appl. Radiat. Iso.*, **18,** 493 (1967). [i] D. D. DeFord and A. W. Davidson, *J. Amer. Chem. Soc.*, **73,** 1469 (1951). [j] J. R. Perumareddi, A. D. Liehr, and A. W. Adamson, *ibid.*, **85,** 249 (1963). [k] This work. [l] H. Baadsgaard and W. D. Treadwell, *Helv. Chim. Acta*, **38,** 1669 (1955). [m] Taken in part from C. K. Jørgensen, *Mol. Phys.*, **2,** 309 (1959). [n] M. Anbar and E. J. Hart, unpublished results cited in M. Anbar and P. Neta, *J. Appl. Radiat. Iso.*, **18,** 493 (1967). [o] W. M. Latimer, "Oxidation Potentials," 2nd ed, Prentice-Hall, Inc., New York, N. Y., 1952, p 217.

Our results are summarized in Table I. They are corrected for the retention of nitrogen by the collection system (0.58 μmoles) and for incomplete absorption of light by the actinometer solution at wavelengths greater than 254 mμ. The per cent photolysis has been calculated from the nitrogen yield, assuming that hydroxyl radical oxidized a second molecule of complex. The reaction is a likely one, in view of the high oxidation potential for OH, $\epsilon^0 = 2.0$ v for $OH + e^- = OH^-$ [18] and, moreover, this is known to occur in the cases of $Fe(CN)_6^{4-}$ (see ref 5, 19) and of $Mo(CN)_8^{4-}$.[20] Secondary photolysis is probably not important for the systems involving the cyano complexes, as the products are less absorbing to light around 250 mμ than are the starting complexes (but not at longer wavelengths, as noted further below). In the case of $IrCl_6^{3-}$, however, the photolysis products absorb strongly at the irradiating wavelength, and even with only 6% reaction, some secondary photolysis could have occurred. The tabulated quantum yield value may thus be somewhat low because of such partial diversion of light absorption to products. However, our best result for $Fe(CN)_6^{4-}$ is in agreement with the quantum yield value of 0.66 reported by Airey and Dainton,[5] although less so with other literature values of 1.00[7] and 0.35.[6] Some of these discrepancies may, however, arise from the different methods used in arriving at limiting $\phi_{e_{aq}^-}$ values.

We do believe, however, that our ϕ_{N_2} values are limiting ones, that is, that e⁻(aq) scavenging by N_2O was always essentially complete. Thus in the case of ferrocyanide, it has been shown[5] that the limiting ϕ_{N_2} is reached at a much lower concentration of N_2O than was used here. Also, in the case of our most reactive cyano complex, $Mo(CN)_8^{4-}$, ϕ_{N_2} did not change (within the experimental error estimated at *ca.* 15%) on lowering the N_2O concentration by some 30% (see Table I).

The similar possible complication with the $IrCl_6^{3-}$ system is that the product, $IrCl_6^{2-}$, is a very effective electron scavenger. The reported rate constant is 2×10^{10} M^{-1} sec^{-1} (ref 21) and that for $IrCl_5(H_2O)^-$, although it apparently is not known, could be of this order. Even so, the relative concentrations of N_2O and of products were such that scavenging by these products should not have been important, and our ϕ_{N_2} value should therefore be the limiting one.

Finally, in the experiment with $Mo(CN)_8^{4-}$ using light of wavelength greater than 300 mμ, no evolution of nitrogen could be detected. The upper limit given

---

(18) W. M. Latimer, "Oxidation Potentials," 2nd ed., Prentice-Hall, Inc., New York, N. Y., 1952, p 48.

(19) J. Rabani and M. S. Matheson, *J. Phys. Chem.*, **70,** 761 (1966).

(20) B. K. Sharma, *Can. J. Chem.*, **46,** 2757 (1968).

(21) M. Anbar and E. J. Hart, unpublished data cited in M. Anbar and P. Neta, *J. Appl. Radiat. Iso.*, **18,** 493 (1967).

for ϕ_{N_2} is estimated from the quantum yield found for the terminal blue product, $MoO(OH)(CN)_4^{3-}$ [22] of 0.14 at 363 mμ,[23] as well as from the amount of nitrogen estimated to be retained by the collection system, and hence the maximum nonobserved amount.

Photolysis Products. The nominal reaction for photoelectron production is that given by eq 3, and in

$$ML_n^z \xrightarrow{h\nu} ML_n^{z+1} + e_{aq}^- \qquad (3)$$

the presence of N_2O, the overall process might be expected to be that of eq 4. Were the alternative fate

$$2ML_n^z + N_2O + H_2O \xrightarrow{h\nu} 2ML_n^{z+1} + 2OH^- + N_2 \qquad (4)$$

of OH radicals their combination to give H_2O_2, this last would presumably be oxidized by ML_n^{z+1} to give oxygen, according to eq 5. This last type of

$$2ML_n^{z+1} + H_2O_2 \longrightarrow 2H^+ + O_2 + 2ML_n^z \qquad (5)$$

reaction is evidently not important for our systems as in no case was oxygen detected in the collected gas.

In the case of $Fe(CN)_6^{4-}$, solutions photolyzed under conditions yielding e_{aq}^- showed absorption changes (*e.g.*, a developing peak at 415 mμ) indicating the formation of $Fe(CN)_6^{3-}$. Others[3,5-7] have also found $Fe(CN)_6^{3-}$ to be produced, at least as the principal product. Analysis of our observed spectral changes gives a ratio of $Fe(CN)_6^{3-}$ to nitrogen of 1.6:1, however, instead of the 2:1 ratio expected from eq 4 and found by others.[5] We have not been able to identify the source of the discrepancy, but as a precaution, potassium persulfate was added to the water, prior to its final distillation, in the work with the other systems. The intent was to make doubly sure that trace impurities oxidizable by hydroxyl radical would be eliminated, although no other evidence for such was actually found.

Irradiation of $Ru(CN)_6^{4-}$ at 254 mμ in the presence either of air or of N_2O led to an increase in absorption at 310 mμ, due to a developing maximum, and a decrease at shorter wavelengths. This change in absorption spectrum is not that anticipated for $Ru(CN)_6^{3-}$, which is reported to show four absorption bands in the region of 300–455 mμ, rather than a single one.[24] Furthermore, addition of saturated silver nitrate solution did not give the red-brown precipitate reported to be characteristic of $Ru(CN)_6^{3-}$, although a white precipitate derived from $Ru(CN)_6^{4-}$ did form.[24] As a minimum conclusion, we feel that $Ru(CN)_6^{3-}$ is not the sole photolysis product.

Complications in product analysis were also found in the case of $Mo(CN)_8^{4-}$. Here, $Mo(CN)_8^{3-}$ should definitely be stable over the period of the experiments, yet the final spectra of solutions of $Mo(CN)_8^{4-}$ irradiated at 254 mμ in the presence of N_2O are quite similar to the initial one. Further, in separate experiments, 254-mμ irradiation of 1×10^{-3} M solutions to about 10% photolysis is found to lead to a prompt general increase in absorption in the 300–550-mμ region. Yet on standing, the absorption returned to essentially that of the original solution, within a several hour period at 25°. Analysis of the promptly produced spectrum determined that $Mo(CN)_8^{3-}$ is at least not the sole product. However, from the measured ϕ_{N_2}, the increased absorption is such as to require the product species to have an extinction coefficient greater than about 500 M^{-1} cm^{-1} in this wavelength region. Such high absorption is more indicative of a Mo(V) than of a Mo(IV) compound (compare, for example, the spectra of $Mo(CN)_8^{4-}$ and $Mo(CN)_8^{3-}$, ref 11). In aerated solutions, less initial increase in absorption occurs. Prolonged irradiation leads to some decomposition, as evidenced by a general decrease in absorption.

The behavior of 254-mμ irradiated solutions of $W(CN)_8^{4-}$ is similar to that for solutions of $Mo(CN)_8^{4-}$. There is a general increase in absorption in the 310–400 mμ region, with the absorption maximum decreasing from 370 mμ to shorter wavelengths. Again, $W(CN)_8^{3-}$ should be stable under our conditions, yet there is a dark return towards that of the original solution. The return is slower than that with $Mo(CN)_8^{4-}$ systems, taking about a day at 25°, and is less complete. The behavior of aerated solutions is now about the same as those containing N_2O. Although the direction of shift of the 370-mμ maximum, and the molar absorption coefficient of the product, estimated from ϕ_{N_2}, are similar to those expected for $W(CN)_8^{3-}$ as product, there are quantitative discrepancies. This species thus could not have been the sole product.

Finally, the 254-mμ photolysis of N_2O containing solutions of $IrCl_6^{3-}$ led to spectral changes consistent with the presence of both $IrCl_6^{2-}$ and $IrCl_5(H_2O)^-$ (or $IrCl_5(OH)^{2-}$) (see ref 25 and 26), with the latter the more abundant product. However, $IrCl_6^{2-}$ is reported to be photosensitive,[27] and the presence of pentachloroiridium(IV) species could be attributed to secondary photolysis. In any event, the total Ir(IV) content of the irradiated solutions could definitely be established, and the ratio of Ir(IV) to N_2 produced was close to 2:1. Reaction 3 may well be essentially correct for this system. Finally, the spectra of the irradiated solutions are relatively stable, showing only small dark changes over a week's period.

---

[22] S. J. Lippard and B. J. Russ, *Inorg. Chem.*, 6, 1943 (1967).

[23] A. W. Adamson and J. R. Perumareddi, *ibid.*, 4, 247 (1965).

[24] D. D. DeFord and A. W. Davidson, *J. Amer. Chem. Soc.*, 73, 1469 (1951).

[25] I. A. Poulsen and C. S. Garner, *ibid.*, 84, 2032 (1962).

[26] C. K. Jørgensen, *Mol. Phys.*, 2, 309 (1959).

[27] T. P. Sleight and C. R. Hare, *Inorg. Nucl. Chem. Lett.*, 4, 165 (1968).

A general observation for all of the systems containing N_2O is that an increase in pH occurs on irradiation. However, because of the low concentration that would be present, it was not possible to determine if this pH change is due to released cyanide ion in some cases, or is entirely due to hydroxide ion produced by reaction 4.

Discussion

Photoelectron production by transition metal coordination compounds has been a rare phenomenon; the only previously reported case being that of $Fe(CN)_6^{4-}$. We believe the present combined flash photolysis and N_2O scavenging results to certify not only the similar behavior of other cyano complexes, but also, with the example of $IrCl_6^{3-}$, to show that the process is not unique to complex cyanides. It may, in fact, eventually prove to be quite common for transition metal complexes.

It was noted in our earlier communication[9] that in selecting systems for study, we were guided by certain criteria. These are (a) that the irradiation should be in the wavelength region of a CT band of the complex; (b) that there exist a reasonably stable complex of the same stoichiometry and one higher valence state; (c) and that there should not exist a stable valence state of the same stoichiometry and one lower oxidation number.

Considering the reasons in reverse order, (c) applies primarily to flash photolysis studies. In order to observe the e_{aq}^- transient with our equipment, it is essential that scavenging be minimized, and we feel that the existence of an easily attainable lower valence state of the complex would ensure that excessive scavenging would occur. Criterion (b) follows from energetic considerations. If the next higher valence state is not known, at least to the extent of being observable as an electrode reaction, we considered it doubtful if light quanta corresponding to wavelengths accessible in aqueous media would have sufficient energy to bring about reaction (3); implied in this reasoning is also that the one higher oxidation state should be stable in the same stoichiometry as the parent complex, as otherwise the activation energy for ejection of an electron might be excessively large relative to those of other possible photochemical reaction modes.

Criterion (b) can be put on a more quantitative basis, in terms of the actual systems studied. The estimated standard oxidation potential for e_{aq}^- is about 2.5 V,[28] so that in combination with the standard potentials given in Table I, that for reaction 3 falls in the range of -3 to -3.5 V. The energy requirement for reaction 3 should be greater than the reversible standard free energy, and the indicated required wavelength of 300–350 mμ is undoubtedly close to a maximum one. The data of Table I are suggestive on this point, in that there is an approximate inverse correlation between ϕ_{N_2} and ϵ^0 for the $ML_n^z - ML_n^{z+1}$ couple. An additional aspect that may influence the quantum yield is the overall charge on the complex. The system, $Fe^{2+}(aq)$, has an oxidation potential close to that of $Mo(CN)_8^{4-}$; however, the quantum yield reported for photoelectron production with 254 mμ radiation is about four times smaller than that for $Mo(CN)_8^{4-}$.[5] A high overall negative charge may thus facilitate the formation of e_{aq}^-.

The first criterion followed from a general conclusion that we have reached, namely that the photochemistry of coordination compounds derives usually from specific excited state chemistries rather than from hot ground state molecules produced during deexcitation (see ref 8 and 29). We thus associate photoelectron production with an excited state in which electron density has moved either towards the periphery of the complex or into the adjacent solvent. Absorptions of this type have been termed charge transfer to ligand (CTTL) or charge transfer to solvent (CTTS) (see ref 8). Conversely, if photoreduction of the central metal ion occurs, as with many Co(III) complex ammines, the band involved would by this criterion be considered to be charge transfer to metal (CTTM) in type. Where ligand field or d–d bands are irradiated, the general observation so far has been that substitution type reactions predominate.[8] We thus do assume that the electronic nature of an excited state is qualitatively deducible from that of the chemical reaction to which the state is precursor; criterion (a) above is simply an application of this assumption.

From the spectroscopic and theoretical point of view, absorption bands which lie in the blue or ultraviolet, which are too intense reasonably to be ascribed to d–d transitions, and which are not present in the isolated ligand nor can be attributed to a chelate ring system, are more or less automatically called CT. Those for the Co(III) amines have been labeled CTTM on qualitative theoretical as well as other grounds (see ref 30, for example), while the intense ultraviolet bands of $Fe(CN)_6^{4-}$ have been viewed as either CTTL or CTTS in nature. The CTTL assignment has been argued as the better one in view of the lack of major solvent affect on the spectrum.[6] No specific treatment of the CT bands of $Mo(CN)_8^{4-}$ or $W(CN)_8^{4-}$ appears extant;[8] we regard them as CTTL or CTTS in view of their photochemistry. A tentative assignment of the CT bands of $IrCl_6^{3-}$ has been made as involving considerable ligand to metal character.[26] Our observation

---

(28) M. S. Matheson, "Solvated Electron," Advances in Chemistry Series No. 50, American Chemical Society, Washington, D. C., 1965, p 47.

(29) A. W. Adamson, *J. Phys. Chem.*, 71, 798 (1967).

(30) T. M. Dunn, "Modern Coordination Chemistry," J. Lewis and R. G. Wilkins, Ed., Interscience Publishers, Inc., New York, N. Y., 1960, p 294.

of photoelectron production at least suggests that a theoretical reexamination would be desirable.

Returning to criterion (a) above, it does seem correct that photoelectron production is confined to CT type excited states. Longer wavelength irradiation of $Fe(CN)_6^{4-}$ and of $Mo(CN)_8^{4-}$ leads to aquation rather than e_{aq}^- production.[31-33] Our present observation in the case of $Mo(CN)_8^{4-}$ is that ϕ_{N_2} drops to the vanishing point if the irradiation is at wavelengths above 300 mμ.

The remaining aspect of the present investigation concerns the nature of the immediate photochemical act. While the spectra of the photolyzed solutions indicated the presence of oxidized complex, with the possible exception of the $Fe(CN)_6^{4-}$ system, species in addition to ML_n^{x+1} of eq 3 generally seemed to be present. In the case of $IrCl_6^{3-}$, the products clearly are $IrCl_6^{2-}$ and $IrCl_5(H_2O)^-$; with the cyano complexes, species of the type $ML_{n-1}(H_2O)^{x+2}$ or $ML_{n-1}(H_2O)^{x+1}$ could have been present, with some post irradiation redox reaction with the released cyanide ion. We were unable to determine, however, if the production of such alternatively ligated forms occurs as a primary step, through secondary photochemical reactions, or possibly through secondary thermal reactions with radical species such as OH. Their formation by ordinary thermal aquation reactions can, however, definitely be ruled out.

Acknowledgments. We wish to thank Dr. P. D. Fleischauer and Mr. P. Natarajan for their technical assistance; and Mr. T. Meyers for help with the mass spectral analyses and Dr. D. Meyerstein for performing the pulse radiolysis experiments. Helpful discussions with Professors A. B. Burg and W. K. Wilmarth are acknowledged with appreciation. Finally but not least, we are grateful for support from the U. S. Army Research Office, through Contract DA-31-124-ARO-D-343.

---

(31) S. Ohno, *Bull. Chem. Soc. Jap.*, **40**, 1765 (1967).

(32) S. Emschwiller and J. Legros, *Compt. Rend.*, **261**, 1535 (1965).

(33) L. Moggi, F. Bolleta, V. Balzani, and F. Scandola, *J. Inorg. Nucl. Chem.*, **28**, 2589 (1966) (and preceding papers); W. Jacob, A. Samotus, Z. Stasicka, and A. Golebiewski, *Z. Naturforsch.*, **21B**, 819 (1966) (and preceding papers).

Ultrasonic Investigation of the Conformal Changes of Bovine Serum Albumin in Aqueous Solution[1a]

by L. W. Kessler[1b] and F. Dunn

Bioacoustics Research Laboratory, University of Illinois, Urbana, Illinois 61801 (*Received May 13, 1969*)

The excess ultrasonic absorption and the speed of sound were measured in aqueous solutions of bovine serum albumin (a globular protein which undergoes marked configurational change with pH) at 20° over the frequency range 0.3 to 163 MHz and over the pH range 2.3 to 11.8. A sharp increase in the excess absorption is found outside the range $4.3 < \mathrm{pH} < 10.5$. The effect is reversible throughout this range and is more pronounced at the lower frequencies. The increase in the absorption below pH 4.3 appears to be correlated with the intermediate N-F′ transition discussed by Foster and the change above pH 10.5 is thought to correspond with expansion of the molecule. At neutral pH, the ultrasonic absorption spectrum and the velocity dispersion are indicative of a broad distribution of relaxation processes. The magnitude of the ultrasonic absorption over the range $4.3 < \mathrm{pH} < 10.5$ is attributed to the perturbation of the solute–solvent equilibrium by the sound wave. Based on data at 20°, between 2.4 and 50 MHz, the frequency spectrum of the absorption increase at pH 3.5 over that at pH 7.0 may be described by a single relaxation process whose characteristic frequency is 2.2 MHz. Based on measurements of the velocity of sound at pH 7.0, the bulk modulus of BSA has been found to be 3.86×10^9 n/m^2.

Introduction

The spatial configuration assumed by a macromolecule within the environment of solvent molecules plays an important role in determining the hydrodynamic properties of the solution,[2a] as well as the chemical activity of the solute molecule. It appears that in cellular processes, for example, the transport of molecules across the protoplasmic membrane is related, in some complex manner, to the spatial geometry of the transported molecule as well as to the spatial arrangement of the lipoprotein complex constituting the cell membrane.[2b] Thus, it is within the realm of profitable investigation to explore methods which have the potential of providing information about molecular configuration and changes in molecule structure. Ultrasonic techniques have already been employed successfully to observe the dynamic equilibrium between multiple isomeric forms of molecules and to arrive at more complete kinetic descriptions of chemical and structural reactions whose relaxation times are comparable to the period of the ultrasonic wave.[3,4] The adiabatic propagation of a longitudinal acoustic wave through a fluid medium results in time-varying, localized changes in pressure, density, and temperature. Thus, the wave motion may perturb molecular equilibria at rates which depend upon the sound frequency.[5] For a nonideal fluid, this leads to a time lag between an applied pressure and the ensuing change in density. Consequently, molecular energy level populations are perturbed at the expense of acoustic wave energy, and the process is referred to as absorption. Ultrasonic absorption spectroscopy is useful for studying fast reactions having rate constants over the range from 10^{-9} sec to 10^{-4} sec.[6] The reader unacquainted with ultrasonic technology may wish to consult ref 4 and 6 for details of theory and experimental methods for determining absorption and velocity, and for current reviews of measurements on liquids, including biological media.

Only a few biologically important macromolecules have been subjected to thorough ultrasonic examination. For both hemoglobin,[7] a globular protein, and dextran,[8,9] a random coil molecule, the interaction between solvent and solute is probably the principal mechanism of acoustic absorption. The pressure variation associated with the sound wave perturbs the equilibrium distribution of solvent molecules that are weakly bonded to the solute, and, since rearrangement

---

(1) (a) Portions of this work were extracted from the Thesis submitted by the first-named author in partial fulfillment of the requirements for the Ph.D. degree in Electrical Engineering, University of Illinois, 1968. (b) Research Department, Zenith Radio Corporation, 6001 W. Dickens, Chicago, Ill. 60639.

(2) (a) C. Tanford, "Physical Chemistry of Macromolecules," John Wiley & Sons, Inc., New York, N. Y. (1961); (b) A. C. Giese "Cell Physiology," W. B. Saunders Co., Philadelphia, Pa., 1962.

(3) J. Lamb "Physical Acoustics," Vol. II, Part A, W. P. Mason, Ed., Academic Press, New York, N. Y., 1965, Chapter 4.

(4) M. Eigen and L. deMayer, "Technique of Organic Chemistry," Vol. 8, Part 2, S. L. Friess, E. S. Lewis, and A. Weissberger, Ed., Interscience Publishers, New York, N. Y., 1963.

(5) K. F. Herzfeld and T. A. Litovitz, "Absorption and Dispersion of Ultrasonic Waves," Academic Press, New York, N. Y., 1959.

(6) See for example, F. Dunn, P. D. Edmonds, and W. J. Fry, *Absorption and Dispersion of Ultrasound in Biological Media*, in "Bioelectronics," H. P. Schwan, Ed., McGraw-Hill Book Co., Inc., New York, N. Y., 1969.

(7) E. L. Carstensen and H. P. Schwan, *J. Acoust. Soc. Amer.*, **31**, 305 (1959).

(8) L. W. Kessler, M.S. Thesis, Univ. of Illinois, Urbana, Ill., 1966.

(9) S. A. Hawley and F. Dunn, *J. Chem. Phys.*, **50**, 3523 (1969).

of the solvent molecules does not occur instantaneously, absorption results. Of those biomacromolecules studied, hemoglobin can be made to undergo configurational changes,[2a] although ultrasonic spectroscopy has not been employed to study them. Polyglutamic acid, a synthetic polypeptide that can undergo a configurational change from helix coil to random coil in aqueous solution, has been examined ultrasonically by several investigators.[10,11,12] Schwarz[10] has shown that the ultrasonic absorption shows a sharp maximum at the midpoint of the helix coil transition and that theoretically this effect should be most pronounced at the relaxation frequency. According to his estimated value of 10^{-7} sec as the mean relaxation time at the midpoint of the transition, the mean relaxation frequency is 1.6 MHz. Lewis,[11] on the other hand, was not able to observe the absorption maximum corresponding to the helix coil transition and attributed the observed absorption to solvation phenomena. Saksena, *et al.*[12] have observed the absorption maximum but have calculated that the relaxation time is smaller than that predicted by Schwarz by a factor of approximately 10. Zana, *et al.*,[13] have investigated the absorption in nonaqueous solutions of several synthetic polypeptides that were made to undergo helix coil transitions, and, although the results obtained do not indicate that the helix coil transition is the principal mechanism of absorption, definite changes in the absorption are observed with changes in the molecular configuration.

Bovine serum albumin, a globular protein which undergoes a complex conformal change with pH in aqueous solution, was chosen for study because many of its physical and chemical properties have been rather well characterized by numerous investigations.[14] Briefly, the bovine serum albumin molecule has a compact structure within the pH range $4.3 < \text{pH} < 10.5$ and an expanded structure outside that region. Although the nature of the conformal change has not yet been determined exactly, it is reasonable that the unfolding of the BSA molecule which results in the expanded structure may somehow involve a helix–coil transition. This is suggested by optical rotation and dispersion experiments in which the apparent helix content of bovine serum albumin changes with pH.[14]

Experimental Section

Bovine serum albumin (BSA) Fraction V powder, Lot 82268, was obtained from General Biochemicals and maintained at −7° until used. Fraction V grade material was used for this investigation since it is more readily available than the purest grade in the large quantities necessary for this investigation. The solution was prepared by placing the BSA on the surface of a quantity of singly distilled water sufficient to prepare a solution of concentration 0.04 to 0.1 g/cc. The flask was then placed in the refrigerator until mixing of the two components was complete, usually accomplished overnight. The solution was filtered twice through type A glass fiber filters (Gelman Instrument Co.) in order to remove foreign particles larger than 0.3μ diameter, and after filtration the solution was maintained at 8° until used. Generally, the acoustic experiments were started within a few hours after the solutions were prepared. The concentration of each protein solution was determined with a Beckman Model DU spectrophotometer using the extinction coefficient determined by Cohn, *et al.*,[15] *viz.*, $[\mathrm{E}]_{1\,\mathrm{cm}}{}^{1\%} = 6.6$ at 280 mμ.

The pH of each solution was changed in steps ranging from 0.2 to 0.5 pH unit by the addition of known quantities of standard volumetric solutions of HCl and KOH. During this procedure, the solutions were stirred gently with a magnetic stirring bar to minimize pH gradients. Measurements of pH were made to within ±0.1 pH unit, in the temperature range 19 to 23°, with a Beckman Model H-2 glass electrode pH meter which was standardized with accurate buffer solutions at pH 4, 7, and 9. Ultrasonic absorption and velocity measurements were not begun on the BSA solutions until at least 15 min after a pH change was made, which allowed sufficient time for the temperature to reach the desired value and also allowed the BSA molecules to reach configurational equilibrium.[16] The titrations were carried out in two stages using separate solutions, *i.e.*, the pH was varied from neutral to about 2.3 for one set of solutions and from neutral to about 11.8 for the second set of solutions. This was considered the maximum pH range allowable to avoid possible damage to the sample chamber. For a particular set of experiments, the neutral solution was examined first, and then, after the investigation at either pH 2.3 or pH 11.8 the solution was titrated back to neutral for comparison with the first measurement.

The amplitude of a plane, progressive sinusoidal wave decays exponentially as it propagates through a lossy, homogeneous, infinitely extended medium according to

$$P(x,t) = P_0 \exp(-ax) \exp i(\omega t - kx) \qquad (1)$$

where P is the instantaneous value of the acoustic pressure amplitude as a function of distance x and time t, a is the absorption coefficient, ω is the angular frequency, and k is the wave number. The pulse technique employed in this study to measure the absorption coefficient in liquids simulates the free field condition

---

(10) G. Schwarz, *J. Mol. Biol.*, **11**, 64 (1965).

(11) T. B. Lewis, Ph.D. Thesis, M.I.T., Cambridge, Mass., 1965.

(12) T. K. Saksena, B. Michels, and R. Zana, *J. Chim. Phys.*, **65**, 597 (1968).

(13) R. Zana, R. Cerf, and S. Candau, *ibid.*, **60**, 869 (1963).

(14) J. F. Foster "Plasma Proteins," F. W. Putnam, Ed., Academic Press, New York, N. Y., 1960, Chapter 6.

(15) E. J. Cohn, W. L. Hughes, and J. H. Weare, *J. Amer. Chem. Soc.*, **69**, 1753 (1947).

(16) C. Tanford, J. G. Buzzel, D. G. Rands, and S. A. Swanson, *ibid.*, **77**, 6421 (1955).

expressed by eq 1 for finite sample sizes, provided that the pulse length in the medium is short compared with the acoustic path length. In addition, the error in the absorption coefficient due to the spectrum of frequencies associated with a pulse train is negligible if the pulse is at least $30\pi/\omega$ sec in length.[17]

Two techniques were employed to measure the absorption coefficient to within 5% over the frequency range from 0.3 to 163 MHz. The first technique,[18] an automated version of that described by Pellam and Galt,[17] can be employed for frequencies greater than 9 MHz, for the transducer diameter available (1 in.), where diffraction effects are small. Over the frequency range from 9 to 69 MHz, two matched 3 MHz fundamental frequency X-cut quartz transducers are set parallel and coaxial to each other in the liquid to be studied. Each transducer is edge mounted with its front face in direct contact with the liquid and its back face exposed to an air-filled cavity. One transducer emits pulses of ultrasonic energy while the other transducer detects acoustic pulses. The acoustic path length is varied by displacing one transducer relative to the other at constant velocity. The amplitude of the received acoustic pulse varies according to eq 1 (where x is the instantaneous acoustic path length) and the electrical pulse from the receiving transducer is recorded on a logarithmic chart recorder whose paper displacement is slaved to the moving transducer. Over the frequency range 75 to 165 MHz, a pair of 15 MHz fundamental, X-cut quartz transducers bonded to fused quartz delay rods are substituted for the 3 MHz transducers. Velocity measurements are performed by electronically measuring the length of time required to change the acoustic path length by 100 wavelengths of sound. Details of this system can be found in ref 18 and 19.

At frequencies below 9 MHz, the technique described above for measuring the absorption coefficient and velocity of sound requires unreasonably large diameter transducer elements to minimize diffraction effects. These effects arise because the requirement of plane waves, as described by eq 1, is only approximated by a finite size transducer and the approximation deteriorates as the wavelength of sound approaches the diameter of the transducer. A comparison technique, described by Carstensen,[20] in which the acoustic properties of the sample liquid are determined relative to those of a known reference liquid, minimizes diffraction effects. In the present study, water served as a convenient reference liquid since its absorption coefficient and velocity of sound have already been determined accurately.[21,22] Two compartments of a double chamber tank are separated by an acoustically transparent window and are filled, respectively, with the reference liquid and the sample liquid. Two 3 in. diameter 0.3 MHz fundamental frequency ceramic transducers are placed in the respective chambers and face each other through the window. The transducers are mounted coaxially parallel and are supported a fixed distance apart on a sliding carriage. The acoustic measurements are made by varying the relative amounts of sample and reference liquids in the acoustic path by moving the carriage along the axis of sound propagation. If the velocity of sound in the sample liquid is within a few per cent of that in the reference liquid, then varying the relative amounts of each within the acoustic path produces little change in the acoustic path length and consequently only a negligible diffraction effect. Details of this technique are to be found in ref 19 and 20.

Results

The ultrasonic absorption in aqueous solutions of BSA was measured as a function of pH from 2.3 to 11.8 at six frequencies ranging from 2.39 MHz to 50.25 MHz at 20°. The data are presented in terms of the excess frequency-free absorption per unit concentration, *i.e.*

$$A = \Delta a/cf^2 \qquad (2)$$

where c is the concentration of solute in grams per cubic centimeter of solution and Δa is the difference in the absorption coefficients between the solution and the solvent. The absorption coefficient of the solvent found by Pinkerton[21] has been used to evaluate Δa. In aqueous solutions of BSA, the excess absorption has been shown to increase linearly with concentration at least to about 0.1 g/cc in the pH region where expansion of the molecule is known not to occur,[18] Figure 1.

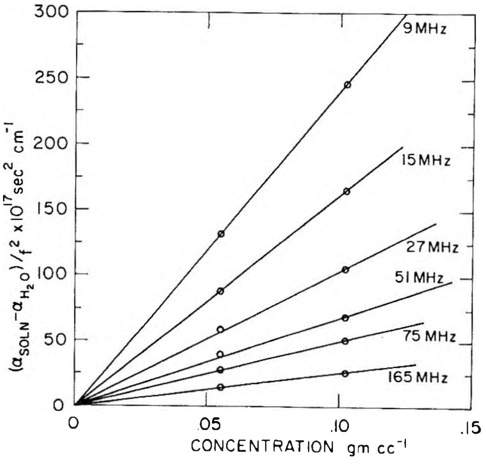

Figure 1. Concentration dependence of acoustic absorption of BSA at 20.0° in an aqueous solution of 0.15 *M* KCl.

---

(17) J. R. Pellam and J. K. Galt, *J. Chem. Phys.*, **14,** 608 (1946).

(18) S. A. Hawley, Ph.D. Thesis, Univ. of Illinois, Urbana, Ill., 1966.

(19) L. W. Kessler, Ph.D. Thesis, Univ. of Illinois, Urbana, Ill., 1968.

(20) E. L. Carstensen, *J. Acoust. Soc. Amer.*, **26,** 858 (1954).

(21) J. M. M. Pinkerton, *Proc. Phys. Soc.*, **B62,** 129 (1949).

(22) M. Greenspan and C. E. Tschiegg, *J. Acoust. Soc. Amer.*, **31,** 75 (1959).

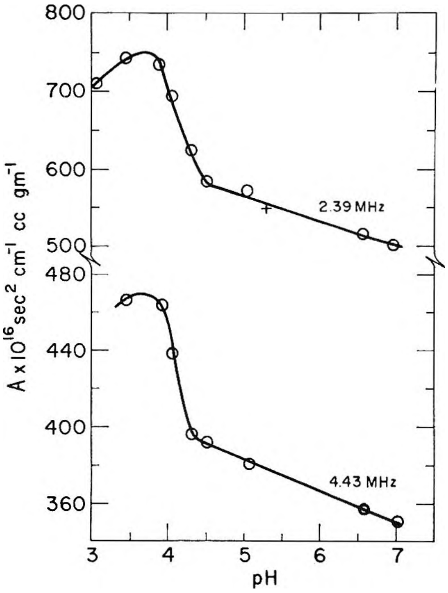

Figure 2. Ultrasonic absorption titration of BSA in an aqueous solution at 19.9° (+ indicates back titration).

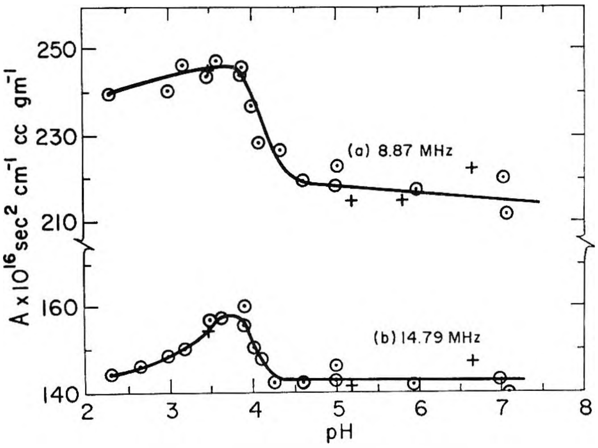

Figure 3. Ultrasonic absorption titration of BSA in an aqueous solution at 20.0° (+ indicates back titration).

This implies that contributions to the absorption arising from possible intermolecular interactions are not important, and that in this region, as far as the ultrasonic wave is concerned the solution may be considered equivalent to one which is infinitely dilute.

The excess frequency-free absorption is plotted as a function of pH for the acid titration in Figures 2, 3, and 4 and it is clear that within experimental error the ultrasonic absorption changes reversibly with changes of pH. This is reasonable on the basis of the previously observed reversibility of other properties of BSA in aqueous solution over the same pH range.[14] The very small effect on the absorption of the formation of KCl as a result of back titration[19] has been corrected in all the figures. As the BSA solution is made acidic, the absorption increases by a small amount until the pH reaches about 4.3. Beyond this point, there is an abrupt increase in A which is markedly greater at lower frequencies than at higher frequencies. The velocity of sound in the solution was also measured as a function of pH at 2.39 MHz and the result for the acid titration is presented in Figure 5. In this figure, Δc_n is the difference between velocity of sound in the solution and that in the solvent, divided by the solute concentration. For the purpose of this calculation, changes in the velocity of sound in water were assumed to be negligible with changes of pH compared with changes in the velocity of sound in the solution.[19] The resulting curve exhibits a minimum at about pH 4.1 which is also the approximate midpoint of the abrupt absorption increase.

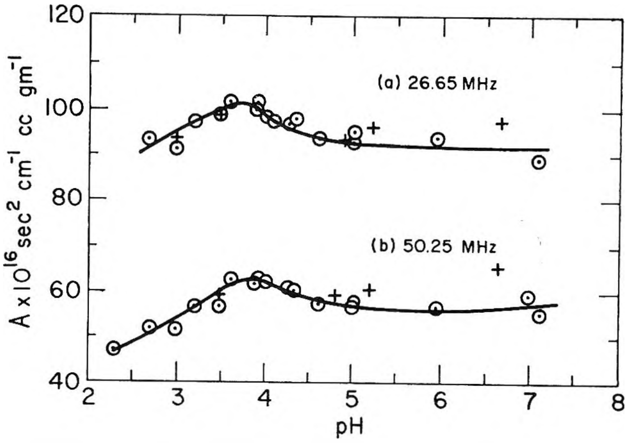

Figure 4. Ultrasonic absorption titration of BSA in an aqueous solution at 20.0° (— indicates back titration).

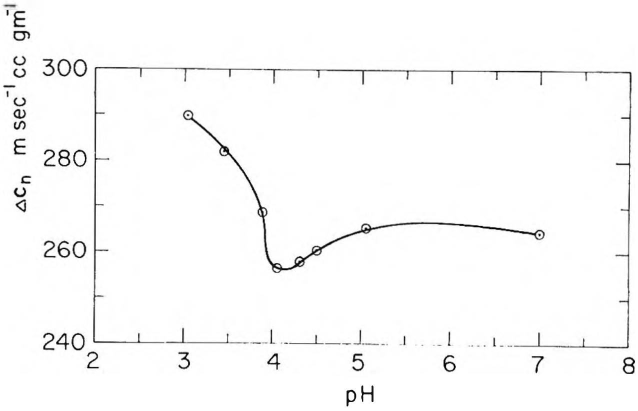

Figure 5. Ultrasonic velocity titration of BSA in an aqueous solution at 19.9° (BSA concentration 0.092 g/cc).

Ultrasonic titration on the alkaline side shows a somewhat greater increase in the absorption coefficient than at acid pH, an example of which is shown in Figure 6. As the alkalinity of the solution is increased from pH 7, the variation of A with pH is small up to about pH 10 where A increases rapidly. The alkaline effect is also reversible over the pH range investigated. Further, as with the acid titration, the effect is more pronounced at lower frequencies. The velocity of sound, on the other hand, was found to increase monotonically with increasing alkalinity.

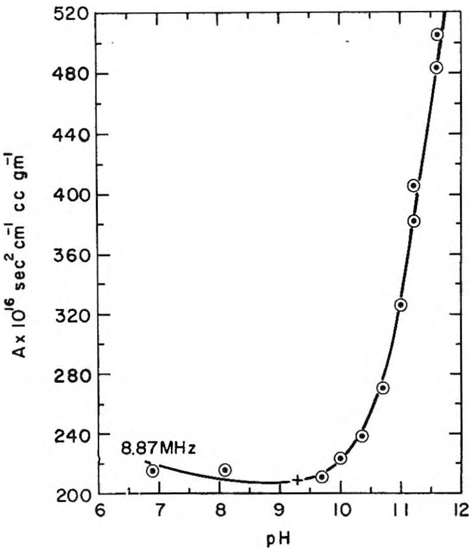

Figure 6. Ultrasonic absorption titration of BSA in an aqueous solution (+ indicates back titration).

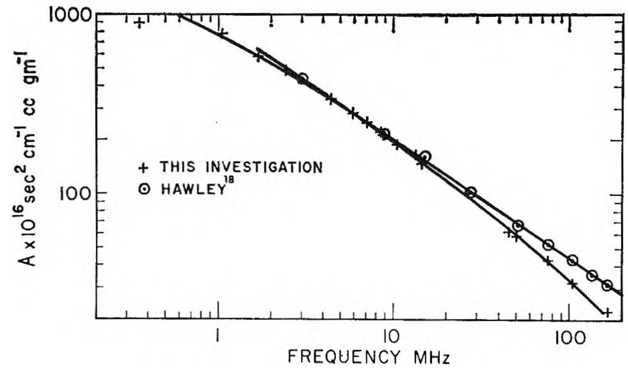

Figure 7. Ultrasonic absorption spectrogram at pH 7 and 20.0°.

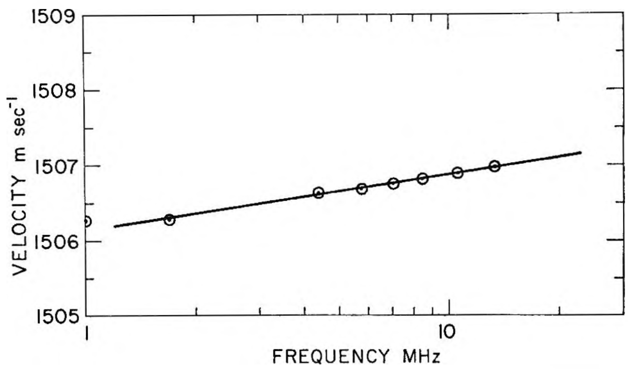

Figure 8. Velocity dispersion in an aqueous solution of BSA at pH 7 and 19.9°. BSA concentration, 0.092 g/cc. The velocity of sound in pure solvent at 19.9° is 1482.35 m/sec.

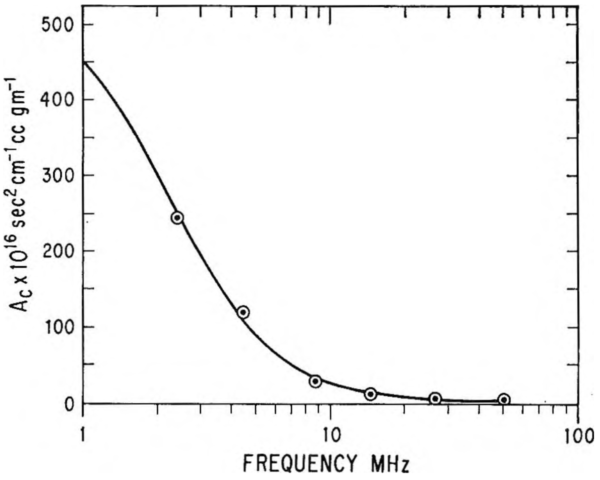

Figure 9. Spectrogram of absorption difference between pH values 3.5 and 7.0, compiled from data in Figures 2, 3, and 4.

The frequency dependence of A was measured over the frequency range from 0.3 to 163 MHz by the techniques indicated above and a composite of all the data, at neutral pH, is shown in Figure 7. Over the frequency range covered, a broad distribution of relaxation times may be necessary to characterize the absorption behavior. The presence of velocity dispersion further indicates the relaxational behavior of the absorption over this frequency range, Figure 8. In order to relate changes in the relaxational properties of BSA in aqueous solution with molecular conformal changes, the variation of the absorption coefficient as a function of frequency is examined. It is evident from Figures 2-6 that there are two sharp transition regions, one which is completely delineated in the acid pH region, and a second, in the alkaline pH region, which extends beyond the range of these measurements. If the following definition is made, $A_c = A(\text{pH } 3.5) - A(\text{pH } 7.0)$, then the frequency spectrum of A_c is described, approximately, by a single relaxation process as shown in Figure 9. The best fit single relaxation curve was determined by the method of "least squares" for an equation of the form

$$A_c = \frac{a_c}{1 + (f/f_0)^2} + b_c \qquad (3)$$

where a_c, b_c, and f_0 are constants, f_0 being the characteristic relaxation frequency. For eq 3, f_0 = 2.2 MHz, a_c = 543 × 10^{-16} sec^2 cc/cm g and b_c = 2.2 × 10^{-16} sec^2 cc/cm g.

The absorption coefficient was determined as a function of temperature from 15 to 38° and at two pH values *viz.*, 7.0 and 2.9. Higher temperatures were avoided since above 40° irreversible denaturation of the molecule can occur.[23] For absorption due to either shear or bulk viscosity, η, the temperature dependence of the absorption coefficient is given by Eyring[24] as

$$\alpha = \frac{2\omega^2}{3\rho_0 c_0^3}\left[\eta \exp\frac{\Delta F}{RT}\right] \qquad (4)$$

---

(23) J. F. Foster and J. T. Yang, *J. Amer. Chem. Soc.*, **77**, 3895 (1955).

(24) H. Eyring, *J. Chem. Phys.*, **4**, 263 (1936).

where ρ_0 and c_0 are the density of the medium and velocity of sound respectively, ΔF is the activation energy, R is the gas constant and T is the absolute temperature. This relation is valid if the period of the acoustic wave does not approach a characteristic time constant associated with a relaxation process. Table I lists the apparent activation energies determined for a solution of 0.05 g/cc of BSA in water. In all cases, the apparent activation energy is less than that for pure water. At pH 7.0, ΔF is independent of frequency, within the experimental error, as it is for water. However, for low pH values, ΔF is a strong function of frequency which indicates the presence of additional relaxation phenomena.

Table I: Apparent Activation Energy of BSA in Aqueous Solution (Concn, 0.05 g/cc)

pH	f(MHz)	ΔF, kcal/mol
7.0	8.87	2.19
7.0	14.79	2.23
7.0	26.65	2.26
2.9	8.87	0.671
2.9	14.79	1.35
2.9	26.65	1.70
Water	All	4.23

Discussion

In order to account for the magnitude of the excess absorption coefficient at neutral pH, quantitative consideration is given to (1) dynamic shear viscosity of prolate ellipsoidal molecules in solution; (2) frictional losses associated with relative motion between the solute and solvent particles; (3) scattering of the acoustic waves by the solute particles; and (4) mode conversion of the longitudinal acoustic wave into rapidly decaying transverse acoustic waves at the solute–solvent interfaces. Such consideration[19] shows that, collectively, the above mechanisms of absorption account for only a small percentage of that observed. An investigation of the dynamic shear viscoelasticity of BSA in glycerol and water mixtures was reported by Allis and Ferry[25] in the frequency range from 0.04 to 400 Hz and the dynamic shear viscosity observed did not agree with theories of rotational relaxation. It is suggested by these authors that the origin of the viscoelasticity in BSA does not arise from orientation of the molecule by the shear stresses but primarily from an intramolecular flexibility not otherwise observable. However, a reexamination of the contribution of shear viscosity, taking into account this discrepancy, does not alter significantly the results presented here.

As a result of the above considerations it is concluded that the structural (bulk) viscosity of the solution is the principal factor responsible for the ultrasonic absorption. The distribution of relaxation times and the velocity dispersion indicate structural relaxation[26] and the same mechanism is thought to be present in aqueous solutions of other biomacromolecules, *viz.*, hemoglobin,[7] and dextran.[27] A reasonable description of the observed phenomena has been given by Andreae, *et al.*,[28] for a nonelectrolyte dissolved in water. The short range structure of water rapidly breaks down as solute molecules are dissolved. Water molecules, which bind to the solute molecules in hydration layers, reach an equilibrium state with the unbound solvent molecules and it is this equilibrium which is perturbed by the sound wave and gives rise to absorption.

In order to understand the observed changes of the ultrasonic absorption coefficient that occur with changes in pH, a brief resumé of the physical-chemical properties of BSA in aqueous solution is presented. It has been generally recognized that serum albumin molecules undergo marked reversible structural changes as the pH of the environment is altered, although the exact nature of these changes remains unclear.[14] Within the range $4.3 < \text{pH} < 10.5$, each BSA molecule behaves as an undeformable solid particle whose shape can be approximated by a prolate ellipsoid. Outside this range, it was thought that a simple swelling of the compact globular structure was responsible for the observed increase in optical rotation,[29] in viscosity,[30] and in other physical parameters until Tanford, *et al.*,[16] discovered a distinct stepwise change in the intrinsic viscosity, $[\eta]$, as the pH decreased below 4.3. Specifically, between pH 4.3 and 4.0, $[\eta]$ increases sharply by about 22% and between pH 3.5 and 2.8 an 84% increase occurs. This two-step process was observed when the BSA was suspended in 0.15 *M* KCl and was not observed at low ionic strengths. It should be noted that the ionic strength of the Fraction V material supplied by the manufacturer is high. In nearly the same pH region as the smaller increase in $[\eta]$, A increases abruptly between pH 4.4 and 3.8. There is no change in A corresponding to the 84% increase in $[\eta]$ below pH 3.5. This suggests that if the same mechanism is responsible for both the first increase in A and the increase in $[\eta]$ at pH 4.3, then a separate mechanism which does not affect the ultrasonic properties of the solution is responsible for the larger increase in $[\eta]$. Tanford, *et al.*,[16] propose that the complete expan-

---

(25) J. W. Allis and J. D. Ferry, *J. Amer. Chem. Soc.*, **87**, 4681 (1965).

(26) T. A. Litovitz and C. M. Davis, "Physical Acoustics," Vol. II, Part A, W. P. Mason, Ed., Academic Press, New York, N. Y., 1965, Chapter 5.

(27) S. A. Hawley, L. W. Kessler, and F. Dunn, *J. Acoust. Soc. Amer.*, **38**, 521 (1965).

(28) J. H. Andreae, P. D. Edmonds, and J. F. McKellar, *Acustica*, **15**, 74 (1965).

(29) B. Jirgensons, *Arch. Biochem. Biophys.*, **39**, 261 (1952).

(30) J. T. Yang and J. F. Foster, *J. Amer. Chem. Soc.*, **76**, 1588 (1954).

sion of BSA occurs in at least three distinct stages. As the pH is decreased a structural change occurs from a compact form to an "expandable form." At lower pH, the molecule expands physically, and for $\mathrm{pH} < 4$, a small time-dependent increase in the viscosity occurs. This last stage is attributed to possible slow aggregation of the molecules.

Aggregation has been observed in aqueous BSA solutions at acid pH by many investigators. According to Williams and Foster,[31] the principal aggregate is the dimer and it has a maximum concentration at pH 3.3. Below pH 3.0 or above pH 3.5, the rate and extent of dimerization is diminished and these investigators conclude that the turbidity, or cloudiness of the solution that occurs below the isoelectric point which is usually attributed to aggregation, is due to the liberation of a lipid impurity that is carried along with the BSA molecule. Since the abrupt change of the ultrasonic absorption coefficient does not occur in the neighborhood of pH 3.3, it is unlikely that the acoustic disturbance is associated with dimerization. If the impurity itself was involved in the absorption mechanism, then some correlation should have been observed with liberation of this material, which occurred above pH 4.3.

The stepwise expansion process and more recent evidence of a two-step change in the rotational relaxation time occurring at pH 4.1 and pH 3.6[32] support the N–F transformation theory proposed by Aoki and Foster[33,34] and Foster.[14] The N state is the compact rigid form of the molecule which exists between pH 4.3 and 10.5. It is thought to be composed of two pairs of globular subunits held together tightly with each member of a pair held to its partner by hydrophobic bonds. The two pairs of subunits are then bonded to one another electrostatically to make up a four unit globule. As the pH of the BSA solution is reduced below its isoelectric point, electrostatic repulsion forces the molecule to separate into two units linked by flexible chains. This is the so-called F′ state or "intermediate F" form. This state, which corresponds to Tanford's "expandable form," occurs in the same region as the observed ultrasonic effect. As the pH is reduced below 3.6, electrostatic forces become strong enough to overcome the hydrophobic bonds and each unit pair separates. This configuration of the molecule, which consists of four subunits interconnected by flexible linkages, is known as the F state.

Weber and Young[35] subjected acidified BSA to short enzymatic digestion and found that the BSA molecule was split into one large and two smaller globular fragments, a total of three instead of four subunits. With this evidence and with the hydrodynamic properties obtained by others, Bloomfield[36] determined a suitable three subunit model for BSA which consists of a central sphere, of radius 26.6 Å and two flanking spheres of radius 19 Å each. The hydrodynamic properties of this model agree well with those experimentally observed at pH 3.6. However, this model does not account for any stepwise expansion process. It is possible, however, that a combination of Bloomfield's model and Foster's could do so. For example, assume that the N state is composed of a single pair of hydrophobically bonded subunits which is electrostatically bonded to a third, larger subunit. The F′ state and F state would correspond to the flanking spheres of Bloomfield's model.

At this point it is proposed that the observed absorption increase at acid pH over that at neutral pH is related to the $\mathrm{N} \rightleftharpoons \mathrm{F}'$ transformation and that the best estimate of the relaxation time of this reaction that can be made on the basis of this study is $\tau_{\mathrm{NF}'} = 0.72 \times 10^{-7}$ sec. (This was calculated from the simple relation $\tau_{\mathrm{NF}'} = {}^1/_{2\pi f_0}$.) The transformation $\mathrm{F}' \rightleftharpoons \mathrm{F}$ is too slow to be observed with the ultrasonic frequencies employed in this investigation.

Figure 5 shows that the reduced velocity exhibits a minimum at pH 4.1. If the expansion of BSA occurs by separation of the globular units without certain changes to the globular units themselves, as implied by the fragmentation experiments of Weber and Young,[35] then it may be assumed, to a first approximation, that the elastic moduli and densities of these units remain constant. Urick,[37] under the simplifying assumption that a solution can be considered homogeneous to the sound wave, derived the following equation for the velocity of sound in a solution, C_x.

$$C_x = C_0\left(\frac{1}{(1 + \phi\sigma_K)(1 + \phi\sigma_\rho)}\right)^{1/2} \tag{5}$$

where

$$\sigma_K = \frac{K_0 - K_1}{K_0}; \quad \sigma_\rho = \frac{\rho_1 - \rho_0}{\rho_0}$$

In eq 5, the subscripts 0 and 1 correspond to the solvent and solute, respectively, K is the bulk modulus, ρ is the density and ϕ is the volume fraction of the solution occupied by solute. At 2.39 MHz, pH 7.0 and 20°, $C_0 = 1482.4$ m/sec and $C_x = 1506.5$ m/sec when the solute concentration is 9.18%. If a reasonable value for ρ_1 is taken as 1.33 (see page 307 of ref 1) then $\sigma_\rho = 0.33$ and $\sigma_K = -0.77$. If K_0 is 2.18×10^9 n/m² then the bulk modulus of BSA is 3.86×10^9 n/m². It follows from eq 5, under the assumption stated above, that the minimum at pH 4.1 corresponds to a net decrease in the volume fraction of molecules in solution,

---

(31) E. J. Williams and J. F. Foster, *J. Amer. Chem. Soc.*, **82**, 3741 (1959).

(32) C. L. Riddiford and B. R. Jennings, *J. Chem. Soc.*, **88**, 4359 (1966).

(33) K. Aoki and J. F. Foster, *J. Amer. Chem. Soc.*, **79**, 3385 (1957).

(34) K. Aoki and J. F. Foster, *ibid.*, **79**, 3393 (1957).

(35) G. Weber and L. B. Young, *J. Biol. Chem.*, **239**, 1424 (1964).

(36) V. Bloomfield, *Biochem.*, **5**, 684 (1966).

(37) R. J. Urick, *J. Appl. Phys.*, **18**, 983 (1947).

which could result from a reduction of the protein hydration. This is reasoned physically as follows. In the N state, each gram of protein is associated with approximately 0.2 g of bound water molecules. If, when the molecule assumes the intermediate F′ state, the hydration layer remains intact, then the internal rotational freedom possessed by the separated globular units would be suppressed and a decrease in the rotational relaxation time would not be observed. As pH decreases below 4.1, the velocity of sound increases monotonically due, in part, to the increased velocity in the solvent alone, and, in part, to the changes in the chemical nature of the solvent and solute at low pH.[38]

The change in the ultrasonic absorption coefficient for pH > 10.5 is more difficult to correlate with molecular events than it is for pH < 4.3 since very little experimental work on the nature of the alkaline expansion has been reported in the literature. Weber[39] and Tanford, *et al.*,[16] suggest that both the acid and alkaline expansions are similar; however, no other experimental evidence has been presented to substantiate this. Abrupt decreases of the rotational relaxation time of BSA were observed by Weber[39] at pH 3.6 and pH 11.2. It has been observed[14] that at pH 3.6, BSA begins to expand rapidly with decreasing pH, and thus it is reasonable to assume that expansion is also rapid with pH changes above 11.2. The ultrasonic titrations at acid pH and alkaline pH are similar in that the absorption coefficient begins to increase above pH 3.6 and below pH 11.2, *i.e.*, before the molecule actually expands. For pH < 3.6, no correspondence is evident between expansion and A; however, for pH > 11.2, A is increasing sharply which implies that the mechanisms responsible for the absorption increase may be different in each region. Further evidence to support this is the sharp contrast between the velocity titrations at acid and alkaline pH. Tanford and Buzzell[40] have measured $[\eta]$ to pH 10.5 and found that no observable change occurs between pH 9.3 and pH 10.5 whereas here it has been shown that A increases significantly. Further correlation of the ultrasonic absorption increase for pH > 10.5 must await further details of the nature of the alkaline expansion.

Acknowledgment. The authors acknowledge gratefully the support of this research in part by a grant from the Institute of General Medical Sciences, National Institutes of Health, and in part by the Office of Naval Research, Acoustics Program. The authors also wish to extend their appreciation to G. Weber for his numerous and helpful discussions, to S. A. Hawley for his valuable suggestions regarding preparation of this manuscript, and to P. D. Edmonds for the use of his computer program for determining the best fit single relaxation curve.

(38) H. A. Saroff, *J. Phys. Chem.*, **61**, 1364 (1957).

(39) G. Weber, *Biochem. J.*, **51**, 155 (1952).

(40) C. Tanford and J. G. Buzzell, *J. Phys. Chem.*, **60**, 225 (1956).

Enthalpy and Entropy of Sublimation of Tetraphenyltin and Hexaphenylditin. The Bond Dissociation Energy of Sn–C and Sn–Sn[1]

by D. Keiser and A. S. Kana'an

Department of Chemistry, Western Michigan University, Kalamazoo, Michigan 49001 *(Received May 15, 1969)*

The vapor pressures of solid tetraphenyltin and hexaphenylditin have been measured directly by measurements of the torsional recoil of a suspended effusion cell, P_τ, and indirectly by measurement of the mass effusion, P_K. The results of the sublimation pressures in atmospheres are: For tetraphenyltin the torsional recoil yields in the range 428–454°K $\log_{10} P = (12.942 \pm 0.753) - (7963 \pm 33)T^{-1}$; the mass effusion yields in the range 393–461°K $\log_{10} P_K = (12.816 \pm 0.131) - (7927 \pm 56)T^{-1}$. For hexaphenylditin the torsional recoil yields in the range 463–503°K $\log_{10} P = (14.087 \pm 0.276) - (9373 \pm 42)T^{-1}$; the mass effusion yields in the range 444–503°K $\log_{10} P_K = (14.082 \pm 0.124) - (9399 \pm 59)T^{-1}$. The cited errors are standard deviations generated in the least-squares analyses. The average ratio P_τ/P_K is of the order of 1.10; the deviation from unity represents a systematic difference between the two procedures. The enthalpies and entropies of sublimation derived from the measurements are 36.3 ± 0.3 kcal mol^{-1} and 58.6 ± 0.6 eu for tetraphenyltin at 433°K and 43.0 ± 0.3 kcal mol^{-1} and 64.4 ± 0.6 eu for hexaphenylditin at 475°K, respectively. The average bond dissociation energy, $\bar{E}$(Sn–C) is calculated to be 55.8 ± 1.7 kcal mol^{-1}, and the bond dissociation energy of Sn–Sn in hexaphenylditin is calculated to be 36.3 ± 2.4 kcal mol^{-1}.

Introduction

In recent years there has been a notable increase in the accumulated thermochemical data for organometallic compounds. However, there is a lack of reliable and systematic study of the vapor pressures of related compounds to elucidate the relationship between their thermal and structural properties. In this paper the thermochemical quantities associated with the sublimation of tetraphenyltin and hexaphenylditin are reported. The average bond dissociation energy of Sn–C in these compounds and the bond energy of Sn–Sn in hexaphenylditin are derived.

In the present investigation the vapor pressures of tetraphenyltin and hexaphenylditin have been determined from the simultaneous measurements of the torsional recoil and the rate of mass effusion in the temperature ranges 405–461 and 443–503°K, respectively. The vapor pressure of $SnPh_4$ has been previously studied in the temperature range 298–315°K.[2] The vapor pressure of Sn_2Ph_6 has not been cited in the literature in any temperature range.

Experimental Section

Apparatus. The apparatus is essentially similar to that described by McCreary and Thorn[3] except for an automatic semimicro recording-vacuum balance (Ainsworth, RV-AUI) and the furnace. Only details unique to the present study are mentioned.

Torsion Fibers. Tungsten wires 0.038 mm in diameter and 35.6 cm long, served as torsion fibers. The torsional constant was determined by using the assembly as a torsional pendulum, according to the procedure described by Myles.[4] The measured constants and characteristics of the cylinders of known moment of inertia, used in the calibration, are listed in Tables I and II. The cited errors in mass, diameter, and time are those estimated from the precision of these measurements. The propagated error in τ, ±0.01 dyn cm rad^{-1}, compares well with the differences obtained from repeated measurements.

Table I: Measurements of the Torsional Constant Parameters of the Ring of the Torsion Pendulum

Parameter	Aluminum ring[a]	Brass ring[a]
Inside diameter, cm	5.398	5.392
Outside diameter, cm	5.716	5.720
Mass, g	11.9604	39.4653
Moment of inertia, g cm^2	92.411	304.830

[a] Errors: mass, 3×10^{-5} g; diameter, 5×10^{-3} cm; time, 0.01 sec; torsional constant (propagated), 1×10^{-2} dyn cm rad^{-1}.

Cells. Two sets of effusion cells machined from brass and aluminum were used. An aluminum cell, 12.7 mm in diameter and 38 mm long, consisted of three sections. The central section joined each of the two end sections by means of tapered joints. The central section, 16 mm diameter, had a tapered key-

---

[1] This paper is based on work presented by D. Keiser to the School of Graduate Studies, Western Michigan University in partial fulfillment of the requirements of a M.A. degree in Chemistry.

[2] A. S. Carson, R. Cooper, and D. R. Stranks, *Trans. Faraday Soc.*, **58**, 2125 (1962).

[3] J. R. McCreary and R. J. Thorn, *J. Chem. Phys.*, **48**, 3290 (1968).

[4] K. M. Myles, *Trans. AIME*, **230**, 736 (1964).

Table II: Calibration Measurements of Tungsten Wire (diameter, 0.038 mm; length, 35.6 cm)

Experiment	Ring material	Time per oscillation, sec[a] With ring	Time per oscillation, sec[a] Without ring	Torsional constant[a] dyne cm rad^{-1}
4	Brass	117.589	26.497	0.916$_9$
4	Aluminum	66.119	19.518	0.914$_2$
5	Aluminum	66.273	19.537	0.909$_7$
6	Aluminum	66.608	19.593	0.900$_2$
7	Aluminum	66.725	19.685	0.897$_6$

[a] See footnote *a*, Table I.

way machined traversely across the upper side. A brass cell, of the same over-all dimensions, consisted of one piece. The central part, 16 mm in diameter and 12.5 mm long, accommodated the tapered keyway. The cell end openings were fitted with tapered plugs. In both sets a cell was connected to the torsion assembly by means of a dovetail matching the keyway in the main body of the cell. The characteristics of the cells, listed in Table III, were measured microscopically. The transmission factors for mass effusion and for torsional recoil are based on the tabulations of DeMarcus and Hopper[5a] and Schulz and Searcy,[5b] respectively.

Table III: Parameters of Effusion Cells

Cell no.	Diameter of orifices, cm × 10^2	Moment arm cm × 10^2	Clausing factor	Pressure factor
	Set I: Brass Cells[a]			
3B	8.91	89.97	0.8982	0.9289
	9.28	90.86	0.9018	0.9316
4B	11.54	89.18	0.9196	0.9447
	11.41	90.07	0.9187	0.9441
	Set II: Aluminum Cells[b]			
1A	8.23	158.25	0.7847	0.8365
	8.21	154.40	0.7844	0.8363
2A	9.86	156.21	0.8131	0.8609
	9.79	160.63	0.8121	0.8600
3A	12.15	160.52	0.8427	0.8854
	12.04	158.20	0.8413	0.8842

[a] All orifice lengths were 10.16 × 10^{-2} cm. [b] All orifice lengths were 22.86 × 10^{-2} cm.

Heating Chamber and Furnace. A Pyrex tube, 67 mm i.d. and 40 cm long, enclosed the suspended cell. The tube was connected to the main apparatus *via* an O-ringed Pyrex flange. This heating chamber was immersed in an air-fluidized sand bath (Tecam, type SBS4). The temperature of the bath was controlled through a relayed thermoregulator immersed in the sand bath. The heating chamber was jacketed with a brass cylinder, without direct contact. This arrangement was essential to eliminate direct contact with the fluidized sand, which otherwise could cause undesirable vibration of the system. Also the brass cylinder served as a heat sink which improved thermal stabilization.

Temperature Measurement. Temperatures of the effusion cell were considered to be those of a calibrated chromel–alumel thermocouple, suspended in a fixed position inside the heating chamber. The thermocouple hot junction was about 3 mm above the upper side of the cell. The relation between the potential of this thermocouple (reference thermocouple) and the temperature inside the cell was established in the following way. A standard thermocouple was inserted into an equivalent stationary cell, located in the same position of the cell used in an actual experiment. With the apparatus evacuated to a pressure of about 10^{-6} Torr, the reference and standard thermocouples were intercompared over a wide temperature range including the temperatures reported in this work. The standard thermocouple was initially standardized against the freezing temperatures of lead, zinc, aluminum, and copper. The resulting relation of the temperature *vs.* emf of the thermocouple derived from the linear relations for both operations, the calibration and standardization is

$$T(°\mathrm{K}) = 279.2_6 + 24.3_8 V_r \qquad (1)$$

where V_r is the emf in millivolts for the reference thermocouple. During a typical experiment lasting 2 hr, the temperature was constant within ±0.2°.

Chemicals. Samples of Alfa's tetraphenyltin and hexaphenylditin were purified by repeated recrystallization, from benzene solutions, prior to use. The melting points of the purified samples actually used were 225–227° for $SnPh_4$ and 230–232° for Sn_2Ph_6.

Procedure. Prior to an experiment the effusion cell was outgassed under reduced pressure of the order of 10^{-6} Torr at 250°. The weight of the suspension system excluding the cell was recorded. This was necessary to determine the fraction of effusate which condensed on the suspension system and to correct the rate of effusion accordingly. For such correction it was assumed that the condensed fraction was constant for all times and temperatures involved. In a typical experiment of a total weight loss of 370 mg the weight of the suspension system increased by about 20 mg or what corresponds to less than 6% of the total weight loss. The amount of starting material was 0.6–0.8 g.

After the system was evacuated to a pressure of the order of 10^{-6} Torr, the sample was degassed by raising the temperature gradually, first to about 425°K for 2 hr and finally to the highest temperature of

---

(5) (a) W. C. DeMarcus and E. H. Hopper, *J. Chem. Phys.*, **23**, 1344 (1955); (b) D. A. Schulz and A. W. Searcy, *ibid.*, **36**, 3099 (1962).

interest. After 10 min at this temperature, during which the weight loss was approximately 20 mg, the temperature was lowered and vapor pressure measurements were performed at randomly selected temperatures. The rate of effusion was recorded at each temperature after equilibration had occurred as indicated by the steady rate of weight loss. The angular deflection at the same temperature was obtained from measurements of the angular displacement of the reflected light beam on the scale of the optical lever system.[4] The deflection and temperature were recorded every 15 min during the time of an effusion measurement at a given temperature. The residual pressure in the system was maintained between 10^{-6} and 10^{-5} Torr at all times.

During the course of investigation of each compound the melting points and the infrared spectra of the original sample, the condensed effusate and the residue were compared. Such observations confirmed the simple sublimation of the samples.

Results and Treatment of Data

Calculations. The saturated vapor pressures in equilibrium with solid tetraphenyltin and hexaphenylditin were determined from the simultaneous measurements of the rate of effusion and the torsional recoil. The vapor pressures were calculated according to the familiar equations of mass effusion[6] and torsional recoil.[7] In the calculation of P_K the molecular weight of the monomer of the corresponding compound has been employed. The calculated vapor pressures were analyzed by the least-squares method to establish the linear Clausius–Clapeyron equations. The second-law enthalpies and entropies of sublimation were calculated from the parameters A and B of these equations.

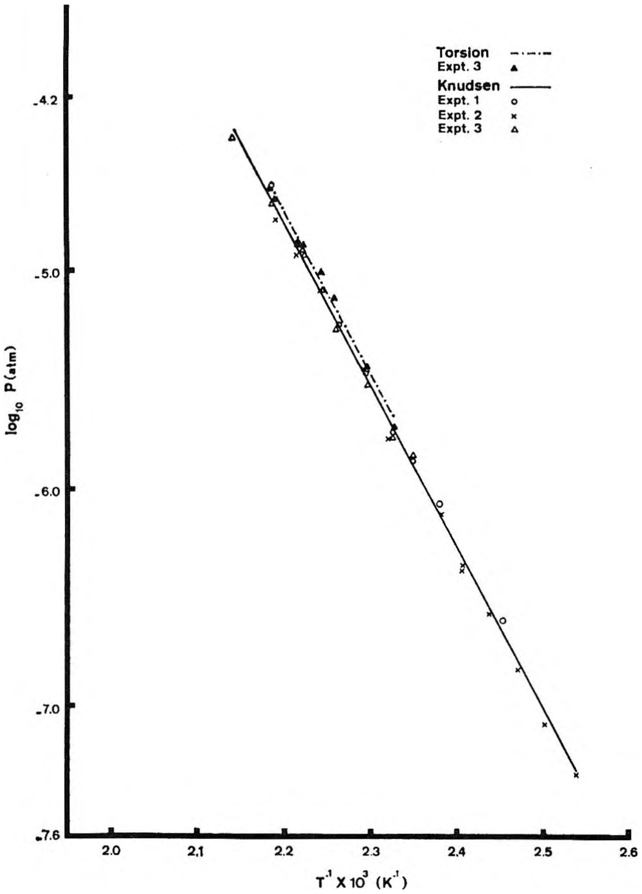

Figure 1. Torsion- and Knudsen-effusion data for tetraphenyltin.

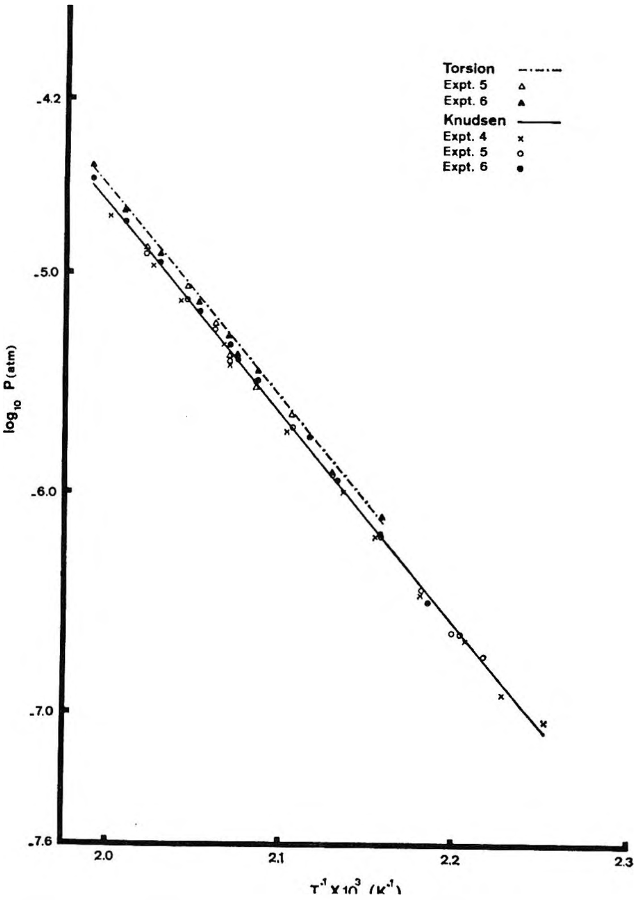

Figure 2. Torsion- and Knudsen-effusion data for hexaphenylditin.

Results. The results of Knudsen-effusion and torsional-recoil measurements of the sublimation pressures are presented in Table IV and Figures 1 and 2. The cited errors are the standard deviations obtained in the least-squares analyses. Also listed in Table IV are the results of the least-squares analysis of the combined points of the indicated sets of experiments. In this averaging approach the points having the largest residuals were successively rejected in each analysis. In the case of $SnPh_4$ five points were removed (two points from each of experiments 1 and 2

---

(6) See, for instance, J. L. Margrave in "Physicochemical Measurements at High Temperatures," J. O'M. Bockris, J. L. White, and J. D. Mackenzie, Ed., Butterworths Scientific Publications, London, 1959, pp 225–246.

(7) See, for instance, R. D. Freeman, in "The Characterization of High Temperature Vapors," J. L. Margrave, Ed., John Wiley & Sons, Inc., New York, N. Y., 1967, pp 152–192.

Table IV: Torsion- and Knudsen-Effusion Results ($\log_{10} P(\text{atm}) = A - BT^{-1}$)

Method	Expt-cell no.	A	B	Temp. range, °K	$P_{\bar{T}} \times 10^6$, atm	$\bar{T}$, °K
			Tetraphenyltin			
Knudsen	1-3B	12.737 ± 0.264	7882 ± 114	407–454	3.418	433
Knudsen	2-4B	12.579 ± 0.213	7837 ± 88	394–453	3.019	
Knudsen	3-1A	12.591 ± 0.435	7829 ± 193	424–461	3.236	
Torsion	3-1A	12.942 ± 0.753	7963 ± 33	428–454	3.568	
Knudsen	1, 2, 3	12.816 ± 0.131	7927 ± 56	393–461	3.358	
			Hexaphenylditin			
Knudsen	4-2A	13.690 ± 0.217	9222 ± 32	444–500	1.879	475
Knudsen	5-3A	14.068 ± 0.232	9392 ± 109	451–495	1.978	
Torsion	5-3A	14.178 ± 0.944	9431 ± 454	469–495	2.107	
Knudsen	6-1A	14.296 ± 0.222	9493 ± 107	457–503	2.047	
Torsion	6-1A	14.006 ± 0.220	9330 ± 107	463–503	2.312	
Knudsen	4, 5, 6	14.082 ± 0.124	9399 ± 59	444–503	1.971	
Torsion	5, 6	14.087 ± 0.276	9373 ± 42	463–503	2.262	

Table V: Thermodynamic Properties of Tetraphenyltin and Hexaphenylditin

	Tetraphenyltin		Hexaphenylditin	
	Knudsen	Torsion	Knudsen	Torsion
T, °K	433	433	475	475
$\Delta \bar{H}_T°$, kcal mol^{-1}	36.3 ± 0.3	36.4 ± 0.2	43.0 ± 0.3	42.9 ± 0.2
$\Delta \bar{S}_T°$, eu	58.6 ± 0.6	59.2 ± 3.4	64.4 ± 0.6	64.5 ± 1.3
$\Delta \bar{H}_{298}°$, kcal mol^{-1}	38.5 ± 1.0	38.6 ± 0.9	45.0 ± 1.0	44.9 ± 0.9

and one point from experiment 3). In the case of Sn_2Ph_6 two points were removed (one point from each of experiments 5 and 6). Such a test indicated that all experiments for a given compound are reliable, even though systematic errors are probably present. Such systematic errors are encountered in the various measurements of vapor pressures. For both compounds there occurs a linear correlation of $\Delta S°$ *vs.* $\Delta H°$, both derived from the linear least-squares analysis of log P *vs.* T^{-1}. Thorn and coworkers[8–10] have demonstrated the same linear correlation in their vapor pressures measurements. The underlying principle discussed by Thorn[11] reveals that the errors encountered in the vapor pressure measurements are, in the sense of $\Delta H°$ *vs.* $\Delta S°$, systematic rather than random.

Thermodynamic Properties. Thermodynamic properties derived from the linear least-squares analyses of the data, summarized in Table IV, are given in Table V. Additional thermodynamic properties derived from the measurements associated with sublimation are the enthalpies of formation of the gaseous molecules, the average bond dissociation energy, $\bar{E}(Sn-C_6H_5)$, and the bond dissociation energy, $E(Sn-Sn)$. To calculate these quantities the following auxiliary data were employed.

Enthalpy of Formation of $SnPh_4$. The heat of combustion of $SnPh_4$, at 298°K, was measured by Pope and Skinner[12] to be -3177.7 ± 0.8 kcal/mol^{-1}. For the enthalpy of formation they calculated the value $\Delta H_f°(SnPh_4, s, 298°K) = 98.5 \pm 0.9$ kcal/mol^{-1}. The above value of the enthalpy of formation and the corrected enthalpy of sublimation $\Delta H_{sub}°(SnPh_4, 298°K) = 38.5 \pm 1.0$ kcal mol^{-1}, yield the enthalpy of formation of the vapor, $\Delta H_f°(SnPh_4, g, 298°K) = 137.0 \pm 2.0$ kcal mol^{-1}.

Enthalpy of Formation of Phenyl Radical and Sn(g). Fielding and Pritchard[13] reported for the enthalpy of formation of the phenyl radical the value $\Delta H_f°(Ph\cdot, g) = 72.0 \pm 2.0$ kcal mol^{-1}. The value for the enthalpy of formation of Sn(g) is $\Delta H_f°(Sn, g) = 72.2 \pm 0.5$ kcal mol^{-1}.[14]

Enthalpy of Formation of Sn_2Ph_6. The heat of combustion of Sn_2Ph_6 was measured by Lautsch, *et al.*,[15] to be -4848.5 ± 7.0 kcal mol^{-1}. For the enthalpy of formation they reported the value $\Delta H_f°$-

---

[8] J. R. McCreary and R. J. Thorn, *J. Chem. Phys.*, **50**, 3725 (1969).

[9] A. S. Kana'an, J. R. McCreary, D. E. Peterson, and R. J. Thorn, *High Temp. Sci.*, **1**, 222 (1969).

[10] J. R. McCreary, S. A. Russoul, and R. J. Thorn, *ibid.*, in press.

[11] R. J. Thorn, *ibid.*, in press.

[12] A. E. Pope and H. A. Skinner, *Trans. Faraday Soc.*, **60**, 1402 (1964).

[13] W. Fielding and H. O. Pritchard, *J. Phys. Chem.*, **66**, 821 (1962).

[14] R. Hultgren, R. L. Orr, P. D. Anderson, and K. K. Kelley, "Selected Values of Thermodynamic Properties of Metals and Alloys," John Wiley & Sons, Inc., New York, N. Y., 1963, p 262.

(Sn_2Ph_6, s) = 160.3 kcal mol^{-1}. Using this value and the corrected enthalpy of sublimation $\Delta H_{sub}°$(Sn_2Ph_6, 298°K) = 45.0 ± 1.0 kcal mol^{-1}, the enthalpy of formation of the vapor is calculated to be $\Delta H_f°$(Sn_2Ph_6, g) = 205.3 ± 1.0 kcal mol^{-1}.

The Average Bond Dissociation Energy of Sn–C. The average bond dissociation energy, $\bar{E}$(Sn–C) in tetraphenyltin is calculated from the enthalpy change for the process

$$SnPh_4(g, 298°K) \longrightarrow Sn(g, 298°K) + 4Ph\cdot(g, 298°K)$$

The calculated value, using the above thermodynamic data, is $\bar{E}$(Sn–C) = 55.8 ± 1.7 kcal mol^{-1}.

The Bond Dissociation Energy of Sn–Sn in Hexaphenylditin. The bond dissociation energy E(Sn–Sn) is calculated from the enthalpy change for the process

$$2SnPh_4(g, 298°K) \longrightarrow Sn_2Ph_6(g, 298°K) + 2Ph\cdot(g, 298°K)$$

The above enthalpy change is represented approximately by

$$\Delta H° = 2\bar{E}(Sn–C) - E(Sn–Sn) = 75.3 \pm 1 \text{ kcal mol}^{-1}$$

The bond dissociation energy of Sn–Sn is calculated to be E(Sn–Sn) = 36.3 ± 2.4 kcal mol^{-1}.

Discussion and Conclusions

The vapor pressure and enthalpy of sublimation of tetraphenyltin at 298°K reported by Carson, *et al.*,[2] are 8.32×10^{-12} atm and 15.85 kcal mol^{-1}, respectively. When the above values are inserted into the Clausius–Clapeyron equation

$$\ln P(\text{atm}) = \Delta S°/R - \Delta H°/RT \qquad (2)$$

the entropy of sublimation is calculated to be 2.49 eu and the Clausius–Clapeyron equation parameters A and B are 0.544 and 3464, respectively. A comparison of these parameters with those derived from the least-squares analysis of the combined data of the present work shows a marked disagreement between the data of these two investigations. This disagreement is not explainable in terms of dissociative sublimation in the present study. The agreement, within experimental errors, between the simultaneous measurements of the vapor pressure by Knudsen effusion, assuming monomer vapor species, and by torsional recoil rules out such possibility.

The enthalpy of sublimation of tetraphenyltin reported by Carson, *et al.*,[2] is too low relative to the corresponding values for polyphenyl compounds of group III. The enthalpy of sublimation reported in this paper is in good agreement with that expected for tetraphenyl compounds of group IV according to the discussion below. Also the low value of the entropy of sublimation derived from their data is practically an impossible value for a process such as $SnPh_4(s) \rightarrow SnPh_4(g)$. Probably they encountered an error associated with incomplete condensation of the effusate.

The enthalpies of sublimation of planar hydrocarbons such as anthracene and pyrene correspond to a value of *ca.* 1.75 kcal mol^{-1} per carbon atom.[16] The corresponding value for nonplanar molecules of related symmetry is expected to be lower than the cited value of planar molecules. Greenwood, *et al.*,[17] reported relatively high values for the enthalpies of sublimation of triphenylgallium (32.9 ± 0.9 kcal mol^{-1}) and triphenylindium (33.6 ± 0.4 kcal mol^{-1}) and a low value for triphenylboron (26.6 ± 0.3 kcal mol^{-1}). They inferred that in triphenylgallium and triphenylindium it is possible that a crystal structure similar to that of the planar organic molecules exists and that in triphenylboron steric interference of the three phenyl rings may be responsible for their nonplanarity with the B–C skeleton. Other nonplanar molecules of low enthalpy of sublimation are triphenylarsenic (23.5 ± 1.0 kcal mol^{-1}), triphenylantimony (25.4 ± 1.0 kcal mol^{-1}),[18] and triphenylmethane (24.1 ± 1.0 kcal mol^{-1}).[19] From these limited examples it is surmised that for such nonplanar molecules the enthalpy of sublimation corresponds to a value of *ca.* 1.4 ± 0.1 kcal mol^{-1} per carbon atom. In accordance with this conclusion, tetraphenyltin is expected to have $\Delta H_{sub}°$ = 33.6 ± 2.4 kcal mol^{-1}. This value agrees with the enthalpy of sublimation obtained from the sublimation studied of this work.

Other approximation rules which lead to values for the enthalpy of sublimation of tetraphenyltin which are in good agreement with the values reported in this paper are the additivity rule for lattice energy of organic crystals[20] and the additivity of the enthalpy of sublimation in terms of uniquely defined group increments.[21] According to the first Aihara[20] assigned an allotment of 9 kcal mol^{-1} per phenyl group. Bondi[21] assigned a value of 10 kcal mol^{-1} per phenyl group and an approximate value of 1.5 kcal mol^{-1} per tetravalent tin in alkyl compounds. However, Bondi[21] pointed out that his rule is expected to err consistently on the high side

The derived average bond dissociation energy, $\bar{E}$(Sn–C) in tetraphenyltin when incorporated in the

---

(15) W. F. Lautsch, A. Tröber, W. Zimmer, L. Mehnen, W. Linck, H. M. Lehmann, H. Brandenburger, H. Körner, H. J. Metzschker, K. Wagner, and R. Kaden, *Z. Chem.*, **3**, 415 (1963).

(16) R. S. Bradley and T. G. Cleasby, *J. Chem. Soc.*, 1690 (1953).

(17) N. N. Greenwood, P. G. Perkins, and M. E. Twentyman, *ibid.*, 2109 (1967).

(18) H. A. Skinner in "Advances in Organometallic Chemistry," Vol. 2, F. G. A. Stone and R. West, Ed., Academic Press, New York, N. Y., 1964, pp 49–114.

(19) G. R. Cuthbertson and H. A. Bent, *J. Amer. Chem. Soc.*, **58**, 2000 (1936).

(20) A. Aihara, *Bull. Chem. Soc. Jap.*, **32**, 1242 (1959).

(21) A. Bondi, *J. Chem. Eng. Data*, **8**, 371 (1963).

derivation of the bond dissociation energy, E(Sn–Sn) in hexaphenylditin gave a value of 36.3 ± 2.4 kcal mol^{-1}. This value is in agreement with that expected in organometallic compounds of tin. Cottrell[22] cited a value of E(Sn–Sn) = 39.0 kcal mol^{-1} in hexamethylditin based on the work of Pedley, *et al.*[23]

The differences between P_τ and P_K may be attributable to systematic difference between the two methods. The average ratio P_τ/P_K is of the order of 1.10 for the present system. This value is within the range of 1.07–1.15 found by other investigators[3,24–26] for the simultaneous measurements of the vapor pressure of substances known to vaporize as monomers.

Acknowledgments. The authors wish to acknowledge partial support for equipment and supplies through grants to A.S.K. by Western Michigan University, Faculty Research Funds, and the Petroleum Research Funds administered by the American Chemical Society.

---

[22] T. L. Cottrell, "The Strengths of Chemical Bonds, 2nd ed, Butterworths Scientific Publications, London, 1958, p 259.

[23] J. B. Pedley, H. A. Skinner, and C. L. Chernick, *Trans. Faraday Soc.*, **53**, 1612 (1957).

[24] R. D. Freeman and A. W. Searcy, *J. Chem. Phys.*, **22**, 762 (1954).

[25] G. M. Rosenblatt and C. E. Birchenall, *ibid.*, **35**, 788 (1961).

[26] J. H. Kim and A. Cosgarea, Jr., *ibid.*, **44**, 806 (1966).

Adsorption on Hydroxylated Silica Surfaces

by M. L. Hair and W. Hertl

Research and Development Laboratory, Corning Glass Works, Corning, New York 14830 *(Received May 19, 1969)*

Adsorption isotherms have been measured by volumetric, gravimetric, and spectroscopic techniques on silica surfaces which have been modified so as to contain only freely vibrating hydroxyl groups, or only H-bonded hydroxyl groups, or no hydroxyl groups. For most of the adsorbates the freely vibrating hydroxyl group is the strongest surface adsorption site, and adsorption on this site accounts for the major part of the adsorption which takes place at low pressures. Hydrocarbon adsorbates interact with these free OH groups an a 1:1 basis. The nonhydrocarbon compounds studied interact on a 1:1 basis when only a single OH is connected to a surface silicon atom, but on a 1:2 basis when the freely vibrating surface hydroxyl groups have a geminal configuration. Mutually H-bonded surface OH groups interact only slightly with lone-pair and hydrocarbon adsorbates. This slight interaction takes place only with the weakly H-bonded OH groups. Water behaves differently from the other adsorbates in that it interacts strongly with the H-bonded OH groups. The formation of the first and second layers of adsorbed water can be observed as plateaus in the absorption isotherm. The adsorption properties of silica containing a preadsorbed layer of water were also studied. When adsorption takes place on this "wet" silica, the amount adsorbed is increased. This adsorbed water thus acts as a specific adsorption site for other molecules.

Introduction

The surface of silica and adsorption on that surface has been the subject of many investigations. Infrared studies, in particular, have led to an acceptable picture of that surface as containing siloxane groups, hydrogen-bonded hydroxyl groups, and free hydroxyl groups which may be either single or geminal.[1]

It has been shown that specific adsorption occurs on the surface silanol groups.[2,3] The specific adsorption on these groups has been measured spectroscopically and heats of adsorption have been obtained.[4] These measurements, however, apply only to the free hydroxyl groups and ignore any other adsorption which may place on the surface, such as on the H-bonded OH groups. Specific adsorption refers here to an adsorbed molecule which has a relatively high heat of adsorption and is probably localized on a given adsorption site.

Under normal atmospheric conditions the silica surface also contains adsorbed water. It has been suggested that water adsorbs preferentially on the H-bonded OH groups.[1] For practical reasons it is important to know what effect this adsorbed water has on the adsorbent properties of silica, since small quantities of adsorbed water are known to have a great effect in either accelerating or poisoning the rate of catalytic reactions on surfaces. Also, water has been used as a liquid phase in gas–liquid chromatography.[5]

---

[1] M. L. Hair, "Infrared Spectroscopy in Surface Chemistry," Marcel Dekker, Inc., New York, N. Y., 1967.

[2] A. V. Kiselev, *Quart. Rev.* (London), *XV*, 99 (1961).

[3] M. R. Basila, *J. Chem. Phys.*, **35**, 1151 (1961).

[4] W. Hertl and M. L. Hair, *J. Phys. Chem.*, **72**, 4676 (1968).

In order to understand properly the nature of the silica surface, three questions remain to be answered: (1) to what total extent does adsorption take place on silica, (2) is the additional adsorption specific to a given site and, if so, what site, and (3) what effect does adsorbed water have on the absorption properties of silica?

To answer these questions, adsorption isotherms have been measured by volumetric, gravimetric, and spectroscopic techniques on silica surfaces which have been modified in a variety of ways. These modifications have been arranged so as to allow adsorption studies on either the freely vibrating or the H-bonded OH groups on the surface, individually, without the complication arising from the simultaneous presence of both types of OH groups.

The treatments result in a sparse covering of the specific adsorption sites and the population of the surface OH groups is less than one-third of that associated with a completely hydrated silica. This minimizes the effects of lateral interactions between adsorbate molecules and allows the data to be easily interpreted. The silica used is a nonporous material, selected to minimize any capillary effects. It should be emphasized that most silicas employed in adsorption studies are microporous and contain many more hydroxyl groups on the surface than the simplified silica employed here.

Experimental Section

1. Measurement of Isotherms. The volumetric isotherms were obtained on a standard instrument used for measuring BET surface areas. The gravimetric isotherms were obtained on an Ainsworth recording balance, connected to a conventional vacuum rack. Spectroscopic isotherms were obtained by measuring the decrease in intensity of the band due to the free OH groups. The silica sample was mounted in a compensated cell, so as to cancel out any absorption due to gas phase bands.

2. Modification of Silica Surface. The silica used in these experiments was Cab-O-Sil (Cabot Co., Boston) and had a BET surface area of 160 m^2/g. No significant surface area changes occur on heating this silica to 800°. The following pretreatments were used. (a) The silica was heated to 800°. The surface contains only free OH groups (Figure 1a). (b) The silica was heated to 800° and then methylated with Me_3SiCl. The surface contains no OH groups; only siloxane linkages and the organic methyl groups (Figure 1b). (c) The silica was soaked in HNO_3 for 16 hr, heated to 520°, and then methylated with Me_3SiCl. This surface contains vicinal H-bonded OH groups but no free OH groups (Figure 1c). (d) The untreated silica was exposed to several Torr of water vapor before the desired adsorbate was added to the system. The surface contains free OH groups, H-bonded OH groups, and adsorbed water.

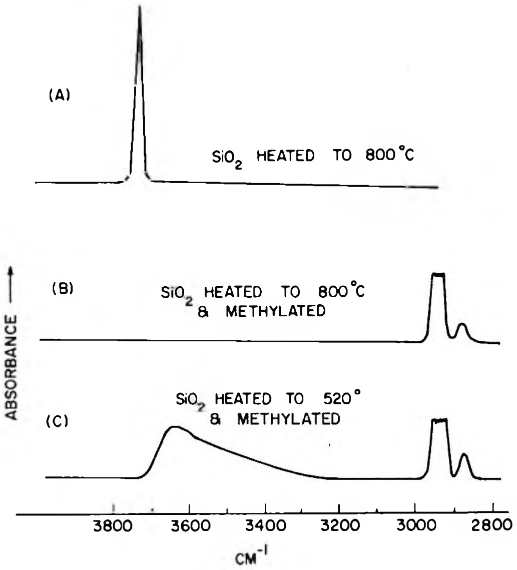

Figure 1. Spectra of silicas with modified surfaces which were used in adsorption experiments: A, silica heated to 800°, surface contains free OH groups; B, silica heated to 800° and methylated, surface contains methyl groups but no OH groups; C, silica heated to 520° and methylated, surface contains H-bonded OH groups and methyl groups.

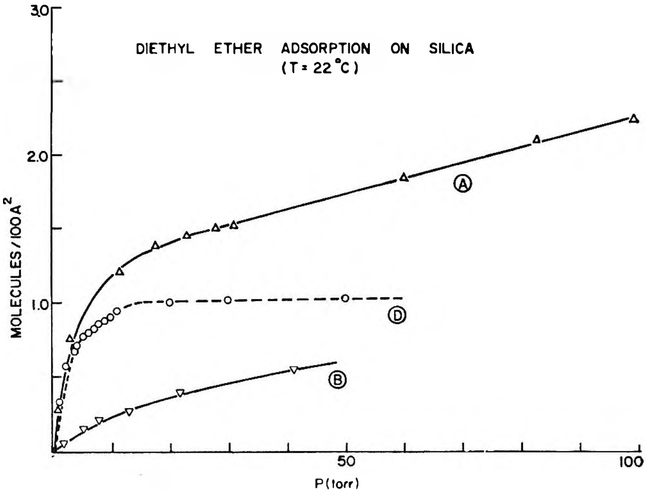

Figure 2. Diethyl ether adsorption isotherms on silica at 24°: A, volumetric isotherm on silica containing only free OH groups; B, volumetric isotherm on dehydroxylated silica; D, spectroscopically measured isotherm on free OH groups.

Results and Discussion

Figures 2, 3, and 4 give the volumetric and spectroscopic isotherms for diethyl ether, acetone, and benzene obtained on the surfaces containing only free OH groups (sample a) and on completely dehydroxylated surfaces (sample b).

Figures 5–9 give the gravimetric isotherms obtained for hexane, triethylamine, pyridine, methanol, and

---

(5) B. L. Karger and A. Hartkopf, *Anal. Chem.*, **40**, 215 (1968).

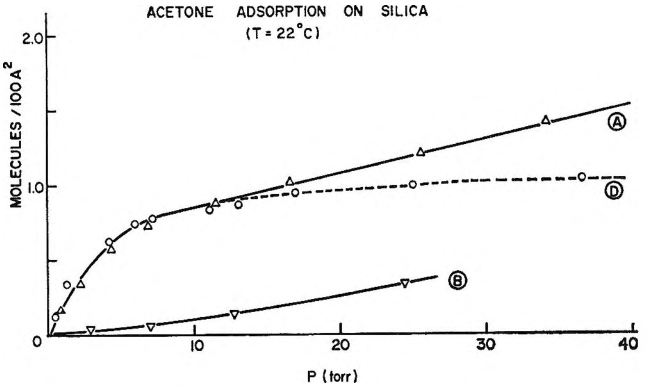

Figure 3. Acetone adsorption isotherms on silica at 22°: A, volumetric isotherm on silica containing only free OH groups; B, volumetric isotherm on dehydroxylated silica; D, spectroscopically measured isotherm on free OH groups.

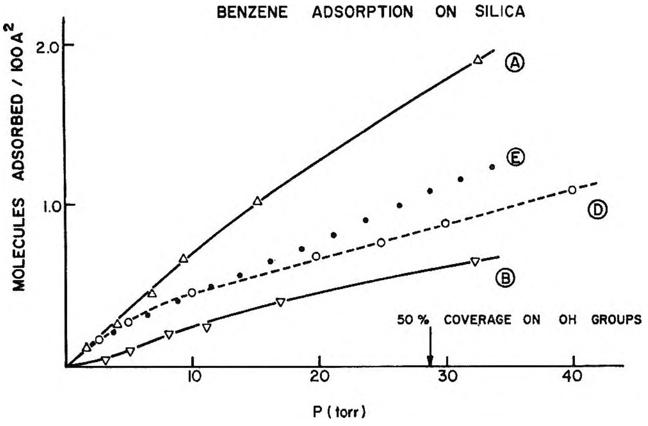

Figure 4. Benzene adsorption isotherms on silica at 24°: A, volumetric isotherm on silica containing only free OH groups; B, volumetric isotherm on dehydroxylated silica; D, spectroscopically measured isotherm on free OH groups; E, arithmetic difference of curves A and B.

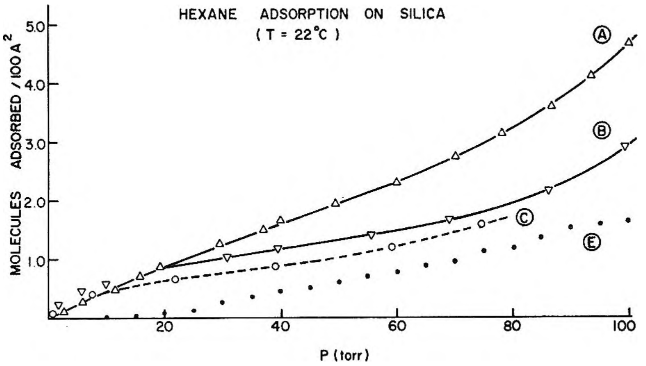

Figure 5. Hexane adsorption isotherms on silica at 22°: A, gravimetric isotherm on silica containing only free OH groups; B, gravimetric isotherm on dehydroxylated silica; C, gravimetric isotherm on silica containing only H-bonded OH groups; E, arithmetic difference of curves A and B.

water on surfaces containing only free OH groups, or only vicinal H-bonded OH groups, or on completely dehydroxylated surfaces.

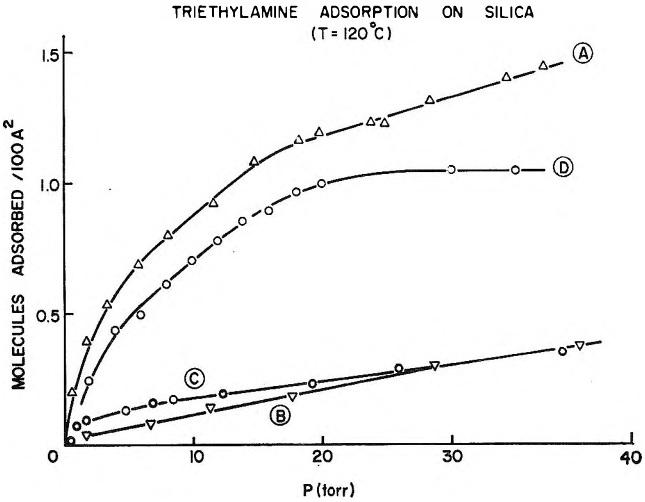

Figure 6. Triethylamine adsorption isotherms on silica at 120°: A, gravimetric isotherm on silica containing only free OH groups; B, gravimetric isotherm on dehydroxylated silica; C, gravimetric isotherm on silica containing only H-bonded OH groups; D, spectroscopically measured isotherm on free OH groups.

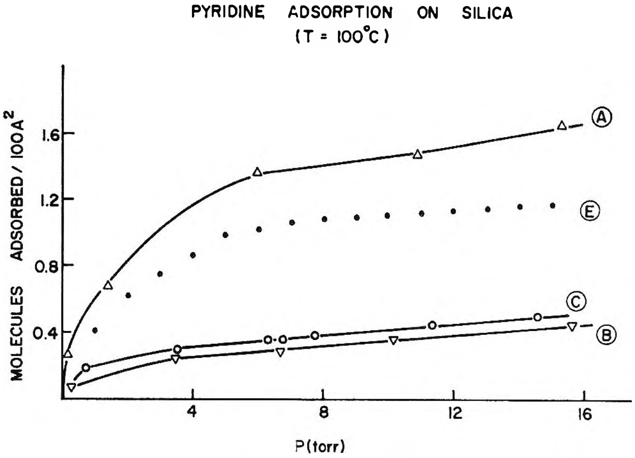

Figure 7. Pyridine adsorption isotherms on silica at 100°: A, gravimetric isotherm on silica containing only free OH groups; B, gravimetric isotherm on dehydroxylated silica; C, gravimetric isotherm on silica containing only H-bonded OH groups; E, arithmetic difference of curves A and B.

The discussion is subdivided so as to consider adsorption on freely vibrating OH groups, adsorption on H-bonded OH groups, adsorption of water and methanol, and adsorption on "wet" surfaces.

Adsorption on Freely Vibrating OH Groups. In all cases, considerably more adsorption takes place on the surfaces containing free OH groups than takes place on the surfaces containing no OH groups. This is in agreement with Kiselev's findings in an earlier study.[2]

The spectroscopically determined isotherms give the coverage on the free OH groups only. In order to compare these isotherms with those determined gravimetrically and volumetrically it is necessary to know the total number of freely vibrating OH groups present on the

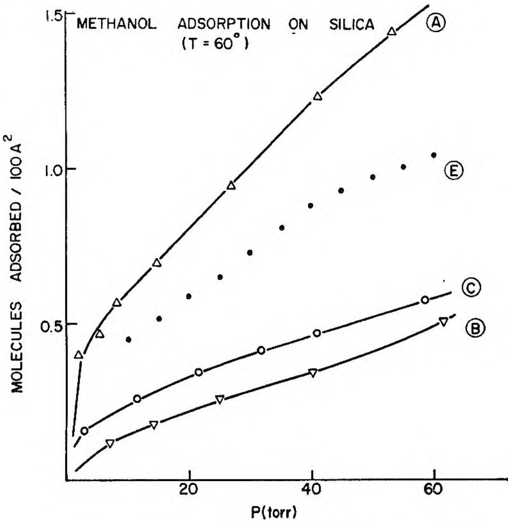

Figure 8. Methanol adsorption isotherms on silica at 60°: A, gravimetric isotherm on silica containing only free OH groups; B, gravimetric isotherm on dehydroxylated silica; C, gravimetric isotherm on silica containing only H-bonded OH groups; E, arithmetic difference of curves A and B.

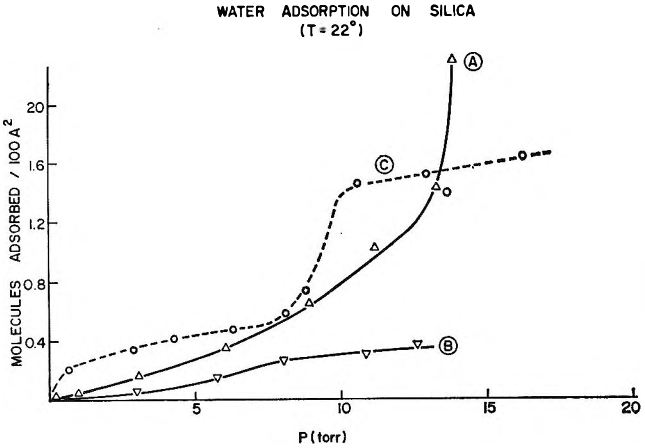

Figure 9. Water adsorption isotherms on silica at 22°: A, gravimetric isotherm on silica containing only free OH groups; B, gravimetric isotherm on dehydroxylated silica; C, gravimetric isotherm on silica containing only H-bonded OH groups.

surface. This quantity was determined gravimetrically in the vacuum recording balance by measuring the weight increase of a sample of silica (sample a) which reacted with methanol vapor according to the equation

$$\mathrm{Si_s{-}OH + CH_3OH = Si_s{-}O{-}CH_3 + H_2O}$$

Complete reaction was checked spectroscopically. From the weight gain and the known surface area, a value of 1.70 OH groups/100 Å² was calculated. This is in good agreement with the value of 1.6 OH groups/100 Å² calculated by residual chlorine analyses following chlorosilane reactions with silica[6,7] and also with previous literature values.[8,9] It has been shown that about 40% of these hydroxyl groups are isolated (*i.e.*, $\mathrm{Si_s{-}OH}$) and 60% of these groups are geminal $\left(\textit{i.e.},\ \mathrm{Si_s}\Big\langle\begin{matrix}\mathrm{OH}\\ \mathrm{OH}\end{matrix}\right)$[5]. Thus, on each 100 Å² of surface, about 0.68 group is single whereas about 1.02 exist in the form of 0.51 pairs.

If the amount adsorbed on the dehydroxylated surface is substracted from the amount adsorbed on the surface containing only free OH groups, then the difference corresponds to adsorption on the free hydroxyl groups only. This should be identical with the spectroscopically determined isotherm, which measures the coverage on the OH groups only. In the case of hexane (Figure 5), this is indeed the case. However, with the nonhydrocarbon compounds the amount of adsorption corresponds to a value of 1.2 sites/100 Å² (Figures 2, 3, and 6). This value of 1.2 sites, however, is just the sum of the number of single OH groups (0.68) plus the number of geminal pairs (0.51). Thus, whereas in the case of the hydrocarbon compound each free OH group acts as a specific adsorption site, in the case of the nonhydrocarbon compounds the geminal pairs appear to act as a single site, so that one adsorbate molecule adsorbs on each geminal pair.

This differentiation between the hydrocarbon and nonhydrocarbon compounds is interesting in view of results obtained from other studies.[4] It had been found that the frequency shifts observed when nonhydrocarbon compounds adsorb on free OH groups are a function of the heat of adsorption on these groups, whereas with the hydrocarbon compounds the heats of adsorption were all similar and the frequency shift could be correlated with the ionization potentials of the adsorbates, but not with the heats of adsorption. Benzene is again anomalous. In the previous study of adsorption on freely vibrating silanol groups, it was found that of the 23 compounds studied, all of them except benzene adsorbed and gave a symmetrical perturbed OH peak whose frequency was essentially independent of coverage. With benzene, however, the perturbed OH band was asymmetric and this perturbed band shifted to lower frequencies as coverage was increased. The present data for benzene are summarized in Figure 4. At low coverages (up to 15 Torr) the spectroscopic isotherm coincides with the isotherm for adsorption on free OH groups. Above this coverage, however, more benzene is adsorbed than can be accounted for by 1:1 adsorption of free OH groups, and this deviation becomes greater as the pressure is increased.

Adsorption on Vicinal H-Bonded OH Groups. Comparison of the isotherms in Figures 5, 6, and 7 shows

---

[6] M. L. Hair and W. Hertl, *J. Phys. Chem.*, **73**, 2372 (1969).

[7] B. Evans and T. E. White, *J. Catal.*, **11**, 336 (1968).

[8] J. B. Peri and A. L. Hensley, *J. Phys. Chem.*, **72**, 2926 (1968).

[9] V. Ya. Davydov, A. V. Kiselev, and L. T. Zhuravlev, *Trans. Faraday Soc.*, **60**, 2254 (1964).

that the presence of the H-bonded OH groups has only a slight effect on the amount of adsorption taking place, the isotherms falling quite close to those obtained on the completely dehydroxylated surfaces. With hexane (Figure 5) a slightly lesser amount of adsorption occurs on the surface with H-bonded OH groups than on a dehydroxylated surface; with the other adsorbates a slightly larger amount of adsorption takes place. This suggests that there is a specific interaction between the lone-pair adsorbents and the H-bonded hydroxyls and a consequent increase in the amount adsorbed at any given pressure. Note, however, that this effect is slight in comparison to the effect of the freely vibrating OH groups. In the case of hexane, there is no such interaction. Indeed, the implication is that the presence of the H-bonded hydroxyls reduces adsorption on the surface.

Spectra were also taken on sample b (containing only H-bonded OH groups) in the presence of various adsorbates. Two typical spectra are shown in Figure 10. With hexane no interaction is noted on the H-bonded OH groups, but with the other adsorbates the high-frequency side of the H-bonded OH band is perturbed and the perturbed band is observed at a lower frequency. This is in agreement with the conclusions reached above, in that the presence of these groups on the surface enhanced the degree of adsorption slightly except in the case of hexane.

That no perturbation of the H-bonded OH groups was observed when hexane adsorbs on the surface means that the mutual interaction between these adjacent OH groups is greater than that between the OH groups and hexane. With the other adsorbates a perturbation is observed, which means that the interaction with some of the OH groups is greater than the mutual interaction between the OH groups. It should be noted, however, that only those H-bonded OH groups which cause the absorption at the high-frequency end of the band are perturbed. This is perhaps predictable, since hexane causes a frequency shift of the freely vibrating hydroxyl group band of only 30 cm^{-1}, whereas, with the other adsorbates, the perturbations are greater than 100 cm^{-1} and the position of the maximum band intensity of the H-bonded OH groups is about 100 cm^{-1} lower than that of the freely vibrating OH group.

When adsorption occurs on freely vibrating OH groups, the perturbed band is usually symmetrical.[4] The H-bonded OH band is very strongly skewed toward the lower frequency end. This immediately suggests that there is a distribution of vicinal OH bond distances.[10] The closer the distance, the stronger is the H-bonding interaction, and thus the greater is the frequency shift. At the high-frequency end of the band, the distance between these hydroxyls becomes relatively great and only a weak H-bond exists. The spectra shown in Figure 10 confirm that the perturbation occurs at the high-frequency end of the band.

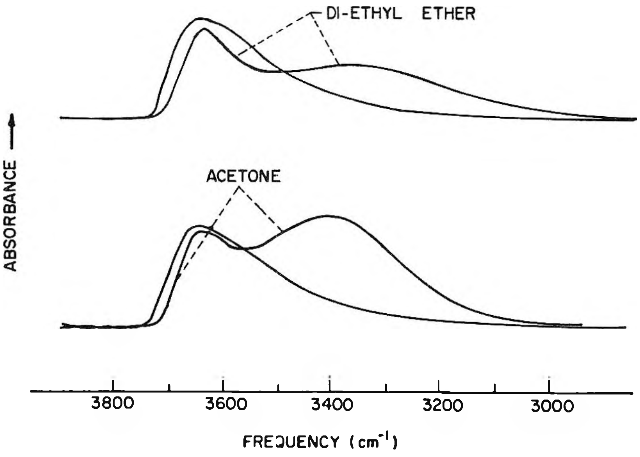

Figure 10. Spectra showing interaction of adsorbed diethyl ether and adsorbed acetone with H-bonded OH groups.

Adsorption of Water and Methanol. The hydroxyl containing compounds (water and methanol) behave somewhat differently than the other adsorbates in that the presence of H-bonded OH groups on the surface has a large effect on the amounts adsorbed. In view of the correlations found between the amount adsorbed and the number of freely vibrating hydroxyl groups in the case of the lone-pair electron and hydrocarbon adsorptions, it is of interest to compare the water adsorption values with the surface concentration of the vicinal H-bonded OH groups.

To determine this quantity a sample of silica was soaked in NHO_3, dried in air at 130°, and mounted in the vacuum recording balance. The sequence of thermal and vacuum treatments as well as the observed weight changes are given in Table I.

Table I: Gravimetric Changes on SiO_2 as a Function of Thermal Treatment[a]

Treatment	ΔW, mg	Molecules of water/100 Å^2
Evacuated at 25°	−30	−5.5
Evacuated at 150°	−1.8	−0.33
Heated to 520° in air	−1.5	−0.27
Heated to 800° in air	−3.0	−0.55
Standing at 25° in air for 60 hr	6.6	1.20

[a] SiO_2 sample = 1.1442 g, surface area = 160 m^2/g.

After the physically adsorbed water is removed, the weight changes on silica are usually ascribed to the condensation of the H-bonded OH groups to produce a siloxane linkage and water. Thus, from Table I, it can be seen that the surface concentration of the vicinal H-bonded OH groups on the silica used in these experi-

---

(10) L. R. Snyder and J. W. Ward, *J. Phys. Chem.*, **70**, 3941 (1966).

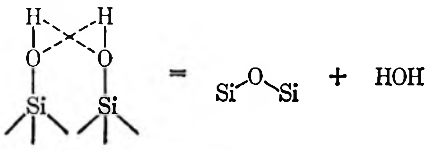

ments (sample c, heated to 520° prior to methylation, then used as the adsorbent) is 0.55 pair of OH groups per 100 Å^2, or a total of 1.1 H-bonded OH groups per 100 Å^2.

Comparison of the isotherms given in Figures 8 and 9 for water and methanol with those shown in Figures 2–7 for the other adsorbates shows that more molecules are adsorbed on the hydroxylated surface than on the dehydroxylated surface. The difference here lies in the role of the H-bonded OH groups. With the other adsorbates these groups had only a small effect on the extent of adsorption. With methanol there is a moderate enhancement in adsorption when these groups are present, but with water, the effect is dramatic. At low pressures more water is adsorbed on this surface than on the surface with free OH groups. At higher pressures the amount adsorbed on the surface with H-bonded OH groups levels off, but on the surface with free OH groups condensation is apparently taking place. On the surface with H-bonded OH groups the isotherm has two almost flat portions. The first plateau occurs at a coverage of about 0.5 molecule/100 Å^2 and the second plateau at about 1.6 molecules/100 Å^2. The value of 0.5 molecule/100 Å^2, however, is just the number of H-bonded OH pairs present on the surface (*cf.* Table I). The second plateau is at a value three times as great. The conformation of the adsorbed water can be visualized as

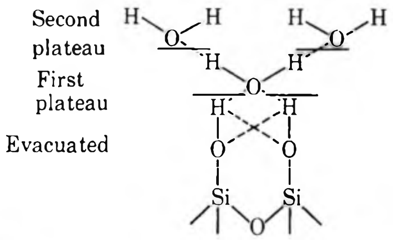

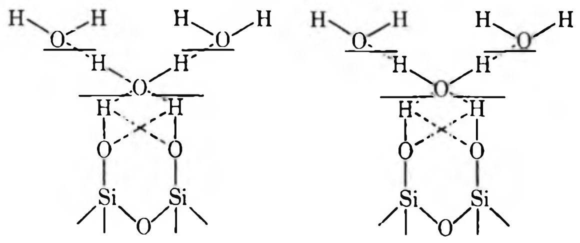

When only freely vibrating OH groups are present on the surface no plateau is observed on the isotherm. It is concave upward throughout, and condensation takes place at a value of $p/p_0 \simeq 0.7$. Just prior to the condensation the surface coverage is about 1.5 molecules of H_2O/100 Å^2. This is approximately the total number of freely vibrating OH groups present on this surface. Thus, as soon as each hydroxyl group has a molecule of water adsorbed on it, condensation takes place, probably around the water molecules already present.

Adsorption on Wet Silica Surfaces. Hydroxylated silica, when exposed to atmospheric water vapor, adsorbs large amounts of water (*cf.* Table I). Various adsorbates were added to silica which contained adsorbed water. In no case did the presence of adsorbed water on the surface decrease the surface concentration of the added adsorbate, but, on the contrary, it had the effect of enhancing the amount of adsorption.

In order to compare the amounts of adsorbates present on the "wet" and "dry" silica, the following experiments were carried out. A wet silica sample was placed in the compensated spectroscopic cell and evacuated briefly, leaving an observable amount of molecular water on the surface. A low pressure of the adsorbate was then added and spectra were taken of the bands which arise due to the adsorbate molecules (*i.e.*, C–H bands, N–H bands, ring vibration bands, and C=O bands). The silica disk was then dried at 800° and the experiment repeated. Thus, for any one adsorbent, the same sample of silica was used. By comparing the intensities of the bands observed, it is possible to estimate the amount of adsorbent present on the surface. This procedure was carried out using benzene, triethylamine, pyridine, acetone, ammonia, and aniline, and the results are given in Table II. For the narrow sharp bands, peak intensities were used to measure the surface concentrations; for the broad bands, areas under the bands were measured.

Table II: Adsorbate Bands and Their Intensities

Compound	Adsorbate bands (cm^{-1}) used for intensity measurements	(Intensity adsorbed wet)/(intensity adsorbed dry)
Benzene	3030, 3065, 3100	1.0–1.33
Et_3N	2940, 2985	1.25–1.50
Pyridine	1440, 1600	1.25–1.42
Acetone	1710, 1695	>1.40
Ammonia	3325, 3410	1.7 → 3.5
Aniline	1465, 1495, 1600 3400, 3325	1.6 –2.5

It is immediately evident that, with the possible exception of benzene, there is more adsorbate present on the wet silica than on the dry silica. In a very rough way the amounts present parallel the solubilities of the adsorbates in water.

This conclusion is in apparent disagreement to conclusions reached by Snyder,[11] who examined the adsorption of aromatic hydrocarbons on "wet" silica using a liquid chromatographic technique, and some comment

---

(11) L. R. Snyder, *J. Phys. Chem.*, **67**, 2622 (1963).

is in order. It should be pointed out that Snyder's conclusions were based on the adsorption of aromatic hydrocarbons containing ten or more carbon atoms. Hydrocarbon adsorption on surface silanols has been shown to proceed by a different mechanism to that of lone pair compounds;[4] *i.e.*, $\Delta\nu$ is related to ionization potential rather than ΔH. The increased adsorption noted on our "wet" surfaces is significant only for lone-pair compounds at low coverage. Moreover, benzene which is anomalous in all our experiments is also anomalous in Synder's work, which is predicated upon the fact that larger aromatic molecules are required before the adsorbate can be considered to "see a more or less average surface energy" and obey the Langmuir equation. The two conclusions are not in disagreement but point out the care that must be taken in interpreting adsorption on a molecular basis. Concentration of surface sites and size of the adsorbate molecule are of the utmost importance.

With the exception of acetone, no new bands were observed between the wet and dry silica samples. In particular, the N–H stretching bands of adsorbed ammonia occurred at the same frequencies on both wet and dry surfaces. In both cases, a small band was observed at 1630 cm^{-1}, which is ascribed to the bending vibration of NH_3,[12] but no band was observed at 1680 or 1400 cm^{-1} which would arise due to NH_4^+. It thus appears that the ammonia adsorbed on the wet surface is not ionized. It must be remembered, however, that the "wet" surface contains only one monolayer or less of adsorbed water.

Acetone shows a strong band at 1695 cm^{-1} on the wet silica which does not appear on the dry silica. This is shown in Figure 11b. The adsorption of acetone onto a dry silica surface proceeds *via* a hydrogen-bonding interaction between the oxygen of the carbonyl group and the proton associated with the freely vibrating surface silanol. The C=O vibration is perturbed from its gas-phase frequency of 1725 cm^{-1} to about 1705 cm^{-1}. At low pressures the band at 1695 cm^{-1} is initially strong; but, as the pressure of the adsorbate is increased, the band at 1710 cm^{-1} begins to grow, followed by a band at 1720 cm^{-1}. The band at 1710 cm^{-1} is attributable to acetone which is hydrogen-bonded to a freely vibrating surface hydroxyl group and the band at 1720 cm^{-1} can be assigned to acetone which is nonspecifically adsorbed on the surface.

The band at 1695 cm^{-1} is more difficult to assign. Although it is possible that it could be assigned to the C=C grouping which would be present if the ketone assumed its enolic form, no comparable changes in the C–H regions could be detected, nor did addition of D_2O cause the rapid deuterium exchange which would be expected if the enolic form existed. In view of this, it seems likely that the 1695-cm^{-1} band can be assigned to an interaction between the acetone and the surface water, and therefore this lower frequency C=O peak should be observable in an acetone–water mixture. To show this, a series of spectra were taken of acetone–water mixtures (Figure 11a). These spectra clearly show that the C=O frequency decreases as the amount of water increases. Whether this is due to a specific interaction between the C=O group and a water molecule or only a frequency shift due to the solvent is not clear. However, the presence of water lowers the C=O frequency to precisely the same value that is observed on the wet silica surface. No changes in C–H band frequencies were observed between the pure acetone and the acetone–water mixtures. Thus, if any enol form is present, it is not detectable spectroscopically.

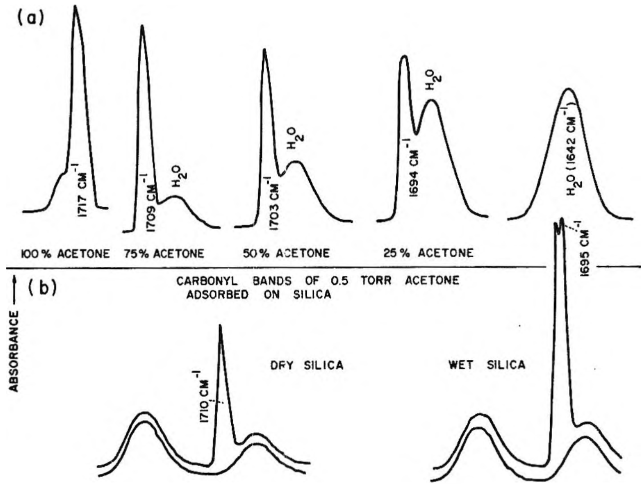

Figure 11. B, spectra of the carbonyl bands of acetone which is adsorbed on a dry and on a wet silica surface; A, spectra of acetone–water mixtures showing shift of the carbonyl frequency with increasing amount of water.

The interpretation of the spectroscopic data is dependent on the assumption that the extinction coefficients are independent of surface coverage. In an attempt to clarify these results a series of gravimetric adsorption experiments were carried out in which about 1.2-1.4 $H_2O/100$ Å^2 were first added to the silica and then the desired gas (benzene, ammonia, and acetone) was added to the system. The silica was then heated to 800°, and the adsorptions were repeated but without the addition of water. The observed weight changes are given in Table III.

Table III: Ratios of Amounts Adsorbed on Wet and Dry SiO_2

Adsorbate	Weight change on wet surface/ weight change on dry surface
Benzene	1.2–1.3
Ammonia	1.5
Acetone	1.0–1.1

---

[12] K. Nakamoto, "Infrared Spectra of Inorganic and Coordination Compounds," John Wiley & Sons, Inc., New York, N. Y., 1963.

It can be seen that in accord with the spectroscopic results, a substantially larger amount of ammonia adsorbs on the wet surface than on the dry surface, and a slightly larger amount of benzene adsorbs on the wet surface than on the dry surface. With acetone, however, the weight changes recorded for adsorption on the wet and dry surfaces were approximately the same. In view of this, a further series of spectroscopic experiments was carried out in which ammonia and acetone were adsorbed at a constant ambient partial pressure onto silica which contained varying amounts of adsorbed water. The data are given in Table IV.

Table IV: Adsorption on SiO_2 Containing Various Amounts of Preadsorbed Water

	Intensity >C=O (1710 cm^{-1})
Acetone (partial pressure = 20 Torr)	
Wet, evacuated sample	1.13
+ 2 Torr of H_2O	1.09
+ 5 Torr of H_2O	1.04
+ 10 Torr of H_2O	1.03
+ 15 Torr of H_2O	1.01
Dried at 800°	0.98
Acetone (partial pressure = 7 Torr)	
Wet, evacuated sample	1.18
+ 2 Torr of H_2O	1.16
+ 10 Torr of H_2O	0.97
Dried at 800°	0.84
Ammonia (partial pressure = 20 Torr)	
	Intensity >N-H (3325, 3410 cm^{-1})
Wet, evacuated sample and with up to 15 Torr of added water	0.14
Dried at 800°	0.04

When acetone or ammonia was adsorbed the spectra showed that both the free OH group and the high-frequency end of the H-bonded OH groups (on the wet samples) were perturbed. Owing to the intensity of the perturbed OH bands, it is not possible to observe directly the changes in intensity of the stretching vibrations due to the adsorbed water (~3500 cm^{-1}). However, the water bending vibration at 1650 cm^{-1} can be observed and it was found that when the acetone was added to a silica sample containing adsorbed water, there was a marked decrease in the band due to the molecular water. Thus, when acetone adsorbs on the wet surface, some of the adsorbed water is displaced from the surface and, therefore, any gravimetric data obtained on such wet surfaces must be suspect.

The apparent discrepancy between the gravimetric and spectroscopic results can be attributed to the displacement of some of the adsorbed water by the adsorbing acetone. It is not possible to say if the water was displaced from the free OH groups, the H-bonded OH groups, or the siloxane surface.

Consideration of the data given in the previous sections suggests a model for the effect of adsorbed water on the enhanced adsorption of other molecules. On the dry surface the freely vibrating hydroxyl groups are strong adsorption sites, particularly with lone pair adsorbates

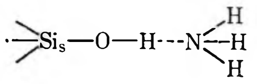

strong H-bond

Adjacent sites which are close together are strongly H bonded to each other and cannot form a hydrogen bond with a lone-pair adsorbate. When they are far apart, however, the weak H bond allows slight interaction

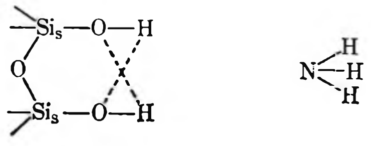

little or no interaction

Water, however, is able to interact with these H-bonded groups to give a structured species

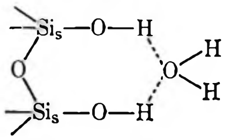

Lone pair adsorbates can now interact with the adsorbed water by H bonding, in the usual way, and thus

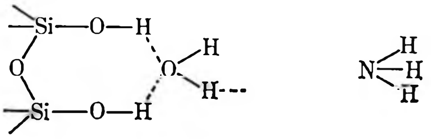

the excess water provides for increased adsorption.

The adsorption isotherm for the total amount of adsorption on the surface represents the sum of these various specific and nonspecific physical adsorptions. It is clear that in attempting to interpret the thermodynamics of adsorption on such surfaces it is necessary to isolate the various surface interactions. The interactions appear to be dependent on the specific orbitals involved in forming the physical bond with the surface rather than on molecular considerations, and thus the problems associated with applying molecular thermodynamic parameters to the overall adsorption which takes place on a surface are apparent.

Acknowledgment. The authors thank Miss E. R. Herritt and Mr. J. A. Gabel for assistance in the experimental work.

Visible Circular Dichroism of Planar Nickel Ion Complexes of Peptides and Cysteine and Derivatives[1]

by Joyce Wen Chang and R. Bruce Martin

Department of Chemistry, University of Virginia, Charlottesville, Virginia 22901 *(Received May 20, 1969)*

Planar, diamagnetic nickel ion complexes of peptides composed of L-amino acid residues typically exhibit negative circular dichroism extrema from 450 to 490 mμ. These minima appear about 50 mμ to longer wavelengths than the absorption maxima at 410–450 mμ due to d–d transitions on the nickel ion. Positive CD extrema also appear near the absorption maxima if histidyl residues are involved in the chelate rings or when bulky amino acid side chains are present in the amino terminal residue. The identity of CD sign for adjacent positions about a chelate ring observed in nickel ion complexes of Gly-Gly-L-Ala and Gly-L-Ala-Gly cannot be accounted for by any octant rule. A hexadecant rule accommodates the results for planar complexes by dividing the coordination plane perpendicularly into eight sectors centering on the metal ion and assigning opposite signs to adjacent sectors. Small side chains for L-amino acid residues then fall into sectors of the same sign regardless of position in a peptide. Four d–d transitions are identified in the circular dichroism for planar complexes of nickel ion and cysteine and derivatives.

Introduction

In a solution containing equimolar amounts of nickel ion and a tripeptide such as triglycine, the addition of 3 equiv of base results in nickel ion promoted amide-hydrogen ionizations yielding a yellow complex containing one amino, two ionized amide nitrogen, and one carboxylate donor atoms arranged in a planar array about nickel ion. For a solution containing equimolar amounts of nickel ion and a tetrapeptide, the addition of 4 equiv of base results in three amide-hydrogen ionizations and yields one amino and three amide nitrogen donor atoms about the nickel ion in a planar complex.[2,3] This paper reports the circular dichroism (CD) occurring in the d–d transitions of diamagnetic[4] nickel ion complexes with optically active derivatives of triglycine and tetraglycine. Ionization of the peptide hydrogens yields planar, *trans* amide bonds which provide a relatively rigid chelate framework for amino acid side chains. As a result of knowledge of side chain disposition, conclusions may be drawn about features of optical properties in planar nickel ion complexes.

Only planar nickel ion complexes yield significant CD in the visible region of the spectrum, and of the common amino acids, only cysteine induces this configuration. This paper also presents the CD results for diamagnetic[5] nickel ion complexes of cysteine and derivatives. The research reported here furnishes model compound studies for the interactions of nickel ion at the N-terminal and sulfhydryl groups of proteins.

Experimental Section

Ligands employed in this research were obtained from Cyclo Chemical Corporation, Mann Research Laboratories, and Calbiochem. Cary 11 and Cary 14R spectrophotometers were used for absorption measurements. Circular dichroism was measured on a Durrum-Jasco ORD/UV-5 recording spectropolarimeter with a CD attachment. The long wavelength limit of CD measurements is about 700 mμ. The absorbance of solutions for CD measurements was 1 to 1.5, made by varying concentrations and cell lengths from 1 to 50 mm. For each CD curve, a base line was obtained by using the identical cell and distilled water under the same conditions as the sample. The CD scale was calibrated periodically by setting the scale deflection at 0.0097 absorption unit for a 1 mg/ml aqueous solution of *d*-10-camphorsulfonic acid in a 10-mm cell. All CD magnitudes are reported as the difference in molar absorptivity based on nickel ion concentration between left and right circularly polarized light. These differential molar absorptivities are designated as $\Delta\epsilon$. Areas under CD curves were evaluated with the aid of a

---

(1) This paper is abstracted from the Ph.D. Thesis (1967) of Joyce Wen Chang, and the research was supported by a grant from the National Science Foundation.

(2) R. B. Martin, M. Chamberlin, and J. T. Edsall, *J. Amer. Chem. Soc.*, **82**, 495 (1960).

(3) M. K. Kim and A. E. Martell, *ibid.*, **89**, 5138 (1967). This paper confirms the results and conclusions of our earlier study in ref 2. Their statement that we have drawn opposite conclusions about the "simultaneous" ionizations in nickel complexes of triglycine and tetraglycine is incorrect. Determination of equilibrium constants for ionizations that occur in a less than statistical manner is a legitimate procedure, and their relative values present a quantitative expression of the cooperative nature of the transition from octahedral to square planar geometry about nickel ion. These authors also report a second formation constant for nickel ion and diglycine more than five times greater than the first formation constant. This unlikely interpretation may be modified by allowing for amide hydrogen ionization, as has been done.[2]

(4) R. Mathur and R. B. Martin, *J. Phys. Chem.*, **69**, 668 (1965).

(5) R. B. Martin and R. Mathur, *J. Amer. Chem. Soc.*, **87**, 1065 (1965).

Table I: Circular Dichroism of Nickel Ion Complexes of Peptides Composed of L-Amino Acid Residues

Peptide	Circular dichroism				Absorption	
	$m\mu$	$\Delta\epsilon$	$m\mu$	$\Delta\epsilon$	$m\mu$	ϵ
Alaninamide	416	−0.50	510	−0.09	430	60
Prolinamide	410	−0.10	496	−1.10	434	65
Gly-Ala-NH_2			480	−0.67	448	40
Gly-Phe-NH_2			460	−0.84	453	60
Gly-His	430	+2.08	488	−1.92	450	110
Gly-Gly-Ala			475	−0.85	430	180
Gly-Ala-Gly			475	−1.12	429	190
Ala-Gly-Gly			490	−0.11	428	228
Ala-Ala-Ala			470	−2.10	427	275
Gly-Ala-Leu			470	−2.20	428	178
Gly-Gly-Leu-NH_2			454	−1.62	408	162
Gly-Gly-Leu			465	−1.38	425	95
Gly-Leu-Gly			475	−1.30	430	110
Leu-Gly-Gly	420	+0.16	490	−0.29	425	110
Leu-Leu-Leu			478	−2.28	426	144
Val-Gly-Gly	420	+0.15	486	−0.30	428	240
Pro-Gly-Gly	422	+0.98	490	−0.38	430	172
Gly-Gly-Phe-NH_2	400	−1.18	470	−0.88	410	126
Gly-Gly-Phe	425	−1.62	Shoulder		430	225
Gly-Phe-Gly			475	−0.90	430	156
Gly-Phe-Phe			475	−2.84	430	196
Phe-Gly-Gly	432	+1.22			432	205
Phe-Phe-Phe			480	−3.04		

planimeter. All experiments were performed at room temperature, near 23°.

Results

The differential molar absorptivities obtained for the CD of square-planar nickel ion complexes of L-amino acid amides and peptides are recorded in Table I. The first two entries refer to 2:1 amide–nickel ion complexes of net zero charge. Solutions containing amide and nickel ion in equimolar amounts show disproportionation to give the 2:1 complexes. All other entries of Table I contain peptide and nickel ion in a 1:1 ratio. The two dipeptide amide chelates bear a net zero charge. In order to induce the yellow color indicative of a square-planar nickel ion complex in a solution containing equimolar amounts of glycylhistidine and nickel ion, sufficient base must be added to yield a complex of net −1 charge.[6] All tripeptide and tripeptide amide chelates in Table I refer to complexes bearing one unit of net negative charge. Circular dichroism curves have been presented for some of the complexes in Table I.[7]

A striking feature of the nickel–peptide complexes of Table I is the narrow range of wavelengths appearing in each column. Wavelengths of extrema in CD in the second column extend only from 400 to 430 mμ, of minima in the third column, from 450 to 520 mμ or from 450 to 490 mμ if the first two entries are excluded, and of absorption maxima in the third column, from 410 to 450 mμ. It is also possible to conclude that a weaker absorption band occurs near 500 mμ in the alaninamide complex. The low molar absorptivities for absorption (all less than 300) indicate that only d–d transitions occur in this wavelength region. No charge-transfer transitions of higher absorptivities occur above 270 mμ in these nickel ion–peptide complexes.

With but one exception, all the chelates in Table I exhibit a negative CD extremum listed in the third column at a wavelength about 50 mμ longer than the absorption maximum tabulated in the last column. This negative CD may be taken as indicative of L-amino acid residues in nickel ion–peptide chelates. A negative sign is also observed in the square-planar Ni(L-1,2-diaminopropane)$_2$ complex in nitromethane solvent where,[8] at the 460 mμ minimum, $\Delta\epsilon = -0.15$, less than the value for the alaninamide complex where the chelate rings should be less puckered. Rather infrequently, a CD extremum of variable sign, listed in the second column of Table I, appears at a wavelength slightly less than the absorption maximum. Except for the glycylhistidine complex, which possesses a unique structure,[6] positive values appear in the second column of Table I only when bulky side chains occur in N terminal amino acid residues. A similar sign reversal to positive CD with bulky groups takes place in some of the corresponding cupric ion chelates.[9] The tetrahedral nitrogen at the N terminus of peptides is much less rigid than the nickel ion bound, planar, trigonal nitrogens in the deprotonated peptide bonds.

---

[6] R. B. Martin and J. T. Edsall, *J. Amer. Chem. Soc.*, **82**, 1107 (1960).

[7] G. F. Bryce and F. R. N. Gurd, *J. Biol. Chem.*, **241**, 1439 (1966).

[8] B. Bosnich, J. H. Dunlop, and R. D. Gillard, *Chem. Commun.*, 274 (1965).

[9] J. M. Tsangaris and R. B. Martin, in preparation.

In addition to the $\Delta\epsilon$ values calculated at the CD extrema and reported in Table I, areas under many of the curves were also evaluated. The areas may be scaled so as to be directly comparable to the $\Delta\epsilon$ values in Table I. The scaled areas for the 6th (Gly-Gly-Ala) through 13th (Gly-Leu-Gly) entries in Table I are −0.74, −1.16, −0.10, −2.11, −2.25, −1.58, −1.33, and −1.38, respectively. The agreement between these scaled areas and the $\Delta\epsilon$ values recorded in Table I is excellent and usually within experimental error of the measurements. We conclude that for a relatively uniform CD peak of one sign, calculation of the differential molar absorptivity, $\Delta\epsilon$, at the extrema is equivalent to evaluating the area.

In order to compare areas with $\Delta\epsilon$ for partially cancelling, oppositely signed CD peaks, scaled areas for the nickel ion complexes of Leu-Gly-Gly, Val-Gly-Gly, and Pro-Gly-Gly were calculated employing the same scale factor used above. The respective pairs of scaled areas obtained are +0.08, −0.19; +0.07, −0.20; and +0.57, −0.19. These scaled areas are only 50 to 65% of the $\Delta\epsilon$ values recorded in Table I for the same complexes. It is apparent that the partial cancellation of positive and negative portions of a CD curve results in greater diminution of areas than of $\Delta\epsilon$ values read at extrema. We conclude that for a partially cancelling, oppositely signed CD curve, the differential molar absorptivities, $\Delta\epsilon$, read at each extremum, are better indicators of the rotational strengths of the transitions than are the areas under each signed curve. Only for two transitions yielding a skewed curve with CD of the same sign would the area appear to be a better measurement of total rotational strength than $\Delta\epsilon$, though the problem of resolution remains. For the reasons advanced in this and the preceding paragraph, $\Delta\epsilon$ values rather than areas will be employed in discussing CD results. No conclusions in the Discussion section would be altered, however, if areas instead of $\Delta\epsilon$ values were utilized.

In Table II are recorded the results for the deep red, divalent nickel ion complexes of L-cysteine and derivatives. In all cases, a sufficient amount of base has been added so that all carboxylate, amino, and sulfhydryl groups are in their basic forms and all complexes are fully formed. The molar ratio of ligands to nickel ion is either 2:1, if only one kind of ligand molecule is present, or 1:1:1 for the mixed complexes of optically active ligand and either ethylenediamine or β-mercaptoethylamine, and as specified in Table II for the glutathione (γ-glutamylcysteinylglycine) complexes. All molar absorptivities and differential molar absorptivities are quoted on the basis of nickel ion concentration.

Absorption spectra results for cysteine and cysteine ester complexes may be summarized by noting that the molar absorptivity per sulfhydryl group at absorption maxima or at shoulders on absorption curves in the complexes ranges from 15 to 18 at 580–590 mμ, and from 51 to 58 at 470–485 mμ. It is more variable at 380–390 mμ as this last absorption band is underlaid by charge-transfer absorption with maxima further into the ultraviolet region. The only exception is the cysteine methyl ester–mercaptoethylamine mixed complex which exhibits greater absorption intensity in the visible region. Though the sulfhydryl groups determine the nature of the absorption band, substitution of oxygen for nitrogen donors displaces absorption maxima to longer wavelengths as shown by the complexes of N-acetylcysteine in Table II. The longest wavelength absorption maximum for the N-acetylcysteine and some other complexes in Table II is not easily resolved though another band appears to be present in the absorption spectra.

The CD results for the three L-cysteine complexes of Table II may be summarized by noting that the $\Delta\epsilon$/mol of optically active ligand is +0.20 to +0.22 at 525–535 mμ; −0.24 to −0.31 at 450–455 mμ, and −0.05 to −0.07 at 390–395 mμ. Corresponding to the long

Table II: Circular Dichroism of Nickel Ion Complexes of L-Cysteine and Derivatives[a]

	Circular dichroism		Absorption	
	mμ	$\Delta\epsilon$	mμ	ϵ
Cysteine, 2:1	535	+0.45	590 s	30
	455	−0.62	475	116
	390	−0.11	390 s	90
Cysteine and mercaptoethylamine	525	+0.20	590 s	35
	455	−0.30	470	109
	395	−0.07	390 s	270
Cysteine and ethylenediamine	525	+0.20		
	450	−0.24	470	57
	390	−0.05	385 s	75
Cysteine ethyl ester, 2:1	580	+0.21	580 s	35
	490	+0.14	480	104
	410	−0.04	390 s	150
Cysteine methyl ester, 2:1	580	+0.22		
	500	+0.19	484	110
	420	−0.03		
Cysteine methyl ester and mercaptoethylamine	570	+0.11		
	505	+0.23	485	170
	425	−0.09	380	380
Cysteine methyl ester and ethylenediamine	585	+0.08		
	490	+0.06	478	57
N-Acetylcysteine, 2:1	610	+0.04		
	525	−0.20	525	
	460	−0.07		
	400	+0.35	415	
Glutathione, 1:1	620	+0.16		
	540	+0.50		
	470	−0.40		
1.5:1			630 s	55
	495	+0.32	520 s	100
	415 s	−0.18	410	300
2:1	620	+0.25		
	490	+0.18	560 s	90
	380	−0.72	420	285

[a] Small s designates shoulder.

wavelength absorption band, an irresolvable, weak, positive CD band seems to appear at about 600 mμ in the cysteine complexes. For the cysteine ester complexes, $\Delta\epsilon$/mol of optically active ligand is +0.08 to +0.11 at 570–585 mμ and +0.06 to +0.10 at 490–505 mμ. The exception, as in the absorption spectra summary, is the cysteine methyl ester–mercaptoethylamine mixed complex, which again yields higher values. Excluding the last complex, the nearly constant values of $\Delta\epsilon$/mol of optically active ligand in the pure 2:1 and mixed 1:1:1 nickel ion complexes of cysteine and its esters indicate that the contributions to the optical activity of two chelate rings with asymmetric centers are independent and additive. The sign of the CD for the first charge-transfer band at <360 mμ is positive for all cysteine complexes and negative for all cysteine ester complexes. A 2:1 complex of D-penicillamine and nickel ion gave a CD curve similar to that of the 2:1 L-cysteine complex but with opposite signs, greater magnitudes, and a shift toward shorter wavelengths.

Solutions containing equimolar ratios of nickel ion and either cysteine, cysteine esters, or N-acetylcysteine were also studied and gave CD magnitudes of the same sign pattern as the 2:1 complexes but with usually more than half the intensity. Since the nature of the complexes present in such solutions is uncertain, they are not mentioned again. A titration performed in a solution containing a 2:1 molar ratio of N-acetylcysteine and nickel ion gave no evidence for ionization of an amide hydrogen.

The results reported in Table II for glutathione all refer to complexes where 3 equiv of base has been added for each mole of glutathione of zero net charge. Additional experiments were performed where more and less than 3 equiv of base per mole of glutathione was added in the case where the glutathione to nickel ion molar ratio is 2:1. A solution with excess base containing base, glutathione, and nickel ion in 8:2:1 molar ratios, respectively, exhibits a CD which does not differ in character from the 6:2:1 containing solution reported in Table II. A solution with less base in which the molar ratios are 4:2:1 yields a weak CD consistent with the predominance of nickel ion at the γ-glutamyl locus rather than at sulfhydryl group in solutions of low pH and excess glutathione.[10] Binding of nickel ion solely at the γ-glutamyl locus provides an octahedral field about the metal ion so that only weak CD is expected. Substitution of S-methylglutathione for glutathione yields a solution which is not red and does not display CD. Addition of 20% additional nickel ion to a solution containing 3 equiv of base per mole of glutathione so that the molar ratios are 3:1:1.2 yields CD similar to the first entry for glutathione in Table II, suggesting that the sulfhydryl binding site is nearly saturated with nickel ion in the last, relatively high pH, solution.

Discussion

As a first approximation, the planar nickel ion–peptide complexes in Table I may be described by the D_{4h} symmetry point group. Though no molecule with an asymmetric carbon may belong to this symmetry group, it does represent the microsymmetry of the four donor atoms about the nickel ion. Except for the expected shift to shorter wavelengths, the similarity of the CD for tripeptide amides with the tripeptides in Table I suggests that the substitution of nitrogen for oxygen donors produces no qualitative changes.

The relative energies of 3d orbitals in square-planar nickel ion complexes is particularly difficult to ascertain in the peptide complexes because all three d–d transitions are closely spaced. For nitrogen and oxygen donors, a likely order of increasing energies for the 3d orbitals in square planar nickel ion complexes is $xz \sim yz < z^2 < xy < x^2 - y^2$, where the x and y coordinates are directed along the metal–donor atom bonds in the complex plane.[11] In the D_{4h} symmetry point group the above ordering is described by the representations $e_g < a_{1g} < b_{2g} < b_{1g}$. For the d^8 nickel ion, the three spin-allowed, one electron d–d transitions in order of increasing energy are $b_{1g} \leftarrow b_{2g}$ ($A_{2g} \leftarrow A_{1g}$), $b_{1g} \leftarrow a_{1g}$ ($B_{1g} \leftarrow A_{1g}$), and $b_{1g} \leftarrow e_g$ ($E_g \leftarrow A_{1g}$). For brevity we designate these transitions as A, B, and E, respectively. Of these three transitions, the medium energy one labeled B is magnetic dipole-forbidden while the high and low energy transitions are magnetic dipole-allowed. Circular dichroism should therefore be strongest in the A and E transitions and be weakest in the B transition to the extent that an effective D_{4h} microsymmetry determines the magnetic dipole selection rules.

Free amino acids other than cysteine are incapable of producing square-planar nickel complexes and yield an octahedral field about the nickel ion. The only magnetic dipole allowed d–d transition of paramagnetic octahedral nickel ion complexes of most amino acids occurs at wavelengths longer than 900 mμ. Since these wavelengths are well beyond the range of the instrument employed and because the magnetic dipole forbidden transitions do not yield easily measurable CD, only ligands that yield diamagnetic square-planar nickel ion complexes are reported in this paper. Circular dichroism in the ultraviolet spectral region for the peptide complexes has been reported.[12]

If the above ordering of transition energies is correct, the CD minima in the third column of Table I for the peptide complexes are assigned to the A transition

---

[10] R. B. Martin and J. T. Edsall, *J. Amer. Chem. Soc.*, **81**, 4044 (1959).

[11] H. B. Gray and C. J. Ballhausen, *ibid.*, **85**, 260 (1963).

[12] J. M. Tsangaris, J. W. Chang, and R. B. Martin, *ibid.*, **91**, 726 (1969). The opposition in sign and similarity in magnitude of the CD observed for the strong absorption bands near 240 mμ and those of the d–d region suggest that an electric dipole–magnetic dipole interaction should be considered as a model for production of optical activity in peptide–nickel ion complexes.

(450–520 mμ) and the CD extrema in the second column to the E transition (410–430 mμ). The higher energy B and E transitions account for the absorption maxima at about 50 mμ shorter wavelength than the lower energy A transition in the nickel ion–peptide complexes.

For series of alanyl tripeptides, the CD for the A transition recorded in Table I is an additive function of independent contributions from the three positions in the chelate ring. The sum of the Δε values for the A transition in the nickel complexes of Gly-Gly-Ala, Gly-Ala-Gly, and Ala-Gly-Gly is −2.08 while the observed value for the Ala-Ala-Ala complex is an identical value (within experimental error) of −2.10. Similarly the observed Δε = −2.20 for Gly-Ala-Leu is close to the sum of −2.50 for the values for Gly-Gly-Leu and Gly-Ala-Gly. The good agreement between calculated and observed Δε values indicates that each L-amino acid residue contributes independently to optical activity in these complexes. An identical conclusion is reached if areas instead of Δε values are compared.

The relative magnitudes of the CD for the alanyl tripeptides may be rationalized. The expectation from simple resonance arguments that the ionized amide group bound to the metal ion through the nitrogen atom is planar is confirmed by an X-ray diffraction study.[13] A side chain on the central amino acid residue of a tripeptide is bounded by two such relatively rigid groups. A side chain on the carboxyl terminal residue is bounded by one ionized amide and one more weakly bound carboxylate group. Examination of dipeptide maps reveals that an equatorial position is not possible for a side chain in the middle or carboxyl terminal residues in the chelate due to steric hindrance with the oxygen atom of the preceding residue.[14] Only a side chain on the amino terminal residue of a tripeptide complex does not suffer this hindrance and an equatorial disposition is allowed. In combination with the greater flexibility of a tetrahedral amino over a trigonal amide nitrogen atom, a side chain in an amino terminal position may take up several conformations over a wider arc than its counterparts in middle or carboxyl terminal positions.

Application of the above argument to the experimental results indicates that side chains in near axial conformations yield greater CD than those in near equatorial conformations. This result indicates that the plane of the chelate ring is a nodal surface for generation of optical activity.

The magnitude additivity and sign identity observed for the CD of the set of alanyl tripeptides cannot be accounted for in terms of an octant rule. Any octant rule predicts that the Gly-L-Ala-Gly tripeptide complex should exhibit a sign opposite to that of the other two tripeptide complexes containing an L-alanyl residue in the terminal positions. In order to account for sign identity and magnitude additivity in the set of four L-alanyl containing tripeptides, a hexadecant rule is applied. A hexadecant or set of 16 sectors is formed by perpendicularly dividing space above the plane of the chelate ring illustrated in Figure 1 into 8 sectors centering on the metal ion. All adjacent sectors are assigned opposite signs, including the second set of 8 sectors located beneath the chelate plane. Most of the atoms of the chelate rings other than hydrogen are in the nodal plane and do not contribute to the optical activity. The signs of Figure 1 are assigned so that the methyl groups of the L-alanyl tripeptide side chains all appear in negative hexadecants. It is not possible to place all three methyl groups of the tripeptide complex composed of L-amino acid residues into octants of the same sign if an octant rule is employed. The hexadecant figure has been mentioned with regard to chromophores belonging to the D_{4h} symmetry point group.[15] Pseudoscalar representations for the C_{2h} or C_s point groups, which simply assign one sign above the chelate plane and another below, may also account for most of the results reported here. These principles have also been applied to copper(II)[9,16] and palladium(II)[17] complexes of amino acids and peptides.

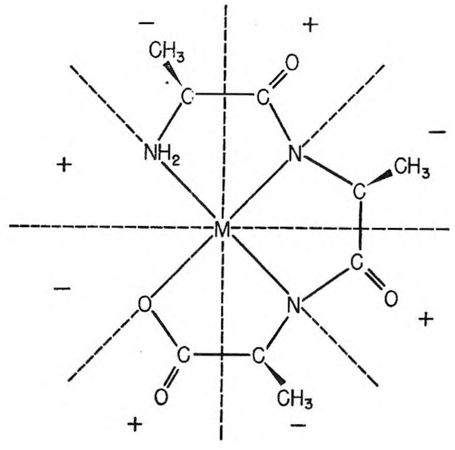

Figure 1. Nickel ion complex of L-Ala-L-Ala-L-Ala after peptide hydrogen ionization. Superimposed is the upper half of hexadecant above the plane of the chelate ring. Opposite signs of adjacent sectors are chosen so that methyl side chains of the L-alanine residues appear in negative hexadecants.

The sum of the Δε values for the nickel complexes of the three tripeptides containing one leucyl residue in Table I is −2.81, which is distinctly greater than the observed value of −2.28 for the Leu-Leu-Leu complex. (For the same complexes the sum of the scaled areas is −2.82 and that for the last tripeptide is −2.31.) For the phenylalanyl set of tripeptides the sum of Δε values

---

(13) H. C. Freeman, J. M. Guss, and R. L. Sinclair, *Chem. Commun.*, 485 (1968).

(14) S. J. Leach, G. Némethy, and H. A. Scheraga, *Biopolymers*, **4**, 369 (1966).

(15) J. A. Schellman, *J. Chem. Phys.*, **44**, 55 (1966).

(16) R. B. Martin, J. M. Tsangaris, and J. W. Chang, *J. Amer. Chem. Soc.*, **90**, 821 (1968). Hexadecant seems a more appropriate name than the double octant employed earlier.

(17) E. W. Wilson, Jr. and R. B. Martin, *Inorg. Chem.*, in press.

or areas for the three tripeptides containing one phenylalanyl residue is less than half the observed values for the Phe-Phe-Phe complex. The fault for these discrepancies may be placed on the tripeptide complexes containing a bulky N-terminal L-amino acid residue. In the first comparison, the Leu-Gly-Gly complex exhibits partially cancelling positive and negative CD components which will also be reflected in the Leu-Leu-Leu complex. Reference to Table I shows that the observed value of $\Delta\epsilon = -2.84$ for the Gly-Phe-Phe complex is not substantially greater than $\Delta\epsilon = -2.52$ for the sum of the values for the Gly-Phe-Gly and Gly-Gly-Phe complexes, especially if a small additional contribution is permitted for skewness in the last case. Thus when complexes not containing the bulky phenylalanyl residue in an N-terminal position are considered, acceptable additivity comparisons are obtained.

When a bulky side chain is introduced into an amino terminal position the chelate ring may no longer be planar. Contributions to optical activity from the different transitions may then be weighted differently. Bulkier side chains in flexible amino terminal residues adopt equatorial positions, which should be increasingly favored as the size of the side chain increases. Any resultant chelate ring puckering adds a conformational contribution to the optical activity which is observed to be of opposite sign to the vicinal contribution and hence reduces the magnitude of the negative CD.

Both absorption spectra and circular dichroism results for the cysteine esters in Table II show three absorption bands at about 580, 490, and 400 mμ. The three cysteine complexes exhibit bands in the same wavelength regions in absorption spectra, but the 490-mμ absorption band is split in CD into a positive band near 530 mμ and a negative one at 450 mμ. The degenerate E transition is the only one of the three mentioned at the beginning of the Discussion section which can undergo this splitting, and the order of increasing energies as strongly suggested by the CD results is $A < E < B$ for 2S and 2N donor systems. As with the peptide complexes, the E transition involving ϵ_g orbitals and out of chelate plane π bonding seems to be the most sensitive to ligand conformation.

The temptation to conclude on the basis of its large negative extremum at about 450 mμ that cysteine is bound to nickel ion through different donor atoms than its esters which do not exhibit the negative CD peak must be resisted. Logarithms of first formation constants for nickel ion and cysteine and its esters are comparable and exceed 10, while that for mercaptopropionic acid is but 5.2, indicating that the primary binding sites in cysteine and its esters are the sulfhydryl and amino groups.[18] In addition, the absorption spectra reported in Table II for the nickel ion complexes of cysteine and its esters are similar in wavelength and intensity, indicating identical 2S and 2N donor atoms in contrast to the shifts of peaks to longer wavelengths observed in the thioglycolate complex for 2S and 2O donors.[19]

Since it is established that both cysteine and its esters are bound to the metal ion predominantly through 2S and 2N donor atoms, what is the reason for the marked splitting of the E transition into positive and negative CD components in cysteine while this transition exhibits only a positive CD for the esters? Absence of super-acid catalysis in the nickel ion promoted hydrolysis of cysteine ethyl ester strongly indicates no binding of the ester function to the metal ion.[20] Though formation constants of nickel ion are greater for cysteine than for its esters, at least some of this additional stability for cysteine is due to a correspondingly greater basicity. We suggest that the splitting of the E band in the CD of cysteine compared to the absence of splitting in cysteine esters is due to biasing of the carboxylate function due to its weak binding in an already strong complex above and below the plane of the chelate ring of 2N and 2S donors. If both carboxylate functions in a 2:1 complex of L-cysteine are to interact simultaneously above and below the plane of the chelate ring, then the N and S donors must be in a *cis* arrangement. In absence of this additional interaction a *trans* arrangement may be preferred in the esters.

At wavelengths greater than 450 mμ, the CD of the cysteine ester complexes is positive and that of the cysteine complexes both positive and negative, while that of N-acetylcysteine is predominantly negative and unique. Absorption maxima for the nickel ion complex of N-acetylcysteine appear at wavelengths similar to those of the thioglycolate complex,[19] suggesting that the ligand is bound through S and O donors. This interpretation is consistent with the absence of amide hydrogen ionization in the N-acetylcysteine–nickel ion complex. The uniqueness of the CD of the N-acetylcysteine complex suggests that none of the other cysteine complexes of Table II takes up a structure with sulfhydryl and oxygen donors where the oxygen atoms are from the carboxylate side of cysteine. This conclusion should also apply to the substitution of nitrogen for oxygen in a carboxamide linkage.

The 1:1 glutathione–nickel ion complex exhibits a CD pattern similar to that of cysteine while the 2:1 complex more nearly resembles that of cysteine esters. Absorption spectra maxima appear in regions suggestive of S and O rather than S and N donors. The solution containing glutathione and nickel ion in a 1.5:1 molar ratio exhibits a CD that is not the average of solutions containing 1:1 and 2:1 molar ratios, indicating that more than two complexes are present in these solutions.

---

[18] J. M. White, R. A. Manning, and N. C. Li, *J. Amer. Chem. Soc.*, **78**, 2367 (1956); Q. Fernando and H. Freiser, *ibid.*, **80**, 4928 (1958).

[19] D. L. Leussing, *ibid.*, **81**, 4208 (1959); D. L. Leussing, *Inorg. Chem.*, **2**, 77 (1963).

[20] H. L. Conley, Jr. and R. B. Martin, *J. Phys. Chem.*, **69**, 2923 (1965).

In addition to the sulfhydryl group, the γ-glutamyl locus is also a metal ion binding site in glutathione, and a variety of mixed complexes may form.

Another goal of these studies is to determine the CD characteristics to be expected of nickel ion when combined with the N-terminus or sulfhydryl groups of proteins. From the results reported here, interaction of nickel ion at the N-terminus of a protein so that amide hydrogens are ionized is expected to give an absorption maximum near 400–430 mμ and a negative CD extremum near 450–490 mμ with a possibility of a positive CD extremum near the absorption maximum when bulky groups appear in N-terminal positions or histidyl groups are involved in the chelate rings. Though the nickel ion complexes of cysteine and glutathione yield absorption maxima and negative CD extrema at less than 500 mμ as do the peptide complexes, coordination of nickel ion at the sulfhydryl groups of proteins should be distinguished by absorption and positive CD extrema at wavelengths longer than 500 mμ. Application of these model compound results to nickel ion association with proteins has been made.[21]

---

[21] J. M. Tsangaris, J. W. Chang, and R. B. Martin, *Arch. Biochem. Biophys.*, **103**, 53 (1969).

The Effect of Charge Scavengers on Radiation-Induced Isomerization of Stilbene in Cyclohexane

by Robert R. Hentz and H. P. Lehmann

Department of Chemistry and the Radiation Laboratory,[1] University of Notre Dame, Notre Dame, Indiana 46556

(Received June 2, 1969)

Effects of electron scavengers (benzyl acetate, $C_6H_5NO_2$, N_2O, CH_3Cl, and CO_2) and cation scavengers (NH_3 and piperidine) on radiation-induced isomerization of *trans*-stilbene in cyclohexane were studied; all but CO_2 suppress $G_{t\rightarrow c}$. Effects of the electron scavengers are discussed in relation to empirical equations for quantitative description of the nonhomogeneous kinetics of charge scavenging in γ-irradiated liquid alkanes. Results are consistent with a model in which isomerization is initiated by electron capture by stilbene with subsequent isomerization *via* stilbene excited states formed in neutralization of stilbene anions by cyclohexane and stilbene cations. The observed absence of any effect of CO_2 on $G_{t\rightarrow c}$ is attributed to stilbene excitation in reaction of CO_2^- with a stilbene cation. Study of the radiation-induced isomerization of *cis*-stilbene is affected by the extreme sensitivity of *cis*-stilbene isomerization to sample-preparation procedures. Though very large values previously reported for $G_{c\rightarrow t}$ in benzene could not be reproduced, present results in both benzene and cyclohexane confirm an appreciable catalytic contribution; in cyclohexane, $G_{c\rightarrow t} = 7.4$ for 0.2 M *cis*-stilbene, and $G_{c\rightarrow t}/G_{t\rightarrow c}$ exceeds the corresponding quantum-yield ratio by more than a factor of 4 for 0.1 M stilbene. Participation of ionic processes in the catalytic contribution is indicated by suppression of $G_{c\rightarrow t}$ by various charge scavengers. A pronounced catalytic effect is observed with C_2H_5Br and SF_6 (probably *via* Br and an SF_x radical from neutralization of the anions formed by electron capture); *e.g.*, $G_{c\rightarrow t} \approx 5500$ for 0.01 M C_2H_5Br and 0.2 M *cis*-stilbene in cyclohexane.

Introduction

In a previous study,[2] concentration dependence of the radiation-induced isomerization of *trans*-stilbene in cyclohexane was found to be remarkably similar to that of $G(N_2)$[3] in radiolysis of N_2O–*c*-C_6H_{12} solutions[4] and to that of $G(H_2)$ in radiolysis of HI–*c*-C_6D_{12} solutions.[5] In the studies cited,[4,5] $G(N_2)$ and $G(H_2)$ were identified with electron-scavenging reactions of the solutes N_2O and HI, respectively. Furthermore, isomerization yields are suppressed by CCl_4,[2] an effective electron scavenger,[6] in such a way as to suggest a competition between CCl_4 and stilbene for an isomerization precursor. Consequently, it was suggested that radiation-induced isomerization of stilbene in cyclohexane is initiated by capture of an electron by stilbene, with subsequent isomerization *via* stilbene excited states produced in charge-neutralization reactions. Conformity of the stilbene-isomerization data to an electron-capture mechanism also is indicated by a theoretical treatment of the nonhomogeneous kinetics of charge scavenging in γ-irradiated alkanes.[7]

---

[1] The Radiation Laboratory of the University of Notre Dame is operated under contract with the U. S. Atomic Energy Commission. This is AEC Document No. COO-38-679.

[2] R. R. Hentz, D. B. Peterson, S. B. Srivastava, H. F. Barzynski, and M. Burton, *J. Phys. Chem.*, **70**, 2362 (1966).

[3] The symbol G denotes a yield in molecules *per* 100 eV absorbed by the system.

[4] G. Scholes and M. Simic, *Nature*, **202**, 895 (1964).

[5] J. R. Nash and W. H. Hamill, *J. Phys. Chem.*, **66**, 1097 (1962).

[6] *Cf.* J. Roberts and W. H. Hamill, *ibid.*, **67**, 2446 (1963), and earlier papers cited therein.

The present work was directed specifically to elucidation of the role of ionic processes in radiation-induced isomerization of *trans*-stilbene in cyclohexane. For such a purpose, the effect of a number of cation and electron scavengers on the radiation-induced isomerization has been studied. The results are discussed in relation to empirical equations proposed for quantitative description of the nonhomogeneous kinetics of charge scavenging in γ-radiolysis of liquid alkane solutions.[8,9] A similar study has been reported of the effect of electron scavengers on radiation-induced luminescence from scintillators in cyclohexane.[10] Six electron scavengers were shown to quench scintillator luminescence in a manner very similar to the effect of the electron scavengers and scintillators on $G(N_2)$ from N_2O–*c*-C_6H_{12} solutions. It was concluded that the luminescence mechanism involves a sequence of ionic reactions identical with that proposed for stilbene isomerization.

In the initial study of radiation-induced stilbene isomerization in benzene and cyclohexane,[2] the ratio $G_{c \to t}/G_{t \to c}$ increased with increase in stilbene concentration becoming considerably larger than the corresponding quantum yield ratio obtained in photochemical studies. Consequently, an ionic chain was postulated to contribute in isomerization of *cis*-stilbene[11] to the thermodynamically favored *trans*-stilbene.[12] Subsequently, values of $G_{c \to t}$ in benzene up to 210 were reported[13] in support of a chain or catalytic contribution to *cis*-stilbene isomerization. The present paper includes a reexamination of the radiation-induced isomerization of *cis*-stilbene in both benzene and cyclohexane.

Experimental Section

Materials. Scintillation grade *trans*-stilbene of Matheson Coleman and Bell was purified by recrystallization. Purification procedures for benzene (Fisher Certified) and cyclohexane (Phillips Petroleum Co.) have been described.[2,10] The *cis*-stilbene was supplied by Aldrich Chemical Co. A yellow coloration was removed by elution through an alumina column with *n*-pentane or petroleum ether. After vacuum distillation on a Nester-Faust annular Teflon spinning-band column at 140°, the only detectable impurity was $<0.1\%$ *trans*-stilbene.

Nitrobenzene (Fisher pure grade), 2-propanol (Baker analytical grade), triethylamine (Aldrich Chemical Co.), and piperidine (Eastman Organic Chemicals) were purified by distillation. Benzyl acetate (Aldrich Chemical Co. Puriss grade) and ethyl bromide (Columbia Organic Chemicals) were used as supplied. Purification procedures for the gases CO_2, SF_6, NH_3, N_2O, and CH_3Cl (all from Matheson Co.) have been described.[10,14]

Procedures. The procedures for preparation of deaerated samples and γ irradiation were essentially the same as described previously.[10,14] Concentration of a gas in cyclohexane solution was calculated from the known amount of gas in the vessel, the volumes of vessel ($\sim$10 ml) and solution (3 ml), and the following Ostwald solubility coefficients: $\beta(N_2O)^{15} = 2.62$ at 23°, $\beta(SF_6)^{16} = 1.22$ at 25°, $\beta(CO_2)^{17} = 1.72$ at 25°, and $\beta(CH_3Cl)^{18} \approx 3.6$ at 25°. In the case of NH_3, vessels with 3 ml of solution and $\sim$0.5 ml of gas space were used with $\beta^{14} = 2.0$ at 24°.

Careful cleaning and masking of all vessels were required by the extreme sensitivity of *cis*-stilbene isomerization to sample-preparation procedures (presumably attributable to certain impurities) and the sensitivity of both isomerizations to light. Pyrex vessels were cleaned with chromic acid, ammonia, and distilled water in succession and then were heated to the annealing temperature. Finally, vessels were heated on the vacuum line just before introduction of the solutions.

Solutions were analyzed on a Beckman GC-5 gas chromatograph with a flame-ionization detector. A $^1/_8$-in. × 12-ft stainless-steel column was packed with nonacid-washed 60–80 mesh Chromosorb G coated with 3% silicone gum rubber. The column was operated at 170° with helium carrier gas; temperatures of injection port and detector were 200°.

Solutions were irradiated at room temperature in a 4-kCi ^{60}Co source at a dose rate to the Fricke dosimeter solution, based on $G(Fe^{3+}) = 15.6$, of 1.51×10^{18} eV ml^{-1} min^{-1}. Dose to a particular solution was calculated by correction for the electron density relative to that of the dosimeter.

---

[7] A. Hummel, *J. Chem. Phys.*, **48**, 3268 (1968).

[8] J. M. Warman, K.-D. Asmus, and R. H. Schuler, Advances in Chemistry Series, No. 82, American Chemical Society, Washington, D. C., 1968, p 25.

[9] S. J. Rzad, R. H. Schuler, and A. Hummel, *J. Chem. Phys.*, in press.

[10] R. R. Hentz and R. J. Knight, *J. Phys. Chem.*, **72**, 1783 (1968).

[11] R. A. Caldwell, D. G. Whitten, and G. S. Hammond, *J. Amer. Chem. Soc.*, **88**, 2659 (1966), have suggested that, on the contrary, $G_{t \to c}$ is reduced by an increase in self-quenching of excited *trans*-stilbene with increase in *trans*-stilbene concentration.

[12] G. Fischer, K. A. Muszkat, and E. Fischer, *J. Chem. Soc., B*, 1156 (1968), report $\sim$0.2% *cis*-stilbene at thermal equilibrium.

[13] R. R. Hentz, K. Shima, and M. Burton, *J. Phys. Chem.*, **71**, 461 (1967).

[14] R. R. Hentz and W. V. Sherman, *ibid.*, **72**, 2635 (1968).

[15] S. Sato, R. Yugeta, K. Shinsaka, and T. Terao, *Bull. Chem. Soc. Jap.*, **39**, 156 (1966).

[16] G. Archer and J. H. Hildebrand, *J. Phys. Chem.*, **67**, 1830 (1963).

[17] J. Gjaldbaeck, *Acta Chem. Scand.*, **7**, 534 (1953).

[18] Estimated from data for other organic solvents in A. Seidell and W. F. Linke, "Solubilities of Inorganic and Organic Compounds," supplement to 3rd ed, D. Van Nostrand Co., Inc., New York, N. Y., 1952, p 575.

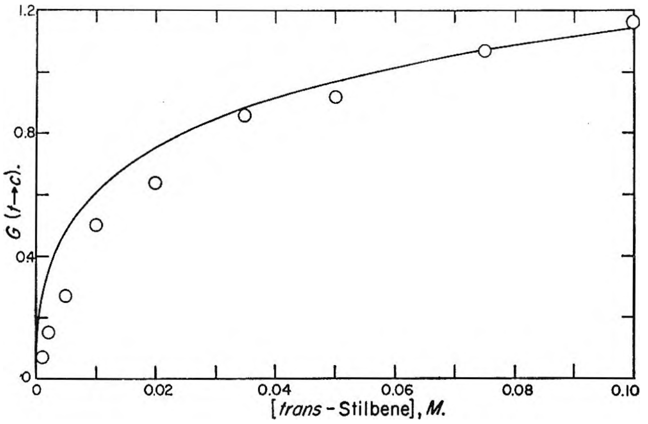

Figure 1. Radiation-induced isomerization of *trans*-stilbene in cyclohexane. Experimental points, ○. Curve is calculated from eq III.

Results

trans-Stilbene in Cyclohexane. All values of $G_{t\rightarrow c}$ were calculated from plots of yield *vs.* dose that were linear through the origin; doses were in the range (1.7–7.5) × 10^{19} eV ml^{-1}. Results presented in Figure 1 for $G_{t\rightarrow c}$ *vs.* *trans*-stilbene concentration in cyclohexane agree reasonably well with those reported previously.[2] Effects of the electron scavengers CH_3Cl,[19] nitrobenzene,[20] N_2O,[19] benzyl acetate,[19] and CO_2[19] on $G_{t\rightarrow c}$ are shown in Figures 2 and 3. Study of the effects of SF_6[19] and C_2H_5Br[19] was precluded by nonlinearity of yield–dose plots owing to a catalytic effect of these solutes on the radiation-induced isomerization (see the following section). Piperidine and NH_3[21] were used as cation scavengers with results shown in Figure 4.

The following results were obtained in benzene solutions with excitation of benzene at 2537 Å: (1) presence of 0.44 *M* NH_3 had no effect on isomerization of 0.03 *M* *trans*-stilbene; (2) presence of 0.3 *M* N_2O had no effect on isomerization of 0.05 *M* *trans*-stilbene, and no N_2 was produced in the presence or absence of *trans*-stilbene. Results obtained in solutions with excitation of *trans*-stilbene at 3130 Å were as follows: (1) presence of 0.08 *M* NH_3 had no effect on isomerization of 0.01 *M* *trans*-stilbene in benzene; (2) presence of 0.05 *M* C_2H_5Br had no effect on isomerization of 0.01 *M* *trans*-stilbene in cyclohexane; (3) presence of 0.3 *M* N_2O had no effect on isomerization of 0.1 *M* *trans*-stilbene in cyclohexane, and no N_2 was produced. It is concluded from such results that the solutes used in this work do not affect excited states of benzene or stilbene but function only as charge scavengers.

cis-Stilbene in Benzene and Cyclohexane. Previously reported values[13] of $G_{c\rightarrow t}$ in benzene up to 210 could not be reproduced in the present work. In preliminary experiments, results for radiation-induced isomerization of *cis*-stilbene were not reproducible and scatter of results on yield–dose plots precluded determinations of $G_{c\rightarrow t}$. Subsequently, large isomerization yields were found in some blank experiments in which an unirradiated portion of a *cis*-stilbene solution had been prepared by an identical procedure at the same time and

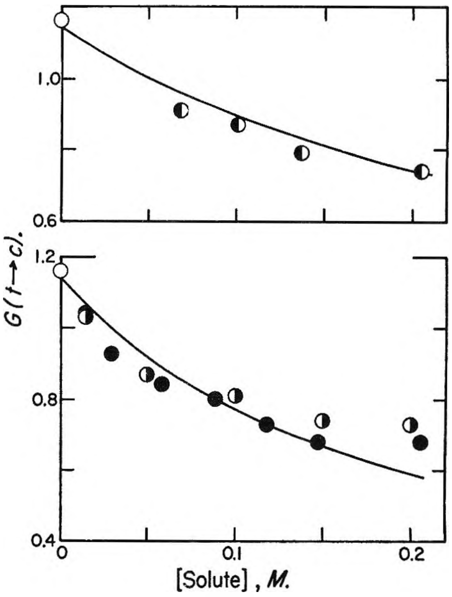

Figure 2. Effects of CH_3Cl, ◐; N_2O, ●; and benzyl acetate, ◑ on radiation-induced isomerization of 0.1 *M* *trans*-stilbene in cyclohexane. Curves are calculated from eq IV with $\alpha_2(CH_3Cl) = 5.6\ M^{-1}$ and $\alpha_2(N_2O) = \alpha_2(\text{benzyl acetate}) = 10\ M^{-1}$.

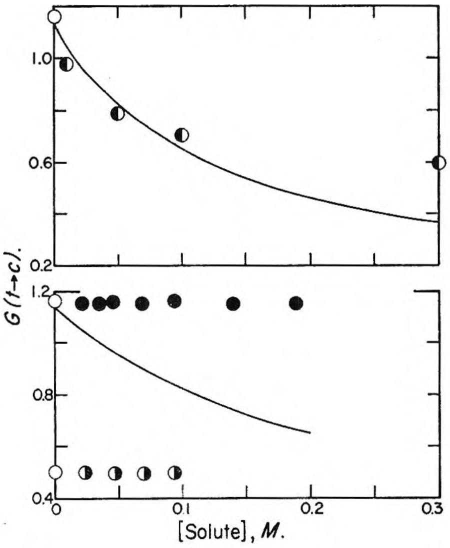

Figure 3. Effects of nitrobenzene and CO_2 on radiation-induced isomerization of *trans*-stilbene in cyclohexane: ◐, nitrobenzene in 0.1 *M* *trans*-stilbene; ●, CO_2 in 0.1 *M* *trans*-stilbene; ◑, CO_2 in 0.01 *M* *trans*-stilbene. Curves are calculated from eq IV with $\alpha_2(\text{nitrobenzene}) = 16\ M^{-1}$ and $\alpha_2(CO_2) = 8\ M^{-1}$.

---

[19] Consult ref 8 and 10 for papers in which the solute has been characterized as an electron scavenger.

[20] Nitrobenzene data are from unpublished work of K. Shima; W. V. Sherman, *J. Chem. Soc.*, **A599**, (1966), has characterized nitrobenzene as an electron scavenger.

[21] F. Williams, *J. Amer. Chem. Soc.*, **86**, 3954 (1964).

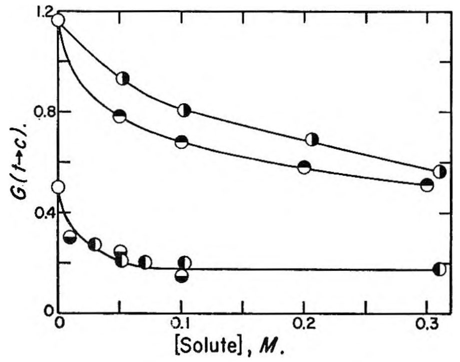

Figure 4. Effect of cation scavengers on radiation-induced isomerization of *trans*-stilbene in cyclohexane: NH_3 in 0.1 *M*, ◑, and 0.01 *M*, ◐, *trans*-stilbene solutions; piperidine in 0.1 *M*, ◓, and 0.01 *M*, ◒, *trans*-stilbene solutions.

analyzed at the same time as irradiated portions of the same solution. In the previous work[13] that gave very large values of $G_{c\rightarrow t}$, isomerization yields in irradiated solutions were corrected only for the *trans*-stilbene concentration present in a portion of stock solution analyzed at the same time as irradiated solutions. Thus, isomerization produced by the sample-treatment procedure may have contributed to the large values of $G_{c\rightarrow t}$ reported.

After standardization of sample-preparation procedures, as described in the Experimental Section, the yield–dose plots shown in Figure 5 were obtained. The zero-dose yields in Figure 5 are for unirradiated solutions prepared and analyzed in the same way and at the same time as the irradiated solutions. The results previously reported[13] as very large values of $G_{c\rightarrow t}$ also are presented in Figure 5 as yield–dose plots. Values of $G_{c\rightarrow t}$ corresponding to slopes of the lines in Figure 5 are given in Table I. Values obtained from the solid lines in Figure 5 (*cf.* Table I) are within 40% of those reported in the initial paper[2] except for the ~3-fold larger value of 11.2 for 0.6 *M* *cis*-stilbene.

Table I: Radiation-Induced Isomerization of *cis*-Stilbene in Benzene

[c-St], *M*	$G_{c\rightarrow t}$[a]
0.02	2.2[b]
0.05	2.8
0.20	2.8
0.40	3.5 (11)
0.60	11.2 (72)[b]

[a] Values *not* in parentheses correspond to slopes of the *solid* lines in Figure 5; those in parentheses correspond to slopes of the broken lines in Figure 5. [b] Based on data reported in ref 13 (*cf.* Figure 5).

The effects of cation and electron scavengers on radiation-induced isomerization of *cis*-stilbene in cyclohexane are shown in Table II. All values of $G_{c\rightarrow t}$ were calculated from initial slopes of yield–dose plots (through the zero-dose yield) for doses in the range (1.3–9.0) × 10^{18} eV ml.$^{-1}$ The value of $G_{c\rightarrow t} = 7.4$ for 0.2 *M* *cis*-stilbene is an average of seven determinations (each from a yield–dose plot) that gave values in the range 5.4–9.4. Of particular interest are the pronounced catalytic effects of C_2H_5Br and SF_6 on radia-

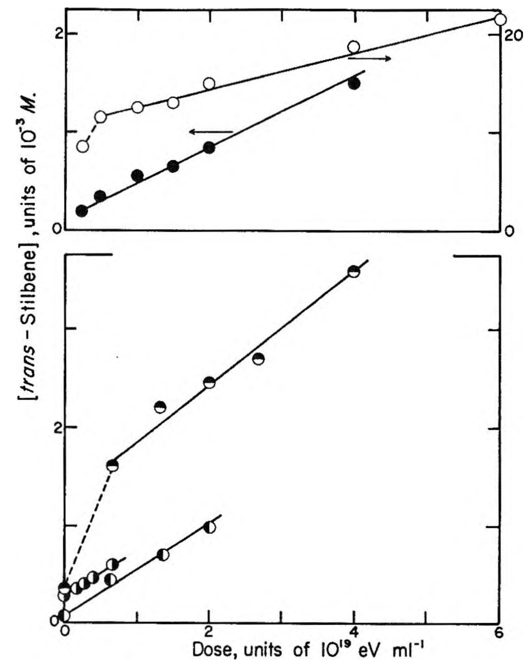

Figure 5. Dose dependence of *trans*-stilbene formation in solutions of *cis*-stilbene in benzene: ○, 0.6 *M* (data from ref 13); ●, 0.02 *M* (data from ref 13); ◓, 0.4 *M*; ◑, 0.2 *M*; ◐, 0.05 *M*.

Table II: Effects of Additives on Radiation-Induced Isomerization of *cis*-Stilbene in Cyclohexane

[c-St], *M*	Additive	Concn, *M*	$G_{c\rightarrow t}$[a]
0.1			4.6
0.2			7.4 ± 2.0[b]
0.4			8.7
0.2	C_2H_5Br	0.001	~2.8 × 10^2
0.2		0.01	~5.5 × 10^3
0.2		0.05	>8.2 × 10^3
0.2		0.1	>1.3 × 10^4
0.2	SF_6	0.07	4.5 × 10^2
0.2	$C_6H_5NO_2$	0.05	2.20
0.2		0.1	1.14
0.2		0.2	1.04
0.2	Piperidine	0.05	1.65
0.2		0.2	1.46
0.2	2-Propanol	0.2	2.76
0.2	$(C_2H_5)_3N$	0.2	1.62
0.2	Piperidine + $C_6H_5NO_2$	0.1 0.1	0.85

[a] Calculated from initial slopes of yield–dose plots (through the zero-dose yield) for doses in the range (1.3–9.0) × 10^{18} eV ml^{-1}. [b] Average, with range, of values from seven yield–dose plots.

tion-induced isomerization of *cis*-stilbene in cyclohexane.

Discussion

trans-Stilbene in Cyclohexane. Schuler and coworkers[8,9] have proposed the empirical equation

$$G_s = G_{fi} + G_{gi}\sqrt{\alpha S}/(1 + \sqrt{\alpha S}) \qquad \text{(I)}$$

for quantitative description of the nonhomogeneous kinetics of charge scavenging in γ-irradiated liquid alkanes. In eq I, S denotes molarity of the scavenger; the yield of scavenged electrons or cations is denoted by G_s, that of geminate ion pairs (*i.e.*, those sibling cation-electron pairs whose members do not escape from their mutual coulombic fields) by G_{gi}, and that of free ion pairs (those that do escape geminate recombination) by G_{fi}. The parameter α in eq I characterizes the reactivity of a scavenger and is considered proportional to the specific rate of the charge-scavenging reaction.

That stilbene is an effective electron scavenger has been shown by identification of the anion in methyl tetrahydrofuran glasses[22] irradiated at 77°K and by its effect in suppression of $G(N_2)$ from irradiated solutions of N_2O in cyclohexane[20] and benzene.[23] If isomerization of *trans*-stilbene is initiated by electron capture, as suggested,[2] eq I should be applicable to the calculation of isomerization yields in the form

$$G_{t\rightarrow c} = \phi_{t\rightarrow c}[\beta_{fi}G_{fi} + \beta_{gi}G_{gi}\sqrt{\alpha_1 S_1}/(1 + \sqrt{\alpha_1 S_1})] \qquad \text{(II)}$$

In eq II, S_1 refers to *trans*-stilbene, $\phi_{t\rightarrow c}$ represents the quantum yield for isomerization from excited states of *trans*-stilbene, and β represents an average probability of stilbene excitation by neutralization of stilbene anions in the reactions

$$C^+ + S_1^- \longrightarrow C + S_1^* \qquad (1)$$

$$S_1^+ + S_1^- \longrightarrow S_1 + S_1^* \qquad (2)$$

in which C denotes cyclohexane.

Formation of the cation of *trans*-stilbene (IP = 7.95 eV[24]) can occur by charge transfer from the cation of cyclohexane (IP = 9.88 eV[25]). The value of β_{gi} in eq II is determined by the relative contributions of reactions 1 and 2 (with values of β_1 and β_2, respectively) to neutralization of stilbene anions by their geminate cations in a particular solution; in all solutions, at the dose rates used, $\beta_{fi} = \beta_2$. The reaction

$$S_1^+ + e^- \longrightarrow S_1^* \qquad (3)$$

is assumed to make a negligible contribution to the yield of excited stilbene molecules. Justification for such an assumption (*cf.* ref 10) is based on the observation that values of α for good electron scavengers are at least 10-fold larger than those for cation scavengers.[7-9]

A value of $\phi_{t\rightarrow c} = 0.50$ has been reported for both the lowest excited singlet state and the triplet state of *trans*-stilbene.[26] Use of such a value in eq II with $\alpha_1 = 16\ M^{-1}$ (a reasonable choice for a good electron scavenger[8]), $G_{fi} = 0.10$,[27] $G_{gi} = 3.9$,[8] and $\beta_{fi} = \beta_{gi} = 1$ gives

$$G_{t\rightarrow c} = 0.50[0.10 + 3.9\sqrt{16S_1}/(1 + \sqrt{16S_1})] \qquad \text{(III)}$$

The curve calculated from eq III (*cf.* Figure 1) agrees quite well with the data for *trans*-stilbene concentrations greater than 0.03 M. However, below 0.03 M, the ratio of experimental to calculated values decreases continuously with decrease in concentration. Although other factors also may be involved, the relation $\beta_2 > \beta_1$ provides a plausible interpretation of such behavior. For $\beta_2 > \beta_1$, β_{gi} decreases as *trans*-stilbene concentration decreases because of the decreasing participation of reaction 2 in neutralization of stilbene anions by their geminate cations.

As shown in Figures 2–4, the radiation-induced isomerization of *trans*-stilbene in cyclohexane is suppressed by all cation and electron scavengers used except CO_2. Such a result strongly indicates the participation of ionic processes in the isomerization mechanism. If the *only* effect of a second scavenger, S_2, on the radiation-induced isomerization is competition with *trans*-stilbene for electrons (*i.e.*, electron capture by S_2 yields *no* isomerization and there is no electron transfer between solutes), then the isomerization yield can be represented by[8-10]

$$G_{t\rightarrow c} = 0.50[0.10 + 3.9\sqrt{16S_1 + \alpha_2 S_2}/(1 + \sqrt{16S_1 + \alpha_2 S_2})] \times 16S_1/(16S_1 + \alpha_2 S_2) \qquad \text{(IV)}$$

for the condition $\beta_1 = \beta_2 = 1$ (and, therefore, $\beta_{fi} = \beta_{gi} = 1$). For 0.1 M *trans*-stilbene, agreement is quite good between $G_{t\rightarrow c}$ calculated from eq III (equivalent to eq IV with $S_2 = 0$) and the experimental value (*cf.* Figure 1). Consequently, even for $\beta_1 \neq \beta_2$, eq IV is a good approximation for 0.1 M *trans*-stilbene solutions if β_{gi} does not change appreciably over the range of S_2 concentrations used.

Curves calculated from eq IV for 0.1 M *trans*-stilbene solutions of the electron scavengers are included in Figures 2 and 3 with the values of α_2 used given in the captions. The values of α_2 for CH_3Cl and CO_2 are those obtained by Schuler and coworkers;[8] values for the other scavengers were chosen to give an approximate fit of the calculated curve to the data. The calculated curve for CH_3Cl is in reasonable accord with the

---

(22) F. S. Dainton and G. A. Salmon, *Proc. Roy. Soc.* (London), **A285**, 319 (1965); T. Shida and W. H. Hamill, *J. Chem. Phys.*, **44**, 4372 (1966).

(23) R. R. Hentz and W. V. Sherman, *J. Phys. Chem.*, **73**, 2676 (1969).

(24) G. Briegleb and J. Czekalla, *Z. Elektrochem.*, **63**, 6 (1959).

(25) K. Watanabe, T. Nakayama, and J. Mottl, *J. Quant. Spectrosc. Radiat. Transfer*, **2**, 369 (1962).

(26) S. Malkin and E. Fischer, *J. Phys. Chem.*, **68**, 1153 (1964).

(27) A. O. Allen and A. Hummel, *Discussions Faraday Soc.*, **36**, 95 (1963); G. R. Freeman, *J. Chem. Phys.*, **39**, 988 (1963).

results; however, $\alpha_2(N_2O) = 10\ M^{-1}$ used in Figure 2 differs significantly from $\alpha_2(N_2O) = 16\ M^{-1}$ obtained by Schuler and coworkers.[8] Certain of the assumptions and approximations involved in the use of eq IV probably contribute to such a disagreement and to the deviation evident in Figure 2 at the highest concentration of N_2O. At the higher concentrations of N_2O, benzyl acetate, and nitrobenzene in Figures 2 and 3, the experimental values of $G_{t \to c}$ appear to be approaching a plateau. Such behavior may result from a contribution of either or both of the reactions

$$S_2^- + S_1 \longrightarrow S_2 + S_1^- \quad (4)$$

$$S_2^- + S_1^+ \longrightarrow S_2 + S_1^* \quad (5)$$

with a small but nonzero value of β_5. Results available in the literature, particularly for the liquid phase, are not adequate for appraisal of the possibility or probability of reactions 4 and 5 for N_2O, benzyl acetate, or nitrobenzene. However, Schuler and coworkers[8] present evidence for reaction 4 between CH_3Cl^- and C_2H_5Br in cyclohexane.

The absence of any effect with CO_2 in 0.01 M or 0.1 M *trans*-stilbene solutions (*cf.* Figure 3) is very surprising. Electron scavenging by CO_2 has been reported by Sagert,[28] and the value $\alpha_2(CO_2) = 8\ M^{-1}$ was determined by Schuler and coworkers.[8] Johnson and Albrecht[29] have assigned an esr signal in 3-methylpentane glass at 77°K to CO_2^- with an ionization potential of 2.3–2.9 eV. Thus, the absence of any effect, as shown in Figure 3, must be attributed tentatively to participation of reaction 5 and a rather fortuitous set of values for the various α and β parameters involved. Support for such a suggestion is provided by the reported observation[30] of naphthalene phosphorescence on warming a hydrocarbon glass in which CO_2^- and $C_{10}H_8^+$ were the only ions present at 77°K. Also, in study of the effect of electron scavengers on radiation-induced luminescence from scintillators in cyclohexane,[10] CO_2 was remarkably less effective in luminescence quenching than in suppression of $G(N_2)$ from cyclohexane solutions of N_2O.

Suppression of *trans*-stilbene isomerization by the cation scavengers NH_3 and piperidine, as shown in Figure 4, provides particularly strong support for the proposed ionic mechanism. Evidently, isomerization is precluded by replacement of C^+ and S_1^+ in eq 1 and 2 with a cation of the scavenger. Available evidence indicates that ammonia (IP = 10.15 eV[25]) scavenges cyclohexane cations by proton transfer.[14,21] In the case of piperidine (IP = 9.15 eV[31]), charge transfer also is possible. Because the ionization potential of piperidine exceeds that of stilbene, charge transfer from a cyclohexane cation to piperidine should result in little or no reduction in the isomerization yield. However, piperidine is at least as effective as NH_3 in suppression of $G_{t \to c}$ (*cf.* Figure 4). Consequently, it appears that scavenging of cyclohexane cations by piperidine occurs largely, perhaps entirely, by proton transfer. Because the nonhomogeneous kinetics of competitive cation scavenging in the solutions studied cannot be simply approximated[9] by an equation such as eq IV, curves have not been calculated for comparison with the data in Figure 4.

cis-Stilbene in Benzene and Cyclohexane. Though the very large values previously reported[13] for $G_{c \to t}$ in benzene could not be reproduced, the values in Table I are generally larger than the initially reported[2] values for explanation of which an ionic chain mechanism was postulated. Present values obtained for $G_{c \to t}$ in cyclohexane are appreciably larger than those initially reported;[2] *e.g.*, compare $G_{c \to t} = 7.4$ for 0.2 M *cis*-stilbene in Table II with $G_{c \to t} = 2.6$ in ref 2. It should be noted that $\phi_{c \to t}/\phi_{t \to c} < 1$,[26,32] whereas $G_{c \to t} = 4.6$ in 0.1 M *cis*-stilbene as compared to $G_{t \to c} = 1.16$ in 0.1 M *trans*-stilbene (*cf.* Table I and Figure 1). Susceptibility of *cis*-stilbene isomerization to catalysis is illustrated by the extreme sensitivity to sample-preparation procedures and the effect of small concentrations of either SF_6 or C_2H_5Br on $G_{c \to t}$, as shown in Table II. In sum, the results indicate that $G_{c \to t}$, particularly at higher concentrations, includes an appreciable but poorly reproducible catalytic contribution and, therefore, does not provide a reliable measure of the yield of stilbene excited states.

In view of the apparent sensitivity of the radiation-induced isomerization of *cis*-stilbene to various sources of chain initiation and termination, detailed mechanistic speculation is not justified. Catalysis by C_2H_5Br is attributed plausibly to Br[33] produced *via* dissociative electron capture and subsequent neutralization of Br^-. Catalysis of radiation-induced 2-butene isomerization by SF_6 has been observed in the gas phase[34] and in liquid benzene.[35] Hummel[34] attributes such catalysis to SF_6^-; however, the well-known efficacy of C_6H_5S as an isomerization catalyst[36] suggests involvement of a perfluorothio radical (SF_x) formed as a consequence of neutralization. The suppression of $G_{c \to t}$ by cation and electron scavengers other than SF_6 and C_2H_5Br (*cf.*

---

[28] N. H. Sagert, *Can. J. Chem.*, 46, 336 (1968).

[29] P. M. Johnson and A. C. Albrecht, *J. Chem. Phys.*, 44, 1845 (1966).

[30] B. Brocklehurst and R. D. Russell, *Nature*, 213, 65 (1967).

[31] J. Collin, *Z. Elektrochem.*, 64, 936 (1960).

[32] G. S. Hammond, J. Saltiel, A. A. Lamola, N. J. Turro, J. S. Bradshaw, D. O. Cowan, R. C. Counsell, V. Vogt, and C. Dalton, *J. Amer. Chem. Soc.*, 86, 3197 (1964).

[33] M. S. Kharasch, J. V. Mansfield, and F. R. Mayo, *ibid.*, 59, 1155 (1937); H. Steinmetz and R. M. Noyes, *ibid.*, 74, 4141 (1952).

[34] R. W. Hummel, *Nature*, 218, 1050 (1968).

[35] R. B. Cundall and W. Tippett, Advances in Chemistry Series, No. 82, American Chemical Society, Washington, D. C., 1968, p 387.

[36] M. A. Golub, *J. Amer. Chem. Soc.*, 81, 54 (1959); *J. Polymer Sci.*, 25, 373 (1957).

Table II), though not susceptible to simple interpretation, does indicate that (as originally suggested[2]) ionic processes also play a role in the catalytic contribution to $G_{c \to t}$.

Relative Cross Sections for the Quenching of Hg($^1P_1$) Atoms[1]

by Albrecht Granzow, Morton Z. Hoffman, and Norman N. Lichtin

Department of Chemistry, Boston University, Boston, Massachusetts 02215 *(Received June 4, 1969)*

Resonance emission at λ 1849 Å was measured at right angles to a λ 1849 Å source as a function of quenching gas pressure in a system containing Hg vapor at room temperature. The emission intensity varied with pressure in accordance with the Stern–Volmer relationship. Cross sections for the quenching of Hg($^1P_1$) relative to N_2 were calculated from the relative slopes of the Stern–Volmer plots for 12 gases (including Ne and Ar) with molecular weights ranging from 2 to 200. The relative quenching cross sections fell in the range 0.2–3.0 and generally increased with increasing molecular weight. Quenching by He was not detectable. The relatively small differences in these values stand in contrast to the much larger differences in quenching cross sections for Hg($^3P_1$). A number of relative quenching cross sections at λ 2537 Å were measured in the same apparatus and agreed with literature values.

Introduction

Although there is substantial uncertainty in the absolute values of the cross sections for the quenching of Hg($^3P_1$) to the $^3P_0$ or $^1S_0$ states, relative cross sections are known quite precisely for a large number of quenching gases.[2] The rare gases have very low cross sections. The quenching efficiencies of other gases vary over a wide range and depend drastically on molecular structure. Correlations between magnitude of the cross section and availability of vibrational energy levels have not been successful and there appears to be no *a priori* way of predicting whether quenching of the Hg($^3P_1$) will occur to the $^3P_0$ or $^1S_0$ state.

In contrast, data on the quenching of Hg($^1P_1$) are extremely sparse. Mori[3] examined the Hg($^1P_1$)-photosensitized decomposition of CO_2 and, by assuming a simple mechanism, calculated an apparent quenching cross section, the value of which depended upon the choice of the uncertain value of the imprisonment lifetime of the $^1P_1$ state. Whatever the absolute value of the quenching cross section, it was recognized that it was larger than the corresponding value for Hg($^3P_1$). Ruland and Pertel[4] came to a similar conclusion for ethylene. The Hg($^1P_1$)-photosensitization of hydrocarbons has led to some estimates of relative quenching cross sections. The quenching cross section of isobutane is reported[5] to be 1.6 times that of propane while the ratio with Hg($^3P_1$) is 3.1.[2] The quenching efficiency of cyclobutane is 1.9 times that of cyclobutane-d_8 compared to the value of 3.8 at λ 2537 Å.[6] We have already reported[7] that N_2 and CO are equally efficient quenchers of λ 1849 Å resonance fluorescence while quenching by He is not detectable and is probably less than one-tenth as efficient. In contrast, CO is 21.5 times as efficient as N_2 in quenching Hg($^3P_1$).[2] The data all indicate that energy transfer from Hg($^1P_1$) is less selective than from Hg($^3P_1$).

This paper reports the extension of the measurement of the quenching of λ 1849 Å resonance fluorescence to a total of thirteen cases.

Experimental Section

The details of the apparatus have already been described.[7] Incident λ 1849 Å radiation from a low-pressure Hg resonance lamp was isolated from the λ 2537 Å line by means of a γ-irradiated LiF filter and impinged upon the fluorescence cell containing a small quantity of liquid Hg and a plane quartz window at right angles to the incident beam. The intensity of the λ 1849 Å resonance fluorescence was measured using a monochromator and photocell with oscilloscopic readout.

---

[1] Supported by the Air Force Office of Scientific Research under Contract AF-AFOSR-765-67. Presented to the Division of Physical Chemistry at the 156th National Meeting of the American Chemical Society, Atlantic City, N. J., Sept 1968, Abstract PHYS 133.

[2] J. G. Calvert and J. H. Pitts, Jr., "Photochemistry," John Wiley and Sons, Inc., New York, N. Y., 1966, pp 74–77.

[3] Y. Mori, *Bull. Chem Soc. Jap.*, **34**, 1128 (1961).

[4] N. L. Ruland and R. Pertel, *J. Amer. Chem. Soc.*, **87**, 4213 (1965).

[5] R. A. Holroyd and T. E. Pierce, *J. Phys. Chem.*, **68**, 1392 (1964).

[6] E. G. Spittler and G. W. Klein, *ibid.*, **72**, 1432 (1968).

[7] A. Granzow, M. Z. Hoffman, N. N. Lichtin, and S. K. Wason, *ibid.*, **72**, 3741 (1968).

The region between the window of the cell and the slit of the monochromator and the monochromator itself were continuously purged with dry N_2. The total light path through the fluorescence cell was 1.5 cm. All experiments were performed at room temperature (23°). Comparative experiments at λ 2537 Å were performed using a No. 7910 Corning filter in place of the LiF filter. A number of measurements were performed employing a fluorescence cell with 180° geometry and a total light path of 9.5 cm.

Linde high-purity N_2 was further purified as previously described.[7] Distilled water, Matheson NH_3 and N_2O, Airco Dry Ice, and Fisher Spectroscopic Grade c-C_6H_{12} were subjected to three freeze (−196°)-pump–thaw cycles. Airco 99.95% H_2, Matheson Research Grade He, Ne, CH_4, C_2H_4, and CO, Linde prepurified Ar, and K and K Laboratories c-C_4F_8 were used without further purification. Pure Lab of America high-purity grade Hg was used.

Data

The intensity of λ 1849 Å resonance emission from the cell was determined as a function of the pressure of the various gases. Because the emission was not detectably broadened over the range of gas pressures employed, the peak height of the emission was taken as representative of the intensity. Linear Stern–Volmer plots of (emission intensity)$^{-1}$ *vs.* pressure were reported previously.[7] In principle, the ratio of the slopes of such lines should represent the ratio of the quenching rate constants. However, the uncertain role of radiation imprisonment required that the technique be tested with quenching systems, the relative cross sections of which were known with good precision. Analogous quenching measurements at λ 2537 Å were performed with H_2, He, Ne, NH_3, N_2, CO, and CH_4.[8] Stern–Volmer treatment of the intensities at gas pressures from 10^{-3} to at least 50 Torr and normalization of the slopes[9] to that for nitrogen gave relative quenching rate constants from which the relative quenching cross sections presented in Table I were calculated.[10] The extent of the agreement of these values and those reported in the literature[2] establishes the validity of the technique at λ 2537 Å. Extrapolation of the validity to λ 1849 Å is based on the reasonable assumption that the 100-times shorter radiative lifetime of Hg($^1P_1$), compared to that of Hg($^3P_1$), does not introduce any complicating features.

Table I: Relative Cross Sections for the Quenching of Hg($^3P_1$) Atoms

Quencher	σ^2_{2537} (N_2 = 1.0) This work[a]	Lit.[b]
H_2	25	31.4
He	0.0	0.0
Ne	0.0	0.0
CH_4	1.1[c]	0.31
NH_3	14	15.4
CO	23	21.5

[a] Estimated error limits ±10%. [b] See ref 2. [c] See ref 8.

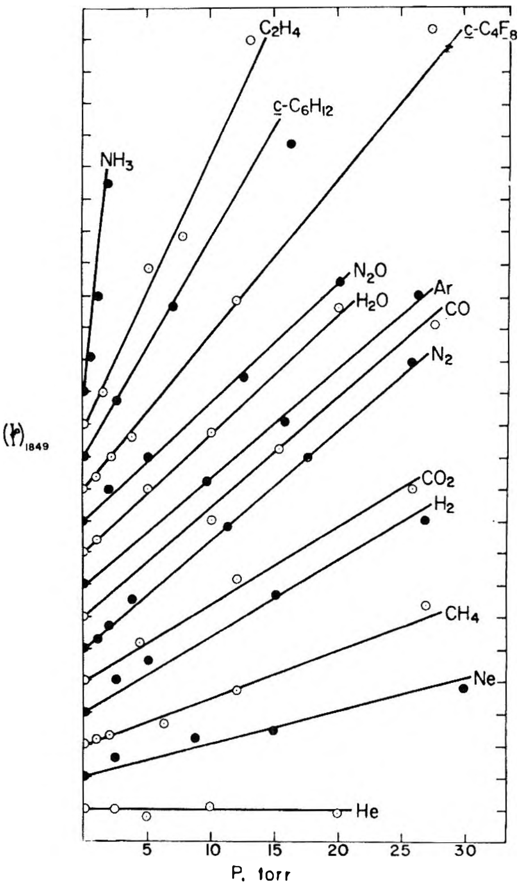

Figure 1. Stern–Volmer plots of quenching data. Each division of ordinate scale represents one unit. Positions of lines with respect to ordinate scale are arbitrary.

Stern–Volmer plots of the quenching data at λ 1849 Å are shown in Figure 1. In most cases the points represent averages of replicated experiments. The estimated error limits of the data are of the order of ±10%. In the case of NH_3 and C_2H_4, the direct absorption of λ 1849 Å radiation had to be taken into account; for all other gases, absorption at this wavelength may be neglected. The data for NH_3 and C_2H_4 were first corrected for absorption using published values of extinction coefficients.[11,12] The uncertainties in the latter values are reflected in the range of the corrected

---

(8) We thank Mr. V. Madhavan for carrying out the measurements on CH_4. His source of λ 2537 Å radiation was less intense than that used in the work reported here resulting in a decrease in signal-to-noise ratio. The error in the CH_4 is probably greater than the 10% limits estimated for the other data.

(9) The Stern–Volmer slope in this experiment is the ratio of the quenching rate constant to a quantity which, due to imprisonment of radiation, is *not* the rate constant for fluorescence. This quantity is a constant for fixed geometry, wavelength, and irradiation conditions and disappears in the evaluation of *relative* quenching rate constants at both λ 2537 Å and λ 1849 Å.

(10) Reference 2, p 73.

quenching data for these gases. Relative quenching cross section values are given in Table II.

Table II: Relative Cross Sections for the Quenching of Hg($^1P_1$) Atoms

Quencher	M_Q	σ^2_{1849} (N_2 = 1.0)[a]	σ^2_{2537} (N_2 = 1.0)[b]
H_2	2	0.2	31
He	4	0.0	0.0
CH_4	16	0.3	0.3
NH_3	17	0.8–1.6[c]	15
H_2O	18	0.9	5.2
Ne	20	0.3	0.0
CO	28	1.0	21
C_2H_4	28	1.0–2.0[c]	135
Ar	40	1.1	0.0
CO_2	44	0.9	13
N_2O	44	1.3	66
c-C_6H_{12}	78	3.0	75
c-C_4F_8	200	2.8	...

[a] Estimated error limits ±10%. [b] See ref 2. [c] Range reflects the uncertainty in the extinction coefficient at λ 1849 Å.

Quenching data for N_2, CO, and Ar obtained in the fluorescence cell with 180° geometry gave Stern–Volmer plots with virtually identical slopes, in good agreement with the measurements taken with the standard 90° configuration.

Discussion

The results confirm the previous observations that Hg($^1P_1$) is far less selective than Hg($^3P_1$) in the transfer of energy leading to the quenching of resonance fluorescence or phosphorescence. The small dependence of σ^2_{1849} on the molecular mass but not the chemical nature of the quenching gas stands in stark contrast to the sharp variations of σ^2_{2537} which have been correlated[13] with the electron donating properties of the quencher through the formation of a well-defined collision complex with the electrophilic Hg($^3P_1$) atom. Even the rare gases display this trend although the quenching efficiencies of He and Ne are less than those of other gases of comparable mass. The quenching of Hg($^1P_1$) by Ne and Ar implies the conversion of electronic to translational energy since these monatomic species do not have electronic energy levels accessible within the 6.67 eV energy range available from Hg($^1P_1$).

The data provide no firm basis for lengthy speculation on the mechanistic details of the quenching process. However, the quenching by Ne and Ar and the apparently simple dependence of σ^2_{1849} on molecular mass suggests that there is a common, major, quenching mechanism for all the gases studied. With the diatomic and polyatomic gases, other quenching mechanisms can operate simultaneously and, although probably responsible for only a minor portion of the total quenching, may lead to the chemical and scintillation effects observed in Hg($^1P_1$) photosensitization.

(11) E. Tannenbaum, E. M. Coffin, and A. J. Harrison, *J. Chem. Phys.*, **21**, 311 (1953).

(12) L. C. Jones, Jr., and L. W. Taylor, *Anal. Chem.*, **27**, 228 (1955).

(13) H. E. Gunning and O. P. Strausz, "Advances in Photochemistry," Vol. 1, W. A. Noyes, Jr., G. S. Hammond, and J. H. Pitts, Jr., Ed., Interscience Publishers, New York, N. Y., 1963, p 209.

The Prediction of the Properties of Mixed Electrolytes from Measurements on Common Ion Mixtures

by P. J. Reilly and R. H. Wood

Department of Chemistry, University of Delaware, Newark, Delaware 19711 *(Received June 5, 1969)*

An equation predicting the free energy enthalpy and volume of a general mixture of electrolytes has been derived. The equation, developed from the work of Friedman, predicts the properties of the mixed electrolyte solution from a knowledge of the properties of pure electrolytes and common ion mixtures. The equation allows for all possible pairwise interactions and will be most accurate when all of the electrolytes are of the type normally considered to be fully dissociated. The equation has been used to derive a general form of the cross-square rule. This general form applies to any mixture of salts whether the mixture is symmetric or asymmetric.

Introduction

In a recent paper Wood and Anderson[1] using Friedman's[2] approach for mixed electrolytes showed that the properties of charge-symmetric mixtures of electrolytes could be predicted from measurements on pure electrolytes and on common ion mixtures. The equation was based on pair and triplet interactions and neglected only like-charged triplets. The equation has an advantage over the equation proposed earlier by Scatchard[3] because, for heats and volumes of mixing, it is expressed more directly in terms of the experimental measurements. The equations of Wood and Anderson have been tested on heats of mixing and have proved accurate.[4] Guggenheim[5] has proposed an equation which includes only pairwise interactions. Recently, Scatchard[6] has extended his treatment to cover charge-asymmetric mixtures. The present paper reports the extension of the Wood and Anderson equations to include charge-asymmetric mixtures.

Theory

The treatment developed in this paper allows the free energy, or any related property, of a mixed electrolyte solution to be calculated if the properties of the pure electrolytes and of the common ion mixtures are known.

The excess free energy of mixing ($\Delta_m G^{ex}$) for a common ion mixture containing 1 kg of solvent, formed at constant ionic strength by mixing a solution of ions 1 and 3 in y kg of solvent with a solution of ions 2 and 3 in $(1 - y)$ kg of solvent, is found to obey an equation of the form[2]

$$\Delta_m G^{ex} = RTI^2 y(1 - y)[g_0 + (1 - 2y)g_1] \qquad (1)$$

where g_0 and g_1 are constants characteristic of the mixture.

Friedman[2] suggests that the excess free energy is governed by the change in the concentrations of ion pairs and triplets in the mixing process. The excess free energy then depends on B_u—a constant characteristic of the species u, and $\Delta_m C^u$—the change in the concentration product of the species u when the mixture is formed. The excess free energy must therefore obey an equation of the form

$$\Delta_m G^{ex} = RT \sum B_u \Delta_m C^u \qquad (2)$$

(Note that for the purposes of this derivation we are neglecting the difference between molal and molar concentration scales. In addition, we are neglecting the difference between mixing at constant solvent activity and mixing at constant pressure. The approximations involved are discussed in Friedman's book.)

A species formed by a pair of ions of type 2 is represented by u = 020 while an ion pair formed by an ion of type 1 with an ion of type 3 means that u = 101. For the species u, the concentration product in each solution is equal to the product of the concentration of the ions in the species multiplied by the mass of solvent in the solution. To evaluate $\Delta_m C^u$, the concentration product in each solution is calculated and the initial values are subtracted from the final value. If the mixing is performed at constant ionic strength, I, by mixing y kg of solvent containing ions 1 and 3 with $(1 - y)$ kg of solvent containing ions 2 and 3 to form 1 kg of solvent containing ions 1, 2, and 3, then the compositions of each of the three solutions are as shown in Table I. To calculate $\Delta_m C^{002}$, one squares the concentration of ion 3 in the final solution and multiplies by the mass of solvent. From this one subtracts y

---

[1] R. H. Wood and H. L. Anderson, *J. Phys. Chem.*, **70**, 992 (1966).

[2] H. L. Friedman, "Ionic Solution Theory," Interscience Publishers, New York, N. Y., 1962; H. L. Friedman, *J. Chem. Phys.*, **32**, 1134, 1351 (1960).

[3] G. Scatchard and S. S. Prentiss, *J. Amer. Chem. Soc.*, **56**, 2314, 2320 (1934); G. Scatchard, *ibid.*, **83**, 2636 (1961).

[4] R. H. Wood and H. L. Anderson, *J. Phys. Chem.*, **70**, 1877 (1966).

[5] E. A. Guggenheim, *Trans. Faraday Soc.*, **62**, 3446 (1966).

[6] G. Scatchard, *J. Amer. Chem. Soc.*, **90**, 3124 (1968).

Table I

	Concn, ion 1	Concn, ion 2	Concn, ion 3	Mass of solvent, kg
Initial solution 1	$\frac{2I}{Z_1(Z_1 - Z_3)}$	0	$\frac{-2I}{Z_3(Z_1 - Z_3)}$	y
Initial solution 2	0	$\frac{2I}{Z_2(Z_2 - Z_3)}$	$\frac{-2I}{Z_3(Z_2 - Z_3)}$	$1 - y$
Final solution	$\frac{y2I}{Z_1(Z_1 - Z_3)}$	$\frac{(1 - y)2I}{Z_2(Z_2 - Z_3)}$	$\left\{\frac{-y2I}{Z_3(Z_1 - Z_3)} \frac{-(1 - y)2I}{Z_3(Z_2 - Z_3)}\right\}$	1

multiplied by the square of the concentration of ion 3 in solution 1 and $(1 - y)$ multiplied by the square of the concentration of ion 3 in solution 2, *i.e.*

$$\Delta_m C^{002} = 1\cdot\left(-y\frac{2I}{Z_3(Z_1 - Z_3)} - (1 - y)\frac{2I}{Z_3(Z_2 - Z_3)}\right)^2 - y\left(\frac{-2I}{Z_3(Z_1 - Z_3)}\right)^2 - (1 - y)\left(\frac{-2I}{Z_3(Z_2 - Z_3)}\right)^2 = -4y(1 - y)I^2\frac{(Z_1 - Z_2)^2}{Z_3^2(Z_1 - Z_3)^2(Z_2 - Z_3)^2}$$

By this process, the following values of $\Delta_m C^u$ for various ion pairs are obtained

$$\Delta_m C^{200} = -4y(1 - y)I^2/Z_1^2(Z_1 - Z_3)^2$$

$$\Delta_m C^{020} = -4y(1 - y)I^2/Z_2^2(Z_2 - Z_3)^2$$

$$\Delta_m C^{002} = -4y(1 - y)I^2(Z_1 - Z_2)^2/Z_3^2(Z_1 - Z_3)^2 \times (Z_2 - Z_3)^2$$

$$\Delta_m C^{110} = 4y(1 - y)I^2/Z_1Z_2(Z_1 - Z_3)(Z_2 - Z_3)$$

$$\Delta_m C^{101} = -4y(1 - y)I^2(Z_1 - Z_2)/Z_1Z_3(Z_1 - Z_3)^2 \times (Z_2 - Z_3)$$

$$\Delta_m C^{011} = 4y(1 - y)I^2(Z_1 - Z_2)/Z_2Z_3(Z_1 - Z_3) \times (Z_2 - Z_3)^2$$

where Z_1, Z_2, and Z_3 are the charges of ions 1, 2, and 3, respectively (ion 3 is the ion common to both salts).

Applying eq 2 to the $\Delta_m C^u$ above, one finds that the excess free energy due to pairs has the form[2]

$$\Delta_m G^{ex}_{pairs} = RTI^2y(1 - y)g_{pairs}$$

where

$$\frac{g_{pairs}}{4} = \frac{-B^{200}}{Z_1^2(Z_1 - Z_3)^2} - \frac{B^{020}}{Z_2^2(Z_2 - Z_3)^2} - \frac{(Z_1 - Z_2)^2B^{002}}{Z_3^2(Z_1 - Z_3)^2(Z_2 - Z_3)^2} + \frac{B^{110}}{Z_1Z_2(Z_1 - Z_3)(Z_2 - Z_3)} - \frac{(Z_1 - Z_2)B^{101}}{Z_1Z_3(Z_1 - Z_3)^2(Z_2 - Z_3)} + \frac{(Z_1 - Z_2)B^{011}}{Z_2Z_3(Z_1 - Z_3)(Z_2 - Z_3)^2} \quad (3)$$

Thus, pairs contribute only to the symmetrical term in eq 1.

The effect of triplet formation is more complicated since, in general, triplets generate extra y dependence—*i.e.*, contribute to g_1 as well as to g_0. The values of $\Delta_m C^u$ for the various triplets are

$$\Delta_m C^{300} = -8y(1 - y)I^3[1 + y]/Z_1^3(Z_1 - Z_3)^3$$

$$\Delta_m C^{030} = -8y(1 - y)I^3[2 - y]/Z_2^3(Z_2 - Z_3)^3$$

$$\Delta_m C^{003} = 8y(1 - y)I^3[2Z_1 + Z_2 - 3Z_3 - (Z_1 - Z_2)y](Z_1 - Z_2)^2/Z_3^3(Z_1 - Z_3)^3(Z_2 - Z_3)^3$$

$$\Delta_m C^{210} = 8y(1 - y)I^3[y]/Z_1^2Z_2(Z_1 - Z_3)^2(Z_2 - Z_3)$$

$$\Delta_m C^{120} = 8y(1 - y)I^3[1 - y]/Z_1Z_2^2(Z_1 - Z_3)(Z_2 - Z_3)^2$$

$$\Delta_m C^{201} = 8y(1 - y)I^3[Z_2 - Z_3 - (Z_1 - Z_2)y]/Z_1^2Z_3(Z_1 - Z_3)^3(Z_2 - Z_3)$$

$$\Delta_m C^{021} = 8y(1 - y)I^3[2Z_1 - Z_2 - Z_3 - (Z_1 - Z_2)y]/Z_2^2Z_3(Z_1 - Z_3)(Z_2 - Z_3)^3$$

$$\Delta_m C^{111} = -8y(1 - y)I^3[Z_1 - Z_3 - (Z_1 - Z_2)y]/Z_1Z_2Z_3(Z_1 - Z_3)^2(Z_2 - Z_3)^2$$

$$\Delta_m C^{102} = 8y(1 - y)I^3[Z_1 + Z_2 - 2Z_3 - (Z_1 - Z_2)y](Z_1 - Z_2)/Z_1Z_3^2(Z_1 - Z_3)^3(Z_2 - Z_3)^2$$

$$\Delta_m C^{012} = -8y(1 - y)I^3[2Z_1 - 2Z_3 - (Z_1 - Z_2)y](Z_1 - Z_2)/Z_2Z_3^2(Z_1 - Z_3)^2(Z_2 - Z_3)^3$$

It seems likely that triplets formed from two anions and one cation and *vice versa* will be more important than triplets formed from three ions of the same charge type. As a first approximation, one need only consider the influence of $\Delta_m C^{201}$, $\Delta_m C^{021}$, $\Delta_m C^{111}$, $\Delta_m C^{102}$, and $\Delta_m C^{012}$, which contribute to g_1 as well as g_0 unless Z_1 and Z_2 have the same value. The approximate values of g_0 and g_1 are given by eq 4 and 5.

$$g_0 = g_{pairs} + \frac{4I}{Z_3(Z_1 - Z_3)(Z_2 - Z_3)} \times \left\{\frac{(-Z_1 + 3Z_2 - 2Z_3)B^{201}}{Z_1^2(Z_1 - Z_3)^2} + \frac{(3Z_1 - Z_2 - 2Z_3)B^{021}}{Z_2^2(Z_2 - Z_3)^2} - \frac{(Z_1 + Z_2 - 2Z_3)B^{111}}{Z_1Z_2(Z_1 - Z_3)(Z_2 - Z_3)} + \frac{(Z_1 - Z_2)}{Z_3(Z_1 - Z_3)(Z_2 - Z_3)} \times \left[\frac{(Z_1 + 3Z_2 - 4Z_3)B^{102}}{Z_1(Z_1 - Z_3)} - \frac{(3Z_1 + Z_2 - 4Z_3)B^{012}}{Z_2(Z_2 - Z_3)}\right]\right\} \quad (4)$$

$$g_1 = \frac{4I(Z_1 - Z_2)}{Z_3(Z_1 - Z_3)(Z_2 - Z_3)}\left\{\frac{B^{201}}{Z_1^2(Z_1 - Z_3)^2} + \frac{B^{021}}{Z_2^2(Z_2 - Z_3)^2} - \frac{B^{111}}{Z_1Z_2(Z_1 - Z_3)(Z_2 - Z_3)} + \frac{(Z_1 - Z_2)}{Z_3(Z_1 - Z_3)(Z_2 - Z_3)}\left[\frac{B^{102}}{Z_1(Z_1 - Z_3)} - \frac{B^{012}}{Z_2(Z_2 - Z_3)}\right]\right\} \quad (5)$$

Experimentally it is found that ion pairs are often much more important than triplets in mixed electrolyte solutions.[1,2,7] If triplets are neglected, it becomes possible to calculate the excess free energy—and hence, the total free energy—of any solution. Thus for a solution containing m_i^{M} moles of cation M_i with charge Z_i^{M}, m_j^{X} moles of anion X_j with charge Z_j^{X}, etc., in each kilogram of solvent it will be shown that the free energy is given by

$$G = \sum_{l=1}^{l=i}\sum_{m=1}^{m=j} \frac{E_l^{\mathrm{M}}E_m^{\mathrm{X}}Z_{lm}}{2EI} G^{\circ}{}_{\mathrm{M}_l\mathrm{X}_m} + \frac{RT}{4E}\sum_{k=2}^{k=i}\sum_{l=1}^{l=(k-1)}\sum_{m=1}^{m=j} E_k^{\mathrm{M}}E_l^{\mathrm{M}}E_m^{\mathrm{X}}Z_{km}Z_{lm}g_{\mathrm{M}_k\mathrm{M}_l}{}^{\mathrm{X}_m} + \frac{RT}{4E}\sum_{k=1}^{k=i}\sum_{l=2}^{l=j}\sum_{m=1}^{m=l-1} E_k^{\mathrm{M}}E_l^{\mathrm{X}}E_m^{\mathrm{X}}Z_{kl}Z_{km}g_{\mathrm{X}_l\mathrm{X}_m}{}^{\mathrm{M}_k} \tag{6}$$

where

$$E_l^{\mathrm{M}} = Z_l^{\mathrm{M}}m_l^{\mathrm{M}}$$

$$E_l^{\mathrm{X}} = -Z_l^{\mathrm{X}}m_l^{\mathrm{X}} \tag{6a}$$

$$E = \sum_{k=1}^{k=i} E_k^{\mathrm{M}} = \sum_{l=1}^{l=j} E_l^{\mathrm{X}} \tag{6b}$$

$$Z_{km} = Z_k^{\mathrm{M}} - Z_m^{\mathrm{X}} \tag{6c}$$

$$2I = \sum_{k=1}^{k=i} Z_k^{\mathrm{M}}E_k^{\mathrm{M}} - \sum_{l=1}^{l=j} Z_l^{\mathrm{X}}E_l^{\mathrm{X}} \tag{6d}$$

$G^{\circ}{}_{\mathrm{M}_l\mathrm{X}_m}$ is the free energy of pure $\mathrm{M}_l\mathrm{X}_m$ while $g_{\mathrm{M}_k\mathrm{M}_l}{}^{\mathrm{X}_m}$ and $g_{\mathrm{X}_l\mathrm{X}_m}{}^{\mathrm{M}_k}$ are the values of g_0, from eq 4, for the mixing of M_k and M_l in the presence of X_m, and the mixing of X_l and X_m in the presence of M_k, respectively.

Equation 6 is equivalent to forming the mixed electrolyte solution by mixing quantities of solutions of each of the salts $\mathrm{M}_1\mathrm{X}_1$, $\mathrm{M}_1\mathrm{X}_2$, $\cdots$ $\mathrm{M}_i\mathrm{X}_j$ such that the final solution contains m_1^{M} moles of M_1, m_2^{M} moles of M_2, etc. The quantity of $\mathrm{M}_i\mathrm{X}_j$ solution to be taken is $(E_i^{\mathrm{M}}E_j^{\mathrm{X}}Z_{ij}/2EI)$ kg of solvent and the concentrations of M_i and X_j are $(ZI/Z_i^{\mathrm{M}}Z_{ij})$ and $(-ZI/Z_j^{\mathrm{X}}Z_{ij})$ molal, respectively.

The excess free energy of mixing is given by the second and third terms of eq 6 and it may be shown that the equation correctly predicts the excess free energy, due to pairwise interactions, as follows.

1. The excess free energy of mixing generated by an ion M_p interacting with another ion of the same type may be calculated by substituting the relevant portion of eq 4 into eq 6 and simplifying by use of eq 6a to 6d, *i.e.*

$$\Delta_{\mathrm{m}}G^{\mathrm{ex}} = -\frac{RT}{4E}\sum_{l=1}^{l=(p-1)}\sum_{m=1}^{m=j} E_p^{\mathrm{M}}E_l^{\mathrm{M}}E_m^{\mathrm{X}}Z_{pm}Z_{lm}\frac{4B^{pp}}{(Z_p^{\mathrm{M}})^2(Z_{pm})^2} - \frac{RT}{4E}\sum_{k=(p+1)}^{k=i}\sum_{m=1}^{m=j} E_k^{\mathrm{M}}E_p^{\mathrm{M}}E_m^{\mathrm{X}}Z_{km}Z_{pm}\frac{4B^{pp}}{(Z_p^{\mathrm{M}})^2(Z_{pm})^2} - \frac{RT}{4E}\sum_{l=2}^{l=j}\sum_{m=1}^{m=(l-1)} E_p^{\mathrm{M}}E_l^{\mathrm{X}}E_m^{\mathrm{X}}\, Z_{pl}Z_{pm}\frac{4(Z_l^{\mathrm{X}} - Z_m^{\mathrm{X}})^2B^{pp}}{(Z_p^{\mathrm{M}})^2(Z_{pl})^2(Z_{pm})^2}$$

$$= -\frac{RT}{E}\frac{B^{pp}E_p^{\mathrm{M}}}{(Z_p^{\mathrm{M}})^2}\left\{\sum_{k=1}^{k=i}\sum_{m=1}^{m=j} E_k^{\mathrm{M}}E_m^{\mathrm{X}}\frac{Z_{km}}{Z_{pm}} - E_p^{\mathrm{M}}E + E\sum_{m=1}^{m=j}\frac{Z_m^{\mathrm{X}}E_m^{\mathrm{X}}}{Z_{pm}} - \left[\sum_{m=l}^{m=j} Z_m^{\mathrm{X}}E_m^{\mathrm{X}}\right]\left[\sum_{m=1}^{m=j}\frac{E_m^{\mathrm{X}}}{Z_{pm}}\right]\right\}$$

$$= \frac{RT}{E}\frac{B^{pp}E_p^{\mathrm{M}}}{(Z_p^{\mathrm{M}})^2}\left\{E_p^{\mathrm{M}}E - 2I\sum_{m=1}^{m=j}\frac{E_m^{\mathrm{X}}}{Z_{pm}}\right\}$$

The excess free energy of mixing may also be calculated from the actual difference between interactions in the initial and final solutions. Since the interaction in a solution is given by the product of the kilograms of solvent times the molalities of the interacting ions and RTB^{u} we have the interaction in the final solution equal to

$$RTB^{pp}(m_p^{\mathrm{M}})^2$$

The initial solutions include solutions of M_p in combination with each anion. The concentration of M_p in each of these solutions is $(2I/Z_p^{\mathrm{M}}Z_{pm})$ while the quantity of solution taken is such that the mass of solvent in each is $E_p^{\mathrm{M}}E_m^{\mathrm{X}}Z_{pm}/2EI$. The interaction of M_p with itself in each of these solutions is

$$RTB^{pp}\left(\frac{2I}{Z_p^{\mathrm{M}}Z_{pm}}\right)^2\frac{E_p^{\mathrm{M}}E_m^{\mathrm{X}}Z_{pm}}{2EI}$$

The excess free energy of mixing due to the interaction is obtained by subtracting from the value of the interaction in the final solution, the sum of the interactions in the initial solutions. Hence

$$\Delta_{\mathrm{m}}G^{\mathrm{ex}} = RTB^{pp}\left\{(m_p^{\mathrm{M}})^2 - \sum_{m=1}^{m=j}\left(\frac{2I}{Z_p^{\mathrm{M}}Z_{pm}}\right)^2 \times \frac{E_p^{\mathrm{M}}E_m^{\mathrm{X}}Z_{pm}}{2EI}\right\}$$

$$= RT\,B^{pp}\left\{\frac{(E_p^{\mathrm{M}})^2}{(Z_p^{\mathrm{M}})^2} - \frac{2I}{E}\frac{E_p^{\mathrm{M}}}{(Z_p^{\mathrm{M}})^2}\sum_{m=1}^{m=j}\frac{E_m^{\mathrm{X}}}{Z_{pm}}\right\}$$

$$= \frac{RT}{E}\frac{B^{pp}E_p^{\mathrm{M}}}{(X_p^{\mathrm{M}})^2}\left\{E_p^{\mathrm{M}}E - 2I\sum_{m=1}^{m=j}\frac{E_m^{\mathrm{X}}}{Z_{pm}}\right\}$$

This result agrees with the prediction of the equation and, from the symmetry of eq 6, it is obvious that the same result will apply to the interaction between two X_r ions.

---

(7) R. H. Wood and R. W. Smith, *J. Phys. Chem.*, **69**, 2974 (1965).

2. The second type of interaction is that of an ion, M_p, with another ion of the same charge type, M_q. The excess free energy due to this interaction may be estimated from eq 4 and 6 as before, *i.e.*

$$\Delta_m G^{ex} = \frac{RT}{4E} \sum_{m=1}^{m=j} E_p{}^M E_q{}^M E_m{}^X Z_{pm} Z_{qm} \frac{4B^{pq}}{Z_p{}^M Z_q{}^M Z_{pm} Z_{qm}}$$

$$= \frac{RT}{E} \frac{E_p{}^M}{Z_p{}^M} \frac{E_q{}^M}{Z_q{}^M} B^{pq} \sum_{m=1}^{m=j} E_m{}^X$$

$$= RT \frac{E_p{}^M}{Z_p{}^M} \frac{E_q{}^M}{Z_o{}^M} B^{pq}$$

Direct calculation of the effect of this interaction, from the compositions of the solutions, gives

$$\Delta_m G^{ex} = RTm_p{}^M m_q{}^M B^{pq}$$

$$= RT \frac{E_p{}^M}{Z_p{}^M} \frac{E_q{}^M}{Z_q{}^M} B^{pq}$$

This result agrees with that given by eq 6 and from the symmetry of eq 6 it is obvious that the interaction of two anions X_r and X_s will be correctly predicted.

3. The third and final type of pairwise interaction is between a cation, M_p, and an anion, X_r. Proceeding as before, we find that eq 4 and 6 yield

$$\Delta_m G^{ex} = -\frac{RT}{4E} \sum_{l=1}^{l=(p-1)} E_p{}^M E_l{}^M E_r{}^X Z_{pr} Z_{lr} \times \frac{4(Z_p{}^M - Z_l{}^M)B^{pr}}{Z_p{}^M Z_r{}^X (Z_{pr})^2 Z_{lr}} +$$
$$\frac{RT}{4E} \sum_{k=(p+1)}^{k=i} E_k{}^M E_p{}^M E_r{}^X Z_{kr} Z_{pr} \times \frac{4(Z_k{}^M - Z_p{}^M)B^{pr}}{Z_p{}^M Z_r{}^X Z_{kr} (Z_{pr})^2} +$$
$$\frac{RT}{4E} \sum_{m=1}^{m=(r-1)} E_p{}^M E_r{}^X E_m{}^X Z_{pr} Z_{pm} \times \frac{4(Z_r{}^X - Z_m{}^X)B^{pr}}{Z_p{}^M Z_r{}^X (Z_{pr})^2 Z_{pm}} -$$
$$\frac{RT}{4E} \sum_{l=(r+1)}^{l=j} E_p{}^M E_l{}^X E_r{}^X Z_{pl} Z_{pr} \times \frac{4(Z_l{}^X - Z_r{}^X)B^{pr}}{Z_p{}^M Z_r{}^X Z_{pl} (Z_{pr})^2}$$

$$= \frac{RT}{E} \frac{E_p{}^M}{Z_p{}^M} \frac{E_r{}^X}{Z_r{}^X} \frac{B^{pr}}{Z_{pr}} \left\{ \sum_{k=1}^{k=i} Z_k{}^M E_k{}^M - Z_p{}^M E - \sum_{l=1}^{l=j} Z_l{}^X E_l{}^X + Z_r{}^X E \right\}$$

$$= \frac{RT}{E} \frac{E_p{}^M}{Z_p{}^M} \frac{E_r{}^X}{Z_r{}^X} \frac{B^{pr}}{Z_{pr}} \{2I - Z_{pr}E\}$$

The magnitude of the actual interaction in the system may also be calculated as follows.

$$\Delta_m G^{ex} = RTB^{pr} \left\{ m_p{}^M m_r{}^X - \frac{2I}{Z_p{}^M Z_{pr}} \frac{(-2I)}{Z_r{}^X Z_{pr}} \times \frac{E_p{}^M E_r{}^X Z_{pr}}{2EI} \right\}$$

$$= RTB^{pr} \left\{ \frac{E_p{}^M}{Z_p{}^M} \frac{E_r{}^X}{Z_r{}^X} + \frac{2I}{Z_{pr}E} \frac{E_p{}^M}{Z_p{}^M} \frac{E_r{}^X}{Z_r{}^X} \right\}$$

$$= \frac{RT}{E} \frac{E_p{}^M}{Z_p{}^M} \frac{E_r{}^X}{Z_r{}^X} \frac{B^{pr}}{Z_{pr}} \{2I - Z_{pr}E\}$$

Hence, in all possible situations the equation correctly predicts the ion-pair interactions.

If the cations all have the same charge, Z^M, and the anions all have the same charge, Z^X, the equation will correctly predict triplet interactions (except for triplets composed of three cations or three anions). In this case, g_1 vanishes and g_0 of eq 4 becomes

$$g_0 = \frac{4}{Z_1{}^2(Z_1 - Z_3)^2} \left\{ -B^{200} - B^{020} + B^{110} + \frac{2I}{Z_3(Z_1 - Z_3)} [B^{201} + B^{021} - B^{111}] \right\} \quad (7)$$

(since $Z_1 = Z_2$).

In this special case, E is equal to $2I/(Z^M - Z^X)$. Equation 6 may then be written as

$$G = \sum_{l=1}^{l=i} \sum_{m=1}^{m=j} \frac{E_l{}^M E_m{}^X (Z^M - Z^X)^2}{4I^2} G^\circ{}_{M_l X_m} + \frac{RT}{8I} \sum_{k=2}^{k=i} \sum_{l=1}^{l=(k-1)} \sum_{m=1}^{m=j} E_k{}^M E_l{}^M E_m{}^X (Z^M - Z^X)^3 \times g_{M_k M_l}{}^{X_m} + \frac{RT}{8I} \sum_{k=1}^{k=i} \sum_{l=2}^{l=j} \sum_{m=1}^{m=(l-1)} E_k{}^M E_l{}^X E_m{}^X \times (Z^M - Z^X)^3 g_{X_l X_m}{}^{M_k} \quad (8)$$

The triplet interactions may be divided into two classes. The first class of triplets contains three different ions, *e.g.*, M_p, M_q, and X_r. Combination of the restricted equations (7 and 8) gives the excess free energy of mixing due to this triplet as

$$\Delta_m G^{ex} = -\frac{RT}{8I} E_p{}^M E_q{}^M E_r{}^X (Z^M - Z^X)^3 \times \frac{8IB^{pqr}}{(Z^M)^2 Z^X (Z^M - Z^X)^3}$$

$$= -RT \frac{E_p{}^M E_q{}^M E_r{}^X}{(Z^M)^2 Z^X} B^{pqr}$$

The actual interaction in the solution gives

$$\Delta_m G^{ex} = RTm_p{}^M m_q{}^M m_r{}^X B^{pqr}$$

$$= -RT \frac{E_p{}^M E_q{}^M E_r{}^X}{(Z^M)^2 Z^X} B^{pqr}$$

The second class of triplet interactions are those between two ions of the same type, *e.g.*, M_p, and an ion of the opposite charge type, *e.g.*, X_r. The excess free energy of mixing due to this triplet is given by eq 7 and 8 as

$$\Delta_m G^{ex} = \frac{RT}{8I} \sum_{k=(p+1)}^{k=i} E_k{}^M E_p{}^M E_r{}^X (Z^M - Z^X)^3 \times \frac{8IB^{ppr}}{(Z^M)^2 Z^X (Z^M - Z^X)^3} + \frac{RT}{8I} \sum_{l=1)}^{l=(p-1)} E_l{}^M E_p{}^M E_r{}^X (Z^M - Z^X)^3 \times \frac{8IB^{ppr}}{(Z^M)^2 Z^X (Z^M - Z^X)^3}$$

$$= RT \frac{E_p{}^M E_r{}^X}{(Z^M)^2 Z^X} B^{ppr} \{E - E_p{}^M\}$$

The actual interaction indicated from the composition of the solutions gives the following amount of excess free energy of mixing.

$$\Delta_m G^{ex} = RTB^{ppr} \left\{ m_p{}^M m_p{}^M m_r{}^M - \left[\frac{2I}{Z^M(Z^M - Z^X)}\right]^2 \frac{(-2I)}{Z^X(Z^M - Z^X)} \frac{E_p{}^M E_r{}^X (Z^M - Z^X)^2}{4I^2} \right\}$$

$$= RTB^{ppr} \left\{ \frac{-(E_p{}^M)^2 E_r{}^X}{(Z^M)^2 Z^X} + \frac{2IE_p{}^M E_r{}^X}{(Z^M)^2 Z^X (Z^M - Z^X)} \right\}$$

$$= RT \frac{E_p{}^M E_r{}^X}{(Z^M)^2 Z^X} B^{ppr} \{E - E_p{}^M\}$$

Thus in this special case the equation correctly predicts the effect of both pairs and these triplets. It can be shown that eq 8 is identical with the equation of Wood and Anderson for the case where all the electrolytes are of the same charge type.

Discussion

Equation 6 correctly predicts all pairwise interactions for any mixture of electrolytes. For mixtures containing only a single class of electrolytes (*e.g.*, 1–1 or 2–1 salts) all triplets, except those formed by three ions of the same charge type, are correctly predicted. For other mixtures, the triplet terms are only partially accounted for. This means that the equation will not be as accurate for mixtures containing several classes of electrolytes but since pairwise interactions are often predominant,[1,7] it should be a good first approximation.

The present equations differ from Scatchard's equations in that the properties of the pure electrolytes are not represented by power series and the components of the mixed electrolyte solution are specified by the first term in eq 6. This term specifies the amount of each component from which the mixture is formed. By collecting terms in Scatchard's equation into terms representing the properties of the pure electrolytes of our component rule ($G°_{M_lX_m}$ terms in eq 6) and terms representing measurements on two salt common ion mixtures (the $g_{M_kM_l}{}^{X_m}$ terms of eq 6) one should obtain the present equation.

The advantage of the present equation is that for heats and volumes of mixing it is more directly expressed in terms of experimental quantities. To show this, the analog of eq 6 for heats of mixing is needed. This is

$$H = \sum_{l=1}^{l=i} \sum_{m=1}^{m=j} \frac{E_l{}^M E_m{}^X Z_{lm}}{2EI} H°_{M_lX_m} + \frac{RT}{4E} \sum_{k=2}^{k=i} \sum_{l=1}^{l=(k-1)} \sum_{m=1}^{m=j} E_k{}^M E_l{}^M E_m{}^X Z_{km} Z_{lm} h_{M_kM_l}{}^{X_m} + \frac{RT}{4E} \sum_{k=1}^{k=i} \sum_{l=2}^{l=j} \sum_{m=1}^{(m=l-1)} E_k{}^M E_l{}^X E_m{}^X Z_{kl} Z_{km} h_{X_lX_m}{}^{M_k}$$

where RTh_0 is the heat of mixing analog of RTg_0 and

$$H°_{M_lX_m} = m_{M_lX_m} \varphi_L(M_lX_m)$$

In this equation $H°_{M_lX_m}$ is obtained by measuring the heat of dilution of the pure electrolyte. Similarly, $h_{M_kM_l}{}^{X_m}$ is measured by one heat of mixing (M_kX_m with M_lX_m) at a molal ionic strength equal to that of the multicomponent mixture.

The final equations do not show it but in deriving the present equation the concept that any mixture of electrolytes can be formed by a series of common-ion mixings was very important. The mixing scheme involves picking a cation and, with it as a common ion, mixing all the anions to get the final anion mixture. This process is repeated for each cation and the final mixture is then made by mixing the cations in the presence of the common mixture of anions. This concept makes it clear that it is only necessary to predict heats of mixing ions in the presence of a common mixture of ions in order to predict the properties of any mixed electrolyte. It was a consideration of this mixing scheme that led to the component rule expressed in the first term of eq 6.

The general equations may be used to investigate the cross-square rule[8] and to predict the limitations of the conventional form of the rule. The cross-square rule has usually been applied to mixtures of 1–1 electrolytes. If the four salts formed from two cations and two anions are mixed in pairs, it is found that the sum of the excess free energy of mixing of the four common ion mixings is equal to the sum of the two mixings in which there is no common ion. If one represents the mixings as the sides and diagonals of a square as below, then the sum of the sides (square) mixings is equal to the sum of the diagonal (cross) mixings.

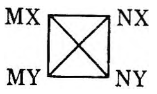

---

[8] T. F. Young, Y. C. Wu, and A. A. Krawetz, *Discussions Faraday Soc.*, **24**, 37, 77, 80 (1957).

In the general case, the influence of the charge of each ion must be taken into account. If one takes quantities of solution containing equal masses of solvent (*e.g.*, 0.5 kg) and if each solution has the same ionic strength (I) the excess free energy of mixing generated in the pairwise mixings is as follows.

1. The excess free energy of mixing for the common anion mixture MX–NX is

$$\Delta_m G^{ex} = {}^1/_4 RTI^2 g_{MN}{}^{X}$$

2. The excess free energy generated by mixing M and N in the presence of the common anion Y is

$$\Delta_m G^{ex} = {}^1/_4 RTI^2 g_{MN}{}^{Y}$$

3. The first common cation mixture, MX–MY, generates excess free energy as below

$$\Delta_m G^{ex} = {}^1/_4 RTI^2 g_{XY}{}^{M}$$

4. The final common-ion mixture is NX–NY which gives the following quantity of excess free energy

$$\Delta_m G^{ex} = {}^1/_4 RTI^2 g_{XY}{}^{N}$$

(In the above the effect of the small RTg_1 term is neglected.) The excess free energy of mixing involved in the two cross mixings may be calculated from the general equation (eq 6).

The total free energy of the mixture of MX and NY is given by

$$G = \frac{(Z^N - Z^Y)G°_{MX} + (Z^M - Z^Y)G°_{MY} + (Z^N - Z^X)G°_{NX} + (Z^M - Z^X)G°_{NY}}{2(Z^M + Z^N - Z^X - Z^Y)} + RTI^2\left[\frac{(Z^N - Z^X)g_{MN}{}^{X} + (Z^M - Z^Y)g_{MN}{}^{Y} + (Z^M - Z^Y)g_{XY}{}^{M} + (Z^N - Z^X)g_{XY}{}^{N}}{4(Z^M + Z^N - Z^X - Z^Y)}\right]$$

The excess free energy of mixing is the difference between the total free energy of the mixture and the free energy of the components. In this case, the components are MX and NY so the excess free energy is

$$\Delta_m G^{ex} = G - {}^1/_2 G°_{MX} - {}^1/_2 G°_{NY} = \frac{-(Z^M - Z^X)G°_{MX} + (Z^M - Z^Y)G°_{MY} + (Z^N - Z^X)G°_{NX} - (Z^N - Z^Y)G°_{NY}}{2(Z^M + Z^N - Z^X - Z^Y)} + RTI^2\left[\frac{(Z^N - Z^X)g_{MN}{}^{X} + (Z^M - Z^Y)g_{MN}{}^{Y} + (Z^M - Z^Y)g_{XY}{}^{M} + (Z^N - Z^X)g_{XY}{}^{N}}{4(Z^M + Z^N - Z^X - Z^Y)}\right]$$

Similarly, the excess free energy of mixing for the salt pair MY–NX is

$$\Delta_m G^{ex} = \frac{(Z^M - Z^X)G°_{MX} - (Z^M - Z^Y)G°_{MY} - (Z^N - Z^X)G°_{NX} + (Z^N - Z^Y)G°_{NY}}{2(Z^M + Z^N - Z^X - Z^Y)} + RTI^2\left[\frac{(Z^M - Z^X)g_{MN}{}^{X} + (Z^N - Z^Y)g_{MN}{}^{Y} + (Z^M - Z^X)g_{XY}{}^{M} + (Z^N - Z^Y)g_{XY}{}^{N}}{4(Z^M + Z^N - Z^X - Z^Y)}\right]$$

These two results show how eq 6 predicts the excess free energy of the cross mixings from a knowledge of the common ion (square) mixings.

The sum of the cross-mixings therefore gives the excess free energy of mixing as

$$\left[\Delta_m G^{ex}{}_{MX-NY} + \Delta_m G^{ex}{}_{MY-NX}\right] = {}^1/_4 RTI^2 \times \{(Z^M + Z^N - 2Z^X)g_{MN}{}^{X} + (Z^M + Z^N - 2Z^Y)g_{MN}{}^{Y} + (2Z^M - Z^X - Z^Y)\,g_{XY}{}^{M} + (2Z^N - Z^X - Z^Y)\,g_{XY}{}^{N}\}/\{(Z^M + Z^N - Z^X - Z^Y)\} \quad (9)$$

The cross-square rule is now seen to apply in its original form if the four salts are from the same class of electrolytes (1–1, 2–1, etc.). If the salts are from different classes, then the cross-square rule must be modified to include the charge factors shown in eq 9. The general relation between the cross and square mixings is that the sum of the excess free energy in the cross mixings is equal to a weighted sum of the excess free energy in the square mixings, *i.e.*

$$(Z^M + Z^N - Z^X - Z^Y)(\Delta_m G^{ex}{}_{MX-NY} + \Delta_m G^{ex}{}_{MY-NX}) = (Z^M + Z^N - 2Z^X)\Delta_m G^{ex}{}_{MX-NX} + (Z^M + Z^N - 2Z^Y)\Delta_m G^{ex}{}_{MY-NY} + (2Z^M - Z^X - Z^Y)\Delta_m G^{ex}{}_{MX-MY} + (2Z^N - Z^X - Z^Y)\Delta_m G^{ex}{}_{NX-NY}$$

Conclusion

The equations presented in this paper allow the free energy and related properties of a mixed electrolyte solution to be calculated from the properties of single electrolyte solutions combined with knowledge of common-ion mixtures. The cross-square rule has been extended to charge-asymmetric mixtures. The following paper gives an example of the use of these equations to predict the heat of formation of charge-asymmetric mixture of three salts.

Acknowledgment. The authors gratefully acknowledge the support of this work by the Office of Saline Water, U. S. Department of the Interior.

Heats of Mixing Aqueous Electrolytes. VIII. Prediction and Measurement of Charge-Asymmetric Mixtures of Three Salts[1]

by R. H. Wood, M. Ghamkhar, and J. D. Patton

Department of Chemistry, University of Delaware, Newark Delaware 19711 *(Received June 5, 1969)*

The heats of mixing aqueous solutions of alkaline earth chlorides with aqueous solutions of mixtures of two alkali metal chlorides at constant molal ionic strength have been measured at 25°. The results are compared with the prediction of the equation of Reilly and Wood and show that the prediction is accurate below 1 *m* and still useful at 3 *m*. A thermodynamic cycle is used to explore the approximation inherent in the use of the equation for mixtures of three cations. The results confirm the conclusion of Wood and Smith that like-charged pair interactions are often larger than triplet interactions.

Introduction

Wood and Anderson,[2] using Friedman's[3] approach to mixed electrolytes, derived an equation for predicting multi-component mixtures providing that all electrolytes in the mixture were of the same charge-type. These equations were shown to be quite accurate by measurements on mixtures of three salts.[4] Recently, Reilly and Wood[5] have extended the equation of Wood and Anderson to charge-asymmetric mixtures. As a test of the accuracy of this equation, the present paper reports measurements on charge-asymmetric mixtures of three salts.

Experimental Section

The calorimetric technique and the preparation of the stock solutions have been described elsewhere.[6–8]

The experimental data were fitted by the method of least squares to the equation

$$\Delta H_{\mathrm{m}}(\text{cal/kg of solvent}) = RTI^2y(1 - y)[h_0 + (1 - 2y)h_1] \quad (1)$$

where I is the molal ionic strength and y is the ionic strength fraction of either magnesium chloride or barium chloride, h_0 is a measure of the magnitude of the interaction, and h_1 is a measure of the skew of the interaction. The heats of mixing were measured in the range y = 0–0.2 and y = 0.8–1.0. Any points which differed from the least-squares fit by more than about twice the standard deviation were rejected.

Discussion

The results of the measurements of the heat of mixing a 50–50 mol % mixture of two alkali metal chlorides with an alkaline earth chloride are given in Table I. These mixtures can be considered as a mixture of a 1–1 electrolyte with a 2–1 electrolyte. As a result, the same trend to more positive values of RTh_0 as the molal ionic strength decreases, observed for mixtures of two salts,[7,8] should be seen in these results. Table I shows that indeed RTh_0 at $I = 1$ is always larger than RTh at $I = 2$ or 3.

The results in Table I can be predicted from measurements on mixtures of two salts by using the equation of Reilly and Wood[5]

$$H = \sum_{l=1}^{l=i}\sum_{m=1}^{m=j} E_l^{\mathrm{M}}E_m^{\mathrm{X}}(Z_l^{\mathrm{M}} - Z_m^{\mathrm{X}})H^\circ_{\mathrm{M}_l\mathrm{X}_m}/2EI +$$
$$(RT/4E)\sum_{k=2}^{k=i}\sum_{l=1}^{l=(k-1)}\sum_{m=1}^{m=j} E_k^{\mathrm{M}}E_l^{\mathrm{M}}E_m^{\mathrm{X}}(Z_k^{\mathrm{M}} - Z_m^{\mathrm{X}})(Z_l^{\mathrm{M}} - Z_m^{\mathrm{X}})h_{\mathrm{M}_k\mathrm{M}_l}{}^{\mathrm{X}_m} +$$
$$(RT/4E)\sum_{k=1}^{k=i}\sum_{l=2}^{l=i}\sum_{m=1}^{m=(l-1)} E_k^{\mathrm{M}}E_l^{\mathrm{X}}E_m^{\mathrm{X}}(Z_k^{\mathrm{M}} - Z_l^{\mathrm{X}})(Z_k^{\mathrm{M}} - Z_m^{\mathrm{X}})h_{\mathrm{X}_l\mathrm{X}_m}{}^{\mathrm{M}_k} \quad (2)$$

where E_k^{M} is the concentration of cation k in equivalents per kilogram of solvent, Z_k^{M} is the charge on cation k, $E = \Sigma_k E_k^{\mathrm{M}} = -\Sigma_m E_m^{\mathrm{X}}$, and $H^\circ_{\mathrm{M}_l\mathrm{X}_m}$ is the heat content of the pure electrolyte $\mathrm{M}_l\mathrm{X}_m$ in calories per kilogram of solvent. Note that

$$H^\circ_{\mathrm{M}_l\mathrm{X}_m} = m^\circ_{\mathrm{M}_l\mathrm{X}_m}\phi_{\mathrm{L}}(\mathrm{M}_l\mathrm{X}_m) \quad (3)$$

where $m^\circ_{\mathrm{M}_l\mathrm{X}_m}$ is the molality of the salt $\mathrm{M}_l\mathrm{X}_m$ when its ionic strength is equal to I. The nomenclature in this equation is convenient for the derivation of the equations but can be simplied to

---

[1] Presented at the symposium on "Structure of Water and Aqueous Solutions" in honor of Professor T. F. Young, University of Chicago, Chicago, Ill., June 1969.

[2] R. H. Wood and H. L. Anderson, *J. Phys. Chem.*, **70**, 992 (1966).

[3] (a) H. L. Friedman, *J. Chem. Phys.*, **32**, 1134, 1351 (1960); (b) H. L. Friedman, "Ionic Solution Theory," Interscience Publishers, Inc., New York, N. Y., 1962.

[4] R. H. Wood and H. L. Anderson, *J. Phys Chem.*, **70**, 1877 (1966).

[5] P. J. Reilly and R. H. Wood, *ibid.*, **73**, 4292 (1969).

[6] R. H. Wood and R. W. Smith, *ibid.*, **69**, 2974 (1965).

[7] R. H. Wood, J. D. Patton, and M. Ghamkhar, *ibid.*, **73**, 346 (1969).

[8] R. H. Wood and M. Ghamkhar, *ibid.*, **73**, 3959 (1969).

Table I: Heat of Mixing 50–50 Mol % Alkali Chloride Mixtures with Magnesium Chloride and Barium Chloride

Salt mixture	I^a	RTh_0,[b] cal/kg ional^2	RTh_1, cal/kg ional^2	N^c
LiCl·KCl–MgCl$_2$	3	26.9 ± 0.1	−1.7 ± 0.2	16
	2	41.7 ± 0.1	−2.8 ± 0.2	16
	1	57 ± 1	−4 ± 2	8
	0.5	67 ± 2	−5 ± 2	8
LiCl·CsCl–MgCl$_2$	3	21.17 ± 0.1	−1.1 ± 0.1	14
	2	34.4 ± 0.1	−2.6 ± 0.2	7
	1	58.6 ± 0.7	−1 ± 1	8
	0.5	83 ± 1	−5 ± 2	7
KCl·CsCl–MgCl$_2$	3	−22.7 ± 0.1	5.9 ± 0.2	14
	2	15.3 ± 0.1	0.7 ± 0.1	15
	1	54.3 ± 0.5	−3.0 ± 0.7	8
	0.5	94 ± 1	−6 ± 2	8
LiCl·NaCl–BaCl$_2$	3	−14.5 ± 0.2	−1.2 ± 0.3	8
	1	4 ± 1	−3 ± 2	8
LiCl·KCl–BaCl$_2$	3	−17.2 ± 0.5	1.5 ± 5	8
	1	−0.4 ± 1	−2 ± 2	8
NaCl·KCl–BaCl$_2$	3	5.2 ± 0.1	−0.9 ± 0.2	12
	1	4.7 ± 1	−2 ± 2	8

[a] Molal ionic strength of the solutions. [b] Units are calories per kilogram of solvent per ional squared. This gives ΔH_m in calories per kilogram of solvent. [c] Number of experimental points.

$$H(\text{cal/kg}) = \sum_{\text{M,X}} E_\text{M}E_\text{X}(Z_\text{M} - Z_\text{X})m^\circ{}_{\text{MX}}\phi_\text{L}(\text{MX})/2EI + (RT/4E)\sum_{\text{M>N,X}} E_\text{M}E_\text{N}E_\text{X}(Z_\text{M} - Z_\text{X})(Z_\text{N} - Z_\text{X})h_{\text{MN}}{}^\text{X} + (RT/4E)\sum_{\text{X>Y,M}} E_\text{M}E_\text{X}E_\text{Y}(Z_\text{M} - Z_\text{X})(Z_\text{M} - Z_\text{Y})h_{\text{XY}}{}^\text{M} \quad (4)$$

where the summation with M > N means that the sum is over all M and N such that M > N. This takes each $h_{\text{MN}}{}^\text{X}$ term only once.

For the mixing of 0.5 kg of a 50–50 mixture of LiCl and KCl with 0.5 kg of MgCl$_2$, we get

$$\Delta H_\text{m}(\text{calcd}) = H(\text{LiCl}\cdot\text{KCl}\cdot\text{MgCl}_2) - (^1/_2)H(\text{MgCl}_2) - (^1/_2)H(\text{LiCl}\cdot\text{KCl}) \quad (5)$$

where each H is calculated by eq 4.

The initial MgCl$_2$ solution at a molal ionic strength, I, has $m_{\text{MgCl}_2} = I/3$, $E_\text{Mg} = 2m = 2I/3 = E_\text{Cl} = E$, and $m^\circ{}_{\text{MgCl}_2} = I/3$ so that from eq 4

$$H(\text{MgCl}_2) = (2I/3)(2I/3)[2 - (-1)](I/3)\phi_\text{L} \times (\text{MgCl}_2)/2(2I/3)I = (I/3)\phi_\text{L}(\text{MgCl}_2) \quad (6)$$

The initial LiCl–KCl solution at a molal ionic strength of I has $m_\text{Li} = m_\text{K} = I/2 = E_\text{Li} = E_\text{K}$, $m_\text{Cl} = I = E_\text{Cl} = E$, and $m^\circ{}_\text{LiCl} = m^\circ{}_\text{KCl} = I$ so that

$$H(\text{LiCl–KCl}) = (I/2)I[1 - (-1)]I\phi_\text{L}(\text{LiCl})/2I^2 + (I/2)I[1 - (-1)]I\phi_\text{L}(\text{KCl})/2I^2 + (RT/4I)(I/2)(I/2)I[1 - (-1)][1 - (-1)]h_{\text{LiK}}{}^\text{Cl} = (I/2)\phi_\text{L}(\text{LiCl}) + (I/2)\phi_\text{L}(\text{KCl}) + (I^2/4)RTh_{\text{LiK}}{}^\text{Cl} \quad (7)$$

The final solution at a molal ionic strength of I has $m_\text{Li} = m_\text{K} = I/4 = E_\text{Li} = E_\text{K}$; $E_\text{Mg} = 2m_\text{Mg} = I/3$, and $E_\text{Cl} = m_\text{Cl} = E = (I/2) + (I/3) = 5I/6$. The molalities of the pure electrolytes at the same ionic strength, I, are the same as before. Applying eq 4 gives

$$H(\text{LiCl}\cdot\text{KCl}\cdot\text{MgCl}) = (I/3)(5I/6)[2 - (-1)](I/3) \times \phi_\text{L}(\text{MgCl}_2)/[2(5I/6)I] + (I/4)(5I/6)[1 - (-1)]I\phi_\text{L}(\text{LiCl})/(2(5I/6)I] + (I/4)(5I/6)[1 - (-1)]I\phi_\text{L}(\text{KCl})/[2(5I/6)I] + (RT/[4(5I/6)]) \times \{(I/3)(I/4)(5I/6)[2 - (-1)][1 - (-1)]h_{\text{MgLi}}{}^\text{Cl} + (I/3)(I/4)(5I/6)[2 - (-1)][1 - (-1)]h_{\text{MgK}}{}^\text{Cl} + (I/4)(I/4)(5I/6)[1 - (-1)][1 - (-1)]h_{\text{LiK}}{}^\text{Cl}\} = (I/6)\phi_\text{L}(\text{MgCl}_2) + (I/4)\phi_\text{L}(\text{LiCl}) + (I/4)\phi_\text{L}(\text{KCl}) + (I^2/8)RTh_{\text{MgK}}{}^\text{Cl} + (I^2/8)RTh_{\text{MgLi}}{}^\text{Cl} + (I^2/16)RTh_{\text{LiK}}{}^\text{Cl} \quad (8)$$

Substituting eq 6, 7, and 8 into eq 5 gives

Table II: Test of the Equation for Predicting Three-Salt Mixtures

Salt mixture		I^a 0.5	1.0	2.0	3.0
LiCl·KCl–MgCl$_2$	RTh (calcd)[b]	70	58.5	42.8	32.7
	RTh (exptl)[c]	67	57	41.7	26.9
LiCl·CsCl–MgCl$_2$	RTh (calcd)	82	57.3	37.6	26.1
	RTh (exptl)	83	58.6	34.4	21.2
KCl·CsCl–MgCl$_2$	RTh (calcd)	88[d]	51.3	15.0	−8.6
	RTh (exptl)	94	54.3	15.3	−22.7
LiCl·NaCl–BaCl$_2$	RTh (calcd)		4.7		−9.5
	RTh (exptl)		4		−14.5
LiCl·KCl–BaCl$_2$	RTh (calcd)		−4.8		−12.8
	RTh (exptl)		−0.4		−17.2
NaCl·KCl–BaCl$_2$	RTh (calcd)		48.3		7.8
	RTh (exptl)		47		5.2

[a] Molal ionic strength of the solutions. [b] Calculated by eq 11. [c] Experimental value from Table I. [d] Based on an extrapolated value $RTh_0 = 11.0 \pm 4$ for the KCl–CsCl mixing at $I = 0.5$.

Table III: Heat of Mixing Alkali Chlorides in the Presence of a Common Concentration of Alkali Metal Chloride

Salt pair		I^a 0.5	1.0	2.0	3.0
LiCl·MgCl$_2$–KCl·MgCl$_2$	RTh_0 (exptl)[b]	−16 (−15)[d]	−17.6	−21.1	−29.1
	RTh_0 (calcd)[c]	−13.5	−16.0	−20.1	−23.3
LiCl·MgCl$_2$–CsCl·MgCl$_2$	RTh_0 (exptl)	−42	−47.3	−56.8	−62.1
	RTh_0 (calcd)	−43.0	−47.7	−53.8	−57.3
KCl·MgCl$_2$–CsCl·MgCl$_2$	RTh_0 (exptl)	9[e]	4.6	1.6	−14.6
	RTh_0 (calcd)	2.8	1.6	0.7	−0.4
LiCl·BaCl$_2$–NaCl·BaCl$_2$	RTh_0 (exptl)		20.5		9.4
	RTh_0 (calcd)		21.2		14.4
LiCl·BaCl$_2$–KCl·BaCl$_2$	RTh_0 (exptl)		−11.6		−27.6
	RTh_0 (calcd)		−16.0		−23.3
NaCl·BaCl$_2$–KCl·BaCl$_2$	RTh_0 (exptl)	(−11)[d]	−10.9		−10.9
	RTh_0 (calcd)	−9	−9.6		−8.4

[a] Molal ionic strength of the solutions. [b] From eq 20. [c] From eq 21. [d] Values in parentheses are from direct experimental measurements of the heat of mixing the alkali metal chlorides in the presence of a common concentration of alkaline earth chloride. [e] Based on an extrapolated value $RTh_0 = 11.0 \pm 4$ for the KCl–CsCl mixing at $I = 0.5$.

$$\Delta H_m(\text{calcd}) = [(I/6)\phi_L(\text{MgCl}_2) + (I/4)\phi_L(\text{LiCl}) + (I/4)\phi_L(\text{KCl}) + (I^2/8)RTh_{\text{MgK}}{}^{\text{Cl}} + (I^2/8)RTh_{\text{MgLi}}{}^{\text{Cl}} + (I^2/16)RTh_{\text{LiK}}{}^{\text{Cl}}] - (1/2)[(I/3)\phi_L(\text{MgCl}_2)] - (1/2)[(I/2)\phi_L(\text{LiCl}) + (I/2)\phi_L(\text{KCl}) + (I^2/4)RTh_{\text{LiK}}{}^{\text{Cl}}] = (I^2/8)RTh_{\text{MgK}}{}^{\text{Cl}} + (I^2/8)RTh_{\text{MgLi}}{}^{\text{Cl}} - (I^2/16)RTh_{\text{LiK}}{}^{\text{Cl}} \quad (9)$$

The calculated heat of mixing for this mixture from eq 1 is

$$\Delta H_m(\text{calcd}) = (I^2/4)RTh(\text{calcd}) \quad (10)$$

Combining eq 9 and 10 gives

$$RTh(\text{calcd}) = (^1/_2)RTh_{\text{MgK}}{}^{\text{Cl}} + (^1/_2)RTh_{\text{MgLi}}{}^{\text{Cl}} - (^1/_4)RTh_{\text{LiK}}{}^{\text{Cl}} \quad (11)$$

This equation comes out to be the same as the one derived earlier for charge-symmetric mixtures.[4] It was not clear that this would be so without the complete derivation. The equation is understandable because the experimental heat is made up of one-half the heat of mixing KCl with MgCl$_2$, one-half the heat of mixing LiCl with MgCl$_2$, and one-fourth the heat of *unmixing* LiCl and KCl.

Table II shows a comparison of RTh(calcd) with RTh(exptl) from Table I. The values of RTh_0 in eq 11 were taken from the literature. The magnesium chloride with alkali metal chloride data are from Wood, Patton, and Ghamkhar[7] and the barium chloride with alkali metal chloride data are from Wood and Ghamkhar.[8] The heats of mixing two alkali metal chlorides are taken from Wu, Smith, and Young (at I = 1 only),[9]

---

[9] Y. C. Wu, M. B. Smith, and T. F. Young, *J. Phys. Chem.*, 69, 1868 (1965).

Scheme I

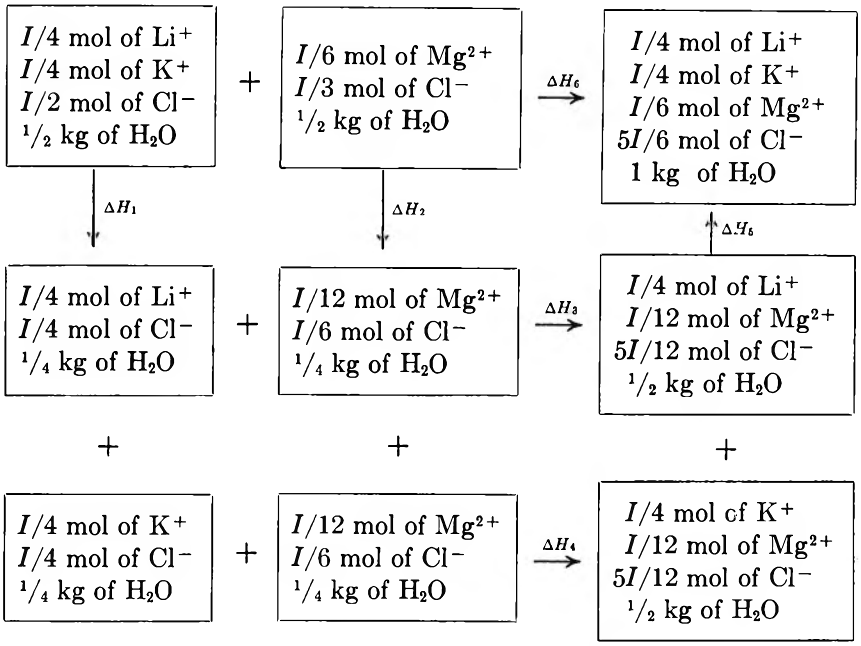
I/4 mol of Li+
I/4 mol of K+
I/2 mol of Cl−
1/2 kg of H2O
+
I/6 mol of Mg2+
I/3 mol of Cl−
1/2 kg of H2O
ΔH6
I/4 mol of Li+
I/4 mol of K+
I/6 mol of Mg2+
5I/6 mol of Cl−
1 kg of H2O
ΔH1
ΔH2
ΔH5
I/4 mol of Li+
I/4 mol of Cl−
1/4 kg of H2O
+
I/12 mol of Mg2+
I/6 mol of Cl−
1/4 kg of H2O
ΔH3
I/4 mol of Li+
I/12 mol of Mg2+
5I/12 mol of Cl−
1/2 kg of H2O
+
+
+
I/4 mol of K+
I/4 mol of Cl−
1/4 kg of H2O
+
I/12 mol of Mg2+
I/6 mol of Cl−
1/4 kg of H2O
ΔH4
I/4 mol of K+
I/12 mol of Mg2+
5I/12 mol of Cl−
1/2 kg of H2O

Stern and Anderson (LiCl with NaCl and NaCl with KCl),[10] and Levine, Bhatt, Ghamkhar, and Wood (LiCl with KCl, LiCl with CsCl, and KCl with CsCl).[11] The value of RTh_0 for KCl with CsCl at $I = 0.5$ was extrapolated from the high concentration data.

A comparison of the experimental and calculated values of RTh_0 confirms the predictive value of the equation of Reilly and Wood.[5] At the lower concentrations ($I = 0.5$ and 1.0), all except two of the predictions are within the estimated experimental error. At the highest concentrations, the errors are larger but the equation is still useful. This behavior is just what is expected since the equation of Reilly and Wood does not take all of the triplet interactions into account and these become more important as the concentration increases.

The approximations involved in the general equation, when applied to the present results, are illustrated by the thermodynamic cycle shown in scheme I. The mixing to be predicted, ΔH_6, is calculated from the cycle

$$\Delta H_6 = \Delta H_1 + \Delta H_2 + \Delta H_3 + \Delta H_4 + \Delta H_5 \quad (12)$$

Using eq 1 and remembering that ΔH in calories equals ΔH in cal/kg times the weight of the solvent, we have

$$\Delta H_1(\text{cal}) = -(^1/_2)RTI^2(^1/_4)h_{\text{LiK}}{}^{\text{Cl}} \quad (13)$$

$$\Delta H_2(\text{cal}) = 0 \quad (14)$$

$$\Delta H_3(\text{cal}) = (^1/_2)RTI^2(^1/_4)h_{\text{MgLi}}{}^{\text{Cl}} \quad (15)$$

$$\Delta H_4(\text{cal}) = (^1/_2)RTI^2(^1/_4)h_{\text{MgK}}{}^{\text{Cl}} \quad (16)$$

The final term, ΔH_5, is the heat of mixing Li^+ with K^+ in the presence of a constant concentration of both Cl^- and Mg^{2+} ions. It is easily shown that a common ion does not contribute to pairwise interactions so that, as a first approximation, ΔH_5 can be estimated as the heat of mixing Li^+ with K^+ in the presence of Cl^-. Since the concentrations of Li^+ and K^+ ions are one-half what they would be in pure LiCl and KCl solutions, their pairwise interactions in the $MgCl_2$ solutions will be one-fourth as large as in the pure solutions.[5] Thus

$$\Delta H_5(\text{cal}) \simeq (1)(RTI^2(^1/_4)h_{\text{LiK}}{}^{\text{Cl}})(^1/_4) \quad (17)$$

Substituting eq 13–17 into eq 12 gives

$$\Delta H_m(\text{calcd}) = (I^2/8)RTh_{\text{MgK}}{}^{\text{Cl}} + (I^2/8)RTh_{\text{MgLi}}{}^{\text{Cl}} - (I^2/16)RTh_{\text{LiK}}{}^{\text{Cl}} \quad (18)$$

This is identical with eq 9 which was derived from the general equation. The only approximation involved is in the calculation of ΔH_5 by eq 17.

The accuracy of this approximation can be tested by calculating an experimental value of the heat of reaction 5 using the same thermodynamic cycle.

$$\Delta H_5(\text{exptl}) = \Delta H_6 - \Delta H_1 - \Delta H_2 - \Delta H_3 - \Delta H_4 \quad (19)$$

Using eq 1, 13, 14, 15, and 16 gives an experimental value of RTh_0 for reaction 5.

$$RTh_0(\text{exptl}) = RTh_{\text{LiK,Mg}}{}^{\text{Cl}} - (^1/_2)RTh_{\text{MgLi}}{}^{\text{Cl}} - (^1/_2)RTh_{\text{MgK}}{}^{\text{Cl}} + (^1/_2)RTh_{\text{LiK}}{}^{\text{Cl}} \quad (20)$$

where $RTh_{\text{LiK,Mg}}{}^{\text{Cl}}$ is RTh_0 for the reaction of LiCl·KCl with $MgCl_2$ as given in Table I. The calculated value of RTh_0 for reaction 5 derived from eq 17 is

---

[10] J. H. Stern and C. W. Anderson, *J. Phys. Chem.*, **68**, 2528 (1964).

[11] A. S. Levine, N. Bhatt, M. Ghamkhar, and R. H. Wood, *J. Chem. Eng. Data*, in press.

$$RTh^0(\text{calcd}) = (^1/_4)RTh_{\text{LiK}}{}^{\text{Cl}} \qquad (21)$$

Table III shows a comparison of the experimental and calculated values of RTh_0. The experimental data needed for this calculation are the same as those needed for the calculation of eq 11 (see Table II) and the same sources of data were used.[7-11]

As expected, the differences between experimental and calculated values in Table III are the same as in Table II, except for round-off errors.

Two direct experimental measurements of the heat of mixing alkali metal chlorides in the presence of a common concentration of alkaline earth chloride are also reported in Table III. The direct experimental value of RTh_0 for the $LiCl \cdot MgCl_2$–$KCl \cdot MgCl_2$ mixing ($RTh_0 = -15 \pm 2$) is in excellent agreement with the value from the thermodynamic cycle ($RTh_0 = -16$) and this serves as a check on the accuracy of all of the measurements in the cycle. The direct experimental value of RTh_0 for the $NaCl \cdot BaCl_2$–$KCl \cdot BaCl_2$ at $I = 0.5$ ($RTh_0 = -11 \pm 1$) is in excellent agreement with the value calculated by eq 21 ($RTh_0 = -9$) using the data of Wood and Smith[6] for the NaCl–KCl mixing at $I = 0.5$.

Young and coworkers found that to a first approximation the heat of mixing alkali metal halides with a common anion or a common cation was independent of the common ion.[9,12] Wood and Smith[6] showed that the reason for this was that the heat of reaction was mainly due to the interaction of pairs of cations. Wood and Anderson[2] found that the approximation was still valid for the Cl^-–Br^- interaction with Mg^{2+} as the common ion. The results of Table III show that the approximation is quite good even in the presence of both a common anion (Cl^-) and a common cation (Mg^{2+}).

The fact that this is a pairwise interaction is demonstrated by the need for a factor of $^1/_4$ in eq 21. Since the Li^+ and Na^+ concentrations are halved in going from a mixture of LiCl with KCl to a mixture of $LiCl \cdot MgCl_2$ with $KCl \cdot MgCl_2$, the interaction of the two ions is reduced by $^1/_4$.

Acknowledgments. The authors gratefully acknowledge the support of this work by the Office of Saline Water, U. S. Department of the Interior. The authors also wish to thank Miss Nalini Bhatt for help with the calorimetric measurements.

---

(12) T. F. Young, Y. C. Wu, and A. A. Krawetz, *Discussions Faraday Soc.*, **24**, 37, 77, 80 (1957).

Sublimation of Ammonium Perchlorate[1]

by Christiane Guirao and F. A. Williams

Department of Aerospace and Mechanical Engineering Sciences, University of California, San Diego, La Jolla, California *(Received June 6, 1969)*

Various models are discussed theoretically for the sublimation mechanism of pure ammonium perchlorate. It is concluded that the results of the careful experiments performed by Russell-Jones, on the pressure dependence of the sublimation rate of pressed pellets at 270°, may be influenced by continuing low-temperature decomposition. On the basis of various considerations it is inferred that for deflagration at pressures between 20 and 100 atm, equilibrium for a dissociative sublimation process is likely to exist at the interface between the gaseous and condensed phases.

1. Introduction

Because ammonium perchlorate (NH_4ClO_4, denoted herein as AP) enjoys widespread use as an oxidizer in composite solid propellants, its decomposition has now been studied more thoroughly than that of any other oxygen-rich salt. Instead of producing a complete understanding of AP decomposition, this great volume of research has revealed that AP can behave in a bewildering variety of ways. Isothermal samples decompose to form primarily H_2O, O_2, Cl_2, and N_2O at atmospheric pressure and at temperatures between approximately 150 and 350° (the "low-temperature" decomposition),[2] while they decompose to form primarily H_2O, O_2, Cl_2, and NO at atmospheric pressure and at temperatures between approximately 350 and 420° (the "high-temperature" reaction).[2] At higher temperatures, isothermal decomposition experiments are difficult to perform since, after a brief induction period, samples experience either thermal explosion or rapid deflagration.[3] Pure AP can support a steady deflagration at atmospheric pressure if its initial temperature exceeds approximately 270°[4,5] and at room temperature for pressures above roughly 20 atm.[6] The primary deflagration products, roughly in the order of decreasing abundance, are H_2O, O_2, NO, HCl, Cl_2, N_2O, and N_2[5] differing from the adiabatic equilibrium composition which is H_2O, O_2, HCl, N_2 with very small amounts of Cl_2.[7] Dissociative sublimation into NH_3 and $HClO_4$ apparently can occur at all temperatures and pressures but is easiest to observe at subatmospheric pressures since it becomes relatively more predominant than other processes (*e.g.*, low-temperature decomposition) as the pressure is decreased.[2,8]

---

[1] This work was supported by the Air Force Office of Scientific Research under Project THEMIS, Contract F44620-68-C-0010.

[2] L. L. Bircumshaw and B. H. Newman, *Proc. Roy. Soc., Ser. A*, **227**, 115, 228 (1954).

The process of deflagration, at grain temperatures and pressures encountered in solid propellant rocket motors, probably is the AP decomposition process of greatest practical importance. Since it has been argued that in these deflagration processes residence times of the condensed material at elevated temperatures are too short for the low-temperature or high-temperature reactions to proceed appreciably, sublimation is likely to be the dominant interphase process during deflagration. In view of the fact that a thorough understanding of deflagration cannot be attained unless conditions are known at the interface between the gas and the condensed material, studies of the sublimation process, *per se*, should be ascribed a high priority on any practically motivated list of research topics. The present paper addresses the problem of ascertaining the sublimation mechanism of AP.

2. Dissociative *vs.* Associative Sublimation

As discussed, for example, in the comprehensive review by Hall and Pearson,[7] observations of AP sublimation date back to the works of Dodé in 1935. One of the first questions that arose in these studies was whether the over-all process was dissociative. The earliest thoughts favored dissociation,[9] but later the possible occurrence of associated sublimation products was raised.[10,11] Because of the uncertainty, various tests were performed to ascertain whether dissociation was present.[12-15] Each such investigation concluded that the process was dissociative. Extrapolation of these results to conditions of linear pyrolysis[16-18] and deflagration, by use of the ubiquitous activation energy of 30 kcal/mol,[7,11,19,20] suggest that it is unlikely that associative sublimation will occur even at these higher pressures and temperatures. Although the case is not yet airtight even at lower pressures, the most reasonable course at present is to assume dissociative sublimation under all conditions. The work reported herein is based on this premise.

3. Work of Jacobs and Russell-Jones

The largest single body of information on the sublimation process, *per se*, was obtained by Russell-Jones[8] who, under the direction of P. W. M. Jacobs, performed measurements at pressures from vacuum to atmospheric and at temperatures from 220 to 380°. Results of these studies have been reported by Davies, Jacobs, and Russell-Jones[19] and by Jacobs and Russell-Jones.[20] Many different types of AP were tested, ranging from single crystals to loose powder, with reagents obtained from three different suppliers. It was established that crystals behave in essentially the same manner as pressed pellets, and most of the experiments were performed with cylindrical pressed pellets of various sizes. First the low-temperature reaction was allowed to proceed to presumed completion, then rates of weight loss under isothermal conditions were recorded. Vacuum sublimation rates were measured from 218 to 270°, sublimation rates at atmospheric pressure were measured from 270 to 380°, and sublimation rates between 7.75 Torr and 1 atm were measured at 270°. Values for surface evaporation

---

(3) A. Glasner and A. Makovley, *J. Chem. Soc.*, 1606 (1965).

(4) J. Powling, "The Combustion of Ammonium Perchlorate-Based Composite Propellants: A Discussion of Some Recent Experimental Results," Explosives Research and Development Establishment, Report No. 15/R/65, July 1965.

(5) E. A. Arden, J. Powling, and W. A. W. Smith, *Combust. Flame*, **6**, 21 (1962).

(6) J. B. Levy and R. Friedman, "Further Studies of Pure Ammonium Perchlorate Deflagration," Eighth International Symposium on Combustion, 1962, The Williams and Wilkins Co., Baltimore, Md., pp 663–672.

(7) A. R. Hall and G. S. Pearson, "Ammonium Perchlorate: A Review of Its Role in Composite Propellant Combustion," Rocket Propulsion Establishment Technical Report, No. 67/1, Jan 1967; to appear in *Oxidation and Combustion Reviews*.

(8) A. Russell-Jones, "The Thermal Decomposition of Some Inorganic Perchlorates," Ph.D. Thesis, University of London, Oct 1964.

(9) L. L. Bircumshaw and T. R. Phillips, *J. Chem. Soc.*, 4741 (1957).

(10) A. W. Galwey and P. W. M. Jacobs, *ibid.*, 837 (1959).

(11) W. Nachbar and F. A. Williams, "On the Analysis of Linear Pyrolysis Experiments," Ninth International Symposium on Combustion, 1962, Academic Press, New York, N. Y., pp 345–356.

(12) S. H. Inami, W. A. Rosser, and H. Wise, *J. Phys. Chem.*, **67**, 1077 (1963).

(13) A. S. Tompa, G. B. Wilmot, and J. L. Mack, "Matrix Isolation and Infrared Determination of the Vapor Species of NH_4ClO_4," Symposium on Molecular Structure and Spectroscopy, The Ohio State University, 1962.

(14) J. B. Levy, *J. Phys. Chem.*, **66**, 1092 (1962).

(15) S. H. Inami and H. Wise, to be published in *Conbust. Flame*.

(16) J. Powling, "Experiments Relating to the Combustion of Ammonium Perchlorate-Based Propellants," Eleventh International Symposium on Combustion, 1966, The Combustion Institute, Pittsburgh, Pa., pp 447–456.

(17) M. Guinet, "Vitesse Linéaire de Pyrolyse du Perchlorate d'-Ammonium en Ecoulement Unidimensionel," La Recherche Aerospatiale, No. 109, Nov–Dec 1965.

(18) W. H. Andersen and R. F. Chaiken, "The Detonability of Solid Composite Propellants, Part 1," Tech. Mem. 809, Aerojet-General Corp., Azusa, Calif., Jan 1959.

(19) J. V. Davies, P. M. W. Jacobs, and A. Russell-Jones, *Trans. Faraday Soc.*, **63**, 1737 (1967).

(20) P. W. M. Jacobs and A. Russell-Jones, *J. Phys. Chem.*, **72**, 202 (1968).

coefficients were deduced from the experimental results, and it was inferred that the evaporation coefficient is pressure dependent. A surface diffusion model was proposed for explaining this pressure dependence.[20] The question of whether surface diffusion is an important step in the sublimation mechanism bears direct relevance to the interface condition in deflagration since elevated pressures enhance the degree of surface adsorption. The present paper addresses this question by considering a variety of models for the sublimation of pellets under the conditions of the Russell-Jones experiments.

4. Chemical Mechanism of Sublimation

The most reasonable sublimation mechanism appears at present to be

$$NH_4^+(c) + ClO_4^-(c) \rightleftarrows NH_3(a) + HClO_4(a) \rightleftarrows NH_3(g) + HClO_4(g) \quad (1)$$

where (c) denotes a crystalline lattice position, (a) identifies an adsorbed molecule, and (g) denotes a gaseous molecule. Equation 1 is similar to that given by Russell-Jones,[8] who argued that the proton-transfer process may be the rate-controlling step. If proton transfer is rate controlling under all nonequilibrium conditions, the best way to describe sublimation rates is in terms of adsorption equilibria and pressure-independent rate constants for proton transfer on the surface; evaporation coefficients should not be introduced, and surface diffusion processes cannot affect sublimation rates. The later consideration of surface diffusion[8,20] therefore carries with it the view that proton transfer is not always rate controlling. Since there is some evidence that NH_3 is strongly adsorbed[12,19] and might in fact migrate through the crystal by means of a series of proton jumps,[21] it appears that the proton transfer may occur rather readily and that NH_3 desorption may be the rate-controlling step. Arguments[22] that the heat of adsorption is likely to be comparable with the heat of vaporization are not necessarily true if NH_3 is strongly chemisorbed. If a desorption step is rate controlling, then it is proper to analyze sublimation rates in terms of evaporation coefficients. For the models considered in the present paper, it will be assumed that the proton-transfer process always maintains equilibrium; both desorption processes will be allowed to depart from equilibrium.

5. Critique of Theory of Jacobs and Russell-Jones

Jacobs and Russell-Jones[20] assume that a cylindrical pellet can be approximated as a sphere whose radius is denoted by a. The density ρ of the sphere is presumed to remain constant, and a is treated as a decreasing function of time. While they recognize that sublimation is dissociative, Jacobs and Russell-Jones state that since in the steady state the flux of NH_3 through the gas phase must equal that of $HClO_4$, it is sufficient to consider an effective mean gas phase flux of AP and to analyze a system for which there is only one gaseous sublimation product which possesses a mean diffusion coefficient D. An evaporation coefficient β is introduced for this sublimation product, and an equation for the time dependence of a is then developed which allows for molecules leaving the surface, returning to the surface, and diffusing through the gas. By a method somewhat different from that of Monchick and Reiss,[23] the analysis accounts for limiting cases in which the ratio of the sphere radius to molecular mean free path Δ is large or small and also provides approximate results when this ratio is of order unity. The final expression for the fractional weight loss, $\delta \equiv 1 - (a/a_0)^3$ (where a_0 is the value of a at time $t = 0$), reduces to the contracting-volume expression, $1 - (1 - \delta)^{1/3} \propto t$, under vacuum conditions and to the expression for diffusion-controlled vaporization, $1 - (1 - \delta)^{2/3} \propto t$, under conditions of surface equilibrium. Three parameters appear in the final expression, $X_1 \equiv \Delta/a_0$, $X_2 \equiv (D/\nu\beta\Delta) - 1$, and $X_3 \equiv Dmn_0/a_0^2\rho$, where ν is an average value for the component of the molecular velocity normal to the solid surface in the gas phase, m is the molecular weight of AP, and n_0 is the equilibrium concentration of the subliming species in the gas phase. All weight-loss data were fitted extremely well by a least-squares criterion in which X_1, X_2, and X_3 were treated as adjustable parameters.

We believe that objections may be raised against assuming an effective mean gaseous sublimation product. From kinetic theory, accounting only for the effect of molecular weight and collision diameter and assuming a Lennard-Jones collision diameter of ~10 Å for $HClO_4$, we estimate that the diffusion coefficient of NH_3 through N_2 exceeds that of $HClO_4$ through N_2 by a factor of approximately 4.5. The consequent tendency for $HClO_4$ to achieve a higher concentration than NH_3 in the gas phase at the pellet surface may be of quantitative but not qualitative significance.[24] More important qualitatively is the fact that the surface evaporation coefficients for NH_3 and $HClO_4$ may differ by orders of magnitude. This can lead to sur-

---

(21) H. Wise, "Electrical Conductivity of Solid Ammonium Perchlorate," Stanford Research Institute, Menlo Park, Calif., Rept. 15, Sept 1966.

(22) R. D. Schultz and A. O. Dekker, "Transition-State Theory of the Linear Rate of Decomposition of Ammonium Perchlorate," Sixth International Symposium on Combustion 1956, Reinhold Publishing Corp., New York, N. Y., pp 618–628.

(23) L. Monchick and H. Reiss, *J. Chem. Phys.*, 22, 831 (1954).

(24) Later in section 13, fitting the slope of the curve in Figure 2 to eq 25, we get for the ratio $D_{NH_3\text{-air}}/D_{HClO_4\text{-air}}$ a value of ~25, which would result in an appreciably greater tendency toward diffusive separation of species in the gas phase. This experimentally inferred value is based on a calculation of the binary diffusion coefficient for NH_3-air, which uses a kinetic theory formula with a Lennard-Jones intermolecular potential. We note that such calculations of transport properties typically are uncertain by 50% and that therefore a corresponding uncertainty exists in the value of the ratio of the diffusion coefficients.

face equilibrium for one species while the other experiences a surface rate process. It appears to be of interest to investigate in a general way the peculiarities that can result from this type of dissociative sublimation. All of the models discussed in this paper allow for two different sublimation products in the gas phase.

Although there is an esthetic satisfaction in constructing a unified theory which exhibits as limiting cases both vacuum sublimation and diffusion-controlled sublimation, there are also arguments for not doing so. While accurate formulas for sublimation rates can be obtained if either $a_0/\Delta \ll 1$ or $a_0/\Delta \gg 1$, the regime of transition between continuum and free molecule flow, $a_0/\Delta \simeq 1$, cannot be analyzed accurately. Currently unresolved questions concerning the appropriate exact definition of Δ, the character of the nonequilibrium molecular velocity distribution function, etc., arise in the transition regime. A theory including transition contains aspects that are inherently less precise than the aspects of a theory restricted to the limiting cases. Moreover, for existing AP sublimation experiments, it is not obviously essential to consider the transition regime, because it is not clear that the experiments enter it. For vacuum sublimation experiments, at temperatures below 270°, $a_0/\Delta < 1$ and vacuum theory should suffice, while for sublimation experiments at pressures above 7 Torr, $a_0/\Delta > 10^2$, and departures from continuum flow should not become observable before δ reaches 0.999, a condition which is not achieved experimentally. For these reasons we have chosen to restrict our theoretical considerations to the two limiting cases. In interpreting vacuum sublimation experiments, we neglect gas phase diffusion processes. For the more general theoretical considerations presented in subsequent sections, we are concerned only with interpreting experiments performed at pressures above 7 Torr and therefore assume that $a_0/\Delta \gg 1$.

6. Equilibrium Vapor Pressure and Rate Observations at Pressures above 7 Torr

Although general theoretical considerations may be of some intrinsic interest, we are concerned principally with AP. During the theoretical deliberations, it is therefore desirable to keep in mind experimentally observed facts about AP sublimation. These facts are summarized here.

The equilibrium sublimation pressure measurements of Inami, Rosser, and Wise[12] yield a heat of dissociative sublimation of 58 ± 2 kcal/mol. Under the assumption that the partial pressure of NH_3 is equal to that of $HClO_4$, their sum, the sublimation pressure P, was found experimentally to be given in mm by the equation

$$\log P = -6283.7/T + 10.56 \tag{2}$$

where the units of T are °K. The value of P varies roughly from 3×10^{-2} Torr at 250° to 3 Torr at 350°.

For the isothermal weight-loss experiments of Russell-Jones, a rate constant k may be defined as

$$k \equiv -\lim_{t \to 0} \frac{d}{dt}[(1 - \delta)^{1/3}] \tag{3}$$

If the contracting volume equation were valid, then k would be the rate constant in that equation; since experimentally the contracting volume equation is not valid under 1 atm of air in the temperature range 304–375°, k is merely a constant indicative of the early time rate of weight loss. Figure 1 shows the values of k obtained from the data of Jacobs and Russell-Jones[20] for sublimation at atmospheric pressure and at temperatures between 304 and 375°. The first and most important observation to be made from Figure 1 is that the activation energy is approximately 30 kcal/mol, just as for vacuum sublimation. The second observation is that the value of k depends on the initial weight of the pellet: k decreases as the sample size is increased. Since only three sizes were used, it is difficult to draw an accurate conclusion concerning the dependence of k on a_0, although $k \propto a_0^{-n}$, with $^3/_2 \leq n \leq 3$, would apparently be consistent with the data. Third it has been stated[20] that the formula

$$1 - (1 - \delta)^{1/2} = k't \tag{4}$$

(k' = constant) fits this atmospheric pressure data over a wider range of weight loss ($0 \leq \delta \leq 0.93$ in one case) than does any other simple power formula.

Seven data points at 270° for pressures between 7.75 and 760 Torr produce the rate constant curve shown in Figure 2. The value of k appearing here is that defined in eq 3. The formula

$$k = A + (B/p) \tag{5}$$

fits these data well, and the constants A and B are definitely both positive.

Our objective in the following sections will be to see if any simple theory agrees with these observations.

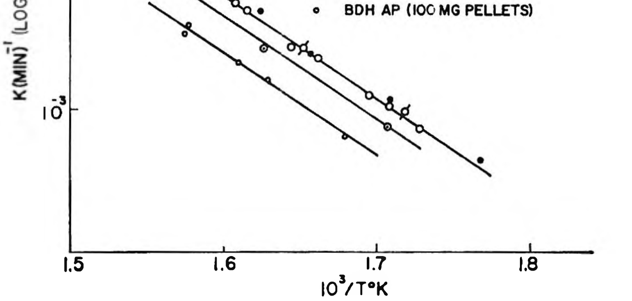

Figure 1. Arrhenius plots for the sublimation of ammonium perchlorate, using rate constants derived from the "contracting volume" equation; data from ref 20.

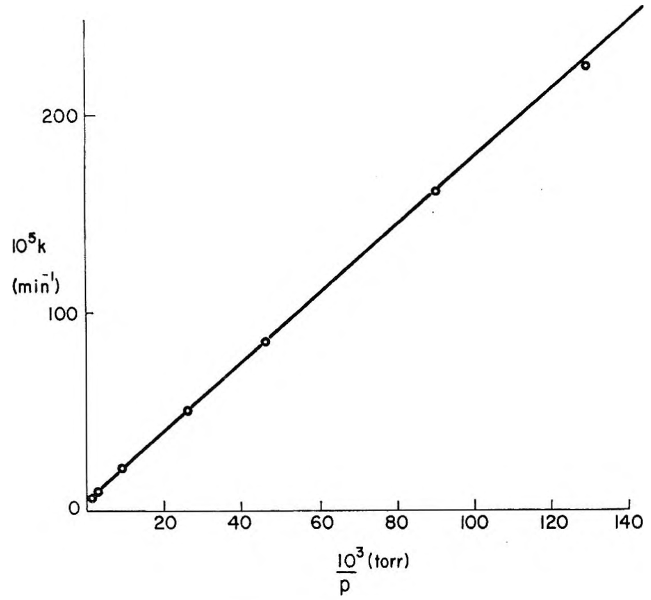

Figure 2. Dependence of rate of sublimation of BDH (British Drug House) AP on air pressure at 270°.[20]

7. A General Model for Dissociative Sublimation in an Inert Atmosphere

Let us consider the hypothetical dissociative sublimation process

$$AB(c) \rightleftarrows A(a) + B(a) \rightleftarrows A(g) + B(g)$$

for a sphere of radius a under steady-state conditions. Sublimation will be assumed to occur in an atmosphere consisting of an inert gaseous species C which is capable of being adsorbed on the surface. The concentration n_C of species C in the gas is assumed to be very large compared with that of species A and B at the surface of the sphere, *i.e.*, $p/RT = n_C \gg n_A$, n_B where R is Boltzmann's constant. Two kinds ($i = 1, 2$) of adsorption sites will be permitted to exist on the surface, and each site will be permitted to adsorb both species A and B. Our belief is that real surfaces contain practically an infinite number of different kinds of sites, and our hope is that variations in site characteristics can be modeled with sufficient accuracy by considering only two kinds. We might remark that models considering surface diffusion necessarily require at least two kinds of sites. We do not consider surface diffusion in the present theories.

The number of molecules of species k per second leaving the surface of the sphere from sites of type i is

$$Q_{ki} = 4\pi a^2 f_i[\omega_{ki}\theta_{ki} - \nu_k\alpha_{ki}(1 - \theta_i)n_k];$$
$$k = \text{A, B, C};\ i = 1, 2 \qquad (6)$$

where f_i is the fraction of the surface identifiable as sites of kind i ($f_2 = 1 - f_1$), ω_{ki} is the number of molecules of type k per unit area per second that would enter the gas from a surface of kind i completely covered with molecules of type k, θ_{ki} is the fraction of surface sites of kind i occupied by molecules of type k, $\theta_i \equiv \Sigma_k\ \theta_{ki}$ is the total occupied fraction of surface sites of kind i, ν_k is the average component of molecular velocity normal to the surface for molecules of type k in the gas, α_{ki} is the probability that a gaseous molecule of type k striking an unoccupied surface site of kind i adheres to the surface, and n_k is the number of molecules of type k per unit volume in the gas at the surface. We insist that f_i, ω_{ki}, and $\nu_k\alpha_{ki}$ represent fundamental structure or rate constants which are independent of p. Equation 6 simply constitutes a molecular flux count at the surface.

It is reasonable to assume that the distance between surface sites of different kinds is small compared with a gas phase diffusion distance. Then, the solution of the relevant diffusion equation in the gas shows that

$$Q_k \equiv Q_{k1} + Q_{k2} = 4\pi a D_{kC} n_k;\ k = \text{A, B} \qquad (7)$$

where D_{kC} is the binary diffusion coefficient for the species pair k and C which varies inversely with p. Of course

$$Q_{Ci} = 0;\ i = 1, 2 \qquad (8)$$

and steady sublimation requires

$$Q_{Ai} = Q_{Bi};\ i = 1, 2 \qquad (9)$$

Equilibrium for the first step in the reaction requires

$$\theta_{Ai}\theta_{Bi}/(1 - \theta_i)^2 = K_i;\ i = 1, 2 \qquad (10)$$

where the equilibrium constants K_i depend only on temperature T. The constants K_i can be related to the equilibrium constant for concentrations for the over-all sublimation process

$$K_n = n_{A0}n_{B0} = (P/2RT)^2 \qquad (11)$$

through the equilibrium identities

$$K_n = K_i\omega_{Ai}\omega_{Bi}/\nu_A\nu_B\alpha_{Ai}\alpha_{Bi};\ i = 1, 2 \qquad (12)$$

The subscript 0 on n_k identifies equilibrium, and the equilibrium vapor pressure P appears in eq 2 for AP.

A mass balance for the sphere yields

$$Q_k = -(\rho/m)4\pi a^2(\mathrm{d}a/\mathrm{d}t);\ k = \text{A, B} \qquad (13)$$

where ρ/m is the molecule (AB) number density of the solid. Equations 6 through 10 can be thought of as 14 equations in the 14 unknowns Q_{ki}, θ_{ki}, n_A, and n_B; solution of these equations followed by substituting into eq 13 yields an explicit expression for $\mathrm{d}a/\mathrm{d}t$ in terms of a and constants that are presumed known.

By eliminating n_k between eq 6 and 7, we obtain

$$Q_k = \frac{4\pi a \dfrac{D_{kC}}{\nu_k}\left[\dfrac{f_1\omega_{k1}\theta_{k1} + f_2\omega_{k2}\theta_{k2}}{f_1\alpha_{k1}(1 - \theta_1) + f_2\alpha_{k2}(1 - \theta_2)}\right]}{1 + \dfrac{D_{kC}/a\nu_k}{f_1\alpha_{k1}(1 - \theta_1) + f_2\alpha_{k2}(1 - \theta_2)}};\ k = \text{A, B} \qquad (14)$$

When solutions for θ_{kl} have been obtained, eq 14 can be substituted into eq 13 to yield an expression for the rate of weight loss. To understand the kinds of results that can ensue, it is instructive to investigate limiting cases.

8. Diffusion-Controlled Limit with One Kind of Site

If $f_2 = 0$ (*i.e.*, $f_1 = 1$) and if

$$D_{kC}/a\nu_k\alpha_{k1}(1 - \theta_1) \ll 1;\ k = \mathrm{A, B} \tag{15}$$

then it can be shown that eq 6 through 14 reduce to

$$Q_k = 4\pi a\sqrt{D_{AC}D_{BC}K_n};\ k = \mathrm{A, B}$$

which results in

$$1 - (1 - \delta)^{2/3} = vt;\ v = (2m/a_0^2\rho)\sqrt{D_{AC}D_{BC}K_n} \tag{16}$$

after substitution into eq 13 and integration. The exponent $^2/_3$ is the expected value for surface equilibrium and a diffusion-controlled process. It may be noted that the effective one-component diffusion coefficient is the geometric mean. Equation 15 states that the diffusion-controlled limit is achieved when the diffusion rate through the gas is small compared with the rate at which molecules return to the surface, for each species separately.

9. Rate-Controlled Limit With One Kind of Site

If $f_2 = 0$ (*i.e.*, $f_1 = 1$) and if

$$D_{kC}/a\nu_k\alpha_{k1}(1 - \theta_1) \gg 1;\ k = \mathrm{A, B} \tag{17}$$

then it can be shown that eq 6 through 14 yield

$$1 - (1 - \delta)^{1/3} = vt;\ v = \frac{m}{a_0\rho}\left\{\frac{1}{\omega_A} + \frac{1}{\omega_B} + (K_n\nu_A\nu_B\alpha_A\alpha_B)^{-1/2}[1 + (\nu_C\alpha_C p/\omega_C RT)]\right\}^{-1} \tag{18}$$

This contracting volume equation contains the effect of retardation due to adsorption of inerts. For sufficiently strong adsorption

$$v = (K_n\nu_A\nu_B\alpha_A\alpha_B)^{1/2}(mRT\omega_C/\alpha_C\nu_C\rho a_0 p)$$

which varies inversely as pressure. If adsorption is negligible, then

$$[\omega_A^{-1} + \omega_B^{-1} + (K_n\nu_A\nu_B\alpha_A\alpha_B)^{-1/2}]^{-1}$$

is the effective number of molecules per unit area per second leaving the surface, which would appear in a single species model. The term containing K_n enters because of the requirement of equilibrium in the "proton-transfer" process.

10. Equilibrium for One Species and Rate Control for the Other, with One Kind of Site

With $f_2 = 0$ (*i.e.*, $f_1 = 1$), it is interesting to consider the case

$$D_{AC}/a\nu_A\alpha_{A1}\ (1 - \theta_1) \ll 1;\quad D_{BC}/a\nu_B\alpha_{B1}(1 - \theta_1) \gg 1 \tag{19}$$

which may well be attained if the two species have widely differing evaporation coefficients. These hypotheses lead to a cubic equation for θ_1 whose solution exhibits a variety of different behaviors for da/dt. One of the more interesting behaviors occurs when $\theta_{C1} \ll \theta_{A1}$, $\theta_{C1} \ll \theta_{B1}$, $K_n\nu_B\alpha_B D_{AC} \ll a\omega_B^2$, and $K_1 a\omega_B\nu_A\alpha_A \ll \omega_A D_{AC}$. In this case

$$1 - (1 - \delta)^{1/2} = vt;\quad v = (3m/2a_0^{3/2}\rho)\sqrt{D_{AC}K_n\nu_B\alpha_B} \tag{20}$$

A somewhat similar result occurs if, instead, $\theta_{C1} \approx 1$; here

$$1 - (1 - \delta)^{1/2} = vt;\quad v = (3m/2a_0^{3/2}\rho)\sqrt{D_{AC}K_n\nu_B\alpha_B\omega_C RT/\nu_C\alpha_C p} \tag{21}$$

Equation 20 requires negligible inert adsorption while eq 21 holds whenever there is strong inert adsorption. Both equations exhibit the contracting area formula in agreement with eq 4. In both cases, it is reasonable to assume that the primary temperature dependence of v arises from K_n and that therefore the equilibrium sublimation pressure data for AP would yield an activation energy of 30 kcal/mol for v, in agreement with experiment. The variation of v with a_0 lies within experimental uncertainty for both equations. However, eq 20 predicts that $v \propto p^{-1/2}$, in contradiction with eq 5, and eq 21 predicts that $v \propto p^{-1}$, thereby requiring $A = 0$ in eq 5. If Figure 2 did not indicate so strongly that $A > 0$, then eq 21 might well explain the AP sublimation rate experiments. The interpretation would be that species A represents strongly adsorbed NH_3 which is essentially in equilibrium while species B represents weakly adsorbed $HClO_4$ which experiences a surface rate process.

11. Two Types of Sites with Inert Adsorption on Only One

We have performed calculations which demonstrate that if both $f_1 \neq 0$ and $f_2 \neq 0$, then there exist enough unknown parameters in the theory to fit the existing AP data. Although the fit is possible, it is somewhat "unnatural" in that eq 13 and 14 have a noticeable tendency to produce formulas of the form $k = Af(p)/[1 + Bg(p)]$ which do not reduce easily to eq 5. Usually inherent in eq 13 and 14 is a continuous decrease in $dk/d(1/p)$ with increasing $(1/p)$ rather than the extended range of essentially constant slope exhibited in Figure 2. Thus, some aspects of the physical bases of the resulting correlations are undesirable.

12. A Wire Mesh Model

Since a fine weblike residue in the shape of the original pellet remained after completion of each sublimation test,[8] instead of leaving a sphere or cylinder that contracts, the low-temperature reaction may produce a wire meshlike structure that sublimes through a decrease in the wire diameter. It may be assumed that all wires have the same diameter b and that the sum l of the lengths of all wires in the mesh remains constant. Then eq 6 is replaced by

$$Q_{ki} = \pi l b f_i[\omega_{ki}\theta_{ki} - \nu_k\alpha_{ki}(1 - \theta_i)n_k];$$
$$k = \mathrm{A, B, C};\ i = 1, 2 \quad (22)$$

and eq 13 becomes

$$Q_k = -(\pi\rho l b/2m)\mathrm{d}b/\mathrm{d}t;\ k = \mathrm{A, B} \quad (23)$$

We postulate rate-controlled vaporization (adsorption rates small compared with desorption rates), no inert adsorption on sites of kind 1, and strong inert adsorption on sites of kind 2. Then, diffusion becomes unimportant, eq 7 becomes irrelevant, and eq 8 through 12 remain valid. The fractional weight loss becomes $\delta = 1 - (b^2/b_0^2)$, and it can then be shown that

$$1 - (1 - \delta)^{1/2} = vt;$$
$$v = (m/\rho b_0)\{f_1[(K_n\nu_A\nu_B\alpha_{A1}\alpha_{B1})^{-1/2} + \omega_{A1}^{-1} + \omega_{B1}^{-1}]^{-1} + f_2[(K_n\nu_A\nu_B\alpha_{A2}\alpha_{B2})^{-1/2} \times (1 + (\nu_C\alpha_{C2}p/\omega_{C2}RT)) + \omega_{A2}^{-1} + \omega_{B2}^{-1}]^{-1}\} \quad (24)$$

This result agrees well with all of the weight-loss experimental results summarized in section 6, and its basis possesses much physical appeal. However, for reasons given in the following section, we prefer a different explanation of the observations on AP sublimation.

13. Equilibrium with Falsification by Continuing Low-Temperature Reaction

It is remarkable how closely the data in Figure 2 correspond to values of k calculated by assuming a diffusion-controlled process with surface equilibrium. If eq 16 were valid, then from eq 3 we would find

$$k = \frac{v}{2} = (m/a_0^2\rho)\sqrt{K_nD_{AC}D_{BC}} = \begin{cases} 2 \times 10^{-5}\ \mathrm{min}^{-1} \text{ at } p = 760 \text{ Torr} \\ 200 \times 10^{-5}\ \mathrm{min}^{-1} \text{ at } p = 7.75 \text{ Torr} \end{cases} \quad (25)$$

by using the value $K_n = 2 \times 10^{-18}$ mol^2/cm^6 at 270° obtained from eq 2 and 11 and $\sqrt{D_{AC}D_{BC}} = (0.1/p)$ cm^2/sec (with p measured in atmospheres). Figure 2 appears to imply that there is a pressure-independent additive contribution to v of about 5×10^{-5} min^{-1}, above that given by eq 25.

Since there is strong evidence for surface equilibrium in the experiment of Inami, Rosser, and Wise[12] and since the ease of mass transfer appears to be roughly the same for ref 12 and for Figure 2, it is difficult to escape the conclusion that dissociative sublimation will maintain surface equilibrium in Figure 2. The atmosphere was flowing helium at 1 atm in ref 12 but stagnant air at 10^{-2} to 1 atm in Figure 2. At equal pressures, flowing helium will allow mass transfer rates that are perhaps an order of magnitude larger than those permitted by stagnant air. Since diffusion rates vary inversely with pressure, by ignoring differences in sample size we would find that the diffusion rate in Figure 2 varies from an order of magnitude greater than that of ref 12 at the lowest pressure to an order of magnitude less than that of ref 12 at the highest pressure. If the characteristic diffusion length is taken to be the granule size in ref 12, then the diffusion length is roughly two orders of magnitude below that of Figure 2, and one would conclude that for all the data in Figure 2 the diffusion rate ($\sim aD$) is less than that of ref 12. One can obtain the opposite conclusion by using the total sample size to estimate the characteristic diffusion length of ref 12. Thus there is uncertainty, but on the average it appears unlikely that the ease of mass transfer from the sample is very much greater in Figure 2 than in the experiment of ref 12. Therefore, explanations of Figure 2 requiring rate processes for dissociative sublimation of one or more species on one or more kinds of sites (*e.g.*, the explanations offered in sections 9 through 12) are objectionable.

A way to fit data such as that exhibited in Figure 2 is to allow a material to leave the surface whose flow is not inhibited by the diffusion which retards the flow of dissociation products. If a surface decomposition process were to occur in addition to dissociation, then the decomposition products would not experience inhibition by diffusion, since the decomposition is irreversible. A small amount of decomposition would not be noticed in the experiments of Inami, Rosser, and Wise[12] since they measured only condensed sublimate and did not monitor their sample weight loss. However, the decomposition would affect the results shown in Figure 2.

One can therefore construct a one-site model with eq 15 applicable for dissociation products. However, decomposition is also permitted to occur, so that eq 13 is replaced by

$$Q_k + Q_D = -(\rho/m)4\pi a^2(\mathrm{d}a/\mathrm{d}t);\ k = \mathrm{A, B} \quad (26)$$

where

$$Q_D = 4\pi a^2\omega_D \quad (27)$$

in which ω_D, the fundamental rate constant for decomposition (number of AB molecules decomposed per unit area per second) is a function only of temperature.[25] Analysis then shows that

$$1 - (1 - \delta)^{1/3} + C\log_e\left[1 - \frac{1 - (1 - \delta)^{1/3}}{1 + C}\right] = vt;$$
$$C = (D_{AC}D_{BC}K_n)^{1/2}/\omega_Da_0;\ v = \omega_Dm/\rho a_0 \quad (28)$$

---

(25) If the decomposition were retarded by adsorption, then ω_D might depend on θ_k as well. We ignore this possibility and do not offer an explanation for deceleration of low-temperature decomposition.

which yields

$$k = (m/a_0\rho)[\omega_D + (D_{AC}D_{BC}K_n)^{1/2}a_0^{-1}] \qquad (29)$$

for the k defined in eq 3.

Let us choose to interpret ω_D as the rate of a continuing low-temperature decomposition reaction. Then, since the activation energy for the low-temperature reaction was found to be approximately[7] 30 kcal/mol, the activation energy of k in eq 29 will be 30 kcal/mol in agreement with the sublimation experiments performed at atmospheric pressure. The dependence of k on a_0 in eq 29 is not inconsistent with experimental observations. The weight loss as a function of time, given by eq 28, also agrees quite well with experiment, as can be seen from the representative curves shown in Figures 3 and 4; the agreement is certainly as good as eq 4 and appears to be as good as the least-squares fit of Jacobs and Russell-Jones[20] (see section 5). Finally, eq 29 is in precisely the same form as eq 5. Thus the results summarized in section 6 can all be explained. The best fit to the data yields $\omega_D = 2 \times 10^{-9}$ mol/(cm^2 sec) at 270°.

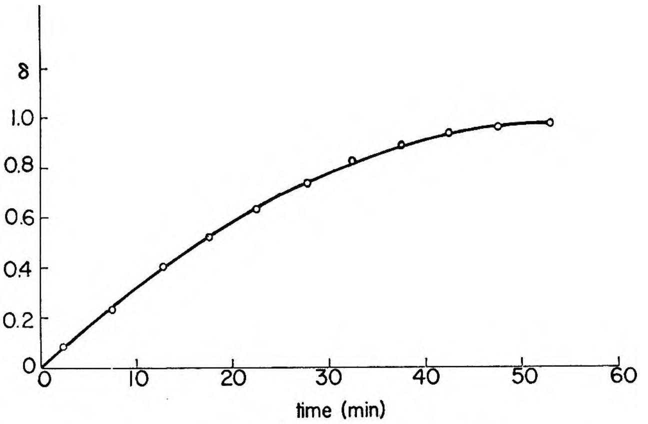

Figure 3. Sublimation of BDH AP in 1 atm of air at 375°.

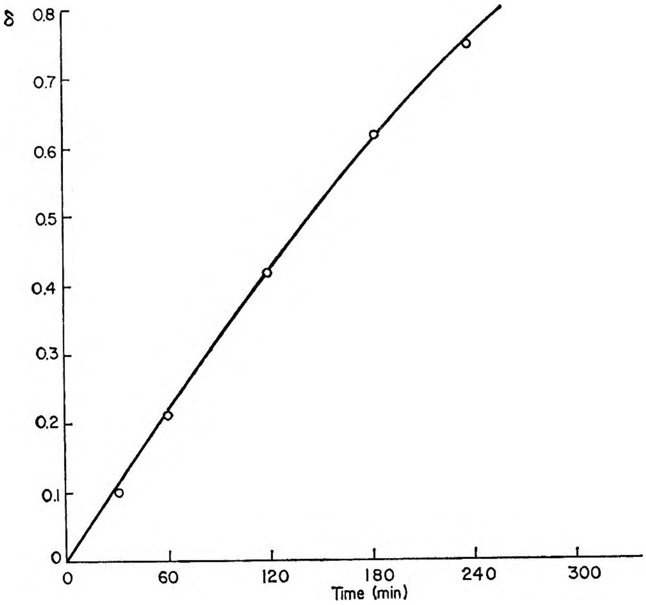

Figure 4. Sublimation of BDH AP in 11 Torr of air at 270°.

One might object to identifying ω_D with the low-temperature reaction since it is commonly stated that the low-temperature reaction ceases after 30% of the sample has been consumed. However, the times of observation[2,19] in the experiments which established this result were short compared with the time over which the sample would lose an appreciable amount of mass for the values of ω_D obtained herein. *The present* ω_D *is to be interpreted as the limiting long-time value of the rate of the low-temperature reaction,* and numerically it is not inconsistent with any of the previous experiments on the low-temperature reaction. We might also remark that values quoted for the extent of decomposition in the low-temperature reaction are influenced by pretreatment with $HClO_4$ and NH_3,[2,19] so there is nothing fundamentally inviolable about 30%.

Since the present interpretation requires that some noncondensable gases be produced in the sublimation weight-loss experiments of Russell-Jones, it is important to study the experimental technique of ref 8 to see whether these gases would have been detected. The sublimation weight-loss experiments at subatmospheric pressures were performed in a closed system in which noncondensable gases would produce a pressure rise. The pressure rise would be most easily observable at the lowest pressure, ~7 Torr. The system contained 10 l. of "ballast," and it is not clear whether the ballast was opened or closed during the weight-loss measurements. We estimate that over the entire running time of the experiment at 270°, the pressure increase would be of the order of 0.03 Torr if the ballast were open and less than 3 Torr if the ballast were closed. It seems that the relatively small amounts of noncondensable gases produced might easily escape detection since the reported accuracy for pressure measurements is ±1 Torr.

The explanation of the sublimation experiments presented here should be considered to be an alternative to that offered by Jacobs and Russell-Jones.[20] The theory in ref 20 is internally self-consistent and may be correct. We believe that the data support the present interpretation as strongly as that of ref 20. For example, the weight-loss rates at 270° are so slow that it was reasonable to carry out observations only for $\delta < 0.5$, and therefore use of the k data in Figure 2 should provide practically as much true information as a least-squares fit to the weight-loss curve. Also, a detailed least-squares fit may retain some information arising from random experimental errors and does not provide an indication of the extent of uncertainty arising from random experimental error. The theory of Jacobs and Russell-Jones requires appreciable chemisorption of N_2 or O_2 on the AP surface, while the present theory permits inert adsorption but does not require it. We are aware of no independent evidence supporting strong chemisorption of N_2 or O_2 on AP.

14. Interpretation of Weight-Loss Measurements for Vacuum Sublimation

In discussing their vacuum sublimation measurements performed between 220 and 270°, Jacobs and Russell-Jones[20] employ an effective one-component evaporation coefficient β defined essentially as

$$\beta = ka_0p/\bar{\nu}m\sqrt{K_n} \tag{30}$$

where $\bar{\nu}$ is an average molecular velocity (normal to the surface) for the dissociation products. The experiments seem to us to yield $\beta = (3.5 \pm 1) \times 10^{-2}$, with appreciable scatter but no apparent temperature dependence over this temperature range. Since under vacuum conditions sublimation rates are so high that the continuing low-temperature reaction is negligible, the interpretation of these experiments as surface rate-controlled sublimation seems quite reasonable to us, and our dissociative sublimation formulas with equilibrium for proton transfer yield

$$\beta = (\sqrt{\nu_A\nu_B/\bar{\nu}})\sqrt{\alpha_{A1}\alpha_{B1}} \times \\ [1 + \sqrt{K_n\nu_A\nu_B\alpha_{A1}\alpha_{B1}}(\omega_{A1}{}^{-1} + \omega_{B1}{}^{-1})]^{-1} \tag{31}$$

Thus, proton-transfer equilibrium can complicate the fundamental significance of β, although it still depends at most on temperature. The derivation of eq 31 is reproduced in the Appendix as an illustration of calculations. If θ_{A1} and θ_{B1} are small compared with unity, then eq 31 reduces simply to

$$\beta = (\sqrt{\nu_A\nu_B/\bar{\nu}})\sqrt{\alpha_{A1}\alpha_{B1}} \tag{32}$$

which shows that β is essentially the geometric mean of the evaporation coefficients for NH_3 and $HClO_4$. The data are consistent, for example, with $\alpha_{NH_3} = 1$, $\alpha_{HClO_4} = 10^{-3}$.

One may alternatively choose to assume that proton transfer is a rate process. In that case

$$\beta = \omega_T/(\bar{\nu}\sqrt{K_n}) \tag{33}$$

where ω_T is the number of proton transfers per unit surface area per second.

15. Inferences Concerning Deflagration and Linear Pyrolysis

Jacobs[26] has reviewed linear pyrolysis experiments with an eye toward using his surface-diffusion model in interpreting them. Here we wish to consider the implications of the alternative explanation offered in section 13, for these high-temperature, high-pressure experiments.

One cannot be certain of the importance of the "low-temperature reaction" (ω_D of section 13) at elevated temperatures. If we assume that the observed activation energy can be used to extrapolate the rate ω_D to deflagration temperatures, then we find that $\omega_D \approx 5 \times 10^{-5}$ mol/(cm^2 sec) at 870°K, a representative surface temperature for deflagration. This corresponds to a linear regression rate of roughly 5×10^{-3} g/(cm^2 sec) or 2×10^{-3} cm/sec which is about two orders of magnitude below representative deflagration or linear pyrolysis rates at this temperature. Thus, one is inclined to infer that ω_D is unimportant under typical conditions of deflagration or linear pyrolysis. The sublimation process seems likely to be dominant.

Whether the sublimation will be in equilibrium (section 13) or rate controlled (section 14) depends on surface temperature, pressure, and the effective diffusion distance. The elevated temperature and elevated pressure (for deflagration or pyrolysis as compared with sublimation experiments) favor equilibrium, while the diffusion distance probably decreases, favoring a rate process. The temperature and pressure effects combined tend to make equilibrium about 10^6 times more likely in deflagration at 70 atm and 600° than in sublimation at 1 atm and 270°. It therefore seems highly unlikely that the diffusion distance in deflagration can be small enough to cause deflagration to exhibit a greater tendency toward a surface rate process than is exhibited in the equilibrium sublimation experiments; diffusion lengths less than 10^{-6} cm would be required. Similar estimates indicate that surface equilibrium conditions probably also prevail for pyrolysis experiments. Pyrolysis or deflagration at subatmospheric pressures may conceivably be surface rate controlled, as inferred in the most recent work of Powling.[16] However, at pressures above 1 atm, Powlings's data[16] appear to be equally consistent with a surface equilibrium or surface rate process, and the present considerations favor surface equilibrium under these conditions.

Acknowledgment. We wish especially to thank P. W. M. Jacobs, W. Nachbar, E. W. Price, and H. Wise for highly informative and cooperative discussions during the course of this work.

Appendix

Derivation of Eq 31. With one kind of site and rate-controlled sublimation

$$Q_k = 4\pi a^2\omega_{k1}\theta_{k1}; \quad k = A, B \tag{A-1}$$

Since $Q_A = Q_B$ in steady state

$$\omega_{A1}\theta_{A1} = \omega_{B1}\theta_{B1} \tag{A-2}$$

Equilibrium for proton-transfer states

$$\frac{\theta_{A1}\theta_{B1}}{(1 - \theta_1)^2} = K_1 = K_n\nu_A\nu_B\alpha_{A1}\alpha_{B1}/\omega_{A1}\omega_{B1} \tag{A-3}$$

---

[26] P. W. M. Jacobs and J. Powling, *Combust. Flame*, **13**, 71 (1969).

where the last equality arises from the definition of the equilibrium constant K_n.

Since $\theta_1 = \theta_{A1} + \theta_{B1}$, solution of eq A-2 and A-3 for θ_{A1} and θ_{B1} yields

$$\theta_{A1} = \left[1 + \frac{\omega_{A1}}{\omega_{B1}} + \sqrt{\frac{\omega_{A1}}{K_1\omega_{B1}}}\right]^{-1};$$

$$\theta_{B1} = \left[1 + \frac{\omega_{B1}}{\omega_{A1}} + \sqrt{\frac{\omega_{B1}}{K_1\omega_{A1}}}\right]^{-1} \qquad \text{(A-4)}$$

Equation A-1 implies that $Q_k = 4\pi a^2\sqrt{\omega_{A1}\theta_{A1}\omega_{B1}\theta_{B1}}$, whence eq A−4 provides the expression

$$Q_k = 4\pi a^2[\omega_{A1}{}^{-1} + \omega_{B1}{}^{-1} + (K_1\omega_{A1}\omega_{B1})^{-1/2}] \qquad \text{(A-5)}$$

Since

$$Q_k = (\rho/m)4\pi a^2(\mathrm{d}a/\mathrm{d}t) \qquad \text{(A-6)}$$

and $(1 - \delta)^{1/3} = a/a_0$, we see that $k \equiv -\mathrm{d}(1 - \delta)^{1/3}/\mathrm{d}t$ is given by

$$k = (m/\rho a_0)[\omega_{A1}{}^{-1} + \omega_{B1}{}^{-1} + (K_1\omega_{A1}\omega_{B1})^{-1/2}]^{-1} \qquad \text{(A-7)}$$

Substitution of eq 30 and A-3 into this formula yields eq 31.

Extinction Coefficient of Azulene Anion Radical and the Yield of Scavengeable Electron in γ-Irradiated Organic Glass

by Tadamasa Shida

The Institute of Physical and Chemical Research, Yamatomachi, Kitaadachi-gun, Saitama, Japan

(Received June 16, 1969)

γ Irradiation of azulene in 2-methyltetrahydrofuran at 77°K produces azulene anion radicals which exhibit an absorption band at 440 mμ. The increase of the anion band is in proportion to the decrease of azulene band at 687 mμ. Knowing the extinction coefficient of the 687-mμ band at 77°K as 168.3 l. mol^{-1} cm^{-1}, the extinction coefficient of the anion band was determined to be 6.78×10^3 l. mol^{-1} cm^{-1}. The G value of total scavengeable electron for the matrix was determined as 2.53 on the basis that all scavengeable electrons react with azulene to form its anion.

Introduction

Determination of extinction coefficients of transient species is of considerable importance both from the theoretical and the practical viewpoints. In such occasions as electrolysis, flash photolysis, pulse radiolysis, and radiolysis of low-temperature rigid solutions, transient absorptions of intermediate products are observed, and yet usually their concentration cannot be assessed because of the lack of data on extinction coefficients.

Among other reactive species, anion radicals require careful treatment in the quantitative determination because they react rapidly with oxygen and other impurities in most cases. Since many anion radicals have an extinction coefficient of the order of 10^4 to 10^5 l. mol^{-1} cm^{-1}, the concentration of radical must be kept at 10^{-4} to 10^{-5} mol l.$^{-1}$ when their absorbance is measured in a 1-cm absorption cell. In such a low concentration a trace of impurity may easily cause serious trouble. In a few cases, however, extinction coefficients of anion radicals have been reported. Hoijtink,[1] Weissman,[2] and Hamill[3] produced aromatic hydrocarbon anions by alkali metal reduction and determined the extinction coefficient by a titration method or by weighing the reactant hydrocarbons. The discrepancy of the results among these authors may reflect the difficulty encountered in the treatment of a small amount of anion radicals.

γ Irradiation of frozen rigid solutions for the production of solute anions has been established by Hamill and his coworkers.[4] In this method electrons ejected by ionization from matrix molecules are utilized to react with solute molecules which are sparsely doped in the rigid 2-methyltetrahydrofuran (MTHF) matrix at 77°K. Depending on the solute either the electron attachment

---

[1] P. Balk, G. J. Hoijtink, and J. W. H. Schreurs, *Rec. Trav. Chim.*, **76**, 813 (1957).

[2] D. E. Paul, D. Lipkin, and S. I. Weissman, *J. Amer. Chem. Soc.*, **78**, 116 (1956).

[3] M. R. Ronayne, J. P. Guarino, and W. H. Hamill, *ibid.*, **84**, 4230 (1962).

[4] P. S. Rao, J. R. Nash, J. P. Guarino, M. R. Ronayne, and W. H. Hamill, *ibid.*, **84**, 500 (1962).

$$S + e^- \longrightarrow S^- \quad (1)$$

or the attachment with dissociation

$$AB + e^- \longrightarrow A + B^- \quad (2)$$

takes place. Therefore, if the solute undergoes type 1 reaction, measurements of the decrease in the absorbance of solute ($-\Delta O.D._S$) and the simultaneous increase in the absorbance of anion ($\Delta O.D._{S^-}$) will yield the extinction coefficient of anion (ϵ_{S^-}) provided that the extinction coefficient of solute (ϵ_S) is known beforehand.

The principle is simple, and the method should be superior to those involving chemical analyses because it eliminates possible decomposition of the anion during its formation and determination. However, the crux is in the choice of solute because the absorption spectra of S and S^- must be well separated so that the decrease in S and the increase in S^- may be measured accurately. Moreover, severe restrictions are imposed on the magnitude of ϵ_S and ϵ_{S^-}. First, to scavenge thermal electrons by reaction 1 the solute concentration should be about 10 m*M* or higher; therefore, if ϵ_S is too high, say 10^4 l. mol^{-1} cm^{-1}, the initial absorbance of solute ($O.D._S{}^\circ$) in a 1-cm optical cell will be immeasurably high. Second, ϵ_S cannot be too small either. A low ϵ_S requires a high initial concentration for a sizable initial absorbance. However, since the irradiation cannot be dosed unlimitedly, $-\Delta O.D._S$ *vs.* $O.D._S{}^\circ$ will become vanishingly small if the initial solute concentration is too high. Finally, ϵ_{S^-}, on the other hand, should be high enough to enable the accurate measurement of $O.D._{S^-}$ at a practical level of irradiation dose.

Azulene was found to satisfy all these requirements, absorption spectra of parent molecule and its anion being conveniently located in the visible spectral region.

The purpose of the present paper is twofold: the first is the determination of the extinction coefficient of azulene anion at 440 mμ, and the second is the estimation of total yield of scavengeable electron in reaction 1. The latter has been reported as 2.5–3.0 by Hamill for the MTHF matrix on the basis of ϵ of biphenyl and naphthalene anions determined by a chemical analysis. The present work attempts to confirm the reported value because the *G* value has a considerable meaning in radiation chemistry and also because once it is established, extinction coefficients of any anions obtainable by reaction 1 can be calculated on the assumption that all electrons corresponding to the *G* value are scavenged at sufficiently high solute concentrations.

Experimental Section

Commercially available azulene was purified by repeating sublimation under vacuum; MTHF was purified by a method similar to Dainton and Salmon's[5] and was kept in contact with a potassium–sodium alloy sphere under vacuum. The storage bulb was furnished with greaseless stopcocks to prevent contamination with lubricants. Azulene solutions in MTHF were transferred to quartz (Suprasil) cells of 1 cm, 2 mm, and 0.5 mm in thickness and were degassed by the freeze–thaw–reflux technique. The thickness of the cells was calibrated by measuring the absorbance of suitable solutions (a peak at 328 mμ of 1,4-diphenylbutadiene in ethanol) in the cells. The absorption spectra at 77°K before and after γ irradiation were measured on a Cary spectrophotometer, Model 14 RI. A 12,000-Ci Co^{60} source was used for irradiation. Dosimetry was carried out using the Fricke

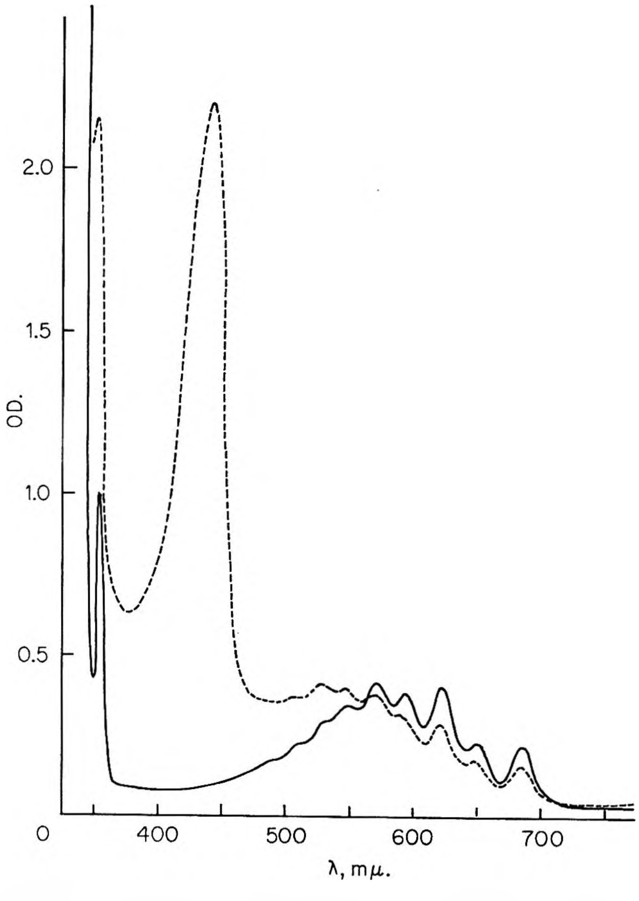

Figure 1. Absorption spectra of azulene in MTHF at 77°K before and after γ irradiation. Azulene (3.4 m*M*) in MTHF at 24° was frozen at 77°K in a 2.00-mm optical cell, and the spectrum was recorded at 77°K (solid curve). After γ irradiation with the dose of 9.20 × 10^{19} eV/g, the sample was photobleached with light of λ >690 mμ to eliminate the superposing absorption of residual $(e^-)_t$. The resulting spectrum is in the broken curve.

---

(5) F. S. Dainton and G. A. Salmon, *Proc. Roy. Soc.*, **A285**, 319 (1964).

solution which was positioned identically with the azulene samples in a Dewar. To simulate the liquid nitrogen, n-butyl alcohol, whose density matches with that of liquid nitrogen, was filled in the Dewar. The density of MTHF at 77°K was calculated to be 1.057 from the density at room temperature[6] and the volume contraction which amounted to 19.6% of the volume at 24°.

ϵ's of the visible bands of azulene molecule were determined as follows. A 1–5-mg sample of azulene was weighed with a microbalance and dissolved in 1.00 ml of MTHF at 24.0° in air. The absorption of solutions in 1.5-mm cells was measured immediately in air at the room temperature and then at 77°K. Omission of degassing eliminated possible pumping loss of highly volatile azulene. The molar extinction coefficients at 24° and 77°K were found to be 113.2 and 168.3, respectively, for the peak at about 690 mμ. Due to the sharpening of absorption bands, the ϵ at 77°K is higher than that at room temperature by about 48% even after correcting the volume contraction upon cooling.

Results

Azulene Solutions in MTHF. When azulene solutions (>30 mM) in MTHF were irradiated at 77°K, an absorption band appeared at 440 mμ whose absorbance increased linearly with the irradiation dose (Figures 1 and 2). The linearity was sustained up to 9.0×10^{19} eV/g of dose for a solution of 60 mM of azulene. As the concentration of azulene was lowered, part of electrons not scavenged by azulene appeared as the solvent-trapped electron, designated as $(e^-)_t$ hereafter, which was evidenced by its characteristic absorption band in the near-ir region ($\lambda_{max} \sim 1.2\ \mu$).[5] Figure 3 shows the competitive relation between the electron band at 1.2 μ and the 440-mμ band. For samples of concentrations less than 30 mM, optical bleaching with infrared light ($\lambda > 690$ mμ) eliminated the residual electron and enhanced the absorbance of the visible band as the two concave curves in Figure 3 show. The absorbance of the visible band after the ir bleaching was found to be proportional to the decrease in the absorbance of azulene bands (Figure 1). Readability of the small change in the azulene bands was improved by employing a 1-cm optical cell in place of the 2-mm cell. Since the peak at 687 mμ is well separated from the band at 440 mμ, the change at 687 mμ was taken to be purely due to the disappearance of azulene molecule. As will be shown in the next section, possible background absorptions due to the radiation decomposition of matrix molecules are negligible in the visible region. The ϵ of the 440-mμ band was then obtained by the relation, $\epsilon_{440}/\epsilon_{687} = \Delta\text{O.D.}_{440}/-\Delta\text{O.D.}_{687}$. The average of six determinations gave $\epsilon_{440} = 6782$, with the standard deviation of 114.

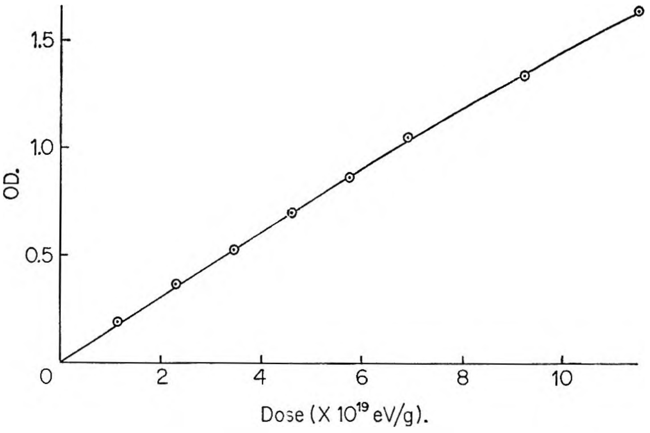

Figure 2. Absorbance of the azulene anion band at 440 mμ as a function of irradiation dose. Azulene (60 mM) in MTHF was irradiated in a 0.50-mm cell at 77°K. The initial slope of the curve gives the value of $G\epsilon = 1.72 \times 10^4$ (molecules/100 eV) (l. mol^{-1} cm^{-1}), where ϵ is the extinction coefficient of the band at 440 mμ.

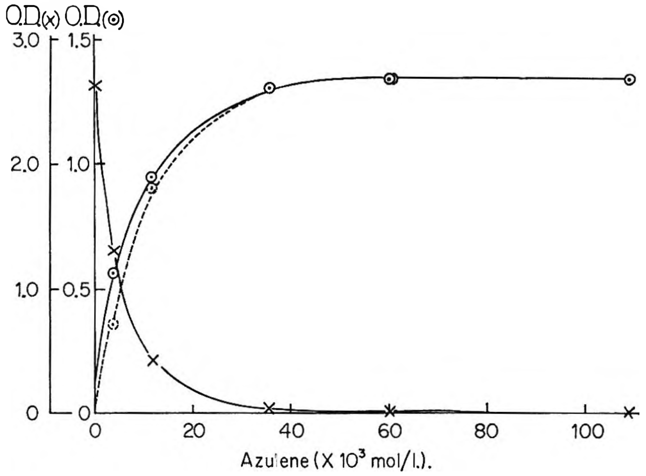

Figure 3. Absorbances of the azulene anion band (⊙) and the $(e^-)_t$ band (×) as plotted against the concentration of azulene. The solid concave curve is for the absorption in 0.50-mm cells immediately after γ irradiation (dose = 9.2×10^{19} eV/g), and the broken curve is for the absorption after a subsequent photobleaching of the $(e^-)_t$ band with ir light.

Pure MTHF. Extensive studies on the γ-irradiated pure MTHF glass were carried out by Dainton and Salmon[5] and Hamill, *et al.*[7] Supplementary data for the growth of 1.2-μ band with dose are shown in Figure 4. The deviation from the linearity is noticeable at the dose of 2×10^{19} eV/g compared with 9×10^{19} eV/g for the 60 mM azulene solution (Figure 2). From the initial slope of the curve in Figure 4 $G\epsilon$ is obtained as 4.92×10^4 (molecules/100 eV)(l. mol^{-1} cm^{-1}) in comparison with a previous value of 4.37 ×

---

[6] G. M. Bennett and W. G. Philip, *J. Chem. Soc.*, 1937 (1928).

[7] J. P. Guarino and W. H. Hamill, *J. Amer. Chem. Soc.*, **86**, 777 (1964).

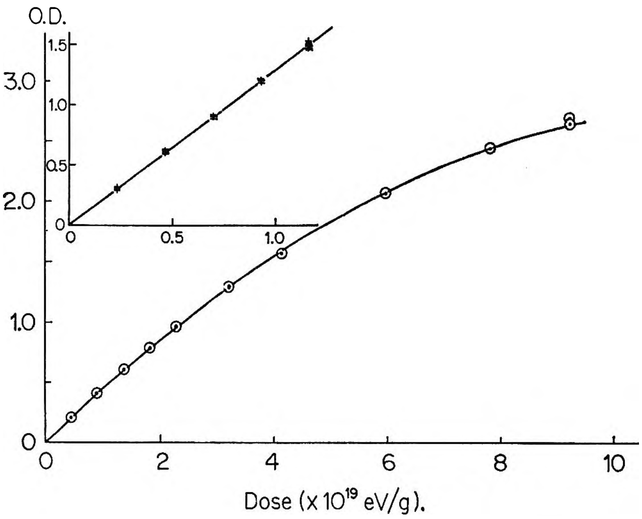

Figure 4. Absorbance of the $(e^-)_t$ band at 1.20 μ as a function of irradiation dose. Pure degassed MTHF in a 0.5-mm cell was irradiated successively at 77°K. The inset enlarges the initial portion of the curve which was obtained with samples in 1.5-mm cells in place of 0.5 mm (units are the same for both figures).

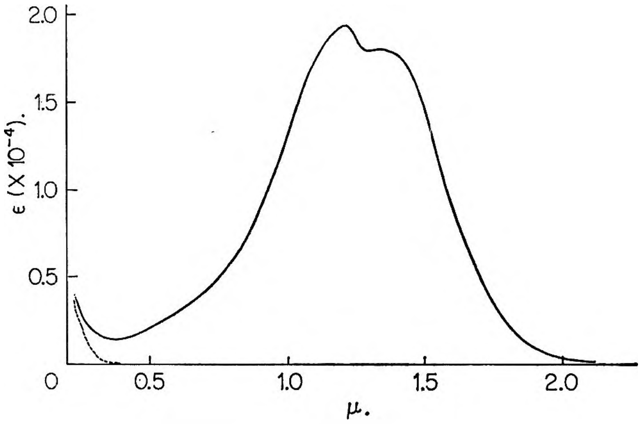

Figure 5. Absorption spectrum of the $(e^-)_t$ band in MTHF at 77°K. The spectrum in solid curve was obtained as a difference of the absorptions before and after irradiation. The broken curve shows the residual absorption after the photobleaching of the irradiated sample with ir light. ε's were determined by normalizing to $\epsilon_{1.2\mu} = 1.94 \times 10^4$ (see text).

10^4 (molecules/100 eV)(l. mol^{-1} cm^{-1}) for the absorbance at 1.25 μ.[5,8]

Discussion

Azulene anion radical has been produced for the esr study by electrolysis[9] and by alkali metal reduction.[10] Sioda, using a polarographic method, observed a broad absorption spectrum ascribable to the anion in solutions under electrolysis.[11] By measuring the electric current simultaneously he made an estimation for ε at room temperature obtaining ε ~3200 for the λ_{max} at 444 mμ. The similarity of the 440-mμ band in the present work with Sioda's observation and the reciprocal relation of the band with the $(e^-)_t$ band as shown in Figure 3 convince us that the 440-mμ band is due to the azulene anion radical. The much smaller ε determined by Sioda is not incompatible with the ε in this work because of the sharpening of absorption bands at the low temperature. As mentioned above, ϵ_{687} of azulene molecule increases by about 50% at 77°K compared with the value at room temperature.

It is fortunate that the anion band is on the short wavelength side of the first band of azulene molecule where the absorption due to azulene is relatively small and smooth. In most contrary cases molecular absorptions are overshadowed by the tailing absorption of anion bands lying at longer wavelengths, and the subtle decrement of the molecular absorption is practically immeasurable.

Since the present method of determining ε excludes possible errors in the assessment of the ion, the ε obtained above should be reliable. However, due to the sharpening of spectra, ε's at 77°K may not always be applicable for the absorption at room temperature. The temperature-independent oscillator strength should be more versatile, which is estimated to be approximately 9.3×10^{-2} for the 440-mμ band.

Based on ϵ_{440} 6.78×10^3 at 77°K, the *G* value of total scavengeable electron can be obtained as 2.53 from the level-off absorbance of the anion band in Figure 3. Once the *G* value is established, ε of any anions formed by reaction 1 can be determined on the assumption that all electrons corresponding to the *G* value are scavenged at level-off concentrations of the solute. For example, biphenyl as a solute in MTHF exhibited curves similar to those in Figure 3, and the limiting absorbance of biphenyl anion gave $\epsilon_{(C_6H_5)_2^-} = 3.93 \times 10^4$ l. mol^{-1} cm^{-1} for the peak maximum at 410 mμ, which is in fair agreement with the value of 3.7×10^4 determined by a chemical method.[3]

If all the scavengeable electrons become $(e^-)_t$ in the absence of solutes, the *G* value of $(e^-)_t$ will be 2.53 and the ε of $(e^-)_t$ at 1.20 μ is calculated as 1.94×10^4 from the product, $G\epsilon = 4.92 \times 10^4$ determined above. Figure 5 displays ε obtained in this way. The spectrum in Figure 5 gives the oscillator strength of $(e^-)_t$ as 0.58, which is comparable with a rough estimation of 0.8 by Hamill, *et al.*[7]

Acknowledgment. The author is indebted to Dr. Masashi Imamura for helpful discussions.

(8) Referring to the spectrum in Figure 5, the corresponding value for 1.20 μ would be 4.55×10^4, which is still about 8% lower than the value determined in this work.

(9) I. Bernal, P. H. Rieger, and G. K. Fraenkel, *J. Chem. Phys.*, **37**, 1489 (1962).

(10) A. H. Reddoch, *ibid.*, **41**, 444 (1964).

(11) R. Sioda, *Bull. Acad. Pol. Sci., Ser. Sci. Chim.*, **14**, 579 (1966).

Optical and Electron Spin Resonance Studies on Photolyzed and Radiolyzed Tetraphenylhydrazine and Related Compounds

by Tadamasa Shida and Akira Kira

The Institute of Physical and Chemical Research, Yamatomachi, Kitaadachi-gun, Saitama, Japan

(*Received June 16, 1969*)

Ultraviolet and γ irradiation of tetraphenylhydrazine in rigid matrices at 77°K induces the following modes of decomposition, respectively.

$$(C_6H_5)_2NN(C_6H_5)_2 + h\nu \longrightarrow 2(C_6H_5)_2N\cdot$$

$$(C_6H_5)_2NN(C_6H_5)_2 + e^- \longrightarrow (C_6H_5)_2N\cdot + (C_6H_5)_2N^-$$

The radical pair in the photolysis has a spin–spin interaction as manifested by esr spectra, but it is not responsible for the electronic absorption band in the near-infrared region, contrary to the proposal by Kommandeur, *et al.* Flash photolysis of tetraphenylhydrazine in benzene solution at room temperature yields the diphenyl nitrogen radical which disappears by second-order kinetics with a rate constant of 2.5×10^7 l. mol^{-1} sec^{-1}. Diphenylhydrazine in γ-irradiated matrices undergoes the dissociative electron attachment $(C_6H_5)_2NNH_2 + e^- \rightarrow (C_6H_5)_2N^- + \cdot NH_2$, while dicarbazyl captures an electron to form the anion radical. The anion is stable at 77°K but dissociates upon bleaching with visible light into a carbazyl radical and a carbazyl anion. The extinction coefficient at 77°K was estimated for the following intermediate species, $(C_6H_5)_2N\cdot$, $(C_6H_5)_2N^-$, dicarbazyl anion, and carbazyl radical.

Introduction

Since the pioneering work by Lewis and Lipkin[1] on the photolysis of tetraphenylhydrazine (TPH) in the rigid matrix, there have been relatively few reports on the subject. Recently, Garofano and Santangelo[2] and Wiersma and Kommandeur[3] confirmed that TPH dissociates upon uv illumination into two diphenyl nitrogen radicals, $(C_6H_5)_2N\cdot$. The work by the latter group clearly indicates that the geminate radicals in a cage has a spin–spin interaction giving rise to a doublet esr spectrum at 3300 G and a weak forbidden absorption at 1650 G. The same authors proposed that the radical pair was also responsible for a broad optical absorption in the near-ir region which they interpreted in terms of an intermolecular charge transfer between the radicals. Since the conclusion depends entirely on a calculation for electronic states of the radical pair which seems to have some room for argument in the choice of molecular arrangement and other parameters, we have reinvestigated the system along with related systems using several experimental techniques.

Since the findings in the present work are rather discursive, a brief summary is presented here for the convenience of preliminary understanding. (1) TPH photodissociates into two diphenyl nitrogen radicals both in solutions at room temperature and in rigid matrices at 77°K. The radical exhibits absorption bands with λ_{max} ~450 and 770 mμ. The radical pair in the rigid matrix does not yield any new absorption band proper to the pair formation. (2) γ-Irradiated TPH in the rigid methyltetrahydrofuran (MTHF) matrix produces a diphenyl nitrogen radical and a diphenylamide ion by a dissociative electron attachment. The amide ion is identified by a strong absorption band at 380 mμ. In alcoholic matrices the amide ion reacts subsequently with the matrix alcohol according to the reaction

$$(C_6H_5)_2N^- + ROH \longrightarrow (C_6H_5)_2NH + RO^-$$

(3) Upon γ irradiation, *asym*-diphenylhydrazine in the MTHF matrix undergoes the reaction

$$(C_6H_5)_2NNH_2 + e^- \longrightarrow (C_6H_5)_2N^- + \cdot NH_2$$

(4) Photolysis of dicarbazyl in the rigid matrix leads to the homolytic dissociation similar to TPH. As in the case of TPH no absorption of intermolecular nature was detected. (5) Dicarbazyl in the γ-irradiated MTHF matrix captures electrons without dissociation contrary to THP, but optical bleaching of the anion radical causes a dissociation similar to TPH.

Experimental Section

Materials. TPH was prepared according to the method described in a standard textbook[4] and was purified by recrystallization from a methanol–benzene mixture. Dicarbazyl was synthesized from carbazole and potassium permanganate.[5] *asym*-Diphenylhydrazine (DPH) was obtained by neutralizing the aqueous solution of commercially available DPH hydrochloride with a concentrated sodium hydroxide solution. The free base purified by recrystallization from cold ligroin could be kept under vacuum without significant deterioration.

---

(1) G. N. Lewis and D. Lipkin, *J. Amer. Chem. Soc.*, **64**, 2801 (1942).

(2) T. Garofano and M. Santangelo, *Ric. Sci.*, **4**, 75 (1964).

(3) D. W. Wiersma and J. Kommandeur, *Mol. Phys.*, **13**, 241 (1967).

(4) T. Wieland, "Die Praxis des Organischen Chemikers," W. Gruyter & Co., Berlin, 1958.

Photolysis and Radiolysis. Transient spectra of flash photolysis were recorded on photoplates, Fuji Neopan SS sheet (ASA 100), or displayed on an oscilloscope using photomultiplier tubes, Hamamatsu R-106 and R-136 for the visible region and R-196 for the near-ir. Cylindrical quartz cells (10 cm) were used as the optical absorption cell. Steady-state uv illumination was performed using a 500-W high-pressure mercury point source, Ushio USH 500. A 12-kCi Co^{60} γ-ray source was used for radiolysis.

Optical and Esr Measurements. Optical absorption spectra of rigid solutions at 77°K were measured with a Cary spectrophotometer Model 14 RI. Optical cells, 1.5 mm thick, made of Suprasil quartz were used for the low-temperature experiments. A JEOLCO (Japan Electron Optics Laboratories Co. Ltd.) esr spectrometer with a 100-kHz modulation was employed for esr measurements.

Results

Tetraphenylhydrazine. Flash Photolysis. TPH solution (1.0 m*M*) in deaerated benzene was photolyzed at room temperature with a flash of 64 J. A transient absorption was observed in the visible and the near-ir regions. The visible band photographed on a plate is displayed at the left side of Figure 1, whereas the absorption in the near-ir region recorded photoelectrically is reproduced at the right. Figure 2 shows the linear relation between the reciprocal of absorbances at 450 and 720 mμ and the time elapsed after the end of flash. If the same species is responsible for the absorption bands at about 450 and 770 mμ in Figure 1, the product of the initial absorbance multiplied by the slope of the curves in Figure 2 must be equal for the two wavelengths measured. From Figure 2 the products are calculated as 4.7×10^2 for 450 mμ and 4.6×10^2 for 720 mμ, substantiating the assumption of the same species.

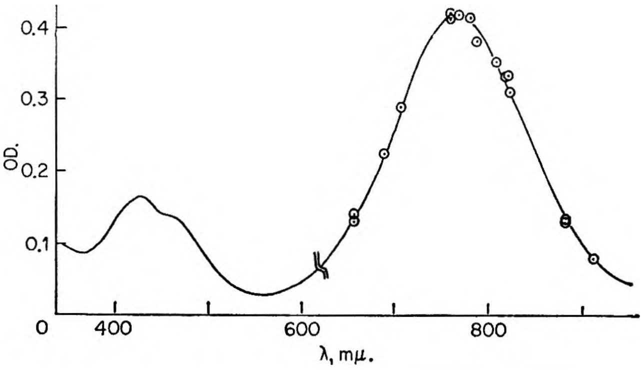

Figure 1. Transient spectrum of flash-photolyzed TPH (1 m*M*) in deaerated benzene. The absorption at 330–630 mμ was photographed 50 μsec after the flash, while the absorption at longer wavelengths was obtained from the optical density recorded on an oscilloscope. The two portions of spectrum were jointed by normalizing the optical density in the region of 600–650 mμ.

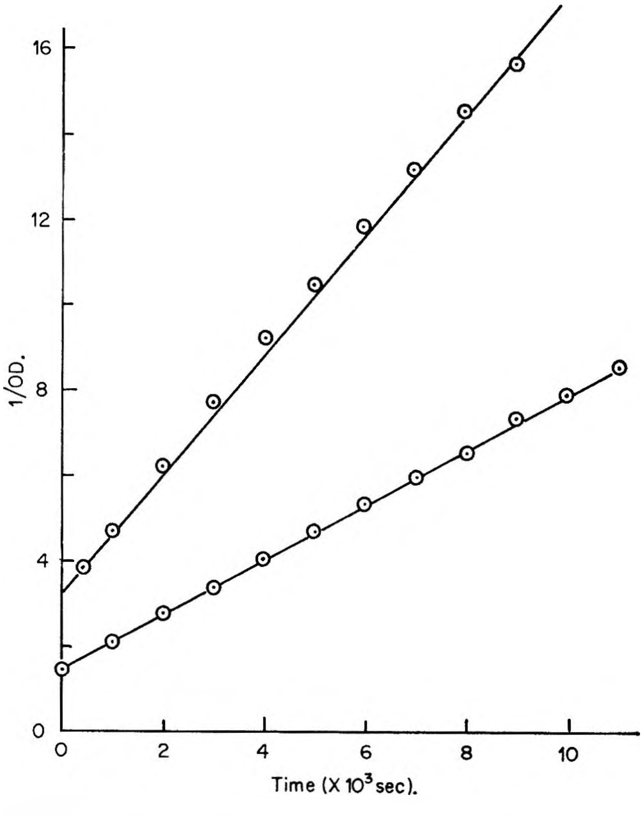

Figure 2. Second-order test of the decay of transient absorption in Figure 1. The upper and lower lines correspond to the decay at 450 and 720 mμ, respectively.

Photolysis at 77°K. Steady-state uv illumination was also carried out for TPH in MTHF at 77°K. The spectrum observed is illustrated in the upper part of Figure 3, which agrees with the spectrum reported by the previous workers[2,3] and also with that in Figure 1. For TPH in EPA (5:5:2 volume mixture of ether, isopentane, and ethanol) solutions photolyzed at 90°K, Lewis and Lipkin foundf our different species, A, B, C, and X in their designation and identified them, respectively, with TPH cation radical, diphenyl nitrogen radical, diphenyl nitrogen cation, and an unspecified product.[1] We were unable to reproduce their result for the TPH–MTHF solution photolyzed at 77°K, but the absorptions at 700–800 and at <470 mμ (D band in their symbolism), assigned by Lewis to the diphenyl nitrogen radical, are comparable with the spectrum shown in Figure 3.

---

[5] W. H. Perkin, Jr., and S. H. Tucker, *J. Chem. Soc.*, 119, 216 (1921).

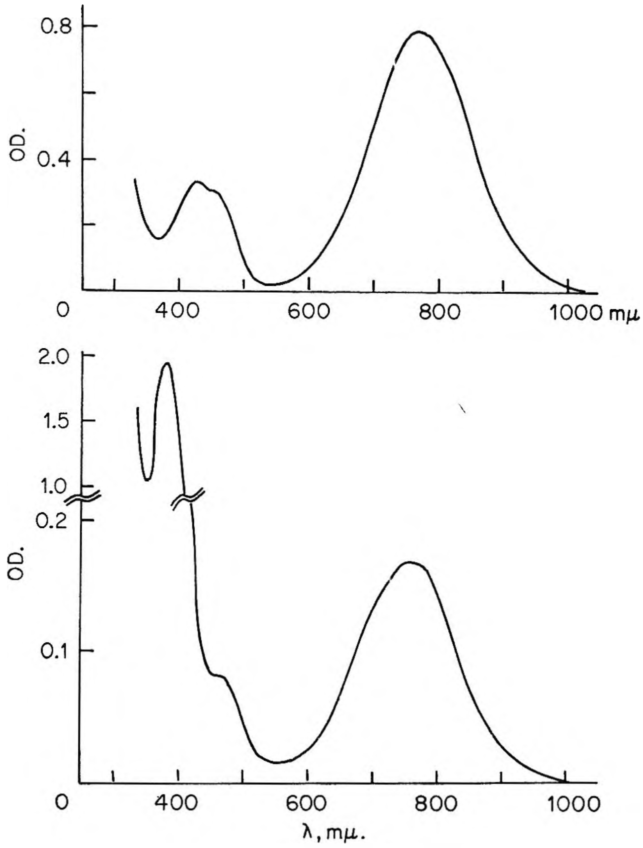

Figure 3. Absorption spectra of TPH (10 mM) in MTHF uv-illuminated (upper) and γ-irradiated (lower) at 77°K. For photolysis the sample was exposed to uv light of $\lambda > 290$ mμ for 40 sec. Samples immediately after γ irradiation exhibited a broad absorption band due to the unscavenged electron whose λ_{max} is at about 1.2 μ. Photobleaching the sample with ir light eliminated the electron band and revealed the three bands shown in the lower spectrum (dose = 1.1×10^{19} eV/g).

Esr spectra of uv illuminated TPH in MTHF glass coincided with those previously reported.[2,3] Both the allowed and forbidden ($\Delta m_s = 2$) absorptions due to the radical pair were observed. The upper spectrum of Figure 4 shows the allowed band at about 3300 G.

Radiolysis at 77°K. γ Irradiation of pure MTHF glass at 77°K produces a strong absorption band with the $\lambda_{max} \sim 1.2$ μ which is attributed to the solvent-trapped electron,[6] $(e^-)_t$. As TPH was added in MTHF, the $(e^-)_t$ band was suppressed, and three new bands appeared at 380, 400–500, and 770 mμ. Optical bleaching of the irradiated sample with ir light ($\lambda > 690$ mμ) eliminated the residual $(e^-)_t$ band and enhanced the absorbance of the three bands. At TPH concentrations higher than *ca.* 80 mM the electron band did not appear, and the absorbance of the three bands attained level-off values (Figure 5). The spectrum after the photobleaching appears in the lower part of Figure 3. Comparison with the upper spectrum indicates that the bands at 400–500 and 770 mμ are common to photolyzed and radiolyzed

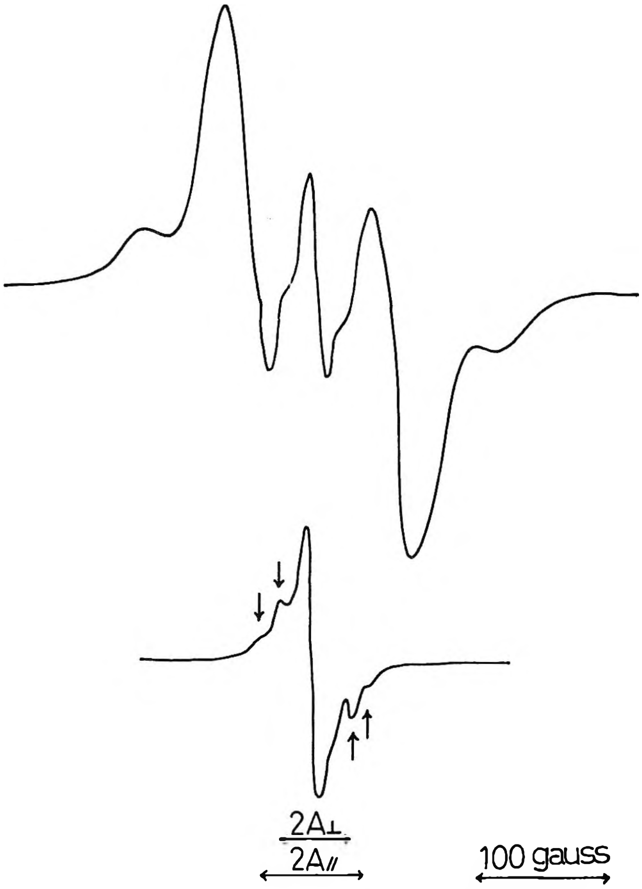

Figure 4. Esr spectra of TPH (50 mM) in MTHF uv-illuminated (upper) and γ-irradiated (lower) at 77°K. Both samples were green. The lower spectrum was obtained by subtracting the superposing spectrum of MTHF radical (dose = 1.1×10^{19} eV/g).

samples. The 380-mμ band, on the other hand, is unique to radiolysis. Another difference between the uv-illuminated and γ-irradiated samples is the effect of carbon tetrachloride added with TPH in the MTHF matrix; all the three bands in radiolyzed solutions decreased as the chloride was added whereas the two bands in photolyzed samples were not affected by the presence of the second solute (Figure 6).

Parallel experiments of γ irradiation were performed with ethanol matrix in place of MTHF. In the alcoholic matrix the band at 380 mμ was not produced, and only two bands were observed at 400–500 mμ and at about 750 mμ which are similar to those observed for the photolyzed TPH in MTHF matrix. The 750-mμ band is related to the 770-mμ band in MTHF, the shift by *ca.* 20 mμ being attributed to the general solvent effect.

The difference between the photolyzed and radiolyzed samples is remarkable also in the esr results. γ-Irradiated TPH in MTHF produced a triplet esr spectrum superposed with the known spectrum of MTHF

---

(6) F. S. Dainton and G. A. Salmon, *Proc. Roy. Soc.*, **A285**, 319 (1965).

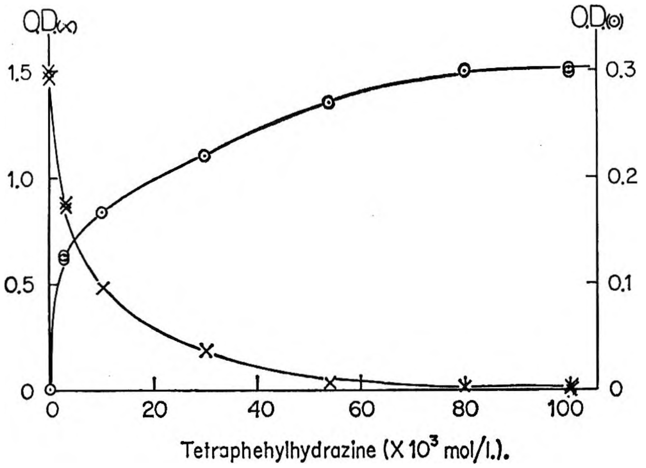

Figure 5. Optical densities of the 770-mμ band (⊙), right ordinate, and the $(e^-)_t$ band (×), left ordinate, as a function of the concentration of TPH. The plots in the circle were obtained after optical bleaching of the irradiated sample with ir light (dose = 1.1×10^{19} eV/g).

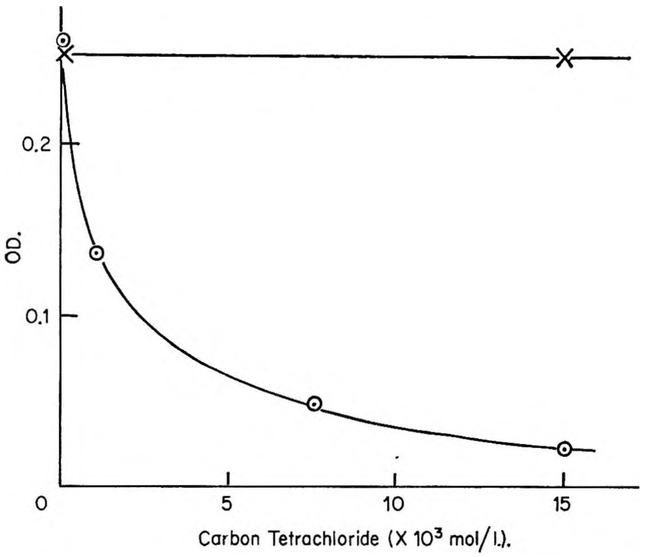

Figure 6. Effect of the addition of carbon tetrachloride on the optical density of 770-mμ band. CCl_4 was added to TPH (15 mM) in MTHF, and the solutions were irradiated at 77°K to the dose of 2.3×10^{19} eV/g (⊙). The chloride suppressed not only the optical density of the 770-mμ band as shown above but that of the $(e^-)_t$ band and the two other TPH bands in Figure 3. In contrast with the radiolysis, CCl_4 does not affect the photolysis (×).

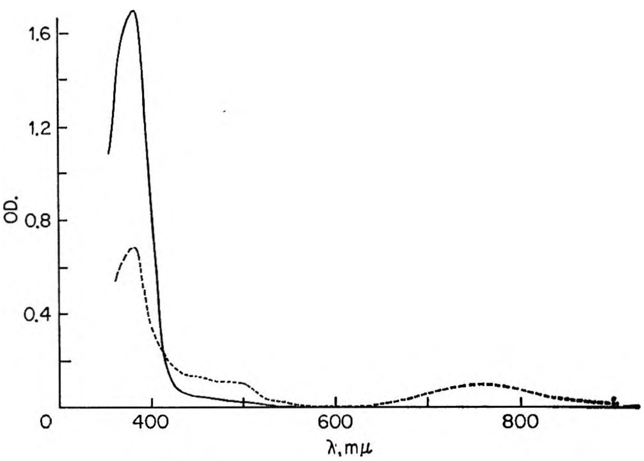

Figure 7. Absorption spectra of γ-irradiated DPH (76 mM) in MTHF at 77°K: solid curve, after irradiation with the dose of 4.0×10^{18} eV/g; broken curve, after bleaching of the irradiated sample with near-uv ($\lambda > 350$ mμ).

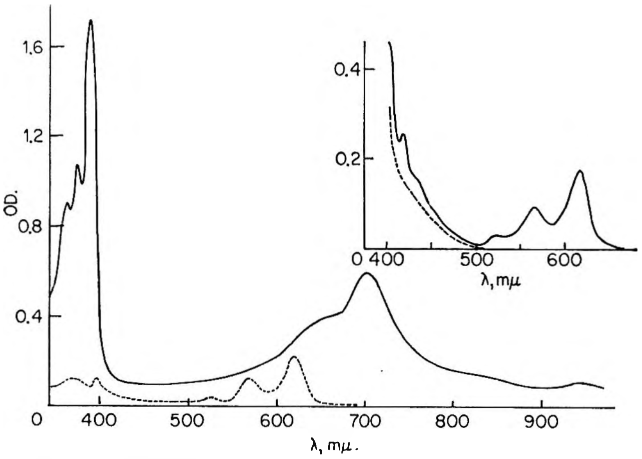

Figure 8. Absorption spectra of dicarbazyl (20 mM) in MTHF at 77°K: solid curve, after irradiation with the dose of 1.1×10^{19} eV/g; broken curve, after subsequent bleaching of the irradiated sample with light of $\lambda > 420$ mμ; inset, after uv illumination for 60 min with uv light of $\lambda > 290$ mμ. The broken curve indicates absorptions due to unspecified decomposition products from the solute.

radical.[6] Figure 4 (lower spectrum) shows the triplet component obtained after subtracting the spectrum of the solvent radical. In contrast with the photolyzed sample (upper spectrum of Figure 4) the spectral band width of the triplet is in the order of magnitude of hyperfine interaction. The half-field absorption observed for the photolyzed sample was not detected with the irradiated sample.

asym-Diphenylhydrazine. DPH in MTHF matrix yielded on γ irradiation an absorption band at 380 mμ at the sacrifice of the $(e^-)_t$ band. Bleaching with light of $\lambda > 350$ mμ diminished the band and produced two bands at about 450 and 770 mμ (Figure 7).

The esr spectrum of irradiated DPH (60 mM) in MTHF coincided exactly with the spectrum of the MTHF radical, and no new absorption due to the solute DPH was detected.

Dicarbazyl. The inset of Figure 8 demonstrates the spectrum of uv-illuminated dicarbazyl in MTHF matrix. Though no attempt was made to determine the quantum yield, the efficiency of photolysis was quite low compared with that of TPH under the same condition (compare the illumination time indicated in the caption). The brilliant luminescence observed for the dicarbazyl under illumination is consistent with the poor yield of photodecomposition.

The spectrum of γ-irradiated dicarbazyl in MTHF is shown in Figure 8. When the irradiated sample was exposed to light of $\lambda > 420$ mμ, the spectrum changed from the solid to the broken curve, the latter being unmistakably identified with the spectrum in the inset. Exposure of unirradiated samples to the visible light, of course, did not induce any spectral change.

Discussion

Tetraphenylhydrazine. Since the finding by Hausser and Murrell of π–π complexes between like radicals,[7] similar radical pairs have been reported by several authors.[8,9] Esr studies by Wiersma and Kommandeur on TPH in rigid matrices unambiguously show that the radicals in a cage are paired in the triplet state of a two-spin system. Their interpretation on electronic absorption spectra, however, is less persuading because of the arbitrariness involved in the calculation for energy levels. They regarded the 770-mμ band as due to the intermolecular charge resonance, and the band at 450 mμ was assigned to the first band of the monomeric radical affected slightly by the pair formation.

The matrix isolation method used in photochemistry is also useful in radiation chemistry. In matrices such as MTHF the radiation energy is primarily consumed for the ionization of matrix molecules and what we observe for the irradiated frozen sample is mainly reactions between ejected electrons and sparsely dispersed solute molecules. In what follows we will show that TPH in an irradiated matrix undergoes exclusively the dissociative electron attachment

$$(C_6H_5)_2NN(C_6H_5)_2 + e^- \longrightarrow (C_6H_5)_2N\cdot + (C_6H_5)_2N^- \quad (1)$$

Of the three bands shown in Figure 3 (lower spectrum) the bands at 400–500 and 770 mμ are assigned to the monomeric diphenyl nitrogen radical produced by reaction 1, while the 380-mμ band is assigned to the diphenylamide ion. The reasoning for this assignment is as follows. First, all the three appears at the expense of $(e^-)_t$ band, and the electron-scavenging carbon tetrachloride prevents their appearance competitively. Second, the result that the 380-mμ band appears in MTHF but not in alcoholic matrix can be accounted for by assigning the band to the amide ion and assuming that the ion reacts with alcohol as

$$(C_6H_5)_2N^- + ROH \longrightarrow (C_6H_5)_2NH + RO^- \quad (2)$$

Third, the result of a DPH–MTHF system discussed in the next section also supports the assignment of the amide ion. Lewis and Lipkin synthesized lithium diphenylamide for their photolytic study and found that a strong absorption sets in at about 400 mμ.[1] Though they did not see the λ_{max}, the feature of their spectrum is similar to the 380-mμ band. They also pointed out that the amide ion decomposes in alcohol according to reaction 2 because of the higher basicity of the amide.

A strong indication of reaction 1 is seen in the esr result; in spite of the absence of the doublet esr spectrum due to the radical pair (upper spectrum in Figure 4) in γ-irradiated samples, both 450- and 770-mμ bands appear in the radiolyzed sample as well as in the photolyzed solution. This indicates that the 770-mμ band is not proper to the radical pair but is an attribute to the monomeric radical. The esr triplet spectrum in γ-irradiated samples may be attributed to the monomer radical produced by reaction 1. Although not quite unambiguous, the vestigial bumps indicated by the small arrows in Figure 4 may be due to the anisotropy of hyperfine interaction of the nitrogen in the radical. If this is the case, hyperfine coupling constants parallel and perpendicular to the static magnetic field are crudely estimated as $A_{\parallel} = 40$ and $A_{\perp} = 29$ G from the spectrum. Based on these constants the s and p characters of the electron on the nitrogen can be calculated as 0.06 and 0.24, respectively, by the standard procedure. Thus, about 30% of the electron is localized on the nitrogen, and the rest is distributed over the two phenyl groups.

The absorption bands observed for the flashed solution are now ascribed to the radical produced by the homolysis at the N–N bond of TPH. The second-order decay of both bands is then understood in terms of bimolecular combination of the radicals.

Since the yield of electron participating in reaction 1 is known to be $G = 2.53$,[10] one can estimate from the level-off absorbance in Figure 5 the molar extinction coefficient of the three bands as 3.9×10^3, 1.5×10^3, and 4.5×10^4 l. mol^{-1} cm^{-1} at 770, 450, and 380 mμ, respectively. In the calculation the volume contraction on cooling has been corrected accordingly. Using the ϵ_{770} thus determined, the rate constant for the second-order disappearance of diphenyl nitrogen radical in the flashed sample is obtained as $k = 2.5 \times 10^7$ l. mol^{-1} sec^{-1}.

asym-Diphenylhydrazine. The result of radiolysis of DPH in MTHF can be explained by a reaction similar to reaction 1

$$(C_6H_5)_2NNH_2 + e^- \longrightarrow (C_6H_5)_2N^- + \cdot NH_2 \quad (3)$$

The band at 380 mμ in Figure 7 coincides with the band assigned to the same ion produced by reaction 1. The effect of the near-uv illumination is accounted for by the reaction

$$(C_6H_5)_2N^- + h\nu\ (\lambda > 350\ m\mu) \longrightarrow (C_6H_5)_2N\cdot + e^- \quad (4)$$

---

(7) K. H. Hausser and J. N. Murrell, *J. Chem. Phys.*, **27**, 500 (1957).

(8) M. Itoh and S. Nagakura, *J. Amer. Chem. Soc.*, **89**, 3959 (1967).

(9) T. J. Schaafsma and J. Kommandeur, *Mol. Phys.*, **14**, 525 (1968).

(10) T. Shida, to be published.

The ejected electron will decompose another DPH molecule by reaction 3 reproducing the amide ion. If the electron were subject only to the above cyclic change, the intensity of the 380-mμ band would not diminish. In fact, part of the electrons disappear by reacting with positive species produced by irradiation. The ratio of the decrement at 380 mμ *vs.* the increment at 770 mμ in Figure 7 is roughly 11:1, whereas the ratio of $\epsilon_{380}/\epsilon_{770}$ in Figure 3 is also about 11:1. This means that the photoexcitation of amide ion almost exclusively results in the ejection of electrons by reaction 4.

The NH_2 radical produced in reaction 3 should be detected by its characteristic esr spectrum.[11] Despite a careful search for the spectrum the observed spectrum indicated the presence of only the MTHF radical. The NH_2 radical is considered to react with a matrix molecule to produce NH_3 and a radical of the matrix molecule. The reason why reaction 3 is favored over the fragmentation into $(C_6H_5)_2N\cdot$ + NH_2^- may be in that the electron affinity of $(C_6H_5)_2N\cdot$ is possibly higher than that of NH_2 radicals and that the difference, $EA((C_6H_5)_2N\cdot) - EA(NH_2)$, may overcome the difference, $S(NH_2^-) - S((C_6H_5)_2N^-)$, where EA and S stand for electron affinity and solvation energy, respectively.

Dicarbazyl. Since the N–N bond in dicarbazyl is similar to that of TPH, comparative studies were carried out for dicarbazyl also. If dicarbazyl behaved analogously to TPH, carbazyl radicals should be formed both in photolyzed and radiolyzed samples. Since the spectrum of a photolyzed sample agrees with that of the γ-irradiated sample after the subsequent photobleaching (Figure 8 and the inset), we presume that the spectrum immediately after γ irradiation is due to dicarbazyl anion radicals and that photoexcitation of the anion leads to a heterolysis (see reaction 5) analogous to reaction 1. The assignment of the anion radical is supported by the competitive relation with the $(e^-)_t$ band and the preventive effect of electron scavengers such as carbon tetrachloride. The extensive conjugation over the carbazole ring would stabilize the anion radical, whereas the corresponding

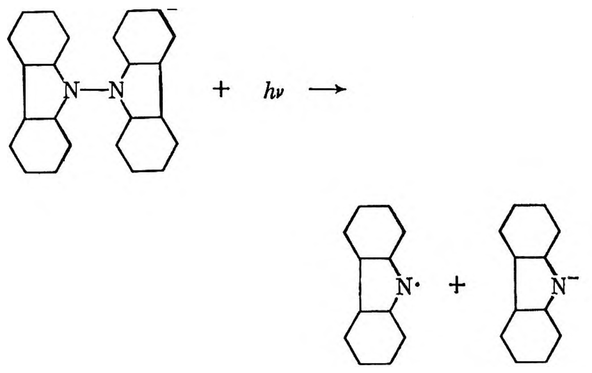

(5)

TPH anion radical dissociates instantly even at 77°K. Assuming that all electrons of the yield of $G = 2.53$ are scavenged by dicarbazyl to produce the anion radical, ε's of the ion are calculated as 2.2×10^4 and 7.8×10^3 l. mol^{-1} cm^{-1} at 390 and 700 mμ, respectively. If reaction 5 is the only fate of the anion upon photoexcitation, the ε of carbazyl radical is also obtained from the broken curve in Figure 8 which is 2.9×10^3 l. mol^{-1} cm^{-1} at 617 mμ. For the photolyzed sample no extra band was observed at wavelengths longer than 650 mμ, indicating again that the radical pair does not interact strongly enough to yield the charge resonance band.

Compared with the spectrum of diphenyl nitrogen radical the spectrum of carbazyl is nicely structured probably owing to the planarity of the radical. In a previous paper we reported the absorption spectrum of a radical derived from acridan

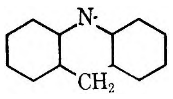

which closely resembles the spectrum of carbazyl radical.[12]

Acknowledgment. The authors wish to thank Dr. Masashi Imamura for his interest in this work.

---

[11] S. N. Foner, E. L. Cochran, V. A. Bowers, and C. K. Jen, *Phys. Rev. Lett.*, **1**, 91 (1958).

[12] T. Shida and A. Kira, *Bull. Chem. Soc. Jap.*, **42**, 1197 (1969).

Excitation of Molecular Vibration on Collision. Oriented Nonlinear Encounters

by Hyung Kyu Shin

Department of Chemistry, University of Nevada, Reno, Nevada *(Received June 17, 1969)*

The theory of vibrational energy transfer in oriented nonlinear collisions between a diatomic molecule and an atom is investigated. The classical energy transfer, ΔE_v, and vibrational transition probabilities, p_{nm}, are dependent on the impact parameter b and orientation angle Θ as well as on the initial collision velocity v. The N_2 + He collision is chosen for numerical examples. While only the head-on collinear collisions are of importance at low v, ΔE_v becomes appreciable for nonzero-impact parameter encounters at higher v ($>5 \times 10^5$ cm/sec). For the oscillator initially in the ground state, p_{0m} has a minimum value at a velocity such that $\Delta E_v = m\hbar\omega$; thus, in high-velocity collisions p_{01} decreases as v increases, while multilevel transitions become more probable. At high-velocities, p_{01} increases to a maximum value and then decreases as b increases; a similar situation can occur in $0 \rightarrow 2$ ($0 \rightarrow 3$ and so on) at still higher velocities. The p_{nm} values are very small for $b > \sigma$, where σ is the Lennard-Jones potential parameter. Nonlinear encounters up to $b/\sigma \simeq 0.8$ need to be considered in calculating the effective cross section Q_{01}. A brief discussion of rotational excitation is also made.

Introduction

The problem of vibrational energy transfer in simple collision systems such as BC + A and BC + BC has received attention in the past several years in a number of important papers.[1-3] New insight can now be obtained on energy transfer cross sections, particularly with respect to their dependence on the various parameters which characterize the collision. Some recent studies have involved exact calculation of vibrational transition probabilities. Of such studies, Secrest and Johnson's quantum mechanical approach[4] and Kelley and Wolfsberg's classical one[5] represent important contributions to this field.

A large amount of theoretical work, including the above-mentioned studies, has been done with the model of a diatomic molecule (BC) interacting with an atom (A) which is approaching BC along its line of oscillation or with another BC molecule collinearly. However, such a simple collision model is not a good one on which to base realistic calculation of energy transfer. A preferable treatment involves consideration of the nonlinear collision model. Nonlinear collisions are conveniently described in terms of an impact parameter b, defined as the distance separating asymptotes to the trajectories of the colliding partners. Furthermore, BC may be in any rotational orientation, so that molecular orientation should be introduced into the collision model.[6] It appears that a realistic attempt to solve the collision problem should be based on the "oriented nonlinear" collision model.

In the present paper we formulate a procedure for evaluating the vibrational energy transfer ΔE_v with such a model, in order to show how nonzero-impact parameters and oriented encounters affect the collision process. We assume that the Lennard-Jones (L-J) interaction law represents interactions between the colliding atoms.

Collision Model and Perturbation Energy

The interaction model is shown in Figure 1. The assumed form of the interaction potential in terms of the coordinates defined in the figure is

$$U(r_1,r_2) = 2D \sum_{i=1}^{2}[(\sigma/r_i)^{12} - (\sigma/r_i)^6] \qquad (1)$$

where $r_{1,2}^2 = r^2 \mp 2(d + x)rS_{2,1} \cos \Theta + (d + x)^2S_{2,1}^2$, $S_{1,2} = m_{B,C}/(m_B + m_C)$, and D, σ are the L-J potential parameters. The quantity d is the equilibrium bond distance of BC and x is the vibrational amplitude. In the collinear configuration the interaction between A and the nearest atom of BC is much greater than that of A and the other atom; *i.e.*, in C–B + A, the B–A interaction is the greatest. However, for nonlinear encounters the C–A interaction becomes important also. At $\Theta = \pi/2$, the B–A and C–A interactions contribute equally to the collision process; and for $\pi/2 < \Theta < 3\pi/2$, the C–A interaction becomes most important. Therefore, we must introduce both pair-wise interactions in deriving the overall interaction energy. The detailed description of the oriented encounters can be conveniently introduced in the interaction model as shown in Figure 1. The effect of nonzero-impact parameter encounters can be accounted for by introducing the centrifugal energy into eq 1.

It is often assumed that an exponential interaction such as $U(r_i) = C_1\Sigma_i[\exp(-r_i/a) - C_2 \exp(-r_i/2a)]$, where C_1, C_2, and a are potential parameters, is a reasonable representation of the collision. When such a potential is used, it turns out that the determination

---

(1) K. Takayanagi, *Progr. Theoret. Phys.* (Kyoto), **25**, 1 (1963).

(2) K. Takayanagi, *Advan. At. Mol. Phys.*, **1**, 149 (1965).

(3) D. Rapp and T. Kassal, *Chem. Rev.*, **69**, 61 (1969).

(4) D. Secrest and B. R. Johnson, *J. Chem. Phys.*, **45**, 4556 (1966).

(5) J. D. Kelley and M. Wolfsberg, *ibid.*, **44**, 324 (1966).

(6) H. Shin, *ibid.*, **49**, 3964 (1968).

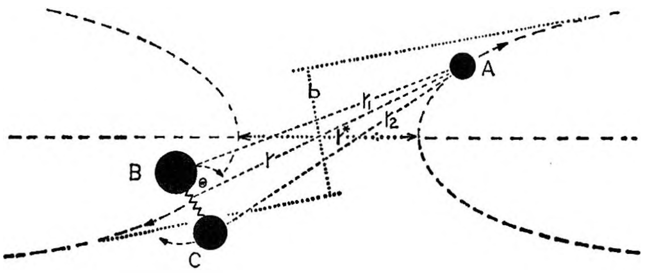

Figure 1. Collision geometry.

of the force parameter a is a difficult problem. One of the most widely used procedures is to calculate a by fitting the exponential to the L-J potential curves.[3,7] When such a value for a is used, the calculated vibrational transition probability based on the exponential potential should not be greatly different from the probability calculated with the L-J potential since the exponential potential is numerically "almost" identical with the L-J potential in the most probable region of energy transfer. This situation has been discussed in a recent paper for head-on collisions.[8]

For large interaction distances such that $r \gg d/2$, we can approximate

$$r_{1,2}^{-12} = r^{-12}\left[1 \pm 12\left(\frac{d+x}{r}\right)S_{2,1}\cos\Theta + (84\cos^2\Theta - 6)\left(\frac{d+x}{r}\right)^2 S_{2,1}^{\,2}\right]$$

$$r_{1,2}^{-6} = r^{-6}\left[1 \pm 6\left(\frac{d+x}{r}\right)S_{2,1}\cos\Theta + (24\cos^2\Theta - 3)\left(\frac{d+x}{r}\right)^2 S_{2,1}^{\,2}\right]$$

The overall interaction energy can then be shown to be

$$U(r,x,\Theta) = 4D\left[\left(\frac{\sigma}{r}\right)^{12} - \left(\frac{\sigma}{r}\right)^{6}\right] + 24D\left[\left(\frac{\sigma}{r}\right)^{12} - \frac{1}{2}\left(\frac{\sigma}{r}\right)^{6}\right](S_2 - S_1)\left(\frac{d+x}{r}\right)\cos\Theta + 4D\left[(42\cos^2\Theta - 3)\left(\frac{\sigma}{r}\right)^{12} - \left(12\cos^2\Theta - \frac{3}{2}\right)\left(\frac{\sigma}{r}\right)^{6}\right](S_1^{\,2} + S_2^{\,2})\left(\frac{d+x}{r}\right)^2 \qquad (2)$$

where the third- and higher-order terms in $(d + x)/r$ are neglected. Because of the model of individual atom–atom interactions, the portion of $U(r,x,\Theta)$ which determines the translational motion of the collision system is dependent on the orientation angle; *i.e.*, the r motion is dependent on Θ. In using eq 2 to calculate the energy transfer, only the leading part of the x-dependent term is retained, *i.e.*, the linear term in x.

Vibrational Energy Transfer Per Collision

A standard treatment of the dynamics of an encounter starts with the derivation of $r(t)$ from the equation of motion in the form

$$t = \left(\frac{\mu}{2}\right)^{1/2}\int_{r^*}^{r}\frac{\mathrm{d}r}{\left[E - E\left(\frac{b}{r}\right)^2 - U(r,0,\Theta)\right]^{1/2}} \qquad (3)$$

where $U(r,0,\Theta)$ is obtained from eq 2 by setting $x = 0$, E is the initial relative kinetic energy, and the centrifugal energy term is represented by $E(b/r)^2$. The symbol μ represents the reduced mass of the collision system and r^* is the largest root of the radical in the denominator. If we considered the relative motion of A with respect to the center of mass of BC, then $U(r,0,\Theta)$ should be replaced by the simple form $4D[(\sigma/r)^{12} - (\sigma/r)^6]$ in eq 3. An analytical expression of the classical trajectory for such a model is already known.[9] However, during both the approach and the recession of the colliding partners the r motion is affected by the relative orientation of BC, and eq 3 explicitly considers such a deformation of the trajectory.

Equation 3 can be divided into two parts

$$t = i\left(\frac{\mu}{2}\right)^{1/2}\left\{\int_0^{r^*}\frac{\mathrm{d}r}{\left[U(r,0,\Theta) + E\left(\frac{b}{r}\right)^2 - E\right]^{1/2}} - \int_0^{r}\frac{\mathrm{d}r}{\left[U(r,0,\Theta) + E\left(\frac{b}{r}\right)^2 - E\right]^{1/2}}\right\} \qquad (4)$$

In the region of strong interaction the second integral can be evaluated to give the result

$$t = i\tau - i(\mu/2D)^{1/2}(\sigma/14)(r/\sigma)^7 \qquad (5)$$

where τ is the collision time defined by[9]

$$\tau = \left(\frac{\mu}{2}\right)^{1/2}\int_0^{r^*}\frac{\mathrm{d}r}{\left[U(r,0,\Theta) + E\left(\frac{b}{r}\right)^2 - E\right]^{1/2}} \qquad (6)$$

For a purely classical oscillator with no initial vibrational energy, the transfer of vibrational energy due to a collision with a particle is given by[1,3]

$$\Delta E_{\mathrm{v}} = \frac{1}{2M}\left|\int_{-\infty}^{\infty}F(t)\exp(i\omega t)\mathrm{d}t\right|^2 \qquad (7)$$

where $F(t)$ is the time-dependent driving force acting on the oscillator and M is the reduced mass of BC. This expression, according to Takayanagi,[1] also represents the phase-averaged energy transfer if the oscillator has initial vibrational energy. For the collision of a heavy molecule and a light atom, Kelley and Wolfsberg[5] showed that ΔE_v calculated from eq 7 agrees satisfactorily with the exact results over a wide range of incident kinetic energies. For example, they showed that $\Delta E_v/\Delta E_{\text{exact}} \simeq 1.14$ over the energy range from 0.3174 to 20.31 eV for $m_B = m_C = 12$ and $m_A = 2$ based on the zero-impact parameter collinear interaction model with a purely repulsive exponential potential. For 24-24 + 2 the ratio is 1.06 at $E = 1.269$ eV. It should also be noted that for collisions such as 1-12 + 13 and 1-12 + 24, $\Delta E_v/\Delta E_{\text{exact}}$ is less than 1.1 at the same energy. Our present formulation and discussion are therefore *restricted* to collision systems of such combinations of the masses. It is shown in ref 5 that eq 7 gives excessive values of ΔE_v compared to ΔE_{exact} for B–C + A in which m_C is very small compared to m_A.

---

(7) K. F. Herzfeld and T. A. Litovitz, "Absorption and Dispersion of Ultrasonic Waves," Academic Press, Inc., New York, N. Y., 1959, Chapter 7.

(8) H. Shin, *J. Chem. Phys.*, **48**, 3644 (1968).

(9) E. E. Nikitin, *Opt. Spektrosk.*, **6**, 141 (1959); *Opt. Spectry.*, **6**, 93 (1959).

The perturbation force is, from eq 2

$$F[r(t)] = 24(D/\sigma)(S_2 - S_1)\cos\Theta[(\sigma/r)^{13} - {}^1\!/_2(\sigma/r)^7] + 8(Dd/\sigma^2)(S_1^2 + S_2^2)[(42\cos^2\Theta - 3) \times (\sigma/r)^{14} - (12\cos^2\Theta - {}^3\!/_2)(\sigma/r)^8] \quad (8)$$

in which the r–t relationship is given by eq 5. Since

$$\int_{-\infty}^{\infty}(t - i\tau)^{-g}\exp(i\omega t)\mathrm{d}t = \frac{2\pi(i\omega)^g}{\omega\Gamma(g)}\exp(-\omega\tau)$$

we find

$$\Delta E_v = (2/M)[(6d\pi\mu\omega/7)(S_1^2 + S_2^2)(\cos^2\Theta - {}^1\!/_{14})]^2 \times \left[1 - \left(\frac{4\cos^2\Theta - {}^1\!/_2}{14\cos^2\Theta - 1}\right)\frac{1}{\Gamma({}^8\!/_7)\gamma^{6/7}} + \left(\frac{14D\gamma}{d\sigma\mu\omega^2}\right) \times \left(\frac{S_1 - S_2}{S_1^2 + S_2^2}\right)\left(\frac{\cos\Theta}{\cos^2\Theta - {}^1\!/_{14}}\right) \times \left(1 - \frac{2\gamma^{6/7}}{\Gamma({}^{13}\!/_7)}\right)\right]^2 \exp(-2\omega\tau) \quad (9)$$

where $\gamma = (\omega a/14)(\mu/2D)^{1/2}$. This expression becomes simpler for collision systems with a homonuclear ($S_1 = S_2 = {}^1\!/_2$) or a very asymmetric ($S_2 \ll S_1 \simeq 1$) molecule; *i.e.*, for collisions involving a homonuclear diatomic molecule, the second squared quantity in eq 9 reduces to

$$\left[1 - \left(\frac{4\cos^2\Theta - {}^1\!/_2}{14\cos^2\Theta - 1}\right)\frac{1}{\Gamma({}^8\!/_7)\gamma^{6/7}}\right]^2$$

The second term in this expression is due to the inclusion of the attractive potential $-4D\Sigma_i(\sigma/r_i)^6$ in $U(r_i)$ and is generally less than 0.2. Thus, if this term is neglected, the angle-dependence of the preexponential part of ΔE_v is simply $(\cos^2\Theta - {}^1\!/_{14})^2 \simeq \cos^4\Theta$.

We shall now derive the collision time to complete the formulation of ΔE_v. From eq 6 in the region of strong interaction, we have

$$\tau = \left(\frac{\mu}{2}\right)^{1/2}\left[\lim_{V^*\to\infty}\int_E^{V^*}\frac{r'(V)\mathrm{d}V}{(V - E)^{1/2}}\right] \quad (10)$$

where the effective potential is $V = U(r,0,\Theta) + E(b/r)^2$, $r(V)$ is the function inverse to V, and $r'(V)$ is its derivative. The inverse derivative can be obtained as

$$r'(V) = -V^{-13/12}\sum_{i=0}^{\infty}\alpha_i V^{-i};\ i = 0, {}^1\!/_2, {}^5\!/_6, 1, \ldots \quad (11)$$

where

$$\alpha_0 = (\sigma/12)(4D\rho_1)^{1/12},\ \alpha_{1/2} = -(7\sigma/144)(4D)^{7/12}\rho_2\rho_1^{-6/12}$$

$$\sigma_{5/6} = (11/144)(E/\sigma)(4D\ \rho_1)^{-1/12}b^2, \ldots$$

$$\rho_1 = 1 + 6(S_2 - S_1)(d/r^*)\cos\Theta + (42\cos^2\Theta - 3)(S_1^2 + S_2^2)(d/r^*)^2$$

$$\rho_2 = 1 + 3(S_2 - S_1)(d/r^*)\cos\Theta + (12\cos^2\Theta - {}^3\!/_2)(S_1^2 + S_2^2)(d/r^*)^2$$

By combining eq 11 with eq 10 we obtain the collision time for specific molecular orientation

$$\tau = \left(\frac{\mu}{2}\right)^{1/2}\sum_{i=0}^{\infty}\alpha_i\left[\lim_{V^*\to\infty}\int_E^{V^*}\frac{\mathrm{d}V}{V^{13/12+i}(V - E)^{1/2}}\right] \quad (12)$$

in which the integral may be converted into the Eulerian integral $B(q,p) = \int_0^1 x^{p-1}(1 - x)^{q-1}\mathrm{d}x$ and calculated to be

$$\tau = \frac{\Gamma({}^7\!/_{12})}{\Gamma({}^1\!/_{12})}\left(\frac{\pi\mu}{2}\right)^{1/2}\frac{\sigma(4D\rho_1)^{1/12}}{E^{7/12}} \times \left[1 - \frac{1}{72}\left(\frac{\Gamma({}^1\!/_{12})}{\Gamma({}^7\!/_{12})}\right)^2\left(\frac{D}{E}\right)^{1/2}\frac{\rho_2}{\rho_1^{1/2}}\right] + \frac{5}{144}\frac{\Gamma({}^5\!/_{12})}{\Gamma({}^{11}\!/_{12})}\left(\frac{\pi\mu}{2}\right)^{1/2}\frac{b^2}{\sigma(4D)^{1/12}\rho_1^{1/6}E^{5/12}} \quad (13)$$

The second term in the square brackets represents the contribution of the attractive potential to the vibrational energy transfer. The first term is due to the repulsive part of $U(r,0,\Theta)$ which dominates the overall collision dynamics. The last term results from the centrifugal force and determines the importance of nonlinear (or indirect) encounters. For the zero-impact parameter collisions this term vanishes, while for large b the term becomes very large and thus it results in an inefficient energy transfer process. All three terms are dependent on the orientation angle Θ. We also note that when E becomes very large the collision time approaches zero and ΔE_v reduces to the preexponential term in eq 9.

Numerical Consideration and Discussion

For numerical examples, we take N_2 + He (14-14 + 4) collisions for which the following potential parameters are chosen: $D = 30.56k$, $\sigma = 3.123$ Å, $d = 1.094$ Å, $\omega = 4.445 \times 10^{14}$ ergs. The first two parameters

Table I: Calculated Values of $\Delta E_v/\hbar\omega$

$v \times 10^{-5}$, cm/sec	Θ, deg	b/σ							
		0	0.2	0.4	0.6	0.8	1.0	1.2	1.5
3	0	1.76(−5)[a]	1.16(−5)	3.31(−6)	4.11(−7)	2.22(−8)	5.19(−10)	5.26(−12)	1.12(−15)
	30	1.23(−5)	7.95(−6)	2.15(−6)	2.45(−7)	1.15(−8)	2.28(−10)	1.89(−12)	2.77(−16)
	45	7.51(−6)	4.72(−6)	1.18(−6)	1.16(−7)	4.57(−9)	7.11(−11)	4.37(−13)	3.73(−17)
	60	2.77(−6)	1.66(−6)	3.63(−7)	2.86(−8)	8.15(−10)	8.40(−12)	3.13(−14)	1.06(−18)
	90	1.01(−6)	5.90(−7)	1.16(−7)	7.71(−9)	1.73(−10)	1.32(−12)	3.39(−15)	5.79(−20)
4	0	2.35(−3)	1.69(−3)	6.32(−4)	1.22(−4)	1.23(−5)	6.41(−7)	1.73(−8)	2.24(−11)
	30	1.57(−3)	1.11(−3)	3.98(−4)	7.16(−5)	6.50(−6)	2.97(−7)	6.83(−9)	6.59(−12)
	45	8.74(−4)	6.07(−4)	2.03(−4)	3.30(−5)	2.58(−6)	9.74(−8)	1.77(−9)	1.11(−12)
	60	2.67(−4)	1.79(−4)	5.39(−5)	7.30(−6)	4.44(−7)	1.21(−8)	1.49(−10)	4.55(−14)
	90	7.27(−5)	4.75(−5)	1.32(−5)	1.56(−6)	7.91(−8)	1.70(−9)	1.56(−11)	2.77(−15)
5	0	4.52(−2)	3.44(−2)	1.52(−2)	3.89(−3)	5.77(−4)	4.97(−5)	2.47(−6)	9.93(−9)
	30	2.90(−2)	2.18(−2)	9.30(−3)	2.24(−3)	3.05(−4)	2.35(−5)	1.02(−6)	3.22(−9)
	45	1.51(−2)	1.12(−2)	4.52(−3)	9.98(−4)	1.20(−4)	7.92(−6)	2.85(−7)	6.27(−10)
	60	4.11(−3)	2.95(−3)	1.09(−3)	2.07(−4)	2.03(−5)	1.02(−6)	2.65(−8)	3.19(−11)
	90	1.02(−3)	6.98(−4)	2.25(−4)	3.40(−5)	2.42(−6)	8.11(−8)	1.27(−9)	6.10(−13)
6	0	3.08(−1)	2.43(−1)	1.20(−1)	3.74(−2)	7.26(−3)	8.83(−4)	6.71(−5)	5.85(−7)
	30	1.92(−1)	1.50(−1)	7.24(−2)	2.13(−2)	3.84(−3)	4.25(−4)	2.88(−5)	2.03(−7)
	45	9.64(−2)	7.43(−2)	3.41(−2)	9.31(−3)	1.51(−3)	1.46(−4)	8.38(−6)	4.36(−8)
	60	2.42(−2)	1.82(−2)	7.74(−3)	1.86(−3)	2.52(−4)	1.93(−5)	8.39(−7)	2.60(−9)
	90	5.16(−3)	3.81(−3)	1.53(−3)	3.34(−4)	3.96(−5)	2.56(−6)	9.03(−8)	1.90(−9)
7	0	1.21	9.86(−1)	5.31(−1)	1.90(−1)	4.49(−2)	7.04(−3)	7.31(−4)	1.13(−5)
	30	7.42(−1)	5.98(−1)	3.13(−1)	1.07(−1)	2.37(−2)	3.43(−3)	3.22(−4)	4.13(−6)
	45	3.59(−1)	2.85(−1)	1.44(−1)	4.60(−2)	9.30(−2)	1.19(−3)	9.67(−5)	9.49(−7)
	60	8.53(−2)	6.64(−2)	3.13(−2)	8.93(−3)	1.54(−3)	1.61(−4)	1.02(−5)	6.37(−8)
	90	1.71(−2)	1.31(−2)	5.87(−3)	1.54(−3)	2.37(−4)	2.13(−5)	1.12(−6)	4.99(−9)
8	0	3.35	2.78	1.60	6.37(−1)	1.75(−1)	3.34(−2)	4.40(−3)	1.50(−4)
	30	2.01	1.66	9.34(−1)	3.56(−1)	9.27(−2)	1.64(−2)	1.97(−3)	4.00(−5)
	45	9.52(−1)	7.76(−1)	4.20(−1)	1.51(−1)	3.62(−2)	5.75(−3)	6.06(−4)	9.69(−6)
	60	2.16(−1)	1.73(−1)	8.83(−2)	2.87(−2)	5.97(−3)	7.92(−4)	6.70(−5)	7.11(−7)
	90	4.16(−2)	3.28(−2)	1.60(−2)	4.83(−3)	9.03(−4)	1.04(−4)	7.52(−6)	5.89(−8)
9	0	7.33	6.20	3.76	1.63	5.06(−1)	1.12(−1)	1.78(−2)	6.06(−4)
	30	4.35	3.66	2.16	9.05(−1)	2.66(−1)	5.54(−2)	8.12(−3)	2.36(−4)
	45	2.01	1.67	9.61(−1)	3.80(−1)	1.04(−1)	1.96(−2)	2.55(−3)	5.99(−5)
	60	4.44(−1)	3.62(−1)	1.97(−1)	7.11(−2)	1.71(−2)	2.74(−3)	2.91(−4)	4.72(−6)
	90	8.27(−2)	6.66(−2)	3.47(−2)	1.17(−2)	2.56(−3)	3.63(−4)	3.33(−5)	4.10(−7)

[a] Numbers in parentheses denote the power of 10; *e.g.*, 1.76(−5) = 1.76 × 10^{-5}.

are obtained by use of the combining rule.[10] A complete numerical illustration must consider the dependence of ΔE_v on the initial relative collision energy, the orientation angle, and the impact parameter. It is convenient to calculate $\Delta E_v/\hbar\omega$, the energy that would have been absorbed by a classical oscillator driven by the force $F(t)$, divided by one quantum of energy for the true quantum oscillator. It is interesting to note that when $\Delta E_v \ll \hbar\omega$, the quantum mechanical transition $(0 \rightarrow 1)$ probability per collision is essentially identical with $\Delta E_v/\hbar\omega$ itself.[3] The calculated values of $\Delta E_v/\hbar\omega$ for N_2 + He are tabulated in Table I for various values of Θ and b as a function of the initial velocity $v = (2E/\mu)^{1/2}$. The orientation angles chosen are in the first quadrant. In general, $\Delta E_v/\hbar\omega$ rapidly decreases as the collision configuration becomes different from the zero-impact parameter collinear case. This variation is shown in Figure 2 for a collision velocity of 7 × 10^5 cm/sec, which corresponds to 0.889 eV. For any particular impact parameter, the collinear configuration is most effective for energy transfer and the perpendicular configuration least effective. At higher velocities and small b, ΔE_v exceeds $\hbar\omega$. Table I also shows that as the collision velocity increases, the contribution of oriented nonlinear encounters becomes more and more important.

The effective inelastic scattering cross section Q_{nm} for the $n \rightarrow m$ transition equals the vibrational transi-

---

(10) J. O. Hirschfelder, C. F. Curtiss, and R. B. Bird, "Molecular Theory of Gases and Liquids," John Wiley and Sons, Inc., New York, N. Y., 1964, p 168.

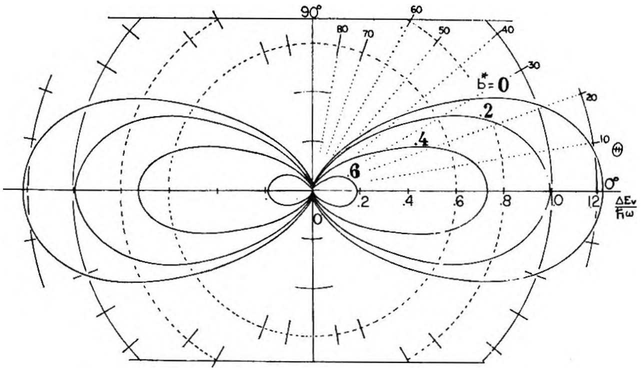

Figure 2. Orientation dependence of $\Delta E_v/\hbar\omega$ for various impact parameters ($b^* = b/\sigma$) at 7 × 10^5 cm/sec.

tion probability per collision p_{nm} integrated over all impact parameters

$$Q_{nm} = 2\pi \int_0^\infty p_{nm}\, b\, \mathrm{d}b \tag{14}$$

Treanor[11] has obtained, based on Kerner's solution,[12] the exact semiclassical transition probabilities for a potential linear in x. A similar expression has been obtained by Shin[13] from the second-order perturbation solution of the time-independent Schrödinger equation for the harmonic oscillator driven by $F(r)$, eq 8. The result[13] is

$$p_{nm} = \exp(\epsilon_0)\, \epsilon_0^{|m-n|} \frac{1}{m!\, n!}\left[\sum_{j=0}^{\infty} \frac{(-1)^j (k+j)!\, \epsilon_0^{\,j}}{(|m-n|+j)!\, j!}\right]^2 \tag{15}$$

where $\epsilon_0 = \Delta E_v/\hbar\omega$ and k is the larger of m, n. In the present model, ΔE_v explicitly contains information about the effect of Θ and b on the energy transfer, while in the previous studies[4,5,11,13] it is derived for the linear collision model. Bartlett and Moyal's phase-space method[14] for the harmonic oscillator under the perturbing potential $xF(t)$ is equivalent to Treanor's procedure.

When the oscillator is initially in the ground state, the transition probability given by eq 15 reduces to

$$p_{0m} = \epsilon_0^{\,m} \exp(\epsilon_0)/m! \tag{16}$$

which becomes $\epsilon_0^{\,m}/m!$ for $\epsilon_0 \ll 1$. A general expression for $\epsilon_0 \ll 1$ is

$$p_{nm} = \begin{cases} \dfrac{\epsilon_0^{\,n-m}}{[(n-m)!]^2}\left(\dfrac{n!}{m!}\right); & m \leqslant n \\[2ex] \dfrac{\epsilon_0^{\,m-n}}{[(m-n)!]^2}\left(\dfrac{m!}{n!}\right); & m \geqslant n \end{cases} \tag{17}$$

If we use $\Delta E_v/\hbar\omega$ for p_{01} in these expressions, we obtain

$$Q_{0m} = \frac{2\pi}{m!}\int_0^\infty \left(\frac{\Delta E_v}{\hbar\omega}\right)^m b\, \mathrm{d}b \tag{18}$$

when $\epsilon_0 \ll 1$. By combining eq 9 and 13 the energy transfer is found to be

$$\frac{\Delta E_v}{\hbar\omega} = \frac{1}{2M\hbar\omega}\left(\frac{6d\pi\mu\omega}{7}\right)^2\left(\cos^2\Theta - \frac{1}{14}\right)^2 \times \left[1 - \left(\frac{4\cos^2\Theta - {}^1/_2}{14\cos^2\Theta - 1}\right)\frac{1}{\Gamma({}^8/_7)\gamma^{{}^8/_7}}\right]^2 \times \exp[-K_1E^{-{}^7/_{12}} + K_2E^{-{}^{13}/_{12}} - K_3E^{-{}^5/_{12}}(b/\sigma)^2] \tag{19}$$

where K's represent the coefficients of τ given by eq 13 and are dependent on Θ. Then, denoting the preexponential part of eq 19 by G, we obtain

$$Q_{0m} = \pi\sigma^2(G/m!mK_3)E^{{}^5/_{12}} \exp(-mK_1E^{-{}^7/_{12}} + mK_2E^{-{}^{13}/_{12}}) \tag{20}$$

For $n \rightarrow n + 1$ and $n \rightarrow n + 2$ transitions, the cross sections are, respectively

$$Q_{n,n+1} = \pi\sigma^2[(n+1)G/K_3]E^{{}^5/_{12}} \exp(-K_1E^{-{}^7/_{12}} + K_2E^{-{}^{13}/_{12}}) \tag{21}$$

$$Q_{n,n+2} = \pi\sigma^2[(n+1)(n+2)G^2/4K_3]E^{{}^5/_{12}} \times \exp(-2K_1E^{-{}^7/_{22}} + 2K_2E^{-{}^{13}/_{12}}) \tag{22}$$

Before making calculations of transition probabilities and effective cross sections we consider the dependence of the collision time on Θ and b as well as on v. In Figure 3 the τ–v relationship is shown for Θ = 0°. The period of vibration τ_v ($= 2\pi/\omega$) is 1.41 × 10^{-14} sec and also shown in the figure for comparison. The exponential part of the vibrational energy transfer given by eq 9 can then be written as $\exp(-4\pi\tau/\tau_v)$ [*cf.* ref 3]. At low velocities, where $\tau \gg \tau_v$, the energy transfer is small because the oscillator can adjust adiabatically to the perturbation caused by the incident particle. In this case, eq 16 and 17 may be used to calculate vibrational transition probabilities from the semiclassical approximation. As the velocity increases, the collision time decreases and become shorter than τ_v, particularly for small b encounters, implying that when the oscillator is struck by the incident particle at such velocities, large vibrational excitation is produced. Calculations also show that for a fixed b the difference between $\tau(0°)$ and $\tau(90°)$ is almost independent of the collision velocity; for b/σ = 0.2, 0.4, and 0.6, the ratio $\tau(0°)/\tau(90°)$ has the values 1.12, 1.09, and 1.04, respectively. At larger b, $\tau(0°)$ becomes smaller than $\tau(90°)$; *e.g.*, $\tau(0°)/\tau(90°) \simeq 0.94$ and 0.88 at $b/\sigma = 1$ and 1.5, respectively, showing a slight dependence on v. Although $\tau(90°)$ is smaller than $\tau(0°)$ for $b \lesssim \sigma$, $\Delta E_v(90°)$ is always very small compared to $\Delta E_v(0°)$

---

(11) C. E. Treanor, *J. Chem. Phys.*, **43**, 532 (1965); **44**, 2220 (1966).

(12) E. Kerner, *Can. J. Phys.*, **36**, 371 (1958).

(13) H. Shin, *Chem. Phys. Lett.*, **3**, 195 (1969).

(14) M. S. Bartlett and J. E. Moyal, *Proc. Cambridge Phil. Soc.*, **45**, 545 (1949).

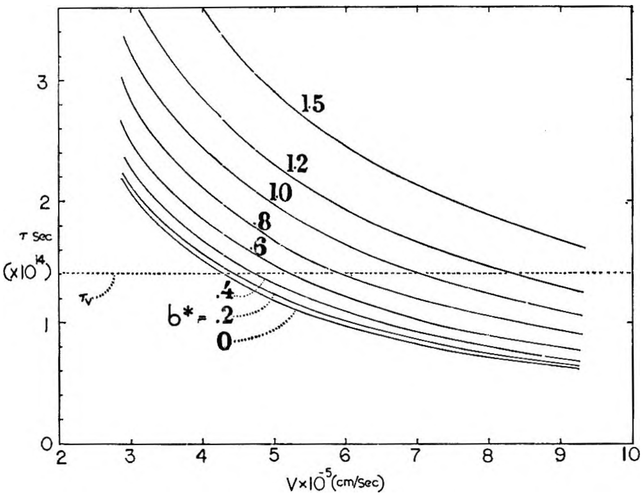

Figure 3. The collision time τ as a function of v. The dashed line represents the vibrational period τ_v.

because of the preexponential part (see eq 9), which decreases rapidly as Θ increases from 0° (see Table I).

At higher velocities (*e.g.*, $>5 \times 10^5$ cm/sec in Table I), the condition $\epsilon_0 \ll 1$ is not satisfied. At 5×10^5 cm/sec, $\epsilon_0 = 4.52 \times 10^{-2}$ and $p_{01} = 4.32 \times 10^{-2}$, but at 6×10^5 cm/sec, $\epsilon_0 = 0.308$ and $p_{01} = 0.226$; Θ and b are zero for both examples. An interesting result is obtained for p_{01} at high velocities. At 8×10^5 cm/sec, p_{01} is greatly different from $\Delta E_v/\hbar\omega$, and first increases to a maximum value and then decreases as b increases for $\Theta < 30°$, while for larger Θ it always decreases. Furthermore, for the zero-impact parameter p_{01} is the largest at $\Theta = 45°$. As long as $\epsilon_0 \lesssim 1$, all p_{0m} values always decrease as b and Θ increase. On the other hand, if $\epsilon_0 > 1$, some of the p_{0m} decrease while others first increase then decrease as b and Θ increase from zero. This situation will be discussed further below.

At higher velocities where ΔE_v may exceed $\hbar\omega$, the excitation of the oscillator to higher quantum states becomes increasingly probable. For example, when $\Theta = 0°$ and $b = 0$, $\epsilon_0 = 3.34$ at $v = 8 \times 10^5$ cm/sec; thus the oscillator which was initially in the ground state received sufficient energy to jump up to the third or fourth vibrational state, bypassing the first and second states. With $\epsilon_0 = 3.34$ we find: $p_{01} = 0.117$, $p_{02} = 0.197$, $p_{03} = 0.219$, and $p_{04} = 0.184$. The transition probability p_{0m} becomes largest at a velocity such that $\Delta E_v = m\hbar\omega$ with $p_{0m}{}^{\max} = m^m \exp(-m)/m!$; *e.g.*, $p_{01}{}^{\max} = 0.368$. Therefore, p_{01} is small at higher velocities, where all types of transitions are possible. In Figure 4, p_{0m} values for $m = 0, 1, 2, 3$, and 4 are shown at $b = 0$ and $\Theta = 0°$. In the figure, the b-dependence of the vibrational transition probabilities is also shown. We again chose the $0 \rightarrow 1$ transition at the most probable configuration for energy transfer. The plot is p_{01} *vs.* v for $b < \sigma$. As b increases, the position of the maximum value of p_{01} shifts toward higher velocities. Since the b-dependence of ΔE_v is equal to

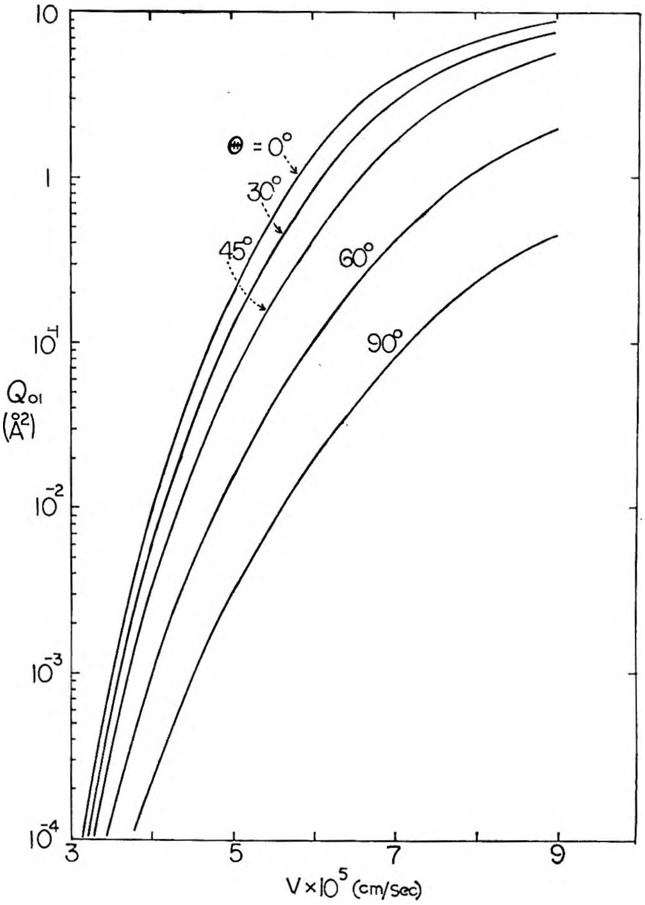

Figure 4. Calculation of p_{0m}. The solid curves represent p_{01} for different values of b^* at $\Theta = 0°$. The multilevel transition probabilities for the head-on collinear collision are shown by dashed curves.

$\exp[-\text{constant} \times E^{-5/12}(b/\sigma)^2]$, the transition probabilities rapidly decrease as b becomes larger than σ.

For high-velocity collisions the effective cross section must be evaluated numerically from eq 14 and 15. In Figure 5 the calculated values of Q_{01} are plotted as a function of v for various molecular orientations. For $\epsilon_0 \lesssim 10^{-3}$ the cross section can be determined analytically by use of eq 20. For Figure 5, Simpson's rule was used for numerical integration whenever necessary. For the $0 \rightarrow 1$ transition, both ΔE_v and Q_{01} are dominated by head-on collinear collisions, but nonzero-impact parameter collisions play an important role at higher velocities. The latter situation results because p_{01} becomes smaller than multilevel transition probabilities at such velocities. At 8×10^5 cm/sec, for the collinear configurations, the collisions with $0.3 < b/\sigma < 0.7$ are most effective for $0 \rightarrow 1$. For $\Theta = 30°$, the range is $0 < b/\sigma < 0.5$ and for 45° it is $0 = b/\sigma < 0.4$. For larger Θ (*i.e.*, close to 90°) only the direct encounters are of importance for vibrational energy transfer.

In the above we considered vibrational–translational energy transfer assuming that the transfer of rotational energy in collisions is a relatively easy process. The magnitude of rotational quantum is $E_r = 2Bj$, where j

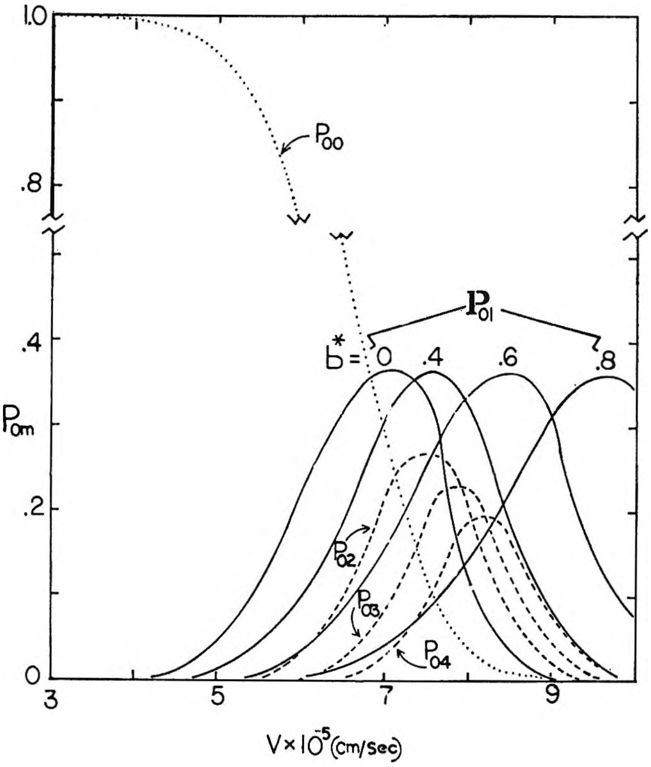

Figure 5. The effective cross section Q_{01} for various collision orientations.

is the rotational quantum number and $B = \hbar^2/2I$, I being the moment of inertia. Then, $E_r \simeq \hbar/\tau$ is the condition for an efficient exchange of rotational and translational energy, while $E_r \gg \hbar/\tau$ is the condition for an inefficient energy transfer.[15] Since the rotational constant B has values ranging from 60.8 for H_2 to 0.037 cm^{-1} for I_2 and the collision time is $\sim 10^{-13}$ sec so that $\hbar/\tau \simeq 40$ cm^{-1}, it is obvious that the latter condition is not fulfilled for the lower rotational levels of molecules other than H_2, HD, and D_2 and except for these molecules the collisional transfer of energy between rotational and translational degrees of freedom should be efficient.[16] The rotational constant of N_2 is 2 cm^{-1}.

Because we considered the vibrational energy transfer in oriented nonlinear collisions, however, it should be worthwhile to comment on the problem of rotational excitations. The interaction potential derived above is particularly suited for studying such a problem and we show the formulation of rotational transition probabilities using "the sudden approximation," which was developed by Bernstein and Kramer[17] based on the Alder–Winther theory[18] of Coulomb excitation. According to this approach the rotational transition probability for $jm \rightarrow j'm'$ may be expressed as

$$p_{jm,j'm'} = \left|\left\langle j'm'\left|\exp\left[-\frac{i}{\hbar}\int_{-\infty}^{\infty} V(t)\mathrm{d}t\right]\right|jm\right\rangle\right|^2 \quad (23)$$

where j, m are the rotational and magnetic quantum numbers of the molecule. By use of the basic relations given in Bernstein's papers, the action integral $\int_{-\infty}^{\infty} V(t)$. d$t$ can be readily evaluated [*e.g.*, see eq 4 of ref 17a]. The complete expression of the integral for the interaction potential given by eq 2 with $x = 0$ is

$$\int_{-\infty}^{\infty} V(t)\mathrm{d}t = -\frac{3D\pi\sigma}{2v}\left[\frac{21}{32}\left(\frac{\sigma}{b}\right)^{11} - \left(\frac{\sigma}{b}\right)^{5}\right] + \frac{5D\pi d^2}{4v\sigma}(S_1^2 + S_2^2)\left[\frac{693}{320}\left(\frac{\sigma}{b}\right)^{13} - \frac{3}{2}\left(\frac{\sigma}{b}\right)^{7}\right] - \frac{24D\pi d}{v}(S_1 - S_2)\left[\frac{1155}{2048}\left(\frac{\sigma}{b}\right)^{12} - \frac{5}{32}\left(\frac{\sigma}{b}\right)^{6}\right]\sin\theta \times \cos\phi - \frac{45045}{512}\frac{D\pi d^2}{v\sigma}(S_1^2 + S_2^2)\left(\frac{\sigma}{b}\right)^{13} \times \left(\frac{1}{13}\cos^2\theta + \sin^2\theta\cos^2\phi\right) + \frac{735}{16}\frac{D\pi d^2}{v\sigma}(S_1^2 + S_2^2) \times \left(\frac{\sigma}{b}\right)^{7}\left(\frac{1}{8}\cos^2\theta + \sin^2\theta\cos^2\phi\right) \quad (24)$$

where θ, ϕ are the orientation angles of *the molecule*. In this lengthy expression, the angle-dependent terms will only contribute to the probability. It may be noted that the so-called anisotropic parameter "q" found in the work of Bernstein does not appear in the present model.

For the collision between a homonuclear diatomic molecule and an atom, the transition probability is then

$$p_{jm,j'm'} = |\langle j'm'|\exp[-iK(\alpha\cos^2\theta + \beta\sin^2\theta\cos\phi)]|jm\rangle|^2 \quad (25)$$

with $K = 84D\pi d^2/\hbar v\sigma$, $\alpha = 0.040(\sigma/b)^{13} - 0.034(\sigma/b)^7$, and $\beta = 0.523(\sigma/b)^{13} - 0.273(\sigma/r)^7$. For a simple numerical illustration, we consider $00 \rightarrow 20$ in N_2 + He. For this process eq 25 reduces to

$$p_{00,20} = (5/16\pi^2)[J_0(K|\beta|/2)]^2 \times \left\{\left|\int_0^1 (3x^2 - 1)\cos(K|\alpha - \beta|x^2)\mathrm{d}x\right|^2 + \left|\int_0^1 (3x^2 - 1)\sin(K|\alpha - \beta|x^2)\mathrm{d}x\right|^2\right\} \quad (26)$$

where J_0 is the Bessel function. For $b > \sigma, |\beta| \gg |\alpha|$ and the magnitude of the sine integral dominates the other. As an example, we calculate $p_{00,20}$ for several b/σ values at $v = 1.2 \times 10^5$ cm/sec, which corresponds to the average (relative) velocity of N_2 + He at 300°. For $b \simeq \sigma$ the integrals in eq 26 were evaluated by use of

---

(15) B. Stevens, "Collisional Activation in Gases," Topic 19, Vol. 3, of "The International Encyclopedia of Physical Chemistry and Chemical Physics," Pergamon Press, London, 1967, pp 12–16.

(16) T. L. Cottrell and J. C. McCoubrey, "Molecular Energy Transfer in Gases," Butterworth and Co., Ltd., London, 1961, Chapter 5.

(17) (a) K. H. Kramer and R. B. Bernstein, *J. Chem. Phys.*, **40**, 200 (1964); (*b*) *ibid.*, **44**, 4473 (1966). Also see P. Pechukas and J. C. Light, *ibid.*, **44**, 3897 (1966), for comments on the validity of the sudden approximation applied to the rotational excitation problem.

(18) K. Alder and A. Winther, *Kgl. Danske Videnskab. Selskab., Mat.-Fys. Medd.*, **32**, No. 8 (1960).

Simpson's rule, while for $b/\sigma > 1.5$ for which $\alpha - \beta \ll 1$ the trigonometric functions were expanded in power series and the first three terms were taken. We find a maximum value of $p_{00,20} \simeq 0.05$ at $b/\sigma = 1.25$. As b/σ increases or decreases from this value, the transition probability decreases rapidly; *e.g.*, it is only 0.002 at $b/\sigma = 1.75$. However, at this velocity the amount of energy transferred per collision in the vibrational–translational process is negligibly small; $\Delta E_v/\hbar\omega$ is smaller than 10^{-10} even for $b/\sigma = 0$. Although it is a different collision system, it should be informative to note that in N_2–N_2, the rotational collision number is only about 7 at room temperature,[19] while the vibrational collision number is as large as 8×10^8 at 476°.[20] The latter number may be estimated to increase by more than two orders of magnitude at room temperature.

Although we do not attempt to solve $p_{jm,j'm'}$ for heteronuclear diatomic molecules, a straightforward formulation can be obtained from eq 24 and 25. In this case, the magnitude of the matrix element is dominated by the part resulting from the term containing $\sin\theta\cos\phi$ in eq 24 and we can write

$$p_{jm,j'm'} = |\langle j'm'|\ \exp(iz\sin\theta\cos\phi)|jm\rangle|^2 \qquad (27)$$

where

$$z = \frac{24D\pi d}{\hbar v}(S_1 - S_2)\left[\frac{1155}{2048}\left(\frac{\sigma}{b}\right)^{12} - \frac{5}{32}\left(\frac{\sigma}{b}\right)^{6}\right]$$

For 00 → $j'm'$, the essential part of the matrix element appears as a combination of integrals of the type

$$\int_0^{2\pi}\int_0^{\pi} \exp(iz\sin\theta\cos\phi)\cos^{2n+1}\theta\sin\theta\, d\theta\, d\phi$$

which can be evaluated as[21] $2\pi\,(2/z)^{n+1}\Gamma(n+1)J_{n+1}(z)$. However, in this collision system, it should be important to introduce in eq 2 the energy term representing the interaction between a polar molecule, having a dipole moment $\bar{\mu}$ and a quadrupole moment $\bar{Q}$, and a polarizable atom[22] $U'(r,\Theta) = -(6\bar{\alpha}\bar{\mu}\bar{Q}/r^7)\cos^2\Theta$, where $\bar{\alpha}$ is the polarizability of the atom.

Acknowledgments. This work was supported by the Directorate of Chemical Sciences, the U. S. Air Force Office of Scientific Research, under Grant AFOSR-68-1354. The author is indebted to Professor R. C. Fuson for many helpful suggestions.

---

[19] Reference 16, p 81.

[20] M. C. Henderson, *J. Acoust. Soc. Amer.*, 34, 349 (1962).

[21] G. N. Watson, "Theory of Bessel Functions," 2nd ed, Cambridge University Press, Cambridge, England, 1966, p 375.

[22] P. W. Anderson, *Phys. Rev.*, **80**, 511 (1950).

Mass Spectrometric Determination of the Proton Affinities of Various Molecules

by Max A. Haney and J. L. Franklin

Department of Chemistry, Rice University, Houston, Texas 77001 *(Received June 24, 1969)*

The proton affinities of a number of simple molecules have been determined by a combination of techniques. Observation of proton transfer reactions between molecules establishes a relative order of proton affinities. Absolute values are then estimated by an empirical method involving measurement of translational energies of products of an ion–molecule reaction. The proton affinities found by these two methods are consistent with each other and with values obtained from appearance potentials. The proton affinities range from 126 kcal/mol for methane to 211 kcal/mol for methylamine.

Introduction

Previous mass spectrometric determinations of proton affinities have used either one of two methods. In the first method, the heat of formation of the protonated species is obtained from its appearance potential as a fragment ion. The proton affinity is then calculated according to the relation

$$\text{P.A.(M)} = \Delta H_f(\text{H}^+) + \Delta H_f(\text{M}) - \Delta H_f(\text{MH}^+) \qquad (1)$$

The proton affinities of olefins and a few simple carbonyl compounds have been determined in this manner from the heats of formation of the appropriate carbonium ions.[1-3] NH_4^+, H_3O^+, and H_3S^+ have also been analyzed by this method.[4] The method suffers from the

---

[1] A. G. Harrison, A. Irko, and D. Van Raalte, *Can. J. Chem.*, 44, 1625 (1966).

[2] K. M. A. Rafaey and W. A. Chupka, *J. Chem. Phys.*, 48, 5205 (1967).

[3] M. S. B. Munson and J. L. Franklin, *J. Phys. Chem.*, 68, 3191 (1964).

[4] M. A. Haney and J. L. Franklin, *J. Chem. Phys.*, 50, 2028 (1969).

usual liabilities of appearance potentials, *e.g.*, possibility of excess energy and identification of fragment neutrals. More importantly, the protonated species of many interesting molecules do not occur as fragment ions.

The second method involves the occurrence or nonoccurrence of ion–molecule reactions to place limits upon the proton affinity. The original supposition was that if an ion–molecule reaction occurs in the mass spectrometer, it must be exothermic ($\Delta H° \leq 0$), while if it does not occur, it is endothermic.[5] Neither of these assumptions can be true for ion–molecule reactions in general. Endothermic reactions may occur if the reactant ion is internally excited. If the excitation arises from the ionization process, the participation of excited states can be determined by comparing the electron or proton energy thresholds for reactant and product ions. The detection of excited reactants is not so simple when the reactant ion is itself the product of an exothermic reaction. For example, the following reaction is observed in a mixture of water and formaldehyde[6]

$$H_3O^+ + CH_2O \longrightarrow CH_2OH^+ + H_2O \qquad (2)$$

Friedman and coworkers[7] have justifiably criticized the use of this reaction to place an upper limit to the proton affinity of water, because the H_3O^+ likely retains a considerable portion of the heat of the reaction from which it is formed.

By now it is well known that the second assumption of method 2 is incorrect. Many plausible exothermic ion–molecule reactions do not occur at all, or only with a very slow rate. However, most of these cases can be explained by the competition of other processes, especially charge exchange. For the special class of reactions involving simple transfer of a proton between stable molecules as in reaction 2 and its reverse, no competing process is usually possible. It therefore appears plausible to postulate that the nonoccurrence of a reaction of this type is sufficient evidence of its endothermicity. For example, we conclude that the proton affinity of formaldehyde is greater than that of water because the reverse of reaction 2 is not observed.[6]

The results of a recent study[8] suggest a third method for obtaining estimates of proton affinities. The relative translational energies of the products of several exothermic ion–molecule reactions of the type

$$RH^+ + RH \longrightarrow RH_2^+ + R \qquad (3)$$

were examined. The ratio of translational energy to heat of reaction was found to be nearly constant at ~0.2 for most of the reactions studied. If the heat of reaction can be estimated by measuring the translational energy of the products, the proton affinity of the molecule RH can be calculated from the thermochemical relation

$$\text{P.A.(RH)} = \Delta H_f(\text{H}^+) + \Delta H_f(\text{R}) - \Delta H_f(\text{RH}^+) - \Delta H° \qquad (4)$$

We have used this method in conjunction with method 2 and with previous results by the appearance potential method to determine the proton affinities of a variety of simple molecules.

Experimental Section

All work was performed on a Bendix Model 12 time-of-flight mass spectrometer equipped with the ion–molecule reaction source. This instrument and the method of measuring translational energies have been described elsewhere.[8] Chemicals were usually common reagent grade. The mass spectra of all compounds were checked for interfering impurities before use.

Results

The procedure for the second method was to introduce a pair of gases into the source at pressures of 30–50 μ and at low electron energies. Under these conditions, the mass spectrum consisted mostly of the two protonated molecules. The reaction time was

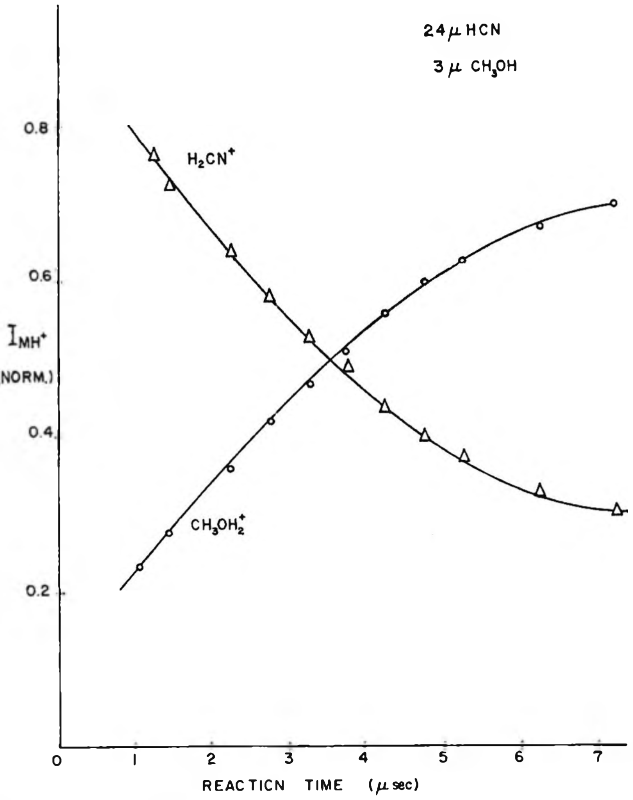

Figure 1. Illustration of method 2 for molecules having different proton affinities.

---

(5) V. L. Tal'rose, *Pure Appl. Chem.*, **5**, 455 (1962).

(6) J. L. Beauchamp and S. E. Buttrill, Jr., *J. Chem. Phys.*, **48**, 1783 (1968).

(7) M. DePas, J. J. Leventhal, and L. Friedman, *ibid.*, **49**, 5543 (1968).

(8) J. L. Franklin and M. A. Haney, *J. Phys. Chem.*, **73**, 2857 (1969).

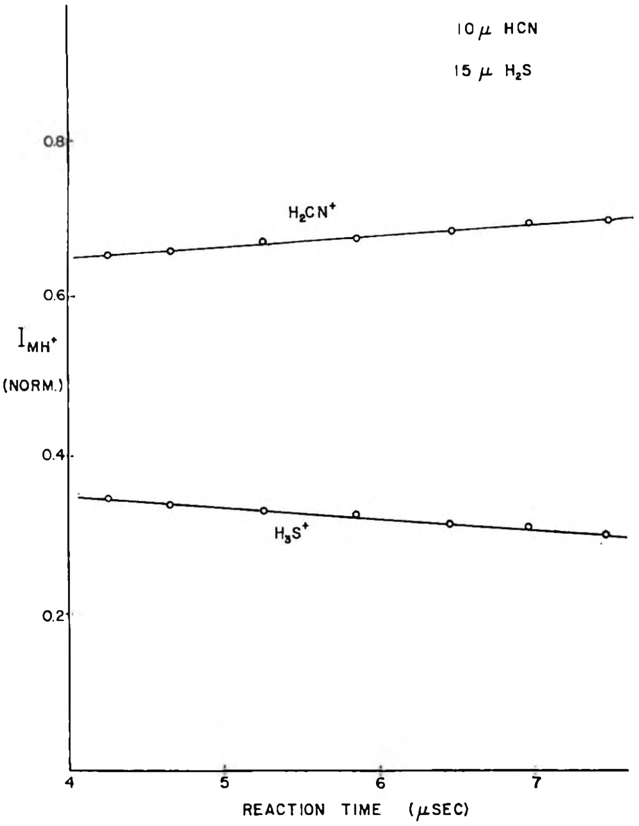

Figure 2. Illustration of method 2 for molecules having similar proton affinities.

then increased by delaying the ion drawout pulse and the relative intensities of the two peaks were observed. The results are illustrated for the case of methanol and hydrogen cyanide in Figure 1. The rise of $CH_3OH_2^+$ and fall of H_2CN^+ indicate that $CH_3OH_2^+$ does not transfer a proton to HCN. According to the previous postulate, this means that the proton affinity of methanol is greater than that of hydrogen cyanide. In a few cases, the relative intensities of the two peaks changed only a little or not at all with increasing reaction time. This situation is illustrated in Figure 2. We conclude that proton transfer is occurring in both directions and the proton affinities must be very nearly equal.

This method established the relative order of proton affinities listed in column 1 of Table I. The order was internally consistent; *i.e.*, any molecule would transfer a proton to any other molecule above it in the table. Those pairs of molecules which had indistinguishable proton affinities are marked with brackets. The series from dimethyl ether through acetaldehyde is particularly interesting. Here it was observed that any adjacent pair had indistinguishable proton affinities, while nonadjacent pairs were distinguishable. This overall consistency is important because it helps verify the working postulate that any exothermic proton transfer of this type will occur.

Table I: Proton Affinities (in kcal/mol)

Decreasing order	$\bar{T}_c$	Estimated $-\Delta H°$ of reaction 3	P.A. by eq 4	Best P.A.
CH_3NH_2	1.8	9	211	211 ± 3
NH_3				207 ± 3[a]
CH_3COCH_3	1.2	6	188	188 ± 2
CH_3OCH_3	2.4	12	189	187 ± 1
PH_3	4.2	21	186	186 ± 1
CH_3CN	3.2	16	135	186 ± 1
CH_3SH	2.0	10	189	185 ± 1
CH_3CHO				185 ± 1[b]
C_6H_6				183 ± 3[c]
CH_3OH	3.8	19	182	182 ± 3
HCOOH				179 ± 3[c]
HCN	4.4	22	139	170 ± 3
H_2S				170 ± 3[a]
HCHO				168 ± 1[b]
H_2O				165 ± 3[a]
CH_3Cl	1.8	9	164	164 ± 3
HI	~0	0	145	145 ± 3
CO				142 ± 3[d]
HCl	1.6	8	141	141 ± 3
HBr	1.5	7	140	140 ± 3
CH_4				126 ± 1[e]

[a] Ref 4. [b] Ref 2. [c] See text. [d] Ref 12. [e] M. S. B. Munson and F. H. Field, *J. Amer. Chem. Soc.*, **87**, 3294, (1965).

The average translational energies of the RH_2^+ ions, $\bar{E}_i$, were measured and inserted in eq 5 to obtain the total translational energy of the products in the center-of-mass.

$$\bar{T}_c = \left[\bar{E}_i - \frac{m_i}{M}\,(^3/_2kT)\right]\frac{M}{M_n} \qquad (5)$$

m_i is the mass of RH_2^+, m_n is the mass of R, M is their sum, and $\bar{T}_c$ is the relative translational energy of the products calculated on the assumption that a long-lived complex is formed.[8] The estimated heat of reaction 3 was obtained by multiplying $\bar{T}_c$ by a factor of 5. These values are given in column 3 of Table I. Column 4 lists the proton affinities obtained from these estimates by eq 4. All of these values are reasonably consistent with the relative order established independently by method 2 except for CH_3CN and HCN. Reaction 3 for both of these molecules is very exothermic. It is possible, therefore, that electronic excitation of CN or CH_2CN is responsible for the low fraction of translational energy observed. Fortunately, method 2 sufficiently limits the proton affinities of these two molecules. The proton affinity of benzene could not be determined by method 3 because reaction 3 in this case would be endothermic by at least 20 kcal/mol and hence would not be observed. One other molecule of interest in which method 3 is inapplicable is formic acid. The heat of formation of the neutral product is in sufficient doubt that no value of the proton affinity is given in column 4.

The proton affinities of several molecules are assumed to be known through previous determinations by method 1. These known values provide reference points in the ordered list of column 1. The values in column 4 were carefully compared with these reference values and with the relative order to arrive at the "best" proton affinities given in column 5. The errors for the reference molecules were taken from the quoted works. The errors for the others were estimated by overall comparison of the values in column 4 with the relative order and with the reference values.

Discussion

Acetone. The value of 188 kcal/mol is in excellent agreement with that obtained by Rafaey and Chupka[2] by photoionization of isopropyl alcohol, 186 kcal/mol.

PH_3. The value of 186 appears indisputable since the proton affinity is definitely between that of acetone and acetaldehyde. This is about 20 kcal/mol less than that of ammonia, the analog of phosphine. The difference is in accord with solution chemistry where phosphine is found to be a much weaker base than ammonia.[9] It is noteworthy that hydrogen sulfide has a slightly higher proton affinity than its comparable analog, water.

C_6H_6. Since benzene does not undergo reaction 3, the proton affinity of benzene was taken to be 183 kcal/mol on the basis of its position in the relative order. This is considerably larger than any value previously published. Franklin, Lampe, and Lumpkin[10] determined $A_P(C_6H_7^+)$ from 1,3 cyclohexadiene and deduced a proton affinity of 150 kcal/mol for benzene. In a more recent study Franklin and Carroll[11] determined $A_P(C_6H_7^+)$ from 1,4- and 1,3-cyclohexadiene and 1,3,5-hexatriene and deduced values for the proton affinity of benzene to be 159, 162, and 167 kcal/mol, respectively. These results could not be corrected for excess energy and so must be taken as lower limits of the proton affinity of benzene. The present, much higher value is in keeping with this.

HCOOH. We measured the appearance potential of $HCOOH_2^+$ from ethyl formate as 11.61 eV, in excellent agreement with the values previously reported.[1] This appearance potential yields a proton affinity of 161 kcal/mol, which seems quite low and is in disagreement with the relative order established by method 2. The translational energy of the $HCOOH_2^+$ fragment at threshold was found to be 1.1 kcal/mol. Using this value in the equations previously given,[4,12] we find 18 kcal/mol excess energy. Correcting the appearance potential for the excess energy yields a proton affinity of 179 kcal/mol, a value which is consistent with the limitations imposed by method 2. Ros[13] performed MO-SCF calculations on the possible isomers of protonated formic acid and found that the proton is preferentially attached to the carbonyl oxygen rather than the hydroxyl oxygen. If acetaldehyde and formic acid are considered substituted formaldehyde, we note that the methyl group raises the proton affinity by 17 kcal/mol, whereas the hydroxyl group raises it by only 11 kcal/mol. This reflects the relative inductive effects of the two substituents.

Another illustration of substituent effects is shown in Table II. Note that the difference is nearly constant at about 16 kcal/mol for the group of methyl-substituted compounds having proton affinities in the range 182–186 kcal/mol. However, the difference is 23 kcal/mol for CH_3Cl and only 4 kcal/mol for CH_3NH_2. Apparently, methyl substitution has a greater effect the lower the proton affinity.

Table II: Effect of Methyl Substitution on Proton Affinity

X	P.A.(HX), kcal/mol	P.A.(CH_3X) kcal/mol	Difference, kcal/mol
NH_2	207	211	4
CN	170	186	16
SH	170	185	15
HCO	168	185	17
OH	185	182	17
Cl	141	164	23

Proton transfer reactions have long been a favorite subject of solution chemistry. This work is probably of more importance to gas-phase ion chemistry, especially the technique called chemical ionization.[14] The determination of proton affinities should extend this field and open the way toward quantitative study.

Conclusions

The use of ion–molecule reactions to determine the relative order of proton affinities is valid for proton transfers of the type described. Empirical estimation of the heat of a proton transfer reaction by measuring the translational energy produced is a feasible technique for obtaining absolute values of the proton affinity.

Acknowledgment. The authors wish to express their gratitude to the Robert A. Welch Foundation for support of this work and to the National Aeronautics and Space Administration for the research fellowship of M. A. H.

---

(9) J. R. Wazer, "Phosphorus and Its Compounds," Vol. I, Interscience, New York, N. Y., 1958.

(10) J. L. Franklin, F. W. Lampe, and H. E. Lumpkin, *J. Amer. Chem. Soc.*, 81, 3152 (1959).

(11) J. L. Franklin and S. R. Carroll, *ibid.*, to be published.

(12) M. A. Haney and J. L. Franklin, *Trans. Faraday Soc.*, 65, 1794 (1969).

(13) P. Ros, *J. Chem. Phys.*, 49, 4902 (1968).

(14) F. H. Field, *Accounts Chem. Res.*, 1, 42 (1968).

Singlet–Triplet Absorption Bands of Methyl-Substituted Ethylenes[1]

by Michiya Itoh[2] and Robert S. Mulliken[3]

Institute of Molecular Biophysics, Florida State University, Tallahassee, Florida 32306 and
Laboratory of Molecular Structure and Spectra, Department of Physics, University of Chicago, Chicago, Illinois 60637
(Received June 25, 1969)

In the absorption spectra of the methylated ethylenes propene and 2-methylpropene in the gas state plus 70 atm of oxygen, banded structures are found which can be identified as triplet ← singlet (T ← N) transitions analogous to that found for ethylene itself. A similar absorption but without structure is found for *trans*-butene. At shorter wavelengths, and also even at longer wavelengths in 2-methyl-2-butene and in 2,3-dimethyl-2-butene vapor in the presence of 70 atm of oxygen, relatively strong absorption was found which can probably be attributed to contact charge-transfer transitions from the ethylene to O_2. This absorption defeated attempts to determine by oxygen enhancement whether the extremely weak bands which have been observed by others at 2100–2500 Å on the long wavelength side of the Rydberg bands of the methylated ethylenes are the triplet ← singlet analogs of the Rydberg bands. To determine the location of the T ← N bands of 2-methyl-2-butene and 2,3-dimethyl-2-butene, enhancement in the liquid state by CH_2Br_2 was used.

Introduction

Writing the normal state (N) electron configuration of ethylene as ---- π^2, the first excited states are a triplet (T) and a singlet (V) of respective vertical excitation energies 4.6 and 7.6 eV, both of configuration -----$\pi\pi^*$, and another singlet, a Rydberg state (R) with vertical energy 7.1 eV.[4] States analogous to R and V are also known in the alkyl-substituted ethylenes. The V ← N bands, and to a greater extent the R ← N bands, are progressively shifted to longer wavelengths with each additional alkyl substitution.

In the absorption spectra of ethylene and the alkylated ethylenes, the V ← N band system is very strong, the R ← N system moderately strong, the T ← N system[5,6] extremely weak. In the methylated ethylenes, absorption bands very much weaker than the R ← N systems, and at somewhat longer wavelengths (2100–2500 Å) have long been known,[7] although the possibility that they may be due to impurities has not been entirely disproved. These bands if genuine can be ascribed to the transition T_R ← N, where T_R means the triplet Rydberg state corresponding to the singlet Rydberg state R.[8] The vibrational spacing in these bands (about 1400 cm^{-1}) is approximately the same as in the R ← N bands and their positions, which correspond to an energy separation of 0.7 eV between T_R and R levels, are in good agreement[9] with theoretical expectation. A proposal by Berry[10] that the tentative T_R ← N bands may be analogous to the π^* ← n transition in formaldehyde has been shown not to be correct.[4]

The T ← N band was first discovered by Reid[5] in the absorption spectrum of a 1.4-m path in liquid ethylene. This identification was confirmed by Evans[6] using a mixture of ethylene at 50 atm and oxygen at 25 atm; it is well known that oxygen causes marked intensification of otherwise weak singlet–triplet transitions. The present paper originated in an attempt to use the oxygen-intensification technique to confirm the triplet–singlet nature of the tentative T_R ← N bands in several methylated ethylenes. We found new weak absorption bands, but only in the wavelength region where T ← N bands should occur. Relatively strong absorption also occurred in the T_R ← N wavelength region, but it was entirely continuous—no bands could be identified. We attribute this absorption to contact charge-transfer transitions, which as well as triplet ← singlet bands are known to be brought out by oxygen.[11]

Experimental Section

We have investigated the near-ultraviolet absorption of propene, 2-methylpropene, and *trans*-butene in the gas phase by the oxygen enhancement method using a high-pressure optical cell, and that of 2-methyl- and 2,3-dimethyl-2-butene in the liquid state using the external heavy atom effect[12] of CH_2Br_2. Commercial research grade cylinders (The Matheson Co., Inc.) were

---

(1) This research was assisted by a contract between the Division of Biology and Medicine, U. S. Atomic Energy Commission and the Florida State University, and by the Office of Naval Research, Physics Branch, under Contract No. N00014-67-A-0285-0001 with theUniversity of Chicago.

(2) Faculty of Pharmaceutical Sciences, University of Tokyo, Bunkyo-ku, Tokyo, Japan.

(3) To whom requests for reprints should be addressed.

(4) See A. J. Merer and R. S. Mulliken, *Chem. Rev.*, **69**, 639 (1969).

(5) C. Reid, *J. Chem. Phys.*, **18**, 1299 (1950).

(6) D. F. Evans, *J. Chem. Soc.*, 1735 (1960).

(7) W. J. Potts, *J. Chem. Phys.*, **23**, 65 (1955).

(8) R. S. Mulliken, *ibid.*, **33**, 1597 (1960). Before the discovery[5,6] of the T ← N bands, it had been thought that the bands now attributed to T_R ← N were T ← N bands.

(9) P. G. Wilkinson and R. S. Mulliken, *ibid.*, **23**, 1895 (1955).

(10) R. S. Berry, *ibid.*, **38**, 1934 (1963).

(11) Cf. H. Tsubomura and R. S. Mulliken, *J. Amer. Chem. Soc.*, **82**, 5966 (1960).

(12) M. Kasha, *J. Chem. Phys.*, **20**, 71 (1952).

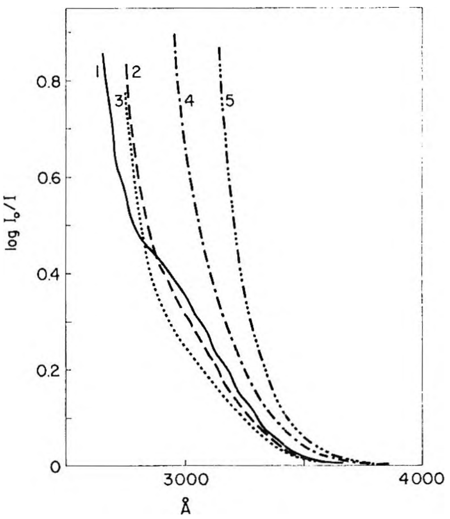

Figure 1. Absorption spectra of oxygen at 70 atm pressure and several methylethylenes (~6.5 cm cell): (1) propene, ~10 atm; (2) 2-methylpropene, ~1.5 atm; (3) *trans*-butene, ~1.0 atm; (4) 2-methyl-2-butene, ~0.5 atm (vapor pressure at room temperature); (5) 2,3-dimethyl-2-butene, ~0.2 atm (vapor pressure at room temperature).

used without further purification for the three gaseous samples, and API standard samples were used for the other two methylated ethylenes. Absorption spectra of propene, 2-methylpropene, and *trans*-butene in the gas phase with oxygen at 70 atm pressure were taken at room temperature with a Cary recording spectrophotometer 14 M. A high-pressure optical cell with a light path of approximately 6.5 cm was used.

Results

The spectra of several methylethylenes are shown in Figure 1. A weak absorption band with vibrational structure was observed in propene and in 2-methylpropene, and a very weak band without structure in *trans*-butene. There is no reasonable doubt that the bands shown in curves 1–3 in Figure 1 are due to T ← N transitions, especially since the vibrational spacing, 960–970 cm^{-1} in both propene and 2-methylpropene, is almost identical with that of ethylene as reported by Reid[5] and Evans.[6]

However, there was also relatively very strong absorption beginning near 4000 Å in the case of 2-methyl- and 2,3-dimethyl-2-butene with compressed oxygen gas (curves 4 and 5 in Figure 1). Contact charge-transfer absorption between methylethylenes and oxygen should shift to longer wavelengths with decrease in ionization potentials of the methylethylene; these vary from 10.507 to about 8.3 eV[13] in going from ethylene to 2,3-dimethyl-2-butene. The relatively strong absorption beginning near 4000 Å in the 2-methyl- and 2,3-dimethyl-2-butenes, and also *trans*-butene, may probably be ascribed to contact charge-transfer absorption masking the weak T ← N bands, and at shorter wavelengths the T_R ← N bands. In the cases of propene, 2-methylpropene, and *trans*-butene, the increasingly intense absorption at wavelengths beginning at almost 2600–2700 Å may also probably be attributed to charge-transfer absorption, or perhaps also to V ← N absorption.

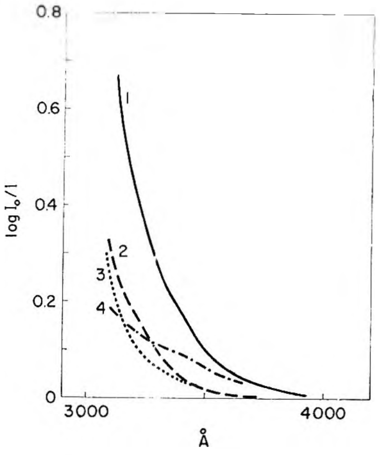

Figure 2. Absorption spectra of 2-methyl-2-butene plus CH_2Br_2: (1) 2-methyl-2-butene and CH_2Br_2, 1:1 mixture, (5-cm cell); (2) 2-methyl-2-butene (2.5-cm cell); (3) CH_3Br_2 (2.5-cm cell); (4) absorption spectrum obtained by subtracting curves 2 and 3 from curve 1.

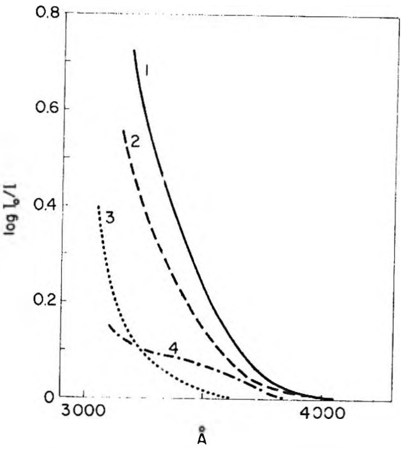

Figure 3. Absorption spectra of 2,3-dimethyl-2-butene plus CH_2Br_2: (1) 2,3-dimethyl-2-butene and CH_2Br_2, 1:1 mixture (5-cm cell); (2) 2,3-dimethyl-2-butene (2.5-cm cell); (3) CH_2Br_2 (2.5-cm cell); (4), absorption spectrum obtained by subtracting curves 2 and 3 from curve 1.

We also examined the spectra of 1:1 mixed solutions of 2-methylbutene and of 2,3-dimethyl-2-butene with methylene bromide. In each case a weak absorption band was obtained by subtracting the individual absorptions of CH_2Br_2 and the methylethylene from that of the mixed solution, see Figures 2 and 3. It seems to us that these absorption bands can be identified as T ← N bands enhanced by the heavy atom effect. Possible charge-transfer bands between the methylethylenes and CH_2Br_2 should be at much shorter wave-

---

[13] Roughly estimated from the data of *trans*-butene (9.13 eV) and 3-methyl-2-butene (8.67 eV); see K. Watanabe, T. Nakayama and J. Mottl, *J. Quant. Spectrosc. Radiat. Transfer*, 2, 369 (1962).

Table I: Absorption Maxima of V ← N and T ← N bands, and the T–V Energy Separations

	V ← N (λ_{max}, cm^{-1})	T ← N (λ_{max}, cm^{-1})	T–V (eV)
Ethylene	61,400[a]	37,000[e]	3.0[e]
Propene	57,800[b]	33,900	2.96
2-Methylpropene	53,100[c]	33,000	(2.3)
trans-Butene	56,270[c]	32,800	2.9
2-Methyl-2-butene	56,340[b] (53,000)[d]	29,850[f]	2.87[f]
2,3-Dimethyl-2-butene	53,500[c] (52,250)[d]	29,400[f]	2.82[f]

[a] P. G. Wilkinson and H. L. Johnston, *J. Chem. Phys.*, **18**, 190 (1950). [b] L. C. Jones, Jr., and L. W. Taylor, *Anal. Chem.*, **27**, 228 (1955). [c] J. T. Cary and L. W. Pickett, *J. Chem. Phys.*, **22**, 599, 1266 (1954). [d] Data in solution, see ref 7. [e] See ref 6. [f] Data from the CH_2Br solution.

lengths. On the other hand, the considerable absorption shown by the liquid methylethylenes themselves (curve 1 in Figures 2 and 3) may perhaps be ascribed to the relatively weak long wavelength tail of the V ← N transition; in ethylene itself this absorption begins at almost 2700 Å.

Table I summarizes the absorption maxima estimated from the spectra and also gives the T–V energy separation in the several ethylenes, using the liquid state data in the case of 2-methyl- and 2,3-dimethyl-2-butene. Table I shows that this energy separation decreases slowly with increase in the number of alkyl substituents, as seems reasonable.

Acknowledgment. M. I. wishes to thank Professor Michael Kasha for giving him an opportunity to work at Florida State University during the period January 1 to March 30, 1968.

Heats of Dilution at 25° of Aqueous Solutions of the Bolaform Electrolyte $[Bu_3N\text{-}(CH_2)_8\text{-}NBu_3]X_2$[1]

by **Siegfried Lindenbaum**

Chemistry Division, Oak Ridge National Laboratory, Oak Ridge, Tennessee 37830 *(Received June 27, 1969)*

Apparent molal heat contents, ϕ_L, are reported for the fluoride, chloride, and bromide salts of the bolaform electrolytes, octane-1, 8-bis(tri-*n*-butylammonium) dihalides, ($DiBuX_2$), at 25°. These values of ϕ_L are compared with previously reported values of ϕ_L for tetra-*n*-butylammonium halides. For this comparison heats of dilution of Bu_4NCl have been repeated with greater accuracy and in more detail to confirm that there are no anomalies in the ϕ_L *vs.* concentration curve corresponding to minima observed by others in partial and apparent molal volume studies. Heats of dilution of Bu_4NF are reported for the first time, and for the concentration range available this salt has larger values of ϕ_L than any previously studied 1-1 electrolyte. The comparison between the univalent electrolytes Bu_4NX and the divalent $DiBuX_2$ on an equivalental basis shows that aqueous solutions of the divalent electrolytes have slightly lower values of equivalental heat content. This lowering is attributed to the decreased hydrocarbon solvent interaction for the octyl chain connecting the two nitrogen atoms.

Introduction

Thermodynamic[2-5] measurements and transport[6] properties of tetra-*n*-butylammonium halides have suggested that cation–cation pairing and aggregation occur in aqueous solutions of tetrabutylammonium halides. It has been suggested[7] that the bolaform electrolytes $[Bu_3N\text{-}(CH_2)_8\text{-}NBu_3]X_2$, ($DiBuX_2$), may serve as a model for a Bu_4N^+ cation–cation pair. Partial molal volume measurements by Broadwater and Evans[7] reproduce the general features of the partial molal volumes previously determined by Wen and Saito[4] for Bu_4NBr solutions. The values obtained and the minima in the partial molal volume *vs.* concentration curves for both of these systems suggest that these two compounds have similar aqueous solution properties.

---

[1] Research sponsored by the U. S. Atomic Energy Commission under contract with the Union Carbide Corporation.

[2] S. Lindenbaum and G. E. Boyd, *J. Phys. Chem.*, **68**, 911 (1964).

[3] S. Lindenbaum, *ibid.*, **70**, 814 (1966).

[4] W.-Y. Wen and S. Saito, *ibid.*, **68**, 2639 (1964).

[5] R. H. Wood and H. L. Anderson, *ibid.*, **71**, 1871 (1967).

[6] D. F. Evans and R. L. Kay, *ibid.*, **70**, 366 (1966).

[7] T. L. Broadwater and D. F. Evans, *ibid.*, **73**, 164 (1969).

It is the purpose of this work to measure the heats of dilution of $DiBuX_2$ aqueous solutions and to compare the results with heats of dilution of Bu_4NX. Measurements of heats of dilution have been reported previously[3] for Bu_4NCl and Bu_4NBr. These measurements have been repeated in greater detail for Bu_4NCl, and the values for Bu_4NF are reported here for the first time.

Experimental Section

$DiBuBr_2$ was prepared as described by Broadwater and Evans.[7] Gravimetric bromide analysis yielded 24.86 ± 0.01% compared to a calculated value of 24.87%. The chloride salt was prepared by treating a solution of the bromide with freshly prepared silver hydroxide; the filtrate was treated with a stoichiometric amount of hydrochloric acid, the solution was evaporated, and the salt dried under vacuum. The salt was recrystallized from acetone–ether mixtures, dried under vacuum at 25°, and analyzed gravimetrically for chloride: Found, 12.78; Calcd, 12.80; mp ~50°. Fluoride solutions, $DiBuF_2$ and Bu_4NF, were prepared by accurately neutralizing the hydroxide solutions prepared from the pure bromides. No attempt was made to prepare the dry fluoride salts. Tetra-*n*-butylammonium chloride was recrystallized and analyzed as previously described.[2]

The calorimetric system and technique was somewhat improved over that described in a previous publication.[3] A 10,000-ohm thermistor was used as the temperature-sensing element to provide greater temperature sensitivity, and the Wheatstone bridge was provided with better shielding to reduce electrical noise. The temperature sensitivity was such that 1 cm on the strip chart recorder corresponded to 5×10^{-5}°. In order to obtain convenient temperature drift rates for the calorimetric measurements, the temperature of the calorimeter was raised 0.1° above that of the bath, so that the reaction temperature was 25.1 ± 0.05° for all of the reported values of ϕ_L. Heats of solution of tris(hydroxymethyl)aminomethane (THAM) in 0.1 *N* HCl were determined periodically to test the accuracy of the calorimetric measurements. After appropriate temperature corrections, a value of 7106 ± 13 cal/mol was obtained at 25° and a final concentration of 0.04 *m*, in good agreement with values of 7104 and 7107 published by Irving and Wadsö[8] and Gunn,[9] respectively.

Results

The calorimetric data are given in Tables I–V. Q in calories per mole is the heat absorbed on dilution from initial concentration, m_1 (mol/kg of solvent), to final concentration, m_2, and ϕ_L in calories per mole is the apparent molal heat content. The correction from m_2 to infinite dilution was calculated according to the equation of Guggenheim and Prue.[10]

Table I: Heat of Dilution of Tetrabutylammonium Fluoride Solutions at 25°

m_1	$m_2 \times 10^3$	$-Q$	ϕ_L
0.1135	1.793	332	360
0.1135	1.772	322	348
0.3009	4.459	870	918
0.3009	3.652	868	910
0.4809	1.982	1436	1464
0.4809	1.956	1460	1488
0.4809	2.080	1421	1455
0.7379	2.933	2298	2335
0.7379	2.909	2301	2337
1.053	2.601	3455	3489
1.053	2.465	3453	3486
1.404	2.856	4766	4802
1.404	3.128	4760	4798
1.837	1.558	6336	6359
1.837	1.510	6334	6356
1.837[a]	1.825	6331	6356

[a] The highest concentration for which a measurement of ϕ_L is reported is close to the solubility limit. The clathrate hydrate crystallizes from slightly more concentrated solutions at 25°.[10] From 0.1135 to 1.837 *m*: $\phi_L = 64.7 + 2502.4m +9\ 92.3m^2 - 266.5m^3$; standard deviation of fit, $\sigma = 10.6$.

$$\phi_L = \frac{\nu}{2} S_H |Z_+ Z_-| I^{1/2} \left[(1 + I^{1/2})^{-1} - \frac{\sigma(I^{1/2})}{3} \right] - 2.303RT^2 \frac{dB}{dT} m\nu_+\nu_- \qquad (1)$$

where S_H is the theoretical limiting slope, $\nu = \nu_+ + \nu_-$, ν_+ and ν_- are the number of positive and negative ions produced by the dissociation of one molecule of electrolyte, Z_+ and Z_- are the charges on the ions, I is the ionic strength, and $\sigma(I^{1/2})$ is a special function[11] defined by

$$\sigma(I^{1/2}) = \frac{3}{I^{3/2}} [1 + I^{1/2} - (1 + I^{1/2})^{-1} - 2 \ln(1 + I^{1/2})] \qquad (2)$$

Values for dB/dT were estimated from the activity coefficients of the univalent tetrabutylammonium salts according to the method of Pitzer and Brewer.[11] Activity coefficient data for the $DiBuX_2$ salts are not available; the dB/dT values of the corresponding tetrabutylammonium salt were therefore used to calculate the correction to infinite dilution. The errors introduced by this assumption are well within the experimental errors in the calorimetry.

---

(8) R. J. Irving and I. Wadsö, *Acta Chem. Scand.*, **18**, 195 (1964).

(9) S. Gunn, *J. Phys. Chem.*, **69**, 2902 (1965).

(10) E. A. Guggenheim and J. E. Prue, *Trans. Faraday Soc.*, **50**, 710 (1954).

(11) K. S. Pitzer and L. Brewer, "Thermodynamics," 2nd ed, McGraw-Hill Book Co., Inc., New York, N. Y., 1961, p 394.

Table II: Heat of Dilution of Tetrabutylammonium Chloride Solutions at 25°

m_1	$m_2 \times 10^3$	$-Q$	ϕ_L
0.1001	1.606	185	201
0.1001	1.595	186	202
0.2011	3.162	373	395
0.2011	2.920	368	389
0.2982	4.607	588	614
0.2982	4.481	589	614
0.4007	5.336	828	854
0.4007	5.685	827	854
0.5049	1.897	1084	1102
0.5049	1.917	1092	1110
0.6964	2.457	1587	1607
0.6964	2.713	1591	1611
0.9011	2.904	2154	2175
0.9011	3.099	2151	2172
1.025	3.608	2489	2512
1.025	2.837	2491	2512
1.256	2.535	3151	3171
1.256	3.089	3144	3165
1.365	3.304	3422	3444
1.365	3.080	3433	3454
1.506	3.030	3814	3835
1.506	2.816	3811	3832
1.506	3.421	3815	3837
1.707	2.451	4320	4340
1.707	3.107	4323	4344
1.807	3.057	4564	4589
1.807	2.139	4581	4599
1.983	2.777	4974	4995
1.983	2.311	4981	5000
2.047	2.409	5105	5124
2.047	2.798	5104	5123
2.047	2.187	5120	5139
2.291	1.255	5613	5628
2.291	3.479	5595	5617
2.479	2.196	5949	5968
2.479	2.372	5951	5970
2.644	2.095	6214	6232
2.644	2.622	6220	6240

From 0.5 to 2.6 m: $\phi_L = -192.1 + 2374.9m + 425.5m^2 - 153.4\,m^3$; standard deviation of fit, $\sigma = 10.2$.

Table III: Heat of Dilution of DiBuF$_2$ Solutions at 25°

m_1	$m_2 \times 10^3$	$-Q$	ϕ_L
0.2183	0.972	2,280	2,344
0.2183	0.963	2,282	2,346
0.4928	1.270	5,912	5,981
0.4928	1.210	5,878	5,946
0.8716	1.722	10,148	10,223
0.8716	1.608	9,928	10,001
2.128	0.582	20,344	20,393
2.128	0.822	20,802	20,860
3.230	1.282	25,336	25,395
3.230	0.477	24,598	24,644

Table IV: Heat of Dilution of DiBuCl$_2$ Solutions at 25°

m_1	$m_2 \times 10^3$	$-Q$	ϕ_L
0.2503	1.681	1,299	1,391
0.5023	1.846	3,285	3,382
0.5023	1.777	3,300	3,395
1.009	2.340	7,495	7,603
1.009	1.762	7,472	7,565
1.973	2.167	12,570	12,674
1.973	1.358	12,553	12,637
3.496	3.112	15,398	15,520
5.046	0.892	16,307	16,375
5.046	1.049	16,511	16,585
7.502	0.566	17,026	17,082
10.090	0.535	17,650	17,704
10.090	0.705	17,616	17,678

Table V: Heat of Dilution of DiBuBr$_2$ Solutions at 25°

m_1	$m_2 \times 10^3$	$-Q$	ϕ_L
0.1747	1.830	508	605
1.1747	2.176	495	600
0.5230	1.865	2,987	2,995
0.5230	1.663	2,899	2,992
0.9911	1.760	5,944	6,040
0.9911	2.611	5,940	6,055
1.998	3.130	9,774	9,899
1.998	2.699	9,764	9,881
2.973	2.306	11,393	11,501
2.973	1.319	11,394	11,477
4.999	1.587	12,579	12,669
4.999	2.415	12,619	12,729
6.043	0.432	12,736	12,786
6.043	0.249	12,779	12,787
7.992	1.349	12,910	12,994
7.992	1.103	12,913	12,990
9.968	0.656	12,579	12,669
9.968	0.562	12,619	12,729

Discussion

The apparent molal heat contents for tetrabutylammonium fluoride given in Table I are the largest values of ϕ_L reported for a 1–1 electrolyte for the concentration range covered by the measurements. These values are much larger than those for the corresponding chloride and bromide salts. It has been shown[12] in a study of X-ray diffraction from aqueous solutions of tetrabutylammonium fluoride that this salt is effective in increasing the amount of hydrogen bonding in the solution. This is in good agreement with previous suggestions based on less direct thermodynamic evidence.[13] In a study of X-ray diffraction from aqueous solutions of ammonium halides,[14] it has also been shown that halide ions reduce the number, and increase the length of hydrogen bonds in solution, and this effect increases with increasing anion size. If, as has been previously suggested, the apparent molal heat content is a measure of increased hydrogen bonding of the solvent,[3] then it might be expected that increasing the anion size will decrease the value of ϕ_L due to the partial cancellation of

---

(12) A. H. Narten and S. Lindenbaum, *J. Chem. Phys.*, in press.

(13) H. S. Frank, *Z. Phys. Chem.*, (Leipzig), **228**, 364 (1965).

(14) A. H. Narten, *J. Phys. Chem.*, in press.

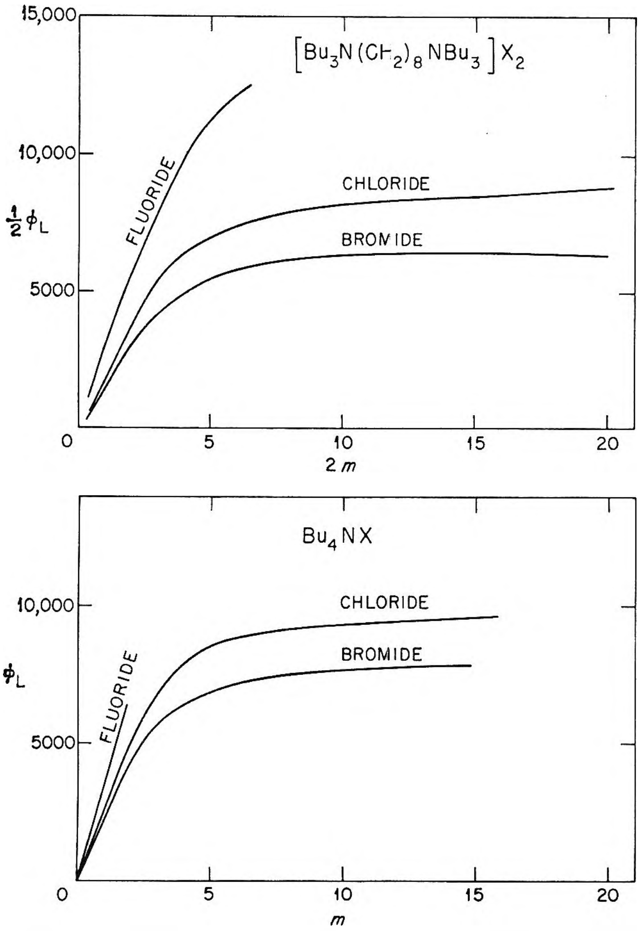

Figure 1. Apparent molal heat contents of $[Bu_3N(CH_2)_8NBu_3]$ difluoride, dichloride, and dibromide and apparent molal heat contents of Bu_4N fluoride, chloride, and bromide. Values of ϕ_L for Bu_4NBr and for Bu_4NCl above 2.7 *m* are taken from ref 3.

the hydrogen-bond formation caused by the tetraalkylammonium ion.

Measurements of apparent, ϕ_V, and partial molal, $\bar{V}_2$, volumes of tetraalkylammonium halides[15] have shown that a minimum as a function of concentration in these quantities occurs for the larger tetraalkylammonium salts. A careful examination of earlier published data on heats of dilution[3] reveals inflections in the ϕ_L and $\bar{L}_2$ data in the approximate concentration range corresponding to the minima in the ϕ_V curves. It was not clear whether these inflections were real or artifacts due to scatter in the data.[16] For this reason, heats of dilution of tetrabutylammonium chloride solutions were carefully repeated with greater accuracy and in more detail over the concentration range 0.1–2.6 *m*. No inflections or other anomalies are observable in the concentration range of interest. In fact, it was possible to represent accurately the data from 0.5 to 2.6 *m* by a cubic equation obtained by the method of least squares. The ϕ_L curves for the bolaform electrolytes are compared with those of the corresponding univalent salts in Figure 1. The curves for the divalent salts compared on an equivalental basis all fall slightly below those of the corresponding Bu_4NX salt. They are, however, very nearly superimposable after normalization of the ordinates. It has already been suggested that the large values of ϕ_L for tetraalkylammonium halides are in large part a measure of the heat evolved due to the promotion of additional hydrogen bonding of the water molecules in the vicinity of the hydrocarbon chains. Whereas $DiBu^{2+}$ ion has the same length of hydrocarbon chain per unit charge as a Bu_4N^+ ion, less contact with the solvent is possible since one end of a butyl chain is protected from contact with the aqueous solvent. The slightly lower values of ϕ_L for the bolaform electrolyte are therefore not unreasonable. This study provides additional evidence for the contention that the thermodynamic properties of aqueous solutions of $DiBuX_2$ are very similar to those of Bu_4NX. Volume of mixing studies[17,18] on tetraalkylammonium salt solutions have lent themselves to interpretation in terms of cation–cation pair formation, and volume studies on $DiBuX_2$ solutions[7] have supported the idea that this salt may serve as a model for such a pair. Qualitatively, the ϕ_L values reported here may also be interpreted in this manner. However, these data cannot be used as *evidence* for the existence of cation–cation pairs in Bu_4NX solutions because the contribution to the thermodynamic properties of the solution by such pair formation is not known. Small-angle X-ray scattering experiments on aqueous Bu_4NX and $DiBuX_2$ solutions are in progress[19] to investigate the possibility of ion pair or micelle formation and will be discussed in a later report.

---

(15) W.-Y. Wen and S. Saito, *J. Phys. Chem.*, **68**, 2639 (1964).

(16) Thanks are due to Dr. Wen-Yang Wen for pointing out this problem.

(17) W.-Y. Wen and K. Nara, *J. Phys. Chem.*, **71**, 3907 (1967).

(18) W.-Y. Wen, K. Nara, and R. H. Wood, *ibid.*, **72**, 3048 (1968).

(19) R. W. Hendricks and S. Lindenbaum, Abstracts, 157th National Meeting of the American Chemical Socity, Minneapolis, Minn., April 1969, No. 34.

Relationships between Arrhenius Activation Energies and Excitation Functions

by Rodney L. LeRoy[1]

Department of Chemistry, University of Colorado, Boulder, Colorado 80302 *(Received June 30, 1969)*

Analytical expressions are derived which relate the Arrhenius activation energy to the energy dependent reaction cross section or excitation function. Results are presented for reactions which proceed with and without a threshold energy. It is shown that the activation energy for neutral–neutral reactions may display a strong temperature dependence, and that activation energies determined in thermal studies of ion–molecule reactions can commonly be expected to be either positive or negative, and strongly temperature dependent. Particular attention is given to recent rate measurements for the exchange reactions of atomic hydrogen with molecular hydrogen, and an attempt is made to derive excitation functions from these results. Three general formulations of the excitation function are used. These reflect the forms which have been suggested by experiments and by theoretical calculations. In particular one class of functions is found to be able to accurately reproduce the available data on the energy dependence of the reaction cross section for neutral–neutral reactions, and representative data for ion-impact induced fragmentation reactions. A second class of functions is introduced to include the special case of hard spheres which require a critical energy along the line of centers to react, while a final class adequately reproduces data for many ion–molecule processes.

Introduction

Much of the interesting information about an elementary chemical reaction can be summarized in its excitation function or energy dependent reaction cross section. Considerable progress is now being made towards devising "non-classical" experiments which will allow such excitation functions to be determined directly.[2–5] Also, calculations performed by Monte Carlo averaging over quasi-classical trajectories have made it possible to predict excitation functions for some simple systems.[6,7] All of the results which have been obtained for neutral reactions suggest that the excitation function rises from zero at some critical value of the relative translational energy of the reagents—the threshold energy. This function then passes through a maximum, and decreases towards zero again as the energy is further increased.[4,6,7] Also it is well established[8] that the excitation function for most ion–molecule processes is a monotonically decreasing function of energy.

Menzinger and Wolfgang[9] have recently examined the relationship between the Arrhenius activation energy, E_{exp}, and the more fundamental excitation function for reaction. In the present paper we extend their results. Three general analytical formulations of the energy dependence of the reaction cross section are suggested, and E_{exp} and the bimolecular rate constant $k(T)$ are derived for each of these.

Theory

The Arrhenius activation energy is defined by the relation

$$E_{\mathrm{exp}} = RT^2 \frac{\mathrm{d} \ln k(T)}{\mathrm{d}T} \tag{1}$$

where T is the absolute temperature of the reaction mixture, R is the universal gas constant, and $k(\mathrm{T})$ is the bimolecular rate constant, given by [9,10]

$$k(T) = \left(\frac{2}{RT}\right)^{3/2} \frac{1}{(\pi\mu)^{1/2}} \int_0^\infty E\sigma(E)e^{-E/RT}\,\mathrm{d}E \tag{2}$$

Here E and μ are the relative translational energy and the reduced mass respectively of the collision partners, and $\sigma(E)$ is the excitation function for reaction.[11]

---

[1] Address requests for reprints to Department of Chemistry, Yale University, New Haven, Connecticut 06520.

[2] (a) M. Menzinger and R. Wolfgang, *J. Chem. Phys.*, **50,** 2991 (1969); (b) E. F. Greene and J. Ross, *Science*, 159, 587 (1968).

[3] A. Kuppermann and J. M. White, *J. Chem. Phys.*, **44,** 4352 (1966).

[4] R. Wolfgang, in "Progress in Reaction Kinetics," Vol. 3, G. Porter, Ed., Pergamon Press, New York, 1965, p 97; *Ann. Rev. Phys. Chem.*, **16,** 15 (1965).

[5] "Ion–Molecule Reactions in the Gas Phase," R. F. Gould, Ed., Vol. 58, American Chemical Society Publications, Washington, D. C., 1966.

[6] M. Karplus, R. N. Porter, and R. D. Sharma, *J. Chem. Phys.*, **43,** 3259 (1965).

[7] M. Karplus, R. N. Porter, and R. D. Sharma, *J. Chem. Phys.*, **45,** 3871 (1966).

[8] See, for example, C. F. Giese and W. B. Maier, *J. Chem. Phys.*, **39,** 739 (1963).

[9] M. Menzinger and R. Wolfgang, *Angew. Chem.*, **8,** 438 (1969).

[10] M. Eliason and J. O. Hirschfelder, *J. Chem. Phys.*, **30,** 1426 (1959).

[11] Note that we do not significantly restrict our considerations by treating only bimolecular processes. This is because the Arrhenius activation energy for a chemical reaction generally reflects the temperature dependence of the rate of an elementary collisional activation step, whatever the overall reaction order.[9]

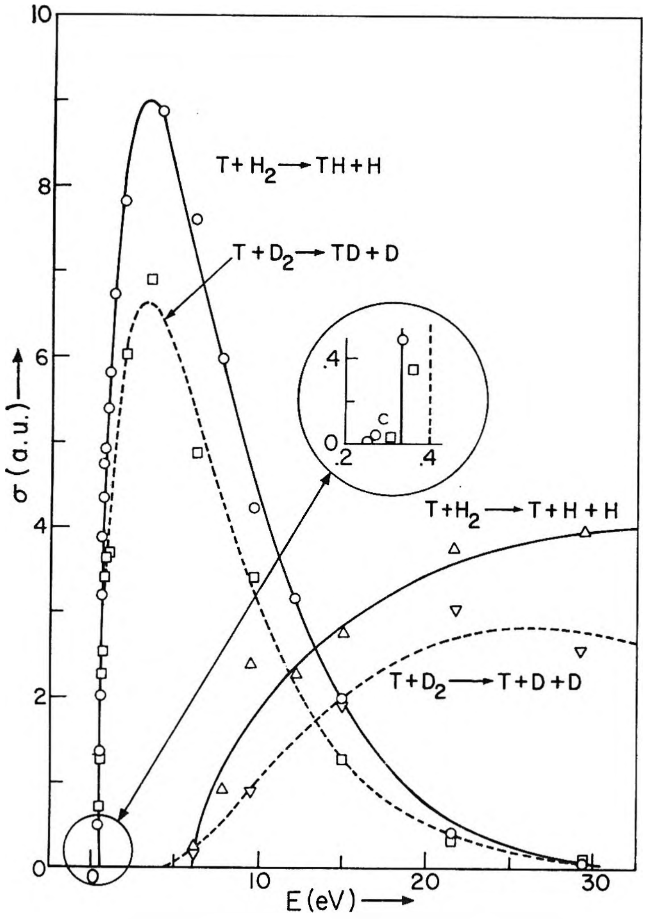

Figure 1. Excitation functions for the reactions of atomic tritium with molecular hydrogen and deuterium. The points were obtained by Monte Carlo averaging over quasi-classical trajectories,[7,13] and the curves through the data correspond to the best least-squares fits of class I excitation functions. The lower three points for the exchange reaction with hydrogen and the lower two points for the exchange reaction with deuterium (see insert), were omitted in the fitting procedure. The derived class I parameters are recorded in Table I.

Equations 1 and 2 are evaluated below for three general classes of functions. These can be used to describe most of the forms of the excitation function which have been postulated.

Class I.

$$\sigma(E) = C(E - E_0)^n e^{-m(E-E_0)} \quad (E \geqslant E_0)$$

and (3)

$$\sigma(E) = 0 \quad (E < E_0)$$

where $m,n \geqslant 0$. These functions increase from 0 at $E = E_0$. The rising portion is concave upward when n is greater than 1, and is convex upward when n has a value between 0 and 1. The exponential term causes the excitation function to pass through a maximum[12] as the energy E increases, and then to decrease at a rate determined by the parameter m. In the simple case where $n = m = 0$, $\sigma(E)$ becomes a step function.

The best fits of class I functions to some experimental and theoretical excitation functions for neutral–neutral reactions are presented in Figures 1 to 3. The excitation functions of Figure 1 for the reactions of atomic tritium with hydrogen and deuterium were obtained from trajectory calculations.[7,13] The fit seems quite good, except for the exchange reactions in the vicinity of the reaction threshold (insert, Figure 1). Although the number of calculated trajectories in this region may be too small for the Monte Carlo averages to be reliable,[14] they indicate structure which class I functions can not reproduce. Such structure is negligible when compared with the

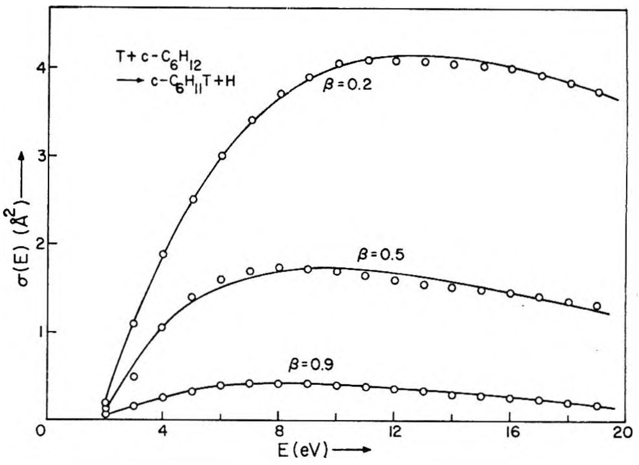

Figure 2. Excitation functions for the displacement reaction of of atomic tritium with cyclohexane. The data is taken from Menzinger and Wolfgang,[2a] who derived it by assuming that the total reaction probability is 3.5 times the probability of reaction to form c-$C_6H_{11}T$. The different curves correspond to different values of the energy loss parameter β. Parameters of the class I functions drawn through the data are recorded in Table I.

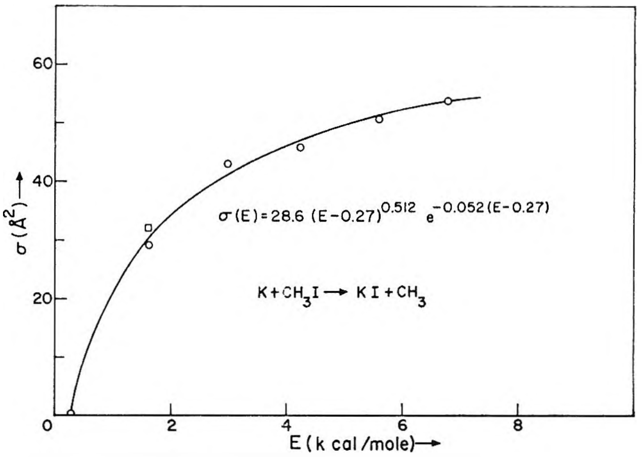

Figure 3. Excitation function for the reaction of potassium with methyl iodide.[2b] The circled points were deduced from measurements of elastically scattered potassium, and the squared point from measurements of reactively scattered potassium iodide.

---

[12] The maximum of class I excitation functions occurs at $E = E_0 + n/m$.

[13] R. N. Porter kindly provided the original quasi-classical results which were used in plotting $\sigma(E)$ for the exchange reactions treated in ref 7.

[14] R. N. Porter, private communication.

Table I: Parameters of Class I Functions Plotted in Figures 1 and 2

Figure	Data	C, Å^2 eV^{-n}	n	m, eV^{-1}	E_0, eV
1	$T + H_2 \rightarrow TH + H$	2.55	0.57	0.21	0.33
1	$T + D_2 \rightarrow TD + D$	1.90	0.58	0.22	0.40
1	$T + H_2 \rightarrow T + H + H$	0.263	0.59	0.018	6.07
1	$T + D_2 \rightarrow T + D + D$	0.291	1.60	0.074	4.59
2	$T + c\text{-}C_6H_{12}$; $\beta = 0.2$	1.14	0.92	0.085	1.88
2	$T + c\text{-}C_6H_{12}$; $\beta = 0.5$	0.74	0.80	0.102	1.94
2	$T + c\text{-}C_6H_{12}$; $\beta = 0.9$	0.13	1.28	0.188	1.51

overall excitation function, but it could have a significant effect on the low temperature thermal rate constants for these reactions.

Figure 2 presents three of the excitation functions which Menzinger and Wolfgang derived from an analysis of their beam studies of the hot atom reaction of atomic tritium with solid cyclohexane.[2a] The curves correspond to three different values of the energy loss parameter β. Parameters of the excitation functions which were used in fitting curves to the data of Figures 1 and 2 are listed in Table I.

The excitation function for the reaction of potassium with methyl iodide is plotted in Figure 3. These data were obtained by Greene and Ross[2b] in a molecular beam study of the angular distribution of elastically scattered potassium, and of reactively scattered potassium iodide.

It is evident from Figures 1 to 3 that class I functions can quite satisfactorily describe the energy dependence of the available excitation functions for neutral reactions. In Figure 4 (bottom curve) we show that this class of functions can give an equally good description of the excitation function for an ion-impact induced dissociation reaction. The illustrated data were obtained by Vance and Bailey[15] for the impact of molecular hydrogen ions on hydrogen molecules. In addition eq 3 has been fitted with comparable success to the numerous excitation functions reported by Maier[16] for analogous processes.

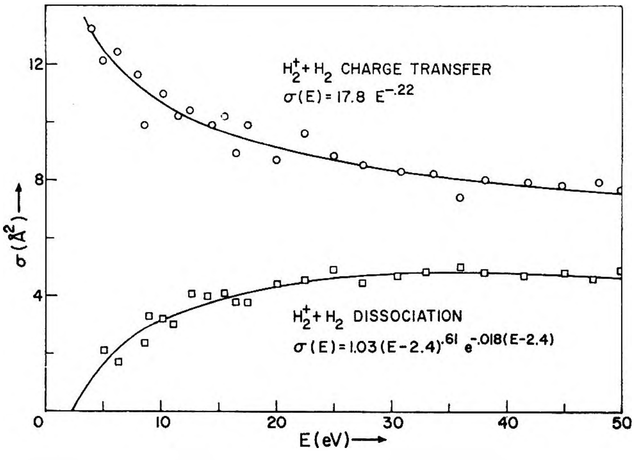

Figure 4. Excitation functions for the inelastic scattering of H_2^+ on molecular hydrogen[15]. The cross section for ion impact induced dissociation (bottom curve) is reproduced by a class I function, while that for charge exchange (top curve) is well represented by a class III function.

Substituting $\sigma(E)$ from eq 3 into eq 1 and 2 gives analytical expressions for the bimolecular rate constant $k(T)$ and for E_{exp}

$$k(T) = C\left(\frac{8RT}{\pi\mu}\right)^{1/2} \frac{(RT)^n e^{-E_0/RT}}{(1 + mRT)^{n+2}} [\Gamma(n + 2) + \Gamma(n + 1)(1 + mRT)E_0/RT] \quad (4)$$

and

$$E_{\text{exp}} = E_0 + RT(n + {}^1/_2) - \frac{m(n + 2)(RT)^2}{1 + mRT} - \frac{E_0}{(n + 1) + (1 + mRT)E_0/RT} \quad (5)$$

where $\Gamma(n + 1)$ and $\Gamma(n + 2)$ are gamma functions.[17] When m is set equal to zero, eq 5 becomes equivalent to the expression quoted by Menzinger and Wolfgang.[9]

$$E_{\text{exp}} = E_0 + RT\left(n - {}^1/_2 + \left[1 + \frac{E_0}{(n + 1)RT}\right]^{-1}\right) \quad (6)$$

Class II

$$\sigma(E) = C\frac{(E - E_0)^n}{E} e^{-m(E-E_0)} \quad (E \geqslant E_0)$$

and

$$\sigma(E) = 0 \qquad (E < E_0) \quad (7)$$

These functions are similar in form to those of class I. However they are introduced here in order to include the well known excitation function for the collision of hard spheres which require a critical relative translational energy E_0, measured along their line of centers, in order to react.[10] The form of eq 7 for this special case is

$$\sigma(E) \propto (1 - E_0/E) \quad (E \geqslant E_0) \quad (8)$$

and

$$\sigma(E) = 0 \qquad (E < E_0)$$

---

[15] D. W. Vance and T. L. Bailey, *J. Chem. Phys.*, **44**, 486 (1966).

[16] W. B. Maier, *ibid.*, **41**, 2174 (1964).

[17] See for example the tables of $\Gamma(x)$ in "Handbook of Mathematical Functions," M. Abramowitz and I. A. Stegun, Ed., Dover Publications, Inc., New York, N. Y., 1965, p 267.

Substitution of the general class II function into eq 2 yields

$$k(T) = C\left(\frac{8RT}{\pi\mu}\right)^{1/2}\frac{(RT)^{n-1}\Gamma(n+1)e^{-E_0/RT}}{(1+mRT)^{n+1}} \qquad (9)$$

and the activation energy assumes a particularly simple form

$$E_{\mathrm{exp}} = E_0 + RT(n - {}^1/_2) - \frac{m(n+1)(RT)^2}{1+mRT} \qquad (10)$$

For the hard sphere excitation function of eq 8 ($n = 1$, $m = 0$), eq 10 reduces to the well known result[10,18]

$$E_{\mathrm{exp}} = E_0 + RT/2 \qquad (11)$$

It is also interesting to note that if the excitation function has the unlikely form

$$\sigma(E) \propto (E - E_0)^{1/2}/E \quad (E \geqslant E_0)$$

and

$$\sigma(E) = 0 \qquad (E < E_0) \qquad (12)$$

then the experimental activation energy calculated from eq 10 will be identically equal to the threshold energy E_0. This latter observation was made by Karplus, Porter, and Sharma.[6]

Class III

$$\sigma(E) = CE^n \quad (E \geqslant E_0)$$

and

$$\sigma(E) = 0 \quad (E < E_0) \qquad (13)$$

The best known example of this type of function is the Langevin cross section,[19] $\sigma(E) \propto E^{-1/2}$, which applies for close collisions between low energy ions and polarizable molecules. Typical fits of class III functions to measured cross sections for ion–molecule processes are illustrated in Figure 4 (top curve) and Figure 5.

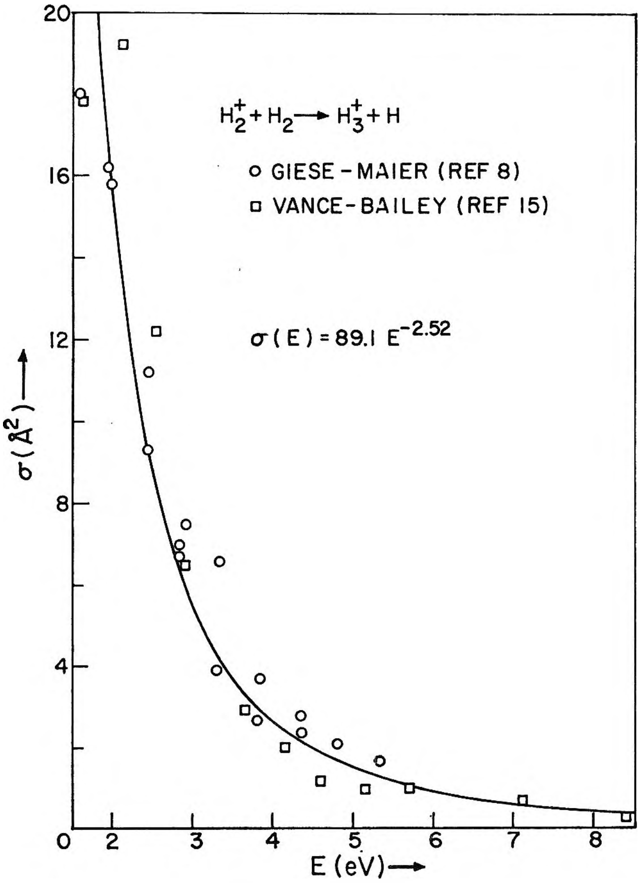

Figure 5. Excitation function for the ion–molecule reaction of H_2^+ with molecular hydrogen. Data of both Giese and Maier[8] and Vance and Bailey[15] are plotted, and all the data are well represented by a class III function.

For these functions, solution of eq 1 and 2 gives

$$k(T) = C\left(\frac{8RT}{\pi\mu}\right)^{1/2}(RT)^n[\Gamma(n+2) - \gamma(n+2,E_0/RT)] \qquad (14)$$

and

$$E_{\mathrm{exp}} = RT(n + {}^1/_2) + E_0\frac{(E_0/RT)^{n+1}e^{-E_0/RT}}{\Gamma(n+2) - \gamma(n+2,E_0/RT)} \qquad (15)$$

where $\gamma(n + 2,E_0/RT)$ is an incomplete gamma function.[20,21]

For integer and half-integer values of n, E_{exp} is expressed in terms of analytical and tabulated functions in the Appendix. We only record here the expression which applies when $\sigma(E)$ is the Langevin cross section ($n = -{}^1/_2$) for an endoergic process

$$E_{\mathrm{exp}} = E_0\frac{(E_0/RT)^{1/2}e^{-E_0/RT}}{\dfrac{(\pi)^{1/2}}{2}[1 - erf(E_0/RT)^{1/2}] + (E_0/RT)^{1/2}e^{-E_0/RT}} \qquad (16)$$

Reaction with No Threshold Energy

For reactions which occur with no threshold energy, the class I and II excitation functions become

$$\sigma(E) = CE^n e^{-mE} \qquad (17)$$

Examples of this form will be discussed below. When the excitation function is given by eq 17 E_{exp} is nonzero, having the form

$$E_{\mathrm{exp}} = RT(n + {}^1/_2) - \frac{m(n+2)(RT)^2}{1+mRT} \qquad (18)$$

where n and m are greater than zero.

---

(18) W. J. Moore, "Physical Chemistry," 3rd ed., Prentice-Hall, Inc., Englewood Cliffs, N. J., 1962, p 278.

(19) P. Langevin, *Ann. Chim. Phys.*, **5**, 245 (1905); G. Gioumousis and D. P. Stevenson, *J. Chem. Phys.*, **29**, 294 (1958).

(20) The incomplete gamma function is defined and plotted on pages 260 and 261 of ref 17, and is discussed more fully in ref 21.

(21) F. G. Tricomi, *Ann. Mat.*, **31**, 263 (1950).

Discussion

The results presented above offer several formal relationships between the Arrhenius activation energy and the excitation function for reaction. It should be emphasized, however, that by making use of eq 2 we assume that the velocities of the reactant molecules are distributed according to the Maxwell–Boltzmann function. In fact this will only be true if $\sigma(E)$ (and thus the reaction rate) is small enough that collisions can maintain an equilibrium distribution of translational energies. Menzinger and Wolfgang[9] have discussed some of the consequences of a departure from equilibrium.

Secondly, it is important to realize that the excitation function is different for each vibrational and rotational state of the reagent molecules.[6] Thus the overall excitation function for a reaction represents an appropriate temperature dependent average over all possible microscopic processes. Assuming functional forms such as those given in eq 3, 7, and 13 to be temperature independent is an approximation.

In spite of these limitations, it is instructive to examine the variation of E_{exp} with temperature. E_{exp}/E_0 is plotted against RT/E_0 in Figure 6a for three class I functions which correspond to reasonable (see Figures 1 to 3) values of the parameters n and m. The activation energy shows a strong temperature dependence in each case. At very high temperatures, the activation energy calculated for class I and II functions will always become negative, provided m is not equal to zero. This is because the average translational energy will, in the limit, exceed the average energy at which reaction occurs. This is particularly obvious if m is sufficiently large that the energy dependence of the reaction cross section approaches a delta function. Then the values of E_{exp} predicted by eq 5 and 10 both approach

$$E_{\text{exp}} = E_0 - 3RT/2 \tag{19}$$

Most neutral reactions are studied at temperatures which are low enough that $RT \ll E_0$. In this limit

$$E_{\text{exp}} \simeq E_0 + RT(n - {}^1/_2) \tag{20}$$

for both class I and II functions. Thus we might expect the activation energy to be constant at low temperatures and to vary slightly with increasing temperature, the sign of the temperature coefficient depending on whether n is greater or less than one half. It is interesting to note that n is close to 0.5 for the reaction of potassium with methyl iodide (Figure 3) and for the exchange reactions of Figure 1 (see Table I).

Figure 6b illustrates the temperature dependence of E_{exp} for some class III functions. Since these functions can describe the excitation function for ion–molecule reactions (see Figures 4 and 5), low or zero values of E_0 and correspondingly high values of RT/E_0 can easily be encountered experimentally. Thus, for ion–molecule reactions whose excitation functions correspond to values of n less than $-{}^1/_2$, Figure 6 suggests that thermal studies could often yield a negative temperature dependence of the reaction rate (*i.e.*, E_{exp} negative). In fact

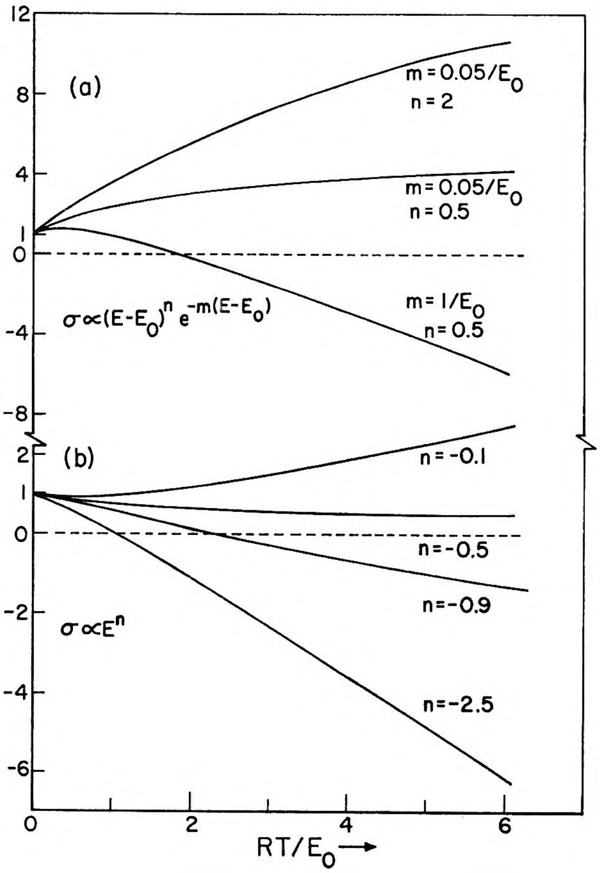

Figure 6. Typical variations of the Arrhenius activation energy with reaction temperature for class I (top) and class III (bottom) functions.

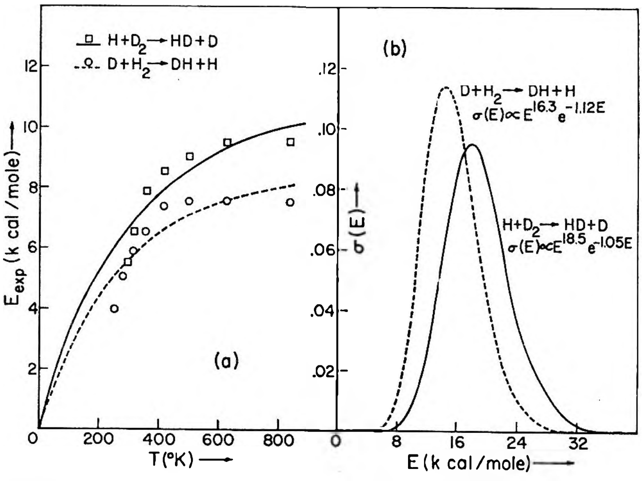

Figure 7. Activation energies for the reactions of H with molecular deuterium, and D with molecular hydrogen, taken from the data of Westenberg and de Haas.[23] The curves through the data are drawn from eq 18, using the parameters of the excitation functions presented in Figure 7b. These functions are normalized so that the area under each curve is unity.

if there is no threshold energy for reaction, eq 15 becomes simply

$$E_{\text{exp}} = (n + {}^1/_2)RT \tag{21}$$

and the Arrhenius activation energy will always be negative when n is less than -0.5. It is difficult to estimate how common such low values of n might be, but the result $\sigma(E) \propto E^{-2.52}$ for the reaction

$$H_2^+ + H_2 \longrightarrow H_3^+ + H \tag{22}$$

(Figure 5) confirms that $n < -0.5$ is feasible.

Finally we shall comment briefly on the nonlinearity of Arrhenius plots which has recently been found for the exchange reactions of atomic with molecular hydrogen.[22,23] These measurements indicate that the thermal activation energy for these reactions rises sharply at low temperatures, approaching a constant value as the temperature is increased. This conflicts directly with the result which would be predicted by eq 20 even though, in the temperature range where E_{exp} is varying rapidly, RT is considerably lower than the lowest barrier height indicated by the experimental activation energies (*i.e.*, $RT \ll 6$ kcal/mol). This suggests that the actual threshold energy for reaction must be considerably lower than 6–10 kcal/mol. Such a low threshold could be due to quantum mechanical tunneling—a possibility which D. J. LeRoy and his coworkers discuss in detail[22]—or to the finite reaction probabilities at low energies which are revealed by the quasi-classical trajectory calculations (see Figure 1, insert, and Figure 4 of ref 6). Most likely the experimental results reflect both of these effects.

Menzinger and Wolfgang[9] suggest that the effect of quantum mechanical tunneling on an excitation function might be approximated if that function has zero threshold energy, and rises as E^n where n is relatively large. In Figure 7 we test whether such a function can be responsible for the observed temperature dependence of the rates of the hydrogen exchange reactions. Specifically we attempt to reproduce the experimental results with a class I function for which $E_0 = 0$ (eq 17).

Experimental values of E_{exp}, taken from Westenberg and de Haas' data[23,24] for the reactions

$$H + D_2 \longrightarrow HD + D \tag{23}$$

$$D + H_2 \longrightarrow DH + H \tag{24}$$

are plotted in Figure 7a. Equation 18 has been fitted to this data by least-squares (solid and broken curves, Figure 7a), and the excitation functions calculated from the resulting parameters[26] are plotted in Figure 7b. The curves in Figure 7a approximate the experimental values of E_{exp} reasonably well at high temperatures, while at low temperatures they show the same trend as the experimental data, but are consistently too high. Thus it is likely that the simple function of eq 17 is not sufficiently versatile to describe in detail the excitation functions for the hydrogen exchange reactions at low energies. However qualitative agreement is obtained, and it is possible to derive "reasonable" excitation functions from the experimental rate measurements. In particular it is interesting to note that a very small contribution to the excitation function at low energies can result in a dramatic temperature dependence of the Arrhenius activation energy at low temperatures.

Finally we should comment that the experimental temperature dependence of E_{exp} could certainly be reproduced using an excitation function of the form

$$\sigma(E) = \left(\sum_{i=1}^{k} C_i E^{i-1}\right) E^n e^{-mE} \tag{25}$$

where k is as large as is necessary. We have not attempted such a fit because the experimental data are not sufficiently precise to guarantee that the resulting excitation function will be unique.

Acknowledgments. I am grateful to Professor Richard Wolfgang for encouraging me to pursue this problem, and to Professors Richard Porter and D. J. LeRoy for several invaluable discussions. Mr. Calvin Blakley assisted with the early calculations. This work was made possible by the support of the U. S. Atomic Energy Commission and the National Aeronautics and Space Administration, and also by the National Research Council of Canada through the award of a Postdoctoral Fellowship.

Appendix. Relationships between E_{exp} and E_0 for Class III Excitation Functions Corresponding to Integer and Half-Integer Values of n

(*a*) *n Integer*

$$E_{\text{exp}} = RT(n + {}^1/_2) + E_0 \frac{(E_0/RT)^{n+1}}{(n+1)! \sum_{i=0}^{n+1} \left[\left(\frac{E_0}{RT}\right)^i \Big/ i!\right]} \qquad (n \geqslant -1)$$

$$E_{\text{exp}} = RT(n + {}^1/_2) + RTe^{-E_0/RT}/E_1\left(\frac{E_0}{RT}\right) \qquad (n = -2)$$

---

(22) W. R. Schulz and D. J. LeRoy, *J. Chem. Phys.*, **42**, 3869 (1965); B. A. Ridley, W. R. Schulz, and D. J. LeRoy, *ibid.*, **44**, 3344 (1966); D. J. LeRoy, B. A. Ridley, and K. A. Quickert, *Discussions Faraday Soc.*, **44**, 92 (1967).

(23) A. A. Westenberg and N. de Haas, *J. Chem. Phys.*, **47**, 1393 (1967).

(24) The earlier results of D. J. LeRoy and his collaborators[22] for reaction 24 give lower values of E_{exp} at low temperatures. However the rate constants determined by these workers were likely somewhat high due to back diffusion of the molecular reactant.[25] The resulting errors are more serious at low temperatures.

(25) D. J. LeRoy, private communication.

(26) Note that the thermal rate constants are almost completely insensitive to the form of the excitation function above, say, 12 kcal/mol, so the derived functions of Figure 7b have little significance above this energy.

and

$$E_{\mathrm{exp}} = RT(n + {}^1/_2) + E_0 \frac{(E_0/RT)^{n+1}(-n-2)!}{(-1)^{n+2}\left[e^{E_0/RT}E_1\left(\frac{E_0}{RT}\right) - \sum_{i=0}^{-n-3} \frac{(-1)^i i!}{(E_0/RT)^{i+1}}\right]} \quad (n \leqslant -3)$$

$E_1(z)$ is the exponential integral,[27] given by

$$E_1(z) = \int_z^{\infty} \frac{e^{-y}}{y}\,\mathrm{d}y$$

(*b*) *n Half-Integer*

$$E_{\mathrm{exp}} = RT(n + {}^1/_2) + E_0 \frac{(E_0/RT)^{n+1}}{\prod_{j=0}^{n+{}^1/_2}(j + {}^1/_2)\left\{(\pi)^{{}^1/_2}\left[1 - erf\left(\frac{E_0}{RT}\right)^{{}^1/_2}\right]e^{E_0/RT} + \sum_{i=0}^{n+{}^1/_2}\frac{(E_0/RT)^{i+{}^1/_2}}{\prod_{j=0}^{i}(j + {}^1/_2)}\right\}} \quad (n \geq -{}^1/_2)$$

$$E_{\mathrm{exp}} = \left(\frac{RTE_0}{\pi}\right)^{{}^1/_2} \frac{e^{-E_0/RT}}{1 - erf\left(\frac{E_0}{RT}\right)^{{}^1/_2}} - RT \quad (n = -{}^3/_2)$$

and

$$E_{\mathrm{exp}} = RT(n + {}^1/_2) + E_0 \frac{(E_0/RT)^{n+1}\prod_{i=1}^{-n-{}^3/_2}({}^1/_2 - i)}{(\pi)^{{}^1/_2}e^{E_0/RT}\left[1 - erf\left(\frac{E_0}{RT}\right)^{{}^1/_2}\right] - 2\sum_{i=1}^{-n-{}^3/_2}\left[\frac{\prod_{j=1}^{i}({}^3/_2 - j)}{(E_0/RT)^{i-{}^1/_2}}\right]} \quad (n \leqslant -{}^5/_2)$$

---

(27) The exponential integral $E_1(z)$ is discussed and tabulated on pages 228–243 of ref 17.

Quantum Yield of Photonitrosation of Cyclohexane in Homogeneous System

by Hajime Miyama, Kuya Fukuzawa, Noriho Harumiya,

Basic Research Laboratory, Toyo Rayon Co., Ltd., Tebiro, Kamakura, Japan

Yoshikazu Ito, and Shigeru Wakamatsu

Nagoya Laboratory, Toyo Rayon Co., Ltd., Minato-ku, Nagoya, Japan *(Received June 30, 1969)*

Quantum yield of photonitrosation of cyclohexane was measured in a homogeneous system, where the oxime hydrochloride formed was dissolved by adding chloroform to the reaction mixture. Obtained values were 0.80 ± 0.06 at 365 mμ, 0.79 ± 0.06 at 436 mμ, and 0.97 ± 0.13 at 578 mμ. These results were discussed from the mechanistic viewpoint.

In a previous study,[1] we have measured the quantum yield of photonitrosation of cyclohexane by using an integrating sphere to remove the effect of light scattering by the precipitated oxime hydrochloride and obtained a value of 0.72 independent of wavelengths. However, an estimated experimental error was as high as ± 20%. In order to obtain the more accurate value, chloroform which is inert to nitrosyl chloride and dissolves the oxime hydrochloride was added to the reaction mixture and the measurement was performed at 365, 436, and 578 mμ, in a homogeneous system by using conventional techniques.

Experimental Section

A conventional optical system for measuring quantum yield was used and its schematic diagram is shown in Figure 1. The reaction vessel was a quartz cylinder (5 cm in diameter and 5 cm long) with flat quartz surfaces at both ends and kept at a constant temperature in an air bath. As the light source, a high-pressure mercury lamp of 2 KW was used in combination with various Toshiba glass filters and an aqueous solution of copper sulfate to obtain monochromatic light. That is, UV-DIC was used to obtain the light of 365 mμ, a combination of V-V 40, V-Y 42, and a 1% aqueous solution of copper sulfate for 436 mμ, and a combination of V-O58 and a 1% aqueous solution of copper sulfate for 578 mμ. The absorption characteristics of the glass-filters are shown in Figure 2.

Absolute light intensities at 365 and 436 mμ, were measured by using a potassium ferrioxalate actinometer,[2] and that at 578 mμ, by a Reinecke's salt actinometer.[3] Since the latter actinometer was considered less reliable than the former one, a Kip & Zonen thermopile CA1 calibrated by the potassium ferrioxalate actinometer was used also at 578 mμ, giving the same results as those obtained with the chemical actinometer. Light absorption by the reaction system during the reaction was followed by means of the thermopile equipped with a recorder.

Commercial cyclohexane was washed with concentrated sulfuric acid, water, sodium hydroxide and water dried over calcium chloride, refluxed over metallic sodium, and distilled in an argon atmosphere. Chloroform of the first grade was washed with water, dried with calcium chloride, and distilled. Hydrogen chloride in cylinder was used after being dried by passage through a calcium chloride tube.

The quantitative analysis of the product of the photonitrosation was carried out by converting cyclohexanone oxime formed into chloronitrosocylohexane (CNC) by treatment with chlorine, and measuring the absorption of CNC spectrophotometrically.[1] Since CNC was invariably present to some extent in the original product, the same analysis without the chlorine treatment was carried out as a control.

The experimental procedure was as follows. An equal volume mixture of cyclohexane and chloroform was saturated with hydrogen chloride, and a definite quantity of nitrosyl chloride was bubbled into the mixture. This solution was then introduced into the reaction vessel. All of these operations were carried out in an argon atomsphere. The photoreaction was carried out at 24° for a given time, and the products were analyzed as described above. Since the dark reaction observed in the previous study[1] did not occur because of the high purity of the reactants used in the present system, no correction for the dark reaction was made.

Results and Discussion

Results obtained at 365 mμ, 436 mμ, and 578 mμ are shown in Tables I, II, and III, respectively. Here, the quantum yield was calculated by dividing the sum of the quantities of the oxime and CNC by the light quantity absorbed during the reaction. The reason for adopting the sum of the oxime and CNC is that the CNC present in the reaction mixture is derived from the oxime ac-

---

(1) H. Miyama, N. Harumiya, Y. Ito, and S. Wakamatsu, *J. Phys. Chem.*, **72**, 4700 (1968).

(2) C. A. Parker, *Proc. Roy. Soc.*, **A220**, 104 (1953).

(3) E. E. Wegner and A. W. Adamson, *J. Amer. Chem. Soc.*, **88**, 394 (1966).

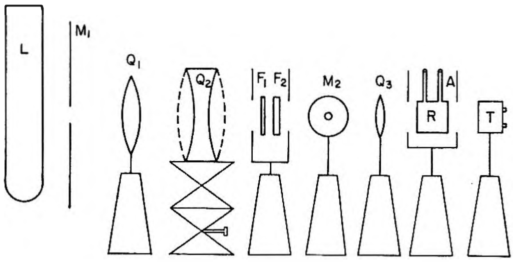

Figure 1. Schematic diagram of experimental apparatus L, light source, M_1 and M_2, mask; Q_1 and Q_2, quartz condenser lense, F_1, glass filter; F_2, copper sulfate filter; Q_3, quartz collimating lense; R, reaction vessel; A, air bath; T, thermopile.

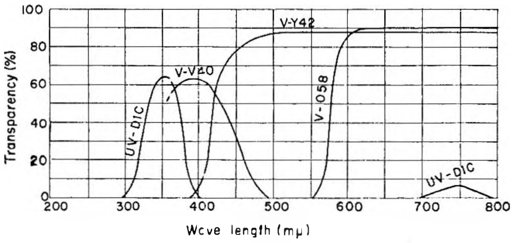

Figure 2. Absorption characteristics of glass filters.

Table I: Results at 365 mμ

Reaction time, min	NOCl, weight%	CNC,[a] %	Quantum yield	
120	0.76	100	0.86	Av 0.80 ± 0.07
240	0.62	100	0.84	
240	0.54	76.4	0.84	
121	0.68		0.78	
100	0.71		0.67	
181	0.30	50	0.77	Av 0.81 ± 0.06
242	0.25	50	0.88	
242	0.35	10.7	0.86	
120	0.35	5.9	0.74	
240	0.35	2.9	0.77	
362	0.35	24.0	0.80	
120	0.35		0.88	
121	0.35		0.83	
100	0.38		0.74	
			Overall av 0.80 ± 0.06	

[a] Molar per cent expressed by [CNC]/([oxime] + [CNC]) × 100(%).

Table II: Results at 436 mμ

Reaction time, min	NOCl, weight%	CNC, %	Quantum yield	
120	0.76	100	0.71	Av 0.78 ± 0.06
120	0.81	87.0	0.85	
100	0.80		0.80	
100	0.71		0.75	
60	0.27	10.8	0.78	Av 0.80 ± 0.07
121	0.27	10.9	0.81	
183	0.27	9.7	0.84	
240	0.27	20.7	0.84	
121	0.31	84.7	0.84	
180	0.30	65	0.85	
180	0.38	28.8	0.88	
120	0.37		0.67	
120	0.37		0.75	
120	0.37		0.68	
120	0.35		0.81	
120	0.35		0.82	
101	0.38		0.81	
100	0.38		0.85	
302	0.38		0.74	
			Overall av 0.79 ± 0.06	

cording to the following reaction. In fact, this reaction

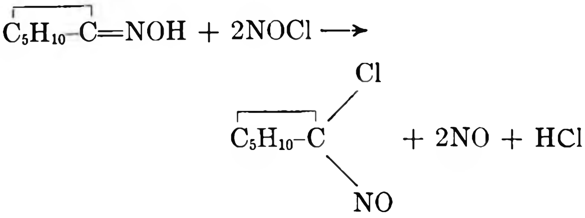

$$C_5H_{10}C{=}NOH + 2NOCl \longrightarrow C_5H_{10}C(Cl)(NO) + 2NO + HCl \qquad (I)$$

was observed in our preliminary experiments and also reported by other researchers.[4] These tables show that the higher the concentration of nitrosyl chloride the larger the amount of CNC produced in the mixture. In the previous study[1], this reaction was hardly observed because the oxime hydrochloride had precipitated and the concentration of nitrosyl chloride was low.

Table I shows that no significant difference in quantum yield is present between the cases of high and low concentrations of nitrosyl chloride at 365 mμ and that an average quantum yield is 0.80 ± 0.06. Table II shows a similar tendency and an average quantum yield at 436 mμ is 0.79 ± 0.06. On the contrary, Table III shows that the quantum yield at 578 mμ is 0.77 ± 0.07 when the nitrosyl chloride concentration is high and 0.97 ± 0.13 when it is low. From these results, the following main features are obtained; (1) the quantum yield does not exceed unity, (2) the higher the concentration of nitrosyl chloride, the larger the amount of CNC produced during the reaction, and (3) the quantum yields at 365 mμ and 436 mμ are about 0.8 independent of the nitrosyl chloride concentration, while that at 578 mμ is close to unity for the low concentration and equal to 0.77 for the high concentration.

The first feature suggests that a chain mechanism is not adequate as discussed in the previous reports.[1,5] The second is to be expected on the consideration of the reaction I.

The third is very interesting and will be discussed below from the mechanistic viewpoint. Since the absorption of CNC begins at about 530 mμ and has a maximum at 650 mμ, CNC does not decompose at shorter wavelengths. However, at longer wavelengths, CNC

---

(4) E. Müller, H. G. Padeken, M. Salamon, and G. Fiedler, *Chem. Ber.*, 98, 1893 (1965).

(5) K. Fukuzawa and H. Miyama, *J. Phys. Chem.*, 72, 371 (1968).

decomposes photochemically.[6] Therefore, when the nitrosyl chloride concentration is high at a longer wavelength, CNC derived from the oxime *via* reaction I decomposes photochemically and this lowers the apparent quantum yield. Also, as proposed by Müller *et al.*,[4] there is a possibility that different mechanisms are operating at shorter and longer wavelengths.

Table III: Results at 578 mμ

Reaction time, min	NOCl, weight%	CNC, %	Quantum yield	
40	0.82	97.6	0.73	
35	0.82	95.6	0.72	
37.5	0.82		0.79	
21	0.61	92.5	0.77	
42	0.61	100	0.83	
64	0.61	98.0	0.68	
90	0.61	100	0.70	
120	0.61	96.2	0.72	
40	0.71		0.69	
40	0.71		0.68	
60	0.65	100	0.77	
61	0.65	100	0.80	
30	0.56		0.92	Av 0.77 ± 0.07
62	0.56		0.76	
91	0.56		0.83	
122	0.56		0.73	
94	0.78		0.80	
61	0.93		0.76	
63	0.81		0.82	
30	0.72		0.76	
46	0.72		0.78	
60	0.72		0.82	
73	0.62		0.75	
61	0.76		0.63	
61	0.78		0.89	
120	0.22	2.5	1.02	
180	0.22	3.9	1.09	
240	0.22	21.7	1.23	
300	0.22	14.9	1.22	
124	0.20	13.5	0.88	
180	0.20	27.9	0.87	
243	0.20	26.6	0.88	
185	0.31	24.0	1.06	
241	0.31	96.8	1.23	
30	0.20		1.00	
45	0.20	77.4	0.86	
60	0.20	78.2	0.89	
75	0.20	90.0	0.80	
91	0.20	76.1	0.85	
241	0.22	13.3	0.83	
105	0.33	29.5	1.10	
63	0.25		1.10	Av 0.97 ± 0.13
90	0.25		1.05	
120	0.25		1.05	
30	0.30		0.81	
46	0.30		0.96	
60	0.30		0.95	
30	0.32		0.72	
45	0.32		0.85	
60	0.32		1.07	
93	0.37		0.86	
91	0.37		0.81	
95	0.37		1.04	
93	0.37		0.98	
90	0.39		0.95	
90	0.39		0.97	
94	0.39		0.96	
91	0.39		0.97	

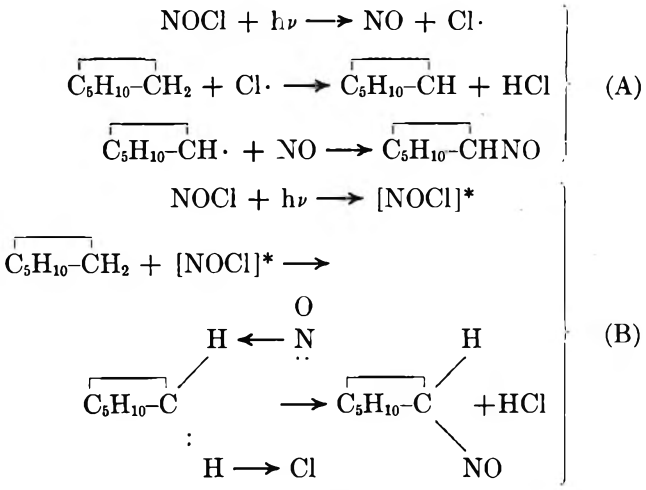

$$NOCl + h\nu \longrightarrow NO + Cl\cdot$$
$$\overline{C_5H_{10}-C}H_2 + Cl\cdot \longrightarrow \overline{C_5H_{10}-C}H + HCl \qquad (A)$$
$$\overline{C_5H_{10}-C}H\cdot + NO \longrightarrow \overline{C_5H_{10}-C}HNO$$
$$NOCl + h\nu \longrightarrow [NOCl]^*$$
$$\overline{C_5H_{10}-C}H_2 + [NOCl]^* \longrightarrow \qquad (B)$$

According to Goodeve *et al.*,[7] the clear band structure of the absorption spectrum of nitrosyl chloride (539~643 mμ) indicates that the nitrlosyl chloride molecule excited by the light of a longer wave length is stable though for only a very short time. Therefore, it may be reasonable to assume that a photo-excited molecule [NOCl]* reacts with cyclohexane to give the oxime at longer wave lengths. Both of the mechanisms (A) and (B) should give quantum yields of unity unless other side reactions occur. In this regard, the following possibilities might have to be considered with the mechanism (A).

$$NOCl + Cl \longrightarrow Cl_2 + NO \qquad (II)$$

$$\overline{C_5H_{10}-C}H_2 + Cl\cdot \longrightarrow \overline{C_5H_{10}-C}HCl + H\cdot \qquad (III)$$

Further, the chlorine molecule absorbs the light of a shorter wave length and decomposes as follows.

$$Cl_2 + h\nu \longrightarrow 2Cl\cdot \qquad (IV)$$

This is followed by a reaction (V) and the above described reactions.

$$Cl\cdot + Cl\cdot \longrightarrow Cl_2 \qquad (V)$$

All of these side reactions occurring at shorter wavelengths lower the quantum yields. On the other hand, the mechanism (B) at longer wavelengths does not give side reactions except (I) occurring at high nitrosyl chloride concentrations. Therefore the quantum yield close to unity obtained at 578 mμ with low nitrosyl chloride concentrations is not considered to be fortuitous.

Acknowledgment. The authors wish to express their thanks to Mr. Sigeshi Ozasa for his help in the experiments.

(6) E. Müller, H. Metzger, and D. Fries, *Chem. Ber.*, **87**, 1449 (1954).

(7) D. F. Goodeve and S. Katz, *Proc. Roy. Soc.*, **A172**, 432 (1939).

The Effects of a Homogeneous Chemical Reaction Preceding Electron Transfer on the Current–Time Curves and Current Integrals Obtained in Controlled-Potential Electrolysis

by Robert S. Rodgers[1] and Louis Meites[1,2]

Department of Chemistry, Polytechnic Institute of Brooklyn, Brooklyn, New York *(Received July 17, 1969)*

This paper deals with controlled-potential electrolyses in which an elctroactive substance Ox is formed from an inactive substance Y by a homogeneous chemical reaction and then undergoes a mass-transfer-controlled reduction at the electrode surface. When the occurrence of the homogeneous reaction can be detected, its extent in the diffusion layer will generally be negligible. It is shown how the rate and equilibrium constants of this reaction affect the slopes of the two straight lines into which a plot of ln *i* *vs.* *t* can be dissected and the partial current integrals corresponding to these lines.

Introduction

Recent research in our laboratory has prompted a closer examination of the current–time curves and current integrals obtained in the controlled-potential electroreduction of an electroactive species, Ox, in slow equilibrium with an electroinactive species Y

$$\mathrm{Y} \underset{k_b}{\overset{k_f}{\rightleftarrows}} \mathrm{Ox} \xrightarrow{+ne} \mathrm{Red} \tag{1}$$

It has already been shown[3,4] that a plot of log *i* *vs.* *t* can be dissected into two straight lines, since

$$i = C_1 \exp(R_1 t) + C_2 \exp(R_2 t) \tag{2}$$

There has, however, been no formal consideration of either the current integrals that correspond to the two linear segments or the reaction within the diffusion layer. Both of these matters are considered here on the basis of the mathematical model of Karp and Meites.[5]

Previous treatments of the mechanism described by eq 1 were based on the Nernst diffusion-layer assumption. This assumes that the concentration profiles of Ox and Red are linear within the unstirred diffusion layer next to the electrode surface. This is equivalent to assuming that there is no interconversion of Y and Ox within the diffusion layer. In fact, however, when the rate of the chemical reaction is comparable to the rate of mass transport, much of the current arises from the reduction of Ox produced chemically within the diffusion layer. When this is so, the concentration profile of Ox cannot be linear within the diffusion layer.

Theory

Karp and Meites[5] outlined a mathematical treatment that takes account of reactions occurring within the diffusion layer and does not assume that the concentration profiles within that layer are always linear. In this paper their treatment is applied to the mechanism described by eq 1. We assume that the electrolysis is carried out on the plateau of the wave of Ox, so that the electron-transfer step is very rapid.

Karp and Meites assume that the solution is homogeneous everywhere except within a layer δ cm thick adjacent to the electrode surface. The concentrations of Ox and Y in the bulk of the solution, where $x > \delta$, are given by

$$\frac{\mathrm{d}C_{\mathrm{Ox}}^{\mathrm{b}}}{\mathrm{d}t} = k_f C_{\mathrm{Y}}^{\mathrm{b}} - k_b C_{\mathrm{Ox}}^{\mathrm{b}} - \frac{DA}{V}\left(\frac{\partial C_{\mathrm{Ox}}}{\partial x}\right)_{x=\delta^-} \tag{3}$$

$$\frac{\mathrm{d}C_{\mathrm{Y}}^{\mathrm{b}}}{\mathrm{d}t} = -k_f C_{\mathrm{Y}}^{\mathrm{b}} + k_b C_{\mathrm{Ox}}^{\mathrm{b}} - \frac{DA}{V}\left(\frac{\partial C_{\mathrm{Y}}}{\partial x}\right)_{x=\delta^-} \tag{4}$$

C is a concentration in mol-cm^{-3}, k_f and k_b are first- or pseudo-first-order rate constants in sec^{-1}, V is the volume of the solution in cm^3, and A is the electrode area in cm^2. The diffusion coefficients of Y and Ox are assumed to be equal and are both represented by D (cm^2-sec^{-1}). The superscript b denotes the bulk of the solution, and the subscript $x = \delta^-$ denotes that the "left derivative" of C is to be evaluated.

Within the diffusion layer, $0 < x < \delta$, the concentrations are given by

$$\frac{\partial C_{\mathrm{Ox}}}{\partial t} = D\frac{\partial^2 C_{\mathrm{Ox}}}{\partial x^2} + k_f C_{\mathrm{Y}} - k_b C_{\mathrm{Ox}} \tag{5}$$

---

[1] Department of Chemistry, Clarkson College of Technology, Potsdam, N. Y. 13676.

[2] To whom correspondence and requests for reprints should be addressed.

[3] A. J. Bard and E. Solon, *J. Phys. Chem.*, **67**, 2326 (1963).

[4] R. I. Gelb, B.S. in Chem. Thesis, Polytechnic Institute of Brooklyn, 1963; R. I. Gelb and L. Meites, *J. Phys. Chem.*, **68**, 630 (1964).

[5] S. Karp and L. Meites, *J. Electroanal. Chem.*, **17**, 253 (1968).

$$\frac{\partial C_{\mathrm{Y}}}{\partial t} = D\frac{\partial^2 C_{\mathrm{Y}}}{\partial x^2} - k_{\mathrm{f}}C_{\mathrm{Y}} + k_{\mathrm{b}}C_{\mathrm{Ox}} \tag{6}$$

subject to the following boundary conditions

$$\left.\begin{aligned}
&C_{\mathrm{Ox}}(x = 0) = 0\\
&C_{\mathrm{Y}}(x = 0) = C_{\mathrm{Y}}^*\\
&C_{\mathrm{Ox}}(x = \delta) = C_{\mathrm{Ox}}^{\mathrm{b}}\\
&C_{\mathrm{Y}}(x = \delta) = C_{\mathrm{Y}}^{\mathrm{b}}\\
&\left(\frac{\partial C_{\mathrm{Ox}}}{\partial x}\right)_{x=0} = \frac{i}{nFAD}\\
&\left(\frac{\partial C_{\mathrm{Y}}}{\partial x}\right)_{x=0} = 0
\end{aligned}\right| \tag{7}$$

where C_{Y}^* denotes the concentration of Y at the surface of the electrode.

Karp and Meites assumed that if the volume $A\delta$ of the diffusion layer is much smaller than the total volume V a steady-state approximation may be made by equating the left-hand sides of eq 5 and 6 to zero. This implies that the shape of the concentration profile remains unchanged throughout the electrolysis. Koutecký and Levich[6] made an almost equivalent assumption in deriving an expression for the limiting current observed with a rotating disc electrode for the mechanism described by eq 1. Their solution corresponds to $t = 0$ here and gives no information about the course of the current-time curve or the behaviors of the partial current integrals, and their method of solution does not permit the use of any of their intermediate equations.

Combining eq 5 and 6 with the boundary conditions of eq 7, and defining $R = [(k_{\mathrm{f}} + k_{\mathrm{b}})/D]^{1/2}$ and $K = k_{\mathrm{f}}/k_{\mathrm{b}} = C_{\mathrm{Ox}}(x,0)/C_{\mathrm{Y}}(x,0)$ [the second of these equalities is equivalent to assuming that the solution is at equilibrium when the electrolysis is begun], we obtain $C_{\mathrm{Ox}}(x,t)$ as a function of the time-dependent variables $C_{\mathrm{Ox}}^{\mathrm{b}}$, $C_{\mathrm{Y}}^{\mathrm{b}}$, C_{Y}^*, and i

$$C_{\mathrm{Ox}}(x,t) = \frac{i\sinh(Rx)}{nFDAR(1 + K)} - \frac{KC_{\mathrm{Y}}^*}{1 + K}\cosh(Rx) + \frac{Kix}{nFDA(1 + K)} + \frac{KC_{\mathrm{Y}}^*}{1 + K} \tag{8}$$

and further

$$\frac{i\delta}{nFDA} + C_{\mathrm{Y}}^* = C_{\mathrm{Ox}}^{\mathrm{b}} + C_{\mathrm{Y}}^{\mathrm{b}} \tag{9}$$

Equation 8 can be differentiated with respect to x to obtain $(\partial C_{\mathrm{Ox}}/\partial x)_{x=\delta^-}$. Then, since

$$\left(\frac{\partial C_{\mathrm{Ox}}}{\partial x}\right)_{x=\delta} + \left(\frac{\partial C_{\mathrm{Y}}}{\partial x}\right)_{x=\delta^-} = \frac{i}{nFDA} \tag{10}$$

descriptions of the time dependences of $C_{\mathrm{Ox}}^{\mathrm{b}}$, $C_{\mathrm{Y}}^{\mathrm{b}}$, and i can be obtained from eq. 3, 4, 8, and 9.

Defining

$$M = \frac{\sinh(R\delta)}{(1 + K)R\delta} + \frac{K}{1 + K}\cosh(R\delta) \tag{11a}$$

$$L = {}^1/_2\left[(\beta + k_{\mathrm{f}})\cosh(R\delta) + \frac{k_{\mathrm{b}} + \dfrac{\beta K(R\delta)^2}{1 + K}}{R\delta}\sinh(R\delta)\right] \tag{11b}$$

and

$$N = \frac{\beta^2 KR\delta}{1 + K}\sinh(R\delta) + \beta k_{\mathrm{f}}\cosh(R\delta) \tag{11c}$$

where the mass-transfer constant β is given by $\beta = DA/V\delta$, the time dependence of the current becomes

$$\frac{i}{nF} = Q_1S_1e^{-S_1t} + Q_2S_2e^{-S_2t} \tag{12}$$

where

$$S_1 = \frac{L + \sqrt{L^2 - MN}}{M} \tag{13a}$$

$$S_2 = \frac{L - \sqrt{L^2 - MN}}{M} = \frac{2L}{M} - S_1 \tag{13b}$$

and Q_1 and Q_2 are the current integrals that correspond to the two linear segments into which the plot of ln i *vs.* t can be dissected. Furthermore,

$$\frac{Q_2}{Q_\infty} = \frac{S_1M - \dfrac{K\beta\cosh(R\delta)}{K + 1}}{2\sqrt{L^2 - MN}} \tag{14}$$

The solution is assumed to be at equilibrium at the start of the electrolysis.

It is instructive to examine the nature of the current-time curve when $R\delta$ is essentially zero, so that $\cosh(R\delta) = 1$, $\sinh(R\delta) = R\delta$, $M = 1$, $L = (k_{\mathrm{f}} + k_{\mathrm{b}} + \beta)/2$, and $N = k_{\mathrm{f}}\beta$. The reaction within the diffusion layer is then inconsequential, and eq 12 becomes

$$\frac{i}{nFC^0V} = \frac{K}{K + 1}\left\{\left[\frac{1}{2} - \frac{k_{\mathrm{f}} + k_{\mathrm{b}} - \beta}{4\sqrt{L^2 - k_{\mathrm{f}}\beta}}\right] \times \exp(-L - \sqrt{L^2 - k_{\mathrm{f}}\beta}) + \left[\frac{1}{2} + \frac{k_{\mathrm{f}} + k_{\mathrm{b}} - \beta}{4\sqrt{L^2 - k_{\mathrm{f}}\beta}}\right] \times \exp(-L + \sqrt{L^2 - k_{\mathrm{f}}\beta})\right\} \tag{15}$$

where C^0 denotes the sum of the initial bulk concentrations of Y and Ox. This is identical with an equation given by Bard and Solon.

Figure 1 shows how the ratio S_2/β depends on k_{f}/β when $R\delta = 0$ for several values of the equilibrium constant K. The quantity S_2 is the absolute value of the slope of the second, less steep, straight-line segment of a

---

(6) J. Koutecký and V. G. Levich, *Zh. Fiz. Khim.*, **32**, 1565 (1958).

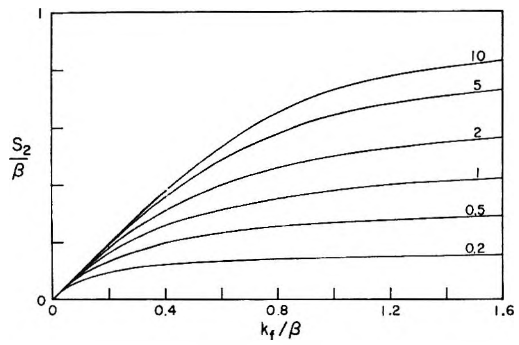

Figure 1. Variation of S_2/β with k_f/β when no reaction occurs in the diffusion layer, so that $R\delta = 0$. The value of the equilibrium constant, $K = [\mathrm{Ox}]/[\mathrm{Y}]$, is given next to each curve.

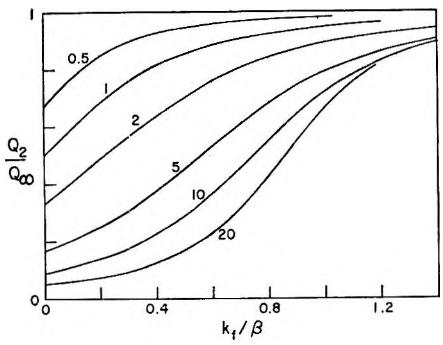

Figure 2. Variation of Q_2/Q_∞ with k_f/β when no reaction occurs in the diffusion layer, so that $R\delta = 0$. The value of the equilibrium constant, $K = [\mathrm{Ox}]/[\mathrm{Y}]$, is given next to each curve.

plot of ln i *vs.* t. If k_f/β is small, $S_2 = k_f$, as intuitively expected. The current late in the electrolysis is then controlled only by the rate at which Y is transformed into the electroactive species Ox. However, S_1, the absolute value of the slope of the steeper linear component of the plot, is given by $S_1 = k_b + \beta$, and thus exceeds β. This is implicit in, but is not clearly indicated by, Figure 4 of the paper by Bard and Solon.[3] If K is fixed, the effect of the reverse reaction becomes more pronounced as k_f and k_b increase, and the value of S_2/β asymptotically approaches $1/(1 + K)$, which is the value expected for a fast preceding equilibrium.

Figure 2 shows how the current integral Q_2, which corresponds to the second linear segment of the plot of ln i *vs.* t, varies with k_f/β when $R\delta = 0$. When $k_f/\beta \ll 1$, Q_2 differs very little from the value that would correspond to the reduction of the Y present initially. Under these conditions it is easy to evaluate K with the aid of current–time data, as was done by Ficker and Meites.[7] However, as k_f/β increases Q_2 deviates more and more from the value corresponding to the initial equilibrium concentration of Y, and the equilibrium constant computed from the current integrals becomes smaller than the true value.

The extent of the reaction within the diffusion layer becomes important either if δ is very large, as is likely to be the case if β is small, or if $k_f + k_b$ is much larger than β. If $(k_f + k_b)/\beta$ is large, Figures 1 and 2 show that Q_2 is essentially equal to the total current integral Q_∞. A plot of ln i *vs.* t consists of a single straight line, whose slope is numerically smaller than β. The concentration of Ox is smaller with the diffusion layer than it is in the bulk of the solution. Hence the rate of the backward reaction is smaller, and the overall rate of disappearance of Y is higher, in the diffusion layer than in the bulk. The slope of a plot of ln i *vs.* t therefore exceeds that predicted by Figure 1, where the reaction within the diffusion layer is insignificant.

Similar effects are noted when $\delta A/V$ is large. Even if it is as large as 0.01, however, the slopes and current integrals differ by less than 2% from those predicted by eq 15, provided that k_f/β does not exceed 1 and that K does not exceed 0.1. If K has a smaller value, a plot of ln i *vs.* t consists of only one straight line if k_f/β is large enough for the reaction in the diffusion layer to be important, and the observations will again agree with the predictions of eq 15. Thus the reaction within the diffusion layer is generally unimportant; it does not change the form of the current–time curve, and it affects the magnitude of the current only when the reaction rates greatly exceed the rate of mass transport. Similarly, Karp and Meites[5] showed that the extent of the chemical reaction occurring within the diffusion layer in an ECE mechanism could be neglected whenever the occurrence of that reaction could be detected at all.

Conclusions

These calculations imply that it will usually be possible to ignore the extent of the chemical reaction within the diffusion layer, and thus to evaluate the equilibrium constant of that reaction in the simple fashion described by Ficker and Meites in most cases where the occurrence of the reaction can be deduced from the current–time curve. As an antidote to excessive optimism, however, it may be pointed out that the range of applicability of the technique is inherently quite narrow.

If K is smaller than about 10^{-2} or larger than about 10^2, so that the initial equilibrium concentrations of Y and Ox are widely disparate, the presence of one of them is likely to escape notice. Even if $K = 1$, if k_f/β is smaller than about 10^{-3} the second segment of a plot of ln i *vs.* t may be cloaked by the background current. These things being so, it is plain that great care is necessary to ensure that the reaction within the diffusion layer can be neglected in any practical case. The corrections that must be applied when it cannot be neglected may be deduced from eq 11, 12, and 13.

---

(7) H. K. Ficker and L. Meites, *Anal. Chim. Acta*, 26, 172 (1962).

Direct Determination of the Extinction Coefficients For Triplet ← Triplet Transitions in Naphthalene, Phenanthrene, and Triphenylene

by Steven G. Hadley and Richard A. Keller

National Bureau of Standards, Washington, D. C. 20234 *(Received June 6, 1969)*

Extinction coefficients for triplet ← triplet absorption have been directly determined for several aromatic hydrocarbons. A high intensity photolysis lamp was used to populate the triplet state and the concentration of triplets was measured by monitoring the depletion of the ground state. The values of the extinction coefficients $\epsilon \times 10^{-4}$ (l. mol^{-1} cm^{-1}) and their estimated uncertainties at the most prominent maximum λ(nm) are: naphthalene-h_8, 4.0 ± 0.6, 414.0; naphthalene-d_8, 4.0 ± 0.6, 414.0; phenanthrene-h_{10}, 3.8 ± 0.6, 492.5; phenanthrene-d_{10}, 3.1 ± 0.5, 492.5; triphenylene-h_{12}, 1.56 ± 0.23, 430.0; and triphenylene-d_{12}, 1.20 ± 0.18, 431.0. For anthracene, $\epsilon_T \geq 9 \times 10^4$ l. mol^{-1} cm^{-1} at 427.3 nm.

Introduction

In this paper we wish to report the direct determination of the extinction coefficients for the strong triplet ← triplet absorption bands, located in the visible region, for the perhydro- and the perdeuterionaphthalenes, -phenanthrenes, -anthracenes, and -triphenylenes. Optical absorptions arising from the metastable triplet state have been the subject of considerable interest over the last two decades. Lower and El-Sayed[1] have reviewed the field through 1964. Little attention has been given to the measurement of the extinction coefficients of these transitions, largely because of the difficulty in determining the concentration of triplets.

Previously we have reported values of these extinction coefficients for four of the above compounds using an indirect method.[2] It is relatively easy to measure the optical density of these bands, but quite difficult to determine the concentration of triplets. Our indirect method required knowledge of the intersystem crossing quantum yield for each of the compounds. As we noted,[2] values of the extinction coefficient obtained in this fashion could be in error due to uncertainty in the intersystem crossing quantum yield. The independent determination of the triplet ← triplet extinction coefficients described here can be combined with our previous technique[2] to directly determine the intersystem crossing yields.[3]

A much more direct approach has been used to measure the extinction coefficients of the triplet ← triplet absorption in the present work. The concentration of triplets has been measured by observing the depopulation of the ground state and assuming that all molecules pumped out of the ground state are in the lowest triplet state. The depopulation was observed by measuring the change in the optical density of the singlet ← singlet absorption following a high intensity light pulse. The time dependence of the singlet ← singlet and triplet ← triplet absorption were simultaneously measured. The technique has the advantage that photochemical decomposition does not interfere with the measurements.

Experimental Section

Preparation of Samples. The perhydronaphthalene, -phenanthrene, and -anthracene were zone refined materials purchased from James Hinton.[4] They were used as received. Perhydrotriphenylene was zone refined in these laboratories. Perdeutero-napthalene, -phenanthrene, and -triphenylene were purchased from Merck Sharp and Dohme, Ltd [4] and were used after sublimation. Perdeuterioanthracene was a gift of W. Siebrand of the National Research Council of Canada. It had been extensively purified and was used as received.

Typical solute concentrations were 10^{-4} to 10^{-6} mol l.$^{-1}$ in a mixture of 30% n-butanol and 70% isopentane, by volume. The solvents were purchased from the Hartman–Leddon, Co.,[4] and were used as received. At 77°K this mixture freezes to a clear rigid glass. Due to solvent contraction, the solute concentration increased by a factor of 1.26 upon cooling from 300 to 77°K.[5] The solute concentration was adjusted so that the optical density of the solution was approximately 0.5 at the maximum of the singlet ← singlet absorption where the depletion was measured.

Apparatus. The apparatus was arranged as shown in Figure 1. The sample was contained in a dewar similar to the one previously described.[2] No liquid

---

(1) S. K. Lower and M. A. El-Sayed, *Chem. Rev.*, **66**, 199 (1966).

(2) R. A. Keller and S. G. Hadley, *J. Chem. Phys.*, **42**, 2382 (1965).

(3) S. G. Hadley and R. A. Keller, *J. Phys. Chem.*, **73**, 4356 (1969).

(4) Certain commercial instruments and materials are identified in this paper in order to adequately specify the experimental procedure. In no case does such identification imply recommendation or endorsement by the National Bureau of Standards, nor does it imply that the instruments or materials identified are necessarily the best available for the purpose.

(5) H. E. Rast, Ph.D. dissertation, University of Oregon, 1964.

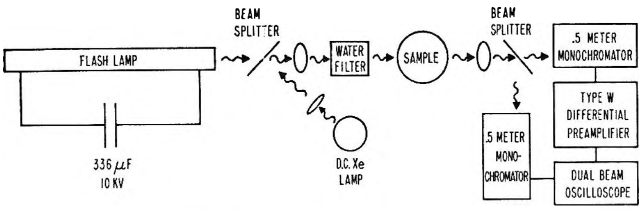

Figure 1. Experimental apparatus used to measure extinction coefficients of triplet ← triplet absorptions.

nitrogen was in the light path. The flash lamp[6] was constructed from a 30 in. long, 1.5 in. o.d., $^1/_8$ in. wall alumina tube with stainless steel electrodes affixed to each end with epoxy resin. The windows were sapphire, 2 in. diameter by $^1/_8$ in. thick. It was found that quartz windows were pitted so badly that they had to be discarded after each discharge of the lamp. After each flash the sapphire windows were removed and cleaned of deposited alumina and electrode material. The capacitor bank contained fourteen 24-μF capacitors obtained from the Telegraph Condenser Co., Ltd.[4] They were connected in parallel, joined together with $^1/_4$-in. by 1-in. copper bars bolted to the electrodes. When charged to 10 kV, the bank held over 16,000 J. The lamp was discharged at this energy to give a light pulse with a $1/e$ width of less than 10^{-4} sec.

Chemical actinometry[7] showed that the lamp's output at wavelengths <400 mm was between 10^{16} and 10^{17} quanta/flash cm^2 into the dewar.

The analytical beam radiation was supplied by a high pressure dc Xe lamp[4] powered by three 12-V automobile batteries. The total noise was less than 1% of the signal when measured with a RC time constant of 2×10^{-3} sec. The time constant of the electronic equipment used in the measurements was always less than 10% of the triplet state lifetime.

Jarrell Ash 0.5-m monochromators[4] were used with either 1P28 or 931A photomultiplier tubes. The monochromator slits were kept narrow compared with the bands being observed. A Corning 7-54 ultraviolet transmitting,[4] visible absorbing filter was used to reduce scattered visible light to a negligible value during the ultraviolet measurements. The beam splitters were quartz windows. This apparatus has the advantage that both the pumping and absorption measurements are made along the same optical axis. Also, both the triplet concentration and triplet ← triplet absorption optical density are determined at the same time. Erroneous optical density measurements can occur if the triplet concentration is not uniform over the area being sampled by the analytical beam. Special care was taken to align the components so that the pumping beam and the analytical beam were coaxial. An Ne–He gas laser was used in this alignment.

A dual-beam oscilloscope was used in measuring the optical densities. The signal from the first monochromator was fed into a Tektronix Type W high gain differential comparator preamplifier[4] to measure the change in the singlet ← singlet absorption due to depletion. Optical density changes as small as 0.005 could be measured in this fashion. The second monochromator monitored the triplet ← triplet absorption. Due to the high optical density of this absorption, a standard preamplifier was used on the second beam. The oscilloscope sweep was triggered by a signal from a photocell activated by light from the flash lamp. Data were taken from photographs of the oscilloscope display.

Procedure. Triplet ← triplet absorption has been observed to overlap the singlet ← singlet absorption. This complicates the measurement of the depletion. In the Appendix it has been shown that[8]

$$\mathrm{OD}(t) = \log \frac{I(\infty)}{I(t)} = (\epsilon_\mathrm{T} - \epsilon_\mathrm{S})C_\mathrm{T}^0 d \exp(-t/\tau_\mathrm{T}) \qquad (1)$$

Here ϵ_T and ϵ_S are the extinction coefficients for triplet ← triplet and singlet ← singlet absorption at a particular wavelength, respectively. C_T^0 is the concentration of triplet state molecules immediately after the pumping lamp is fired. d is the path length and τ_T is the triplet state lifetime. $I(\infty)$ is the intensity of the transmitted beam at a time such that $t \gg \tau_\mathrm{T}$. $I(t)$ is the intensity of the transmitted beam at a time t.

The initial concentration of triplets, C_T^0, can be calculated using eq 1. A value of $(\epsilon_\mathrm{T}^\lambda - \epsilon_\mathrm{s}^\lambda)C_\mathrm{T}^0$ at a particular wavelength λ can be obtained from a plot of log [OD] (t)] *vs.* t. By performing three separate measurements of OD ($t = 0$) at three different wavelengths, λ_1, λ_2, λ_3, one at a singlet ← singlet absorption peak and one at the bottom of the trough on each side, three simultaneous equations are obtained.

$$(\epsilon_\mathrm{T}^{\lambda 1} - \epsilon_\mathrm{S}^{\lambda 1})C_\mathrm{T}^0 d = A \qquad (2)$$

$$(\epsilon_\mathrm{T}^{\lambda 2} - \epsilon_\mathrm{S}^{\lambda 2})C_\mathrm{T}^0 d = B \qquad (3)$$

$$(\epsilon_\mathrm{T}^{\lambda 3} - \epsilon_\mathrm{S}^{\lambda 3})C_\mathrm{T}^0 d = D \qquad (4)$$

By assuming that ϵ_T changes in a linear fashion over the region of the singlet ← singlet absorption, a fourth relationship is obtained

$$(\epsilon_\mathrm{T}^{\lambda 1} - \epsilon_\mathrm{T}^{\lambda 2})/(\epsilon_\mathrm{T}^{\lambda 3} - \epsilon_\mathrm{T}^{\lambda 2}) = (\lambda_1 - \lambda_2)/(\lambda_3 - \lambda_2) \qquad (5)$$

This system of equations can be solved for C_T^0. Under our experimental conditions, the triplet ← triplet bands are from two to three times wider than the singlet–singlet bands. Thus, the assumption of a linear charge in ϵ_T with λ over this small range seems reasonable. The accuracy of this assumption will be demonstrated below. C_T^0 was calculated by solving the system of eq 2, 3, 4, and 5.

Three different flashes of the pumping lamp are

---

(6) L. J. Schoen, *J. Chem. Phys.*, **45**, 2773 (1966).

(7) C. G. Hatchard and C. A. Parker, *Proc. Roy. Soc.*, **A235**, 518 (1956).

(8) Similar considerations are discussed by W. R. Dawson, *J. Opt. Soc. Amer.*, **58**, 222 (1968).

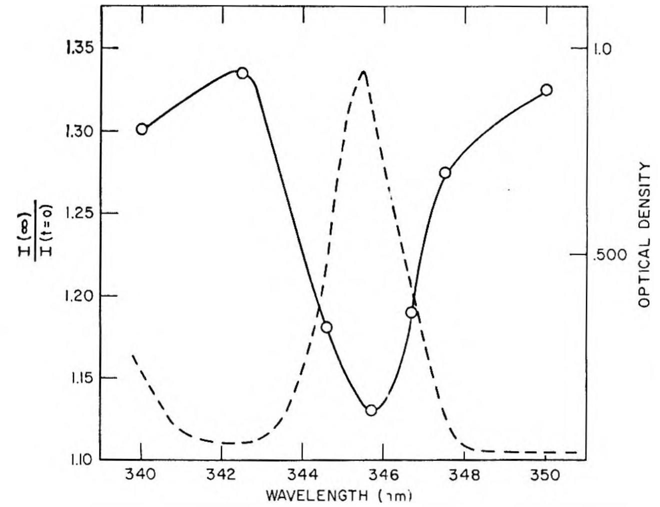

Figure 2. Singlet depletion as a function of wavelength in the region of strong singlet absorption. Singlet ← singlet depletion, ——; singlet ← singlet absorption, - - - -. Left ordinate applies to singlet ← singlet depletion; right ordinate applies to singlet ← singlet absorption.

necessary to obtain A, B, and D. These values are corrected to constant flash intensity by using the data obtained from the second monochromator which monitors the triplet ← triplet absorption. These corrections amounted to not more than ± 10%.

Typical experiment data are presented in Figure 2. $I(\infty)/I(t=0)$ has been plotted as a function of wavelength over the first band in the singlet ← singlet absorption spectrum of phenanthrene-h_{10}. The singlet ← singlet absorption spectrum in this region is also shown. The behavior predicted by eq 1 is followed. It should also be noted that the value of $I(\infty)/I(t=0)$ has about the same value at 342 nm as it does at 350 nm. ϵ_S has about the same value at these two wavelengths, so we can conclude that ϵ_T is also about the same at these two wavelengths. Thus, the assumption of a linear change of ϵ_T over this small wavelength region (28 nm) is justified.

The value of C_T^0 for phenanthrene-h_{10} can be calculated as outlined above by making measurements at 342 nm, 345.5 nm and 350 nm, respectively, and correcting for variations in the flash lamp intensity. The simultaneously measured value of the optical density of the strong triplet ← triplet absorption at 492.5 nm, when used with the value of C_T^0, yields a value of ϵ_T at 492.5 nm.

Results

In Table I are shown the values of the extinction coefficients of the triplet ← triplet absorption and the wavelength of the maximum at which they were determined. All values are at 77°K in a rigid glass. The oscillator strengths were computed by changing the previously reported oscillator strengths[2] by the same factor that the extinction coefficients were observed to change. For reference, the triplet ← triplet absorption spectra of naphthalene, phenanthrene, and triphenylene are shown in Figure 3 with the extinction coefficients reported in this work. Typical ground state depletions were about 3% for naphthalene, 13% for phenanthrene, 9% for triphenylene, and 42% for anthracene.

To check the validity of assuming a linear change in ϵ_T over the region where the ground-state depletion was measured, the concentration of triplet state molecules was determined over two different singlet ← singlet absorption regions for the perhydro- and perdeuterionaph-

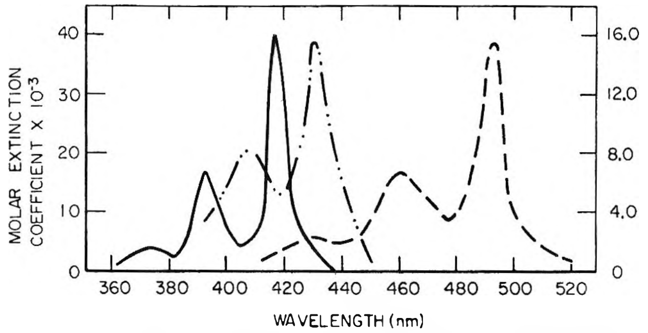

Figure 3. Triplet ← triplet absorption spectra: naphthalene, ——, phenanthrene, - - - -; triphenylene, —·—: Left ordinate applies to naphthalene and phenanthrene, right ordinate applies to triphenylene.

Table I: Extinction Coefficients of Triplet ← Triplet Absorption

Molecule	$\epsilon_T \times 10^{-4}$ l. mol^{-1} cm$^{-1\,a,b}$	λ_T, nm^c	λ_S, nm^c	Triplet oscillator strengths	τ, s^d
Naphthalene-h_8	4.0 ± 0.6	414.0	310.9	0.14	2.3
Naphthalene-d_8	4.0 ± 0.6	414.0	309.7		13.5
Phenanthrene-h_{10}	3.8 ± 0.6	492.5	345.3	0.15	3.4
Phenanthrene-d_{10}	3.1 ± 0.5	492.5	344.7		12.2
Triphenylene-h_{12}	1.56 ± 0.23	430.0	334.3	0.11	13.8
Triphenylene-d_{12}	1.20 ± 0.18	431.0	334.1		17.3

[a] Log of (I_0/I) to the base ten was used to compute these values. [b] Estimated error. [c] Wavelength of maximum absorption, λ_T, and wavelength of band where depletion was measured, λ_S. [d] Error extimated at ±20%. These values are included for reference only. Data were not taken over sufficient time interval to make the numbers particularly accurate. [e] λ_S refers to the band which was used to measure the depletion.

thalenes and -triphenylenes. It was found that the extinction coefficients determined at two different singlet ← singlet bands were the same within the experimental error. The phenanthrenes were studied at only one singlet ← singlet absorption region because the triplet ← triplet extinction coefficient was constant over the region where the depletion was measured.

The rate of depopulation of the lowest triplet state was found to be equal to the rate of repopulation of the ground state singlet for the perhydro- and perdeuterionaphthalenes, -phenanthrenes and -triphenylenes. This indicates that is is most likely that the only state involved in the depopulation is the triplet state. Any state with a lifetime much shorter than τ_T will not affect our measurements as this state will have decayed to the ground state before the concentration of singlets was measured. No measurable depopulation with a lifetime much greater than τ_T (such as photochemical decomposition) was observed. In all cases, for the above molecules the OD of the sample before the flash was equal to the OD of the sample ten triplet-state lieftimes after the flash.

However, for perhydro- and perdeuterioanthracene it was observed that the ground state was repopulated faster than the triplet was depopulated. Evidently, some process other than triplet → ground state decay was repopulating the ground state with a lifetime somewhat shorter than τ_T. No permanent changes in the sample were observed. In an attempt to reduce the possibility of photoionization the solvent was changed to 3-methylpentane and a Corning 0-54 filter[4] was inserted immediately behind the flash lamp. This filter absorbs all radiation more energetic than 32,000 cm^{-1}. These changes were found to have no effect on the results. The ground state was still repopulated faster than the triplet state was depopulated even though processes more energetic than 47,000 cm^{-1} were very unlikely. $E_T + 32{,}000\ \text{cm}^{-1}$ is less than 47,000 cm^{-1}. Even with this difficulty our measurements show that $\epsilon_T \geq 9 \times 10^4\ \text{l. mol}^{-1}\ \text{cm}^{-1}$ at 427.3 nm. Note that the technique of measuring the rate of repopulation of the ground state enabled us to detect this extraneous process. This process would not have been detected with steady-state measurements and would have lead to an error in the results.

The error in this work has been estimated at ±15%. This results largely from the rather small magnitude of the singlet ← singlet absorption and subsequent difficulties in obtaining data. The values of ϵ_S used in the calculation are also uncertain to about ±5%. This is due to both the uncertainty in concentration of solute arising from contraction of the solvent upon cooling and the uncertainty in the optical density values needed to calculate it. It is reassuring that the extinction coefficients for the perhydro and perdeuterio forms are identical within the experimental error. The wavelength of the triplet ← triplet absorption maximum is uncertain within about ±0.5 nm, due to the broad nature of the absorption. The chief error that could enter into these measurements would be nonuniform triplet distribution over the monitoring beam. This can occur when the excitation and analytical beams are not on the same optical axis. Special care was taken to align the components so that the two beams were coaxial.

A systematic error can occur in these experiments due to the special photoselected nature of the system produced. The flash lamp preferentially selects those molecules whose singlet ← singlet transition moments are parallel to electric vector of the pumping radiation. This results in a nonrandom distribution in both the remaining singlet state molecules and in the triplet state molecules. It can be shown that when nonpolarized light is used in the measurements these effects are less than 10%.[2]

Discussion

In Table II the results obtained in this work have been compared with other recent data. The values of Brinen[9] were obtained using an esr technique for measuring the concentration of triplet state molecules. His experimental conditions were similar to ours. Within the experimental uncertainty, our values and Brinen's are in very good agreement. Lavalette[10] has also measured the extinction coefficients of these bands using the technique of McClure.[11] His values are in fairly good agreement. Astier and Meyer[12] have recently reported values of $\epsilon_T = 4.5 \pm 0.5 \times 10^4\ \text{l. mol}^{-1}\ \text{cm}^{-1}$ for naphthalene. This was determined under experimental conditions similar to ours. They also used a ground state depletion measurement to determine the concentration of triplets. For anthracene they report $\epsilon_T = 9 \times 10^4\ \text{l. mol}^{-1}\ \text{cm}^{-1}$. Their experimental technique did not permit measurement of the lifetime of the triplet state or the rate of repopulation of the ground state.

E. J. Land[13] has published values of ϵ_T for several aromatic hydrocarbons based upon an energy transfer technique. The values are listed in Table II. His values are all relative to the extinction coefficient of the benzophenone ketyl radical. There appears to be some doubt as to the value of the standard in this work. Bowers and Porter[14] have used a technique similar to ours, except that they performed their studies in liquid paraffin at room temperature. The only molecule where a comparison can be made to our work is phenanthrene-h_{10}. Their value of ϵ_T is $2.4 \pm 0.2 \times 10^4\ \text{l. mol}^{-1}\ \text{cm}^{-1}$ which is to be compared with our value of $3.8 \pm 0.6 \times 10^4\ \text{l. mol}^{-1}\ \text{cm}^{-1}$. The difference may very

---

(9) J. S. Brinen, *J. Chem. Phys.*, **49**, 586 (1968).

(10) D. Lavalette, *Compt. Rend.*, **279**, (1968).

(11) D. S. McClure, *J. Chem. Phys.*, **19**, 670 (1951).

(12) R. Astier and Y. H. Meyer in "The Triplet State," A. B. Zahlan, *et al.*, Ed., Cambridge University Press, London, 1967.

(13) E. J. Land, *Proc. Roy. Soc.*, **A305**, 457 (1968).

(14) P. G. Bowers and G. Porter, *ibid.*, **A299**, 348 (1967).

Table II: Comparison of Reported ϵ_T Values[g]

Molecule	This work[a]	Brinen[b,c]	D. Lavalette[d,f]	Others
Naphthalene-h_8	4.0 ± 0.6			2.26 ± 0.56[b]
Naphthalene-d_8	4.0 ± 0.6	3.19	2.33 ± 0.65	4.5[c]
Phenanthrene-h_{10}	3.8 ± 0.6	4.15		2.10 ± 0.52[e,b]
Phenanthrene-d_{10}	3.1 ± 0.5	4.29	2.04 ± 0.11	2.4 ± 0.2[f,b]
Triphenylene-h_{12}	1.56 ± 0.23	1.65	1.68 ± 0.03	
Triphenylene-d_{12}	1.20 ± 0.18			

[a] Estimated error. [b] Estimated uncertainty of ±20%. [c] J. S. Brinen, *J. Chem. Phys.*, **49,** 586 (1968). [d] D. Lavalette, *Compt. Rend.*, 279 (1968); [e] E. J. Land, *Proc. Roy. Soc.* **A305,** 457 (1968). [f] Significance of stated error not clearly specified by authors. [g] l. mol^{-1} cm^{-1} × 10^4. [h] P. G. Bowers and G. Porter, *Proc. Roy. Soc.* **A299,** 348 (1967). [i] R. Astier and Y. H. Meyer, in "The Triplet State," A. B. Zahlan, *et al.*, Ed., Cambridge University Press, London, 1967.

well be due to the sharpening of the band at the lower temperature, which will increase the value of the extinction coefficient. Bowers and Porter report a value of $\epsilon_T = 6.3 \pm 0.5 \times 10^4$ l. mol^{-1} cm^{-1} for anthracene-h$_{10}$ while we report $\epsilon_T > 9 \times 10^4$ l. mol^{-1} cm^{-1}. Direct comparisons are more difficult here, however the difference may very well be due to the difference in temperature in the two experiments.

Conclusions

A technique has been developed making possible the accurate determination of triplet ← triplet extinction coefficients. All quantities needed in the calculation of these extinction coefficients can be experimentally determined; no assumption regarding quantum yields or relative measurements are needed. It is applicable to molecules which have a triplet state lifetime as short as 1×10^{-3} seconds. Overlapping absorption from either photochemical decomposition or triplet ← triplet absorption has no effect.

In a following publication we report on values of the singlet → triplet intersystem crossing quantum yields using these extinction coefficients.

Acknowledgment. The authors wish to thank the many members of the staff of the National Bureau of Standards for the loan of much of the equipment used in this work.

Appendix

For a mixture of singlet and triplet molecules absorbing at the same wavelength Beer's Law is

$$\log \frac{I_0}{I} = (\epsilon_S C_S + \epsilon_T C_T)d \qquad (6)$$

where ϵ_S and ϵ_T are the singlet and triplet extinction coefficients, respectively. C_S and C_T are the concentration of singlets and triplets. d is the path length. The time dependence of the singlet and triplet concentrations after excitation will be given by

$$C_S = C_S^1 - C_T^0 \exp(-t/\tau_T) \qquad (7)$$

$$C_T = C_T^0 \exp(-t/\tau_T) \qquad (8)$$

C_S^1 is the initial concentration of singlets and C_S^0 and C_T^0 are the concentrations of singlets and triplets at $t = 0$. Combining eq 6, 7, and 8

$$\log \frac{I_0}{I(t)} = [\epsilon_S C_S^1 - \epsilon_S C_T^0 \, 3\mathrm{xp}(t/\tau_T) + \epsilon_T C_T^0 \exp(-t/\tau_T)]d \qquad (9)$$

At $t >>> \tau_T$, eq 9 becomes

$$\log \frac{I_0}{I(\infty)} = \epsilon_S C_S^1 d \qquad (10)$$

which when substituted into eq 9 yields

$$\Delta\mathrm{od}(t) = \log \frac{I(\infty)}{I(t)} = (\epsilon_T - \epsilon_S) C_T^0 d \exp(-t/\tau_T) \qquad (11)$$

Direct Determination of the Singlet → Triplet Intersystem Crossing Quantum Yield in Naphthalene, Phenanthrene, and Triphenylene

by Steven G. Hadley and Richard A. Keller

National Bureau of Standards, Washington, D. C. 20234 *(Received June 6, 1969)*

Radiationless singlet → triplet intersystem crossing quantum yields have been directly determined. The technique used depends upon using previously determined extinction coefficients to relate the optical density of the triplet ← triplet absorption and the absolute intensity of the light used to generate triplet state molecules to the intersystem crossing quantum yield. The quantum yields at 77°K in a rigid matrix and their estimated uncertainties were found to be naphthalene-h_8, 0.25 ± 0.05; naphthalene-d_8, 0.25 ± 0.05; phenanthrene-h_{10}, 0.35 ± 0.07; phenanthrene-d_{10}, 0.45 ± 0.09; triphenylene-h_{12}, 0.54 ± 0.11; and triphenylene-d_{12}, 0.88 ± 0.18. No significant deuterium isotope effects were noted on the intersystem crossing quantum yields.

Introduction

Intersystem crossing quantum yields have been directly determined for the perhydro- and perdeuterio-naphthalenes, -phenanthrenes, and -triphenylenes. The intersystem crossing quantum yield can be defined as

$$\Phi_{ISC} = k_{ISC}(k_{ISC} + k_f + k_r)^{-1} \tag{1}$$

where k_{ISC} is the first order rate constant for intersystem crossing between the singlet and triplet manifolds. k_f and k_r are the first-order rate constants for the radiative (fluorescence) and the radiationless deactivation of the first excited singlet, other than to the triplet state, respectively. Similar quantum yields can be defined for fluorescence, Φ_f, and radiationless deactivation of the first excited singlet, Φ_r. In the absence of photodecomposition, the sum $\Phi_{ISC} + \Phi_f + \Phi_r = 1$. Φ_{ISC} can be related to the optical density of the triplet ← triplet absorption by the relationship we have previously derived.[1]

$$\mathrm{OD} = \epsilon_T \tau_T \Phi_{ISC} i_0 \tag{2}$$

Here ϵ_T is the extinction coefficient of the triplet ← triplet absorption, τ_T is the lifetime of the triplet state, and i_0 is the absolute intensity of the excitation light absorbed by the system. This relationship allows the accurate determination of Φ_{ISC}, because all the other parameters in eq 2 can be determined experimentally. Good values of ϵ_T have just recently been determined by us[2] and by other workers[3-7] and it is now possible to use this relation to obtain accurate quantum yields. It is desirable to determine quantum yields in a fashion such as this, for all the difficulties involved in collecting emitted light are circumvented and no standards are needed for comparison.

Experimental Section

Values of OD/i_0 were obtained using the apparatus shown in Figure 1. A Bausch and Lomb[8] grating monochromator was used to isolate different regions of the emission from a 200 W high pressure mercury lamp. For the experiments performed on the naphthalenes, the 290 to 305 nm region was isolated; for the phenanthrenes and triphenylenes the 300 to 315-nm region was used.

The concentration of the samples was such that over 95% of the light was absorbed. A Corning 7-54 (visible absorbing, ultraviolet passing) filter was used to reduce the scattered light. These samples were prepared in a solution of 30% *n*-butanol-70% isopentane which was frozen to a rigid glass at 77°K in the previously described dewar.[1] The triplet ← triplet absorption was monitored using a tungsten filament lamp. A small value of i_0 was used to avoid depletion of the ground state and this necessitated the use of a differential comparator preamplifier in conjunction with an oscilloscope[2] to detect the relatively weak absorption due to the triplet ← triplet transition. A 1P28 photomultiplier was used on a Jarrell Ash 0.5-m Ebert monochromator[8] as a detector. The beam splitters were quartz windows. The optical density was measured by observing the change in the transmitted beam when the mercury lamp was blocked. The display on the oscilloscope was photographed and both the optical density and the triplet lifetime, τ_T were determined.

A second monochromator was used to measure the

---

(1) R. A. Keller and S. G. Hadley, *J. Chem. Phys.*, **42**, 2382 (1965).

(2) R. A. Keller and S. G. Hadley, *ibid.*, **42**, 2382 (1965).

(3) J. S. Brinen, *ibid.*, **49**, 586 (1968).

(4) D. Lavalette, *Compt. Rend.*, **B**, **279**, (1968).

(5) E. J. Land, *Proc. Roy. Soc.* **A305**, 457 (1968).

(6) P. G. Bowers and G. Porter, *ibid.*, **A299**, 348 (1967).

(7) R. Astier and Y. H. Meyer in "The Triplet State," A. B. Zahlan, *et al.*, Ed., Cambridge University Press, London, 1967.

(8) Certain commercial instruments and materials are identified in this paper in order to adequately specify the experimental procedure. In no case does such identification imply recommendation or endorsement by the National Bureau of Standards, nor does it imply that the instrument or materials identified are necessarily the best available for the purpose.

Table I: Summary of the Experimental Results

Molecule	$(OD/i_0) \times 10^{-8}$,[b] cm² einstein⁻¹	$\epsilon_T \times 10^{-4}$,[a] [c] l. mol⁻¹ cm⁻¹	τ_T,[a] S	Φ_{ISC}[d]	$(OD/i_0)^c \times 10^{-7}$,[a]$/\tau_T$, cm²/einstein
$C_{10}H_8$	0.249 ± 0.021	4.0 ± 0.6	2.45 ± 0.2	0.25 ± 0.05	1.02 ± 0.09
$C_{10}D_8$	1.61 ± 0.15	4.0 ± 0.6	16.2 ± 1.6	0.25 ± 0.05	0.99 ± 0.09
$C_{14}H_{10}$	0.555 ± 0.043	3.8 ± 0.6	4.2 ± 0.4	0.35 ± 0.07	1.32 ± 0.1
$C_{14}D_{10}$	2.04 ± 0.12	3.1 ± 0.5	14.5 ± 1.4	0.45 ± 0.09	1.41 ± 0.08
$C_{18}H_{12}$	1.45 ± 0.17	1.56 ± 0.23	17.1 ± 1.7	0.54 ± 0.11	0.85 ± 0.1
$C_{18}D_{12}$	2.33 ± 0.35	1.20 ± 0.18	22.1 ± 2.2	0.88 ± 0.18	1.05 ± 0.16

[a] Estimated uncertainty. [b] Error based upon 95% confidence limits. [c] S. G. Hadley and R. A. Keller, *J. Phys. Chem.*, **73**, 4351 (1969). [d] Uncertainty estimated at ±20%.

relative output of the mercury lamp–monochromator combination. Neutral density screens were placed immediately after the 7-54 filter to vary the magnitude of i_0. Plots of triplet ← triplet absorption optical density against relative i_0 fit a straight line with zero intercept. The absolute magnitude of i_0 was measured by removing the sampler dewar and inserting a cell containing a ferrioxlate actinometer. The cell was masked to prevent edge effects. The recommended actinometry procedure was followed.[9, 10]

Results

The measured values of OD/i_0 and τ_T are shown in Table I. The values of ϵ_t used in the calculation are also included. Table I shows the values of Φ_{ISC} calculated from this data. The error shown in the values of OD/i_0 is the 95% confidence interval; it is about ±10%.

The formulas used to arrive at this value were 95%

$$s = \left(\sum_i \frac{(x_i - \bar{x})^2}{n - 1}\right)^{1/2}$$

confidence interval $= \bar{x} \pm t\frac{s}{\sqrt{n}}$, x_i represents the measurement, $\bar{x}$ the mean, and n the number of measurements. Tables of the t coefficient are available in standard texts on statistics. Sample sizes ranged from 3 to 6. The values of τ_T are reproducible to about ±5%. The error in ϵ_t has been estimated at ±15%. This represents a total error of ±15 to 20% in the values of Φ_{ISC}.

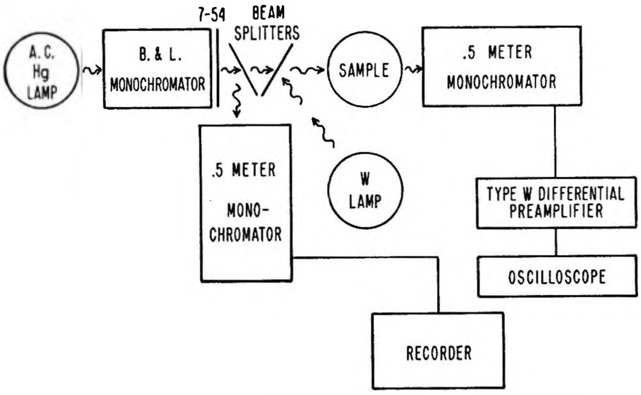

Figure 1. Experimental apparatus used to measure OD/i_0.

A systematic error can enter into measurements of Φ_{ISC} by this technique. The measured optical density of the triplet ← triplet absorption is not for a random distribution of molecules but for a special photoselected distribution. We have considered this problem in more detail and it can be shown that when nonpolarized light is used for excitation and for detection of triplet states the error does not exceed 10%.[11] Quantitative corrections for this effect are difficult because of the mixed polarization present in the absorption bands.

Gueron, Eisinger, and Shulman[12] have reported a relative measurement of the intersystem crossing quantum yields of triphenylene-h₁₂ and naphthalene-h₈ in a rigid medium at 77°K using an esr technique. Their relative technique determined that

$$(\Phi_{ISC}{}^{C_{18}H_{12}})/(\Phi_{ISC}{}^{C_{10}H_8}) = 2.09$$

Our ratio, 2.18, is in excellent agreement with this number. There is little known about fluorescence quantum yields in rigid glasses at 77°K. Good measurements are difficult to make at room temperature and the low temperature just compounds the difficulties. Φ_f's have been determined by Kellogg and Bennett[13] at 77°K using an energy transfer technique under experimental conditions similar to ours. Gilmore, Gibson, and McClure[14] have also measured values of Φ_f under similar experimental conditions. Both sets of values are shown in Table II. From these data it would appear that $\Phi_f + \Phi_{ISC}$ at 77°K in a rigid medium is less than unity for naphthalene and phenanthrene, indicating direct radiationless deactivation of the first excited singlet to the ground state. However, our data alone does *not* indicate this; it must be combined with

---

(9) J. Lee and H. H. Seliger, *J. Chem. Phys.*, **40**, 519 (1964).

(10) C. G. Hatchard and C. A. Parker, *Proc. Roy. Soc.*, **A220**, 104 (1953); **A235**, 518 (1956).

(11) R. A. Keller and S. G. Hadley, submitted for publication.

(12) M. Gueron, J. Eisinger, and R. G. Shulman, *Mol. Phys.*, **14**, 111 (1968).

(13) R. E. Kellogg and R. G. Bennett, *J. Chem. Phys.*, **41**, 3042 (1964).

(14) E. H. Gilmore, G. E. Gibson, and D. S. McClure, *ibid.*, **20**, 829 (1952); **23**, 399 (1955).

Table II: Comparison of Values of Φ_{ISC} and Φ_f under Various Experimental Conditions

Molecule	Φ_{ISC}, 77° K[a,i]	Φ_f, 77°K[b]	Φ_f, 77°K[c]	Φ_f, 77°K[d]	Φ_f, 298°K[e]	Φ_{ISC}, 298°K[f]	Φ_{ISC}, 298°K[g]	Φ_{ISC}, 298°K[e]	Φ_{ISC}, 298°K[h]
$C_{10}H_8$	0.25 ± 0.05		0.55	0.55	0.21	0.40		0.71	0.8
$C_{10}D_8$	0.25 ± 0.05	0.47							
$C_{14}H_{10}$	0.35 ± 0.07	0.12			0.13	0.76	0.70	0.80	0.85
$C_{14}D_{10}$	0.45 ± 0.07	0.10							
$C_{18}H_{12}$	0.54 ± 0.11	0.15	0.53		0.09	0.95		0.89	
$C_{18}D_{12}$	0.88 ± 0.18	0.14							

[a] This work. [b] R. E Kellogg and R. G. Bennett, *J. Chem. Phys.*, **41**, 3042 (1964). [c] E. H. Gilmore, G. E. Gibson, and D. S. McClure, *ibid.*, **20**, 829 (1952); **23**, 399 (1955). [d] B. Stevens and M. F. Thomaz, *Chem. Phys. Letters*, **1**, 549 (1968). [e] C. A. Parker and T. A. Joyce, *Trans. Faraday Soc.*, **62**, 2785 (1966). [f] A. A. Lamola and G. S. Hammond, *J. Chem. Phys.*, **43**, 2129 (1965). [g] P. G. Bowers and G. Porter, *Proc. Roy. Soc.*, **A299**, 348 (1967). [h] A. R. Horrocks and F. Wilkinson, *ibid.*, **A306**, 257 (1968). [i] Estimated uncertainties.

values of Φ_f at 77°K. Quantum yields are quite difficult to determine and there are no generally accepted values. Until this situation is remedied, it will be difficult to know with any degree of certainty whether or not $\Phi_r = 0$ for these systems. For the triphenylenes $\Phi_f + \Phi_{ISC}$ appears to be unity within the experimental error.

Hammond and Lamola[15] have reported values of Φ_{ISC} measured at room temperature in fluid solution using a triplet state sensitized *cis–trans* isomerization as a detector. More recently they have noted some of the difficulties with this chemical method.[16] Parker and Joyce[17] have obtained similar values, with the exception of naphthalene, using an independent technique. Horrocks and Wilkinson[18] have measured Φ_{ISC} for several aromatic hydrocarbons in fluid solution at room temperature. The only systems which both we and they studied are naphthalene-h_8 and phenanthrene-h_{10}, where their values of Φ_{ISC} are 0.8 and 0.85, respectively. Bowers and Porter[19] have recently reported values of Φ_{ISC} determined in a manner similar to ours except that their work was done in fluid solution at room temperature. The only molecule we have both investigated is phenanthrene-h$_{10}$, for which they measured $\Phi_{ISC} = 0.70 \pm 0.12$. This is to be compared with our value of 0.35 ± 0.07. The values of all these workers are compared with ours in Table II.

The values of Φ_{ISC} measured by these workers at *room temperature* are generally significantly larger than those we have determined for naphthalene and phenanthrene at 77°K. It is quite probable that this difference can be attributed entirely to the difference in temperature. Recent evidence indicates that intersystem crossing in many molecules is a thermally activated process.[20–24] This is exemplified by the fact that fluorescence quantum yields[24] and fluorescence lifetimes[20–23] increase at lower temperatures. In fact, the fluorescence lifetime of naphthalene is about 2.7 times greater at 77°K in an alcoholic rigid glass than it is at room temperature.[23] If a value of 0.2 is chosen for Φ_f at room temperature the increased lifetime indicates a value of $\Phi_f = 0.5$–0.6 at low temperature, a result which is in good agreement with those in ref 13 and 14. The increase in Φ_f at low temperatures means that $\Phi_{I.C.}$ at 77°K must be much less than $\Phi_{I.C.}$ at room temperature and tends to explain the differences shown in Table II.

It is possible to derive an expression which relates $\Phi_{I.C.}$ at room temperature to $\Phi_{I.C.}$ at 77°K.

$$\frac{k_{I.C.}{}^{300}}{k_{I.C.}{}^{77}} = \frac{\tau_f{}^{77}}{\tau_f{}^{300}} \frac{\Phi_{I.C.}{}^{300}}{\Phi_{I.C.}{}^{77}} \tag{3}$$

It is tempting to use the values in Table II to calculate the ratio of the intersystem crossing rate constants for naphthalene.

$$\frac{k_{I.C.}{}^{300}}{k_{I.C.}{}^{77}} = 2.7 \times \frac{0.85}{0.25} = 9.2 \tag{4}$$

The final question posed by our data is whether there is a real deuterium isotope effect on the singlet → triplet intersystem crossing quantum yield. It is not necessary to know the magnitude of the extinction coefficients for this comparison, but if it is assumed that the extinction coefficients are the same for the perhydro and perdeuterio forms (from our data[2] they appear to be the same) then only real differences in the intersystem crossing yields will be shown in the quantity $(OD/i_0)\tau_T$.

---

(15) A. A. Lamola and G. S. Hammond, *J. Chem. Phys.*, **43**, 2129 (1965).

(16) L. M. Stephenson, *et al.*, *J. Amer. Chem. Soc.*, **88**, 3665 (1966).

(17) C. A. Parker and T. A. Joyce, *Trans. Faraday Soc.*, **62**, 2785 (1966).

(18) A. R. Horrocks and F. Wilkinson, *Proc. Roy. Soc.*, **A306**, 257 (1968).

(19) P. G. Bowers and G. Porter, *ibid.*, **A299**, 348 (1967).

(20) R. G. Bennett and P. J. McCarten, *J. Chem. Phys.*, **44**, 1969 (1966).

(21) B. Stevens, M. F. Thomaz, and J. Jones, *ibid.*, **46**, 405 (1967).

(22) B. Stevens and M. F. Thomaz, *Chem. Phys. Letters*, **1**, 535 (1968).

(23) B. Stevens and M. F. Thomaz, *ibid.*, **1**, 549 (1968).

(24) J. L. Kropp and W. R. Dawson, paper presented at the International Conference on Molecular Luminescence, Loyola University, Chicago, Illinois, August 20–23, 1968.

These parameters are shown in Table I. They are the same within the experimental error for the naphthalenes and phenanthrenes. Within the limits of our stated error, there appears to be no isotope effect for naphthalene and phenanthrene. The apparent isotope effect for triphenylene is just outside of our experimental uncertainty and may not be significant.

The values of OD/i_0 reported in this work are in good agreement with those that we previously reported.[1] The discrepancies are probably due to light not absorbed by the sample but counted by the actinometer in the previous work. This is most noticeable in the case of the naphthalenes where it is difficult to find the correct solution filter.

Conclusions

Singlet → triplet intersystem crossing quantum yields have been directly measured for three pairs of perhydro and perdeuterio aromatic compounds at 77°K. No significant isotope effect was observed. The technique is limited to systems where the extinction coefficient for triplet ← triplet absorption is known. It has the advantages that no assumption regarding relative standards is necessary and it is not necessary to collect and measure the intensity of emitted light. In principle the method can be extended to any compound with an observable triplet ← triplet absorption spectrum.

The Molecular *g* Values, Magnetic Susceptibility Anisotropies, and Molecular Quadrupole Moments in Propynal

by R. C. Benson, R. S. Scott, and W. H. Flygare

Noyes Chemical Laboratory, University of Illinois, Urbana, Illinois *(Received June 19, 1969)*

The high-field rotational Zeeman effect has been studied in propynal. The molecular g values are $g_{aa} = -0.553 \pm 0.002$, $g_{bb} = -0.040 \pm 0.002$, and $g_{cc} = -0.015 \pm 0.001$. The magnetic susceptibility anisotropies, in units of 10^{-6} erg/(G^2 mol), are $2\chi_{aa} - \chi_{bb} - \chi_{cc} = 4.4 \pm 0.8$ and $-\chi_{aa} + 2\chi_{bb} - \chi_{cc} = 9.0 \pm 1.6$. (The a and b axes are in the molecular plane with the angle between the a axis and the near linear C≡C—C link of about 12.6°). Although only the relative signs of the g values are determined experimentally, the above signs are conclusively assigned on the basis of the molecular quadrupole moments. The molecular quadrupole moments, in units of 10^{-26} esu cm^2, are $Q_{aa} = 3.1 \pm 1.3$, $Q_{bb} = 1.1 \pm 2.2$, and $Q_{cc} = -4.2 \pm 2.4$. Using the above g values and magnetic susceptibility anisotropies in conjunction with the known molecular structure, the diagonal elements of the paramagnetic susceptibility tensor and the anisotropies in the second moment of the electronic charge distribution may be calculated. They are $\chi_{aa}^{p} = 38.7 \pm 0.1$, $\chi_{bb}^{p} = 259.3 \pm 1.2$, and $\chi_{cc}^{p} = 270.1 \pm 0.8$, all in units of 10^{-6} erg/(G^2 mol); and $\langle a^2\rangle - \langle b^2\rangle = 51.6 \pm 0.5$, $\langle b^2\rangle - \langle c^2\rangle = 4.3 \pm 0.7$, and $\langle c^2\rangle - \langle a^2\rangle = -55.9 \pm 0.4$, all in units of 10^{-16} cm^2.

I. Introduction

Molecular Zeeman studies in a relatively large number of diamagnetic molecules have led to considerable information about the electronic charge distribution and the magnetic properties in molecules.[1-3]

In rotational Zeeman studies the first- and second-order magnetic field effects lead, respectively, to a measurement of the molecular g values and the anisotropies in the total magnetic susceptibility tensor elements in the principal inertial axis system. The diagonal elements of the paramagnetic susceptibility tensor, which are determined from the g values and the molecular structure, can be combined with the anisotropies in the total magnetic susceptibility to give anisotropies in the ground-state second moment of the electronic charge distribution. The molecular quadrupole moments are directly determined from the g values and the total magnetic susceptibility anisotropies. If the bulk magnetic susceptibility is known, the diagonal elements in the total and diamagnetic susceptibility tensors, and the individual second mo-

---

(1) For results of various ring compounds see D. H. Sütter and W. H. Flygare, *J. Amer. Chem. Soc.*, **91**, 4063 (1961), and R. C. Benson and W. H. Flygare, *J. Chem. Phys.*, **51**, 3087 (1969), and references therein.

(2) For results of inorganic molecules, see R. G. Stone, J. M. Pochan, and W. H. Flygare, *Inorg. Chem.*, **8**, 2647 (1969).

(3) For results of symmetric tops see R. L. Shoemaker and W. H. Flygare, *J. Amer. Chem. Soc.*, **91**, 5417 (1969); D. VanderHart and W. H. Flygare, *Mol. Phys.*, in press; and J. M. Pochan, R. G. Stone, and W. H. Flygare, *J. Chem. Phys.*, in press.

ments of the electronic charge distribution may also be obtained.

In this paper, we report the molecular Zeeman results for propynal and compare them to similar molecules which have been studied previously.

II. Experimental Section

The microwave spectrometer and high-field electromagnet have been described in detail previously.[4] Briefly, the spectrometer is a relatively standard system employing 5-kHz Stark modulation, and the magnet is of a rectangular design in which the gap is variable to accommodate different wave guide sizes. In this work the 12 × 72 in. flat poles were used, and the measurements were in a X-band and C-band wave guide with the microwave electric field parallel to the magnetic field ($\Delta M_J = 0$) and in a X-band wave guide with the microwave electric field perpendicular to the magnetic field ($\Delta M_J = \pm 1$). The magnetic fields employed were about 21000 G and were measured using a Rawson–Lush Type 920 rotating coil gaussmeter which is periodically calibrated with a nmr gaussmeter and is consistently accurate to better than 0.02%. The field homogeneity using the X-band wave guide enabled the field to be measured to better than 0.05%, while using the C-band wave guide, 0.10% accuracy is achieved.

The zero-field microwave spectrum of propynal has been previously studied.[5,6] Propynal was synthesized by oxidation of the corresponding alcohol, 2-propyn-1-ol,[7] and was then vacuum distilled at −78°.

The theory of the rotational Zeeman effect in an asymmetric top has been given by Hüttner and Flygare,[8] who have derived the following expression for the rotational energy levels in the presence of a magnetic field (in the absence of nuclear spin)

$$E(J,M_J) = -{}^1\!/_2\chi H^2 - \frac{\mu_0 M_J H}{J(J+1)} \sum_g g_{gg}\langle J_g^2\rangle - H^2\left[\frac{3M_J^2 - J(J+1)}{J(J+1)(2J-1)(2J+3)}\right]\sum_g (\chi_{gg} - \chi)\langle J_g^2\rangle \quad (1)$$

$\chi = {}^1\!/_3(\chi_{aa} + \chi_{bb} + \chi_{cc})$ is the average magnetic susceptibility with χ_{aa}, χ_{bb}, and χ_{cc} being the components along the principal inertial axes in the molecule. H is the external magnetic field, μ_0 is the nuclear magneton, J and M_J are the rotational quantum numbers, g_{gg} is the molecular g value along the gth principal inertial axis, and $\langle J_g^2\rangle$ is the average value of the squared rotational angular momentum (in units of $\hbar^2$) along the gth principal inertial axis. Since only energy differences are observed, the $-{}^1\!/_2\chi H^2$ term cancels out.

The values of $\langle J_g^2\rangle$ are calculated using the rotational constants from the previous assignment: A = 68026.60 MHz, B = 4826.223 MHz, and C = 4499.612 MHz.[6] There are three magnetic anisotropy parameters; however, only two are linearly independent and they are arbitrarily chosen to be $2\chi_{aa} - \chi_{bb} - \chi_{cc}$ and $-\chi_{aa} + 2\chi_{bb} - \chi_{cc}$. Thus, these magnetic susceptibility anisotropies and the absolute values and relative signs of the three g values can be directly measured, giving five independent Zeeman parameters.

III. Results

A. Molecular g Values and Magnetic Susceptibility Anisotropies. The observed rotational Zeeman transitions in propynal are listed in Table I. The $M = |0 \rightarrow 1|$ transitions in the $1_{11} \rightarrow 2_{12}$ and $1_{10} \rightarrow 2_{11}$ rotational transitions were of low intensity, and the accuracy of their frequency shifts was therefore decreased. Thus, only strong lines were used in the least-squares analysis of the five Zeeman parameters. (These are marked with an asterisk (*) in Table I.) The resultant Zeeman parameters are listed in Table II. Although only the relative signs of the g values are obtained experimentally, it will be shown below that the signs given in Table II are correct.

B. Molecular Quadrupole Moments. A general expression relating the five parameters listed in Table II to the molecular quadrupole moments has been given by Hüttner, Lo, and Flygare[9]

$$Q_{zz} = \frac{|e|}{2}\sum_n Z_n(3z_n^2 - r_n^2) - \frac{|e|}{2}\left\langle 0\left|\sum_i (3z_i^2 - r_i^2)\right|0\right\rangle = -\frac{h|e|}{8\pi M}\left[\frac{2g_{zz}}{G_{zz}} - \frac{g_{xx}}{G_{xx}} - \frac{g_{yy}}{G_{yy}}\right] - \frac{2mc^2}{|e|N}(2\chi_{zz} - \chi_{xx} - \chi_{yy}) \quad (2)$$

$|e|$ is the electronic charge, Z_n is the charge of the nth nucleus, and z_n and z_i are the nuclear and electronic center of mass coordinates summed over all n nuclei and i electrons. $\langle 0|\ |0\rangle$ indicates the ground electronic state average value. M is the proton mass, G_{zz} is the rotational constant along the zth principal inertial axis, c is the speed of light, m is the electron mass and N is Avogadro's number. Substituting the five Zeeman parameters from Table II into eq 2 gives two sets of Q for either choice of the signs of the g values. (The a and b axes are in the molecular plane with the angle between the a axis and the C≡C—C chain about 12.6°.)

---

[4] W. H. Flygare, W. Hüttner, R. L. Shoemaker, and P. D. Foster, *J. Chem. Phys.*, **50**, 1714 (1969).

[5] J. A. Howe and J. H. Goldstein, *ibid.*, **23**, 1223 (1955).

[6] C. C. Costain and J. R. Morton, *ibid.*, **31**, 389 (1959).

[7] N. J. Leonard, Ed., *Org. Syn.*, **36**, 66 (1956).

[8] W. Hüttner and W. H. Flygare, *J. Chem. Phys.*, **47**, 4137 (1967).

[9] W. Hüttner, M. K. Lo, and W. H. Flygare, *ibid.*, **48**, 1206 (1968).

Table I: The Rotational Zeeman Splittings in Propynal[a]

Transition	$M_L \rightarrow M_U$	$\Delta\nu_{\text{exptl}}$,[b] kHz	$\Delta\nu_{\text{calcd}}$, kHz	$\Delta\nu_{\text{exptl}} - \Delta\nu_{\text{calcd}}$, kHz
$0_{00} \rightarrow 1_{01}$	$0 \rightarrow -1$*	−398	−429	+31
$\nu_0 = 9325.82 \pm 0.03$ MHz	$0 \rightarrow 1$*	+480	+462	+18
$H = 21257$ G				
$1_{11} \rightarrow 2_{12}$	$+1 \rightarrow 0$		−4686	
$\nu_0 = 18325.662 \pm 0.03$ MHz	$0 \rightarrow -1$	−1592	−1724	+132
$H = 21162$ G	$1 \rightarrow 2$*	−1002	−1032	+30
	$-1 \rightarrow -2$*	+1108	+1108	0
	$0 \rightarrow 1$	+1838	+1787	+51
	$-1 \rightarrow 0$		+4476	
$1_{11} \rightarrow 2_{12}$	$1 \rightarrow 0$		−4688	
$\nu_0 = 18325.625 \pm 0.03$ MHz	$0 \rightarrow -1$		−1725	
$H = 21172$ G	$1 \rightarrow 2$*	−1000	−1032	+32
	$-1 \rightarrow -2$*	+1140	+1108	+32
	$0 \rightarrow 1$	+1625	+1788	−63
	$-1 \rightarrow 0$		+4478	
$1_{01} \rightarrow 2_{02}$	$1 \rightarrow 0$		−484	
$\nu_0 = 18650.31 \pm 0.03$ MHz	$-1 \rightarrow -2$*	−430	−435	−5
$H = 21160$ G	$0 \rightarrow -1$*		−422	−8
	$-1 \rightarrow 0$		+403	
	$1 \rightarrow 2$*	+450	+450	0
	$0 \rightarrow 1$*		+464	−14
$1_{10} \rightarrow 2_{11}$	$1 \rightarrow 0$		−4685	
$\nu_0 = 18978.72 \pm 0.03$ MHz	$0 \rightarrow -1$	−2120	−2033	−87
$H = 21163$ G	$1 \rightarrow 2$*	−875	−866	−9
	$-1 \rightarrow -2$*	+840	+870	−30
	$0 \rightarrow 1$	+1750	+1881	−131
	$-1 \rightarrow 0$		−4881	
$1_{10} \rightarrow 2_{11}$	$1 \rightarrow 0$		−4688	
$\nu_0 = 18978.71 \pm 0.035$ MHz	$0 \rightarrow -1$	−2125	−2035	−90
$H = 21181$ G	$1 \rightarrow 2$*	−870	−867	−3
	$-1 \rightarrow -2$*	−830	+871	−41
	$0 \rightarrow 1$	+1760	+1883	−123
	$-1 \rightarrow 0$		+4885	
$2_{12} \rightarrow 3_{13}$	$2 \rightarrow 1$		−2600	
$\nu_0 = 27487.54 \pm 0.03$ MHz	$1 \rightarrow 0$		−1800	
$H = 21256$ G	$0 \rightarrow -1$	−980	−1036	+56
	$2 \rightarrow 3$*	−307	−346	+39
	$-1 \rightarrow -2$*		−308	+1
	$1 \rightarrow 2$*	+335	+380	−45
	$-2 \rightarrow -3$*		+385	−50
	$0 \rightarrow 1$	+1020	+1071	−51
	$-1 \rightarrow 0$	+1632	+1726	−94
	$-2 \rightarrow -1$			
$0_{00} \rightarrow 1_{01}$				
$\nu_0 = 9325.846 \pm 0.025$ MHz	$0 \rightarrow 0$*	−46	−38	−8
$H = 22842$ G				
$0_{00} \rightarrow 1_{01}$				
$\nu_0 = 9325.823 \pm 0.008$ MHz	$0 \rightarrow 0$*	−37	−33	−4
$H = 21115$ G				
$1_{11} \rightarrow 2_{12}$	$1 \rightarrow 1$*	−2853	−2904	+53
$\nu_0 = 18325.558 \pm 0.01$ MHz	$0 \rightarrow 0$*	+22	−4	+18
$H = 21230$ G	$-1 \rightarrow -1$*	+2772	+2765	+7
$1_{10} \rightarrow 2_{11}$	$1 \rightarrow 1$*	−2759	−2750	−9
$\nu_0 = 18978.788 \pm 0.01$ MHz	$0 \rightarrow 0$*	−96	−52	−44
$H = 21150$ G	$-1 \rightarrow -1$*	+2844	+2898	−54
$2_{12} \rightarrow 3_{13}$	$2 \rightarrow 2$*	−1500	−1494	−6
$\nu_0 = 27487.45 \pm 0.02$	$1 \rightarrow 1$*	−740	−730	−10
$H = 21295$ G	$0 \rightarrow 0$*	0	− 1	+1
	$-1 \rightarrow -1$*	+685	+692	−7
	$-2 \rightarrow -2$*	+1315	+1349	−34

[a] The first column on the left identifies the ΔM_J transition. The transitions used in the least-squares analysis to give the Zeeman parameters in Table III are marked with an asterisk (*). The calculated frequencies are obtained using these parameters and eq 1. The magnetic field (in gauss) and zero-field frequencies are listed under the rotational transition designation. [b] The experimental frequencies are quoted to the nearest kHz since they are the average of several scans. The uncertainties in $\Delta\nu_{\text{exptl}}$ range from 10 to 60 kHz.

Table II: Zeeman Parameters, Molecular Quadrupole Moments, and Anisotropies in the Second Moment of the Electronic Charge Distribution in Propynal[a]

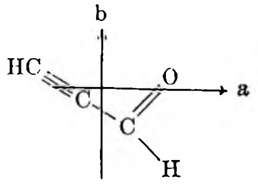

$g_{aa} = -0.553 \pm 0.002$
$g_{bb} = -0.040 \pm 0.002$
$g_{cc} = -0.015 \pm 0.001$
$2\chi_{aa} - \chi_{bb} - \chi_{cc} = 4.4 \pm 0.8$
$-\chi_{aa} + 2\chi_{bb} - \chi_{cc} = 9.0 \pm 1.6$
$Q_{aa} = 3.1 \pm 1.3$
$Q_{bb} = 1.1 \pm 2.2$
$Q_{cc} = -4.2 \pm 2.4$
$\langle a^2 \rangle - \langle b^2 \rangle = 51.6 \pm 0.5$
$\langle b^2 \rangle - \langle c^2 \rangle = 4.3 \pm 0.7$
$\langle c^2 \rangle - \langle a^2 \rangle = -55.9 \pm 0.4$
$\chi_{aa}^{p} = 38.7 \pm 0.1$
$\chi_{bb}^{p} = 259.3 \pm 1.2$
$\chi_{cc}^{p} = 270.1 \pm 0.8$

[a] The a and b axes are in the molecular plane. The magnetic susceptibilities are in units of 10^{-6} erg/(G^2 mol), the molecular quadrupole moments are in units of 10^{-26} esu cm^2, and values of $\langle a^2 \rangle - \langle b^2 \rangle$ are in units of 10^{-16} cm^2.

The two sets of Q, in units of 10^{-26} esu cm^2, are: g values all negative

$$Q_{aa} = 3.1 \pm 1.3$$
$$Q_{bb} = 1.1 \pm 2.2 \qquad (3)$$
$$Q_{cc} = -4.2 \pm 2.4$$

g-values all positive

$$Q_{aa} = -8.1 \pm 1.3$$
$$Q_{bb} = -11.3 \pm 2.2 \qquad (4)$$
$$Q_{cc} = +19.4 \pm 2.4$$

A comparison of the above molecular quadrupole moments to those of similar molecules (see Table III) indicates that eq 3 is correct. Comparing the Q_{yy} values indicates that Q_{yy} for propynal should be near zero and certainly should not be a large negative value as in eq 4. Also, the Q_{zz} values in formaldehyde and the acetylenic molecules are all positive due to the protons. Thus, it is expected that Q_{zz} for propynal would definitely be positive and near the values for formaldehyde and fluoroacetylene. This is also in contradiction to the values in eq 4. In addition, the negative values in eq 3 are in agreement with the known negative g val-

Table III: Magnetic Susceptibilities and Molecular Quadrupole Moments for Molecules Similar to Propynal

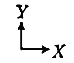	$\chi_{zz} - \chi_{yy}$[a]	$\chi_{zz} - \frac{1}{2}(\chi_{xx} + \chi_{yy})$[a]	Q_{xx}[b] Q_{yy} Q_{zz}	Reference
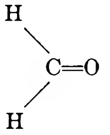	9.6 ± 1.1	-12.0 ± 1.8	1.3 ± 0.8 -0.6 ± 0.7 -0.7 ± 0.8	9
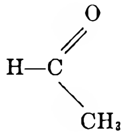	-0.5 ± 1.3	-8.8 ± 2.0	$+1.0 \pm 0.9$ -1.2 ± 1.5 $+0.2 \pm 1.8$	11
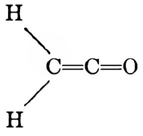	-1.62 ± 0.4	$+2.6 \pm 0.6$	-0.7 ± 0.3 $+3.8 \pm 0.4$ -3.1 ± 0.4	10
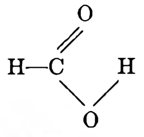	-2.0 ± 0.3	-6.4 ± 0.4	$+5.1 \pm 0.3$ -5.3 ± 0.3 $+0.2 \pm 0.3$	12
HC≡C—F	-0.86 ± 0.02	$+0.43 \pm 0.01$	$Q_{zz} = 3.96 \pm 0.14$	c
HC≡C—CH$_3$	-7.7 ± 0.14	$+3.85 \pm 0.7$	$Q_{zz} = 4.82 \pm 0.23$	d
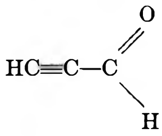	-1.5 ± 0.8	-6.7 ± 1.2	$+3.1 \pm 1.3$ $+1.1 \pm 2.2$ -4.2 ± 2.4	This work

[a] Units of 10^{-6} erg/(G^2 mole). [b] Units of 10^{-26} esu cm.^{2} [c] R. L. Shoemaker and W. H. Flygare, *Chem. Phys. Lett.*, **2**, 610 (1968). [d] R. L. Shoemaker and W. H. Flygare, *J. Amer. Chem. Soc.*, **91**, 5417 (1969).

ues for formaldehyde,[9] ketene,[10] acetaldehyde,[11] and formic acid.[12] Therefore, the g values in eq 3 are correct.

C. Anisotropies in the Second Moment of the Electronic Charge Distribution. The anisotropies in the center of mass average values of x^2, y^2, and z^2 for the electronic charge distribution are determined from the results of Table II and the known molecular structure.[6]

The total magnetic susceptibility, χ_{xx}, along any axis is a sum of diamagnetic, χ_{xx}^{d}, and paramagnetic, χ_{xx}^{p}, components defined by

$$\begin{aligned} \chi_{xx} &= \chi_{xx}^{p} + \chi_{xx}^{d} \\ \chi_{xx}^{d} &= \frac{-e^2N}{2mc^2}\left\langle 0\middle|\sum_i (y_i^2 + z_i^2)\middle|0\right\rangle \\ \chi_{xx}^{p} &= \frac{-e^2N}{2mc^2}\left[\frac{hg_{xx}}{8\pi G_{xx}M} - {}^1/_2\sum_n Z_n(y_n^2 + z_n^2)\right] \end{aligned} \tag{5}$$

The average values of the second moment of the electronic charge distributions are defined as

$$\begin{aligned} \langle x^2\rangle &= \langle 0|\sum_i x_i^2\, 0\rangle \\ \langle y^2\rangle &= \langle 0|\sum_i y_i^2|0\rangle \\ \langle z^2\rangle &= \langle 0|\sum_i z_i^2|0\rangle \end{aligned} \tag{6}$$

The anisotropies of the second moments are related to the observables in Table II and the known molecular structure according to the following expression

$$\begin{aligned} \langle y^2\rangle - \langle x^2\rangle = \sum_n Z_n(y_n^2 - {} \\ x_n^2) + \frac{h}{4\pi M}\left(\frac{g_{yy}}{G_{yy}} - \frac{g_{xx}}{G_{xx}}\right) - \frac{4mc^2}{3e^2\mathrm{N}}[(2\chi_{yy} - {} \\ \chi_{xx} - \chi_{zz}) - (2\chi_{xx} - \chi_{yy} - \chi_{zz})] \end{aligned} \tag{7}$$

The values of $\sum_n Z_n a_n^2$, $\sum_n Z_n b_n^2$, and $\sum_n Z_n c_n^2$ are given below (in units of 10^{-16} cm^2); the uncertainties are based on the uncertainties in the structure given in ref 6.

$$\begin{aligned} \sum_n Z_n a_n^2 &= 56.9412 \pm 0.07 \\ \sum_n Z_n b_n^2 &= 5.0286 = 0.02 \\ \sum_n Z_n c_n^2 &= 0 \pm 0 \end{aligned} \tag{8}$$

The above values along with the measured g values and magnetic susceptibility anisotropies are substituted into eq 7 to obtain the second moment anisotropies which are listed in Table II.

The bulk susceptibility for propynal has apparently not been measured so the individual elements of the second moment of the electronic charge distribution and the individual elements in the total and diamagnetic susceptibility tensors cannot be calculated. Only the individual elements in the paramagnetic susceptibility tensor may be directly obtained from the five Zeeman parameters in Table II and the known molecular structure. These numbers are substituted into eq 5 to obtain the χ_{gg}^{p} values which are listed in Table II.

IV. Discussion

The molecular g values, magnetic susceptibility anisotropies, and molecular quadrupole moments have been obtained for propynal. The molecular quadrupole moments have been compared in section III to similar molecules which are listed in Table III. It was noted that the positive value for Q_{xx} in propynal is about the same as that in formaldehyde and fluoroacetylene, indicating the presence of the positive protons along the x axis. The large negative value for Q_{zz} is significantly larger than that in formaldehyde and slightly larger than that in ketene. This is expected since the electron density along the z axis should increase as the number of π bonds increase.

The in-plane magnetic susceptibility anisotropy $(\chi_{xx} - \chi_{yy})$ and the difference between the out-of-plane and the average in-plane susceptibilities, $\chi_{zz} - {}^1/_2(\chi_{xx} + \chi_{yy})$, are also listed in Table III for propynal and similar molecules. A test of the additivity of group susceptibilities is available since propynal is essentially acetylene + formaldehyde. $\chi_{zz} - {}^1/_2(\chi_{xx} + \chi_{yy})$ for methylacetylene should be nearly equal (to 10%) to that of acetylene assuming the methyl group is almost isotropic. The sum of $\chi_{zz} - {}^1/_2(\chi_{xx} + \chi_{yy})$ for methylacetylene and formaldehyde gives $-8.2 \pm 2.0\ 10^{-6}$ erg/(G^2 mol) for propynal as compared to the experimental value of $-6.7 \pm 1.2\ 10^{-6}$ erg/(G^2 mol). Due to the large errors in the susceptibility values for propynal and formaldehyde the agreement is adequate and does not refute the possibility of group additivity rules.

Acknowledgment. The support of the National Science Foundation is gratefully acknowledged.

---

(10) W. Hüttner, W. H. Flygare, and P. D. Foster, *J. Chem. Phys.*, **49**, 1710 (1969).

(11) W. Hüttner and W. H. Flygare, *Trans. Faraday Soc.*, **65**, 1953 (1969).

(12) S. G. Kukolich and W. H. Flygare, *J. Amer. Chem. Soc.*, **91**, 2433 (1969).

Electron Transfer from Dimeric Dianions of α-Methylstyrene to Benz[*e*]pyrene

by H. Tokunaga, J. Jagur-Grodzinski, and M. Szwarc

Department of Chemistry, State University College of Forestry at Syracuse University, Syracuse, New York 13210

(Received July 24, 1969)

Electron transfer from dimeric dianion of α-methylstyrene, ${}^{-}\alpha\alpha^{-}$, to benz[*e*]pyrene, Bp, leads to the formation of benzpyrene radical-anion, $\mathrm{Bp}^{-}\cdot$. The reaction was studied in THF at 25° in the presence of an excess of Na^{+}, $\mathrm{BPh_4}^{-}$. The kinetic results confirmed the mechanism previously proposed for the analogous reactions involving anthracene or pyrene, *viz.*

$$^{-}\alpha\alpha^{-} + \mathrm{Bp} \rightleftarrows {}^{-}\alpha\alpha\mathrm{Bp}^{-},\ K_{\mathrm{A}}$$

$$^{-}\mathrm{Bp}\alpha\alpha^{-} + \mathrm{Bp} \rightleftarrows {}^{-}\mathrm{Bp}\alpha\alpha\mathrm{Bp}^{-},\ K_{\mathrm{A}}'$$

$$^{-}\alpha\alpha\mathrm{Bp}^{-} \underset{k_{-1}}{\overset{k_1}{\rightleftarrows}} {}^{-}\alpha\alpha\cdot + \mathrm{Bp}\cdot^{-} \tag{1}$$

$$^{-}\alpha\alpha\cdot \xrightarrow{k_2} \alpha + \alpha\cdot^{-} \tag{2}$$

It was shown that $K_{\mathrm{A}} \approx 700\ M^{-1}$, $K_{\mathrm{A}}' \approx 600\text{–}700\ M^{-1}$, and $2k_1 = 5 \times 10^{-2}\ M^{-1}\ \mathrm{sec}^{-1}$. The spectrum of the complex ${}^{-}\alpha\alpha\mathrm{Bp}^{-}$ was recorded. The dependence of the observed constants on the electron affinity of the acceptor is discussed.

Extensive studies of electron-transfer reactions from dimeric dicarbanions to aromatic acceptors were carried out in our laboratory during the last few years.[1-4] The reactions involving dimeric dicarbanions of α-methylstyrene,[5] proceed by three steps. Denoting by A the aromatic acceptor, the overall process is described by the equations

$$\bar{\mathrm{C}}(\mathrm{CH_3})(\mathrm{Ph}).\mathrm{CH_2}.\mathrm{CH_2}\bar{\mathrm{C}}(\mathrm{CH_3})(\mathrm{Ph}) = {}^{-}\alpha\alpha^{-}$$

$$^{-}\alpha\alpha^{-} + \mathrm{A} \rightleftarrows {}^{-}\alpha\alpha\mathrm{A}^{-},\ K_{\mathrm{A}}$$

$$^{-}\mathrm{A}\alpha\alpha^{-} + \mathrm{A} \rightleftarrows {}^{-}\mathrm{A}\alpha\alpha\mathrm{A}^{-},\ K_{\mathrm{A}}'$$

$$^{-}\alpha\alpha\mathrm{A}^{-} \underset{k_{-1}}{\overset{k_1}{\rightleftarrows}} {}^{-}\alpha\alpha\cdot + \mathrm{A}\cdot^{-} \tag{1}$$

$$^{-}\alpha\alpha\cdot \xrightarrow{k_2} \alpha + \alpha\cdot^{-} \tag{2}$$

$$\alpha\cdot^{-} + \mathrm{A} \longrightarrow \alpha + \mathrm{A}\cdot^{-} \tag{3}$$

or

$$\alpha^{-}\cdot + {}^{-}\alpha\alpha\cdot \longrightarrow \alpha + {}^{-}\alpha\alpha^{-} \quad \text{(both fast)}$$

${}^{-}\alpha\alpha\mathrm{A}^{-}$ and ${}^{-}\mathrm{A}\alpha\alpha\mathrm{A}^{-}$ are the adducts in which a covalent bond is established between the carbanion and the aromatic hydrocarbon, a new carbanion, or its delocalized analog, being produced.

The interesting feature of these systems arises from the fact that the decomposition of the monoadducts leads to the final electron transfer and to the formation of the radical ion, $\mathrm{A}\cdot^{-}$ (though the reversible reaction 1), while the decomposition of the diadduct, contributes only little, if at all, to the formation of the radical ions. This peculiarity is due to the facile decomposition of the intermediate dimeric radical ions, ${}^{-}\alpha\alpha\cdot$, which provides a sink driving the equilibrium (1) to the right. The reformation of the C=C double bonds in the resulting α-methylstyrene, α, and in its radical ion, $\alpha\cdot^{-}$, is the driving force responsible for the rapid decomposition of ${}^{-}\alpha\alpha\cdot$. On the other hand, the diadduct, if decomposed produces ${}^{-}\mathrm{A}\alpha\alpha\cdot$

$$^{-}\mathrm{A}\alpha\alpha\mathrm{A}^{-} \rightleftarrows {}^{-}\mathrm{A}\alpha\alpha\cdot + \mathrm{A}^{-}\cdot \tag{4}$$

which dissociates slowly because only one C=C bond is gained in the reaction giving ${}^{-}\mathrm{A}\alpha\cdot + \alpha$. The reversibility of (4) and the absence of an efficient sink makes, therefore, the diadduct relatively stable.

The above peculiarity leads to the unusual behavior of the system. The initial rate of $\mathrm{A}\cdot^{-}$ formation at a constant $[{}^{-}\alpha\alpha^{-}]_0$ first *increases* and then *decreases* as the initial concentration of A is raised. This is due, of course, to the increasing conversion of the reactive ${}^{-}\alpha\alpha\mathrm{A}^{-}$ into the less reactive ${}^{-}\mathrm{A}\alpha\alpha\mathrm{A}^{-}$ wich is caused by the increase in $[\mathrm{A}]_0$.

The equilibria leading to the formation of ${}^{-}\mathrm{A}\alpha\alpha^{-}$ and ${}^{-}\mathrm{A}\alpha\alpha\mathrm{A}^{-}$ are established in a fraction of a second.[6] Decomposition (1) is relatively fast in the initial stage of the reaction; when [A·⁻] is exceedingly low this is the rate-determining step. The stationary state is established within a second or two, and reaction 2 becomes the rate-determining step when [A·⁻] is sufficiently large. The overall reaction is autoretarded by A·⁻ as shown in ref 3 and 4.

---

(1) (a) J. Jagur, M. Levy, M. Feld, and M. Szwarc, *Trans. Faraday Soc.*, **58**, 2168 (1962); (b) J. Jagur-Grodzinski and M. Szwarc, *Proc. Roy. Soc.*, **A288**, 224 (1965).

(2) D. Gill, J. Jagur-Grodzinski, and M. Szwarc, *Trans. Faraday Soc.*, **60**, 1424 (1964).

(3) J. Jagur-Grodzinski and M. Szwarc, *ibid.*, **59**, 2305 (1963).

(4) S. C. Chadha, J. Jagur-Grodzinski, and M. Szwarc, *ibid.*, **65**, 1074 (1969).

(5) These processes were studied in THF and, hence, the carbanions and radical ions are present as the relevant ion pairs and not free ions. However, for the sake of brevity, the counterions (Na^{+} or K^{+}) are omitted in the equations.

(6) R. Lipman, J. Jagur-Grodzinski, and M. Szwarc, *J. Amer. Chem. Soc.*, **87**, 3005 (1965).

The above system was investigated for A = anthracene[3] and A = pyrene;[4] detailed kinetic study led to the constants for anthracene, $K_A > 10^5\ M^{-1}$; $k_1 \times 10^2$ 0.9–1.6 sec^{-1}; relative k_{-1}, 1.0; relative electron affinity of A, 0.642 and for pyrene, $K_A = 120\ M^{-1}$; $k_1 \times 10^2$ of, 1.1–1.5 sec^{-1}; relative k_{-1} 1.2; and relative electron affinity of A, 0.529. (See ref 7 for the relative electron affinities of aromatic hydrocarbons.)

The similarity of the k_1, k_{-1} (and, therefore, also of K_1) for the reactions involving anthracene and pyrene raised the question of whether or not there is a genuine internal compensation which makes k_1, k_{-1}, and K_1 independent of the electron affinity of the acceptor. In search of the answer, we investigated a similar system involving [e]-benzypyrene, Bp, as the acceptor; its electron affinity (0.484 V) is lower than that of either anthracene (0.642 V) or pyrene (0.529 V). As will be seen from the data presented herewith, the constants $k_1 = 2.5 \times 10^{-2}$ and the relative value of $k_{-1} = 0.4 \times 10^{-2}$ are different, although not appreciably different, from those obtained for the other two systems.

The reaction of $^-\alpha\alpha^-$ with benz[*e*]pyrene, Bp, leads to the rapid formation of the adducts $^-\text{Bp}\alpha\alpha^-$ and $^-\text{Bp}\alpha\alpha\text{Bp}^-$ and eventually it yields Bp·⁻ radical-ions. Its kinetic was investigated at 25° in THF using the sodium salt of $^-\alpha\alpha^-$ in the presence of an excess of $\text{Na}^+\ \text{BPh}_4^-$. The presence of the latter decreased the dissociation of the $^-\alpha\alpha^-$ salt into free ions, and, therefore, any complications which could be caused by the presence of free ions were eliminated. A few experiments were performed with the potassium salt of $^-\alpha\alpha^-$. Flow and stop-flow techniques were applied in our studies, the experimental details being given in ref 3 and 4.

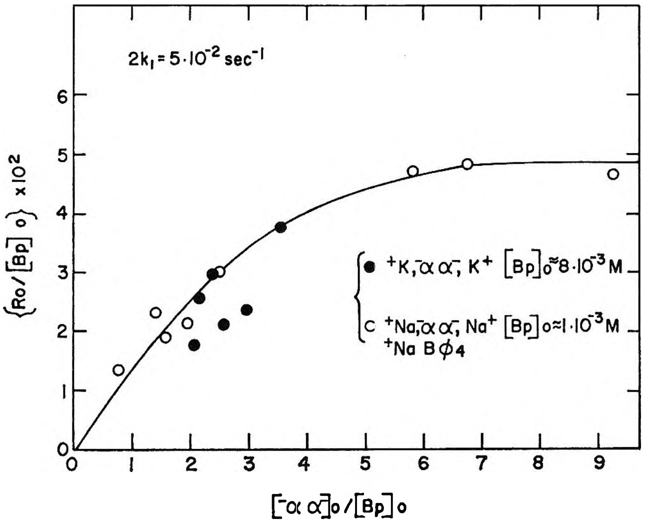

Figure 1. Dependence of $R_0/[\text{Bp}]_0$ on $[^-\alpha\alpha^-]_0/[\text{Bp}]_0$. ○, sodium salt; ●, potassium salt. Asymptotic value gives $2k_1 = 5.0 \times 10^{-2}\ M^{-1}\ \text{sec}^{-1}$.

Table I: $\text{Na}^+, {}^-\alpha\alpha^-\text{Na}^+$ + Benz[*e*]pyrene → [e]-Benzpyrene$\cdot, {}^-\text{Na}^+$ + ... in THF with Excess of $\text{Na}^+, \text{BPh}_4^-$ at 25°

$[^-\alpha\alpha^-]_0 \times 10^3$ *M*	$[\text{Bp}]_0 \times 10^3$ *M*	$[^-\alpha\alpha^-]_0/[\text{Bp}]_0$	$R_0 \times 10^6$ $M^{-1}\ \text{sec}^{-1}$	$R_0/[\text{Bp}]_0 \times 10^2\ \text{sec}^{-1}$
0.67	0.89	0.755	1.19	1.34
1.51	0.925	1.40	2.12	2.29
1.47	0.95	1.56	1.76	1.86
1.80	0.97	1.96	1.94	2.12
2.40	0.97	2.48	2.89	2.98
5.60	0.96	5.82	4.52	4.70
6.54	0.97	6.76	4.66	4.81
7.63	0.82	9.26	4.50	4.65
	$\text{K}^+, {}^-\alpha\alpha^-, \text{K}^+$ + Benz[*e*]pyrene			
16.0	7.76	2.06	13.5(?)	1.75(?)
16.4	7.57	2.17	19.2	2.54
21.0	8.22	2.56	17.3(?)	2.10(?)
17.5	7.12	2.46	20.7	2.91
22.7	7.72	2.94	18.1(?)	2.34(?)
20.6	5.80	3.55	21.7	3.74

The absorption spectrum of the benzpyrene radical ion, Bp·⁻, shows maxima at $\lambda_{\max}$ 413 mμ (ϵ 0.97 × 10^4), 457 mμ (ϵ 1.72 × 10^4), 505 mμ (ϵ 0.67 × 10^4) and 1062 (ϵ 0.32 × 10^4). The absorption of the group αBp^- was determined by mixing $^-\alpha\alpha^-$ with a large excess of Bp (8–9 fold) and observing the spectrum of the resulting mixture in the flow (*i.e.*, less than 0.1 sec after the onset of the reaction). The new absorption peaks observed under these conditions, and attributed to αBp^-, have maxima at $\lambda_{\max}$ 426 mμ (ϵ 1.1 × 10^4) and $\lambda_{\max}$ 630 mμ (ϵ 0.42 × 10^4). The quoted extinction coefficients are based on the assumption that the conversion of $^-\alpha\alpha^-$ into $^-\text{Bp}\alpha\alpha\text{Bp}^-$ is virtually completed (this has been justified by *a posteriori* calculations).

The initial rate of Bp·⁻ formation, R_0, was determined in stop-flow experiments as the tangent of the conversion curve at $t \approx 1$ sec. The pertinent data are collected in Table I. The analysis of the proposed kinetic scheme shows that $R_0/[\text{Bp}]_0$ tends to $2k_1$ when $[^-\alpha\alpha^-]_0/[\text{Bp}]_0$ becomes large. This is shown in Figure 1 and the results lead to $2k_1 = 5.0 \times 10^{-2}\ M^{-1}\ \text{sec}^{-1}$. For the ratio $[\text{Bp}]_0/[^-\alpha\alpha^-]_0$ not too large, the formation of $^-\text{Bp}\alpha\alpha\text{Bp}^-$ may be neglected and then the equation

$$K_A = x/([^-\alpha\alpha^-]_0 - x)([\text{Bp}]_0 - x)$$

---

(7) J. Chaudhuri, J. Jagur-Grodzinski, and M. Szwarc, *J. Phys. Chem.*, 71, 3063 (1967).

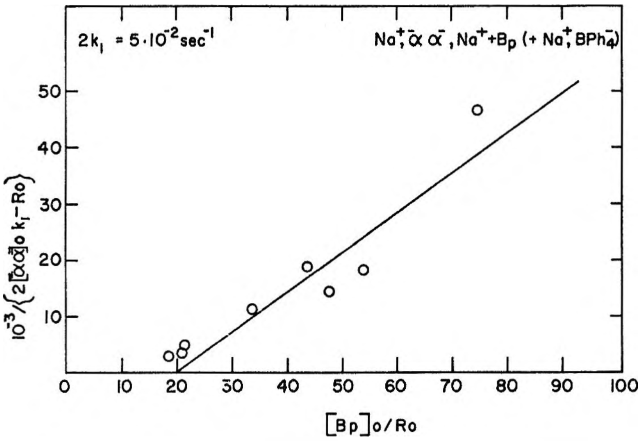

Figure 2. Dependence of $1/\{2k_1[^-\alpha\alpha^-]_0 - R_0\}$ on $[Bp]_0/R_0$. The intercept on x-axis and slope of the least-square line are 20 and 700, respectively.

where $x = [^-\alpha\alpha Bp^-]_e$ combined with $R_0 = 2k_1 x$ leads to

$$1/\{2k_1[^-\alpha\alpha^-]_0 - R_0\} = K_A[Bp]_0/R_0 - K_A/2k_1.$$

The plot of $1/\{2k_1[^-\alpha\alpha^-]_0 - R_0\}$ *vs.* $[Bp]_0/R_0$ calculated for $2k_1 = 5 \times 10^{-2}$ is shown in Figure 2. The slope of the least-square line gives $K_A = 700\ M^{-1}$ and the intercept leads then to $2k_1 = 5 \times 10^{-2}\ M^{-1}\ sec^{-1}$ demonstrating the self consistency of our approach.

In the presence of a sufficient excess of Bp, virtually all $^-\alpha\alpha^-$ are converted into $^-\alpha\alpha Bp^-$ or $^-Bp\alpha\alpha Bp^-$ adducts (*i.e.*, $[^-\alpha\alpha^-]_e \approx 0$). If we assume that only the decomposition of $^-\alpha\alpha Bp^-$ contributes then to R_0, we may calculate the equilibrium constant K_A' from the equation

$$K_A' = \frac{2k_1[^-\alpha\alpha^-]_0/R_0 - 1}{[Bp]_0 - 2[^-\alpha\alpha^-]_0 + R_0/2k_1}$$

The pertinent data are given in Table II and lead to $K_A' = 600\text{–}750\ M^{-1}$; *i.e.*, close to the value of K_A.

Table II: Na^+, $^-\alpha\alpha^-$, $Na^+ + Bp \rightarrow Bp\cdot^- + \ldots$ in THF, with Excess of Na^+, BPh_4^- at 25°

$[^-\alpha\alpha^-]_0 \times 10^3$ M	$[Bp]_0 \times 10^3$ M	$[Bp]_0/[^-\alpha\alpha^-]_0$	$R_0 \times 10^6$ $M^{-1}\ sec^{-1}$	$K_A'\ M^{-1}$
1.19	8.50	7.2	1.03	750
1.10	9.5	8.7	1.00	600

Accepting thus derived values of K_A and K_A', we may check whether $[^-\alpha\alpha^-]_e$ is indeed negligible under conditions given in Table II. The calculations fully confirm our assumption, the equilibrium concentration of $^-\alpha\alpha^-$ is 3–5% of its initial concentration.

Discussion

The results of this investigation confirmed again the the proposed mechanism of the electron transfer process from $^-\alpha\alpha^-$ to an aromatic acceptor. Two adducts are formed, *viz.*, $^-Bp\alpha\alpha^-$ and $^-Bp\alpha\alpha Bp^-$, but only the monoadduct substantially contributes to the overall reaction. The equilibrium constants of the adducts formation seems to be similar for both additions, *i.e.*, $K_A \approx K_A'$

$$^-\alpha\alpha^- + Bp \rightleftarrows {}^-\alpha\alpha Bp^-, \qquad K_A = 700\ M^{-1}$$

$$^-Bp\alpha\alpha^- + Bp \rightleftarrows {}^-Bp\alpha\alpha Bp^-, \quad K_A' \sim 600\text{–}700\ M^{-1}$$

It appears that the reaction taking place on one end of $^-\alpha\alpha^-$ hardly affects the rate of the addition to the other end. The same conclusion has been drawn previously from the studies of the anthracene addition.[3]

The equilibrium constants of the addition do not seem to be correlated with the electron affinity of the acceptor. Thus $K_A = 10^5$, 120, and 700 M^{-1} for anthracene, pyrene, and benz[*e*]pyrene, respectively, whereas the relative electron affinities in V are 0.642, 0.529, and 0.484. Apparently some other factors (steric?) determine the free energy of the adduct formation. However, it is interesting to note that the decomposition of $^-\alpha\alpha Bp^-$ into $^-\alpha\alpha\cdot + Bp\cdot^-$ is slightly faster than the analogous decomposition of the anthracene adduct. Although the electron affinity of anthracene is much higher than that of benz[*e*]pyrene, and this should facilitate the dissociation, the same factor increases the stability of the adduct and thus slows down the dissociation. The net result of this opposing tendency nearly compensates them and thus the magnitude of k_1 remains constant within a factor of 2 or 3.

Acknowledgment. We gratefully acknowledge the financial support of this work by the National Science Foundation and the Petroleum Research Fund administered by the American Chemical Society. We appreciate the help of Mr. Gideon Levin in the last stages of this research.

The Study of the Thermal Decomposition of Methyl-Substituted Amine-Type Perchlorates

by William A. Guillory and Morgan King

Naval Ordnance Research, Naval Ordnance Station, Indian Head, Maryland 20640 *(Received May 26, 1969)*

The thermal decompositions of the methyl-, dimethyl-, and trimethylammonium perchlorates have been studied over the temperature range 130–320° by use of a Bendix time-of-flight mass spectrometer. All three methyl-substituted amine salts decompose principally *via* $(CH_3)_nNH_{4-n}ClO_4 \rightarrow (CH_3)_nNH_{3-n} + HClO_4$, in addition to some heterogeneous decomposition. Perchloric acid, formed upon dissociation, appears to undergo limited decomposition to ClO_2 and HCl.

Introduction

The thermal decomposition of ammonium perchlorate (AP) has been exhaustively studied.[1] Over the temperature range from 130 to 200°, the salt undergoes simple dissociation into NH_3 and $HClO_4$, presumably by a proton transfer process. However, above 200° other modes of decomposition occur which do not yield $HClO_4$ as a final product.

It has been suggested by Mack and Wilmot[2] that an approximate proportional relationship might exist between the relative vaporization temperatures of amine salts and the pK_a values of their corresponding bases in aqueous solution. Therefore, the substitution of methyl groups for hydrogen atoms in the ammonium cation should lead to higher dissociation temperatures because of the stabilizing effect of methyl groups with respect to the proton transfer mechanism. As a consequence, reactions of the evaporated products from simple dissociation could be studied under Knudsen conditions at higher temperatures; of particular interest are reactions involving $HClO_4$. This study revealed that such a proportional relationship as suggested above does exist in the case of the methyl-substituted amine-type perchlorates. In addition, $HClO_4$ produced as an evaporated product remains relatively stable up to 320°.

Experimental Section

Materials. The various methyl-substituted amine salts were prepared by titrating aqueous solutions of the methyl-substituted amines against a slightly diluted solution of 70 wt % $HClO_4$ using a methyl red indicator. The water was removed by liquid nitrogen cryo-pumping for 2 days. The methyl-substituted amine salts were recrystallized twice with a hot ethanol solution and a few drops of H_2O. The salts were then filtered and placed in a 60° oven for 2 hr. The 70 wt % $HClO_4$ was obtained from Allied Chemical. Prior to each $HClO_4$ run, the 70 wt % $HClO_4$ sample was pumped until the mass spectrum revealed peaks due solely to $HClO_4$ and no H_2O from the sample.

Mass Spectrometric Method. The mass spectral observations were performed with a Bendix time-of-flight mass spectrometer (Model 12-101) with the modified S-12-101 source in conjunction with a heater inlet system. The heater inlet system consisted of a 2-in. diameter copper tube soldered to a stainless steel flange that adapted directly to the bottom of the source cross. The Pyrex glass sample tubes were mounted axially to the inlet system about 6 cm below the entrance slit. Further details of the experimental setup have been described previously.[3] The inlet system used for the comparison spectrum of $HClO_4$ was all glass with two Teflon stopcocks in series for pressure monitoring. The delivery tube was attached to a flange that was mounted to the bottom of the source cross such that the sample came into contact with only glass and Teflon.

Results

Methylammonium Perchlorate (MAP). The thermal decomposition of MAP under free-evaporation conditions was studied over the temperature range 150 to 257°. New features in the spectrum appeared at approximately 150°. The prominent features are indicative of two major products, $HClO_4$ and CH_3NH_2.[4] Other products formed in small quantities were N_2O, H_2O, and, possibly, O_2 and N_2 (Figure 1).

However, one striking feature of the spectrum was the apparent change in the cracking pattern of $HClO_4$ as the temperature was increased. The peaks due to the 67–69 isotopic pair were dominant below approximately 176°. Above 176°, there was a reversal in the relative

---

[1] A. R. Hall and G. S. Pearson, "A Review of Ammonium Perchlorate Combustion," Ministry of Technology, London, Jan 1967.

[2] J. L. Mack and G. B. Wilmot, *J. Phys. Chem.*, 71, 2155 (1967).

[3] W. A. Guillory, J. L. Mack, and M. King, *ibid.*, 73, 4370 (1969).

[4] "American Petroleum Institute Research Project 44, Mass Spectral Data," Serial No. 1123.

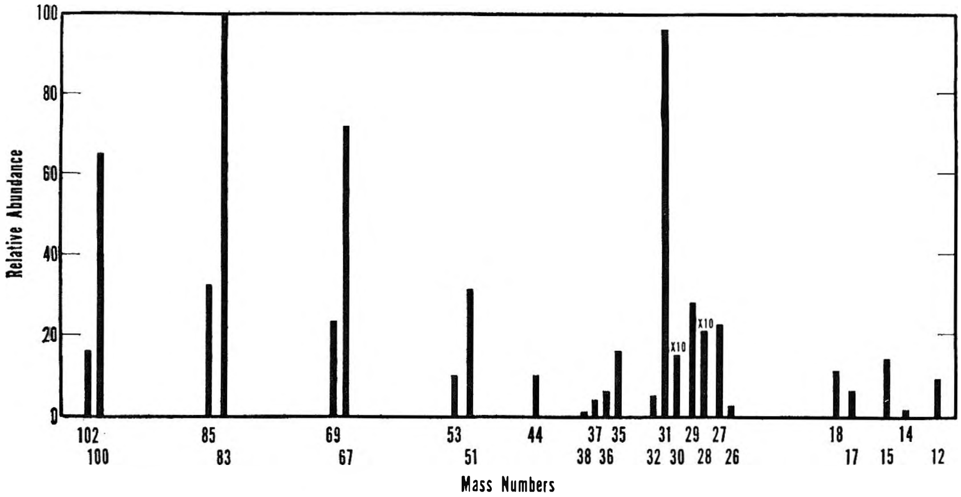

Figure 1. Mass spectrum of thermally dissociated methylammonium perchlorate at 230° [free-evaporation experiment].

peak heights of the 67–69 and 83–85 isotopic pairs, such that the 83–85 pair became the dominant peaks in the isotopic pattern (reversal effect). The peaks then remained proportional as the temperature was further increased. The true $HClO_4$ cracking pattern was shown to be the one observed at high temperatures as proven by a comparison spectrum of $HClO_4$ alone (Figure 2).

Dimethylammonium Perchlorate (*DMAP*). The thermal decomposition of DMAP under free evaporation and Knudsen conditions was studied over the temperature range from 165 to 290°. The resulting spectra showed little difference between the two conditions. The products spectrum at 190° is shown in Figure 3. The major features observed are those due to $HClO_4$, $(CH_3)_2NH$,[5] a chlorine–oxygen species, and their degradation products. There is also production of some H_2O, O_2, N_2, HCl, NO_2, and, possibly, N_2O.

When comparing the spectrum of $HClO_4$ with the DMAP chlorine isotopic peaks, one notices that the 67–69 and 51–53 pairs are not proportional to the $HClO_4$ parent peak (100–102). These two pairs remained greater than their sole contribution from $HClO_4$ over the entire temperature range.

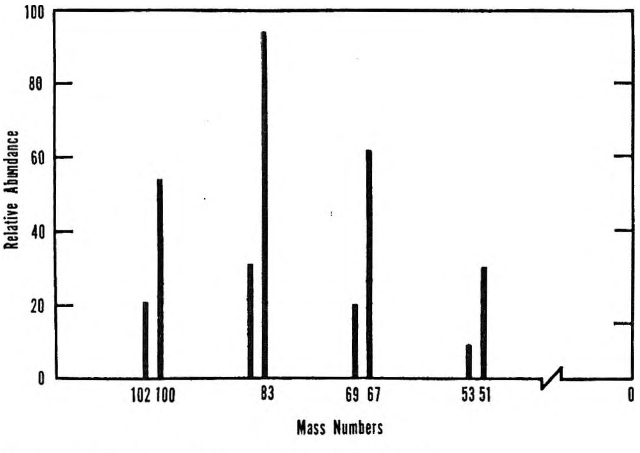

Figure 2. Mass spectrum of perchloric acid.

Trimethylammonium Perchlorate (*TMAP*). The thermal decomposition of solid TMAP was studied in both a free-evaporation and a Knudsen cell over the temperature range 250–320°. The products spectrum is shown in Figure 4. The major features observed are those due to $HClO_4$, $(CH_3)_3N$,[6] and their degradation products. In addition, some HCl, N_2O, O_2, N_2, and H_2O were formed. The Knudsen experiments revealed that there was no tendency toward further gas-phase reactions between the evaporated products. Again, the so-called "reversal effect" was observed.

Discussion

All three of the methyl-substituted amine salts appear to decompose principally to the corresponding methyl-substituted amine and $HClO_4$ *via*

$$(CH_3)_nNH_{4-n}ClO_4 \longrightarrow (CH_3)_nNH_{3-n} + HClO_4 \quad (1)$$

where n ranges from 1 to 3. In each case there is an additional mode of decomposition giving rise to small contributions of HCl, NO_2, H_2O, O_2, N_2, and some N_2O.

The substitution of methyl groups into the cation does appear to stabilize these perchlorate salts. This stability is indicated by the higher dissociation temperatures as the number of methyl groups increases. This observation supports the suggestion that one should observe this trend where decomposition occurs *via* proton transfer.[2]

The Knudsen experiments revealed that $HClO_4$ and the various methyl-substituted amines are relatively stable with respect to each other in the gas phase over the temperature ranges investigated.

The most striking feature in the spectra of the vaporized salts was the so-called "reversal effect" in the

(5) See ref 4, Serial No. 1124.

(6) See ref 4, Serial No. 1127.

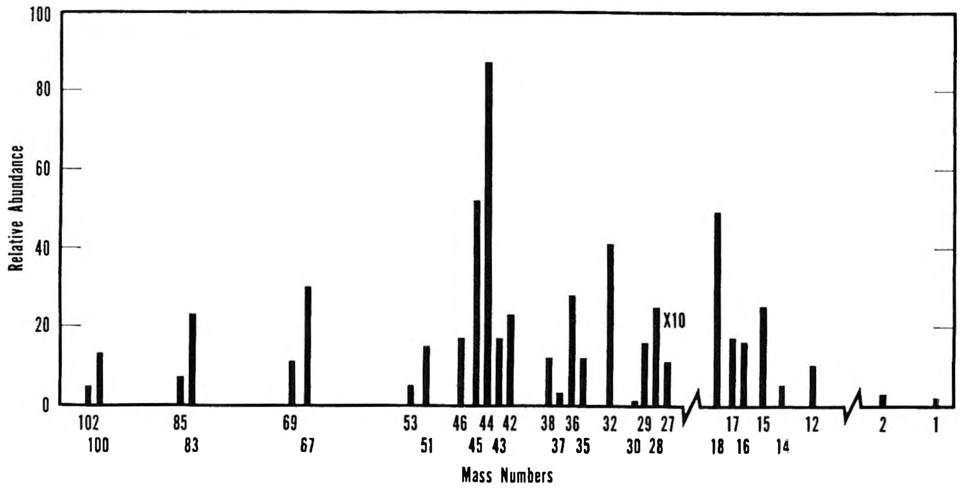

Figure 3. Mass spectrum of thermally dissociated dimethylammonium perchlorate at 190° [free-evaporation experiment].

cracking pattern of $HClO_4$. Upon closer examination of the isotopic peaks, it can be shown that this effect is due to the production of ClO_2. This species has also been observed by Pellet and Saunders[7] upon laser flashing an AP sample and in the thermal decomposition of NH_4ClO_4.[3] Since this effect is observed in all of these perchlorate systems, it would appear to arise from a common component, namely $HClO_4$. Apparently, HCl and ClO_2 production results from the heterogeneous decomposition of $HClO_4$ on the salt surface as suggested by Pellet and Saunders.[7]

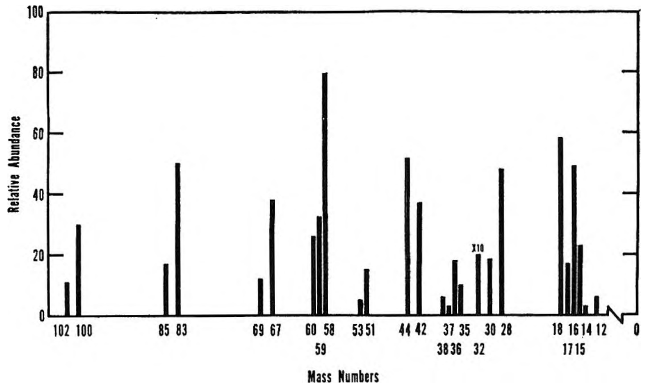

Figure 4. Mass spectrum of thermally dissociated trimethylammonium perchlorate at 300° [Knudsen experiment].

Conclusion

The thermal decompositions of methyl-,dimethyl-, and trimethylammonium perchlorates occur principally by dissociation into perchloric acid and the corresponding methyl-substituted amine. The dissociation temperatures increase with increasing methyl substitution into the ammonium cation. Experiments with a Knudsen cell revealed that practically no reactions occur between the evaporated products. Perchloric acid appears to undergo limited decomposition in all cases leading to HCl and ClO_2 production.

Acknowledgments. This work funded under the Foundation Research Program of the Naval Ordnance Systems Command. The authors wish to express their appreciation to Dr. George Wilmot and Dr. Julius Mack, who read the manuscript and made helpful suggestions.

---

(7) G. L. Pellet and A. R. Saunders, "Heterogeneous Decomposition of Ammonium Perchlorate-Catapult Mixtures Using Pulsed Laser Mass Spectrometry," presented at the AIAA Sixth Aerospace Sciences Meeting (Jan 1967), NASA Langely Research Center, Hampton, Va.

The Thermal Decomposition of Ammonium Chlorate

by **W. A. Guillory, M. King, and J. L. Mack**

Naval Ordnance Research, Naval Ordnance Station, Indian Head, Maryland 20640 *(Received April 18, 1969)*

The thermal decomposition of ammonium chlorate has been studied over the temperature range 75 to 120°. Two decomposition processes were identified; one process yields ammonia and chlorine dioxide as the principal products. The other process yields as major products N_2, H_2O, Cl_2, and NH_4NO_3. All the products and intermediates listed, with the exception of NH_4NO_3, were identified by mass spectrometry and additionally the identification of NH_4NO_3, ClO_2, HNO_3, H_2O and NH_3 were confirmed by their infrared spectra. On the basis of the observed intermediates and products formed, a reaction sequence is suggested.

Introduction

In the course of infrared studies[1] performed on the vaporization of various perchlorate salts, the thermal decomposition of methylammonium perchlorate gave significant product absorptions which were not characterized. Two particularly interesting pairs of absorptions with the appropriate $^{35}Cl/^{37}Cl$ intensity ratio occurred at 1180–1168 cm^{-1} and 1128–1114 cm^{-1}. These absorptions are suggestive of chlorine–oxygen or chlorine–hydrogen–oxygen species. Since the observed absorptions did not fit any known chlorine–oxygen species, other possibilities were considered. One likely species is $HClO_3$, since the chlorine–oxygen stretching frequencies would be expected to shift to lower frequencies relative to $HClO_4$,[2] presumably caused by the accumulation of positive charge on the Cl atoms as oxygens are successively added.

Assuming that ammonium chlorate thermally decomposes as do the perchlorate salts,[1] one would expect the following

$$NH_4ClO_3 \longrightarrow NH_3 + HClO_3 \qquad (1)$$

The combined use of matrix-isolation infrared and mass spectroscopy has shown that this mode of decomposition probably does occur in part.

Experimental Section

Materials. Ammonium chlorate (AC) was prepared by mixing approximately stoichiometric quantities of solutions of $Ba(ClO_3)_2 \cdot H_2O$ (99.9% pure) and $(NH_4)_2SO_4$ (99.5% pure) and titrating to the $BaSO_4$ end point. The barium sulfate precipitate was then filtered and the resulting solution was again tested for excess sulfate or barium ion. The water was pumped away and the residue recrystallized from ethanol. Ammonium chlorate decomposes upon standing at room temperature to produce N_2, Cl_2, H_2O, and NH_4NO_3. However, freshly prepared samples stored at −5° remained stable indefinitely. The nitric acid (71 wt %) and ammonium nitrate (99.5% purity) obtained from the Allied Chemical Company were used without further purification.

Infrared Method. The experimental procedure was essentially the same as previously described[1] except for the addition of glass beads to the sample to prevent sputtering. Ammonium chlorate was slowly heated between 75 and 120°, and the decomposition products were matrix-isolated on an infrared transmitting window between 7 and 10°K. The matrix material in all experiments was nitrogen. The spectrum was recorded with a double-beam grating spectrophotometer over the region 250–4000 cm^{-1}.

A comparison spectrum of matrix-isolated nitric acid was obtained by depositing the 71 wt % HNO_3 directly onto the cold window from an all-glass delivery system (N_2/HNO_3 was approximately 500/1). The vapor pressure of the 71 wt % nitric acid is 2–3 Torr at room temperature, and its rate of delivery was controlled by two stopcocks in series.

Mass Spectrometric Method. The mass spectral observations were performed with a Bendix time-of-flight mass spectrometer, Model 12-101, with the modified S-12-101 source. A rhenium filament was used in all the experiments performed. The heater-inlet system (Figure 1) consisted of a 2-in. diameter copper tube soldered to a stainless steel flange that adapted directly to the bottom of the source cross. Four electrical feedthroughs in the flange allowed measurement of the temperature with a chromel–alumel thermocouple and electrical current to be delivered to the tantalum heater coil surrounding the sample cell. The thermocouple was placed on the outer wall of the sample holder adjacent to the sample and was surrounded by two concentric tantalum radiation shields. The Pyrex sample tube was mounted axially to the inlet system about 6 cm below the entrance slit. In order to reduce collisions and reactions occurring in the source region, a liquid nitrogen trap was placed above the source cross. This feature also proved valuable in obtaining a reduced mass spectral background.

---

[1] J. L. Mack and G. B. Wilmot, *J. Phys. Chem.*, 71, 2155 (1967).

[2] M. M. Rochkind and G. C. Pimentel, *J. Chem. Phys.*, 42, 1361 (1965).

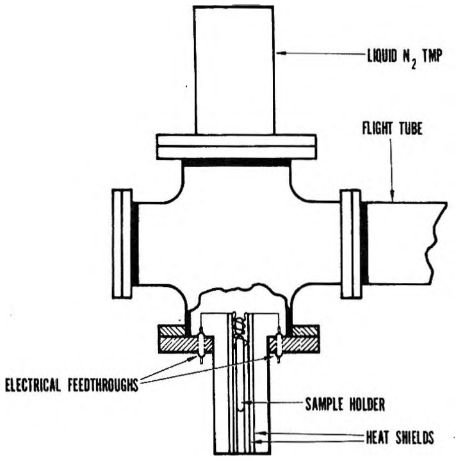

Figure 1. The heater-inlet system used with the mass spectrometric experiments.

Two types of sample holders were used in the mass spectrometric investigation. One was an open Pyrex tube, 10 mm diam × 10 mm length (one end closed), approximating free evaporation and allowing decomposition products to be fed directly into the source; the other was a Knudsen cell which allowed collisions to occur between the products of decomposition before being fed into the mass spectrometer source region.

The procedure then was simply to heat the sample slowly, measure the temperature and pressure, and record the mass spectrum.

Results

Mass Spectrometric Study. AC Free Evaporation Experiment. As ammonium chlorate was gradually heated above room temperature, the pressure increased. However, it was kept within the working range of the mass spectrometer by use of a nitrogen cold trap above the electron source. The first indication of decomposition of NH_4ClO_3 occurred at approximately 75°, where the 67 (ClO_2^+), 46 (NO_2^+), and 17 (NH_3^+) peaks began to grow. As the temperature was raised further, growth patterns corresponding to H_2O, Cl_2, and N_2 were observed. A "pressure burst" consistently occurred at approximately 87° regardless of the quantity or compactness of the sample. The spectrum of the species existing at 89° just after the "pressure burst" is shown in Figure 2. This products spectrum indicated very large production of N_2 with correspondingly smaller concentrations of H_2O, HNO_3, and Cl_2. Other products observed in even lesser concentrations are NH_3, ClO_2, N_2O, HCl, and probably NCl_3.

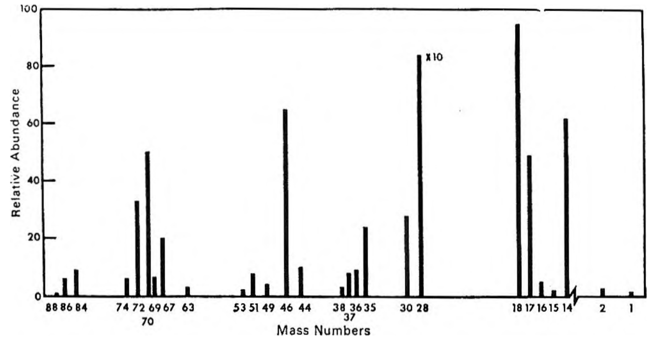

Figure 2. Mass spectrum of thermally dissociated ammonium chlorate at 89° (free evaporation experiment).

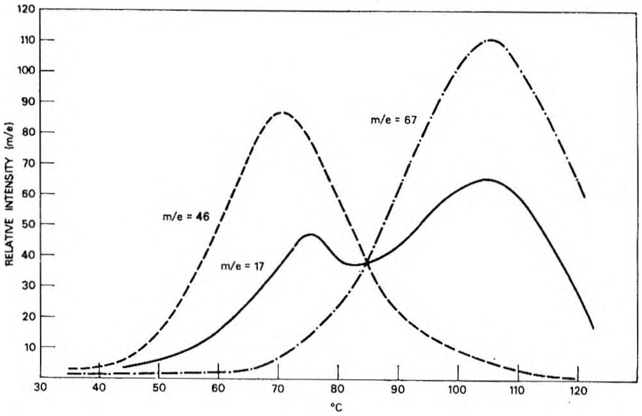

Figure 3. Variation of m/e 46, 67, and 17 *vs.* T, °C, for the pretreated NH_4ClO_3 sample.

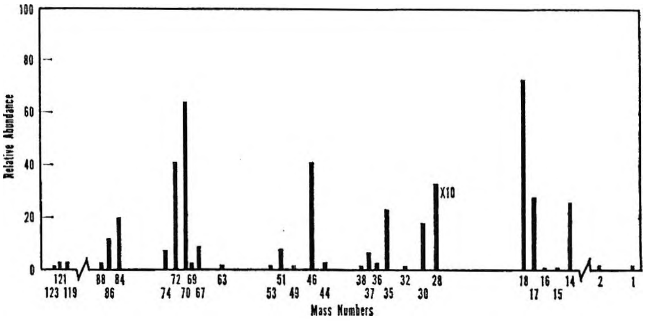

Figure 4. Mass spectrum of thermally dissociated ammonium chlorate at 88° (Knudsen type experiment).

Freshly prepared samples of NH_4ClO_3 were "pretreated" by slowly heating the salt on a vacuum line until the "pressure burst" occurred. After this point was reached, the sample continued to exhibit a "fountain effect" for a few minutes as if small pressurized voids throughout the sample were rupturing. The residue gradually cooled after the burst occurred and infrared KBr pellet analyses confirmed the existence of NH_4ClO_3 and NH_4NO_3. The conversion to NH_4NO_3 was roughly 20% as approximated by their infrared absorptions.

A "pretreated" sample of AC was slowly heated (1°/min) while recording the mass spectrum. Over the temperature range 50 to 80° the mass spectrum revealed products due to NH_3 and HNO_3 with very small contributions of N_2, Cl_2, and H_2O, probably from some unruptured voids. A comparison experiment of solid NH_4NO_3 was performed and the results were essentially the same as those obtained with the "pretreated" sample of NH_4ClO_3 over the temperature interval 50

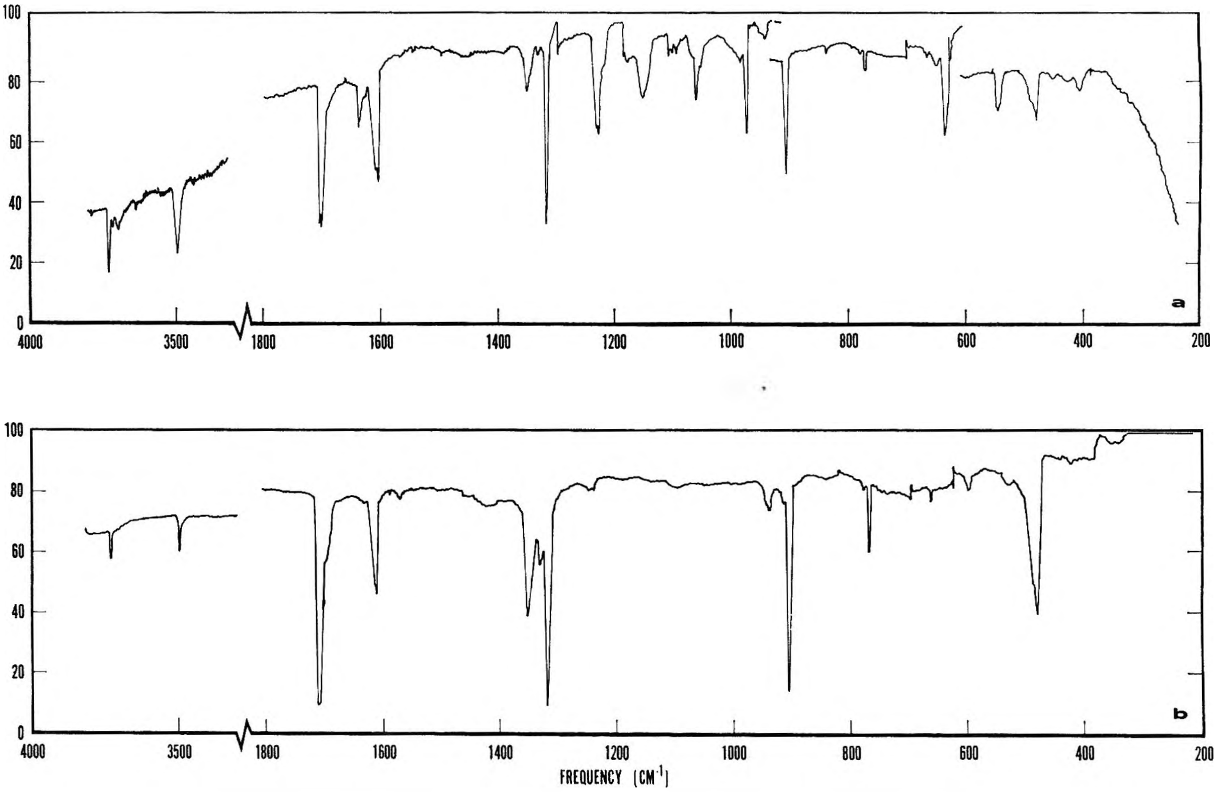

Figure 5. a, Absorption spectrum of the vapor products from thermally decomposed ammonium chlorate; b, absorption spectrum of 71% nitric acid.

to 80°. Over the temperature range 80 to 120°, the spectrum revealed features due principally to ClO_2, NH_3, possibly OH, and very small contributions of N_2, O_2, Cl_2, HCl, and H_2O. The "pretreated" sample did not experience a "pressure burst." These results are summarized in Figure 3.

Table I: Summary of the Absorptions Obtained from the Thermal Decomposition of Ammonium Chlorate

Absorption frequency, cm^{-1}	Intensity	Assignment
3730	m	H_2O
3700	w	$(H_2O)_2$ or OH (?)
3490	m	HNO_3
1700	vs	HNO_3
1632	w	NH_3
1599	s	H_2O
1345	m	HNO_3
1313	vs	HNO_3
1225	s	?
1150	m	?
1105	w	ClO_2
1055	m	?
970	m	NH_3
945	w	ClO_2
900	s	HNO_3
830	vw	?
765	w	HNO_3
645	vw	?
630	m	?
540	m	?
475	m	HNO_3
450	vw	ClO_2
403	w	?

AC Knudsen Experiment. The products spectrum of thermally decomposed ammonium chlorate using the Knudsen cell is shown in Figure 4. The spectrum indicates again very large production of N_2 with lesser relative amounts of H_2O, HNO_3, and Cl_2. The amount of HCl and ClO_2 relative to Cl_2 decreases slightly. There is a virtual absence of NH_3. In turn, significant new features occurring in the 120, 86, and 50 mass regions do so in isotopic ratios which are consistent with a cracking pattern of NCl_3.

Experiments with "pretreated" samples were carried out with a Knudsen cell. The results were similar to those obtained in the case of free evaporation, where NH_4NO_3 and NH_4ClO_3 decomposed over different temperature ranges and no "pressure burst" occurred.

Infrared Study. A typical absorption spectrum of the products from heated ammonium chlorate is shown in Figure 5a, and the data are listed in Table I.

In practically all of the infrared experiments performed, absorptions due to nitric acid were by far the strongest observed. The spectrum of 71 wt % matrix-isolated nitric acid is shown in Figure 5b; it can be compared with the spectrum of the vapor species obtained from heated NH_4ClO_3. Other products ob-

Table II: Summary of the Mass Spectral and Infrared Absorption NH_4ClO_3 ("Pretreated") Decomposition Results (Free Evaporation Experiment)

Species	Relative concn[a]	Infrared absorption
N_2	Small	...
H_2O	Small	Obsd
HNO_3	Large	Obsd
Cl_2	Small	...
NH_3	Moderate	Obsd
ClO_2	Large	Obsd
N_2O	Small	Obsd
HCl	Small	Not obsd[b]
$HClO_3$	Small[c]	Not obsd[b]
NCl_3	Small	Unconfirmed

[a] Relative concentrations as determined from ion currents. [b] Probably due to low concentration. [c] The small concentration of $HClO_3$ occurring at the same *m/e* of NCl_2 did not allow its positive identification.

served in the infrared such as ClO_2, NH_3, and N_2O were confirmed from their matrix-isolated spectra.[3]

The unknown absorptions in Table I do not appear to be chlorine-containing species since no resolvable pattern of isotopic shifts was observed, although the broadness of some of these absorptions could possibly account for this fact. In fact, two fundamental absorptions of NCl_3 in CCl_4 have been reported at 642 and 538 cm^{-1}.[4] However, the relative spectral intensities are so different from the observations of this work that it is very difficult to ascertain whether some of the unknown absorptions were due to NCl_3, in particular 645 and 540 cm^{-1}. Polymeric absorptions of HNO_3 were also compared with the unidentified features but did not correlate with the bands in question. Practically every stable oxide of nitrogen and some unstable oxides were compared for possible identification, but none corresponded to the unknown frequencies.

The experimental results obtained with the "pretreated" material were in general agreement with those obtained by mass spectroscopy and infrared analyses of the "untreated sample." The combined results of mass and infrared spectroscopy of the decomposition processes are summarized in Table II.

Discussion

Analysis of the experimental results seems to indicate that the NH_4ClO_3 crystals are formed with defective sites and small interior voids in the lattice. Apparently, the unstable nature of the salt is caused by decomposition at these defective sites. The products of this decomposition process are NH_4NO_3, Cl_2, H_2O, and N_2. When this process occurs near or in the interior voids of the crystal lattice, these products remain trapped.

As the partially decomposed salt is heated above room temperature, an additional process becomes significant at approximately 50°. The dissociation of NH_4NO_3 *via*

$$NH_4NO_3(c) \longrightarrow NH_3(g) + HNO_3(g) \qquad (2)$$

is similar to the liquid dissociation process[5] and confirmed in this work with an experiment involving the evaporation of pure NH_4NO_3. There is additionally a small contribution from NH_4NO_3 decomposition giving rise to N_2O as observed previously[5]

$$NH_4NO_3(c) \longrightarrow N_2O(g) + 2H_2O(g) \qquad (3)$$

Thus, the dissociation and decomposition (eq 2 and 3) products are also trapped.

As NH_4ClO_3 is further heated, disruption of the crystal lattice occurs releasing the trapped gases from the interior voids and giving rise to the observed "pressure burst."

Prior to this disruptive process, the trapped gases probably react to some extent giving rise to other observed products such as NCl_3 and HCl, as confirmed by the Knudsen experiments.

$$2NH_3(g) + 6Cl_2(g) \longrightarrow 2NCl_3(g) + 6HCl(g) \quad (4)$$

Hydrogen chloride formed by this reaction would react rapidly with NH_3 yielding NH_4Cl and thus significantly contribute to the decrease in HCl and the virtual absence of NH_3 in Figure 4.

The products resulting from NH_4ClO_3 decomposition as identified from the infrared work are ClO_2 and NH_3. This decomposition process generally becomes significant at approximately 80°, but it was always complicated by the "pressure burst" which occurred. Therefore, by "pretreating" the sample, we were able to study the decomposition of NH_4ClO_3 without the complicating side reactions.

The "pretreated" sample consisted of a mixture of NH_4NO_3 and NH_4ClO_3 with very few, if any, defective sites, since no "pressure burst" was observed. The results of the experiments performed using this sample revealed that the decomposition ranges of the two salts occurred over different temperature intervals and were apparently independent of each other. The modes of NH_4NO_3 decomposition have been described, *i.e.*, eq 2 and 3.

The combined results of mass spectral and infrared matrix-isolation data indicate that the decomposition of NH_4ClO_3 appears to occur *via*

$$NH_4ClO_3 \longrightarrow NH_3 + HClO_3 \qquad (1)$$

and subsequent decomposition of the acid, possibly initiated by splitting off an OH radical.

$$HClO_3 \longrightarrow ClO_2 + OH \qquad (5)$$

---

(3) M. M. Rochkind and G. C. Pimentel, *J. Chem. Phys.*, **46**, 4481 (1967).

(4) J. C. Carter, R. F. Bratton, and J. F. Jackovitz, *ibid.*, **49**, 3751 (1968).

(5) W. A. Rosser, Jr., S. H. Inami, and H. Wise, *J. Phys. Chem.*, **67**, 1753 (1963).

This mode of decomposition is analogous to that suggested for the $HClO_4$ decomposition[6] and observed in the pulsed laser decomposition of NH_4ClO_4.[7]

Although the presence of OH from this source would be masked by NH_3 in the mass spectrometer, the NH_3^+/NH_2^+ ratio was greater than the normal ratio observed for NH_3 alone (after correcting for H_2O). This could indicate possible additional contribution from the OH radical.

The results of the Knudsen experiments compared to those of free-evaporation seem to indicate that very little reaction occurred between the sublimed products of NH_4ClO_3 dissociation.

Conclusion

The dissociation of ammonium chlorate appears to proceed *via* a proton-transfer mechanism: $NH_4ClO_3(c) \rightarrow NH_3 + HClO_3$, with subsequent decomposition of the acid to produce ClO_2 as the major product. The gaseous products of the dissociation process do not show any tendency to undergo further reaction. The energy of activation for the dissociation process has been determined as 17 kcal/mol.

No evidence was obtained for the existence of an NH_4ClO_3 vapor phase species.

Acknowledgments. This work was funded under the Foundation Research Program of the Naval Ordnance Systems Command. The authors would also like to express their appreciation to Dr. George Wilmot for reading the manuscript and making valuable suggestions.

---

(6) J. B. Levy, *J. Phys. Chem.*, **66**, 1092 (1962).

(7) G. L. Pellet and A. R. Saunders, AIAA Sixth Aerospace Sciences Meeting, New York, N. Y., 1968.

NOTES

Ion–Solvent Interactions. Conductance and Nuclear Magnetic Resonance Studies of Sodium Tetrabutylaluminate in the Presence of Benzene and Toluene

by C. N. Hammonds, T. D. Westmoreland, and M. C. Day[1]

Department of Chemistry, Louisiana State University, Baton Rouge, Louisiana 70803

(Received May 26, 1969)

The importance of solvent interactions on the behavior of ionic solutions is well recognized. Their effects on ionic conductance and extent of ion-pair formation were clearly pointed out by Gilkerson[2] and have been extensively studied by several research groups.[3-7] More recently there has been considerable interest in the effects of such interactions on the rates of anionic polymerization reactions in the presence of various alkali metal counterions.[8] Although these studies have generally been carried out in ethereal solvents such as tetrahydrofuran (THF) and dimethoxyethane (DME), some studies have been made in the nonpolar solvents cyclohexane[9,10] and benzene.[11]

There can be no question that specific complexation occurs between the smaller alkali metal cations and basic solvents such as THF and DME and that this affects the rates of anionic polymerization reactions, but the possibility of specific complexation of alkali metal cations with aromatic solvents such as benzene has not been determined although the effect of benzene on anionic polymerization rates has been studied and the possibility of such complexation has been proposed.[9]

Using cyclohexane as an inert solvent and sodium tetrabutylaluminate ($NaAlBu_4$) as a source of the sodium ion, we have recently shown that it is possible to study the specific solvation of the sodium ion by bases such as THF using nmr[12] and conductance[13] techniques. We report here the use of these techniques in the study

---

(1) Reprint requests should be sent to M. C. Day.

(2) W. R. Gilkerson, *J. Chem. Phys.*, **25**, 1199 (1956).

(3) R. M. Fuoss, *et al.*, *J. Phys. Chem.*, **69**, 2576 (1965), and many others in the series.

(4) C. A. Kraus, *J. Chem. Educ.*, **35**, 324 (1958).

(5) W. R. Gilkerson and J. B. Ezell, *J. Amer. Chem. Soc.*, **89**, 808 (1967).

(6) T. E. Hogen-Esch and J. Smid, *ibid.*, **88**, 318 (1966).

(7) A. D'Aprano and R. Triolo, *J. Phys. Chem.*, **71**, 3474 (1967).

(8) T. Shimomura, J. Smid, and M. Szwarc, *J. Amer. Chem. Soc.*, **89**, 5743 (1967).

(9) J. E. L. Roovers and S. Bywater, *Can. J. Chem.* **46**, 2711 (1968).

(10) F. S. Dainton, *et al.*, *Makromol. Chem.*, **89**, 257 (1965).

(11) J. E. L. Roovers and S. Bywater, *Trans. Faraday Soc.*, **62**, 701 (1966).

(12) E. Schaschel and M. C. Day, *J. Amer. Chem. Soc.*, **90**, 503 (1968).

(13) C. N. Hammonds and M. C. Day, *J. Phys. Chem.*, **73**, 1151 (1969).

of the system $NaAlBu_4$–cyclohexane with both benzene and toluene.

Experimental Section

The nmr and conductance measurements and the preparation of $NaAlBu_4$ have been previously reported.[12,13] The proton magnetic resonance spectra were obtained at ~37° and the conductance measurements were made at 25.00 ± 0.05°.

All solvents were purchased as reagent or higher grade chemicals. Cyclohexane, benzene, and toluene were refluxed over sodium–potassium alloy and distilled under a dry nitrogen atmosphere with an 80% return to the distillation column. All solvents were stored over sodium chips in vacuum-tight flasks in a nitrogen drybox.

Standard solutions of $NaAlBu_4$ were prepared by dissolving the salt in the bulk solvent cyclohexane. Aliquot portions of this solution were withdrawn and added to a series of 100-ml volumetric flasks which were fitted with outer caps to prevent contamination by the ground-glass joint lubricant. Coordinating agents were added by weight to the flasks to give the appropriate mole ratio of coordinating agent to salt, and the solutions were diluted with the bulk solvent at 25.00 ± 0.05° in a constant temperature bath by means of a closed dilution apparatus fitted to the flask.

Results and Discussion

In a solvent of low dielectric constant such as cyclohexane, $NaAlBu_4$ can be considered to exist as an ion-pair or higher aggregate. On the addition of a complexing agent such as tetrahydrofuran, a complex with the sodium ion is formed. Based on the distinctive nmr and conductance behavior observed in earlier studies, we have proposed the equilibrium

$$\text{Na}\cdot\text{THF}^+, \text{X}^- + 3\text{THF} = \text{Na}\cdot4\text{THF}^+, \text{X}^-$$

in which the 1:1 complex is assumed to be totally in the complexed form.

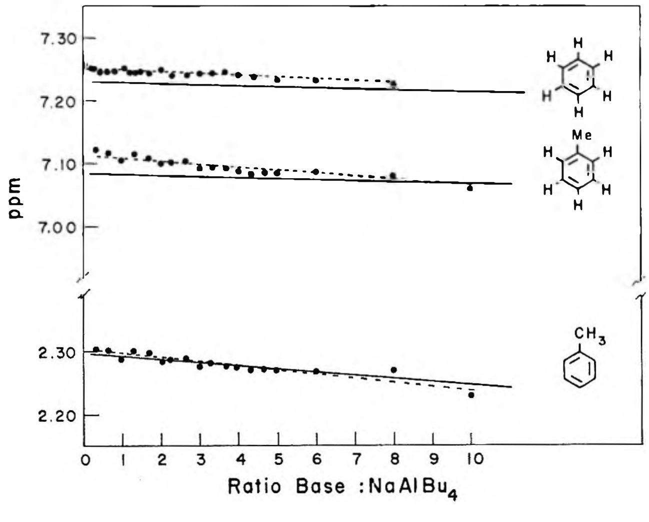

Figure 1. Chemical shifts in the benzene and toluene proton signals as a function of the mole ratio, base:$NaAlBu_4$. Solid line represents the corresponding signals in the absence of salt.

A summary of the application of these methods to the study of possible complexation of the sodium ion by benzene and toluene is shown in Figures 1 and 2. In Figure 1, the chemical shifts of the indicated protons are shown for both toluene and benzene as a function of the mole ratio of base to $NaAlBu_4$ using cyclohexane as a solvent with a salt concentration of 0.20 *M*. The corresponding chemical shifts in the absence of the salt are seen to be very nearly coincident with those in the presence of the salt, indicating that concentration effects are responsible for the chemical shifts. The absence of any inflection points along with the fact that there is no significant change in the chemical shift in the presence or absence of $NaAlBu_4$ indicates that no specific complex exists between the sodium ion and benzene or toluene.

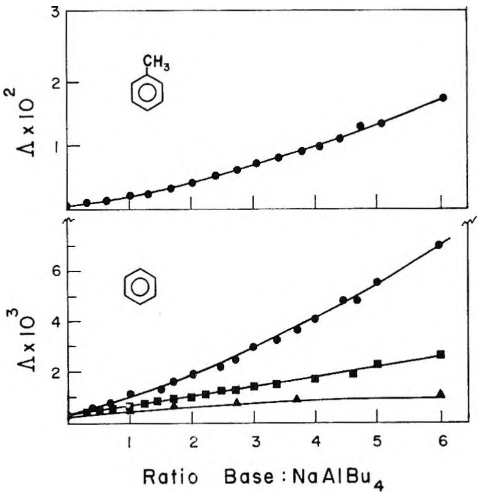

Figure 2. Equivalent conductance of $NaAlBu_4$ in cyclohexane–base mixtures as a function of mole ratio, base:salt; salt concentration (benzene): ●, 0.2023 *M*; ■, 0.1032 *M*; ▲, 0.04776 *M*; salt concentration (toluene) = 0.1994 *M*.

The analogous conductance data are shown in Figure 2 where the equivalent conductance of $NaAlBu_4$ in cyclohexane as a function of base to salt ratio is given, respectively, for benzene and toluene. In contrast to the behavior observed in the presence of a coordinating solvent such as THF,[13] no inflection points are noted in these curves. Rather, the regular increase in equivalent conductance is most reasonably attributed to an increase in solvent dielectric constant. Thus, the conductance data substantiate the nmr studies, and we conclude that the sodium ion does not form a specific complex with either benzene or toluene at 25°.

Based on general observations of ion–solvent interactions and cation size, it can reasonably be assumed that complexation also does not occur with the larger alkali metal cations. Attempts to carry out analogous studies on the lithium ion were unsuccessful because of the inability to find a lithium salt that is soluble in a saturated hydrocarbon solvent.

Acknowledgment. Support of this work by National Science Foundation Grant Gp6421 and a National Science Foundation Science Faculty Fellowship for C. N. Hammonds is gratefully acknowledged.

Negative Ions Produced by Electron Capture in Phosphine

by M. Halmann and I. Platzner

Isotope Department, The Weizmann Institute of Science, Rehovot, Israel *(Received January 3, 1969)*

Negative ions, PH_2^-, PH^-, P^-, and H^- had been produced by electron impact on phosphine in the mass spectrometer.[1] Their appearance potentials were measured by the retarding potential difference method, but only in the resonance electron capture region, below 10 eV.[2] In the present work, measurements have been extended up to electron energies of 75 eV, covering also the region of ion pair formation. The new data, together with previous results on positive primary[3] and secondary[4] ions, enable a more complete description of the various processes of electron capture and ionization.

Experimental Section

Experiments were performed with an Atlas CH-4 mass spectrometer, using the normal electron impact ionization chamber (Type AN4). The highest ion currents at the ion collector were about 10^{-11} A.

Appearance potentials were calculated from the observed ionization efficiency curves by linear extrapolation to zero ion current, using the steepest section of the increasing curve for each process. Each curve was measured at least twice, and at three different gas pressures (2, 5, and about 10 Torr in the inlet reservoir).

The electron energy was measured with a Hewlett-Packard Model 3440 A digital voltmeter connected between the filament and the ion chamber. For calibration of the electron energy scale the appearance potentials of O^- by electron capture and ion pair formation in carbon monoxide (9.60 and 20.9 eV) were used. Results given in Table I include the average of the observed appearance potentials and their probable errors.

Phosphine was prepared by thermal decomposition of phosphorous acid.[4b]

Results and Discussion

Ionization efficiency curves for the ions H^-, PH_2^-, PH^-, and P^- in the mass spectrum of phosphine are shown in Figure 1. The curves show both the sharp maxima due to resonant electron capture, as well as the gradual onset of ion pair formation. Appearance potentials derived from these curves for resonant capture and ion pair formation are presented in Table I, and are compared with previously reported results on the resonant capture.[2]

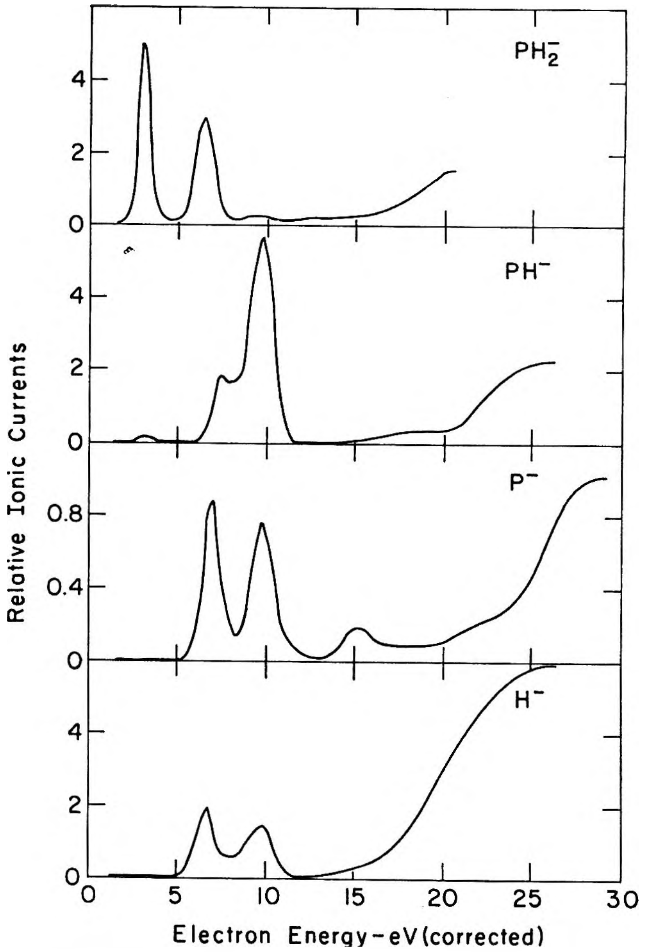

Figure 1. Ion current (in arbitrary units) as a function of electron energy (in eV) for the negative ions in the mass spectrum of phosphine.

On the basis of the observed appearance potentials we are able to propose some conclusions on the reactions of phosphine in the ion source (see Table I). The conclusions are based on the following values for the ionization potentials *I*, electron affinities *EA*, and bond dissocia-

---

[1] O. Rosenbaum and H. Neuert, *Z. Naturforsch.*, **9a**, 990 (1954).

[2] H. Ebinghaus, K. Kraus, W. Müller-Duysing, and H. Neuert, *ibid*, **19a**, 732 (1964).

[3] H. Neuert and H. Clasen, *ibid.*, **7a**, 410 (1952); M. Halmann, *J. Chem. Soc.*, 3270 (1962); J. Fischler and M. Halmann, *ibid.*, 31 (1964); F. E. Saalfeld and H. Svec, *Inorg. Chem.*, **2**, 46 (1963); Y. Wada and R. W. K. Kiser, *ibid.*, **3**, 174 (1964); A. A. Sandoval, H. C. Moser and R. W. Kiser, *J. Phys. Chem.*, **67**, 125 (1963); T. P. Fehlner and R. B. Callen, in "Mass Spectrometry in Inorganic Chemistry," J. L. Margrave Ed., Advances in Chemistry Series, No. 72, American Chemical Society, Washington, D. C., 1968, p. 181.

[4] (a) A. Giardini-Guidoni and G. G. Volpi, *Nuovo Cimento*, **17**, 919 (1960); (b) M. Halmann and I. Platzner, *J. Phys. Chem.*, **71**, 4522 (1967).

Table I: Appearance Potentials (in eV) for Negative Ions by Electron Impact on Phosphine

Ion	Lit.[a] obsd	Present work		Process type	Tentative mechanism $PH_3 + e^- \rightarrow$
		obsd	calcd		
H^-	3		3.0	Resonance	$H^- + PH_2$
	5.4 ± 0.1	5.4 ± 0.1	4.8	Resonance	$H^- + P + H_2$
	7.5 ± 0.2	7.5	6.0	Resonance	$H^- + PH + H$
		16.3 ± 0.1	15.4	Ion pair	$H^- + P^+ + H_2 + e^-$
PH_2^-	2.3 ± 0.1	2.2 ± 0.1		Resonance	$PH_2^- + H$
	5.2 ± 0.2	5.2 ± 0.1		Resonance	$(PH_2^-)^*$
		8		Resonance	
		15.8 ± 0.2		Ion pair	$PH_2^- + H^+ + e^-$
PH^-	2.1 ± 0.2	2.2 ± 0.2		Resonance	$PH^- + H_2$
	6.3 ± 0.2	6.3 ± 0.1		Resonance	$PH^- + 2H$
	8.1 ± 0.3	8.2 ± 0.2		Resonance	$(PH^-)^* + 2H$
		19.8 ± 0.1		Ion pair	$PH^- + H^+ + H + e^-$
P^-	5.7 ± 0.2	5.8 ± 0.2	4.8	Resonance	$P^- + H_2 + H$
	8.3 ± 0.3	8.4 ± 0.2	9.3	Resonance	
		13.4 ± 0.2		Resonance	
		22.6 ± 0.1	22.9	Ion pair	$P^- + H^+ + 2H + e^-$

[a] Reference 2.

tion energies D, all in eV,[5a-d] $I(H) = 13.595$; $I(P) = 10.55$; $I(H_2) = 15.43$; $EA(H) = 0.747$; $EA(P) = 0.77$ and $D(H\text{-}H) = 4.476$. For the P–H dissociation energy in phosphine, an average value (the "bond energy term") of $D(P\text{-}H) = 3.35$ eV is obtained from thermochemistry.[5b] For $D(PH_2\text{-}H)$ and $D(PH\text{-}H)$, the energies required to break the first and second P–H bond in phosphine, values of 3.8 and 2.9 eV have been proposed.[6] A decrease in dissociation energy from the first to the other bonds has been observed in various hydrides. In the case of ammonia, $D(NH_2\text{-}H)$, $D(NH\text{-}H)$, and $D(N\text{-}H)$ are 4.46, 3.9, and 3.7 eV, respectively.[5d] Similarly for water[5a] and hydrogen sulfide,[5c] the values of $D(H\text{-}OH)$, $D(O\text{-}H)$, $D(H\text{-}SH)$, and $D(S\text{-}H)$ are 5.114, 4.35, 3.9, and 3.6 eV, respectively.

H^- ions. The intense resonance peak at 5.4 eV can be accounted for by the reaction

$$PH_3 + e \longrightarrow H^- + P + H_2 \qquad (1)$$

for which the calculated appearance potential is 4.8 eV.

The threshold of ion-pair formation, at 16.3 eV, can best be described by the process

$$PH_3 + e \longrightarrow H^- + P^+ + H_2 + e \qquad (2)$$

for which $AP(H^-) \geq 15.4$ eV.

The observed appearance potential of H^- as an ion pair, at 16.3 eV, is thus 0.9 eV higher than the calculated minimal energy. The excess may appear in either vibrational or kinetic energy of the fragments. For the first appearance potential of the positive ion, P^+, values of 16.0 ± 1, 16.5, 16.7 ± 1 and 17.2 have been reported.[3]

PH_2^- ions. The first two resonance capture maxima are sharp and resolved peaks, the third is a very shallow one. The appearance of the ion at 2.2 eV may be attributed to the reaction

$$PH_3 + e \longrightarrow PH_2^- + H \qquad (3)$$

Hence $EA(PH_2) \geqslant 1.6$ eV.

The second and third peaks appearing at 5.2 and 8 eV may be due to processes

$$PH_3 + e \longrightarrow (PH_2^-)^* + H \qquad (4)$$

where $(PH_2^*)^-$ are yet unknown excited states of the anion, which only slowly (lifetime > 10^{-6} sec) decay to the neutral PH_2 radical and an electron. An analogous explanation has been suggested for the second resonant peak of NH_2^- in the mass spectrum of ammonia.[5d] Only the following reaction is possible for the 15.8 eV onset of PH_2^- in the ion-pair region

$$PH_3 + e \longrightarrow PH_2^- + H^+ + e \qquad (5)$$

Hence $EA(PH_2^-) \geq 1.6$ eV. The shallow shoulder between 9 and 15 eV may be due to resonant capture processes yielding excited hydrogen atoms (see below).

PH^- ions. The first maximum, at 2.2 eV, is a very weak one and the two other peaks, at 6.3 and 8.2 eV, are

---

(5) (a) G. Herzberg, "Molecular Spectra and Molecular Structure," I, "Spectra of Diatomic Molecules," 2nd ed., 1950; II "Electronic Spectra of Polyatomic Molecules" D. Van Nostrand Co., Inc., Princeton, N. J., 1960; (b) T. L. Cottrell, "The Strength of Chemical Bonds," 2nd ed., Butterworth and Co. Publishers, Ltd., London, 1958; (c) C. J. Schexnayder, Jr., " Tabulated Values of Dissociation Energies, Ionization Potentials and Electron Affinities for some Molecules," National Aeronautics and Space Administration, TN-D 1791, May, 1963; (d) J. E. Collin, M. J. Hubin-Franskin and L.-d'Or in "Advances in Mass Spectrometry," Vol. 4, E. Kendric, Ed., Institute of Petroleum, London, 1968, p 713.

(6) D. Kley and K. H. Welge, *Z. Naturforsch*, **20a**, 124 (1965).

not resolved completely. The appearance of the ion at 2.2 eV may be due to the reaction

$$PH_3 + e \longrightarrow PH^- + H_2 \qquad (6)$$

Hence, $EA(PH) \geq 0.1$ eV. The stronger peak at 6.3 eV fits the reaction

$$PH_3 + e \longrightarrow PH^- + 2H \qquad (7)$$

which results in $EA(PH) \geq 0.4$ eV.

The intense peak of PH^- at 8.2 eV is more difficult to explain. Possibly it is due to formation of an excited, long-lived ($>10^{-6}$ sec) PH^- ion. In the ion pair formation region, the reaction proposed is

$$PH_3 + e \longrightarrow PH^- + H^+ + H + e \qquad (8)$$

leading to $EA(PH) \geq 0.5$ eV.

P^- ions. Three resonance maxima are observed. For the lowest peak appearing at 5.8 eV, the reaction

$$PH_3 + e \longrightarrow P^- + H_2 + H \qquad (10)$$

requires $AP(P^-) \geq 4.8$ eV.

The second peak, starting at about 8.4 eV, cannot be due to the process

$$PH_3 + e \longrightarrow P^- + 3H \qquad (11)$$

which would acquire $AP(P^-) \geq 9.3$ eV. The intensity of this peak is linearly related to the gas pressure in the ion source. Thus it is not a secondary ion-molecule reaction product. Possibly this P^- peak is due to process 10, but involving kinetic and internal excitation of the fragments.

The reaction proposed for the ion pair formation is

$$PH_3 + e \longrightarrow P^- + H^+ + 2H + e \qquad (12)$$

Thus, $AP(P^-) \geq 22.9$ eV, in good agreement with the observed value, 22.6 eV.

The steep increase in ion currents in the ion-pair region for PH_2^-, PH^- and P^- is preceeded by a 3-4 eV wide section of shallow shoulders and broad maxima. We propose that the processes in this region may be due to a series of successive excitations of the newly formed hydrogen atom to different atomic levels, converging in the limit to ionization to H^+ (reactions 5, 8, and 12.) These processes are therefore analogous to the Lyman series in the atomic spectrum of hydrogen. In the atomic spectrum the first line (Lyman-α) appears at 10.15 eV above the ground level, and the ionization limit occurs at 13.53 eV. Thus we expect that the onset for the process forming the excited H atoms should be in each case at 3.4 eV below the onset of the ion-pair processes. As seen in the figure, the onset of such shoulders can be discerned at about 3 eV below the steep onset for ion-pair production.

Competitive Reactions of Recoil Tritium Atoms with Methysilanes and Alkanes

by S. H. Daniel and Yi-Noo Tang

Department of Chemistry, Texas A & M University, College Station, Texas 77843

(Received January 13, 1969)

Although the reactions of recoil tritium atoms with carbon-skeletal molecules have been extensively studied, the corresponding work for the reactions with silicon-skeletal molecules is barely initiated.[1-3] In 1967, Cetini and coworkers studied the recoil tritium reactions with monosilane and concluded that (a) monosilane is more reactive than methane probably because of the weaker Si–H bonds, and (b) kinetic theory for hot atom reactions as proposed by Wofgang, *et al.*, can be extended to silane systems.[4]

Earlier studies on methylsilanes which were either published or submitted for publication during the process of this research included the results of Witkin and Wolfgang's work on tetramethyl-, trimethyl-, and monomethylsilanes, and the work on the first two molecules by Tominaga, Hosaka, and Rowland.[5,6] In the present work, we would like to report recoil tritium reactions with tetra-, tri-, and the previously unstudied dimethylsilanes in one-component systems, as well as in two-component mixtures with their corresponding member of the alkane series. With these competitive studies, we can directly and quantitatively evaluate the relative reactivities of recoil tritium reactions with the silicon-skeletal and carbon-skeletal compounds.

Experimental Section

Recoil tritium atoms were produced by employing the nuclear transmutation $He^3(n,p)H^3$ for the gas phase reactions and $Li^6(n,\alpha)H^3$ for the liquid phase studies. Gas samples containing He^3, methylsilane, and other additives were prepared with a high vacuum system. For scavenged samples, 5-10 cm of oxygen was added. For liquid samples, the components were condensed into capillary tubes containing a small amount of LiF. I_2 or DPPH were used as liquid phase scavengers. These samples were irradiated at the Texas A & M University Nuclear Science Center Research Reactor with a neutron flux of 1×10^{12} neutrons/(cm^2 sec) for 30 min.

The analysis of tritium-labeled products after irra-

---

(1) R. Wolfgang, *Progr. Reaction Kinetics*, **3**, 97 (1965).

(2) R. Wolfgang, *Ann. Rev. Phys. Chem.*, **16**, 15 (1965).

(3) F. Schmidt-Bleek and F. S. Rowland, *Angew. Chem., Intern. Ed.*, **3**, 769 (1964).

(4) G. Getini, O. Gambino, M. Castiglioni, and P. Volpe, *J. Chem. Phys.*, **46**, 89 (1967).

(5) J. Witkin and R. Wolfgang, *J. Phys. Chem.*, **72**, 2631 (1968).

(6) T. Tominaga, A. Hosaka, and F. S. Rowland, *ibid.*, **73**, 465 (1969).

Table I: Relative Yields of Products from Recoil Tritium Reactions with Methylsilanes[a]

Reacting Compound	O_2, mole %	HT	CH_3T	T-for-H substitution	T-for-CH_3 substitution	Reference
$(CH_3)_2SiH_2$	10	168 ± 3	13 ± 1	100	9.4 ± 0.3	This work
$(CH_3)_3SiH$	10	157 ± 2	13 ± 1	100	8.8 ± 0.4	This work
	1	227	18	100	7.7	Ref 5
$(CH_3)_4Si$	10	97 ± 2	15 ± 1	100	6.7 ± 0.3	This work
	5	99	14	100	5	Ref 6
	1	167	20	100	6.4	Ref 5

[a] Relative to T-for-H substitution reaction as 100.

Table II: Calculation of Specific Activity Ratio per Bond for Methylsilanes and Alkanes from Recoil Tritium Competitive Reactions

Methylsilanes, cm	Alkanes, cm	Obsd activity (first aliquot)		Sp act ratio (first aliquot) methylsilane/alkane	Sp act ratio (whole sample)	Av sp act ratio per bond
		Methylsilane-*t*	Alkane-*t*			
$(CH_3)_4Si$	$(CH_3)_4C$					$(CH_3)_4Si$/
37.7	36.9	278,000	192,800	1.17	1.17 ± 0.02	$(CH_3)_4C$
34.6	36.7	183,800	166,700	1.17	1.17 ± 0.02	1.17 ± 0.02
$(CH_3)_3SiH$	$(CH_3)_3CH$					$(CH_3)_3SiH$/
36.0	39.3	33,750	26,100	1.29	1.30 ± 0.02	$(CH_3)_3CH$
37.0	43.6	89,100	88,350	1.29	1.22 ± 0.04	1.26 ± 0.06
$(CH_3)_2SiH_2$	$(CH_3)_2CH_2$					$(CH_3)_2SiH_2$/
34.8	35.4	159,550	104,600	1.55	1.55 ± 0.01	$(CH_3)_2CH_2$
35.2	35.1	148,200	96,800	1.53	1.55 ± 0.02	1.55 ± 0.02

diation was performed by radio-gas chromatography.[7] The majority of the separations was performed with a 50-ft dimethyl sulfolane (DMS) column at 25° which separates well all the methylsilanes. A 50-ft safrole column was also used. However, for the competition experiments, an additional 30-ft DMS column was connected in series with the 50-ft one in order to get a clean separation between the silanes and the hydrocarbons. A 50-ft propylene carbonate column (coated on alumina) at 0° was used to separate dimethylsilane from propane. It also separates HT and CH_3T.

The methylsilanes were obtained from Peninsular Chemical Co. while the hydrocarbons were obtained from the Matheson Co. with an impurity level less than 0.5%. He^3 with a tritium content of less than $2 \times 10^{-11}\%$ was obtained from Monsanto Research Corp.

Results and Discussion

The primary reactions of recoil tritium atoms with methylsilanes are the abstraction of and the substitution for hydrogens, and the reaction at the Si–C bond to give either CH_3T or a formation of the corresponding Si–T bond. These reactions are illustrated below with dimethylsilane as an example.

(a) H-abstraction

$$(CH_3)_2SiH_2 + T^* \longrightarrow \left\{\begin{array}{ll} HT + CH_3SiH_2CH_2\cdot & (1a) \\ HT + (CH_3)_2SiH\cdot & (1b) \end{array}\right.$$

(b) T-for-H substitution

$$(CH_3)_2SiH_2 + T^* \longrightarrow \left\{\begin{array}{ll} CH_2TSiH_2CH_3 + H & (2a) \\ (CH_3)_2SiHT + H & (2b) \end{array}\right.$$

(c) reactions at Si–C bond

$$(CH_3)_2SiH_2 + T^* \longrightarrow CH_3T + CH_3SiH_2\cdot \qquad (3)$$

$$(CH_3)_2SiH_2 + T^* \longrightarrow CH_3SiH_2T + CH_3\cdot \qquad (4)$$

From the one-component systems of the methylsilanes, $(CH_3)_nSiH_{4-n}$, every expected primary product has been experimentally detected as an appreciable yield. These include HT, CH_3T, $(CH_3)_{n-1}SiH_{4-n}T$ and $(CH_3)_nSiH_{4-n}$-*t* as illustrated above in reactions 1 to 4 in the case of $(CH_3)_2SiH_2$. The experimental results are as shown in Table I, together with the previously published data from ref 5 and 6 for comparison.

For the tetramethylsilane system, the agreement between our data and those from ref 6 is excellent. When allowance is made for different oxygen concentrations, there is basically no disagreement between our data on trimethyl- and tetramethylsilane with those of ref 5.

However, data in Table I are relative to the T-for -H substitution reaction in methylsilanes as an

---

[7] J. K. Lee, E. K. C. Lee, B. Musgrave, Y.-N. Tang, J. W. Root, and F. S. Rowland, *Anal. Chem.*, **34**, 741 (1962).

Table III: Comparison of Normalized Product Yields of Methylsilanes and Corresponding Alkanes from Recoil Tritium Reactions[a]

Molecule	HT	T-for-H substitution	CH_3T	T-for-CH_3 substitution	Total yield
$(CH_3)_2CH_2$	185	100	10.9	4.5	300
$(CH_3)_2SiH_2$	260	155	20.2	14.6	450
$(CH_3)_3CH$	192	100	14.1	3.0	309
$(CH_3)_3SiH$	198	126	16.4	11.1	352
$(CH_3)_4C$	139	100	21.0	2.5	263
$(CH_3)_4Si$	114	117	17.5	7.8	256

[a] Values for alkanes come from ref 1.

arbitrary standard. Their values cannot be directly compared with those of the hydrocarbon systems unless the two systems can be normalized. The normalization factor for each methylsilane–alkane pair can be obtained by carrying out a two-component competition reaction between the pair and calculate their specific reactivity ratio.

For such competiton runs, 1:1 mixtures of the pairs $(CH_3)_2SiH_2$–C_3H_8, $(CH_3)_3SiH$–i-C_4H_{10}, and $(CH_3)_4Si$–$(CH_3)_4C$ were studied. Table II shows the experimental data of these competitions together with the calculation which gives the specific activity ratio for T-for-H substitution in silane over that in the corresponding hydrocarbon for the above three pairs. Their values are, respectively, 1.55 ± 0.02, 1.26 ± 0.06, and 1.17 ± 0.02 with the tetramethyl compounds showing the least difference in T-for-H substitution reactivity.

A liquid competition of the $(CH_3)_4Si$–$(CH_3)_4C$ system shows a specific activity ratio of 1.21 ± 0.07 which is similar to the 1.17 gas phase value. This fact coupled with the low yield of CH_2TI detected in the I_2-scavenged systems indicates that either the decomposition of the primary products is not serious or these two compounds decompose to a similar degree, or both.[8,9] Therefore the gas phase relative yields can be used to represent the ratio of the primary hot yields, at least as a first approximation. Consequently, by assuming that the moderating abilities of the molecules in each pair are similar, the observed data for the individual methylsilanes were normalized to those of alkanes by multiplying them by the above specific activity ratios. The results of each pair, as shown in Table III, can then be directly compared.

The major conclusion to these competition experiments is the quantitative comparison of the reactivities of alkylsilanes and their corresponding hydrocarbons. The values in Table III clearly show that the total reactivities of $(CH_3)_4Si$ and $(CH_3)_4C$ are approximately the same, quantitatively confirming the estimation of Tominaga, *et al.* However, for the other two pairs, our data show that $(CH_3)_3SiH$ and $(CH_3)_2SiH_2$ are, respectively, about 20 and 50% more reactive than their hydrocarbon counterparts, qualitatively in agreement with what Witkin and Wolfgang suggested. But, yields from compounds containing Si–H bonds may remain slightly sensitive to the scavenger concentration even at the level of 10% O_2.[6]

As for the comparison of the individual yields, the specific reactivity ratios show that the average T-for-H substitution in methylsilanes is about 20–50% more reactive than the corresponding reaction in hydrocarbons.

The HT yields indicate that hydrogen abstraction at the C–H bonds in tetramethylsilane is only 0.82 times as likely as those in neopentane. The close relationship between HT yields from recoil tritium reactions and bond dissociation energies has been well established by a series of studies in C_2D_4 moderating systems.[10,11] The value 0.82 indicates that the C–H bond dissociation energy in tetramethylsilane is larger than 99 kcal/mol and is probably around 101 kcal/mol.[10] For the other two pairs, the data indicate that H abstraction is about the same for both isobutane and trimethylsilane, but, on the average, it is easier to abstract from dimethylsilane than from propane.

Data in Table III reveal that the total reactivities at the Si–C bonds are always higher than those at the corresponding C–C bonds. Moreover, if we use R–CH_3 to represent both the methylsilanes and the alkanes, the ratios of CH_3T/RT from methylsilanes are always much smaller than those from their corresponding hydrocarbons although the R's from the silanes always have the larger mass. For example, the CH_3T/RT ratio from tetramethylsilane is 2.2 while that from neopentane is 8.4. This observation might be attributed to the incoming T being closer to the normal bond angle of the Si–T than it is to the C–T bond, and to the slower bending vibration of the Si–T bond as proposed by Witkin and Wolfgang.[5] However, other effects might also be operating such as the following: (a) the larger size of Si in comparison with that of C and therefore a higher chance to collide with the incoming T; (b) the availability and direct use of d orbitals of Si; and (c) the electropositive nature of Si. But, it is not possible from the present data to determine what the correct explanations are.

Acknowledgments. The authors wish to thank Dr. F. S. Rowland of the University of California, Irvine,

---

[8] E. K. C. Lee and F. S. Rowland, *J. Amer. Chem. Soc.*, **85**, 897 (1963).

[9] Y.-N. Tang, E. K. C. Lee, and F. S. Rowland, *ibid.*, **86**, 1280 (1964).

[10] J. W. Root, W. Breckenridge, and F. S. Rowland, *J. Chem. Phys.*, **43**, 3694 (1965).

[11] E. Tachikawa and F. S. Rowland, *J. Amer. Chem. Soc.*, **90**, 4767 (1968).

and Dr. D. H. O'Brien of Texas A & M University for their helpful discussions. This research was supported by the Research Council and the Chemistry Department of Texas A & M University. It is also partially supported by Research Corporation. Acknowledgment is also made to the donors of the Petroleum Fund (PRF-1447-G), administered by the American Chemical Society, for partial support of this research.

Photoconductivity of Electron Acceptors.

II. 2,7-Dibromofluoren-$\Delta^{9\alpha}$-malononitrile

by Tapan K. Mukherjee

Energetics Branch, Air Force Cambridge Research Laboratories, Bedford, Massachusetts 01730 *(Received February 20, 1969)*

In our previous work[1] on the photoconductivity in nitro derivatives of fluoren-$\Delta^{9\alpha}$-malononitrile it was noted that, in the case of the 2,7-dinitro derivative (DDF; X = NO_2), the maximum photocurrent was obtained by excitation with energy less than that required to raise the photoconductor to the first singlet state. The exact reason for this difference was not clearly understood. Replacement of the NO_2-group by a heavy atom would enhance the probability of direct singlet–triplet transition. If the S → T transition is involved in any way in the generation of photocarriers, then one would expect the photocurrent maximum to be shifted to a wavelength considerably longer than the first singlet–singlet absorption band. To test this possibility, 2,7-dibromo-$\Delta^{9\alpha}$-malononitrile (DBF, X = Br) was synthesized, and its light absorption and photoconductivity characteristics were studied.[2]

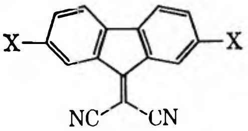

DBF, synthesized from 2,7-dibromofluorenone[3] by the previously described procedure,[1] was purified by repeated crystallization from dimethylformamide, ethyl acetate, and chloroform[4] (red crystals, mp 346–348°). Spectroscopic and photoconductivity measurements were performed as before.[1]

Results and Discussion

In methylene dichloride, DBF shows a low intensity broad absorption between 550–425 mμ (maximum at 480 mμ; log E, 2.49). Due to the limited solubility of DBF, the solvent dependence of the absorption spectrum could not be studied. Hence, the assignment of the low energy transition (480 mμ) as a π–π^* state was done by indirect means.

A comparison of the absorption spectra of DBF and fluoren-$\Delta^{9\alpha}$-malononitrile (X = H) with those of 2,7-dibromofluorenone and fluorenone (Table I) shows that the long wavelength peaks are of similar intensities. From theoretical molecular orbital calculations[5] and other experimental evidence,[6] the weak absorption near 380 mμ in fluorenone has been assigned to a π–π^* state, rather than to a n–π^* state as previously thought. By analogy, the band at 420 mμ in 2,7-dibromofluorenone is assigned the π–π^* level. It is also known that the well characterized n–π^* bands in aldehydes and ketones disappear when carbonyl oxygen (=O) atom is replaced by dicyanomethylene group[7] $\left(=C\begin{matrix}CN\\CN\end{matrix}\right)$. The positions and the intensities of the first low-energy bands that appear in the products have the properties of π–π^* transitions.[8] Table I also shows that in DBF, the low energy band is red-shifted compared to the unsubstituted fluoren-$\Delta^{9\alpha}$-malononitrile. Similar red shift was observed in fluorenone with the electron donating substituent in the "two" position, and was considered a good test of π–π^* transition.[9]

Table I: Absorption Spectra in Methylene Dichloride

Compound	mμ (log E)
Fluorenone	380 (2.42), 327 (3.00) 310 (3.28)
2,7-Dibromofluorenone	420 (2.72), 312 (3.68) 310 (3.79)
Fluoren-$\Delta^{9\alpha}$-malononitrile (X = H)	435 (2.51), 365 (3.45) 350 (3.53), 295 (3.35)
DBF (X = Br)	480 (2.49), 360 (4.25) 348 (4.29), 317 (4.22)

The absorption spectrum of the vacuum evaporated film (Figure 1) of DBF shows some vibrational structure in the long wavelength region. All peaks are somewhat red-shifted compared to those of the solution spectrum. Since the excited singlet levels in the crystals are often found to be lower than the singlet levels in solution by a few tenths of an electron volt,[10] the difference between the solid and solution spectrum is not unexpected.

---

(1) T. K. Mukherjee, *J. Phys. Chem.*, **70**, 3848 (1966).

(2) The monobromo derivative, as well as the 2,7-diamino and 2,7-dihydroxy derivatives were found to be nonphotoconductive. 2,7-Dibromofluorenone did not yield any photocurrent.

(3) Ch. Courtot, *Ann. Chim.*, **14**, 99 (1930).

(4) *Anal.* Calcd. for $C_{16}H_6Br_2N_2$: C, 49.77; H, 1.56; Br, 41.40; N, 7.25. Found: C, 49.70; H, 1.80; Br, 41.15; N, 7.28. The upper limit of purity was ascertained from a single spot on TLC and maximum molecular extinction coefficient. Repeated melting of a sample showed some decomposition, hence zone refining was not attempted.

(5) H. Kuroda and T. L. Kunii, *Theor. Chim. Acta*, **9**, 51 (1967).

(6) K. Yoshihara and D. R. Kearns, *J. Chem. Phys.*, **45**, 1991 (1966).

(7) E. Campaigne, R. Subramaya, and D. R. Maulding, *J. Org. Chem.*, **28**, 623 (1963). There are a large number of examples scattered in the literature.

(8) This test of π–π^* transition may be used as a supplement to the oximation test described by Yasihara and Kearns in ref 6.

(9) A. Kuboyama, *Bull. Chem. Soc. Jap.* **37**, 1540 (1964).

(10) F. Gutman and L. E. Lyons, "Organic Semiconductors," John Wiley and Sons, Inc., New York, N. Y., 1967, Table I, p 653.

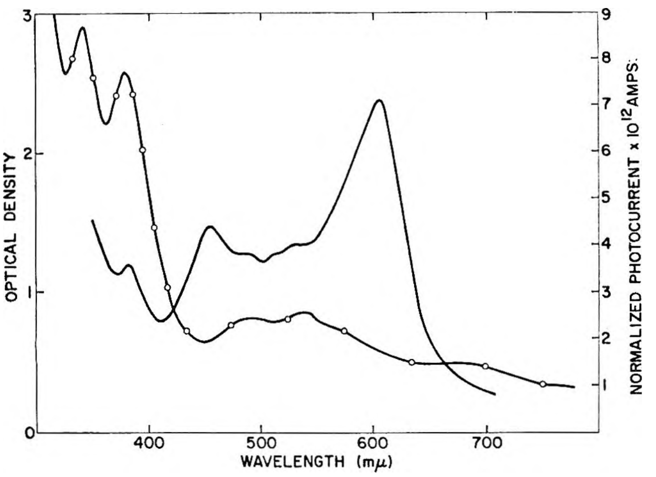

Figure 1. Spectral response of surface photoconductivity of 2,7-dibromofluoren-$\Delta^{9\alpha}$-malononitrile at 200 V. ———, Absorption spectrum of vacuum deposited film, —O—O—.

Like most other molecular crystals, DBF is a high resistance semiconductor ($\rho_{\text{bulk}} = 2 \times 10^{15}$ ohm cm), and it is a weaker photoconductor compared to DDF.[11] The surface photocurrent in air was about 35% lower than that in vacuum, a behavior reminescent of the 2,7-dinitro derivative. The surface photocurrent spectrum is also shown in Figure 1. Reading from the low energy side, one notices that the photocurrent maximum at 610 mμ is about 0.26 eV lower than the first absorption maximum at 550 mμ. There is some evidence of vibrational structure in the photocurrent action spectrum. The height of the photocurrent peak at 610 mμ increased monotonically with the applied field (60–500 V). Although the solid absorption spectrum shows a weak tail towards the longer wavelength, the photocurrent drops rather sharply. This behavior, coupled with the proximity of the absorption and photocurrent peaks, is suggestive of the fact that the charge carriers in DBF may be generated within the singlet–singlet energy threshold of this compound.[12]

---

[11] Under the conditions described in ref 1.

[12] It has not been possible to detect the triplet level in DBF, either from the absorption spectrum in heavy atom solvent or from emission spectroscopy.

Potentiometric Titration of Stereoregular Poly(acrylic acids)

by Yoshikazu Kawaguchi and Mitsuru Nagasawa

Department of Applied Chemistry, Nagoya University, Furocho, Chikusa-ku, Nagoya, 464, Japan

(Received March 14, 1969)

Theoretical treatment of the problem of potentiometric titration of polyelectrolytes, having a uniform distribution of ionizable groups of one kind, leads to an expression for the pH of the solution

$$\text{pH} = \text{p}K_0 - \log[(1 - \alpha)/\alpha] + 0.434e\psi/kT \quad (1)$$

where ψ is the electrostatic potential at the point on the molecule from which the proton is removed, pK_0 the intrinsic ionization constant of the group and α is the degree of ionization. Since the magnitude of ψ is dependent on the effects of nearest charged groups, the potentiometric titration curves reflect the local conformation of the polyions and, therefore, one may expect to find a difference between the potentiometric titration curves of linear polyelectrolytes which have different local conformations in solution.

Many quantitative studies were carried out with poly(L-glutamic acid) to find its conformational change in neutralization and to estimate the molecular parameters from analysis of the potentiometric titration curves. For linear polyelectrolytes, too, it was predicted from potentiometric titration curves that isotactic poly(methacrylic acid), p(MAA), may have locally helical conformation, whereas syndiotactic p(MAA) has the planar zigzag conformation.[1] Therefore, it would be desirable to confirm the locally helical structure of isotactic p(MAA) using an independent experimental method. Unfortunately, no such method has been found. On the other hand, recent nmr studies show that isotactic poly(acrylic acid), p(AA), appears to have locally helical structure in solution due to the strong electrostatic repulsion between charged groups.

The purpose of the present paper is to show that a detectable difference can be observed between the potentiometric titration curves of isotactic p(AA) which was shown by nmr studies to have a helical conformation and those of syndiotactic p(AA) which presumably has a planar zigzag conformation. Concerning the difference between ionization constants of carboxyl group of isotactic and atactic p(AA), Miller, *et al.*,[2] detected no difference but Sakaguchi, *et al.*,[3] reported that syndiotactic p(AA) is a stronger acid than atactic p(AA). The present work supports the conclusion of the latter authors.

Experimental Section

Samples. Isotactic poly(methyl acrylate), p(MA), was polymerized with lithium aluminum hydride at −78° in toluene for 20 hr *in vacuo*. The polymerization product was poured into methanol containing 10% HCl. P(MA) thus obtained was purified by repeated precipitation from its chloroform solution with methanol. The degree of tacticity, calculated from the nmr spectrum of the methylene groups using the method of

---

(1) M. Nagasawa, T. Murase, and K. Kondo, *J. Phys. Chem.*, **69**, 4005 (1965).

(2) M. L. Miller, K. O'Donnel, and K. Skogman, *J. Colloid Sci.*, **17**, 649 (1962).

(3) Y. Sakaguchi, J. Nishino, M. Okuyama, H. Shobayashi, M. Shimada, R. Nomura, and Y. Ito, *Kobunshi Kagaku*, **24**, 25 (1967).

Matsuzaki, *et al.*,[4] was found to be $i = 0.96$. The nmr spectrum of the sample was shown previously.[5] Purified p(MA) was hydrolyzed in acetone–water mixture with NaOH under nitrogen gas atmosphere at 30°. Sodium polyacrylate, p(NaA), thus produced, was purified by repeated precipitation from its aqueous solution with methanol. The degree of hydrolysis was 100% when calculated from dry weight and acid group content of the sample. Syndiotactic p(AA), whose degree of tacticity was $s = 0.71$,[6] was kindly provided by Professor Matsuzaki of Tokyo University. The molecular weight of isotactic and syndiotactic p(NaA) was 9.5×10^4 and 10.4×10^4, respectively, if calculated from $[\eta]$ in 0.1 N NaBr solution at 25° using the equation as obtained for conventional p(NaA).[7]

$$[\eta] = 3.12 \times 10^{-4} M^{0.755} \qquad (2)$$

The sodium salts of all samples were converted to acid forms by passing them through a mixed-bed ion-exchange resin column of Amberlite IR-120 and 400.

pH Measurement. A Beckman 1019 pH research meter was used with NBS standard buffers. The titration was carried out in a nitrogen atmosphere at room temperature (25 ± 1°) using standard NaOH solutions (0.25 M) delivered with a Tesa microburet. The polymer concentration used was 0.01 N and the initial volume of the sample solution was 40 ml.

Calculation of ψ. The method has been reported by Kotin and Nagasawa in a previous paper.[8] The values used here were recalculated with more precise mesh using a HITAC 5020 E electronic computer. No detectable disagreement was found between the previously calculated results and the present ones.

Results and Discussion

Figure 1 shows the potentiometric titration curves of both stereoregular p(AA) carried out at 0.01 N polymer concentration in 0.01 and 0.1 N NaCl solutions. It is clear that the isotactic p(AA) is a weaker acid than syndiotactic p(AA). Moreover, a clear difference is observed between the behavior of the two forms of p(AA) with increasing degree of ionization; the curves of syndiotactic p(AA) are slightly inflected as was pointed out in a previous paper,[1] whereas such inflections are almost undetectable in the titration curves for isotactic p(AA).

It is very difficult to verify unambiguously that the observed difference between the potentiometric titration curves of isotactic and syndiotactic p(AA) is due to the difference in their conformations because of the lack of the theory on potentiometric titration of flexible polyelectrolytes. Only if the chain is fairly stiff so that a rod-like model is applicable can the experimental potentiometric titration curves be quantitatively compared with theory. In comparison between a theory and experiments, it was reported that p(MAA) appears to have a stiff chain, whereas p(AA) may be more flexible;[1] consequently, quantitative agreement between theory and experiments could not be obtained for p(AA). In order to prove that the difference in potentiometric titration behavior of stereoregular polyelectrolytes is really due to the difference in their conformations, therefore, it is preferable to determine the conformation of isotactic p(MAA) by using an independent method such as nmr. Unfortunately, however, it is not possible to determine the conformation of isotactic p(MAA) by nmr because there is no α-proton in the molecule. On the other hand, it was shown by nmr that isotactic p(AA) has an almost helical conformation in solution,[5] but here since the chain is flexible,

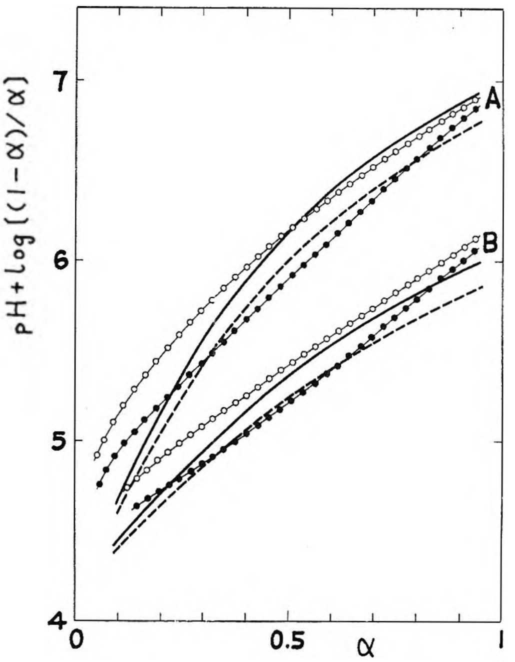

Figure 1. The potentiometric titration curves of isotactic and syndiotactic poly(acrylic acid)s at 25 ± 1°. NaCl concentrations: A, 0.0100 N; B, 0.100 N. The white and black circles show experimental data of the isotactic and syndiotactic forms, respectively. The thick solid lines and the thick broken lines are the values calculated by Kotin and Nagasawa for isotactic and syndiotactic forms, respectively.

---

(4) K. Matsuzaki and T. Uryu, *Kogyo Kagaku Zasshi*, **70**, 24 (1967).

(5) Y. Muroga, I. Noda, and M. Nagasawa, *J. Phys. Chem.*, **73**, 667 (1969).

(6) K. Matsuzaki, T. Uryu, and H. Shiraki, Polymer Symposium in Matsuyama, Japan, 1968.

(7) I. Noda, T. Tsuge, and M. Nagasawa, to be published.

(8) L. Kotin and M. Nagasawa, *J. Chem. Phys.*, **36**, 873 (1962).

the potentiometric titration curves of p(AA) cannot fully be analyzed by current theories.

Nevertheless, if we compare the theoretical curves for rod-like molecules with experimental results of p(AA) over the whole range of degrees of ionization, it appears safe to conclude that the difference between the potentiometric titration curves of the two stereoregular p(AA)'s shown in Figure 1, is due to the difference in their conformations. We can see a clear difference between the two curves except at high degrees of ionization, where the curves of syndiotactic p(AA) are slightly inflected upward and both curves tend to coincide. Taking into account the discussion in the previous paper,[1] the upward inflection of syndiotactic p(AA) at high degrees of ionization is caused by the flexibility of the p(AA) chain, that is, due to the contribution of the free energy change, $\Delta A(\alpha)$, accompanying the expansion of the polyion coil to the total free energy change in dissociation. In the potentiometric titration curves of isotactic p(AA), such inflection is not observed; the backbone chain of isotactic p(AA) may be stiffer than syndiotactic p(AA) presumably because of helix formation. Therefore, it is our opinion that the coincidence between both potentiometric titration curves of isotactic and syndiotactic p(AA) at high degrees of ionization can occur in spite of the difference in their conformations. Strictly speaking, since the theoretical curves are obtained for the samples at infinite dilution, the experimental data should be extrapolated to infinite dilution to be compared with the theoretical curves. However, it was confirmed that the relative behavior or features of the potentiometric titration curves is not changed with dilution.

In the calculation of theoretical curves of isotactic p(AA), we use 5.5 Å for radius of rod, 2.06 Å for distance between carboxylic groups, and 0.72 for degree of helix, independently of α[5] In his recent nmr study on isotactic p(AA), Yoshino[9] reported more precise dependence of nmr parameters on degree of ionization using deuterated p(AA). From his data, the degree of helix must increase slightly with α. Even though his data are used, the calculated curve is little affected. Thus, taking into account both results in this paper and the previous one,[1] we may conclude that isotactic polyelectrolyte has a helical structure in solution because of the electrostatic repulsion between ionized groups. This is in good contrast with the fact that, the helical structure of poly(L-glutamic acid) is collapsed by electrostatic repulsion if it is ionized. Moreover, due to the presence of a methyl group, the helical structure of isotactic p(MAA) may be more stable than isotactic p(AA).

Acknowledgment. The authors are indebted to Professor Matsuzaki for supplying the syndiotactic poly(acrylic acid).

---

[9] T. Yoshino, Polymer Symposium in Matsuyama, Japan, 1968.

Instability of Sorption Complexes in Synthetic Faujasites

by Lothar Riekert

Mobil Research and Development Corporation, Research Department, Central Research Division, Princeton, New Jersey 08540

(Received March 19, 1969)

Sorption isotherms in synthetic faujasite zeolites were investigated, and it was observed that the amount of sorbate in the solid decreases spontaneously under certain conditions, although the pressure of the gas increases. This instability appears to be of general interest because it indicates that the uptake of the sorbate can induce changes in the structure of the solid.

Experimental Section

The synthetic HY zeolite was obtained by calcination of NH_4Y at 400°. The parent NH_4Y had the composition $((NH_4)_{0.95}Na_{0.05}AlO_2)\cdot(SiO_2)_{2.87}$. NaY had the composition $(NaAlO_2)\cdot(SiO_2)_{2.76}$. Both zeolites consisted of crystals of about 1 μm diameter.

The sorption measurements were performed by recording the change of the pressure in a closed system, using a capacitance pressure transducer. A calibrated volume of gas was opened at time zero to a smaller vessel containing the zeolite sample. The amount of gas taken up by the solid was determined on the basis of the ideal gas law, correction being made for the dead space in the sample vessel. By repeating this experiment with increasing initial pressures, the equilibrium isotherm and the kinetics of sorption in each step were obtained. The sorbent was degassed before the experiment at 350° for at least 6 hr until a static pressure of less than 10^{-4} Torr was reached in the system.

Results

The results obtained with CO_2 in HY at $-80°$, particularly the instability mentioned, are illustrated in Figures 1 and 2. Figure 1 shows the amount, s, of CO_2 in the solid at equilibrium as a function of the CO_2 pressure in the gas. After degassing and cooling the solid to $-80°$, the points 1, 2, and 3 were successively obtained (line a). In the next step a maximum uptake corresponding to point 4 is reached, but this state is unstable; here the amount of sorbate in the solid decreases spontaneously as shown by the solid lines in Figure 2. The pressure p increases simultaneously until equilibrium is reached at point 5, because the volume is constant and the system is closed. The approach to this equilibrium point is much slower than the approach to the other equilibrium states, where it follows typically the pattern shown by the dotted lines in Figure 2. Subsequently, points 6 and 7 were obtained in sorption (s increasing) and points 8, 9, and

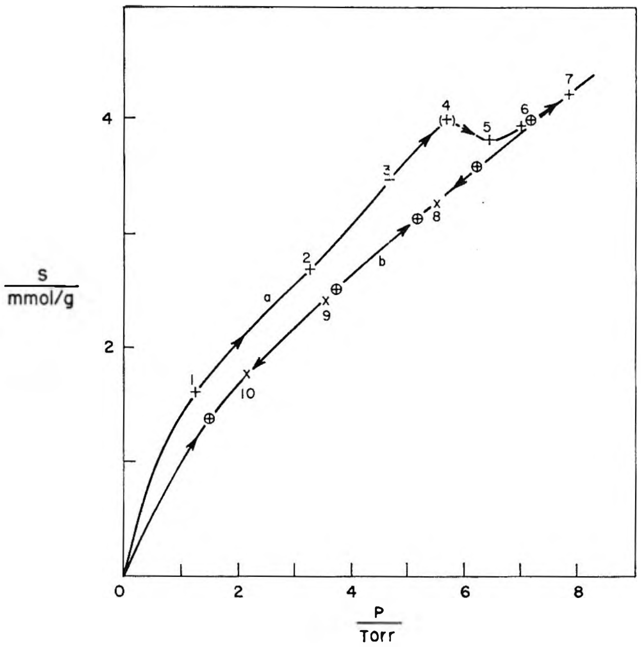

Figure 1. Sorption of CO_2 at −80° in HY: (a) in the metastable state; (b) in the stable state.

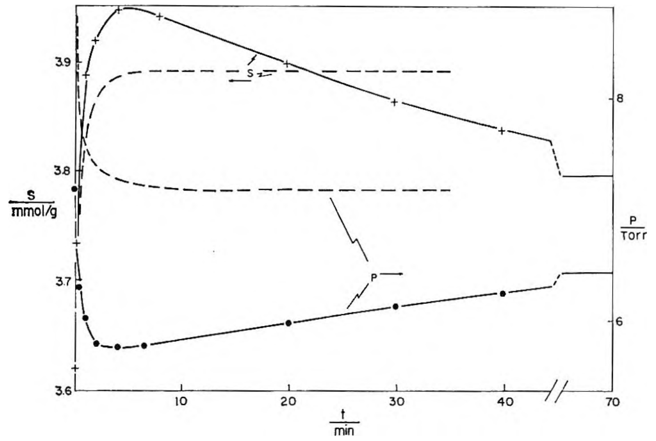

Figure 2. Solid lines: kinetics of spontaneous desorption of CO_2 from HY at −80° and about 30% of saturation; dotted lines: kinetics of sorption of CO_2 in HY after stabilization and evacuation, in the same region of pressure and saturation.

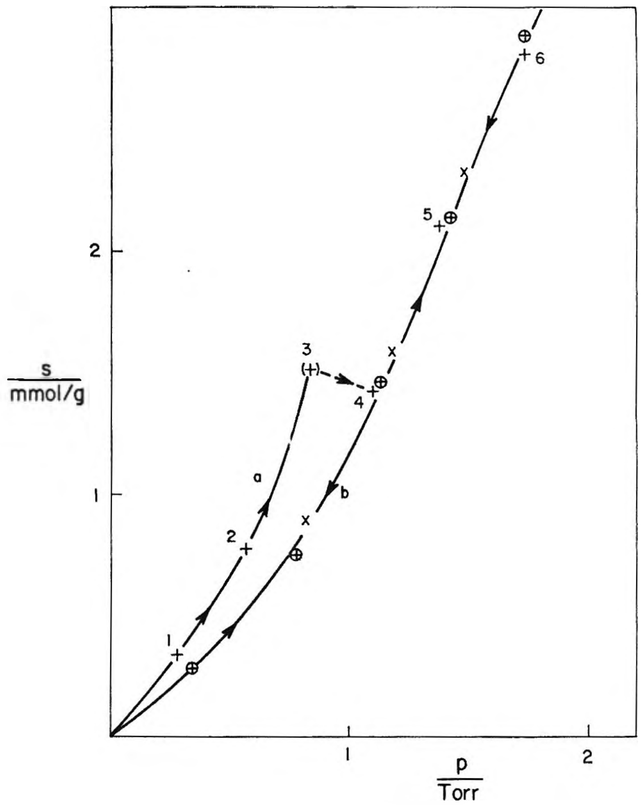

Figure 3. Sorption of C_2H_6 at −80° in NaY: (a) in the metastable state; (b) equilibrium points in the stable state.

10 in desorption (s decreasing). The p–s diagram shows a loop that is inverted compared to a normal hysteresis loop; s in sorption is higher than s in desorption at equal pressure. The sorbent was then evacuated at −80° and, subsequently, the points marked ⊕ were obtained in sorption (s increasing). They fall together with the points 7, 8, 9, and 10, on the same equilibrium line (b). This equilibrium line is now stable and can be reproduced repeatedly in sorption and desorption as long as the solid is kept at −80°. However, if the solid was evacuated at 300° and cooled down to −80° again, then the original sequence including the instability around 30% (corresponding to roughly one CO_2 molecule per aluminum atom in the solid) of saturation and the "inverted hysteresis" was repeated. The same type of instability and "inverted hysteresis" was also observed when C_2H_6 was sorbed into the NaY zeolite at −80° after cooling from 300°. The isotherms for this system in the metastable and stable state are shown in Figure 3. The instability occurred at point 3, the stable isotherm (line b) was obtained afterwards in sorption and desorption at −80°. In both systems the behavior was found to be reproducible. The instability was observed each time after the zeolites had been degassed at 300° and cooled to −80° within rather narrow ranges (±5%) of pressure and degree of saturation. In both systems the behavior was also reproduced with fresh samples of the same materials.

Discussion

There are two different states of the sorbent, characterized by different sorption behavior (lines a and b in Figure 1) at the same composition and temperature. These two states must be distinguished by a difference in structure.

The observation of a hysteresis loop that is inverted compared to the normal case (gas uptake at increasing pressures being higher here than at decreasing pressures) and is nonrecurring under isothermal conditions, as well as the phenomenon of spontaneous desorption (Figure 2), present some interest from a thermodynamic viewpoint. The direction of the flux of CO_2 is reversed when the spontaneous desorption begins. The chemical potential of CO_2 in the solid must then increase at this moment, while the pressure and therefore also the chemical potential of CO_2 in the gas reach a minimum and begin to increase at the same time. The chemical potential of the zeolite has to decrease simultaneously, since the Helmholtz free energy of the closed system can only decrease at constant temperature and constant volume, indicating that an irreversible transition in the solid occurs. Line a in Figure 1, therefore, represents states of the solid that are metastable relative to the equilibrium states at the same composition (s) and temperature represented by line b. A transition from a metastable to a stable state at constant composition must involve some spatial rearrangement of the particles in the solid. In other words, if the inverted hysteresis loop were a perfect cycle, the solid after evacuation being in exactly the same state as initially, then it should be possible to run through the same cycle repeatedly at constant temperature, and a *perpetuum mobile* of the second kind could be constructed. Since this possibility is excluded (only one cycle in the p–s diagram is possible at constant temperature, which cannot be perfect), the state of the solid initially and after completion of the loop must be different at the same composition. A change in structure, however minor, must have occurred.

The transition from the metastable to the stable state at −80° must be exothermic because it can be reversed at 300°. The metastable state becomes unstable at −80° if a certain critical amount of sorbate is present.

Polymorphic transitions have been observed in many silicate systems.[1,2] Different polymorphous forms are generally characterized by different optical or thermal properties; in the systems described here a monotropic transition, which is induced at a certain concentration of guest molecules, changes the sorption properties of the solid.

A dependence of the equilibrium lattice positions of cations in zeolites on temperature has been observed by Smith, Bennett, and Flanigen;[3] a change of the equilibrium positions of the constituents of the solid upon introduction of a sorbate has been found by Smith[4] and by Meier and Shoemaker.[5]

Acknowledgment. The author is indebted to G. H. Kühl and H. S. Sherry for providing the synthetic zeolite materials.

---

(1) W. Eitel, "Silicate Science," Vol. III, Academic Press, New York, N. Y., 1965, p 44 ff.

(2) F. C. Kracek in "Phase Transformations in Solids," R. Smoluchowski, J. E. Mayer, and W. A. Weyl, Ed., John Wiley & Sons, New York, N. Y., 1951, p 257.

(3) J. V. Smith, J. M. Bennett, and E. M. Flanigen, *Nature*, **215**, 241 (1967).

(4) J. V. Smith, *J. Chem. Soc.*, 3759 (1964).

(5) W. M. Meier and D. P. Shoemaker, *Z. Kristallogr.*, **123**, 357 (1966).

Analysis of Dielectric Measurements in the Presence of a Small Departure from Debye Behavior[1a]

by Edward H. Grant[1b]

Electromedical Division, The Moore School of Electrical Engineering, University of Pennsylvania, Philadelphia, Pennsylvania 19104

(Received July 29, 1969)

The purpose of this note is to suggest methods by which any given set of dielectric data may best be examined in order to detect small deviations from a single relaxation time. To achieve this, some of the previously published material[2a] will be drawn upon but new ideas will be also presented. The emphasis will be on simple analytical techniques not requiring the use of a computer so that a set of results can be quickly tested for departures from the Debye theory. Once Debye behavior is contraindicated, a computer may be necessary to fit the data to the appropriate relaxation function.

In general, if a given set of dielectric data will not fit a single relaxation time, the explanation is usually given in terms of a distribution of relaxation times, or a subsidiary overlapping dispersion, or both. The most convenient procedure to adopt for the present purpose is to choose a commonly used distribution function and examine its effect on various well known expressions which are valid when the Debye equations hold. The particular distribution function chosen is unimportant since *departure* from Debye behavior is the point at issue; for convenience the Cole–Cole[3] function (which is probably the one most widely used) will be used.

The Cole–Cole equations are normally written in the form

$$\epsilon' = \epsilon_\infty + (\epsilon_0 - \epsilon_\infty)\frac{\left[1 + x^{1-\alpha}\sin\dfrac{\alpha\pi}{2}\right]}{1 + 2x^{1-\alpha}\sin\dfrac{\alpha\pi}{2} + x^{2(1-\alpha)}} \tag{1}$$

$$\epsilon'' = \frac{(\epsilon_0 - \epsilon_\infty)x^{1-\alpha}\cos\dfrac{\alpha\pi}{2}}{1 + 2x^{1-\alpha}\sin\dfrac{\alpha\pi}{2} + x^{2(1-\alpha)}} \tag{2}$$

---

(1) (a) This work was supported by NIH Grant HE-01253 NONR-551(52); (b) on leave of absence from Queen Elizabeth College, London.

(2) (a) E. H. Grant, T. J. Buchanan, and H. F. Cook, *J. Chem. Phys.*, **25**, 156 (1957).

(b) H. P. Schwan, *Z. Naturforsch.*, **9a**, 35 (1954).

(3) K. S. Cole and R. H. Cole, *J. Chem. Phys.*, **9**, 341 (1941).

where $x = \omega\tau_m$ and τ_m is the most probable relaxation time. Alternatively $x = \lambda_m/\lambda = f/f_m$. The other symbols have their usual significance. If α is small and points are considered where the dispersion is appreciable ($0.1 < x < 10$) one may write $x^\alpha = 1 + \alpha \ln x$ which makes eq 1 and 2 considerably easier to handle by removing the fractional indices. The modified expressions are

$$\epsilon' = \epsilon_\infty + \frac{(\epsilon_0 - \epsilon_\infty)\left(1 + \frac{1}{2}\alpha x\pi\right)}{1 + \alpha x(\pi - 2x \ln x) + x^2} \tag{3}$$

$$\epsilon'' = \frac{(\epsilon_0 - \epsilon_\infty)x(1 - \alpha \ln x)}{1 + \alpha x(\pi - 2x \ln x) + x^2} \tag{4}$$

which, it must be emphasized, hold for values of α less than about 0.05 and for values of ϵ' and ϵ'' taken within the dispersion region corresponding to the range of x defined as above.

Assuming these conditions, expressions 3 and 4 can be rearranged to form the four following equations

$$\epsilon' - \frac{\epsilon''^2}{\epsilon_0 - \epsilon'} = \epsilon_\infty + (\epsilon_0 - \epsilon_\infty)\frac{\alpha\pi}{2}x^{-1} \tag{5}$$

$$\epsilon' + \frac{\epsilon''^2}{\epsilon' - \epsilon_\infty} = \epsilon_0 - (\epsilon_0 - \epsilon_\infty)\frac{\alpha\pi}{2}x \tag{6}$$

$$\frac{\lambda\epsilon''}{\epsilon' - \epsilon_\infty} = \lambda_m - \lambda\alpha x^2\left(\frac{\pi}{2} + x^{-1}\ln x\right) \tag{7}$$

$$\frac{\lambda(\epsilon_0 - \epsilon')}{\epsilon''} = \lambda_m + \lambda\alpha\left(\frac{\pi}{2} - x \ln x\right) \tag{8}$$

The final term in each of these equations shows the effect of a small α on standard expressions used for deriving the important dispersion parameters when a single relaxation time is present. In a previous publication[2a] the effect of a small α on the values of the left hand side of eq 5–7 has also been considered, but the resulting equations were unwieldy and difficult to handle due to the presence of terms containing $x^{1-\alpha}$ These difficulties are removed by making the derivations from eq 3 and 4 rather than 1 and 2.

Clearly, the usefulness of any of the above four equations depends upon the part of the dispersion region where the experimental points are available, since the terms containing α also contain x. For example, using eq 8 in conjunction with readings taken previously by the author[2a,4] on water at 0.86, 1.26, and 3.225 cm the left hand side becomes 1.74 ± 0.02, 1.77 ± 0.03, and 1.94 ± 0.07 cm, respectively. The quoted errors are appropriate to ±1% in ϵ' and ±2% in ϵ''. The three corresponding values of $\lambda\alpha\ (\pi/2 - x \ln x)$ are $0.11\ \alpha$, $1.3\ \alpha$, and $6.2\ \alpha$ which on substitution gives α lying in the range of 0.02 to 0.04. The precise value of α is of minimal importance however; the relevant observation is that the trend is away from single relaxation time behavior. Full discussions of the dielectric behavior of water appear elsewhere.[2a,2b,4]

For completeness it is worth noting that at frequencies well away from the relaxation frequency the curves for ϵ' against $\ln x$ become indistinguishable over a fair range of values of α. On the other hand, the differences between the ϵ'' curves for various values of α actually become more enhanced as $x \gg 1$ or $x \ll 1$ which makes these conditions very suitable for locating a small α, as was pointed out by Schwan.[2a] In these circumstances

$$\epsilon'' = (\epsilon_0 - \epsilon_\infty)x^{1-\alpha} \quad (f \ll f_m) \tag{9}$$

$$\epsilon'' = (\epsilon_0 - \epsilon_\infty)x^{-(1-\alpha)} \quad (f \gg f_m) \tag{10}$$

A logarithmic plot of ϵ'' against frequency or wavelength produces a straight line of slope (1-α); a similar plot can be deduced if values are available for conductivity rather than ϵ''.

Near the center of the dispersion the curves of ϵ'' against $\ln x$ lie almost on top of one another for the very small values of α being considered, and examination of eq 4 shows that one value of exists on either side of the central maximum where ϵ'' is the same for all values of α between 0 and about 0.05. This isobathic point is obtained by solving the equation $(x^2 - 1) \ln x = \pi x$ which gives the result $x = 3.1$ or 0.323.

In this note only small departures from Debye behavior have been considered; the case for a larger spread of relaxation times having been dealt with previously.[5-8]

Acknowledgment. Thanks are due to Professor H. P. Schwan for his comments on the material contained in this paper and for providing the facilities for the author's stay at the University of Pennsylvania.

(4) E. H. Grant and R. Shack, *Brit. J. Appl. Phys.*, **18**, 1807 (1967).

(5) Robert H. Cole, *J. Chem. Phys.*, **23**, 493 (1955).

(6) C. Brot, *Compt. Rend.*, 19, 397 (1959).

(7) G. Williams, *J. Phys. Chem.*, **63**, 534 (1959).

(8) V. A. Santerelli, J. A. MacDonald, and C. Pine, *J. Chem. Phys.*, **46**, 2367 (1967).

Line-Width Effects in the Electron Spin Resonance Spectrum of the 2,5-Dimethylhydroquinone Cation Radical

by Paul D. Sullivan[1] and James R. Bolton

Department of Chemistry, University of Minnesota,
Minneapolis, Minnesota 55455 *(Received April 3, 1969)*

As part of a study on the temperature dependence of the coupling constants of several cation radicals,[2a] the

---

[1] Department of Chemistry, Ohio University, Athens, Ohio.

[2] (a) J. R. Bolton and P. D. Sullivan, unpublished results; (b) P. D. Sullivan and J. R. Bolton, *J. Amer. Chem. Soc.*, **90**, 5366, (1968).

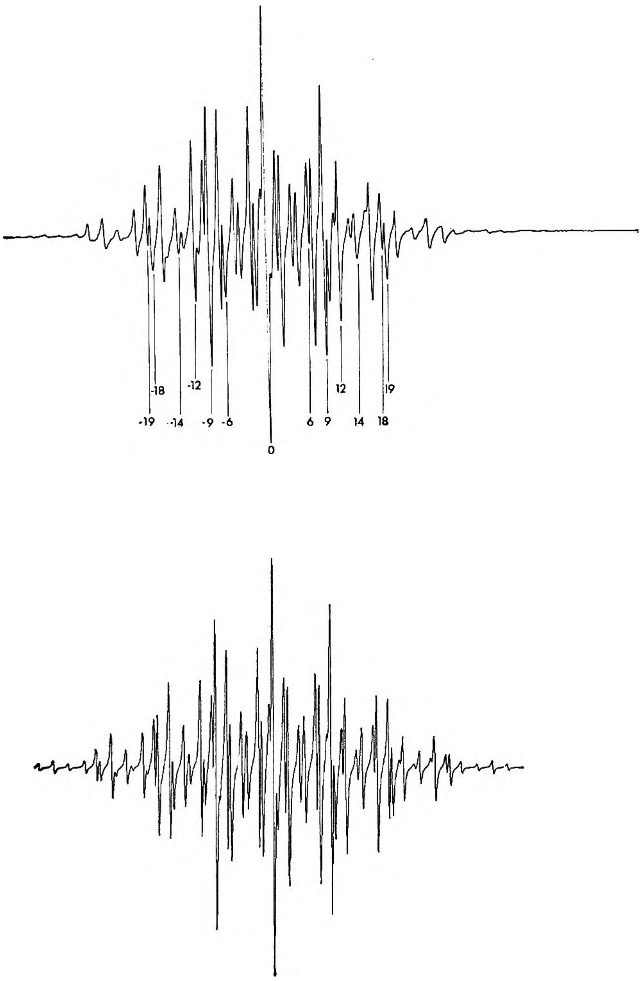

Figure 1. The esr spectrum (top) of the cation radical of 2,5-dimethylhydroquinone at 25°. Line numbers are indicated in the figure. A simulated spectrum (bottom) with a constant line width of 100 mG.

Table I: Experimental and Calculated Amplitudes for the 2,5-Dimethylhydroquinone Cation Radical at 25°

Line no.	$\tilde{M}_{CH_3}$[a]	$\tilde{M}_{CH}$	$\tilde{M}_{OH}$	Degeneracy, calcd,	Exptl relative widths,[b] 25°	Calcd relative widths[c]
+19	1	1	1	15	1.18	
+18	2	0	0	24	1.53	1.56
+16	1	0	1	30	1.19	
+14	1	−1	1	15	1.35	
+12	1	1	0	30	1.01	0.98
+9	1	0	0	60	1.11	1.14
+7	0	0	1	40	1.08	
+6	1	−1	0	30	1.42	1.44
+3	0	1	0	40	1.06	1.09
+2	1	0	−1	30	1.15	
0	0	0	0	80	1.00	1.00
−2	−1	0	+1	30	1.24	
−3	0	−1	0	40	1.03	1.09
−6	−1	+1	0	30	1.45	1.44
−7	0	0	−1	40	1.04	
−9	−1	0	0	60	1.13	1.14
−12	−1	−1	0	30	1.00	0.98
−14	−1	+1	−1	15	1.35	
−16	−1	0	−1	30	1.18	
−18	−2	0	0	24	1.55	1.56
−19	−1	−1	−1	15	1.15	

[a] See B. L. Barton and G. K. Fraenkel, *J. Chem. Phys.*, **41,** 695 (1964) for explanation of spectral index numbers. [b] Normalized to the center line, which is assumed to have a line width independent of the modulating mechanisms. Relative widths were determined from relative amplitudes after corrections for overlap. [c] Calculated from eq (1) with $A = 0.14$, $B = 0.09$, $C = -0.21$.

esr spectrum of the 2,5-dimethylhydroquinone cation radical was examined over the temperature range −70 to +25°. At the lowest temperatures line-width effects due to anisotropic dipolar and g tensor interactions were observed.[2b] At the higher temperatures (25°, see Figure 1), the spectrum is totally symmetric about the center line, however, a comparison of the experimental amplitudes with those predicted show certain deviations (Table I and Figure 1). First the lines arising from the methyl protons only (*i.e.*, $\tilde{M}_{CH_3} = \pm3, \pm2, \pm1, 0, \tilde{M}_{CH} = \tilde{M}_{OH} = 0$) broaden symmetrically away from the center with an approximately quadratic dependence on $\tilde{M}_{CH_3}$ (*cf.* line no's ±18, ±9, 0 in Table I). Second, lines with $\tilde{M}_{CH_3}$ and $\tilde{M}_{CH}$ of the same sign have greater amplitudes than those with quantum numbers of opposite sign (compare line no's, ±12 with ±6, and ±19 with ±14 in Table I and Figure 1). These results cannot be explained in terms of the anisotropic dipolar and g tensor interactions.[3] It can be shown by observing the changes in line amplitudes with temperature that these effects are negligible at 25°, except perhaps for a small effect on lines associated with the hydroxyl protons. Most simply, the results may be explained in terms of "in-phase modulations."[3] Thus if the two methyl groups have splitting constants which are instantaneously equivalent at all times but which are modulated between two limiting values, then the line widths would be proportional to $(\tilde{M}_{CH_3})^2$. Also if we assume that there is an "in-phase modulation" of the CH protons but that this modulation is "out of phase" with that of the methyl-group modulations (with respect to the absolute values of the methyl and CH proton splitting constants), the second effect is explained. That is, as the absolute value of the methyl group splitting constant increases the absolute value of the CH proton splitting constant decreases, thus making $|a_{CH_3}{}^H| + |a_{CH}{}^H| \cong$ constant. In relaxation matrix theory terms, the line widths would be expressed by[3]

$$T_2{}^{-1}(\tilde{M}_{CH_3},\tilde{M}_{CH}) = A(\tilde{M}_{CH_3})^2 + B(\tilde{M}_{CH})^2 + C\tilde{M}_{CH_3}\cdot\tilde{M}_{CH} + T_{2,0}{}^{-1} \quad (1)$$

where, A, B, and C are spectral densities.[3] A least-squares fit of the experimental data for lines with $\tilde{M}_{OH}$

(3) G. K. Fraenkel, *J. Phys. Chem.*, **71,** 139 (1967).

$= 0$, gives values for A, B, and C of 0.14 ± 0.01, 0.09 ± 0.03 and −0.21 ± 0.02 respectively (see also Table I).

The physical explanation of this phenomenon is not straightforward. It is known that hydroxyl groups in hydroquinone and duroquinol are "fixed" at low temtemperatures and are "rotating" at high temperatures. It is presumed that the existence of only one distinct spectrum for 2,5-dimethylhydroquinone at low temperatures is due to the presence of the *trans* form only.[2] We may therefore speculate that it is the rotation of the hydroxyl groups at higher temperatures which cause the observed effects. The interesting point is, however, that for an "in-phase modulation" of the methyl and ring protons, both hydroxyl groups are required to rotate in an *instantaneously equivalent manner*. One wonders if, in fact, this may be a manifestation of a "cog-wheel" effect between the hydroxyl and methyl groups. Alternatively it may be that a more complex motion may also contribute to the observed line-width variations.

It is appropriate to mention that an apparently similar effect has been observed for the cation radical of 1,4-dideuteroxy, 2,3-dimethylnaphthalene at *low* temperatures, although in this case, due to the complexity of the spectrum it is more difficult to analyze in detail. It should also be noted that it has not been possible to study the cation radical of 2,3-dimethylhydroquinone at high temperatures due to the instability of this radical.

Acknowledgment. Research supported in part by Grant No. NSF-GP-8416 from the National Science Foundation. Equipment partially funded by the National Science Foundation through Grant No. GP-6991.

Steric Effects in the Decomposition of Halogenated Nitrobenzene Anion Radicals

by Wayne C. Danen, Terry T. Kensler,
J. G. Lawless, M. F. Marcus, and M. D. Hawley

Department of Chemistry, Kansas State University, Manhattan, Kansas 66502 *(Received April 16, 1969)*

Numerous nitroaromatic compounds have now been successfully reduced to their corresponding anions in aprotic solvents.[1] Although many of these radicals are sufficiently stable to permit recording of their electron spin resonance (esr) spectra, a group of halogen-substituted nitroaromatic radicals constitutes a notable exception. For example, the reduction of the three isomers of iodonitrobenzene in dimethylformamide[2] and acetonitrile[3] gives not the corresponding iodonitrobenzene anion radicals, but rather the anion radical of nitrobenzene. Evidence was presented recently which indicates that this electrochemical reduction is an over-all two-electron process.[4] The initial one-electron reduction of an iodonitrobenzene was shown to give its anion radical which loses iodide ion to yield the corresponding nitrophenyl radical (eq 1)

$$IC_6H_4NO_2 + e \rightleftharpoons [IC_6H_4NO_2]^{\cdot -} \rightleftharpoons [C_6H_4NO_2]\cdot + I^- \quad (1)$$

Nitrobenzene is then formed by the abstraction of a hydrogen atom from either the solvent or the supporting electrolyte by the nitrophenyl radical

$$[C_6H_4NO_2]\cdot + SH \longrightarrow C_6H_5NO_2 + S\cdot \quad (2)$$

The subsequent one-electron reduction of nitrobenzene to its anion radical at slightly more negative potential completes the over-all two-electron process

$$C_6H_5NO_2 + e \rightleftharpoons C_6H_5NO_2^{\cdot -} \quad (3)$$

It was observed during the course of the earlier work that the *o*-iodo- and *o*-bromonitrobenzene anion radicals decomposed considerably more rapidly than their *meta* and *para* isomers. Those observations suggested that further studies should be made into the relationship between stability of the halogenated nitrobenzene anion radical and steric interactions. The results of such a study are reported herein.

Table I summarizes the electrochemical data for the compounds studied. Data for nonhalogenated nitrobenzenes are included for comparison. As the results for compounds 3, 4, 6, and 9–11 indicate, placement of a methyl group adjacent to the nitro group decreases the stability of the anion radical as evidenced by the enhanced rate of halide loss from a nonsterically affected position. For example, substitution of a methyl group in the 6 position of 3-iodonitrobenzene causes a 30-fold increase in the rate of iodide loss in the anion radical. Substitution of two methyl groups adjacent to the nitro group in 4-iodonitrobenzene results in a 280-fold increase in the rate of iodide loss. As expected from carbon–halogen bond energies, loss of halide ion from the 4-halogeno-2,6-dimethylnitrobenzene anion radicals is more rapid for iodide than for bromide (compare compounds 9 and 10). Loss of chloride is not observed electrochemically from any of the anion radicals.

Twisting of the nitro group by alkyl substituents in nitrobenzene anion radicals has been shown to be

---

(1) D. H. Geske, J. L. Ragle, M. A. Bambanek, and A. L. Balch, *J. Amer. Chem. Soc.*, **86**, 987 (1964).

(2) T. Kitagawa, T. P. Layloff, and R. N. Adams, *Anal. Chem.*, **35**, 1086 (1963).

(3) T. Fujinaga, Y. Deguchi, and K. Umemoto, *Bull. Chem. Soc. Jap.*, **37**, 822 (1964).

(4) J. G. Lawless and M. D. Hawley, *J. Electroanal. Chem.*, **21**, 365 (1969).

Table I: Substituent Effects on Nitrobenzene and Nitrobenzene Anion Radicals in Dimethylformamide

Compound	Substituent	$-E_{p/2}$ *vs.* sce, V	$-\Delta$, mv	k, sec^{-1} [d]	Anion radical coupling constant a_N[a] g
1	H	1.06			10.32
2	2-Iodo	0.95		8×10^4	
3	3-Iodo	0.94		3.1×10^{-1} [b]	
4	4-Iodo	1.00		9×10^{-1} [b]	
5	2-Bromo	1.03	100[c]	1.1×10^2 [b]	
6	4-Bromo	0.98		4×10^{-3}	
7	2-Chloro	1.05	60	10^{-2}	
8	4-Chloro	0.99		10^{-2}	
9	2,6-Dimethyl-4-iodo	1.19	180[c]	2.5×10^2	
10	2,6-Dimethyl-4-bromo	1.27	170	1.0	
11	3-Iodo-6-methyl	1.04	60[c]	9.8	
12	4-Iodo-3-methyl	1.00		1.4	
13	3-Iodo-4-methyl	1.00		2.3	
14	3-Bromo-4-methyl	0.98		8.5×10^{-2}	
15	3-Bromo-4-*t*-butyl	0.96		1.5×10^{-1}	
16	4-Bromo-3-methyl	1.00		1.3×10^{-2}	
17	4-Bromo-3-*t*-butyl	0.96		3.1	
18	4-Methyl	1.13			10.79
19	4-*t*-Butyl	1.13			
20	2,6-Dimethyl	1.36	180		17.8
21	3-*t*-Butyl	1.10			
22	2-Methyl	1.18	60		11.0
23	3-Methyl	1.09			10.4

[a] Data in acetonitrile taken from ref 1. [b] Data taken from ref 4. [c] See text for procedure on calculation. [d] Relative average deviation is less than 5%.

accompanied by a marked increase in the nitrogen coupling constant (Table I) and a decrease in the spin density on the ring.[1,5] The increased steric interaction in substituted nitrobenzene anion radicals is also reflected in the reduction potentials. From values for *ortho* substituents[6] and the value of the reaction constant determined from *p*- and *m*-substituted nitrobenzenes (ρ = 0.36 V), the reduction potentials for *o*-substituted nitrobenzenes in the absence of steric interactions can be predicted. The difference, Δ, between the predicted and observed reduction potentials for *o*-substituted nitrobenzenes can be taken as a qualitative measure of the extent of increased steric interaction in the anion radical.[7] In the case of *o*-nitrotoluene, Δ_{o,CH_3} is determined to be -60 mV (1.4 kcal), a value in agreement with a previously reported result for *o*-nitrotoluene in acetonitrile.[1] $\Delta_{o,Cl}$ is measured as -60 mV in *o*-chloronitrobenzene, a result which is anticipated since the van der Waals radii of the methyl group and chlorine atom are nearly equal ($r_{v,Cl}$ = 1.75 Å and r_{v,min,CH_3} = 1.72 Å).[8] Placement of two methyl groups adjacent to the nitro group, as in 2,6-dimethylnitrobenzene (see also compounds 9 and 10), causes additional steric interaction of 4.1 kcal ($\Delta_{2,6\text{-dimethyl}} = -180$ mV) in the anion radical.

Direct calculations of steric interactions with other substituted nitrobenzenes can be made if the electrode process is chemically and electrochemically reversible. Although all the nitrobenzenes satisfy the electrochemical reversibility requirement, several halogenated anion radicals, including the anion radicals of *o*-bromo- and *o*-iodonitrobenzene, eliminate halide ion sufficiently rapidly so as to preclude a direct estimate of their interaction from reduction potentials alone.[9] While the results from alkyl-substituted nitrobenzenes would

---

(5) An increase in the nitrogen coupling constant alone should not be taken as an indication of halogenated nitrobenzene anion radical instability, since the addition of a hydroxylic solvent causes an increase in radical stability as well as an increase in the nitrogen coupling constant. See for example, P. Ludwig, T. Layloff, and R. N. Adams, *J. Amer. Chem. Soc.*, **86**, 4568 (1964); J. Q. Chambers, III, T. Layloff, and R. N. Adams, *J. Phys. Chem.*, **68**, 661 (1964).

(6) P. Zuman, "Substituent Effects in Organic Polarography," Plenum Press, New York, N. Y., 1967, Chapter 3.

(7) The steric interaction, Δ, will be zero if the energy changes in going from the planar to the twisted configurations are equal for both the anion radical and the neutral species. Since $\Delta = E°_{\text{planar}} - E°_{\text{twisted}}$ are all negative in the present study, the loss of resonance interaction of the nitro group is larger in the anion radical than in the neutral molecule. The actual loss of resonance interaction is probably somewhat greater than those estimates indicate, since twisting of the nitro group should increase solvation of the anion radical, causing an anodic shift in the reduction potential.

(8) M. Charton, *J. Amer. Chem. Soc.*, **91**, 615 (1969).

(9) In the case of an irreversible chemical reaction subsequent to electron transfer, the cyclic voltammetric peak potential, E_p, is shifted anodically by 30 mV for every tenfold increase in the rate constant. For 2,6-dimethyl-4-iodonitrobenzene anion radical a rate constant of 250 sec^{-1} and a potential scan rate of 87-mV/sec shift the peak potential anodically by approximately 64 mV. Loss of bromide ion in 4-bromo-2,6-dimethylnitrobenzene is sufficiently slow so as not to shift the peak significantly. For a full discussion of chemical reactions subsequent to electron transfer and their effect upon the location of peak potentials, see R. S. Nicholson and I. Shain, *Anal. Chem.*, **36**, 706 (1964).

suggest that the difficulty of reduction should increase in the order of increasing size of the *ortho* halogen substituent, the order of the reduction potentials is reversed and a "positive *ortho* effect" is observed. However, if the effect of the rate of the irreversible loss of halide ion upon the location of the reduction potenital is taken into consideration,[9] the expected order for the standard reduction potential is obtained ($E_{1/2}$ = -1.12 V and $\Delta_{o,\mathrm{Br}} = -100$ mV). Thus, while steric interaction increases with increasing size of the *ortho*-substituted halogen, this also facilitates the loss of halide ion. The anodic shift caused by the enhanced rate of halide elimination more than compensates for the cathodic shift that would normally accompany increased steric interaction. Although our present equipment does not permit the direct determination of rate constants in excess of 500 $\sec^{-1}$, a lower limit of 8×10^4 $\sec^{-1}$ can be estimated for the elimination of iodide ion from *o*-iodonitrobenzene anion radical if one assumes that

$$|\Delta_{o,\mathrm{I}}| \geq |\Delta_{o,\mathrm{Br}}| \text{ and } |E_{1/2}(o\text{-iodonitrobenzene})| \geq |E_{1/2}(o\text{-bromonitrobenzene})|$$

The results above clearly show that twisting of the nitro group from the plane of the benzene ring enhances the rate of loss of halide ion. As expected, the substitution of alkyl groups adjacent to the halogen also assists elimination of halide ion. In the case of the alkyl-substituted 4-bromonitrobenzenes, the rate of bromide loss increases with increasing size of the substituent in the 3 position: $r_{\mathrm{v,H}} = 1.20$ Å, $k = 4 \times 10^{-3}$ $\sec^{-1}$; $r_{\mathrm{v,min,CH_3}} = 1.72$ Å, $k = 8.5 \times 10^{-2}$ $\sec^{-1}$; and $r_{\mathrm{v,min,}t\text{-butyl}} = 2.44$ Å, $k = 3.1$ $\sec^{-1}$.[8] A similar order in rate of halide loss is observed in the 3-bromo-4-alkylnitrobenzenes (compare compounds 14 and 15). Substitution of a methyl group in the 3 position of 4-iodonitrobenzene increases the rate of iodide loss by a factor of 1.5. The similar addition of a methyl group to the 4 position of 3-iodonitrobenzene is more effective, causing an eightfold enhancement in the rate constant.

Experimental Section

Rate constants for the elimination of halide ion from halogenated nitrobenzene anion radicals were determined by a chronoamperometric technique. Details of the experimental procedure and of the instrumentation have been described previously.[4] All studies were made at 23 ± 0.5° in purified dimethylformamide. The supporting electrolyte for the iodonitrobenzenes was 0.1 *F* tetraethylammonium iodide; the remaining halogenated and alkyl-substituted nitrobenzenes were studied in 0.1 *F* tetraethylammonium perchlorate. The rate constants for the elimination of bromide ion from anion radicals of bromonitrobenzenes were unaffected by change of the anion of tetraethylammonium salt from perchlorate to bromide.

Compounds 1–8, 11–13, 18, 22, and 23 were commercially available samples. Of these compounds, 2 was sublimed and 11–13 were purified further by repeated recrystallizations. 4-Bromo-2,6-dimethylnitrobenzene was prepared by nitration of 3,5-dimethylacetanilide,[10] followed by deacylation, diazotization with HBr and $NaNO_2$, and reaction of the diazonium salt with Cu_2Br_2. Recrystallization from ethanol and subsequent sublimation gave a low yield of the desired product (mp 63–64°). 2,6-Dimethyl-4-iodonitrobenzene was prepared analogously using KI to convert the diazonium salt into the iodide (mp 59–61°, decomposing with light). Compounds 14 and 16 were prepared by diazotization of the corresponding amines with 48% HBr and $NaNO_2$. Treatment of the resulting salts with an HBr solution of Cu_2Br_2 gave solid products which were washed with NaOH and H_2O and recrystallized from ethanol (mp compound 14, 77–77.5°; mp compound 16, 78.5–79.5°). 3-Bromo-4-*t*-butylnitrobenzene was prepared by nitration of *t*-butylbenzene,[11] followed by bromination[12] of the 4-nitro-*t*-butylbenzene to give 15 (mp 93–94°). Compound 17 was prepared from compound 15 by reduction with Fe and HCl, the product subsequently being deaminated with HCl, $NaNO_2$, and H_3PO_2.[13] The resulting *o*-bromo-*t*-butylbenzene was then nitrated according to the procedure described in the literature.[14]

Acknowledgments. Acknowledgment is made to the donors of the Petroleum Research Fund, administered by the American Chemical Society, for partial support of this work (Grant PRF No. 1123-Gl) and to the Kansas State University Bureau of General Research.

---

[10] K. Ibbotson and J. Kenner, *J. Chem. Soc.*, 1260 (1923).

[11] D. Craig, *J. Amer. Chem. Soc.*, 57, 195 (1935).

[12] M. H. Klouwen and H. Boelens, *Rec. Trav. Chim., Pays-Bas*, 79, 1022 (1960).

[13] M. Crawford and F. H. C. Stewart, *J. Chem. Soc.*, 4443 (1952).

[14] P. B. D. de la Mare and J. T. Harvey, *ibid.*, 131 (1957).

The Kinetics of the Hydrolysis of the Dichromate Ion. V. General Acid Catalysis

by R. Baharad, Berta Perlmutter-Hayman, and Michael A. Wolff[1]

Department of Physical Chemistry, Hebrew University, Jerusalem, Israel

(Received July 28, 1969)

The hydrolysis of the dichromate ion

$$Cr_2O_7^{2-} + H_2O \rightleftharpoons 2HCrO_4^- \qquad \text{(I)}$$

---

[1] Department of Chemistry, Brandeis University, Waltham, Mass.

is known to be catalyzed by bases and by nucleophiles,[2,3] and the laws governing this catalysis have been discussed.[2] The reaction is also acid-catalyzed, and the catalytic constant k_{H^+} has been determined.[4,5] In order to get some insight into the mechanism of the acid catalysis, we considered it desirable to determine whether this catalysis is general or specific.

Because of the high value of k_{H^+}, the hydrogen ion makes the dominant contribution to the observed reaction rate, unless its concentration is very low. In buffer solution, this concentration is given by the expression $K_a[HA]/[A^-]$ (where K_a is the dissociation constant of the general acid HA). We see that when the acid is fairly strong, we may have to use impracticably high concentrations of A^- in order to suppress the contribution of H^+ sufficiently for general acid catalysis to make itself felt. On the other hand, when the acid is very weak, its *anion* has a high catalytic constant[2] and its contribution to the observed rate is apt to obscure any catalytic effect which the acid may have. We compromised on acetic acid and chloroacetic acid, employing a ratio of salt to acid <1 in the first case, and >1 in the second.

Procedure

(*a*) *Experimental Technique.* We used the same experimental procedures as those described earlier,[2] except that in the rapid mixing technique[6] we used a Hamilton 725 LL syringe equipped with a bayonet socket. This socket prevents the needle from coming loose under pressure. Therefore, a finer needle than previously can be used (Luer 21 HL instead of 19 HL). This increases the linear velocity of the injected liquid, and hence the efficiency of mixing. The recorder was employed when the half-times were >3.5 sec; for shorter half-times ($3.5 > \tau_{1/2} > 0.17$) we used an oscilloscope.[6] For experiments at pH 7, the wavelength was 370 mμ; in acid solution it was 385 mμ. The dichromate concentration was $\sim 3.3 \times 10^{-4}$ M. The temperature was 25°.

(*b*) *Methods of Calculation.* For the reversible reaction we are dealing with we can again[4] define an observed pseudo-first-order rate constant k_{obsd} by

$$k_{obsd} = \frac{d \ln (D_t - D_\infty)}{dt} = \frac{d \ln (x_\infty - x_t)}{dt} \quad (1)$$

where D_t and D_∞ are the optical densities at time t, and at the end of the reaction, respectively, and the x's are the corresponding amounts of dichromate hydrolyzed, measured in moles per liter. From this we calculate k, the pseudo-first-order rate constant of the forward reaction, using an approximate expression employed earlier (eq 3 of ref 4). In the present case, where the concentration of CrO_4^{2-} is negligibly small, and the ratio $P \equiv [HCrO_4^-]/([HCrO_4^-] + [CrO_4^{-2}])$ equals unity, that expression takes the form

$$k_{obsd}/k = 1 + 4(1.5x_\infty + 0.5x_0)/K_I \quad (2)$$

where K_I is the equilibrium constant of reaction I, and x_0 the value of x at zero time.[7]

The rate constant k thus obtained is composed of k_{H_2O}, the contribution of the "spontaneous" reaction, and the sum of the various catalytic constants k_{H^+}, k_{A^-}, and k_{HA}, each multiplied by the appropriate catalyst concentration.

Results

(*a*) *Acetic Acid.* We carried out two series of experiments, both at $[Na^+] = 0.2$ M, kept constant by the addition of sodium nitrate. In the first series, the ratio of salt to acid was 0.175 and the pH was 4.0, whereas in the second the ratio was 0.40 and the pH 4.36. The highest acid concentration employed was 0.855 and 0.50 M, respectively.

Taking the value of K_I at our ionic concentration[8] as $K_I = 2.5 \times 10^{-2}$ M, we obtain from eq 2, $k_{obsd}/k \simeq 1.09$ at $[Na^+] = 0.2$ M, *i.e.*, the back reaction contributes $\sim 9\%$ to the observed rate. In Figure 1 we plotted k against acetate concentration, at the two values of pH. For the sake of comparison, we also present the influence of acetate in the absence of acid, at pH 7, taken from our previous paper.[4] Straight lines are seen to be obtained, their slopes increasing significantly with increasing relative acid concentration. Quantitatively, the slopes are equal to $k_{CH_3COO^-}$, $(k_{CH_3COO^-} + k_{CH_3COOH}/0.4)$ and $(k_{CH_3COO^-} + k_{CH_3COOH}/0.175)$, respectively. Using[4] $k_{CH_3COO^-} = 1.92$, we obtain, $k_{CH_3COOH} = 1.06$ M^{-1} sec^{-1}.

The intercepts at zero acid concentration are due to the contributions of water and of hydrogen ion. Taking[4] $k_{H_2O} = 0.03$ sec^{-1}, we obtain $k_{H^+} \simeq 1.05 \times 10^4$ M^{-1} sec^{-1} at $[Na^+] = 0.2$.

(*b*) *Chloroacetate.* The catalytic constant of the chloroacetate ion is not reported in the literature, and therefore had to be determined. We carried out the measurement in the presence of $[Na^+] = 1$ M, in order to be able to apply chloroacetate in large excess over chloroacetic acid (see section (*c*)). The sodium ion concentration was again regulated by the addition of sodium nitrate. The pH was 7, achieved by phosphate buffer at a total phosphate concentration of 10^{-2} M. As a result of 3 experiments at chloroacetate concentrations between 0.24 to 0.32 M we obtained $k_{\mathrm{CH_2ClCOO^-}} = 0.28$ M^{-1} sec^{-1} (See also Figure 2, lower line, where k is plotted against [$\mathrm{CH_2ClCOO^-}$].)

---

[2] B. Perlmutter-Hayman and M. A. Wolff, *J. Phys. Chem.*, **71**, 1416 (1967), where earlier literature is quoted.

[3] Y. Egozy and A. Loewenstein, *J. Magnetic Resonance*, **1**, 494 (1969).

[4] B. Perlmutter-Hayman, *J. Phys. Chem.*, **69**, 1736 (1965), where earlier literature is quoted.

[5] J. A. Jackson and H. Taube, *ibid.*, **69**, 1844 (1965).

[6] B. Perlmutter-Hayman and M. A. Wolff, *Israel J. Chem.*, **3**, 155 (1965).

[7] The use of eq 2, instead of the exact equation $d \ln (x_\infty - x_t)/dt = k[1 + 4(x_\infty + x_t)/K_I]$ (eq 2 of ref 4), is justified provided the contribution of the back reaction is small and no great error is introduced by replacing $(x_\infty + x_t)$ by its mean value, thus treating k_{obsd} as a true constant during any given run.

[8] B. Perlmutter-Hayman and Y. Weissmann, *Israel J. Chem.*, **6**, 17 (1968).

(*c*) *Chloroacetic Acid.* The value of $k_{\mathrm{CH_2ClCOOH}}$ was determined in a solution where the ratio salt to acid was 8:1, and the concentration of the acid varied from 0.024 to 0.118 M. The pH was 3.8, and the sodium ion concentration was again kept constant at 1 M by the addition of sodium nitrate. Taking the value of K_I at this ionic strength[8] as $K_I = 1.8 \times 10^{-2}$ M we obtain from eq 2, $k_{\mathrm{obs}}/k \simeq 1.12$ at [$\mathrm{Na^+}$] = 1.0 M. In Figure 2 we plotted k against [$\mathrm{CH_2ClCOO^-}$] (upper line). The slope of the straight line obtained is equal to ($k_{\mathrm{CH_2ClCOO^-}} + k_{\mathrm{CH_2ClCOOH}}/8.1$). From this we obtain $k_{\mathrm{CH_2ClCOOH}} = 20$ M^{-1} sec^{-1}. Furthermore, assuming[9] $k_{\mathrm{H_2O}} \simeq 0.06$ sec^{-1} we obtain from the intercept, $k_{\mathrm{H^+}} \simeq 0.55 \times 10^4$ M^{-1} sec^{-1} at [$\mathrm{Na^+}$] = 1.0 M.

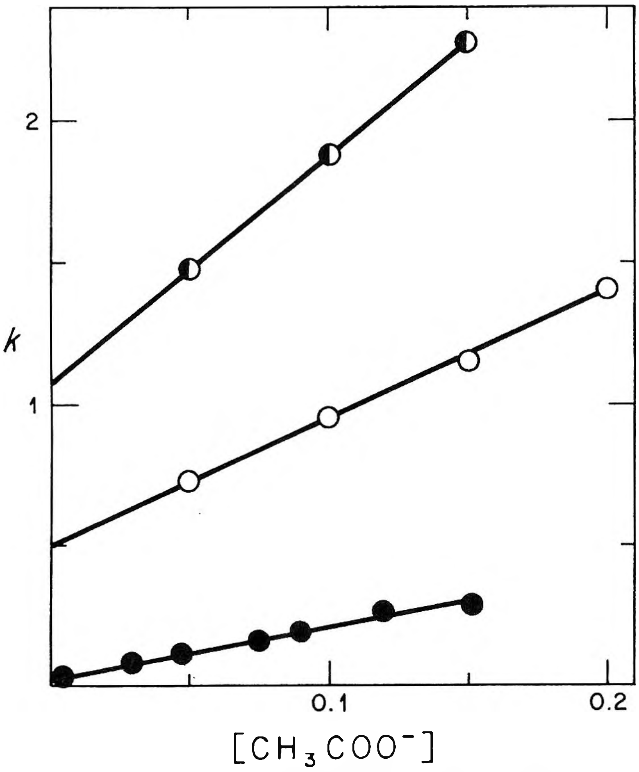

Figure 1. The dependence of the rate constant on acetate concentration at pH 4 (half-filled circles), 4.36 (open circles), and ~7 (dots).

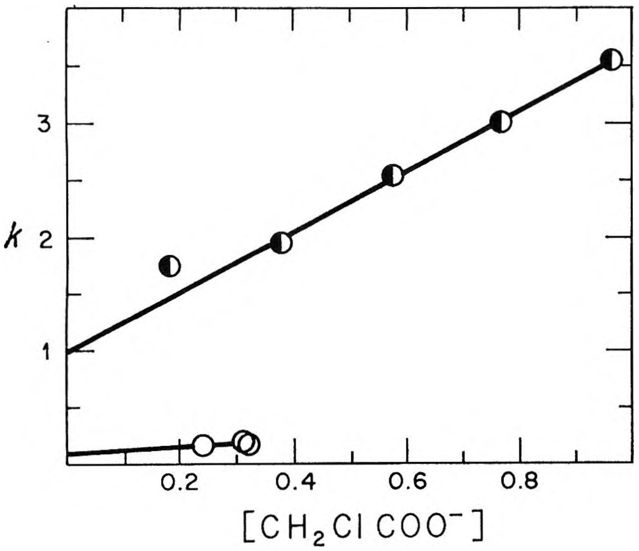

Figure 2. The dependence of the rate constant on chloroacetate concentration at pH 3.8 (half-filled circles) and ~7 (open circles).

Discussion

(*a*) *Comparison with Previous Results.* In our previous paper,[4] in addition to the experiments at pH 7 from which $k_{\mathrm{CH_3COO^-}}$ had been calculated, we also reported results at lower pH. The fact that the contribution of acetic acid had remained undetected does however not contradict the present findings. At pH > 5.5, the contribution of the acid to the observed rate is <10%, whereas at pH <5, the reaction is too fast for reliable results to be obtained with the technique applied at the time.

The pK of chloroacetic acid is 2.85. Comparison of $k_{\mathrm{CH_2ClCOO^-}}$ with the values of k_{N} for other monovalent anions of acids of comparable strength[2] (such as $\mathrm{HCO_3^-}$ or $\mathrm{H_2PO_4^-}$) shows the value of 0.28 M^{-1} sec^{-1} to lie in the range expected for a base which has no special nucleophilic properties.

The values of $k_{\mathrm{H^+}}$ and their downward trend with increasing ionic strength are in good agreement with our previous results.[4]

(*b*) *Mechanism of the Acid Catalysis.* Our results show the acid catalysis to be general rather than specific, the catalytic constant increasing with increasing acid strength in accordance with the Brønsted catalytic law. We therefore have to look for a mechanism involving rate determining proton transfer. Now, the protonation of the terminal oxygens to form $\mathrm{HCr_2O_7^-}$ is very fast and therefore cannot be rate determining. The possible protonation of the formally uncharged, bridging oxygen would be expected to proceed more slowly and might thus constitute the rate-determining step. We suggest that this protonation facilitates the heterolytic fission of a chromium–oxygen bond in a "fast" following reaction; the $\mathrm{CrO_3}$ thus remaining can be visualized as $\mathrm{H_2O \cdot CrO_3}$ which will form $\mathrm{H^+}$ and $\mathrm{HCrO_4^-}$ immediately (I). Alternatively, the fission might be envisaged as a concerted mechanism (II) where $\mathrm{CrO_3}$ adds $\mathrm{OH^-}$, facilitated by the proximity of the conjugate base. A similar rate determining protonation of the

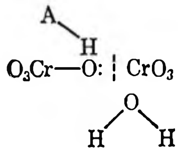

I

or

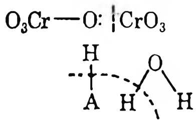

II

---

[9] B. Perlmutter-Hayman and Y. Weissmann, *J. Phys. Chem.*, 71, 1409 (1967).

bridging oxygen has been suggested for the acid-catalyzed decomposition of pyrophosphite[10] and of isohypophosphate.[11] A slightly different mechanism, involving five-coordinated Cr(VI), has recently been proposed for the formation (and decomposition) of the mixed anhydride [hydrogen chromatophosphate]$^{2-}$, a reaction which is both general acid- and general base-catalyzed.[12] It has further been suggested[12] that this mechanism is likely to resemble that of the dimerization of hydrogen chromate. This latter suggestion seems strengthened by the present findings. On the other hand, a mechanism for the general base catalysis involving rate determining proton transfer cannot account for *nucleophilic* catalysis. We would then have to conclude that pure base catalysis and nucleophilic catalysis follow different paths,[13] the latter involving direct attack of the nucleophilic A^- on the chromium-oxygen bond to form a mixed anhydride CrO_3A^- which rapidly hydrolyzes. When we first suggested this mechanism for the base catalysis[14] we had been unaware of the existence of such a substance, $HCrPO_7^{2-}$, as an identifiable species.[15] In the meantime many examples of mixed anhydrides have been reported in the literature.[12,16] This seems to strengthen our early suggestion as applied to nucleophilic catalysis.

---

(10) R. E. Mesmer and R. L. Carroll, *J. Amer. Chem. Soc.*, **88**, 1381 (1966).

(11) R. L. Carroll and R. E. Mesmer, *Inorg. Chem.*, **6**, 1137 (1967).

(12) S. A. Frennesson, J. K. Beattie, and G. P. Haight, Jr., *J. Amer. Chem. Soc.*, **90**, 6018 (1968).

(13) The existence of two distinct mechanisms might explain the large scatter in the Edwards plot of our catalytic constants (Figure 2 of ref 2, where the x axis should read P/H, and *not* pK_a!). We are indebted to Professor J. O. Edwards for suggesting this possibility.

(14) A. Lifshitz and B. Perlmutter-Hayman, *J. Phys. Chem.*, **65**, 2098 (1961), where the intermediate is termed CrO_3B.

(15) F. Halloway, *J. Amer. Chem. Soc.*, **74**, 224 (1952).

(16) D. G. Lee and R. Stuart, *J. Amer. Chem. Soc.*, **86**, 3051 (1964); J. G. Mason and A. D. Kowalek, *Inorg. Chem.*, **3**, 1248 (1964); G. P. Haight, D. C. Richardson, and N. H. Coburn, *ibid.*, **3**, 1777 (1964); G. P. Haight, E. Perchonock, F. Emmenegger, and G. Gordon, *J. Amer. Chem. Soc.*, **87**, 3835 (1965); J. Y. Tong and R. L. Johnson, *Inorg. Chem.*, **5**, 1902 (1966); G. P. Haight, M. Rose, and J. Preer, *J. Amer. Chem. Soc.*, **90**, 4809 (1968).

Electron Impact Studies of Stannous Chloride and Stannic Chloride

by A. S. Buchanan, D. J. Knowles,

Department of Physical Chemistry, University of Melbourne,
Parkville, Victoria, Australia 3052

and D. L. Swingler

Division of Chemical Physics, CSIRO Chemical Research
Laboratories, Clayton, Victoria, Australia *(Received April 18, 1969)*

Ionization efficiency (I.E.) curves produced by electron impact are difficult to interpret and usually give ionization potentials (I.P.) and appearance potentials (A.P.) that are a few tenths of an electron volt high.

Further inaccuracies are introduced in measuring the vapors over heated inorganic salts by the small ion currents and other experimental difficulties. Nevertheless data obtained by this method are worth recording when no other information is available. As part of a study of the vapor phase reactions of metal halides, the IE curves of $SnCl_2$ and $SnCl_4$ were measured and are discussed below.

Experimental Section

The quadrupole mass spectrometer used was essentially that described by Hastie and Swingler.[1] The Knudsen cell assembly had an inlet below the shutter to admit gases into the system. The gas flow was regulated by a vacuum leak (Edwards No. LKB2).

The $SnCl_2$ was contained in a silica-lined, silver Knudsen cell, the vapors from which were passed through the shutter, ionized by transverse electron impact, passed through the mass filter and collected on an electron-multiplier (EMI No. 9603B gain 10^5 at 3kV). The $SnCl_4$ was admitted below the shutter *via* the Edwards leak.

$SnCl_2$ (BDH anhydrous) was heated in the Knudsen cell to *ca.* 150° and pumped for at least 12 hr before an IE curve was measured. $SnCl_4$ (Fluka reagent grade) was purified by trap-to-trap distillation before use.

Ion currents were measured at 0.2 V intervals of the electron accelerating voltage. The point on the plot of log ion current *vs.* electron energy at which it deviates from a straight line was taken as the relevant I.P. or A.P.[2,3] The electron energy scale in the figures was calibrated using the convenient background peak of H_2O, or from added argon. Cross checks between the reference gases were always within ± 0.2 eV of the accepted values. Worthwhile semilog plots could only be obtained for the more abundant ions and where only a single process occurred. The other A.P.'s were estimated to lie within the limits given by examination of the direct I.E. plots.

Results and Discussions

I.E. curves are given in Figures 1 and 2 and the results assembled in Table I.[4–8] The calculated A.P. values

---

(1) J. W. Hastie and D. L. Swingler, to be published.

(2) R. E. Honig, *J. Chem. Phys.*, **16**, 105 (1948).

(3) J. D. Morrison, *ibid.*, **99**, 1305 (9951).

(4) C. E. Moore, "Atomic Energy Levels," National Bureau of Standards Circular 467, U. S. Government Printing Office, 1958.

(5) H. B. Gray, "Electrons and Chemical Bonding," W. A. Benjamin Inc., New York, N. Y., 1965, p 34.

(6) A. G. Gaydon. "Dissociation Energies and Spectra of Diatomic Molecules," 2nd ed, Chapman and Hall, London, 1953.

(7) G. Herzberg, "Molecular Spectra and Molecular Structure, I. Spectra of Diatomic Molecules," 2nd ed, New York, N. Y., 1960.

(8) R. C. Ferber, "Heats of Dissociation of Gaseous Chlorides," LA2841, TID-4900, UC-4, Chem., 19th Ed.

Table I: Appearance Potentials

Ion	Parent molecule		Reaction postulated	A.P., eV measd	A.P., eV calcd[a]
$SnCl_2^+$	$SnCl_2$	(i)	$SnCl_2 + e \rightarrow SnCl_2^+ + 2e$	[b]10.1 ± 0.4	
$SnCl^+$	$SnCl_2$	(ii)	$SnCl_2 + e \rightarrow SnCl^+ + Cl + 2e$	[b]11.3 ± 0.4	
Sn^+	$SnCl_2$	(iii)	$SnCl_2 + e \rightarrow Sn^+ + 2Cl + 2e$	15.8 ± 1.0	15.4
		(iv)	$SnCl_2 + e \rightarrow Sn^+ + Cl_2 + 2e$	12.8 ± 1.0	12.9
		(v)	$SnCl_2 + e \rightarrow Sn^+ + Cl^- + Cl + e$	—	11.8
$SnCl_4^+$	$SnCl_4$	(vi)	$SnCl_4 + e \rightarrow SnCl_4^+ + 2e$	[b]11.5 ± 0.4	
$SnCl_3^+$	$SnCl_4$	(vii)	$SnCl_4 + e \rightarrow SnCl_3^+ + Cl + 2e$	[b]12.2 ± 0.4	
$SnCl_2^+$	$SnCl_4$	(viii)	$SnCl_4 + e \rightarrow SnCl_2^+ + 2Cl + 2e$	16.0 ± 1.0	15.5
		(ix)	$SnCl_4 + e \rightarrow SnCl_2^+ + Cl_2 + 2e$	13.6 ± 1.0	13.0
		(x)	$SnCl_4 + e \rightarrow SnCl_2^+ + Cl^- + Cl + e$	—	11.9
$SnCl^+$	$SnCl_4$	(xi)	$SnCl_4 + e \rightarrow SnCl^+ + 3Cl + 2e$	17.7 ± 1.0	16.6
		(xii)	$SnCl_4 + e \rightarrow SnCl^+ + Cl_2 + Cl + 2e$	14.4 ± 1.0	14.1
		(xiii)	$SnCl_4 + e \rightarrow SnCl^+ + Cl^- + 2Cl + e$	12.5 ± 1.0	13.0
		(xiv)	$SnCl_4 + e \rightarrow SnCl^+ + Cl^- + Cl_2 + e$	—	10.5
Sn^+	$SnCl_4$	(xv)	$SnCl_4 + e \rightarrow Sn^+ + 4Cl + 2e$	22.2 ± 1.0	20.7
		(xvi)	$SnCl_4 + e \rightarrow Sn^+ + Cl_2 + 2Cl + 2e$	?	18.2
		(xvii)	$SnCl_4 + e \rightarrow Sn^+ + Cl^- + 3Cl + e$	?	17.1
		(xviii)	$SnCl_4 + e \rightarrow Sn^+ + 2Cl_2 + 2e$	?	15.7
		(xix)	$SnCl_4 + e \rightarrow Sn^+ + Cl^- + Cl_2 + Cl + e$	?	14.6

[a] Using values I.P.(Sn) = 7.3 eV[4], E.A. (Cl) = 3.6 eV[5], $D(Cl_2)$ = 2.5 eV[6], D(Sn–Cl) = 3.6 eV[7], 3.2 eV[6], D^0 ($SnCl_4$) = 13.4 eV[8], D^0 ($SnCl_2$) = 8.1 eV[8] and the experimental measurements of reactions (i) and (ii). [b] Semilog treatment.

enable a reasonable assignment to be made of the reactions producing the ions. In all calculations it is assumed that the ions are produced in their ground states with no kinetic energy.

$SnCl^+$ ($SnCl_2$). From A.P.[$SnCl^+$ ($SnCl_2$)], I.P. (SnCl) can be calculated since I.P.(SnCl) ⩽ A.P.-[$SnCl^+$ ($SnCl_2$)] − D(Cl–SnCl) and D(Cl–SnCl) = D°($SnCl_2$) − D(SnCl) = 8.1 − 3.6 = 4.5 or 8.1 − 3.2 = 4.9 according as Herzberg's[7] or Gaydon's[6] value is taken for D(Sn–Cl). Hence I.P.(SnCl) ⩽ 6.8 or 6.4 ±0.6. Since individual points in the I.E. curve were measured at 0.2-V intervals and the D(Sn–Cl) value is not very accurate it is felt that the error limit chosen is more realistic than the ±0.1 claimed by Hastie, *et al.*,[9] for their results on this apparatus.

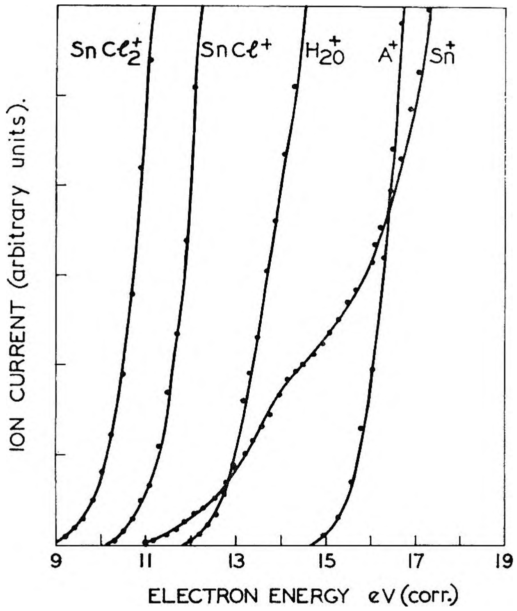

Figure 1. Ionization efficiency curves for $SnCl_2$.

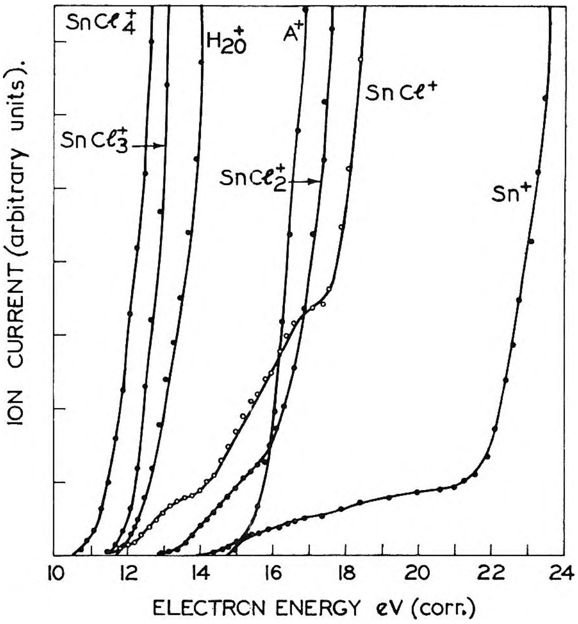

Figure 2. Ionization efficiency curves for $SnCl_4$.

Sn^+ ($SnCl_2$). For this ion the main process is clearly reaction iii but at least one lower energy process is also occurring, the possibilities being reactions iv and v, iv being indicated as the most likely. This is

---

(9) J. W. Hastie, H. Bloom and J. D. Morrison, *J. Chem. Phys.*, **47**, 1580 (1967).

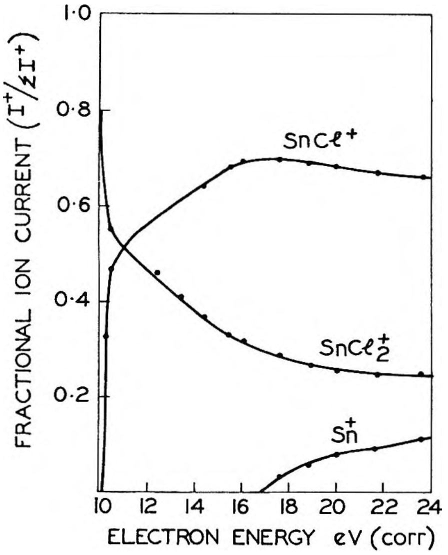

Figure 3. Fragmentation pattern for $SnCl_2$.

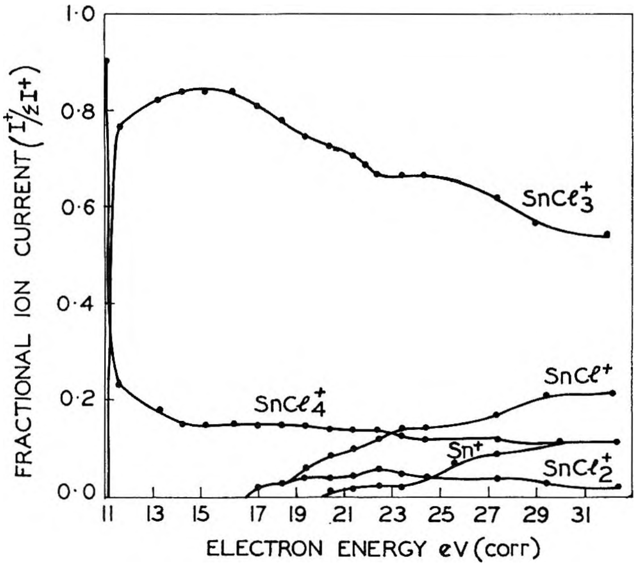

Figure 4. Fragmentation pattern for $SnCl_4$.

contrasted to the case of $PbCl_2$,[9] where the lower energy process is seen to be the ion-pair production, the process involving the production of Cl_2 being either absent or masked.

$SnCl_3^+$ ($SnCl_4$). For reaction vii I.P.($SnCl_3$) is given by A.P.[$SnCl_3^+$ ($SnCl_4$)] − $D(Cl_3Sn\text{–}Cl)$. The bond dissociation energy is not known, but a rough estimate can be taken as equal to $^1/_2[D°(SnCl_4) - D°(SnCl_2)]$, *i.e.*, 2.7 eV. Hence, I.P.($SnCl_3$) $\leqslant 12.2 - 2.7 = 9.5$ eV.

$SnCl_2^+$ ($SnCl_4$). The value of this A.P. is equal to I.P.($SnCl_2$) + $D(Cl_2 - SnCl_2)$. The latter term is known accurately, *i.e.*, $D°(SnCl_4) - D°(SnCl_2) = 5.3$ eV and the value of I.P.($SnCl_2$), measured above from this work, gives a calculated A.P.[$SnCl_2^+$ ($SnCl_4$)] = 15.5 eV indicating that reaction viii is the major process producing this ion. The I.E. curve indicates a lower energy process also; this is seen as reaction ix.

$SnCl^+$ ($SnCl_4$). The I.E. curve indicates two lower energy processes as well as the major one. The latter is seen as reaction xi, A.P.[$SnCl^+$ ($SnCl_4$)] = I.P.(SnCl) + $D°(SnCl_4) - D(SnCl) = 16.6$ eV. As the onset is somewhat higher than this value, the process may require some excess energy. The lower energy processes are predicted to be xii and xiii.

Sn^+ ($SnCl_4$). For Sn^+($SnCl_4$), as with $SnCl_2^+$-($SnCl_4$) and $SnCl^+$($SnCl_4$), the I.E. curve indicates the presence of lower energy processes but these are indefinite. The reason for this may well be twofold, *viz* small dissociative ionization cross-sections and overlapping of possible processes. The major process, postulated as reaction xv, A.P.[Sn^+ ($SnCl_4$)] = $D°(SnCl_4)$ + I.P.(Sn) = 20.7 eV, has its onset at some 1–1.5 eV higher than this, hence there exists the possibility that this process also requires some excess energy.

The fragmentation patterns of $SnCl_4$ and $SnCl_2$ are shown in Figures 3 and 4. As is the case with a number of analogous systems,[9–11] the processes ii and vii have the greatest ionization cross-sections for most of the electron energy range. It is interesting to note that once sufficiently high electron energies are reached, processes involving production of species with odd numbers of electrons are more favored, similar to the case in hydrocarbon systems.

Conclusions

The I.P. value determined here for the radical SnCl may give some insight as to its structure. The I.P. of around 6.8 eV is very close to the energy required to remove the first 5p electron from Sn itself (7.3 eV). This suggests that the Sn–Cl bond is essentially covalent, the electron being removed from a relatively unperturbed atomic p orbital on the Sn atom.

No doubt the bond would exhibit some ionic character due to the electronegativity differences between the atoms. Pauling[12] gives a correlation between ionic character and electronegativity difference which indicates that the Sn–Cl bond would have *ca.* 0.3 ionic character whereas a later study of Dailey and Townes,[13] based on quadrupole coupling data and the electronegativities of Huggins[14] gives the bond *ca.* 0.55 ionic character. Similar values apply for the diatomic PbCl.

Any prediction as to the extent to which this polarity may effect the energy of the lone electron on the tin would be nothing more than speculation.

(10) D. B. Chambers, F. Glocking, and M. Weston, *J. Chem. Soc.*, A, 1759 (1967).

(11) R. H. Vought, *Phys. Rev.*, 71, 93 (1947).

(12) L. Pauling, "Nature of the Chemical Bond," Cornell University Press, Ithaca, N. Y., 1940, p 70.

(13) B. P. Dailey and C. H. Townes, *J. Chem. Phys.*, 23, 118 (1955).

(14) M. L. Huggins, *J. Amer. Chem. Soc.*, 75, 4123 (1953).

If the molecule was in the ionic state Sn^+Cl^-, the energy required to remove the electron from essentially Sn^+, would be expected to be closer to the second I.P. of Sn, namely 14.6 eV, even allowing for an offsetting effect of the positive charge on the Sn by the negative charge on the Cl.

Hastie, *et al.*'s,[9] opinion that PbCl is ionic, based on similar I.P. arguments, is, in our view, debatable.

This work tends to favor the value of 3.6 eV for D(Sn–Cl) though a recent paper[15] favors that of 3.2 eV.

Acknowledgments. The authors wish to thank Dr. A. J. C. Nicholson and Dr. C. G. Barraclough for their many helpful discussions. Two of us, (A. S. B. & D. J. K.), would also like to thank Dr. A. L. G. Rees for the hospitality extended in the laboratories of the Division of Chemical Physics, C.S.I.R.O.

(15) Yu. Ya. Kuryakov, *Vestn. Mosk. Univ. Khim.*, **23**(3), 21 (1968).

Deuterium Sulfide as an Electron Scavenger in the Radiolysis of Liquid Saturated Hydrocarbons

by P. T. Holland and J. A. Stone

Chemistry Department, Queen's University, Kingston, Ontario, Canada

(Received April 21, 1969)

The use of deuterium sulfide as a radical and ion scavenger in the radiolysis of organic liquids has been advocated by Henglein.[1,2] Ausloos[3,4] has used hydrogen sulfide as a free radical scavenger in gas phase radiolysis and photolysis of hydrocarbons. Bone and Futrell[5] observed both proton transfer and charge transfer from propane ions to hydrogen sulfide in the ion source of a mass spectrometer. We have studied the radiolysis of saturated hydrocarbons in the liquid phase with varying concentrations of D_2S as solute and find that it is also an electron scavenger.

Von Meissner and Henglein[1] suggest that D_2S reacts by both H atom scavenging and charge transfer in liquids of low dielectric constant

$$H\cdot + D_2S \longrightarrow HD + DS\cdot \quad (1)$$

$$RH^+ + D_2S \longrightarrow RH + D_2S^+ \quad (2)$$

$$D_2S^+ + e \longrightarrow D_2 + S \quad (3)$$

In support of reaction 3 they find that the D_2 yield is reduced to a very low value by N_2O whereas the HD yield is relatively unchanged. In a single series of experiments it should therefore be possible to obtain the yields of both H atoms and positive ions. Our HD and D_2 yields from D_2S in n-hexane agree with those reported by von Meissner and Henglein.[1] However, we obtain similar HD and D_2 yields from D_2S in cyclohexane, the gas phase ionization potential of which is about 0.5 eV less than that of H_2S.[6] In solid cyclohexane at 77°K, $G(D_2)$ is the same as in the liquid at 298°K, although G(HD) is lower. For example, $G(D_2)$ is 1.0 for 1 mol % of D_2S, a yield much higher than those usually associated with charge transfer processes occurring in the solid phase[7] but one more consistent with electron scavenging.[8] The usual diagnostic test for electron scavenging, which we have applied, is the reduction of $G(N_2)$ obtained when solutions containing N_2O are irradiated with a second solute.[9]

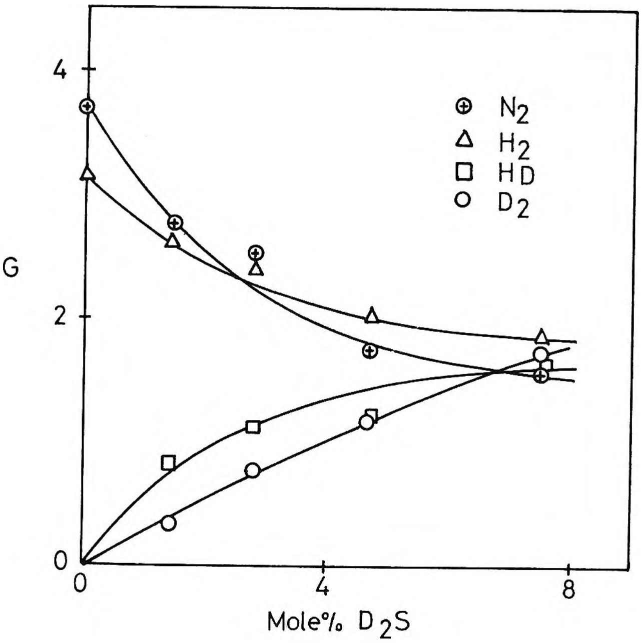

Figure 1. The yields of gaseous products from the radiolysis of liquid n-hexane containing N_2O (0.44 mol %) and D_2S at 298°K.

Liquid n-hexane containing 0.44 mol % N_2O was irradiated at 298°K with ^{60}Co γ rays at a dose rate of 6.2×10^{17} eV/ml min to a total dose of 9.5×10^{18} eV/ml. The gaseous volume in the Pyrex sample tube was less than 5% of the liquid volume. The yields of D_2, HD, H_2, and N_2 obtained with various D_2S concentrations are presented in Figure 1.

(1) Von G. Meissner and A. Henglein, *Ber. Bunsenges. Phys. Chem.*, **69**, 264 (1965).

(2) J. Pukies, A. Henglein, and G. Meissner, *Z. Phys. Chem.*, **57**, 177 (1968).

(3) P. Ausloos and S. G. Lias, *J. Chem. Phys.*, **44**, 521 (1966).

(4) R. Gordon, Jr. and P. Ausloos, *ibid.*, **46**, 4823 (1967).

(5) L. I. Bone and J. H. Futrell, *ibid.*, **47**, 4366 (1967).

(6) K. Watanabe, T. Nakayama, and J. Mottl, U. S. Department of Commerce Office Technical Service Report, **158**, 319, 1959.

(7) J. A. Stone, *Can. J. Chem.*, **46**, 3531 (1968).

(8) N. H. Sagert, *ibid.*, **46**, 89 (1968).

(9) W. V. Sherman, *J. Chem. Soc.*, 599 (1966).

N_2O scavenges electrons to yield N_2 and O^-[10]

$$e + N_2O \longrightarrow N_2O^- \longrightarrow N_2 + O^- \qquad (4)$$

$G(N_2)$ is reduced with increasing D_2S concentration but at the same time $G(H_2 + HD + D_2 + N_2)$ remains constant. A reaction of an electron with D_2S yielding D_2 and HD must be superceding a similar one with N_2O. The results of Sagert and Blair[11] show that at the N_2O concentration we employ, almost all the N_2 arises from reaction 4 and very little, if any, from the secondary reaction

$$O^- + N_2O \longrightarrow N_2 + O_2^- \qquad (5)$$

which increases $G(N_2)$ in gas phase radiolysis of saturated hydrocarbons by 55% above G(electrons).[12] It is to be noted that at 3 mol % D_2S, $G(N_2)$ is less than one half its value in the absence of D_2S. A Stern–Volmer type plot using the N_2 yields shown in the figure gives $k_{e+N_2O}/k_{e+D_2S} = 6$. The same value is obtained with cyclohexane as solvent.

A possible mechanism for the production of D_2 *via* electron capture is that given by von Meissner and Henglein[1] as the mechanism operating in irradiated aqueous D_2S solutions

$$\begin{tikzcd} & & D_2 + S^- \\ D_2S + e \arrow[r] & D_2S^- \arrow[ur] \arrow[dr] & \\ & & D + HS^- \end{tikzcd}$$

The D atom will be scavenged by D_2S to give D_2.

Von Meissner and Henglein[1] rejected the idea of electron capture by D_2S in saturated hydrocarbon solvents with low dielectric constants since the effects of solvation are not great enough to overcome the activation energy of 1.56 eV observed for the formation of SH^- in the gas phase.[13] If this argument holds, then the extrapolation of the appearance potential of negative species from gas to liquid phase is not valid for the system under discussion.

Electron capture by D_2S explains two inconsistencies found in the radiolysis of this solute in cyclohexane and *n*-hexane. (a) Whereas the addition of the efficient proton acceptors ethanol-*d* and ammonia-d_3 to liquid cyclohexane does not lead to any increase in the total hydrogen yield[14,15], the addition of D_2S causes an increase which at 5 mol % is ~1 G unit. This increase can now be attributed to the reactions of D_2S with electrons which do not normally participate in hydrogen production. Such increased yields are found with HI[16] and HCl[17] as electron scavengers. (b) Freeman[18] has made theoretical calculations of positive ion scavenging in liquid hydrocarbons. He finds that agreement between theory and experiment can be obtained for the D_2S–*n*-hexane system only if a reduced mobility is assumed for the negative entity. We have found that with the same basic theory the D_2 yields can be accounted for by an inefficient electron scavenging mechanism without any positive charge transfer.

Although we have shown that electron capture by D_2S occurs we cannot say whether positive charge scavenging occurs at the same time. The results of Bone and Futrell[5] suggest that both charge exchange and proton transfer might occur. However a limiting $G(D_2)$ of ~3 at high D_2S concentration as found by von Meissner and Henglein[1] is consistent with electron scavenging being the sole process for the production of D_2.

Acknowledgment. This work was supported by the National Research Council of Canada and Atomic Energy of Canada Ltd, Commercial Products.

---

[10] G. R. A. Johnson and J. M. Warman, *Trans. Faraday Soc.*, **61**, 1709 (1965).

[11] N. H. Sagert and A. S. Blair, *Can. J. Chem.*, **45**, 1351 (1967).

[12] J. M. Warman, *J. Phys. Chem.*, **71**, 4066 (1967).

[13] K. Jäger and A. Henglein, *Z. Naturforsch.*, **21a**, 1251 (1966).

[14] F. Williams, *J. Amer. Chem. Soc.*, **86**, 3954 (1964).

[15] J. W. Buchanan and F. Williams, *J. Chem. Phys.*, **44**, 4377 (1966).

[16] J. R. Nash and W. H. Hamill, *J. Phys. Chem.*, **66**, 1097 (1962).

[17] P. J. Dyne, *Can. J. Chem.*, **43**, 1080 (1965).

[18] G. R. Freeman, *J. Chem. Phys.*, **46**, 2822 (1967).

Field Independence of Photoinjection into Hydrocarbon Solution

by A. Prock and M. Djibelian

Department of Chemistry, Boston University, Boston, Massachusetts 02215 *(Received April 31, 1969)*

Photoinjection from rhodium electrode into hydrocarbon solutions has been reported previously,[1] where a simple thermodynamic analysis based on energy requirements led to an estimate of solvation energies of anionic species. Objections were later raised in private communication that the effect of the large applied electric field was not taken into account. That is, under high enough electric field strength there would be sufficient potential drop across the Helmholtz double layer for a nonnegligible amount of energy to be coupled into the electrode reaction. The solvation energy calculated without accounting for this energy would be too high. The question is, are we missing an energy term under the conditions of the experiment?

This note describes experiments on one of our previous systems which carries photoinjection measurements down to 1% of the original applied voltage, or

---

[1] A. Prock, M. Djibelian, and S. Sullivan, *J. Phys. Chem.*, **71**, 3378 (1967).

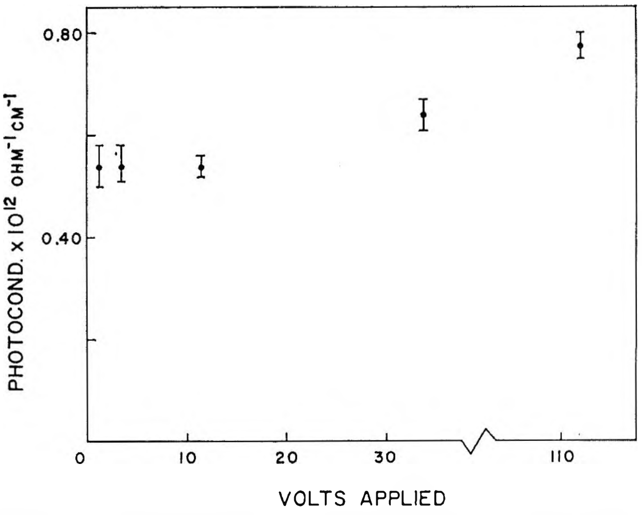

Figure 1. Apparent photoconductivity ($\Delta I_{ph}/V_{app}$) *vs.* applied voltage for 0.10 *M* anthracene in benzene under white light. A 200-W super pressure mercury lamp plus water and saturated $NaNO_2$ filter supplies light of λ > 404 nm.

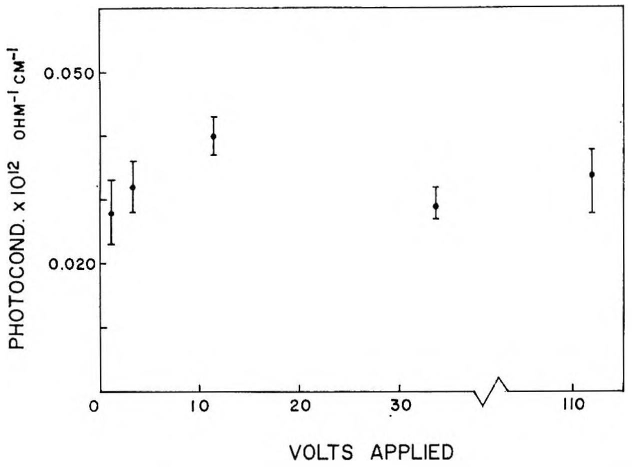

Figure 2. Apparent photoconductivity ($\Delta I_{ph}/V_{app}$) *vs.* applied voltage under same conditions as in Figure 1, with the addition of a Schott 546 nm filter with HBW of 27 nm to produce incident green light.

about 4% of the original applied field strength. The system studied was anthracene in benzene, the system which is best from the aspect of showing very low photocurrent for reversed polarity, *i.e.*, the rhodium electrode positive. The system has been described previously; the electrode spacing was reduced to 0.010 cm, and applied voltage was in the range 1.14–112 V. White light (λ > 404 nm) and green light (λ = 546 nm, HW = 27 nm) was obtained using a 250-W super pressure mercury lamp with filters, and red light (λ = 660 nm, HW = 60 nm) was supplied by a 450-W xenon lamp, with filters. Figures 1 and 2 present data of apparent conductivity change (photoconductivity) as a function of applied voltage for the white light and for the green light. It appears that the photoinjection effect shows no tendency to vanish as the applied voltage decreases towards zero. The graph for red light is not presented but shows similar behavior. The original conclusion concerning this work, which ignored the effect of the electric field, is strongly supported by this result.

The lowest applied voltage used in these experiments is judged to be low enough to make negligible the electric field contribution to the energetics of the reaction on the following basis. A simple calculation given below shows that even for 10 V applied, the diffuse double layer thickness is around 2500 Å. Taking the Helmholtz double layer to be around 5 Å, we find that of the 5 V applied between bulk solution and an electrode, then at most only the fraction, 5/2500 of the voltage, or 10 mV, appears across the Helmholtz double layer to aid energetically in the transfer of charge. For such low conductivity media, applied voltages of even tens of volts would not be very effective in energy transfer at the electrode, but since the amount of energy coupled rises with the square of applied voltage, then at some hundreds of volts applied the field should supply considerable energy to the discharge process.

The calculation of double-layer thickness under applied field is based on the differential equation of forced diffusion.[2,3] We retain all terms in the equation, and assume further that in the dark the positive current equals the negative current. This is reasonable since it is almost certain that the dark current is caused by traces of impurity. The usual definitions are D, diffusion coefficient; n_+, n_-, ionic concentrations, dark; μ, mobility, assumed the same for both ions; and φ, potential. The forced diffusion equations are for the one-dimensional problem

$$J_+ = -De\frac{dn_+}{dx} - \mu e\frac{d\varphi}{dx}n_+ \tag{1}$$

$$J_- = De\frac{dn_-}{dx} - \mu e\frac{d\varphi}{dx}n_- \tag{2}$$

For steady state the divergence of the sum vanishes. Along with the relation $D/\mu = kT/e$, the result is

$$\text{div } J_T = 0 = -De\frac{d^2}{dx^2}(n_+ + n_-) - \frac{De^2}{kT}\frac{d^2\varphi}{dx^2}(n_+ + n_-) - \frac{De^2}{kT}\frac{d\varphi}{dx}\frac{d}{dx}(n_+ + n_-) \tag{3}$$

Equations 1 and 2 are subtracted and the result set equal to zero to obtain an evaluation of the third term in eq 3. This latter equation can then be put into the form

$$\frac{d^2q}{dx^2} + \frac{q}{\lambda^2} = 0, \text{ where } \lambda = \frac{\lambda_0}{\left[1 + \left(\lambda_0\frac{e}{kT}\frac{d\varphi}{dx}\right)^2\right]^{1/2}} \tag{4}$$

---

(2) A. Prock and G. McConkey, "Topics in Chemical Physics," Elsevier, Amsterdam, 1962, p 242.

(3) J. Gavis, *J. Chem. Phys.*, 41, 3787 (1964).

Charge density, q, is $e(n_+ - n_-)$. The length, λ_0, is the double layer thickness under no externally applied field.

$$\lambda_0^{-2} = \frac{4\pi e^2}{\epsilon kT}(n_+ + n_-) \cong \frac{8\pi e^2 n^0_\pm}{\epsilon kT}$$

In our system, where conductivity is so low ($<10^{-14}$ ohm^{-1} cm^{-1}) it is estimated that this length is in excess of 0.01 cm.[4] The correction to λ_0 is a function of position, strictly speaking, but we take the field strength $d\varphi/dx$, to be virtually constant. This is based on observed Ohm's law dependence of benzene solutions of some ionic species.[3,5] For the cell geometry described, it turns out that the last term in the denominator far exceeds unity for even 1 V applied so that the formula becomes

$$\lambda = \frac{1}{40E_0}$$

where E_0, the applied field strength, is expressed in practical units of V/cm. The double layer thickness in the presence of a field is seen to be dependent only on the field strength.

Acknowledgment. The authors wish to express their thanks to Professor M. Szwarc, Director of the Polymer Research Center at Syracuse University, for kindly pointing out the necessity for performing this work. The work of M. D. was supported by the National Science Foundation, Grant GP 7094.

---

[4] A. Prock, *Rev. Sci. Instrum.*, **36**, 949 (1965).

[5] W. A. LaVallee, Thesis, Chemistry Department, Boston University, unpublished results.

Substituent Effects on the Nuclear Magnetic Resonance Spectra of Ethyl Acetates

by Lana S. Rattet and J. H. Goldstein

Department of Chemistry, Emory University, Atlanta, Georgia 30322

(Received May 7, 1969)

Nuclear magnetic resonance (nmr) techniques have been successfully applied in the study of nonequivalence between the methylene protons in acetal and substituted acetals ($Z-CH(OCH_2-CH_3)_2$, Z = CH_3, CH_2Cl, CH_2Br, $CHCl_2$, $CHBr_2$, and CCl_3).[1] In particular, changes in the differences of the methylene chemical shifts and $^{13}C-H$ coupling parameters have made it possible to relate quantitatively such nonequivalence to the group electronegativity of the substituent Z. Moreover, the results indicate that, in all likelihood, substituent effects of this type are transmitted along the bond system. The previous techniques and approaches have now been applied to the equivalent methylene protons of a series of ethyl esters of substituted acetic acids (I), leading to results similar to those previously obtained.

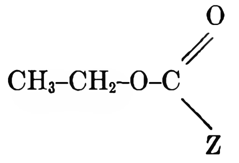

(I)

Z = CWXY where W, X, Y = H_X, Cl or Br

Sample preparation, nmr analysis and computational phases are identical to those of the earlier study. However, in order to establish the quality of the work involved, we may note that root-mean-square deviations between theoretical and experimental frequencies averaged to 0.045 Hz for the proton patterns and ~0.05 Hz for the satellite patterns, employing the parameters given in Table I. In all compounds studied, both upfield and downfield methylene $^{13}C-H$ satellite patterns were obtained, with resulting ^{13}C isotope shifts of the order of 0.1–0.2 Hz. The estimated probable errors in the vicinal couplings are +0.03 Hz, and in the remainder of the parameters are ±0.05 Hz.

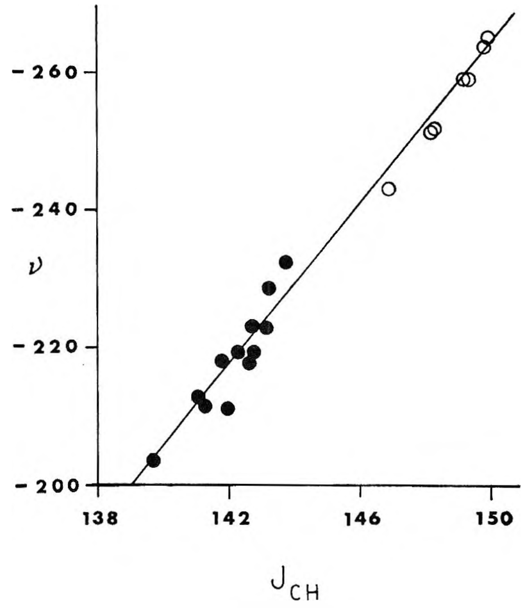

Figure 1. Chemical shift *vs.* $^{13}C-H$ couplings of the ethoxy methylene protons of six acetals (closed circles) and seven ethyl acetates (open circles). Both parameters are in Hz. Shifts are relative to internal TMS at 60 MHz.

The results of this work tend to substantiate the conclusions drawn in our earlier study. For example, examination of Table I reveals a marked dependence

---

[1] L. S. Rattet and J. H. Goldstein, "Organic Magnetic Resonance," to be published.

[2] H. E. Huheey, *J. Org. Chem.*, **31**, 2365 (1966).

Table I: Parameters of Ethyl Acetate and Ethyl Haloacetates[a]

Z^b	ν_{CH_3}	ν_{CH_2}	J_{vic}	$J(CH_A)$	ν_{H_X}	a'^c
CH_3	−242.83	−71.78	7.13	146.84	−116.44	7.50
CH_2Br	−251.16	−76.04	7.11	148.12	−232.19	8.38
CH_2Cl	−251.62	−75.93	7.09	148.18	−244.03	8.38
$CHBr_2$	−258.69	−80.35	7.10	149.11	−356.48	9.12
$CHCl_2$	−258.93	−80.04	7.12	149.24	−363.91	9.20
CCl_3	−264.89	−83.95	7.11	149.85		9.96

[a] All values are in Hz. Chemical shifts are relative to internal TMS at 60 MHz. [b] Nomenclature used is shown in structure (I). [c] Values from Ref. 2 or calculated using the equations therein.

of four spectral parameters upon the degree of halogen substitution in group Z. As this behavior is similar to that of the acetals, we have used the same approaches as employed in that study.

Table II shows the results of correlations attempted with Huheey's group electronegativity parameter, a'.[2] We observe that the slopes (N) of the regression equations on the respective acetals, given in the last column, are in good agreement with those of the acetates. Furthermore, the parallel behavior of the methylenic ^{13}C–H couplings and chemical shifts with respect to a', is analogous to that found in the acetals. This linearity with a' also appears with the methyl and H_X shift values.

It has been previously demonstrated that, in the absence of appreciable anisotropy effects, a linear relation between the chemical shift of a proton and the corresponding bonded ^{13}C–H coupling exists.[3–5] Figure 1 shows that such a relation also exists for the acetals and the acetates. From this it appears that the carbonyl group in the acetates enhances the effect of the electron-withdrawing group, Z, on the shifts and ^{13}C–H couplings.

Structural studies of simple esters indicate a preferred conformation of this class of compounds, as shown in (II)[6]. This conformation would tend to minimize any direct field interactions from the group Z.

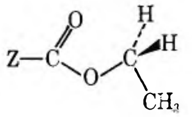

II

Table II: Statistical Parameters for Empirical Correlation

$Y = M_k + N_k a'$

	Acetates			
Y	M	N	Correlation coefficient	Acetals[a] N
$J(CH_2)$	137.7	1.243	0.991	1.226[b]
ν_{H_X}	996.3	−147.8	0.998	−156.6
ν_{CH_2}	−175.3	−9.067	0.998	−8.865[b]
ν_{CH_3}	−34.10	−5.015	0.998	−3.564

[a] Values from ref 1. [b] Average of the two methylene values.

Therefore, the observations made in this study support the conclusion that, insofar as nmr parameters can be employed to measure such effects, transmission of inductive effects from Z occurs primarily through a polarization of electrons through five bonds.

As was also true in the case of the acetals,[1,7] J_{vic} is essentially constant (*i.e.*, 7.11 ± 0.02 Hz) throughout the series. Thus, either the substituent effect on this parameter is negligible or is being cancelled out by some unknown effect.

(3) J. H. Goldstein and G. S. Reddy, *J. Chem. Phys.*, **36**, 2644 (1962).

(4) G. S. Reddy and J. H. Goldstein, *ibid.*, **38**, 2736 (1963).

(5) G. S. Reddy and J. H. Goldstein, *ibid.*, **39**, 3509 (1963).

(6) G. J. Karabatsos, N. Hsi, and C. E. Orzech, *Tetrahedron Lett.*, **1966**, 4639.

(7) L. S. Rattet, A. D. Williamson, and J. H. Goldstein, *J. Mol. Spectrosc.*, **26**, 281 (1968); *J. Phys. Chem.*, **72**, 2954 (1968).

Comparison of Methylene Radical Insertion Reactions with the Si–H Bonds of Methylsilane, Dimethylsilane, and Trimethylsilane[1a]

by W. L. Hase,[1b] W. G. Brieland,[1c] and J. W. Simons

Chemistry Department, New Mexico State University,
Las Cruces, New Mexico 88001 (*Received May 14, 1969*)

It has been shown that singlet methylene radicals, formed from the photolysis of diazomethane (DM) at 3660 Å, insert into the Si–H bonds 8.9 times faster than into the C–H bonds of methylsilane.[2] Previous studies have revealed that singlet methylene radicals insert almost statistically into the various types of C–H bonds of the alkanes with a slight selectivity for the C–H

---

(1) (a) The National Science Foundation is gratefully acknowledged for financial support; (b) NDEA Predoctoral Fellow; (c) NSF Undergraduate Research participant during the summer of 1968.

(2) C. J. Mazac and J. W. Simons, *J. Amer. Chem. Soc.*, **90**, 2484 (1968).

bonds on the more highly substituted carbon.[3–7] Thus, we report a gas-phase study of the reaction of singlet methylene radicals with dimethylsilane and trimethylsilane in order to determine the effect on the Si–H insertion of increasing methyl substitution on silicon, and varying the energy of the methylene radical. In order to study only singlet methylene radical insertion reactions, oxygen was added as a radical scavenger. Oxygen scavenges ground triplet state methylene radicals[8] as well as any other triplet or doublet radicals which are formed in the system.[9–15]

The reaction mixtures were photolyzed in seasoned Pyrex vessels for 2 hr at the highest pressure and up to 20 hr for the lowest pressures. The analyses of the products were done by gas–liquid phase chromatography. The analytical column used consisted of 25 ft of 30% dibutylphthalate on chromosorb and 4 ft of didecylphthalate on chromosorb. Calibration mixtures similar to the reaction mixtures were used to calibrate the column for the measured products.

Table I:[a] Insertion Product Ratios from the 3660-Å Photolyses of Diazomethane–Dimethylsilane Mixtures

P_{DMS}	$P_{CH_2N_2}$	%O_2	TMS/MES
74.44	14.88	27	2.48
20.30	1.88	10	2.27
14.34	1.88	31	2.36
8.49	0.99	11	2.02
8.20	1.44	12	2.26
6.90	1.06	29	2.32
3.79	0.52	11	2.34
3.63	0.52	11	2.27
2.91	0.58	27	2.39

[a] All pressures are in centimeters.

Table II:[a] Insertion Product Ratios from the 3660-Å Photolyses of Diazomethane–Trimethylsilane Mixtures

P_{TMS}	$P_{Neopentane}$	P_{Butane}	$P_{CH_2N_2}$	%O_2	TEMS/ EDMS
0.273	0.168	...	0.098	16	0.81
0.053	...	0.069	0.024	17	0.75
0.051	...	0.065	0.019	16	0.79
0.048	...	0.061	0.014	28	0.78
0.051	0.043	...	0.029	22	0.79
0.049	...	0.051	0.019	17	0.80
0.030	...	0.029	0.012	16	0.89
0.054	...	...	0.012	14	0.81
0.022	...	0.017	0.005	12	0.80
0.014	0.014	...	0.009	17	0.79
0.010	0.010	...	0.008	24	0.82
0.010	0.010	...	0.003	12	0.81
0.018	...	...	0.004	16	0.80
0.014	...	...	0.002	11	0.79

[a] All pressures are in centimeters.

Table III:[a] Insertion Product Ratios from the 4358-Å Photolyses of Diazomethane–Trimethylsilane Mixtures

P_{TMS}	$P_{CH_2N_2}$	%O_2	TEMS/ EDMS
4.10	0.622	14	0.81
0.218	0.036	18	0.81
0.148	0.036	20	0.76
0.147	0.018	12	0.79
0.068	0.009	10	0.78
0.025	0.003	12	0.80
0.019	0.002	12	0.78
0.012	0.002	12	0.78

[a] All pressures are in centimeters.

Experiments were done to test for a possible dark reaction between oxygen and the silanes. There were no products of interest observed in the dark reactions.

Dimethylsilane System. The results for the dimethylsilane/diazomethane photolyses at 3660 Å in the presence of oxygen are given in Table I. It is seen that the trimethylsilane to methylethylsilane ratio (TMS/MES), which represents the total Si–H to C–H insertion ratio, is invariant over the pressure range studied. The average of the TMS/MES ratios in Table I is 2.3 ± 0.1, which yields a per-bond ratio of Si–H to C–H insertion of 6.9 ± 0.3.

Trimethylsilane System. The tetramethylsilane to ethyldimethylsilane ratios (TEMS/EDMS) obtained from photolyses of trimethylsilane–diazomethane mixtures at 3660 Å in the presence of oxygen and added neopentane or butane are given in Table II. An important observation is that the TEMS/EDMS ratio is constant, 0.80 ± 0.01, independent of the identity and proportions of the gas mixture, total pressure, and of

---

(3) G. Z. Whitten and B. S. Rabinovitch, *J. Phys. Chem.*, **69**, 4348 (1965).

(4) R. W. Carr, Jr., *ibid.*, **70**, 1970 (1966).

(5) M. L. Halbertstadt and J. R. McNesby, *J. Amer. Chem. Soc.*, **89**, 3417 (1967).

(6) B. M. Herzog and R. W. Carr, Jr., *J. Phys. Chem.*, **71**, 2688 (1967).

(7) J. W. Simons, C. J. Mazac, and G. W. Taylor, *ibid.*, **72**, 749 (1968).

(8) R. L. Russell and F. S. Rowland, *J. Amer. Chem. Soc.*, **90**, 1671 (1968).

(9) J. W. Simons and B. S. Rabinovitch, *J. Phys. Chem.*, **68**, 1322 (1964).

(10) F. H. Dorer and B. S. Rabinovitch, *ibid.*, **69**, 1952 (1965).

(11) S. Ho, I. Unger, and W. A. Noyes, Jr., *J. Amer. Chem. Soc.*, **87**, 2297 (1965).

(12) H. M. Frey, *Chem. Commun.*, 260 (1965).

(13) R. W. Carr, Jr., and G. B. Kistiakowsky, *J. Phys. Chem.*, **70**, 118 (1966).

(14) B. S. Rabinovitch, K. W. Watkin, and D. F. Ring, *J. Amer. Chem. Soc.*, **87**, 4960 (1965).

(15) R. F. W. Bader and J. I. Generosa, *Can. J. Chem.*, **43**, 1631 (1965).

amounts of added oxygen in the range of 10–30%. The Si–H to C–H per-bond insertion ratio is 7.2 ± 0.1. The results for the trimethylsilane–diazomethane photolyses at 4358 Å in the presence of oxygen are given in Table III. The TEMS/EDMS ratio is constant, 0.79 ± 0.01, independent of the total pressure and oxygen proportions. The corresponding Si–H to C–H bond insertion ratio is 7.1 ± 0.1. Thus, within experimental error, the relative rates of singlet methylene insertion into the Si–H and C–H bonds of dimethylsilane and trimethylsilane are the same and independent of wavelength. These values are about 25% lower than that found earlier[2] for the SiH/C–H insertion ratio for methylsilane.[2] It is possible that this rather small difference is due to systematic errors between the different studies.

Comparison of the Si–H to C–H bond insertion ratio for trimethylsilane at 3660 and 4358 Å, shows that there is no real difference in the selectivity of singlet methylene radicals from diazomethane photolyses at 3660 and 4358 Å toward the Si–H bond and C–H bonds of trimethylsilane. This invariance in selectivity is in agreement with the invariance in selectivity found toward the primary, secondary, and tertiary C–H bonds of the alkanes in this laboratory[7] and by Herzog and Carr.[6]

The higher reactivity of Si–H bonds toward singlet methylene radical insertion relative to C–H bonds is probably due to a combination of effects related to the larger Si–H bond length, opposite polarity of the Si–H bond, and slightly lower Si–H bond dissociation energy. Recent work on H atom abstraction from silanes by methyl radicals,[16] hot tritium atom reactions with silanes,[17] and electron impact appearance potential measurements on silanes[18] indicate that Si–H bond dissociation energies are in general only slightly lower than C–H bond dissociation energies and that these small differences lead to significant reaction kinetic effects.

In the alkane systems, C–H bonds to the more highly substituted carbon are slightly more reactive toward singlet methylene insertion, while in the various methyl silane systems the reactivities of the different Si–H bonds are nearly the same, with the Si–H bonds to the least substituted silicon atom appearing to be slightly more reactive. If it is assumed that the preexponential factors for insertion of methylene radicals into the Si–H bonds of methylsilane, dimethylsilane, and trimethylsilane are the same, (which may not be the case), and that activation energy differences are due to bond energy differences, one would conclude that the Si–H bond dissociation energies in dimethylsilane and trimethylsilane are nearly the same, while that in methylsilane is possibly slightly lower. Comparing this possible trend of Si–H bond dissociation energies, primary $\lesssim$ secondary $\sim$ tertiary, one could speculate that the amount of resonance stabilization of the dimethylsilyl and trimethylsilyl radicals is small compared to the resonance stabilization of the analogous isopropyl and *t*-butyl radicals.

[16] (a) J. A. Kerr, D. H. Slater, and J. C. Young, *J. Chem. Soc.* **A**, 134 (1967); (b) T. N. Bell and B. B. Johnson, *Aust. J. Chem.*, **20**, 1545 (1967); (c) O. P. Strausz, E. Jakubowski, H. S. Sandhu, and H. E. Gunning, private communication.

[17] F. S. Rowland, A. Hosaka, and T. Tominga, *J. Phys. Chem.*, **73**, 465 (1969).

[18] (a) S. J. Band, I. M. T. Davidson, and C. A. Lambert, *J. Chem. Soc.*, **A**, 2068 (1968), and references therein; (b) W. C. Steele, L. D. Nichols, and F. G. A. Stone, *J. Amer. Chem. Soc.*, **84**, 4441 (1962); (c) G. G. Hess, F. W. Lampe, and L. H. Sommer, *ibid.*, **87**, 5327 (1965).

Further Consideration of the Moving Boundary Experiment for the Measurement of Transference Numbers

by Richard J. Bearman[1]

Department of Physical and Inorganic Chemistry,
University of New England, Armidale, N.S.W., 2351, and
Research School of Physical Sciences, Australian National University,
Canberra, A.C.T. 2600, Australia

and L. A. Woolf

Research School of Physical Sciences, Australian National University,
Canberra, A.C.T. 2600, Australia (*Received June 9, 1969*)

In a significant paper, Milios and Newman[2] recently reformulated the theory of the moving boundary experiment. For the case where the density below the moving boundary varies linearly with solute concentration, they derived a "volume correction" by using a rigorous form for the regulating function in conjunction with general equations of mass balance.

For situations where partial molar volumes are spatially constant everywhere, Bearman[3] earlier derived the classical Lewis volume correction by observing that an average velocity, the *volume velocity*, must then also be uniform throughout the system.

In the present note we derive the Newman–Milios correction,[4] by applying Bearman's method to the case where partial molar volumes are necessarily constant only below the moving boundary. We then show that the methods of Milios and Newman and of Bearman are quite equivalent when applied to the systems considered in their respective papers.

---

[1] Correspondence should be addressed to Department of Chemsitry, University of Kansas, Lawrence, Kan. This research was supported in part by a grant from the Office of Saline Water of the U. S. Department of Interior to the University of Kansas. R. J. B. is also grateful to the ARGC for a travel grant which enabled his commutation between Armidale and Canberra.

[2] P. Milios and J. Newman, *J. Phys. Chem.*, **73**, 298 (1969).

[3] R. J. Bearman, *J. Chem. Phys.*, **36**, 2432 (1962).

[4] We interpret the acknowledgment given on p 44 of the reference given in footnote 8 to mean that the derivation reported in the reference of footnote 2 is due chiefly to Newman. We therefore choose to refer to the volume correction of the latter reference as the "Newman–Milios correction."

The Regulating Function

From eq M2, M3, M5, and M9,[5a] Milios and Newman derive the general form[5b] for the regulating function (eq M17). Since their starting equations are equivalent to eq B2.4c and B2.6 (including the ensuing discussions), and B3.4, the theory of Bearman leads rigorously to the identical result. The discrepancy between eq M17 and Bearman's equation for the regulating function, eq B5.3, is only superficial and disappears when it is noted that Bearman should have cancelled $\bar{v}_0/\bar{v}_0'$, the ratio of partial molar volumes of solvent above and below the boundary, which was unity, according to his assumption of constancy of partial molar volumes.

Evidently, the path of derivation followed by Milios and Newman is superior because it shows clearly that the regulating function is valid whether or not the partial molar volumes are constant.

Sufficient Conditions for the Lewis and Newman–Milios Corrections

Bearman obtained the Lewis correction for the solvent velocity by assuming constancy of partial molar volumes to extend from the bottom electrode through the moving boundary. In the next paragraph, we show that the Bearman method leads to the Newman–Milios correction, eq M28, under the weaker assumption that the partial molar volumes are spatially constant below the moving boundary.

For simplicity, the derivations of Milios and Newman and of Bearman each proceeded through consideration of specific systems, which, unfortunately, were different. However, when due allowance is made for the differences, eq M28 follows from eq B5.1 and the general form of the regulating function (*N.B.* $a = 1/\bar{v}_0'$ by eq 5 and 6 below). Since we have shown the method of derivation of the regulating function in the preceding section, all we have left to show is that eq B5.1 remains valid under the weaker assumption. But that is simple, for eq B5.1 follows from eq B4.1 through B 4.6 applied beneath the boundary, and these are valid in the present context: equations B4.1–B4.5 are thermodynamic and hydrodynamic identities, and eq B4.6 holds below the boundary because the partial molar volumes are assumed to be constant beneath it.

In other words, the condition of constancy of volume velocity below the boundary leads to the Newman–Milios correction whereas the condition of constancy of volume velocity throughout the system leads to the Lewis correction. The second condition is a special case of the first, so we deduce that the Newman–Milios correction reduces to the Lewis correction when the volume velocity is everywhere constant.[6]

Equivalence of the Approaches of Milios and Newman and of Bearman

The methods of both Milios and Newman and of Bearman lead to the Newman–Milios correction. Bearman makes the assumption that the partial molar volumes of both solvent and solute are spatially constant below the moving boundary, while Milios and Newman make the thermodynamic assumption that below the boundary

$$c_0 = a + bc_B \tag{1}$$

where c_0 is the concentration of solvent, c_B is the concentration of electrolyte, and a and b are constants. One may well ask why the two different assumptions lead to the same result.

The answer is that they are equivalent. Milios and Newman nearly state this (ref 2, p 302) when they point out that our eq 1 (their eq 23) implies that the partial molar volume of solvent is constant below the boundary. However, they do not state that the partial molar volume of solute must then also be constant. Moreover, they especially stress the usefulness of eq 1, which obscures its limitations to all but the most perceptive readers. Therefore, we now prove very explicitly that the only class of salt solutions satisfying both assumptions are those with thermodynamically constant partial molar volumes.

Into eq 1 we substitute the relations $c_0 = x_0/(x_0\bar{v}_0 + x_B\bar{v}_B)$ and $c_B = x_B/(x_0\bar{v}_0 + x_B\bar{v}_B)$, where x's are mole fractions and $\bar{v}$'s are partial molar volumes, and obtain

$$x_0 = a(x_0\bar{v}_0 + x_B\bar{v}_B) + bx_B \tag{2}$$

Twice differentiating eq 2 with respect to $x_B = 1 - x_0$ leads, at constant temperature and pressure, with the aid of the thermodynamic identity[7]

$$x_B\frac{\partial \bar{v}_B}{\partial x_B} = -x_0\frac{\partial \bar{v}_0}{\partial x_B} \tag{3}$$

to

$$\frac{\partial \bar{v}_B}{\partial x_B} = \frac{\partial \bar{v}_0}{\partial x_B} \tag{4}$$

For the simultaneous validity of eq 3 and 4 we must have

$$\frac{\partial \bar{v}_B}{\partial x_B} = \frac{\partial \bar{v}_0}{\partial x_B} = 0 \tag{5}$$

Hence $\bar{v}_B$ and $\bar{v}_0$ are thermodynamic constants.

---

(5) (a) We prefix equations from the paper of Milios and Newman with an "M" and equations from the paper of Bearman with a "B;" (b) advocated earlier by L. J. M. Smits and E. M. Duyvis, *J. Phys. Chem.*, **70**, 2747 (1966), and *ibid.*, **71**, 1168 (1967), and, still earlier, by G. S. Hartley, *Trans. Faraday Soc.*, **30**, 648 (1934).

(6) An alternative sufficient condition for the Lewis correction to be valid is for the partial molar volumes below the boundary to be constant, and, simultaneously, $\bar{v}_0 = \bar{v}_0'$, without the partial molar volumes being constant through the boundary. Hence, despite the implication of Bearman to the contrary, the constancy of partial molar volumes through the boundary is not a necessary condition for the validity of the Lewis correction.

(7) For example, derivable from R. J. Bearman and B. Chu, "Problems in Chemical Thermodynamics," Addison-Wesley Publishing Co., Reading, Mass., 1967, p 109, eq 4.29.

The thermodynamic constancy of the partial molar volumes below the boundary implies their spatial constancy, so that the Bearman method yields the Newman–Milios correction. At first sight it is conceivable that there may be spatial uniformity even though eq 1 is not obeyed. In that case, it would seem that the method of Bearman gives the Newman–Milios correction whereas the method of Milios and Newman is not applicable. However, as Milios pointed out in his thesis,[8] there inevitably will be concentration gradients in the neighborhood of the electrode; and these are sufficient to also destroy the applicability of the Bearman theory unless the partial molar volumes are constant wherever there are concentration gradients below the moving boundary.

Thus far, we have shown that equivalent assumptions are used in the approaches of Milios and Newman and of Bearman in deriving the Newman–Milios correction. To complete the demonstration of the equivalence of the two theoretical methods, we note that they both lead to the regulating function[9a] and, when the partial molar volumes are constant through the liquid junction, also to the Lewis correction.[9b]

Conclusions

We have shown that the approach of Bearman, like that of Milios and Newman, leads to the general form of the regulating function and to the Lewis and Newman–Milios corrections. Because the assumption of constancy of partial molar volumes below the moving boundary is well concealed in the method of Milios and Newman and because they do not show the constancy of volume velocity, which links the theory of the moving boundary to the theory of mutual diffusion,[10a] we tend to prefer the Bearman approach.[10b]

We are less confident than Milios and Newman that forcing experimental thermodynamic data for c_0 to assume the form of eq 1 "does not greatly limit the usefulness of the transference number equation." In essence, such a force-fit replaces the assumption that partial molar volumes are constant through the boundary by the assumption that they are constant below the boundary. The new assumption undoubtedly represents an improvement since it concerns a binary, rather than a ternary, solution, but a quantitative estimate of the extent of improvement has not yet been obtained.

---

[8] P. Milios, "A Theoretical Analysis of the Moving Boundary Measurement of Transference Numbers," Masters Thesis, University of California, Berkeley, Sept 1967 (UCRL-17807), p 21.

[9] (a) Demonstrated in the fourth paragraph of this note; (b) Demonstrated in the preceding section for the case of Bearman and in the reference of footnote 2 for the case of Milios and Newman.

[10] (a) *Cf.* J. G. Kirkwood, R. L. Baldwin, P. J. Dunlop, L. J. Gosting, and G. Kegeles, *J. Chem. Phys.*, **33**, 1505 (1960), especially section III; (b) It is entirely possible, however, that for the case of vertical electrodes, briefly mentioned by Milios and Newman, the mass balance technique may prove to be more useful.

Electron Paramagnetic Resonance of Nitrosodisulfonate Ion with Oxygen-17 and Sulfur-33 in Natural Abundance

by J. B. Howell and Douglas C. McCain

Department of Chemistry, University of California, Santa Barbara, California 93106 *(Received June 11, 1969)*

The epr spectrum of the nitrosodisulfonate ion $(SO_3)_2NO^{-2}$, has been frequently studied, and except for the sulfur-bonded $^{17}O(S-^{17}O)$, coupling constants have been reported for all atoms in the ion.[1] Recently the nitrogen-bonded $^{17}O(N-^{17}O)$ was seen after chemical preparation with labeled oxygen.[2] Line width variations allowed the relative signs of the nitrogen and $N-^{17}O$ coupling constants to be determined.

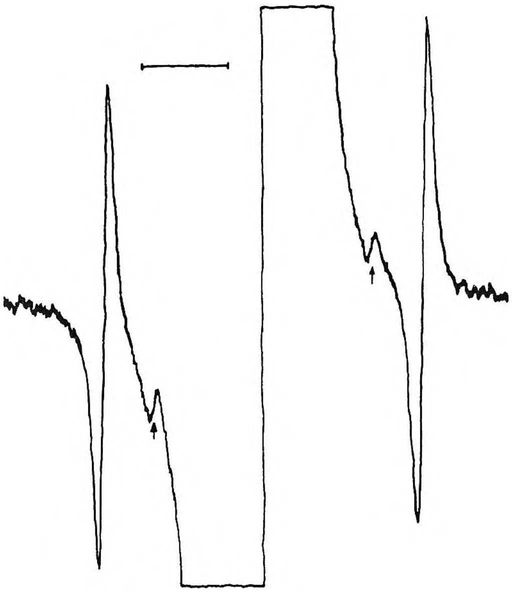

Figure 1. A part of the spectrum of $(SO_3)_2NO^{2-}$ showing the central ^{14}N line ($m_N = 0$) off scale, two ^{33}S lines ($m_S = \pm^3/_2$) and two ^{17}O lines ($m_O = \pm^5/_2$) marked by arrows. Magnetic field increases to the left. The horizontal line represents 1 G.

We have obtained the spectrum of a very dilute solution of purified $K_2(SO_3)_2NO$ dissolved in deoxygenated dimethyl sulfoxide (DMSO). The weak lines in Figure 1 are assigned to the outermost, $m = \pm^5/_2$, of the six lines derived from interaction with the ^{17}O nuclear spin in an ion with one ^{14}N. Assignment of these lines to any other set in the ^{17}O multiplet would predict lines displaced farther out from the center of the multiplet in positions where no lines are observed. Statistically, these ^{17}O lines should be about one-tenth the intensity of ^{33}S lines, and very nearly this ratio is

---

[1] J. J. Windle and A. K. Wiersema, *J. Chem. Phys.*, **39**, 1139 (1963).

[2] Z. Luz, B. L. Silver, and C. Eden, *ibid.*, **44**, 4421 (1966).

Table I: Summary of Hyperfine Interactions in $(SO_3)_2NO_2^{2-}$

Nucleus	a, G	Sign of the spin density[d]
^{14}N	$13.0^{a,b}$	+
^{33}S	-1.29 ± 0.04^{c}	−
N–^{17}O	-20.7 ± 0.2^{b}	+
S–^{17}O	$\pm 0.53 \pm 0.04^{c}$	?

[a] Reference 1. [b] Reference 2. [c] This work. [d] A positive spin density represents unpaired electron polarization parallel to the net polarization of the ion.

observed. Under conditions of best resolution, the next set of ^{17}O lines, $m = \pm ^3/_2$, can just be seen as poorly resolved shoulders on the innermost ^{33}S lines. We measure for S–^{17}O a coupling constant $a_0 = 0.53 \pm 0.04$ G. (See Table I.)

The line width of the low-field ^{14}N transition is about 0.125 G at room temperature and very great dilution, but both modulation frequency (100 KHz) and magnet inhomogeneities make some contribution, so the natural line width is probably less than 0.10 G. For better signal-to-noise ratio, coupling constants were measured at higher concentrations with line widths of about 0.135 G. No variation in ^{17}O line widths with m is observed, so the sign of the coupling constant cannot be determined from our data.

We have also remeasured the ^{33}S hyperfine spectrum which has fully resolved outer lines, $m = \pm ^3/_2$, and partially resolved shoulders for $m = \pm ^1/_2$. We find a coupling constant $a_S = 1.29 \pm 0.04$ G in DMSO. The previously reported value[1] was 1.25 G measured in water and D_2O. We also find a systematic line width variation with m. The low-field lines within any ^{33}S multiplet are invariably narrower than the high-field lines. Line width ratios can be measured quite accurately from a derivative spectrum. When the observed line widths and line width ratios are fitted to an equation of the form[2]

$$1/T_2(\tilde{m}_N,\tilde{m}_S) = K_N\tilde{m}_N^2 + L_N\tilde{m}_N + K_S\tilde{m}_S^2 + L_S\tilde{m}_S + C + E\tilde{m}_S\tilde{m}_N$$

where the spectral index numbers $\tilde{m}_S$ and $\tilde{m}_N$ are arbitrarily taken as negative on the low-field side of the spectrum, we obtain

$$K_N = 1.3 \times 10^5 \text{ sec}^{-1}$$

$$L_N = 1.4 \times 10^5 \text{ sec}^{-1}$$

$$K_S\tilde{m}_S^2 + C = 2.0 \times 10^6 \text{ sec}^{-1}$$

$$L_S = 2.0 \pm 0.3 \times 10^4 \text{ sec}^{-1}$$

$$E = 1.0 \pm 0.3 \times 10^4 \text{ sec}^{-1}$$

The term E is positive so both $a_N\rho_N$ and $a_S\rho_S$ must have the same sign. Since the signs of the coupling constant, a_N, and spin density, ρ_N, on ^{14}N are both known to be positive,[2] we conclude that $a_S\rho_S$ must also be positive.

A complete analysis of this effect[2-4] to determine the sign of ρ_S requires a knowledge of the geometry of molecular electronic wave functions. For simplicity we may assume that almost all of the spin density in the ion is localized on the nitrogen and oxygen atoms in $p\pi$ orbitals. A nucleus, i, which has a small coupling constant and which is adjacent to a p orbital with high spin density on atom j, should normally have a negative spectral density term $j_{i,j}^{(D)}$ if the product of the gyromagnetic ratios, $\gamma_i\gamma_j$, is positive.[3] This term, $j_{N,S}^{(D)}$ is probably negative in $(SO_3)_2NO^{2-}$ although there is a possibility that the NO bond may not lie in the SNS plane.[5] If $j_{N,S}^{(D)}$ is negative and a_N is positive, then both a_S and ρ_S must be negative and the electronic polarization at the sulfur atom is opposite to that of the whole ion. A similar result is found with hydrogen in aromatic hydrocarbon ions where the polarization is also opposite to the whole ion polarization and where the hydrogen, like the sulfur in $(SO_3)_2NO^{2-}$, is σ-bonded to a π system containing unpaired electrons.

Acknowledgment. We wish to thank the Petroleum Research Fund for supporting this work.

(3) J. H. Freed and G. K. Fraenkel, *J. Chem. Phys.*, **40**, 1815 (1964).

(4) A. Hudson and G. R. Luckhurst, *Chem. Rev.*, **69**, 191 (1969).

(5) J. Lajzérowicz-Bonneteau, *Acta Cryst.*, **B24**, 196 (1968).

Methyl Radical Reactions in Aqueous Solutions. I. Hydrogen Abstraction from Acetone

by Issam A. I. Taha and Robert R. Kuntz

Department of Chemistry, University of Missouri at Columbia, Columbia, Missouri 65201 *(Received June 18, 1969)*

The rate of methyl radical reaction with acetone in the photolysis of aqueous solutions has been reported previously.[1] Methane and ethane are formed by free-radical steps in which reactions 1 and 2 are of the most importance. If these are the only sources of methane and ethane, then the relative rate of hydrogen abstraction by the methyl radical may be determined by using eq I.

$$CH_3 + CH_3COCH_3 \longrightarrow CH_4 + CH_2COCH_3 \quad (1)$$

$$CH_3 + CH_3 \longrightarrow C_2H_6 \quad (2)$$

$$\frac{R_{CH_4}}{R_{C_2H_6}^{1/2}} = \frac{k_1[CH_3COCH_3]}{k_2^{1/2}} \quad (I)$$

(1) D. H. Volman and L. W. Swanson, *J. Amer. Chem. Soc.*, **82**, 4141 (1960).

Previous studies in liquid acetone[2] and in the gas phase[3] indicated a strong dependence of this product ratio on light intensity due to radical disproportionation reactions of the methyl radical which enhance the methane yield. Volman and Swanson[1] considered reaction 3 as the additional source of methane and corrected eq I to include this source. The Arrhenius

$$CH_3 + CH_3CO \longrightarrow CH_4 + CH_2CO \qquad (3)$$

parameters resulting from this treatment differed considerably from the well-known gas-phase values, and these differences could not be accounted for on the basis of diffusion corrections alone. In addition to the acetyl radical, the acetonyl, CH_2COCH_3, and the dimethyl carbinol, $CH_3C(OH)CH_3$, radicals have been characterized in the photolysis of pure acetone and acetone solutions containing hydrogen donors[4] and must be considered as potential disproportionation partners of the methyl radical. It has been suggested that the disproportionation of the acetonyl radical with the methyl radical is an important source of methane in the gas-phase photolysis.[3] This laboratory, in the investigation of acetone photolysis as a source of methyl radicals in aqueous solutions, has found it possible to work at low intensities such that the disproportionation reaction is no longer a significant fate of the methyl radical. Under these conditions, the methane contribution from this source may be ignored in the determination of rate parameters for the methyl radical.

Experimental Section

The reaction cell was a Vycor cylinder 13.5 cm in length and 1.9 cm in diameter attached through a graded seal to a Pyrex tube suitable for connection to the vacuum system. The irradiation zone was restricted to a 9.7-cm length of the tube by shielding. Acetone was spectroquality reagent obtained from Matheson Coleman and Bell and purified by bulb-to-bulb distillation before use. Water was deionized, distilled from permanganate, and then doubly distilled.

Samples were prepared by placing 20 ml of the purified water in the reaction cell and degassing by gentle cavitation after making the vacuum connections. The desired amount of acetone was degassed independently and distilled into a reaction vessel side arm before sealing. The cell was placed inside a quartz jacket through which thermostated water was passing. Photolysis was performed inside the coils of a low-pressure mercury lamp with a Vycor envelope. The effective wavelength under these conditions is 2537 Å. The solution was stirred during photolysis using a magnetic stirring bar and an induction technique.

Intensity studies were made using the combination of a variable transformer on the primary side of the lamp transformer and a copper screen wrapped around the water jacket of the cell. Actinometry was performed with the uranyl oxalate actinometer using the modification of Pitts, *et al.*,[5] and the method of equivalent optical density. The rate of oxalate destruction was linear with optical density over the concentration range of 3×10^{-5} to 2.5×10^{-4} M for uranyl oxalate, and this line was extrapolated to a zero intercept. Measurements at concentrations of 2.5×10^{-4} to 1×10^{-3} M were nearly constant at the intensity corresponding to total light absorption. The quantum yield data presented in this report are based on the assumption that the quantum yield for oxalate decomposition in the uranyl oxalate actinometer is unchanged over the entire concentration range. This assumption appears to be reasonable on the basis of the consistency of values in the higher range which overlaps the concentrations that are commonly used, and the expected derived intensity behavior over the lower range.

After photolysis, the reaction cell was attached to the vacuum system. Gaseous products were removed from the solution by gentle cavitation and caused to flow through a cold trap maintained at −119°. The noncondensed gases, which included methane, ethane, and carbon monoxide, were pushed into a sample loop of a thermal conductivity chromatograph by a number of cycles with a Toepler pump and analyzed on a Porapak Q column.

Results and Discussion

The excited singlet state of acetone produced in the 3130-Å photolysis of acetone undergoes intersystem crossing to the triplet state with nearly unit efficiency in condensed systems.[6] An evaluation of the importance of triplet acetone in the present study at 2537 Å was made by adding an efficient trap of triplet acetone, ethanol (USP, 200 proof, U. S. Industrial Chemicals Co.)[4] to the system and observing the yields of radical products. The decrease of methane and ethane yields when ethanol is added is shown in Figure 1. The virtual elimination of these products at high ethanol concentrations is consistent with a mechanism in which the excited triplet state is the major precursor to radical products. The subsequent processes are presumed to be identical with those observed at 3130 Å.[4,6]

The yields of methane, ethane, and in some instances carbon monoxide were measured as a function of acetone concentration, absorbed light intensity, and temperature. These data are presented in Table I. The quantum yields of methane and ethane varied over a

---

[2] R. Pieck and E. W. R. Steacie, *Can. J. Chem.*, **33**, 1304 (1955).

[3] B. deB. Darwent, M. J. Allard, M. F. Hartman, and L. J. Lange, *J. Phys. Chem.*, **64**, 1847 (1960).

[4] H. Zeldes and R. Livingston, *J. Chem. Phys.*, **45**, 1946 (1966).

[5] J. N. Pitts, J. D. Margerum, R. P. Taylor, and W. Brum, *J. Amer. Chem. Soc.*, **77**, 5499 (1955).

[6] R. F. Borkman and D. R. Kearns, *J. Chem. Phys.*, **44**, 945 (1966).

Table I: Methane, Ethane, and CO Yields in the Photolysis of Acetone[a]

10^2[Ac], mol/l.	$I_a \times 10^{10}$, E/(cc sec)	ϕ_{CH_4}	$\phi_{C_2H_6}$	
		Temp, 25°		
1.25	2.29	0.125	0.0186	
2.50	4.57	0.121	0.0091	
3.00	5.43	0.095	0.0036	
3.75	6.34	0.106	0.0046	
4.50	6.87	0.105	0.0049	
5.00	7.01	0.116	0.0035	
2.50	315[e]	0.0267	0.0210	ϕ_{CO} = 0.000318 0.000342 0.000390
		Temp, 35°		
2.50	0.797[b]	0.745	0.0518	
3.75	1.10[b]	0.641	0.0189	
5.00	1.22[b]	0.481	0.0069	
2.50	4.57	0.225	0.0218	
2.50	4.57	0.239	0.0227	
3.00	5.43	0.221	0.0181	
3.75	6.34	0.241	0.0153	
4.50	6.87	0.239	0.0116	
5.00	7.01	0.135	0.0029	
5.00	7.01	0.144	0.0029	
1.25	5.05[c]	0.125	0.0419	
1.25	5.05[c]	0.119	0.0330	
2.50	10.1[c]	0.196	0.0359	
3.00	12.0[c]	0.127	0.0150	
3.75	14.0[c]	0.200	0.0187	
5.00	15.5[c]	0.146	0.0081	
5.00	15.5[c]	0.146	0.0075	
1.25	39.5[d]	0.0637	0.0405	
2.50	78.7[d]	0.0630	0.0224	
3.00	93.6[d]	0.0585	0.0161	
4.50	119[d]	0.0643	0.0121	
1.25	158[e]	0.0432	0.0619	
1.25	158[e]	0.0437	0.0595	
2.00	254[e]	0.0253	0.0131	
2.50	315[e]	0.0450	0.0371	
2.50	315[e]	0.0514	0.0450	
3.00	374[e]	0.0323	0.0158	
3.75	437[e]	0.0480	0.0265	
4.00	452[e]	0.0424	0.0178	
5.00	483[e]	0.0445	0.0136	
		Temp, 45°		
1.00	1.86	0.254	0.0386	
2.00	3.69	0.236	0.0140	
3.75	6.34	0.178	0.0035	
4.50	6.87	0.186	0.0034	
		Temp, 55°		
1.25	2.29	0.264	0.0175	
2.50	4.57	0.241	0.0040	
3.00	5.43	0.250	0.0059	
3.75	6.34	0.218	0.0030	
4.50	6.87	0.246	0.0030	
5.00	7.01	0.220	0.0020	
5.00	7.01	0.201	0.0016	

[a] Several lamp intensities were used to vary the absorbed light intensity, which was measured relative to full lamp intensity at 110 V on the transformer primary. [b] Intensity, 0.00725. [c] Intensity, 0.032. [d] Intensity, 0.25. [e] Intensity, 1.00. Unmarked entries were determined at a relative intensity of 0.0145.

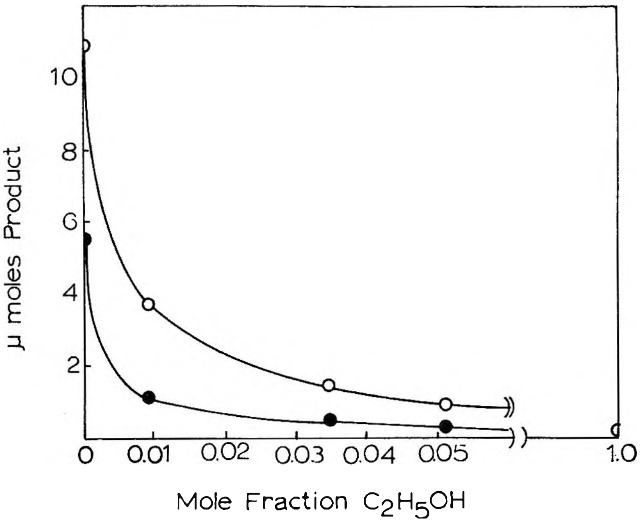

Figure 1. Effect of ethanol on the methane and ethane yields from the photolysis of 0.025 *M* acetone solutions: ○, CH_4; ●, $C_2H_6 \times 10$.

wide range as a function of intensity. The highest values of methane yields, $\phi_{CH_4} = 0.7$, were obtained at the lowest lamp intensity. The quantum yields at high intensity approach 10^{-2}, which is in agreement with earlier work.[1] Carbon monoxide was analyzed under the high-intensity conditions using a molecular sieve column. It is a minor product of this photolysis amounting to about 1% of the methane yield under these conditions.

The intensity variation data at 35° give straight lines when $R_{CH_4}/R_{C_2H_6}{}^{1/2}$ is plotted against [CH_3COCH_3]. The results of the least-mean-square treatment of these data are summarized in Table II. The intercepts appear to be randomly scattered about the origin and may be considered to be zero within the experimental error. The result of forcing the lines to intersect the origin causes no more than a 10% change in the reported slopes. Therefore subsequent kinetic plots were forced to conform to eq I (*i.e.*, lines were forced to pass through the origin). The apparent rate constant ratios given by the slopes at different light intensities remain essentially constant in the lower intensity region indicating a negligible contri-

Table II: Effect of Intensity on Apparent Values of $k_1/k_2{}^{1/2}$

Relative intensity	Slope[a]	Intercept[a]
0.00725	1.38 ± 0.00	−0.4 ± 0.1
0.0145	1.37 ± 0.04	−0.2 ± 0.0
0.032	1.28 ± 0.04	−0.3 ± 0.1
0.25	1.35 ± 0.00	+0.4 ± 0.1
1.00	1.66 ± 0.03	+0.1 ± 0.0

[a] Parameters for the least-mean-squares treatment of intensity variation data where $R_{CH_4}/R_{C_2H_6}{}^{1/2}$ = slope X[CH_3COCH_3] + intercept.

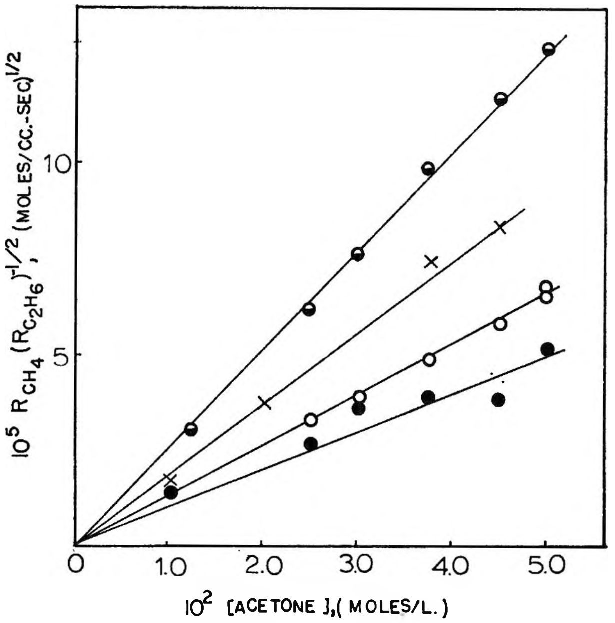

Figure 2. Acetone concentration and temperature effect on the ratio $R_{CH_4}/R_{C_2H_6}^{1/2}$: ●, 25°; ○, 35°; ×, 45°; ⊖, 55°.

bution of sources of methane other than reaction 1. At the highest intensity, which is of the same magnitude as those used in the previous study,[1] a noticeable increase in the apparent rate constant was found. This result may be explained by an increase in methane production due to the emphasis on the importance of radical–radical reactions (including disporportionation) at high intensities. Correction for methane production by reaction 3 using the rate of CO production as a measure of acetyl radical concentration was not attempted since CO is a minor product under these conditions and since corrections for other likely disproportionation reactions (reactions 4 and 5) cannot

$$CH_3 + CH_2COCH_3 \longrightarrow CH_4 + CH_2COCH_2 \quad (4)$$

$$CH_3 + CH_3C(OH)CH_3 \longrightarrow CH_4 + CH_3COCH_3 \quad (5)$$

be made in a satisfactory manner.

Subsequent determinations were restricted to the relative intensity of 0.0145 at which radical–radical reactions for the methyl radicals are minor processes for methyl radical disappearance as evidenced by the low ethane yields compared to the methane yields. The variables in eq I are plotted as a function of temperature in Figure 2, and the resulting rate constant ratios are compared with the previous values in Table III. The Arrhenius plot of this data is shown in Figure 3. The rate constant ratio may be expressed as

$$\log k_1/k_2^{1/2} = 4.47 \pm 0.05 - \frac{1335 \pm 18}{T}$$

The preexponential factor is in reasonable agreement with the gas-phase value of log A = 4.85.[7] The gas-phase activation energy of this reaction has been reported to be 9.7 kcal/mol,[7] which compares to $E_1 - 0.5\,E_2 = 6.14$ kcal/mol in this study. If E_2 is assumed to be the temperature coefficient for the viscosity of water which varies from 3.2 to 4.0 kcal/mol in the temperature range of these experiments,[8] then $E_1 = 6.1 + 1.8 = 7.9$ kcal/mol, which compares favorably with the gas-phase value. It deviates considerably, however, from the value reported earlier in which the disproportionation was not completely accounted for.

Table III: Effect of Temperature on the Abstraction of Hydrogen from Acetone by Methyl Radicals

T, °C	$k_1/k^{1/2}$, [cc/(mol sec)]$^{1/2}$	$k_1/k_2^{1/2}$, [cc/(mol sec)]$^{1/2a}$
25	1.00	0.77(27°)
35	1.34	
45	1.86	1.47(49°)
55	2.56	1.56(73°)

[a] Values taken from ref 1.

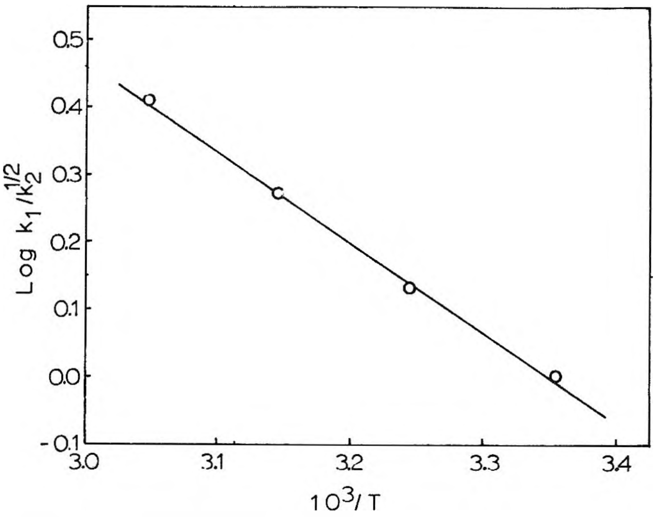

Figure 3. Arrhenius plot of $k_1/k_2^{1/2}$.

This rate constant ratio for the hydrogen abstraction from acetone by the methyl radical in aqueous solution appears to be nearly independent of other sources of methane and thus is a more accurate representation of the rate parameters than was previously available. It demonstrates that the low-intensity photolysis of acetone in aqueous solutions is a convenient technique for the production and study of methyl radicals in these systems. Further studies are underway to characterize the reaction rates of methyl radicals with other solutes.

Acknowledgment. This research was supported in part by NIH Grant No. RH-00321. The authors are indebted to Dr. Wynn Volkert for helpful preliminary investigations.

(7) A. F. Trotman-Dickenson and E. W. R. Steacie, *J. Chem. Phys.*, **18**, 1097 (1950).

(8) L. Korson, W. Drost-Hanson, and F. J. Millero, *J. Phys. Chem.*, **73**, 34 (1969).

Solubility of Gases in Mixtures of Nonpolar Liquids

by R. G. Linford and J. H. Hildebrand

Department of Chemistry, University of California, Berkeley, California 94720 *(Received June 19, 1969)*

Several experimental determinations have been published[1] of the solubility of gases in mixtures of polar liquids, but the more fundamental problem of their solubility in nonpolar liquid mixtures appears to have been attacked only in a theoretical paper by O'Connell and Prausnitz.[2]

This investigation was undertaken in order to ascertain whether a successful regular solution correlation of values of the solubility of a gas in a series of pure liquids with their solubility parameters is applicable also to its solubility in mixtures of two of these liquids.

A relationship between the logarithm of solubility of a gas and the solubility parameters of solvents was pointed out by Hildebrand[3] in 1954 and subsequently expanded in later papers.[4]

The lines for log x_2 (x_2 = mole fraction of gas) *vs.* δ_1, the solubility parameters of the solvents, proved to be curved. Hildebrand[5] showed in 1967 that straight lines result by using $\delta_1{}^2$ instead of δ_1. In the case of Ar, for which values of x_2 are most abundant and accurate, the straight line extends through the whole range from C_7F_{16} to CS_2, with values of $\delta_1{}^2$ from 37 to 100.

Table I: Solubility of Gases, Mole Fraction, x_2 at 1 Atm and 25°, in Mixtures of (1) Benzene, Mole Fraction x_1, with (3) $CCl_2F \cdot CClF_2$, and Square of Solubility Parameter of the Mixed Solvent, $\delta_{1-3}{}^2$, Calculated from δ_2 and δ_3 by Eq 1

	x_1	$10^4 x_2$	$\delta_{1-3}{}^2$, (cal/cc)$^{1/2}$
H_2	1.000	2.58[a]	83.5
	0.695	3.96	70.0
	0.341	5.35	58.5
	0	6.55[e]	50.0
Ar	1.000	8.77[b]	83.5
	0.650	16.0	68.5
	0.348	22.2	58.5
	0	30.5[d]	50.0
C_2F_6	1.000	11.06[e]	83.5
	0.674	40.55	69.5
	0.359	85.8	59.0
	0	149.4[e]	50.0
C_2H_6	1.000	151.0[c]	83.5
	0.776	193.2	73.5
	0.510	238.0	63.5
	0.260	265.4	56.0
	0	285.8[e]	50.0

[a] H. W. Cook, D. N. Hansen, and B. J. Alder, *J. Chem. Phys.*, **26**, 748 (1957). [b] H. L. Clever, R. Battino, J. H. Saylor, and P. M. Gross, *J. Phys. Chem.*, **61**, 1078 (1957). [c] J. Horiuti, *Sci. Papers, Inst. Phys. Chem. Research, Tokyo*, **17**, No. 341, 125 (1931). [d] H. Hiraoka and J. H. Hildebrand, *J. Phys. Chem.*, **68**, 213 (1964). [e] Determined for this study by R. G. Linford; details to be published.

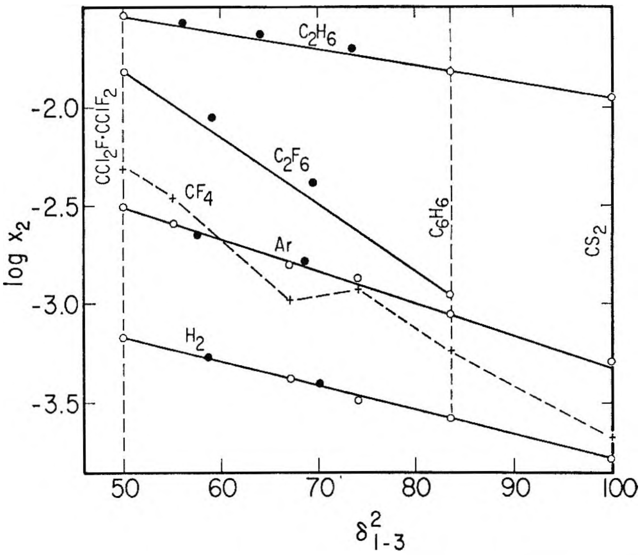

Figure 1. Linear correlation between the solubility of a gas, x_2, and the solubility parameters of solvents: open circles, pure liquids; closed circles, mixtures of (1) benzene with (3) $CCl_2F \cdot CClF_2$.

Scott[6] in 1950 proposed calculating a solubility parameter for a solvent mixture as the volume fraction average of the parameter of the pure liquids. We follow our convention of designating a "solute," in this case a gas, by subscript 2, and use subscripts 1 and 3 for the pure solvent liquids. The solubility parameters of our liquid mixtures are calculated by

$$\delta_{1-3} = \frac{\delta_1\Phi_1 + \delta_3\Phi_3}{\Phi_1 + \Phi_3} \tag{1}$$

where the Φ's are volume fractions.

Gordon and Scott[7] applied this equation to solutions of phenanthrene in mixtures of cyclohexane and methylene iodide. Smith, Walkley, and Hildebrand[8] determined the solubility of iodine in mixtures of C_7F_{16} and CCl_4 and found eq 1 to be applicable.

In this paper, we report determinations of the solubility of H_2, Ar, C_2H_6, and C_2F_6 in mixtures of benzene and $CCl_2F \cdot CClF_2$, "Freon 113." We selected this pair of liquids because they are nonpolar, noncomplexing with the above gases, and very different in solvent power as indicated by their solubility parameters, 9.15 (cal cm^{-3} mol^{-1})$^{1/2}$ for benzene and 7.05 for the Freon. The latter figure is a revision of one given in ref 4; we now have for its heat of vaporization 35.07 cal g^{-1} from Du Pont Bulletin FST-1; from this and the molal volume, 119.9 cm^3 at 25°, we obtain the new value for its solubility parameter given above.

---

(1) R. Battino and H. L. Clever, *Chem. Rev.*, **66**, 395 (1966).

(2) J. P. O'Connell and J. M. Prausnitz, *Ind. Eng. Chem. Fundamentals*, 3, 347 (1964).

(3) J. H. Hildebrand, *J. Phys. Chem.*, **57**, 671 (1954).

(4) J. H. Hildebrand and R. L. Scott, "Regular Solutions," Prentice-Hall, Englewood Cliffs, N. J., 1962.

(5) J. H. Hildebrand, *Proc. Nat. Acad. Sci. U. S.*, **57**, 542 (1967).

(6) R. L. Scott and J. H. Hildebrand, "Solubility of Nonelectrolytes," Reinhold Publishing Corp., New York, N. Y., 1950; 2nd ed., Dover Publications, New York, N. Y., 1964, p 201.

(7) L. J. Gordon and R. L. Scott, *J. Amer. Chem. Soc.*, **74**, 4138 (1952).

(8) E. B. Smith, J. Walkley, and J. H. Hildebrand, *J. Phys. Chem.*, **63**, 703 (1959).

The two solvents were "Spectroquality," from Matheson Coleman and Bell. The mixtures were degassed in the apparatus by repeated freezing and evacuating; their composition was determined from the density of a degassed sample. The gases were of the highest purity commercially obtainable; they were dried before use. Solubilities were determined in the apparatus designed by Dymond and Hildebrand[9] and since used extensively.

Table I gives our measured values of the solubility of the four gases in the two pure liquids and 2 or 3 mixtures at 25°, together with values of $\delta_{1-3}{}^2$. Figure 1 plots log x_2 *vs.* $\delta_{1-3}{}^2$ for the mixtures (solid circles) and the pure liquids (open circles) with points added for other pure liquids in order to illustrate the linear relationship existing in both cases.

We included C_2F_6 in order to learn whether its solubility in mixtures of liquids would show peculiarities such as are seen in the zig-zag line for CF_4 in different pure liquids. We see only that the points for C_2F_6 in the two mixtures are not so close to the line joining the points for the pure liquids as they are for the other gases.

We conclude that the linear relation between the solubility of a gas as log x_2 in pure liquids and the square of their solubility parameters is equally valid for its solubility in liquid mixtures if their solubility parameters are calculated as volume fraction averages of the parameter of the component liquids.

Acknowledgment. This research was supported by the National Science Foundation.

---

[9] J. H. Dymond and J. H. Hildebrand, *Ind. Eng. Chem. Fundamentals*, 6, 130 (1967).

The Limiting Behavior of the Integrand in the Robinson and Sinclair Equation

by Chai-fu Pan

Department of Chemistry, Alabama State University, Montgomery, Alabama 36101

(Received June 26, 1969)

The isopiestic vapor pressure method of studying aqueous solutions gives directly the osmotic coefficient of the solution and the activity coefficient of the solute can be calculated by means of some form of the Gibbs–Duhem equation. One convenient form is the Robinson and Sinclair equation[1]

$$\ln \gamma = \ln \gamma_R + \ln R + 2\int_{m_R=0}^{m_R} \frac{R-1}{\sqrt{\gamma_R m_R}}\, d\sqrt{\gamma_R m_R} \tag{1}$$

where γ is the activity coefficient, R denotes the reference electrolyte, m is the molal concentration, and R is the isopiestic ratio. The integrand in eq 1 can be evaluated by graphical methods. In the case of the reference and the test electrolytes are 1:1 salts, it is stated[2] that the limiting value of the integrand in this equation is zero. This, however, has not been proved, nor has the behavior of the integrand for electrolytes of other charge type been investigated. The problem, however, can be solved.

The limiting Debye–Hückel equation for the osmotic coefficient is[3]

$$\phi - 1 = -\frac{2.303}{3\sqrt{2}} A|Z_+Z_-|^{3/2}\nu^{1/2}m^{1/2} \tag{2}$$

where ϕ is the osmotic coefficient, Z is the charge number, ν is the number of ions per molecule of electrolyte, and for aqueous solutions at 25°, $A = 0.5107$ mol$^{-1/2}$ kg$^{1/2}$.

The condition for equilibrium in an isopiestic experiment is

$$\nu_R m_R \phi_R = \nu m \phi$$

or

$$R = \frac{\nu_R m_R}{\nu m} = \frac{\phi}{\phi_R} \tag{3}$$

From eq 2 and 3 and with the limiting behavior $\gamma_R \rightarrow 1$, $\phi_R \rightarrow 1$, and $m/m_R \rightarrow \nu_R/\nu$ when $m_R \rightarrow 0$, we obtain

$$\lim_{m_R \rightarrow 0} \frac{R-1}{\sqrt{\gamma_R m_R}} = 0.2773\nu_R{}^{1/2}\{|Z_+Z_-|_R{}^{3/2} - |Z_+Z_-|^{3/2}\} \tag{4}$$

for an aqueous solution at 25°. The limiting value in eq 4 is obviously zero if both electrolytes are of the same charge type. If the reference electrolyte is of the 1:1 charge type and the other is of the 2:1 charge type, the limiting value is −0.716.

An example can be cited to show the validity of this derivation. The isopiestic measurements of Stokes[4] on calcium chloride solutions, with sodium chloride as reference salt, include data for four solutions between

---

[1] R. A. Robinson and D. A. Sinclair, *J. Amer. Chem. Soc.*, 56, 1830 (1934).

[2] R. A. Robinson and R. H. Stokes, "Electrolyte Solutions," revised ed, Butterworth and Co. Ltd., London, 1965, pp 180, 181.

[3] G. N. Lewis and M. Randall (revised by K. S. Pitzer and L. Brewer), "Thermodynamics," 2nd ed, McGraw-Hill Book Co., Inc., New York, N. Y., 1961, pp 338, 339.

[4] R. H. Stokes, *Trans. Faraday Soc.*, 41, 637 (1945).

Table I: Values of $(1 - R)/\sqrt{\gamma_{NaCl} \cdot m_{NaCl}}$ as a Function of m_{NaCl} for both the Isopiestic and the Emf Measurements of Sodium Chloride and Calcium Chloride Solutions

$\sqrt{m_{NaCl}}$	m_{NaCl}	m_{CaCl_2}	$(1 - R)$	$\gamma_{NaCl} \cdot m_{NaCl}$	$(1 - R)/(\gamma_{NaCl} \cdot m_{NaCl})^{1/2}$
From Emf Measurements					
0.080	0.0064	0.004462	0.0438	0.07673	0.5708
0.160	0.0256	0.01831	0.0679	0.1484	0.4575
0.240	0.0576	0.04174	0.0800	0.2157	0.3709
0.320	0.1024	0.07431	0.0814	0.2910	0.2797
From Isopiestic Measurements					
0.354	0.1255	0.0908	0.0786	0.3102	0.2534
0.398	0.1586	0.1148	0.0790	0.3455	0.2287
0.550	0.3034	0.2156	0.0618	0.4721	0.1309
0.624	0.3901	0.2742	0.0515	0.5199	0.0991

0.09 and 0.27 m_{CaCl_2}. From these, values of $(1 - R)/(\gamma_{NaCl} \cdot m_{NaCl})^{1/2}$ can be calculated (Table I). Gordon, *et al.*,[5,6] from emf and transference number measurements, have calculated osmotic coefficients for both sodium chloride and calcium chloride solutions. For example, Janz and Gordon give $\phi = 0.9414$ for a 0.0576 m solution of sodium chloride. By interpolation in the data of McLeod and Gordon, a solution of 0.04174 m calcium chloride has the same vapor pressure as this sodium chloride solution. In this way, values of $(1 - R)/(\gamma_{NaCl} \cdot m_{NaCl})^{1/2}$ were calculated for four pairs of solutions (Table I).

Figure 1 is the plot of $(1 - R)/\sqrt{\gamma_R m_R}$ against $\sqrt{m_R}$ for both the isopiestic and the emf measurements of calcium chloride solutions. The extrapolation in Figure 1 shows that the integrand in eq 1 does approach -0.716. Suppose we did not have Gordon's data for calcium chloride below 0.1 m and had only the points from Stokes' work; to know the limiting value is -0.716 is useful, but it does not completely solve the problem of filling in the curve between 0 and 0.1 m. In fact, there is much need for more work of Gordon's type for extrapolations in the dilute region.

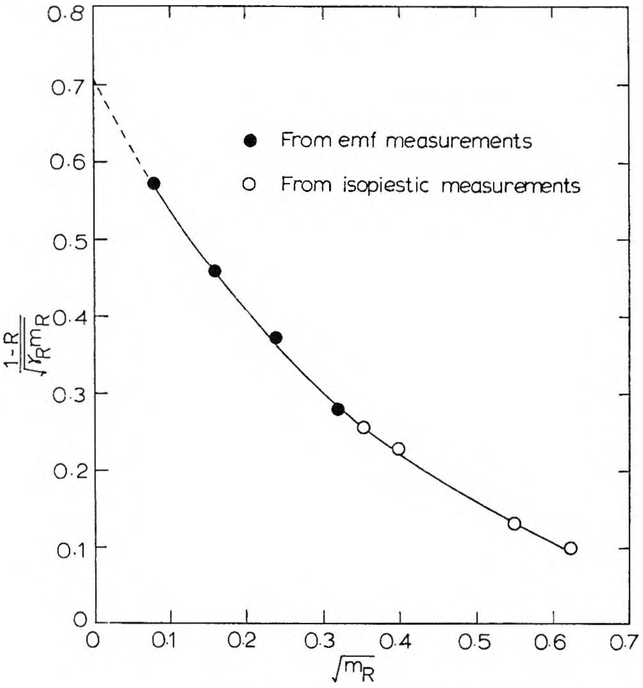

Figure 1. Plot of $(1 - R)/\sqrt{\gamma_R m_R}$ *vs.* $\sqrt{m_R}$ for calcium chloride solutions (R = NaCl).

Acknowledgment. The author wishes to thank Professor R. A. Robinson for suggesting improvements in the manuscript, and Professor C. W. McDonald for helpful discussions.

(5) G. J. Janz and A. R. Gordon, *J. Amer. Chem. Soc.*, **65**, 218 (1943).

(6) H. G. McLeod and A. R. Gordon, *ibid.*, **68**, 58 (1946).

Identification of the Photochemically Active Species in Sulfur Dioxide Photolysis within the First Allowed Absorption Band

by Sachiko Okuda, T. Navaneeth Rao,
David H. Slater, and Jack G. Calvert

Chemistry Department, The Ohio State University, Columbus, Ohio 43210

(Received June 23, 1969)

Recently the photochemistry of sulfur dioxide has been studied extensively by several research groups.[1-4] The rate constants for the quenching reactions of the photoexcited singlet (${}^1SO_2$) and triplet (${}^3SO_2$) states of sulfur dioxide have been reported.[1-3] A small fraction of the SO_2-quenched molecules of sulfur dioxide excited at 3130 Å[5,6] or 2537 Å[6] react to form sulfur trioxide[7]

---

(1) (a) H. D. Mettee, *J. Chem. Phys.*, **49**, 1784 (1968); (b) H. D. Mettee, *J. Phys. Chem.*, **73**, 1071 (1969).

(2) S. J. Strickler and D. B. Howell, *J. Chem. Phys.*, **49**, 1947 (1968).

(3) (a) T. N. Rao, S. S. Collier, and J. G. Calvert, *J. Amer. Chem. Soc.*, **91**, 1609 (1969); (b) T. N. Rao, S. S. Collier, and J. G. Calvert, *ibid.*, **91**, 1616 (1969).

(4) J. N. Discoll and P. Warneck, *J. Phys. Chem.*, **72**, 3736 (1968).

(5) T. C. Hall, Jr., "Photochemical Studies of Nitrogen Dioxide and Sulfur Dioxide," Ph.D. Thesis, Univ. Calif., Los Angeles, 1953.

(6) P. J. Warneck, G. C. A. Technology Division, Bedford, Mass., personal communication to one of the authors.

(7) The present experimental evidence suggests but certainly does not require that the oxidation product of SO_2 formed photochemically is SO_3. All analytical systems which have been employed in the previous and present study depend on analysis for SO_4^{2-} formed by reaction of the product with water. Direct spectroscopic evidence for SO_3 formation in this system has never been reported to our knowledge; the fact that the ultraviolet and infrared spectra of SO_3 are uncertain and appear to contain no highly characteristic structure complicates its unambiguous identification. Conceivably, the primary product may be a metastable dimer of SO_2 ($O_2S\text{–}O\text{–}S\text{–}O$) or even the reactive tetroxide of sulfur (SO_4). Until further more definitive evidence of the nature of the SO_2 photoproducts is available, we will assume that SO_4^{2-} arises from the simplest, traditionally proposed product, SO_3.

($\Phi_{SO_3} \cong 0.04$,[5] 0.05[6]). At wavelengths greater than 2180 Å photodissociation of sulfur dioxide is energetically impossible, and it is probable that sulfur trioxide formation in this case results from an oxygen atom exchange reaction involving one of the electronically excited states of sulfur dioxide (SO_2^*)

$$SO_2^* + SO_2 \longrightarrow SO_3 + SO$$

It is surprising in view of the extensive kinetic data now available on the reactions of excited states of sulfur dioxide that the spin state of the excited molecule involved in reaction 10 cannot be determined. The work reported here provides this information for the first time.

The previous studies are consistent with the following reaction mechanism for SO_2 photolysis within the first allowed absorption band

$$SO_2 + h\nu \longrightarrow {}^1SO_2 \qquad (1a)$$

$${}^1SO_2 + SO_2 \longrightarrow (2SO_2) \qquad (1b)$$

$$\longrightarrow {}^3SO_2 + SO_2 \qquad (2)$$

$${}^1SO_2 \longrightarrow SO_2 + h\nu_f \qquad (3)$$

$$\longrightarrow SO_2 \qquad (4)$$

$$\longrightarrow {}^3SO_2 \qquad (5)$$

$${}^3SO_2 \longrightarrow SO_2 + h\nu_p \qquad (6)$$

$$\longrightarrow SO_2 \qquad (7)$$

$${}^3SO_2 + SO_2 \longrightarrow (2SO_2) \qquad (8)$$

The indeterminant product ($2SO_2$) in reactions 1 and 8 can be ground-state sulfur dioxide, SO_3 and SO, and/or possibly some other chemical products which do not regenerate any excited state of sulfur dioxide.[7] Although estimates of the rate constants for each of the reactions 1–8 have been made and quantum yields of sulfur trioxide determined, it remains impossible to establish the nature of the precursor to sulfur trioxide formation from the existing data. This can be seen from the following considerations. The above mechanism and recent data from sulfur dioxide photolyses at 2875 Å, 25°, and $P_{SO_2} \geq 200\ \mu$, suggest that the ratio of concentrations of triplet to excited singlet sulfur dioxide is given by[3a]

$$[{}^3SO_2]/[{}^1SO_2] \cong k_2/k_8 \cong 72$$

The rate constant data show that the rate of quenching of ${}^3SO_2$ is much slower than that for ${}^1SO_2$ in irradiated sulfur dioxide[3a]

$$\frac{\text{rate of } {}^3SO_2 \text{ quenching by } SO_2}{\text{rate of } {}^1SO_2 \text{ quenching by } SO_2} = \frac{[{}^3SO_2]k_8}{[{}^1SO_2]k_1} \cong 0.090$$

Since the measured quantum yield of sulfur trioxide is less than 0.09 (0.04–0.05), the quenching rate data do not shed any light on the state or states responsible for the sulfur trioxide formation. Either one or both could contribute to it.

In our previous work it was found that low pressures of biacetyl quenched efficiently the excited triplet sulfur dioxide molecules by energy transfer, reaction 9.

$${}^3SO_2 + Ac_2 \longrightarrow SO_2 + {}^3Ac_2 \qquad (9)$$

Under the same conditions the concentration of singlet molecules was not affected detectably.[3a] It became evident that a series of chemical experiments utilizing pure SO_2 and SO_2–biacetyl mixture photolyses could define the nature of the reactive excited state of sulfur dioxide.

We have determined the rates of photochemical formation of sulfur trioxide in a flow system using pure SO_2 (740 mm) and SO_2 (737 mm)–biacetyl (3.3 mm) mixtures at 25°. The data are summarized in Figure 1. There is a marked lowering of the rate of SO_3 formation in runs with added biacetyl. This lowering is not an artifact associated with the presence and reaction of the carbonyl compound with sulfur oxides, since within the experimental error there is no effect on the rate of sulfur trioxide formation with added acetone (9.5 mm) in the sulfur dioxide (730 mm). In this case of course the triplet energy (80.5 ± 1.5 kcal/mol)[8] is much higher than that of the sulfur dioxide (73.7 kcal/mole),[9] and triplet energy transfer from sulfur dioxide to acetone is expected to be very slow. The rate of sulfur trioxide formation is lowered with biacetyl addition to about 65% of that with pure sulfur dioxide photolysis. This result is in good agreement with that expected if the ${}^3SO_2$ is the only reactive precursor to sulfur trioxide formation. From the rate constants for reactions 8 and 9 measured previously ($k_8/k_9 = 2.7 \times 10^{-3}$),[3a] it can be calculated that about 63% of the triplet SO_2 molecules and less than 1% of the singlet molecules would be quenched by biacetyl addition at the concentrations employed here.

The present data lead to a somewhat higher estimate of the quantum yield of sulfur trioxide formation than that reported by Hall[5] and Warneck[6]; from the data of Figure 1, $\Phi_{SO_3} = 0.08 \pm 0.02$ for the band of wavelengths employed here (3126–2537 Å). This value is surprisingly close to our recent estimate of the quantum yield of triplet sulfur dioxide formation at 2875 Å; $\Phi_{^3SO_2} = 0.080 \pm 0.014$. The near equality of these two quantities may be somewhat fortuitous since the quantum yield of ${}^3SO_2$ may be wavelength dependent. However, all of the present data do establish that the ${}^3SO_2$ molecule is the dominant chemically active species which leads to sulfur trioxide in sulfur dioxide photolysis within the first allowed absorption band. The data further suggest that practically all of the triplets formed in the photolysis of pure sulfur dioxide at high pressures react to give sulfur trioxide product.

---

[8] R. F. Borkman and D. R. Kearns, *J. Chem. Phys.*, **44**, 945 (1966).

[9] G. Herzberg, "Molecular Spectra and Molecular Structure. III. Electronic Spectra and Electronic Structure of Polyatomic Molecules," D. Van Nostrand Co., Princeton, N. J., 1966, p 605.

The present results, coupled with considerations of energy requirements and spin conservation, favor the following more detailed description of reaction 8a.

$$^3SO_2 + SO_2 \longrightarrow SO_3 + SO(^3\Sigma^-) \qquad (8a)$$

With vibrationally relaxed triplet molecules, reaction 8a is exothermic by 26.1 kcal/mol. We are attempting to test the mechanism and the stoichiometry suggested by (8a) through kinetic spectroscopy of the presumed product SO using a doubled ruby laser to excite directly the triplet state of sulfur dioxide through absorption within a forbidden singlet–triplet band of SO_2.[10]

It will be most interesting to determine the spin state responsible for sulfinic acid formation in sulfur dioxide–hydrocarbon mixture photolysis. In this case the quantum yields of product climb from 0.006 for methane to 0.26 with pentane.[11] Unless a chain reaction is involved here, the singlet excited state must be an important reactant in this case, since the quantum yield of triplet sulfur dioxide formation is only 0.08.[3a] We are planning to investigate this system in an analogous fashion to that used in this study.

Experimental Section

The photolyses were carried out in a cylindrical quartz cell (4.4 cm diameter, 5.2 cm length). The initiating light was generated from a medium-pressure mercury arc (Hanovia, Type A, 673, 500 W), filtered through a Corning filter 7–54 (9863). The relative intensities of the different wavelengths of light absorbed by the SO_2 were as follows: 3126–32, 39%; 3022–28, 18%; 2967, 12%; 2894, 4%; 2804, 6%; 2753, 2%; 2700, 2%; 2652–5, 8%; 2571, 2%; and 2537 Å, 6%. Practically all of the light at each of the wavelengths was absorbed by sulfur dioxide in the pure SO_2, SO_2–Me_2CO, and SO_2–Ac_2 mixture photolyses and almost none by biacetyl or acetone for these conditions. Tank sulfur dioxide (Matheson Co.) was dried, freed from dust, and then passed through the photolysis cell at a rate of 10 cc/min. The SO_2 excess and the fraction of SO_3 product which remained gaseous flowed into two bubblers which were placed in series; each bubbler contained 10 cc of an aqueous solution (10% ethanol) which was 0.1 M in $HgCl_2$ and 1 M in HCl. Following the run, nitrogen gas (20 cc/min) was used to flush the system for 20 min.

The cell and associated glass tubing leading to the traps was disassembled after each run and the walls washed with small portions of the mercuric chloride solution. The stable complex formed between the mercuric chloride and sulfur dioxide retarded the thermal oxidation of SO_2 to SO_3 during analysis. The trap solutions and the wash solutions from the cell and tubing were analyzed separately by adding 210 mg of $BaCl_2 \cdot 2H_2O$ solid to each 10 cc of solution while it was magnetically stirred. The apparent optical density (usually 0.05–0.3) of the $BaSO_4$ suspension at 475 mμ was measured on a spectrophotometer after a regulated period of time. Calibration of the analytical system was made using known amounts of soluble sulfate salt under identical conditions. The method gave excellent reproducibility on known solutions.[12] Scatter observed in the photochemical data is believed to be a consequence of the difficulties inherent in the quantitative transport of SO_3 product to the analytical system. Usually the majority of the SO_3 product (~85%) appeared in the first trap with the majority of the remaining product divided between the cell and the connecting tubing between the cell and traps.

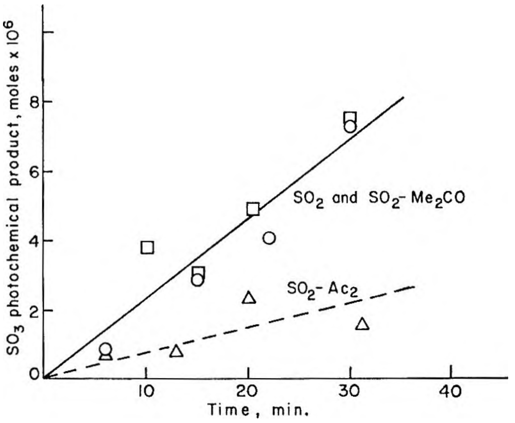

Figure 1. The time dependence of the product SO_3 (measured as SO_4^{2-}) which is formed photochemically (3126–2537 Å) in pure SO_2 at 740 mm, circles; in mixtures of SO_2 (730 mm) and acetone (9.5 mm), squares; and in mixtures of SO_2 (737 mm) and biacetyl (3.3 mm), triangles. Temperature, 25°; intensity of light absorbed by SO_2, 2.9 × 10^{16} quanta/sec.

In runs with added carbonyl compound the SO_2 gas was partially saturated with the desired vapor by leading the gas over a sample of either the pure biacetyl at 0° or acetone at −3.2°. About 30% of saturation was achieved for these conditions; the composition of the mixtures from run to run was found to be very reproducible. Analysis of the biacetyl–SO_2 mixtures was carried out by phosphorescence excitation using standard mixtures of Ac_2 and SO_2 and the Turner spectrophosphorimeter (Model 210). The acetone–SO_2 mixtures were analyzed chromatographically on a 10-ft Porapak-Q temperature-programmed column.

In the runs with added biacetyl and acetone a larger part of the SO_3 was found in the solution prepared from the cell washings. Apparently the polar vapors accentuated the condensation of SO_3 in these cases. Following the analysis of a given run and before each new run, the cell and connecting tubing were washed thoroughly, dried, reassembled, and evacuated overnight at a pressure of less than 10^{-4} mm.

---

[10] The absorption spectrum of SO has been observed in the flash photolysis of SO_2 by R. G. W. Norrish and G. A. Oldershaw, *Proc. Roy. Soc.*, **A249**, 498 (1959); however, in this study the authors attribute SO formation largely to the direct photodissociation of SO_2 at wavelengths shorter than 2200 Å present in the flash and to the photolysis of some high energy isomer of SO_2.

[11] F. S. Dainton and K. J. Ivin, *Trans. Faraday Soc.*, **46**, 374 (1950).

[12] The analytical system was based in part on the work of H. J. Keily and L. B. Rogers, *Anal. Chem.*, **27**, 759 (1955).

Dark runs were made which were identical in other respects with the photochemical runs. The amount of SO_3 derived from these experiments was considerably smaller than that formed photochemically and was very reproducible. For a dark run of given duration the amount of SO_3 formed thermally was the same for pure SO_2, SO_2–Me_2CO, and SO_2–Ac_2 mixtures within the experimental error. Correction for SO_3 formed thermally has been made in the data for the photochemical runs shown in Figure 1.

Actinometry was carried out using the potassium ferrioxalate system.[13] Correction was made in the quantum yield calculations for the 3650–60 and 3341-Å light present in the photolysis beam which was absorbed by the actinometer solutions but not by the SO_2. The light intensity absorbed by sulfur dioxide was essentially constant throughout the series of runs: 2.9×10^{-16} quanta/sec (3126–2537 Å).

Acknowledgment. The authors acknowledge gratefully the support of this work through a research grant from the National Air Pollution Control Administration, U. S. Department of Health, Education, and Welfare, Public Health Service, Arlington, Va. We are indebted to Professor Paul Urone (University of Colorado) for helpful suggestions which formed the basis for the development of the analytical system employed, and Dr. James W. Gall, who performed the SO_2–acetone mixture analyses.

---

[13] C. G. Hatchard and C. A. Parker, *Proc. Roy. Soc.*, **A235**, 518 (1956).

Anion Exchange of Metal Complexes.

XIX.[1] Volumetric Studies of the Exchanger in Mixed Solvents

by Y. Marcus,

Department of Inorganic and Analytical Chemistry, The Hebrew University, Jerusalem, Israel

J. Naveh, and Mayo Nissim

Israel Atomic Energy Commission, Nuclear Research Center-Negev, Israel *(Received June 30, 1969)*

In a recent paper[2] we reported the selective swelling of a divinylbenzene polystyrene–methylene–trimethylammonium salt copolymer (Dowex-1) in several aqueous organic solvent mixtures. This information is essential for an understanding of the factors affecting the sorption of metal complexes on the exchanger, which is of great practical importance. The applicability of anion exchange of metal complexes in mixed solvents depends, among other factors, on the rate of particle diffusion and on the dimensional stability of the column of resin, and these quantities depend, in turn, on the specific volume of the exchanger and on the solvent composition.

It is further expected that some useful information concerning the interaction of the water and organic solvent with resin functional groups can be obtained from a study of the partial molar volumes of these components as a function of composition. These, again, are obtainable from the specific volumes.

A study has therefore been undertaken of the density of the swollen resin, in equilibrium with a mixed solvent of known composition. The densities of 4 and 8% cross-linked resins in chloride form were measured in water and in aqueous methanol, ethanol, *n*-propyl alcohol, acetone, and formamide, at 22°.

Experimental Section

Densities were measured in 25-ml picnometers at 22 ± 1°, the displaced liquid being the equilibrium solution itself, the density of which was separately measured. In this way there is no fear from changes in the composition when the density of the swollen resin is measured. The effect of the temperature variations on the densities were within the reported experimental precision.

The characterization of the resin and other materials, the procedure for drying the resin, and other operations have been reported.[2]

Calculations

The specific volume, that is the volume per gram of dry chloride form of resin of a resin sample swollen in a mixed solvent, is given by

$$\bar{V} = \bar{V}_R + n_S\bar{V}_S' + n_W\bar{V}_W' \qquad (1)$$

where $\bar{V}_R$ is the specific volume of the resin skeleton with its functional groups, assumed invariant with solvent composition, n_S and n_W are the specific numbers of moles of solvent (S) and water (W), and V_S' and V_W' are the partial molar volumes, respectively. The specific swollen volume is obtained experimentally as

$$\bar{V} = (1.000 + n_S M_S + n_W M_W)/\bar{d} \qquad (2)$$

where M_S and M_W are the molecular weights and $\bar{d}$ the measured density of the swollen resin. The molar volume of the solvent in the resin is now obtained from

$$\bar{V}' = (\bar{V} - \bar{V}_R)/(n_S + n_W) = \bar{x}_S\bar{V}_S' + \bar{x}_W\bar{V}_W' \qquad (3)$$

while a reference molar volume is calculated as

$$V' = (n_S M_S + n_W M_W)/d(n_S + n_W) \qquad (4)$$

---

[1] Previous paper in series: Y. Marcus and E. Eyal, *J. Inorg. Nucl. Chem.*, submitted, 1969.

[2] Y. Marcus and J. Naveh, *J. Phys. Chem.*, **73**, 591 (1969).

Table I: Densities, Molar Volumes, and Molar Contraction of Aqueous Ethanol in Dowex-1 X-4 Chloride

x_S	$\bar{x}_S$	d, mg/ml	$n_S + n_W$, mmol/g	$n_SM_S + n_WM_W$, mg/g	$\bar{d}$, mg/ml	$\bar{V}'$ ml/mol	$-\Delta\bar{V}'$, ml/mol
0.1	0.135	950	55.5	1175	1052	21.0	1.26
0.2	0.190	933	52.8	1125	1046	21.4	1.36
0.3	0.205	929	48.0	1070	1044	22.6	1.42
0.4	0.230	921	42.8	990	1043	23.5	1.56
0.5	0.260	914	37.3	895	1042	24.6	1.64
0.6	0.305	901	32.1	810	1042	26.1	1.93
0.7	0.350	888	26.5	727	1040	28.7	2.07
0.8	0.485	860	22.9	680	1033	31.7	2.75
0.9	0.675	827	20.1	717	1008	40.0	2.93
~1.0	0.870	799	18.0	875	963	58.0	2.61

Table II: Molar Contractions of Solvents in Chloride-Form Anion Exchangers Swollen by the Neat Solvents (in ml/mol)

	Water		Methanol	Ethanol	n-Propyl alcohol	Acetone	Formamide
X-4[b]	2.60[a]	0.59	2.3	2.0		5.3	0.3
X-8[b]	2.42[a]	0.89	3.2	3.3	2.7	6.5	0.5
V[0c]	18.0		40.3	58.2	75.0	73.5	39.8

[a] Perchlorate form. [b] Nominal cross-linking. [c] Molar volume of the pure solvent.

where d is the density of a mixed solvent having a mole fraction $\bar{x}_S$ of solvent, $\bar{x}$ being the equilibrium mole fraction in the resin. The molar solvent contraction in the resin is now defined as

$$\Delta\bar{V}' = \bar{V}' - V' \tag{5}$$

and it measures the change of volume the solvent of composition $\bar{x}_S$ undergoes when it enters the resin. If the contraction ($\Delta\bar{V}'$ being negative) is thought to be due to electrostriction, then the partial molal electrostriction of the water in the resin is obtained from

$$\Delta\bar{V}_W' = \Delta\bar{V}' - \bar{x}_S(d\Delta\bar{V}'/d\bar{x}_S) \tag{6}$$

Results

The values of $\bar{V}_R$ required for the calculation (eq 3) were obtained by dodecane displacement[2] and are 898 μl/g for 4% cross-linked resin and 907 μl/g for 8% cross-linked resin.

Table I shows the quantities obtained experimentally ($\bar{x}$, d, and $\bar{d}$) and by calculation ($\bar{V}'$ and $\Delta\bar{V}'$) for one of the systems studied. The experimental accuracy attained can be estimated from these data. All the data obtained are shown in Figure 1 as plots of $\Delta\bar{V}'$ against $\bar{x}_S$. Unfortunately, the region above $\bar{x}_S = 0.9$ could not be measured, since the resin could not be dried completely in all cases. Since the curves are rather steep at high mole fractions of the solvent, the initial partial molar electrostriction of the solvent, $\lim \Delta\bar{V}_S'$ ($\bar{x}_S \rightarrow 1$), could not be calculated exactly. It could, however, be estimated to within 0.2 ml/mol by extrapolation of the curves to $\bar{x}_S = 1$, and is shown in Table II for the various solvents at the two cross-linkings studied.

Discussion

The use of picnometry in resin density measurements is well established,[3,4] although other methods such as sedimentation,[5] buoyancy weighing,[6] or microscopy[7] are also applicable. The former method was adequate for our purposes, and because of the good but still limited reproducibility of the resin samples, a precision in the densities higher than ±1 mg/ml was not warranted. Hydrocarbons are standard displacement fluids for water-swollen resins[3,4] and have also been used for dry resins.[2,4] We have observed a small amount of swelling (~2%) with dodecane for the dry resin, which was neglected.

The results in Table I and in Figure 1 show that the solvent in the resin contracts as compared to a solvent of similar composition outside the resin. The molar contraction increases as the concentration of the organic component increases. Since, however, the average molar volume of the solvent, V', increases also, the relative contraction $\Delta\bar{V}'/V'$ does not change very much in the water-rich region (at least for methanol, ethanol, and formamide). Indeed, the relative con-

---

(3) H. P. Gregor, K. M. Held, and J. Bellin, *Anal. Chem.*, **23**, 620 (1951).

(4) K. W. Pepper, D. Reichenberg, and D. K. Hale, *J. Chem. Soc.*, 3129 (1952).

(5) M. G. Suryaraman, Ph.D. Thesis, University of Colorado, 1962; M. G. Suryaraman and H. F. Walton, *Science*, **131**, 829 (1960).

(6) D. H. Freeman, private communication, 1962; G. Dickel, private communication, 1969.

(7) D. H. Freeman and G. Scatchard, *J. Phys. Chem.*, **69**, 70 (1965).

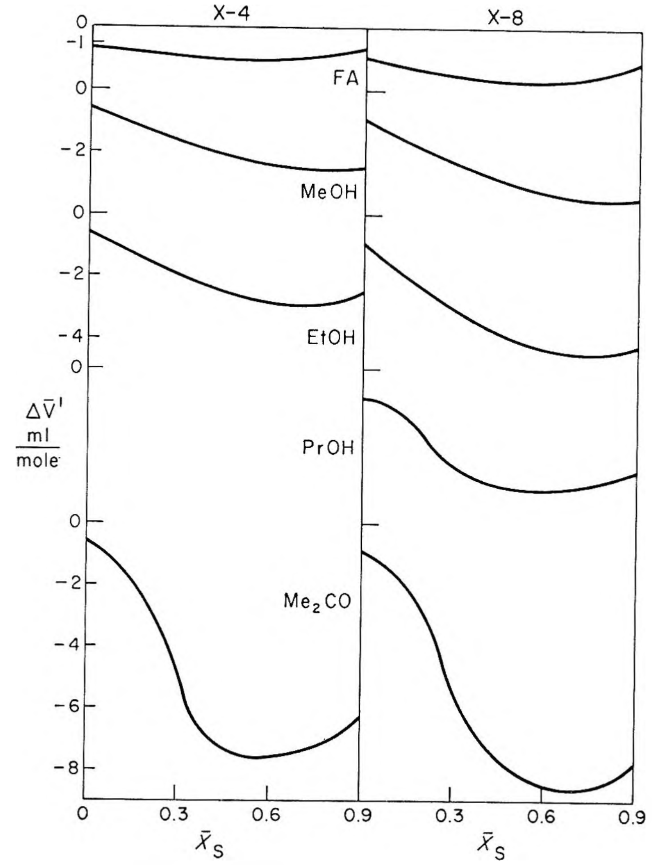

Figure 1. The molar contraction of solvents swelling X-4 (left hand side) and X-8 (right hand side) chloride form Dowex-1, as a function of solvent composition *inside the resin*. FA, formamide; MeOH, methanol; EtOH, ethanol; PrOH, *n*-propyl alcohol; Me$_2$CO, acetone.

traction decreases for all solvents when the concentration of water diminishes below *ca.* 40%.

The limiting molar contraction (Table II) is highest for acetone both absolutely and relatively, the relative contraction decreasing in the order (for X-8 resin) acetone > methanol > ethanol > water > propanol > formamide.

The contraction of water in a swollen cation exchange resin has been ascribed to electrostriction.[4,8–11] A molar contraction of water as high as 1.15 ml/mol has been noted for the H$^+$ or Mg^{2+} forms of a polystyrenesulfonate resin as an average at relative humidities of above 45%. The first molecule of water sorbed per functional group in a cation exchanger suffers even more electrostriction than that,[8] but as swelling proceeds, and as soon as there is some free water in the system, the partial molar volume of water becomes again equal to its molar volume in the pure state.

In the present case of mixed aqueous–organic solvents in anion exchangers, electrostriction is again larger for the less highly swollen form of the resin, *i.e.*, perchlorate compared with chloride (data for water in Table II), and X-8 resin compared with X-4 (for cation exchangers the cross-linking effect is small[9]). As the concentration of water decreases in the resin, the partial molar electrostriction of water $\Delta\bar{V}_W'$, estimated by the intercept method, becomes very large. This points to a strong preferential hydration of the ions in the resin. That means that even if the total sorption of solvent in the resin may not show a great preference to water at low water concentrations,[2] whatever water is present is in the vicinity of the ions and is influenced by their electric field. The higher the positive slope of the right-hand part of the curves in Figure 1, the stronger is the effect.

It is puzzling that acetone should show such a large contraction. Its carbonyl group must interact strongly with the resin, permitting it a much denser packing than in the neat liquid or in aqueous solutions, but there is no apparent reason for this. The consequence of this, however, is that exchange in acetone-swollen resins becomes very slow, which is a disadvantage when the enhanced selectivity of the resin for anions in acetone[1] is to be utilized.

(8) K. W. Pepper and D. Reichenberg, *Z. Elektrochem.*, **57**, 183 (1953).

(9) H. P. Gregor, B. R. Sundheim, K. M. Held, and M. H. Waxman, *J. Coll. Sci.*, **7**, 511 (1952); H. P. Gregor, F. Gutoff, and J. I. Bergman, *ibid.*, **6**, 245 (1951).

(10) G. E. Boyd and B. A. Soldano, *Z. Elektrochem.*, **57**, 162 (1953).

(11) E. Högfeldt, *Acta Chem. Scand.*, **12**, 182 (1958).

Electron Spin Resonance Study of Ultraviolet-Irradiated Di-*t*-butyl Peroxide in the Frozen State[1]

by P. Svejda and D. H. Volman

Department of Chemistry, University of California, Davis, California 95616 *(Received July 8, 1969)*

Recently, Krusic and Kochi[2] have shown that the photolysis of liquid solutions of di-*t*-butyl peroxide in alkyl hydrocarbons yields esr spectra of the hydrocarbon radicals produced *via* hydrogen atom abstraction, presumably by the *t*-butoxy radical formed in the primary process. Independently, Adams[3] reported the esr spectra of α-hydroxy alkyl radicals formed in the photolysis of liquid solutions of di-*t*-butyl peroxide in alcohols or alcohols and isooctane. In the photolysis of solid solutions of the peroxide in 3-methylpentane, Shida[4] observed the spectrum of methyl radicals, at-

(1) This investigation was supported by a grant from the National Science Foundation.

(2) (a) P. J. Krusic and J. K. Kochi, *J. Amer. Chem. Soc.*, **90**, 7155 (1968); (b) J. K. Kochi and P. J. Krusic, *ibid.*, **90**, 1757 (1968).

(3) J. Q. Adams, *ibid.*, **90**, 5363 (1968).

(4) T. Shida, *J. Phys. Chem.*, **72**, 723 (1968).

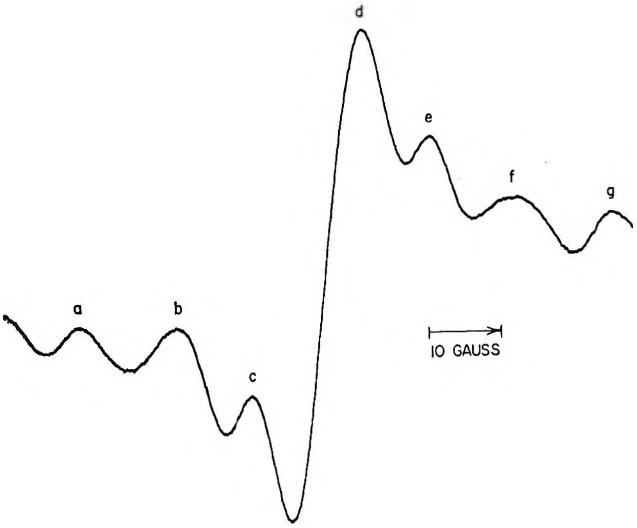

Figure 1. Electron spin resonance spectrum of di-*t*-butyl peroxide irradiated 5 min at 77°K.

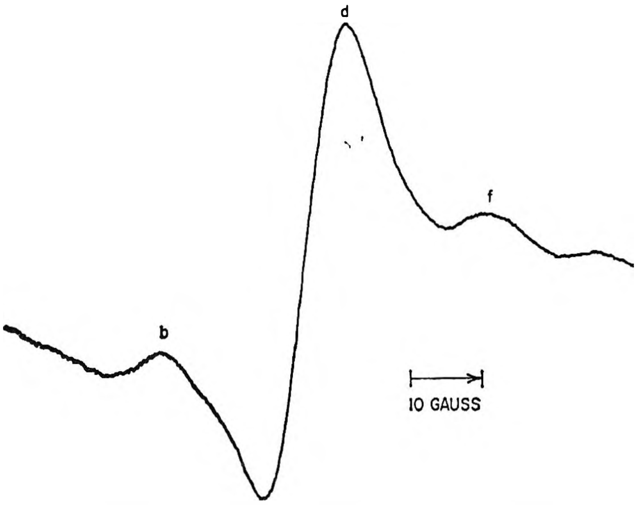

Figure 2. Electron spin resonance spectrum of di-*t*-butyl peroxide, irradiated 5 min at 77°K, after 72 hr at 77°K.

tributed to the decomposition of *t*-butoxy radicals, and of 3-methylpentyl radicals, attributed to H-atom abstraction. In the photolysis of the peroxide at −70°, Weiner and Hammond[5] found the esr spectrum of *t*-butoxy radicals. In contrast, Ingold and Morton[6] found no free radicals by esr in the uv irradiation of the peroxide at 77°K and Maguire and Pink[7] found no free radicals in the uv irradiation of the peroxide or solutions of the peroxide in hydrocarbons at 77°K.

For the photolysis of di-*t*-butyl peroxide,[8] the following reactions yielding different free radicals are postulated

$$\mathrm{(CH_3)_3COOC(CH_3)_3} + h\nu \longrightarrow \mathrm{2(CH_3)_3CO\cdot} \qquad (1)$$

$$\mathrm{(CH_3)_3CO\cdot} \longrightarrow \mathrm{CH_3COCH_3} + \mathrm{\cdot CH_3} \qquad (2)$$

$$\mathrm{\cdot R_1[(CH_3)_3CO\cdot\ or\ \cdot CH_3]} + \mathrm{(CH_3)_3COOC(CH_3)_3} \longrightarrow \mathrm{R\dot{C}H_2[(CH_3)_3COOC(CH_3)_2\dot{C}H_2]} + \mathrm{R_1H} \qquad (3)$$

For the initial stages of photolysis where reactions involving products are negligible, three free radicals are expected: $\mathrm{(CH_3)_3CO\cdot}$, $\mathrm{\cdot CH_3}$, $\mathrm{R\dot{C}H_2}$. In esr studies which we have carried out on uv-irradiated frozen samples of di-*t*-butyl peroxide, evidence for all three radicals was obtained. Moreover, the results yield a striking confirmation of the postulated photochemical mechanism.

Di-*t*-butyl peroxide, purified by vpc, at 77°K irradiated at 254 nm for 5 min gave the esr spectrum shown in Figure 1. Evidence for the three free radicals is present. Peaks a, c, e, and g are a 1:3:3:1 quartet with an average spacing of 25 G, characteristic for $\mathrm{\cdot CH_3}$. Peaks b, d, and f, are a triplet, *ca.* 1:6:1 intensity ratios with average spacing of 24 G. $\mathrm{R\dot{C}H_2}$ would give a 1:2:1 triplet with this spacing. *t*-Butoxy radicals give a singlet esr spectrum.[5] Thus the intensity ratios observed for b, d, and f are indicative of a singlet superimposed on a triplet. This argument is reinforced by the fact that the intensity ratios observed in the frozen state are never more than the theoretical values and quite often less. After 72 hr storage at 77°K, the spectrum shown in Figure 2 was obtained. The methyl radical spectrum is virtually absent while the intensity of the central line has increased and the intensity of the outer lines of the triplet has decreased. This can occur through the previously postulated photolysis reaction[8c]

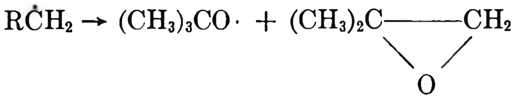

$$\mathrm{R\dot{C}H_2} \rightarrow \mathrm{(CH_3)_3CO\cdot} + \mathrm{(CH_3)_2C\underset{O}{\diagdown\!\diagup}CH_2} \qquad (4)$$

If the irradiated sample was warmed rather than stored at 77°K, similar results were obtained. Upon raising the temperature to 87°K, the methyl radical spectrum disappeared in a few minutes. The center line did not diminish in intensity at temperatures up to about 115°K but was weakening appreciably at 150°K and was gone when the temperature reached 185°K.

Ingold and Morton[6] reported that traces of *t*-butyl hydroperoxide, a common impurity in di-*t*-butyl peroxide, give rise to peroxy radicals on uv irradiation. The central line of our esr spectrum has a *g* value of 2.004, indentical with that reported for the *t*-butoxy radical, while the *t*-butyl peroxy radical has a *g* value of 2.015.[5] The absence of peroxy radicals in our spectrum thus indicates both that they are not formed in the photolysis of the peroxide and that the results cannot be attributed to impurities.

Our results are explicable if one takes into account that, if the excess energy of the quantum is equiparti-

---

(5) S. Weiner and G. S. Hammond, *J. Amer. Chem. Soc.*, **91**, 2182 (1969).

(6) K. U. Ingold and J. R. Morton, *ibid.*, **86**, 3400 (1964).

(7) W. J. Maguire and R. C. Pink, *Trans. Faraday Soc.*, **63**, 1097 (1967).

(8) (a) L. M. Dorfman and Z. W. Salsburg, *J. Amer. Chem. Soc.*, **73**, 255 (1951); (b) D. H. Volman and W. M. Graven, *ibid.*, **75**, 3112 (1953); (c) G. R. McMillan, *ibid.*, **82**, 2422 (1960).

tioned between two *t*-butoxy free radicals, each radical will have about 36 kcal of excess energy. In the solid at low temperature, dissipation of this energy will be relatively slow and, hence, decomposition to yield methyl radical or H-atom abstraction by "hot" radicals can occur.

The absence of the spectrum of radicals, other than those resulting from H-atom abstraction for the studies in liquid solutions,[2,3] is obviously due to the rapid reaction of *t*-butoxy radicals at these temperatures. Our results on storage of an irradiated sample at 77°K or warming are in agreement with those of Weiner and Hammond[5] indicating a short lifetime for alkyl relative to alkoxy radicals in the frozen solid. The results of Shida[4] are consistent with our observation that methyl radicals are formed by decomposition of excited *t*-butoxy radicals and that *t*-butoxy radicals abstract hydrogen atoms at 77°K. One can only speculate on the reasons for the negative results obtained in the other studies.[6,7] It may, however, be observed that in both of these investigations, irradiations were carried out with the sample in the cavity with, perhaps, low intensity sources, experimental conditions which could lead to weak absorption and, hence, undetectable signals.[9]

NOTE ADDED IN PROOF. M. C. R. Symons [*J. Amer. Chem. Soc.*, (9) 91, 5924 (1969)] has suggested on theoretical grounds that the spectrum found by Weiner and Hammond[5] is not that of the *t*-butoxy radical but is instead that of the ozonide radical, $(CH_3)_3COOO$, possibly formed by the reaction of *t*-butoxy with molecular oxygen. These arguments would apply also to the central line of our spectra although we thoroughly excluded dissolved gases from our samples. However, a possible source of oxygen may be from a primary process in the photolysis for which Frey [*Proc. Chem. Soc.*, 385 (1959)] has given evidence.

A Redetermination of the Thermoelectric Properties of the Bismuth–Bismuth Bromide System[1]

by Jordan D. Kellner,[2] S. J. Yosim, and L. E. Topol

Atomics International Division of North American Rockwell Corp., Canoga Park, California 91304 *(Received March 6, 1969)*

The initial and steady-state thermoelectric potentials of bismuth–bismuth halides were determined previously[3a,b] in this laboratory. The steady-state potentials per degree of thermal gradient $(\Delta E/\Delta T)_{st}$ were unusually large in dilute metal solutions; *e.g.*, for the Bi–BiBr$_3$ system it was as high as $-16{,}000$ μV/deg at 1% Bi. (The sign of the thermoelectric potential corresponds to the sign of the hot electrode and is consistent with the higher activity of Bi$^+$ in the hot side.) This was attributed to the Soret effect. However, in more recent experiments carried out in this laboratory it was shown that these high potentials were not due to the Soret effect but from a compositional change caused by distillation of the solvent.

This investigation reports evidence for this conclusion as well as a redetermination of the thermoelectric power of Bi–BiBr$_3$ solutions in cells in which no vapor was transported across the temperature gradient.

Experimental Section

Bismuth tribromide and bismuth metal were treated as described previously.[3a,b] The cell in which a vapor path existed across the thermal gradient has been described elsewhere.[3b] In addition, three types of cells in which no vapor transport was permitted across the thermal gradient were used.

The first, in which most of the Soret redeterminations were measured, was a vertical one. These cells were constructed from 10-mm diameter Pyrex tubing at one end of which a tungsten disk of approximately equal diameter was sealed. A tungsten lead was joined to the disk with silver paint and Sauereisen cement and a chromel–alumel thermocouple contacted the disk. A thermocouple well and a tungsten electrode were sealed into the tube about 1 cm above the tungsten disk. Temperature gradients ranging mostly from 1 to 7° were imposed on the cell between the tungsten disk and the upper electrode. To minimize convection, thoria powder (100 mesh), an inert high-density material, was added to the cell. It was within this layer of powder at the bottom of the cell that the thermal and concentration gradients were established. Experiments with the redesigned cells were run under argon and *in vacuo*. An experiment was also run in a cell containing 50-mesh sintered glass powder as a convection inhibitor instead of thoria powder.

The second type of cell was also a vertical one where a medium porosity glass frit between the tungsten wire electrodes was used to maintain the thermal and concentration gradients.

The third type, because of its shape, was designated as a J-cell and contained a vertical, medium-porosity frit at the bottom between the tungsten wire electrodes. After both sides of the cell were loaded with the appropriate amounts of salt and metal, the cell was evacuated and sealed off. Since no vapor connection was present, no salt distilled from the hot to the cold side.

Results and Discussion

The results of the following experiments suggest that the large voltages are caused by distillation.

(1) Cells similar to those used in the previous studies[3a,b] (*i.e.*, with a vapor path between the hot and

---

[1] This research was supported in part by the U. S. Atomic Energy Commission.

[2] Hamilton Standard Division, United Aircraft Corp., Windsor Locks, Conn. 06096.

[3] (a) J. D. Kellner, *J. Phys. Chem.*, **70**, 2341 (1966); (b) J. D. Kellner, *ibid.*, **71**, 2434 (1967).

Table I: Initial and Steady-State Thermoelectric Potentials of Bi–$BiBr_3$ Cells

Run	Mol % Bi	Temp, °C	$(\Delta E/\Delta T)_{in}$,[a] μV/deg	$(\Delta E/\Delta T)_{st}$,[a] μV/deg	Cell type
1	3	450	+10 ± 10[b]	+40 ± 3[b]	1[d]
2	3	400	0 ± 5	+50 ± 10	1[c,d]
3	3	400	0 ± 2	+23 ± 2	1[c,d]
4	3	500	0 ± 4	+50 ± 8	3[d]
5	5	430	−37 ± 7	−9 ± 9	1
		395	−45 ± 2	−13 ± 3	
		300	−65 ± 7	−40 ± 10	
6	10	416	−53 ± 4	−33 ± 3	
		327	−74 ± 1	−68 ± 1	1[d]
		270	−84 ± 1	−79 ± 6	
7	10	400	−80 ± 5	−53 ± 15	2[d]
8	20	440	−72 ± 5	−52 ± 2	1
9	20	400	−66 ± 1	−50 ± 3	1[d]
10	30	415	−34 ± 1	−32 ± 2	1
		300	−84 ± 4	−83 ± 2	1
11	50	390	+35 ± 5	+35 ± 5	1

[a] These values are not corrected for the thermoelectric potential contribution of the tungsten electrodes. This correction would add about +8 to +14 μV/deg for the temperature range 270–500°. [b] The ± symbol indicates the range of values obtained for the conditions described. [c] Sintered glass powder used instead of thoria. [d] Vacuum instead of argon.

cold compartments) and containing 3% Bi were filled with $^1/_2$ and $^2/_3$ atm of argon. For both cells, the attainment of potentials half those of the steady-state value took twice as long and the steady-state thermoelectric potentials (−5 to −7 mV/deg) were about $^1/_2$ to $^1/_3$ of the earlier values.

(2) Changes in melt level were observed visually in several cells with ΔT's of 10° or more. Refluxing in the cells should give rise to a decrease in the melt level of the hot half-cell if the flow back through the frit is slow relative to the distillation rate.

(3) An experiment was run with a cell of different geometry. The vapor-phase connection tube was the same size as before (about 10 mm) but the diameter of the solution chambers was about 50% larger. Thermoelectric effects of only −1000 μV/deg were measured with this cell.

(4) In a cell with no vapor connection between the hot and cold compartments (the J-cell) a steady-state thermoelectric potential of about 50 μV/deg for 3% Bi–$BiBr_3$ was obtained. In addition, the sign of the potential was positive, opposite to that measured in the vapor-phase cells.

Thus, it appears that the large thermoelectric powers reported earlier[3a,b] for the Bi–BiX_3 systems were not due to the Soret effect but rather to a distillation process. This is plausible since the solvent $BiBr_3$ (boiling point = 453°) has an appreciable vapor pressure at the temperatures of measurement. Further, the solute BiBr is known to have only a slight vapor pressure[4] at these temperatures and should not be transported through the vapor in any significant amount. Thus it is concluded that the $BiBr_3$ distills to the cold side of the cell, and solution flows through the frit from the cold to the hot compartment due to the resulting hydrostatic head. This results in the solute being diluted in the cold side and concentrated in the hot side, forming a concentration cell. The unexpected result is that the distillation is sufficient to yield a significant steady-state potential even at a temperature difference of only 1° where the difference in vapor pressure of the $BiBr_3$ at the temperatures of these experiments, *e.g.*, 400°, is only 7 Torr.

Since the above thermocell effect arises from distillation, it should not be a unique property of the Bi–BiX_3 systems; any aqueous or nonaqueous ionic system containing one volatile and one nonvolatile component should behave similarly. An experiment was performed to confirm that an aqueous solution could be unmixed by the above distillation mechanism. An aqueous blue $CuSO_4$ solution in a U-tube with a frit at the bottom and a tube connecting the two legs in the vapor phase at the top was monitored visually. One side of the apparatus was heated slowly; a head of colorless liquid soon formed in the cool leg, and after several hours that side of the cell became completely colorless.

In another experiment, a Cu–CuCl cell was run. With ΔT's of 5 to 10° the voltage increased and reached steady-state values of over 100 mV. The hot electrode was positive in agreement with the higher copper ion activity being present at this electrode.

Redetermination of the Thermoelectric Potentials. Since the previous Soret results for solutions of low metal composition were in error, the thermoelectric potentials of the Bi–$BiBr_3$ system were measured in vertical cells with no vapor path across the thermal gradient. The results are shown in Table I where it can be seen that the steady-state thermoelectric potentials are smaller by as much as 2 orders of magnitude and less negative when no vapor phase transport can occur. In general, the emf's are not sufficiently reproducible to warrant a quantitative discussion. However, the fact that the sign of the steady-state potential is, in general, less negative than the initial potential indicates that the lower-valent Bi species has accumulated in the cold side of the cell in contrast to previous results[3a,b] in which the hot side became enriched with this species. As before, the amount of thermal diffusion decreased with increasing bismuth concentration until it was essentially zero. This behavior is again attributed to the electron exchange mechanism which becomes important in solutions of 30% or more Bi and renders a Bi$^+$ indistinguishable from a Bi^{3+} as far as diffusion is concerned.

---

(4) D. Cubicciotti, *J. Phys. Chem.*, 64, 1506 (1960).

Recently, Ichikawa and Shimoji[5] measured the thermoelectric powers of these solutions. Their absolute values for the steady-state thermoelectric powers of dilute solutions were considerably smaller than those reported earlier.[3b] For example, in a 10 mol % solution they report $(\Delta E/\Delta T)_{st}$ to be -340 μV/deg, while the value reported in reference 3b was -5000 μV/deg. They attributed the difference to the graphite electrodes used instead of tungsten.[3b] However, we found that results with the vapor path cells were the same with graphite or tungsten electrodes. Our explanation of their smaller results is that their experiments were run in argon, which decreases the distillation rate, and the vapor path in their cell is longer. As noted above, we obtained smaller absolute thermoelectric potentials when our vapor path cells contained argon. Thus their results must also be considered to be in error due to vapor-phase transport.

---

(5) K. Ichikawa and M. Shimoji, *Ber. Bunsenges. Phys. Chem.*, **71**, 1149 (1967).

On the Surface Tension of Fused Salt Mixtures

by George L. Gaines, Jr.

General Electric Research and Development Center, Schenectady, New York 12301 *(Received June 6, 1969)*

Despite the availability[1] of extensive experimental data on the surface tension of fused salt mixtures, there seems to be little theoretical basis for their interpretation.

Several workers have noted that deviations from linear or ideal mixing expressions can be correlated with differences in ionic radii.[2-5] The importance of ionic size in the thermodynamic properties of fused salt mixtures has also been recognized.[6]

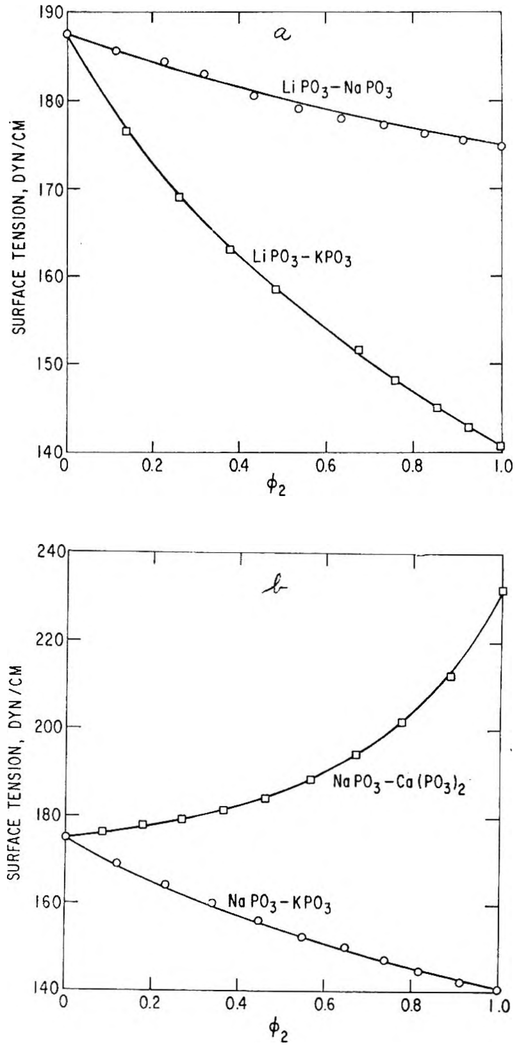

Figure 1. Surface tension of (a) $LiPO_3$–$NaPO_3$, $LiPO_3$–KPO_3 and (b) $NaPO_3$–KPO_3, $NaPO_3$–$Ca(PO_3)_2$ mixtures, at 1000°, plotted against volume fraction of second component. Points, data of Nijjhar and Williams;[10] lines, eq 1 with constants listed in Table I.

I have found recently[7] that equations based on simple lattice model calculations give good fits for the concentration dependence of surface tension in a wide variety of liquid mixtures. Comparison of several sets of data for fused salt mixtures with these equations also shows

---

(1) I. D. Sokolova and N. K. Voskresenskaya, *Russ. Chem. Rev.*, **35**, 500 (1966).

(2) N. K. Boardman, A. R. Palmer, and E. Heymann, *Trans. Faraday Soc.*, **51**, 277 (1955).

(3) J. L. Dahl and F. R. Duke, *J. Phys. Chem.*, **62**, 1142 (1958).

(4) G. Bertozzi and G. Sternheim, *ibid.*, **68**, 2908 (1964).

(5) G. Bertozzi, *ibid.*, **69**, 2606 (1965).

(6) O. J. Kleppa and L. S. Hersh, *J. Chem. Phys.*, **34**, 351 (1961); G. N. Papatheodorou and O. J. Kleppa, *ibid.*, **47**, 2014 (1967).

(7) G. L. Gaines, Jr., *Trans. Faraday Soc.*, **65**, 2320 (1969).

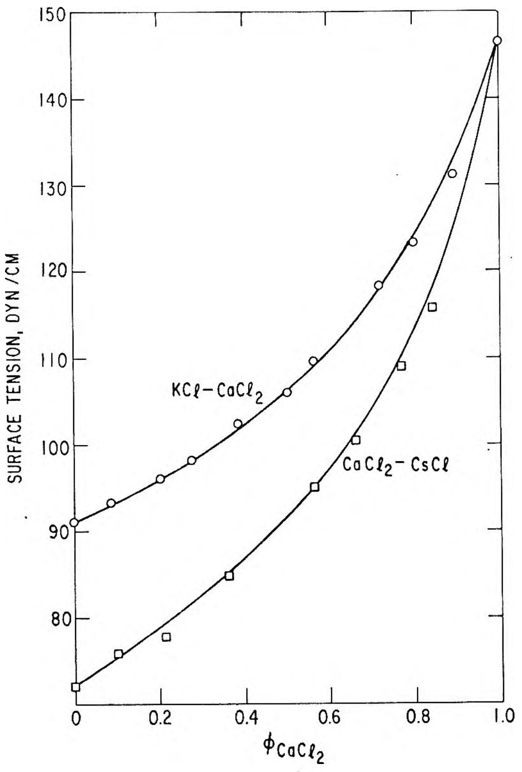

Figure 2. Surface tension of KCl-CaCl$_2$ and CaCl$_2$-CsCl mixtures, at 900°, plotted against volume fraction of CaCl$_2$. Points, data of Lehman[11] lines, eq 1 with constants listed in Table I.

excellent agreement. In this communication, this observation is presented and its implications are discussed.

Treatment of Data and Results

Defay, Prigogine, and their collaborators[8] have developed equations for the surface tension of mixtures of molecules of different sizes, using a lattice model. I have used a simple extension of their athermal solution case, adding a single energy parameter in the derivation.[9] The resulting equations are

$$\gamma = \gamma_1{}^0 + \frac{kT}{a}\left[\ln\frac{\varphi_1{}^s}{\varphi_1} + \frac{r-1}{r}(\varphi_2{}^s - \varphi_2)\right] - \frac{\beta}{a}(\varphi_2)^2 =$$

$$\gamma_2{}^0 + \frac{kT}{ra}\left[\ln\frac{\varphi_2{}^s}{\varphi_2} + (r-1)(\varphi_2{}^s - \varphi_2)\right] - \frac{\beta}{a}(\varphi_1)^2 \qquad (1)$$

and

$$\frac{\varphi_1{}^s}{\varphi_1} = \left(\frac{\varphi_2{}^s}{\varphi_2}\right)^{1/r} \exp\frac{(\gamma_2{}^0 - \gamma_1{}^0)a}{kT} \exp\frac{\beta}{kT}(1 - 2\varphi_1)$$

where φ_i = volume fraction of component i in bulk, $\varphi_i{}^s$ = volume fraction of component i in surface layer, r = ratio of size of component molecules, a = area per molecule (of smaller size) in surface lattice, γ = surface tension of mixture, $\gamma_i{}^0$ = surface tension of pure component i, and β is the energy parameter. If β is adjustable, these equations can be fitted to experimental data as previously described.[7,9]

Table I: Fit of Eq 1 to Surface Tension of Fused Salt Mixtures

System[a]	a, Å^2	r	Best β/kT	Max deviation, dyn/cm
		Phosphates 1000°		
Li–Na	16.8	1.157	0.034	See Figure 1
Li–K	16.8	1.407	0.129	
Na–K	18.5	1.215	0.112	
Na–Ca	18.5	1.697	0.523	
		Chlorides 900°		
K–Ca	19.38	1.064	0.390	See Figure 2
Ca–Cs	20.2	1.222	0.442	
		Nitrates 400°		
Li–K[b]	16.55	1.365	0.194	0.2
Li–Rb[b]	16.55	1.518	0.293	0.2
Li–Cs	16.55	1.695	0.338	0.5
Li–Ag	16.55	1.112	0.198	0.4
Na–K	18.06	1.198	0.070	0.1
Na–Rb	18.06	1.333	0.121	0.4
Na–Cs	18.06	1.488	0.168	0.2
K–Rb	20.37	1.112	0.030	0.1
K–Cs	20.37	1.242	0.005	0.3
Ag–Na	17.77	1.024	0.285	0.6
Ag–K	17.77	1.227	0.473	0.3
Ag–Rb	17.77	1.365	0.482	0.4
Ag–Cs	17.77	1.524	0.392	0.8
		Carbonates 900°		
Na–K	20.09	1.345	0.167	0.5

[a] Salt listed first in each pair has smaller molar volume and is considered "solvent." [b] Indicates minimum in experimental data.

Data for several mixtures of metaphosphates,[10] chlorides,[11] nitrates,[4] and carbonates[12] were selected for test. Mole fractions were converted to volume fractions using the densities of the pure components, assuming no volume change on mixing. Density data (extrapolated where necessary) were taken from the literature.[12,13]

The constants $a = (V_1{}^m/N)^{2/3}$ and $r = (V_2{}^m/V_1{}^m)$ were evaluated from the molar volumes (V^m) using the same density values. Fitting of (1) to the data was ac-

---

(8) I. Prigogine and J. Marechal, *J. Colloid Sci.*, **7**, 122 (1952); R. Defay, *J. Chim. Phys.*, **51**, 299 (1954); R. Defay, I. Prigogine, A. Bellemans, and D. H. Everett, "Surface Tension and Adsorption," John Wiley and Sons, Inc., New York, N. Y., 1966, Chapter 13.

(9) G. L. Gaines, Jr., *J. Phys. Chem.*, **73**, 3143 (1969).

(10) R. S. Nijjhar and D. J. Williams, *Trans. Faraday Soc.*, **64**, 1784 (1968).

(11) D. S. Lehman, *Diss. Abstr.*, **20**, 1192 (1959).

(12) G. J. Janz and M. R. Lorenz, *J. Electrochem. Soc.*, **108**, 1052 (1961).

(13) (a) Phosphates, D. J. Williams, *J. Soc. Glass Tech.*, **43**, 352T (1959); (b) Chlorides and nitrates, G. J. Janz, "Molten Salts Handbook," Academic Press, New York, N. Y., 1967.

complished by numerical approximation using computer programs,[14] as previously described.[7,9]

The data for phosphate and chloride mixtures, for which a considerable number of points over the whole concentration range are available, are plotted in Figures 1 and 2. Parameters used to plot the solid lines, according to (1), are given in Table I. For the nitrates and carbonates, experimental results for only 3 or 4 different compositions in each system are given in the sources used. For this reason, plots are not shown, but the best values of β required to fit the data are given in Table I, along with the maximum deviations between the experimental and calculated values.

Discussion

In all of the common anion systems examined, agreement between experimental results and the composition dependence predicted by (1) is within experimental error. Furthermore, the required values of β are, in all cases but one, less than $0.5kT$. One reciprocal system, KCl–NaI,[15] was also examined, but quantitative agreement with (1) was not obtained. It would also obviously be impossible to obtain agreement with the highly structured surface tension isotherms obtained in such systems as $KBr–CdCl_2$.[16]

Clearly, the application of (1) to fused salt mixtures is theoretically indefensible. The present results, however, suggest that these equations may have utility as empirical interpolation formulas. Moreover, the fact that such good fits are obtained, when the salt molar volumes differ by up to 70%, may imply that the entropy calculation inherent in the derivation of (1) does have some relevance to fused salt systems. It is suggested, therefore, that a lattice model calculation allowing for disparate ionic size might be usefully incorporated in a valid theoretical treatment of the thermodynamic properties of fused salt mixtures.

---

(14) Programs, in BASIC, available from the author on request.

(15) H. Bloom, F. G. Davis, and D. W. James, *Trans. Faraday Soc.* 56, 1179 (1960).

(16) R. B. Ellis, J. E. Smith, W. S. Wilcox, and E. H. Crook, *J. Phys. Chem.*, 65, 1186 (1961).

Concentration Dependence of Heats of Transfer between Heavy and Normal Water[1]

by Jerome Greyson and Harriet Snell

Rocketdyne Division, North American Rockwell Corporation, Canoga Park, California *(Received July 11, 1969)*

In a recent publication, determinations of entropies of transfer for alkaline earth chlorides passing between heavy and normal water were reported.[2] Based on the values, it was concluded that with the exception of magnesium, the alkaline earth cations behave as structure breakers in the transfer process, with the order of effectiveness being $Ba^{2+} > Sr^{2+} > Ca^{2+} > Mg^{2+}$. The structure-breaking characteristics were attributed to long-range interactions with bulk solvent (Samoilov's "distant hydration"[3]) as contrasted to primary solvation, the effects of which, it was suggested, cancel in the transfer between the isotopic solvents. As an argument in support of the conclusion, it was pointed out that distant hydration, as a primary influence in the transfer process, should lead to a strong concentration dependence for the entropies of transfer. That is, as the concentration of bulk solvent decreases relative to that of solvent engaged in primary solvation, the absolute value of the entropy of transfer would be expected to decrease also; and indeed, although not stated explicitly, such decreases in transfer entropy were observed by Wu and Friedman in measurements of concentration effects for some alkali halides.[2,4] Thus, the purpose of the work reported in this note is to investigate the concentration dependence of the entropy of transfer and the influence of distant hydration in solutions of alkaline earth chlorides. However, since it has been noted in all the related work reported to date that the entropy of transfer for salts passing between heavy and normal water is dominated by the heat of transfer, even in concentrated solutions, inferences relative to structure effects can be made from heat measurements alone.[2,4,5] Therefore, the measurements reported here are limited to a determination of the concentration dependence of the heat of transfer only.

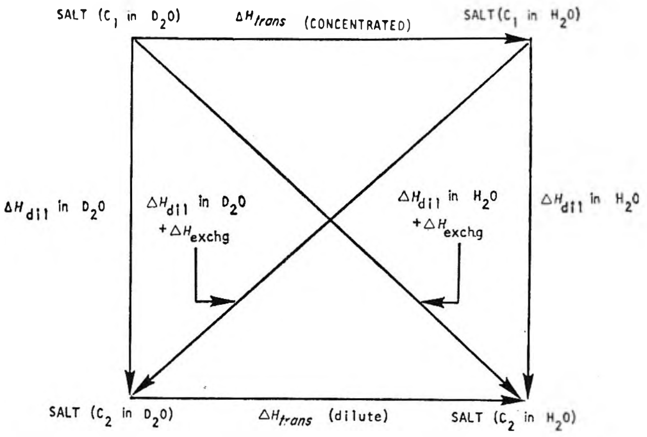
SALT (C_1 in D_2O)
ΔH_{trans} (CONCENTRATED)
SALT(C_1 in H_2O)
ΔH_{dil} in D_2O
ΔH_{dil} in D_2O $+\Delta H_{exchg}$
ΔH_{dil} in H_2O $+\Delta H_{exchg}$
ΔH_{dil} in H_2O
SALT (C_2 in D_2O)
ΔH_{trans} (dilute)
SALT (C_2 in H_2O)

Figure 1. Schematic of dilution processes for measurement of ΔH_{trans}.

---

(1) This research was supported by the Research Division of the Office of Saline Water, U. S. Department of the Interior, under Contract No. 14-01-0001-1701.

(2) J. Greyson and H. Snell, *J. Phys. Chem.*, 73, 3208 (1969).

(3) O. Ya. Samoilov, "Structure of Aqueous Solutions," Consultants Bureau, New York, N. Y. 1965, pp 74–82.

(4) Y. C. Wu and H. L. Friedman, *J. Phys. Chem.*, 70, 166 (1966).

(5) E. M. Arnett and D. R. McKelvey, "Solvent Interactions," J. Coeffee and C. D. Ritchie, Ed., Interscience Publications, New York, N. Y., in press.

Table I: Concentration Dependence of the Heat of Transfer for the Process: Salt (D_2O) → Salt (H_2O)

Salt	Concentration[a]	ΔH, cal/mol	Concentration[a]	ΔH, cal/mol
$MgCl_2$	0.0480	−751 ± 25	5.17	−634 ± 30
$CaCl_2$	0.0491	−1050 ± 25	5.29	−824 ± 24
$SrCl_2$	0.0302	−1220 ± 21	3.00	−1014 ± 20
$BaCl_2$	0.0140	−1363 ± 29	1.40	−1228 ± 29

[a] Concentration units are mol/55.5 mol of solvent.

The experimental procedure entailed measurements of heat effects associated with the dilution of concentrated heavy and normal water solutions according to the processes shown in Figure 1. As can be seen from the schematic, measurements of the vertical and diagonal processes lead to values for the heats of transfer in both the concentrated and dilute solutions. The measurements were carried out in the LKB precision calorimeter described before.[2] However, the measurement procedure was varied to conform to the processes in Figure 1. Solutions were prepared such that the concentrations before dilution were equal in both solvents, and dilution volumes were selected such that concentrations were equal in both solvents after the dilution experiments. Concentrated solutions were prepared in duplicate, and a single dilution heat was measured for each process shown in Figure 1 and for each solution by diluting it approximately 100-fold.

Except for $MgCl_2$, the salts used to prepare the concentrated solutions were the same as described before.[2] For preparation of the $MgCl_2$ solutions, the anhydrous salt was obtained from K & K Laboratories. A chloride assay indicated it to be 97.7% $MgCl_2$; it was used without further purification.

Since the diagonal processes in Figure 1 include the heat resulting from the exchange reaction

$$H_2O(l) + D_2O(l) = 2HDO(l)$$

measurements of the magnitude of the exchange heat were made by diluting each of the solvents with a 100-fold volume of the other. The equilibrium constant for the exchange reaction is $K = 4.20$ at 25°.[6] Thus, at H/D and D/H ratios of 100/1, the reaction is essentially complete, and the dilution heat is equal to the heat per mole of water isotope reacted. Two dilution experiments at each of the H/D ratio extremes were carried out. The mean value obtained from the measurements was 31 ± 2 cal, in good agreement with Doehlemann and Lange's[7] value of 32 cal/mol and Skripov and Povyshev's[8] value of 33.4 ± 1 cal/mol. The value 31 cal/mol was used to correct the heats measured in the diagonal processes of Figure 1.

Heats of transfer resulting from differences among the various dilution processes are shown in Table I along with the values of the initial and final concentrations for each of the solutions. The heat values for the dilute solutions of $BaCl_2$ and $SrCl_2$ are in good agreement with those obtained from the integral heat measurements reported before.[2] The dilute solution transfer heats for the $MgCl_2$ and $CaCl_2$ solutions are, within the experimental reproducibility, somewhat lower than those obtained from the integral heat measurements.[2] The discrepancy between the two measurements probably arises from the extreme hygroscopic character of $CaCl_2$ and $MgCl_2$. Neither salt can be simply dehydrated and must be synthesized in the anhydrous form. To avoid a lengthy preparative procedure for these measurements, the $MgCl_2$ was obtained commercially and could have contained a small amount of water as one of its impurities. The $CaCl_2$ had been prepared for the measurements reported earlier[2] and probably absorbed a small amount of water in storage.

It is to be noted, from the data in Table I, that for all the salts, a reduction in absolute value for the transfer heat occurs with increased solution concentration. Since the transfer entropy is dominated by the heat, the data indicate that a reduction in solvent structure breaking occurs with increased salt concentration. Thus, the data are consistent with the conclusion stated before, that distant hydration is responsible for the structure-breaking effects exhibited by the alkaline earth chlorides in transferring between heavy and normal water.

---

(6) A. Narten, *J. Chem. Phys.*, **41**, 1318 (1964).

(7) E. Doehlemann and E. Lange, *Z. Elektrochem.*, **41**, 539 (1935).

(8) V. P. Skripov and L. V. Povyshev, *Soviet Phys. JETP*, **8**, 903 (1959).

COMMUNICATIONS TO THE EDITOR

The Spectrophotometric Determination of Association Constants for $CuSO_4$ and $Cu(en)_2S_2O_3$

Sir: Some years ago we[1] studied the formation in aqueous solution of the ion pairs $CuSO_4$ and $Cu(en)_2S_2O_3$ (en = ethylenediamine) by measuring the optical densities of the appropriate constant ionic strength mixtures. For each ion pair, a range of values of K was obtained from these optical densities,[2] the precise value depending on the activity coefficient assumption employed. However, Hemmes and Petrucci, who recently made similar measurements, argue[3] that spectrophotometry can yield unambiguous (although not very precise) values of these association constants.

Their arguments are that, for each ion pair, plots of $\log K' + 8A\sqrt{I}/1 + Bd\sqrt{I}$ *vs.* I for different values of d converge as $I \to 0$ and that, for $CuSO_4$, these plots give a value of K which agrees with "the conductance value." The first argument undoubtedly shows the calculation of K from K' to be insensitive to the activity coefficient assumption used. However, to prove that spectrophotometry gives an unambiguous value of K one must *also* show that values of K' derived by this method do not depend on one's activity coefficient assumption. Thus, consideration must be given to the role of the activity coefficient in the calculation of K' from optical densities, a point not discussed by Hemmes and Petrucci.

To calculate K' from optical densities one needs a figure for $\Delta\epsilon$, the difference between the extinction coefficients of the ion pair and the free ions. Since this quantity is generally unknown, it must be determined simultaneously with K' by finding a value of $\Delta\epsilon$ which gives figures for K' such that K is constant. Since $K = K'/(\gamma_\pm)^2$, an activity coefficient assumption is required in this operation. Moreover, for species like $CuSO_4$ and $Cu(en)_2S_2O_3$, the value of $\Delta\epsilon$ which is obtained from the optical densities of a given set of solutions can be shown to depend on the assumption made about the variation of $\gamma_\pm$ within the set. With different assumptions about this variation, different values of $\Delta\epsilon$ and different sets of values of K' may be obtained *from the same set of optical densities.* For example, in our studies of $CuSO_4$ and $Cu(en)_2S_2O_3$, we considered the possibility that, at constant I

$$\log \gamma_\pm = \log \gamma_\pm^0 + \alpha b \qquad (1)$$

with $\gamma_\pm^0$, α constants (*cf.* Harned's rule) and b the concentration of $SO_4^{2-}/S_2O_3^{2-}$. We found that the value of $\Delta\epsilon$ which was consistent with the optical densities of one of our sets of solutions depended on the figure assumed for α. Unless this quantity was arbitrarily fixed, a range of values of $\Delta\epsilon$ was consistent with such a set of optical densities. Further, with this range of values of $\Delta\epsilon$ a range of values of K' was obtained for a given solution. Hemmes and Petrucci obtained K' by a graphical method[4] which assumes $\gamma_\pm$ to be constant at constant I and thus fixes α at zero. It is therefore not surprising that they obtained a unique value of K' for each of their solutions. However, since activity coefficients are not necessarily strictly constant at constant I,[5] α may well *not* be zero.

Table I

	α	$10^3/\Delta\epsilon$	$K_0'^c$
A	$3.4\ M^{-1}$	8.1 cm M	$42.8 \pm 1.0\ M^{-1}$
B	$0\ M^{-1}$	6.3^a cm M	$35.3 \pm 0.9\ M^{-1}$
C	$0\ M^{-1}$	5.8^b cm M	$31.3 \pm 0.8\ M^{-1}$
D	$-1.25\ M^{-1}$	4.9 cm M	$26.6 \pm 0.5\ M^{-1}$

[a] The mean of the figures in Table III, ref 2. [b] Our estimate of the slope of the plot of $^{ab}/D - D'$ *vs.* $(a + b - x)$. [c] Mean deviations indicated by ±.

Table II

$10^3\ a/M$	$10^3\ b/M$	$10^3\Delta(A)^a$	$10^3\Delta(B)^a$	$10^3\Delta(C)^a$	$10^3\Delta(D)^a$
2.63	4.00	−2	0	−1	0
2.63	8.00	+1	+3	+2	+3
2.63	12.00	0	+1	+1	0
2.63	16.00	+2	+1	+2	+1
2.63	20.00	+3	+1	+3	+2
2.63	24.00	−1	−5	−2	−4
2.63	28.00	−1	−4	0	−3

[a] $(\Delta = (D - D')_{calcd} - (D - D')_{obsd})$. $(D - D')_{obsd}$ from Table II, ref 3.

We have analyzed Hemmes and Petrucci's optical data[6] for $Cu(en)_2S_2O_3$ assuming eq 1 to apply at constant I and find that the values of $\Delta\epsilon$ and K' which

---

(1) R. A. Matheson, *J. Phys. Chem.*, **69**, 1537 (1965); (b) R. A. Matheson, *ibid.*, **71**, 1302 (1967).

(2) $K = ({}^{a}CuSO_4)/({}^{a}Cu^{2+}\,{}^{a}SO_4^{2-})$ or $({}^{a}Cu(en)_2S_2O_3)/({}^{a}Cu(en)_2^{2+}\,{}^{a}S_2O_3^{2-})$. The corresponding concentration quotients will be denoted by K'.

(3) P. Hemmes and S. Petrucci, *J. Phys. Chem.*, **72**, 3986 (1968).

(4) Discussed in ref 1b.

(5) See, *e.g.*, R. A. Robinson and R. H. Stokes, "Electrolyte Solutions," Butterworth and Co., Ltd., London, 1965, Chapter 15.

(6) Table II, ref 2.

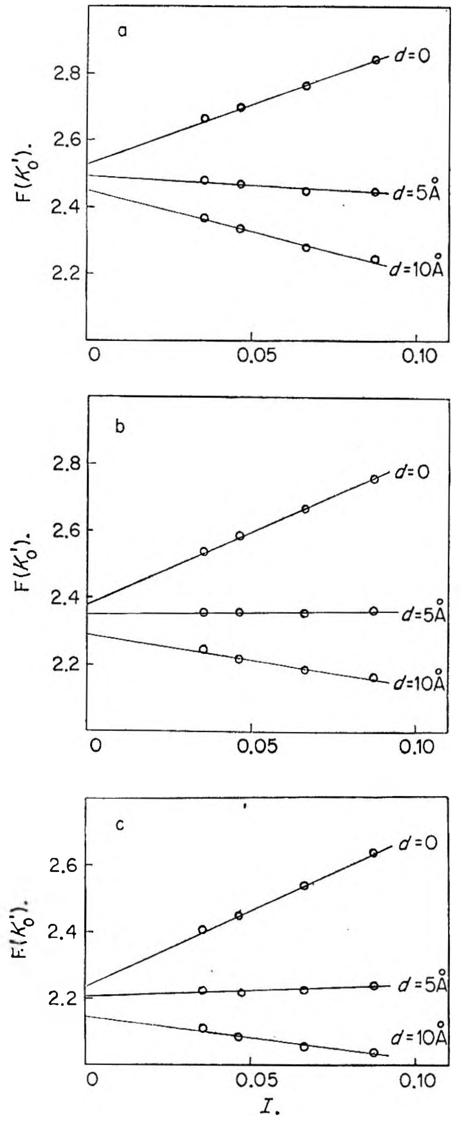

Figure 1.

are consistent with the results for any one of their sets of solutions depend on the figure assumed for α and, unless this is zero, differ from the values originally obtained by these authors. Table I lists some values of $1/\Delta\epsilon'$ α and K_0' (defined below) which are consistent with their data for solutions of I = 0.0875 M. Although the values of $1/\Delta\epsilon$ corresponding to the three figures for α are very different, each gives rise to a set of K' values such that log K_0' = log K' − $2\alpha b$ is constant and therefore (*cf.* eq 1) $K'/(\gamma_\pm)^2$ is constant. Of course if $\alpha \neq 0$, K' is not constant and *cannot be expected to be constant.* We have also used each of the sets of K_0' α and $\Delta\epsilon$ in Table I to calculate the concentrations of $Cu(en)_2S_2O_3$ and the values of $D - D'$ for all the solutions with I = 0.0875 M. The results (see Table II) confirm that these four sets of parameters differ little in their consistency with the experimental optical densities of these solutions. It seems that unique values of $1/\Delta\epsilon$ and K' cannot be obtained from these optical densities unless some arbitrary restriction is placed on $\gamma_\pm$, *e.g.*, if α is fixed at zero. The position can be shown to be similar in the case of Hemmes and Petrucci's other solutions for which different values of α again given different figures for $1/\Delta\epsilon$ and K'. Thus, if α is not arbitrarily fixed, Hemmes and Petrucci's optical densities produce a range of values of K_0' at each I. However K_0'[7] varies with I and there remains the possibility that the extrapolation procedure used by Hemmes and Petrucci may produce a definite figure for K despite the ambiguity in K_0'. We have therefore constructed plots of $F(K_0') = \log K_0' + 8A\sqrt{I}/1 + Bd\sqrt{I}$ *vs.* I for d = 0, 5, and 10 Å using values of K_0' calculated from Hemmes and Petrucci's optical densities for their solutions of I = 0.0335, 0.0465, 0.0664, and 0.0875 M[8] assuming (a) $\alpha = 3.4\ M^{-1}$, $10^3/\Delta\epsilon = 8.1$ cm M; (b) $\alpha = 0$, $10^3/\Delta\epsilon = 6.3$ cm M; and (c) $\alpha = -1.25\ M^{-1}$, $10^3/\Delta\epsilon = 4.9$ cm M. In each case (see Figures 1a, 1b, and 1c) the plots for the three values of d converge satisfactorily as $I \rightarrow 0$. However, the limits to which they extrapolate correspond to different values of K (275 to 347 M^{-1} for Figure 1a, 195 to 246 M^{-1} for 1b, and 141 to 178 M^{-1} for 1c). Evidently, this extrapolation does not eliminate the ambiguity which results from the dependence of K' and $\Delta\epsilon$ upon the activity coefficient assumption used to calculate these quantities from the experimental data.

In regard to the agreement between Hemmes and Petrucci's figure for $CuSO_4$ and "the conductance value," it is in our view misleading to speak of "the conductance value" when, for electrolytes like $CuSO_4$, the value of K which is obtained from conductances depends on the assumptions made in the calculations.[9]

---

[7] $K_0' = \lim_{b \to 0} K'$ for the constant ionic strength series in question.

[8] The set of solutions with I = 0.109 was not considered because the points for this set diverged from the original graphs (Figure 2, ref 2).

[9] J. E. Prue, "Ionic Equilibria," Pergamon Press, Ltd., London 1966, Chapter 3.

Department of Chemistry,
The University of Otago
Dunedin, New Zealand

R. A. Matheson

Received April 28, 1969

On the Reliability of the Spectrophotometric Determination of Association Constants. The Case of $CuSO_4$ and $Cu(en)_2S_2O_3$

Sir: We wish to start our answer from the concluding point of Dr. Matheson's statements,[1a] namely from the claimed unsuitability of the conductance method to determine a unique value of association for electrolytes like $CuSO_4$.

---

[1] (a) R. A. Matheson, *J. Phys. Chem.*, 4425 (1969); (b) J. E. Prue, "Ionic Equilibria," Pergamon Press, Ltd., London, 1966.

By analyzing the data by the Fuoss–Onsager equation[2] for associated electrolytes, or more precisely by using the so-called "y–x" method, values of $K_A = 191$ M^{-1} and $a = 5.7$ Å have been obtained.[3] By starting the calculation with an arbitrary value of a (1 or 14 Å, for example) rapid (two or three cycles) convergence to the above values of a and K_A is obtained. The claimed ambiguity[1b] of the calculation was based on the possible fit of the data to the Fuoss–Onsager equation[2] by imposing a range of values of a and therefore of $J(a)$ at the expense of K_A. This ambiguity arises *only by imposing and keeping constant the parameter a.*

The above should be enough to sustain our spectrophotometric work for $CuSO_4$ given the fact that our data extrapolate to the conductance value for $I = 0$. Since, however, this would not justify our result for $Cu(en)_2S_2O_3$ and, more important, would leave the generality of the use of the spectrophotometric method open to question, the following discussion is presented.

It is only because of the arbitrary assumption[4] of the validity of the Harned rule for a three-component system

$$\log \gamma = \log \gamma_0 + \alpha b \qquad \text{(I)}$$

that the expression

$$\frac{ab}{D - D'} = \frac{a + b - x}{\Delta\epsilon l} + \frac{1}{\Delta\epsilon l K'} \qquad \text{(II)}$$

is transformed into a three-parameter equation in $\Delta\epsilon$, K'_0, and α

$$\frac{ab}{D - D'} = \frac{a + b - x}{\Delta\epsilon l} + \frac{\exp(-4.606\alpha b)}{\Delta\epsilon l K'_0} \qquad \text{(III)}$$

making impossible its graphical or analytical solution unless some assumption on α is retained. Our contention in this matter is that the above procedure[4] (retention of formula I with large values of α and consequent assumption of the failure of the ionic strength principle) is as arbitrary as the assumption of the ionic principle itself.

Therefore, in this range of ionic strengths ($I = 0.04$ to 0.1) one should prove that the results for $\Delta\epsilon$ and K' strongly depend on the internal composition of the mixture at the same value of the ionic strength. In order to clarify this matter, we have measured the optical density differences of solutions containing a moles of $Cu(ClO_4)_2$, b moles of Li_2SO_4 (or Cs_2SO_4), and c moles of $LiClO_4$ (or $CsClO_4$) and the reference solution containing a moles of $Cu(ClO_4)_2$ and enough $LiClO_4$ (or $CsClO_4$) to reach the same ionic strength. Small quantities of $HClO_4$ to repress the hydrolysis of Cu_{aq}^{2+} have also been added.

The difference with previous determinations[4,5] has been the substitution of Na^+ with Li^+ (or Cs^+) at the same ionic strength I. The results are reported in Table I in the form of the calculated K' and $10^3/\Delta\epsilon$.[6]

Table I: Values of K' (M^{-1}) and $10^3/\Delta\epsilon$ (M, cm) at Different Ionic Strengths I, for the Various Mixtures Investigated

Species	I, M	K', M^{-1}	$10^3/\Delta\epsilon$, M cm
$Cu^{2+} + SO_4^{2-}$	0.041[a]	36.3[a]	4.2[a]
	0.041[b]	43.7[b]	4.8[b]
	0.070[a]	21.8[a]	3.7[a]
	0.070[c]	28.4[c]	4.0[c]
	0.070[d]	28.1[d]	4.5[d]
$Cu(en)_2^{+2} + S_2O_3^{-2}$	0.0465[e]	45.4[e]	5.9[e]
	0.0465[f]	50.8[f]	6.3[f]
	0.0875[e]	29.3[e]	4.5[e]
	0.0875[f]	35.7[f]	6.4[f]
	0.0273[g]	54.2[g]	5.2[g]
	0.0273[h]	64.1[h]	6.2[h]
	0.0338[g]	47.5[g]	5.8[g]
	0.0664[g]	31.1[g]	5.3[g]
	0.0664[f]	43.7[f]	6.5[f]

[a] This work, $Cu(ClO_4)_2 + Li_2SO_4 + LiClO_4$. [b] Matheson's results,[4] $Cu(ClO_4)_2 + Na_2SO_4 + NaClO_4$. [c] Previous work,[5] $Cu(ClO_4)_2 + Na_2SO_4 + NaClO_4$. [d] This work, $Cu(ClO_4)_2 + Cs_2SO_4 + CsClO_4$. [e] This work, $Cu(en)_2(ClO_4)_2 + Na_2S_2O_3 + LiClO_4$. [f] Previous work,[5] $Cu(en)_2(ClO_4)_2 + Na_2S_2O_3 + NaClO_4$. [g] This work, $Cu(en)_2(ClO_4)_2 + Na_2S_2O_3 + CsClO_4$. [h] Matheson's results, $Cu(en)_2(ClO_4)_2 + Na_2S_2O_3 + NaClO_4$ (R. A. Matheson, *J. Phys. Chem.*, **71**, 1302 (1967).

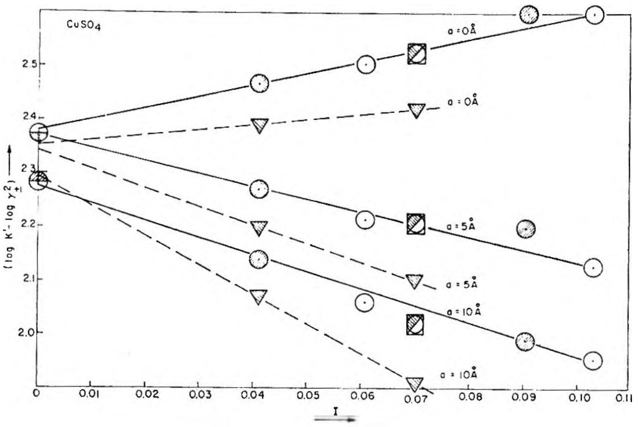

Figure 1. $CuSO_4$ in water at 25°: ●, Matheson's results;[4] ⊙, previous work by the same authors;[5] ▼, present work substituting Na^+ for Li^+; ▨, present work substituting Na^+ for Cs^+; ⊖, conductance result by the Shedlowsky method;[7] ⊖, conductance result by the Fuoss–Onsager theory[3].

It can be seen that differences indeed exist, the values of K'(Li) differing by 17% at $I = 0.04$ and by 24% at $I = 0.07$ with respect to the previous determinations

---

(2) R. M. Fuoss and F. Accascina, "Electrolytic Conductance," Interscience Publishers, New York, N. Y., 1959.

(3) G. Atkinson, M. Yokoi, and C. J. Hallada, *J. Amer. Chem. Soc.*, **83**, 1570 (1961); C. J. Hallada, Ph.D. Thesis, University of Michigan, Ann Arbor, Mich., 1960.

(4) R. A. Matheson, *J. Phys. Chem.*, **69**, 1537 (1965).

(5) P. Hemmes and S. Petrucci, *ibid.*, **72**, 3986 (1968).

(6) The original data for optical density differences can be obtained from the authors upon request.

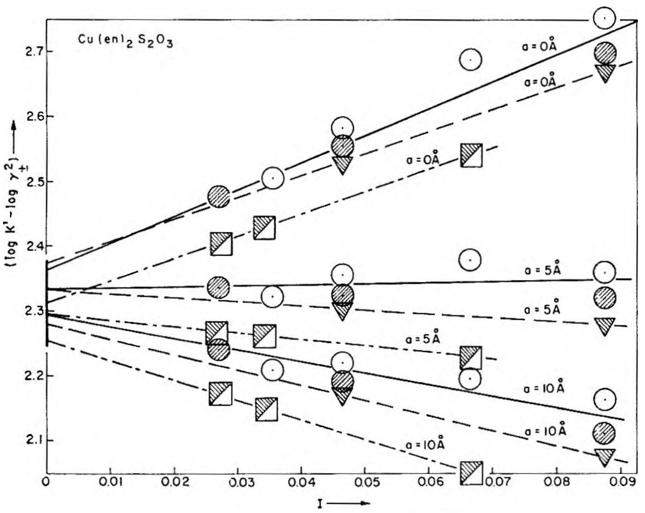

Figure 2. Cu(en)$_2$S$_2$O$_3$ in water at 25°: ◍, Matheson's results (R. A. Matheson, *J. Phys. Chem.*, **71**, 1302 (1967)); ○, previous work by the same authors;[5] ▼, present work substituting NaClO$_4$ for LiClO$_4$ ▨, present work substituting NaClO$_4$ for CsClO$_4$.

K'(Na). The values of K'(Cs) are instead very similar to the previous determined K'(Na). (The symbols K'(Na), K'(Li), and K'(Cs) refer to the cation other than Cu^{2+} used.)

However, when the same plot as before[5] is constructed (Figure 1), namely the ($\log K' - \log \gamma_{\pm}^2$) is reported *vs.* I (where $\gamma_{\pm}^2$ is calculated from the Debye–Hückel relation for various arbitrary values of a), the convergence to $I = 0$ is obtained for K(Li) $= 215 \pm 20$ M^{-1} with respect to the previous[5] K(Na) $= 225 \pm 25$ M^{-1}. In Figure 1 the results by conductance calculations at $I = 0$ for K are also reported.[6] The Shedlowski method gives[7] $K = 233$ M^{-1}, while the Fuoss–Onsager theory gives[3] $K = 191$ M^{-1}. The use of these two forms of the conductance theory gives a range of results comparable with the dispersion of the spectrophotometric results.

The same procedure as above has been applied to the Cu(en)$_2^{2+}$ + S$_2$O$_3^{2-}$ ions. For this case, more complex mixtures have been used, namely optical density differences of solutions of Cu(en)$_2$(ClO$_4$)$_2$, Na$_2$S$_2$O$_3$, and LiClO$_4$ (or Cu(en)$_2$(ClO$_4$)$_2$, Na$_2$S$_2$O$_3$, and CsClO$_4$) the first and Cu(en)$_2$(ClO$_4$)$_2$, LiClO$_4$ (or Cu(en)$_2$(ClO$_4$)$_2$, CsClO$_4$) the reference have been measured. The results are reported in Table I. The differences in K'(Li, Na) are 11% and 18% with respect to K'(Na) at $I = 0.046$ and $I = 0.0875$ M. For K'(Cs, Na) a difference of 15.4% and 29% at $I = 0.0273$ and $I = 0.0664$ with respect to K' (Na) is observed (Table I).

However also in this case when a plot of ($\log K' - \log \gamma_{\pm}^2$) *vs.* I is constructed (Figure 2) the graph extrapolates to K(Li, Na) $= 215 \pm 25$ M^{-1} and K(Cs, Na) $= 192 \pm 14$ M^{-1} with respect to the previous determination[5] K(Na) $= 220 \pm 20$ M^{-1}. *It is quite clear that in the above the condition $\alpha = 0$ has been tacitly imposed.* The differences among the three sets of results indicate the departure of one solution from this condition with respect to the other solutions at the same ionic strength. The only point left to be considered is that *α be large and similar for the three sets of solutions of different internal composition at the same ionic strength.* This is the same as saying that the breakdown of the principle of ionic strength occurs to almost the same extent and in the same direction for the various mixtures investigated. This is extremely unlikely given the different character of Li$^+$, Na$^+$, and Cs$^+$ ions.

(7) B. B. Owen and R. W. Gurry. *J. Amer. Chem. Soc.*, **60**, 3074 (1938).

DEPARTMENT OF CHEMISTRY
POLYTECHNIC INSTITUTE OF BROOKLYN
BROOKLYN, NEW YORK

PAUL HEMMES
SERGIO PETRUCCI

RECEIVED JUNE 19, 1969

On the Determination of Average Pore Size of Membranes

Sir: Recently, a method for estimating the average pore radius of a membrane from electroosmotic and hydrodynamic permeability measurements has been suggested by Rastogi, *et al.*[1] The phenomenological coefficients L_{11} and L_{12} are expressed in terms of classical theory as

$$(L_{11}/T) = (n\pi r^4)/(8\eta d) \tag{1}$$

$$(L_{12}/T) = (nr^2D\zeta)/(4\eta d) \tag{2}$$

where (L_{11}/T) is the hydrodynamic flow (cm^3/sec) induced by unit pressure (dyn/cm^2), (L_{12}/T) is the electroosmotic flow (cm^3/sec) per volt, n is the number of pores of radius r in the membrane, D is the dielectric constant of the pore liquid of viscosity η, d is the length of the pore, and ζ is the ζ potential. Dividing eq 1 by eq 2 gives an equation for r, *viz.*

$$r = \sqrt{(2D\zeta L_{11})/(\pi L_{12})} \tag{3}$$

In the classical work of physiologists described elsewhere[2] and reviewed recently by Solomon,[3] the pore radius expressed in simple terms without the corrections for steric hindrance and molecular sieving is given by

$$r = \sqrt{8\eta L_p(d/A)_w} \tag{4}$$

where $L_p = (L_{11}/T)$, d is the pore length, and A is the pore area for the passage of water, w.

Evaluation of r by eq 3 calls for three measurements (L_{11}/T), (L_{12}/T), and ζ. On the contrary, derivation

(1) R. P. Rastogi, K. Singh, and S. N. Singh, *Indian J. Chem.*, **6**, 466 (1968).

(2) N. Lakshminarayanaiah, *Chem. Rev.*, **65**, 539 (1965).

(3) A. K. Solomon, *J. Gen. Physiol.*, **51**, 335s (1968).

of a value for r by eq 4 requires only two measurements, L_p and $(A/d)_w$. In both cases, values used for D and η for the pore liquid are the values known for the bulk liquid.

Rastogi, *et al.*, in a recent paper,[4] derived values for r for a number of Pyrex sinters using a value of 0.07 V for ζ derived from electrophoretic measurements in which suspensions of Pyrex particles were used. How relevant the value of ζ derived this way is to ζ appearing in eq 2–3 is unknown. In classical work, it is considered that the electrophoretic velocity is equal to the velocity of electroosmosis, both obeying the equation of Helmholtz–Smoluchowski.[5] This obedience is possible only if the electrokinetic properties of both suspensions and sinters are identical. Protein adsorption on both particles and sinters is recommended to make them electrokinetically equal. No such or other procedure is mentioned in the work of Rastogi and coworkers[1,4] and so the values of r derived should be considered suspect unless proven otherwise.

In order to obviate this lack of relevance and to eliminate the third electrophoretic measurement, the Helmholtz–Smoluchowski equation for electroosmosis, *viz.*

$$\zeta = (4\pi\eta k V_e 300^2)/(Di) \qquad (5)$$

where ζ is in volts, k is the specific conductance of the pore liquid (ohm^{-1} cm^{-1}), V_e is the volume of liquid flowing (cm^3/sec), and i is the current (A), can be used to evaluate ζ. Substitution of the following values taken from the work of Rastogi, *et al.*, for acetone–Pyrex system gave a value of 1.2 mV for ζ (5.3×10^{-7} has been used for k): $\eta = 0.284 \times 10^{-2}$ P[6]; $D = 19.7$[6]; k (pure acetone) $= 2 \times 10^{-8}$ at 18°,[7] $= 6 \times 10^{-8}$ at 25°,[7] $\approx 1.2 \times 10^{-7}$ ohm^{-1} cm^{-1} at 35° (calculated); k (acetone–Pyrex system) $= 5.3 \times 10^{-7}$, *i.e.*, $R = 1.157 \times 10^5$ ohm,[6] $A = 4.9$ cm^2,[6] $d = 0.3$ cm,[4] $V_e = 24.25 \times 10^{-3}$ cm^3 sec^{-1} at 200 V,[4] and $i = (200/1.157) \times 10^{-5} = 1.73 \times 10^{-3}$ A. This value for ζ is too low compared to a value of 70 mV derived from electrophoretic measurements.[8] The value of 1.2 mV will be further reduced if the value of k for pure acetone is used in the calculations. This discrepancy between the ζ values, *i.e.*, 70 and 1.2 mV, can be attributed to the differences in the electrokinetic properties of the particles and the sinter. Therefore eq 3, as suggested and used by Rastogi and coworkers,[1,4] is not reliable for estimating the values for r. Instead, electroosmotic and hydrodynamic permeability measurements alone are sufficient to derive a value for r. Equation 5 may be written as

$$\zeta = (L_{12}/T)E(4\pi\eta k)/(Di) \text{ (es units)} \qquad (6)$$

Substitution of this in eq 3 gives

$$r = \sqrt{8\eta(L_{11}/T)kE/i} \qquad (7)$$

Use of the values given above and that of (L_{11}/T), *i.e.*, 0.96×10^{-6} cm^5 dyn^{-1} sec^{-1},[4] gives a value of 1.7×10^{-5} cm for r as opposed to the value of 3×10^{-4} cm obtained by Rastogi, *et al.*[4] The k value used in this calculation was 1.2×10^{-7}; r will have a value of 3.7×10^{-5} cm if 5.3×10^{-7} is used for k.

A trivial manipulation, *i.e.*, $(kE/i) = (d/A)$, shows that eq 7 is equivalent to eq 4 where k is the specific conductance of the pore liquid.

It should be emphasized that the equivalence of eq 4 and 7 can only be true when the membrane matrix contributes little to the conductance of the pore liquid. This is so only when the pore radius is very large compared to the thickness of the electrical double layer. So it should be expected that in the case of "tight" membranes whose matrix contains a number of fixed ionic groups, the relation $kE/i = kR = d/A$ cannot be valid. The ratio of pore length to pore area, *i.e.*, (d/A), has been determined by Lakshminarayanaiah[9] for a polyethylene–polystyrene graft copolymer membrane containing sulfonic acid groups using tritiated water in the manner described in the literature.[2] The value was 0.24 cm^{-1}. The factor kR for the membrane is difficult to evaluate since the pore liquid in the membrane was water ($k = 10^{-6}$ ohm^{-1} cm^{-1}) in which SO_3^- groups attached to the membrane matrix were submerged. The membrane resistance (thickness $\approx 150\ \mu$ and area ≈ 0.3 cm^2) was about 5–10 ohm. The product kR is therefore about $5\text{–}10 \times 10^{-6}$. If a value of about 5×10^{-2} corresponding to an aqueous 0.5 N electrolyte solution is taken for k, then kR will be about 0.24; k for the membrane in H^+ form is about 10^{-2}. This means that conduction is mostly taking place along the polymer chains and is similar to the phenomenon of surface conduction. Consequently, eq 7 cannot be used for measuring r of "tight" ion-exchange membranes whose pore radius is about 7 Å,[9] a little bigger than the thickness of the electrical double layer.

Acknowledgment. The writing of this communication has been supported in part by Public Health Service Grant NB-08163.

(4) R. P. Rastogi, K. Singh, and M. L. Srivastava, *J. Phys. Chem.*, **73**, 46 (1969).

(5) J. Th. G. Overbeek in "Colloid Science," H. R. Kruyt, Ed., Vol. I, Elsevier Publishing Co. Inc., New York, N. Y., 1952, p 224.

(6) R. P. Rastogi and K. M. Jha, *Trans. Faraday Soc.*, **62**, 585 (1966).

(7) N. A. Lange, "Handbook of Chemistry," 10th ed, McGraw-Hill Book Company, Inc., New York, N. Y., 1961, p 1209.

(8) R. P. Rastogi and B. M. Misra, *Trans. Faraday Soc.*, **63**, 2926 (1967).

(9) N. Lakshminarayanaiah, *Biophys. J.*, **7**, 511 (1967).

DEPARTMENT OF PHARMACOLOGY N. LAKSHMINARAYANAIAH
UNIVERSITY OF PENNSYLVANIA
PHILADELPHIA, PENNSYLVANIA 19104

RECEIVED JUNE 11, 1969

The Chemistry of Nuclear Recoil Fluorine-18 Atoms. II. Energetic F-for-F and Ring-Attack Reactions in Perfluorocyclanes

Sir: Recoil ^{18}F atoms undergo novel high energy chemical reactions including F-for-F substitution (1), F-for-H, and F-for-CH_3 replacement (2)[1–3]

$$^{18}F^* + RF \xrightarrow{\text{F-for-F}} R^{18}F + {}^{19}F \qquad (1)$$

$$^{18}F^* + RX \xrightarrow{\text{F-for-X}} R^{18}F + X \qquad (2)$$

in which X = H or $\dot{C}H_3$. Recent recoil ^{18}F studies with CH_3CF_3 have shown that $\bar{E}^{vib}(R^{18}F)$ from (1) is in the range of 11–12 eV.[1c–2] We have studied the ^{18}F recoil chemistry of perfluorocyclanes in an attempt to provide corroborative evidence about the energetics for (1) as well as characterizations for the hot ^{18}F abstraction (3) and ring-attack (4) reactions[4]

$$^{18}F^* + RF \xrightarrow{\text{F-to-F}_2} F^{18}F + \cdot R \qquad (3)$$

$$^{18}F^* + c\text{-}C_xF_{2x} \longrightarrow n\text{-}\dot{C}_xF_{2x}{}^{18}F \qquad (4)$$

The basic method has been described.[1c,1d] Here the inorganic ^{18}F was measured through successive treatment of samples with granulated Cu metal (for $F^{18}F$), and anhydrous K_2CO_3 (for $H^{18}F$), followed by NaI(Tl) scintillation detection of the ^{18}F annihilation photopeak. High-pressure runs to 100 atmospheres were carried out with gaseous CF_4–perfluorocyclane mixtures in 1–10-cm^3 stainless steel vessels.

Our results suggest that efficient incorporation of ^{18}F into perfluorocyclanes occurs *via* (1) resulting in the formation of highly excited $R^{18}F$ species. In all previous studies of F-for-F substitution, the product distributions have indicated extensive unimolecular decomposition associated with (1).[1b–1d] Such unimolecular processes are conveniently investigated through pressure variation experiments, and our pressure-dependent c-C_4F_8 data are shown in Figure 1. The decomposition mechanisms that we have identified are[2]

$$\begin{aligned}
(c\text{-}C_3F_5{}^{18}F)^\dagger &\xrightarrow{S} c\text{-}C_3F_5{}^{18}F && (5)\\
&\xrightarrow{D_1} :CF^{18}F + C_2F_4\\
&\xrightarrow{D_2} C_2F_3{}^{18}F + :CF_2\\
(c\text{-}C_4F_7{}^{18}F)^\dagger &\xrightarrow{S} c\text{-}C_4F_7{}^{18}F && (6)\\
&\xrightarrow{D_1} :CF^{18}F + C_3F_6\\
&\xrightarrow{D_2} c\text{-}C_3F_5{}^{18}F + :CF_2\\
&\xrightarrow{D_3} C_2F_3{}^{18}F + C_2F_4
\end{aligned}$$

Experimental half-fugacities for c-$C_4F_7{}^{18}F$ and c-$C_3F_5{}^{18}F$ stabilization were 12.0 ± 0.5 and 75 ± 25 atm.[5] The corresponding low-pressure yields and critical decomposition energies were 30.0 ± 0.5% (3.22 eV)[6] and 0.00% (1.67 eV).[7] Thus, about 30% of the products from (1) in perfluorocyclanes were formed with $\bar{E}^{vib}(R^{18}F)$ below 3.2 eV, but none were formed below about 1.7 eV.[8] Decomposition mechanism (6-D2) for c-$C_4F_7{}^{18}F$ contrasts with the earlier finding that perfluoropropylene (C_3F_6, E_a = 3.77 eV), not c-C_3F_6, was formed along with C_2F_4 (E_a = 3.22 eV).[6a,9]

Simple Kassel calculations based upon Figure 1 provide an $\bar{E}^{vib}(c\text{-}C_4F_7{}^{18}F)$ value of 8.8 to 10.5 (±2.0) eV, in good agreement with available $CH_3CF_2{}^{18}F$ and $CF_3{}^{18}F$ results.[1b–1d,10,11] This calculation cannot be regarded as wholly definitive, however, for several reasons; the Kassel parameters for c-C_4F_8 are not well known,[6,10] and quantitative extrapolations of unimolecular kinetic theories to energies as high as 12 eV involve untested assumptions.[1c,1d,10e] In view of these

---

[1] (a) J. F. J. Todd, N. Colebourne, and R. Wolfgang, *J. Phys Chem.*, 71, 2875 (1967); (b) Y. N. Tang, T. Smail, and F. S. Rowland *J. Amer. Chem. Soc.*, **91**, 2130 (1969); (c) N. J. Parks, C. F. McKnight, and J. W. Root, *Chem. Eng. News*, Sept. 15, 42 (1969); (d) C. F. McKnight and J. W. Root, *J. Phys. Chem.*, submitted for publication.

[2] The symbols include: *, translational excitation; †, vibrational excitation; $\bar{E}^{vib}(R^{18}F)$, the average $R^{18}F$ vibrational energy from (1); S and D, product stabilization and decomposition.

[3] Y. N. Tang and F. S. Rowland, *J. Phys. Chem.*, **71**, 4576 (1967).

[4] Ring attack (4) is the alicyclic equivalent of alkyl replacement (2).

[5] (a) Fugacity corrections involved the acentric parameter method, ref 5b, 5c; (b) K. S. Pitzer and L. Brewer, "Thermodynamics," originally by G. N. Lewis and M. Randall, 2nd ed, McGraw-Hill Book Co. Inc., New York, N. Y., 1961, pp 605–634; (c) R. C. Reid and T. K. Sherwood, "The Properties of Gases and Liquids," 2nd ed, McGraw-Hill Book Co. Inc., New York, N. Y., 1966, pp 45–113 and 300–370.

[6] (a) J. N. Butler, *J. Amer. Chem. Soc.*, **84**, 1393 (1962); (b) A. Lifshitz, H. F. Carroll, and S. H. Bauer, *J. Chem. Phys.*, **39**, 1661 (1963).

[7] B. Atkinson and D. McKeagan, *Chem. Commun.*, 189 (1966).

[8] R. R. Pettijohn, K. A. Krohn, C. F. McKnight, N. J. Parks, and J. W. Root, manuscripts in preparation.

[9] (a) The earlier analysis (ref 6a) involved calibration standards obtained *via* pyrolysis of Teflon, which proceeds through formation of $:CF_2$ and C_2F_4 (ref 9b). c-C_3F_6 is now known to be formed under these conditions (ref 9c–9f). Our analysis (ref 9g) separated C_3F_6 and c-C_3F_6 by 2 min, and confirmation of (6-D2) was based upon carrier-addition techniques; (b) E. E. Lewis and M. A. Naylor, *J. Amer. Chem. Soc.*, **69**, 1968 (1947); (c) M. Lenzi and A. Mele, *J. Chem. Phys.*, **43**, 1974 (1965); (d) N. Cohen and J. Heicklen, *J. Phys. Chem.*, **70**, 3082 (1966); (e) J. M. Birchall, R. N. Haszeldine, and D. W. Roberts, *Chem. Commun.*, 287 (1967); (f) N. C. Craig, T. N. Hu, and P. H. Martyn, *J. Phys. Chem.*, **72**, 2234 (1968); (g) S. A. Greene and F. M. Wachi, *Anal. Chem.*, **35**, 928 (1963).

[10] (a) Kassel *S* parameters within a fluorohydrocarbon series increase with fluorine substitution (ref 10b–10d). c-$C_3F_xH_{6-x}$ values range from 13.0 to 21.0 (x = 0 to x = 4), and $C_2F_xH_{6-x}$ values range from 9.0 to 18.0 (x = 0 to x = 6), corresponding to active participation of *all* vibrational modes for the fully fluorinated species. By analogy an *S* value of 30.0 was assigned for c-C_4F_8. The A = 2.1 × 10^{16} sec^{-1} and E_a = 3.22, 3.77 eV values have been well established (ref 6). A collision diameter of 5.73 Å was calculated for c-C_4F_8 using the modified corresponding states method of Root (ref 8, 10f). The 8.8 and 10.5 eV-values for $\bar{E}^{vib}(c\text{-}C_4F_7{}^{18}F)$ correspond to the 3.22 and 3.77-eV E_a values, respectively. (b) A. Maccoll, *Chem. Rev.*, **69**, 33 (1969); (c) F. P. Herbert, J. A. Kerr, and A. F. Trotman-Dickenson, *J. Chem. Soc.*, 5710, (1965); (d) S. W. Benson and G. Haugen, *J. Phys. Chem.*, **69**, 3898 (1965); (e) D. W. Placzek, B. S. Rabinovitch, and G. Z. Whitten, *J. Chem. Phys.*, **43**, 4071 (1965); (f) J. W. Root, Ph.D. Dissertation, University of Kansas, 1964.

reservations, the present semiquantitative agreement between $\bar{E}^{vib}(R^{18}F)$ values for c-$C_4F_7{}^{18}F$ and CH_3-$CF_2{}^{18}F$ was somewhat unexpected. The present values are also supported by the observation that $CF_3{}^{18}F$ from (1) undergoes extensive decomposition by a mechanism that is endoergic by 9.3 eV.[1b–1d,8,11]

The search for products from (3) was negative in both c-C_4F_8 and n-C_4F_{10}, but extensive ring attack (4) was indicated for both c-C_3F_6 and c-C_4F_8. Measurements of the radical products from (4) were carried out through H_2S scavenging,[1d,8,12] and the product distributions indicated that the primary n-$\dot{C}_3F_6{}^{18}F$ and n-$\dot{C}_4F_8{}^{18}F$ radicals underwent extensive unimolecular decomposition under our experimental conditions. This is illustrated in Figure 1 for n-$\dot{C}_4F_8{}^{18}F$. Although we conclude that excess internal energy is associated with (4),[12] any quantitative interpretation of the pressure dependence data would require kinetic background information that is presently unavailable. At low pressures the yield of decomposition products from n-$\dot{C}_4F_8{}^{18}F$ radicals approaches the F-for-F yield in c-C_4F_8 (93 ± 5% from Figure 1). Because of its very long vpc retention time, the n-$C_4F_8{}^{18}FH$ from scavenged, stabilized n-$\dot{C}_4F_8{}^{18}F$ was not measured, so that this 93% relative yield represents a lower limiting value. The ring-attack yield from c-C_3F_6 (including *measured* n-$C_3F_6{}^{18}FH$) was roughly twice the F-for-F substitution yield.

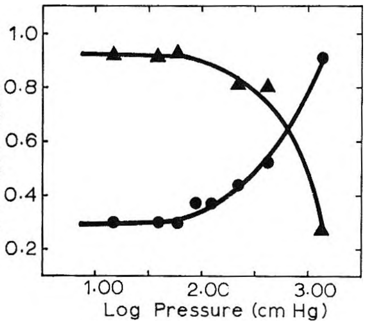

Figure 1. F-for-F and ring-attack yield data for c-C_4F_8. Experimental points: ●, c-$C_4F_7{}^{18}F/(S + D)$; ▲, $(n$-$\dot{C}_4F_8{}^{18}F)^{\dagger}/(S + D)$ in which (S + D) denotes the sum of c-$C_4F_7{}^{18}F$ (S) plus all decomposition products (D = D1 + D2 + D3 from eq 6) and $(n$-$\dot{C}_4F_8{}^{18}F)^{\dagger}$ denotes the sum of decomposition products from (4).

This postulate of extensive ring attack (4) is in marked contrast to the alkyl-replacement *vs.* substitution trends previously reported for recoil ^3H atoms.[4] Whereas T-for-H substitution yields in hydrocarbons typically exceed T-for-R alkyl-replacement yields by factors of about 4,[13] the reverse trend has been characteristic of *every* ^{18}F recoil system that we have investigated, including C_2–C_6 perfluoroalkanes, mixed C_2–C_4 haloalkanes, and perfluorocyclanes;[1c,1d,8] similar results have been reported from an earlier study with 1,3-dimethylcyclobutane.[3] From the present results we conclude that *recoil ^{18}F reacts preferentially with the carbon–carbon bonds in perfluorocyclanes by at least a factor of 2 on a per-bond basis* [(C–C):(C–F) > (93/4):(100/8)].

Acknowledgment. Stimulating discussions with Professors B. S. Rabinovitch, University of Washington, and D. L. Bunker, University of California, Irvine, gifts of fluorine chemicals from Dr. D. C. England and Dr. J. R. Martin of DuPont, cooperation from the Crocker Nuclear Laboratory staff, and support from the United States Atomic Energy Commission are gratefully acknowledged.[14]

---

(11) (a) Our recent results indicate that $CF_3{}^{18}F$ from (1) undergoes *stepwise* decomposition to $\dot{C}F_2{}^{18}F$, and then to $:CF^{18}F$, so that the *minimum* energy associated with $:CF^{18}F$ formation is 9.3 eV. $\Delta H_f°$ [Species, g, 298°K] values in kcal/mol (and ref) include: CF_4, −224.1; CF_3H, −166.7 (11b); F, 15.5 (11c); H, 52.1 (11d); $:CF_2$, −39.7 (11e); and $\cdot CF_3$, −112.4 (11i); (b) J. R. Lacher and H. A. Skinner, *J. Chem. Soc., A*, 1034 (1968); (c) V. H. Dibeler, J. A. Walker, and K. E. McCulloh, *J. Chem. Phys.*, **50**, 4592 (1969); (d) S. W. Benson, *J. Chem. Educ.*, **42**, 502 (1965); (e) This $:CF_2$ value is the average of recent reported values (ref 10f–10h); (f) K. F. Zmbov, O. Manuel Uy, and J. L. Margrave, *J. Amer. Chem. Soc.*, **90**, 5090 (1968); (g) A. P. Modica and J. E. LaGraff, *J. Chem. Phys.*, **44**, 3375 (1966); (h) A. P. Modica and J. E. LaGraff, *ibid.*, **43**, 3383 (1965). (i) This $\cdot CF_3$ value was calculated from data for fluoroform dissociation (ref 11b, 11d, 11j); (j) J. C. Amphlett and E. Whittle, *Trans. Faraday Soc.*, **64**, 2130 (1968).

(12) (a) J. D. Kale and R. B. Timmons, *J. Phys. Chem.*, **72**, 4239 (1968). (b) Bond dissociation energies for CF_3–H, C_2F_5–H, n-C_3H_7–H, and H_2S are 4.61 ± 0.02, 4.46 ± 0.04, 4.42 ± 0.04, and 3.93 ± 0.07 eV (ref 11j, 12c) so that *maximum* n-$\dot{C}_xF_{2x}{}^{18}FH$ excitation energies from reactions of n-$\dot{C}_xF_{2x}{}^{18}F$ radicals with H_2S are 0.68, 0.53, and 0.49 (±0.08) eV for $x = 1$ to $x = 3$. Because the corresponding E_a values lie within the range 2.5 ± 0.2 eV (ref 10b), H_2S scavenging cannot have induced further decomposition of the products from (4) unless the scavenged radicals already contained *at least* 2 eV of vibrational excitation. (c) T. F. Palmer and F. P. Lossing, *J. Amer. Chem. Soc.*, **84**, 4661 (1962).

(13) (a) D. Urch and R. Wolfgang, *ibid.*, **83**, 2982 (1961); (b) J. W. Root, *J. Phys. Chem.*, **73**, 3174 (1969).

(14) This research was supported under Atomic Energy Commission Contract No. AT-(11-1)-34, Agreement 158.

(15) To whom inquiries should be addressed at Crocker Nuclear Laboratory and Department of Chemistry, University of California, Davis, Calif. 95616.

DEPARTMENT OF CHEMISTRY
UNIVERSITY OF CALIFORNIA,
DAVIS, CALIFORNIA 95616

CHARLES F. MCKNIGHT
JOHN W. ROOT[15]

RECEIVED JULY 14, 1969

ADDITIONS AND CORRECTIONS

1965, Volume 69

G. Z. Whitten and B. S. Rabinovitch: The Chemically Activated Decomposition of *n*-Butane and of Isobutane.

Page 4353. In Table IV, the values given under k_{exptl} should all be reduced by a factor of 10. Their description in the text in terms of collision rate at a given pressure remains correct. We thank Professor J. W. Simons for calling our attention to this error.—B. S. Rabinovitch.

1967, Volume 71

H. Selig, C. W. Williams, and G. J. Moody: The Refractive Indices, Densities, and Dielectric Constants of IF_7 and IOF_5.

Page 2741. In a recent communication [C. J. Schack, D. Pilipovich, S. N. Cohz, and D. F. Sheehan, *J. Phys. Chem.*, **72,** 4697 (1968)] it was pointed out that the density of liquid IOF_5 reported earlier [H. Selig, C. W. Williams, and G. J. Moody, *ibid.*, **71**, 2739 (1967)] may be inaccurate because it depended on incorrect vapor pressure data [N. Bartlett and L. E. Levchuck, *Proc. Chem. Soc.*, 342 (1963)]. We have recalculated our density values for liquid IOF_5 using the two newly reported vapor pressure points for liquid IOF_5 (Schack, *et al.*). The correct density of liquid IOF_5 over the range 7–25° is represented by the equation

$$d = (2.6600 \pm 0.0005) - (0.00482 \pm 0.0000)t$$

The vapor pressure equation for IF_7 reported by Selig, Williams, and Moody remains unchanged.—C. W. Williams and H. Selig

1968, Volume 72

P. L. Luisi and P. Pino: Conformational Properties of Optically Active Poly-α-olefins in Solution.

Page 2402. In Table I, second column, the first line should read 180 instead of 300 and the second line should read 300 instead of 180. In Table II, first column, the S_2 and S_1 should be interchanged.—P. Pino and P. L. Luisi.

Jiri Janata and Harry B. Mark, Jr.: The Reduction of Aromatic Hydrocarbons. II. Polarographic Study of the Effect of Proton Donors.

Pages 3617 and 3619. The rate constant in eq 11 should be expressed in l. mol^{-1} sec^{-1} and therefore the coefficient 10^{-3} in eq 13 should be deleted. Consequently, values of k in Figures 1 and 2 and estimated values of k for hydroquinone and resorcinol should be multiplied by a factor of 10^{-3}. As a result of this error, the assumed conditions for reaction layer approximation are not fulfilled for slow protonation reaction (curves 1–3 in Figures 1 and 2). Other results and conclusions are unaffected.—Jiri Janata and Harry B. Mark, Jr.

Y. C. Wu, R. M. Rush, and G. Scatchard: Osmotic and Activity Coefficients for Binary Mixtures of Sodium Chloride, Sodium Sulfate, Magnesium Sulfate, and Magnesium Chloride in Water at 25°. I. Isopiestic Measurements on the Four Systems with Common Ions.

Pages 4049 and 4050. In Tables I–IV z is used for the osmolality fraction as defined on p 4048. On pp 4049 and 4050 the same symbol is used for the valence of an ion. The only ambiguity occurs in the first paragraph of the second column of p 4050. In the factor $-2/z_+z_-$ the symbol z refers to the valence of the ion.

Page 4050. In Table VI the heading for the second column of figures should be $Na_2SO_4(A)$–$MgSO_4(B)$.

Page 4052. The title for Table VII should be "Values of the Parameters Q_{AB} and Q_{BA}." The headings for columns two and three are reversed. The heading for column two should be Q_{AB} and for column three Q_{BA}.—Richard M. Rush.

Fumikatsu Tokiwa: Solubilization Behavior of a Polyoxyethylene Sulfate Type of Surfactant in Connection with the Micellar Charge.

Page 4332. In Figure 2, the graduation of α should be added on the right-hand ordinate; from the bottom of this figure α should be 0.3, 0.4, 0.5, and 0.6.—Fumikatsu Tokiwa.

Norio Ise, Hideo Hirohara, Tetsuo Makino, and Ichiro Sakurada: Ionic Polymerization under an Electric Field. XII. Living Anionic Polymerization of Styrene in the Binary Mixtures of Benzene and Tetrahydrofuran.

Page 4544. Column 1, line 6 from the bottom, "and CaH_2 was cooled to the melting point" should read "and CaH_2, cooled to the melting point."

Page 4548. Column 2, line 12 from the top, "true case" should read "true cause."—N. Ise.

1969, Volume 73

T. L. Broadwater and D. Fennell Evans: Partial Molal Volume of $[Bu_3N\text{-}(CH_2)_4\text{-}NBu_3]Br_2$, a Large Bolaform Electrolyte, in Water at 10 and 25°.

Page 167. We wish to add the following acknowledgment. *Acknowledgment.* This work was supported by Contract No. 14-01-0001-1281 with the Office of Saline water, U. S. Department of the Interior.—D. Fennell Evans.

Eugene M. Holleran: A Dimensionless Constant Characteristic of Gases, Equations of State, and Intermolecular Potentials.

Page 171. In Table III, the value of T_B^* at $\gamma = 20$ should be 2.506 instead of 2.368.

Page 173. Equation 13 should read

$$Z = 1 + k_B[(B/V_B)\delta + (C/C_B)\delta^2 + \ldots]$$

rather than the published form.—Eugene M. Holleran.

K. J. Hole and M. F. R. Mulcahy: The Pyrolysis of Biacetyl and the Third-Body Effect on the Combination of Methyl Radicals.

Page 185. Professor B. S. Rabinovitch has drawn the authors' attention to an error in one of the points plotted in Figure 7. The value of log $p_{1/2}$ at 760°K (log T = 2.88) derived from the work of Krech and Price (ref 48) on the combination of methyl radicals in the presence of benzene is incorrectly given as 1.0. It should be 2.0. This does not affect any conclusion drawn in the paper.—M. F. R. Mulcahy.

T. R. Beck: "Electrocapillary Curves" of Solid Metals Measured by Extensometer Instrument.

Page 468. All of the potentials in the text should be with respect to the standard hydrogen electrode, s.h.e., rather than as shown (SCE is correct in Figure 2).—T. R. Beck.

Paul Ehrlich and Robert H. Fariss: Negative Partial Molal Volumes in the Critical Region. Mixtures of Ethylene and Vinyl Chloride.

Page 1165. The pressure referred to in the legend of Figure 3 should read 69.0 atm.

Page 1166. There should be a decimal point before the last digit in the first column of Table I; *i.e.*, the proper pressures are 69.0, 71.7, and 69.9 atm.

Page 1166. The pressures referred to in the second and fourth paragraphs should read 70 atm.—PAUL EHRLICH.

Y. C. Wu, R. M. Rush, and G. Scatchard: Osmotic and Activity Coefficients for Binary Mixtures of Sodium Chloride, Sodium Sulfate, Magnesium Sulfate, and Magnesium Chloride in Water at 25°. II. Isopiestic and Electromotive Force Measurements on the Two Systems without Common Ions.

Pages 2048, 2049, and 2052. In Table I, z is used for the osmolality fraction as defined on p 2048. On pp 2049 and 2052 the same symbol is used for the valence of an ion. The only ambiguity occurs in the first paragraph of text of the first column of p 2049. In the factor $-2/z_+z_-$ the symbol z refers to the valence of the ion.

Page 2049. In eq 6 the first term of the second line should be $\beta_{AB}^{(0)}y_B$.—RICHARD M. RUSH.

AUTHOR INDEX *to Volume 73, 1969*

Abraham, R. J. Medium Effects in Rotational Isomerism. VI. Inclusion of Dipole–Dipole Interactions in Polar Sovents 1192
Abrams, L., and Allen, A. O. Radiolysis of Ethanol Adsorbed on Silica 2741
Abrams, L., and Sutherland, J. W. Infrared Study of the Radiolysis of Carbon Dioxide, Ammonia, and Hydrogen Adsorbed on Silica 3160
Ache, H. J., and Wolf, A. P. Production and Reactivity of Carbon-11 in Solid Compounds 3499
Ache, H. J. See Finn, R. D., 3928; Wu, Y., 2424
Ackermann, R. J., Rauh, E. G., and Chandrasekharaiah, M. S. A Thermodynamic Study of the Urania–Uranium System 762
Ackermann, R. J., and Rauh, E. G. The Vapor Pressure of Liquid Uranium; Effects of Dissolved Tantalum, Phosphorus, Sulfur, Carbon, and Oxygen 769
Ackermann, T. See Neumann, E., 2170; Ruterjans, H., 986
Adami, L. H. See O'Neil, J. R., 1553
Adams, R. N. See Marcoux, L. S., 2611
Adamson, A. W., Vogler, A., and Lantzke, I. Photochemistry of Complex Ions. VII. *trans*-4-Stilbenecarboxylatopentaamminecobalt(III) Ion 4183
Adamson, A. W. See Waltz, W. L., 4250
Adman, E., and Margulis, T. N. Crystal and Molecular Structure of *cis*-1,3-Cyclobutanedicarboxylic Acid 1480
Affsprung, H. E. See Lynch, R. L., 3273
Agrawal, M. C. See Mehrotra, U. S., 1996
Ahlert, R. C. See Vogl, W. F., 2304
Ahluwalia, J. C. See Subramanian, S., 266
Ahmed, S. M. Studies of the Double Layer at Oxide–Solution Interface 3546
Albrecht, A. C. See Cadogan, K. D., 1868
Albright, J. G. Two Semiempirical Equations Which Relate Viscosity and the Intradiffusion Coefficients for Multicomponents Systems 1280
Alei, M., Jr., and Florin, A. E. Proton Magnetic Resonance Study of Water–Ammonia Proton Exchange in Water–Ammonia Solutions Containing Added Potassium Hydroxide 857
Alei, M., Jr., and Florin, A. E. The Nature of Water Species in Water–Ammonia Solutions as Inferred from Proton and Oxygen-17 Nuclear Magnetic Resonance Observations 863
Algar, B. E. See Stevens, B., 1711
Allan, G. G., and Neogi, A. Macromolecular Organometallic Catalysis 2093
Allen, A. O. See Abrams, L., 2741; Capellos, C., 3264; Gebicki, J. M., 2443
Allulli, S. Solubilities of Ammonia in Alkali Nitrate and Perchlorate Melts 1084
Alwitt, R. S. A Contribution to the Theory of Dielectric Dispersion of Colloidal Particles 1052
Alwitt, R. S. A Dielectric Dispersion of Paper Impregnated with a Glycol Electrolyte 1056
Amdur, S. Determination of Water Activities of Dilute Electrolyte Solutions 1163
Ander, S. M. See Schmidt, K. H., 2846
Anders, L. R. Study of the Energetics of Ion–Molecule Reactions by Pulsed Ion Cyclotron Double Resonance 469
Andersen, T. N., Anderson, J. L., and Eyring, H. The Nature of Fresh Metal Surfaces in Aqueous Solutions 3562
Anderson, B. A. See Berlin, E., 303
Anderson, D. K. See Kett, T. K., 1262, 1268
Anderson, J. L. See Andersen, T. N., 3562
Andrade, J. R. See Vidulich, G. A., 1621
Andrews, L. Infrared Spectra and Bonding in the Sodium Superoxide and Sodium Peroxide Molecules 3922
Andrews, L., and Frederick, D. L. Infrared Spectra of the Dichloro- and Dibromophosphinyl Radicals in Solid Argon 2774
Angell, C. A. See Moynihan, C. T., 2287
Angell, C. L., and Howell, M. V. Infrared Spectroscopic Investigation of Zeolites and Adsorbed Molecules. IV. Acetonitrile 2551
Anson, F. C., Martin, R. F., and Yarnitzky, C. Creation of Nonequilibrium Diffuse Double Layers and Studies of Their Relaxation 1835
Appleby, A., and Schwarz, H. A. Radical and Molecular Yields in Water Irradiated by γ Rays and Heavy Ions 1937
Ard, J. S. See Susi, H., 2440
Arel, M. See Desnoyers, J. E., 3346
Arkell, A. Matrix Infrared Studies of OF Radical Systems 3877
Armistead, C. G., Tyler, A. J., Hambleton, F. H., Mitchell, S. A., and Hockey, J. A. The Surface Hydroxylation of Silica 3947
Arnason, B. Equilibrium Constant for the Fractionation of Deuterium between Ice and Water 3491
Arnold, R. Temperature Dependence of Electroosmotic Water Transport through Cation-Exchange Membranes. The Effect of Proton Jumping 1414
Arnold, S. J., and Kimbell, G. H. Reactions of Shock-Heated Carbon Disulfide–Argon Mixtures. I. Light Emission 3751
Arzoumanidis, G. G., and O'Connell, J. J. Electrocatalytic Oxidation of D-Glucose in Neutral Media with Electrodes Catalyzed by 4,4′,4′′,4′′′-Tetrasulfophthalocyaninemolybdenum Dioxide Salts 3508
Asai, K., Takaya, K., and Ise, N. Mean Activity Coefficient of Polyelectrolytes. XI. Activity Coefficients of Various Salts of Polyacrylic Acid and Carboxymethylcellulose 4071
Asmus, K.-D., and Fendler, J. H. The Use of Sulfur Hexafluoride to Determine $G(e^-_{D_2O})$ and Relative Reaction Rate Constants in D_2O 1583
Asmus, K.-D. See Warman, J. M., 931
Asmus, T. W., and Houser, T. J. Pyrolysis Kinetics of Acetonitrile 2555
Assink, R. A., and Jonas, J. Calculation of Rotational Diffusion Constants for Anisotropic Reorientation by the Modified Hill Method 2445
Atkinson, G. See Staples, B. R., 520
Avery, H. E., Hayes, D. M., and Phillips, L. Reactions of Acetyl and Methyl Radicals with Nitric Oxide 3498
Avitabile, G., Ganis, P., and Petraccone, V. The Crystal and Molecular Structure of 1,3,5,7-Tetramethylcycloocta-*cis,cis,cis,cis*-1,3,5,7-tetraene 2378

Baba, K., Fujimura, T., and Kamiyoshi, K. The Dielectric Relaxation of Binary Liquid Mixtures 1146
Back, R. A. See Terao, T., 3884
Bacon, W. E., and Brown, G. H. X-Ray Diffraction Studies of Mono- and Polynuclear Thorium(IV) Ions in Aqueous Perchlorate Solutions 4163
Badachhape, R. B. See Wood, J. L., 3139
Baharad, R., Perlmutter-Hayman, B., and Wolff, M. A. The Kinetics of the Hydrolysis of the Dichromate Ion. V. General Acid Catalysis 4391
Bahnick, D. A., Bennett, W. E., and Person, W. B. A Spectroscopic Study of Some CBr_4 Complexes 2309
Bailey, M. G., and Dixon, R. S. The Molecular Hydrogen Yield in Irradiated 2-Propanol Vapor 2451
Bailey, R. E., and Cady, G. H. Nuclear Magnetic Resonance Studies of Heptafluorobutyric Acid Micelle Formation 1612
Bakale, G., and Gillis, H. A. The Radiolysis of Solutions of Ethylene in Ethane 2178
Baker, R. T. K., and Wolfgang, R. L. On the Occurrence of Simultaneous Double Displacement in Hot-Hydrogen Reactions 3478
Balakrishnan, I. See Srinivasan, T. K. K., 2071
Balasubramanian, D. See Subramanian, S., 266
Baldwin, W. H., Raridon, R. J., and Kraus, K. A. Properties of Organic–Water Mixtures. X. Activity Coefficients of Sodium Chloride at Saturation in Water Mixtures of Polyglycols and Polyglycol Ethers at 50° 3417
Baliga, B. T., and Whalley, E. Effect of Pressure on the Rate of Hydrolysis of Methyl and Isopropyl Bromides 654
Bard, A. J. See Valenzuela, J. A., 779

Barefoot, R. D. See Tompa, A. S., 435
Barker, N. T. See Johnsen, R. H., 3204
Barnartt, S. See Johnson, C. A., 3374
Barradas, R. G., and Hermann, E. W. Electrocapillary Studies in Aqueous Lithium Chloride Solutions 3619
Bartle, K. D., and Jones, D. W. Proton Chemical Shifts and the Reactivity of Polynuclear Aromatic Hydrocarbons 293
Basch, H., and Ginsberg, A. P. A Molecular Orbital Description of TcH_9^{2-} 854
Bates, R. G. See Paabo, M., 3014
Batt, L. Comment on the Communication "Acetone Formation in the Pyrolysis of Acetaldehyde" 2091
Batten, R. C. See Stanley, E. M., 1187
Baum, E. J. See Párkányi, C., 1132
Baumgartner, E. See Fernández-Prini, R., 1420
Baur, M. E., Horsma, D. A., Knobler, C. M., and Perez, P. Dielectric Constant and Refractive Index of Weak Complexes in Solution 641
Baybarz, R. D. See Nugent, L. J., 1177, 1540
Bayes, K. D. See Williamson, D. G., 1232
Bayley, P. M., Nielsen, E. B., and Schellman, J. A. The Rotatory Properties of Molecules Containing Two Peptide Groups: Theory 228
Beard, H. R. See Prenzlow, C. F., 969
Bearman, R. J., and Woolf, L. A. Further Consideration of the Moving Boundary Experiment for the Measurement of Transference Numbers 4403
Beauchamp, A. L. See Benoit, R. L., 3268
Beaven, G. H. See Gratzer, W. B., 2270
Beck, T. R. "Electrocapillary Curves" of Solid Metals Measured by Extensometer Instrument 466
Beggs, D. P., and Lampe, F. W. Ionic Reactions in Gaseous Mixtures of Monosilane and Acetylene 3307
Beggs, D. P., and Lampe, F. W. Ionic Reactions in Gaseous Mixtures of Monosilane and Ethylene 3315
Beggs, D. P., and Lampe, F. W. Ionic Reactions in Gaseous Mixtures of Monosilane with Methane and Benzene 4194
Bell, G. M. See Levine, S., 3534
Bell, J. T., Thompson, C. C., and Helton, D. M. The High-Temperature Spectra of Aqueous Transition Metal Salts. I. Praseodymium and Neodymium Nitrate to 356° 3338
Benedetti, E., Corradini, P., and Pedone, C. The Crystal and Molecular Structure of the *trans*-3,6-Dimethyl-2,5-piperazinedione (L-Alanyl-D-alanyl-2,5-diketopiperazine) 2891
Benerito, R. R., Ziifle, H. M., and Berni, R. J. Kinetics of the Fluoroboric Acid Catalyzed Hydrolysis of Butadiene Diepoxide 1216
Ben-Naim, A. See Stillinger, F. H., Jr., 900
Bennett, W. E. See Bahnick, D. A., 2309
Bennion, B. C., Tong, L. K. J., Holmes, L. P., and Eyring, E. M. Kinetics of Sodium Lauryl Sulfate Micelle Dissociation by a Light-Scattering Temperature-Jump Technique 3288
Benoit, R. L., Beauchamp, A. L., and Deneux, M. Equilibria between Silver, Chloride, and Bromide Ions in Sulfolane 3268
Bensasson, R. See Potashnik, R., 1912
Benson, G. C. See Boublik, T., 2356
Benson, R. C., Scott, R. S., and Flygare, W. H. The Molecular g Values, Magnetic Susceptibility Anisotropies, and Molecular Quadrupole Moments in Propynal 4359
Benson, S. W. See Cruickshank, F. R., 733
Beran, J. A., and Kevan, L. Semiempirical Calculation of Molecular Polarizabilities and Diamagnetic Susceptibilities of Fluorocarbons, Substituted Fluorocarbons, Ethers, Esters, Ketones, and Aldehydes 3860
Beran, J. A., and Kevan, L. Molecular Electron Ionization Cross Sections at 70 eV 3866
Berlin, E., Anderson, B. A., and Pallansch, M. J. Sorption of Water Vapor and of Nitrogen by Genetic Variants of α_{s1}-Casein 303
Bernal, I. See Brennan, T., 443
Berni, R. J. See Benerito, R. R., 1216
Bettman, M., and Peters, C. R. The Crystal Structure of $Na_2O \cdot MgO \cdot 5Al_2O_3$ with Reference to $Na_2O \cdot 5Al_2O_3$ and Other Isotypal Compounds 1774
Beutel, J., Ruszkay, R. J., and Brennan, J. F. Quinone Photoreduction. I. A Mathematical Model 3240
Beutel, J. See Brennan, J. F., 3245
Bevan, R. B., Jr. See Busey, R. H., 1039
Bhatnagar, O. N., and Criss, C. M. Thermodynamic Properties of Nonaqueous Solutions. VI. Enthalpies of Solution of Some Tetraalkylammonium Iodides in Water and N,N-Dimethylformamide at 25° 174
Bhattacharyya, S. K., and Purohit, G. B. Effect of Pressure on the Rate of Acid-Catalyzed Hydration of Crotonic Acid 3278
Biagini, E. See Russo, S., 378
Biegler, T., and Woods, R. Analysis of Isotherms with Coverage-Dependent Heats of Chemisorption 3502
Bielski, B. H. J., and Gebicki, J. M. Electron Spin Resonance Studies of the Mechanism of Interaction between Nitrogen Dioxide and Olefinic Solvents 1402
Biloen, P., Fransen, T., Tulp, A., and Hoytink, G. J. Ultraviolet and Conductance Data Pertinent to the Clustering of Terphenyl Radical Anions with Sodium Cations in THF Solutions 1581
Biordi, J. C. The Behavior of Nitrogen Atoms in the Presence of Nitrosyl Chloride 3163
Birss, F. W. See Messmer, R. P., 2085
Bissell, R. See Hoffmann, R., 1789
Bist, H. D., and Person, W. B. Spectroscopic Studies of the Triethylamine–I_2 System in *n*-Heptane and in *p*-Dioxane 482
Blachford, J. A Theory of the Secondary Electroviscous Effect for Nonidentical Particles 3512
Blachford, J., Chan, F. S., and Goring, D. A. I. The Secondary Electroviscous Effect. Paths of Approach of Two Charged Spheres in a Viscous Medium 1062
Blanchette, P. P. See Vidulich, G. A., 1621
Blaser, S. See Weiler, R., 4147
Blauer, J. A., McMath, H. G., and Jaye, F. C. The Thermal Dissociation of Chlorine Trifluoride behind Incident Shock Waves 2683
Bloch, F. W., and MacKenzie, D. R. Radiolysis of Cyclic Fluorocarbons. II. Perfluoroaromatics at Elevated Temperatures 552
Blount, H. N. See Herman, H. B., 1406; Winograd, N., 3456
Blyholder, G., and Neff, L. D. Structure of Surface Species on Cobalt 3494
Bockris, J. O'M., Gileadi, E., and Stoner, G. E. The Anodic Oxidation of Saturated Hydrocarbons. A Mechanistic Study 427
Boden, D. P. See Mukherjee, L. M., 3965
Bolton, J. R. See Sullivan, P. D., 4387
Bonner, O. D., and Kim, S.-J. The Osmotic and Activity Coefficients of Some Dibolaform Electrolytes 1367
Bonner, O. D., Kim, S. J., and Torres, A. L. A Comparison of the Osmotic and Activity Coefficients of Some Solutes in Structured Solvents 1968
Bordewijk, P., Gransch, F., and Böttcher, C. J. F. The Dielectric Behavior of Mixtures of Heptanol-1 and Heptanol-4 and the Fluid Structure of the Monoalcohols 3255
Borello, E., Zecchina, A., Morterra, C., and Ghiotti, G. Infrared Study of Carbon Monoxide, Oxygen, and Carbon Dioxide Adsorption on Chromia–Silica. I. Carbon Monoxide 1286
Borello, E. See Zecchina, A., 1292, 1295
Bothner-By, A. A., and Cox, R. H. The Estimation of Vicinal Phosphorus-31–Hydrogen and Nitrogen-14–Hydrogen Spin–Spin Coupling Constants in Single Conformers 1830
Bothner-By, A. A. See Cox, R. H., 2465
Böttcher, C. J. F. See Bordewijk, P., 3255
Boublik, T., Lam, V. T., Murakami, S., and Benson, G. C. The Excess Thermodynamic Functions of Cyclopentane–Carbon Tetrachloride Mixtures 2356
Boudart, M. See Delgass, W. N., 2970
Bowden, M. J., and O'Donnell, J. H. Dehydration of Barium Methacrylate in Air 2871
Bowen, L. H. See Kalfoglou, G., 2728
Boyd, G. E. See Brown, L. C., 396
Boyd, R. H. See Hirko, R. J., 1990
Boyington, R. L. See Masterton, W. L., 2761
Boyle, J. W., Ghormley, J. A., Hochanadel, C. J., and Riley, J. F. Production of Hydrated Electrons by Flash Photolysis of Liquid Water with Light in the First Continuum 2886
Braddock, J. N. See Wood, R. H., 1673
Brainard, A. J. The Behavior of Entropy at Low Temperatures 940
Braunstein, J. Comment on Complex Ion Equilibria in Molten Salt Mixtures 754
Braunstein, J. See Tripp, T. B., 1984

Brecher, C., and French, K. W. Comparison of Aprotic Solvents for Nd^{3+} Liquid Laser Systems: Selenium Oxychloride and Phosphorus Oxychloride ... 1785
Breiter, M. W. Processes Occurring during the Interaction of Carbon Monoxide with Platinized Platinum at Potentials of the Hydrogen Region ... 3283
Breivogel, F. W., Jr. Solvent Exchange Rates of Solvent–Metal Complexes for Fe^{3+} in N,N-Dimethylformamide, Acetonitrile, and Ethanol for Ni^{2+} in Ethanol by Proton Magnetic Resonance ... 4203
Brennan, J. F., and Beutel, J. Quinone Photoreduction. II. The Mechanism of Photoreduction of 9,10-Phenanthrenequinone and 2,*t*-Butyl-9,10-anthraquinone in Ethanol ... 3245
Brennan, J. F. See Beutel, J., 3240
Brennan, T., and Bernal, I. The Crystal and Molecular Structure of Tris(diethyldithiocarbamato)cobalt(III) ... 443
Bresler, E. H., and Wendt, R. P. Onsager's Reciprocal Relation. An Examination of Its Application to a Simple Membrane Transport Process ... 264
Brieland, W. G. See Hase, W. L., 4401
Broadwater, T. L., and Evans, D. F. Partial Molal Volume of $[Bu_3N\text{–}(CH_2)_8\text{–}NBu_3]Br_2$, a Large Bolaform Electrolyte, in Water at 10 and 25° ... 164
Broadwater, T. L., and Evans, D. F. Transport Processes in Hydrogen Bonding Solvents. III. The Conductance of Large Bolaform Ions in Water at 10 and 25° 3985
Bronskill, M. J., Wolff, R. K., and Hunt, J. W. Subnanosecond Observations of the Solvated Electron ... 1175
Bronstein, H. R. Electromotive Force Measurements on Solutions of Rare Earth Metals in Their Molten Halides. I. The Cerium–Cerium Chloride, Praseodymium–Praseodymium Chloride, and Neodymium–Neodymium Chloride Solutions ... 1320
Broussard, L. The Disproportionation of Wustite ... 1848
Brower, K. R., Peslak, J., Jr., and Elrod, J. A Correlation of Molecular Flexibility with Volume and Heat of Mixing of Organic Solutes with Water and a Glycol–Water Mixture ... 207
Brown, G. H. See Bacon, W. E., 4163
Brown, L. C., and Boyd, G. E. Production of Perchlorate and Chlorite Ions in Crystalline Potassium Chlorate Irradiated with Cobalt-60 γ Rays ... 396
Brown, R. J. S. Empirical Expressions for Viscosity and Proton Spin-Lattice Relaxation Times for Water from −10 to +140° ... 3157
Brownlee, R. T. C., English, P. J. Q., Katritzky, A. R., and Topsom, R. D. Infrared Intensities as a Quantitative Measure of Intramolecular Interaction. VII. The ν_{13} Band near 1500 Cm^{-1} in Monosubstituted and *para*-Disubstituted Benzenes ... 557
Broze, M., and Luz, Z. Oxygen-17 Spin–Spin Coupling with Manganese-55 and Carbon-13 ... 1600
Brummer, S. B. See Gancy, A. B., 2429; Taylor, A. H., 2397
Brundage, R. S. See Prenzlow, C. F., 969
Bryant, J. T. See Chan, S. C., 2464
Bryant, R. G. Nuclear Magnetic Resonance Study of Concentrated Lithium Chloride Solutions ... 1153
Buchanan, A. S., Knowles, D. J., and Swingler, D. L. Electron Impact Studies of Stannous Chloride and Stannic Chloride ... 4394
Bucher, J. J., and Diamond, R. M. Extraction of HClO$_4$ and HReO$_4$ by Dilute Solutions of Tributyl Phosphate in Carbon Tetrachloride, Isooctane, and 1,2-Dichloroethane ... 675
Bucher, J. J., and Diamond, R. M. Extraction of HClO$_4$ and HReO$_4$ by Dilute Solutions of Tributyl Phosphate in Benzene, *sym*-Triethylbenzene, and Chloroform ... 1494
Buchowski, H. Evidence of Chain Association of Benzoic Acid in Benzene? ... 3520
Budde, W. L. The Rates of Methanolysis of Several Organosilazanes ... 3718
Buenker, R. J., and Peyerimhoff, S. D. Theoretical Study of the Geometry, Reactivity, and Spectrum of Cyclopropane ... 1299
Bunker, D. L., and Chang, T.-S. A Parametric Study of Bimolecular Exchange Reactions ... 943
Bunton, C. A., and Robinson, L. Micellar Effects on Acidity Functions ... 4237
Burdett, J. K. See Current, J. H. 3504, 3505
Burgin, M. See Johnsen, R. H., 3204
Burkhart, M. J., and Newton, T. W. The Kinetics of the Reaction between Vanadium(II) and Neptunium(IV) in Aqueous Perchlorate Solutions ... 1741
Burkhart, R. D. Radical–Radical Reactions in Different Solvents. Propyl, Cyclohexyl, and Benzyl Radicals 2703
Burkhart, R. D., and Merrill, J. C. Photo- and Thermal Initiator Efficiency of 2,2′-Azobisisobutyronitrile at 25° ... 2699
Burlamacchi, L., and Tiezzi, E. An Electron Paramagnetic Resonance Study of Inner- and Outer-Sphere Equilibria of Manganese(II) in Water Solution ... 1588
Burnelle, L. See Olsen, J. F., 2298
Burnett, L. J. See Nugent, L.J., 1177, 1540
Busey, R. H., Sprague, E. D., and Bevan, R. B., Jr. Enthalpy of Hydrolysis of Rhenium Trichloride. Enthalpy and Free Energy of Formation of Rhenium Sesquioxide ... 1039
Busse, H. G. A Spatial Periodic Homogeneous Chemical Reaction ... 750
Butler, J. N., Cogley, D. R., and Synnott, J. C. Effect of Water on the Kinetics of the Solid Lithium–Lithium Ion Reaction in Propylene Carbonate ... 4026
Butler, J. N. See Synnott, J. C., 1470
Butler, R. S. See Schmidt, R. L., 1117
Buxton, G. See Laming, F. P., 867

Cadogan, D. F., Conder, J. R., Locke, D. C., and Purnell, J. H. Concurrent Solution and Adsorption Phenomena in Chromatography. II. System Alcohols–Squalane ... 708
Cadogan, D. F., and Purnell, J. H. Concurrent Solution and Adsorption Phenomena in Chromatography. III. The Measurement of Formation Constants of H-Bonded Complexes in Solution ... 3849
Cadogan, K. D., and Albrecht, A. C. Polarized Triplet–Triplet Absorption Spectra in Three Benzene Derivatives ... 1868
Cady, G. H. See Bailey, R. E., 1612
Calvert, J. G. See Okuda, S., 4412
Campbell, G. M. Thermodynamic Properties of Plutonium Nitride by Galvanostatic Potential Determination ... 350
Campbell, J. R., and Nancollas, G. H. The Crystallization and Dissolution of Strontium Sulfate in Aqueous Solution ... 1735
Cantu, A. A. See Matsen, F. A., 2488
Capellos, C., and Allen, A. O. Ionization of Liquids by Radiation Studied by the Method of Pulse Radiolysis. II. Solutions of Triphenylmethyl Chloride ... 3264
Capellos, C., and Swallow, A. J. Aspects of the Pulse Radiolysis and γ Radiolysis of Alkyl Iodides and Their Mixtures ... 1077
Cargioli, J. See Frankel, L. S., 91
Carlisle, T. L. See Deming, R. L., 1762
Carlson, K. D. See Cohen, I., 1356
Carlton, T. S., and Harker, A. B. Kinetics of the Reaction of Hydrogen Iodide with Tetrafluoroethylene.. 3356
Carman, P. C. Transport in Concentrated Solutions of 1:1 Electrolytes ... 1095
Carr, R. W., Jr. See Eder, T. W., 2074
Carroll, B. See Freeman, E. S., 751
Cash, D. L. See Larson, D. L., 2814
Cassatt, J. C. See Pasternack, R. F., 3814
Castle, J. E., and Surman, P. L. The Self-Diffusion of Oxygen in Magnetite. The Effect of Anion Vacancy Concentration and Cation Distribution ... 632
Catone, D. L. See Matijević, E., 3556
Cercek, B., and Kongshaug, M. Hydrogen Ion Yields in the Radiolysis of Neutral Aqueous Solutions ... 2056
Chakravorty, K., Pearson, J. M., and Szwarc, M. Photolysis of 1,1,1-Trifluoromethylazocyclopropane. The Fate of the N·N-*c*-C$_3$H$_5$ Radical ... 746
Chan, F. S. See Blachford, J., 1062
Chan, S. C., Rabinovitch, B. S., Spicer, L. D., and Bryant, T. J. Dipolar Orientation Effect in Collisional Energy Transfer ... 2464
Chan, W. See Jones, R. A., 3693
Chandler, W. L., and Dinius, R. H. Nuclear Magnetic Resonance Study of Hydrogen Bonding in Ethanol ... 1596
Chandrasekharaiah, M. S. See Ackermann, R. J., 762
Chang, E. See Justice, B. H., 333
Chang, J. W., and Martin, R. B. Visible Circular Dichroism of Planar Nickel Ion Complexes of Peptides and Cysteine and Derivatives ... 4277
Chang, T.-S. See Bunker, D. L.,943
Chantooni, M. K., Jr. See Kolthoff, I. M., 4029
Charney, E. See Tsai, L., 2462
Chen, C. L. See Wen, W.-Y., 2895

Chen, C. Y. S., and Swenson, C. A. Self-Association of Some Lactams 1363
Chen, C. Y. S., and Swenson, C. A. The Ultraviolet Absorption Spectra of Lactams 1642
Chen, C. Y. S., and Swenson, C. A. Infrared Spectral Studies on Lactams as *cis–trans* Models for the Peptide Bond 2999
Cheong, K.-K., Fu, Y.-C., Robins, R. K., and Eyring, H. Absorption, Optical Rotatory Dispersion, and Circular Dichroism Studies on Some Sulfur-Containing Ribonucleosides 4219
Child, W. C., Jr. See Deming, R. L., 1762
Childs, C. W. Equilibria in Dilute Aqueous Solutions of Orthophosphates 2956
Chiu, Y.-C., and Genshaw, M. A. A Study of Anion Adsorption on Platinum by Ellipsometry 3571
Choudhury, P. K. See Das, B., 3413
Chow, L. C., and Martire, D. E. Thermodynamics of Solutions with Liquid Crystal Solvents. II. Surface Effects with Nematogenic Compounds 1127
Chowdhury, D. M., and Harris, G. M. Thermal and Neutron Irradiation Effects on the Rate of Racemization of d-$K_3Cr(C_2O_4)_3 \cdot 2H_2O$ in the Solid State 3366
Christe, K. O. Comments on "The Electrical Conductivity of Boron Trifluoride in Pure and Mixed Halogen Fluorides," by M. S. Toy and W. A. Cannon 2792
Christensen, H. See Nielsen, S. O., 3171; Pagsberg, P., 1029
Christian, S. D. See Lynch, R. L., 3273; Taha, A. A., 3430; Tucker, E. E., 3820
Christie, J. R. See Copeland, J. L., 1205
Chrysochoos, J. Pulse-Radiolysis Studies of p-Hydroxyphenylpropionic Acid 4188
Ciferri, A. See Gliozzi, A., 3063
Clark, A. See Finch, J. N., 2234
Clark, L. W. Further Studies on the Decarboxylation of n-Hexylmalonic Acid in Polar Solvents 438
Clearfield, A., Duax, W. L., Medina, A. S., Smith, G. D., and Thomas, J. R. On the Mechanism of Ion Exchange in Crystalline Zirconium Phosphates. I. Sodium Ion Exchange of α-Zirconium Phosphate 3424
Cobble, J. W. See Gardner, W. L., 2017, 2021, 2025
Coburn, T. T. See Harmon, K. M., 2939
Coetzee, J. F. See Springer, C. H., 471
Cogley, D. R. See Butler, J. N., 4026
Cohen, I., and Carlson, K. D. Density Distributions and Chemical Bonding in Diatomic Molecules of the Transition Metals 1356
Cole, D. L. See Holmes, L. P., 737; Owen, J. D., 3918; Rich, L. D., 713
Companion, A. L. Crystal Field Activation Energies of Hexaaquo Transition Metal Complexes 739
Compton, L. E., Gole, J. L., and Martin, R. M. Kinetics of Hot Hydrogen Atoms from H_2S Photodissociation at 1850 Å 1158
Compton, L. E., and Martin, R. M. Photodissociation Dynamics. Production of $I^*(^2P_{1/2})$ Atoms in the Photolysis of Hydrogen Iodide 3474
Conder, J. R., Locke, D. C., and Purnell, J. H. Concurrent Solution and Adsorption Phenomena in Chromatography. I. General Considerations 700
Conder, J. R. See Cadogan, D. F., 708
Conner, W. C., and Kokes, R. J. Addition of Hydrogen–Deuterium Mixtures to Ethylene over Chromia and Zinc Oxide 2436
Conway, B. E., and Gordon, L. G. M. Entropy and Structural Effects in the Electrochemical Adsorption of Pyridine at Mercury 3609
Conway, B. E., and Gordon, L. G. M. Some Common Problems with the Double Layer and Ionic Solutions. An Introductory Paper 3523
Copeland, J. L., and Christie, J. R. Effects of High-Pressure Helium, Argon, and Nitrogen on the Viscosity of Fused Sodium Nitrate 1205
Cordes, E. H. See Dunlap, R. B., 361, 1898
Corradini, P. See Benedetti, E., 2891
Costantino, L. See Vitagliano, V., 2456
Cotton, D. J. Shereshefsky's Equation and Binary-Solution Surface Tension 270
Cox, R. H. Effect of Cation on the Nuclear Magnetic Resonance Spectrum of Fluorenyl Carbanion 2649
Cox, R. H., and Bothner-By, A. A. Proton Magnetic Resonance Spectra of Tautomeric Substituted Pyridines and Their Conjugate Acids 2465
Cox, R. H. See Bothner-By, A. A., 1830
Crawford, B. L., Jr. See Fujiyama, T., 4040
Creekmore, R. W., and Reilley, C. N. Nuclear Magnetic Resonance Determination of Hydration Numbers of Electrolytes in Concentrated Aqueous Solutions 1563
Crickard, K., and Skinner, J. F. Negative Viscosity *B* Coefficients in Nonaqueous Solvents 2060
Criss, C. M. See Bhatnagar, O. N., 174
Cronan, C. L., and Schneider, F. W. Cooperativity and Composition of the Linear Amylose–Iodine–Iodide Complex 3990
Cross, R. J., Jr. See Wolfgang, R., 743
Crowell, T. I., and Hankins, M. G. The Hydrolysis of Thiocyanic Acid. I. Dependence of Rate on Acidity Function 1380
Cruickshank, F. R., and Benson, S. W. The Carbon–Hydrogen Bond Dissociation Energy in Methanol 733
Cubicciotti, D. See Keneshea, F. J., 3054
Cukrowski, A. S. The Diaphragm Cell Method for the Investigation of Thermal and Self-Thermal Diffusion in Liquid Electrolyte Solutions 6
Cummins, S. M. See Harmon, K. M., 2939
Cundall, R. B., Evans, G. B., and Land, E. J. Rate Constants for Quenching of Biacetyl Triplets in Benzene 3982
Cunningham, G. P. See Kay, R. L., 3322
Current, J. H., and Burdett, J. K. Infrared Spectra of $\cdot CCl_3$ and $\cdot CCl_2Br$ Isolated in an Argon Matrix 3504
Current, J. H., and Burdett, J. K. The Structure and Bonding in Methyl and Substituted Methyl Radicals 3505
Currie, J. A., and Dole, M. Specific Heat of Synthetic High Polymers. XIII. Amorphous Polystyrene 3384
Curthoys, G. See Elkington, P. A., 2321
Cyvin, B. N., and Cyvin, S. J. Mean Amplitudes of Vibration of Comparatively Large Molecules. III. Isotopic Anthracenes 1430
Cyvin, S. J. See Cyvin, B. N., 1430

Dahlqvist, K.-I., and Forsén, S. Application of Density Matrix Methods to the Study of Spin Exchange. I. The Barrier to Internal Rotation in N-Acetylpyrrole 4124
Dalla Lana, I. G. See Deo, A. V., 716
Danen, W. C., Kensler, T. T., Lawless, J. G., Marcus, M. F., and Hawley, M. D. Steric Effects in the Decomposition of Halogenated Nitrobenzene Anion Radicals 4389
Daniel, S. H., and Tang, Y.-N. Competitive Reactions of Recoil Tritium Atoms with Methylsilanes and Alkanes 4378
Daniels, M. Radiation Chemistry of the Aqueous Nitrate System. III. Pulse Electron Radiolysis of Concentrated Sodium Nitrate Solutions 3710
Daniels, M., and Wigg, E. E. Radiation Chemistry of the Aqueous Nitrate System. II. Scavenging and pH Effects in the Cobalt-60 γ Radiolysis of Concentrated Sodium Nitrate Solutions 3703
Dantzler, E. M., and Knobler, C. M. Interaction Virial Coefficients in Fluorocarbon Mixtures 1335
Dantzler, E. M., and Knobler, C. M. Complex Formation in Benzene–Hexafluorobenzene Vapor Mixtures 1602
D'Aprano, A., and Fuoss, R. M. Electrolyte–Solvent Interaction. XIX. Solvation by Molecular Picric Acid 223
D'Aprano, A., and Fuoss, R. M. Electrolyte–Solvent Interaction. XX. Picric Acid in Mixtures of Acetonitrile and Basic Solvents 400
Darbari, G. S., and Petrucci, S. Ultrasonic Absorption in Hydrated Melts. I. Systems of $Ca(NO_3)_2 \cdot 4H_2O$ and Its Mixtures with Water 921
Darnell, A. J., McCollum, W. A., and Yosim, S. J. The Electrical Conductivities of Molten Bismuth Chloride, Bismuth Bromide, and Bismuth Iodide at High Pressure 4116
Daruwala, J. See Swarbrick, J., 2627
Darwent, B. deB. See Flores, A. L., 2203; Timmons, R. B., 2208
Das, B., Ray, A. K., and Choudhury, P. K. Unperturbed Dimension of Sodium Cellulose Xanthate 3413
Das, J. See Guilbault, G. G., 2243
Dauerman, L., Salser, G. E., and Tajima, Y. A. Comment on "The Thermal Dissociation of Oxygen Difluoride. I. Incident Shock Waves" 1621
Davenport, J. E., and Miller, G. H. Photolysis of Perfluorocyclobutane 809
Davies, G., and Kustin, K. The Stoichiometry and Kinetics of Manganese(III) Reactions with Hydrazine and the Methylhydrazines in Acid Perchlorate Solution. 2248

Davis, G. T. See Hull, L. A., 2142, 2147

Dawson, W. R., and Kropp, J. L. Radiative and Radiationless Processes in Aromatic Molecules. Coronene and Benzcoronene ... 963

Dawson, W. R., and Kropp, J. L. Radiationless Deactivation and Anomalous Fluorescence of Singlet 1,12-Benzperylene ... 1752

Dawson, W. R. See Kropp, J. L., 1747

Day, A. F. See Horne, R. A., 2782

Day, M. C. See Hammonds, C. N., 1151; 4374; Hohn, E. G., 3880

De Boelpaep, J. See Verbeke, O. B., 4076

Defay, R. See Sanfeld, A., 4047

deHaas, N. See Westenberg, A. A., 1181

DeLancey, G. B. Analysis of Multicomponent Diaphragm Cell Data ... 1591

Delgass, W. N., Garten, R. L., and Boudart, M. Dehydration and Adsorbate Interactions of Fe–Y Zeolite by Mössbauer Spectroscopy ... 2970

Dembinski, G. W. See Yates, D. J. C., 911

Deming, R. L., Carlisle, T. L., Lauerman, B. J., Muckerman, J. T., Muirhead, A. R., and Child, W. C., Jr. Dissociation Pressures and Compositions of Quinol Clathrates of Methane and Methyl Fluoride ... 1762

DeMore, W. B. Reactions of $O(^1D)$ with Hydrocarbons in Liquid Argon ... 391

DeMore, W. B., and Jacobsen, C. W. Formation of Carbon Trioxide in the Photolysis of Ozone in Liquid Carbon Dioxide ... 2935

Dempsey, E. The Calculation of Madelung Potentials for Faujasite-Type Zeolites. I ... 3660

Dempsey, E., Kuhl, G. H., and Olson, D. H. Variation of the Lattice Parameter with Aluminum Content in Synthetic Sodium Faujasites. Evidence for Ordering of the Framework Ions ... 387

Deneux, M. See Benoit, R. L., 3268

Dent, A. L., and Kokes, R. J. Hydrogenation of Ethylene by Zinc Oxide. I. Role of Slow Hydrogen Chemisorption ... 3772

Dent, A. L., and Kokes, R. J. Hydrogenation of Ethylene by Zinc Oxide. II. Mechanism and Active Sites ... 3781

Deo, A. V., and Dalla Lana, I. G. An Infrared Study of the Adsorption and Mechanism of Surface Reactions of 1-Propanol on γ-Alumina and γ-Alumina Doped with Sodium Hydroxide and Chromium Oxide ... 716

Desnoyers, J. E., Arel, M., Perron, G., and Jolicoeur, C. Apparent Molal Volumes of Alkali Halides in Water at 25°. Influence of Structural Hydration Interactions on the Concentration Dependence ... 3346

Devanathan, M. A. V. See Tilak, B. V., 3582

DeVore, J. A., and O'Neal, H. E. Heats of Formation of the Acetyl Halides and of the Acetyl Radical ... 2644

Dewald, R. R. The Conductance of Solutions of Cesium in Liquid Ammonia ... 2615

Diamond, R. M. See Bucher, J. J., 675, 1494

DiCarlo, E. N., Stronski, R. E., and Varga, C. E. The Microwave Absorption of Several Metal Acetylacetonates in Benzene Solution ... 3433

Dickerson, D. G. See Pocker, Y., 4005

Dickinson, C. See Holden, J. R., 1199

Diel, R. E. See Graham, L. L., 2696

Dinius, R. H. See Chandler, W. L., 1596

Ditz, J. M., Hill, C. G., Jr., and Reid, R. C. Hydrogen Atom Permeation through Solid Hydrocarbons at 77°K ... 3756

Dixon, R. S. See Bailey, M. G., 2451

Djibelian, M. See Prock, A., 4398

Doepker, R. D. Gas-Phase Photolysis of Methylcyclopropane at 1470 and 1236 Å ... 3219

Doepker, R. D., and Hill, K. L. Vacuum-Ultraviolet Photolysis of the C_4H_6 Isomers. II. 1,2-Butadiene ... 1313

Dole, M. See Currie, J. A., 3384

Dombrowski, L. J., Groncki, C. L., Strong, R. L., and Richtol, H. H. Transient and Photoproduct Studies of Bianthrone and Substituted Bianthrones ... 3481

Donaldson, G. W., and Johnston, F. J. The Reaction of Colloidal Sulfur with Sulfite ... 2064

Dorer, F. H. Energy Partitioning in Photochemical Reactions. The Photolysis of 4-Methyl-1-pyrazoline ... 3109

Dorfman, L. M. See Neta, P., 413

Doue, F., and Guiochon, G. The Mechanism of Pyrolysis of Some Normal and Branched C_6 to C_9 Alkanes. Composition of Their Pyrolysis Products ... 2804

Doughty, D. A., and Dwiggins, C. W., Jr. A Nuclear Magnetic Resonance Study of the Association of Porphyrins in Chloroform Solution. Mesoporphyrin IX Dimethyl Ester and Its Nickel Chelate ... 423

Douglass, D. C., and Frisch, H. L. Isothermal Diffusion in Some Two- and Three-Component Systems in Terms of Velocity Correlation Functions ... 3039

Draganić, I. G., Nenadovic, M. T., and Draganić, Z. D. Radiolysis of $HCOOH + O_2$ at pH 1.3–13 and the Yields of Primary Products in γ Radiolysis of Water ... 2564

Draganić, I. G. See Draganić, Z. D., 2571

Draganić, Z. D., and Draganić, I. G. On the Origin of Primary Hydrogen Peroxide Yield in the γ Radiolysis of Water ... 2571

Draganić, Z. D. See Draganić, I. G., 2564

Drost-Hansen, W. See Korson, L., 34

Daux, W. L. See Clearfield, A., 3424

Dube, D. C., and Parshad, R. Application of Böttscher's Formula to Dielectric Behavior of Liquid Mixtures and a New Method of Deducing Dipole Moments in Liquid and Vapor States ... 3236

Duda, L. J., Sigelko, W. L., and Vrentas, J. S. Binary Diffusion Studies with a Wedge Interferometer ... 141

Duewer, W. H. See Keenan, A. G., 212

Dunlap, R. B., and Cordes, E. H. Secondary Valence Force Catalysis. VIII. Catalysis of Hydrolysis of Methyl Orthobenzoate by Anionic Surfactants ... 361

Dunlap, R. B., Ghanim, G. A., and Cordes, E. H. Secondary Valence Force Catalysis. IX. Catalysis of Hydrolysis of *para*-Substituted Benzaldehyde Diethyl Acetals by Sodium Dodecyl Sulfate ... 1898

Dunn, F. See Kessler, L. W., 4256

Dunn, L. A., and Marshall, W. L. Electrical Conductances of Aqueous Sodium Iodide and the Comparative Thermodynamic Behavior of Aqueous Sodium Halide Solutions to 800° and 4000 Bars ... 723

Dunn, L. A., and Marshall, W. L. Electrical Conductances and Ionization Behavior of Sodium Chloride in Dioxane–Water Mixtures at 100° ... 2619

Durigon, D. D. See Sandler, Y. L., 2392

Dwiggins, C. W., Jr. See Doughty, D. A., 423

Eargle, D. H., Jr. Hyperfine Splittings in the Anion Radical of Thianthrene 5,5,10,10-Tetroxide and Molecules of Related Symmetry ... 1854

Eder, T. W., and Carr, R. W., Jr. Triplet Methylene. Determination of Yields from CH_2Co Photolysis and Extent of Nonstereospecific Addition to 2-Butenes ... 2074

Edwards, R. K. See Veleckis, E., 683

Egghart, H. C. 3d Transition Metal Complexes in Molten Potassium Thiocyanate Solution ... 4014

Ehlert, T. C. Bonding in C_1 and C_2 Fluorides ... 949

Ehrlich, P., and Fariss, R. H. Negative Partial Molal Volumes in the Critical Region. Mixtures of Ethylene and Vinyl Chloride ... 1164

Eick, H. A. See Haschke, J. M., 374

Eliason, R. See Kreevoy, M. M., 1088

Elkington, P. A., and Curthoys, G. Heats of Adsorption on Carbon Black Surfaces ... 2321

Ellingsen, T., and Smid, J. Studies of Contact and Solvent-Separated Ion Pairs of Cabanions. VI. Conductivities and Thermodynamics of Dissociation of Fluorenyl Alkali Salts in Tetrahydrofuran and Dimethoxyethane ... 2712

Elliott, J. J. See Yates, D. J. C., 911

Ellzey, M. L. See Matsen, F. A., 2495

Elrod, J. See Brower, K. R., 207

Emerson, M. F. See Holtzer, A., 26

Endicott, J. F. The Effects of Magnetic Exchange Interactions on the Rates of Electron-Transfer Reactions ... 2594

English, P. J. Q. See Brownlee, R. T. C., 557

Ensley, K. See Fuller, E. N., 3679

Eppstein, L. B. Isotope Effects in the Diffusion of ^{12}C- and ^{14}C-Substituted Molecules in the Liquid Phase ... 269

Esdaile, J. D. Order of Univariants around a Three-Component Invariant Point ... 1884

Espersen, W., and Kreilick, R. W. Magnetic Resonance Studies of a Series of Phenoxy Radicals. Substituent and Steric Effects on Spin Distributions ... 3370

Evans, D. F., and Gardam, P. Transport Processes in Hydrogen-Bonding Solvents. II. Conductance of Tetraalkylammonium Salts in 1-Butanol and 1-Pentanol at 25° ... 158

Evans, D. F. See Broadwater, T. L., 164, 3985; Kay, R. L., 3322

Evans, G. B. See Cundall, R. B., 3982

Evans, J. C., and Lo, G. Y-S. Vibrational Spectra of the Hydrogen Dihalide Ions. V. $BrHBr^-$ at 20°K....... 448
Eyring, E. M. See Bennion, B. C., 3288; Holmes, L. P., 737; Owen, J. D., 3918; Rich, L. D., 713
Eyring, H. See Andersen, T. N., 3562; Cheong, K.-K., 4219

Fagley, T. F., and Oglukian, R. L. The Solvolysis of Phthalic Anhydride in Dioxane–Water Mixtures...... 1438
Fanelli, A. J. See Grabar, D. G., 3514; Rauch, F. C., 1604
Farina, R. D. The Electric Moment of Dichlorobis(pyridine)cobalt(II) Complex.......................... 1619
Fariss, R. H. See Ehrlich, P., 1164
Farnham, S. B. See Tucker, E. E., 3820
Farnum, D. G. See Hoffmann, R., 1789
Fay, D. P., Litchinsky, D., and Purdie, N. Ultrasonic Absorption in Aqueous Salts of the Lanthanides....... 544
Fay, D. P., and Purdie, N. Calorimetric Determination of the Heats of Complexation of the Lanthanide Monosulfates $LnSO_4^+$.................................... 3462
Fehlner, T. P., and Mappes, G. W. A Mass Spectrometric Investigation of the Low-Pressure Pyrolysis of Borane Carbonyl. The Bond Dissociation Energy of Diborane.. 873
Feinstein, M. E., and Rosano, H. L. The Influence of Micelles on Titrations of Aqueous Sodium and Potassium Soap Solutions.............................. 601
Feldberg, S. Theory of Regenerative Second-Order Mechanisms in Chronoamperometry. The Paradox of Disproportionation.............................. 1238
Feldberg, S. W. See Kissel, G., 3082; Marcoux, L. S., 2611; Nelson, R. F., 2623
Fellner-Feldegg, H. The Measurement of Dielectrics in the Time Domain.................................. 616
Fendler, J. H. See Asmus, K.-D., 1583
Fenger, J. See Pagsberg, P., 1029
Fernández-Prini, R., Baumgartner, E., Liberman, S., and Lagos, A. E. Tracer Diffusion and Activity Coefficients of Counterions in Aqueous Solutions of Polyelectrolytes.. 1420
Fieldhouse, S. A., and Peat, I. R. The Sign of the ^{11}B-^{19}F Coupling Constant in Boron Trifluoride and Related Compounds.. 275
Filseth, S. V. The Mercury $6(^3P_1)$ Photosensitized Decomposition of Methyl Ethyl Ether................. 793
Finch, J. N., and Clark, A. The Effect of Water Content of Silica–Alumina Catalyst on 1-Butene Isomerization and Polymerization.......................... 2234
Finegold, H. Temperature-Dependence Nuclear Magnetic Resonance Studies of a Very Strongly Coupled Spin System. Ethylene Sulfite.................... 4020
Finn, R. D., Ache, H. J., and Wolf, A. P. Chemical Effects Following $N^{14}(n,p)C^{14}$ in Magnesium Nitride... 3928
Fischer, H. Electron Spin Resonance of Transient Alkyl Radicals during Alkyllithium–Alkyl Halide Reactions.. 3834
Flanagan, T. B. See Holleck, G. L., 285
Fletcher, A. N. The Effect of Carbon Tetrachloride upon the Self-Association of 1-Octanol.............. 2217
Fletcher, A. N. The Effect of Hydrogen Bonding upon the Autoxidation Kinetics of Tetrakis(dimethylamino)ethylene.. 3686
Flores, A. L., and Darwent, D. deB. The Photochemical Decomposition of Nitrosyl Fluoride......... 2203
Florin, A. E. See Alei, M., Jr., 857, 863
Flurry, R. L., Jr. Molecular Orbital Theory of Electron Donor–Acceptor Complexes. II. Charged Donors and Acceptors.. 2111
Flurry, R. L., Jr., and Politzer, P. Molecular Orbital Theory of Electron Donor–Acceptor Complexes. III. The Relationship of State Energies and Stabilization Energies to the Charge-Transfer Transition Energy.... 2787
Flygare, W. H. See Benson, R. C., 4359
Fong, D.-W., and Grunwald, E. Acid Dissociation in Acetone–Water Mixtures. An Anomalous Medium Effect When London Dispersion Forces Are Large...... 3909
Fong, D.-W. See Grunwald, E., 650
Forsén, S. See Dahlqvist, K.-I., 4124
Fraenkel, G. See Jones, A. J., 1624
Franceschetti, D. R. See Fried, V., 1476
Frankel, L. S. A Nuclear Magnetic Resonance Study of the Effect of Charge on Solvent Orientation of a Series of Chromium(III) Complexes...................... 3897
Frankel, L. S., Klapper, H., and Cargioli, J. The Effects of Solvent and Temperature on Magnetically Nonequivalent Methylene Protons in Asymmetric Phosphorus Compounds............................ 91
Frankel, S., and Mysels, K. J. The Bursting of Soap Films. II. Theoretical Considerations............. 3028
Franklin, J. L., and Haney, M. A. Translational Energies of Products of Exothermic Ion–Molecule Reactions.. 2857
Franklin, J. L. See Haney, M. A., 4328
Franks, F., and Reid, D. S. Ionic Solvation Entropies in Mixed Aqueous Solvents......................... 3152
Fransen, T. See Biloen, P., 1581
Frech, K. J. See Hutchings, D. A., 3167
Frederick, D. L. See Andrews, L., 2774
Freeman, E. S., and Carroll, B. Reply to "Interpretation of the Kinetics of Thermogravimetric Analysis"... 751
Freeman, E. S. See Rudloff, W. K., 1209
French, K. W. See Brecher, C., 1785
Freund, T. Electron Injection into Zinc Oxide........ 468
Fried, V., Franceschetti, D. R., and Gallanter, A. S. Thermodynamic Properties of the System Carbon Tetrachloride–Tetrachloroethylene................. 1476
Friedman, H. L. See Krishnan, C. V., 1572, 3934
Friedman, M. H., and Unger, H. J. Light-Induced Boiling of Blackened Liquids...................... 1634
Frisch, H. L. See Douglass, D. C., 3039
Fu, Y.-C. See Cheong, K.-K., 4219
Fujimura, T. See Baba, K., 1146
Fujita, H. A New Approximation to the Sedimentation Equilibrium Equation for Polydisperse Nonideal Solutions.. 1759
Fujiwara, S. See Haraguchi, H., 3467
Fujiyama, T., and Crawford, B. L., Jr. Vibrational Intensities. XX. Band Shapes of Some Fundamentals of Methyl Iodide-d_3...................... 4040
Fukuzawa, K. See Miyama, H., 4345
Fuller, E. N., Ensley, K., and Giddings, J. C. Diffusion of Halogenated Hydrocarbons in Helium. The Effect of Structure on Collision Cross Sections......... 3679
Funabashi, K. See Narita, K., 964
Fuoss, R. M. See D'Aprano, A., 223, 400; McKenzie, I. D., 1501
Furnival, S. See Khanna, S., 2062
Futrell, J. H. See Hughes, B. M., 829

Gagnaire, D., and St-Jacques, M. Nuclear Magnetic Resonance Investigation of α-Phenylethylphosphine... 1678
Gaines, G. L., Jr. The Surface Tension of Polymer Solutions. I. Solutions of Poly(dimethylsiloxanes)... 3143
Gaines, G. L., Jr. On the Surface Tension of Fused Salt Mixtures.. 4421
Gaines, G. L., Jr. See Romagosa, E. E., 3150
Gallanter, A. S. See Freid, V., 1476
Gallivan, J. B. Luminescence Characteristics of Phenyl- and Halophenylnaphthalenes...................... 3070
Gancy, A. B., and Brummer, S. B. The Effect of Solution Concentration on the High-Pressure Coefficient of Ionic Conductance................................ 2429
Ganis, P., Musco, A., and Temussi, P. A. Bond Shift in Cyclooctatetraene and in Tetramethylcyclooctatetraene.. 3201
Ganis, P. See Avitabile, G., 2378
Garcia-Morin, M., Uphaus, R. A., Norris, J. R., and Katz, J. J. Interpretation of Chlorophyll Electron Spin Resonance Spectra................................ 1066
Gardam, P. See Evans, D. F., 158
Gardner, W. L., Jekel, E. C., and Cobble, J. W. The Thermodynamic Properties of High-Temperature Aqueous Solutions. IX. The Standard Partial Molal Heat Capacities of Sodium Sulfate and Sulfuric Acid from 0 to 100°.................................... 2017
Gardner, W. L., Mitchell, R. E., and Cobble, J. W. The Thermodynamic Properties of High-Temperature Aqueous Solutions. X. The Electrode Potentials of Sulfate Ion Electrodes from 0 to 100°. Activity Coefficients and the Entropy of Aqueous Sulfuric Acid... 2021
Gardner, W. L., Mitchell, R. E., and Cobble, J. W. The Thermodynamic Properties of High-Temperature Aqueous Solutions. XI. Colorimetric Determination of the Standard Partial Molar Heat Capacity and Entropy of Sodium Chloride from 100 to 200°........ 2025
Garfinkel, H. M. Electrochemical Properties of Glass Membranes in Molten Salts......................... 1766
Garland, J. K. See Mahan, K. I., 1247; Schroeder, J. W., 1252; Weeks, R. W., Jr., 2508
Garnett, J. L. See Hodges, R. J., 1525

Garrison, W. M. See Peterson, D. B., 1568

Garrod, J. E., and Herrington, T. M. Dilute Solution of Two Nonelectrolytes in a Solvent 1877

Garten, R. L. See Delgass, W. N., 2970

Gary-Bobo, C. M., and Weber, H. W. Diffusion of Alcohols and Amides in Water from 4 to 37° 1155

Gauss, E. J., and Gilman, T. S. The Electric Moments of the Halotrifluoroethylenes 3969

Gebicki, J. M., and Allen, A. O. Relationship between Critical Micelle Concentration and Rate of Radiolysis of Aqueous Sodium Linoleate 2443

Gebicki, J. M. See Bielski, B. H. J., 1402

Genshaw, M. A. See Chiu, Y.-C., 3571

Gerardi, G. J. See Holleran, E. M., 525, 528

Gershfeld, N. L. See Muramatsu, M., 1157

Geske, D. H. See Sehlossel, R. H., 71

Ghamkhar, M. See Wood, R. H., 346, 3959, 4298

Ghanim, G. A. See Dunlap, R. B., 1898

Ghiotti, G. See Borello, E., 1286; Zecchina, A., 1292, 1295

Ghormley, J. A. See Boyle, J. W., 2886

Giaque, W. F. See Lamoreaux, R. H., 755; Siemens, P. R., 149

Gibbard, H. F., Jr. A New Analytical Treatment of Heats of Dilution of Electrolyte Solutions 2382

Gibbs, E. See Pasternack, R. F., 3814

Giddings, J. C., and Schettler, P. D. General Nonequilibrium Theory of Chromatography with Complex Flow Transport 2577

Giddings, J. C. See Fuller, E. N., 3679; Schettler, P. D., 2582

Gielen, R. See Verbeke, O. B., 4076

Gilbert, B. C., and Gulick, W. M., Jr. Oxygen-17 Hyperfine Splitting in an Iminoxy Radical 2448

Gileadi, E. See Bockris, J. O'M., 427

Gillbro, T., Kinell, P.-O., and Lund, A. Free Radical Formation in Hydrocarbon Crystals by γ Irradiation. Electron Spin Resonance Spectra of Some Alkyl Radicals 4167

Gillespie, M. D. See O'Connell, J. P., 2000

Gilligan, T. J., III. See Vidulich, G. A., 1621

Gillis, H. A. See Bakale, G., 2178

Gilman, T. S. See Gauss, E. J., 3969

Gingerich, K. A. Gaseous Phosphorus Compounds. III. Mass Spectrometric Study of the Reaction between Diatomic Nitrogen and Phosphorus Vapor and Dissociation Energy of Phosphorus Mononitride and Diatomic Phosphorus 2734

Ginsberg, A. P. See Basch, H., 854

Giordano, W. P. See Hull, L. A., 2147

Gliozzi, A., Morchio, R., and Ciferri, A. Transport Properties of Collagen Membranes 3063

Glover, D. E., and Hollenberg, J. L. Absolute Intensity of Thin-Film C_6H_6(s) from Reflectance and Transmittance near 680 Cm^{-1} 889

Golden, S. See Matalon, S., 3098

Goldschmidt, C. R. See Postashnik, R., 3170

Goldstein, J. H. See Rattet, L. S., 4400; Schmidt, R. L., 1117

Gole, J. L. See Compton, L. E., 1158

Golubovic, A. Photoconductive Properties of Aceanthraquinoxaline and Related Pyrazines 1352

Goodin, R. D. See Herndon, W. C., 2793

Gopal, R., and Siddiqi, M. A. A Study of Ion–Solvent Interaction of Some Tetraalkylammonium and Common Ions in N-Methylacetamide from Apparent Molal Volume Data 3390

Gordon, J. E., and Thorne, R. L. Proton Nuclear Magnetic Resonance Solvent Shifts in Aqueous Electrolyte Solutions. I. Behavior of Internal References 3643

Gordon, J. E., and Thorne, R. L. Proton Nuclear Magnetic Resonance Solvent Shifts in Aqueous Electrolyte Solutions. II. Mixtures of Two Salts. Additivity and Nonlinearity of Shifts 3652

Gordon, L. G. M. See Conway, B. E., 3223, 3609

Gore, E. S., and Gutowsky, H. S. The Dissociation of Lithium and Sodium Tetramethylaluminate in Solution 2515

Goring, D. A. I. See Blachford, J., 1062

Gough, S. R., and Price, A. H. The Dielectric Properties of Pyridine Complexes with Dichloro- and Trichloroacetic Acids 459

Grabar, D. G., Rauch, F. C., and Fanelli, A. J. Observation of a Solid–Solid Polymorphic Transformation in 2,4,6-Trinitrotoluene 3514

Graham, L. L., and Diel, R. E. Nuclear Magnetic Studies of Internal Rotation in Aliphatic Tertiary Amides 2696

Gransch, F. See Bordewijk, P., 3255

Grant, D. M. See Jones, A. J., 1624

Grant, E. H. Analysis of Dielectric Measurements in the Presence of a Small Departure from Debye Behavior 4386

Granzow, A., Hoffman, M. Z., and Lichtin, N. N. Relative Cross Sections for the Quenching of Hg($^1P_1$) Atoms 4289

Gratzer, W. B., and Beaven, G. H. Effect of Protein Denaturation of Micelle Stability 2270

Gray, B. F. See Yang, C. H., 3395

Graybeal, J. D., and Green, P. J. Nuclear Quadrupole Resonance Zeeman Study of Polycrystalline Group IVa Tetrachlorides 2948

Graybeal, J. D., and McKown, R. J. Nuclear Quadrupole Resonance in Barium Chloride Dehydrate 3156

Greatorex, D., Kemp, T. J., and Roberts, J. P. Reactions of Radiation-Excited States of Tetramethyl-*p*-phenylenediamine with Electron Acceptors 1616

Green, M. E., and Yafuso, M. Correction to "A Study of the Noise Generated during Ion Transport across Membranes" 1626

Green, P. J. See Graybeal, J. D., 2948

Greene, J. H. See Tao, S. J., 882

Gregg, S. J., and Ramsay, J. D. F. A Study of the Adsorption of Carbon Dioxide by Alumina Using Infrared and Isotherm Measurements 1243

Gregory, N. W. See Williams, R. C., 623

Greyson, J., and Snell, H. The Influence of the Alkaline Earth Chlorides on the Structure of Water 3208

Greyson, J., and Snell, H. Concentration Dependence of Heats of Transfer Between Heavy and Normal Water 4423

Griffith, O. H. See Roeder, S. B. W., 3510

Griffiths, P. R., Schuhmann, P. J., and Lippincott, E. R. High-Temperature Equilibria from Plasma Sources. II. Hydrocarbon Systems 2532

Griffiths, P. R. See Weiffenbach, C. K., 2526

Grimison, A., Sipson, G. A., Sanchez, M. T., and Jhaveri, J. Electron Attachment by Pyridine and the Diazines in γ Radiolysis. Experimental and Theoretical Consideration 4064

Grimley, R. T., and Joyce, T. E. A Technique for the Calibration of High-Temperature Mass Spectrometers 3047

Groncki, C. L. See Dombrowski, L. J., 3481

Grossman, M., Semeluk, G. P., and Unger, I. Fluorescent Yields of 1,2,3,4-Tetrahydronaphthalene Excited in the 2850–3100-Å Region 1149

Grossman, M., Semeluk, G. P., and Unger, I. Correction to "Fluorescent Yields of 1,2,3,4-Tetrahydronaphthalene Excited in the Region 2850–3100 Å" 3175

Grossweiner, L. I. See Youtsey, K. J., 447

Grunwald, E., and Fong, D.-W. Acidity and Association of Aluminum Ion in Dilute Aqueous Acid 650

Grunwald, E. See Fong, D.-W., 3909; Leung, C. S., 1822

Gubbins, K. E. See Shoor, S. K., 312, 498

Guilbault, G. G., and Das, J. Chemisorption Reactions of Diisopropylmethyl Phosphonate with Transition Metal Salts 2243

Guillory, W. A., and King, M. The Study of the Thermal Decomposition of Methyl-Substituted Amine-Type Perchlorates 4367

Guillory, W. A., King, M., and Mack, J. L. The Thermal Decomposition of Ammonium Chlorate 4370

Guiochon, G. See Doue, F., 2804

Guirao, C., and Williams, F. A. Sublimation of Ammonium Perchlorate 4302

Gulick, W. M., Jr. See Gilbert, B. C., 2448; Schlossel, R. H., 71

Gupta, A. R. See Jeevanandum, M., 2472

Gupta, S. K. Thermal Stabilities of Tungsten Oxyiodides 4086

Gutmann, F. See Rembaum, A., 513

Gutowsky, H. S. See Gore, E. S., 2515

Guzzo, A. V., and Pool, G. L. Energy Transfer to the Triplet Level of All-*trans* Retinal 2512

Haase, R. Activity Coefficients for Ionic Melts 1160

Haase, R. Reply to the Comments on the Paper "Activity Coefficients for Ionic Melts" 4023

Hackerman, N. See Niki, K. K., 1023

Hadley, S. G., and Keller, R. A. Direct Determination of the Singlet → Triplet Intersystem Crossing Quantum Yield in Naphthalene, Phenanthrene, and Triphenylene 4351

Hadley, S. G., and Keller, R. A. Direct Determination of the Extraction Coefficients For Triplet ← Triplet Transitions in Naphthalene, Phenanthrene, and Triphenylene 4356
Hafemann, D. R., and Miller, S. L. The Clathrate Hydrates of Cyclopropane 1392
Hafemann, D. R., and Miller, S. L. The Deuteriohydrates of Cyclopropane 1398
Hagiwara, Z. Elution System of the Rare Earths with EDTA Eluent 3102
Hahn, H. K. J. See Lambrecht, R. M., 2779
Hair, M. L., and Hertl, W. Reactions of Chlorosilanes with Silica Surfaces 2372
Hair, M. L., and Hertl, W. Adsorption on Hydroxylated Silica Surfaces 4269
Hale, J. M. Electrode Reactions Involving Electronically Excited States of Molecules 3196
Halmann, M., and Platzner, I. Negative Ions Produced by Electron Capture in Phosphine 4376
Hambleton, F. H. See Armistead, C. G., 3947
Hamill, W. H. A Model for the Radiolysis of Water 1341
Hamill, W. H. See Louwrier, P. W. F., 1702, 1707; Sawai, T., 2750, 3452
Hammonds, C. N., and Day, M. C. Ion–Solvent Interactions. Relation to Solvent Dielectric Constant 1151
Hammonds, C. N., Westmoreland, T. D., and Day, M. C. Conductance and Nuclear Magnetic Resonance Studies of Sodium Tetrabutylaluminate in the Presence of Benzene and Toluene 4374
Haney, M. A., and Franklin, J. L. Mass Spectrometric Determination of the Proton Affinities of Various Molecules 4328
Haney, M. A. See Franklin, J. L., 2857
Haniger, G. A., Jr., and Lee, E. K. C. Benzene-Photosensitized Phosphorescence Emission from Biacetyl. Competitive Quenching by π-Bonded Molecules 1815
Haninger, G. A., Jr. See Lee, E. K. C., 1805
Hankins, M. G. See Crowell, T. I., 1380
Hansen, R. S. See Rye, R. R., 1667
Happ, J. W. See Janzen, E. G., 2335
Haraguchi, H., and Fujiwara, S. Aluminum Complexes in Solution as Studied by Aluminum-27 Nuclear Magnetic Resonance 3467
Hargraves, W. A., and Kresheck, G. C. The Partial Molal Volume of Several Alcohols, Amino Acids, Carboxylic Acids, and Salts in 6 M Urea at 25° 3249
Harker, A. B. See Carlton, T. S., 3356
Harkins, C. G., Shang, W. W., and Leland, T. W. Relation of the Catalytic Activity of MgO to Its Electron Energy States 130
Harland, P., and Thynne, J. C. J. The Electron Attachment Cross Section for Hexafluoroacetone 2791
Harland, P., and Thynne, J. C. J. Ionization and Dissociation of Pentafluorosulfur Chloride by Electron Impact 4031
Harmon, K. M., Cummins, S. M., and Coburn, T. T. Carbonium Ion Salts. XIV. The Chromogenic Transition of Hydroxytroppenylium Bromide 2939
Harrington, R. E. See Sarquis, J. L., 1685
Harris, G. M. See Chowdhury, D. M., 3366
Harrison, A. G. See Herod, A. A., 3189
Hart, E. J. See Nielsen, S. O., 3171
Hartstein, A. M., and Windwer, S. Electrical Conductivity of Tetraalkylammonium Halides in 1,3-Diaminopropane 1549
Harumiya, N. See Miyama, H., 4345
Haschke, J. M., and Eick, H. A. The Vaporization Thermodynamics of Europium Monoxide 374
Hase, H., and Kevan, L. Paramagnetic Relaxation of Radiation-Produced Electrons in Annealed Glassy and Polycrystalline Alkaline Ices 3290
Hase, W. L., Brieland, W. G., and Simons, J. W. Comparison of Methylene Radical Insertion Reactions with the Si–H Bonds of Methylsilane, Dimethylsilane, and Trimethylsilane 4401
Hashizume, G. See Motooka, I., 3012
Haskell, R. W. A Thermodynamic Model of Dipole–Dipole and Dipole–Induced Dipole Interactions in Polar Mixtures 2916
Hastie, J. W., and Margrave, J. L. Ionization Potentials, Electronic and Molecular Structures of Metal Halides from Extended Hückel Theory 1105
Hasty, R. A. The Rate of Reaction of Methyl Iodide and Hydrazine in Aqueous Solution 317
Hasty, R. A., and Sutter, S. L. The Rate of Reaction of Methyl Iodide with Substituted Hydrazines in Aqueous Solutions 3154
Hawke, J. G., and Trout, G. J. The Phase-Change Induced Decomposition of Methyl Alcohol 3521
Hawley, M. D. See Danen, W. C., 4389
Hayashi, K. See Tsuji, K., 2345
Hayes, D. M. See Avery, H. E., 3498
Hayes, R. G. See Keller, E., 3901
Hayon, E. See Neta, P., 4207; Simic, M., 3794, 4214
Hazelrigg, M. J., Jr., and Politzer, P. The Electronic Density Distributions in Carbon Monoxide, Carbonyl Sulfide, and Carbon Dioxide 1008
Heidt, L. J. See Landi, V. R., 2361
Helton, D. M. See Bell, J. T., 3338
Hemmes, P., and Petrucci, S. On the Reliability of the Spectrophotometric Determination of Association Constants. The Case of CuSO$_4$ and Cu(en)$_2$S$_2$O$_8$ 4426
Hempel, J. C., and Matsen, F. A. Luminescence of Chromium(III) Compounds 2502
Hentz, R. R., and Lehmann, H. P. The Effect of Charge Scavengers on Radiation-Induced Isomerization of Stilbene in Cyclohexane 4283
Hentz, R. R., and Sherman, W. V. Charge Scavenging and Energy Transfer in γ Radiolysis of Benzene Solutions 2676
Hentz, R. R., and Wickenden, D. K. An Electron Spin Resonance Study of Radiation-Induced Centers of Chemical Activity in a Silica–Alumina Gel 817
Hentz, R. R., and Wickenden, D. K. The Radiation-Induced Isomerization of Cyclohexane on Silica–Alumina 1608
Hepler, L. G. See Millero, F. J., 2453
Hercules, D. M. See Werner, T. C., 2005
Heric, E. L. On a Criterion for Rejection of Formation Constants of Weak Complexes 3496
Herman, H. B., and Blount, H. N. Chronocoulometric Measurement of Chemical Reaction Rates. The ECE Mechanism at Plane and Spherical Electrodes 1406
Hermann, A. M. See Rembaum, A., 513
Hermann, E. W. See Barradas, R. G., 3619
Herndon, W. C., and Goodin, R. D. Misstatements of Thermodynamic Properties of Tetracyanoethylene–Aromatic Donor Molecular Compounds 2793
Herod, A. A., and Harrison, A. G. Effect of Kinetic Energy of the Ionic Reactions in Propylene and Cyclopropane 3189
Herrington, T. M. See Garrod, J. E., 1877
Herron, J. T., and Huie, R. E. Rates of Reaction of Atomic Oxygen (O^{3}P). Experimental Method and Results for Some C$_1$ to C$_5$ Chloroalkanes and Bromoalkanes 1326
Herron, J. T., and Huie, R. E. Rates of Reaction of Atomic Oxygen. II. Some C$_2$ to C$_8$ Alkanes 3327
Herron, J. T., and Penzhorn, R. D. Mass Spectrometric Study of the Reactions of Atomic Oxygen with Ethylene and Formaldehyde 191
Hertl, W. See Hair, M. L., 2372, 4269
Hesselink, F. T. On the Density Distribution of Segments of a Technically Adsorbed Macromolecule 3488
Hildebrand, J. H. See Linford, R. G., 4410
Hill, C. G., Jr. See Ditz, J. M., 3756
Hill, K. L. See Doepker, R. D., 1313
Hillenbrand, L. J. The Absorption and Incorporation of Oxygen by Lead Sulfide at Room Temperature 2902
Hills, G. The Compact Double Layer as a Function of Temperature and Pressure 3591
Hiltner, P. A., and Krieger, I. M. Diffraction of Light by Ordered Suspensions 2386
Hirko, R. J., and Boyd, R. H. The Activity Coefficients of Solutes in Acid Solutions. III. The Relative Activity Coefficients of the Silver and Halide Ions in Aqueous Sulfuric and Perchloric Acid Solutions 1990
Hirota, K., Niwa, Y., and Yamamoto, M. Comment on the Paper "Charge Distribution in Some Alkanes and Their Mass Spectra" 464
Hirota, K. See Kera, Y., 3973
Hisatsune, I. C., Passerini, R., Pichai, R., and Schettino, V. Thermal Isomerization of the Maleate Ion in Potassium Halide Matrices 3690
Hisatsune, I. C., and Zafonte, L. A Kinetic Study of Some Third-Order Reactions of Nitric Oxide 2980
Hobbs, J. R. See Owens, C. W., 1956
Hobson, J. P. Physical Adsorption Isotherms Extending from Ultrahigh Vacuum to Vapor Pressure 2720

Hochanadel, C. J. See Boyle, J. W., 2886
Hockey, J. A. See Armistead, C. G., 3947
Hodges, R. J., and Garnett, J. L. The Homogeneous Platinum(II)-Catalyzed Exchange of Hydrogen in Polycyclic Aromatic Hydrocarbons and Heterocyclic Molecules 1525
Hodgkins, J. E. See Leubner, I. H., 2545
Hofer, L. J. E. See Manes, M., 584
Hoffman, M. Z. See Granzow, A., 4289
Hoffmann, R., Bissell, R., and Farnum, D. G. The Balance of Steric and Conjugative Effects in Phenyl-Substituted Cations, Radicals, and Anions 1789
Hoffsommer, J. C. See Sager, W. F., 4155
Hogue, J. W., III, and Levy, J. B. The Reaction between Nitric Oxide and Bistrifluoromethyl Peroxide 2834
Höhn, E. G., Olander, J. A., and Day, M. C. Ion–Solvent Interactions. Infrared Studies of Solvation of the Sodium Ion 3880
Holden, J. R., and Dickinson, C. The Crystal Structure of N-(β,β,β-Trifluoroethyl)-N,2,4,6-tetranitroaniline 1199
Hole, K. J., and Mulcahy, M. F. R. The Pyrolysis of Biacetyl and the Third-Body Effect on the Combination of Methyl Radicals 177
Holian, J. See Peterson, D. B., 1568
Holland, P. T., and Stone, J. A. Deuterium Sulfide as an Electron Scavenger in the Radiolysis of Liquid Saturated Hydrocarbons 4397
Holleck, G. L., and Flanagan, T. B. The Mechanism for Exchange between Aqueous Solutions and Deuterium Gas on Palladium Surfaces 285
Hollenberg, J. L. See Glover, D. E., 889
Holleran, E. M. A Dimensionless Constant Characteristic of Gases, Equations of State, and Intermolecular Potentials 167
Holleran, E. M. The Unit Compresssibility Law and Corresponding-States Behavior of Hydrogen Sulfide 3700
Holleran, E. M., and Gerardi, G. J. The Unit Compressibility Law for Mixtures 525
Holleran, E. M., and Gerardi, G. J. Corresponding States of CH_4, CF_4, and Their Mixtures 528
Holmes, E. O., Jr. Calculation of the Wavelength Maxima for Some Triphenylmethane Dye Carbonium Ions 273
Holmes, L. P., Silzars, A., Cole, D. L., Rich, L. D., and Eyring, E. M. Methyl Red Dissociation Kinetics in Dilute Aqueous Solution 737
Holmes, L. P. See Bennion, B. C., 3288
Holtzer, A., and Emerson, M. F. On the Utility of the Concept of Water Structure in the Rationalization of the Properties of Aqueous Solutions of Proteins and Small Molecules 26
Honig, J. M. See Loehman, R. E., 1781
Hoover, G. P., Robinson, E. A., McQuate, R. S., Screiber, H. D., and Spencer, J. N. Temperature Dependence of the Molar Absorptivity of the OH Stretching Vibration 4027
Hoover, T. B. The N-Methylpropionamide–Water System. Densities and Dielectric Constants at 20–40°. 57
Horne, R. A., Day, A. F., and Young, R. P. Ionic Diffusion under High Pressure in Porous Solid Materials Permeated with Aqueous, Electrolytic Solution 2782
Horsma, D. A. See Baur, M. E., 641
Hosaka, A. See Tominaga, T., 465
Hosoya, H. See Nogami, T., 2670
Houser, T. J. See Asmus, T. W., 2555
Howell, J. B., and McCain, D. C. Electron Paramagnetic Resonance of Nitrosodisulfonate Ion with Oxygen-17 and Sulfur-33 in Natural Abundance 4405
Howell, M. V. See Angell, C. L., 2551
Howell, P. A. Sorption Studies of Polypyrrolidone, Nylon 4 2294
Hoytink, G. J. See Biloen, P., 1581
Huang, Y. K. On the Tait Equation of Compressibility for Solids 2459
Hughes, B. M., Tiernan, T. O., and Futrell, J. H. Ionic Reactions in Unsaturated Compounds. IV. Vinyl Chloride 829
Huie, R. E. See Herron, J. T., 1326, 3327
Huisman, F., and Mysels, K. J. The Contact Angle and the Depth of the Fee-Energy Minimum in Thin Liquid Films. Their Measurement and Interpretation 489
Hull, L. A., Davis, G. T., Rosenblatt, D. H., and Mann, C. K. Oxidations of Amines. VII. Chemical and Electrochemical Correlations 2142
Hull, L. A., Giordano, W. P., Rosenblatt, D. H., Davis, G. T., Mann, C. K., and Milliken, S. B. Oxidations of Amines. VIII. Role of the Cation Radical in the Oxidation of Triethylenediamine by Chlorine Dioxide and Hypochlorous Acid 2147
Hunt, J. W. See Bronskill, M. J., 1175
Hunter, R. J. See Meakins, R. J., 112
Huntress, W. T., Jr. A Nuclear Magnetic Resonance Study of Anisotropic Molecular Rotation in Liquid Chloroform and in Chloroform–Benzene Solution 103
Hutchings, D. A., Taylor, J. E., and Frech, K. J. Homogeneous Gas-Phase Pyrolyses Using a Wall-less Reactor. II. The Absolute Evaluation of Surface Effects with Neopentane 3167

Ichikawa, M. See Sudo, M., 1174
Iida, S., and Imai, N. Hydrogen Ion Titration and Sodium Ion Activity of Tropomyosin Solutions 75
Ikeda, S. See Kishi, K., 15, 729, 2559
Iles, D. H. See Mingins, J., 2118
Imai, N. See Iida, S., 75
Infelta, P. P., and Schuler, R. H. The Rate of Hydrogen Abstraction by $CF_3\cdot$ and $C_2F_5\cdot$ in Liquid Cyclohexane 2083
Inokuchi, H. See Tsuda, M., 1595
Inoue, H. See Yasunaga, T., 477
Inoue, Y., and Yasumori, I. Carbon-14 Tracer Study of Active Sites on Cold-Worked Palladium Catalyst 1618
Ise, N. See Asai, K., 4071; Okubo, T., 1488
Isomoto, A. See Shiga, T., 1139
Ito, Y. See Miyama, H., 4345
Itoh, M., and Mulliken, R. S. Singlet–Triplet Absorption Banns of Methyl Substituted Ethylenes 4332
Iwasaki, M. See Toriyama, K., 2663, 2919

Jacobsen, C. W. See DeMore, W. B., 2935
Jagur-Grodzinski, J. See Tokunaga, H., 4364
Jaitly, J. N. See Meites, T., 3801
James, T. L., and Kula, R. J. A Comparison of the Protein Affinities of Neutral Oxygen and Sulfur in Chelating Ligands 634
Janauer, G. E., and Turner, I. M. The Selectivity of a Polystyrenebenzyltrimethylammonium-Type Anion Exchange Resin for Alkenesulfonates 2194
Jansoone, V. See Verbeke, O. B., 4076
Janzen, E. G., and Happ, J. W. Electron Spin Resonance of Substituted Pyridine N-Oxide Radical Anions. Aromatic Nitroxides 2335
Jaye, F. C. See Blauer, J. A., 2683
Jeevanandam, M., and Gupta, A. R. Nitrogen Isotope Effect in Transition Metal Hexaamine Complex–Ammonia Systems. A Theoretical Consideration 2472
Jekel, E. C. See Gardner, W. L., 2017
Jenkins, A. E. See Jostsons, A., 749
Jennings, K. R. See Scott, P. M., 1513, 1521
Jhaveri, J. See Grimison, A., 4064
Johnsen, R. H., Barker, N. T., and Burgin, M. Studies on Iodine as a Scavenger in Irradiated Hydrocarbons and Hydrocarbon–Alcohol Solutions 3204
Johnson, C. A., and Barnartt, S. Constant-Potential Reactions at Cylindrical Electrodes 3374
Johnson, H. W., Jr. See Sebastian, J. F., 455
Johnson, R. L. See Perona, M. J., 2091
Johnson, T. W. See Muller, N., 2042, 2460
Johnston, F. J. See Donaldson, G. W., 2064
Jolicoeur, C. See Desnoyers, J. E., 3346
Jonas, J. See Assink, R. A., 2445
Jonas, V. See Neuman, R. C., Jr., 3177
Jones, A. J., Grant, D. M., Russell, J. G., and Fraenkel, G. Carbon-13 Magnetic Resonance. Phenyllithium and Phenylmagnesium Bromide 1624
Jones, D. W. See Bartle, K. D., 293
Jones, F. T., and Loebl, E. M. The Orthohydrogen–Parahydrogen Conversion and Hydrogen–Deuterium Equilibration on Sodium Tungsten Bronzes 894
Jones, R. A., Chan, W., and Venugopalan, M. Studies of Water Vapor Dissociated by Microwave Discharges at Low Flow Rates. I. Effect of Residence Time in the Traversed Volume on Product Yields at Liquid Air Temperature 3693
Jordan, C. F. See Stefani, A. P., 1257
Jostsons, A., and Jenkins, A. E. The Configurational Entropy of Titanium Monoxide 749
Joyce, T. E. See Grimley, R. T., 3047

Judeikis, H. S., and Siegel, S. Light Absorption and Triplet-State Concentrations in Depopulated Systems ... 2036
Justice, B. H., Westrum, E. F., Jr., Chang, E., and Radebaugh, R. Thermophysical Properties of the Lanthanide Oxides. IV. Heat Capacities and Thermodynamic Properties of Thulium(III) and Lutetium(III) Oxides. Electronic Energy Levels of Several Lanthanide(III) Ions ... 333
Justice, B. H., and Westrum, E. F., Jr. Thermophysical Properties of the Lanthanide Oxides. V. Heat Capacity, Thermodynamic Properties, and Energy Levels of Cerium(III) Oxide ... 1959

Kachhwaha, O. P. See Kapoor, R. C., 1627
Kainosho, M. Removal of Spin-Spin Coupling by the Addition of Paramagnetic Metal Complexes ... 3516
Kaiser, R. S. See Reeves, R. L., 2279
Kale, J. D. See LeFevre, H. F., 1614
Kalfoglou, G., and Bowen, L. H. Osmotic and Activity Coefficients of the Group V Tetraphenyl Salts in Aqueous Solution ... 2728
Kamel, A. M. See Mikhail, R. Sh., 2213
Kamiyoshi, K. See Baba, K., 1146
Kana'an, A. S. See Keiser, D., 4264
Kanekar, C. R., Khetrapal, C. L., and Nipankar, S. V. Proton Magnetic Resonance in Octahedral Complexes of Iron(II) and Cobalt(III) with α,α'-Dipyridyl ... 276
Kant, A. See Lin, S.-S., 2450
Kapoor, R. C., Kachhwaha, O. P., and Sinha, B. P. Oxidation Kinetics of Thioglycolic Acid by Ferricyanide Ion In Acid Medium ... 1627
Karaulic, D. B. See Susic, M. V., 1975
Kass, W. J., and Yankwich, P. E. Three-Element Reaction Coordinates and Intramolecular Kinetic Isotope Effects ... 3722
Kataoka, N., and Kon, H. The Electron Spin Resonance of Low-Spin Isocyanide Complexes of Cobalt(II). I. Halides ... 803
Katritzky, A. R. See Brownlee, R. T. C., 557
Katz, J. J. See Garcia-Morin, M., 1066
Kawaguchi, Y., and Nagasawa, M. Potentiometric Titration of Stereoregular Poly(acrylic acids) ... 4382
Kawahara, Y. Decomposition of Hydrocarbons in a Microwave Discharge. I. Methane. Effect of Power 1648
Kay, R. L., Evans, D. F., and Cunningham, G. P. The Conductance of Large Hydrophobic Ions in Water, Methanol, and Acetonitrile at 25° ... 3322
Kay, R. L., Vidulich, G. A., and Pribadi, K. S. A Reinvestigation of the Dielectric Constant of Water and Its Temperature Coefficient ... 445
Kay, R. L. See Springer, C. H., 471
Kay, W. B. See Kreglewski, A., 3359
Keenan, A. G., and Duewer, W. H. Silver and Sodium Ion Transport Numbers into Pyrex from Binary Nitrate Melts ... 212
Keiser, D., and Kana'an, A. S. Enthalpy and Entropy of Sublimation of Tetraphenyltin and Hexaphenylditin. The Bond Dissociation Energy of Sn–C and Sn–Sn ... 4264
Keller, E., and Hayes, R. G. Electron Paramagnetic Resonance Study of the Anion Radical of Phenyl Methyl Sulfone and of 4-Nitrophenyl Methyl Sulfone ... 3901
Keller, O. L., Jr. See Nugent, L. J., 1540
Keller, R. A. See Hadley, S. G., 4351, 4356
Kelley, R. D., Klein, R., and Scheer, M. D. The *cis-trans* Effect in the H-Atom Addition to Olefins ... 1169
Kelley, R. V. See McNesby, J. R., 789
Kellner, J. D., Yosim, S. J., and Topol, L. E. A Redetermination of the Thermoelectric Properties of the Bismuth–Bismuth Bromide System ... 4419
Kelly, C. C., and Wijnen, M. H. J. Competitive Chlorination of 1- and 2-Chloropropane ... 2447
Kelly, J. J. See Mukherjee, L. M., 580
Kemp, T. J. See Greatorex, D., 1616
Keneshea, F. J., and Cubicciotti, D. The Thermodynamic Properties of Gaseous Niobium Chlorides ... 3054
Kensler, T. T. See Danen, W. C., 4389
Kera, Y., and Hirota, K. Infrared Spectroscopic Study of Oxygen Species in Vanadium Pentoxide with Reference to Its Activity in Catalytic Oxidation ... 3973
Kerr, G. T. Chemistry of Crystalline Aluminosilicates. VI. Preparation and Properties of Ultrastable Hydrogen Zeolite Y ... 2780
Kessler, L. W., and Dunn, F. Ultrasonic Investigation of the Conformal Changes of Bovine Serum Albumin in Aqueous Solution ... 4256
Ketelaar, J. A. A. See Kwak, J. C. T., 94
Kett, T. K., and Anderson, D. K. Multicomponent Diffusion in Nonassociating, Nonelectrolyte Solutions ... 1262
Kett, T. K., and Anderson, D. K. Ternary Isothermal Diffusion and the Validity of the Onsager Reciprocal Relations in Nonassociating Systems ... 1268
Kevan, L. See Beran, J. A., 3860, 3866; Hase, H., 3290
Keyser, R. M., and Williams, F. Characterization of Trapped Electrons in γ-Irradiated Hydrocarbon Polymers by Electron Spin Resonance and Optical Absorption Spectroscopy ... 1623
Khanna, S., Furnival, S., and Winkler, C. A. The Reaction of Active Nitrogen with Phosphorus Vapor ... 2062
Khetrapal, C. L. See Kanekar, C. R., 276
Khulbe, K. C. See Mann, R. S., 2104
Kim, H. Combined Use of Various Experimental Techniques for the Determination of Nine Diffusion Coefficients in Four-Component Systems ... 1716
Kim, S.-J. See Bonner, O. D., 1367, 1968
Kimbell, G. H. See Arnold, S. J., 3751
Kinell, P.-O., Lund, A., and Shimizu, A. Electron Spin Resonance Studies of Irradiated Heterogeneous Systems. V. Naphthalene, Anthracene, Phenanthrene, and Biphenyl Adsorbed on Porous Silica Gel ... 4175
Kinell, P.-O. See Gillbro, T., 4167
King, E. J. Volume Changes for Ionization of Formic, Acetic, and *n*-Butyric Acids and the Glycinium Ion in Aqueous Solution at 25° ... 1220
King, M. See Guillory, W. A., 4367, 4370
King, S.-T., and Overend, J. The Importance of Lone-Pair Electrons in the Intramolecular Potential Function of Group V. Hydrides and Trihalides ... 406
Kinser, H. B. See Schaad, L. J., 1901
Kira, A. See Shida, T., 4315
Kirby, E. P. See Steiner, R. F., 4130
Kishi, K., and Ikeda, S. Ultraviolet Studies of the Adsorption of β-Diketones on Evaporated Metal Films ... 15
Kishi, K., and Ikeda, S. Ultraviolet Studies for the Adsorption of 8-Quinolinol on Evaporated Metal Films. 729
Kishi, K., and Ikeda, S. Ultraviolet Study for the Adsorption of Pyridine and 2,2'-Bipyridyl on Evaporated Metal Films ... 2559
Kissel, G., and Feldberg, S. W. Disproportionation of the Technetate Ion in Aqueous Alkaline Media. An Electrochemical Study ... 3082
Klapper, H. See Frankel, L. S., 91
Klein, D. J. See Matsen, F. A., 2477
Klein, R., and Scheer, M. D. Reaction of $O(^3P)$ with 2-Methyl-2-pentene at Low Temperatures and Its Implication for the Transition State ... 1598
Klein, R. See Kelley, R. D., 1169; Scheer, M. D., 597
Knobler, C. M. See Baur, M. E., 641; Dantzler, E. M., 1335, 1602
Knowles, D. J. See Buchanan, A. S., 4394
Kobayashi, M. See Motooka, I., 3012
Koehler, W. H., and Lagowski, J. J. Metal–Ammonia Solutions. V. Optical Properties of Solutions in the Intermediate Concentration Region ... 2329
Kokes, R. J. See Conner, W. C., 2436; Dent, A. L., 3772, 3781
Kolak, N. See Mutijević, E., 3556
Kolthoff, I. M., and Chantooni, M. K., Jr. The Homoconjugation Constant of Picric Acid in Acetonitrile 4029
Kon, H. See Kataoka, N., 803
Kondo, Y. See Tasaka, M., 3181
Kongshaug, M. See Cercek, B., 2056
Koob, R. D. Methylene Produced in the Vacuum-Ultraviolet Photolysis of Propane ... 3168
Korson, L., Drost-Hansen, W., and Millero, F. J. Viscosity of Water at Various Temperatures ... 34
Kowalak, A., Kustin, K., and Pasternack, R. F. Relaxation Spectra of Nickel(II)– and Cobalt(II)–Picolinic Acid Complexes ... 281
Kratochvil, B. See Yeager, H. L., 1963
Kratohvil, S. See Matijević, E., 564
Kraus, K. A. See Baldwin, W. H., 3417
Kreevoy, M. M., Landholm, R. A., and Eliason, R. The Distribution of Hydrogen Isotopes between $H_2PO_4^-$ and Water in Partially Deuterated Solutions ... 1088
Kreglewski, A. On the Second Virial Coefficient of Real Gases ... 608
Kreglewski, A., and Kay, W. B. The Critical Constants of Conformal Mixtures ... 3359
Kreilick, R. W. See Espersen, W., 3370
Kresheck, G. C. An Alternate Interpretation of the

Mechanism of Self-Association of Urea in Dilute Aqueous Solution 2441
Kresheck, G. C. See Hargraves, W. A., 3249
Krieger, I. M. See Hiltner, P. A., 2386
Krishna, B., Prakash, B., and Mahadane, S. V. Dielectric Study of Esters in Benzene. Barrier to Internal Rotation and Molecular Configuration 3697
Krishnamurthy, S. S., and Soundararajan, S. Charge Distribution in and Dipole Moments of Some Aliphatic Alcohols 4036
Krishnan, C. V., and Friedman, H. L. Solvation Enthalpies of Various Nonelectrolytes in Water, Propylene Carbonate, and Dimethyl Sulfoxide 1572
Krishnan, C. V., and Friedman, H. L. Solvation Enthalpies of Various Ions in Water, Propylene Carbonate, and Dimethyl Sulfoxide 3934
Krishnan, P. N., and Salomon, R. E. The Solubility of Hydrogen Chloride in Ice 2680
Kröger, F. A. See Yuan, D., 2390
Kroll, W. R. See Yates, D. J. C., 911
Kropp, J. L., Dawson, W. R., and Windsor, M. W. Radiative and Radiationless Processes in Aromatic Molecules. Pyrene 1747
Kropp, J. L. See Dawson, W. R., 693, 1752
Krostek, W. D. See O'Connell, J. P., 2000
Kuhl, G. H. See Dempsey, E., 387
Kula, R. J. See James, T. L., 634
Kulluk, J. D. See Stern, J. H., 2795
Kummer, J. T. Yao, Y.-F. Y., 2262
Kuntz, R. R. See Taha, I. A. I., 4406
Kuppermann, A. See Truhlar, D. G., 1722
Kurata, M. See Utiyama, H., 1448
Kurland, R. J. See Tewari, K. C., 2853
Kustin, K., and Pasternack, R. F. The Complexation Reactions of Co(II) and Ni(II) with Glycylsarcosine 1
Kustin, K. See Davies, G., 2248; Kowalak, A., 281
Kuwana, T. See Winograd, N., 3456
Kuwata, K. See Nishikida, K., 2239
Kwak, J. C. T., and Ketelaar, J. A. A. Temperature Dependence of the Electrical and Diffusional Mobilities of ^{22}Na and ^{137}Cs in Molten LiNO$_3$, NaNO$_3$, and RbNO$_3$. 94
Kwart, H., Sarner, S. F., and Olson, J. H. Homogeneous Gas-Phase Thermolysis Kinetics. An Improved Flow Technique for Direct Study of Rate Processes in the Gas Phase 4056

Ladd, M. F. C., and Lee, W. H. Studies on Crystalline Hydrates 2033
Lagos, A. E. See Fernández-Prini, R., 1420
Lagow, R. J. See Wood, J. L., 3139
Lagowski, J. J. See Koehler, W. H., 2329; Quinn, R. K., 2326
Lakshminarayanaiah, N. Counterion Transference Numbers in Ion-Exchange Membranes 97
Lakshminarayanaiah, N. On the Determination of Average Pore Size of Membranes 4428
Lal, M., and Swinton, F. L. The Thermodynamic Properties of the Binary System *cis*- Decalin–*trans*-Decalin 2883
Lam, V. T. See Boublik, T., 2356
Lambrecht, R. M., Hahn, H. K. J., and Rack, E. P. Radiative Neutron Capture Organic Yields as an Indication of the State of Aggregation of ICl and I$_2$ in C$_6$-Hydrocarbon Matrices at 77°K 2779
Laming, F. P., Buxton, G., and Wilmarth, W. K. Aqueous Chemistry of Inorganic Free Radicals. VI. The Effect of Oxygen on the Rate of Photolysis of Hydrogen Peroxide in Aqueous Solutions Containing Carbon Monoxide 867
Lamoreaux, R. H., and Giauque, W. F. Thermodynamics of Iodine Trichloride. Entropy and Heat Capacity from 15 to 325°K. Composition of the Equilibrium ICl and Cl$_2$ Gas Phase 755
Lampe, F. W. See Beggs, D. P., 3307, 3315, 4194; Potzinger, P., 3912; Schmidt, J. F., 2706
Land, E. J. See Cundall, R. B., 3982
Landholm, R. A. See Kreevoy, M. M., 1088
Landi, V. R., and Heidt, L. J. Flash Photolysis Study of the Mechanism of Ozonide Ion Decay in Basic Aqueous Hydrogen Peroxide 2361
Langer, S. H. See Pratt, G. L., 2095
Lantzke, I. See Adamson, A. W., 4183
Larry, J. R., and VanWinkle, Q. Charge-Transfer Interactions of Chlorophylls a and b and Pheophytins a and b with *sym*-Trinitrobenzene 570
Larson, C. W. See O'Neal, H. E., 1011
Larson, D. T., and Cash, D. L. Ellipsometer Studies of Plutonium Oxidation 2814
Lauerman, B. J. See Deming, R. L., 1762
Laufer, A. H. Photolysis of Ketene. Mechanism of Hydrogen Production and the Reaction of Methylene with Methane 959
Laurentino, R. See Vitagliano, V., 2456
Lawless, J. G. See Danen, W. C., 4389
Lawrence, J., and Parsons, R. Adsorption Isotherms in Mixed Solvent Systems 3577
Lee, E. K. C., Schmidt, M. W., Shortridge, R. G., Jr., and Haninger, G. A., Jr. Fluorescence Quenching by Singlet Energy Transfer. I. From Benzene and Toluene to π-Bonded Molecules 1805
Lee, E. K. C. See Haninger, G. A., Jr., 1815; Rowland, F. S., 4024
Lee, T. P. See Masterton, W. L., 2761
Lee, W. H. See Ladd, M. F. C., 2033
Lee, W. Y., and Treloar, F. E. The Dissociation of Trityl Perchlorate in 1,2-Dichloroethane 2458
LeFevre, H. F., Kale, J. D., and Timmons, R. B. Confirmation of the Inertness of Sulfur Hexafluoride toward Attack by CF$_3$ and CH$_3$ Radicals 1614
LeFevre, H. F., and Timmons, R. B. The Kinetics of the Reaction of Trifluoromethyl Radicals with Ammonia 3854
Lehmann, H. P. The Radiation-Induced Isomerization of Stilbene in 2-Propanol and Acetone 20
Lehmann, H. P. See Hentz, R. R., 4283
Leland, T. W. See Harkins, C. G., 130
LeRoy, R. L. Relationships between Arrhenius Activation Energies and Excitation Functions 4338
Leubner, I. H. Comment on "Observed Phosphorescence Lifetimes and Glass Relaxation at 77°K" 2088
Leubner, I. H., and Hodgkins, J. E. Temperature Dependence of the Phosphorescence Lifetime of Benzene and *n*-Alkylbenzenes between 4.2 and 100°K 2545
Leung, C. S., and Grunwald, E. Substituent Effects in the Ion-Pair Dissociation of Anilinium Acetate and Anilinium *p*-Toluenesulfonate in Acetic Acid 1822
Levanon, H., and Navon, G. The Spectrum and Stability of Oxygen Iodide Charge-Transfer Complex 1861
Levine, S., Bell, G. M., and Smith, A. L. A Theory of the Electrical Capacity of the Inner Region in the Absence of Ionic Adsorption at the Mercury–Water Interface 3534
Levy, J. B. See Hogue, J. W., 2834
Lewis, E. L., and Sicilio, F. Electron Spin Resonance Kinetic Studies of Two Dimethoxymethane Radicals in Aqueous Solution 2590
Lewis, I. C., and Singer, L. S. Electron Spin Resonance Spectroscopy of the 1-Methylphenalenyl and the 1-Phenylphenalenyl Radicals 215
Leyden, D. E., and Morgan, W. R. Proton Exchange Mechanisms of Some Tertiary Benzylamines 2924
Leyden, D. E., and Whidby, J. F. A Nuclear Magnetic Resonance Study of the Photolysis Kinetics of Iminodiacetic Acids in Sulfuric Acid 3076
Li, N. C. See Tewari, K. C., 2853
Liang, K., and Tong, L. K. J. A Diffusion Model for Multiphase Systems with Sorption 3125
Liberman, S. See Fernández-Prini, R., 1420
Libowitz, G. G., and Pack, J. G. The Gadolinium–Hydrogen System at Elevated Temperatures. Vacancy Interactions in Gadolinium Dihydride 2352
Libus, Z., and Sadowska, T. Coordination and Association Equilibria in Aqueous Electrolyte Solutions. I. Osmotic and Activity Coefficients of Divalent Metal Perchlorates 3229
Lichtin, N. N. See Granzow, A., 4289; Suryanarayanan, K., 1384
Lietzke, M. H., and Stoughton, R. W. On the Existence of the Complex AgSO$_4^-$ in Aqueous Solutions 745
Lifton, J. F. See Welch, M. J., 3351
Lin, S.-S., and Kant, A. Dissociation Energy of Fe$_2$ 2450
Lind, J. E., Jr. See Rudich, S. W., 2099
Lindenbaum, S. Heats of Dilution at 25° of Aqueous Solutions of the Bolaform Electrolyte [Bu$_3$N–(CH$_2$)$_8$–NBu$_3$]X$_2$ 4334
Lindstrom, R. E., and Wirth, H. E. Estimation of the Bisulfate Ion Dissociation in Solutions of Sulfuric Acid and Sodium Bisulfate 218
Linford, R. G., and Hildebrand, J. H. Solubility of Gases in Mixtures of Nonpolar Liquids 4410
Ling, A. C., and Willard, J. E. Electrical Conduc-

tivity of 2-Methyltetrahydrofuran and Methylcyclohexane during Warming from 77°K with and without Prior γ Irradiation.... 2408
Lippincott, E. R. See Griffiths, P. R., 2532; Weiffenbach, C. K., 2526
Litchinsky, D. See Fay, D. P., 544
Lo, G. Y-S. See Evans, J. C., 448
Locke, D. C. See Cadogan, D. F., 708; Conder, J. R., 700
Loebl, E. M. See Jones, F. T., 894
Loehman, R. E., Rao, C. N. R., and Honig, J. M. Crystallography and Defect Chemistry of Solid Solutions of Vanadium and Titanium Oxides.... 1781
Loflin, T., and McLaughlin, E. Diffusion in Binary Liquid Mixtures.... 186
Logan, S. R. Temperature Dependence of Reactions of the Hydrated Electron.... 277
Lorquet, J. C. Reply to "Charge Distribution in Some Alkanes and Their Mass Spectra".... 463
Losenicky, Z. The Thermal Conductivity of Aqueous Solutions of Alkali Hydroxides.... 451
Lossing, F. P. See McAllister, T., 2996
Louwrier, P. W. F., and Hamill, W. H. Intermediates in γ-Irradiated Solutions of Carbon Tetrachloride in Alkanes at 77°K.... 1702
Louwrier, P. W. F., and Hamill, W. H. Charge-Transfer Complexes as Radiolytic Products from Alkyl Halides and Toluene in Alkane Matrices at 77°K.... 1707
Low, M. J. D., and Matsushita, K. Infrared Spectra of the Reactions between Silica and Trimethylaluminum 911
Low, M. J. D. See Morterra, C., 321, 327
Lukacs, J. M., Jr. See Mukherjee, L. M., 580, 3115
Lund, A. See Gillbro, T., 4167; Kinell, P.-O., 4175
Lunsford, J. H. See Wang, K. M., 2069
Luz, Z. See Broze, M., 1600
Lynch, R. L., Christian, S. D., and Affsprung, H. E. Self-Association and Hydration of Cyclopentanone in Carbon Tetrachloride.... 3273
Lyons, P. A. See Shieh, J. C., 3258

MacBeath, M. E., Semeluk, G. P., and Unger, I. Spectrofluorometric Studies. IV. Some New Aspects of the Photochemistry of Monofluorobenzene.... 995
MacCallum, J. R., and Tanner, J. Interpretation of the Kinetics of Thermogravimetric Analysis.... 751
Macedo, P. B. See Weiler, R., 4147
Machin, W. D. The Apparent Molecular Area of Adsorbed Carbon Tetrachloride.... 1170
MacIntyre, F., and Winchester, J. W. Phosphate Ion Enrichment in Drops from Breaking Bubbles.... 2163
Mack, J. L. See Guillory, W. A., 4370
MacKenzie, D. R. See Bloch, F. W., 552
MacNeil, K. A. G., and Thynne, J. C. J. Negative Ion Formation in Carbon Disulfide and Carbonyl Sulfide.... 2960
Magenheimer, J. J., Varnerin, R. E., and Timmons, R. B. The Photochemistry of Methylamine at 1470 Å.. 3904
Mahadane, S. V. See Krishna, B., 3697
Mahan, K. I., and Garland, J. K. The Reactions of Recoil Tritium with Propene in the Liquid Phase.... 1247
Malbin, M. D., and Mark, H. B., Jr. The Electrochemiluminescence of the Diphenylanthracene Radical Anion.... 2786
Malbin, M. D., and Mark, H. B., Jr. The Reduction of Aromatic Hydrocarbons. IV. The Effects of a Proton Donor on Preannihilation Electrochemiluminescence.... 2992
Maloney, K. M. The Deexcitation Probability of a Surface.... 3158
Maloney, K. M., Pavlou, S. P., and Rabinovitch, B. S. Kinetic Isotope Effects in Nonequilibrium Thermal Unimolecular Systems. Ethyl Isocyanide-d_5.... 2756
Maloney, K. M., and Rabinovitch, B. S. The Thermal Isomerization of Isocyanides. Variation of Molecular Parameters. Ethyl Isocyanide.... 1652
Manes, M., and Hofer, L. J. E. Application of the Polanyi Adsorption Potential Theory to Adsorption from Solution on Activated Carbon.... 584
Mann, C. K. See Hull, L. A., 2142, 2147
Mann, R. S., and Khulbe, K. C. Hydrogenation of Methylacetylene over Platinum and Iridium Catalysts. 2104
Mappes, G. W. See Fehlner, T. P., 873
Marcoux, L. S., Adams, R. N., and Feldberg, S. W. Dimerization of Triphenylamine Cation Radicals. Evaluation of Kinetics Using the Rotating Disk Electrode.... 2611
Marcus, M. F. See Danen, W. C., 4389
Marcus, S. H., and Miller, S. I. A Proton Magnetic Resonance Solute–Solute Correlation. Solvent Interactions with the Sulfhydryl Proton.... 453
Marcus, Y., and Naveh, J. Anion Exchange of Metal Complexes. XVII. The Selective Swelling of the Exchanger in Mixed Aqueous–Organic Solvents.... 591
Marcus, Y., Naveh, J., and Nissim, M. Anion Exchange of Metal Complexes. XIX. Volumetric Studies of the Exchanger in Mixed Solvents.... 4415
Margrave, J. L. See Hastie, J. W., 1105; Wood, J. L., 3139; Zmbov, K. F., 3008
Margulis, T. N. See Adman, E., 1480
Mark, H. B., Jr. See Malbin M. D., 2786, 2992; McCoy, L. R., 953, 2764
Marshall, R. W., and Nancollas, G. N. The Kinetics of Crystal Growth of Dicalcium Phosphate Dihydrate... 3838
Marshall, W. L. See Dunn, L. A., 723, 2619; Quist, A. S., 978; Yeatts, L. B., 81
Martin, R. B. See Chang, L. W., 4277
Martin, R. F. See Anson, F. C., 1835
Martin, R. M. See Compton, L. E., 1158, 3474
Martire, D. E. See Chow, L. C., 1127
Masterton, W. L., Lee, T. P., and Boyington, R. L. The Solubility of Aromatic Hydrocarbons in Aqueous Solutions of Complex Ion Electrolytes.... 2761
Mataga, N., Obashi, H., and Okada, T. Electronic Excitation Transfer from Pyrene to Perylene by a Very Weak Interaction Mechanism.... 370
Matalon, S., Golden, S., and Ottolenghi, M. On the Nature of the Visible Absorption Bands in Metal–Amine Solutions.... 3098
Matheson, R. A. The Thermodynamics of Electrolyte Equilibria in Media of Variable Water Concentration... 3635
Matheson, R. A. The Spectrophotometric Determination of Association Constants for $CuSO_4$ and $Cu(en)_2S_2O_3$.... 4425
Matijević, E., Kolak, N., and Catone, D. L. Interactions of Silver Halides with Metal Chelates and Chelating Agents.... 3556
Matijević, E., Kratohvil, S., and Stickels, J. Counterion Complexing and Sol Stability. I. Coagulation Effects of Aluminum Salts in the Presence of Fluoride Ions.... 564
Matijević, E. See Stryker, L. J., 1484
Matsen, F. A., and Cantu, A. A. Spin-Free Quantum Chemistry. VII. The Slater Determinant.... 2488
Matsen, F. A., and Ellzey, M. L. Spin-Free Quantum Chemistry. VIII. The Crystal Field Problem.... 2495
Matsen, F. A., and Klein, D. J. Spin-Free Quantum Chemistry. VI. Spin Conservation.... 2477
Matsen, F. A. See Hempel, J. C., 2502
Matsushita, K. See Low, M. J. D., 908
Matwiyoff, N. A. See Zeltmann, A. H., 2689
Mayer, S. W. Estimation of Activation Energies for Nitrous Oxide, Carbon Dioxide, Nitrogen Dioxide, Nitric Oxide, Oxygen, and Nitrogen Reactions by a Bond-Energy Method.... 3941
McAllister, T., and Lossing, F. P. Free Radicals by Mass Spectrometry. XLI. Ionization Potential and Heat of Formation of PH_2 Radical.... 2996
McAlpine, I., and Sutcliffe, H. The Radiolysis of Trifluoroiodomethane in the Gas Phase.... 3215
McCain, D. C. See Howell, J. B., 4405
McCollum, W. A. See Darnell, A. J., 4116
McCoy, L. R., and Mark, H. B., Jr. Catalytic Polarographic Current of a Metal Complex. VI. Correlation of the Nickel(II)-o-Phenylenediamine Prewave Height with the Surface Concentration of theLigand... 953
McCoy, L. R., and Mark, H. B., Jr. Catalytic Polarographic Current of Metal Complex. VII. Determination of the Charge of the Electroactive Species for the o-Phenylenediamine–Nickel(II) Prewave.... 2764
McEntee, W. R., and Mysels, K. J. The Bursting of Soap Films. I. An Experimental Study.... 3018
McGee, H. A., Jr. See Sessa, P. A., 2078
McGee, T. H., and Waring, C. E. The Kinetics of the Thermal Decomposition of Hexafluoroazomethane and the Reaction of CF_3 Radicals with Methyl Ethyl Ketone.... 2838
McIntyre, J. D. E. The Kinetics of Heterogeneous Catalytic Electrode Reactions. II. Charge-Transfer Kinetics.... 4102
McIntyre, J. D. E. On the Distinction between the

Kinetics of Parallel and Heterogeneous Catalytic Electrode Reactions 4111
McKenzie, I. D., and Fuoss, R. M. Conductance of Potassium Nitrate and Silver Nitrate in Dioxane–Water Mixtures at 25° 1501
McKnight, C. F., and Root, J. W. The Chemistry of Nuclear Recoil Fluorine Atoms. II. Energetic F-for-F and Ring-Attack Reactions in Perfluorocyclanes 4430
McKown, R. J. See Graybeal, J. D., 3156
McLaughlin, E. See Loflin, T., 186
McMath, H. G. See Blauer, J. A., 2683
McNesby, J. R., and Kelley, R. V. High-Temperature Vacuum Ultraviolet Photolysis of *n*-Butane 789
McQuate, R. S. See Hoover, G. P., 4027
Meakins, R. J., Stevens, M. G., and Hunter, R. J. A Comparison of Triethyl- and Trimethylammonium Headgroups in the Adsorption of *n*-Alkyl Quaternary Ammonium Ions at the Mercury Surface 112
Meany, J. E. The Reversible Tautomerization of Acetylacetone Enol. I. Metal Ion Catalysis 3421
Meany, J. E. See Pocker, Y., 1857, 2879
Mears, W. H., Rosenthal, E., and Sinka, J. V. Physical Properties and Virial Coefficients of Sulfur Hexafluoride 2254
Medina, A. S. See Clearfield, A., 3424
Mehrotra, U. S., Agrawal, M. C., and Mushran, S. P. Kinetics of the Reduction of Hexacyanoferrate(III) by Ascorbic Acid 1996
Meites, L. See Meites, T., 3801; Rodgers, R. S., 4348
Meites, T., Meites, L., and Jaitly, J. N. A Simple Differential Thermometric Technique for Measuring the Rates of Chemical Reactions in Solutions 3801
Melton, B. F., and Pollak, V. L. Proton Spin Relaxation and Exchange Properties of Hydrated Chromic Ions in H_2O and H_2O–D_2O Mixtures 3669
Merrill, J. C. See Burkhart, R. D., 2699
Messmer, R. P., and Birss, F. W. An Analysis of the Origin of a Misconception Regarding the Triplet State 2085
Mettee, H. D. Foreign Gas Quenching of Sulfur Dioxide Vapor Emission 1071
Meyer, F. Plane Specificity in the Reaction of Methanol and Ethanol Vapor with Clean Germanium 3844
Meyer, W. C., and Woo, J. T. K. Nuclear Magnetic Resonance Study of Hydrogen Bonding between Methyl N-Vinylcarbamate and Dimethyl Sulfoxide 2989
Meyer, W. C., and Woo, J. T. K. Nuclear Magnetic Resonance Study of Methyl N-Vinylcarbamate Self-Association 3485
Meyerstein, D., and Mulac, W. A. Reduction of Cobalt(III) Complexes by Monovalent Zinc, Cadmium, and Nickel Ions in Aqueous Solutions 1091
Mikhail, R. S., and Kamel, A. M. The Pore Structure of Cadmium Oxide 2213
Milakovic-Vucelic, V. See Susic, M. V., 1975
Milios, P., and Newman, J. Moving Boundary Measurement of Transference Numbers 298
Mill, T., and Stringham, R. The Photoxidation of *t*-Butyl Iodide at Low Temperatures 282
Miller, G. H. See Davenport, J. E., 809
Miller, J. T., Jr. See Parts, L., 3088
Miller, S. I. See Marcus, S. H., 453
Miller, S. L. See Hafemann, D. R., 1392, 1398
Millero, F. J. The Partial Molal Volume of Ions in Various Solvents 2417
Millero, F. J., Wu, C., and Hepler, L. G. Thermodynamics of Ionization of Acetic and Chloroacetic Acids in Water–Ethanol Mixtures 2453
Millero, F. J. See Korson, L., 34
Milliken, S. B. See Hull, L. A., 2147
Mingins, J., Owens, N. F., and Iles, D. H. Properties of Monolayers at the Air–Water Interface. I. The Effect of Spreading Solvent on the Surface Pressure of Octadecyltrimethylammonium Bromide 2118
Mitchell, R. E. See Gardner, W. L., 2012, 2025
Mitchell, S. A. See Armistead, C. G., 3947
Miura, M. See Yasunaga, T., 477
Miyama, H., Fukuzawa, K., Harumiya, N., Ito, Y., and Wakamatsu, S. Quantum Yield of Photonitrosation of Cyclohexane in Homogeneous System 4345
Miyazima, G., Utsumi, Y., and Takahashi, K. Carbon-13 Nuclear Magnetic Resonance Spectroscopy. I. The Coupling Constants between Carbon-13 and Protons through Two Bonds 1370
Mohilner, D. M. Double-Layer Effects in the Kinetics of Heterogeneous Electron Exchange Reactions 2652
Momma, N., and Yasumori, I. Langmuir–Hinshelwood Mechanism as Revealed by Thermal Desorption Study. The Catalytic Decomposition of Methyl Formate on Copper Surface 1179
Moniz, W. B. Analysis of the Proton Nuclear Magnetic Resonance Spectrum of Trimethylene Selenide 1124
Moniz, W. B., and Poranski, C. F., Jr. Nitrogen-14 Nuclear Magnetic Resonance Determination of the Quadrupole Coupling Constants of Methyl Isocyanide and Ethyl Isocyanide 4145
Monroe, N. M. See Schroeder, J. W., 1252
Morchio, R. See Gliozzi, A., 3063
Morgan, L. O. See Zeltmann, A. H., 2689
Morgan, W. R. See Leyden, D. E., 2924
Mori, Y. See Takita, S., 2929
Morimoto, T., Nagao, M., and Tokuda, F. The Relation between the Amounts of Chemisorbed and Physisorbed Water on Metal Oxides 243
Morimoto, T. See Nagao, M., 3809
Morris, E. R., and Thynne, J. C. J. Hydrogen Atom Abstraction from Silane, Trimethylsilane, and Tetramethylsilane by Methyl Radicals 3294
Morterra, C., and Low, M. J. D. Reactive Silica. I. The Formation of a Reactive Silica by the Thermal Collapse of the Methoxy Groups of Methylated Aerosil 321
Morterra, C., and Low, M. J. D. Reactive Silica. II. The Nature of the Surface Silicon Hydrides Produced by the Chemisorption of Hydrogen 327
Morterra, C. See Borello, E., 1286; Zecchina, A., 1292, 1295
Morton-Blake, D. A. Electron Paramagnetic Resonance of Cupric Acetate: Irradiation-Induced Spin Pairing 2964
Motooka, I., Hashizume, G., and Kobayashi, M. Studies of the Grinding of Condensed Phosphates. VI. The Effect of Grinding on the Heat of Solution of Sodium Trimetaphosphate 3012
Moulton, D. M. Comments on the Paper "Activity Coefficients for Ionic Melts" 4022
Moynihan, C. T., Smalley, C. R., Angell, C. A., and Sare, E. J. Conductance, Viscosity, Density, Proton Magnetic Resonance Spectra, and Glass Transition Temperatures of Calcium Nitrate Tetrahydrate–Cadmium Nitrate Tetrahydrate Melts. An Ideal Fused Salt System 2287
Muckerman, J. T. See Deming, R. L., 1762
Muirhead, A. R. See Deming, R. L., 1762
Mukerjee, P. Hydrophobic and Electrostatic Interactions in Ionic Micelles. Problems in Calculating Monomer Contributions to the Free Energy 2054
Mukherjee, L. M., and Boden, D. P. Equilibria in Propylene Carbonate. I. Viscosity and Conductance Studies of Some Lithium and Quaternary Ammonium Salts 3965
Mukherjee, L. M., Kelly, J. J., Richards, M., and Lukacs, J. M., Jr. Equilibria in Pyridine. II. Behavior of Some Monovalent Silver Salts in Pyridine 580
Mukherjee, L. M., and Lukacs, J. M., Jr. Equilibria in Pyridine. III. Behavior of Silver Bromide and Silver Bromide–Hydrobromic Acid Mixtures in Pyridine 3115
Mukherjee, T. K. Charge-Transfer Donor Abilities of O,O′-Bridged Biphenyls 3442
Mukherjee, T. K. Photoconductivity of Electron Acceptors. II. 2,7-Dibromofluoren-$\Delta^{9\alpha}$-malonitrile 4381
Mulac, W. A. See Meyerstein, D., 1091
Mulcahy, M. F. R. See Hole, K. J., 177
Müller, K. See Wroblowa, H., 3528
Muller, N., and Johnson, T. W. Investigation of Micelle Structure by Fluorine Magnetic Resonance. III. Effect of Organic Additives on Sodium 12,12,12-Trifluorododecyl Sulfate Solutions 2042
Muller, N., and Johnson, T. W. Temperature Measurement in Fluorine Magnetic Resonance Spectroscopy 2460
Mulliken, R. S. See Itoh, M., 4332
Munari, S. See Russo, S., 378
Murakami, S. See Boublík, T., 2356
Muramatsu, M., and Gershfeld, N. L. Adhesive Forces in Mixed Films of Cholesterol and Octadecyl Sulfate as Detected by Desorption 1157
Muroga, Y., Noda, I., and Nagasawa, M. Nuclear Magnetic Resonance Investigation of Conformations of Isotactic Polyelectrolytes in Aqueous Solution 667
Murty, T. S. S. R., and Pitzer, K. S. Trifluoroacetic Acid. Nature of Association in Dilute Solutions in Nonpolar Solvents 1426

Musco, A. See Ganis, P., 3201
Mushran, S. P. See Mehrotra, U. S., 1996
Myers, M. B. See Ward, A. T., 1374
Mysels, K. J. See Frankel, S., 3028; Huisman, F., 489; McEntee, W. R., 3018

Nagai, S., Ohnishi, S., and Nitta, I. The Proton Hyperfine Coupling in the Methyl-Substituted Phenyl Radicals 2438
Nagakura, S. See Nogami, T., 2670
Nagao, M., and Morimoto, T. Differential Heat of Adsorption and Entropy of Water Adsorbed on Zinc Oxide Surface 3809
Nagao, M. See Morimoto, T., 243
Nagasawa, M. See Kawaguchi, Y., 4382; Muroga, Y., 667; Suzuki, Y., 797; Tasaka, M., 3181
Nancollas, G. H. See Campbell, J. R., 1735; Marshall, R. W., 3838
Narita, K., and Funabashi, K. A Theoretical Study of Alkane Positive Ions in γ-Irradiated Organic Solids 964
Narula, S. P. See Paul, R. C., 741
Naveh, J. See Marcus, Y. 591, 4415
Navon, G. See Levanon, H., 1861
Neff, L. D. See Blyholder, G., 3494
Nelson, R. D., Jr., and White, C. E. The Electric Dipole Moment of Aluminum Tris(2,4-pentanedionate) 3439
Nelson, R. F., and Feldberg, S. W. Chronoamperometric Determination of the Rate of Dimerization of Some Substituted Triphenylamine Cation Radicals 2623
Nemeth, A., and Sawyer, R. F. The Overall Kinetics of High-Temperature Methane Oxidation in a Flow Reactor 2421
Nenadovic, M. T. See Draganic, I. G., 2564
Neogi, A. See Allan, G. G., 2093
Neta, P., and Dorfman, L. M. Pulse-Radiolysis Studies. XIV. Rate Constants for the Reactions of Hydrogen Atoms with Aromatic Compounds in Aqueous Solution 413
Neta, P., Simic, M., and Hayon, E. Pulse Radiolysis of Aliphatic Acids in Aqueous Solutions. I. Simple Monocarboxylic Acids 4207
Neta, P. See Simic, M., 3794, 4214
Neuman, R. C., Jr., Woolfenden, W. R., and Jonas, V. The Effect of Hydrogen Bonding on the Barrier to Rotation about Amide Bonds 3177
Neumann, E., and Ackermann, T. Thermodynamic Investigation of the Helix–Coil Transition of a Polyribonucleotide System 2170
Newman, J. Migration in Rapid Double-Layer Charging 1843
Newman, J. See Milios, P., 298
Newton, T. W. See Burkhart, M. J., 1741
Ng, W. Y., and Walkley, J. The Partial Molal Volume of Gases Dissolved in Nonpolar Solvents 2274
Nielsen, E. B. See Bayley, P. M., 228
Nielsen, S. O., Pagsberg, P., Hart, E. J., Christensen, H., and Nilsson, G. Absorption Spectrum of the Hydrated Electron from 200 to 250 nm 3171
Nielsen, S. O. See Pagsberg, P., 1029; Rabani, J., 3736
Niki, K. K., and Hackerman, N. The Effect of Normal Aliphatic Alcohols on Electrode Kinetics 1023
Nilsson, G. See Nielsen, S. O., 3171; Pagsberg, P., 1029
Nipankar, S. V. See Kanekar, C. R., 276
Nishikida, K., and Kuwata, K. Photolytic Conversion of Free-Radical Species in Some Esters and Ethers as Studied by Electron Spin Resonance 2239
Nissim, M. See Marcus, Y., 4415
Nist, B. J. See Pocker, Y., 2879
Nitta, I. See Nagai, S., 2438
Niwa, Y. See Hirota, K., 464
Nobilione, J. M. See Stern, J. H., 928
Noda, I. See Muroga, Y., 667; Suzuki, Y., 797
Nogami, T., Yoshihara, K., Hosoya, H., and Nagakura, S. Charge-Transfer Interaction and Chemical Reaction. I. Reaction of Aniline with Chloranil 2670
Norris, J. R., and Weissman, S. I. Studies of Rotational Diffusion Through the Electron–Electron Dipolar Interaction 3119
Norris, J. R. See Garcia-Morin, M., 1066
Northcott, D., and Robertson, R. E. The Secondary Deuterium Isotope Effect in the Ionization of Trimethylamine-d_9 in Water 1559
Nowak, E. J. Catalysis of the Reduction of Supported Nickel Oxide 3790
Nozaki, H. See Toyoshima, Y., 2134
Nugent, L. J., Baybarz, R. D., and Burnett, J. L. Electron-Transfer Spectra and the II–III Oxidation Potentials of Some Lanthanide and Actinide Halides in Solution 1177
Nugent, L. J., Burnett, J. L., Baybarz, R. D., Werner, G. K., Tanner, S. P., Tarrant, J. R., and Keller, O. L., Jr. Intramolecular Energy Transfer and Sensitized Luminescence in Actinide(III) β-Diketone Chelates 1540

Obashi, H. See Mataga, N., 370
O'Connell, J. J. See Arzoumanidis, G. G., 3508
O'Connell, J. P., Gillespie, M. D., Krostek, W. D., and Prausnitz, J. M. Diffusivities of Water in Nonpolar Gases 2000
O'Deen, L. A. Sre Watkins, K. W., 4094
O'Donnell, J. H. See Bowden, M. J., 2871
Oglukian, R. L. See Fagley, T. F., 1438
Ohmura, T. See Yokohata, A., 4013
Ohnishi, S. See Nagai, S., 2438
Okada, T. See Nataga, N., 370
Okamura, S. See Tsuji, K., 2345
Okubo, T., and Ise, N. The Solubilities of Naphthalene and Biphenyl in Aqueous Polymer Solutions 1488
Okuda, S., Rao, T., Slater, D. H., and Calvert, J. G. Identification of the Photochemically Active Species in Sulfur Dioxide Photolysis within the First Allowed Absorption Band 4412
Olander, J. A. See Hohn, E. G., 3880
Oldham, K. B., and Topol, L. E. Electrochemical Investigation of Porous Media. III. Theory of Galvanostatic Methods 1462
Oldham, K. B. See Topol, L. E., 1455
Olsen, J. F., and Burnelle, L. The Electronic Structure of Carbon Suboxide 2298
Olson, D. H. See Dempsey, E., 387
Olson, J. H. See Kwart, H., 4056
O'Neal, H. E., and Larson, C. W. Primary Processes in the Acetone Photochemical System 1011
O'Neal, H. E. See Devore, J. A., 2644
O'Neil, J. R., and Adami, L. H. The Oxygen Isotope Partition Function Ratio of Water and the Structure of Liquid Water 1553
Onishi, T. See Sudo, M., 1174
O'Reilly, D. E., Santiago, F. D., and Squires, R. G. Paramagnetic Resonance and Phosphorescence of Chromia–Silica Catalyst with Chemisorbed Oxygen 3172
Orttung, W. H. Calculation of the Mean-Square Dipole Moments and Proton Fluctuation Anisotropy of Hemoglobin at Low Ionic Strength 418
Orttung, W. H. The Kerr Effect Optical Dispersion of Hemoglobin. A Molecular Interpretation 2908
Österberg, R. Proton Equilibria of Glycylglycylglycine and Glycylhistidylglycine in the Solvent 5 Volume % Water in Methanol 2230
Ostreko, L. A. See Watkins, K. W., 2080
Ostroff, A. G., Snowden, B. S., Jr., and Woessner, D. E. Viscosities of Protonated and Deuterated Water Solutions of Alkali Metal Chlorides 2784
Ottolenghi, M. See Matalon, S., 3098; Potashnik, R., 1912, 3170; Shuali, U., 3445
Overend, J. See King ,S.-T., 406
Owen, J. D., Eyring, E. M., and Cole, D. L. A Kinetic Investigation of an Isomerization of Aqueous Lysozyme near Neutral pH 3918
Owens, C. W., and Hobbs, J. R. Behavior of Recoil Sulfur-35 in Mixed Crystals of Potassium Chloride–Potassium Bromide 1956
Owens, N. F. See Mingins, J., 2118
Owzarski, P. C., and Ranz, W. E. Structured Liquids near Platinum Electrodes 3628

Paabo, M., and Bates, R. G. Dissociation of Deuteriocarbonate Ion in Deuterium Oxide from 5 to 50° 3014
Pace, E. L. See Smith, J. H., 2368, 4232
Pack, J. G. See Libowitz, G. G., 2352
Pagsberg, P., Christensen, H., Rabani, J., Nilsson, G., Fenger, J., and Nielsen, S. O. Far-Ultraviolet Spectra of Hydrogen and Hydroxyl Radicals from Pulse Radiolysis of Aqueous Solutions. Direct Measurement of the Rate of H + H 1029
Pagsberg, P. See Nielsen, S. O., 3171
Pallansch, M. J. See Berlin, E., 303
Pan, C. The Limiting Behavior of the Integrand in the Robinson and Sinclair Equation 4411
Panckhurst, M. H. Comment on "Conductance of Thallous Chloride in Dioxane–Water Mixtures at 25°" 2097

Párkányi, C., Baum, E. J., Wyatt, J., and Pitts, J. N., Jr. Physical Properties and Chemical Reactivity of Alternant Hydrocarbons and Related Compounds. XVI. Electronic Absorption and Phosphorescence Spectra of Aryl Phenyl Ketones 1132
Parshad, R. See Dube, D. C., 3236
Parsons, R. See Lawrence, J., 3577
Parts, L., and Miller, J. T., Jr. The Reaction of Nitrosonium Nitrate with Isobutylene at 77–195°K 3088
Passerini, R. See Hisatsune, I. C., 3690
Pasternack, R. F., Gibbs, E., and Cassatt, J. C. The Complexation Kinetics of Leucine with Nickel(II), Cobalt(II), and Copper(II) 3814
Pasternack, R. F. See Kowalak, A., 281; Kustin, K., 1
Patel, C. K. See Patel, J. R., 3224
Patel, J. R., Patel, C. K., Patel, K. C., and Patel, R. D. Application of Ullman and Eizner–Ptitsyn Theories to Polyelectrolyte Solutions 3224
Patel, K. C. See Patel, J. R., 3224
Patel, R. D. See Patel, J. R., 3224
Patton, J. D. See Wood, R. H., 346, 4298
Paul, R. C., Singla, J. P., and Narula, S. P. Transference Numbers and Ionic Solvation of Lithium Chloride in Dimethylformamide 741
Pausak, S. V. See Susic, M. V., 1975
Pavlou, S. P. See Maloney, K. M., 2756
Payne, R. The Electrical Double Layer in Amide Solvents 3598
Pearson, J. M. See Chakravorty, K., 746
Pearson, R. G. See Waltz, W. L., 1941
Peat, I. R. See Fieldhouse, S. A., 275
Peddle, G. J. D. See Redl, G., 1150
Pedone, C. See Benedetti, E., 2891
Peers, A. M. Ion–Molecule Reactions in Propene 4141
Pennock, B. E., and Schwan, H. P. Further Observations on the Electrical Properties of Hemoglobin-Bound Water 2600
Penzhorn, R. D. See Herron, J. T., 191
Perez, P. See Baur, M. E., 641
Perlmutter-Hayman, B. See Baharad, R., 4391
Perona, M. J., Setser, D. W., and Johnson, R. L. Identification of the Competitive Elementary Reaction of Hydrogen Atoms with Chlorine Monoxide by Infrared Chemiluminescence 2091
Perona, M. J. See Pritchard, G. O., 2944
Perron, G. See Desnoyers, J. E., 3346
Person, W. B. See Bahnick, D. A., 2309; Bist, H. D., 482
Peslak, J., Jr. See Brower, K. B., 207
Peters, C. R. See Bettman, M., 1774
Peterson, D. B., Holian, J., and Garrison, W. M. Radiation Chemistry of the α-Amino Acids. γ Radiolysis of Solid Cysteine 1568
Petraccone, V. See Avitabile, G., 2378
Petrucci, S. See Darbari, G. S., 921; Hemmes, P., 4426
Peyerimhoff, S. D. See Buenker, R. J., 1299
Phillips, L. Acetone Formation in the Pyrolysis of Actaldehyde. Decomposition Reactions of the Isopropoxyl Radical 2090
Phillips, L. See Avery, H. E., 3498
Pichai, R. See Hisatsune, I. C., 3690
Pierce, C. Localized Adsorption on Graphite and Absolute Surface Areas 813
Pitts, J. N., Jr. See Párkányi, C., 1132
Pitzer, K. S. See Murty, T. S. S. R., 1426
Platzner, I. See Halmann, M., 4376
Pocker, Y., and Dickerson, D. G. The Hydration of Propionaldehyde, Isobutyraldehyde, and Pivalaldehyde. Thermodynamic Parameters, Buffer Catalysis, and Transition State Characterization 4005
Pocker, Y., and Meany, J. E. The Reversible Hydration of 2- and 4-Pyridinecarboxaldehydes. III. Solvent Deuterium Isotope Effects 1857
Pocker, Y., Meany, J. E., Nist, B. J., and Zadorojny, C. The Reversible Hydration of Pyruvic Acid. I. Equilibrium Studies 2879
Politzer, P. See Flurry, R. L., Jr., 2787; Hazelrigg, M. J., Jr., 1008
Pollak, V. L. See Melton, B. F., 3669
Pool, G. L. See Buzzo, A. V., 2512
Poranski, C. F., Jr. See Moniz, W. B., 4145
Potashnik, R., Goldschmidt, C. R., and Ottolenghi, M. Photoionization of Charge-Transfer Systems. The Pyromellitic Dianhydride–Mestiylene Complex 3170
Potashnik, R., Ottolenghi, M., and Benasson, R. Photoionization and Delayed Fluorescence in Liquid Solutions of N,N,N′,N′-Tetramethyl-*p*-phenylenediamine 1912
Potzinger, P., and Lampe, F. W. An Electron Impact Study of Ionization and Dissociation of Monosilane and Disilane 3912
Prakash, B. See Krishna, B., 3697
Pratt, G. L., and Langer, S. H. The Gas Chromatographic Chemical Reactor. The Unimolecular Dissociation of Dicyclopentadiene 2095
Prausnitz, J. M. See O'Connell, J. P., 2000
Prenzlow, C. F., Beard, H. R., and Brundage, R. S. Argon–Ethylene Layer Formation on Graphitized Carbon Black 969
Pressley, G. A., Jr. See Steck, S. J., 1000
Pribadi, K. S. See Kay, R. L., 445
Price, A. H. See Gough, S. R., 459
Price, E. See Tompa, A. S., 435
Prins, A., and van den Tempel, M. Composition and Elasticity of Thin Liquid Films 2828
Pritchard, G. O., and Perona, M. J. The Decomposition of Vibrationally Excited 1,1,2,2-Tetrafluoro-1-chloroethane 2944
Prock, A., and Djibelian, M. Field Independence of Photoinjection into Hydrocarbon Solution 4398
Proudlock, W., and Rosenthal, D. Acid–Base Equilibria in Concentrated Salt Solutions. V. Activity Coefficients of Nonelectrolytes and Equilibria Involving Some Uncharged Bases in Lithium Chloride Solutions 1965
Pryor, W. A., and Tonellato, U. The Use of Tritiated H_2S as a Radical Scavenger in the γ Radiolysis of Organic Liquids 850
Purdie, N. See Fay, D. P., 544, 3462
Purnell, J. H. See Cadogan, D. F., 708, 3849; Conder, J. R., 700
Purohit, G. B. See Bhattacharyya, S. K., 3278

Quadrifoglio, F. See Temussii, P. A., 4227
Quinlan, K. P. Proton Ejection in Photoactive Quinone Systems 2058
Quinn, R. K., and Lagowski, J. J. Metal–Ammonia Solutions. IV. Spectra of Dilute Metal–Ammonia Solutions 2326
Quiring, W. J. See Simmie, J. M., 3830
Quist, A. S., and Marshall, W. L. The Electrical Conductances of Some Alkali Metal Halides in Aqueous Solutions from 0 to 800° and at Pressures to 4000 Bars .. 978

Rabani, J., and Nielsen, S. O. Absorption Spectrum and Decay Kinetics of O_2^- and HO_2 in Aqueous Solutions by Pulse Radiolysis 3736
Rabani, J. See Pagsberg, P., 1029; Shuali, U., 3445
Rabinovitch, B. S. See Chan, S. C., 2464; Maloney, K. M., 1652, 2756
Rack, E. P. See Lambrecht, R. M., 2779
Radebaugh, R. See Justice, B. H., 333
Rajbenbach, L. A. Radiolysis of Solutions of Perfluorocarbons in *n*-Hexane 356
Ramdas, S. See Rao, C. N. R., 672
Ramsay, J. D. F. See Gregg, S. J., 1243
Ranz, W. E. See Owzarski, P. C., 3628
Rao, C. N. R., Rao, G. V. S., and Ramdas, S. Phase Transformations and Electrical Properties of Bismuth Sesquioxide 672
Rao, C. N. R. See Loehman, R. E., 1781
Rao, G. V. S. See Rao, C. N. R., 672
Rao, K. V. S. R. See Shankar, J., 52
Rao, T. N. See Okuda, S., 4412
Raridon, R. J. See Baldwin, W. H., 3417
Rastogi, R. P., Singh, K., and Singh, H. P. Heats of Transport of Gases. I 2798
Rastogi, R. P., Singh, K., and Singh, S. N. Nonlinear Phenomenological Equation for Electroosmosis 1593
Rastogi, R. P., Singh, K., and Srivastava, M. L. Cross-Phenomenological Coefficients. XI. Nonlinear Transport Equation 46
Rattet, L. S., and Goldstein, J. H. Substituent Effects on the Nuclear Magnetic Resonance Spectra of Ethyl Acetates 4400
Rauch, F. C., and Fanelli, A. J. The Thermal Decomposition Kinetics of Hexahydro-1,3,5-trinitro-*s*-triazine above the Melting Point. Evidence for Both a Gas and Liquid Phase Decomposition 1604
Rauch, F. C. See Grabar, D. G., 3514

Rauh, E. G. See Ackermann, R. J., 762, 769
Ray, A. K. See Das, B., 3413
Reddy, M. P. See Srinivasan, T. K. K., 2071
Redl, G., and Peddle, G. J. D. Direct Observation of Intrinsic Diasterotopic Magnetic Nonequivalence...... 1150
Redpath, J. L., and Simić, M. Effect of Polar Molecules on Reaction of Negative Ions in Radiolysis of Hydrocarbon + Nitrous Oxide Systems in the Gas Phase...... 2809
Reeves, R. L., and Kaiser, R. S. The Protonation of Arylsulfonates in Aqueous Sulfuric Acid. Apparent pK_a Values of Azo Dye Sulfonic Acids from Solubility Measurements...... 2279
Reid, D. S. See Franks, F., 3152
Reid, R. C. See Ditz, J. M., 3756
Reilley, C. N. See Creekmore, R. W., 1563
Reilly, P. J., and Wood, R. H. The Prediction of the Properties of Mixed Electrolytes from Measurements on Common Ion Mixtures...... 4292
Reinecke, M. G. See Sebastian, J. F., 455
Rembaum, A., Hermann, A. M., Stewart, F. E., and Gutmann, F. Electronic Properties of Some TCNQ Complexes...... 513
Rich, L. D., Cole, D. L., and Eyring, E. M. Hydrolysis Kinetics of Dilute Aqueous Chromium(III) Perchlorate.. 713
Rich, L. D. See Holmes, L. P., 737
Richards, M. See Mukherjee, L. M., 580
Richtol, H. H. See Dombrowski, L. J., 3481
Riekert, L. Instability of Sorption Complexes in Synthetic Faujasites...... 4384
Riley, J. F. See Boyle, J. W., 2886
Ristau, W. See Wentworth, W. E., 2126
Roark, J. L., and Smith, W. B. The Proton Magnetic Resonance Spectra of Five *ortho*-Substituted Phenols.... 1043
Roark, J. L., and Smith, W. B. The Nuclear Magnetic Resonance Spectra of Six *ortho*-Substituted Fluorobenzenes...... 1046
Roark, J. L. See Smith, W. B., 1049
Roberts, J. D. See Weigert, F. J., 449
Roberts, J. P. See Greatorex, D., 1616
Robertson, R. E. See Northcott, D., 1559
Robins, R. K. See Cheong, K.-K., 4219
Robinson, E. A. See Hoover, G. P., 4027
Robinson, L. See Bunton, C. A., 4237
Robinson, R. A. An Isopiestic Vapor Pressure Study of the System Potassium Chloride–Sodium Chloride in Deuterium Oxide Solution at 25°...... 3165
Rodgers, R. S., and Meites, L. The Effects of a Homogeneous Chemical Reaction Preceding Electron-Transfer on the Current–Time Curves and Current Integrals Obtained in Controlled-Potential Electrolysis...... 4348
Roeder, S. B. W., Wun, W., and Griffith, O. H. Spin-Lattice Relaxation of Solvents Containing Nitroxide Spin Labels...... 3510
Romagosa, E. E., and Gaines, G. L., Jr. The Surface Tension of Hexamethyldisiloxane–Toluene Mixtures.... 3150
Rooney, R. A. See Wood, R. H., 1673
Root, J. W. Carbon–Carbon Bond Strength Effects in Recoil Tritium Alkyl Replacement Reactions...... 3174
Root, J. W. See McKnight, C. F., 4430
Rosa, E. J., and Schrauzer, G. N. Semiconductor Properties of Transition Metal Chelates of Ligands Derived from α-Dithiodiketones...... 3152
Rosano, H. L. See Feinstein, M. E., 601
Rosenblatt, D. H. See Hull, L. A., 2142, 2147
Rosenthal, D. See Proudlock, W., 1695
Rosenthal, E. See Mears, W. H., 2254
Rosner, D. E. Lifetime of a Highly Soluble Spherical Particle...... 382
Rowland, F. S., Lee, E. K. C., and Tang, Y.-N. Electron Density and Electronegativity Effects in the Substitution for Hydrogen Atoms by Energetic Tritium Atoms from Nuclear Recoil...... 4024
Rowland, F. S. See Tominaga, T., 465
Rudich, S. W., and Lind, J. E., Jr. Friction Constants for Tetra-*n*-propylammonium Tetrafluoroborate...... 2099
Rudloff, W. K., and Freeman, E. S. The Catalytic Effect of Metal Oxides on Thermal-Decomposition Reactions. I. The Mechanism of the Molten-Phase Thermal Decomposition of Potassium Chlorate and of Potassium Chlorate in Mixtures with Potassium Chloride and Potassium Perchlorate...... 1209
Rush, R. M. See Wu, Y. C., 2047
Russell, J. G. See Jones, A. J., 1624
Russo, S., Munari, S., and Biagini, E. Energy Transfer in the Radiolysis of Gaseous Mixtures of Ethylene and Carbon Monoxide...... 378
Ruszkay, R. J. See Beutel, J., 3240
Rüterjans, H., Schreiner, F., Sage, U., and Ackermann, Th. Apparent Molal Heat Capacities of Aqueous Solutions of Alkali Halides and Alkylammonium Salts...... 986
Rye, R. R., and Hansen, R. S. Initial Hydrogenation Activity of Tungsten. Hydrogenation and Self-Hydrogenation of Ethylene...... 1667

Sadowska, T. See Libus, Z., 3229
Sage, U. See Ruterjans, H., 986
Sager, W. F., and Hoffsommer, J. C. Kinetics and Mechanism for the Reaction between Alkyl Hydroperoxides and Tetranitromethane...... 4155
St.-Jacques, M. See Gagnaire, D., 1678
Sakka, S. Coloring of Alkaline Earth Sulfides Induced by Application of Shear...... 2468
Sakurai, H. See Takamuku, S., 1171
Salomon, M. Thermodynamics of Lithium Chloride and Lithium Bromide in Propylene Carbonate...... 3299
Salomon, R. E. See Krishnan, P. N., 2680
Salser, G. E. See Dauerman, L., 1621
Sambhi, M. S. Donor–Acceptor Complexes of 2,3-Dichloro-5,6-dicyanobenzoquinone with Tetrahydrofuran, Tetrohydropyran, and 1,4-Dioxane...... 1584
Sánchez, M. T. See Grimison, A., 4064
Sandblom, J. Liquid Ion-Exchange Membranes with Weakly Ionized Groups. I. A Theoretical Study of Their Steady-State Properties...... 249
Sandblom, J. Liquid Ion-Exchange Membranes with Weakly Ionized Groups. II. The Resistance and Electromotive Force of a Thin Membrane...... 257
Sandler, Y. L., and Durigon, D. D. The Low-Temperature Isotopic Oxygen Equilibration on Oxidized Palladium...... 2392
Sanfeld, A., Steinchen, A., and Defay, R. Surface Orientation in Electrocapillarity...... 4047
Sangster, J. M., and Thynne, J. C. J. Reactions of Radicals Containing Fluorine. V. The Addition of Trifluoromethyl Radicals to Ethylene...... 2746
Santiago, F. D. See O'Reilly, D. E., 3172
Santoro, V., and Spadaccini, G. Charge Distribution in Some Alkanes and Their Mass Spectra...... 462
Sare, E. J. See Moynihan, C. T., 2287
Sarner, S. F. See Kwart, H., 4056
Sarquis, J. L., and Harrington, R. E. Optical Anisotropy and Chain Flexibility in Low-Molecular-Weight Deoxyribose Nucleic Acid from Flow Birefringence Measurements...... 1685
Sawai, T., and Hamill, W. H. Electron Scavenging in Methanol–Water at 77°K...... 2750
Sawai, T., and Hamill, W. H. Evidence for Discrete Changes in Solvation of Trapped Electrons in Rigid Mixtures...... 3452
Sawyer, R. F. See Nemeth, A., 2421
Saxena, M. C. See Shukla, J. P., 2187
Scatchard, G. See Wu, Y. C., 2047
Schaad, L. J., and Kinser, H. B. The Structure of Diimide...... 1901
Schaleger, L. L., and Watamori, N. Kinetics of Acid-Catalyzed Deoxymercuration in Water–Glycerol Mixtures...... 2011
Scheer, M. D., and Klein, R. Low-Temperature Oxygen Atom Addition to Olefins. III. Transition State and the Reaction with *cis* and *trans*-2-Butenes...... 597
Scheer, M. D. See Kelley, R. D., 1169; Klein, R., 1598
Schellman, J. A. See Bayley, P. M., 228
Schettino, V. See Hisatsune, I. C., 3690
Schettler, P. D., and Giddings, J. C. Application of the Nonequilibrium Theory of Chromatography to a Variable Flow Correlation Model of Complex Flow and Coupling...... 2582
Schettler, P. D. See Giddings, J. C., 2577
Schiffrin, D. J. Image Forces at a Mercury–Aqueous Electrolyte Interface...... 1632
Schindler, R. N. See Schurath, U., 456
Schlegel, J. M. The Oxidation of Bromide by Bromate in Fused Alkali Nitrates...... 4152
Schlossel, R. H., Geske, D. H., and Gulick, W. M., Jr. An Electron Spin Resonance Investigation of the Anion Radicals 1,4-Dimethylanthrasemiquinone and 1,4,5,8-Tetramethylanthrasemiquinone...... 71

Schmidt, J. F., and Lampe, F. W. The γ-Ray Radiolysis of Monosilane and Monosilane–Ethylene Mixtures..... 2706
Schmidt, K. H., and Ander, S. M. Formation and Recombination of H_3O^+ and Hydroxide in Irradiated Water........ 2846
Schmidt, M. W. See Lee, E. K. C., 1805
Schmidt, R. L., Butler, R. S., and Goldstein, J. H. The Role of Polar Factors in Collision Complex Models for the Solvent and Concentration Dependence of Nuclear Magnetic Resonance Parameters................ 1117
Schneider, F. W. See Cronan, C. L., 3990
Schönert, H. On the Concentration Dependence of Transport Coefficients in Multicomponent Mixtures.... 62
Schönert, H. Reevaluation of Frictional Coefficients in the System Benzene–Cyclohexane at 25°............ 752
Schrauzer, G. N. See Rosa, E. J., 3132
Schreiber, H. D. See Hoover, G. P., 4027
Schreiner, F. See Ruterjans, H., 986
Schroeder, J. W., Monroe, N. M., and Garland, J. K. Phase Effects on Recoil Tritium Reactions with Benzene 2520
Schroeder, R. R., and Shain, I. Application of the Potentiostatic Method. Determination of the Rate Constant for the Dissociation of Acetic Acid............... 197
Schuhmann, P. J. See Griffiths, P. R., 2532; Weifenbach, C. K., 2526
Schuler, R. H. See Infeta, P. P., 2083; Warman, J. M., 931
Schurath, U., Tiedemann, P., and Schindler, R. N. The Photolysis of Ammonia at 2062 Å in the Presence of Ethylene.................................... 456
Schurr, J. M. Theory of Quasielastic Light Scattering from Chemically Reactive Ionic Solutions............ 2820
Schwan, H. P. See Pennock, B. E., 2600
Schwarz, H. A. Applications of the Spur Diffusion Model to the Radiation Chemistry of Aqueous Solutions 1928
Schwarz, H. A. See Appleby, A., 1937
Scott, A. R. See Singh, A., 2633
Scott, P. M., and Jennings, K. R. The Mercury-Photosensitized Decompositions of Ethyl Fluoride, 1,1-Difluoroethane, and 1,1,1-Trifluoroethane.............. 1513
Scott, P. M., and Jennings, K. R. The Addition of Hydrogen Atoms to Vinyl Fluoride, 1,1-Difluoroethylene, and Trifluoroethylene............................ 1521
Scott, R., and Vinogradov, S. Proton-Transfer Complexes. II. Role of Solvent Polarity and the Specific Solvation of *p*-Nitrophenol–Amine Complexes in Aqueous Solutions.............................. 1890
Scott, R. S. See Benson, R. C., 4359
Sears, J. T. Effect of Density and Electron Scavengers in Nitrous Oxide Radiolysis....................... 1143
Sebastian, J. F., Reinecke, M. G., and Johnson, H. W., Jr. Nuclear Magnetic Resonance Spectra of Some Indole Salts...................................... 455
Seck, J. A. See Welch, M. J., 3351
Seely, G. R. Energetics of the Pyrochlorophyll-Sensitized Photoreduction of Nitro Compounds................ 117
Seely, G. R. The Quenching of Pyrochlorophyll Fluorescence by Nitro Compounds....................... 125
Semeluk, G. P. See Grossman, M., 1149, 3175; MacBeath, M. E., 995
Senior, W. A., and Verrall, R. E. Spectroscopic Evidence for the Mixture Model in HOD Solutions....... 4242
Sessa, P. A., and McGee, H. A., Jr. Mass Spectrum and Molecular Energetics of Krypton Difluoride.......... 2078
Setser, D. W. See Perona, M. J., 2091
Shain, I. See Schroeder, R. R., 197
Shang, W. W. See Harkins, C. G., 130
Shankar, J., Rao, K. V. S. R., and Shastri, L. V. Peroxide Formation in the γ Radiolysis of Aerated Aqueous Solutions of Methyl Iodide........................ 52
Shastri, L. V. See Shankar, J., 52
Sherman, W. V. See Hentz, R. R., 2676
Shida, T. Extinction Coefficient of Azulene Anion Radical and the Yield of Scavengeable Electron in γ-Irradiated Organic Glass.................................. 4311
Shida, T., and Kira, A. Optical and Electron Spin Resonance Studies on Photolyzed and Radiolyzed Tetraphenylhydrazine and Related Compounds........ 4315
Shieh, J. C., and Lyons, P. A. Transport Properties of Liquid *n*-Alkanes.................................. 3258
Shieh, J. J. C. Thermal Diffusion and Segmental Motion in Binary *n*-Alkane Systems..................... 1508
Shiga, T., and Isomoto, A. Aromatic Hydroxylation Catalyzed by Fenton's Reagent. An Electron Paramagnetic Resonance Study. I. Furans............. 1139
Shimizu, A. See Kinell, P.-O., 4175
Shin, H. K. Excitation of Molecular Vibration on Collision. Oriented Nonlinear Encounters............... 4321
Shoor, S. K., and Gubbins, K. E. Solubility of Nonpolar Gases in Concentrated Electrolyte Solutions..... 498
Shoor, S. K., Walker, R. D., Jr., and Gubbins, K. E. Salting Out of Nonpolar Gases in Aqueous Potassium Hydroxide Solutions............................. 312
Shortridge, R. G., Jr. See Lee, E. K. C., 1805
Shuali, U., Ottolenghi, M., Rabani, J., and Yelin, Z. On the Photochemistry of Aqueous Nitrate Solutions Excited in the 195-nm Band....................... 3445
Shukla, D. D. See Shukla, J. P., 2187
Shukla, J. P., Shukla, D. D., and Saxena, M. C. Microwave Absorption and Molecular Structure of Polar Molecules in Solutions. Averaged Mutual Viscosities and Relaxation Times of Some Substituted Benzenes.... 2187
Sicilio, F. See Lewis, E. L., 2590
Siddall, T. H., III, and Stewart, W. E. Kinetics of Rotation around the Aryl–Nitrogen Bond in Some *ortho*-Substituted Acetanilides........................ 40
Siddiqi, M. A. See Gopal, R., 3390
Siegel, S., and Stewart, T. Vacuum-Ultraviolet Photolysis of Polydimethylsiloxane. Gas Yields and Energy Transfer....................................... 823
Siegel, S. See Judeikis, H. S., 2036
Siemens, P. R., and Giauque, W. F. The Entropies of the Hydrates of Sodium Hydroxide. II. Low-Temperature Heat Capacities and Heats of Fusion of $NaOH \cdot 2H_2O$ and $NaOH \cdot 3.5H_2O$............................ 149
Siew, L. C., and Sundheim, B. R. Proton Resonance in Alkali Nitrate Melts................................ 4135
Sigelko, W. L. See Duda, J. L., 141
Silzars, A. See Holmes, L. P., 737
Simic, M., Neta, P., and Hayon, E. Pulse Radiolysis Study of Alcohols in Aqueous Solution................ 3794
Simic, M., Neta, P., and Hayon, E. Pulse Radiolysis of Aliphatic Acids in Aqueous Solutions. II. Hydroxy and Polycarboxylic Acids........................... 4214
Simic, M. See Neta, P., 4207; Redpath, J. L., 2809
Simmie, J. M., Quiring, W. J., and Tschuikow-Roux, E. The Thermal Decomposition of Perfluorocyclobutane in a Single-Pulse Shock Tube...................... 3830
Simons, J. W., and Taylor, G. W. Chemically Activated *cis*-1,2-Dimethylcyclopropane from Photolysis of *cis*-2-Butene–Diazomethane Mixtures in the Presence of Oxygen.. 1274
Simons, J. W. See Hase, W. L., 4401
Simpson, G. A. See Grimison, A., 4064
Singer, L. S. See Lewis, I. C., 215
Singh, A., Scott, A. R., and Sopchyshyn, F. Flash Photolysis of Camphorquinone and Biacetyl........... 2633
Singh, H. P. See Rastogi, R. P., 2798
Singh, K. See Rastogi, R. P., 46, 1593, 2798
Singh, S. N. See Rastogi, R. P., 1593
Singla, J. P. See Paul, R. C., 741
Sinha, B. P. See Kapoor, R. C., 1627
Sinka, J. V. See Mears, W. H., 2254
Skinner, J. F. See Crickard, K., 2060
Slater, D. H. See Okuda, S., 4412
Slepetys, R. A., and Vaughan, P. A. Solid Solution of Aluminum Oxide in Rutile Titanium Dioxide.......... 2157
Sloth, E. N., Stein, L., and Williams, C. W. Mass Spectra of Hydrolyzed Bromine Fluorides............. 278
Smalley, C. R. See Moynihan, C. T., 2287
Smentowski, F. J., and Stevenson, G. R. Temperature-Dependent Electron Spin Resonance Studies. II. Cyclooctatetraene Anion Radical..................... 340
Smid, J. See Ellingsen, T., 2712
Smith, A. L. See Levine, S., 3534
Smith, G. D. See Clearfield, A., 3424
Smith, J. H., and Pace, E. L. An Estimate of the Librational Barrier in the Solid Perfluoroalkanes from Heat Capacity Data.................................... 2368
Smith, J. H., and Pace, E. L. The Thermodynamic Properties of Carbon Tetrafluoride from 12°K to its Boiling Point. The Significance of the Parameter ν.... 4232
Smith, W. B., and Roark, J. L. The Proton Magnetic Resonance Spectra of Several 2-Substituted Pyridines... 1049
Smith, W. B. See Roark, J. L., 1043, 1046
Snell, H. See Greyson, J., 3208, 4423
Snelson, A. Heats of Vaporization of the Lithium Fluoride Vapor Species by the Matrix Isolation Technique... 1919
Snowden, B. S., Jr. See Ostroff, A. G., 2784
Soma, M. See Sudo, M., 1174

Soos, Z. G., and Tobolsky, A. V. A New Function for Dipole Orientation and Rubber Elasticity 2864
Sopchyshyn, F. See Singh, A., 2633
Soundararajan, S. See Krishnamurthy, S. S., 4036
Spadaccini, G. See Santoro, V., 462
Spalding, G. E. A Sensitive Method for Measuring Diffusion Coefficients in Agarose Gels of Electrolyte Solutions 3380
Spencer, H. E. Quantum Yields of Production of Iron(II) and Cobalt(II) in the Photolysis of Solid Potassium Trisoxalatoferrate(III) Trihydrate and Potassium Trisoxalatocobaltate(III) Trihydrate 2316
Spencer, J. N. See Hoover, G. P., 4027
Spicer, L. D. See Chan, S. C., 2464
Sprague, E. D. See Busey, R. H., 1039
Springer, C. H., Coetzee, J. F., and Kay, R. L. Transference Number Measurements in Acetonitrile as Solvent 471
Squires, R. G. See O'Reilly, D. E., 3172
Srinivasan, T. K. K., Balakrishnan, I., and Reddy, M. P. On the Nature of the Products of γ Radiolysis of Aerated Aqueous Solutions of Benzene 2071
Srivastava, M. L. See Rastogi, R. P., 46
Stafford, F. E. See Steck, S. J., 1000
Stanley, E. M., and Batten, R. C. Viscosity of Water at High Pressures and Moderate Temperatures 1187
Staples, B. R., and Atkinson, G. Structure and Electrolyte Properties in Bolaform Electrolytes. III. The Hydrodynamics of Potassium Salts of Several Rigid Bolaform Disulfonic Acids in Dioxane–Water Mixtures at 25° 520
Steck, S. J., Pressley, G. A., Jr., and Stafford, F. E. Mass Spectrometric Investigation of the High-Temperature Reaction of Hydrogen with Boron Carbide 1000
Stefani, A. P., Thrower, G. F., and Jordan, C. F. Solvent Effects in Electroneutral Reactions. II. Diffusion-Controlled Reactions of Ethyl and Trifluoromethyl Radicals 1257
Stein, L. See Sloth, E. N., 278
Steinchen, A. See Sanfeld, A., 4047
Steiner, R. F., and Kirby, E. P. The Interaction of the Ground and Excited States of Indole Derivatives with Electron Scavengers 4130
Stern, J. H., and Kulluk, J. D. Thermodynamics of Aqueous Mixtures of Electrolytes and Nonelectrolytes. VIII. Transfer of Sodium Chloride from Water to Aqueous Urea at 25° 2795
Stern, J. H., and Nobilione, J. M. Thermodynamics of Aqueous Mixtures of Electrolytes and Nonelectrolytes. VII. Enthalpies of Transfer of Perchloric and Hydrochloric Acids from Pure Water to Aqueous Ethylene Glycol and Aqueous Acetic Acid at 25° 928
Stevens, B., and Algar, B. E. The Photoperoxidation of Unsaturated Organic Molecules. IV. The Photosensitized Reaction 1711
Stevens, M. G. See Meakins, R. J., 112
Stevenson, G. R. See Smentowski, F. J., 340
Stewart, F. E. See Rembaum, A., 513
Stewart, T. See Siegel, S., 823
Stewart, W. E. See Siddall, T. H., III, 40
Stickels, J. See Matijević, E., 564
Stillinger, F. H., Jr., and Ben-Naim, A. Relation between Local Structure and Thermodynamic Properties in Aqueous Fluids 900
Stock, T. H. See Wojcik, J. F., 2153
Stone, J. A. See Holland, P. T., 4397
Stoner, G. E. See Bockris, J. O'M., 427
Stoughton, R. W. See Lietzke, M. H., 745; Waggener, W. C., 3518
Stranks, D. R., and Yandell, J. K. Chemical Effects of Charge-Transfer Absorption. I. The Photoinduced Chain Rdaction between Thallium(I) and Thallium(III) 840
Stringham, R. See Mill, T., 282
Strong, R. L. See Dombrowski, L. J., 3481
Stronski, R. E. See DiCarlo, E. N., 3433
Stryker, L. J., and Matijević, E. Counterion Complexing and Sol Stability. II. Coagulation Effects of Aluminum Sulfate in Acidic Solutions 1484
Subramanian, S., Balasubramanian, D., and Ahluwalia, J. C. Nuclear Magnetic Resonance and Thermochemical Studies on the Influence of Urea on Water Structure 266
Sudo, M., Ichikawa, M., Soma, M., Onishi, T., and Tamaru, K. Catalytic Synthesis of Ammonia over the Electron Donor–Acceptor Complexes of Alkali Metals with Graphite or Phthalocyanines 1174
Sullivan, P. D. Temperature-Dependent Methoxyl and Hydroxyl Splitting Constants in the Electron Spin Resonance Spectra of Cation Radicals 2790
Sullivan, P. D., and Bolton, J. R. Line Width Effects in the Electron Spin Resonance Spectrum of the 2,5-Dimethylhydroquinone Cation Radical 4387
Sundheim, B. R. See Siew, L. C., 4135
Surman, P. L. See Castle, J. E., 632
Suryanarayanan, K., and Lichtin, N. N. The Radiolysis of Methanol and Methanolic Solutions. V. The Acid Effect 1384
Susi, H., and Ard, J. S. Hydrophobic Interactions and Hydrogen Bonding of ϵ-Caprolactam in Aqueous Solution 2440
Susic, M. V., Vucelic, D. R., Paūsak, S. V., Karaulic, D. B., and Milakovic-Vucelic, V. Nuclear Magnetic Resonance Method for the Determination of Specific Surface Area. Study of the State of Adsorbed Polar Vapors on Zeolite Linde 5A 1975
Sutcliffe, H. See McAlpine, I., 3215
Sutherland, J. W. See Abrams, L., 3160
Sutter, S. L. See Hasty, R. A., 3154
Suzuki, H. See Tsuda, M., 1595
Suzuki, Y., Noda, I., and Nagasawa, M. The Diffusion of Polyelectrolyte in the Presence of Added Salt 797
Svejda, P., and Volman, D. H. Electron Spin Resonance Study of Ultraviolet-Irradiated Di-*t*-butyl Peroxide in the Frozen State 4417
Swallow, A. J. See Capellos, C., 1077
Swarbrick, J., and Daruwala, J. Thermodynamics of Micellization of Some Zwitterionic N-Alkyl Betaines 2627
Swenson, C. A. See Chen, C. Y. S., 1363, 1642, 2999
Swingler, D. L. See Buchanan, A. S., 4394
Swinton, F. L. See Lal, M., 2883
Synnott, J. C., and Butler, J. N. Solubility and Complex Formation Equilibria of Silver Chloride in Dimethyl Sulfoxide–Water Mixtures 1470
Synnott, J. C. See Butler, J. N. 4026
Szwarc, M. See Chakravorty, K., 746; Tokunaga, H., 4364

Tagata, N. See Utiyama, H., 1448
Taha, A. A., and Christian, S. D. Vapor Pressure Studies of Complex Formation in Solution. I. Trifluoroacetic Acid and Benzophenone in Diphenylmethane 3430
Taha, I. A. I., and Kuntz, R. R. Methyl Radical Reactions in Aqueous Solutions. I. Hydrogen Abstraction from Acetone 4406
Tajima, Y. A. See Dauerman, L., 1621
Takahashi, K. See Miyazima, G., 1370
Takamuku, S., and Sakurai, H. Photolysis of 1,5-Cyclooctadiene Vapor. Molecular Elimination of Ethylene from 1,5-Dienes 1171
Takaya, K. See Asai, K., 4071
Takita, S., Mori, Y., and Tanaka, I. Acetylene Photolysis at 1236 and 1470 Å 2929
Tamaru, K. See Sudo, M., 1174
Tanaka, I. See Takita, S., 2929
Tancredi, T. See Temussi, P. A., 4227
Tang, Y.-N. See Daniel, S. H., 4378; Rowland, F. S., 4024
Tanner, J. See MacCallum, J. R., 751
Tanner, S. P. See Nugent, L. J., 1540
Tao, S. J., and Greene, J. H. Positronium Interactions in Aqueous Oxyacids and Hydrogen Compounds 882
Tarrant, J. R. See Nugent, L. J., 1540
Tasaka, M., Kondo, Y., and Nagasawa, M. Anomalous Osmosis through Charged Membranes 3181
Tatsumoto, N. See Yasunaga, T., 477
Taylor, A. H., and Brummer, S. B. The Adsorption and Oxidation of Hydrocarbons on Noble Metal Electrodes. VIII. Composition of Adsorbed CH_4 and Rate-Limiting Step in the Overall CH_4 to CO_2 Reaction . . 2397
Taylor, G. W. See Simons, J. W., 1274
Taylor, J. E. See Hutchings, D. A., 3167
Tazuke, S. See Tsuji, K., 2345
Temussi, P. A., Tancredi, T., and Quadrifoglio, F. Conformational Rigidity of the Amide Bond. A Variable Temperature Nuclear Magnetic Resonance Study of the System Ag^+–N,N-Dimethylacetamide 4227
Temussi, P. A. See Ganis, P., 3201

Terao, T., and Back, R. A. The Radiation-Induced Isotopic Exchange in Gaseous Hydrogen–Deuterium Mixtures 3884
Tewari, K. C., Li, N. C., and Kurland, R. J. Proton Exchange between Guanidinium Ion and Water in Water–Dimethyl Sulfoxide Mixtures 2853
Thomas, J. R. See Clearfield, A., 3424
Thompson, C. C. See Bell, J. T., 3338
Thorne, R. L. See Gordon, J. E., 3643, 3652
Thrower, G. F. See Stefani, A. P., 1257
Thynne, J. C. J. Negative Ion Formation by Electron Impact in Nitrogen Trifluoride 1586
Thynne, J. C. J. See Harland, P., 2791, 4031; MacNeil, K. A. G., 2960; Morris, E. R., 3294; Sangster, J. M., 2746
Tichý, M., and Zahradník, R. Physical Properties and Chemical Reactivity of Alternant Hydrocarbons and Related Compounds. XVII. Electronic Spectra of Amino and Hydroxy Derivatives of Benzenoid Hydrocarbons 534
Tiedemann, P. See Schurath, U., 456
Tiernan, T. O. See Hughes, B. M., 829
Tiezzi, E. See Burlamacchi, L., 1588
Tilak, B. V. K. S. R. A., and Devanathan, M. A. V. Some Aspects of the Adsorption of Nitrate and Phthalate Ions at the Mercury–Solution Interface 3582
Timm, D., and Willard, J. E. Absence of Hydrogen Atom Production in Radiolysis of Solid Hydrocarbons 2403
Timmons, R. B., and Darwent, B. deB. The Decomposition and Deactivation of Chemically Activated ClNO 2208
Timmons, R. B. See LeFevre, H. F., 1614, 3854; Magenheimer, J. J., 3904
Tobolsky, A. V. See Soos, Z. G., 2864
Tokuda, F. See Morimoto, T., 243
Tokunaga, H., Jagur-Grodzinski, J., and Szwarc, M. Electronic Transfer from Dimeric Dianions of α-Methylstyrene to Benz[*e*]pyrene 4364
Tominaga, T., Hosaka, A., and Rowland, F. S. Recoil Tritium Reactions with Methylsilanes 465
Tompa, A. S., Barefoot, R. D., and Price, E. Hindered Rotation in N-Methylthiourea 435
Tonellato, U. See Pryor, W. A., 850
Tong, L. K. J. See Bennion, B. C., 3288; Liang, K., 3125
Topol, L. E., and Oldham, K. B. Electrochemical Investigation of Porous Media. II. Potentiostatic Experiments 1455
Topol, L. E. See Kellner, J. D., 4419; Oldham, K. B., 1462
Topsom, R. D. See Brownlee, R. T. C., 557
Toriyama, K., and Iwasaki, M. Electron Spin Resonance Spectra of Peroxy Radicals Trapped in a γ-Irradiated Single Crystal of Trifluoroacetamide 2663
Toriyama, K., and Iwasaki, M. Change with Temperature of the Electron Spin Resonance Spectra of ⁓CF_2-CF_2· Trapped in Irradiated Polytetrafluoroethylene 2919
Torres, A. L. See Bonner, O. D., 1968
Toyoshima, Y., and Nozaki, H. Streaming Potential across a Charged Membrane 2134
Trapp, C. See Wasson, J. R., 3763
Treloar, F. E. See Lee, W. Y., 2458
Tripp, T. B., and Braunstein, J. Vapor Pressures of Aqueous Melts. Lithium Nitrate–Potassium Nitrate–Water at 119–150° 1984
Trout, G. J. See Hawke, J. G., 3521
Truhlar, D. G., and Kuppermann, A. Application of the Statistical Phase Space Theory to Reactions of Atomic Hydrogen with Deuterium Halides 1722
Tsai, L., and Charney, E. The Triplet States of α-Dicarbonyls. Camphorquinone 2462
Tschuikow-Roux, E. Some Energetics and the Kassel Fit Parameter s_K in Unimolecular Reactions 3891
Tschuikow-Roux, E. See Simmie, J. M., 3830
Tsuda, M., Inokuchi, H., and Suzuki, H. Reduction of Quinone in Its Charge-Transfer Complex with the Hydrogen Molecule 1595
Tsuda, S. See Yokohata, A., 4013
Tsuji, K., Tazuke, S., Hayashi, K., and Okamura, S. Electron Spin Resonance Study on Irradiated Coordination Compounds of Pyridine and Its Derivatives 2345
Tsuji, K., and Williams, F. Electron Spin Resonance Studies on Trapped Electrons and Free Radicals in γ-Irradiated Isobutyl Vinyl Ether Glasses 4017
Tucker, E. E., Farnham, S. B., and Christian, S. D. Association of Methanol in Vapor and in *n*-Hexadecane. A Model for the Association of Alcohols 3820
Tulp, A. See Biloen, P., 1581
Turner, I. M. See Janauer, G. E., 2194
Tyler, A. J. See Armistead, C. G., 3947

Unger, H. J. See Friedman, M. H., 1634
Unger, I. See Grossman, M., 1149, 3175; MacBeath, M. E., 995
Uphaus, R. A. See Garcia-Morin, M., 1066
Utiyama, H., Tagata, N., and Kurata, M. Determination of Molecular Weight and Second Virial Coefficient of Polydisperse Nonideal Polymer Solutions by the Sedimentation Equilibrium Method 1448
Utsumi, Y. See Miyazima, G., 1370
Uy, O. M. See Zmbov, K. F., 3008

Valenzuela, J. A., and Bard, A. J. Electron Spin Resonance Studies of Hyperconjugation in 2,3-, 2,6-, and 2,7-Dimethylanthracene Cation and Anion Radicals 779
van den Tempel, M. See Prins, A., 2828
VanWinkle, Q. See Larry, J. R., 570
Varga, C. E. See DiCarlo, E. N., 3433
Varnerin, R. E. See Magenheimer, J. J., 3904
Vaslow, F. The Apparent Molal Volumes of the Lithium and Sodium Halides. Critical-Type Transitions in Aqueous Solution 3745
Vaughan, P. A. See Slepetys, R. A., 2157
Veleckis, E., and Edwards, R. K. Thermodynamic Properties in the Systems Vanadium–Hydrogen, Niobium–Hydrogen, and Tantalum–Hydrogen 683
Venugopalan, M. See Jones, R. A., 3693
Verbeke, O. B., Jansoone, V., Gielen, R., and De Boelpaep, J. The Equation of State of Fluid Argon and Calculation of the Scaling Exponents 4076
Verrall, R. E. See Senior, W. A., 4242
Vidulich, G. A., Andrade, J. R., Blanchette, P. P., and Gilligan, T. J., III. Effect of Urea and Ethanol on the Viscosities of Several Aqueous Electrolyte Solutions 1621
Vidulich, G. A. See Kay, R. L., 445
Vijh, A. K. Electrolytic Hydrogen Evolution Reaction on Aluminum, Oxide-Covered Electrodes 506
Vincow, G. See Volland, W. V., 1147
Vinogradov, S. See Scott, R., 1890
Vissers, D. R. A Kinetic Study of Orthophosphate Sorption on Metal Oxides 1953
Vitagliano, V., Laurentino, R., and Constantino, L. Diffusion in a Ternary System with Strong Interacting Flows 2456
Vogl, W. F., and Ahlert, R. C. Optimization of Force Constants for Methane and Argon 2304
Vogler, A. See Adamson, A. W., 4183
Voigt, A. F. See Williams, R. L., 2538
Volland, W. V., and Vincow, G. Hyperfine and *g*-Tensor Anisotropy of the Tropenyl Radical 1147
Volman, D. H. See Svejda, P., 4417
Vrentas, J. S. See Duda, J. L., 141
Vucelic, D. R. See Susic, M. V., 1975

Waggener, W. C., Weinberger, A. J., and Stoughton, R. W. The Near-Infrared Spectrum of Liquid Hydrogen Sulfide 3518
Wakamatsu, S. See Miyama, H., 4345
Walker, R. D., Jr. See Shoor, S. K., 312
Walkley, J. See Ng, W. Y., 2274
Wall, F. T., and Whittington, S. G. The Density Function for End-to-End Lengths of Self-Avoiding Random Walks on a Lattice 3953
Wallach, D. Effect of Fast Internal Rotation on the Nitrogen-14 Nuclear Magnetic Resonance Relaxation Times of the Methylbenzyl Cyanides 307
Waltz, W. L., and Adamson, A. W. Photochemistry of Complex Ions. VIII. Photoelectron Production 4250
Waltz, W. L., and Pearson, R. G. A Pulse Radiolysis Study of Some Cobalt(III) Complexes. Occurrence of Electronically Excited Cobalt(II) Products 1941
Wanders, A. C. M., and Zwietering, Th. N. Calculation of ΔH and K Values from Thermometric Titration Curves 2076
Wang, K. M., and Lunsford, J. H. Electron Paramagnetic Resonance Evidence for the Presence of Aluminum at Adsorption Sites on Decationated Zeolites 2069
Ward, A. T., and Myers, M. B. An Investigation of the Polymerization of Liquid Sulfur, Sulfur–Selenium, and

Sulfur-Arsenic Mixtures Using Raman Spectroscopy and Scanning Differential Calorimetry 1374
Ward, J. W. Hydroxyl Groups on Hydrogen Y Zeolite 2086
Waring, C. E. See McGee, T. H., 2838
Warman, J. M., Asmus, K.-D., and Schuler, R. H. Electron Scavenging in the Radiolysis of Cyclohexane Solutions of Alkyl Halides 931
Wasson, J. R., and Trapp, C. An Electron Spin Resonance Study of Copper(II) O-Alkyl-1-amidinourea Complexes. Properties of the CuN_4^{2-} Chromophore 3763
Watamori, N. See Schaleger, L. L., 2011
Watkins, K. W., and O'Deen, L. A. Kinetics of the Addition of Ethyl, Isopropyl, *n*-Butyl, and Isopentyl Radicals to Ethylene 4094
Watkins, K. W., and Ostreko, L. A. Isomerization of *n*-Hexyl Radicals in the Gas Phase 2080
Weber, H. W. See Gary-Bobo, C. M., 1155
Weeks, R. W., Jr., and Garland, J. K. Gas-Phase Reactions of Cyclohexene with Highly Energetic Tritium 2508
Weiffenbach, C. K., Griffiths, P. R., Schuhmann, P. J., and Lippincott, E. R. High-Temperature Equilibria from Plasma Sources. I. Carbon–Hydrogen–Oxygen Systems 2526
Weigert, F. J., and Roberts, J. D. Two-Bond, Carbon–Proton Coupling in Halogenated Ethylenes 449
Weiler, R., Blaser, S., and Macedo, P. B. Viscosity of a Vitreous Potassium Nitrate–Calcium Nitrate Mixture 4147
Weinberger, A. J. See Waggener, W. C., 3518
Weissman, S. I. See Norris, J. R., 3119
Welch, M. J., Lifton, J. F., and Seck, J. A. Tracer Studies with Radioactive Oxygen-15. Exchange between Carbon Dioxide and Water 3351
Wen, W.-Y., and Chen, C. L. Activity Coefficients for Two Ternary Systems: Water–Urea–Tetramethylammonium Bromide and Water–Urea–Tetrabutylammonium Bromide at 25° 2895
Wendt, R. P. See Bresler, E. H., 264
Wentworth, W. E., and Ristau, W. Thermal Electron Attachment Involving a Change in Molecular Geometry 2126
Werner, G. K. See Nugent, L. J., 1540
Werner, T. C., and Hercules, D. M. The Fluorescence of 9-Anthroic Acid and Its Esters. Environmental Effects on Excited-State Behavior 2005
Westenberg, A. A., and deHaas, N. Absolute Measurements of the $O + C_2H_2$ Rate Coefficient 1181
Westmoreland, T. D. See Hammonds, C. N., 4374
Westrum, E. F., Jr. See Justice, B. H., 333, 1959
Wettack, F. S. Fluorescence of 2-Pentanone 1167
Whalley, E. See Baliga, B. T., 654
Wheelwright, W. J. Preparation of Promethium-147 Metal and Determination of the Density and Melting Point 2867
Whidby, J. F. See Leyden, D. E., 3076
White, C. E. See Nelson, R. D., Jr., 3439
Whittington, S. G. See Wall, F. T., 3953
Wickenden, D. K. See Hentz, R. R., 817, 1608
Wigg, E. E. See Daniels, M., 3703
Wijnen, M. H. J. See Kelly, C. C., 2447
Willard, J. E. See Ling, A. C., 2408; Timm, D., 2403; Wong, P. K., 2226
Williams, C. W. See Sloth, E. N., 278
Williams, F. See Keyser, R. M., 1623; Tsuji, K., 4017
Williams, F. A. See Guirao, C., 4302
Williams, R. C., and Gregory, N. W. The Palladium–Bromine System. The Molecular Composition of Palladium Bromide Vapor 623
Williams, R. L., and Voigt, A. F. Recoil Reaction Products of Carbon-11 in Simple Aromatic Compounds 2538
Williamson, D. G., and Bayes, K. D. Reactions of Oxygen Atoms with Acetylene 1232
Wilmarth, W. K. See Laming, F. P., 867
Winchester, J. W. See MacIntyre, F., 2163
Windsor, M. W. See Kropp, J. L., 1747
Windwer, S. See Hartstein, A. M., 1549
Winkler, C. A. See Khanna, S., 2062
Winograd, N., Blount, H. N., and Kuwana, T. Spectroelectrochemical Measurement of Chemical Reaction Rates. First-Order Catalytic Processes 3456
Wirth, H. E. See Lindstrom, R. E., 218
Wise, H. See Wood, B. J., 1348
Woessner, D. E. See Ostroff, A. G., 2784
Wojcik, J. F., and Stock, T. H. Aqueous Infrared Studies of the Pyridine Carboxylic Acids 2153
Wolf, A. P. See Ache, H. J., 3499; Finn, R. D., 3928
Wolff, M. A. See Baharad, R., 4391
Wolff, R. K. See Bronskill, M. J., 1175
Wolfgang, R., and Cross, R. J., Jr. Intensity Contour Maps in Molecular Beam Scattering Experiments 743
Wolfgang, R. L. See Baker, R. T. K., 3478
Wong, P. K., and Willard, J. E. Reactions of Carbon Dioxide, Sulfur Dioxide, Nitric Oxide, and Alkyl Halides with γ-Irradiated Silica Gel 2226
Woo, J. T. K. See Meyer, W. C., 2989, 3485
Wood, B. J., and Wise, H. The Reaction Kinetics of Gaseous Hydrogen Atoms with Graphite 1348
Wood, J. L., Badachhape, R. B., Lagow, R. J., and Margrave, J. L. The Heat of Formation of Poly(carbon monofluoride) 3139
Wood, R. H., and Ghamkhar, M. Heats of Mixing Aqueous Electrolytes. VII. Calcium Chloride and Barium Chloride with Some Alkali Metal Chlorides 3959
Wood, R. H., Ghamkhar, M., and Patton, J. Heats of Mixing Aqueous Electrolytes. VIII. Prediction and Measurement of Charge-Asymmetric Mixtures of Three Salts 4298
Wood, R. H., Patton, J. D., and Ghamkhar, M. Heats of Mixing Aqueous Electrolytes. VI. Magnesium Chloride with Some Alkali Metal Chlorides 346
Wood, R. H., Rooney, R. A., and Braddock, J. N. Heats of Dilution of Some Alkali Metal Halides in Deuterium Oxide and Water 1673
Wood, R. H. See Reilly, P. J., 4292
Woods, R. See Biegler, T., 3502
Woolf, L. A. See Bearman, R. J., 4403
Woolfenden, W. R. See Neuman, R. C., Jr., 3177
Wroblowa, H., and Muller, K. Isotherms of Contact Adsorption in the Double Layer 3528
Wu, C. See Millero, F. J., 2453
Wu, T. K. Nuclear Magnetic Resonance Studies on Microstructure of Ethylene Copolymers. I. Sequence Distribution in Ethylene–Vinyl Formate Copolymers 1801
Wu, Y., and Ache, H. J. On the Mechanism of the Self-Induced Exchange of Tritium with Halogenated Organic Molecules. I. Halogenated Aromatic Hydrocarbons 2424
Wu, Y. C., Rush, R. M., and Scatchard, G. Osmotic and Activity Coefficients for Binary Mixtures of Sodium Chloride, Sodium Sulfate, Magnesium Sulfate, and Magnesium Chloride in Water at 25°. II. Isopiestic and Electromotive Force Measurements on the Two Systems without Common Ions 2047
Wun, W. See Roeder, S. B. W., 3510
Wyatt, J. See Párkányi, C., 1132

Yafuso, M. See Green, M. E., 1626
Yagil, G. Acid-Base Equilibria and Structure in Two Water–Nonelectrolyte Mixtures 1610
Yamamoto, M. See Hirota, K., 464
Yandell, J. K. See Stranks, D. R., 840
Yang, C. H. Two-Stage Ignition and Self-Excited Thermokinetic Oscillation in Hydrocarbon Oxidation 3407
Yang, C. H., and Gray, B. F. On the Slow Oxidation of Hydrocarbon and Cool Flames 3395
Yankwich, P. E. See Kass, W. J., 3722
Yao, Y.-F. Y., and Kummer, J. T. The Surface Composition of Dilute Solid Solutions of Cesium Chloride in Potassium Chloride 2262
Yarnitzky, C. See Anson, F. C., 1835
Yasumori, I. See Inoue, Y., 1618; Momma, N., 1179
Yasunaga, T., Tatsumoto, N., Inoue, H., and Miura, M. Kinetic Studies of Intramolecular Hydrogen Bonding in Methyl and Ethyl Salicylates and Salicylaldehyde by Means of Ultrasonic Absorption Measurement 477
Yates, D. J. C., Dembinski, G. W., Kroll, W. R., and Elliott, J. J. Infrared Studies of the Reactions between Silica and Trimethylaluminum 911
Yeager, H. L., and Kratochvil, B. Conductance Study of Copper(I) and Silver(I) Salts of Symmetrical Anions in Acetonitrile 1963
Yeatts, L. B., and Marshall, W. L. Apparent Invariance of Activity Coefficients of Calcium Sulfate at Constant Ionic Strength and Temperature in the System $CaSO_4$–Na_2SO_4–$NaNO_3$–H_2O to the Critical Temperature of Water. Association Equilibria 81
Yelin, Z. See Shuali, U., 3445
Yin, T. P. The Kinetics of Spreading 2413
Yokohata, A., Ohmura, T., and Tsuda, S. A De-

chlorination Reaction in the Radiolysis of Aqueous Monochloroacetic Acid Solutions in the Presence of Nitrous Oxide 4013
Yoshihara, K. See Nogami, T., 2670
Yosim, S. J. See Darnell, A. J., 4116; Kellner, J. D., 4419
Young, R. P. See Horne, R. A., 2782
Youtsey, K. J., and Grossweiner, L. I. Photochemical Reactions of Fluorescein Dyes with H_2O_2 447
Yuan, D., and Kröger, F. A. The Sodium Activity in Liquid Sodium—Tin Alloys 2390

Zadorojny, C. See Pocker, Y., 2879
Zafonte, L. See Hisatsune, I. C., 2980
Zahradník, R. See Tichy, M., 534
Zecchina, A., Ghiotti, G., Morterra, C., and Borello, E. Infrared Study of Carbon Monoxide, Oxygen, and Carbon Dioxide Adsorption on Chromia–Silica. III. Carbon Monoxide–Oxygen Interaction 1295
Zecchina, A., Morterra, C., Ghiotti, G., and Borello, E. Infrared Study of Carbon Monoxide, Oxygen, and Carbon Dioxide Adsorption on Chromia–Silica. II. Carbon Dioxide 1292
Zecchina, A. See Borello, E., 1286
Zeltmann, A. H., Matwiyoff, N. A., and Morgan, L. O. Nuclear Magnetic Resonance of Oxygen-17 and Chlorine-35 in Aqueous Hydrochloric Acid Solutions of Cobalt(II). II. Relaxation and Chemical Exchange . . 2689
Ziifle, H. M. See Benerito, R. R., 1216
Zmbov, K. F., Uy, O. M., and Margrave, J. L. Mass Spectrometric Studies at High Temperatures. XXXI. Stabilities of Tungsten and Molybdenum Oxyfluorides . . 3008
Zwietering, Th. N. See Wanders, A. C. M., 2076

SUBJECT INDEX *to Volume 73, 1969*[1]

Aceanthraquinoxaline, and related pyrazines, photoconduction, 1352
Acetanilides, *ortho*-subst., rotation around aryl–N bond, 40
Acetic acid, and chloroacetic acids in H_2O–MeOH, 2453; dissn. kinetics, 197
Acetone, photolysis, 1011, 4406; pyrolysis, 2090, 2091
Acetonitrile, Ag(I) and Cu(I) salts in, 1963; pyrolysis kinetics, 2555; transference in, 471
Acetyl, and CH_3 radicals, rxs. w/ NO, 3498
Acetylene, rx. w/ O atoms, 1232; photolysis, 2929
Acetyl halides, thermo. data, 2645
N-Acetylpyrrole, internal rotation, 4124
Acidity functions, micellar effects, 4237
Actimde(III) β-diketone chelates, luminescence, 1540
Actinide halides, II–III oxid. potentials, 1177
Adsorption, by activated C from soln., 584; *n*-alkyl quaternary ammonium ions on Hg, 112; anions on Pt, 3571; Ar, Kr, Xe on porous Ag, 2720; on carbon black, 2321; chemisorbed and physisorbed H_2O on metal oxides, 243; CO on chromia–silica, 1286, 1295; CO_2 by alumina, 1243; CO_2 on chromia–silica, 1292; contact, in double layer, 3528; β-diketones on metal films, 15; ethylene–Ar on C (graph.), 969; on hydroxylated silica, 4269; localized, on graphite, 813; MeOH and EtOH on, 3844; in mixed solvents, 3577; nitrate and phthalate ions at Hg–soln. interface, 3582; O_2 by PbS, 2902; polar vapors on zeolite 5A, 1975; 1-propanol on γ-alumina, 716; pyridine and 2,2′-bipyridyl on metal films, 2559; pyridine at Hg, 3609; 8-quinolinol on metal films, 729
Agarose gels, of electrolyte solns., diffusion coefficients, 3380
Alcohols, aq., radiolysis, 3794; normal aliphatic, effect on electrode kinetics, 1023
Aliphatic acids, aq., radiolysis, 4207; 4214
Aliphatic alcohols, charge dist., 4036
Alkali halides, aq., thermo. data, 3346
Alkali hydroxide, aq., therm. cond., 451
Alkali metal halides, aq., conductivities, 978; in D_2O and H_2O, thermo. data, 1673
Alkanes, radiolysis, 964
n-Alkanes, binary sys., thermal diffusion, 1508; C_6 to C_9, pyrolysis, 2804; charge dist. and mass spectra, 462, 463, 464; and methylsilanes, rxs. w/ recoil ^3H, 4378; trans. props., 3258
N-Alkyl betaines, micellization, 2627
n-Alkylbenzenes, phosphorescence, 2545
Alkyl halides, and toluene, radiolysis in alkanes, 1707; radiolysis in cyclohexane, 931
Alkyl iodides, radiolysis, 1077
Alkyllithium–alkyl halide rxs., trans. alkyl rads., 3834
n-Alkyl quaternary ammonium ions, ads. on Hg, 112
Aluminum complexes, ^{27}Al soln. nmr, 3467
Aluminum ion, acidity and assn. in aq. acid, 650
Aluminum tris(2,4-pentanedionate), dipole moment, 3439
Amide bonds, barrier to rotation, 3177
Amides, aliphatic tertiary, internal rotation, 2696
Amines, oxid., 2142, 2147
Amine-type perchlorates, methyl-subst., thermal decomp., 4367
Ammonia, catalytic synthesis, 1174; rxs. w/ germania gel, 908
Ammonia–ethylene, photolysis, 456
Ammonium chlorate, thermal decomp., 4370
Ammonium perchlorate, sublimation, 4302
Aniline, rx. w/ chloranil, 2670
Anilinium *p*-toluenesulfonate in HAc, 1822
Anilinium acetate in HAc, 1822
Anion exchange, metal complexes, mixed solvs., 4415; selective swelling of exchanger, 591
Anthracenes, isotopic, harmonic vib. analysis, 1430
9-Anthroic acid, and esters, fluorescence, 2005
Argon, fluid, eqn. of state, 4076
Aromatics, ^{11}C recoil rxs. in, 2538
Arrhenius activation energies, rel. w/ excitation functs., 4338
Aryl phenyl ketones, spectral properties, 1132
Arylsulfonates, in aq. H_2SO_4, thermo. data, 2279
2,2′-Azobisisobutyronitrile, photo- and thermal initiator efficiency 2699

Barium chloride dihydrate, ^{137}Ba and ^{135}Ba nqr, 3156
Barium methacrylate, dehydration in air, 2871
Benzene, amine derivatives, triplet–triplet abs. spectra, 1868; aq., radiolysis, 2071; benzoic acid assn. in, 3520; –cyclohexane, frictional coefficients, 752; –hexafluorobenzene, thermo. data, 1602; –N_2O solns., radiolysis, 2676; phosphorescence, 2545; rxs. w/ recoil ^3H, 1252; thin-film, ir reflectance and trans. spectra, 889
Benzenes, intramol. interaction, 557; microwave abs., 2187
Benzenoid hydrocarbons, electronic spectra, 534
Benzylphosphine, PH_2 from, 2996
1,12-Benzperylene, radiationless deactivation, 1752
Benzylamines, tertiary, H^* exch. mechanisms, 2924
Biacetyl, phosphorescence, 1815; photolysis, 2633; pyrolysis, 177
Biacetyl triplets, in benzene, quenching, 3982
Bianthrones, photolysis, 3481
Biphenyl, in aq. polymers, 1488
Biphenyls, *o*, *o*′-bridged, charge-transfer donor abilities, 3442
2,2′-Bipyridyl, ads. on metal films, 2559
Bismuth, halides, molten conductivities, 4116
Bismuth sesquioxide, phase trans. and elect. properties, 672
Bilsulfate ion, dissn. in H_2SO_4 and $NaHSO_4$, 218
Boiling, light induced, blackened liquids, 1634
Bolaform electrolytes, aq., thermo. data, 4334; thermo. data, 164
Bolaform ions, cond. in H_2O, 3985
Bonding, C_1 and C_2 fluorides, 949; methyl radicals, 3505
Boron carbide, rx. w/ hydrogen, 1000
Borane carbonyl, pyrolysis, 873
Boron trifluoride, ^{11}B–^{19}F coupling constants, 275; conductivity in halogen fluorides, 2792
Bovine serum albumen, aq. conformal changes, 4256
Bromide, oxid. by bromate in alkali nitrates, 4152
Bronzes, Na–W, ortho–parahydrogen conversion and H_2–D_2 equil., 894
Bubbles, phosphate ion enrichment in, 2163
Butadiene diepoxide, hydrolysis, 1216
1,2-Butadiene, vac.–uv photolysis, 1313
n-Butane, photolysis, 789
cis-2-Butene–diazomethane mixtures, photolysis, 1274
t-Butyl iodide, photolysis in $CFCl_3$, 282

Cadmium oxide, pore structure, 2213
Calcium nitrate·$4H_2O$, ultrasonic absorption, 921
Calcium nitrate tetrahydrate–cadmium nitrate tetrahydrate melts, properties, 2287
Calcium sulfate, activity coeffs. in $CaSO_4$–Na_2SO_4–$NaNO_3$–H_2O, 81
Camphorquinone, photolysis, 2633; triplet states, 2462
ϵ-Caprolactam, H bonding, 2440
Carbon, ads. by, from soln., 584; graphite, localized ads. and absolute surface areas, 813
Carbon-11, recoil, rxs. in simple aromatics, 2538; recoil. rxs. w/ solid, 3499
Carbon-14, recoil, rxs. in Mg_3N_2, 3928
Carbon black, graphitized, Ar–ethylene ads., 969
Carbon dioxide, ads. by alumina, 1243; ads. on chromia–silica, 1292
Carbon disulfide, neg. ion formation in, 2960
Carbon disulfide–Ar, shock-heated, light emission, 3751
Carbon–hydrogen bond, dissn. energy, 733
Carbon–hydrogen–oxygen systems, plasma equil., 2526
Carbon monoxide, ads. on chromia–silica, 1286, 1295; interaction w/ platinized Pt, 3283
Carbon suboxide, elect. struct., 2298
Carbon tetrabromide complexes, Raman and uv spectra, 2309
Carbon tetrachloride, ads., apparent mol. area, 1170; in alkanes, radiolysis, 1702
Carbon tetrachloride–tetrachloroethylene, thermo. data, 1476
Carbon tetrafluoride, thermo. data, 4232
Carbonyl sulfide, neg. ion form. in, 2960
Catalysis, metal ion, 3421; metal oxides in thermal decomp. rxs., 1209; by MgO, 130; NiO redn., 3790; organometallic, 2093; sec. valence force, 361; sec. valence force, 1898; silica–alumina, 1-butene isom. and polym., 2234

---

[1] Index prepared by Dr. Jack Opdycke, University of San Diego, College for Men, San Diego, Calif.

Cation radicals, esr, 2790
Cesium, in liq. NH_3, conductance, 2615
Cesium chloride, in KCl, surface composition, 2262
Chemisorption, coverage-dependent, 3502; diisopropylmethyl phosphonate w/ trans. met. salts, 2243
Chlorination, 1- and 2-chloropropane, 2447
Chlorine monoxide, rx. w/ H atoms, 2091
Chlorine trifluoride, thermal dissn., 2683
α-Chloroacrylonitrile, nmr, 1117
Chloroform, and chloroform–benzene, anisotropic mol. rotation, 103
Chlorophyll, esr, 1066
Chloropropane, 1- and 2-, competitive chlorination, 2447
Chlorosilanes, rxs. w/SiO_2 surfaces, 2372
Cholesterol, films, adhesive forces, 1157
Chromatography, concurrent soln. and ads., 700, 708; gen. non-eq. theory, 2577, 2582
Chromia–silica, ir study of ads. on, 1286, 1292, 1295
Chromic ions, hydrated, in H_2O and H_2O–D_2O, 3669
Chromium(III) complexes, solvent orientation, 3897
Chromium(III) cpds., luminescence, 2502
Chromium(III) perchlorate, hydrolysis, 713
Chromogenic transition, hydroxytropenylium bromide, 2939
Chronoamperometry, theory of second-order mech., 1238
Chronocoulometry, kinetics by, 1406
Circular dichroism, visible, nickel ion–peptide complexes, 4277
Cobalt, surface species structure, 3494
Cobalt(II), in aq. HCl, nmr, 2689
Cobalt(III) complexes, aq., radiolysis, 1941; redn. by Zn^+, Cd^+, Ni^+, 1091
Collagen membranes, trans, props., 3063
Colloidal particles, dielectric dispersion, 1052
Complexes, aq. $AgSO_4^-$, 745; Cr(III), solvent orientation, 3897; w/ CuN_4^{2-} chromophore, 3763; donor–acceptor, 2,3-dichloro-5, 6-dicyanobenzoquinone w/ THF, THP and 1,4-dioxane, 1584; e^- donor–acceptor, M.O. theory, 2111, 2787; H-bonded, in soln., 3849; hexaaquo trans. metal, crystal field act. energy, 739; linear amylose–iodine–iodide, 3990; nickel ion–peptide, circ. dichroism, 4277; TCNQ, electronic props., 513; 3d trans. metals, in KCNS(l), 4014; weak, 641; weak, thermo., 3496
Complex ions, photochem., 4183; 4250
Compressibility, unit law, mixtures, 525
Conductance, in acetonitrile, 223; aq. alkali metal halides, 978; BF_3 in halogen fluorides, 2792; bolaform ions in H_2O, 3985; Ce–NH_3(l), 2615; Cu(I) and Ag(I) salts in acetonitrile, 1963; high-pressure ionic, 2429; KNO_3 and $AgNO_3$ in dioxane–H_2O, 1501; large hydrophobic ions in H_2O, MeOH, CH_3CN, 3322; NaCl–dioxane–H_2O, 2619; tetraalkylammonium halides in 1,3-diaminopropane, 1549; tetraalkylammonium salts in 1-butanol and 1-pentanol, 158; TlCl–dioxane–H_2O, 2097
Conductivity, MTHF and MCH from 70°K, 2408; molten $BiCl_3$, $BiBr_3$, BiI_3, 4116; thermal, aq. alkali hydroxide, 451
Coronene, and benzcoronene, fluorescence and phosphorescence, 693
Critical constants, conformal mixtures, 3359
Cross sections, molecular electron, 62 cpds. at 70 eV, 3866
Crotonic acid, acid-catalyzed hydration, 3278
Crystal growth, kinetics, 3838
Crystal structure, *cis*-1,3-cyclobutanedicarboxylic acid, 1480; *tris*(diethyldithiocarbamato) cobalt(III), 443; *trans*-3,6-dimethyl-2,5-piperazinedione, 2891; $Na_2O \cdot MgO \cdot 5Al_2O_3$, 1774; 1,3,5,7-tetramethylcycloocta-*cis*, *cis*, *cis*, *cis*-1,3,5,7-tetraene, 2378; N-(β,β,β-trifluoroethyl)-N,2,4,6-tetranitroaniline, 1199
Cupric acetate, esr, 2964
cis-1,3-Cyclobutanedicarboxylic acid, crys. and mol. structure, 1480
Cyclohexane, photonitrosation, 4345; radiolysis on silica–alumina, 1608
Cyclohexene, rxs. w/ recoil ^3H, 2508
1,5-Cyclooctadiene, photolysis, 1171
Cyclooctatetraene, bond shift, isom., 3201
Cyclooctatetraene anion radical, esr, 340
Cyclopentane–CCl_4, thermo. data, 2356
Cyclopentanone, self assn. and hyd. in CCl_4, 3273
Cyclopropane, clathrate hydrates, 1392, 1398; ionic rxs., 3189; SCF–MO and CI calcs., 1299
Cylindrical electrodes, const.-potential rxs., 3374
Cysteine, radiolysis, 1568

cis-Decalin–*trans*-decalin sys., thermo. data, 2883
Deexcitation probability, surface, 3158
Deoxyribose nucleic acid, optical anisotropy and chain flexibility, 1685
Deuteriocarbonate ion, dissn. in D_2O, 3014
Diaphragm cell data, multicomponent, analysis, 1591
Di-*t*-butyl peroxide, radiolysis, 4417
Dichlorobis (pyridine) cobalt(II) complex, electric moment, 1619
Dichromate ion, hydrolysis, 4391
Dicyclopentadiene, unimol. dissn., 2095
Dielectric behavior, Böttcher's formula app. to liq. mixtures, 3236; heptanol-1 and heptanol-4 mixtures, 3255
Dielectric dispersion, colloidal particles, 1052; glycol electrolyte impreg. paper, 1056
Dielectric properties, data w/ small departure from Debye behavior 4386; esters in benzene, 3697; H_2O, 445; ion–solvent interactions, 1151; meas. in time domain, 616; N-methylpropionamide–H_2O, 57; pyryidine complexes w/ dichloro- and trichloroacetic acids, 459; weak complexes, 641
Dielectric relaxation, binary liq. mixts., 1146
Diffusion, alcohols and amides in H_2O, 1155; binary liq. mixts., 186; binary, study w/ a wedge interferometer, 141; ^{12}C- and ^{14}C- subst. molecules, liq. phase, 269; H_2O in nonpolar gases, 2000; halogenated H.C.'s in He, 3679; high pressure ionic, 2782; isothermal, 2- and 3-component sys., 3039; isothermal ternary, 1268; model for multiphase sys. w/sorption, 3125; multicomponent, 1262; 1591; oxygen in magnetite, 632; polyelectrolyte, 797; thermal, in binary *n*-alkane sys., 1508; thermal in liq. electrolyte solns., 6; ternary system, 2456
Diffusion coefficients, agarose gels of electrolyte solns., 3380; four component systems, 1716; light, ordered suspensions, 2386
Diimide, structure, 1901
Diisopropylmethyl phosphonate, chemisorption w/ trans. met. salts, 2243
β-Diketones, ads. on metal films, 15
trans-3,6-Dimethyl-2,5- piperazinedione, 2891
N,N-Dimethylacetamide-*d*$_3$, internal rotation, 4227
2,3-, 2,6- and 2,7-Dimethylanthracene rads., esr, 779
2,5-Dimethylhydroquinone cation rad., esr, 4387
Dimethoxymethane rads., kinetic data, 2590
Diphenylanthracene, electrochemiluminescence, 2786
Dipole moments, aliphatic alcohols, 4036; aluminum *tris*(2,4-pentanedionate), 3439; liq. and vapor states, 3236
Dipole orientation, a new function for, 2864
Double layer, amide solvs., 3598; common problems, 3523; compact, therodynamics, 3591; contact ads., 3528; diffuse, nonequilib., 1835; oxide–soln. interface, 3546; rapid charging, 1843

Eizner–Ptitsyn theories, polyelectrolyte solns., 3224
Elasticity, rubber, 2864; halotrifluoroethylenes, 3969; Electric moments, dichlorobis (pyridine) cobalt(II) complex, 1919
Electrocapillarity, surface orientation, 4047
Electrocapillary curves, solid metals, 466
Electrocapillary studies, aq. LiCl, 3619
Electrochemiluminescence, diphenylanthracene rad. anion, 2786
Electrochemistry, aq. TcO_4^-, 3082; porous media, 1455, 1462
Electrode rxs., electronically excited molecules, 3196; catalytic, kinetics, 4102, 4111
Electrode sensitivity, boromosilicate glass in molten salts, 1766
Electrodes, cyclindrical, const.-potential rxs., 3374; fresh metal, 3562
Electroluminescence, preannihilation, H^+ donor effect, 2992
Electrolysis, controlled-potential, 4348; hydrogen evolution, 506
Electrolytes, aq., heats of mixing, 3959; aq., hydration nos., 1563; bolaform, 520; dibolaform, thermo. data, 1367; in dioxane-H_2O, 3635; mixed, thermo., 4292; 4298; 1:1, transport, 1095
Electrolyte solns., heat of dilution, 2382; nmr, internal references, 3643, 3652; thermal diffusion, 6
Electron, hydrated, temp. dependence, of rxs., 277; hydrated, uv spectrum, 3171; solvated, subnanosecond observation, 1175
Electron acceptors, photocond., 4381
Electron capture, phosphine, 4376
Electron distributions, CO, SCO, CO_2, 1008
Electron exchange reactions, double-layer effects, 2652
Electron impact study, mono- and disilane, 3912; pentafluorosulfur, 4031; $SnCl_2$ and $SnCl_4$, 4394
Electron injection, into ZnO, 468
Electron ionization cross sections, mol., 62 cpds., 3866
Electrons, trapped, solvation, 3452
Electron scavengers, indole deriv., excited state interaction w/, 4130
Electron transfer, dianions of α-methylstyrene to benz[*e*]pyrene, 4364
Electron-transfer rxs., magnetic exchange effects, 2594
Electron attachment, hexafluoroacetone, 2791
Electronic excitation, trans. from pyrene to perylene, 370

Electronic properties, TCNQ complexes, 513
Electroosmosis, H_2O trans. through cation-exch. membranes, 1414; nonlinear phenom. eqn., 1593
Electroviscous effect, secondary, charged spheres, 1062; secondary, for nonidentical particles, 3512
Energy transfer, collisional, 2464; vibrational, 4321
Esr, alkyl rads during alkyllithium-alkyl halide rxs., 3824; cation rads., 2790; $CF_2CF_2\cdot$, 2919; chlorophyll, 1066; chromia–silica w/ O_2, 3172; Cu(II) O-alky-l-amidinourea complexes, 3763; cupric acetate, 2964; cyclooctatetreane anion rad., 340; 2,3-, 2,6,- and 2,7-dimethylanthracene rads. 779; 1,4-dimethylanthrasemiquinone, 71; 2,5-dimethylhydroquinone cation rad., 4387; hydroxylation of furans, 1139; hyperfine splitting in anion rad. of thianthrene 5,5,10,10-tetroxide, 1854; irradiated H.C.'s on silica gel, 4175; γ-irradiated silica–alumina gel, 817; low-spin Co(II) isocyanide complexes, 803; methyl-subst. phenyl rads., 2438; 1-methylphenalenyl and 1-phenylphenalenyl rads., 215; NO_2 in olefinic solvents, 1402; nitrosodisulfonate ion, 4405; ^{17}O hyperfine splitting in iminoxy rad., 2448; peroxy rads. in trifluoroacetamide, 2663; phenyl methyl sulfone anion rad., 3901; phenoxy rads., 3370; subst. pyridine N-oxide rad. anions, 2335; 1,4,5,8-tetramethylanthrasemiquinone, 71; tropenyl rad., 1147
Esters, in benzene, mol. configuration, 3697; photolysis, 2239
Ethanol, H bonding, 1596; radiolysis, 2741
Ethers, photolysis, 2239
Ethyl acetates, nmr, 4400
Ethylene, alkyl rad. addn., 4094; hydrogenation, 1667; hydrogenation by ZnO, 3772, 3781; mixts. w/ vinyl chloride, critical region, 1164; radiolysis, 2178
Ethylene–CO, radiolysis, 378
Ethylene copolymers, microstructure, 1801
Ethylene sulfite, nmr, 4020
Ethyl isocyanide, thermal decomp., 1652
Ethyl radicals, diffusion-controlled rxs., 1257
Ethylenes, halogenated, two-bond carbon–proton coupling, 449; methyl subst., singlet–triplet abs. bands, 4332
Europium monoxide, thermo. data, 374
Exchange, isotopic, aq. solns. and D_2 on Pd, 285
Exchange rxs., bimolecular, parametric study, 943
Extraction, $HClO_4$ and $HReO_4$, 675

Faujasites, syn. Na, ordering of framework ions, 387
Films, soap, bursting, 3018, 3028; thin liq., 489; thin liq. comp. and elasticity, 2828
Flames, cool, 3395
Fluorenyl alkali salts, in THF and DME, thermo. data, 2712
Fluorenyl carbanion, nmr, 2649
Fluorescein dye-H_2O_2, photolysis, 447
Fluorescence, 9-anthroic and its esters, 2005; coronene and benzcoronene, 693; Hg($^1P_1$), quenching, 4289; 2-pentanone, 1167; pyrochlorophyll, 125; quenching by singlet energy transfer, 1805; 1,2,3,4-tetrahydronophthalene, 1149, 3175
Fluorides, C_1 and C_2, bonding, 949
Fluorine-18, recoil, rxs. w/ perfluorocyclanes, 4430
Fluorobenzenes, 1046
Fluorocarbon mixtures, virial coefficients, 1335
Fluorocarbons, cyclic, radiolysis, 552
Fluoroethanes, Hg-photosens. decomp., 1513
Force constants, intermolecular, CH_4 and Ar, 2304
Formic acid, aq. w/ O_2, radiolysis, 2564
Friction constants, tetra-n-propylammonium tetrafluoroborate, 2099
Furans, hydroxylation, esr study, 1139

Gadolinium–H_2 sys., thermo. data, 2352
Gases, heats of transport, 2798; in nonpolar solvents, 2274; nonpolar, soln. in conc. electrolytes, 498; second virial coeff., 608; thermo. data, 167
Germanium, clean, MeOH and EtOH rxs. w/, 3844
Glass membranes, electrochem. props. in molten salts, 1766
D-Glucose, electrocatalytic oxid., 3508
Glycylglycylglycine and glycylhistidylglycine, proton equil. in MeOH–H_2O, 2230
Glycylsarcosine, rxs. w/ Co(II) and Ni(II), 1
Grinding, effect on Sodium trimetaphosphate, 3012
Group V hydride and trihalide, intermol. pot. funct., 406

Halotrifluoroethylenes, electric moments, 3969
H_2–D_2 mixt., addn. to ethylene, 2436; isotopic exch., 3884
Heating, flash, of liqs., 1634
Hemoglobin, dipole moment and proton fluct. anisotropy, 418
Hemoglobin-bound water, electrical properties, 2600
Heptafluorobutyric acid, micelle formn., 1612
Hexacyanoferrate(III), red. by ascorbic acid, 1996
Hexafluoroacetone, electron attachment cross section, 2791
Hexafluoroazomethane, pyrolysis, 2838
Hexamethyldisiloxane–toluene mixt., surface tension, 3150
2,4,6,2′,4′,6′-Hexanitrodiphenylamine, acid dissn. in acetone–H_2O, 3909
n-Hexylmalonic acid, dicarbox. in polar solvs., 438
n-Hexyl rads., isomerization, 2080
Hot-hydrogen rxs., simult. double displacement, 3478
Hydrates, crystalline, thermo. data, 2033
Hydrocarbon–I_2 solns., radiolysis, 3204
Hydrocarbon–N_2O, radiolysis, 2809
Hydrocarbon polymers, trapped e^-'s, 1623
Hydrocarbons, halogenated, diffusion in He, 3679; halogenated aromatic, ^3H exch., 2424; poly- and heterocyclic, H exchange, 1525; polynuclear aromatic, chem. shifts and reactivity, 293; radiolysis, 4167; sat., anodic oxid., 427; sat. liq., radiolysis, 4397; slow oxid., 3395, 3407; solid, radiolysis, 2403; solid H atom permeation, 3756; solns., photoinjection, 4398
Hydrocarbon systems, plasma equilibria, 2532
Hydrodynamics, rigid salts of bolaform disulfonic acids in dioxane–H_2O, 520
Hydrogen, exch., polycyclic and heterocyclic H.C.'s, 1525; isotopic exch. between aq. solns. and D_2 on pd, 285
Hydrogen atom, abstraction by CH_3 radicals, 3294
Hydrogen atoms, addn. to olefins, 1169; rxs. w/ aq. aromatics, 413; rx. w/ deuterium halides, 1722; rx. w/ graphite, 1348; solid H. C. permeation, 3756
Hydrogen bonding, EtOH, 1596; intramol., 477; Methyl N-vinylcarbamate w/ DMSO, 2989; and rotation about amide bonds, 3177
Hydrogen chloride, solubility in ice, 2680
Hydrogen, electrolytic evolution on aluminum oxide, 506
Hydrogen iodide, photolysis, 3474; rx. w/ tetrafluoroethylene, 3356
Hydrogen peroxide, basic aq., photolysis, 2361; photolysis, 867
Hydrogen sulfide, liq., ir spectrum, 3518; thermo. data, 3700; tritiated, rad. scavenging, 850
p-Hydroxyphenylpropionic acid, radiolysis, 4188
Hydroxytropenylium bromide, chromogenic transition, 2939

Iminodiacetic acid, protolysis in H_2SO_4, 3076
Iminoxy rad., ^{17}O hyperfine splitting, 2448
Indole derivs., excited states, interact. w/ e^- scavengers, 4130
Indole salts, nmr, 455
Indor, halogenated ethylenes, 449
Internal rotation, tertiary amides, 2696
Iodine, and ICl, in C_6-hydrocarbon matrices, 2779
Iodine trichloride, thermo. data, 755
Ion-exchange, Na^+, α-zironium phosphate, 3424; rare earths w/ EDTA eluent, 3102
Ion-exchange membranes, counterion trans. nos., 97; liq., steady-state properties, 249; resistance and EMF, 257
Ionic melts, activity coeffs., 4022, 4023
Ionic solutions, common problems, 3523
Ion–molecule rxs., monosilane–CH_4 and monosilane–benzene, 4194; in propene, 4141; by pulsed ion cyclotron double resonance, 469; translational energies of products, 2857; vinyl chloride, 829
Ions, in various solvents, thermo. data, 2417
Ion–solvent interaction, sodium tetrabutylaluminate, w/ benzene and toluene, 4374; tetraalkylammonium and common ions in N-methylacetamide, 3390
Ir spectra, aq. pyridine carboxylic acid, 2153; $BrHBr^-$, 448; $\cdot CCl_3$ and $\cdot CCl_2Br$ in Ar, 3504; dichloro- and dibromophosphinyl rads., 2774; $H_2S(1)$, 3518; lactams, 2999; methyl iodide-d_3, 4040; NH_3 on germania gel, 908; NaO_2 and Na_2O_2, 3922; reflectance and transmittance, benzene(s) thin films, 889; subst. benzenes, 557; trimethylaluminum rxs. w/ silica, 911
Iron(III) ion, solvent exch., 4203
Isobutyl vinyl ether glasses, radiolysis, 4017
Isobutylene, rx. w/ nitrosonium nitrate, 3088
Iron molecule, Fe_2, dissn. energy, 2450
Isocyanide complexes, low-spin Co(II), esr, 803
Isomerism, rotational, medium effects, 1192
Isotope effect, N, in transition metal hexaamine complex–ammonia sys., 2472

Kerr effect, optical dispersion of hemoglobin, 2908
Ketene, photolysis, 959
Kinetic data, acetonitrile pyrolysis, 2555; acetylacetone enol tautomerization, 3421; alkyl rad. addn. to ethylene, 4094; alkyl hydroperoxides rxs. w/ tetranitromethane, 4155; anodic oxid. of sat. H.C.'s, 427; aq. dimethoxymethane, 2590; aq.

methyl red dissn., 737; aq. O_2^- and HO_2, 3736; bimol. trans. rxs. in O_2, N_2, NO, N_2O, NO_2, CO, CO_2, 3941; bromide oxid. by bromate in alkali nitrates, 4152; butadiene diepoxide hydrolysis, 1216; $CaHPO_4 \cdot 2H_2O$ crystal growth, 3838; $CF_3\cdot$ rx. w/ C_2H_4, 2746; CF_3 rx. w/ NH_3, 3854; CH_4 decomp., 1648; CH_4 oxid. on Pt electrodes, 2397; CH_4 rx. w/ O_2, 2421; CH_3I w/ aq. subst. hydrazines, 3154; CH_3I rx. w/ hydrazine in H_2O, 317; chlorosilanes rxs. w/ SiO_2 surfaces, 2372; by chronocoulometric meas., 1406; Co(II) and Ni(II) rxs. w/ glycylsarcosine, 1; Cr(III) perchlorate hydrolysis, 713; crystallization and dissolution of $SrSO_4$ in H_2O, 1735; decomp. of halogenated nitrobenzene anion rads., 4389; deoxymercuration in H_2O-glycerol, 2011; dicarbox. of *n*-hexylmalonic acid in polar solvs., 438; by differential thermometry, 3801; dissn. of ClF_3, 2683; dissn. of HAc, 197; ethyl isocyanide–d_5, 2756; ethylene hydrogenation by ZnO, 3772, 3781; $Fe(CN)_6^{3-}$ red. by ascorbic acid, 1996; first-order catalytic processes, 3456; gas phase thermolysis rxs., 4056; hexahydro-1,3,5-trinitro-5-triazine, therm. decomp., 1604; hexafluoroazomethane pyrolysis, 2838; *n*-hexyl rad. isom., 2080; H abstraction by $CF_3\cdot$ and $C_2F_5\cdot$, 2083; H atom abstraction by $CH_3\cdot$, 3294; H rx. w/ graphite, 1348; H rxs. w/ aq. aromatics, 413; H^+ exch., between guanidinium ion H_2O, 2853; H^+ exch., in H_2O–NH_3, 857; H^+ exch., in tertiary benzylamines, 2924; HI rx. w/ tetrafluoroethylene, 3356; H_3O^+ rx. w/ OH^-, 2846; hot H at. rxs., 1158; hydration of crotonic acid, 3278; hydration of propionaldehyde, isobutyraldehyde, pivalaldehyde, 4005; hydration of 2- and 4-pyridinecarboxaldehydes, 1857; H bonding, 477; hydrogenation of ethylene, 1667; hyd. of $Cr_2O_7^{2-}$, 4391; hyd. of methyl orthobenzoate by anionic surfactants, 361; hyd. of methyl and isopropyl bromides, 654; hyd. of *para*-subst. benzaldehyde diethyl acetals, 1898; ionic rxs. in monosilane-acetylene and -ethylene mixtures, 3307, 3315; iminodiacetic acids in H_2SO_4, protolysis, 3076; $KClO_3$ (liq.) thermal decomp., 1209; *d*-$K_3Cr(C_2O_4)\cdot 2H_2O$ thermal racemization, 3366; leucine rx. w/ Ni(II), Co(II), Cu(II), 3814; Li(s)–Li^+ rx. in propylene carbonate, 4026; lysozyme isom., 3918; methyl formate decomp. on Cu, 1179; methylacetylene hydrogenation, 2104; Mn(III) rxs. w/ hydrazines, 2248; N(active) rx. w/ P(g), 2062; N atoms rx. w/ ClNO, 3163; Ni(II) and Co(II) rx. w/ picolinate anion, 281; NO rxs. w/ O_2, Cl_2, and Br_2, 2980; NO rx. w/ bistrifluoromethy peroxide, 2834; O atom rxs. w/ C_2 to C_8 alkanes, 3327; ^{15}O exch. between CO_2 and H_2O, 3351; OF_2 dissn., 1621; O^3P) addn. to olefins, 597; (O^3P) rxs. w/ haloalkanes, 1326; O rx. w/ C_2H_2, 1181; O rxs. w/ ethylene and formaldehyde, 191; organosilane methanolysis, 3918; oxidation of amines, 2142, 2147; ozonide ion decay, 2361; perfluorocyclobutane thermal decomp., 3830; photoperoxidation, 1711; phthalic anhydratide solvolysis, 1438; Pu oxid., 2814; pyrolysis of biacetyl, 177; pyrolysis of borane carbonyl, 873; rad.–rad. rxs., 2703; redn. of Co(III) complexes by Zn^+, Cd^+, and Ni^+, 1091; rotation around aryl–N bond in acetanilides, 40; S(colloid) rx. w/ SO_3^{2-}, 2064; shock-heated CS_2–Ar, 3751; sodium lauryl sulfate micelle dissn., 3288; tetrakis(dimethylamino)ethylene autoxidation, 3686; thermal isom. of ethyl isocyanide, 1652; thermal isom. of maleate ion in potassium halides, 3690; thiocyanic acid hydrolysis, 1380; thioglycolic acid rx. w/ ferricyanide, 1627; triphenylamine cation rad. dimerization, 2611, 2623; unimol. rxs., 3891; V(II) rx. w/ Np(IV) in aq. $HClO_4$, 1741; V(II)–V(III) electrode kinetics, 1023
Kinetic isotope effect, ethyl isocyanide-d_5, 2756; intramolecular; 3722
Kinetics, Arrhenius actn. energies and excitation functions, 4338; bimol. trans. rxs., 3941; catalytic electrode rxs., 4102, 4111; electron exchange reactions, 2652; electron-transfer reactions, 2594; H rx. w/ deuterium halides, 1722; spectroelectrochemical meas., 3456; spreading, 2413; three-element rx. coords., 3722; unimol. rxs., 3891
Krypton difluoride, mass spectrum and energetics, 2078

Lactams, ir studies, 2999; self-assn., 1363; uv spectra, 1642
Lanthanide halide, II–III oxide. potentials, 1177
Lanthanide monosulfates, heats of complexation, 3462
Lanthanide oxides, thermo. data, 333, 1959
Laser systems, liquid, Nd^{3+} in $SeOCl_2$ and $POCl_3$, 1785
Lead sulfide, O_2 adsorption, 2902
Leucine, rxs. w/ Ni(II), Co(II), Cu(II), 3814
Light absorption, and triplet state populations, 2036
Light scattering, quasielastic, 2820
Lithium nitrate –KNO_3–H_2O, thermo. data, 1984
Liquid mixtures, binary, dielectric relaxation, 1146
Liquids, structured, 3628
Lithium chloride, in DMF, 741; solns., nmr, 1153
Lithium fluoride, high temperature species, thermo. data, 1919
Lithium and Na halides, aq., thermo. data, 3745
Luminescence, actinide(III) β-diketone chelates, 1540; Cr(III) cpds., 2502; phenyl- and halophenylnaphalenes, 3070
Lysozyme, aq., isom. kinetics, 3918

Macromolecules, terminally ads., density dist., 3488
Madelung potentials, zeolites, 3660
Magnesium(II), aq., thermo. data, 1588
Magnesium chloride, in aq. alkali metal chloride solns., 346
Magnesium nitride, recoil ^{14}C rxs. in, 3928
Magnesium oxide, catalytic activity, 130
Maleate ion, thermal isom. in potassium halide matrices, 3690
Manganese(III), rxs. w/ hydrazines, 2248
Mass spectra, alkanes, 462, 463, 464; hydrolyzed bromine fluoride, 278; KrF_2, 2078
Mass spectrometers, high-temperature, calibration, 3047
Membranes, average pore size, 4428; cation-exch., electroosmatic water trans., 1414; charged, anomalous osmosis, 3181; charged, streaming potential, 2134; collagen, trans. props., 3063; ion-transp. noise, 1626
Mercury, (Hg^1P_1), quenching cross sect., 4289
Mercury–H_2O interface, Stern inner region, 3534
Metal acetylacetonates, microwave abs., 3433
Metal–amine solns., visible spectra, 3098
Metal chelates, interactions of silver halides w/, 3556
Metal complexes, paramagnetic, removal of spin–spin coupling, 3516
Metal halides, electronic and mol. structures, 1105
Metal hydrides, V–H, Nb–H, Ta–H, thermo. data, 683
Metal–NH_3 solns., uv-visible spectra, 2326
Metal oxides, chemisorbed and physisorbed water, 243
Metal perchlorates, metal, thermo. data., 3229
Metal–solution interface, image forces at, 1632
Metal surfaces, fresh, aq. solns., 3562
Methane, CF_4 and CH_4–CF_4, corresp. states, 528; decomposition, 1648; oxid. on Pt electrodes, 2397; rx. w/ O_2, 2421
Methanol, assn., model, 3820; C–H bond dissn. energy, 733
Methanol–H_2O, radiolysis, 2750
Methyl alcohol, phase-change induced decomp., 3521
Methyl benzyl cyanides, ^{14}N nmr, 307
Methyl ethyl ether, photosens. decomp., 793
Methyl formate, cat. decomp., 1179
Methyl iodide, radiolysis, 52; rx. w/ hydrazine, 317; rxs. w/ subst. hydrazines, 3154
Methyl isocyanide, and ethyl isocyanide, ^{14}N nmr, 4145
Methyl, and isopropyl bromides, rate of hydrolysis, 654
Methyl red, aq. dissn., 737
Methyl N-vinyl carbamate, self-assn., 3485
Methylacetylene, hydrogenation, 2104
Methylamine, photochem., 3904
Methylcyclopropane, photolysis, 3219
Methyl iodide-d_3, vibrational intensities, 4040
N-Methylpropionamide–H_2O, densities and dielectric consts., 57
4-Methyl-1-pyrazoline, photolyris, 3109
Methylsilane, dimethylsilane, trimethylsilane, methylene insertion rxs. w/, 4401
Methylsilanes, rxs. w/ recoil tritium, 465
α-Methylstyrene, dimeric dianions, e^- trans. to [e]-benzpyrene, 4364
N-Methylthiourea, hindered rotation, 435
Micellar effects, acidity functions, 4237
Micelle structure, 12,12,12-trifluorododecyl sulfate solns., 2042
Micelles, hystafluorobutyric acid, 1612; influence on titrations of soap solns., 601; ionic, hydrophobic and electrostatic interactions, 2054; sodium lauryl sulfate, dissn., 3288; stability, effect of protein denaturation, 2270
Microwave absorption, metal acetylacetonates, 3433; subst. benzenes, 2187
Microwave discharge, CH_4 decomposition in, 1648; $H_2O(v)$ dissn., 3693
Mixture model, in HOD solns., 4242
Mixtures, unit compressibility law, 525
MO calculations, EH, metal halides, 1105; LCl–SCF, aryl phenyl ketones, 1132; PPP, benzenoid hydrocarbons, 534; SCF and CI, cyclopropane, 1299; TcH_9^{2-}, 854
Mobilities, electrical and diffusional, ^{22}Na, ^{137}Cs in molten $LiNO_3$, $NaNO_3$, $RbNO_3$, 94
Molecular beam experiments, scattering intensity contour maps, 743
Molecular orbital treatment, e^- donor–acceptor complexes, 2111, 2787
Mono- and disilane, ionization and dissn., 3912
Monochloroacetic acid–N_2O, aq., radiolysis, 4013

Monofluorobenzene, photochem., 995
Monolayers, air–water interface, 2118
Monosilane, w/ methane and benzene, ionic rxs., 4194
Monosilane–acetylene, gas mixture, ionic rxs., 3307
Monosilane–ethylene, gas mixtures, ionic rxs., 3315
Mössbauer spectra, Fe–Y zeolite, 2970

NaCl, activities in H_2O-polyglycols and H_2O-polyglycol ethers, 2417
Naphthalene, in aq. polymers, 1488; phenanthrene, singlet-triplet trans., 4356
Naphthalenes, phenyl- and halophenyl-, luminescence, 3070
Naphthalone, phenanthrone, triphenylene, triplet–triplet trans., 4351
Nematogenic liq. crystals, surface effects, 1127
Neopentane, pyrolysis, 3167
Neutron capture, radiative yields, aggregation yields by, 2779
Nickel(II) ion, solvent exch., 4203
Nickel oxide, supported, catalysis, 3790
Nickel(II)-*o*-phenylenediamine, polarographic prewave, 2764; polarography, 953
Niobium chlorides, thermo. data, 3054
Nitric acid, in $LiNO_3$–KNO_3–$NaNO_3$ eutectic, 4135
Nitric oxide, rx. w/ bistrifluoromethyl peroxide, 2834; rxs. w/ acetyl and methyl rads., 3498; rxs. w/ O_2, Cl_2, and Br_2, 2980
Nitrobenzene anion rads., halogenated, decomp. steric effects, 4389
Nitro cpds., pyrochlorophyll-sens. photored., 117
Nitrogen, active, rx. w/ P(g), 2062
Nitrogen atoms, rx. w/ ClNO, 3163
Nitrogen dioxide, in olefinic solvs., esr, 1402
Nitrogen trifluoride, neg. ion form., 1586
Nitrosodisulfonate ion, esr, 4405
Nitrosonium nitrate, rx. w/ isobutylene, 3088
Nitrosyl chloride, photolysis, 2208
Nitrosyl fluoride, photolysis, 2203
Nitrous oxide, radiolysis, 1143
Nmr, N-acetylpyrrole, 4124; ^{27}Al, aluminum complexes in soln., 3467; aq. electrolytes, 1563; aq. electrolytes, 3643, 3652; asym. phosphorus cpds., 91; ^{11}B–^{19}F coupling constants, 275; ^{13}C, phenyllithium and phenylmagnesium bromide, 1624; $CHCl_3$, $CDCl_3$–C_6H_6 $CHCl_3$–C_6D_6, 103; chem. shifts and reactivity of polynuclear aromatic hydrocarbons, 293; α-chloroacrylonitrile, 1117; ^{13}C, coupling through two bonds, 1370; diastereotopic magnetic nonequivalence, 1150; N,N-dimethylacetamide-d_3, 4227; ethyl acetates, 4400; ethylene copolymers, 1801; ethylene sulfite, 4020; ^{19}F, temp. meas. by, 2460; Fe^{3+} and Ni^{2+} solvent exch., 4203; Fe(II) and Co(III) complexes w/ α,α′-dipyridyl, 276; fluorenyl carbanion, 2649; HNO_3 in $LiNO_3$ in $LiNO_3$–KNO_3–$NaNO_3$ eutectic, 4135; indole salts, 455; LiCl solns., 1153; methyl N-vinylcarbamate, 3485; methyl N-vinylcarbamate in DMSO–CCl_4, 2989; N-methylthiourea, 435; micelle structure by, 2042; ^{14}N, methyl and ethyl isocyanide, 4145; ^{14}N, methyl benzyl cyanides, 307; ^{12}O, H_2O–NH_3, 857, 863; ^{17}O, spin–spin coupling w/ ^{55}Mn and ^{13}C, 1600; ^{17}O and ^{35}Cl, aq. Co(II), 2689; phenoxy radicals, 3370; α-phenylethylphosphine, 1678; porphyrins in chloroform, 423; pyridines, 1049; pyridines and conj. acids, 2465; removal of spin–spin coupling, 3516; *ortho*-subst. fluorobenzenes, 1046; *ortho*-subst. phenols, 1043; sulfhydryl proton, 453; trimethylene selenide, 1124; urea in H_2O, 266; vicinal ^{31}P–H and ^{14}N–H coupling in single conformers, 1830
Nqr, ^{137}Ba and ^{135}Ba, in $BaCl_2 \cdot 2H_2O$, 3156; group IVa tetrachlorides, zeeman study, 2948

Octadecyl sulfate, adhesive forces, 1157
Octadecyltrimethylammonium bromide, surface pressure, 2118
1-Octanal, self-assn., CCl_4 effect on, 2217
OH stretching vibration, molar absorptivity *vs.* temp., 4027
Onsager's reciprocal rel., simple membrane trans. processes, 264
Optical dispersion, of hemoglobin, 2908
Organic cpds., mol. flexibility, 207
Organic glasses, radiolysis, 4311, 4315
Orthophosphate, sorption on metal oxides, 1953
Orthophosphates, dil. aq., equil., 2956
Osmosis, anomalous, charged membranes, 3181
Oxygen, isotopic equilibration on oxidized Pd, 2392; $O(^1D)$, rxs. w/ H.C.'s, 391; $O(^3P)$, rx. w/ 2-methyl-2-pentene, 1598; (O^3P), rxs. w/ *cis*- and *trans*-2-butenes, 597; (O^3P), rxs. w/ haloalkanes, 1326; self-diffusion in magnetite, 632
Oxygen-15, exch. between CO_2 and H_2O, 3351
Oxygen-17, spin–spin coupling w/ ^{55}Mn, ^{13}C, 1600
Oxygen atoms, rx. w/ acetylene, 1232; rx. w/ C_2H_2, 1181; rxs. w/ C_2 to C_5 alkanes, 3327; rxs. w/ ethylene and formaldehyde, 191
Oxygen difluoride, thermal dissn., 1621
Oxygen iodide, stability, 1861
Organosilanes, methanolysis, 3718
Oxygen species, in V_2O_5, 3973
Ozone, photolysis in CO_2 liq., 2935

Palladium, cold-worked catalyst, active sites, 1618
Palladium bromide vapor, mol. comp., 623
Pentafluorosulfur, elect. impact study, 4031
2-Pentanone, fluorescence, 1167
Peptide bond, *cis–trans* models, 2999
Perfluoroalkanes, solid, thermo. data, 2368
Perfluorocarbons, in *n*-hexane, radiolysis, 356
Perfluorocyclanes, rxs. w/ recoil ^{18}F, 4430
Perfluorocyclobutane, photolysis, 809; thermal decomp., 3830
Periodic chemical rx., spatial, 750
Phenols, *ortho*-subst., nmr, 1043
Phenomenological coeffs., cross-, 46
Phenoxy radicals, spin distributions, 3370
Phenyl methyl sulfone, anion radical, esr, 3901
Phenyl rads., methyl-subst., hyperfine coupling, 2438
α-Phenylethylphosphine, nmr, 1678
Phosphine, electron capture, 4376
Phosphorescence, benzene and *n*-alkylbenzenes, 2545; benzene-photosensitized, biacetyl, 1815; chromia–silica w/ O_2, 3172; lifetimes and glass relaxation at 77°K, 2088
Phosphorus cpds., asym., high res. nmr, 91; gaseous, thermo. data, 2734
Phenyl-substituted cations, rads. and anions, steric and conjugative effects, 1789
Phenyllithium and phenylmagnesium bromide, nmr, 1624
Photochemistry, aq. nitrate solns., 3445; complex ions, 4183, 4250
Photoconductivity, electron acceptors, 4381
Photoinjection, H.C. solns., 4398
Photoionization, charge-transfer systems, 3170
Photolysis, acetone, 1011, 4406; acetylene, 2929; azoethane, hexafluoroazomethane, 1257; basic aq. H_2O_2, 2361; 1,2-butadiene, 1313; *n*-butane, 789; *cis*-2-butene–diazomethane mixtures, 1274; *t*-butyl iodide in $CFCl_3$, 282; bianthrones, 3481; camphorquinone, biacetyl, 2633; CH_2CO, 2074; ClNO, 2208; complex. ions, 4183, 4250; 1,5-cyclooctadiene, 1171; esters and ethers, 2239; fluorescein dye–H_2O_2, 447; fluoroethanes, 1513, 1521; H_2O, 2886; H_2O_2, 867; HI, 3474; H_2S, 1158; $K_3[Fe(C_2O_4)_3] \cdot 3H_2O$ and $K_3[Co(C_2O_4)_3] \cdot 3H_2O$, 2316; ketene, 959; methyl ethyl ether, 793; methylamine, 3904; methylcyclopropane, 3219; methyl-, dimethyl- and trimethylsilane w/ diazomethane, 4401; 4-methyl-1-pyrazoline, 3109; monofluorobenzene, 995; neopentane, 3167; NH_3–ethylene, 456; O_3 in CO_2 liq., 2935; O_3–H.C.'s in Ar(1), 391; OF_2–CO_2–N_2, at 4°K, 3877; OF_2–N_2O–N_2, at 4°K, 3877; ONF, 2203; perfluorocyclobutane, 809; polydimethylsiloxane, 823; propane, 3168; quinone, 3240, 3245; SO_2, 4412; 1,1,2,2-tetrafluoro-1-chloroethane, 2944; tetraphenylhydrazine, 4315; Tl(I)–Tl(III) solns., 840; 1,1,1-trifluoromethylazocyclopropane, 746; N,N,N′,N′-tetramethyl-*p*-phenylenediamine, 1912
Photonitrosation, cyclohexane, 4345
Photoperoxidation, unsaturated organics, 1711
Photoreduction, quinone, 3240, 3245
Phthalic anhydride, solvolysis, 1438
Picolinic acid, complexes w/ Ni(II) and Co(II), 281
Picric acid, in acetonitrile, 4029; in acetonitrile-basic solvents, 400; solvation by, 223
Plasma sources, C–H–O systems in, 2526; hydrocarbon systems, 2532
Platinum, anion ads. on, 3571
Platinum electrodes, structured liquids near, 3628
Plutonium, oxid. kinetics, 2814
Plutonium nitride, thermo. data, 350
Polarizabilities, molecular fluorocarbons, ethers, esters, ketones, aldehydes, 3860
Polarographic prewave, *o*-phenylenediamine–nickel(II), 2764
Polarography, Ni(II)-*o*-phenylenediamine prewave, 953
Poly(acrylic acids)s, potentiometric titrations, poly(acrylic acids)s, 4382
Poly(carbon monofluoride), heat of form., 3139
Polydimethylsiloxane, photolysis, 823
Poly(dimethylsiloxanes), surface tension of solns., 3143
Polyelectrolytes, activities, 4071; diffusion, 797; isotactic, nmr, 667; tracer diffusion, 1420
Polyelectrolyte solns., and Eizner–Ptitsyn theories, 3224
Polymer solns., mol. wts. and second virial coeffs., 1448
Polypyrrolidone, sorption studies, 2294
Polyribonucleotide system, helix-coil transition, 2170

Polystyrene, amorphous, specific heat, 3384
Polystyrenebenzyltrimethylammonium-type anion-exch. resin, alkanesulfonate selectivity, 2194
Pore structure, CdO, 2213
Porous media, electrochem., 1455, 1462
Porphyrins, assn. in chloroform, 423
Positrons, lifetimes in aq. oxyacids and hydrogen cpds., 882
Potassium chlorate, molten, thermal decomposition, 1209; radiolysis, 396
Potassium chloride-NaCl-D_2O, thermo. data, 3165
Potassium nitrate, cond. in dioxane-H_2O, 1501
Potassium nitrate-$Ca(NO_3)_2$, vitreous, viscosity, 4147
Potassium trisoxalatocobaltate(III) trihydrate, photolysis, 2316
Potassium trisoxalatoferrate(III) trihydrate, photolysis, 2316
Promethium-147, density and m.p., 2867
Propane, photolysis, 3168
1-Propanol, ads. on γ-alumina, 716
2-Propanol, radiolysis, 2451
Propene, ion-molecule rxs., 4141; rxs. w/ recoil ^3H, 1247
Propylene, ionic rxs., 3189
Propylene carbonate, Li(s)-Li^+ rx. in, 4026; LiCl and LiBr in, 3299; lithium and quaternary ammonium salts in, 3965
Propynal, Zeeman effect, 4359
Proteins, and small mol., aq. properties, 26
Protein affinities, neut. oxygen and sulfur in chelating ligands, 634; simple molecules, 4328
Proton ejection, quinone systems, 2058
Proton exchange, H_2O-NH_3, 857
Proton-transfer complexes, solvation, 1890
Pyrochlorophyll-sensitized photoreduction, nitro cpds., 117
Pyrene, radiative and radiationless transitions, 1747
Pyridine, ads. on metal films, 2559; and diazines, radiolysis, 4064; irradiated, coord. cpds. of, esr study, 2345
Pyridine carboxylic acids, aq., ir spectra, 2153
Pyridine N-oxide radical anions, esr, 2335
2- and 4-Pyridinecarboxaldehydes, hydration, 1857
Pyridines, and conj. acids, nmr, 2465; nmr, 1049
Pyrolysis, acetone, 2090, 2091; acetonitrile, 2555; alkanes, 2804; hexafluoroazomethane, 2838
Pyruvic acid, reversible hydration, 2879

Quantum chemistry, spin-free, 2477, 2488, 2495
Quinol clathrates of CH_4 and CH_3F, thermo. data, 1762
8-Quinolinol, ads. on metal films, 729
Quinone, photoreduction, 3240, 3245; redn. in chg.-trans. complex w/ H_2, 1595

Radiolysis, alkanes in organic solvents, 964; alkyl halides in cyclohexane, 931; alkyl halides and toluene in alkanes, 1707; alkyl iodides, 1077; aq. alcohols, 3794; aq. aliphatic acids, 4207, 4214; aq. benzene, 2071; aq. CH_3I, 52; aq. Co(III) complexes, 1941; aq. HCOOH-O_2, 2564; aq. H_2O_2 and H_2 + O_2, 3736; aq. monochloroacetic acid-N_2O, 4013; aq. sodium linoleate, 2443; aq. solns., 1029, 2846; aq. solns., spur diffusion model, 1928; benzene-N_2O solns., 2676; biacetyl-benzene, 3982; CCl_4 in alkanes, 1702; CO_2, NH_3 and H_2 on silica, 3160; coord. cpds. of pyridine, 2345; cyclic fluorocarbons, 552; cyclohexane, 1608; cysteine, 1568; di-*t*-butyl peroxide, 4417; D_2O-SF_6, 1583; EtOH on SiO_2, 2741; ethylene-CO, 378; ethylene-ethane, 2178; glassy and polycrystalline alkaline ices, 3290; H.C. crystals, 4167; H.C. polymers, 1623; H.C.'s on silica gel, 4175; H_2-D_2, 3884; H_2O, 2571; solid hydrocarbons, 2403; H_2O, 1341; hydrocarbon-I_2 solns., 3204; hydrocarbon-N_2O, 2809; *p*-hydroxyphenyl propionic acid, 4188; isobutyl vinyl ether glasses, 4017; $KClO_3$(s), 396; MeOH and MeOH solns., 1384; monosilane and monosilane-ethylene, 2706; MeOH-H_2O, 2750; $NaNO_3$ solns., 3703, 3710; neutral aq. solns., 2056; N_2O, 1143; organic glasses, 4311, 4315; organic liqs. w/ H_2S scavenger, 850; perfluorocarbons in *n*-heptane, 356; 2-propanol, 2451; pyridine, and diazines, 4064; rad. and mol. yields in H_2O, 1937; sat. H.C.'s, 4397; stilbene in cyclohexane, 4283; stilbene in 2-propanol and acetone, 20; TMPD in benzene, 1616; trifluoroacetamide, 2663; trifluoroiodomethane, 3215; triphenylmethyl chloride solns., 3264
Rare earth metals, in their molten halides, 1320
Rare earths, ion-exchange w/ EDTA eluent, 3102
Raman spectra, CBr_4 complexes, 2309; S, S-Se, S-As liqs., 1374
Reorientation, anisotropic, rotational diffusion constants, 2445
Retinal, all-*trans*, energy transfer to, 2512
Rhenium trichloride and sesquioxide, thermo. data, 1039
Ribonucleosides, S-cont., uv spectra, 4219
Rotational diffusion, triplet molecules, 3119
Rotatory properties, theory, molecules containing peptide gps., 228

Salt mixtures, fused, complex ion equilibria, 754; fused, surface tension, 4421
Salts, aq. binary mixtures, thermo. data, 2047
Salt system, fused, ideal, 2287
Sedimentation, polymer solns., 1448
Sedimentation equilibria, polydisperse nonideal solns., 1759
Self-assn., 1-octanol, 2217
Semiconductor properties, trasition metal chelates, 3132
Shear, alkaline sulfide coloring by, 2468
Shereshefsky's eqn., binary-soln. surface tension, 270
Silica, hydroxylated, ads. on, 4269; reactive, from methylated silica, 321, 327; surface hydroxylation, 3947; Silica-alumina catalyst, effect of water content, 2234
Silica-alumina gel, γ-irradiated, esr, 817
Silica gel, γ-irradiated, rxs. w/ CO_2, $^{-}SO_2$, NO, and alkyl halide, 2226
Silver bromide, and AgBr-HBr, in pyridine, 3115
Silver chloride, in DMSO-H_2O, 1470
Silver halides, in aq. H_2SO_4 and $HClO_4$, 1990; interactions w/ metal chelates, 3556
Silver nitrate, cond. in dioxane-H_2O, 1501
Silver salts, monovalent, in pyridine, 580
Singlet-triplet trans., naphthalene, phenanthrene, 4356
Soap films, bursting, 3018, 3028
Sodium cellulose xanthate, chain dimension, 3413
Sodium chloride, aq., thermo. data, 2025; in dioxane-H_2O, conductances, 2619
Sodium hydroxide, hydrates, thermo. data, 149
Sodium iodide, aq., thermo. data to 900° and 4000 bars, 723
Sodium ion, solvation, 3880
Sodium linoleate, radiolysis, 2443
Sodium nitrate, high gas pressure effect on viscosity, 1205
Sodium nitrate solns., radiolysis, 3703, 3710
Sodium peroxide, ir spectrum and bonding, 3922
Sodium tetrabutylaluminate, in benzene and toluene, 4374
Sodium trimetaphosphate, thermo. data, 3012
Sodium-Sn alloys, thermo. data, 2390
Solids, Tait eqn. for compressibility of, 2459
Sols, stability, counterion complexing, 564, 1484
Solubilities, nonpolar gases in aq. KOH, 312
Solubility, Al_2O_3 in TiO_2, 2157; aromatic hydrocarbons, in aq. complex ion electrolytes, 2761; gases in nonpolar liqs., 4410; NH_3 in alkali nitrate and perchlorate melts, 1084
Solvation, various ions in H_2O, propylene carbonate, DMSO, 3934
Solvents, structured, solutions of, 1968
Sorption, in faujasite zeolites, 4384; H_2O by genetic variants of α_{s1}-casein, 303; by Nylon 4, 2294; orthophosphate on metal oxides, 1953;
Spherical highly soluble particle, lifetime, 382
Spin relaxation, proton, Cr(III) in H_2O and H_2O-D_2O, 3669
Spin-lattice relaxation, solvents w/ nitroxide spin labels, 3510
Spin-lattice relaxation times, proton, in H_2O from −10° to +104°, 3157
Spreading, kinetics, 2413
Spur diffusion model, radiolysis of aq. solns., 1928
Squalane-alcohols, chromatography, 708
Statistical mechanics, self-avoiding random walks, 3953
Stern inner region, Hg-H_2O interface, 3534
Stilbene, rad. ind. isom., 20; rad. ind. isom. in benzene, 4283
Streaming potential, across charged membrane, 2134
Strontium sulfate, aq. crystallization and dissolution, 1735
Structure, alkaline earth chloride effect of H_2O, 3208; Co surface species, 3494; *cis*-1,3-cyclobutanedicarboxylic acid, 1480; diimide, 1901; electronic, carbon suboxide, 2298; fluid, monoalcohols, 3255; H_2O 1553; H_2O-nonelectrolytes, 1610; methyl rads., 3505; molecular, tris(diethyldithiocarbamato) cobalt-(III), 443; molecular, metal halides, 1105; molecular and crystal, 2,3,5,7-tetramethylcycloocta-*cis*, *cis*, *cis*, *cis*-1,3,5,7-tetraene, 2378
Sublimation, ammonium perchlorate, 4302
Sulfolane, Ag^+, Cl^-, and Br^- in, 3268
Sulfur, colloidal, rx. w/ SO_3^{2-}, 2064; liq., polymerization, 1374;
Sulfur-35, recoil, in KCl-KBr, 1956
Sulfur dioxide, photolysis, 4412; vapor emission, 1071
Sulfur hexafluoride, inertness to CF_3 and CH_3 rads., 1614; physical data, 2254
Sulfur-Se and S-As, liq. mixtures, polymerization, 1374
Sulfhydryl proton, solvent interactions, 453
Sulfides, alk. earth, coloring by shear, 2468
Sulfuric acid, aq., thermo. data, 2021
Surface tensions, hexamethyldisiloxane-toluene mixtures, 3150; poly(dimethylsiloxanes) solns., 3143
Susceptibilities, diamagnetic, fluorocarbons, ethers, esters, ketones, aldehydes, 3860
Suspensions, ordered, light diffraction, 2386

Swelling, anion exchanger, 591

Tait equation, for solid, 2459
Technetate ion, disproportionation, 3082
Terphenyl rad. anions, clustering w/ Na^+ in THF, 1581
Tetraalkylammonium–halide, conductance in 1,3-diaminopropane, 1549
Tetraalkylammonium iodides, in H_2O and DMF, 174
Tetrachlorides, group IVa, nqr Zeeman study, 2948
1,1,2,2-Tetrafluoro-1-chloroethane, photolysis, 2944
Tetrahedral and fcc lattices, dens. functs. for random walks, 3953
1,2,3,4-Tetrahydronaphthalene, fluorescence yields, 1149
Tetrakis(dimethylamino)ethylene, autoxidation kinetics, 3686
Tetramethylaluminate, Li and Na, dissn. in soln., 2515
Tetramethylcyclooctatetraene, bond shift isom., 3201
N,N,N′,N′-Tetramethyl-*p*-phenylenediamine, delayed fluorescence in liq. solns., 1912
Tetranitromethane, rxs. w/ alkyl hydroperoxide, 4155
Tetraphenyl salts, group V, aq., thermo. data, 2728
Tetraphenyltin and hexaphenylditin, thermo. data, 4264
Tetra-*n*-propylammonium tetrafluoroborate, friction constants, 2099
Thallium(I)–Tl(III), solns., photolysis, 840
Thermal decomp. amine-type perchlorates, 4367
Thermal decomp., NH_4ClO_3, 4370
Thermal electron, attachment, 2126
Thermodynamic data, acetic acid and chloroacetic acids in H_2O–MeOH, 2453; acetyl halides, 2644; ads. on carbon black, 2321; ads. in mixed solvents, 3577; Ag^+, Cl^-, and Br^- in, 3268; AgBr and AgBr–HBr in pyridine, 3115; AgCl in DMSO–H_2O, 1470; AgI sol in acidic $Al_2(SO_4)_3$, 1484; alcohols, amino acids, carboxylic acids, and salts in 6 *M* urea, 3249; alkali metal halides in H_2O and D_2O, 1673; alkaline earth chlorides in H_2O and D_2O, 4423; alkaline earth chloride–H_2O, 3208; alkylammonium salts, 986; aluminum ion in aq. acid, 650; Al_2O_3–TiO_2, 2157; amorphous polystyrene, 3384; amylose–iodine–iodide, 3990; aniline derivatives and naphthalene in aq. LiCl, 1695; aniline rx. w/ chloranil, 2670; anion exchanges in mixed solvs., 4415; aq. alkali halides, 986; aq. alkali halides, 3346; aq. S-alkylthioacetic acids and alkoxyacetic acids, 634; aq. $CaCl_2$ and $BaCl_2$ mixing w/ alkali metal chlorides, 3959; aq. $CuSO_4$ and $Cu(en)_2S_2O_3$, 4425, 4426; aq. electrolytes, 1163; aq. electrolytes, 3635; aq. electrolytes, 4298; aq. formic, acetic, *n*-butyric acid and glycinium ion, 1220; aq. gp. V tetraphenyl salts, 2728; aq. LiCl, 3619; aq. $MgCl_2$–alkali metal chlorides, 346; aq. NaI to 800° and 400 bars, 723; aq. orthophosphates, 2956; aq. polyelectrolytes, 1420; aq. trimethylamine-d_9, 1559; Ar, 4076; Ar, Kr, Xe on Ag, 2720; aromatic hydrocarbons in aq. complex ion electrolytes, 2761; arylsulfonates in aq. H_2SO_4, 2279; benzene–hexafluorobenzene, 1602; benzoic acid in benzene, 3520; Bi–$BrBr_3$ sys., 4419; Bi_2O_3, 672; binary–soln. surface tension, 270; bolaform electrolytes, 4334; boron carbide rxs. w/ hydrogen, 1000; $[Bu_3N–(CH_2)_8–NBr_3]Br_2$, 164; $CaSO_4$–Na_2SO_4–$NaNO_3$–H_2O, 81; CCl_4–C_2Cl_4, 1476; CF_4, 4232; CH_4, CF_4, and CH_4–CF_4, 528; chlorophylls a and b and pheophytins a and b w/ *sym*-trinitrobenzene, 570; compact double layer, 3591; conformal mixtures, 3359; crystalline hydrates, 2033; cyclopentane–CCl_4, 2356; cyclopentanone–CCl_4–H_2O, 3273; cyclopropane clathrate hydrates, 1392, 1298; *cis*-decalin–*trans*-decalin sys., 2883; deuteriocarbonate ion in P_2O, 3014; dibolaform electrolytes, 1367; dil. solns. of $HClO_4$ and $HReO_4$, 675; elect. double layer in amide solvs., 3598; ethylene–vinyl chloride, 1164; EuO, 374; fluorenyl alkali salts in THF and DME, 2712; fluorocarbon mixtures, 1335; fused salt mixts., 4421; gaseous phosphorus cpds., 2734; gases, 167; gases in nonpolar solvents, 2274; Gd–H_2, 2352; glycylglycylglycine and glycylhistidylglycine in MeOH–H_2O, 2230; H-bonded complexes in soln., 3849; HCl in ice, 2680; $HClO_4$ and HCl in H_2O, H_2O–ethylene glycol, H_2O–HAC, 928; $HClO_4$ and $HReO_4$ extraction by dilution TBP solns., 1494; HNDA in acetone–H_2O, 3909; H_2O on ZnO, 3809; H_2O–HDO, 3491; H_2O–nonelectrolytes, 1610; H_2O–urea–Bu_4NBr, 2895; H_2O–urea–Me_4NBr, 2895; HSO_4^- in H_2SO_4 and $NaHSO_4$, 218; H_2S, 3700; hydration of propionaldehyde, isobutyraldehyde, pivalaldehyde, 4005; ICl_3, 755; ionic melts, 1160; ionic melts, 4022, 4023; ionic solvation in mixed aq. solvs., 3152; ions in several solvents, 2417; ion–solvent interactions, 3390; KCl–NaCl in D_2O, 3165; lactam self-assn., 1363; lanthanide monosulfate complexes, 3462; lanthanide oxides, 333; lanthanide oxides, 1959; Li and Na halides, 3745; Li and Na tetramethylaluminate in soln., 2515; LiCl and LiBr in propylene carbonate, 3299; LiF, 1919; $LiNO_3$–KNO_3–H_2O, 1984; lithium and quaternary ammonium salts in propylene carbonate, 3965; MeOH in *n*-hexane, 3820; metal perchlorates, 3229; micellization of *N*-alkyl betaines, 2627; milinium acetate and anilinium *p*-toluenesulfonate in HAc, 1822; monovalent silver salts in pyridine, 580; Na^+, 3880; NaCl (aq.), 2025; NaCl–H_2O–polyglycols and NaCl–H_2O–polyglycol ethers, 3417; NaCl–$MgSO_4$–H_2O and NaCl–$MgSO_4$–H_2O and Na_2SO_4–$MgCl_2$–H_2O, 2047; NaOH hydrates, 149; Na_2SO_4(aq.) and H_2SO_4(aq.), 2017, 2021; naphthalene and biphenyl in aq. polymers, 1488; Na–Sn alloys, 2390; NH_3 in alkali nitrate and perchlorate melts, 1084; niobium chloride, 3054; nematogenic liq. crystal, 1127; nonelectrolytes in H_2O, PC and DMSO, 1572; nonpolar gases in aq. KOH, 312; O_2I^-, 1861; organics in H_2O and glycol–H_2O, 207; oxide–soln. interface, 3546; partially deuterated diacid phosphate, 1088; Pd–Br sys., 623; PH_2 radical, 2996; picric acid in acetonitrile, 4029; picric acid in acetonitrile–basic solvents, 400; poly(carbon monofluoride), 3139; polyribonucleotide system, 2170; proton–transfer complexes, 1890; PuN, 350; pyridine ads. at Hg, 3609; pyruvic acid hydration, 2879; quinol clathrates of CH_4 and CH_3F, thermo. data, 1762; rare earth metals in their molten halides, 1320; $ReCl_3$ and Re_2O_8, 1039; rotational isomers, 1192; salts of polyacrylic acid and carboxymethylcellulose, 4071; SF_6, 2254; silver halides in aq. H_2SO_4 and $HClO_4$, 1990; silver halide sols., 564; solid perfluoroalkanes, 2368; sodium terphenyl in THF, 1581; solutes in structured solvents, 1968; squalane–alcohols, 708; TCNE–aromatic donor cpds., 2793; tetraalkylammonium iodides in H_2O and DMF, 174; tetraphenyltin and hexaphenylditin, 4264; thin liq. films, 489; TiO, 749; trifluoroacetic acid and benzophenone in diphenylmethane, 3430; tropomyosin solns., 75; tungsten and molybdenum oxyfluorides, 3008; tungsten oxyiodides, 4086; U(l) w/ dissolved Ta, P, S, C, O_2, 769; UO_2(s)–U(l), 762; urea in H_2O, 266; urea–H_2O–NaCl, 2795; various ions in H_2O, propylene carbonate, DMSO, 3934; V–H, Nb–H, Ta–H, 683
Thermodynamics, coverage-dependent chemisorption, 3502; data from thermometric titration curves, 2076; electrocapillary sys., 4047; electrolyte solns., 2382; gases in nonpolar liqs., 4410; Hg–aq. electrolyte interface, 1632; ionic micelles, 2054; local structure in aq. fluids, 900; low temp. entropy, 940; mixed electrolytes, 4292; polar mixture, 2916; real gases, 608; Robinson–Sinclair eqn., 4411; three-component invariant point, 1884; two nonelectrolytes in a solvent, 1877; weak complexes, 3496
Thermoelectric properties, Bi–$BiBr_3$ sys., 4419
Thermogravimetric analysis, kinetics, 751
Thermolysis, gas phase, kinetics, 4056
Thermometry, differential rx. rates by, 3801
Thiocyanic acid, hydrolysis, 1380
Thioglycolic acid, rx. w/ ferricyanide ion, 1627
Thorium(IV) ions, mono- and polynuclear, X-ray diffraction studies, 4163
Tin(II) and (IV) chlorides, electron impact study, 4394
Titanium monoxide, config. entropy, 749
Transference, in acetonitrile, 471; counterion, ion-exch. membranes, 97; LiCl in dimethyl formamide, 741; moving boundary exp., 4403; moving boundary meas., 298
Transition metal hexaammine complex–NH_3 sys., N isotope effect, 2472
Transition metals, diatomic bonding, 1356
Transition metal salts, aq., visible spectra, 3338
Transport, conc. 1:1 electrolyte solns., 1095; heats of gas, 2798; nonlinear, equations, 46
Transport processes, bolaform ions in H_2O, 3985; hydrogen-bonding solvs., 158; simple membrane, 264
Transport properties, multicomponent mixts., 62; Ag^+, Na^+, nitrate melts into Pyrex, 212; liq. *n*-alkanes, 3258
Tributyl phosphate, dil. solns., $HClO_4$ and $HReO_4$ extraction by, 1494
Triethylamine–I_2, in *n*-heptane and *p*-dioxane, 482
Trifluoroacetamide, radiolysis, 2663
Trifluoroacetic acid, and benzophenone, in diphenylmethane, 3430; in nonpolar solvents, 1426
Trifluoroiodomethane, radiolysis, 3215
Trifluoromethyl rads., diffusion-controlled rxs., 1257; rxs. w/ NH_3, 3854
1,1,1-Trifluoromethylazocyclopropane, photolysis, 746
Trimethyl selenide, nmr, 1124
Trimethylaluminum, rxs. w/ silica, 911
Trimethylamine-d_9, aq. ionization, 1559
2,4,6-Trinitrotoluene, solid–solid polymorphic transformation, 3514
Triphenylamine cation rad., dimerization, 2611, 2623
Triphenylmethane dye carbonium ions, λ_{max} absorption bands, 273
Triphenylmethyl chloride solns., radiolysis, 3264
Triplet states, Hunds' rule, 2085

Triplet–triplet abs. spectra, amine derivatives of benzene, 1868
Triplet–triplet trans., in naphthalone, phenanthrone, triphenylene, 4351
Tritium, exch. w/ halogenated aromatic hydrocarbons, 2424; recoil, alkyl replacement rxs., 3174; recoil, rxs. w/ benzene, 1252; recoil, rxs. w/ cyclohexene, 2508; recoil, rx. w/ methylsilanes, 465; recoil, rxs. w/ methylsilanes and alkanes, 4378; recoil, rxs. w/ propene, 1247; recoil, subst. for H, 4024
Trityl perchlorate, dissn. in 1,2-dichloroethane, 2458
Tropenyl radical, esr, 1147
Tropomyosin solns., thermo. data, 75
Tungsten oxyiodides, thermal stabilities, 4086

Ultrasonic absorption, aq. lanthanide salts, 544; bovine serum albumin, 4256; hydrate melts, 921
Urania–Uranium sys., thermo. data, 762
Uranium, liq., w/ diss. Ta, P, S, C, O_2, 769
Urea, dil. aq. self-assn., 2441
Urea–H_2O–NaCl, thermo. data, 2795
Uv spectra, CBr_4 complexes, 2309; e^- aq., 3171; H and OH radicals, 1029; lactams, 1642; methyl subst. ethylenes, 4332; S-cont. ribonucleosides, 4219
Uv–visible spectra, dilute metal–NH_3 solns., 2326; triethylamine–I_2 in *n*-heptane and *p*-dioxane, 482

Vanadium (II), rx. w/ Np(IV) in aq. $HClO_4$, 1741
Vanadium oxides, solid solns. w/ titanium oxides, 1781
Vanadium pentoxide, activity in catalytic oxid., 3973
Vinyl chloride, ionic rxs., 829
Viscosities, aq. alkali metal chlorides, 2784; aq. electrolytes, urea and EtOH effect on, 1621
Viscosity, gas pressure effect on, $NaNO_3$, 1205; H_2O, 1187; and intradiffusion coeff. for multicomponent sys., 1280; nonaq. solvs., 2060; vitreous KNO_3–$Ca(NO_3)_2$, 4147; water, 34
Visible spectra, aq. $Pr(NO_3)_3$ and $Nd(NO_3)_3$, 3338; metal–amine solns., 3098; 3d trans. metal complexes in KCNS(1), 4014

Water, D_2O, radiolysis, 1583; dielectric constant, 445; diffusion in nonpolar gases, 2000; hemoglobin-bound, electrical properties, 2600; H_2O–HDO, thermo. data, 3491; HOD solns., mixture model, 4242; liq., structure, 1553; in NH_3, 863; photolysis, 2886; radiolysis, 1341, 2571; radiolysis, 2571; structure and properties of aq. proteins, 26; vapor, dissn. by microwave discharges, 3693; viscosity, 34; viscosity, 1187; on ZnO, thermo. data, 3809
Wustite, disproportionation, 1848

X-Ray diffraction studies, mono- and polynuclear thorium(IV) ions, 4163

Zeeman effect, propynal, 4359
Zeolite, decationated, Al at ads. sites, 2069; Fe–Y, Mössbauer study, 2970; hydrogen Y, OH gps on, 2086; Linde 5A, polar vapors ads. on, 1975
Zeolites, acetonitrile on, 2551; faujasite, Madlung potentials, 3660; faujasites, sorption complexes, 4384
Zeolite Y, hydrogen, preparation and properties, 2780
Zinc oxide, electron injection into, 468
Zirconium phosphates, ion exchange, 3424